



Handbook of

Oil Spill Science and Technology



Edited by
Merv Fingas

WILEY

HANDBOOK OF OIL SPILL SCIENCE AND TECHNOLOGY

HANDBOOK OF OIL SPILL SCIENCE AND TECHNOLOGY

Edited by

MERV FINGAS

Spill Science, Edmonton, Alberta, Canada

WILEY

Copyright © 2015 by John Wiley & Sons, Inc. All rights reserved

Published by John Wiley & Sons, Inc., Hoboken, New Jersey
Published simultaneously in Canada

No part of this publication may be reproduced, stored in a retrieval system, or transmitted in any form or by any means, electronic, mechanical, photocopying, recording, scanning, or otherwise, except as permitted under Section 107 or 108 of the 1976 United States Copyright Act, without either the prior written permission of the Publisher, or authorization through payment of the appropriate per-copy fee to the Copyright Clearance Center, Inc., 222 Rosewood Drive, Danvers, MA 01923, (978) 750-8400, fax (978) 750-4470, or on the web at www.copyright.com. Requests to the Publisher for permission should be addressed to the Permissions Department, John Wiley & Sons, Inc., 111 River Street, Hoboken, NJ 07030, (201) 748-6011, fax (201) 748-6008, or online at <http://www.wiley.com/go/permission>.

Limit of Liability/Disclaimer of Warranty: While the publisher and author have used their best efforts in preparing this book, they make no representations or warranties with respect to the accuracy or completeness of the contents of this book and specifically disclaim any implied warranties of merchantability or fitness for a particular purpose. No warranty may be created or extended by sales representatives or written sales materials. The advice and strategies contained herein may not be suitable for your situation. You should consult with a professional where appropriate. Neither the publisher nor author shall be liable for any loss of profit or any other commercial damages, including but not limited to special, incidental, consequential, or other damages.

For general information on our other products and services or for technical support, please contact our Customer Care Department within the United States at (800) 762-2974, outside the United States at (317) 572-3993 or fax (317) 572-4002.

Wiley also publishes its books in a variety of electronic formats. Some content that appears in print may not be available in electronic formats. For more information about Wiley products, visit our web site at www.wiley.com.

Library of Congress Cataloging-in-Publication Data:

Handbook of oil spill science and technology / edited by Merv Fingas.

pages cm

Includes bibliographical references and index.

ISBN 978-0-470-45551-7 (hardback)

1. Oil spills--Prevention--Handbooks, manuals, etc. 2. Oil spills--Cleanup--Handbooks, manuals, etc.
 3. Oil spills--Management--Handbooks, manuals, etc. 1. Fingas, Mervin, editor.
- TD427.P4H366 2015
628.1'6833--dc23

2014022293

Printed in the United States of America

10 9 8 7 6 5 4 3 2 1

CONTENTS

CONTRIBUTORS	xvii
AUTHOR BIOGRAPHIES	xix
PREFACE	xxvii

PART I RISK ANALYSIS	1
-----------------------------	----------

1 Risk Analysis and Prevention	3
---------------------------------------	----------

Dagmar Schmidt Etkin

- 1.1 Introduction, 3
- 1.2 Executive Summary, 3
- 1.3 Oil Spill Risk Analysis, 4
 - 1.3.1 Defining “Oil Spill Risk”, 4
 - 1.3.2 Factors That Determine the Probability of Spill Occurrence, 5
 - 1.3.3 Probability Distributions of Spill Volume, 9
 - 1.3.4 Determining the Probable Locations and Timing of Spills, 11
 - 1.3.5 Factors That Determine the Consequences/Impacts of a Spill, 11
 - 1.3.6 Spill Impacts: The Effects of Spill Location Type, 16
 - 1.3.7 Measuring Oil Spill Impacts, 18
 - 1.3.8 Interpreting Risk for Policy-Making, 27
- 1.4 Overview of Oil Spill Prevention, 28
 - 1.4.1 Basic Strategies for Spill Prevention, 28
 - 1.4.2 Implementation of Spill Prevention Measures, 29
 - 1.4.3 Effectiveness of Spill Prevention, 29
 - 1.4.4 Spill Fines and Penalties as Deterrents, 31
- References, 34

PART II OIL PROPERTIES	37
-------------------------------	-----------

2 Oil Physical Properties: Measurement and Correlation	39
---	-----------

Bruce P. Hollebone

- 2.1 Introduction, 39
- 2.2 Bulk Properties of Crude Oil and Fuel Products, 39

- 2.2.1 Density and API Gravity, 40
- 2.2.2 Dynamic Viscosity, 41
- 2.2.3 Surface and Interfacial Tensions, 41
- 2.2.4 Flash Point, 42
- 2.2.5 Pour Point, 42
- 2.2.6 Sulfur Content, 42
- 2.2.7 Water Content, 42
- 2.2.8 Evaluation of the Stability of Emulsions Formed from Brine and Oils and Oil Products, 43
- 2.2.9 Evaluation of the Effectiveness of Dispersants on an Oil, 43
- 2.2.10 Adhesion, 44
- 2.3 Hydrocarbon Groups, 44
 - 2.3.1 Saturates, 44
 - 2.3.2 Aromatics, 44
 - 2.3.3 Resins, 44
 - 2.3.4 Asphaltenes, 44
- 2.4 Quality Assurance and Control, 46
- 2.5 Effects of Evaporative Weathering on Oil Bulk Properties, 46
 - 2.5.1 Weathering, 46
 - 2.5.2 Preparing Evaporated (Weathered) Samples of Oils, 47
 - 2.5.3 Quantifying Equation(s) for Predicting Evaporation, 47
- References, 49

PART III OIL COMPOSITION AND PROPERTIES 51

3 Introduction to Oil Chemistry and Properties 53

Merv Fingas

- 3.1 Introduction, 53
- 3.2 The Composition of Oil, 53
 - 3.2.1 SARA, 54
 - 3.2.2 Sulfur Compounds, 58
 - 3.2.3 Oxygen Compounds, 58
 - 3.2.4 Nitrogen Compounds, 69
 - 3.2.5 Metals, 69
 - 3.2.6 Resins, 69
 - 3.2.7 Asphaltenes, 69
- 3.3 Properties of Oil, 75
- References, 76

4 Vegetable Oil Spills: Oil Properties and Behavior 79

Merv Fingas

- 4.1 Introduction, 79
- 4.2 The Oils, 79
- 4.3 Historical Spills, 79
- 4.4 Aquatic Toxicity, 86
- 4.5 Properties of the Oils, 86
- 4.6 Behavior in the Environment, 87
- 4.7 Oxidation, Biodegradation, and Polymerization, 87
- 4.8 Spill Countermeasures, 88
- 4.9 Biofuels, 88
- 4.10 Conclusions, 89
- References, 89

PART IV OIL ANALYSIS	93
5 Chromatographic Fingerprinting Analysis of Crude Oils and Petroleum Products	95
<i>Chun Yang, Zhendi Wang, Bruce P. Hollebone, Carl E. Brown, Zeyu Yang, and Mike Landriault</i>	
5.1 Introduction, 95	
5.1.1 Crude Oils and Refined Petroleum Products, 96	
5.1.2 Chemical Components of Petroleum, 97	
5.2 Introduction to Oil Analysis Techniques, 100	
5.2.1 GC, 100	
5.2.2 GC with Mass Spectrometry, 103	
5.2.3 Ancillary Oil Fingerprinting Techniques, 104	
5.3 Methodology of Oil Fingerprinting Analysis, 105	
5.3.1 Oil Sample Preparation and Separation, 105	
5.3.2 Identification and Quantitation of Target Petroleum Hydrocarbons, 110	
5.3.3 Oil Type Screening by GC–FID, 113	
5.3.4 Aliphatic Hydrocarbons in Petroleum, 117	
5.3.5 Aromatic Hydrocarbons in Petroleum, 130	
5.4 Weathering Effect on Oil Chemical Composition, 141	
5.4.1 Evaporation Weathering, 141	
5.4.2 Biodegradation Weathering, 141	
5.4.3 Photodegradation Weathering, 146	
5.4.4 Assessment of Mass Loss during Weathering, 147	
5.5 Diagnostic Ratios of Target Hydrocarbons, 148	
5.5.1 Molecular Diagnostic Ratios for Oil Identification, 148	
5.5.2 Selection of Diagnostic Ratios, 150	
5.6 Forensic Oil Spill Identification: A Case Study, 151	
5.6.1 Product Type Screening and Determination of Hydrocarbon Groups, 152	
5.6.2 Determination of Oil-Characteristic Alkylated PAHs and Biomarkers, 154	
5.6.3 Comparison of Diagnostic Ratios, 157	
5.6.4 Weathering Check, 157	
5.6.5 Results of Match between Spilled Oils and Candidate Sources, 157	
References, 158	
6 Oil Spill Identification	165
<i>Joan Albaigés, Paul G.M. Kienhuis, and Gerhard Dahlmann</i>	
6.1 Introduction, 165	
6.2 Sampling, 167	
6.2.1 Thick Oil Layers and Tar Balls, 167	
6.2.2 Sampling of Thin Oil Films (Sheens or Slicks), 167	
6.2.3 Taking Oil Samples on Beaches and from Oiled Animals, 169	
6.2.4 Sampling on Board Vessels, 170	
6.3 Sample Handling in the Laboratory, 170	
6.4 Analysis, 171	
6.4.1 Characterization by GC–FID: Level 1, 172	
6.4.2 Characterization by GC–MS: Level 2, 176	
6.5 Conclusions, 198	
References, 202	

PART V OIL BEHAVIOR	205
7 Oil and Petroleum Evaporation	207
<i>Merv Fingas</i>	
7.1 Introduction, 207	
7.2 Review of Historical Concepts, 209	
7.3 Development of New Diffusion-Regulated Models, 213	
7.3.1 Wind Experiments, 213	
7.3.2 Variation with Area, 214	
7.3.3 Variation with Mass, 215	
7.3.4 Evaporation of Pure Hydrocarbons, 215	
7.3.5 Saturation Concentration, 216	
7.3.6 Development of Generic Equations Using Distillation Data, 216	
7.4 Complexities to the Diffusion-Regulated Model, 218	
7.4.1 Oil Thickness, 218	
7.4.2 The Bottle Effect, 219	
7.4.3 Skinning, 220	
7.4.4 Jumps from the 0-Wind Values, 220	
7.5 Use of Evaporation Equations in Spill Models, 220	
7.6 Volatilization, 221	
7.7 Measurement of Evaporation, 221	
7.8 Summary, 221	
References, 222	
8 Water-in-Oil Emulsions: Formation and Prediction	225
<i>Merv Fingas and Ben Fieldhouse</i>	
8.1 Introduction, 225	
8.2 Types of Emulsions, 225	
8.3 Stability Indices, 226	
8.4 Formation of Emulsions, 230	
8.4.1 The Role of Asphaltenes, 230	
8.4.2 The Role of Resins and Other Components, 231	
8.4.3 Methods to Study Emulsions, 232	
8.4.4 The Overall Theory of Emulsion Formation, 233	
8.4.5 The Role of Weathering, 235	
8.5 Modeling the Formation of Water-in-Oil Emulsions, 235	
8.5.1 Older Models, 235	
8.5.2 New Models, 236	
8.5.3 Development of an Emulsion Kinetics Estimator, 250	
8.5.4 Model Certainty, 250	
8.6 Conclusions, 251	
References, 268	
9 Oil Behavior in Ice-Infested Waters	271
<i>Merv Fingas and Bruce P. Hollebone</i>	
9.1 Introduction, 271	
9.2 Spreading on Ice, 271	
9.3 Spreading on or in Snow, 273	
9.4 Spreading under Ice, 273	
9.4.1 Water Stripping Velocity under Ice, 274	
9.5 Spreading on Water with Ice Present, 274	
9.6 The Effect of Gas on Oil-under-Ice Spreading, 275	
9.7 Movement through Ice, 276	

- 9.8 Oil in Leads, 277
- 9.9 Absorption to Snow and Ice, 280
- 9.10 Containment on Ice, 280
- 9.11 Heating Effect of Oil on the Surface of Ice, 280
- 9.12 Oil under Multiyear Ice, 280
- 9.13 Oil in Pack Ice, 281
- 9.14 Growth of Ice on Shorelines and Effect on Oil Retention, 281
- 9.15 Effect of Oil on Ice Properties, 281
- 9.16 Concluding Remarks, 283
- References, 283

PART VI MODELING 285

10 Introduction to Spill Modeling 287

Merv Fingas

- 10.1 Introduction, 287
- 10.2 An Overview of Weathering, 287
- 10.3 Evaporation, 288
- 10.4 Water Uptake and Emulsification, 290
 - 10.4.1 Regression Model Calculation, 291
- 10.5 Natural Dispersion, 293
- 10.6 Summary of Natural Dispersion, 295
- 10.7 Other Processes, 295
 - 10.7.1 Dissolution, 295
 - 10.7.2 Photooxidation, 295
 - 10.7.3 Sedimentation, Adhesion to Surfaces, and Oil–Fines Interaction, 295
 - 10.7.4 Biodegradation, 296
 - 10.7.5 Sinking and Overwashing, 296
 - 10.7.6 Formation of Tar Balls, 297
- 10.8 Movement of Oil and Oil Spill Modeling, 297
 - 10.8.1 Spreading, 297
 - 10.8.2 Movement of Oil Slicks, 298
- 10.9 Spill Modeling, 299
- References, 299

11 Oceanographic and Meteorological Effects on Spilled Oil 301

C.J. Beegle-Krause and William J. Lehr

- List of Symbols, 301
- 11.1 Introduction, 301
- 11.2 Chapter Scope, 302
- 11.3 Atmospheric Boundary Layer, 302
- 11.4 Water Currents, 303
- 11.5 Waves, 304
- 11.6 Sea Spray, 306
- 11.7 Langmuir Cells, 306
- 11.8 Oil Transport, 307
- 11.9 Areas of Active Research, 308
 - 11.9.1 Ice, 308
 - 11.9.2 Lagrangian Coherent Structures, 308
 - 11.9.3 Subsurface Well Blowouts, 308
- References, 309

PART VII DETECTION, TRACKING, AND REMOTE SENSING 311

12 Oil Spill Remote Sensing 313

Merv Fingas and Carl E. Brown

- 12.1 Introduction, 313
- 12.2 Atmospheric Properties, 314
- 12.3 Oil Interaction with Light and Electronic Waves, 314
- 12.4 Visible Indications of Oil, 316
- 12.5 Optical Sensors, 317
 - 12.5.1 Visible, 317
 - 12.5.2 IR, 323
 - 12.5.3 Near IR, 323
 - 12.5.4 UV, 325
- 12.6 Laser Fluorosensors, 325
- 12.7 Microwave Sensors, 326
 - 12.7.1 Radiometers, 326
 - 12.7.2 Radar, 327
 - 12.7.3 Microwave Scatterometers, 331
 - 12.7.4 Surface-Wave Radars, 331
 - 12.7.5 Interferometric Radar, 331
- 12.8 Slick Thickness Determination, 331
 - 12.8.1 Visual Thickness Indications, 331
 - 12.8.2 Slick Thickness Relationships in Remote Sensors, 332
 - 12.8.3 Specific Thickness Sensors, 332
- 12.9 Integrated Airborne Sensor Systems, 333
- 12.10 Satellite Remote Sensing, 334
 - 12.10.1 Optical, 334
 - 12.10.2 Radar, 335
- 12.11 Oil-Under-Ice Detection, 340
- 12.12 Underwater Detection and Tracking, 340
- 12.13 Small Remote-Controlled Aircraft, 344
- 12.14 Real-Time Displays and Printers, 345
- 12.15 Routine Surveillance, 345
- 12.16 Future Trends, 346
- 12.17 Recommendations, 347
- References, 348

13 Detection, Tracking, and Remote Sensing: Satellites and Image Processing (Spaceborne Oil Spill Detection) 357

Konstantinos Topouzelis, Dario Tarchi, Michele Vespe, Monica Posada, Oliver Muellenhoff and Guido Ferraro

- 13.1 Introduction, 357
- 13.2 Oil Spills Detection by Satellite, 358
 - 13.2.1 Optical Remote Sensing, 358
 - 13.2.2 Microwave Remote Sensing, 360
- 13.3 From Research to Operational Services, 366
 - 13.3.1 Historical attempts, 366
 - 13.3.2 Operational Oil Spill Detection, 371
 - 13.3.3 Oil Seepage Detection Aspects, 374
- 13.4 Ancillary Data, 375
 - 13.4.1 Detection Capability, 375
 - 13.4.2 Risk of Pollution, 377
 - 13.4.3 Ship Detection (AIS, LRIT, VMS, Satellite AIS), 377
- 13.5 Summary and Conclusions, 378
- References, 381

14 Detection of Oil in, with, and under Ice and Snow 385

Merv Fingas and Carl E. Brown

- 14.1 Introduction, 385
- 14.2 Overview of Detection of Oil in or under Ice and Snow, 385
 - 14.2.1 Optical Methods, 386
 - 14.2.2 Acoustic Methods, 386
 - 14.2.3 Radio-Frequency Methods, 389
 - 14.2.4 Ground-Penetrating Radar, 390
 - 14.2.5 UHF Radiometer, 391
 - 14.2.6 Nuclear Techniques, 391
 - 14.2.7 Gas Sniffing and Leak Detection, 391
 - 14.2.8 Nuclear Magnetic Resonance, 392
- 14.3 Detection of Surface Oil with Ice: Conventional Techniques, 392
- 14.4 Conclusions, 392
- References, 392

PART VIII OIL SPILLS ON LAND 395

15 Bioremediation of Oil Spills on Land 397

Lisa D. Brown and Ania C. Ulrich

- 15.1 Introduction, 397
- 15.2 Brief Overview of Bioremediation Techniques for Land Oil Spills, 397
 - 15.2.1 *In Situ* versus *Ex Situ*, 397
 - 15.2.2 Biostimulation versus Bioaugmentation, 398
- 15.3 Key Organisms Involved in Biodegradation of Oil Spills on Land, 398
 - 15.3.1 Communities versus Isolates, 399
- 15.4 Environmental Factors Affecting Bioremediation, 399
 - 15.4.1 Temperature, 399
 - 15.4.2 pH, 399
 - 15.4.3 Salinity, 399
 - 15.4.4 Nutrients, 399
 - 15.4.5 Moisture, 400
 - 15.4.6 Redox Environment, 400
 - 15.4.7 Soil Type, 400
- 15.5 *In Situ* Bioremediation Strategies, 400
 - 15.5.1 Bioventing, 401
 - 15.5.2 Enhanced Bioremediation, 401
 - 15.5.3 Monitored Natural Attenuation, 401
- 15.6 *Ex Situ* Land Treatment Techniques, 402
 - 15.6.1 Landfarming and Land Treatment, 402
 - 15.6.2 Biopiles, 403
 - 15.6.3 Organic Amendments, 403
- 15.7 Bioaugmentation Strategies, 404
 - 15.7.1 Key Bacteria Used in Bioaugmentation, 404
 - 15.7.2 Role of Other Organisms, 404
- 15.8 Biostimulation Strategies, 404
 - 15.8.1 Biosurfactants, 404
- References, 405

16 Microbe-Assisted Phytoremediation of Petroleum Impacted Soil: A Scientifically Proven Green Technology 407

Karen E. Gerhardt, Perry D. Gerwing, Xiao-Dong Huang, and Bruce M. Greenberg

- 16.1 Introduction, 407
 - 16.1.1 Overview of Phytoremediation, 407

16.1.2	Developing Microbe-Assisted Phytoremediation as a Remedial Strategy for PHC,	407
16.1.3	Benefits and Challenges of Phytoremediation and Microbe-Assisted Phytoremediation,	411
16.1.4	Successful Field Tests of Phytoremediation,	413
16.2	PGPR-Enhanced Phytoremediation System(s),	413
16.2.1	Development, Proof, and Full-Scale Application of PEPS,	414
16.2.2	Keys to the Success of PEPS,	415
16.3	Case Studies of Full-Scale Petroleum Phytoremediation,	416
16.3.1	Case Study #1: Edson, Alberta,	416
16.3.2	Case Study #2: Peace River, Alberta,	418
16.3.3	Case Study #3: Hinton, Alberta,	419
16.3.4	Case Study #4: Dawson Creek, British Columbia,	420
16.3.5	Overall Conclusions from Case Studies,	420
16.4	Achieving Regulatory Criteria,	421
16.4.1	Optimizing PHC Analytical Protocols for Removal of BOC,	421
16.4.2	Plant Toxicity Testing,	422
16.5	Conclusions,	422
	References,	423

PART IX EFFECTS OF OIL 429

17 Overview of Efforts to Document and Reduce Impacts of Oil Spills on Seabirds 431

Roger C. Helm, Harry R. Carter, R. Glenn Ford, D. Michael Fry, Rocío L. Moreno, Carolina Sanpera and Florina S. Tseng

17.1	Introduction,	431
17.2	Vulnerability,	433
17.3	Effect of Oiling on Individual Birds,	435
17.3.1	External Oil Effects,	435
17.3.2	Internal Oil Effects,	435
17.3.3	Oil Effects on Reproduction,	436
17.4	Rehabilitation and Veterinary Care,	436
17.4.1	Key Considerations in Care,	436
17.4.2	Release Rates,	437
17.4.3	Post-Release Survival and Reproduction,	437
17.4.4	Rehabilitation Process,	438
17.5	Estimating Mortality,	441
17.5.1	Oiled Birds at Sea,	441
17.5.2	Oiled Birds on Land,	442
17.5.3	Cause of Death and Background Deposition,	443
17.6	Long-Term Impacts,	444
17.7	Restoration,	446
17.7.1	<i>Apex Houston</i> Barge Oil Spill, Central California,	446
17.7.2	<i>American Trader</i> Oil Spill, Southern California,	448
	References,	448

18 Overview of Effects of Oil Spills on Marine Mammals 455

Roger C. Helm, Daniel P. Costa, Terry D. DeBruyn, Thomas J. O'Shea, Randall S. Wells, and Terrie M. Williams

18.1	Introduction,	455
18.1.1	Sea Otters,	456
18.1.2	Seals and Sea Lions,	457
18.1.3	Sea Cows,	457

18.1.4	Polar Bears,	457	
18.1.5	Whales, Dolphins, and Porpoises,	457	
18.2	Sea Otters,	458	
18.2.1	External Exposure,	458	
18.2.2	Internal Exposure,	459	
18.2.3	Long-Term Effects,	461	
18.3	Seals and Sea Lions,	461	
18.3.1	Direct Effects,	462	
18.3.2	Vulnerability and Risk,	462	
18.4	Sea Cows,	464	
18.4.1	Direct Effects,	465	
18.4.2	Indirect Effects,	465	
18.5	Polar Bears,	465	
18.5.1	Direct and Indirect Effects,	465	
18.5.2	Vulnerability and Risk,	466	
18.6	Whales, Dolphins, and Porpoises,	467	
18.6.1	Direct Effects,	467	
18.6.2	Vulnerability and Risk,	468	
	References,	471	
19	Oil Spill Impact and Recovery of Coastal Marsh Vegetation		477
	<i>Qianxin Lin</i>		
19.1	Introduction,	477	
19.2	Toxicity and Impact as a Function of Oil Type and Oil Weathering Degree,	477	
19.3	Sensitivity to Oil Varies by Plant Species,	478	
19.4	Effects of Oil Exposure Modes on Severity of Oil Impacts,	479	
19.5	Effects of Oil Spill Cleanup Procedures on Marsh Recovery,	481	
	References,	483	
PART X	NATURAL DISPERSION		485
20	A Review of Natural Dispersion Models		487
	<i>Merv Fingas</i>		
20.1	Introduction,	487	
20.2	The Mackay Approach,	487	
20.3	The Audunson Approach,	489	
20.4	The Delvigne Approach,	490	
20.5	Residence in the Water Column,	492	
20.6	Comparison of the Models,	492	
20.7	Conclusions,	494	
	References,	494	
PART XI	COLD REGION SPILLS		495
21	Arctic and Antarctic Spills		497
	<i>D.M. Filler, Mahlon C. Kennicutt II, I. Snape, Stephen T. Sweet, and Andrew G. Klein</i>		
21.1	Introduction,	497	
21.1.1	Occurrences,	498	
21.1.2	Scale of the Problem,	499	
21.1.3	Environments,	499	
21.1.4	Regulatory Framework,	501	
21.2	Terrestrial Spills,	502	

- 21.2.1 Petroleum Transport and Fate, 502
- 21.2.2 Mitigation and Countermeasures, 506
- 21.2.3 Remediation and Lessons Learned, 506
- 21.3 Marine Spills, 507
 - 21.3.1 Petroleum Transport and Fate, 507
 - 21.3.2 Mitigation and Countermeasures, 508
 - 21.3.3 Remediation and Lessons Learned, 508
- 21.4 Policy, 508
- References, 510

PART XII CASE STUDIES 513

22 The Prestige Oil Spill 515

Joan Albaigés, Ana Bernabeu, Sonia Castanedo, Núria Jiménez, Carmen Morales-Caselles, Araceli Puente, and Lucía Viñas

- 22.1 Introduction, 515
- 22.2 The Ocean and Coastal Dynamics in the NW Iberia and their Influence on the Spill, 516
 - 22.2.1 Oceanographic Conditions, 516
 - 22.2.2 Oil Spill Forecasting, 519
- 22.3 Oil Monitoring and Fate, 521
 - 22.3.1 Fuel Oil Composition, 521
 - 22.3.2 Fuel at Sea, 521
 - 22.3.3 Spatial and Temporal Distribution in Seawater, 525
 - 22.3.4 Continental Shelf Contamination, 526
 - 22.3.5 Accumulation in Biota, 528
- 22.4 The Assessment of Effects, 531
 - 22.4.1 Bioassays under Laboratory Conditions, 531
 - 22.4.2 Field Studies, 532
- 22.5 Environmental Restoration, 537
 - 22.5.1 Oil Recovery at Sea, 537
 - 22.5.2 Coastal Contamination and Cleanup Efforts, 537
 - 22.5.3 Natural Attenuation Processes, 539
- 22.6 Conclusion, 541
- References, 542

23 The Grounding of the *Bahía Paraíso*, Arthur Harbor, Antarctica: Distribution and Fate of Oil Spill Related Hydrocarbons 547

Stephen T. Sweet, Mahlon C. Kennicutt II, and Andrew G. Klein

- 23.1 Introduction and Background, 547
- 23.2 Environmental Sampling, 550
 - 23.2.1 Surface Slicks and Water Column, 550
 - 23.2.2 Intertidal Macroalgae, 550
 - 23.2.3 Intertidal Beaches, 550
 - 23.2.4 Intertidal Limpets, 551
 - 23.2.5 Subtidal Sediments, 553
 - 23.2.6 Impacts on Other Wildlife, 553
- 23.3 Conclusions, 555
- References, 555

24 Tasman Spirit Oil Spill at Karachi Coast, Pakistan 557

Hina Ahsan Siddiqi and Alia Bano Munshi

- 24.1 Introduction, 557
- 24.2 Immediate Response to the Impact: Actions and Remediation, 557

24.2.1	Oil Recovery and Coast Cleaning,	558
24.2.2	Oil Spill Monitoring,	559
24.2.3	Socioeconomic Impact and Damage to Coastal Marine Life Damage,	560
24.2.4	Human Health Impacts,	561
24.3	The DDWP Project by Ministry of Science and Technology (MoST),	561
24.4	Hydrodynamics and Meteorological Data,	562
24.4.1	Oceanographic Conditions,	562
24.4.2	The Assessment of Oil Transport: Numerical Models,	562
24.5	Oil Monitoring and Fate,	564
24.5.1	Oil Composition,	564
24.5.2	Spatial and Temporal Distribution in Seawater,	564
24.5.3	Biota Affected by Oil Pollution,	566
24.5.4	Oil Content of Sediment,	566
24.6	Effects of Oil Impact at the Community Level,	568
24.6.1	The Effects on the Benthic System,	568
24.6.2	The Effects on the Pelagic System,	569
24.7	Bioremediation/Natural Attenuation Processes,	572
24.8	Conclusions,	572
	References,	573

PART XIII APPENDICES 575

APPENDIX A

THE OIL PROPERTIES DATA APPENDIX 577

Bruce P. Hollebone

APPENDIX B

CONVERSIONS 683

Merv Fingas

APPENDIX C

ICE NOMENCLATURE 685

Merv Fingas

INDEX 689

CONTRIBUTORS

Joan Albaigés Department of Environmental Chemistry, IDAEA–CSIC, Barcelona, Spain

C.J. Beegle-Krause SINTEF, Trondheim, Norway

Ana Bernabeu Department of Marine Geosciences, University of Vigo, Vigo, Spain

Carl E. Brown Emergencies Science and Technology Section (ESTS), Environment Canada, Ottawa, Ontario, Canada

Lisa D. Brown Department of Civil and Environmental Engineering, University of Alberta, Edmonton, Canada

Harry R. Carter Carter Biological Consulting, Victoria, BC, Canada

Sonia Castanedo Environmental Hydraulics Institute (IH Cantabria), Universidad de Cantabria, Parque Científico y Tecnológico de Cantabria (PCTCAN), Santander, Spain

Daniel P. Costa Department of Ecology and Evolutionary Biology, University of California, Santa Cruz, CA, USA

Gerhard Dahlmann Bundesamt für Seeschifffahrt und Hydrographie (BSH), Hamburg, Germany

Dagmar Schmidt Etkin Environmental Research Consulting, Cortlandt Manor, NY, USA

Terry D. DeBruyn U.S. Fish and Wildlife Service, Anchorage, AK, USA

Guido Ferraro Maritime Affairs Unit, Institute for Security and Protection of the Citizen – JRC European Commission, Ispra, Italy

Ben Fieldhouse Emergencies Science and Technology Section (ESTS), Environment Canada, Ottawa, Ontario, Canada

D.M. Filler Department of Civil, Environmental, and Construction Engineering, University of Central Florida, Orlando, FL, USA

Merv Fingas Spill Science, Edmonton, Alberta, Canada

R. Glenn Ford R.G. Ford Consulting Company, Portland, OR, USA

Karen E. Gerhardt Department of Biology, University of Waterloo, Waterloo; and Waterloo Environmental Biotechnology Inc., Hamilton, Ontario, Canada

Perry D. Gerwing Earthmaster Environmental Strategies Inc., Calgary, Alberta, Canada

Bruce M. Greenberg Department of Biology, University of Waterloo, Waterloo; and Waterloo Environmental Biotechnology Inc., Hamilton, Ontario, Canada

Roger C. Helm U.S. Fish and Wildlife Service, Science Applications, Falls Church, VA, USA

Bruce P. Hollebone Emergencies Science and Technology Section (ESTS), Environment Canada, Ottawa, Ontario, Canada

Xiao-Dong Huang Waterloo Environmental Biotechnology Inc., Hamilton, Ontario, Canada

Núria Jiménez Department of Environmental Chemistry, IDAEA–CSIC, Barcelona, Spain; and Federal Institute for Geosciences and Natural Resources (BGR), Geozentrum Hannover, Hannover, Germany

Mahlon C. Kennicutt II Department of Oceanography, Texas A&M University, College Station, TX, USA

Paul G.M. Kienhuis Rijkswaterstaat Center for Water Management (RWS-WD), Lelystad, The Netherlands

Andrew G. Klein Department of Geography, Texas A&M University, College Station, TX, USA

Mike Landriault Emergencies Science and Technology Section (ESTS), Environment Canada, Ottawa, Ontario, Canada

William J. Lehr Emergency Response Division, National Oceanic and Atmospheric Administration, Seattle, WA, USA

Qianxin Lin Department of Oceanography and Coastal Sciences, School of the Coast and Environment, Louisiana State University, Baton Rouge, LA, USA

D. Michael Fry U.S. Fish and Wildlife Service, Environmental Contaminants, Pacific Islands Fish and Wildlife Office, Honolulu, HI, USA

Carmen Morales-Caselles Intergovernmental Oceanographic Commission, UNESCO, Paris, France; and Associated Unit of Pathology and Environmental Quality, University of Cádiz & Institute of Marine Sciences in Andalusia (CSIC), Puerto Real, Cádiz, Spain

Rocío L. Moreno Departament de Biologia Animal, Facultat de Biologia, Universitat de Barcelona, Barcelona, Spain

Oliver Muellenhoff Maritime Affairs Unit, Institute for Security and Protection of the Citizen – JRC European Commission, Ispra, Italy

Alia Bano Munshi Centre for Environmental Studies, Pakistan Council of Scientific and Industrial Research (PCSIR), Karachi, Sindh, Pakistan

Thomas J. O'Shea U.S. Geological Survey (Retired), Glen Haven, CO, USA

Monica Posada Maritime Affairs Unit, Institute for Security and Protection of the Citizen – JRC European Commission, Ispra, Italy

Araceli Puente Environmental Hydraulics Institute (IH Cantabria), Universidad de Cantabria, Parque Científico y Tecnológico de Cantabria (PCTCAN), Santander, Spain

Carolina Sanpera Departament de Biologia Animal, Facultat de Biologia, Universitat de Barcelona, Barcelona, Spain

Hina Ahsan Siddiqi Centre for Environmental Studies, Pakistan Council of Scientific and Industrial Research (PCSIR), Karachi, Sindh, Pakistan

Ian Snape Australian Antarctic Division, Environmental Protection and Change Program, Kingston, Tasmania, Australia

Stephen T. Sweet Texas A&M University, College Station, TX, USA

Dario Tarchi Maritime Affairs Unit, Institute for Security and Protection of the Citizen – JRC European Commission, Ispra, Italy

Konstantinos Topouzelis Department of Marine Sciences, University of the Aegean, Mytilene, Greece

Florina S. Tseng Cummings School of Veterinary Medicine, North Grafton, MA, USA

Ania C. Ulrich Department of Civil and Environmental Engineering, University of Alberta, Edmonton, Canada

Michele Vespe Maritime Affairs Unit, Institute for Security and Protection of the Citizen – JRC European Commission, Ispra, Italy

Lucía Viñas Instituto Español de Oceanografía, Centro Oceanográfico de Vigo, Vigo, Spain

Zhendi Wang Emergencies Science and Technology Section (ESTS), Environment Canada, Ottawa, Ontario, Canada

Randall S. Wells Chicago Zoological Society-Mote Marine Laboratory, Sarasota, FL, USA

Terrie M. Williams Center for Ocean Health, University of California, Santa Cruz, CA, USA

Chun Yang Emergencies Science and Technology Section (ESTS), Environment Canada, Ottawa, Ontario, Canada

Zeyu Yang Emergencies Science and Technology Section (ESTS), Environment Canada, Ottawa, Ontario, Canada

AUTHOR BIOGRAPHIES

Dr. Joan Albaigés is Emeritus professor of the Spanish Research Council (CSIC). He established in 1979 at the CSIC (Barcelona), the Department of Environmental Chemistry, where pioneering and internationally well-known research activities on environmental organic chemistry, biogeochemistry of continental and marine waters, and ecotoxicology of organic pollutants started to develop. He spent 10 years as a consultant for the UNEP Regional Seas Program, keeping a personal engagement in promoting marine monitoring programs with developing countries, particularly in Latin America. He was appointed vice-chairman of the Scientific Advisory Committee on the Prestige accident (2002), coordinator of the European Network on Accidental Marine Pollution (Ampera) (2004) and, since 2010, of the ERA-Net “Towards integrated European marine research strategy and programs” (SEAS-ERA), which groups 20 countries. He is also member of the oil spill identification expert group (OSINET) and responsible for the Spanish reference laboratory for oil spill identification. He has contributed over 250 refereed articles to scientific journals, being editor-in-chief of the *International Journal of Environmental Analytical Chemistry*. Prof. Albaigés has been the recipient of several awards, including the Award for Nature Conservation (Osborne Foundation, 1973), the Award for Mass Spectrometry (Hewlett-Packard, 1986), the Monturiol Award for Science Merit (Government of Catalonia, 1989), and the Spanish Research Award on Coastal and Marine Pollution Studies (2007). He has also been elected member of the European Academy of Sciences and Arts, the Academia Europaea, and the Royal Academy of Sciences and Arts (Spain).

Dr. C.J. Beegle-Krause is an oceanographer interested in finding better answers for the Decision Support questions. Most interested in Lagrangian drift problems, such as oil spills, marine debris, and larval fish modeling, she sees that

the greatest need now is to develop new models for oil-in-ice and to leverage new types of analysis, such as Lagrangian coherent structures. Currently, she is a senior researcher at SINTEF in Norway, and previously she was president of Research4D, a small nonprofit in Seattle, WA, and a senior scientist at RPS ASA. Most of her early career was spent in her first position at the NOAA Office of Response and Restoration. She has worked on over 200 spills and was a lead trajectory modeler for the United States during her last 5 years. In 2010, she was recalled to work on the Deepwater Horizon oil spill. Oil spill issues are inherently interdisciplinary, frequently require decisions among trade-offs, and solutions need to be collaborative. She graduated with a B.S. from Caltech in biology, M.S. from University of Alaska Fairbanks in physical oceanography and Ph.D. from the University of Washington in physical oceanography. She also was a member of the U.S. World Cup Team in Fencing.

Dr. Ana Bernabeu is associate professor at the University of Vigo (Spain). She has a Ph.D. on marine science from the University of Cantabria (Spain). Her field of expertise is marine geology and sedimentary dynamics. She has authored about 80 papers (mostly in international journals) and regularly gives presentations and invited talks on these topics in international venues. She has led OILDEBEACH, an important EU effort for the development of an assessment and cleanup protocol of the oil buried in sandy beaches. At present, she is the vice dean for students' mobility and international liaisons at the Marine Science Faculty in the University of Vigo and Associated Editor in the *Journal of Iberian Geology*.

Dr. Carl E. Brown is the manager of the Emergencies Science and Technology Section in the Water Science and Technology Directorate of Environment Canada. Dr. Brown has a doctorate degree in physical chemistry from McMaster

University and a Bachelor of Technology degree in laboratory science from Ryerson Polytechnical University. Prior to joining Environment Canada, Dr. Brown was a research scientist on Natural Sciences and Engineering Research Council (NSERC) Industrial Fellowship with Intera Information Technologies (now Intermap). Dr. Brown has postdoctoral experience as a research associate with the Organic Reaction Dynamics and the Laser Chemistry Groups at the Steacie Institute for Molecular Sciences, at the National Research Council of Canada, and held a Canadian Government Laboratory Visiting Fellowship in Chemistry, with the Laser Chemistry Group, Division of Chemistry, National Research Council of Canada in Ottawa. His specialities include air-borne oil spill sensor development and the application of laser technologies to environmental problems. He has authored over 230 scientific papers and publications. Dr. Brown is the Chemical Science Community of Practice Leader for the Canadian Safety and Security Program (CSSP) led by Defence Research and Development Canada (DRDC) and Public Safety Canada. Dr. Brown is a graduate of the "Government of Canada's Scientists as Leaders Management Development Program." He has twice been awarded Environment Canada's Citation of Excellence in Teamwork, Partnering and Collaboration, in 2010 for the Vancouver Olympic and Paralympic Winter Games Team, and in 2010 for the ESTS Deepwater Horizon Scientific Support Team.

Dr. Lisa D. Brown is an environmental engineer with work experience in reclamation in the Canadian oil sands and in solid waste management, particularly composting. Dr. Brown completed her Ph.D. in geoenvironmental engineering at the University of Alberta, investigating biological treatment options for organic compounds of concern found in oil sands process-affected waters. Dr. Brown is planning to pursue a career in contaminated sites and/or solid waste.

Harry R. Carter is an independent seabird biologist and consultant who has worked widely on the west coast of North America surveying, monitoring, and studying seabird populations, including rare and endangered species. Since the mid-1980s, he has assisted various aspects of work related to oil spills, including injury assessments, determination of population impacts, assessment of survival of rehabilitated birds, and restoration planning and implementation.

Dr. Sonia Castanedo has a Ph.D. in civil engineering. Since 2011, she is associate professor at the University of Cantabria, in the area of hydraulic engineering, and senior researcher at the Environmental Hydraulics Institute (IH Cantabria). To date, her research has focussed primarily on the study of the morphodynamics of estuaries, numerical modeling and hydrodynamic transport of substances (e.g., oil spills and brine), operational oceanography, and coastal hazards assessment. She has been involved in numerous national and international projects and in more than 20 projects for the Spanish ports and coastal administration. She

has published more than 20 papers in peer-reviewed international journals.

Dr. Daniel P. Costa is a distinguished professor of ecology and evolutionary biology at the University of California at Santa Cruz (CA, USA) where he focuses on the ecology and physiology of marine mammals and seabirds in almost every habitat from the Galapagos to Antarctica. Dr. Costa conducted some of the earliest studies evaluating the effects of crude oil on sea otters in the laboratory and field and he participated in the damage assessment phase of the 1989 *Exxon Valdez* and 2010 *DeepWater Horizon* oil spills.

Dr. Gerhard Dahlmann is senior scientist in section Organic Contaminants of the laboratory of the Federal Maritime and Hydrographic Agency (Bundesamt für Seeschifffahrt und Hydrographie, BSH) in Hamburg, Germany. He has been working in the field of oil spill identification since 1978, when he came from the Institute of Fuel Technique, Clausthal-Zellerfeld, which was closely connected at that time to the Institute of Crude Oil Research, Hannover, in order to establish corresponding analytical techniques in the laboratory. At the beginning of the 1980s, pollution by oil was high in German waters. Patches of oil on beaches were frequently observed. After the analytical method was implemented, and especially after GC/MS was available, cooperation with investigating authorities started. Since then, the number of cases, in which spilled oil had to be compared with oil from suspected sources in the framework of criminal proceedings, decreased from more than 120 to about 10–15 per year. Gerhard Dahlmann has written a first publication about the GC/MS method for forensic investigations in cases of oil pollution in 1985, which was followed by publications about the use of the method in single cases. He was the scientific leader of several bigger national and international projects. Findings of these projects were continuously published. He is/was officially participating in international organizations, such as HELCOM, Bonn-Agreement/OTSOPA, and OSPAR-Offshore Industry Committee. In 2005, he became the convenor of the newly established Oil Spill Identification Network of experts within the Bonn-Agreement (Bonn-OSINET), which has got worldwide acceptance, meanwhile.

Dr. Terry D. DeBruyn has over two decades experience in studying and managing bears and his research and management experience includes all three species of North American bears. Between 2008 and 2013, Dr. DeBruyn served as the Polar Bear Project Leader for the U.S. Fish and Wildlife Service in Alaska. He now works for the U.S. Forest Service as the Ecosystems Team Leader in Hiawatha National Forest, Gladstone, Minnesota, USA.

Guido Ferraro, after a degree in Law of the Sea, joined the Italian Coast Guard as aircraft pilot for 15 years. In 1999, he joined the European Commission: first as Seconded National

Expert from the Italian Government and then as permanent staff. He received his Ph.D. on maritime affairs from the University of Ljubljana. All his professional experience is related to maritime issues and he has around 50 scientific publications on this subject.

Ben Fieldhouse is a scientist with 22 years experience in the field of environmental emergencies related to spills of hazardous materials at the Emergencies Science and Technology Section of Environment Canada. He has a B.Sc. in chemistry from York University in Toronto. His primary expertise is the behavior of petroleum crude oils and fuels released into aquatic environments, focussing on the study of water-in-oil emulsions, the impact of oil properties and chemical composition on the behavior of spills on water, and the effectiveness of treating agents as a spill countermeasure. His experience includes a number of field projects and emergency response operations, including large wave-tank trials, in situ burns, remote sensing ground-truthing operations, and contaminated site assessments.

Dr. Dennis M. Filler practices forensic engineering in Alaska and teaches engineering science at the University of Central Florida. He has published in geoenvironmental and cold regions engineering journals, and has a few book chapters on human impacts and bioremediation in cold regions. Current interests include engineering challenges of the far north and professional engineering education.

Dr. Merv Fingas is a scientist focusing on oil and chemical spills. He was a spill researcher in Environment Canada for over 30 years and is currently working privately in Western Canada. Mr. Fingas has a Ph.D. in environmental physics from McGill University and three masters degrees—chemistry, business, and mathematics—all from University of Ottawa. His specialities include spill dynamics and behavior, spill treating agent studies, remote sensing and detection, and in situ burning. He has over 800 papers and publications in the field. In his 40 years' career, he has published eight books on oil and hazardous materials. Dr. Fingas had been editor of the *Journal of Hazardous Materials* for 6 years. He has served on two committees on the U.S. National Academy of Sciences on oil spills including the recent "Oil in the Sea." He is chairman of several ASTM and intergovernmental committees on spill matters.

Dr. R. Glenn Ford is a modeler and biologist whose focus is on the spatial distribution of marine vertebrates, seabird foraging behavior, and the impacts of oil spills on seabirds. Since 1986, he has led modeling efforts to estimate seabird mortality resulting from most major oil spills in U.S. waters, including the 1989 *Exxon Valdez* (AK, USA) and 2010 MC-252 *DeepWater Horizon* oil spills (Gulf of Mexico, USA).

Dr. D. Michael Fry is an avian ecologist and toxicologist whose work has focused on the effects of pesticides, plastics,

polychlorinated biphenyls, and oil spills on wild birds. He is the author of over 50 scientific publications and coauthor of 10 books and book chapters. Dr. Fry was on the faculty of the Department of Avian Sciences at University of California, Davis, for two decades, at the American Bird Conservancy in Washington, DC, and is currently the environmental contaminants specialist for the U.S. Fish and Wildlife Service in Honolulu (HI, USA).

Karen E. Gerhardt is a research associate at the University of Waterloo, and manager of Research and Administrative Services for Waterloo Environmental Biotechnology Inc., a company that has developed and implemented microbe-enhanced phytoremediation systems. Her background includes research projects in plant biology, microbiology, photobiology, and biochemistry. Dr. Gerhardt has been involved in the fields of plant biology and environmental science for over 20 years and has coauthored more than 80 phytoremediation reports and published papers.

Perry D. Gerwing is a specialist in reclamation and contaminated site assessment and remediation. He has worked as an environmental specialist for large oil and gas corporations and environmental consulting firms for over 25 years. He has coauthored and published many scientific papers, and as president of Earthmaster Environmental Strategies Inc., an environmental consulting firm, has spent a number of years developing and implementing successful phytoremediation programs for clients.

Dr. Bruce M. Greenberg is trained as a chemist and biochemist. He is a professor at the University of Waterloo and president of a spin-off company, Waterloo Environmental Biotechnology Inc., which specializes in innovative phytoremediation solutions. He has over 30 years of experience in environmental biology and chemistry, and has published more than 160 papers.

Dr. Roger C. Helm is the Chief, Division of Environmental Quality, and a senior science advisor for the U.S. Fish and Wildlife Service (Service). He co-lead field investigations determining the impact of the 1989 Exxon Valdez oil spill (AK, USA) on nearshore communities and served as science advisor on the natural resource damage assessment (NRDA) on the 2010 MC-252 DeepWater Horizon oil spill (Gulf of Mexico, USA). Dr. Helm has worked as the lead scientist and in his service has pursued more than 30 NRDA and restoration cases involving oil spills and chemical contamination in the United States and internationally. He has coauthored dozens of technical and peer-reviewed publications on the impact of oil on birds and wildlife and coauthored a book *Marine Mammals of California*.

Dr. Bruce P. Hollebone Bruce Hollebone is a chemist with 17 years of experience in the field of chemical and oil spill research and development. He has a Ph.D. in chemistry from

the University of British Columbia. His research interests include the fate and behavior of oil and petroleum products in the environment, including simulation of spill behaviors in the laboratory; the development of new methods for physical and chemical analyses relevant to spills studies; environmental forensics for oil spill suspect-source identification; and environmental emergencies response. He currently works at the Oil Research Laboratory of Environment Canada.

Dr. Xiao-Dong Huang received his bachelor degree in agronomy in 1982 from Agricultural University of Heilongjiang, China, and his M.Sc. and Ph.D. in Biology in 1991 and 1995, respectively, from University of Waterloo of Canada. He was an agronomist from 1982 to 1990 at the Agricultural and Land Reclamation Academy of Heilongjiang Province, China. He spent 2 years at Wright State University of Ohio for postdoctoral research (1996–1998). He was an adjunct professor at the University of Waterloo from 2004 to 2010. From 2009 to present, he has been vice president of Waterloo Environmental Biotechnology Inc. Dr. Huang's research experience in China was in crop protection and hydroponics. He and his group at state farms of Northern China researched and developed systems to reduce the chemical usage in crop protection. His research activities focused on environmental toxicology and phytoremediation since 1989. He has been actively involved in research and development of methods for assessment of contaminants by using plants and engaged in development of phytoremediation systems for removal of persistent organic and inorganic contaminants from soils. Dr. Huang has completed and managed many scientific research and development projects and has extensive field experience on agronomy, environmental chemistry, environmental toxicology, and phytoremediation. He has over 50 referred scientific publications.

Dr. Núria Jiménez is a senior scientist in the Geomicrobiology group at the Federal Institute for Geosciences and Natural Resources (Germany). She holds a Ph.D. in environmental microbiology and biotechnology from the University of Barcelona, where she was assistant professor at the Department of Microbiology. Her main research topics are oil geochemistry and hydrocarbon microbial degradation, under a variety of conditions and environments like contaminated shorelines or groundwaters, oil reservoirs, or coal deposits. She is interested in oil bioremediation and management of microbial communities for biogenic production of methane. Working for the Spanish Research Council, she participated actively in the scientific response program for the *Prestige* oil spill where she developed fingerprinting techniques for oil spill identification and weathering assessment and conducted bioremediation studies on impacted shorelines.

Paul G.M. Kienhuis works at the lab of the Ministry of Environment and Infrastructure and has 35 years'

experience in analytical chemistry. Since 1999, he has been responsible for the identification of waterborne petroleum and petroleum products from the inland waters of the Netherlands and the Dutch part of the North Sea. He has to handle about 25 cases a year ranging from small diesel overruns to large spills of HFO in harbors. Oil spill identification is used to confirm responsibility in illegal discharges, but also to reclaim cleaning costs for contaminated quays and ships in harbors. In 2004, together with Dr. G. Dahlmann (BSH, Hamburg) he started with an annual international ring test for oil spill identification to share and improve knowledge about analytical techniques and limitations in comparing oil samples. In 2005, on request of Bonn Agreement (an agreement by North Sea coastal states to protect the environment), Gerhard Dahlmann and Paul Kienhuis started an oil spill identification expert group (OSINET). OSINET has worked on a now generally accepted method for oil spill identification (CEN/Tr 15522) that has been published by CEN in 2006 and an updated version in 2012.

Dr. Mahlon C. Kennicutt II received a Bachelor of Science degree in chemistry from Union College, Schenectady, NY (1974), and a Ph.D. in oceanography from Texas A&M University, College Station, TX (1980). He was a founding member, worked for 23 years as research scientist, and rose to director of the Geochemical and Environmental Research Group from 1998 to 2004. Dr. Kennicutt was the director of Sustainable Development (2004–2009) and led the Sustainable Coastal Margins Program (SCMP) from 2000 to 2010. He returned to the Oceanography Department and the Environmental Programs in 2009 where he taught oceanography, polar science, and science and policy retiring in 2013. He was a member of the U.S. Department of State delegation to the Antarctic Treaty from 2002 to 2007. Dr. Kennicutt was the U.S. delegate to the Scientific Committee on Antarctic Research (SCAR) from 2003 to 2012 and ex officio member of the U.S. Polar Research Board from 1998 to 2014. He served as a vice president (2004–2008) and president of SCAR (2008–2012). He was the principal investigator of the long-term environmental monitoring program in McMurdo Sound in Antarctica from 2002 to 2014 and has been to Antarctica eight times. He is professor emeritus of oceanography at Texas A&M University and led the first SCAR Antarctic and Southern Ocean Science Horizon Scan in 2014. Professor Kennicutt was named a National Associate of the U.S. National Academy of Sciences for life, awarded the Antarctic Service Medal of the U.S. Antarctic Program, and a geographic feature was officially named Kennicutt Point in 2006.

Dr. Andrew G. Klein is an associate professor in the Department of Geography at Texas A&M University. He received a B.A. from Macalester College and a Ph.D. in geological sciences from Cornell University. His current research interests lie in the application of remote sensing and geographic information science (GISci) techniques to study

the cryosphere. He and his students are currently using remote sensing to monitor tropical glacier recession and he has been actively involved in the development of algorithms to measure snow extent and snow albedo from data collected by NASA's MODIS instrument. He also applies these techniques to study human impacts in Antarctica.

Mike Landriault is a senior research technician in the Emergency Science and Technology Section (ESTS), Environment Canada, Ottawa, Canada. He has worked for over 20 years in oil spill forensic identification and emergency chemical spill analysis. He is a veteran of instrumental analysis using techniques such as gas chromatography and high-performance liquid chromatography–mass spectroscopy. Mr. Landriault received his diploma in chemical engineering technology from Algonquin College, Ottawa, Canada. He has coauthored over 70 academic publications including over 30 peer-reviewed journal articles.

Dr. William J. Lehr is senior scientist at the Office of Response and Restoration of the National Oceanic and Atmospheric Administration (NOAA). He was previously Spill Response Group Leader for the same organization. Dr. Lehr has also served as an adjunct professor for the World Maritime University and oil spill consultant for UNESCO. Dr. Lehr is a world-recognized expert in the field of hazardous chemical spill modeling and remote sensing of oil spills. He has served as guest editor for the journal *Spill Science and Technology* and the *Journal of Hazardous Materials*, and as cochair of the International Oil Weathering Committee. NOAA and the United States Coast Guard have awarded him several medals for his spill response efforts at major spill incidents of national or international significance. He has numerous publications in the field. Dr. Lehr holds a Ph.D. in physics from Washington State University.

Dr. Qianxin Lin is an associate professor of Department of Oceanography and Coastal Sciences, School of the Coast and Environment, Louisiana State University. Dr. Lin has conducted a variety of wetland oil spill–related research projects and accumulated an extensive oil spill–related experience in the past 20+ years. His oil spill related–areas of expertise primarily include factors controlling impact, recovery and fate of oil spills in wetlands, bioremediation, phytoremediation, *in situ* burning and restoration of oil spill–impacted coastal wetlands, and effects of oil spill dispersants on coastal marsh vegetation.

Dr. Carmen Morales-Caselles is a research scientist at the Ocean Pollution Research Program in the Vancouver Aquarium. Currently she is focused on establishing a coastal monitoring program in the Coast of British Columbia to assess the presence of contaminants in sediments and their effects on the marine biota. Other areas of interest include ecotoxicology of persistent pollutants, microplastics, food web modeling, and the development of quality guidelines.

As part of her Ph.D., Morales developed integrated studies to assess oil-contaminated sediments from the Prestige oil spill. She also spent more than 4 years working as a consultant at IOC-UNESCO where she was closely involved in the coordination of an ICAM project on biological marine indicators in Latin America plus other UN initiatives.

Dr. Rocío L. Moreno is a postdoctoral research fellow at the British Antarctic Survey (Cambridge, UK). Together with Dr. Sanpera, she studied the long-term effects of the *Prestige* oil spill on seabirds.

Oliver Muellenhoff joined Shell in January 2012 as remote sensing consultant in the Survey Operations team. Previously he worked for the European Commission Joint Research Centre as scientific/technical support officer in the field of applied remote sensing and for BMT ARGOS as remote sensing specialist which focused on the AgipKCO North Caspian Sea project. Oliver studied geology and obtained a Ph.D. in geosciences from Westphalian Wilhelm's University Muenster in 2004.

Dr. Alia Bano Munshi is a scientist involved in the research of POPS for last 30 years in PCSIR. She is doctorate in marine chemistry from Xiamen University, China. Dr. Alia received a postdoctorate from the Baltic Sea Research Institute, Germany, on a scholarship by DAAD and from Virginia Tech. State University, Blacksburg, Virginia, USA, on a Fullbright scholarship and from the University of HULL, UK. She has more than 50 research publications and papers. Her specialities include polychlorinated biphenyls, polycyclic aromatic hydrocarbons, pesticides, phthalates, alkyl phenols, and steroids in the marine environment. Dr. Alia has four books published in her career. Presently establishing the dioxin testing facility in fish meat with the collaboration of UNIDO.

Dr. Thomas J. O'Shea an emeritus scientist at U.S. Geological Survey, has studied the ecology of sirenians and other mammals and has expertise on the occurrence and effects of environmental contaminants in wildlife. He has authored or coauthored nearly 150 scientific papers, monographs, and books and is currently an associate editor of the journal *Marine Mammal Science*.

Dr. Araceli Puente is biologist and has a Ph.D. in marine sciences from the University of Cantabria. She is currently associate professor at the University of Cantabria and senior researcher at the Environmental Hydraulics Institute. Much of her teaching is linked to the Master of Science in Environmental Management of Water Systems. Her research focuses on the environmental assessment and monitoring of aquatic systems and the description of the spatial–temporal patterns of estuarine and coastal ecosystems, with particular focus on the study of the ecology of benthic communities (invertebrates and macroalgae).

Dr. Carolina Sanpera is a professor at the Department of Animal Biology, University of Barcelona (Spain). Her research focus is on trophic ecology and ecotoxicology of aquatic birds. Together with Rocío Moreno, Dr. Sanpera studied the long-term effects from the *Prestige* oil spill on seabirds.

Dr. Dagmar Schmidt Etkin has 39 years of experience in environmental analysis—14 years investigating issues in population biology and ecological systems, and 25 years specializing in the analysis of oil spills. Since 1999, she has been president of Environmental Research Consulting (ERC), specializing in data analysis, environmental risk assessment, spill response analysis, cost analyses, expert witness research and testimony, and development of comprehensive databases on oil/chemical spills and spill costs. ERC's work focuses on providing regulatory agencies and industry with sound scientific data and perspectives for responsible environmental decision-making. Dr. Etkin received her B.A. in biology from the University of Rochester, and her M.A. and Ph.D. in organismic and evolutionary biology from Harvard University where she specialized in ecological and population biology modeling and statistical analyses. She is a member of the UN Joint Group of Experts on the Scientific Aspects of Marine Protection (GESAMP), the International Maritime Organization (IMO) Marine Environmental Protection Committee Correspondence Group on Environmental Risk Assessment Criteria, and the UNH/NOAA Coastal Response Research Center Working Group on Oil Spill Modeling.

Dr. Hina Ahsan Siddiqi is a scientist of PCSIR (Pakistan Council of Scientific & Industrial Research), is doing research in the field of persistent organic pollutants for past 10 years. Her specialities include pesticides, polychlorinated biphenyls, and polycyclic aromatic hydrocarbons, and relevant monitoring, assessment, and method development. Ms. Hina acquired Ph.D. in analytical chemistry from University of Karachi, Pakistan. Ms. Hina was awarded internship at International Atomic Energy Agency (IAEA) and completed her Ph.D. research at Agrochemical Unit of FAO/IAEA Training & Reference Center for Food and Pesticide Control, Agriculture and Biotechnology Laboratory, Seibersdorf, Austria. Dr. Hina has 20 research publications and papers. She has written many chapters for different books, which are in progress for publishing. Presently, Dr. Hina is engaged in establishing the dioxin testing facility in fish at PCSIR with the collaboration of UNIDO and it would be a first-response organization in the region.

Dr. Ian Snape when not starring in Harry Potter movies, Professor Snape is a principal research scientist at the Australian Antarctic Division. He leads multidisciplinary teams and collaborates with university and industry partners to innovate for low-cost pollution mitigation and remediation. He has published more than 100 papers and book chapters on human impacts in cold regions. His research includes

remediation technology development, risk assessment, wastewater treatment design, and biodiversity conservation. Practical applications from this research are used in the Arctic and Antarctic to reduce the impacts from pollution.

Stephen T. Sweet is a senior research associate in the Geochemical and Environmental Research Group within the College of Geoscience at Texas A&M University. He received a Master of Science degree in oceanography from Texas A&M University in 1988. He also has a Bachelor of Science degree from McGill University. He has spent over 700 days at sea which included participation in submersible dives including the DSRV Alvin. Stephen was a member of the hydrocarbon component of the NSF sponsored quick response team that investigated the grounding of the *Bahia Paraiso* and subsequent oil spill in 1989. He has been deployed to Antarctica for a total of more than 400 days over the course of 13 expeditions and was awarded the Antarctic Service Award in 1989. He is an author of over 50 peer-reviewed scientific publications and over 70 presentations at scientific meetings. His professional interests include the fate and behavior of oil spills, environmental monitoring and assessment, effects of chemicals on the marine environment, hydrocarbon chemistry, gas hydrates, geochemistry, and atmospheric chemistry.

Dario Tarchi graduated in physics in 1990. Since 1993, he has been with the Joint Research Centre of the European Commission, Ispra, Italy, where he joined the scientific team of the European Microwave Signature Laboratory working on the design and experimental validation of data analysis and signal processing algorithms in the field of Synthetic Aperture Radar (SAR), radar interferometry, and radar polarimetry. He was involved in the design and implementation of a ground-based interferometric SAR system (LISA) as well as in the experimental validation of its use for real-time monitoring of natural hazards, such as landslides and snow avalanches. He was also dealing with the problem of detecting oil pollution at sea leading a project on the use of satellite SAR images for the mapping and monitoring of potential oil spill signatures in European Seas. Recently, he joined the Maritime Affairs Unit at JRC, where he is responsible of scientific activities concerning the development of innovative sensors and technologies for maritime surveillance. His main research interests concern the application of radar interferometric techniques for changes detection in natural and man-made objects, the development and testing of novel radar concepts and systems, such as parasitic radar system, noise radar technology, and MIMO radar system for various applications.

Konstantinos Topouzelis graduated from the Department of Environment, University of the Aegean, Hellenic Republic, in 1999. He fulfilled his M.Sc. in "Remote Sensing, Image Processing, and Applications" at the University of Dundee, Scotland, in 2000. In August 2007, he received his Ph.D. from the National Technical University of Athens. His main

research interests include satellite remote sensing applications in the marine environment and satellite imagery processing algorithms. From 2004 to 2008, he worked as scientific officer at the European Commission Joint Research Centre (JRC). His main responsibilities were the detection of illegal ship discharges using SAR data in European waters. He participated in several research projects related to marine pollution monitoring. He has been teaching at the Department of Marine Sciences at the University of the Aegean in the field of remote sensing and its applications in the marine environment since February 2010.

Dr. Florina S. Tseng is the director of the Wildlife Clinic and an associate professor at Tufts Cummings School of Veterinary Medicine in North Grafton (MA, USA). For nearly a decade, Dr. Tseng was the response veterinarian for International Bird Rescue in Berkeley (CA, USA) addressing oiled wildlife care in over 20 major spills.

Dr. Ania C. Ulrich has worked on developing noninvasive biological remediation techniques for contaminated soil and groundwater. Dr. Ulrich's work has dealt with contaminated sites in the United States, Ontario, and Alberta, most notably the 2005 Lake Wabamun CN derailment. As an associate professor at the University of Alberta, Dr. Ulrich is currently investigating the environmental and health impacts of Alberta's oil sands and their water management practices on the surrounding groundwater. Dr. Ulrich's passion for the environment also has a strong familial tie which began with her great grandfather Henry Stelfox (awarded the Julian Crandall Trophy—Canada's most outstanding conservation award in 1954 and the subsequent naming of Mount Stelfox in his honor). She hopes to pass on her passion for the environment to her children.

Michele Vespe is a senior scientist at the NATO Centre for Maritime Research and Experimentation, where he works on traffic knowledge discovery, anomaly detection, and networked radar systems for maritime situational awareness. Until September 2011, he was a Scientific Officer at the European Commission Joint Research Centre developing synthetic aperture radar-based preoperational applications in the maritime domain. He also led exploratory research on passive radar systems. Prior to this, he spent 2 years in industry as a project engineer in the fields of remote sensing, small and medium area surveillance, and data fusion. Dr. Vespe holds a degree in telecommunications engineering from University of Florence (2003) and a Ph.D. in electronic engineering from University College London (2006).

Dr. Lucia Viñas is a senior researcher at Instituto Español de Oceanografía in Vigo, where she is head of the Hydrocarbon Analysis Unit in the Marine Pollution Department. She has a Ph.D. on analytical chemistry from the University of Vigo. She has authored 15 papers related to marine pollution. She participated in the Prestige response

action, leading some of the projects. She is member of several international groups focused on marine pollution assessment such as the ICES_WGMS, the WG Chemicals (CIS of the WFD), MSFD Expert Network on Contaminants, and the OSPAR_MIME Working Group.

Dr. Zhendi Wang is an emeritus research scientist and head of Oil Spill Research Lab at Environment Canada, Government of Canada. He has devoted the last 20 years on the forensic oil and toxic chemical spill research. His specialties and research interests include development of oil spill fingerprinting and tracing technologies; properties, fate, and behavior of oil and other hazardous organics in the environment; characterization and source differentiation of petrogenic, biogenic, and pyrogenic hydrocarbons in oil sands environmental samples; oil burn emission and products study; oil biodegradation; and application of modern analytical techniques to oil and chemical spill studies. Dr. Wang has continually and extensively led and involved in various scientific projects. He has authored or coauthored over 350 publications including 110 international peer-reviewed journal papers, 6 invited journal review articles, 2 books and 16 book chapters, 25 departmental reports, 238 conference proceedings, and other publications. Dr. Wang is the 2009 recipient of "the Award of Citation of Excellence for Excellent Quality of Work" by Environment Canada of Government Canada. He has also received numerous national and international academic honors. He was the editor-in-chief of *Environmental Forensics* (2006–2010). He is adjunct professor for a number of universities. Dr. Wang has received many invitations to speak as a keynote speaker and plenary presenter at international conferences, international agencies, workshops, research institutes, and universities.

Dr. Randall S. Wells is a senior conservation scientist with the Chicago Zoological Society. Dr. Wells directs the Sarasota Dolphin Research Program (FL, USA), the world's longest running study of a dolphin population. His research since 1970 has focused on the ecology, behavior, and health of dolphins and whales, especially with regards to anthropogenic impacts.

Dr. Terrie M. Williams is a professor of ecology and evolutionary biology at the University of California, Santa Cruz (CA, USA). She was the co-director of the Sea Otter Rescue Program following the 1989 *Exxon Valdez* oil spill and continues to conduct research and training regarding the impacts of oil on sea otters and other marine mammals.

Dr. Zeyu Yang is a scientist in the Emergency Science and Technology Section (ESTS), Environment Canada, Ottawa, Canada. She received her Ph.D. in environmental science from Guangzhou Institute of Geosciences, Chinese Academy of Sciences, a master degree in environmental engineering from Huazhong University of Science and Technology of China, and a bachelor degree in chemistry from Hunan

University of China. Her specialties and research interests include fate and behavior of oil and other hazardous organics in environment, development of oil (including biodiesel) spill fingerprinting and tracing technology, development of biomimic methods based on passive sampling techniques for the simulation of bioaccessibility and bioavailability of organic contaminants. She has authored over 50 academic publications, over 30 of them published in the internationally recognized and respected peer-reviewed journals.

Dr. Chun Yang is a scientist in Emergencies Science and Technology Section of Environment Canada, Ottawa, Canada. He has a Ph.D. in analytical chemistry and environmental process from Nanyang Technological University of

Singapore, a master degree in organic-analytical chemistry from Research Centre for Eco-Environmental Sciences of Chinese Academy of Sciences, and a bachelor degree in organic chemistry from Beijing Normal University of China. He has devoted the last 20 years to research on environmental sciences, analytical chemistry, and natural products. Currently, his research in Environment Canada mainly focuses on the emergency chemical spill analysis, chemical fingerprinting of oils (crude oil, oil sands, and refined petroleum products, etc.), environmental forensics of oils and other potential spill candidates, and environmental behaviors of organic pollutants. He has authored over 110 academic publications including over 50 peer-reviewed journal papers and three invited book chapters.

PREFACE

Oil spill studies continue to evolve. While there are few books on the topic, there are regular conferences and symposia. This is the first scholarly book on the topic of oil spills. As such, this book focuses on providing material that is more scholarly and somewhat involved. While every attempt was made to include the essential material, there may be some gaps. The importance of many subtopics changes with time and current spill situations.

All materials in this book, including introductions, have been peer reviewed by at least two persons. The following peer reviewers are acknowledged (in alphabetical order): Dan Anders, Perihan Aysal, Ken Biggar, Robert Bonke, James Botkin, Jennifer Boyce, Joan Bradock, Tom Brody, Carl Brown, Ian Buist, Ron Delaune, Merv Fingas, Anita George-Ares, Lisa Gieg, Ron Goodman, Kurt Hansen, Sarah Harrison, Jocelyn Hellou, Bruce Hollebone, Alan Judd, Tom King, Davor Kvočka, Pat Lambert, Robin Law, Bill Lehr, Ira

Leifer, Christopher Marwood, Jacqui Michel, Harbo Niu, Gloria Pereira, Debra Sinecek-Beatty, Malcolm Spaulding, Scott Stout, Pavel Thalich, Dave Tilden, Sudhakar Tripuranthakam, Milan Vavrek, Zhendi Wang, Chun Yang, and Scott Zengel.

A special thanks goes out to the authors, many of whom put in their own time to complete their chapters. This is especially true because many of the authors were working on the Deepwater Horizon spill during the preparation of this book. This “double-duty” was greatly appreciated. The author’s names appear throughout the text. Following this forward, I have a brief biography of each of them.

I also like to thank the many people who provided support and encouragement throughout this project. I also thank Environment Canada and my former colleagues for help and support. Environment Canada is acknowledged for permission to use materials and photos.

PART I

RISK ANALYSIS

RISK ANALYSIS AND PREVENTION

DAGMAR SCHMIDT ETKIN

Environmental Research Consulting, Cortlandt Manor, NY, USA

1.1	Introduction	3
1.2	Executive Summary	3
1.3	Oil Spill Risk Analysis	4
1.3.1	Defining “Oil Spill Risk”	4
1.3.2	Factors That Determine the Probability of Spill Occurrence	5
1.3.3	Probability Distributions of Spill Volume	9
1.3.4	Determining the Probable Locations and Timing of Spills	11
1.3.5	Factors That Determine the Consequences/Impacts of a Spill	11
1.3.6	Spill Impacts: The Effects of Spill Location Type	16
1.3.7	Measuring Oil Spill Impacts	18
1.3.8	Interpreting Risk for Policy-Making	27
1.4	Overview of Oil Spill Prevention	28
1.4.1	Basic Strategies for Spill Prevention	28
1.4.2	Implementation of Spill Prevention Measures	29
1.4.3	Effectiveness of Spill Prevention	29
1.4.4	Spill Fines and Penalties as Deterrents	31

1.1 INTRODUCTION

Understanding oil spill risk is at the heart of the entire study of oil spills because it encompasses both the likelihood of spills occurring and the nature of those spills, as well as the complex factors that determine the fate and effects of oil in the environments into which it spills. Risk mitigation—reducing risk—is the purpose of spill prevention measures and spill response. Studies of oil behavior, toxicity, ecosystem effects, and organism impacts are related to the consequences side of risk. Studies of spill rates, causes, and prevention strategies are related to the probability side of risk.

1.2 EXECUTIVE SUMMARY

Risk is the probability that an event will occur multiplied by consequences of the event. With regard to oil spills, risk is a combination of the probability that a spill will occur and the consequences or impacts of that spill. Because oil spills can have such different environmental and socioeconomic impacts based on the specific circumstances of each incident, it is important to consider the *type* of spill event that occurs with regard to oil type, volume, source, location, and season and the *impacts* that that kind of spill is likely to have in a given location and season based on the spillage volume and type of oil.

Spill risk analysis involves studying both the probability of occurrence and the impacts that may occur. Event tree analysis or fault tree analysis (FTA) is often used to evaluate the sequences of events that contribute to a spill occurring. In the event that a spill does occur, the spill volume, oil type, geographic location, resources at risk, and spill response effectiveness will determine the degree of impact. State-of-the-art modeling techniques and qualitative evaluations on impacts incorporating knowledge about oil behavior, toxicity, persistence, and adherence along with knowledge on the sensitivities of species, habitats, and shoreline types can provide data on the consequences side of the risk equation. Socioeconomic impacts and the cost of spill response should also be factored into any analysis.

There are many practical applications for spill risk assessments, including contingency planning for response and preparedness, protection of sensitive resources, risk allocation for insurance or taxation, response trade-off evaluation, cost–benefit analyses of oil exploration, production, storage, or transport; developing spill prevention measures; and evaluating alternative courses of action for oil exploration, production, storage, or transport. A scientifically

based risk assessment removes much of the subjectivity in the process.

Evaluating and developing spill prevention measures is arguably the most important application of risk assessments. With significant reductions in spill rates over the last two decades, there have clearly been positive effects of spill prevention programs and measures, such as double hulls on tankers and legislation such as the Oil Pollution Act of 1990 (OPA 90). A greater appreciation and understanding of the consequences of spills, including environmental and socioeconomic impacts and costs, has also contributed immensely to regulatory and voluntary changes that have led to the reduction of spills despite increased usage of oil.

1.3 OIL SPILL RISK ANALYSIS

While “zero risk” of oil spills is apparently the aspiration of the majority of the general public, the concept is nearly an oxymoron. The complete elimination of oil spills is a laudable goal but near impossibility, at least with current practices and available technologies.

The complete elimination or mitigation of oil spill impacts is also a near impossibility given the facts of oil behavior and the challenges of spill response. Despite arduous efforts and favorable circumstances during the response to a spill, there is still bound to be some degree of impact from a spill.

But between “zero risk” and “extreme risk,” there is a broad spectrum that needs to be carefully assessed to develop reasonable and effective spill prevention, preparedness, and response programs and strategies. “Oil spill risk analysis” encompasses the study of all of the factors that affect risk in terms of both probability and consequences. Such analyses allow policy makers to determine the best ways to assign resources to prevention measures to have the greatest effect on reducing spillage, identify the most sensitive resources at risk, and invest in the most effect ways to mitigate spill impacts.

1.3.1 Defining “Oil Spill Risk”

Colloquial usage of the term “risk” often implies only the chance or likelihood that an event will occur, but this is not its complete technical meaning. By its classical definition, “risk” is the probability that an event will occur multiplied by the consequences of that event:

$$\text{Risk}_{\text{event a}} = \text{Probability}_{\text{event a}} \times \text{Consequences}_{\text{event a}}$$

There can be low-probability or exceedingly rare events that have high consequences (e.g., a meteor hitting the earth), as there can be high-probability or very common events that have very low consequences (e.g., spilling a glass of water), as well as all sorts of probabilities and consequences on that spectrum. Often, risk is characterized in a risk matrix, as shown in Figure 1.1. The red-shaded box (high probability–high impact) represents the greatest risk in this highly simplified risk matrix. The orange, yellow, light-green, and dark-green boxes indicate increasingly lower risk.

With regard to oil spills, risk is a combination of the probability that a spill will occur and the consequences or impacts of that spill. Because oil spills can have such different environmental and socioeconomic impacts based on the specific circumstances of each incident, it is important to consider the *type* of spill event that occurs with regard to oil type, volume, source, location, and season and the *impacts* that that kind of spill is likely to have in a given location and season based on the spillage volume and type of oil.

The circumstances of a spill—the source of the spill (e.g., tank ship, pipeline, or tanker truck), the cause of the spill (e.g., vessel collision or pipeline corrosion), the oil type involved (e.g., crude oil or diesel fuel), the amount spilled, location of the spill (political regime, habitat type, and geography), and the season in which the spill occurs (e.g., weather, bird migrations and nesting, tourism, and commercial

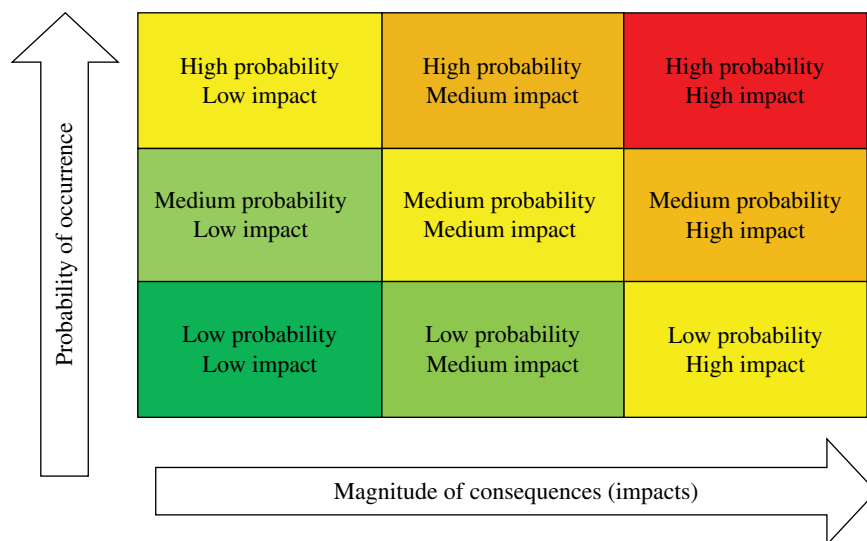


FIGURE 1.1 Basic risk matrix.

fishing)—are all to some extent interrelated with regard to spill scenario probability and all have an effect on the impacts. The source of the spill can be the determinant of the oil type spilled. For example, a tanker truck is much more likely to carry a load of diesel fuel or gasoline than crude oil.

The source also dictates the amount of oil spilled in that the cargo or carrying capacity of the source determines the maximum that can be spilled. A large tank ship might spill as much as 270,000 tonnes of oil, whereas a tank barge will carry a much smaller load, perhaps a maximum of 6500 tonnes. A cargo vessel's bunker capacity is also determined by its size and type. The amount of oil that will spill from a pipeline is determined by the pipeline diameter, the length between shutoff controls, and the pressure of flow. The cause of the spill will also have a determining effect on the spill volume. A vessel grounding or collision has the potential for causing a much larger spill than might be expected from operator error during a fuel transfer operation. A pipeline rupture and explosion will cause a much larger release than a pin-hole-sized hole caused by corrosion. The source type will also to some extent limit the type of location. For example, a large tank ship will not have a spill in a small inland river because it cannot travel in such waters. A tanker truck will not have a spill in offshore marine waters.

1.3.2 Factors That Determine the Probability of Spill Occurrence

The probability of occurrence of a particular spill scenario depends on a large number of factors: source type, cause, location, and season or other measure of timing. There may be a number of serial probabilities at play in determining the

likelihood of a particular type of incident. An example analysis of factors involved in determining the likelihood of tanker spills due to grounding and collisions follows.

1.3.2.1 Probability Event Trees from Historical Data and Engineering Studies

A common way to represent a series of probabilities is as an “event tree.” An example is shown for tankers in Figure 1.2. Probabilities for the event tree are shown in Table 1.1. Calculated probabilities for spills from large-sized double-hulled tankers are shown in Table 1.2 and from the same-sized tanker with a single hull in Table 1.3. A comparison between the single-hulled and double-hulled tanker for the probabilities of spillage with accidents is shown in Table 1.4. A side-impact collision involving a single-hulled large tanker is 3.4 times more likely to result in a spill than one involving a double-hulled tanker. Likewise, side- and bottom-impact collision or a hard grounding is 4.4 and 5.1 times more likely to result in spillage, respectively.

These probabilities apply to an individual tanker operating for a year. To determine the probability of each type of spill occurring in a particular location or for a particular tanker fleet, it is necessary to multiply these probabilities with the number of vessels involved. There are different probabilities associated with each accident type and vessel type and size. For the tanker incidents, the probabilities of accidents and spillage were determined by examining historical data [1], as well as naval engineering studies of impacts and oil outflow [2,3].

1.3.2.2 Analysis of Other Data to Determine Probabilities:

Weather and Seismic Data For predicting spill probabilities for hypothetical situations for which there are no

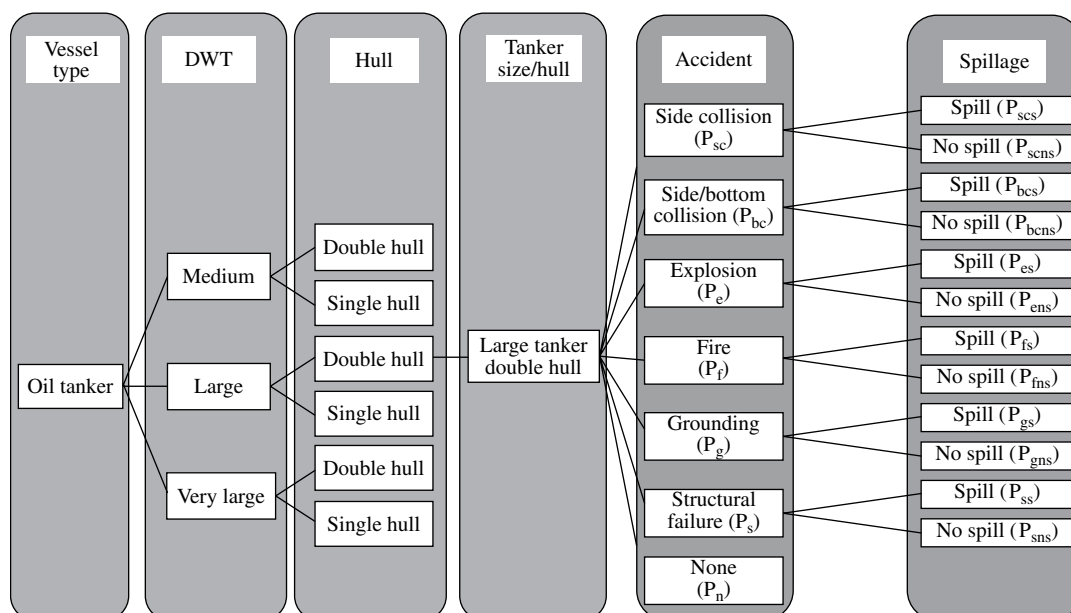


FIGURE 1.2 Event tree for tanker spills.

TABLE 1.1 Event tree probabilities for tanker spills

Event	Probability by tanker size and hull ^a						Source
	Medium ^b		Large ^c		Very large ^d		
	Single hull	Double hull	Single hull	Double hull	Single hull	Double hull	
Accident ^e	2.0E-02		2.0E-02		2.0E-02		[37]
No accident	9.8E-01		9.8E-01		9.8E-01		
Side collision	2.4E-05		4.5E-05		4.5E-05		[2,37]
Spill	6.8E-01	1.5E-01	6.5E-01	1.9E-01	8.1E-01	1.9E-01	[16]
No spill	3.2E-01	8.5E-01	3.2E-01	8.5E-01	1.9E-01	8.1E-01	
S/B collision ^f	5.7E-05		1.1E-04		1.1E-04		[2,37]
Spill	8.1E-01	1.7E-01	7.9E-01	1.8E-01	8.8E-01	2.0E-01	[3]
No spill	1.9E-01	8.3E-01	2.1E-01	8.2E-01	1.2E-01	8.0E-01	
Explosion	2.4E-04		2.3E-04		2.3E-04		[37]
Spill	4.0E-01	4.0E-01	4.0E-01	4.0E-01	4.0E-01	4.0E-01	[5]
No spill	6.0E-01	6.0E-01	6.0E-01	6.0E-01	6.0E-01	6.0E-01	
Fire	1.6E-04		2.3E-04		2.3E-04		[37]
Spill	4.0E-01	4.0E-01	4.0E-01	4.0E-01	4.0E-01	4.0E-01	[5]
No spill	6.0E-01	6.0E-01	6.0E-01	6.0E-01	6.0E-01	6.0E-01	
Grounding ^g	1.6E-04		1.1E-04		1.1E-04		[37]
Spill	9.1E-01	1.8E-01	9.2E-01	1.8E-01	9.3E-01	2.0E-01	[3]
No spill	9.0E-02	7.2E-01	8.0E-02	7.2E-01	7.0E-02	8.0E-01	
Structural failure	2.0E-04		1.5E-04		1.5E-04		[37]
Spill	4.0E-01	4.0E-01	4.0E-01	4.0E-01	4.0E-01	4.0E-01	[5]
No spill	6.0E-01	6.0E-01	6.0E-01	6.0E-01	6.0E-01	6.0E-01	

^aProbability per tanker year of operation for accident rates. Spillage rates per accident based on probability of spillage given incident.^bHandysize (20,000–34,999 DWT) and Handymax (35,000–60,000 DWT).^cPanamax (60,000–79,999 DWT); Aframax (80,000–119,999 DWT).^dVery large crude carriers: 200,000–319,999 DWT; ultra-large crude carriers greater than 320,000 DWT.^ePer vessel trip.^fSide and bottom impact in collision.^gAssumes hard grounding rather than soft-bottom grounding.**TABLE 1.2 Probabilities of spillage for accidents of large-sized double-hull tanker**

Accident event	Probability (per tanker year)		
	Accident	Spill	Accident × spill
Collision with side impact	4.50E-05	1.90E-01	8.55E-06
Collision with side/bottom impact	1.05E-04	1.80E-01	1.89E-05
Explosion	2.30E-04	4.00E-01	9.20E-05
Fire	2.30E-04	4.00E-01	9.20E-05
Hard grounding	1.10E-04	1.80E-01	1.98E-05
Structural failure (non-accident)	1.50E-04	4.00E-01	6.00E-05

Probability per tanker year of operation for accident rates.

TABLE 1.3 Probabilities of spillage for accidents of large-sized single-hull tanker

Accident event	Probability (per tanker year)		
	Accident	Spill	Accident + spill
Collision with side impact	4.50E-05	6.50E-01	2.93E-05
Collision with side/bottom impact	1.05E-04	7.90E-01	8.30E-05
Explosion	2.30E-04	4.00E-01	9.20E-05
Fire	2.30E-04	4.00E-01	9.20E-05
Hard grounding	1.10E-04	9.20E-01	1.01E-04
Structural failure (non-accident)	1.50E-04	4.00E-01	6.00E-05

reliable historical spill or accident data, other approaches may be required. For example, for determining the probability of a weather event of a certain magnitude that might

TABLE 1.4 Comparison of spillage in large-sized single- vs. double-hull tanker

Accident event	Probability of spill (per tanker year)		
	Single hull (SH)	Double hull (DH)	P(SH)/P(DH)
Collision side impact	2.93E-05	8.55E-06	3.4
Collision side/bottom impact	8.30E-05	1.89E-05	4.4
Explosion	9.20E-05	9.20E-05	1.0
Fire	9.20E-05	9.20E-05	1.0
Hard grounding	1.01E-04	1.98E-05	5.1
Structural failure (non-accident)	6.00E-05	6.00E-05	1.0

cause spillage based on engineering studies, historical weather data can be applied.

Table 1.5 gives an example of hurricane data that were applied to determine the likelihood of the toppling of an oil-containing offshore wind turbine generator (WTG) to cause spillage. The analysis indicates that in the last 154 years, there have been 10 hurricanes that have impacted Massachusetts. Five were Category 1 hurricanes on the Saffir–Simpson Hurricane Scale, two were Category 2, and three were Category 3. There have been no Category 4 or 5 hurricanes in Massachusetts in 154 years. Over the next 30 years, there are likely to be two hurricanes that impact the

waters of Massachusetts, potentially including Nantucket Sound (wind farm location). If a hurricane did occur, there is a 46% chance that it would be Category 1, 19% chance that it would be Category 2, and 27% chance that there would be a major hurricane of Category 3. It was concluded that it would be extremely unlikely (0.2 hurricanes) with the damage potential (Category 4 or greater) to topple a WTG in 30 years.

Another potential cause of spillage with the WTGs might be due to seismic activity. Between 1990 and 2001, there were 284 earthquakes recorded in the northeastern United States and eastern Canada. The distribution of magnitudes is shown in Figure 1.3. Nearly 94% of the earthquakes had magnitudes below 3.5, which are generally inconsequential for structural damage. There were three events of 4.7–4.8 magnitude. These earthquakes caused little damage. The probability that there would be an earthquake of at least 4.75 magnitude in the immediate area or within 50km of the project is 0.002 in 5 years, 0.003 in 10 years, and 0.015 in 30 years. The probability of a major earthquake of 7.0 or greater is less than 0.001 in 30 years, based on U.S. Geological Survey earthquake probability models.

Tsunamis occur with undersea earthquakes of at least 7.5 (Richter scale). The recent massively destructive tsunami in Southern Asia followed a 10.0 earthquake. Tsunamis are most common in the Pacific Ocean, but have occurred in the North Atlantic, including one that followed the 1775 Lisbon earthquake. This tsunami was seven meters high in the Caribbean Sea. The probability that there would be an earthquake severe enough to cause a tsunami in Nantucket Sound over the course of 30 years is, for all practical purposes, zero. Tsunamis also rarely occur after extraterrestrial collisions from asteroids or meteors or as a result of massive underwater landslides, which are often related to or caused by earthquakes. The probability of this occurring in Nantucket Sound or near enough to impact coastal waters (CW) in 30 years is also exceedingly small [4].

1.3.2.3 Fault Tree Analysis FTA is another frequently applied technique to determine the probability of a spill occurring under various circumstances. FTA for spills involves analyzing sequences of events that may (or may not) lead up to a system failure (in this case a spill) and

TABLE 1.5 Potential hurricanes in Massachusetts

Hurricane category Saffir–Simpson scale	Winds (km/h)	Annual probability	Potential hurricanes in time period			
			1 year	5 years	10 years	30 years
Category 1	119–153	0.032	0.032	0.162	0.325	0.974
Category 2	154–177	0.013	0.013	0.065	0.130	0.390
Category 3	178–209	0.019	0.019	0.097	0.195	0.584
Category 4	210–249	0.006	0.006	0.032	0.065	0.195
All categories	—	0.070	0.070	0.356	0.715	2.143

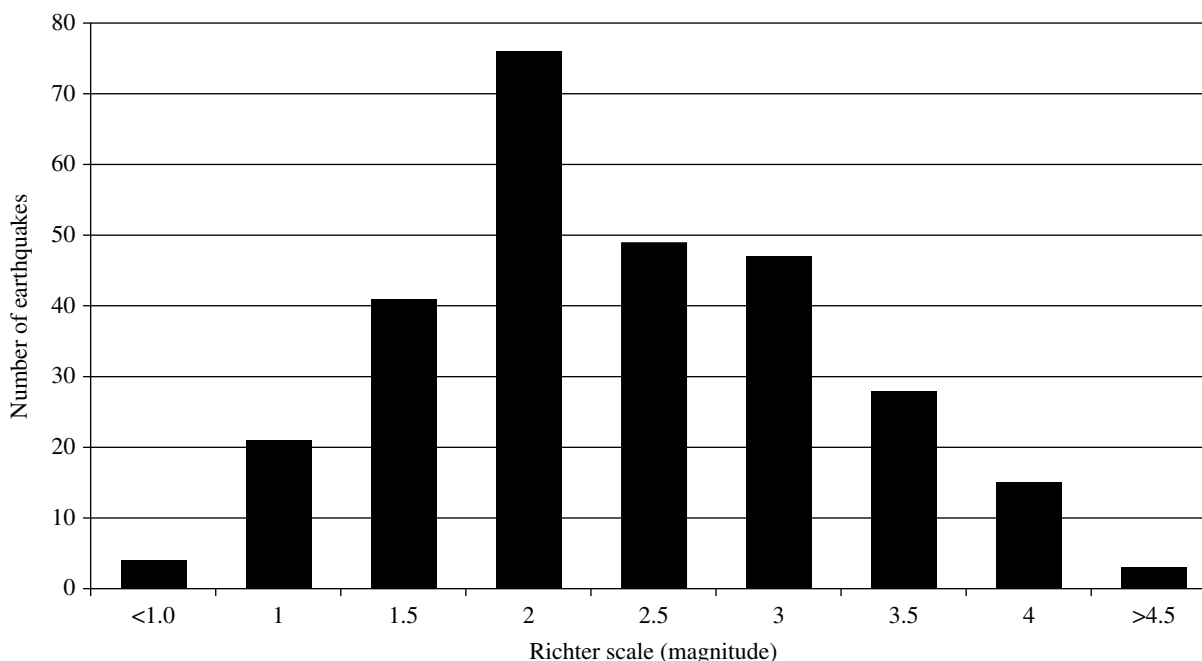


FIGURE 1.3 Number of earthquakes in Eastern US 1990–2001 [13,23]. Lamont Doherty Seismic Network, Columbia University, New York, NY.

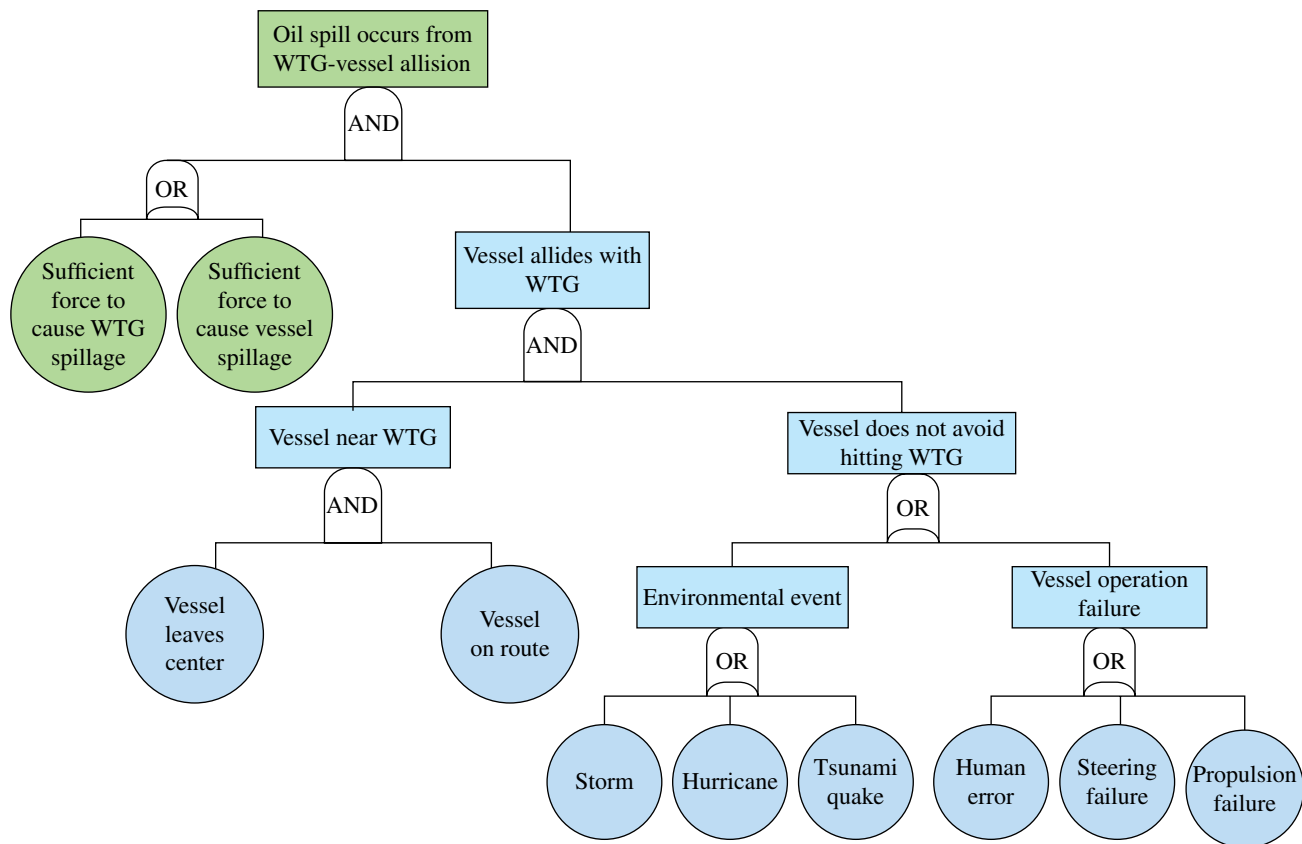


FIGURE 1.4 Fault tree diagram for vessel-WTG Allision analysis [13,23].

TABLE 1.6 Probability of occurrence per vessel trip applied to fault tree analysis [5]

Vessel type	Fault tree basic events per vessel trip							
	Wind turbine generator vicinity		Environmental event			Vessel failure		
	Vessel deviation from course	Vessel in route	Storm	Hurricane	Earthquake Tsunami	Human error	Steering failure	Propulsion failure
A	0.028	1.0	0	0.004731	0.000003	0.00034	0	0
B	0.028	1.0	0	0.000114	0	0.00032	0	0
C	0.028	1.0	0	0.000437	0	0.00032	0	0
D	0.028	1.0	0	0.000038	0	0.00032	0	0
E	0.028	1.0	0	0	0.000017	0.00031	0.00002	0.00003
F	0.042	1.0	0	0	0.000022	0.00047	0.00002	0.00002
G	0.042	1.0	0.0004	0	0.000034	0.00047	0.00002	0.00002
H	0.042	1.0	0.0007	0	0.000020	0.00069	0.00003	0.00003
I	0.042	1.0	0	0.000798	0	0.00044	0.00002	0.00002

A, cruise/dry cargo ships; B, tankers; C, tow/tugboats; D, tank barge; E, ferries; F, commercial fishing vessels; G, charter fishing vessels; H, touring vessels; I, dry cargo barge.

assigning probabilities to each event. Figure 1.4 shows a “fault tree diagram” for an analysis of vessel allisions with WTGs at the wind farm.

Each event (circle) has a probability associated with it (Table 1.6). The blue portions deal with the probability of an allision (i.e., impact of a moving object on a stationary object). The green parts relate to the probability of an oil spill resulting from the allision. The logic behind this diagram is that an oil

spill would occur from a WTG allision only if a vessel allides with the WTG and there is sufficient force to cause spillage from either the vessel or the WTG. The probability of an allision depends on the vessel being in the vicinity of a WTG (WTGs are located proximal to the shipping lane) and the vessel not avoiding hitting the WTG because of an environmental event or a vessel operation failure. The environmental event and vessel failure scenarios each depend on at

least one of three things happening. The probabilities of each independent event are multiplied together to get the probabilities of the sets of circumstances that would lead to a spill. This type of analysis can be applied to a large variety of spill circumstances in which there is some knowledge of the probabilities of occurrence of the relevant sub-events.

The value of conducting a comprehensive location- or situation-specific spill probability analysis for contingency planning and risk management is that it provides an evaluation of the range of possible spill scenarios and the probabilities that they will occur. This will allow for appropriate measures to be taken to address spills that occur, focusing on preparation for spills with the highest likelihood for first-tier responses but also allowing for more complex responses for more rare, but potentially more consequential, spills. The next part of the risk analysis involves analyzing impacts of the various spill scenarios to better determine the complete *risk* (probability \times impacts) of each type of spill scenario to focus particular attention on the highest risk (high probability/high impact) spills for prevention measures and for response planning, recognizing that sometimes smaller spills can cause higher impacts than larger ones if they are in an inopportune location.

Each spill risk analysis requires consideration of the best customized approach to analyzing the probability of spillage, as well as the distributions of spill volumes and scenarios that might occur. Careful consideration needs to be given to the

purpose of the analysis, the degree of risk “tolerance” for the end-user, and the specific ways in which spills might conceivably occur based on the location, potential sources, and time frame.

1.3.3 Probability Distributions of Spill Volume

Determining the probability of a spill occurring is only the first step in assessing risk. The next step is to determine the nature of the spill, including the volume of spillage. Thus, for the tanker spills described earlier, the probabilities only indicate the likelihood of a spill occurring. These probabilities do not indicate whether these are large spills or very small spills.

Each spill that occurs will have a certain volume. This spillage volume is dependent on a number of factors: source size (oil capacity), source condition (e.g., corrosion and engineering), incident cause, and nature of spill cause (e.g., force of impact, and effectiveness and speed of source control, among others).

There is a probability associated with each spill volume, that is, the likelihood that the spill that occurs will be in this volume or volume range. In general, there is a much higher probability of a small spill than a very large spill, as in Figure 1.5 and Table 1.7, which shows an analysis of nearly 75,000 spills in U.S. waters over the course of the 10-year period 1990–1999.

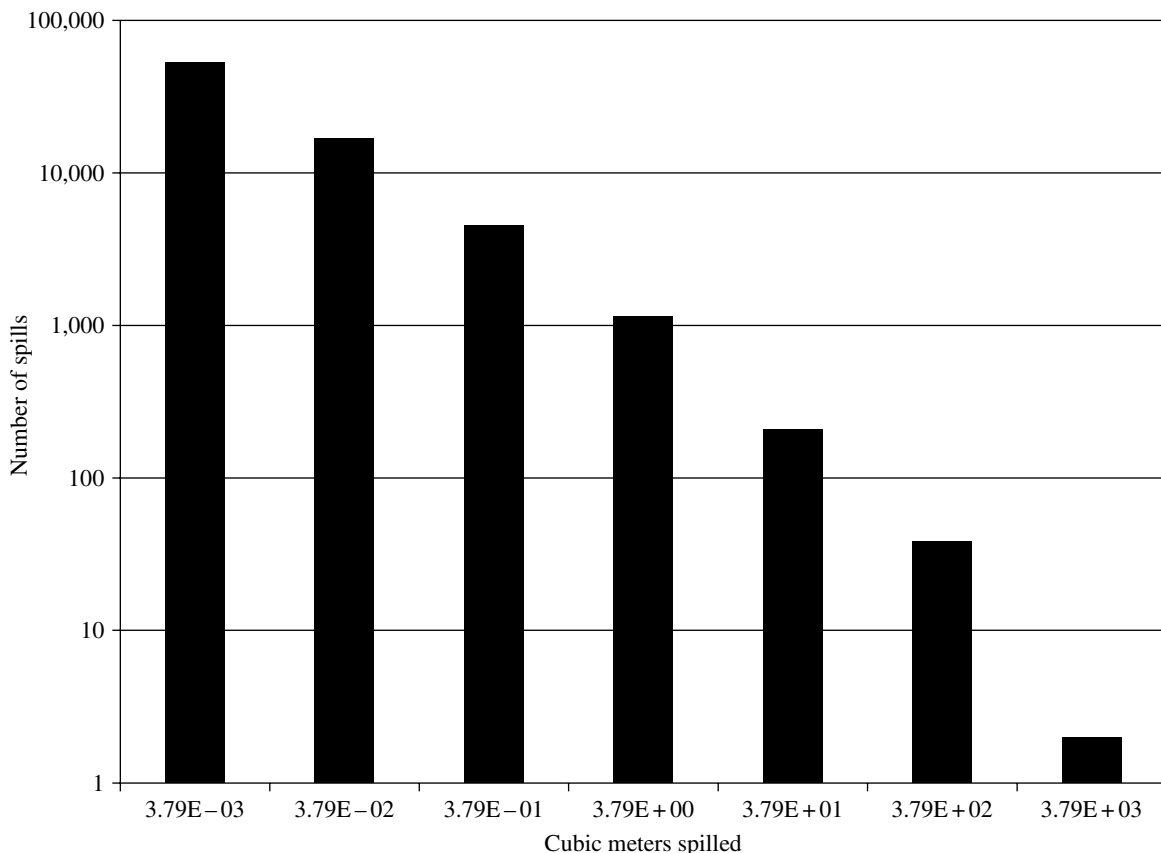


FIGURE 1.5 Oil spills in US waters (1990–1999) (Source: ERC).

1.3.3.1 Probability Distribution Functions The range of spill volume probabilities is often analyzed and presented as a probability distribution function (PDF). A PDF shows the cumulative percentages of spill volumes and the percentile of each spill volume. The n th percentile spill is that spill volume larger than $n\%$ of spills for that source and type and is smaller than $100 - n\%$ of spills. For example, the 90th percentile spill is larger than 90% of spills and only smaller than 10% of spills. These percentages can be used as probabilities for determining the likelihood of a spill being a particular volume when an incident occurs.

The PDF for spill volumes will vary by source type, cause, and other factors. An example of a PDF showing the 90th percentile spills for tanker spills caused by impact accidents

(collisions, allisions, and groundings) and non-accident structural failures is shown in Figure 1.6 and Table 1.8.

Combining the probability of an accident occurring with the probabilities of spill volumes associated with the type of volume for the hypothetical double- or single-hulled tanker results in the probabilities for a large spill ($38,000 \text{ m}^3$ or about the volume of the 1989 Exxon Valdez tanker spill), as shown in Tables 1.9 and 1.10.

For a particular large double-hulled tanker, there is thus a 1.07×10^{-5} probability that there will be a large spill of $38,000 \text{ m}^3$ due to any cause. For a single-hulled large tanker, that probability is 1.67×10^{-5} . Based on these data, there is a 36% reduction in probability with the double hull.

TABLE 1.7 Oil spills in U.S. marine waters (1990–1999) by volume

Spill volume (m^3)	Number of spills	Percent total incidents (%)	Cumulative percentage (%)
0.0038	52,378	69.945	69.945
0.038	16,626	22.202	92.147
0.38	4,491	5.997	98.144
3.8	1,142	1.525	99.669
38.0	208	0.278	99.947
380	38	0.051	99.997
3,800	2	0.003	100.000

1.3.3.2 Incorporating Potential Spillage into Risk Analysis

Analyses of historical data on spills provide a synopsis of what actually happened in the past but do not necessarily provide an accurate picture of what could happen in the future. For contingency planning purposes, potential spillage, especially with respect to worst-case discharges (WCDs), often needs to be evaluated. The theoretical WCD from a source is the total release of all of the oil content of the source (e.g., all of the oil in a fully loaded tanker or storage tank). Obviously, the volume of spillage for the WCD will depend on the carrying capacity of the source.

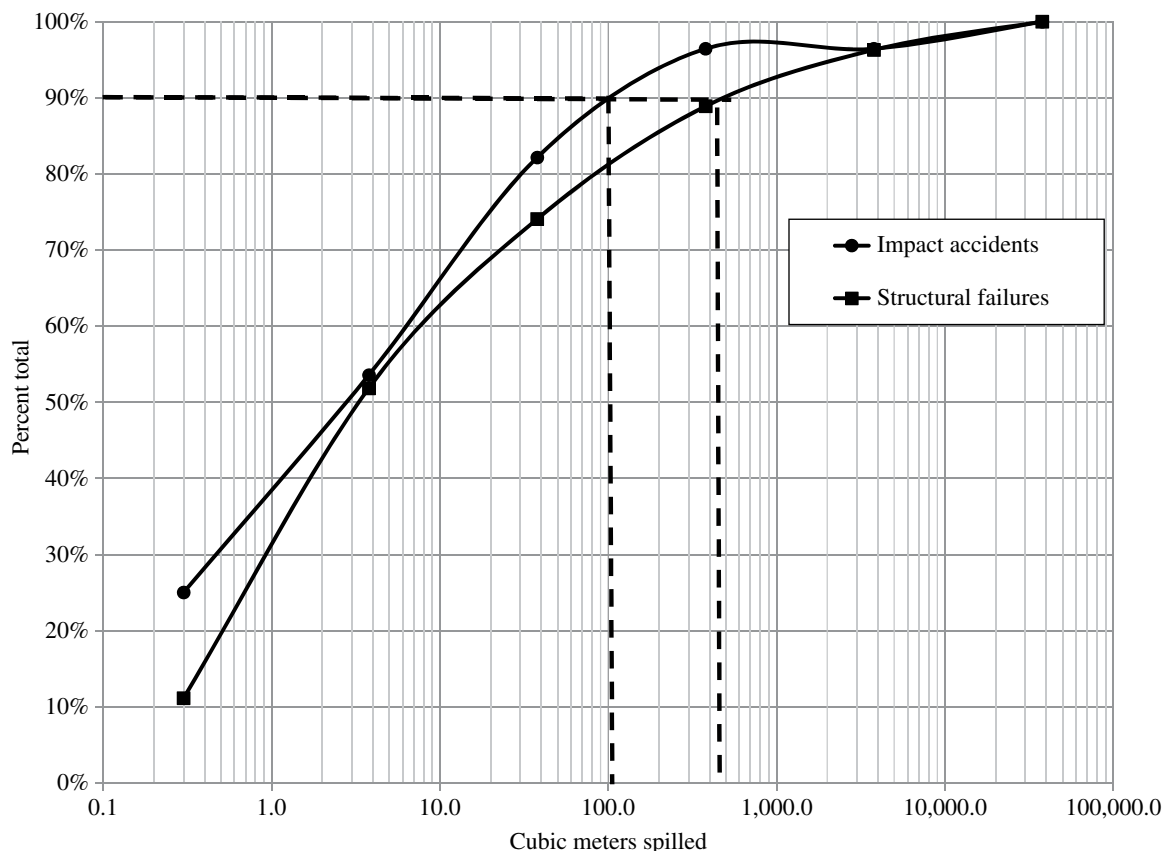


FIGURE 1.6 Probability distribution function of US tanker spills.

In each spill incident, there is the potential for all of the oil to be released from the source up to its total carrying capacity. An analysis of potential spillage for U.S. tanker spills is shown in Figure 1.7, which shows the distribution of actual volumes from historical spills and the volume that each of those spills would have been had each of the spills been WCDs. There is a distribution of volumes because there was a distribution of volumes of carrying capacity (or actual cargo load) in the tankers that were involved in the spill incidents.

1.3.4 Determining the Probable Locations and Timing of Spills

The spill location will be an important factor in determining the impacts of a spill, as will be described in Section 1.3.6. Predicting the locations of likely spill events is another important part of spill risk analysis. Just as there are distributions of probabilities of spills from different sources and spills of different volumes, there are also distributions of spill locations in space and time. Based on spill histories and

patterns of weather, traffic, transport, and other relevant factors, a distribution of spills in space and time may also be established.

An example of analysis for a spatial spill distribution is shown in Figures 1.8 and 1.9 [5]. Figure 1.8 depicts the spatial distribution of vessels in traffic lanes with locations of highest collision probability.

Figure 1.9 indicates the approximate locations of vessel traffic lanes shown in relation to two vessel–vessel collision risk areas considered, WTGs allision risk area, and electric service panel allision risk area that were analyzed for the vessel collision and allision study for the Cape Wind offshore wind project in Nantucket Sound, Massachusetts, USA.

Marine and river traffic lanes and ports are obvious locations to analyze for vessel incidents. For stationary sources, such as pipelines and facilities, the infrastructure of the system needs to be analyzed for determining the likely location of spill incidents.

1.3.5 Factors That Determine the Consequences/Impacts of a Spill

The impacts and consequences of a spill form the other side of the risk equation. Spilled oil can have a broad range of environmental and socioeconomic impacts, along with legal and political ramifications. While each spill is a unique event in terms of consequences and impacts, there are a number of factors that will generally affect the outcome of a spill:

- Oil type
- Spill location with respect to proximity to sensitive resources

TABLE 1.8 Probabilities of spill volume for U.S. tanker spills (1985–2000)

Spill volume (m ³)	Impact accidents		Non-accident structural failure	
	Percent	Cumulative percentage (%)	Percent	Cumulative (%)
0.38	25.0	25.0	11.1	11.1
3.8	28.6	53.6	40.7	51.9
38.0	28.6	82.1	22.2	74.1
380	14.3	96.4	14.8	88.9
3800	0.0	96.4	7.4	96.3
38,000	3.6	100.0	3.7	100.0

TABLE 1.9 Probabilities of large spills for accidents of large double-hull tankers

Accident event	Probability (per tanker year)			
	Accident	Spill	Accident × spill	Large spill (38,000 m ³)
Collision with side impact	4.50E-05	1.90E	8.55E-06	3.1E-07
Collision with side/bottom impact	1.05E-04	1.80E	1.89E-05	6.8E-07
Explosion	2.30E-04	4.00E	9.20E-05	3.4E-06
Fire	2.30E-04	4.00E	9.20E-05	3.4E-06
Hard grounding	1.10E-04	1.80E	1.98E-05	7.1E-07
Structural failure (non-accident)	1.50E-04	4.00E	6.00E-05	2.2E-06

TABLE 1.10 Probabilities of large spills for accidents of large single-hull tankers

Accident event	Probability (per tanker year)			
	Accident	Spill	Accident × spill	Large spill (38,000 m ³)
Collision with side impact	4.50E-05	6.50E	2.93E-05	1.1E-06
Collision with side/bottom impact	1.05E-04	7.90E	8.30E-05	3.0E-06
Explosion	2.30E-04	4.00E	9.20E-05	3.4E-06
Fire	2.30E-04	4.00E	9.20E-05	3.4E-06
Hard grounding	1.10E-04	9.20E	1.01E-04	3.6E-06
Structural failure (non-accident)	1.50E-04	4.00E	6.00E-05	2.2E-06

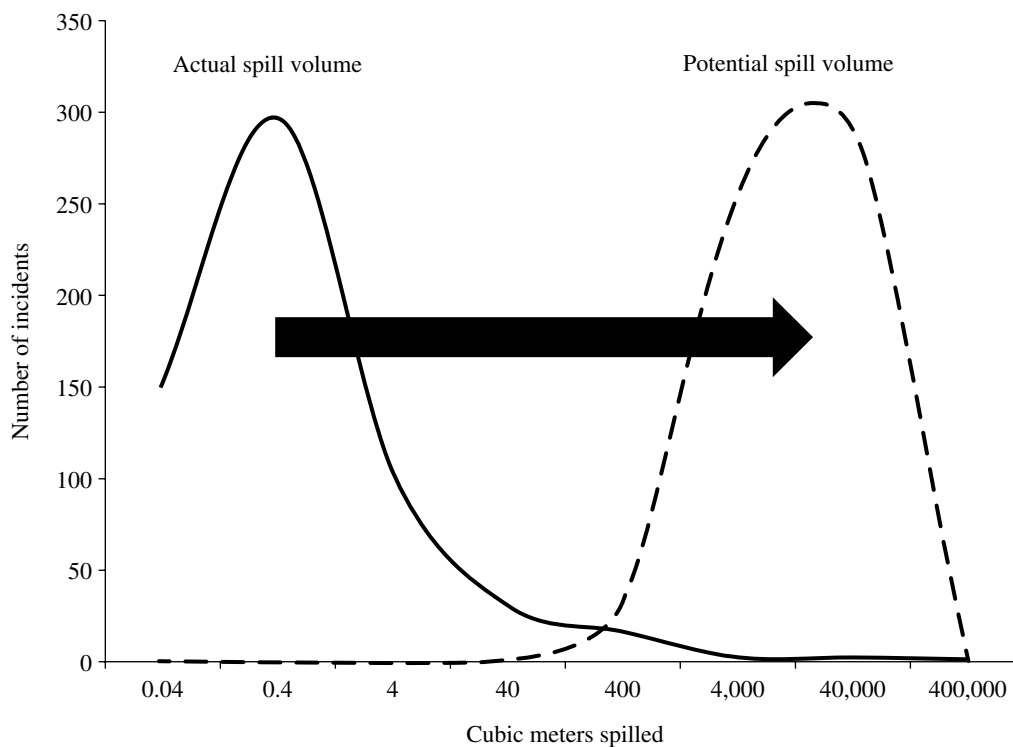


FIGURE 1.7 Actual versus potential spill volume for US tanker spills [5,8].

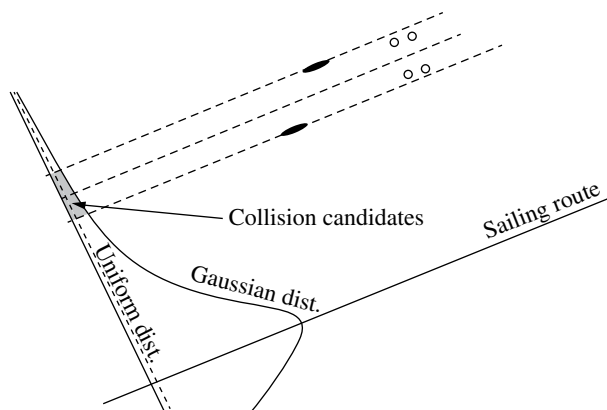


FIGURE 1.8 Geometrical ship distribution in traffic lane [2].

- Environmental conditions (e.g., currents, tides, winds, waves, and weather)
- Sensitive resources (e.g., habitats, flora and fauna, and socioeconomic resources) in vicinity
- Impact mitigation through effective response
- Impacts from response itself

1.3.5.1 Oil Type Different oil types (Table 1.11) vary in their potential for environmental and socioeconomic impacts due to differences in their persistence, toxicity, and coating/mechanical injury effects.

Though each petroleum-based oil has its unique characteristics, for the purpose of modeling and damage or impact estimation, it is useful to put the various oils into one of four basic categories. These categories are generally not only based on the density (specific gravity) of the oils but also incorporate the concentrations of aromatics, which tend to be more toxic and evaporate more easily, versus concentrations of heavier components, which are less toxic but are highly persistent in the environment. Ultimately, these are the factors that will determine short- and long-term impacts on natural and socioeconomic resources.

Volatile distillates include refined petroleum products that are highly toxic but evaporate relatively rapidly, such as gasoline, jet fuel, kerosene, crude condensate, and No. 1 fuel oil. In the United States, this category is called “Group I Oil,” which consists of hydrocarbon fractions at least 50% of which, by volume, distill at a temperature of 340°C and at least 95% of which, by volume, distill at a temperature of 370°C. In general, these oils exhibit the following behavior:

- Highly volatile (evaporate completely within 1–2 days);
- Contain high concentrations of toxic soluble compounds;
- Capable of causing localized, severe impacts to surface and subsurface resources and contaminating drinking water; and
- Generally nearly impossible to clean up with conventional response tools.

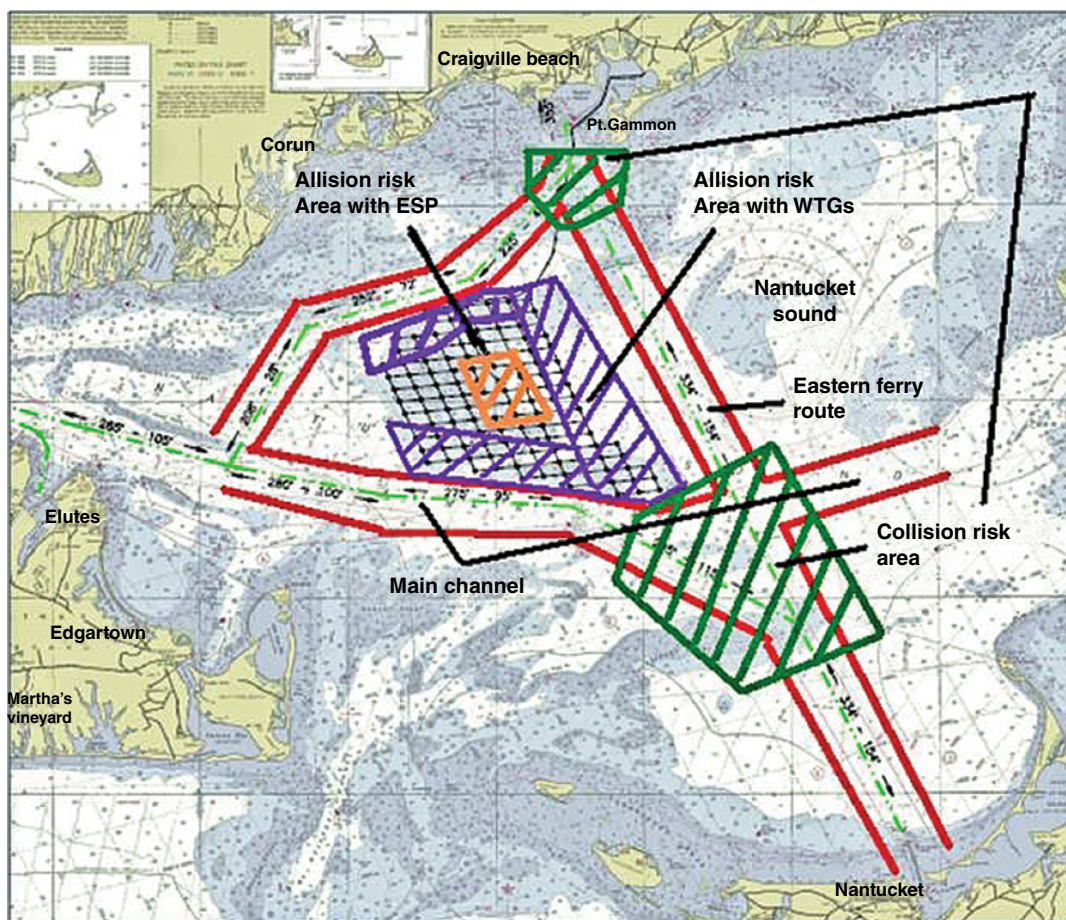


FIGURE 1.9 Vessel collision locations for cape winds facility [15].

TABLE 1.11 Modified oil type persistence classifications

Persistence category ^a	Oil types ^b	Examples in category
Nonpersistent	Volatile distillates	Jet fuel, kerosene, gasoline ^c
Low persistent	Light fuels	Diesel fuel, No. 2 fuel, home-heating oil, marine diesel
Medium persistent	Lube oils	Lubricating oils
	Crude oil	Medium crude oils ^d
Heavy persistent	Heavy oils	Heavy fuel oil; bunker oils Bunker A, Bunker B, and Bunker C; intermediate fuel oil; No. 4 fuel; No. 5 fuel; No. 6 fuel; transmix; residual oils/fuel; waste oil

^aThere is no standard method to determine oil persistence. For example, diesel fuel is sometimes classified as “persistent” and sometimes classified as “non-persistent” [3].

^bThese categories have been used by the EPA in its assessment of impacts of spills from inland facilities regulated by the agency [10].

^cGasoline can be separated out as a separate category if desired.

^dHeavy crude oils have many of the same characteristics as heavy oils, and light crudes tend to be more like light fuels.

The light fuels category incorporates crude oils and refined petroleum products that are not only quite toxic but also contain some persistent components. These oils do not evaporate as readily as volatile distillates. The category includes No. 2 fuel, diesel fuel, light crude oil, gas oil, hydraulic oil, and catalytic feedstock. In the United States, this category is called “Group II Oil,” including crude oil and products that have a specific gravity less than 0.85 (American Petroleum Institute (API°) >35.0). These oils have the following characteristics:

- Moderately toxic and will leave a residue of up to one-third of the spill amount after a few days;
- Contain moderate concentrations of toxic soluble compounds;
- Capable of oiling surface and subsurface resources with long-term contamination potential;
- Generally possible to clean up with effective response tools.

The medium oils category includes crude oils and refined petroleum products that are moderately toxic and moderately persistent, such as most crude oils, lube oil, and intermediate fuel oil. This category would also include synthetic crudes. In the United States, these oils are considered “Group III Oils,” having a specific gravity between 0.85 and less than 0.95 (API° ≤35.0 and >17.5). In general, these oils exhibit the following behavior:

- About one-third will evaporate within 24h;
- Oil contamination can be severe and long-term;
- Oil impacts to waterfowl and fur-bearing mammals can be severe; and
- Cleanup is most effective if conducted quickly.

The heavy oils category includes crude oil and petroleum products that are very persistent, though less toxic. This group includes heavy fuel oil, Bunker C, No. 5 or No. 6 fuel, and heavy crude oils. This category would also include bitumen blends. In the United States, these oils are classified as Group IV, having a specific gravity between 0.95 to and including 1.0 (API° ≤17.5 and >10.0). In general, these oils exhibit the following behavior:

- Heavy oils with little or no evaporation or dissolution;
- Heavy contamination likely;
- Severe impacts to waterfowl and fur-bearing mammals (coating and ingestion);
- Long-term contamination of sediments possible;
- Weathers very slowly; and
- Shoreline and substrate cleanup is difficult under all conditions.

Oil type is an extremely important factor in determining the costs and impacts of spills. The oil type determines the properties of the oil itself and the way in which the oil will behave once it is spilled into the environment. The characteristics of spilled oil are interrelated and can affect response operations in a number of ways. First, the degree to which the oil evaporates, disperses, and dissolves will affect the amount of oil that is available for removal via mechanical containment and recovery, dispersant application, manual removal, or in situ burning. The degree of weathering as well as the oil’s viscosity, density, adhesiveness, and other characteristics will affect the effectiveness of these removal techniques [6].

1.3.5.2 Oil Evaporation Effect on Environmental and Socioeconomic Impacts The most toxic substances in oil (e.g., benzene, toluene, ethylbenzene, and xylene) are also more likely to evaporate and disperse, which reduces the time that they remain concentrated in the aquatic environment. The toxic effects of oil are usually realized in the first hours to days of a spill. Evaporation of the volatile hydrocarbons leaves behind the heavier, more persistent fractions of oil.

Evaporation rates are dependent on temperature with higher evaporation in warmer temperatures.

The more oil that evaporates, the less oil there is to clean up and the less oil that persists in the environment to impact natural and socioeconomic resources. At the same time, the presence of volatile components generally means that there will be at least some toxic impacts from the oil, which translates to environmental and socioeconomic damages as well.

1.3.5.3 Oil Density Effect on Environmental and Socioeconomic Impacts Density, the mass per unit volume of the oil, determines its buoyancy in water. Density is commonly expressed in grams per cubic centimeter (g/cm³).¹ The density of oil increases with weathering (evaporation of volatile hydrocarbon components) and decreasing temperature.

The density of oil affects its buoyancy and the possibility of sinking. Oil will sink if its density is higher than that of the water. It will also sink when it comes in contact with sediment or other particles or debris that makes the mixture heavier than water. Sunken oil presents significant challenges for spill response.

Oil density also affects the rate of natural dispersion with denser oils dispersing more readily. Denser oils also spread faster on the water surface in the early stages of a spill. Denser oils are also more likely to form stable emulsions.² Dispersion, spreading, and emulsion formation all affect spill response costs. While natural dispersion will tend to reduce response costs, as there is less to effectively remove, spreading and emulsion formation both tend to increase costs. With oil spreading, it is more difficult to locate and contain oil for mechanical recovery or to effectively burn or chemically disperse the oil.

1.3.5.4 Oil Viscosity Effect on Environmental and Socioeconomic Impacts Viscosity is a measure of the resistance of oil to flowing once in motion. Oil viscosity increases as weathering progresses and with decreasing temperature. Viscosity is one of the most important properties for spill behavior as it affects spreading—the more viscous the oil, the more slowly it spreads—and emulsification—the more viscous the oil, the more stable the emulsion.

Viscosity also affects the effectiveness of certain spill response measures. Highly viscous oils are very difficult to disperse chemically. Natural dispersion is also significantly reduced in highly viscous oils. More viscous oils are difficult to recover with skimmers and pumps and thus tend to increase response costs.

¹Pure water has a density of 1 g/cm³; seawater generally has a density of 1.03 g/cm³.

²A water-in-oil emulsion is a stable emulsion of small droplets of water incorporated in oil. Oil spills on water may form stable water-in-oil emulsions that can have very different characteristics than the parent crude oil.

1.3.5.5 Interfacial Tension and Environmental and Socioeconomic Impacts Interfacial tension is a measure of the surface forces that exist between the interfaces of the oil and water and the oil and air. Interfacial tensions (oil and air and oil and water) are insensitive to temperature but are affected by evaporation. Interfacial tension affects the rate and type of spreading on the water surface as well as sheen³ formation. Interfacial tension also affects emulsion rates and emulsion stability.

Since chemical dispersants work by reducing the oil and water interfacial tension to allow a given mixing energy⁴ to produce smaller oil droplets, the degree of interfacial tension in an oil will affect the ability of the oil to be chemically dispersed. Oils with high interfacial tensions are more difficult to disperse with chemical dispersing agents and also disperse less naturally. This will tend to limit the effectiveness of dispersants and require more expensive mechanical methods for cleanup.

At the same time, mechanical recovery with oleophilic skimmers (e.g., rope-mop and belt skimmers) work better on oils with moderate to high interfacial tensions. Increased effectiveness of mechanical recovery will generally reduce response costs. The amount of oil recovered offshore (on the water surface) will be greater reducing the amount of oil on the shoreline where cleanup tends to be more labor-intensive and expensive. If more oil can be recovered on the water surface, the less impact on shorelines.

1.3.5.6 Oil Pour Point Effect on Environmental and Socioeconomic Impacts The “pour point” of a particular oil is the lowest temperature at which the oil will still flow at a given rate. The pour point temperature increases with weathering (evaporation of volatile components). Pour point affects spreading on the water surface. Oils that are at temperatures below their pour points will spread only very slowly and are more difficult to disperse. Viscosity increases dramatically at temperatures below the pour point.

Because oils will resist flowing toward skimmers or down-inclined surfaces in skimmers, there are significant challenges in mechanical oil recovery at these temperatures. The solidification of the oil below its pour point also causes problems in storage and transfer. These factors can increase spill response costs because more work needs to be done manually.

1.3.5.7 Adhesiveness Effect on Environmental and Socioeconomic Impacts The adhesiveness of an oil is the degree to which the oil remains on a surface after contact and draining. This character has an effect on spill impacts by way of the amount of oil that will stick to surfaces, including shoreline substrates and structures (e.g., piers, boats, and

seawalls). Higher adhesion increases damage costs and shoreline cleanup costs. At the same time, adhesion can increase the effectiveness of some on-water recovery methods, including the use of oleophilic skimming devices.

1.3.5.8 Emulsification Effect on Environmental and Socioeconomic Impacts A water-in-oil emulsion⁵ is a stable emulsion of small droplets of water incorporated in oil. Oil spills on water may form stable water-in-oil emulsions that can have very different characteristics than the parent crude oil. The tendency to form emulsions, the stability⁶ of those emulsions, and the water content of stable emulsions are all important characteristics of an oil that can affect impacts as well as response.

Emulsification can significantly affect the impacts of a spill and increase the amount of storage capacity required during response and operations. Emulsified oils can be highly persistent in the environment. Strongly emulsified oils are also highly viscous, often with 10–100 times the viscosity of the parent oil. Oils with relatively high concentrations of asphaltenes are most likely to form stable water-in-oil emulsions. Some heavy oils do not easily form emulsions because the high viscosity of the oil prevents the uptake of water. Some light or medium oils do not form an emulsion immediately, but once evaporation occurs and the asphaltene concentration increases, the emulsification process begins and usually proceeds quickly thereafter.

Emulsions can present challenges for all types of response strategies, increasing costs and logistical concerns, such as increases in storage of collected oil (i.e., larger volume with oil/water mixture).

1.3.5.9 Persistence Effect on Environmental and Socioeconomic Impacts The persistence of the oil in the environment can also significantly affect the impacts of a spill as well as the response strategies and costs. Persistence of petroleum-based oils is a very important consideration in assessing the environmental risk of an oil spill and often affects the resources needed for spill recovery and remediation. The heavier, more persistent fractions of oil are those that adhere to the feathers of birds and fur of mammals, as well as to shoreline and wetland communities. For birds and mammals, this coating can cause hypothermia. For organisms living along shoreline or in wetlands, this can cause smothering. Both smothering and hypothermia can result in mortality, which increases environmental damages.

The persistent portions of oil can also coat other surfaces (e.g., tourist beaches, seawalls, marinas, and boats) causing socioeconomic impacts. The persistence of oil and the

³A “sheen” is a very thin layer of oil on the water surface. Rainbow-colored sheens are generally 0.0003 mm thick. Silver sheens are usually about 0.0001 mm thick.

⁴Waves and sea state.

⁵Water-in-oil emulsion is colloquially called “chocolate mousse”.

⁶Emulsion stability can be low, which indicates the emulsion is unstable and will break quickly once removed from the mixing environment; moderate, which means the emulsion will break within a few hours; or high, which means the oil forms a very stable emulsion that is unlikely to break even after standing for 24 h.

degree to which the oil adheres to shoreline substrates and penetrates those substrates will affect the type of shoreline response that is required [1,7]. The labor and resources, as well as disposal, required for shoreline responses will vary by shoreline type, oil type, and degree of oiling, which in turn affect the complexity involved in the cleanup [8,9].

1.3.5.10 Toxicity and Environmental and Socioeconomic Impacts The *toxicity* of the oil determines the adverse effects and mortality of fish, wildlife, and invertebrates after short-term exposure (hours to days). Mortality as well as sublethal effects (e.g., reduced fecundity) is relevant to both environmental impacts and socioeconomic impacts in as much as commercial fisheries, subsistence fishing (particularly important in Tribal Nation areas), and recreational fishing are affected. Different organisms have different tolerances of exposure.

1.3.5.11 Mechanical Injury and Environmental and Socioeconomic Impacts Oil can also cause “mechanical injury” based on its adhesive properties. This injury is caused by coating, fouling, or clogging of organisms and their appendages and apertures, such that movements and behaviors are physically inhibited [10].

1.3.6 Spill Impacts: The Effects of Spill Location Type

The impacts of spills of each oil type will be affected by their individual properties, as well as by the environment into which the oil spills. The characteristics of a spill location also determine impacts in the following ways:

- Hydrodynamics (currents, tides, and wave heights) will affect the way in which spilled oil will travel and spread on the water surface;
- Current velocity and wave height will also affect the degree to which booming, both for shoreline protection and for mechanical containment for on-water oil recovery operations, will be effective;
- Prevailing wind patterns will also affect the way in which the oil spreads and its trajectory on the water surface;
- The water and air temperatures in different seasons will affect the behavior of oil with respect to rates of evaporation and dispersion and viscosity;
- Presence or absence of ice will affect the behavior of the oil and strategies for spill response; and
- Types of shoreline substrates and configurations of the coastline will affect the degree of impacts on shoreline resources, as well as determine the nature of shoreline cleanup response strategies [8].

1.3.6.1 Location Type: Oil Behavior and Potential Effectiveness of Spill Response The effectiveness of the response, in turn, determines the degree to which the

environmental and socioeconomic impacts of the spill can be mitigated or reduced. It is important to remember that a spill response can only mitigate a percentage of the damages from a spill depending on the type of response employed and the efficacy of the oil removal. In most cases, this will represent a small percentage of the oil spillage. Except under highly unusual circumstances (i.e., sheltered waters with little to no current around a pre-boomed dockside vessel), mechanical containment and recovery will remove 3–10%, and occasionally as much as 25%. Dispersant application and in situ burning will have much higher efficacy, though there are limitations to the use of these strategies that need to be considered in response decisions.

Shoreline areas and land-based substrates most sensitive to oiling include those with long oil residency—fine-grained (silt–mud) flats, marshes, and lagoons—as well as shorelines with the greatest potential for penetration and remobilization—coarse-grained (cobble, cobble–boulder mix) substrates [11]. The degree to which oil adheres to and penetrates into various types of shorelines is determined by complex factors [1,7]. The oil-holding capacity of a particular substrate is related to the following:

- Sediment type (porosity and permeability);
- Oil type (viscosity and adhesiveness); and
- Water and air in the pore spaces of the sediment.

Impacts to different shoreline types are summarized in Table 1.12.

The behavior of spilled oil as it first strands on a shoreline or first spills onto or into a substrate depends on a number of interrelated factors: oil type and characteristics (e.g., viscosity); oil thickness on the substrate; time until impact (i.e., degree of weathering); timing with regard to tides; weather during and after the spill; and nearshore wave energy, in the case of spills into water. The adhesiveness of oil to shoreline substrates, in turn, depends on the properties of the oil,

TABLE 1.12 Shoreline substrate types and spill damage implications

Type name	Damage issues
Rock platform	Low penetration and residency; oil will wash off with wave action
Rock cliff	Low penetration and residency; oil will wash off with wave action
Rock with gravel beach	Some penetration and potential remobilization
Rock sand gravel beach	Some penetration and potential remobilization
Rock with sand beach	Some penetration and potential remobilization
Gravel beach	Higher penetration and potential remobilization
Gravel flat	Higher penetration and potential remobilization
Sand gravel beach	Some penetration and potential remobilization
Sand beach	Lower penetration and potential remobilization
Sand gravel flat	Some penetration and potential remobilization
Sand flat	Lower penetration and potential remobilization
Mud flat	Long residency and difficulties with cleanup
Estuary, marsh, lagoon	Long residency and difficulties with cleanup
Man-made (solid)	Lower penetration
Riprap	Higher penetration and remobilization

especially viscosity [12]. The degree of weathering can have a significant impact on the ability of oil to adhere to a substrate. Weathering can also cause emulsification, which can also change the oil viscosity. The degree of emulsification depends on the chemical composition of the oil. The degree of weathering that occurs is related to oil type and environmental conditions. Lighter oils evaporate more quickly than heavier oils. Temperature, wind, light conditions, and other environmental factors can influence the rate of weathering.

Fresh oils tend to be less adhesive than more weathered oils. Light fuels or volatile organic distillates tend to be relatively nonadhesive. Heavier fuels tend to be more adhesive than lighter oils. Penetration into the substrate will also depend on oil type. All other things being equal (e.g., shoreline porosity), heavier oils will penetrate less than lighter oils. Oil viscosity is positively correlated to oil adhesion on the shoreline. Adhesion is inversely related to penetration—the more adhesive an oil, the lower its penetration potential. Oil thickness on the shoreline is a factor of the amount spilled, spill trajectory, oil properties, steepness of the shoreline slope, tidal conditions at the time of shoreline impact, and the porosity of the surface.

Oil behavior at the shoreline or in a substrate is also highly dependent on the substrate characteristics, particularly porosity and permeability. The substrate structure largely determines the degree of oil penetration [13,14]. Penetration will be less in substrates with very fine granules that are packed closely together and greater in more coarsely grained substrates. If the pores are large and interconnected, the substrates will be more “permeable” and allow deeper penetration and lateral movement of the oil through capillary action.

Bedrock is largely impermeable to oil except when the oil is able to enter crevices or fractures in rock surfaces. Gravel tends to have large interconnected pore spaces that will allow oil to readily penetrate. Sand and mud beaches tend to have tightly packed sediments with small pore spaces that are less permeable to oil, though some lighter oils can penetrate. Some substrates have features that can influence oil retention and penetration that are not related to granule size. Tidal flats often have holes from burrowing animals that will allow oil penetration [15]. Oil adhesion can also be influenced by the presence of vegetation, such as in wetlands or mangroves. Ice is another substrate that can cause variations in oil adhesion and penetration based on its nature (tightly packed, granular, smooth, or rough) [16].

Nearshore wave energy can affect the degree of initial deposition and penetration for spills into water [17]. The effectiveness of wave energy in removing or refloating oil is dependent on the permeability of the shoreline substrate, as well as the oil type and weathering condition with respect to adhesiveness. Wave energy can effectively remove oil from a bedrock shoreline where there is little, if any, penetration. Wave action can also cause the shoreline substrate to redistribute itself, as in the case of gravel or sand. This action can

affect the degree of oil retention and refloating. The extent of oiling on the shoreline is also dependent on the tidal stage at the time of oil deposition.

The presence of ice on the water affects spill response in a number of ways. The oil tends to be more viscous, affecting the effectiveness of certain spill response measures. Highly viscous oils are very difficult to disperse chemically. Natural dispersion is also significantly reduced in highly viscous oils. More viscous oils are difficult to recover with skimmers and pumps and thus increase response costs.

At the same time, solid, pack, or broke ice; floes; or brash ice can contain and entrain oil that is spilled on, into, or under the ice. While this sometimes complicates recovery with skimmer and booms, it can also act as a natural containment that isolates spilled oil from the marine environment. Oil spilled under ice will eventually resurface. Recovery can sometimes be safely delayed until winter conditions are more amenable to cleanup operations.

Skimmers used on spills in ice must be able to deal with emulsified, highly weathered oil and oil that is mixed with a good deal of debris, including ice pieces. Sometimes, chemical treatment agents designed to increase viscoelasticity and cohesiveness of oil are added to increase the efficiency of skimmers.

In situ burning is widely touted as the most effective means of removing large volumes of spilled oil on ice and in open water situations. Air pollution and safety issues need to be considered. The use of dispersants in icy water conditions has had mixed results. Issues related to efficacy and potential impacts need to be considered.

Overall, the degree to which an effective spill response can be implemented under the conditions in the spill location may have a significant effect on the impacts and consequences of a spill.

1.3.6.2 Location Type: Oil Trajectory and Fate The trajectory and behavior of the oil will have a large effect on the spill impacts. As discussed in Section 1.3.5, oil type is an important factor in determining the behavior of the oil spilled into water, or on land. In water, surface spreading, evaporation rate, and dissolution or dispersion into the water column are all dependent on oil type, but are also affected by the depth of the oil release (surface or subsurface) and duration and nature of the release (instantaneous, chronic, episodic, or prolonged), water and air temperature, and wind velocity. Wind and current velocity and direction will determine the path or trajectory of the oil, including the probability of the oil impacting sensitive shorelines and other resources. An example of modeling outputs from spill modeling is shown in Figure 1.10.

The model results are then summarized statistically to describe probability and degree of oiling and the time after the spill when each impacted area would be first affected. Exposures to each oil constituent on the water surface, in the water column, and on the shoreline are analyzed over all the simulations to determine the median and worst cases for impacts.

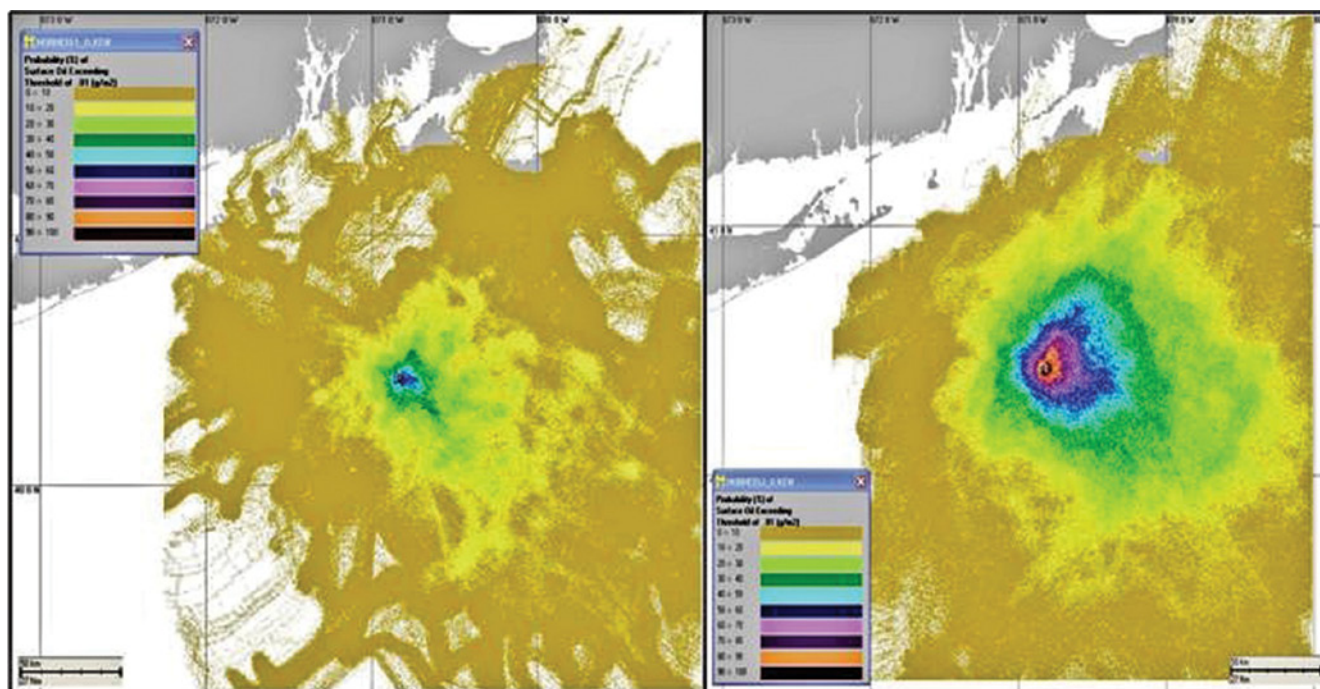


FIGURE 1.10 Hypothetical releases of 17,000 m³ no. 6 fuel [19].

Probabilistic or stochastic modeling, described in greater detail in Chapter 7, provides a means to estimate the probabilities of impact to various resources at risk [18,19].

1.3.6.3 Location Type: Sensitive Resources at Risk The probability of oil impacting sensitive resources depends on the location of the spill in relation to sensitive ecological and socioeconomic resources and the probability that the oil will be carried towards those resources by dispersion and dissolution into the water column or by currents, tides, and winds.

The sensitivity of various resources to oil impacts varies greatly, depending on oil type, particularly the toxicity, persistence, and adherence properties, and the resources themselves. (This is discussed in greater detail in Chapter 7.) There are seasonal factors that need to be considered as well. Wildlife species are often more vulnerable during certain times in their life cycles, such as fish spawning and bird nesting. Socioeconomic resources also have seasonal sensitivities in some cases as with tourist beaches and commercial and recreational fishing.

Spill risk analysis involves a survey of potentially impacted sources in the area of potential oil impact. Environmental sensitivity index (ESI) mapping has been extremely helpful in allowing planners to assess resources at risk. Examples of ESI Maps for Upper Cook Inlet, Alaska, USA, are shown in Figures 1.11 and 1.12. The key to sensitive resources is shown in Figure 1.13. Note the seasonal differences between the spring and winter resource presence and sensitivity.

Socioeconomic resources at risk can also be incorporated into mapping, as shown in Figures 1.14 and 1.15.

After determining the presence of “resources at risk” in a potential spill area, the actual sensitivity of the resources to

the degree of oiling that may occur, as well as the probability that oiling over a sensitivity threshold will occur, needs to be evaluated. If there are sensitive resources in the area of the likely spill impact, but the concentrations of oil are likely to be insignificant or only cause minor damage, the overall risk is low. On the other hand, with some particularly sensitive resources, even relatively small quantities of oil may cause significant impacts. An example of the rankings of species by their LC_{50} to polycyclic aromatic hydrocarbons in crude oils and fuel oils is shown in Figure 1.16. LC_{50} is the concentration at which 50% of the individuals die. The higher the LC_{50} for a species, the less sensitive it is to oil components, which is because it requires a higher concentration of the oil to kill 50% of the individuals.

The degree of impact by different oils will also depend in large part on the degree of contact and the duration of the exposure, particularly with regard to toxicity. The “dose” of oil is a combination of the toxicity of the oil based on its chemical components, the duration of the exposure in time, and the sensitivity of the particular organisms. The volume of spillage and the properties of the oil are important factors in determining dose. An example of an evaluation of species sensitivity to oiling by different oil types for species groups common in Cook Inlet, Alaska, USA, is shown in Table 1.13 [5].

1.3.7 Measuring Oil Spill Impacts

Measuring the impact of oil spills on ecological and socioeconomic resources is a complex science. With such a broad array of potential impacts to sensitive resources—from fish mortality to bird nesting habitat oiling and to disruptions to commercial fishing and tourism—there are many ways to quantify impacts.

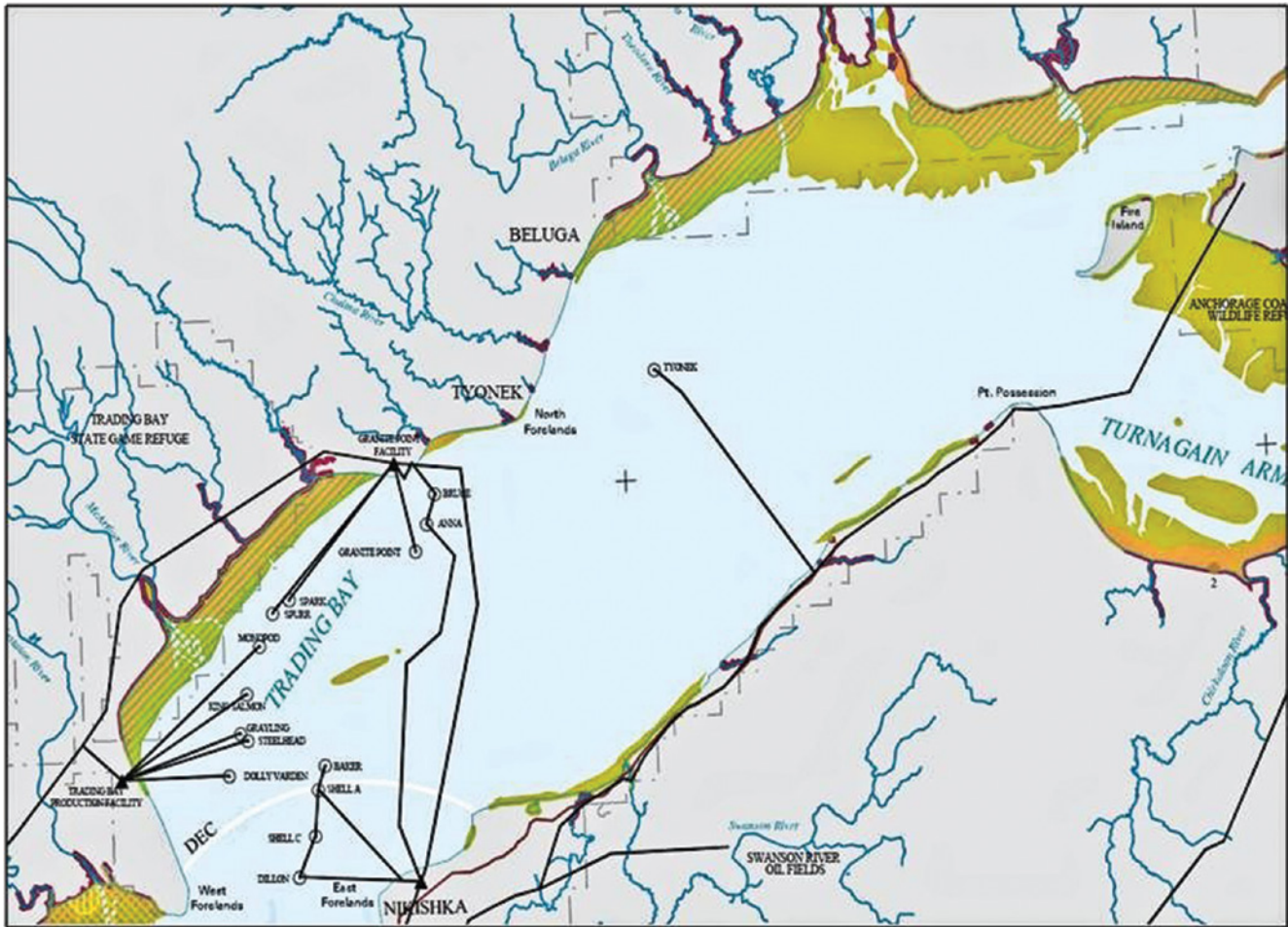


FIGURE 1.11 ESI map of Upper Cook Inlet in winter.

1.3.7.1 Quantifying Ecological Impacts Ecological impacts can be measured with regard to mortality numbers of individuals of different species groups, reductions in ecosystem production, biomass mortality (e.g., kg of fish), changes in the abundance of species, or through a system of natural resource damage assessment (NRDA). NRDA provides a quantification of the cost of restoration of the oiled environment in situ or in another quasi-equivalent location.

Probabilistic oil fates and effects modeling can be used to estimate potential impacts and natural resource damages [20]. The oil fates model uses wind data, current data, and transport and weathering algorithms to calculate mass balance of fuel components in various environmental compartments (water surface, shoreline, water column, atmosphere, sediments, etc.), oil pathway over time (trajectory), surface distribution, shoreline oiling, and concentrations of the fuel components in water and sediments. Exposure of aquatic habitats and organisms to whole oil and toxic components is estimated in the biological model, followed by estimation of resulting acute mortality and ecological losses. Natural resource damages are based on estimated costs to restore equivalent resources and/or ecological services, using Habitat Equivalency Analysis and Resource Equivalency Analysis methods. These

methods can be used to provide a cost (in currency) of ecological impacts.

Another approach to assessing ecological impacts is to rank impacts on a more qualitative scale [5]. An example of a 5-point scale that can be used in risk assessments is as follows:

- Very high impact (VH) (5 points): Long-term impacts (over 5 years) anticipated over a large part of the region and potentially outside of the region and/or significant impacts to threatened species or species indicated for special management. Recovery of populations and ecosystems will take over 5 years, and/or threatened or special-management species will be very significantly impacted at the population level.
- High impact (H) (4 points): Moderate-term impacts (2–5 years) anticipated over a large part of the region or very significant (high) impacts to specific areas of the Inlet. Recovery of populations and ecosystems will take 2–5 years.
- Moderate impact (M) (3 points): Moderate-term impacts (2–5 years) anticipated over a smaller part of the region or significant (high) impacts to specific areas

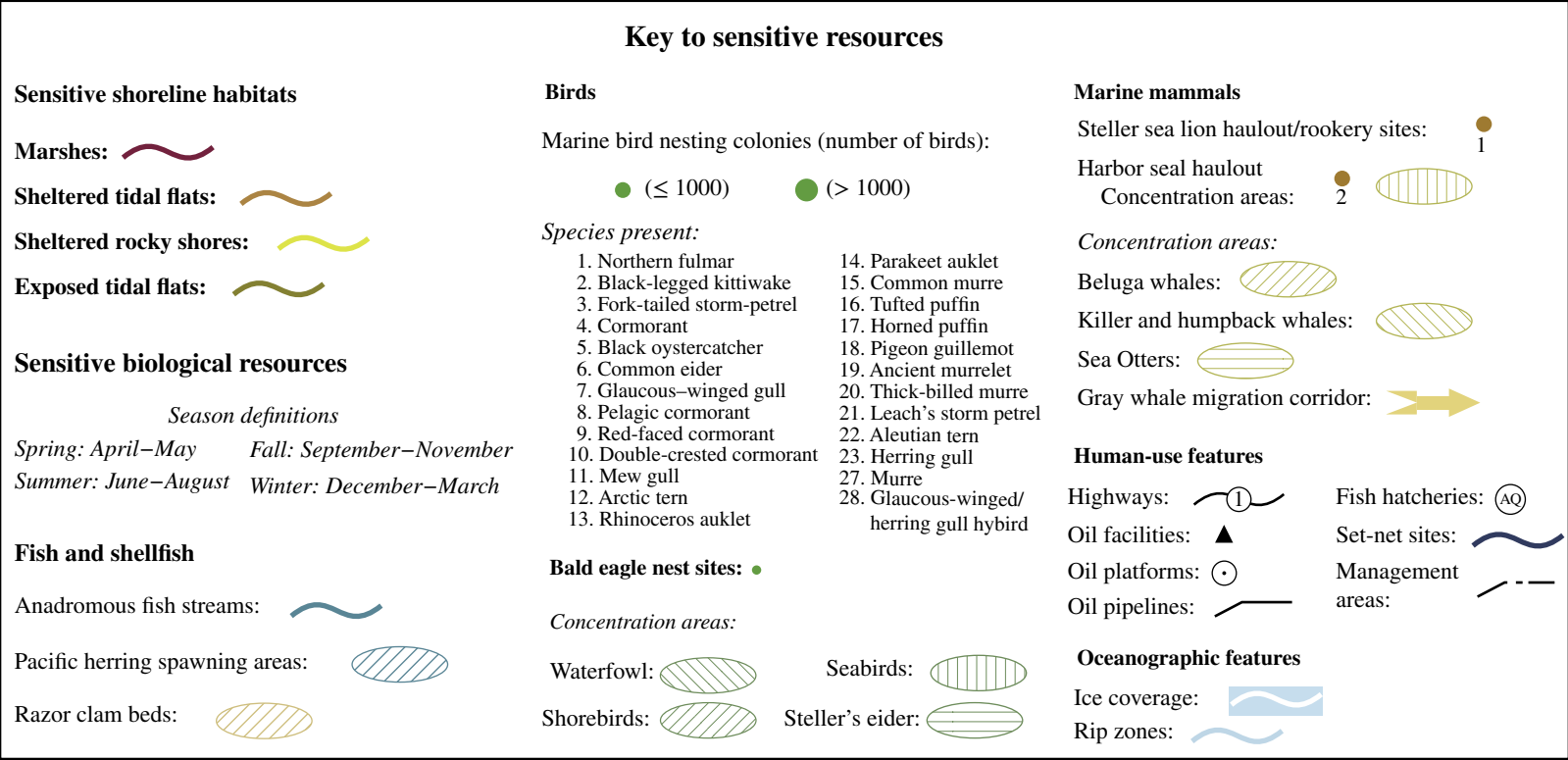


FIGURE 1.13 Key for ESI maps in Figures 1.12 and 1.13.

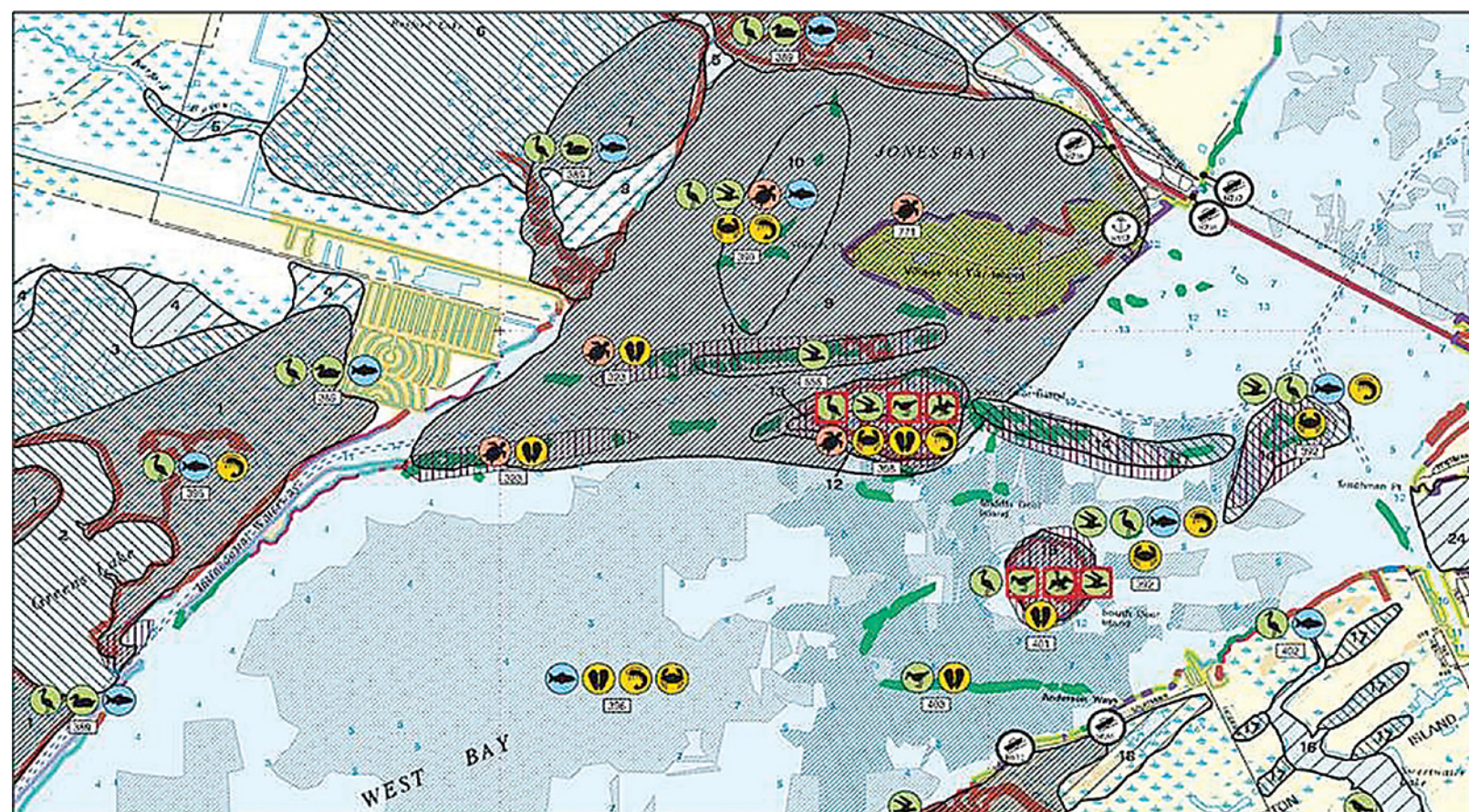


FIGURE 1.14 ESI map from Upper Texas Coast.

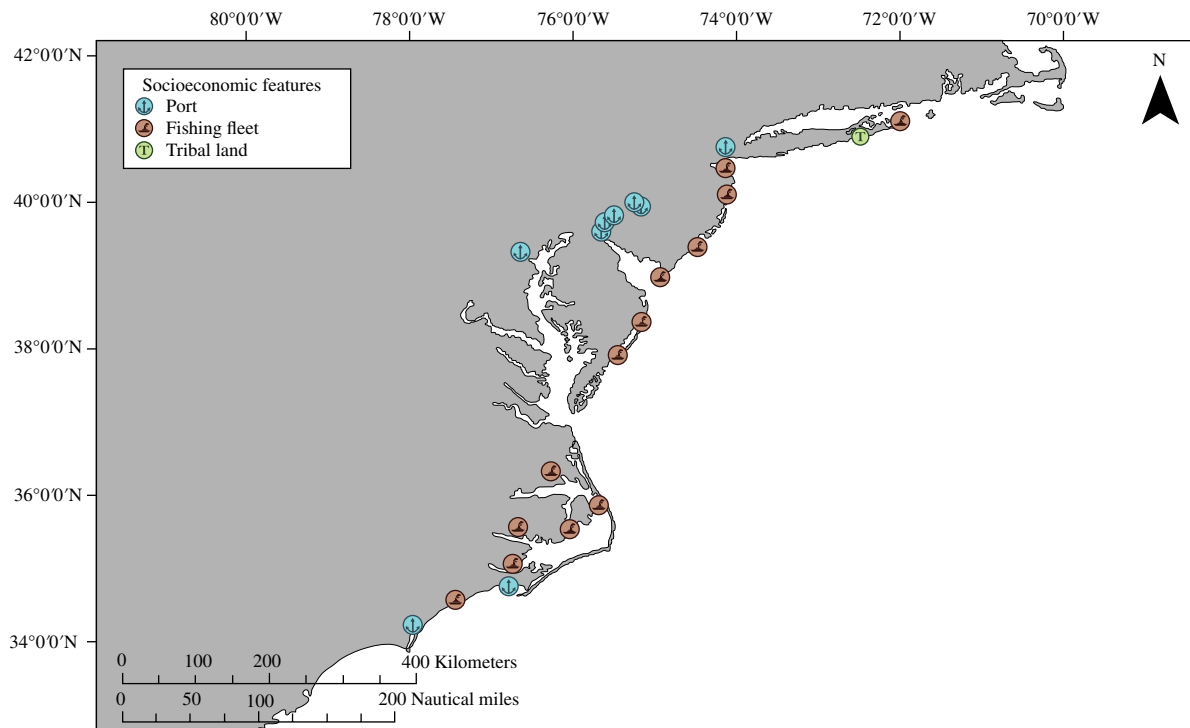


FIGURE 1.15 Sample of socioeconomic resources at risk (North Atlantic, USA).

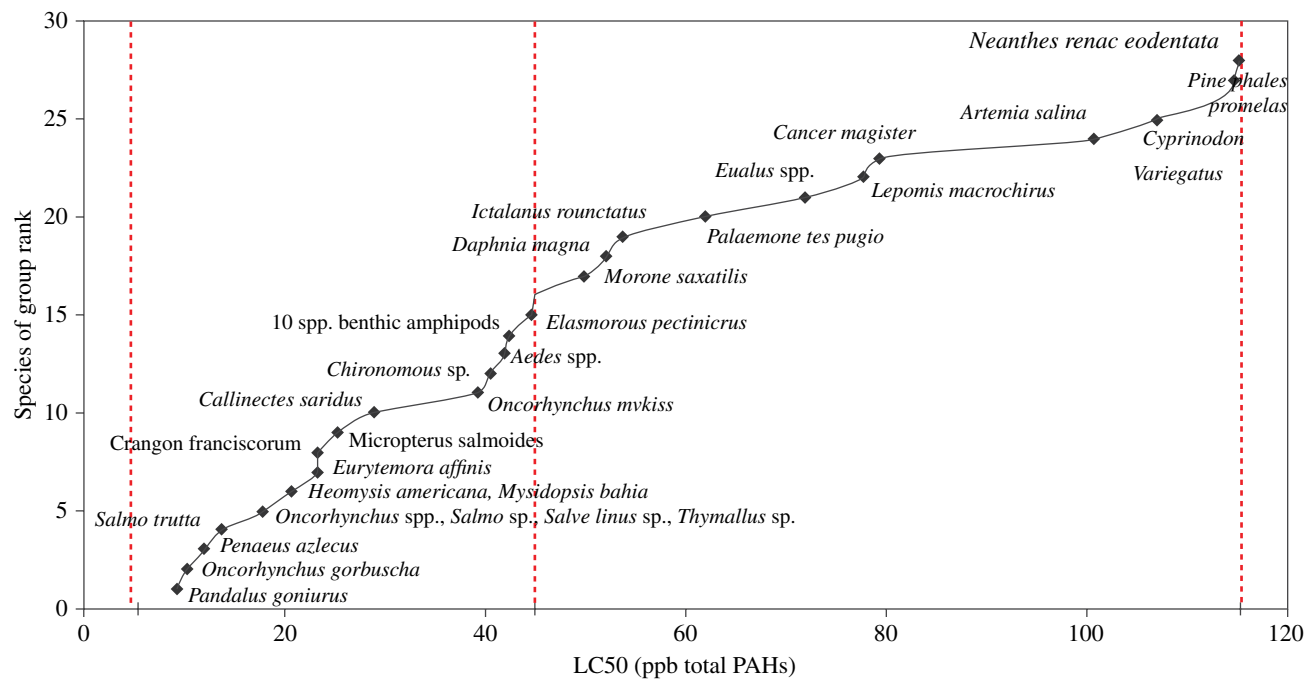


FIGURE 1.16 Species sensitivity rankings to PAHs in crudes and fuel oils. Vertical dashed lines are geometric mean and range for 95% of species [25].

TABLE 1.13 Overall degree of sensitivity to oiling for cook inlet species [38,39]

Oil category	Degree of sensitivity to oiling									
	Fish		Shellfish	Birds				Marine mammals		
	Salmon	Herring	Razor clams	Waterfowl	Seabird	Shorebird	Eider	Otter	Sea lion	Whale
Nonpersistent	H	H	L	L	L	L	L	L	L	L
Low persistent	H	H	M	M	M	L	M	M	M	L
Medium persistent	M	M	H	H	H	M	H	H	H	L
Heavy persistent	L	L	H	H	H	H	H	H	H	L

H, high sensitivity; L, low sensitivity; M, medium sensitivity.

of the region. Recovery of populations and ecosystems will take 2–5 years.

- Low impact (L) (2 points): Significant shorter-term impacts (under 2 years) to a large part of the region or moderate impacts to specific areas of the Inlet. Recovery of populations and ecosystems will take less than 2 years.
- Very low impact (VL) (1 point): Significant shorter-term impacts (under 2 years) to a smaller part of the region or low impacts to larger areas of the region. Recovery of populations and ecosystems will take less than 2 years.

Determining the rate of ecosystem and population recovery is extremely complex. There are a large number of complex and interrelated factors involved in determining short- and long-term consequences of oil spills. There is considerable and legitimate debate in the scientific community about scientific data on short- and long-term recovery rates and the ways in which the results of many spill impact studies and models should be interpreted and applied. A complete analysis generally requires highly complex modeling and studies. The five-point rating system presented earlier and its application to the spill scenarios are based on generalized data analyses on spill impacts based on studies of hundreds of spill case studies and over 1000 spill impact studies.

In determining environmental impacts of hypothetical spills, cultural values placed on impacted environment need to be considered. These can only truly be understood and appreciated by the myriad of stakeholders in the region of concern. While from an ecosystem and a population-level perspective, recovery rates may be similar to those indicated here, the “acceptability” of any degree of environmental impacts from spills will be a matter for stakeholders to consider.

1.3.7.2 Consensus Ecological Risk Assessment In some risk assessment processes, there is greater concern about some resources than others or the concern about resources differs among the stakeholders. A commonly applied approach in these cases is a consensus-based ecological risk assessment (ERA), in which stakeholders rate, rank, and prioritize resources at risk with respect to their sensitivity [21].

ERA is a process through which one can evaluate the possible ecological consequences of human activities and natural catastrophes. An ERA emphasizes the comparison of exposure to a stressor or stressors (i.e., oil and/or the spill response options) with an ecological effect (e.g., population disruption, changes in ecological community structure or function, and toxicological effects). As much as possible, this comparison is made quantitatively, including estimating the probability that the predicted consequences will occur and of the associated severity and magnitude of the effects. Figure 1.17 shows a strategy employed in a number of ERA in the United States.

1.3.7.3 Quantifying Socioeconomic and Response Cost Impacts Besides the environmental impacts, there are also socioeconomic costs that are on the consequences side of the risk equation. Oil spills can have significant impacts on a variety of socioeconomic resources, such as the following:

- Commercial, subsistence, and recreational fishing by causing mortality and/or tainting of fish stocks and interfering with fishing activities;
- Ports and port traffic by interfering with and delaying port traffic and oiling of port facilities;
- Tourism and recreation by oiling of beaches and other coastal property, as well as parks and recreational areas;
- Tribal cultural activities and lands by oiling of water and coastal resources owned by and used by native tribes; and
- Wildlife viewing, diving, and other activities by oiling natural habitats.

Many of these impacts can be quantified to a great extent based on loss of income based on delays and disruptions to commerce and other direct means of putting a currency value on the impact [20]. Other costs, particularly tribal cultural values, are more difficult to quantify. The impacts can also be qualitatively assessed as in the five-point scale previously described. Most impacts will be relatively short-term with the economic resources regaining their original value within a certain period of time, though others may experience a longer impact time.

There are models that can be used to estimate socioeconomic costs of oil spills based on the location type, resources

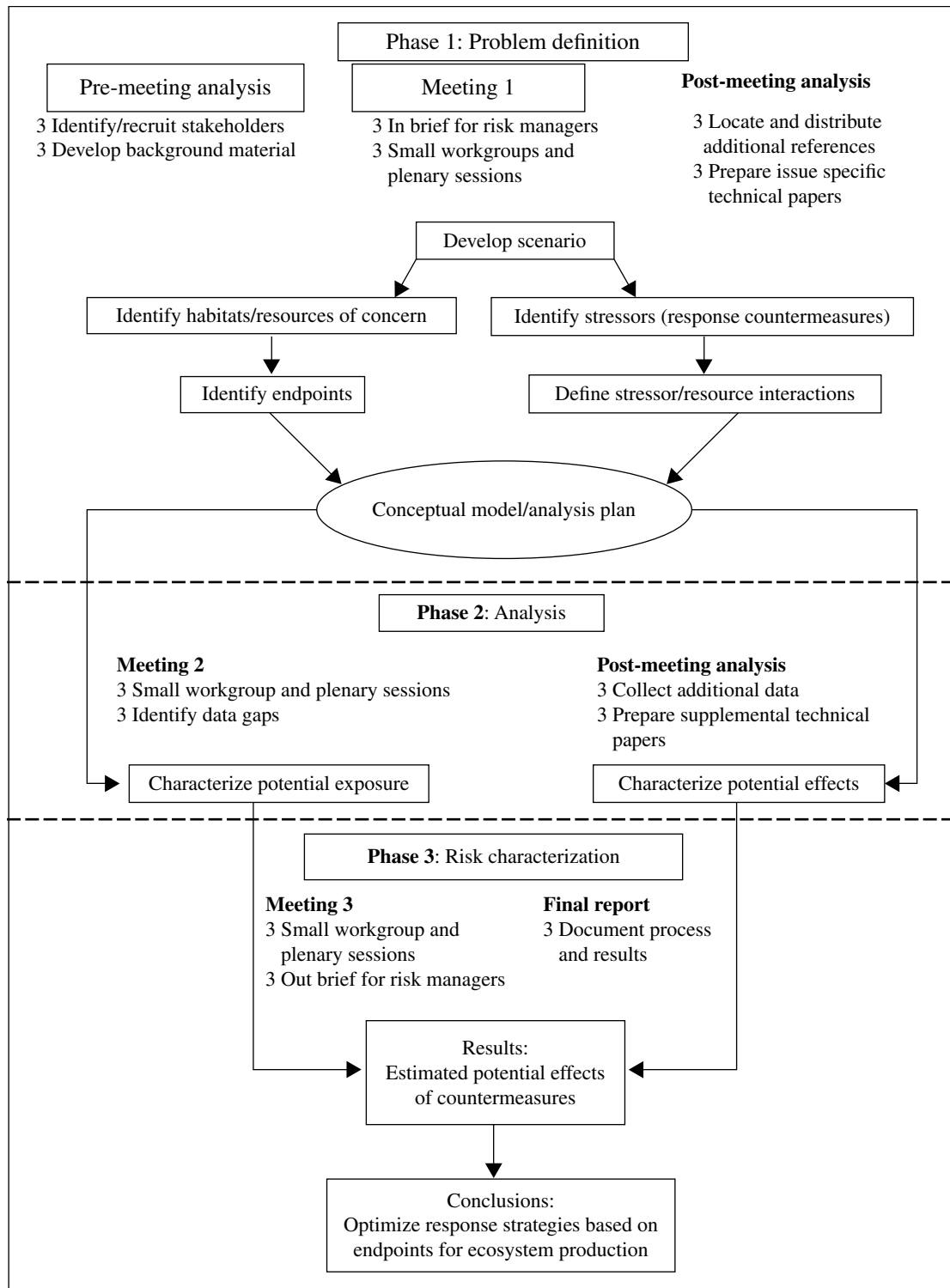


FIGURE 1.17 Consensus ecological risk assessment process [1].

at risk, oil type, and spill volume, including the Basic Oil Spill Cost Estimation Model (BOSCEM) [22,23] and parts of the Oil Spill Response Cost Effectiveness Analytical Tool (OSRCEAT) [24].

A spill incident will also generally require a cleanup response, which can also result in significant costs,

depending on the magnitude of the spill, location, oil type, and method of response. Spill response costs include the cost of equipment, personnel, logistical support, waste disposal, monitoring, and government oversight during the various phases of the spill response operations on, and, in some cases, under the water, on land, and on the shoreline. The BOSCEM

and OSRCEAT models estimate spill response costs based on location factors, oil type, spill volume, and response measures. More precise estimates can be developed by analyzing oil fate and trajectory outputs from modeling and determining the amount of resources and time required for various types of response strategies [6,25,26]. Shoreline response costs can be estimated from algorithms developed from analyses of past spill responses based on the amount of work and resources required to remove oil from different types of shorelines [8,9].

1.3.7.4 Combining Probability of Impact and Degree of Impact For spills on water, the three main categories of risk factors for ecological and socioeconomic resources at risk are as follows:

- Impacts to water column and resources in water column (e.g., fish and invertebrates);
- Impacts to water surface and surface resources (e.g., diving birds and shipping lanes); and
- Impacts to shoreline and shoreline resources (e.g., bird nesting habitats and tourist beaches).

The impacts from an oil spill would depend greatly on the direction in which the oil slick moves, which would, in turn, depend on wind direction and currents at the time of and after the oil release. Impacts are characterized in risk analyses based on the likelihood of any measurable impact, as well as the degree of impact that would be expected if there is an impact. The measure of the degree of impact is based on the median case for which there is at least some impact. The median case is the “middle case”—half of the cases with significant impacts have less impact than this case, and half have more. For each category of ecological and/or socioeconomic resources at risk, risk is defined as follows:

- The probability of oiling over a certain threshold (i.e., the likelihood that there will be an impact to resources over a certain minimal amount); and
- The degree of oiling (the magnitude or amount of that impact).

The ecological and socioeconomic resources at risk for water column impacts include fish, marine mammals, and invertebrates (e.g., shellfish and small organisms that are food for larger organisms in the food chain). These organisms can be affected by toxic components in the oil. The threshold for water column impact to ecological resources at risk is a dissolved aromatic hydrocarbon concentration of 1 ppb (i.e., 1 part total dissolved aromatics per 1 billion parts water). Dissolved aromatic hydrocarbons are the most toxic part of oil. At this concentration and above, one would expect impacts to water column organisms.

After spilling on the water surface, oil will spread rapidly into a relatively thin layer, which will break up into patches

and streams of oil. After some time, the oil spreads out into an extremely thin layer of sheen, which is visible. The threshold level for water surface impacts to socioeconomic resources at risk is 0.01 g/m². At this concentration and above, one would expect impacts to socioeconomic resources on the water surface. Sheen and thin layers of oil tend to have lesser ecological impacts. Ecological resources at risk at the water surface include surface-feeding and diving sea birds, sea turtles, and marine mammals. These organisms can be affected by the toxicity of the oil as well as from coating with oil. The threshold for water surface oiling impact to ecological resources at risk is 10 g/m². At this concentration and above, one would expect impacts to birds and other animals that spend time on the water surface.

On the shoreline, there are differing sensitivities depending on the shoreline type. Shorelines that are difficult to clean and sensitive to the impacts of spill response operations, such as wetlands, are particularly vulnerable [8,9]. The threshold for shoreline oiling impacts to ecological resources at risk is 100 g/m². For socioeconomic impacts, however, a lower threshold of impact should be applied since the visibility of the oil is generally the most important factor in determining socioeconomic impacts. The threshold for impacts to shoreline resources at risk is 1 g/m² [19].

In a risk analysis, for each of the subcategories of resources—water column, water surface, and shoreline—the probability that oiling above a certain threshold will occur needs to be established. This can be achieved through probabilistic or stochastic modeling that provides a range of outcomes for a large number of simulations with variations in winds, currents, and, in some cases, exact locations of release (e.g., over the length of a shipping lane). The percentage of simulation modeling cases in which the assigned impact threshold is reached can be considered the probability of impact the area of concern. These percentages can be divided into general categories, as in a 3- or 5-point scale.

Then, the actual degree of oiling (volume of water column, area of water surface, and length or area of shoreline) over the threshold needs to be determined. Again, this can be accomplished through stochastic modeling. For the degree of oiling, however, there will again be a range of outcomes, for example, different lengths of shoreline that might be oiled. In this case, the “worst” case and/or the “median” case might be selected for further analysis. The worst case of shoreline oiling may mean the case in which the most shoreline was oiled, or the most sensitive shorelines were oiled. In some modeling analyses, the shorelines are “weighted” by sensitivity so that impacts to the most sensitive shorelines (wetlands, marshes, or mangroves) would be weighted more heavily than shorelines with lesser sensitivity (e.g., sandy or rocky) [26]. Again, the degree of oiling can be divided into categories of impact, as shown in the risk matrix in Figure 1.18. The five-scale rankings are given scores of 1–5. Risk scores created by multiplying the

Probability of impact	Degree of impact				
	Very low (1)	Low (2)	Medium (3)	High (4)	Very high (5)
Very high (5)	5	10	15	20	25
High (4)	4	8	12	16	20
Medium (3)	3	6	9	12	15
Low (2)	2	4	6	8	10
Very low (1)	1	2	3	4	5

FIGURE 1.18 Risk matrix for probability and degree of impact to resources.

two 5-point scales can then be divided into risk categories, which are as follows:

- Very low risk: 1–5 points
- Low risk: 6–10 points
- Medium risk: 11–15 points
- High risk: 16–20 points
- Very high risk: 21–25 points

These risks then need to be compared with the actual resources at risk. If there is significant shoreline oiling, but there are no important socioeconomic or ecological resources in the area of impact, for example, the risk can then be categorically reduced to a lower level.

1.3.8 Interpreting Risk for Policy-Making

The results of oil spill risk analyses are incorporated into risk assessments, which involve the process of interpreting that risk for practical purposes, such as the following:

- Contingency planning for response and preparedness for most-probable and worst-case spill scenarios;
- Planning for protection of resources at risk;
- Risk allocation for insurance or taxation;
- Evaluation of trade-offs in decision-making;
- Conducting cost–benefit analyses of oil exploration, production, storage, or transport;
- Developing spill prevention measures; and
- Evaluating alternative courses of action for oil exploration, production, storage, or transport.

A scientifically based risk assessment process, including modeling of potential impacts and analysis of probabilities of impacts to sensitive resources, removes much of the subjectivity in the process. One example of the way in which such an analytical approach was applied for spill risk allocation were the analyses conducted for the state of Washington’s Joint Legislative

TABLE 1.14 Relative spill risk analysis for spills in Washington State [27]

Source type	Historical spillage analyses		Future (2015) analyses	
	Actual spillage	Worst-Case Discharge (WCD) spillage	Actual spillage	WCD spillage
Tank ships	3.78	75.44	3.03	56.93
Tank barges	1.77	6.40	1.77	6.04
Cargo vessels	10.29	15.42	11.32	32.00
Fishing vessels	1.38	2.01	1.38	3.79
Passenger vessels	0.04	0.34	0.04	0.64
Oil terminals	1.40	0.30	1.05	0.42
Pipelines	78.92	0.09	78.98	0.18
Tank trucks	2.39	0.00	2.39	0.01
Marinas/others	0.06	0.00	0.04	0.00
Total	100.00	100.00	100.00	100.00

Audit and Review Committee (JLARC). JLARC was concerned with studying the risk of spills from various sources in the state so that the tax that was levied on the various parts of the industry to support state spill response programs could be better allocated with respect to the risk presented [10,27,28].

Table 1.14 shows the analytical results of that study. The results indicate the percentage of risk (based on risk scoring conducted on probabilities of spills and impacts in different locations across the state). The risk differs by source type, as well as by time frame—past and future. Projected future spillage takes into account changes in patterns of vessel types, fuel used, oil consumption rates, and vessel traffic rates.

Past data indicate that the highest risk is from pipelines. This is because the largest spill in the study time frame was from a pipeline. It is also interesting to note that, based solely on historical data or projected data of actual spillage, tank ships would not be ranked very high with respect to spill risk. If, however, potential WCD scenarios are taken into account, the risk for tankers rises. This is because, while historically there have not been significant tanker spills in the state, there is the potential for a much larger volume of spillage from tankers than from other sources. For the purposes of taxation, the state elected to impose taxes based on past

performance. For the purposes of spill response preparedness, however, the need for higher levels of preparedness is dictated by the potential volume of spillage, even if the probability is exceedingly low.

For contingency planning purposes and for development of spill prevention strategies, risk analyses are extremely important. With limited resources and economic constraints, government and industry officials are often concerned with aiming preparedness and prevention strategies at those measures that will bring the greatest benefit. Weighing the likelihood of spill events and the causes that lead up to them, as well as the potential impacts of hypothetical spill scenarios, can help to guide this process.

In the end, conceptualizing “risk” is often difficult. Industry and government officials are often confronted with a public demand for “zero risk” from oil spills, which is most likely a goal that is not realistically attainable.

High-profile spill events, such as the Deepwater Horizon (Macondo MC252 well blowout) incident, have reawakened the petroleum industry, risk managers, and government officials around the world from a state of relative complacency about the need to quantify risk and prepare for responses to high-consequence, very low-probability spill events, as well as to major spills in general. Public and governmental scrutiny over the appropriateness, effectiveness, and timeliness of the response to this spill of unprecedented magnitude has also called for a review of oil exploration and drilling risks, as well as contingency plans at all levels. With the reexamination of contingency plans and response preparedness in the Deepwater Horizon aftermath comes also an unprecedented opportunity to approach the contingency planning process anew with both the lessons learned from the Deepwater Horizon incident and the benefit of state-of-the-art modeling tools and recent research on spill risk.

1.4 OVERVIEW OF OIL SPILL PREVENTION

There are four basic ways to mitigate oil spill risk: reducing the volume of leakage, improving spill response by increasing the removal rate of oil, preventing oil from entering particularly sensitive locations, and, most importantly, preventing spills from occurring or reducing the probability of spills occurring.

1.4.1 Basic Strategies for Spill Prevention

The most effective way to mitigate oil spill risk is to prevent spills from occurring in the first place, or to reduce the likelihood of spill occurring. Spill prevention encompasses a broad array of tactics that aim to stem the release of oil or in some way impede the series of errors or malfunctions that can lead to a spill event. Prevention measures include such strategies as the following:

- Enclosing stored or transported oil in structures (e.g., tanks, pipelines, and vessels) that are less likely to be breached through outside impact or force (e.g.,

collision and frost heaving) or corrosion or breakage by the use of stronger materials, thicker hulls, or redundant layers (e.g., double hulls and secondary containment);

- Implementing strategies and systems to reduce the likelihood of outside force damage, such as vessel traffic systems to prevent collisions, improved navigational charting to reduce the likelihood of grounding, or marking of underground pipelines to prevent digging damage;
- Improving training of operators to reduce human error in producing, transporting, storing, handling, or using oil;
- Instituting operating procedure that reduces the likelihood of spillage;
- Installing devices to control the flow of oil and prevent overpressured flow as in well blowout preventers;
- Improving maintenance and inspection procedures to detect anomalies in structure, function, and operation that may lead to spillage;
- Relocation or rerouting of oil transport, handling, and storage to locations that are less likely to be the site of events that could lead to spillage; and
- Isolating oil-containing facilities and vessels to prevent sabotage and vandalism that might lead to spillage.

With spill prevention, the *probability* aspect of risk is reduced. The greater the reduction in probability of spillage, the more effective the spill prevention measure will be.

Each of the aforementioned prevention strategies has an impact on the probability of spillage. Other so-called spill prevention measures are really aimed at stemming the flow of an existing oil spill or leak and preventing it from becoming larger. This, in effect, affects the consequences side of the risk equation in that the consequences of a spill are closely related to the volume of spillage. Examples of spill volume reduction measures include such strategies as the following:

- Installing early leak detection systems that will notify operators of spillage or automatically shut the leak off from the system before the leakage becomes larger;
- Conducting salvage and lightering operations on a leaking ship to stabilize the vessel and remove remaining oil;
- Requirements for protective booming around vessels during lightering operations;
- Capping of a well during a blowout; and
- Shutting off a segment of a pipeline system that contains a ruptured pipeline.

Another way to reduce the risk of spills without actually preventing spillage is to affect the location and/or timing of

potential spills. This would also act to reduce risk on the consequences side of the equation. Strategies could include such measures as follows:

- Locating or relocating spill handling facilities, vessels, or pipelines to locations that would have less sensitivity to impacts if a spill were to occur (e.g., rerouting pipelines away from high-consequence areas);
- Conducting oil handling or transporting during times or seasons when sensitive populations are not in the area; and
- Preventing construction of oil facilities (e.g., drilling rigs) in highly sensitive locations.

A corollary of this relocation strategy is the deflection of oil through protective booming during a spill response [29]. This strategy diverts oil from highly sensitive locations (e.g., wildlife areas) to areas that are less sensitive to the impacts of oil. Another example is conducting certain potentially risky operations (e.g., lightering) in locations that are not subject to conditions (e.g., high currents) that might allow significant oil to spread in the event of a spill.

1.4.2 Implementation of Spill Prevention Measures

Many of the spill prevention strategies described are part of voluntary industry initiatives and best-practices programs. In many cases, however, regulations have been imposed to reinforce spill prevention and risk mitigation measures for operators and companies in the oil industry (e.g., oil facility spill prevention regulations and double hulls on tank vessels). In other cases, officials have instituted measures that affect the larger system of oil transport, handling, and storage through the use of regulatory permitting and zoning for the location of facilities, improved vessel traffic and navigational systems, escort tug systems, and others [30]. Local, regional, and national spill response preparedness and contingency planning for spills also affects the larger system.

Regulations for spill prevention often involve fines and penalties for spillers and for those operators that do not abide by the regulatory measures. These fines and penalties are intended to act as deterrents in the event that the spills themselves with regard to costs of cleanup and other losses are not in and of themselves deterrents.

Spill prevention and risk mitigation programs require significant resources and costs for both the regulator and potential spillers with regard to capital expenditures on retrofitting and engineering, as well as costs for maintenance, training, monitoring, inspections, litigation, and enforcement.

Spill prevention regulations range from local permitting and zoning (e.g., locations of gas stations and oil storage facilities) to state or provincial regulations (e.g., storage tank inspection programs), to national laws (e.g., OPA 90 in the United States), and to international conventions (e.g.,

International Convention for the Prevention of Pollution from Ships 1973, as Amended in 1978, known as “MARPOL 73/78”).

1.4.3 Effectiveness of Spill Prevention

The actual effectiveness of spill prevention measures depends on a variety of factors, including the degree of enforcement and compliance with the measures whether they are voluntary best practices or regulated. The effectiveness is also ultimately reliant on the extent to which the prevention measure really addresses the root cause of the spillage and the frequency with which spillage would have occurred without any intervention.

1.4.3.1 Overall Spill Reduction There has clearly been a significant reduction in oil spills across the board on an international basis in the last two decades or more [31]. This reduction has occurred despite the fact that there is more oil consumption and thus more oil production, transport, storage, and handling than previously.

While there are anomalies, such as the unprecedented spillage in the 2010 Deepwater Horizon/Macondo MC252 spill in the Gulf of Mexico, overall, there is a lower volume of spillage and fewer larger incidents occurring. There is also a trend toward the reporting of increasingly smaller incidents as part of a general awareness on the part of the public about impacts of spills, including very small incidents. There are a number of factors that have contributed to this spill reduction trend, which are as follows:

- Implementation and enforcement of prevention-related regulations;
- Better engineering and use of prevention equipment and practices;
- Greater awareness of the public on spill risks;
- Increased environmental responsibility of the oil and shipping industries; and
- Awareness of and reaction to the increasing consequences of spills, including higher response standards and costs, damage liability, and fines and penalties for noncompliance.

1.4.3.2 Double Hulls on Tank Vessels Probably, the most often-cited example of a spill prevention measure is the requirement for double hulls on tank vessels (tank ships or tankers and tank barges). Double hulls are mandated by the year 2015 in U.S. waters by the U.S. OPA 90, legislation enacted largely in reaction to the 1989 Exxon Valdez oil spill in Alaska. International convention followed suit by regulations in MARPOL and related national legislation to require double hulls on international fleets by the year 2026. There has been a continuous phase-in of double hulls with new tanker construction so that the fleets are increasingly double-hulled even before the mandated time.

As described in Section 1.4.3.2, double hulls on tank vessels act to both reduce the probability of spillage from impacts (collisions, allusions, and groundings) and reduce the volume of outflow in the event of a spill. For non-tank vessels, there is no reduction in oil outflow in the event of a spill, but there is a reduced probability that oil will be released as the result of damage from an impact casualty [32,33].

OPA 90 specified double hulls based largely on outflow models and engineering studies that indicated that there would be a 30% reduction in spillage for a 40,000 DWT tanker up to 70% for a 240,000 DWT very large crude carrier [2,34]. Analyses of empirical data showed that there were average reductions of spillage of 62% for tank ships and 20% for tank barges. This analysis confirms that double hulls are effective in reducing oil spillage [35].

Another study on international tanker spills estimated that for the time period 2000–2005, there was a 72% reduction in spills from tankers attributable to double hulls [36]. This reduction included a 49% reduction in small spills (between 7.8 and 780 m³) and an 82% reduction in large spills (780 m³ or larger).

There are, however, trade-offs with regard to safety on double-hulled tankers. An industry survey conducted by National Research Council indicated anecdotally that there were advantages as well as disadvantages of double hulls, as summarized in Table 1.15 [3].

1.4.3.3 Oil Pollution Act of 1990 OPA 90, the comprehensive legislation enacted in the United States in large part in reaction to the 1989 Exxon Valdez spill, established

TABLE 1.15 Advantages and disadvantages of double hulls on tank ships [3]

Function	Advantages	Disadvantages
Cargo operations	<ul style="list-style-type: none"> • Faster cargo discharge and good cargo outturn • Easier and faster cargo tank cleaning 	
Construction		<ul style="list-style-type: none"> • Higher cost • More steel required • Longer construction time
Inspection and maintenance		<ul style="list-style-type: none"> • Higher maintenance cost • Need for continuous monitoring and maintenance of ballast tank coatings
Operational safety		<ul style="list-style-type: none"> • Structural safety concerns over intact stability • Increased stillwater bending moment • Difficult access and ventilation of ballast spaces

stringent requirements for tankers operating in U.S. national waters. While double hulls on tankers were an important part of this legislation, there were other facets that would affect spill rates with regard to pollution liability, compensation, prevention, and spill response.

Perhaps, the most important rules of OPA 90 that effected spill prevention were those related to spiller liability. The regulations in OPA 90 regarding spiller liability are incompatible with the international conventions Civil Liability Convention and International Oil Pollution Compensation Fund Convention and are a major reason for the United States' decision not to become parties to those conventions. OPA 90 set federal limits of spill liability for costs and damages as high as \$1200 per gross ton for vessel over 3000 DWT and unlimited liability in the case of gross negligence.

In addition, OPA 90 allowed states to set their own liability limits that could exceed the federal limits, including unlimited liability. Indeed, of the 24 U.S. coastal states, 16 have unlimited liability. This means that the responsible party (i.e., the "spiller") must pay for any and all costs for cleanup and damages, in addition to any fines and penalties that are imposed by federal and/or state authorities.

A radical departure from international protocol is the liability for natural resource damages. These are damages to ecological systems, habitats, and wildlife species that occur as a result of the spillage of oil. A NRDA is conducted by federal and state officials to determine the degree of damage to the environment and the costs of rehabilitating that environment in the same or similar location to reestablish the habitats and species that were affected by direct mortality and/or by impacts to reproduction and life cycles.

This increased liability for costs and damages coupled with generally increasing costs for spill response and a higher public concern about cleanup standards and spill impacts meant that there was greater risk and more at stake for the oil industry and others handling oil. Theoretically, with more at risk, it would be prudent for operators to increase vigilance about spill prevention and for industry to develop systems and practices that would reduce and prevent spillage even if there were no regulatory incentives.

Analyses of tanker spill rates (and spill rates in general) support this hypothesis in that there were reductions in spillage after OPA 90, which preceded the implementation of some of the more direct means of spill prevention, such as double hulls. A study conducted by Homan and Steiner [40] on the impact of OPA 90 on reducing oil spills indicated that increased liability was a statistically significant factor in reducing spillage. The same study also validated the hypothesis that double hulls were an effective means of reducing spills in tankers. The researchers

calculated that without OPA 90 there would have been 26 large spills ($>38 \text{ m}^3$) in 2004 as opposed to the actual number of five spills. Including much smaller spills, the expected number of spills without OPA 90 would have been over 80% higher than with the legislation (Fig. 1.19).

1.4.3.4 Environmental Protection Agency Spill Prevention, Control, and Countermeasures Program Another study conducted to determine the benefits of the U.S. Environmental Protection Agency's Spill Prevention, Control, and Countermeasures (SPCC) program showed similar results

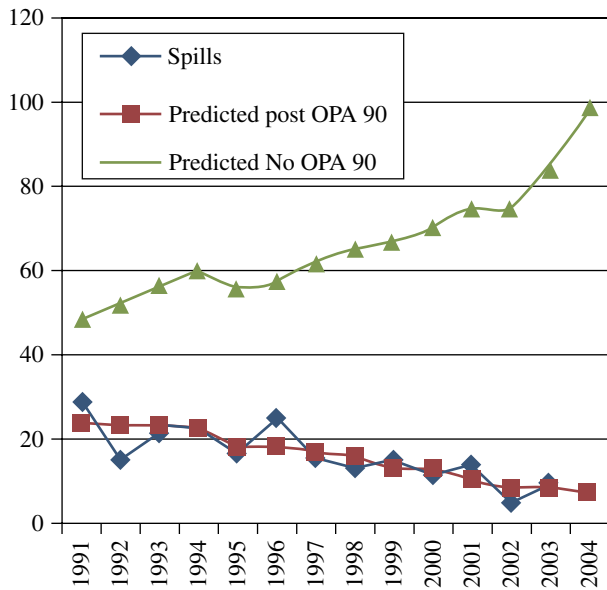


FIGURE 1.19 US spills $>3.8 \text{ m}^3$ with and without OPA 90 [34].

[22]. The SPCC rules affect oil storage and handling facilities that have a total aboveground storage capacity of 5 m^3 or more, store more than 160 m^3 underground, have had a spill of 3.8 m^3 or more, or two spills of more than 0.16 m^3 in a 12-month period. This affects hundreds of thousands of facilities across the United States. SPCC regulations require that facilities adopt a number of strict spill-preventive measures and prepare spill contingency plans.

An analysis of 25 years of spills (1980–2004) showed that spill rate for incidents over 1.9 m^3 decreased significantly despite a 27% increase in oil consumption in the United States over that time period. The number of spills per oil consumption decreased by 50% over 20 years, as shown in Figure 1.20. The benefits of the regulations in terms of spills prevented are shown in Figure 1.21.

1.4.4 Spill Fines and Penalties as Deterrents

Fines and penalties are major components of many spill-preventive regulations around the world. The purpose of these sanctions is to act as deterrents for future incidents as well as to impose on those who have committed offenses. A sample of oil spill fines and penalties for various nations is shown in Table 1.16.

There are no comprehensive studies that definitively determine whether fines and penalties are indeed effective deterrents for oil spills. Certainly, at least theoretically, the amount of the fine or penalty needs to be high enough to exceed the costs of avoiding the spill, whether that means instituting better training programs for operators, improving safety practices, or installing prevention devices, in order to have an actual deterrent effect.

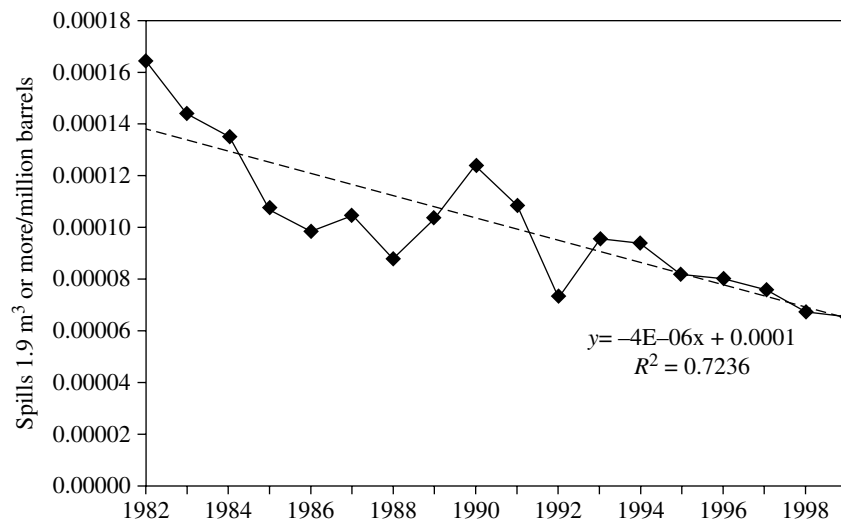


FIGURE 1.20 Number of spills from SPCC facilities per US oil consumption [10].

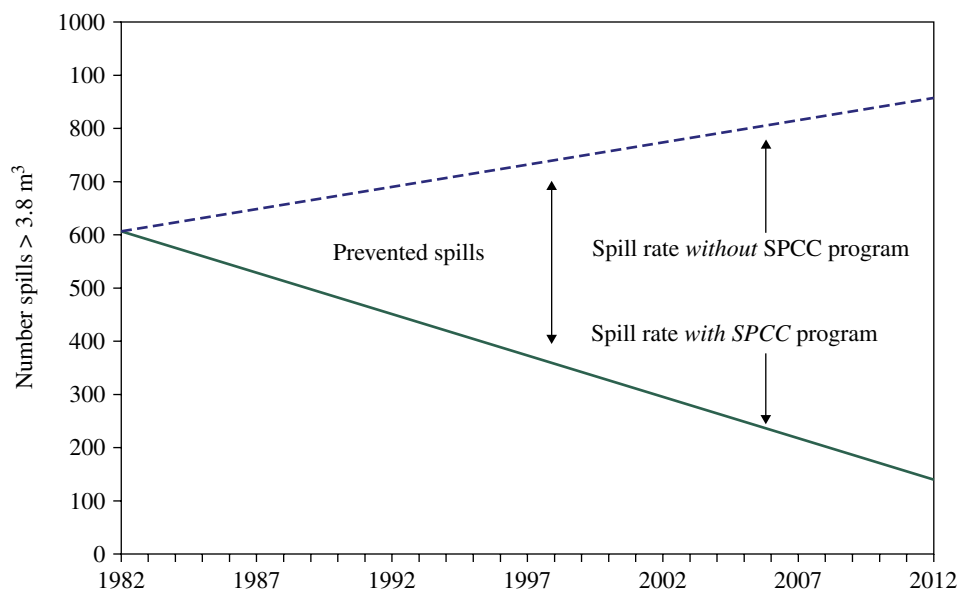


FIGURE 1.21 Facility spillage prevented with SPCC regulations [10].

TABLE 1.16 Sample of marine oil spill fines and penalties

Nation	Marine oil spill law	Fines and penalties
Albania	1991 Law on Environmental Protection	<i>Illegal discharges (individuals):</i> 1000–50,000 Leks [US\$10–500]; <i>Illegal discharges (corporations):</i> 5000–500,000 Leks [US\$100–5000]
Australia	Marine Pollution Act of 1987 No specific law	To Aus\$200,000 [US\$130,907] <i>vessel master</i> <i>State:</i> To 50 million Reals [US\$28 million]; <i>Federal:</i> Additional fines
Brazil	<i>State and federal fines applicable</i>	
Bulgaria	Environmental Protection Act of 1991	<i>Noncriminal pollution offenses:</i> 50,000–3,500,000 Leva [US\$23,000–1,610,000]; <i>Repeat offenses:</i> 100,000–7,000,000 Leva [US\$46,000–3,220,000]; <i>Insignificant violations:</i> To 50,000 Leva [US\$23,000]
Cambodia	Law on Environmental Protection and Natural Resource Management	<i>Failure to allow vessel/facility inspection:</i> 500,000–1 million Riel [US\$129–257]; <i>Repeat offenses:</i> 1–5 million Riel [US\$257–1285]; <i>Pollution and failure to clean up pollution:</i> 1–10 million Riel [US\$257–2570] and/or 1–3 months prison
Canada	Canada Shipping Act Migratory Bird Act (MBA) Fishing Act Canadian Environmental Protection Act	<i>Minor offenses:</i> To C\$250,000 [US\$168,175] and/or 6 months prison; <i>Major offenses:</i> To C\$1 million [US\$672,700] and/or 3 years prison; <i>Under MBA:</i> To C\$520,000 [US\$350,000]
Chile	Navigation Act of 1978	<i>Pollution violations:</i> To 1 million Pesos [US\$1848]; <i>Serious dumping violations:</i> To 5 million Pesos [US\$9240]
China	Marine Environmental Protection Law	<i>Causing pollution:</i> To 100,000 Yuan [US\$11,961]; <i>Failure to report:</i> 1000–5000 Yuan [US\$120–598]; <i>Failure to observe rules for dispersants:</i> 1000–5000 Yuan [US\$120–598]; <i>Oil record book violation or false information:</i> 1000 Yuan [US\$120]
Denmark	Act for the Protection of the Marine Environment	To 2100–5600 Kroner [US\$297–793] <i>ship master</i>
Estonia	Water Act Code of Administrative Offenses Pollution Charge Law Merchant Marine Code	<i>Discharges (individual):</i> To 4430 Kroons [US\$298]; <i>Discharges (corporation):</i> To 114,789 Kroons [US\$7729]; <i>Oil record violations:</i> 1840–3973 Kroons [US\$124–268]; <i>Ship owners:</i> 188,371 Kroons [US\$12,684] per tonne oil discharged
Finland	Act on Protection of the Sea Water Act Act on the Prevention of Pollution from Ships	<i>Individuals:</i> Day fines on the basis of income/blameworthiness; <i>Corporations:</i> 5000–5 million Markka [US\$888–888,000]; <i>Gross negligence/willful misconduct:</i> Fines plus to 6 years prison
France	MARPOL 73/78 Implementation	<i>Large tanker violations:</i> To 1 million Francs [US\$146,228] and up to 2 years prison; <i>Smaller tanker violations:</i> To 300,000 Francs [US\$43,875] and up to 1 year prison
Germany	Penal Code	<i>Intentional discharges:</i> To 10,000 DM [US\$5388] per day or 5 years prison; <i>Administrative fine:</i> To 100,000 DM [US\$53,883]; <i>Oil record violation:</i> To 50,000 DM [US\$26,911]
Greece	Mercantile Marine Law	<i>Most vessel cases:</i> 5,000,000 Drachmas [US\$16,145]; <i>Most serious vessel cases:</i> 250,000,000 Drachmas [US\$807,240]; <i>Onshore facilities (prefecture):</i> To 10,000,000 Drachmas [US\$32,290]; <i>Onshore facilities (national):</i> To 10,000,000 Drachmas [US\$322,896]; <i>Polluters subject to 10 days to 5 years prison (can be bought for 200,000 Drachmas [US\$646] per month)</i>

TABLE 1.16 (Continued)

Nation	Marine oil spill law	Fines and penalties
India	Water Prevention and Control Act of 1974 Environmental Protection Act of 1986	<i>Giving false information:</i> 10,000 Rupees [US\$224] <i>and/or</i> 3 months Prison; <i>Tampering with monitors:</i> 10,000 Rupees [US\$224] <i>and/or</i> 3 months prison; <i>Allowing pollution:</i> 6 months to 6 years prison <i>plus</i> possible fine; <i>Repeat pollution offenses:</i> 1½ to 7 years prison <i>plus</i> possible fine; <i>Other pollution offenses:</i> 10,000 Rupees [US\$224] <i>and/or</i> 3 months prison <i>plus</i> 5000 Rupees [US\$112] per day
Indonesia	Law Concerning Environmental Management	<i>Pollution incidents:</i> 500,000,000 Rupiah [US\$56,000] <i>and</i> up to 10 years prison; <i>Pollution with death/injury:</i> To 750,000,000 Rupiah [US\$84,000]; <i>Negligence:</i> Additional 100,000,000 Rupiah [US\$11,200] <i>and</i> 3 years prison; <i>Negligence with death/injury:</i> Additional 150,000,000 Rupiah [US\$16,800] <i>and</i> 5 years prison
Ireland	Marine Pollution Law	<i>District court cases:</i> To 1000 Punts [US\$1345]; <i>Higher court cases:</i> To 25,000 Punts [US\$33,635]
Japan	Marine Pollution Prevention Law	<i>Intentional spill:</i> To ¥10,000,000 [US\$93,370]; <i>Unintentional but at fault:</i> To ¥5,000,000 [US\$46,685]
Kenya	Merchant Shipping Act	12,050 Shillings [US\$158]
Latvia	Administrative Code	<i>Oil record violations:</i> 250 Lats [US\$426] Latvian master/crew, 500 Lats [US\$853] foreign master/crew; <i>Pollution violations:</i> 250 Lats [US\$426] Latvian master/crew, 2000 Lats [US\$3413] foreign master/crew; <i>Failure to report:</i> 250 Lats [US\$426] Latvian master/crew, 500–3000 Lats [US\$853–5119] foreign master/crew; <i>Administrative fines:</i> 20–250 Lats [US\$34–426] Latvian-flagged vessel; 1162–5812 Lats [US\$1984–9918] foreign-flagged vessel; All violators must pay environmental damage fee of 32 Lats [US\$54] per kg oil spilled <i>plus</i> 2500 Lats [US\$4266] per tonne oil spilled as natural resources tax.
Lithuania	Administrative Law Violation Code	<i>Pollution prevention violations:</i> To 1,000,000 Litas [US\$247,688] <i>plus</i> 5 years prison <i>plus</i> 8000–100,000 Litas [US\$1,982–24,782] <i>or</i> 240 Litas [US\$59] per kg oil spilled
Malaysia	Merchant Shipping (Oil Pollution) Act of 1994 Merchant Shipping Act of 1952	<i>Failure to obey official orders:</i> To 50,000 Ringgit [US\$13,160] per day; Violations of pollution prevention regulations: To 10,000 Ringgit [US\$2632] <i>and/or</i> up to 1 year prison
Mauritius	Ports Act	20,000–400,000 Rupees [US\$788–15,754] depending on cleanup costs
Mexico	Federal Oceans Law General Law of Ecological Balance and Environmental Protection (Ecology Law) National Waters Law General Health Law Ocean Dumping Law Coastal Zone Regulation	<i>Coastal Zone Regulation violations:</i> 50–500 times minimum daily wage (MDW); <i>Ecology Law (marine pollution):</i> 20–20,000 times MDW; <i>National Waters Law wastewater discharges:</i> 100–10,000 times MDW; <i>Ocean Dumping Law violations: Dumping Annex I:</i> 300–1300 Pesos [US\$33–143]; <i>Vessel/platform abandonment:</i> 300–750 Pesos [US\$33–83]; <i>Failure to report emergency dumping:</i> To 750 Pesos
Netherlands	National Maritime Law	To 300,000 Guilders [US\$142,418]
Nigeria	Oil in Navigable Waters Act	<i>Discharges:</i> 2000 Naira [US\$22]; Oil record violation: 1000 Naira [US\$11] <i>and/or</i> 6 months prison; <i>Illegal night transfer operation:</i> 200 Naira [US\$2]; <i>Ballast/waste discharge in harbor:</i> 20 Naira [US\$0.20] per day
Norway	Norwegian Pollution Control Act	<i>Vessel owners:</i> 50,000–120,000 Krona [US\$6347–15,233] <i>and/or</i> 5–10 years prison; <i>Crew:</i> 1-month's salary
Panama	National Maritime Law	To 200,000 Balboas [US\$197,720]
Philippines	Pollution Control Law Marine Pollution Decree	<i>Facility discharges:</i> To 5000 Pesos [US\$1000] per day; <i>Persons responsible:</i> To 1000 Pesos [US\$20] per day <i>and/or</i> 2–6 years prison; <i>Vessel/offshore discharges:</i> 200,000 Pesos [US\$4000] <i>and/or</i> 30 days to 1 year prison
Poland	Act on Marine Areas of Republic of Poland and on Maritime Administration Act on the Prevention of Pollution of the Sea from Ships	<i>Oil dumping violations:</i> 1,000,000 Special Drawing Rights [US\$1,317,289]; <i>Crew/master pollution violations:</i> To 20-months' average national salary
Russia	Instruction for the Prevention of Pollution from Ships	<i>Pollution violations:</i> To 3000 times minimum national salary
Singapore	Prevention of Pollution Sea Act	To Sing\$500,000 [US\$293,028] <i>and/or</i> 2 years prison
South Africa	Marine Pollution (Prevention of Pollution from Ships) Act	<i>Serious offenses:</i> 200,000 Rands [US\$32,693]; <i>Most serious offenses:</i> 500,000 Rands [US\$81,733]
Sweden	Act Concerning Measures for the Prevention of Water Pollution from Ships Ordinance Concerning Measures for the Prevention of Water Pollution from Ships Decree by National Maritime Administration	<i>Day-fines (money-fines for crimes <30 day-fines):</i> <i>Day-fines:</i> 30–150 or if joint punishment for several violations, to 200. Amount of day-fines: 30–1000 Krona [US\$4–121], Joint punishment to 5000 Krona [US\$606]; <i>Money-fines:</i> 100–2000 Krona [US\$12–242], Joint punishment to 5000 Krona [US\$606]
Taiwan	Water Pollution Control Act of 1974	<i>Violations with human fatality:</i> To 300,000 NTD [US\$9000]; <i>Violations with serious harm to humans:</i> To 150,000 NTD [US\$4500]; <i>Other pollution incidents:</i> 30,000–300,000 NTD [US\$900–9000]

(Continued)

TABLE 1.16 (Continued)

Nation	Marine oil spill law	Fines and penalties
Thailand	Enhancement and Conservation of National Environmental Quality Act	<i>Order violations:</i> 100,000 Baht [US\$2476] and/or 1 year prison; <i>Responsible for pollution:</i> 500,000 Baht [US\$12,378] and/or 5 years Prison; <i>False information:</i> 100,000 Baht [US\$2476] and/or 1 year Prison; <i>False information through public media:</i> 500,000 Baht [US\$12,378] and/or 5 years prison; <i>Polluting source owner:</i> 100,000 Baht [US\$2476] and/or 1 year prison
Ukraine	1995 Water Resources Act	To 600,000 Hryvnias [US\$131,901]
United Kingdom	Merchant Shipping (Prevention of Oil Pollution) Regulations of 1996	<i>Magistrate's Court:</i> To £250,000 [US\$409,641]; <i>Crown Court (most serious offenses):</i> unlimited fines
United States	Oil Pollution Act of 1990 Federal Water Pollution Control Act Comprehensive Environmental Response, Compensation, and Liability Act of 1980	<i>Class I civil penalties:</i> To US\$10,000–25,000 maximum; <i>Class II civil penalties:</i> To US\$10,000 per day to US\$125,000 maximum; <i>Judicial civil penalties:</i> To US\$25,000 per day or to US\$1000/bbl (US\$7000/t) spilled; <i>Gross negligence:</i> US\$100,000 minimum to US\$3000/bbl (US\$21,000/t) spilled; Also fines and penalties by state.
Venezuela	Penal Law of the Environment	To 17,150,000 Bolivars [US\$25,000] plus imprisonment
Vietnam	1993 Law on Environmental Protection 1996 Environmental Protection Government Decree	<i>Contingency plan violation:</i> 2–8 million Dong [US\$142–568]; <i>Causing oil spill:</i> 30,000,000–50,000,000 Dong [US\$3550–7100]; <i>Violations with negligence or repeat offenses:</i> Additional 50–100 million Dong [US\$3550–7100]; <i>Failure to report:</i> 50,000–200,000 Dong [US\$4–14]; <i>Failure to report with negligence or repeat offenses:</i> 5–20 million Dong [US\$355–1420]; <i>Failure to remove oil:</i> 50,000–200,000 Dong [US\$4–14]; <i>Failure to remove oil with negligence or repeat offenses:</i> 5–20 million Dong [US\$355–1420]

REFERENCES

- [1] Etkin, D.S., D. French McCay, J. Michel, M. Boufadel, and H. Li, Integrating state-of-the-art shoreline interaction knowledge into spill modeling, *IOSC*, 915, 2008.
- [2] National Research Council (NRC), *Tanker Spills: Prevention by Design*, National Academy Press, Washington, DC, 1991.
- [3] National Research Council (NRC), *Double-Hull Tanker Legislation: An Assessment of the Oil Pollution Act of 1990*, National Academy Press, Washington, DC, 1998.
- [4] Lockridge, P.A., L.S. Whiteside, and J.F. Lander. Tsunamis and tsunami-like waves of the eastern United States, *Science of Tsunami Hazards Int J Tsunami Soc*, 20(3), 120, 2002.
- [5] Etkin, D.S., *Cook Inlet Maritime Risk Assessment: Spill Baseline & Accident Casualty Study. Spill Scenarios and Impacts*, Prepared for Cook Inlet Risk Assessment, Environmental Research Consulting, Cortlandt Manor, NY, April 2008, 2012.
- [6] Etkin, D.S., Comparative methodologies for estimating on-water response costs for marine oil spills, *IOSC*, 1281, 2001.
- [7] Etkin, D.S., D. French McCay, J. Michel, M. Boufadel, and H. Li, Development of a practical methodology for integrating shoreline oil-holding capacity into spill modeling, *AMOP*, 2565, 2008.
- [8] Etkin, D.S., Methodologies for estimating shoreline cleanup costs, *AMOP*, 647, 2001.
- [9] Etkin, D.S., Estimation of shoreline response cost factors, *IOSC*, 1243, 2003.
- [10] French-McCay, D., C.J. Beegle-Krause, J. Rowe, W. Rodriguez, and D.S. Etkin, Oil spill risk assessment—relative impact indices by oil type and location, *AMOP*, 655, 2009.
- [11] Humphrey, B., Persistence of oil in subtidal sediments, *AMOP*, 75, 1983.
- [12] Fingas, M., *The Basics of Oil Spill Cleanup*, Second Edition, Lewis Publishers, New York, 2001.
- [13] Harper, J., G.A. Sergy, and T. Sagayama, Subsurface oil in coarse sediments experiments (SOCSEX II), *AMOP*, 867, 1995.
- [14] Harper, J.R., and G. Sergy, Experimental observations of oil interaction within coarse sediment beaches, *Mar Pollut Bull*, 2007.
- [15] French-McCay, D., Development and application of an oil toxicity and exposure model—OilToxEx, *Environ Toxicol Chem*, 21, 2080–2094, 2002.
- [16] Owens, E.H., and G.A. Sergy, A SCAT manual for Arctic regions and cold climates, *AMOP*, 703, 2004.
- [17] Howard, S., and D.I. Little, Effect of infaunal burrow structure on oil penetration into sediments, *IOSC*, 427, 1987.
- [18] Etkin, D.S., J.A.C. van Rooij, and D. French-McCay, Risk assessment modeling approach for the prioritization of oil removal operations from sunken wrecks, *Interspill*, 2009.
- [19] French-McCay, D., D. Reich, J. Michel, D. Etkin, L. Symons, D. Helton, and J. Wagner, Oil spill consequence analyses of potentially-polluting shipwrecks, *Proceedings of the 35th Arctic and Marine Oilspill Program Technical Seminar*, 2012.
- [20] French-McCay, D., J.J. Rowe, N. Whittier, S. Sankaranarayanan, and D.S. Etkin, Estimation of potential impacts and natural resource damages of oil, *J Hazard Mater*, 107, 11, 2004.
- [21] Aurand, D., L. Walko, and R. Pond, *Developing Consensus Ecological Risk Assessments: Environmental Protection in Oil Spill Response Planning a Guidebook*. United States Coast Guard, Washington, DC, 2000.
- [22] Etkin, D.S., Modeling oil spill response and damage costs, *Proceedings of 5th Biennial Freshwater Spills Symposium*, St. Louis, Missouri, USA, April 6–8, 2004.
- [23] Etkin, D.S., Risk assessment of oil spills to US inland waterways, *Proceedings of 2006 Freshwater Spills Symposium*, Portland, Oregon, USA, May 2–4, 2006.

- [24] Etkin, D.S., Development of an oil spill response cost-effectiveness analytical tool, *AMOP*, 889, 2005.
- [25] Etkin, D.S., D. French-McCay, N. Whittier, S. Subbayya, and J. Jennings, Modeling of response, socioeconomic, and natural resource damage costs for hypothetical oil spill scenarios in San Francisco Bay, *AMOP*, 1075, 2002.
- [26] French-McCay, D., N. Whittier, S. Subbayya, J. Jennings, and D.S. Etkin, Modeling fates and impacts for bio-economic analysis of hypothetical oil spill scenarios in San Francisco Bay, *AMOP*, 1051, 2002.
- [27] Etkin, D.S., D. French-McCay, and C.J. Beegle-Krause, Oil spill risk assessment—probability and impact analyses with future projections, *AMOP*, 683, 2009.
- [28] State of Washington Joint Legislative Audit and Review Committee (JLARC), *Review of Oil Spill Risk and Comparison to Funding Mechanism*, Report 09-2, January 7, 2009, JLARC, Olympia, WA, 2009.
- [29] Etkin, D.S., J. Rowe, S. Sankaranarayanan, D. French McCay, and J. Reichert, Using current analysis to determine efficacy of pre-booming operations, *AMOP*, 355, 2007.
- [30] Herbert Engineering Corp. and Designers and Planners, Inc., *Use of Tugs to Protect Against Oil Spills in the Puget Sound Area*, US Coast Guard Report No. 95522-001, 1999.
- [31] Etkin, D.S., *Analysis of US Oil Spillage*, American Petroleum Institute Publication 356. August 2009. Environmental Research Consulting, Cortlandt Manor, NY, 2009.
- [32] Michel, K., and T.S. Winslow, Cargo ship bunker tanks: designing to mitigate oil spillage, *Society for Naval Architects and Marine Engineers (SNAME) Joint California Sections Meeting*, May 14, 1999.
- [33] Michel, K., and W. Thomas, Cargo ship bunker tankers: designing to mitigate oil spills, *Society for Naval Architects and Marine Engineers (SNAME) Marine Technology*, October 2000.
- [34] Rawson, C., K. Crake, and A.J. Brown, Assessing the environmental performance of tankers in accidental grounding and collision, *Society of Naval Architects and Marine Engineers (SNAME) Transactions*, 1998.
- [35] Yip, T.L., W.K. Talley, and D. Jin, The effectiveness of double hulls in reducing vessel-accident oil spillage, *Mar Poll Bull*, 62(11), 2427, 2011.
- [36] Glen, D., Modelling the impact of double hull technology on oil spill numbers, *Marit Pol Manag*, 37(5), 475, 2010.
- [37] Eliopoulou, E., A. Papanikolaou, P. Diamantis, and R. Hamann, Analysis of tanker casualties after the Oil Pollution Act (USA, 1990), *Proceedings of the Institution of Mechanical Engineers, Part M: Journal of Engineering for the Maritime Environment*, 226, 301–312, 2012.
- [38] Etkin, D.S., Oil spill risk analysis for Cape Wind Energy Project, *IOSC*, 571, 2008.
- [39] Etkin, D.S., *Vessel Allision and Collision Oil Spill Risk Analysis for the Cape Wind Project in Nantucket Sound*. Final Report, Prepared for Cape Wind Associates, LLC, Boston, MA. Environmental Research Consulting, Cortlandt Manor, NY, 2006.
- [40] Homan, A.C., and T. Steiner, OPA 90s impact at reducing oil spills, *Marine Policy*, 32(4), 711, 2008.

PART II

OIL PROPERTIES

OIL PHYSICAL PROPERTIES: MEASUREMENT AND CORRELATION

BRUCE P. HOLLEBONE

Emergencies Science and Technology Section (ESTS), Environment Canada, Ottawa, Ontario, Canada

2.1	Introduction	39
2.2	Bulk Properties of Crude Oil and Fuel Products	39
2.2.1	Density and API Gravity	40
2.2.2	Dynamic Viscosity	41
2.2.3	Surface and Interfacial Tensions	41
2.2.4	Flash Point	42
2.2.5	Pour Point	42
2.2.6	Sulfur Content	42
2.2.7	Water Content	42
2.2.8	Evaluation of the Stability of Emulsions Formed from Brine and Oils and Oil Products	43
2.2.9	Evaluation of the Effectiveness of Dispersants on an Oil	43
2.2.10	Adhesion	44
2.3	Hydrocarbon Groups	44
2.3.1	Saturates	44
2.3.2	Aromatics	44
2.3.3	Resins	44
2.3.4	Asphaltenes	44
2.4	Quality Assurance and Control	46
2.5	Effects of Evaporative Weathering on Oil Bulk Properties	46
2.5.1	Weathering	46
2.5.2	Preparing Evaporated (Weathered) Samples of Oils	47
2.5.3	Quantifying Equation(s) for Predicting Evaporation	47

2.1 INTRODUCTION

The properties of the spilled oil, including the bulk physical properties changes due to weathering, must be immediately available to any spill responder. Models are used to predict the environmental impacts of the spill and guide the selection of various remediation alternatives. These models require the input of oil spill properties. Unfortunately, the properties routinely measured by oil producers and refiners

are not the ones that spill responders need to know most urgently. Questions important to responders include the following:

- The physical properties of the oil and how these will change over time and with weathering;
- How the compositional and bulk property changes affect an oil's behavior and fate;
- If emulsions will form or how the oils uptake water;
- If the oil is likely to submerge;
- The hazard to on-site personnel during cleanup; and
- The oil toxicity to marine or aquatic organisms.

2.2 BULK PROPERTIES OF CRUDE OIL AND FUEL PRODUCTS

Physical properties of the almost limitless variety of crude oils are generally correlated with aspects of chemical composition. Some of these key properties for determining fate and behavior of oil and petroleum products in the environment are viscosity, density, specific gravity (density relative to water), flash point, pour point, distillation, and interfacial tension. Some typical properties of the oils are listed in Table 2.1.

Viscosity is the resistance to flow in a liquid. The lower the viscosity, the more readily the liquid flows. The viscosity of an oil is related to its composition, therefore crude oil has a wide range of viscosities. For example, the viscosity of fresh Federated oil from Alberta is 5 mPa·s, while that of a Sockeye oil from California is 45 mPa·s at 15°C. In general, the greater the fraction of saturates and aromatics and the lower the amount of asphaltenes and resins, the lower the viscosity. As oil weathers, the evaporation of the lighter components leads to increased viscosity.

TABLE 2.1 Typical oil and fuel properties at 15°C

Property	Units	Gasoline	Diesel	Light crude	Heavy crude	Intermediate fuel oil	Bunker C	Crude oil emulsion
Viscosity	mPa · s	0.5	2	5–50	50–50,000	1,000–15,000	5,000–50,000	200,000–1,000,000
Density	g/ml	0.72	0.84	0.78–0.88	0.88–1.00	0.94–0.99	0.96–1.04	0.95–1.0
API gravity		50–65	35–40	30–50	10–30	10–20	5–15	10–15
Interfacial tension	mN/m	27	27	10–30	15–30	25–30	25–35	N/A
Flash point	°C	–35	55–65	–30 to 30	–30 to 60	80–100	>100	>80
Pour point	°C	N/A	–60	–55 to 0	–30 to 30	–10 to 10	5–20	>50

As with other physical properties, viscosity is affected by temperature, with lower temperatures giving higher viscosities. For most oils, the viscosity varies approximately exponentially with temperature. Oils that flow readily at high temperature can become a slow-moving, viscous mass at low temperature. In terms of oil spill cleanup, viscous oils do not spread rapidly, do not penetrate soils readily, and affect the ability of pumps and skimmers to handle the oil. The dynamic viscosity of an oil can be measured by a viscometer using a variety of standard cup-and-spindle sensors at controlled temperatures.

Density is the mass of a unit volume of oil, usually expressed as grams per milliliter (g/ml) or, equivalently, as kilograms per cubic meter (kg/m³). It is used by the petroleum industry to grade light or heavy crude oils. Density is also important because it indicates whether the oil will float or sink in water. As the density of water is 1.0g/ml at 15°C and the density of most oils ranges from 0.7 to 0.99g/ml, oils typically float on water. As the density of seawater is 1.03g/ml, even heavier oils will usually float on it. Only some bitumens have densities greater than water at higher temperatures. However, as water has a minimum density at 4°C and oils will continue to contract as temperature decreases, heavier oils, including heavy crudes and residual fuel oils, may sink in cold waters. Furthermore, as density increases as the light ends of the oil evaporate off, a heavily weathered oil, long after a spill event, may sink, or be prone to overwashing, whereas a fresh oil, immediately after the spill, may have floated readily.

A related measure is specific gravity, an oil's density relative to that of water. As the densities of both water and oil vary differently with temperature, this quantity can be highly variable. The American Petroleum Institute (API) uses the specific gravity of petroleum at 60°F (15.56°C) as a quality indicator for oil. Pure water has an API gravity of 10. Oils with progressively lower specific gravities have higher API gravities. Heavy, inexpensive oils have less than 25 API; medium oils have 25–35°API; and light commercially valuable oils have 35–45°API. API gravities generally vary inversely with viscosity and asphaltene content.

Interfacial tensions are the net stresses at the boundaries between different substances. They are expressed as the increased energy per unit area (relative to the bulk materials), or equivalently as force per unit length. The SI unit

for interfacial tension is milliNewtons per meter (mN/m). Surface tension is thought to be related to the final size of a slick. The lower the interfacial tension of oil with water, the greater the extent of spreading and thinner the terminal thickness of oil. In actual practice, the interfacial tension alone does not appear to account for spreading behavior; environmental effects and other effects become dominant as the slick spreads.

The flash point of an oil is the temperature at which the vapor over the liquid can be ignited. A liquid is considered to be flammable if its flash point is less than 60°C. Flash point is an important consideration for the safety of spill cleanup operations. Gasoline and other light fuels can ignite under most ambient conditions and therefore are a serious hazard when spilled. Many freshly spilled crude oils also have low flash points until the lighter components have evaporated or dispersed. On the other hand, Bunker C and heavy crude oils generally are not flammable when spilled.

The pour point of an oil is the temperature at which no flow of the oil is visible over a period of 5 s from a standard measuring vessel. The pour point of crude oils ranges from –60 to 30°C. Lighter oils with low viscosities generally have lower pour points. As oils are made up of hundreds of compounds, some of which may still be liquid at the pour point, the pour point is not the temperature at which an oil will no longer pour. The pour point represents a consistent temperature at which an oil will pour very slowly and therefore has limited use as an indicator of the state of the oil. For example, waxy oils can have very low pour points but may continue to spread slowly at that temperature and can evaporate to a significant degree.

2.2.1 Density and API Gravity

The density of an oil sample, in g/ml, is best measured using a digital density meter following American Society for Testing and Materials (ASTM) method D 5002 [1]. The instrument is calibrated using air and distilled, degassed water. Acoustically measured densities must be corrected for sample viscosity, as specified by the instrument manufacturer.

API gravity is calculated using the specific gravity of an oil at 60°F (15.6°C) [2]. The oil density at 15.6°C can be estimated by exponential extrapolation from the higher (T_{Hi}) and lower (T_{Lo}) data points if necessary. This is converted to

specific gravity by division by the density of water at 15.5°C, using the following equation:

$$\text{s.g.}^{15.56} = \rho_{\text{Hi}}^T \exp \frac{\left[\left(\ln \rho_{\text{Hi}}^T - \ln \rho_{\text{Lo}}^T \right) (T_{\text{Hi}} - T_{\text{Lo}}) \times (T_{\text{Hi}} - 15.56) + \ln \rho_{\text{Hi}}^T \right]}{\rho(\text{H}_2\text{O})^{15.56}} \quad (2.1)$$

where $\text{s.g.}^{15.56}$ is the specific gravity of the oil or product at 15.56°C (60°F), ρ_{Lo}^T and ρ_{Hi}^T are the measured oil densities at T_{Lo} and T_{Hi} (*high and low temperatures*), respectively, and $\rho(\text{H}_2\text{O})^{15.56}$ is the density of water at 15.56°C. The API gravity is then determined using the formula [2]

$$\text{API} = 141.5/(\text{s.g.}^{15.56}) - 131.5 \quad (2.2)$$

2.2.2 Dynamic Viscosity

The dynamic viscosity of an oil sample, in $\text{mPa} \cdot \text{s}$ or cP, is measured using a rotary viscometer with concentric cylinder geometry and using standard NV and SV1 cup-and-spindle sensors [3]. Check standards of pure ethylene glycol and glycerine can be conveniently used to validate the NV and SV1 methods, respectively.

From a qualitative observation of the oil, either the NV or the SV1 sensor is chosen to measure the sample. The NV sensor is used for oils with viscosities below 100 $\text{mPa} \cdot \text{s}$ and the SV1 sensor for oils above 70–10,000 $\text{mPa} \cdot \text{s}$. For oils with higher viscosity, measurements must be made on cone and plate or parallel plate instruments (see the following text).

For both cases using the rotary viscometer, the measurement cup is filled with sample to the edge of the rotating surface. The sensor is mounted onto the instrument, and the sample volume is adjusted to the proper level. The sample is allowed to equilibrate until the sample temperature probe stabilizes at the measurement temperature and remains stable for 5 min. Samples and sensors are kept chilled at the appropriate temperature prior to use.

For the NV sensor, the rotational shear rate is set at 1000/s and for the SV1 sensor at 50/s. If the oil is observed to be non-Newtonian, single samples are run at shear rates of 1/s, 10/s, and 100/s. In all cases, the sensors are ramped up to speed over a period of 5 min. The viscosity is measured for a subsequent 5 min, sampled once per second. The viscosity reported is the average over the constant-shear rate interval. This may be obtained by the mean of the constant-shear rate interval data or by linear fit to the time–viscosity series if friction-heating has occurred during the measurement. For Newtonian samples, triplicate measurements are averaged and the mean reported as the absolute or dynamic viscosity. For non-Newtonian samples, viscosities are reported for each of the three shear rates.

Viscosities above 50,000 $\text{mPa} \cdot \text{s}$ are measured on a parallel plate rheometer with an air bearing. Measurement

for most oils can be performed with a 35 mm cone/plate geometry with a 4° angle. The instrument is run in a controlled rate mode at a shear rate of 1/s.

2.2.3 Surface and Interfacial Tensions

Surface and interfacial tensions, in mN/m , are normally determined by one of two methods. The de Noüy ring is a common technique, used by many laboratories and has been codified as ASTM method D 971 [4]. It depends on accurate measurement of the maximum force a platinum ring can exert on the surface of a liquid before detachment. A second technique that shows much promise for improved speed and accuracy is the pendant/rising drop method, which depends on shape calculations of a droplet of oil in air or water [5,6].

The values that are important for spill responders include the oil/air, oil/water, and the oil/seawater interfacial tensions. The oil/air interfacial tension is often called surface tension. As interfacial tensions are temperature dependant, it is best to determine these quantities for several temperatures. Two measurements at freezing, 0°C, and ambient temperature, 25°C, allow for a wide range of interpolated values. Measurement at 60°F/15°C also allows determination of common marine temperatures.

2.2.3.1 De Noüy Ring Determination of Interfacial Tensions A measurement apparatus specific to the de Noüy ring test is required. Manual machines are common, but automated systems are now available, which make measurements much quicker and highly repeatable. All measurement equipment, rings, measurement vessels, and transfer and storage containers must be scrupulously clean before measurement. Surface and interfacial tension measurements are very sensitive to contamination by organic chemicals or salts.

For sample/air surface tensions, the instrument is zeroed with measurement ring in air. A small amount of sample, approximately 15 ml, is poured into a vessel of sufficient diameter that the wall effects on the meniscus do not affect the area through which the ring will pass. The ring is dipped into the sample to a depth of no more than 5 mm and then pulled up such that it is just visible on the surface of the liquid. The system is allowed to rest for 30 s. The measurement is initiated, terminating when the upward pulling force on the ring just balances the downward force exerted by the liquid. The apparent surface tension, σ_{APP} is recorded.

For sample/water and sample/brine interfacial tensions, a volume of water or brine is dispensed into the measurement vessel. The ring is dipped 5 mm into the aqueous phase. A small volume of sample is carefully poured down the side of the vessel wall, with great care taken so as to disturb the aqueous/oil interface as little as possible. The overlying layer should be at least 5 mm thick. The ring is then raised to the bottom of the interface and the system is allowed to rest for exactly 30 s. The measurement is started and the apparent

interfacial tension is recorded, σ_{APP} when the force balance is reached.

The apparent surface tension is corrected for mass of the upper phase lifted by the ring during measurement using the Zuidema and Waters correction [4]:

$$\sigma = \sigma_{APP} \left(0.7250 + \sqrt{\frac{1.452\sigma_{APP}}{C^2(D-d)} + 0.04534 - \frac{1.679}{R/r}} \right) \quad (2.3)$$

where σ is the interfacial tension, σ_{APP} is the instrument scale reading, C is the ring diameter, D is the density of the lower phase, d is the density of the upper phase, R is the radius of the du Noüy ring, and r is the radius of the ring wire.

As these measurements depend on temperature, samples, aqueous phases, and glassware should be kept at the measurement temperature for a minimum of 30 min before a determination is made.

2.2.3.2 Pendant/Rising Drop Determination of Interfacial Tensions In this test, the interfacial tension is determined by calculation with comparison to the shape of a drop hanging from the end of a needle. A camera is used to photograph a picture of a drop hanging from a needle. The digital picture is analyzed by software, then a parameterized curve shape is developed, from which the surface tension is calculated [6].

In the case of a liquid–liquid interfacial tension, the surrounding fluid must be clear, so that a good image may be generated. For oil in water, this requires that the oil be suspended in water. However, as most oils are less dense than water, the rising oil bubble, rather than the pendant drop, must be measured. In this case, the image is inverted in software and, instead of the force of gravity, the buoyant force, determined as the fraction of gravity based on the specific gravity of the oil, is used:

$$b = \frac{g(\rho_{\text{water}} - \rho_{\text{oil}})}{\rho_{\text{water}}} \quad (2.4)$$

where b is the buoyant force, g is the acceleration due to gravity, ρ_{water} is the density of water at the measurement temperature, and ρ_{oil} is the oil density.

2.2.4 Flash Point

The flash point of an oil product can be determined by several methods, depending on the oil product and the quantity available. In each method, the flash point is determined by controlled heating of the sample and periodically introducing an ignition source to the vapor over the test fluid until a flash combustion occurs. The two primary method types are open and closed cup, referring to the degree of exposure to the atmosphere. Closed-cup methods are enclosed, resulting in less variability due to ambient conditions. Other variables between methods are rate of heating, frequency of ignition, sample volume, and presence of stirring.

The traditional method for low-viscosity products, including light fuel oils and most fresh crudes, is the Tag closed-cup method. This follows ASTM method D 1310 [7]. While accurate, the Tag method uses a comparatively large volume of oil, 50–70 ml. Heavier products, including intermediate and heavy fuel oils, can be measured by a Pensky–Martins analyzer, following ASTM D 93 [8]. As with the Tag method above, this method uses 50–70 ml of crude oil.

Recently developed methods using continuously closed-cup testers use small volumes between 1 and 2 ml. Light fuels such as gasoline and diesel can be measured by ASTM D6450 [9], while heavier fuels and crude oils are best measured by ASTM D7094 [10], which provides stirring of the sample. Flash point values determined using these new tests remain consistent with the traditional methods, with improved repeatability.

The standard test material for assuring quality control for lower-temperature flash point apparatus historically has been *para*-xylene; however, heavier normal alkane standards, *n*-decane, *n*-undecane, *n*-tetradecane, and *n*-hexadecane, have also been found to be suitable, and offer a wider range of test temperatures [11].

2.2.5 Pour Point

The pour point of an oil sample, in degrees Celsius, can be determined by following ASTM method D 97 for petroleum products and D5853 for crude oils [12]. Sample aliquots are poured into ASTM-approved jars, stopped, and fixed with ASTM-certified thermometers. The temperature regime described in the standard is critical; particularly in waxy oils, with high normal alkane contents, a crust of waxy crystals can form on the surface of the oil as it cools. The ASTM D 97 heating and cooling process for oil is designed to assure that the formation of these microstructures is controlled to give reproducible measurement of the pour point.

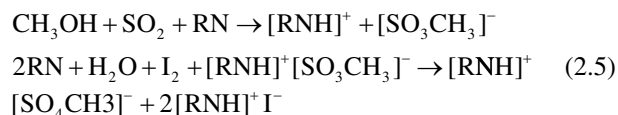
2.2.6 Sulfur Content

The mass fraction of atomic sulfur in oil is conveniently determined using X-ray fluorescence closely following ASTM method D 4294 [13]. In brief, the method is as follows: approximately 3 g of oil is weighed out into standard 31 mm X-ray fluorescence (XRF) cells. The sealed cells are then measured in an XRF spectrometer. The spectrometer response is calibrated using a series of certified reference material standards. Spectra should be corrected for interference by chlorine by subtraction, based on a calibration curve established by the certified reference materials. Matrix effects and X-ray absorption by the base oil can be corrected by subtraction of a spectrum of an oil free of sulfur, such as a mineral or lubricating oil.

2.2.7 Water Content

The mass fraction of water in an oil or an emulsion, expressed as a percentage, is best determined by volumetric Karl Fischer titration, using ASTM method D 4377 [14]. The

Karl Fischer reaction is an amine-catalyzed reduction of water in a methanolic solution:



The amine, RN, or mixture of amines is proprietary to each manufacturer.

An aliquot of approximately 1g of oil is accurately weighed and then introduced to the reaction vessel of the autotitrator. A solution of 1:1:2 (by volume) mixture of methanol:chloroform:toluene is used as a working fluid. Calibrated titrant is then metered out by an autotitrator until the end point is reached. The water content is calculated from the mass of sample and the mass of water implied by the volume of titrant consumed.

2.2.8 Evaluation of the Stability of Emulsions Formed from Brine and Oils and Oil Products

Water-in-oil emulsions are formed in 2.2-l fluorinated vessels on an end-over-end rotary mixer at a rotational speed of 50rpm [15,16].

1. Six hundred milliliters of salt water (3.3% w/v NaCl) is placed in each mixing vessel.
2. Thirty milliliters of oil is added to each vessel for a 1:20 oil:water ratio.
3. The vessels are sealed and placed in the rotary mixer such that the cap of each mixing vessel follows, rather than leads, the direction of rotation. The rotary mixer is kept in a temperature-controlled cold room at 15°C.
4. The vessels and their contents are allowed to stand for approximately 4h before rotation begins, then mixed continuously for 12h.
5. At the conclusion of the mixing time, the emulsions are collected from the vessels for measurement of water content, and the complex modulus. The emulsions are stored at 15°C for 1 week, then observed for changes in physical appearance and remeasured.

Water content of the emulsions should be determined. The Karl Fischer titration method, described earlier, works well for all types of emulsions and water–oil mixtures. The complex modulus of the emulsion is measured on a rheometer using a 35 mm plate–plate geometry. A stress sweep is performed in the range 100–10,000 mPa in the oscillation mode at a frequency of 1 Hz. The complex modulus value in the linear viscoelastic region is reported.

2.2.9 Evaluation of the Effectiveness of Dispersants on an Oil

This method determines the relative ranking of effectiveness for the dispersibility of an oil sample by a dispersant. It is used to either determine the effectiveness of a dispersant

product for a standard crude oil or to test the dispersibility of a crude oil against a standard dispersant. This method follows closely ASTM F 2059 [17].

A premix of 1:25 dispersant:oil is made up by adding oil to 100mg of dispersant. (~2.50 ml of oil in total). Six ASTM-standard swirling conical flasks modified with side spouts containing 120 ml of 33‰ brine are placed into an incubator-shaker. An aliquot of 100 µl of premix is added to the surface of the liquid in each flask, care being taken to not disturb the bulk brine. The flasks are mechanically shaken at 20.0°C with a rotation speed of 150rpm for exactly 20 min. The solutions are allowed to settle for 10 min.

Using the side spout, 30ml of the oil-in-water phase is transferred to a 250 ml separatory funnel, first clearing the spout by draining 3 ml of liquid. The 30ml aliquot is extracted with 3×5 ml of 70:30 (v:v) dichloromethane: pentane, collected into a 25-ml graduated cylinder. Volume is adjusted to 15.0 ml.

A gas chromatograph/flame ionization detector (GC/FID) is used to determine the oil concentration in the solvent. A 900 µl aliquot of the 15-ml solvent extract is combined with 100 µl of internal standard (200 ppm of 5-α-androstane in hexane) in a screw-top injection vial and shaken well. Total petroleum hydrocarbon (TPH) content of the sample is quantified by the internal standard method using the total resolved peak area and the average hydrocarbon response factor over the entire analytical range:

$$\text{RPH} = A_{\text{TOTAL}} / A_{\text{I.S.}} / \text{RRF} \times 20 \times 15 \times 120 / 30 / 0.9 \quad (2.6)$$

where RPH is the resolved petroleum hydrocarbon (mg/ml), A_{TOTAL} is the total resolved peak area, $A_{\text{I.S.}}$ is the internal standard peak area, and RRF is the relative response factor for a series of alkane standards covering the analytical range.

The method is calibrated using a series of six oil-in-solvent mixtures prepared from the premix for each oil. The volume of premix dispersant/oil solution for each standard is selected to represent a percentage efficiency of the dispersed oil. The volume of the premix is then carefully applied to the surface of the brine in a shaker flask and shaken exactly as one of the samples, as described previously. Upon removal from the shaker, however, the entire contents of the flask are transferred to the separatory funnel. This is extracted with 3×20 ml of 70:30 (v:v) dichloromethane: pentane and made up to 60 ml. Chromatographic quantitation is then performed using the formula

$$\text{RPH} = A_{\text{TOTAL}} / A_{\text{I.S.}} / \text{RRF} \times 20 \times 60 \times 30 / 120 / 0.9 \quad (2.7)$$

The RPH values as a function of % effectiveness for the calibration standards are plotted. The sample RPH values are then used to determine the % effectiveness of the dispersant.

Note that these effectiveness percentages are not expected to correlate to real-world dispersibilities. It is important to remember that these values are relative rankings only.

2.2.10 Adhesion

Adhesion to stainless steel is useful to responders in order to judge the “stickiness” of oil to certain drum skimmer configurations as well as numerous other applications. It has been shown that adhesion to different materials is related [18]. A quantitative test has been developed by Environment Canada for this purpose [18,19].

An analytical balance is prepared by hanging an ASTM method D 6 standard penetrometer needle from the balance hook and allowing the apparatus to stabilize and tare. Approximately 80 ml of oil sample is poured into a 100-ml beaker. The beaker is elevated until the oil reaches the top of the stainless steel needle. Care is taken not to go above the needle tip of the apparatus. The needle rests for 30 s immersed in the oil. The beaker is lowered until the needle is clear of the oil. The system is left undisturbed, closed inside a draft shield. After 30 min, the weight of the oil adhering to the needle is recorded. The mass of the oil divided by the surface area of the needle is the adhesion of the oil in g/cm^2 . Typically, four measurements are taken for each oil sample and the mean reported as the final value.

2.3 HYDROCARBON GROUPS

The fate and behavior of crude oils and petroleum products are strongly determined by their chemistries. The main constituents of oils can be grouped into four categories: saturated hydrocarbons (including waxes), aromatics, resins, and asphaltenes.

2.3.1 Saturates

These are a group of hydrocarbons composed of only carbon and hydrogen with no double bonds or aromaticity. They are said to be “saturated” with hydrogen. They may be straight chain (normal), branched, or cyclic. Typically, however, the group of “saturates” refers to the aliphatics generally including alkanes, as well as a small amount of alkenes. The lighter saturates, those with less than approximately C_{18} , make up the components of an oil most prone to weathering. The larger saturates, generally those with more than C_{18} , are termed waxes.

2.3.2 Aromatics

These are cyclic organic compounds that are stabilized by a delocalized π -electron system. They include such compounds as BTEX (benzene, toluene, ethylbenzene, and the three xylene isomers), polycyclic aromatic hydrocarbons (PAHs, such as naphthalene), and some heterocyclic aromatics such as the dibenzothiophenes. Benzene and its alkylated derivatives can constitute several percent in crude oils. PAHs and their alkylated derivatives can also make up as much as a few percent in crude oils.

2.3.3 Resins

This is the name given to a large group of polar compounds in oil. These include hetero-substituted aromatics (typically oxygen- or nitrogen-containing PAHs), acids, ketones, alcohols, and monoaromatic steroids. Because of their polarity, these compounds are more soluble in polar solvents than nonpolar compounds, such as waxes and aromatics, of similar molecular weight.

2.3.4 Asphaltenes

These are a complex mixture of very large organic compounds that precipitate from oils and bitumen by natural processes. For the purposes of this method, these are defined as the fraction that precipitates in *n*-pentane.

The separation of petroleum and its products into these four characteristic groups is known as fractionation. The quantification of the groups is often referred to as SARA analysis, an acronym of the characteristic groups: saturates, aromatics, resins, and asphaltenes. Historically, many techniques have been used to perform this separation including distillation, solvent precipitation (ASTM D6560) [20], treatment with strong acids (ASTM D2006) [21], adsorption (ASTM D2007 and D4124) [22,23], and thin-layer chromatography [24]. For reviews of the methods, see Speight and Becker [24,25]. While excellent methods for the determination of the SARA groups have been developed using thin-layer chromatograph (TLC), there has been continuing interest in alternate test methods based on solvent separation and adsorption techniques [22–24]. Gravimetric methods are typically based on the solubilities of the groups in *n*-pentane, hexane/benzene, and methanol [3]. Such methods can rely on gravimetric determinations of all components, including the saturate and aromatic groups. However, the drawback of such methods is that both saturate and aromatic groups contain significant volatile components. This is particularly true of crude oils and lighter fuels.

More sophisticated methods rely on a combination method involving determination of the saturate and aromatic fractions by gas chromatography, an adaptation of TPH methods, while gravimetrically determining the nonvolatile resin and asphaltene components [26,27].

2.3.4.1 Resin and Asphaltene Gravimetric Determination A 100 ml quantity of *n*-pentane is added to a pre-weighed sample of approximately 5 g of oil. The flask is shaken well and allowed to stand for 30 min [28,26]. The sample is filtered through a 0.45- μm membrane using a minimum of rinsings of *n*-pentane. The precipitate is allowed to dry, then weighed. The weight of the precipitate as a fraction of the initial oil sample weight is reported as the percentage asphaltenes.

The filtrate from the precipitation, the “maltene” fraction, is recovered and made up to 100 ml with *n*-pentane. A 15-g, 1-cm diameter column of activated silica gel is prepared.

The top of the column is protected by a 1-cm layer of sodium sulfate. A 5-ml aliquot of the maltene fraction is loaded onto the column. A 60-ml volume of 1:1 (v:v) benzene:hexane is eluted through the column and discarded. A 60-ml volume of methanol followed by a 60-ml volume of dichloromethane are eluted through the column and combined. The methanol/dichloromethane fractions are reduced by rotary evaporation and blown down to dryness under nitrogen. The mass fraction of this dried eluent, compensating for the volume fraction used, is reported as the percentage of resins in the sample.

2.3.4.2 Resin and Asphaltene Thin-Layer Chromatography Determination While no standard method for this technique exists, it has the advantages over the gravimetric methods of being much faster and requiring much less oil or product. It has the disadvantage of requiring a sophisticated instrument, a TLC with a FID.

A TLC that quantifies analytes developed on silica gel-coated glass rods, such as the Iatroscan Mark 6, is necessary for this method. Briefly, an aliquot of sample dissolved in dichloromethane at a concentration of 1 mg/ml is spotted at a point, the origin, near one end of a rod, the foot of the rod. The rods are then developed by immersion of the feet into a series of solvents to separate the four hydrocarbon groups. The origin points must remain above the liquid surface, but the feet of the rods must be immersed sufficiently to cause solvent to travel up the rods by capillary action.

The first solvent used is *n*-hexane to develop the saturates. Toluene develops the aromatics. Finally, a 95%-dichloromethane 5%-methanol mixture is used to develop the resins. The asphaltenes remain at the spotting origin. The hydrocarbon groups that are not quantified by this method, the saturates and aromatics, are removed by pyrolysis. A known standard is then applied to the chromarod and then quantified using a FID and an internal standard. A sample of 1-octadecanol at 1 mg/ml concentration is a convenient internal standard. This is spotted on the rod just prior to measurement, on the part of the rod pyrolyzed to remove the saturate and aromatic fractions.

The development of the chemicals on the rods critically depends on the conditions. The rods must be developed in tanks to control the vapors in atmosphere. Also temperature and humidity must remain as consistent as possible to achieve reproducible results. When drying after each development, the rods must rest in a controlled humidity chamber.

Resin and asphaltene contents are determined as follows:

$$\% \text{ Resin} = C_{\text{IS}} \times V_{\text{IS}} \times A_{\text{R}} / A_{\text{IS}} \quad (2.8)$$

$$\% \text{ Asphaltene} = C_{\text{IS}} \times V_{\text{IS}} \times A_{\text{A}} / A_{\text{IS}} \quad (2.9)$$

where C_{IS} is the internal standard concentration, V_{IS} is the internal standard volume, A_{IS} is the internal standard area from TLC integration, A_{R} is the resin area from TLC integration, and A_{A} is the asphaltene area from TLC integration.

Note that while saturate and aromatic fractions are separated by the development process, and could in principle be measured by TLC-FID, the drying process between development stages requires significant evaporation. This level of evaporation is significant enough to remove most of the volatile components, which includes a large fraction of both saturates and aromatics (but not the resins or asphaltenes). For this reason, this TLC-FID method is not suitable for saturate or aromatic determination.

2.3.4.3 Saturate and Aromatic Chromatographic Determination This method is adapted and simplified from a previously published method for crude oil and petroleum product determination [27]. An 80 mg/ml solution of oil is prepared in hexane. A 3.0g column of activated silica gel is prepared, topped with 0.5 cm anhydrous sodium sulfate. The column is conditioned with 20 ml of hexane.

An amount of 200 μl of the oil solution, approximately 16 mg of oil, is quantitatively transferred onto the column using an additional 3 ml of hexane to complete the transfer. The eluent is also discarded. Just prior to exposure of the sodium sulfate to the air, 12 ml of hexane is added to the column. The eluent is labeled fraction "F1." F1 is considered to contain all the saturates, including the waxy components in the oil.

The column is then eluted with 15 ml of 1:1 (v:v) benzene/hexane or dichloromethane/hexane. The eluent is collected and labeled fraction "F2." F2 is considered to contain the aromatic compounds in the oil, including the BTEX compounds, other alkylated benzene species, PAHs, and the alkylated PAH homologues.

Half of fractions F1 and F2 are combined. This composite fraction is labeled "F3." This fraction is used for analysis of TPHs.

All the three fractions are concentrated under dry nitrogen. The fractions are then spiked with the internal standard, 100 μl of 200 ppm 5- α -androstane, and made up with hexane to 1 ml.

The analysis for TPHs and saturates is performed by high resolution capillary GC/FID using the following conditions:

Column:	30 m \times 0.32 mm ID HP DB5-HT-fused silica column (0.10 μm film thickness);
Carrier gas:	Helium, 3.0 ml/min, constant flow;
Injection volume:	1.0 μl ;
Injector temperature:	290°C;
Detector temperature:	325°C;
Oven program:	40°C for 2 min, followed by 25°C/min to a final temperature of 340°C, then held for 15 min. The total run time is 29 min.

To calculate the concentration of hydrocarbons in each fraction, the area response attributed to the petroleum hydrocarbons must be determined. This area includes all of the

resolved peaks and unresolved “hump.” This total area must be adjusted to remove the area response of the internal standards and GC column bleed.

Column bleed is the reproducible baseline shift that occurs during the oven cycle of the GC. To determine this area, a hexane blank injection is analyzed before and after every 10 samples to determine the baseline response. The integration baseline is then set at a stable reproducible point just before the solvent peak. This baseline area for the blank run is subtracted from the actual sample run.

The total areas of the chromatograms of F1, F2, and F3 are obtained by integration of all peaks, corrected by removal of the baseline. The area response attributable to the internal standard is calculated. The F3 fraction is used to calculate the TPH values for the oil [27]. The F1 and F2 fractions are used to calculate the total saturate hydrocarbon (TSH) and total aromatic hydrocarbon (TAH) contents. Note that TPH should be within 10% of TSH + TAH.

As not all the oil is passed through the GC column, a simple sum of TSH, TAH, resin, and asphaltene contents will not sum to 100%. This missing portion of the oil, which does not precipitate or get analyzed by the GC method, is approximated by proportionally dividing it into the saturate and aromatic portions. Thus, the saturate content of the oil is commuted using the formula

$$\% \text{Saturates} = \text{TSH} / (\text{TSH} + \text{TAH}) \times (1 - \% \text{Asphaltenes} - \% \text{Resins}) \quad (2.10)$$

Likewise, the aromatic content is computed using the formula

$$\% \text{Aromatic} = \text{TAH} / (\text{TSH} + \text{TAH}) \times (1 - \% \text{Asphaltenes} - \% \text{Resins}) \quad (2.11)$$

Note that the asphaltene and resin contents may be determined by either gravimetric or TLC–FID method described earlier.

For crude oils or products with high water content, it is necessary to dry the sample prior to the gravimetric determination of the hydrocarbon group contents. If a Karl Fischer water content determination can be made, then the composition of the original product can be reported adjusted for the observed water content. If not, the values should be reported as for dried product only.

2.4 QUALITY ASSURANCE AND CONTROL

Most of the physical property methods described here rely on a single instrument and involve a simple measurement with little sample manipulation [27,29]. For these methods, the instruments are calibrated as directed by the manufacturer or the appropriate ASTM method with chemical and/or gravimetric standards as appropriate. In addition, instrumental and operator performance should be monitored by periodic

measurement of check standards. A control chart should be kept for each procedure, for the check or performance standard measurements. The check standard measurements are monitored closely. Failure of the check standard measurement to fall within the smaller of either a historical 95% confidence limit or the appropriate ASTM-required repeatability should result in an investigation of the procedure. This typically includes required instrument maintenance, cleaning, recalibration, and measurement of the check standard until the desired precision and accuracy is reached.

The chromatographic methods described here, including the dispersibility tests and the hydrocarbon group analysis, involve significant sample preparation, followed by a measurement by gas chromatography. Such techniques require a higher level of effort to maintain quality assurance. Check or surrogate samples of either pure materials or certified reference standards should be processed in the same manner as the samples. Calibration should be accomplished with a second, separate set of certified reference materials. Internal standards should also be certified reference materials from reputable suppliers. Surrogate recovery, calibration stability, and internal standard response control charts should all be checked regularly to ensure procedure and measurement accuracy. Chromatograms should be checked to ensure that chromatographic quality, including good peak shape, baseline drift, column bleed, sample carryover and chromatographic resolution, is within acceptable limits.

2.5 EFFECTS OF EVAPORATIVE WEATHERING ON OIL BULK PROPERTIES

Long experience has shown that the physical characteristics and chemical fingerprint of a crude oil can change greatly over the course of a spill incident. These changes have a profound effect on the fate, behavior, and effects of an oil in the environment. The oil may transmute to other states, evaporating, dissolving in water, or condensing to a semisolid residue, each new state having unique behaviors and eventual fates. In order to aid in the estimation and prediction of spill behavior, it is useful to know not only the characteristics of the fresh crude oil but also those of oils at different stages of “weathering” in the environment. Previous work has shown that immediately after a spill, the dominant process of oil weathering is evaporation. The following discussion will focus on the effects of evaporative weathering on changes in oil physical properties and chemical compositions.

2.5.1 Weathering

When oil is spilled, on either water or land, a number of transformation processes operate on the oil. In general, there are two types of transformation processes: the first is weathering, and the second is a group of processes (including *spreading, movement of oil slicks, and sinking and overwashing*) related to the movement of the oil in the environment. Weathering and movement processes overlap, with

weathering strongly influencing how oil moves in the environment and vice versa. These processes depend very much on the type of oil spilled and the weather conditions during and after the spill. Understanding the behavior of spilled oil in the environment is extremely important for development of oil spill models. Today's sophisticated spill models combine the latest information on oil fate and behavior with computer technology to predict where the oil will go, what state it will be in, and when it gets there.

"Weathering" is the term combining a wide variety of physical, chemical, and biological processes that a spilled oil undergoes in the environment. The weathering processes include evaporation, emulsification, natural dispersion, dissolution, microbial degradation, photooxidation, and other processes such as sedimentation and oil-suspended particle interactions.

Weathering has a very significant effect on most bulk oil properties. Unlike the chemical compositions, however, where environmental parameters only effect the rate and type of weathering, bulk properties of the oil are also highly variable depending on the physical conditions. Most important of these is temperature, but other factors such as pressure and the materials with which the oil is in contact also play a role.

As an oil loses mass and changes in composition, several general trends in physical property changes can be observed:

- Density increases approximately linearly with evaporative mass loss. Density decreases approximately linearly with temperature.
- Viscosity increases with increasing weathering, but a simple functional relationship is not easy to develop. Viscosity increases approximately exponentially with decreasing temperature.
- Surface and interfacial tensions tend to increase slightly with increasing weathering.

2.5.2 Preparing Evaporated (Weathered) Samples of Oils

A common technique for simulating weathering in the laboratory is evaporation. While this is only one of the possible processes in the natural environment, it is the dominant one for most spills, particularly in the first few hours or days following a spill. A laboratory oil-weathering technique by rotary evaporation allows for convenient preparation of artificially weathered oils with varying degrees of weight loss. A typical oil-weathering system consists of a rotary evaporator. The bath temperature of the evaporator should be variable from 20 to 100°C ± 0.5°C. The rotation speed should be continuously variable from 10 to 135 rpm.

The following procedure is used to evaporate oils:

1. The water bath is brought to a temperature of 80°C.
2. The empty rotary flask is weighed, and no more than 1/3 the volume of the rotary flask is filled with oil and the flask reweighed.

3. The flask is mounted on the apparatus and the flask partially immersed in the water bath and spun at high speed, at least 120rpm. A constant flow of air through the apparatus should be maintained by a vacuum pump;
4. At set intervals, the sample flask is removed and weighed.

It is convenient to prepare two to three weathered samples for each type of oil measured. With a moderate flow rate through the instrument, evaporation for a duration of 48 h will come within 5–10% of simulating the eventual final state of an oil in the environment. Intermediate fractions of approximately one- and two-thirds of the 48-h loss by weight will simulate approximately the condition of the oil after a few hours to days and a few days to weeks of natural evaporation.

The exact time taken to prepare these intermediate fractions is determined by estimation from the measured fractional mass-loss as a function of time for the 48-h sample. The fractional mass-loss is calculated as follows:

$$\% \text{weathering} = (m_i - m_f) / (m_i) \times 100\%, \quad (2.12)$$

where % *weathering* is the percentage evaporative mass-loss over the 48-h period, m_i is the initial mass of the flask and oil, and m_f is the final mass of the flask and oil. A graph of % *weathering* as a function of time is plotted using the interval-weighing data.

The times for one-third ($t_{1/3}$) and two-thirds ($t_{2/3}$) of the 48-h mass-loss are interpolated from a time-weathering graph. Typical times for $t_{1/3}$ range from 30 min to 2 h and for $t_{2/3}$ from 8 to 12 h.

This technique allows for precise control of the evaporative weight loss for a target oil and can be directly correlated to bulk property and compositional changes of the weathered oil.

2.5.3 Quantifying Equation(s) for Predicting Evaporation

The evaporation kinetics are determined for each oil by measuring the weight loss over time from a shallow dish [30, 31]. Approximately 20g of oil is weighed into a 139 mm petri dish. The oil weight is recorded by an electronic balance accurate to 0.01g at set intervals and collected on a computer logging system. Measurements are conducted in a climate-controlled chamber at 15°C. Temperatures are monitored by a digital thermometer. The evaporation period can last from a few days for light oils to weeks for heavier products.

The time *versus* weight loss data series is fitted to a set of simple equations. The best curve-fit is chosen as the equation for predicting evaporation.

2.5.3.1 Effects of Evaporative Weathering on Crude Oil Density Densities of oils typically increase approximately 5–10% as oil weathers. Cook Inlet, a light oil, changes in

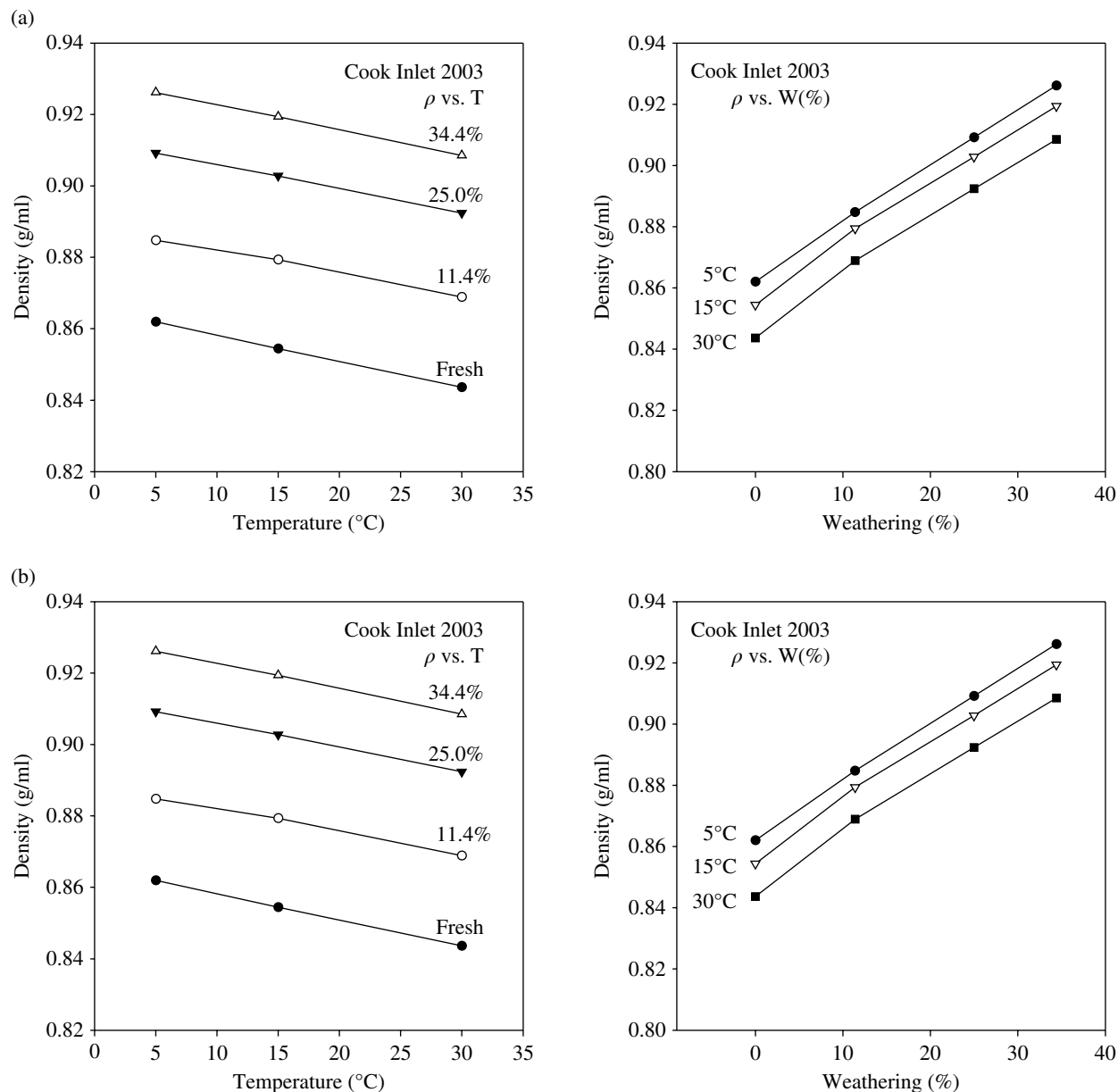


FIGURE 2.1 Density *versus* temperature and weathering for a light (Cook Inlet) (a) and heavy (Platform Elly) (b) crude oil.

density from 0.84 to 0.91 g/ml at 30°C (see Fig. 2.1a), while Platform Elly, a very heavy crude oil, has a fresh density of 0.9531 g/ml and increases to 0.9843 g/ml in its most-weathered state at 30°C (Fig. 2.1b). From Figure 2.1, it can be seen that, to a first approximation, density increases linearly with increasing mass-loss and decreasing temperature. Better extrapolations can be made from log-log extrapolations of both quantities. Note that the uncertainties in density are very small: ± 0.0002 g/ml, approximately 1 part in 5000.

2.5.3.2 Effects of Evaporative Weathering on Crude Oil Viscosity In contrast to most other physical properties, the viscosity of an oil can change by orders of magnitude with

weathering and changes in temperature. For example, the viscosity of Cook Inlet crude changes from 5.8 to 67.0 mPa·s at 30°C (see Fig. 2.2a), while fresh Platform Elly has a viscosity of 1070 mPa·s and reaches 52,280 mPa·s in the most-weathered fraction (Fig. 2.2b). As can be seen from Figure 2.2a and b, the logarithm of viscosity is roughly inversely linear with temperature, but the effects of weathering on viscosity are more complex. Uncertainties in viscosity are $\pm 5\%$.

2.5.3.3 Effects of Evaporative Weathering on Crude Oil Surface and Interfacial Tensions Surface and interfacial tensions have no simple quantitative relationships in general

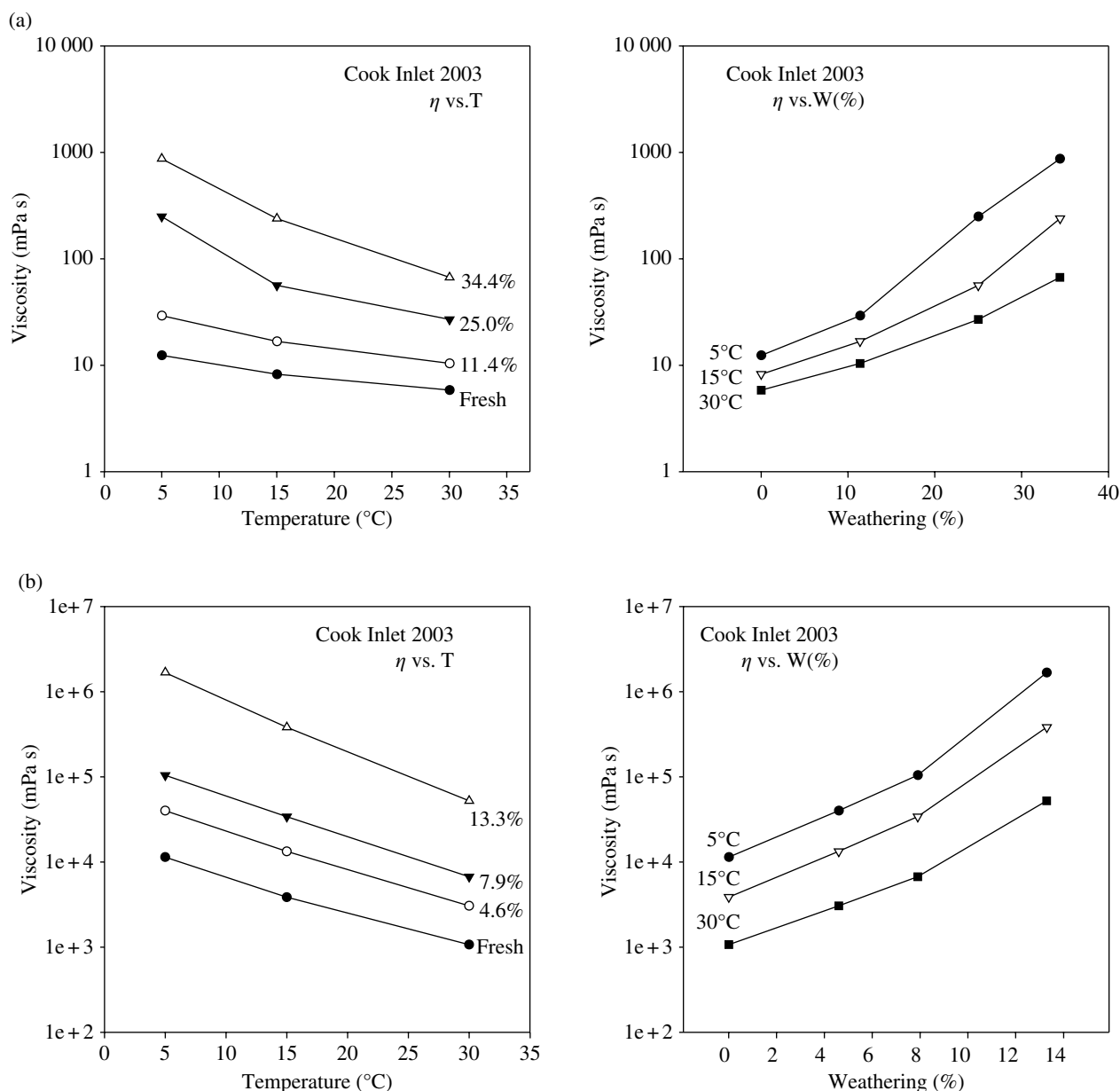


FIGURE 2.2 Viscosity *versus* temperature and weathering for light (Cook Inlet) (a) and heavy (Platform Elly) (b) crude oils.

to either the degree of weathering or the temperature. Surface tensions, however, do not vary greatly from oil to oil; values from 25 to 32 mN/m are typical for almost all types of oil. Interfacial tensions for oil/water and oil/3.3% brine are often marginally lower than the corresponding oil/air surface tension. Oil/brine interfacial tensions are usually somewhat higher than the corresponding oil/(pure) water values. Typical values for both range from 18 to 32 mN/m. Surface and interfacial tensions tend to decrease with temperature and increase with weathering. Care should be taken not to overinterpret to significance of surface and interfacial tension values; however, the errors on these measurements

are relatively large, $\pm 15\%$, and the relative variations of the values are fairly small.

REFERENCES

- [1] ASTM D 5002, *Standard Test Method for Density and Relative Density of Crude Oils by Digital Density Analyzer*, American Society for Testing and Materials, Conshohocken, PA, 2009.
- [2] API 82, American Petroleum Institute (API), *Petroleum Measurement Tables—Volume XI/XII*, American Society for Testing and Materials, West Conshohocken, PA, 1982.

- [3] Jokuty, P., M. Fingas, and S. Whiticar, Oil Analytical Techniques for Environmental Purposes, *AMOP*, 245, 1994.
- [4] ASTM D 971, *Standard Test Method for Interfacial Tension of Oil against Water by the Ring Method*, American Society for Testing and Materials, West Conshohocken, PA, 2009.
- [5] Jokuty, P., M. Fingas, S. Whiticar, and B. Fieldhouse, *A Study of Viscosity and Interfacial Tension of Oils and Emulsions*, Manuscript Report EE-153, Environment Canada, Ottawa, ON, 1995.
- [6] Song, B. and J. Springer, Determination of Interfacial Tension from the Profile of a Pendant Drop Using Computer-Aided Image Processing, *Colloid Interface Sci*, 64, 1996.
- [7] ASTM D1310, *Standard Test Method for Flash Point and Fire Point of Liquids by Tag Open-Cup Apparatus*, American Society for Testing and Materials, West Conshohocken, PA, 2012.
- [8] ASTM D 93, *Standard Test Method for Flash Point by Pensky-Martens Closed Cup Tester*, American Society for Testing and Materials, West Conshohocken, PA, 2009.
- [9] ASTM D 6450, *Standard Test Method for Flash Point by Continuously Closed Cup (CCCFP) Tester*, American Society for Testing and Materials, West Conshohocken, PA, 2009.
- [10] ASTM D 7094, *Standard Test Method for Flash Point by Modified Continuously Closed Cup (MCCCFP) Tester*, American Society for Testing and Materials, West Conshohocken, PA, 2009.
- [11] Montemayor, R.G., J.E. Rogerson, J.C. Colbert, and S.B. Schiller, Reference Verification Fluids for Flash Point Determination, *J Test Eval*, 27, 1999.
- [12] ASTM D 97, *Standard Test Method for Pour Point of Petroleum Oils*, American Society for Testing and Materials, West Conshohocken, PA, 2009.
- [13] ASTM D 4294, *Standard Test Method for Sulfur in Petroleum Products by Energy-Dispersive X-ray Fluorescence Spectroscopy*, American Society for Testing and Materials, West Conshohocken, PA, 2009.
- [14] ASTM D 4377, *Standard Test Method for Water in Crude Oils by Potentiometric Karl Fischer Titration*, American Society for Testing and Materials, West Conshohocken, PA, 2009.
- [15] Fingas, M., B. Fieldhouse, and J. Mullin, Studies of Water-In-Oil Emulsions: Stability and Oil Properties, *AMOP*, 1, 1998.
- [16] Fingas, M. and B. Fieldhouse, Studies on Crude Oil and Petroleum Product Emulsions: Water Resolution and Rheology, *Colloids Surf A*, 67, 2009.
- [17] ASTM F 2059, *Standard Test Method for Laboratory Oil Spill Dispersant Effectiveness Using the Swirling Flask*, American Society for Testing and Materials, West Conshohocken, PA, 2012.
- [18] Jokuty, P., S. Whiticar, K. McRoberts, and J. Mullin, Oil Adhesion Testing—Recent Results, *AMOP*, 9, 1996.
- [19] ASTM D 5, *Standard Test Method for Penetration of Bituminous Materials*, American Society for Testing and Materials, West Conshohocken, PA, 2009.
- [20] ASTM D 6560, *Standard Test Method for Determination of Asphaltenes (Heptane Insolubles) in Crude Petroleum and Petroleum Products*, American Society for Testing and Materials, West Conshohocken, PA, 2011.
- [21] ASTM D 2006, *Method of Test for Characteristic Groups in Rubber Extender and Processing Oils by the Precipitation Method (Withdrawn 1975)*, American Society for Testing and Materials, West Conshohocken, PA, 1965.
- [22] ASTM D 2007, *Standard Test Method for Characteristic Groups in Rubber Extender and Processing Oils and Other Petroleum-Derived Oils by Clay-Gel Absorption Chromatographic Method*, American Society for Testing and Materials, West Conshohocken, PA, 2012.
- [23] ASTM D 4124, *Standard Test Methods for Separation of Asphalt into Four Fractions*, American Society for Testing and Materials, West Conshohocken, PA, 2011.
- [24] Barman, B.N., Hydrocarbon-Type Analysis of Base Oils and Other Heavy Distillates by Thin-Layer Chromatography with Flame-Ionization Detection and by the Clay-Gel Method, *J Chromat Sci*, 219, 1996.
- [25] Speight, J.G., *The Chemistry and Technology of Petroleum*, Marcel Dekker, New York, 2007.
- [26] Hollebone, B., Z. Wang, M. Landriault, and P. Smith, A New Method for the Determination of the Hydrocarbon Groups in Oils: Saturates, Aromatics, Resins and Asphaltenes (SARA), *AMOP*, 31, 2003.
- [27] Wang, Z. D., M. Fingas, and K. Li, Fractionation of ASMB Oil, Identification and Quantitation of Aliphatic Aromatic and Biomarker Compounds by GC/FID and GC/MSD (Parts I and II), *J Chromat Sci*, 361, 1994.
- [28] Becker, J.R., *Asphaltene Test Methods, Crude Oil Waxes, Emulsions and Asphaltenes*, Penn Well Publishing Co., Tulsa, OK, 1991.
- [29] Environment Canada, Oil Properties Database, http://www.etc-cte.ec.gc.ca/databases/OilProperties/oil_prop_e.html, accessed February 15, 2014.
- [30] Fingas, M., The Evaporation of Oil Spills, *AMOP*, 43, 1995.
- [31] Fingas, M., Modeling Evaporation Using Models That Are Not Boundary-layer Regulated, *J Haz Mat*, 27, 2004.

PART III

OIL COMPOSITION AND PROPERTIES

INTRODUCTION TO OIL CHEMISTRY AND PROPERTIES

MERV FINGAS

Spill Science, Edmonton, Alberta, Canada

3.1	Introduction	53
3.2	The Composition of Oil	53
3.2.1	SARA	54
3.2.2	Sulfur Compounds	58
3.2.3	Oxygen Compounds	58
3.2.4	Nitrogen Compounds	69
3.2.5	Metals	69
3.2.6	Resins	69
3.2.7	Asphaltenes	69
3.3	Properties of Oil	75

3.1 INTRODUCTION

Oil is a general term that describes a wide variety of natural substances of plant, animal, or mineral origin and a range of synthetic compounds. This chapter covers crude oil and petroleum products derived from such oils. Crude oils are made up of hundreds of major constituents and thousands of minor ones. As their composition varies, each type of oil or petroleum product has certain unique characteristics or properties. These properties influence how the oil behaves when it is spilled and subsequently determine the fate and effects of the oil in the environment. Oil properties strongly influence the efficiency of cleanup operations.

3.2 THE COMPOSITION OF OIL

Crude oils are complex mixtures of hydrocarbons and hydrocarbons combined with other elements ranging from smaller, volatile compounds to very large, nonvolatile compounds [1]. The mixture of compounds varies with the geological formation of the area in which the crude oil is found. Crude oils are often similar in a given region and when drawn from a similar reservoir. Petroleum products such as gasoline and diesel fuel are mixtures of fewer compounds and are refined

to specific standards. Thus, their properties are more specific and less variable. Crude oil contains many compounds of different sizes and different classes. In fact, there are so many that as time goes by more and more compounds are identified in the oil. Currently, analysts have preliminarily identified up to 17,500 compounds in an oil [2]. In the future, this number will no doubt rise significantly.

Hydrocarbon compounds are composed of hydrogen and carbon, which are the main elements in oils. Oils also contain varying amounts of sulfur; nitrogen; oxygen; and trace metals such as nickel, vanadium, and chromium. This section will detail some of these compounds. In general, the hydrocarbons found in oils are characterized by their structures.

A common and older method of classification is by SARA—saturates, aromatics, resins, and asphaltenes. Figure 3.1 illustrates the SARA classification along with classes of compounds typically found in this overall classification. The saturate group of components in oils consists primarily of alkanes, which are compounds of hydrogen and carbon with the maximum number of hydrogen atoms around each carbon. Thus, the term saturate is used because the carbons are saturated with hydrogen. The saturate group includes straight-chain and branched-chain alkanes and also includes cycloalkanes, which are compounds made up of the same carbon and hydrogen constituents but with the carbon atoms bonded to each other in rings or circles. Straight-chain saturate compounds from C18 and up are often referred to as waxes.

The elemental composition of oil is sometimes of interest. Crude oils have a typical composition [3]:

Carbon: 83–87%
Hydrogen: 10–14%
Sulfur: 0.05–6%
Nitrogen: 0.1–2%
Oxygen: 0.05–1.5%

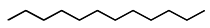
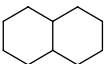
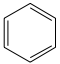
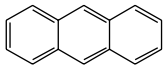
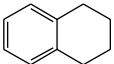
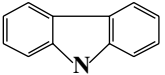
Groupings	Example classes, names, and compounds			
	Chemical class	Alternate name	Description	Example compound
Saturates	Alkanes	Paraffins		Dodecane  $C_{12}H_{26}$
	Cycloalkanes	Naphthenes		Decalin 
	Waxes		<i>n</i> -alkanes C_{18} – C_{80}	
Aromatics	BTEX		Benzene, Toluene, Ethylbenzene, Xylenes	Benzene 
	PAHs			Anthracene 
	Naphthenoaromatics		Combinations of aromatics and cycloalkanes	Tetralin 
Resins	<i>Class of mostly anomalous polar compounds sometimes containing oxygen, nitrogen, sulfur, or metals</i>			Carbazole 
Asphaltenes	<i>Class of large anomalous compounds sometimes containing oxygen, nitrogen, metals, or sulfur</i>			<i>Structures not known</i>

FIGURE 3.1 The typical SARA contents and examples of specific compounds.

TABLE 3.1 Typical composition of some oils and petroleum products

Group	(%—except for metals)			Light crude	Heavy crude	IFO ^a	Bunker C
	Compound class	Gasoline	Diesel				
Saturates		50–60	65–95	55–90	25–80	25–35	20–30
	Alkanes	45–55	35–45	40–85	20–60	10–25	10–20
	Cycloalkanes	5	25–50	5–35	0–10	0–5	0–5
Olefins		5–10	0–10				
Aromatics		25–40	5–25	10–35	15–40	40–60	30–50
	BTEX	15–25	0.5–2.0	0.1–2.5	0.01–2.0	0.05–1.0	0.00–1.0
	PAHs		0–5	10–35	15–40	30–50	30–50
Polar compounds			0–2	1–15	5–40	15–25	10–30
	Resins		0–2	0–10	2–25	10–15	10–20
	Asphaltenes			0–10	0–20	5–10	5–20
Sulfur		0.02	0.1–0.5	0–2	0–5	0.5–2.0	2–4
Metals (in parts per million—ppm)				30–250	100–500	100–1000	100–2000

^aIFO is intermediate fuel oil, which is the residual fraction diluted by diesel fractions.

3.2.1 SARA

The SARA composition of oil is a more general analytical method that defines oils by precipitation and then weight. Newer methods now employ thin-layer chromatography, with the values from both methods varying somewhat. This method is still useful, however, and it provides useful

data both to the refiner and to the environmentalist. Figure 3.1 illustrates the typical compositions designated by SARA and some example compounds. Table 3.1 shows the gross composition of some typical oils and petroleum products. It is noted that the ranges of these compositions vary widely. Saturates are hydrocarbon compounds with the maximum number of hydrogens. Aromatics are

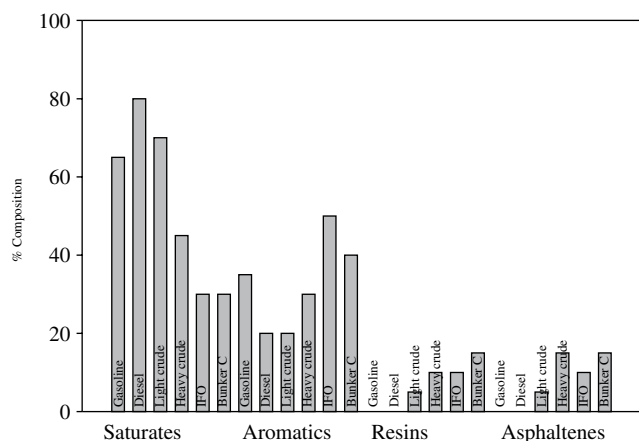


FIGURE 3.2 An illustration of the typical amounts of SARA in various oils and fuels.

hydrocarbon compounds with at least one benzene ring. Resins and asphaltenes are larger compounds containing mostly carbon and hydrogen but containing other elements such as oxygen, sulfur, nitrogen, and metals.

Figure 3.2 shows the SARA composition of some typical oils and petroleum products. It can be seen that SARA content varies widely for the various products. The products illustrated in Figure 3.2 are gasoline, diesel fuel, a light crude oil, a heavy crude oil, an intermediate fuel oil, and Bunker C. These represent a large cross-section of oils and petroleum products and serve to illustrate the broad spectrum of hydrocarbon liquids.

3.2.1.1 Saturates As noted in the general discussion on SARA, saturates are important economical constituents of oils. Saturates are often the most abundant compounds in any oil or petroleum product. Saturates are so-called because they are compounds containing the maximum number of hydrogens.

Alkanes Alkanes, an important part of saturate composition, are hydrocarbons with a chain-like structure and without double bonds or other elements such as sulfur, nitrogen, or oxygen attached [1,3,4]. Alkanes, sometimes called paraffins, are typically the most abundant compounds in crude oils as well as in most fuels such as diesel fuel and gasoline. Most crude oils have anywhere between a few percent up to 30% alkanes. Alkanes are typically the target compounds sought by petroleum producers. It should be noted, however, that larger alkanes are also called waxes, and these are sometimes less desirable from a petroleum producer's point of view.

Normal alkanes are those that are unbranched. All normal and branched alkanes have the generalized molecular formula of C_nH_{n+2} , where n is the number of carbons present. All alkanes are saturated, that is, they contain the most

hydrogen that the configuration can have. The branching potential for alkanes increases as the size of the alkane increases. Table 3.2 shows the typical alkanes contained in crude oils and some fuels [5–12]. Some properties and content of n -alkanes in some crude oils are also shown in this table. Figure 3.3 shows the number of structural isomers possible for pentane, as an example of a typical branched alkane. The column in Table 3.2 indicating the number of isomers shows the possible number of branched compounds. As can be seen in this table, the number of possible branched compounds rises to over one million by the time carbon number 22 is reached. In fact, it is impossible to separate most branched compounds during chemical analysis. Thus, the amount of branched compounds in crude oils may be unknown for some time to come.

Table 3.3 shows the known subdivisions of the SARA contents. Table 3.3 shows that the n -alkanes typically account for about 10% of the saturates. It is suspected that the branched alkanes account for about two to five times that amount and that the cycloalkanes may account for about the same amount as the n -alkanes. Much more analytical work is required to adequately describe the detailed composition of oil.

Cycloalkanes Cycloalkanes, compounds containing rings or cyclic compounds, are also saturated alkanes. These are sometimes called naphthenes. Typical base structures for cycloalkanes are shown in Figure 3.4. Cycloalkanes have the general formula C_nH_{2n} . Figure 3.4 illustrates the three important baseline structures: cyclopentane, cyclohexane, and decahydronaphthalene. These base structures contribute to the majority of the cycloalkanes found in an oil. The smaller cycloalkanes such as cyclopropane and cyclobutane are not common because the smaller-ring carbon bonds have considerable ring strain, being stretched above the normal carbon–carbon tetrahedral angle of 109° . Because of the carbon-to-carbon bond stress, there is no free rotation and thus there are stereoisomers (e.g., cis and trans isomers) for molecules above carbon number 6 (C6). The possible cycloalkanes found in oils are shown in Table 3.4. Because cycloalkanes are low in abundance and may be difficult to separate in chromatographic analysis, there are not much data on their abundance in oils.

3.2.1.2 Alkenes or Olefins The olefins, or unsaturated compounds, are another group of compounds that contain less hydrogen atoms than the maximum possible. Olefins have at least one double carbon-to-carbon bond, which displaces two hydrogen atoms. Significant amounts of olefins are found only in refined products; however, some cyclic alkenes have been observed in crude oils. It should be noted that SARA analysis does not include alkenes and does not specifically provide a method to separate them from many other hydrocarbons.

TABLE 3.2 Typical alkane compounds in oil

Carbon number	Number of isomers	Formula	IUPAC name	Molecular weight	CAS number	Reference	Solubility in water ^a g/l	Reference	SIMS	Levels in ASMB ^b µg/g oil	Reference	Levels in ANS ^c fuel µg/g oil	Levels in diesel fuel µg/g oil	Levels in heavy fuel oil µg/g oil	Reference	Levels in fresh troll crude µg/g	Reference
5	3	C ₅ H ₁₂	Pentane	72.149	109-66-0	[7]	3.9 E ⁻²	[8]	57,71							670	[11]
6	5	C ₆ H ₁₄	Hexane	86.175	110-54-3	[7]	~0.01	[10]	57,71,85							350	[11]
7	9	C ₇ H ₁₆	Heptane	100.202	142-82-5	[7]	~0.003		57,71,85							60	[11]
8	18	C ₈ H ₁₈	Octane	114.229	111-65-9	[7]	0.7 E ⁻³	[10]	57,71,85	5	[5]	6	1	—	[6]	20	[11]
9	35	C ₉ H ₂₀	Nonane	128.255	111-84-2	[7]	1.2 E ⁻⁴	[8]	57,71,85	4	[5]	4	4	—	[6]	20	[11]
10	75	C ₁₀ H ₂₂	Decane	142.282	124-18-5	[7]	~5 E ⁻⁵	[8]	57,71,85	4	[5]	4	11	—	[6]	110	[11]
11	159	C ₁₁ H ₂₄	Undecane	156.309	1120-21-4	[7]	~6 E ⁻⁶	[8]	57,71,85	4	[5]	4	13	0.5	[6]		
12	355	C ₁₂ H ₂₆	Dodecane	170.334	112-40-3	[7]	~2 E ⁻⁶	[8]	57,71,85	4	[5]	4	13	1	[6]		
13	802	C ₁₃ H ₂₈	Tridecane	184.361	629-50-5	[7]	~4 E ⁻⁷	[8]	57,71,85	4	[5]	4	13	1	[6]		
14	1858	C ₁₄ H ₃₀	Tetradecane	198.388	629-59-4	[7]	~3 E ⁻⁷	[8]	57,71,85	4	[5]	3	12	1	[6]		
15	4347	C ₁₅ H ₃₂	Pentadecane	212.415	629-62-9	[7]	~4 E ⁻⁸	[8]	57,71,85	3	[5]	3	12	1	[6]		
16	1.04E+04	C ₁₆ H ₃₄	Hexadecane	226.441	544-76-3	[7]	<6 E ⁻⁶	[8]	57,71,85	3	[5]	3	11	2	[6]		
17	2.49E+04	C ₁₇ H ₃₆	Heptadecane	240.468	629-78-7	[7]			57,71,85	3	[5]	3	9	2	[6]		
18	6.05E+04	C ₁₈ H ₃₈	Octadecane	254.495	593-45-3	[7]			57,71,85	3	[5]	3	7	2	[6]		
19	1.48E+05	C ₁₉ H ₄₀	Nonadecane	268.521	629-92-5	[7]			57,71,85	2	[5]	2	5	2	[6]		
20	3.66E+05	C ₂₀ H ₄₂	Icosane	282.547	112-95-8	[7]	5.8 E ⁻⁶		57,71,85	2	[5]	2	3	2	[6]		
21	9.11E+05	C ₂₁ H ₄₄	Henticosane	296.574	629-94-7	[7]			57,71,85	2	[5]	2	2	2	[6]		
22	2.28E+06	C ₂₂ H ₄₆	Docosane	310.6	629-97-0	[7]			57,71,85	2	[5]	2	1	2	[6]		
23	5.73E+06	C ₂₃ H ₄₈	Tricosane	324.627	638-67-5	[7]			57,71,85	2	[5]	2	0.5	1	[6]		
24	1.45E+07	C ₂₄ H ₅₀	Tetracosane	338.654	646-31-1	[7]			57,71,85	2	[5]	2	0.2	1	[6]		
25	3.68E+07	C ₂₅ H ₅₂	Pentacosane	352.681	629-99-2	[7]			57,71,85	1	[5]	1	—	1	[6]		
26	9.38E+07	C ₂₆ H ₅₄	Hexacosane	366.707	630-01-3	[7]			57,71,85	1	[5]	1	—	1	[6]		
27	2.40E+08	C ₂₇ H ₅₆	Heptacosane	380.734	593-49-7	[7]			57,71,85	1	[5]	1	—	0.5	[6]		
28	6.17E+08	C ₂₈ H ₅₈	Octacosane	394.761	630-02-4	[7]			57,71,85	1	[5]	1	—	0.5	[6]		
29	1.59E+09	C ₂₉ H ₆₀	Nonacosane	408.786	630-03-5	[7]			57,71,85	1	[5]	1	—	—	[6]		
30	4.11E+09	C ₃₀ H ₆₂	Triacontane	422.813	638-68-6	[7]			57,71,85	1	[5]	1	—	—	[6]		

^aApproximate sign (~) indicates solubility values are variable.

^bASMB is Alberta Sweet Mixed Blend crude oil.

^cANS is Alaska North Slope crude oil.

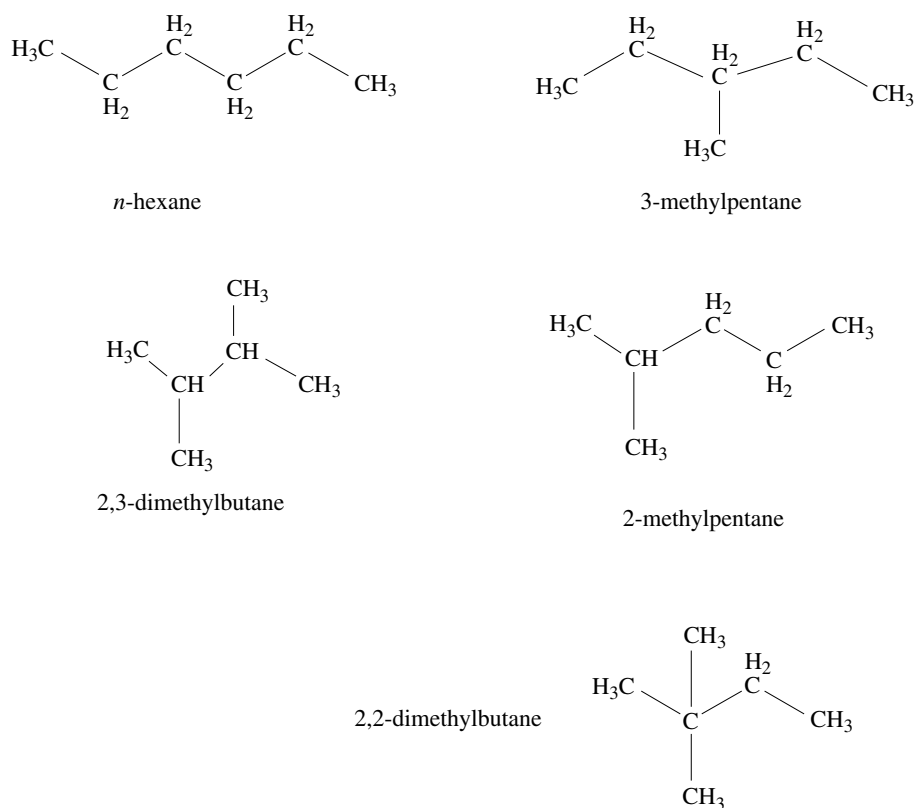


FIGURE 3.3 Illustration of the number of structural isomers for hexane. As the carbon number increases, the number of isomers goes up exponentially.

TABLE 3.3 Gross composition of some crude oils and petroleum products (all values in percent)

	ANS	Arabian Heavy	Arabian Light	ASMB	Cook Inlet	Diesel fuel	Fuel #5	Heavy fuel	Mars TLP
<i>Saturates</i>	75	60.1	75.5	77.3	66.7	88.2	44.2	42.5	58.4
<i>n</i> -alkanes	6.3	7.3	8.5	7.9	7.9	12	3.7	2.8	4.9
<i>Aromatics</i>	15	24.6	15.2	16.8	25.2	10.2	39.5	29	27.5
BTEX and C3	2.2	0.1	1.1	3.1	0.2	1.9	0.3	0.2	0.2
PAHs	1.1	0.9	0.8	1.1	1.2	3	5.6	2.8	1
Estimated UCM ^a		65.7			69.1				
Estimated remainder		10.7			13.5				
<i>Resins</i>	6.1	6.3	5.7	4.2	5.1	1.7	8	15.5	9.5
<i>Asphaltenes</i>	4	9	3.6	1.7	3.1	0	8.4	13	4.7

	Maya	Orimulsion	Platform Elly	Prudhoe Bay	Sockeye	South Louisiana	South Louisiana	Troll	West Delta Block 143	West Texas
<i>Saturates</i>	46.5	44.6	34.6	60.8	49.2	80.8	79.4	66.9	61	78.5
<i>n</i> -alkanes	6.2	0	2.2	6.3	2.6	5.9	7.4	3.6	5.5	9.5
<i>Aromatics</i>	25.4	27.3	32.4	28.3	17.2	12.6	16.9	26.6	26.6	14.8
BTEX and C3	0.1	0	0.1	0.2	0.8	1.2	0.3	0.2	0.2	3.4
PAHs	0.9	0.2	0.4	1.8	0.5	0.9	1.3	1.7	0.9	7.8
Estimated UCM ^a			58.3				76.3	78.9		
Estimated remainder			6				11	9.1		
<i>Resins</i>	12.7	13.3	19.4	7.7	15.1	5.9	3.4	5.8	8.9	6
<i>Asphaltenes</i>	15.5	14.8	13.6	3.2	18.5	0.8	0.4	0.7	3.6	0.7

^aUCM is the GC-unresolved complex molecules as calculated from Wang and Brown [12], by estimating that TPH consists of the total saturates and aromatics.

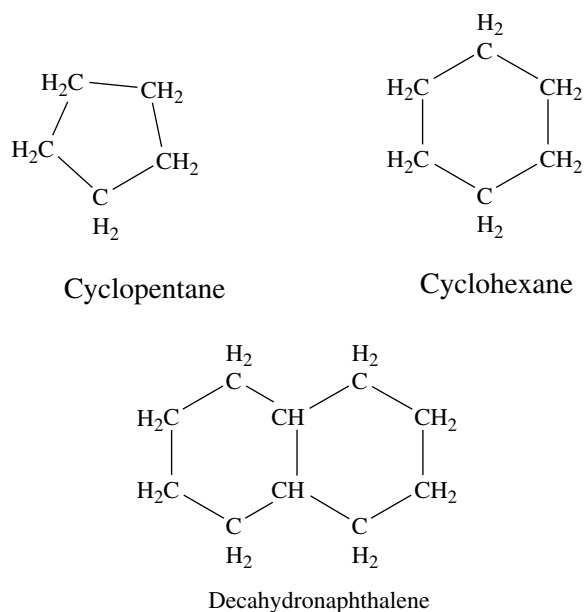


FIGURE 3.4 Typical base structures for cycloalkanes.

3.2.1.3 Aromatic Compounds The aromatic compounds have at least one benzene ring of six carbons. Three carbon-to-carbon double bonds float around the ring, and all six carbons are equivalent and thus provide high stability to the ring. Because of this stability, benzene rings are highly persistent and can have toxic effects on the environment. The most common smaller aromatic compounds found in oil are often referred to as BTEX, or benzene, toluene, ethylbenzene, and xylenes. BTEX compounds and data on them are shown in Table 3.5. Polyaromatic hydrocarbons (PAHs) are compounds consisting of at least two benzene rings. PAHs make up between 0 and 60% of the composition of oil. Common PAHs and their substituted counterparts are shown in Table 3.6. As these are easily separated, there are much data on their presence in oils. These compounds have also been used somewhat as indicators of presence of certain types of oils. There exists a set of compounds designated by the U.S. EPA as priority PAHs [5]. The list of 16 EPA-priority chemicals is shown in Table 3.7, and the list of 34 EPA-priority chemicals is shown in Table 3.8. The concern with these compounds is that many of them are known to be relatively toxic and some to be carcinogenic as indicated in Table 3.7.

Aromatic compounds have the general formula C_nH_{2n-6r} , where r is the number of rings. The amount of aromatics in a typical crude oil varies, but ranges from 0 to 15%. Aromatics are frequently concentrated by distillation in the refining processes into the heavier or residual fractions. Diesel fuel typically contains 5–25% aromatics, while gasoline contains 25–40% aromatics, mostly BTEX compounds. In crude oils, the alkylated compounds occur more frequently than the parent unalkylated rings. This can be of use in identifying the source of contamination as many

PAH pollution sources have more abundant parent compounds than alkylated ones.

3.2.1.4 Naphthenoaromatic Compounds There exists a series of compounds that contain aromatic and cyclic alkane rings. These are not typically analyzed for either petroleum or environmental purposes, and thus there are not a large amount of data on their contents in crude oils or in petroleum products. Table 3.9 shows some of the naphthenoaromatic compounds found in crude oils and petroleum products.

3.2.2 Sulfur Compounds

Sulfur compounds constitute a significant percentage of some crude oils and are also found in petroleum products as an unwanted contaminant [4]. The sulfur compounds found in oils and petroleum are generally found as one of the following four groups:

1. Mercaptans or thiols, with the general structure of $H-S-R$, where R is another hydrocarbon group,
2. Sulfides, with the general structure of $R-S-R$,
3. Thiophenes, with a general structure of a five-membered ring with sulfur as one leg and with two double bonds, or
4. As part of an asphaltene structure, structures which are unknown.

Dibenzothiophenes, as shown in Table 3.10, are often used as forensic markers to track oil spills [6,12]. Table 3.10 also shows the typical sulfur compounds found in oils.

Guadalupe analyzed oils for total sulfur and sulfides [13]. Table 3.11 shows a summary of the results. This table shows that the sulfides and asphaltenes correlate with the total sulfur found in the oil. Nishioka and Tomich developed a method for analyzing oils for thiols noting that many thiols had not yet been identified [14].

Most sulfur compounds in oil are foul-smelling and corrosive. The presence of these compounds lowers the price of the crude oils, as sulfur compounds have to be removed before or during refining. In recent years, the standards for the sulfur content of fuels have been lowered, increasing the expense of refining.

3.2.3 Oxygen Compounds

Oxygen compounds are found in oils and petroleum. Measurement of these compounds is not frequent as they do not have known forensic capability, because they are soluble in water, and because they are more difficult to measure than many hydrocarbons. The common groups of oxygen compounds found in oils are as follows:

1. Naphthenic acids or their salts,
2. Phenols and phenolic compounds,

TABLE 3.4 Cycloalkanes found in oil and petroleum

Carbon number	Formula	IUPAC name	Molecular weight	CAS number	Reference	Solubility in water ^a g/l	Reference	Levels in troll oil µg/g oil	Reference
5	C ₅ H ₁₀	Cyclopentane	70.133	287-92-3	[7]	0.16	[8]	1220	[11]
6	C ₆ H ₁₂	Methylcyclopentane	84.159	96-37-7	[7]	4.1 E ⁻²	[8]	4770	[11]
7	C ₇ H ₁₄	Dimethylcyclopentane	98.186	1	[7]				
8	C ₈ H ₁₆	Trimethylcyclopentane	112.21	2	[7]	~3.7 E ⁻³	[8]		
6	C ₆ H ₁₂	Cyclohexane	84.159	110-82-7	[7]	5.5 E ⁻²	[8]	8180	[11]
7	C ₇ H ₁₄	Methylcyclohexane	98.186	108-87-2	[7]	~1.6 E ⁻²	[8]	18,400	[11]
8	C ₈ H ₁₆	Dimethylcyclohexane	112.213	3	[7]	6 E ⁻³	[8]		
8	C ₈ H ₁₆	Ethylcyclohexane	112.213	1678-91-7	[7]	<6 E ⁻³	[8]		
9	C ₉ H ₁₈	Trimethylcyclohexane	126.239	4	[7]	1.7 E ⁻³	[8]		
10	C ₁₀ H ₁₈	<i>cis</i> -Decahydronaphthalene	138.25	493-01-6	[7]	~8.5 E ⁻⁴	[8]		
10	C ₁₀ H ₁₈	<i>trans</i> -Decahydronaphthalene	138.25	493-02-7	[7]	~8.5 E ⁻⁴	[8]		

^aApproximate sign (~) indicates solubility values are variable.

1 CAS numbers for dimethylcyclopentanes: 1,1—1638-26-2; *cis*-1,2—1192-18-3; *trans*-1,2—822-50-4; *cis*-1,3—2532-58-3; *trans*-1,3—1759-58-6.

2 CAS numbers for trimethylcyclopentanes: 1,1,3—4516-69-2; 1α,2α,4β-1,2,4—4850-28-6; 1α,2β,4α-1,2,4—16883-48-0.

3 CAS numbers for dimethylcyclohexanes: 1,1—590-66-9; *cis*-1,2—2207-01-4; *trans*-1,2—6876-23-9; *cis*-1,3—638-04-0; *trans*-1,3—2207-03-6; *cis*-1,4—624-29-3; *trans*-1,4—2207-04-7.

4 CAS numbers for trimethylcyclohexanes: 1,1,2—7094-26-0; 1,1,3—3073-66-3; 1α,2β,4β-1,2,4—7667-60-9; 1α,3α,5β-1,3,5—1795-26-2.

TABLE 3.5 BTEX compounds found in oils and petroleum

Carbon number	Name	Formula	Molecular weight	CAS number	Reference	Solubility in water ^a g/l	Reference	Levels in				Levels in			
								SIMS	ASMB µg/g oil	Reference	ANS µg/g oil	Levels in diesel fuel µg/g oil	heavy fuel oil µg/g oil	Reference	Levels in troll oil µg/g oil
6	Benzene	C ₆ H ₆	78.112	71-43-2	[7]	~1.8	[8]	78	2300	6	2900	140	40	[6]	510
7	Toluene	C ₇ H ₈	92.139	108-88-3	[7]	0.5–0.6	[8]	92	5300	6	5900	1000	140	[6]	3120
8	Ethyl-benzene	C ₈ H ₁₀	106.165	100-41-4	[7]	0.15–0.2	[8]	106	1600	6	1300	620	60	[6]	1790
8	<i>m</i> -Xylene	C ₈ H ₁₀	106.165	108-38-3	[7]	0.14–0.16	[8]	106	8900 ^b	6	6200 ^b	3800 ^b	400 ^b	[6]	5710
8	<i>o</i> -Xylene	C ₈ H ₁₀	106.165	95-47-6	[7]	0.17–0.2	[8]	106	—	6	—	—	—	[6]	1800
8	<i>p</i> -Xylene	C ₈ H ₁₀	106.165	106-42-3	[7]	~0.16	[8]	106	—	6	—	—	—	[6]	1790
9	1,2,3-trimethyl-benzene	C ₉ H ₁₂	120.191	526-73-8	[7]	~7 E ⁻²	[8]	120	1200 ^b	6	5600 ^b	14,800 ^b	940 ^b	[6]	800
9	1,2,4-trimethyl-benzene	C ₉ H ₁₂	120.191	95-63-6	[7]	5.9 E ⁻²	[8]	120	—	6	—	—	—	[6]	2660
9	1,3,5-trimethyl-benzene	C ₉ H ₁₂	120.191	108-67-8	[7]	~5 E ⁻²	[8]	120	—	6	—	—	—	[6]	1250
9	1-ethyl-2-methyl-benzene	C ₉ H ₁₂	120.191	611-14-3	[7]	~7.5 E ⁻²	[8]	120	—	6	—	—	—	[6]	—
9	1-ethyl-3-methyl-benzene	C ₉ H ₁₂	120.191	—	[7]	—	—	120	—	6	—	—	—	[6]	—
9	1-ethyl-4-methyl-benzene	C ₉ H ₁₂	120.191	622-96-8	[7]	—	—	120	—	6	—	—	—	[6]	—
9	Iso-propyl-benzene	C ₉ H ₁₂	120.191	98-82-8	[7]	5–6 E ⁻²	[8]	120	—	6	—	—	—	[6]	—
9	Propyl-benzene	C ₉ H ₁₂	120.191	103-65-1	[7]	~5 E ⁻²	[8]	120	—	6	—	—	—	[6]	630
10	1,2,3,4-tetramethyl-benzene	C ₁₀ H ₁₄	134.218	488-23-3	[7]	—	—	134	—	6	—	—	—	[6]	—
10	1,2,3,5-tetramethyl-benzene	C ₁₀ H ₁₄	134.218	537-53-7	[7]	—	—	134	—	—	—	—	—	—	—
10	1,2,4,5-tetramethyl-benzene	C ₁₀ H ₁₄	134.218	95-93-2	[7]	3.5 E ⁻³	[8]	134	—	—	—	—	—	—	—
10	1,2-diethyl-benzene	C ₁₀ H ₁₄	134.218	135-01-3	[7]	~7 E ⁻²	[8]	134	—	—	—	—	—	—	—
10	1,3-diethyl-benzene	C ₁₀ H ₁₄	134.218	141-93-5	[7]	—	—	134	—	—	—	—	—	—	—
10	1,4-diethyl-benzene	C ₁₀ H ₁₄	134.218	105-5-5	[7]	~2.5 E ⁻²	[8]	134	—	—	—	—	—	—	—
10	1-ethyl-2,4-dimethyl-benzene	C ₁₀ H ₁₄	134.218	874-41-9	[7]	—	—	134	—	—	—	—	—	—	—
10	1-ethyl-3,5-dimethyl-benzene	C ₁₀ H ₁₄	134.218	934-74-7	[7]	—	—	134	—	—	—	—	—	—	—
10	1-methyl-2-propyl-benzene	C ₁₀ H ₁₄	134.218	1074-17-5	[7]	~1 E ⁻²	[8]	134	—	—	—	—	—	—	—
10	1-methyl-3-propyl-benzene	C ₁₀ H ₁₄	134.218	1074-43-7	[7]	~1 E ⁻²	[8]	134	—	—	—	—	—	—	—
10	1-methyl-4-propyl-benzene	C ₁₀ H ₁₄	134.218	1074-55-1	[7]	~1 E ⁻²	[8]	134	—	—	—	—	—	—	—
10	2-ethyl-1,3-dimethyl-benzene	C ₁₀ H ₁₄	134.218	2870-04-4	[7]	—	—	134	—	—	—	—	—	—	—

10	2-ethyl-1,4-dimethyl-benzene	C ₁₀ H ₁₄	134.218	1758-88-9	[7]		134	
10	3-ethyl-1,2-dimethyl-benzene	C ₁₀ H ₁₄	134.218	933-98-2	[7]		134	
10	4-ethyl-1,2-dimethyl-benzene	C ₁₀ H ₁₄	134.218	934-80-5	[7]		134	
10	Butyl-benzene	C ₁₀ H ₁₄	134.218	104-51-8	[7]	1.2-1.4 E ⁻²	134	
10	Sec-butyl benzene	C ₁₀ H ₁₄	134.218	135-98-8	[7]	1.1-1.8 E ⁻²	134	230 [11]
10	Iso-butyl benzene	C ₁₀ H ₁₄	134.218	538-93-2	[7]		134	
10	<i>m</i> -Cymene	C ₁₀ H ₁₄	134.218	535-77-3	[7]		134	
10	<i>p</i> -Cymene	C ₁₀ H ₁₄	134.218	99-87-6	[7]	~3 E ⁻²	134	
10	Tert-butyl-benzene	C ₁₀ H ₁₄	134.218	98-06-6	[7]	1.8-3 E ⁻²	134	
11	Pentyl-benzene	C ₁₁ H ₁₆	148.245	538-68-1	[7]		148	
11	Iso-pentyl-benzene	C ₁₁ H ₁₆	148.245	2049-94-7	[7]	~3.5 E ⁻³	148	120 [11]
11	Diethyl-trimethyl-benzene	C ₁₁ H ₁₆	148.245		[7]		148	
11	Ethyl-tetramethyl-benzene	C ₁₁ H ₁₆	148.245		[7]		148	
11	Methyl-diethyl-benzene	C ₁₁ H ₁₆	148.245		[7]		148	
11	Methyl-butyl-benzene	C ₁₁ H ₁₆	148.245		[7]		148	
11	Pentamethyl-benzene	C ₁₁ H ₁₆	148.245	700-12-9	[7]	~1.5 E ⁻²	148	
12	C6-benzenes	C ₁₂ H ₁₈	162.271	1077-16-3 ^c	[7]		162	
13	C7-benzenes	C ₁₄ H ₂₀	176.298	1078-71-3 ^c	[7]		176	
14	C8-benzenes	C ₁₆ H ₂₂	190.325	2189-60-8 ^c	[7]		190	

^aApproximate sign (~) indicates solubility values are variable; a range indicates the range of values.

^bQuantitation for all isomers of these compounds.

^cCAS number is applicable to simplest aliphatic compound only.

TABLE 3.6 PAHs and alkylated PAHs found in oils and petroleum

Carbon number	Number of rings	Name	Formula	Abbreviation	Molecular weight	CAS number	Reference	Solubility in water ^a g/l	Reference	SIMS	Levels in ASMB $\mu\text{g/g oil}$	Reference	Levels in ANS $\mu\text{g/g oil}$	Levels in diesel fuel $\mu\text{g/g oil}$	Levels in heavy fuel oil $\mu\text{g/g oil}$	Reference
10	2	Naphthalene	C_{10}H_8	C_N	128.717	91-20-3	[7]	$30\text{--}30\text{ E}^{-3}$	[10]	128	680	[5]	260	820	140	[6]
11	2	Methyl-naphthalene	$\text{C}_{11}\text{H}_{10}$	C_N	142.197	1	[7]	$26\text{--}28\text{ E}^{-3}$	[10]	142	1180	[5]	1000	3700	1300	[6]
12	2	Dimethyl-naphthalene	$\text{C}_{12}\text{H}_{12}$	C_N	156.233	2	[7]	$\sim 2.4\text{ E}^{-3}$	[10]	156	1600	[5]	1800	7000	2900	[6]
12	2	Ethyl-naphthalene	$\text{C}_{12}\text{H}_{12}$	C_N	156.233	3	[7]	$\sim 1\text{ E}^{-2}$	[8]	156	1600	[5]	1800	7000	2900	[6]
13	2	C3-naphthalenes	$\text{C}_{13}\text{H}_{14}$	C_N	170.25	4	[7]	$\sim 1.6\text{ E}^{-3}$	[10]	170	1560	[5]	1700	6600	2900	[6]
14	2	C4-naphthalenes	$\text{C}_{14}\text{H}_{16}$	C_N			[7]			184	450	[5]	820	2800	1400	[6]
14	3	Phenanthrene	$\text{C}_{14}\text{H}_{10}$	C_P	178.229	85-01-8	[7]	$\sim 1\text{ E}^{-3}$	[8]	178	170	[5]	210	440	420	[6]
15	3	C1-phenanthrenes	$\text{C}_{15}\text{H}_{12}$	C_P	192.256	5	[7]	$\sim 7\text{ E}^{-5}$	[8]	192	400	[5]	670	1000	1900	[6]
16	3	C2-phenanthrenes	$\text{C}_{16}\text{H}_{14}$	C_P			[7]			206	400	[5]	710	620	2900	[6]
17	3	C3-phenanthrenes	$\text{C}_{17}\text{H}_{16}$	C_P			[7]			220	160	[5]	490	190	3100	[6]
18	3	C4-phenanthrenes	$\text{C}_{18}\text{H}_{16}$	C_P			[7]			234	60	[5]	300	50	2200	[6]
12	3	Dibenzothiophene	$\text{C}_{12}\text{H}_8\text{S}$	C_D	184.257	132-65-0	[7]	5 E^{-4}	[8]	184	200	[5]	120	70	100	[6]
13	3	C1-dibenzothiophenes	$\text{C}_{13}\text{H}_{10}\text{S}$	C_D			[7]			198	370	[5]	230	110	320	[6]
14	3	C2-dibenzothiophenes	$\text{C}_{14}\text{H}_{12}\text{S}$	C_D			[7]			212	450	[5]	320	100	620	[6]
15	3	C3-dibenzothiophenes	$\text{C}_{15}\text{H}_{14}\text{S}$	C_D			[7]			226	220	[5]	270	40	700	[6]
13	3	Fluorene	$\text{C}_{13}\text{H}_{10}$	C_F	166.218	86-73-7	[7]	$\sim 8\text{ E}^{-5}$	[10]	166	50	[5]	140	570	220	[6]
14	3	C1-fluorenes	$\text{C}_{14}\text{H}_{12}$	C_F	180.245	6	[7]			180	110	[5]	330	800	570	[6]
15	3	C2-fluorenes	$\text{C}_{15}\text{H}_{14}$	C_F			[7]			194	150	[5]	450	760	1000	[6]
16	3	C3-fluorenes	$\text{C}_{16}\text{H}_{16}$	C_F			[7]			208	85	[5]	380	360	940	[6]
18	4	Chrysene	$\text{C}_{18}\text{H}_{12}$	C_C	228.288	218-01-9	[7]	$\sim 1.5\text{ E}^{-6}$	[10]	228	25	[5]	50	<1	380	[6]
19	4	C1-chrysenes	$\text{C}_{19}\text{H}_{14}$	C_C	242.314	7	[7]			242			70	<1	1200	[6]
20	4	C2-chrysenes	$\text{C}_{20}\text{H}_{16}$	C_C			[7]			256			100	<1	1800	[6]
21	4	C3-chrysenes	$\text{C}_{21}\text{H}_{18}$	C_C			[7]			270			80		1400	[6]
20	5	Perylene	$\text{C}_{20}\text{H}_{12}$		252.309	198-55-0	[7]	$\sim 4\text{ E}^{-7}$	[10]	252						

^aApproximate sign (~) indicates solubility values are variable; a range indicates the range of values.

1 CAS numbers for methyl-naphthalenes: **1**—90-12-0; **2**—91-57-6.

2 CAS numbers for dimethyl-naphthalenes: **1,2**—573-98-8; **1,3**—575-41-7; **1,4**—571-58-4; **1,5**—571-61-9; **1,6**—575-43-9; **1,7**—575-37-1; **1,8**—569-41-5; **2,3**—581-40-8; **2,6**—581-42-0; **2,7**—582-16-1.

3 CAS numbers for ethyl-naphthalenes: **1**—1127-76-0; **2**—939-27-5.

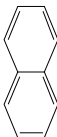
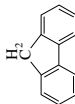
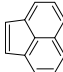
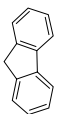
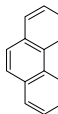
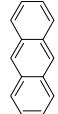
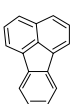
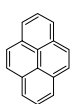
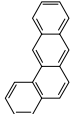
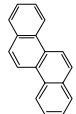
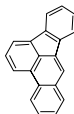
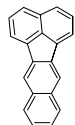
4 CAS numbers for 1,4,5-trimethyl-naphthalene: 2131-41-1.

5 CAS numbers for methyl-phenanthrenes: **1**—832-69-9; **3**—832-71-3; **4**—832-64-4.

6 CAS numbers for methyl-fluorenes: **1**—1730-37-6; **9**—2523-37-7.

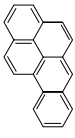
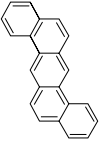
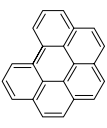
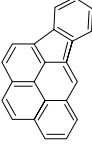
7 CAS numbers for methyl-chrysenes: **3**—3351-31-3; **5**—3697-24-3; **6**—1705-85-7.

TABLE 3.7 EPA top 16 priority PAHs

Compound	Molecular formula	Structure	CAS no.	MW	Reference	Human ^a carcinogenicity	Solubility in water ^b µg/l	Levels in			Levels in				
								Reference	SIMS µg/g oil	ASMB µg/g oil	Reference	Levels in ANS µg/g oil	Levels in diesel fuel µg/g oil	Levels in heavy fuel oil µg/g oil	
Naphthalene	C ₁₀ H ₈		91-20-3	128.171	[7]		~3.5 E ⁻²	[8]	128	250	[6]	260	820	140	[6]
Acenaphthene	C ₁₂ H ₁₀		83-32-9	154.207	[7]		3.4 E ⁻³	[8]	153	16	[6]	13	150	90	[6]
Acenaphthylene	C ₁₂ H ₈		208-96-8	152.192	[7]		~4 E ⁻³	[8]	152	8	[6]	12	35	20	[6]
Fluorene	C ₁₃ H ₁₀		86-73-7	166.218	[7]		~2 E ⁻³	[8]	166	80	[6]	140	560	220	[6]
Phenanthrene	C ₁₄ H ₁₀		85-01-8	178.229	[7]		~1 E ⁻³	[8]	178	140	[6]	210	440	420	[6]
Anthracene	C ₁₄ H ₁₀		120-12-7	178.229	[7]		4-7 E ⁻⁵	[8]	178	2	[6]	3	13	95	[6]
Fluoranthene	C ₁₆ H ₁₀		206-44-0	202.25	[7]		2.7 E ⁻⁴	[8]	202	2	[6]	3	7	40	[6]
Pyrene	C ₁₆ H ₁₀		129-00-0	202.25	[7]		0.9-1.4 E ⁻⁴	[8]	202	18	[6]	8	31	230	[6]
Benz(a)anthracene	C ₁₈ H ₁₂		56-55-3	228.288	[7]	2	0.9-1.3 E ⁻⁵	[8]	228	3	[6]	5	0.3	200	[6]
Chrysene	C ₁₈ H ₁₂		218-01-9	228.288	[7]	1	2-1.6 E ⁻⁶	[8]	228	30	[6]	50	<1	380	[6]
Benzo(b)fluoranthene	C ₂₀ H ₁₂		205-99-2	252.309	[7]	3	~1.5 E ⁻⁶	[8]	252	3	[6]	5	0	50	[6]
Benzo(k)fluoranthene	C ₂₀ H ₁₂		207-08-9	252.309	[7]		~1 E ⁻⁶	[8]	252	3	[6]	1	0	10	[6]

(continued)

TABLE 3.7 (Continued)

Compound	Molecular formula	Structure	CAS no.	MW	Reference	Human ^a carcinogenicity	Solubility in water ^b µg/l	Reference	SIMS	Levels in ASMB µg/g oil	Reference	Levels in ANS µg/g oil	Levels in diesel fuel µg/g oil	Levels in heavy fuel oil µg/g oil	Reference
Benzo(a)pyrene	C ₂₀ H ₁₂		50-32-8	252.309	[7]	4	1.4–3.8 E ⁻⁶	[8]	252	1	[6]	2	0	150	[6]
Dibenz(a,h)anthracene	C ₂₂ H ₁₄		53-70-3	278.346	[7]	4	~1 E ⁻⁶	[8]	278	1	[6]	1	0	20	[6]
Benzo(g,h,i)perylene	C ₂₂ H ₁₂		191-24-2	276.33	[7]		1.8–2.6 E ⁻⁷	[8]	276	3	[6]	3	0	30	[6]
Indeno(1,2,3-cd)pyrene	C ₂₂ H ₁₂		193-39-5	276.33	[7]	2	~2 E ⁻⁷	[8]	276	1	[6]	0.1	0	10	[6]

^aCarcinogenic potency: 1 is a suspected carcinogen, 4 is a known potent carcinogen.^bApproximate sign (~) indicates solubility values are variable; a range indicates the range of values.

TABLE 3.8 EPA 34 priority PAHs

Carbon number	Number of rings	Name	Formula	Abbreviation	Molecular weight	CAS number	Reference	Solubility in water ^a g/l	Reference	U.S. EPA toxicity value ^b	SIMS	Levels in ASMB µg/g oil	Reference	Levels in ANS µg/g oil	Levels in diesel fuel µg/g oil	Levels in heavy fuel oil µg/g oil	Reference
10	2	Naphthalene	C ₁₀ H ₈	NAP	128.171	91-20-3	[7]	~3.5 E-2	[7]	193.47	128	680	[5]	260	820	140	[6]
11	2	1-methyl-naphthalene	C ₁₁ H ₁₀	1MN	142.197	90-12-0	[7]	~2.8 E-2	[7]	72.16	142						
11	2	2-methyl-naphthalene	C ₁₁ H ₁₀	2MN	142.197	91-57-6	[7]	~1.8 E-2	[7]	75.37	142						
12	2	C2-naphthalenes	C ₁₂ H ₁₂	C ₂ N	156.233	1	[7]	1-8 E-3	[7]	30.24	156	1600	[5]	1800	7000	2900	[6]
13	2	C3-naphthalenes	C ₁₃ H ₁₄	C ₃ N	170.25	2	[7]	~2 E-3	[7]	11.1	170	1560	[5]	1700	6600	2900	[6]
14	2	C4-naphthalenes	C ₁₄ H ₁₆	C ₄ N	182.25					4.05	184	450	[5]	820	2800	1400	[6]
12	2	Acenaphthene	C ₁₂ H ₁₀	ACE	154.207	83-32-9	[7]	3.4 E-3	[7]	306.85							
12	2	Acenaphthylene	C ₁₂ H ₈	ACEY	152.192	208-96-8	[7]	~4 E-3	[7]	55.85							
13	3	Fluorene	C ₁₃ H ₁₀	FLU	166.218	86-73-7	[7]	~2 E-3	[7]	39.3	166	50	[5]	140	570	220	[6]
14	3	C1-fluorenes	C ₁₄ H ₁₂	C1F	180.245	3	[7]	~1 E-3	[7]	13.99	180	110	[5]	330	800	570	[6]
15	3	C2-fluorenes	C ₁₅ H ₁₄	C2F						5.3	194	150	[5]	450	760	1000	[6]
16	3	C3-fluorenes	C ₁₆ H ₁₆	C3F						1.92	208	85	[5]	380	360	940	[6]
14	3	Anthracene	C ₁₄ H ₁₀	ANT	178.229	120-12-7	[7]	~1 E-3	[7]	19.13	178	2	[6]	3	13	95	[6]
14	3	Phenanthrene	C ₁₄ H ₁₀	PHE	178.229	85-01-8	[7]	2.7 E-4	[7]	20.72	178	170	[5]	210	440	420	[6]
15	3	C1-phenanthrenes	C ₁₅ H ₁₂	C1P	192.256	4	[7]	~2.7 E-4	[7]	7.44	192	400	[5]	670	1000	1900	[6]
16	3	C2-phenanthrenes	C ₁₆ H ₁₄	C2P						3.2	206	400	[5]	710	620	2900	[6]
17	3	C3-phenanthrenes	C ₁₇ H ₁₆	C3P						1.26	220	160	[5]	490	190	3100	[6]
18	3	C4-phenanthrenes	C ₁₈ H ₁₆	C4P						0.56	234	60	[5]	300	50	2200	[6]
16	4	Fluoranthene	C ₁₆ H ₁₀	FLUOA	202.25	206-44-0	[7]	2.7 E-4	[7]	7.11	202	2	[6]	3	7	40	[6]
16	4	Pyrene	C ₁₆ H ₁₀	PYR	202.25	129-00-0	[7]	0.9-1.4 E-4	[7]	10.11	202	18	[6]	8	31	230	[6]
17	4	C1-fluoranthenes/pyrene	C ₁₇ H ₁₂	C1FP	216.277	5	[7]			4.89							
18	4	Chrysene	C ₁₈ H ₁₂	CHR	228.288	218-01-9	[7]	2-1.6 E-6	[7]	2.04	228	25	[5]	50	<1	380	[6]
19	4	C1-chrysenes	C ₁₉ H ₁₄	C1C	242.314	6	[7]	~6 E-5	[7]	0.86	242			70	<1	1200	[6]
20	4	C2-chrysenes	C ₂₀ H ₁₆	C2C				~3 E-5		0.48	256			100	<1	1800	[6]
21	4	C3-chrysenes	C ₂₁ H ₁₈	C3C						0.17	270			80		1400	[6]
18	4	Benz(a)anthracene	C ₁₈ H ₁₂	BAA	228.288	56-55-3	[7]	0.9-1.3 E-5	[7]	2.23	228	3	[6]	5	0.3	200	[6]
20	5	Pyrene	C ₂₀ H ₁₂	PER	252.309	198-55-0	[7]	4 E-7	[7]	0.9	252	1	[6]	2	0	150	[6]
20	5	Benzo(a)pyrene	C ₂₀ H ₁₂	BAP	252.309	50-32-8	[7]	1.4-3.8 E-6	[7]	0.65	252						
20	5	Benzo(e)pyrene	C ₂₀ H ₁₂	BEP	252.309	192-97-2	[7]		[7]	0.9	252						
20	5	Benzo(b)fluoranthene ^c	C ₂₀ H ₁₂	BBF	252.309	205-99-2	[7]	~1.5 E-6	[7]	0.96	252	3	[6]	5	0	50	[6]
20	5	Benzo(k)fluoranthene ^c	C ₂₀ H ₁₂	BKF	252.309	207-08-9	[7]	~1 E-6	[7]	0.96	252	3	[6]	1	0	10	[6]
22	5	Dibenz(a,h)anthracene	C ₂₂ H ₁₄	DAH	278.346	53-70-3	[7]	~1 E-6	[7]	0.27	278	1	[6]	1	0	20	[6]

(continued)

TABLE 3.8 (Continued)

Carbon number	Number of rings	Name	Formula	Abbreviation	Molecular weight	CAS number	Solubility in water ^a	U.S. EPA toxicity value ^b	Levels in ASMB µg/g oil	Levels in ANS µg/g oil	Levels in diesel fuel µg/g oil	Levels in heavy fuel oil µg/g oil	Reference
22	6	Indeno(1,2,3-cd)pyrene	C ₂₂ H ₁₂	IND	276.33	193-39-5	[7] ~2 E ⁻⁷	[8] 0.28	1	0.1	0	10	[6]
22	6	Benzo(g,h,i)perylene	C ₂₂ H ₁₂	BGP	276.33	191-24-2	[7] 1.8-2.6 E ⁻⁷	[8] 0.44	3	3	0	30	[6]

^aApproximate sign (~) indicates solubility values are variable; a range indicates the range of values.

^bU.S. EPA Chronic Toxicity Value taken from EPA, 2003—smaller numbers indicate higher toxicity.

^cThese two compounds are combined for EPA-34 considerations.

1 CAS numbers for dimethyl-naphthalenes: **1,2**—573-98-8; **1,3**—575-41-7; **1,4**—571-58-4; **1,5**—571-61-9; **1,6**—575-43-9; **1,7**—575-37-1; **1,8**—569-41-5; **2,3**—581-40-8; **2,6**—581-42-0; **2,7**—582-16-1. CAS numbers for ethyl-naphthalenes: **1**—1127-76-0; **2**—939-27-5.

2 CAS numbers for 1,4,5-trimethyl-naphthalene: **2131-41-1**.

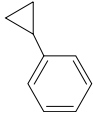
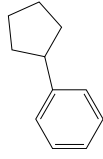
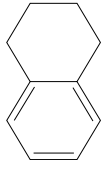
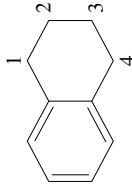
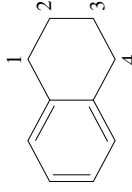
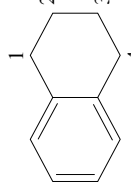
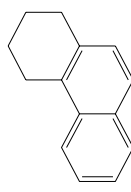
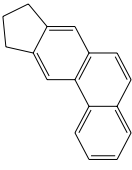
3 CAS numbers for methyl-fluorenes: **1**—1730-37-6; **9**—2523-37-7.

4 CAS numbers for methyl-phenanthrenes: **1**—832-69-9; **3**—832-71-3; **4**—832-64-4.

5 CAS numbers for methyl-pyrenes: **1**—2381-21-7; **2**—3442-78-2.

6 CAS numbers for methyl-chrysenes: **3**—3351-31-3; **5**—3697-24-3; **6**—1705-85-7.

TABLE 3.9 Naphthenoaromatic compounds found in oils

Compound	Molecular formula	Structure	CAS no.	MW	Reference	Solubility in water g/l ^a	Reference	SIMS
Cyclopropylbenzene	C ₉ H ₁₀		873-49-4	118.175	7			118
Cyclopentylbenzene	C ₁₁ H ₁₄		700-88-9	146.229	7			146
1,2,3,4-tetrahydronaphthalene (tetralin)	C ₁₀ H ₁₂		119-64-2	132.202	7	~0.045	8	132
Methyl-1,2,3,4-tetrahydronaphthalene	C ₁₁ H ₁₄		1	146.229	7			146
Dimethyl-1,2,3,4-tetrahydronaphthalene	C ₁₁ H ₁₄		2	160.255	7			160
Trimethyl-1,2,3,4-tetrahydronaphthalene	C ₁₁ H ₁₄		3	174.282	7			174
1,2,3,4-tetrahydraphenanthrene	C ₁₄ H ₁₄		1013-08-7	182.261	7			182
Cyclopentanophenanthrene	C ₁₇ H ₁₄							

^a Solubility values are given as about or approximate if there is variance in the quoted values.

1 CAS number for 1-methyl-1,2,3,4-tetrahydronaphthalene—1559-81-5; 5-methyl—2809-64-5; 6-methyl—1680-561-9.

2 CAS number for 1,5-methyl-1,2,3,4-tetrahydronaphthalene—21564-91-0.

3 CAS number for 1,1,6-methyl-1,2,3,4-tetrahydronaphthalene—475-03-6.

TABLE 3.10 Sulfur compounds found in oils

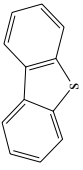
Carbon number	Number of rings	Name	Formula	Molecular weight	CAS number	Reference	Solubility in water g/l	Reference
<i>Sulfides</i>								
2		Dimethyl sulfide	C ₂ H ₆ S	62.134	75-18-3	[7]	6.3 E ⁻³	[10]
4		Diethyl sulfide	C ₄ H ₁₀ S	90.187	352-93-2	[7]	3.1 E ⁻³	[10]
4		Diethyl disulfide	C ₄ H ₁₀ S ₂	122.252	110-81-6	[7]		
6		Dipropyl sulfide	C ₆ H ₁₄ S	118.24	111-47-7	[7]		
8		Dibutyl sulfide	C ₈ H ₁₈ S	146.294	544-40-1	[7]	3.4 E ⁻²	[10]
8		Di- <i>sec</i> -butyl sulfide	C ₈ H ₁₈ S	146.294	626-26-6	[7]		
8		Di- <i>tert</i> -butyl sulfide	C ₈ H ₁₈ S	146.294	107-47-1	[7]		
8		Dibutyl disulfide	C ₈ H ₁₈ S ₂	178.359	629-45-8	[7]		
8		Di- <i>tert</i> -butyl disulfide	C ₈ H ₁₈ S ₂	178.359	110-06-5	[7]	2 E ⁻³	[10]
12		Dihexyl sulfide	C ₁₂ H ₂₆ S	202.399	6294-31-1	[7]		
14		Diheptyl sulfide	C ₁₄ H ₃₀ S	230.453	629-65-2	[7]		
16		Dioctyl sulfide	C ₁₆ H ₃₄ S	258.506	2690-08-6	[7]		
<i>Thiols (mercaptans)</i>								
2		Ethanethiol	C ₂ H ₆ S	62.134	75-08-1	[7]	15	[10]
2		1,2-ethanedithiol	C ₂ H ₆ S ₂	94.199	540-63-6	[7]		
3		1-propanethiol	C ₃ H ₈ S	76.161	107-03-9	[7]		
3		2-propanethiol	C ₃ H ₈ S	76.161	75-33-2	[7]		
3		1,2-propanedithiol	C ₃ H ₈ S ₂	108.226	814-67-5	[7]		
3		1,3-propanedithiol	C ₃ H ₈ S ₂	108.226	109-80-8	[7]		
4		1-butanethiol	C ₄ H ₁₀ S	90.187	109-79-5	[7]	0.59	[10]
4		2-butanethiol	C ₄ H ₁₀ S	90.187	91840-99-2	[7]		
4		1,4-butanedithiol	C ₄ H ₁₀ S ₂	122.252	1191-08-8	[7]		
5		1-pentanethiol	C ₅ H ₁₂ S	104.214	110-66-7	[7]		
5		2-pentanethiol	C ₅ H ₁₂ S	104.214	2084-19-7	[7]		
5		3-pentanethiol	C ₅ H ₁₂ S	104.214	616-31-9	[7]		
6		1-hexanethiol	C ₆ H ₁₄ S	118.24	111-31-9	[7]		
6		2-hexanethiol	C ₆ H ₁₄ S	118.24	1679-06-7	[7]		
6		1,6-hexanedithiol	C ₆ H ₁₄ S ₂	150.305	1191-43-1	[7]		
6	1	1,2-benzenedithiol	C ₆ H ₆ S ₂	142.242	17534-15-5	[7]		
6	1	1,3-benzenedithiol	C ₆ H ₆ S ₂	142.242	626-04-0	[7]		
7	1	Benzenemethanethiol	C ₇ H ₈ S	124.204	100-53-8	[7]		
7		1-heptanethiol	C ₇ H ₁₆ S	132.267	1639-09-4	[7]		
<i>Dibenzothiophenes</i>								
12	3	Dibenzothiophene		184.257	132-65-0	[7]	1.4 E ⁻³	[8]
13	3	C1-dibenzothiophenes	C ₁₂ H ₈ S					
14	3	C2-dibenzothiophenes	C ₁₃ H ₁₀ S			[7]		
15	3	C3-dibenzothiophenes	C ₁₄ H ₁₂ S			[7]		

TABLE 3.11 Guadalupe results on sulfur in oil analysis

Oil	Total sulfur (%)	Asphaltenes (%)	Sulfides (% of total sulfur)
A	3.3	6.3	0.2
B	2.7	21.9	1.5
C	0.9	0.3	0.4

3. Fatty acids and
4. Inclusions in asphaltenes.

Some of the compounds that have been found in oils are shown in Table 3.12. Recent analysis has shown that some of the acid species include complex compounds with two to six aromatic rings and often including sulfur and nitrogen compounds [15]. Porter et al. analyzed several resins and determined the presence of carbazole and similar compounds in these oils [16].

3.2.4 Nitrogen Compounds

Nitrogen compounds are abundant in most crude oils and constitute about 0.1–2 weight percent of the total. Several workers have carried out qualitative and quantitative analyses on nitrogen compounds in oils [17–21]. Nitrogen compounds in oils are often divided into two groups of basic or nonbasic compounds. This division is also useful for separation schemes. Most compounds are present as cyclic compounds as shown in Table 3.13. Furthermore, there is significant nitrogen content in the asphaltenes and in metal-binding compounds such as porphyrins.

3.2.5 Metals

Crude oils and their heavy refined petroleum products often contain significant amounts of metals. Metals are found in oils as one of the following:

1. Inorganic salts,
2. Metal soaps,
3. Organic metal-complex compounds, and
4. Attached to asphaltenes.

Table 3.14 lists the metal contents in several oils. The metals given here are the most common metals identified in oils. In the past, some metals, notably chromium, vanadium, and nickel, were used for crude oil identification. The ratios of these metals have a tendency to remain constant. Further, the ratios of these metals can be used to identify tanks from which the oils may have come, as there is exchange of metals with the tank bodies. At the present time, there is little use of this type of identification as the use of biomarkers is easier and better understood.

Quadros et al. studied the simultaneous measurement of nickel and vanadium in Brazilian and Venezuelan crude

oils [22]. They found that the total nickel in three Brazilian crudes ranged from 9 to 25 $\mu\text{g/g}$ and in three Venezuelan crudes from 29 to 69 $\mu\text{g/g}$. The total vanadium in the same Brazilian crudes ranged from 13 to 32.7 $\mu\text{g/g}$ and in the Venezuelan crudes from 224.7 to 277.0 $\mu\text{g/g}$.

The bonding of metals, particularly nickel, vanadium, iron, and cobalt, into porphyrins is a known source of metal stability in oils. Figure 3.5 shows the porphyrin skeleton. These compounds are residuals of chlorophyll, which has a similar structure.

Metals are concentrated into petroleum residuals and often in the asphalt fractions of the oil. Metals are very low in the diesel fraction and absent in gasoline.

3.2.6 Resins

Resins are polar compounds that are defined by precipitation or by open-column chromatography. The composition of resins is largely unknown. The nitrogen compounds noted earlier may be present in resins, largely as alkylated variants of the basic compounds.

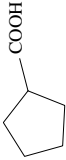
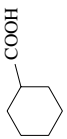
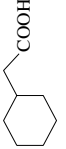
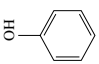
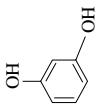
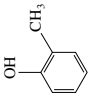
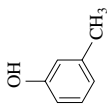
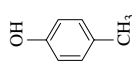
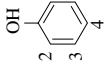
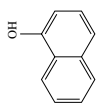
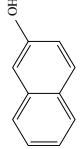
Porter et al. analyzed several resins and determined the presence of carbazole and similar compounds in these oils [16]. They also looked at the average molecular weight of resins using electrospray tandem mass spectrometry. Table 3.15 shows the averages of these molecular weights. It can be seen from this table that the residual resins in diesel are of smaller molecular weight than those in crude oils.

3.2.7 Asphaltenes

The important fact concerning asphaltenes is that currently the structure and composition of this broad class of compounds is unknown [23]. Currently, asphaltenes are defined by their precipitation from oil in pentane, hexane, or heptane. The mass of asphaltenes, typically defined as percentage by weight increases as one uses smaller compounds as solvents. As Mullins points out in his recent volume on the topic that until a number of structures of asphaltenes have been identified, asphaltenes will remain a mystery such as the whole field of genetics before Watson and Crick identified the structure of DNA [24]. Despite recent progress in the field, not one single compound has been positively characterized in the asphaltene mix.

Recent progress on the study of asphaltenes will be summarized later, but includes the fact that for the first time the molecular weight has been found to be about 760, ranging from 500 to 1000 [25]. The aromatic ring system is felt to contain about seven fused rings, with a range of 4–10 rings, and to have a “hand shape” with the alkane chains (fingers) radiating outward from the central fused ring (palm). Further, analysis has been problematic because asphaltene molecules aggregate at low concentrations, typically about 150 mg/l in toluene. These nano-aggregates can range up to 10 or more individual compounds and do not easily lend themselves to analysis or separation.

TABLE 3.12 Oxygenated compounds sometimes found in oils and petroleum

Compound	Molecular formula	Structure	CAS no.	MW	Reference	Solubility in water ^a g/l	Reference
<i>Naphthenic acids</i>							
Cyclopentanecarboxylic acid	C ₆ H ₁₀ O ₂		3400-45-1	114.142	[7]		
Cyclohexanecarboxylic acid	C ₇ H ₁₂ O ₂		98-89-5	128.169	[7]	2	[8]
Cyclohexanecarboxylic acid	C ₈ H ₁₄ O ₂		5292-21-7	142.196	[7]		
<i>Phenols</i>							
Phenol	C ₆ H ₆ O		108-95-2	94.111	[7]	80	[8]
Resorcinol	C ₆ H ₆ O ₂		108-46-3	110.111	[7]	700	[8]
<i>o</i> -Cresol	C ₇ H ₈ O		95-48-7	108.138	[7]	25	[8]
<i>m</i> -Cresol	C ₇ H ₈ O		108-39-4	108.138	[7]	20	[8]
<i>p</i> -Cresol	C ₇ H ₈ O		106-44-5	108.138	[7]	20	[8]
(Dimethyl) xyleneol	C ₈ H ₁₀ O		1	122.164	[7]	4-8	[8]
1-Naphthol	C ₁₀ H ₈ O		90-15-3	144.17	[7]	0.9	[8]
2-Naphthol	C ₁₀ H ₈ O		135-19-3	144.17	[7]	0.7	[8]
<i>Fatty acids</i> Fatty acids	CH ₃ -(CH ₂) _n -COOH	CH ₃ -(CH ₂) _n -COOH	Many	Many			

^aApproximate sign (-) indicates solubility values are variable; a range indicates the range of values; many of these values are the average of several determinations.
1 CAS numbers for dimethylxyleneols—2,3: 526-75-0; 2,4: 105-67-9; 2,5: 95-87-4; 2,6: 576-26-1; 3,4: 95-65-8; 108-69-9.

TABLE 3.13 Table of nitrogen compounds sometimes found in oils and petroleum

Compound	Molecular formula	Structure	CAS no.	MW	Reference	Solubility in water ^a g/l	Reference	Levels in LGO oil as ppm N	Reference	Levels in heavy fuel oil	Reference
Pyrole	C ₄ H ₃ N		109-97-7	67.09	[7]	48	8				
Pyridine	C ₅ H ₅ N		110-86-1	79.101	[7]						
Indole (1-H-indole)	C ₈ H ₇ N		120-72-9	117.149	[7]	3.6–10	8				
Methyl indole	C ₉ H ₉ N		1	131.174	[7]	~0.5	8				
Quinoline	C ₉ H ₇ N		91-22-5	129.159	[7]	~6	8				
Isoquinoline	C ₉ H ₇ N		119-65-3	129.159	[7]						
Methyl quinoline	C ₁₀ H ₉ N		2	143.185	[7]						
Methyl isoquinoline	C ₁₀ H ₉ N		3	143.185	[7]	~1	8				
Dimethyl quinoline	C ₁₁ H ₁₁ N		4	157.212	[7]	1.8	8				
Carbazole	C ₁₂ H ₉ N		86-74-8	167.206	[7]	1.2 E-3	8	38	[18]	7	[21]
Methyl carbazole	C ₁₃ H ₉ N		5	181.233	[7]			Σ190	[18]		
Dimethyl carbazole	C ₁₃ H ₁₁ N							Σ196	[18]		
Trimethyl carbazole	C ₁₄ H ₁₃ N							Σ74	[18]	6	[21]
Tetrahydro carbazole	C ₉ H ₁₁ N		6	171.238	[7]					~4	[21]
Benzo(b)carbazole	C ₁₆ H ₁₁ N										

(continued)

TABLE 3.13 (Continued)

Compound	Molecular formula	Structure	CAS no.	MW	Reference	Solubility in water ^a g/l	Reference	Levels in LGO oil as ppm N	Reference	Levels in heavy fuel oil	Reference
7H-Dibenzo(c,g) carbazole	C ₂₀ H ₁₃ N			267.324	[7]					~4	[21]
Acridine	C ₁₃ H ₉ N			179.217	[7]					~5	[21]
Benzo(a)acridine	C ₁₇ H ₁₁ N									~4	[21]
Dibenzo(a,j)acridine	C ₂₁ H ₁₃ N									~3	[21]

^aApproximate sign (~) indicates solubility values are variable; a range indicates the range of values; many of these values are the average of several determinations.

1 CAS numbers for methyl indoles: 1-methyl, 603-76-9; 2-methyl, 95-20-5; 3-methyl, 83-34-1; 5-methyl, 614-96-0; 7-methyl, 933-67-5.

2 CAS numbers for methyl quinolines: 2-methyl, 91-63-4; 3-methyl, 612-58-8; 4-methyl, 491-35-0; 5-methyl, 7661-55-4; 6-methyl, 91-62-3; 7-methyl, 612-60-2; 8-methyl, 611-32-5.

3 CAS numbers for methyl isoquinolines: 1-methyl, 1721-93-3; 3-methyl, 1125-80-0.

4 CAS numbers for dimethyl quinolines: 2,4-dimethyl, 1198-37-4; 2,6-dimethyl, 877-43-0; 2,7-dimethyl, 93-37-8.

5 CAS numbers for methyl carbazoles: 3-methyl, 4630-20-0; 9-methyl, 1484-12-4.

6 CAS numbers for tetrahydro carbazoles—2,3,4,9: 942-01-8; 1,2,3,4: 635-46-1; 5,6,7,8: 10500-57-9.

TABLE 3.14 Metal content (all content is in ppm—parts per million, < indicates values below detection limit)

Metal	Light fuels					Heavy fuel oils		Refinery intermediates	
	Aviation Gas 80	Aviation Gas 100	Jet A	Jet B	Diesel	Bunker C	IFO-marine	FCC-Heavy Cycle	Heavy reformat
Chromium	<	1.4	<	<	<	<	<	<	<
Copper	1.1	<	<	<	<	<	<	<	<
Iron	<	<	39	13	4.6	3.5	29.5	<	<
Lead	175	795	<	<	<	<	<	<	<
Magnesium	8.2	7.5	9.8	3.6	12.3	23.9	10.2	3.8	10.6
Molybdenum	0.6	<	1.9	<	<	<	<	<	<
Nickel	<	<	<	<	<	8.6	29.5	<	<
Titanium	<	<	2.7	<	<	<	0.6	<	1.2
Vanadium	<	<	<	<	<	42	76.4	<	<
Zinc	<	<	2.4	0.6	1.2	1.6	1.1	0.4	<

Metal	Light crude oils				Heavy crudes				
	Brent	Panuke	Norman Wells	Pitas Point	Oseberg	Ninian	Empire	Iranian Heavy	Maya
Country of origin	UK	Canada	Canada	CA, USA	Norway	UK	CA, USA	Iran	Mexico
Chromium		<	<	<	<	<	<	<	<
Copper		<	<	<	<	<	<	0.6	<
Iron		<	<	10.3	4.2	4.2	39.5	6	<
Lead		<	<	<	<	<	<	<	<
Magnesium		<	<	<	1	<	17.4	8.8	16.7
Molybdenum		<	<	<	<	<	<	<	1.2
Nickel	1	<	3.3	<	3.8	<	<	22.6	46.5
Titanium		<	<	0.6	<	<	105	<	<
Vanadium	6	<	8.7	<	2.7	4	<	81	257
Zinc		<	<	3.3	<	<	<	<	<

Metal	Heavy crudes					Bitumen			
	Lago Medio	Platform Irene	Port Hueneme	Hondo	Dos Cuadras	Carpinteria	California 11	California 15	Cold Lake Bitumen
Country of origin	Venezuela	CA, USA	CA, USA	CA, USA	CA, USA	CA, USA	CA, USA	CA, USA	Canada
Chromium	<	2.3	<	<	<	>	1.5	1.7	<
Copper	<	0.8	<	<	<	<	<	<	<
Iron	<	44	16	30.5	42.1	29.5	21.5	9.1	15.2
Lead	<	<	<	<	<	<	3	3	<
Magnesium	3.8	237	3.1	5.4	16	<	237	8	9
Molybdenum	<	<	0.6	2.3	<	<	4	5.1	3.7
Nickel	5.6	60.5	68	75	62	48.9	106	111	69
Titanium	<	1.1	0.6	1.6	<	<	2.2	2	<
Vanadium	163	238	253	196	70.5	112	245	266	190
Zinc	<	5.1	0.6	0.5	<	4.3	<	<	4.3

Studies up to about 2006 concluded that the molecular weight of asphaltenes varied from about 500 to about 70,000 amu or daltons [23]. More recent studies, using more refined techniques, show that the molecular weight of asphaltenes is smaller than previously thought. One of the problems of determining the molecular weight is the aggregation tendency of asphaltenes. As noted earlier, this is a severe problem for any analysis of asphaltenes. Vapor pressure osmometry, gel permeation chromatography, and

certain introduction methods for mass spectrometry such as laser desorption methods can result in asphaltene aggregation and therefore high molecular weight values. Electrospray ionization Fourier transform ion cyclotron resonance (ESI-FT-ICR) spectroscopy has been successful in studying asphaltenes and other heavy oil components [25]. ESI has been successful as an introduction method for heavy oil component study for both liquid chromatography and ICR chromatography as the analyte molecule is not evaporated,

rather the solvent is. The molecules do not reaggregate as they are charged in the process and electrostatic repulsion keeps them separated. All these methods do not result in separation of the asphaltene mixture, rather just enable a bulk analysis that can lead to some structure indications and idea of the molecular weight.

Groenzin and Mullins report on the use of time-resolved fluorescence depolarization to assess the molecular weight of asphaltenes [24]. This method is basically a look at the decay of fluorescent molecules. Molecular weight is estimated by comparison with the decay rate of molecules of known molecular weight. The results of this analysis show that the typical molecular weight is 750 g/mol and that this varies from about 500 to 1000 g/mol. Interestingly, coal asphaltenes displayed an average molecular weight of about 500 g/mol.

Dr. Yen proposed that asphaltene molecule aggregates are like micelles and will behave like stacks of fused aromatic ring systems [23]. This is now known as the “Yen” model. The micelles will grow to a limiting size and reaggregate into “aggregates” until there is again a limiting size. So there is a double mode of aggregation. Groenzin and Mullins used the sum total of information found to date to propose a structure for one oil asphaltene as shown in Figure 3.6 [24].

Mass spectrometry can yield more information than just a series of peaks for such complicated mixtures. There are two plotting techniques that can yield further information about petroleum mixtures [25]. The Kendrick plot shows the IUPAC (International Union of Pure and Applied Chemistry) 14.0156 mass spacing associated with carbon to show compounds of the same class. The Kendrick mass is defined as

$$\text{Kendrick mass} = \text{IUPAC mass spectrometry mass} \times (14/14.0156) \quad (3.1)$$

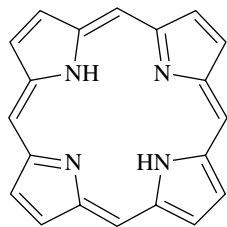


FIGURE 3.5 A typical porphyrin structure. This compound is called porphine.

Using the Kendrick mass thus changes the mass of the CH_2 , the basic hydrocarbon building block, to become exactly 14. A further unit is defined as the Kendrick Mass Defect [25].

$$\text{Kendrick Mass Defect (KMD)} = (\text{nominal mass} - \text{Kendrick mass}) \times 1000 \quad (3.2)$$

Each family of compounds share the same mass defect and thus a plot of KMD versus nominal Kendrick mass yields a graph of the different families of compounds, separated by the number of methylene groups. If one can identify the smaller compounds of a particular family, then the larger members can be identified by summing the methylene groups.

Rodgers and Marshall show how this technique can be used to yield three levels of compositional detail, starting from accurate masses of complex mixtures obtained from FT-ICR MS (mass spectrometry) [25]. First, a plot of class by relative abundance is created. The classes include functional groups such as N, O_2 , NO, O_3 , etc. These functional groups are noted by the unique masses of the heteroatoms. Then for heteroatom, the relative abundance is plotted for the double-bond equivalents (DBE). Then for each DBE grouping, the relative abundance of each carbon atom can be plotted.

The DBE is calculated as

$$\text{DBE} = C - H/2 + N/2 + 1 \quad (3.3)$$

where C , H , and N are the numbers of carbons, hydrogens, and nitrogens, respectively.

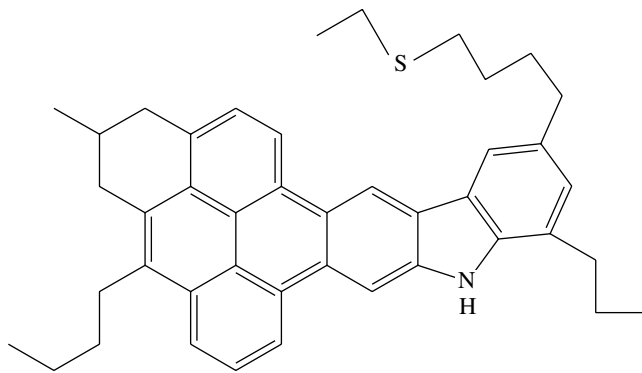


FIGURE 3.6 A hypothetical asphaltene molecule after Mullins et al. [23].

TABLE 3.15 Average molecular weights of resins for various crude oils and petroleum products (from Porter et al. [16])

	Crude oils				Petroleum products					
	Alberta	Maui	Tchat	Alaskan	Arabian Heavy	Hibernia	Mars	Fuel Oil #5	Heating fuel oil	Diesel
Maximum	395	370	382	394	417	410	411	409	405	212
Minimum		361	376	393	408	423	415	404	378	209

Another value that can be used to provide discrimination in the mass spectrum of numbers is the Z number or the total number of heteroatoms:

$$Z \text{ number} = -2(\text{DBE}) + n + 2 \quad (3.4)$$

A simple plot of the KMD versus the nominal Kendrick mass can yield the points of the different compound families by methylene groups.

Another graphing technique that assists in the identification of various compounds is the van Krevelen diagram [24]. A van Krevelen diagram employs the ratio of non-carbon atoms and the H/C ratio to provide discrimination between various compounds.

3.3 PROPERTIES OF OIL

The properties of oil discussed here are viscosity, density, specific gravity, solubility, flash point, pour point, distillation fractions, interfacial tension, and vapor pressure. These properties for the oils noted as examples as given earlier are listed in Table 3.16 [26].

Viscosity is the resistance to flow at a given shear rate. The lower the viscosity, the more readily the liquid flows. For example, water has a low viscosity and flows readily. Molasses with a high viscosity flow slowly. The viscosity of the oil is largely determined by the amount of lighter and heavier fractions that it contains. The greater the percentage of light components such as small saturates and the lesser the amount of asphaltenes, the lower the viscosity. Conversely, oils with a high asphaltene content have high viscosities. Viscosity is affected by temperature, with a lower temperature giving a higher viscosity. For most oils, the viscosity varies as the logarithm of the temperature. Oils that flow readily at high temperatures can become a slow-moving, viscous mass at low temperatures. In terms of oil spill cleanup, viscosity is important. Viscous oils do not spread rapidly, do not penetrate soil as readily, but are difficult to pump and skim.

Density is the mass of a unit volume of oil and is typically expressed in grams per cubic centimeter (g/cm^3). It is the property often used by the petroleum industry to define light or heavy crude oils. The density of fresh water is $1.0 \text{ g}/\text{cm}^3$ at 15°C and the density of most oils ranges from 0.7 to $0.99 \text{ g}/\text{cm}^3$, thus most oils will float on water. As the density of seawater is $1.03 \text{ g}/\text{cm}^3$, even heavier oils will usually float on seawater. The density of oil increases with time, as the light fractions evaporate. When the density of an oil becomes greater than the density of freshwater or seawater, the oil will sink. Sinking is rare and happens only with a few oils, usually residual fuels such as Bunker C or raw products such as bitumen. Significant amounts of oil have sunk in only about 50 incidents out of thousands. However, as heavier and heavier oils are being used more frequently, sinking may become more common in the future.

Specific gravity is another measure of density and is an oil's relative density compared with that of water. If the specific gravity of the oil is greater than 1, it sinks and if less than 1, it floats. Another gravity scale is that of the American Petroleum Institute (API). The API gravity is based on the density of pure water, which has an arbitrarily assigned API gravity value of 10° . Oils with progressively lower specific gravities have higher API gravities. The following is the formula for calculating API gravity:

$$\text{API gravity} = [141.5 \div (\text{oil density at } 15.5^\circ\text{C})] - 131.5 \quad (3.5)$$

Oils with high densities have low API gravities and vice versa.

Oil solubility in water is the measure of how much oil will dissolve in water on a molecular basis. Solubility is important in that the soluble fractions of the oil are sometimes toxic to aquatic life, especially at higher concentrations. As the amount of oil lost to solubility is always small, this is not a large loss mechanism and is typically ignored in mass balance calculations. In fact, the solubility of oil in

TABLE 3.16 Typical oil properties

Property	Units	Gasoline	Diesel	Light crude	Heavy crude	Intermediate fuel oil	Bunker C
Viscosity	mPa-s at 15°C	0.5	2	5–50	50–50,000	1000–15,000	10,000–50,000
Density	g/ml at 15°C	0.72	0.84	0.78–0.88	0.88–1.00	0.94–0.99	0.96–1.04
Flash point	$^\circ\text{C}$	–35	45	–30 to 30	–30 to 60	80–100	>100
Solubility in water	ppm	200	40	10–50	5–30	10–30	1–5
Pour point	$^\circ\text{C}$	NR	–35 to –10	–40 to 30	–40 to 30	–10 to 10	5–20
API gravity		65	35	30–50	10–30	10–20	5–15
Interfacial tension	mN/m at 15°C	27	27	10–30	15–30	25–30	25–35
Distillation fractions	% distilled at						
	100°C	70	1	2–15	1–10	—	—
	200°C	100	30	15–40	2–25	2–5	2–5
	300°C		85	30–60	15–45	15–25	5–15
	400°C		100	45–85	25–75	30–40	15–25
	Residual			15–55	25–75	60–70	75–85

NR, not relevant.

water is so low (generally less than 100 parts per million) that it would be the equivalent of approximately one grain of sugar dissolving in a cup of water. This small amount is important to the environment as even small amounts may be toxic to certain biota.

The flash point of an oil is the temperature at which the liquid oil yields sufficient vapors to ignite upon exposure to an open flame. A liquid is considered to be flammable if its flash point is less than 60 °C. There is a broad range of flash points for oils and petroleum products, many of which are considered flammable, especially when fresh. Gasoline, which is flammable under all ambient conditions, poses a serious fire hazard when spilled. Many fresh crude oils have an abundance of volatile components and may be flammable for as long as 1 day until the more volatile components have evaporated. On the other hand, Bunker C and heavy crude oils generally are not flammable even when freshly spilled.

The pour point of an oil is the temperature at which it takes longer than a specified time to pour from a standard measuring vessel. It is important to note that pour point is not the solidification temperature. As oils are made up of hundreds of compounds, some of which may still be liquid at the pour point, the pour point is not the temperature at which the oil will no longer pour. The pour point represents a consistent temperature at which an oil will pour very slowly from a standard container. Therefore, pour point has limited use as an indicator of the state of the oil. In fact, pour point has been overused in the past to predict how oils will behave in the environment. For example, waxy oils can have very low pour points but may continue to spread slowly at low temperatures and can evaporate to a significant degree. As produced crude oils become heavier, pour point becomes less relevant.

Distillation fractions of an oil represent the fraction (generally measured by volume) of an oil that is boiled off at a given temperature. This data is obtained on crude oils so that oil refineries can adjust parameters to handle the oil. This data also provides environmentalists with useful insights into the chemical composition of oils. For example, while 70% of gasoline will boil off at 100 °C, only about 5% of one selected crude oil will boil off at that temperature and an even smaller amount of a typical Bunker C. The distillation fractions correlate to the composition as well as to other physical properties of the oil. Distillation fraction data are sometimes used as input for estimation equations of evaporation.

The oil–water interfacial tension, sometimes called surface tension, is the force of attraction or repulsion between the surface molecules of oil and water. Together with viscosity, surface tension is one indication of how rapidly and to what extent an oil will spread on water. The lower the interfacial tension with water, the greater the extent of spreading. In actual practice, the interfacial tension must be considered along with the viscosity because it has been found that interfacial tension alone does not account for spreading behavior.

The vapor pressure of an oil is a measure of how the oil partitions between the liquid and gas phase, or how much

vapor is in the space above a given amount of liquid oil at a fixed temperature. Because oils are a mixture of many compounds, the vapor pressure changes as the oil weathers. Vapor pressure is difficult to measure and is not frequently used to assess oil spills. Oil is a mixture of hundreds of compounds, therefore vapor pressure is not entirely relevant to spill control.

While there is a high correlation between the various properties of an oil, these correlations should be used cautiously as oils vary so much in composition. For example, the density of many oils can be predicted using their viscosity values. For other oils, however, this could result in errors. For example, waxy oils have much higher viscosities than would be predicted from their densities. There are several mathematical equations for predicting one property of an oil from another property, but these must be used carefully as there are many exceptions.

REFERENCES

- [1] Kinghorn, R.R.F., *An Introduction to the Physics and Chemistry of Petroleum*, John Wiley & Sons, New York, 1983.
- [2] Fingas, M., Introduction to Oil Chemistry and Properties, Chapter 3, in *Oil Spill Science and Technology*, M. Fingas, Editor, Elsevier Publishers, New York, 51, 2011.
- [3] Speight, J.G., *The Chemistry and Technology of Petroleum*, Fourth Edition, CRC Press, Boca Raton, 2007.
- [4] Neumann, H-J., B. Paczynska-Lahme, and D. Severin, *Composition and Properties of Petroleum*, Halsted Press, New York, 1981.
- [5] Wang, Z., M. Fingas, and K. Li, Fractionation of ASMB Oil and Identification and Quantitation of Aliphatic, Aromatic and Biomarker Compounds by GC/FID and GC/MS, *AMOP*, Calgary, 11, 1993.
- [6] Wang, Z., B.P. Hollebone, M. Fingas, B. Fieldhouse, L. Sigouin, M. Landriault, P. Smith, J. Noonan, and G. Thouin, *Characteristics of Spilled Oils, Fuels and Petroleum Products: 1. Composition and Properties of Selected Oils*, Environment Canada, Ottawa, Ontario, Canada, 2003.
- [7] *Handbook of Chemistry and Physics*, CRC Press, Boca Raton, 2006.
- [8] Yalkowsky, S.H., Y. He, and P. Jain, *Handbook of Aqueous Solubility Data*, CRC Press, Boca Raton, 2010.
- [9] Mackay, D., W.Y. Shiu, and K.C. Ma, *Illustrated Handbook of Physical-Chemical Properties and Environmental Fate for Organic Chemicals*, Vol. 1–5, Lewis Publishers, Boca Raton, 1992.
- [10] Verchueren, K., *Handbook of Environmental Data on Organic Chemicals*, John Wiley & Sons, New York, 2001.
- [11] Faksness, L-G., R.L. Daae, P.J. Brandvik, F. Leivik, and J. F. Borseth, Oil Distribution and Bioavailability Field Experiment—FEX 2009, *Sintef Report A 16584*, Trondheim, Norway, 2010.
- [12] Wang, Z. and C. Brown, Chemical Fingerprinting of Petroleum Hydrocarbons, Chapter 3, in *Environmental*

- Forensic Investigation*, S. Mudge, Editor, CRC Press, New York, 43-115, 2008.
- [13] Gaudalupe, M.F.M., V.A. Castello Branco, and J.C. Schmid, Isolation of Sulfides in Oils, *Organic Geochemistry*, 17, 355, 1991.
- [14] Nishioka, M. and R.S. Tomich, Isolation of Aliphatic Sulfur Compounds in a Crude Oil by a Non-reactive Procedure, *Fuel*, 72, 1007, 1993.
- [15] Tomczyk, N.A., R.E. Winans, J.H. Shinn, and R.C. Robinson, On the Nature and Origin of Acidic Species in Petroleum. 1. Detailed Acid Type Distribution in a California Crude Oil, *Energy Fuels*, 15, 1498, 2001.
- [16] Porter, D.J., P.M. Mayer, and M.F. Fingas, Analysis of Petroleum Resins Using Electrospray Ionization Tandem Mass Spectrometry, *Energy Fuels*, 18, 987, 2004.
- [17] Oliveira, E.C., M.C. Vaz de Campos, M.R.A. Rorigues, V.F. Perez, M.I.S. Melecchi, M.G.R. Vale, C.A. Zini, and E.B. Caramao, Identification of Alkyl Carbazoles and Alkyl Benzocarbazoles in Brazilian Petroleum Derivatives, *Journal of Chromatography. A*, 1105, 186, 2006.
- [18] Li, N., X. Ma, Q. Zha, and C. Song, Analysis and Comparison of Nitrogen Compounds in Different Liquid Hydrocarbon Streams Derived from Petroleum and Coal, *Energy Fuels*, 24, 5539, 2010.
- [19] Von Muehlen, C., E.C. de Oliveria, C.A. Zini, E.B. Caramao, and P.J. Mariott, Characterization of Nitrogen-Containing Compounds in Heavy Gas Oil Petroleum Fractions Using Comprehensive Two-Dimensional Gas Chromatography Coupled to Time-of-Flight Mass Spectrometry, *Energy Fuels*, 24, 3572, 2010.
- [20] Zhang, Y., C. Xu, Q. Shi, S. Zhao, K.H. Chung, and D. Hou, Tracking Neutral Nitrogen Compounds in Subfractions of Crude Oil Obtained by Liquid Chromatography Separation Using Negative-Ion Electrospray Ionization Fourier Transform Ion Cyclotron Resonance Mass Spectrometry, *Energy Fuels*, 24 (12), 6321, 2010.
- [21] Dutriez, T., J. Borras, M. Courtiade, D. Thiebaut, H. Dulot, F. Bertoncini, and M-C. Hennion, Challenge in the Speciation of Nitrogen-Containing Compounds in Heavy Petroleum Fractions by High Temperature Comprehensive Two-Dimensional Gas Chromatography, *Journal of Chromatography. A*, 24 (11), 3190, 2011.
- [22] Quadros, D.P.C, E.S. Chaves, F.G. Lepri, D.L.G. Borges, B. Welz, H. Becker-Ross, and A.J. Curtius, Evaluation of Brazilian and Venezuelan Crude Oil Samples by Means of the Simultaneous Determination of Ni and V as Their Total and Non-volatile Fractions Using High-Resolution Continuum Source Graphite Furnace Atomic Absorption Spectrometry, *Energy Fuels*, 5907, 2010.
- [23] Mullins, O.C., E.Y. Sheu, A. Hammami, and A.G. Marshall, Editors, *Asphaltenes, Heavy Oils and Petroleomics*, O.C. Springer Publications, New York, 2007.
- [24] Groenzin, H. and O.C. Mullins, Asphaltene Molecular Size and Weight by Time-Resolved Fluorescence Depolarization, Chapter 2, in *Asphaltenes, Heavy Oils and Petroleomics*, O.C. Mullins, E.Y. Sheu, A. Hammami, and A.G. Marshall, Editors, Springer Publications, New York, 17, 2007.
- [25] Rodgers, R.P. and A.G. Marshall, Petroleomics: Advanced Characterization of Petroleum-Derived Materials by Fourier Transform Ion Cyclotron Resonance Mass Spectrometry (FT-ICR MS), Chapter 3, in *Asphaltenes, Heavy Oils and Petroleomics*, O.C. Mullins, E.Y. Sheu, A. Hammami, and A.G. Marshall, Editors, Springer Publications, New York, 63, 2007.
- [26] Wang, Z., B.P. Hollebone, Chun Yang, B. Fieldhouse, M. Fingas, and M. Landriault, *Oil Composition and Properties for Oil Spill Modelling*, Environment Canada, Ottawa, Ontario, Canada, 2004.

VEGETABLE OIL SPILLS: OIL PROPERTIES AND BEHAVIOR

MERV FINGAS

Spill Science, Edmonton, Alberta, Canada

4.1	Introduction	79
4.2	The Oils	79
4.3	Historical Spills	79
4.4	Aquatic Toxicity	86
4.5	Properties of the Oils	86
4.6	Behavior in the Environment	87
4.7	Oxidation, Biodegradation, and Polymerization	87
4.8	Spill Countermeasures	88
4.9	Biofuels	88
4.10	Conclusions	89

4.1 INTRODUCTION

Vegetable oil spills can have serious environmental consequences, often similar to those of petroleum-based oils [1, 2]. The primary effects are on the surface organisms, particularly on birds, which can be devastated by a single spill. While the surface oil can cause damage to birds and intertidal organisms, there remain significant differences between vegetable oil and petroleum oil spills. This paper will explore some of these differences. First, vegetable oil spills are not very soluble in water and their measured aquatic toxicity is low. The most significant effect on aquatic life is smothering. Second, the fate of the oil is quite different. Vegetable oils do not evaporate to a significant degree, they do not form water-in-oil emulsions, nor do they disperse in water.

Attention in the last decade has been focused on vegetable oil spills by a number of spill incidents such as in Vancouver Harbour and an extensive review of the topic by the U.S. Environmental Protection Agency [3,4]. Despite the early experiences with vegetable oil spills, vegetable oil spills were suggested to be a useful test material because they were thought to be innocuous [5]. Vegetable oils have also been suggested by a number of proponents to remove petroleum oil residues from beaches [6].

4.2 THE OILS

Canola is a type of rapeseed developed in the 1970s and has become a common source of food oil [7–9]. The original rapeseed oil contained more erucic acid, an undesirable and harmful substance [10]. Canola oil contains less than 2% erucic acid. About 40% of the seed is oil by weight of which only about 6% is unsaturated fat, the lowest of the vegetable oils. In addition to use as a food product, canola is used in industrial lubricants [11]. Erucic acid, typically present as glycerol trierucate, may be extracted and used in industrial lubricants as well. Canola is now the number one vegetable oil used and produced in Canada. It is second in the United States.

The second-most important oil in North America, most important in the United States, is soybean oil [9]. The third-most commercially important oil is corn oil. Many other oils are used and transported because of their special properties and uses.

The fatty acid composition of some common oils is shown in Table 4.1 [12]. The fatty acid composition of the oils dictates their properties and behavior.

The oils often are complemented with antioxidants [13]. The most common is butylated hydroxytoluene (BHT). The frequently used antioxidants are shown in Table 4.2. Antioxidants complicate the long-term behavior of oils as they will slow or stop biodegradation and other oxidative processes.

4.3 HISTORICAL SPILLS

The historical spills found in the literature are summarized in Table 4.3 with details given in the following.

A spill of about four million liters of soybean oil entered the Minnesota River in 1963 [4,14]. This spill resulted in the

TABLE 4.1 Fatty acid content of vegetable oils

Fatty acid	Structural Symbol	Oil types						
		Canola	Soybean	Corn	Sunflower	Peanut	Palm	Olive
		Percentage composition						
Myristic	14:00	<0.2	0.4	<0.1	<0.5	<0.4	0.5–6	0.05
Palmitic	16:00	2–6	7–14	8–19	3–10	6–16	32–59	7–20
Palmitic	9c15:1	<0.6	<0.5	<0.5	<1	<1	<0.6	0.3–4
Stearic	18:00	1–2	1.5–6	0.5–4	1–10	1–7	1.5–8	0.5–4
Oleic	9c18:1	50–66	19–30	19–50	14–65	35–72	27–52	56–83
Linoleic	9c,12c-18:2	18–30	44–62	34–62	20–75	13–45	5–14	3.5–20
α -Linoleic	9c,12c,15c-18:3	6–14	4–11	<2	<0.7	<1	<1.5	<1.5
Arachidic	20:00	0.1–1	<0.1	<1	<1.5	1–3	<1	
Eicosenoic	9c-20:1	0.1–4	<0.1	<0.5	<0.5	0.5–2		
Behenic	22:00	<0.5		<0.5	<1	1–5		

TABLE 4.2 Antioxidants used in vegetable oils

Trade name	Abbreviation	IUPAC (International Union of Pure and Applied Chemistry) name	Structure
Butylated hydroxyanisole	BHA	2- <i>tert</i> -Butyl-4-hydroxyanisole	
Butylated hydroxytoluene	BHT	2,6-bis(1,1-Dimethylethyl)-4-methylphenol	
<i>tert</i> -Butylhydroquinone	TBHQ	2-(1,1-Dimethylethyl)-1,4-benzenediol	
Propyl gallate, octyl gallate, or dodecyl gallate		Propyl 3,4,5-trihydroxybenzoate or octyl or dodecyl	
Vitamin C		2-Oxo-L-threo-hexono-1,4-lactone-2,3-enediol	
Tocopherol or vitamin E		Includes tocopherols and tocotrienols— α tocopherol form shown	

TABLE 4.3 Historical vegetable oil spills

Place	Year	Oil	Location	Spill quantity (t)	Source	% recovered	Environmental issues	Unusual behavior	Reference
Minnesota River	1962–1963	Soy	River	3500–5000	Pipeline rupture under river ice		>5000 birds, >200 animals, and ~6000 fish killed		[14]
South Africa	1973	Anchovy	Bay				>100,000 clams and >10,000 lobsters killed		[15]
South Africa	1974	Fish	Marsh		Leaking pipeline		>5800 birds killed		[16]
USA	1977	Soy			Leaking rail car		Some birds killed		[17]
USA	1978	Canola		Two small spills			Some birds killed		[17]
Fanning Island—Pacific Ocean	1978	Palm and coconut	Coral reef	10,000	MV <i>Lindenbank</i>		Fish, crustaceans, etc., affected	Thick deposits (~10cm) on shore, long persistence	[18]
The Netherlands	1988	Various	Sea to shore		Mystery spill		Thousands of birds died		[19]
Vancouver Harbour	1989	Canola	Harbor	2	Leak from ship loading		>50 birds killed	Formed mineral oil-like slick	[20]
Wales	1991	Sunflower	Sea to shore	1,500	MV <i>Kimya</i>		Mussels killed	Polymerized on shore, most lost at sea and sunk	[21]
Georgia, United States	1994	Soy	Lake Lanier	20	Release from plant	~90%	Little		[22]
English Channel	1997	Palm kernel	Sea to shore	900	MT <i>Allegra</i>	~3%	Little	Formed large blobs from 10 to 100cm, skin oxidized	[23,24]
Monterey Bay, CA	1997	Unknown	Sea to shore	<8	Mystery spill		~400 birds killed		[25,26]
Gulf of Mexico, USA	1998	Mixed	Sea to shore	50	MV <i>Rosellen</i>		Little		[27]
Vancouver Harbour	1998	Canola	Harbor	4	Storage tank overflow	~50%	>300 birds killed		Ross, P. (private communication, April, 2001)
Hong Kong	1998	Canola	Sea	400	MV <i>Matsukaze</i> accident		Little		[27]
Mississippi River, USA	1998	Palm	River	460	MV <i>Champion Trader</i> accident	4%	Little		[28–30]
Vancouver Harbour	1999	Canola	Harbor	<230	Loss from pipe to ship	<10%	>200 birds killed		Ross, P. (private communication, April, 2001)
Vancouver Harbour	1999–2000	Canola	Harbor	Four small spills					Ross, P. (private communication, April, 2001)
Vancouver Harbour	2000	Canola	Harbor	20		~50%	~20 birds killed		Ross, P. (private communication, April, 2001)
South Africa	2007	Sunflower	Wetland	250	Storage facility	~70%	Inhibition of algae growth, low biological oxygen demand (BOD)		Ross, P. (private communication, April, 2001)

death of or severe effects on 5300 birds; about 177 muskrats; 26 beavers; and other wildlife including turtles, skunks, and squirrels. Even domestic animals such as cows and dogs were affected. The spill also caused the loss of about 7000 fish.

A spill of soybean oil from a leaking rail car occurred in 1977 in the United States [17]. Twenty-six birds were recovered, although many more were believed to have been affected. In 1978, the same authors noted a spill of rapeseed oil. This latter spill affected a number of birds, but this was not quantifiable. A third spill was noted in 1978 as well. Seven barrels of canola oil were spilled. Again, a number of birds were affected.

Russell and Carlson describe an edible oil spill that occurred on a tropical island, Fanning island, about 1500 km west of Hawaii and in the middle of the Pacific Ocean [18]. The ship, *Lindenbank*, was carrying miscellaneous cargo and vegetable oils and products. About 10,000 tons of vegetable oils and related products were released onto the shoreline. Much of the oil was palm oil and coconut oil, and this created slicks up to 10 cm thick on the beaches. This oil persisted on the beaches for several weeks. Similar effects to those of crude oil spills were noted. Fish, crustaceans, and mollusks were killed, and there was excessive growth of algae. The counts of dead organisms varied, but on some beaches, more dead crustaceans were found and on others, mollusks and sometimes dead fish. The animal kill was attributed to asphyxiation and clogging of the digestive tract. Furthermore, there was a lesser abundance of fish off the waters that were highly contaminated with the oils. The increased algae growth was attributed to the elimination of competitors and the increased fertilization from the vegetable oil and its breakdown products. Recovery of the shoreline communities progressed over 11 months, with climax communities becoming evident at the year point.

Smith and Herunter describe a canola oil spill in Vancouver Harbour in 1989 [20]. The 1800L of canola oil killed 39 birds outright. Forty-nine birds were captured and cleaned and 23 were released. The number of actual casualties would be much higher than these numbers. Smith and Herunter note that reduced feeding as a result of the contact was significant in increasing the vulnerability of the birds to hypothermia. Figures 4.1, 4.2, 4.3, 4.4, 4.5, and 4.6 show pictures of a canola oil spill in Vancouver Harbour.

Thousands of seabirds, mostly guillemots and razor-bills, died as a result of a mystery spill of vegetable oils and nonylphenol in 1998 off the Netherlands [19]. The birds showed signs of emaciation and plume damage, such as seen in petroleum oil spills. Necropsy also showed some liver damage.

A cargo of sunflower oil was spilled off the coast of Wales in 1991, from the tanker *Kimya* [21,22]. However, the sunflower oil polymerized and it could still be seen 7 years after the spill. The preliminary investigation showed an enhanced concentration of linoleic and oleic acids in mussel tissue. At



FIGURE 4.1 A spill of canola oil in Vancouver Harbor. This spill shows that canola oil will spread similar to petroleum oil.



FIGURE 4.2 A close-up of part of the canola spill noted in Figure 4.1. In this case, the oil has not weathered much and appears gray as it normally is in bulk.



FIGURE 4.3 Another close-up of the canola spill noted in Figure 4.1. Here, the oil is more weathered and appears darker. This could also be due to the pickup of organic matter.



FIGURE 4.4 A view of a canola slick that has picked up some organic matter.

sites close to the wreck, lipid levels were as much as 35 times levels in other areas. There was some evidence of metabolism of the lipids by mussels.

A 20,000l spill of low-grade soybean oil occurred north of Atlanta, GA, on September 26, 1994 [14]. The oil spilled into a small stream and then into an impoundment. Fortunately, the oil was contained and was removed by skimmers and vacuum trucks. There was no wildlife damage

reported as the area was small and little wildlife was in the area at the time.

On April 23, 1996, more than 30,000L of soybean oil was released at a vegetable oil refinery in Macon, Georgia [14]. The oil flowed into a small stream where some workers noted the spill and contained much of it quite quickly. The oil was removed using skimmers and vacuum trucks. Again, there was little wildlife damage because of



FIGURE 4.5 A canola slick being recovered using oil spill booms and skimmer.



FIGURE 4.6 A canola slick on open water mingling with log booms.

the small area of the spill and because little wildlife was in that industrial area.

On October 1, 1997, the tanker, *Allegra*, spilled 900 tons of palm oil in the English Channel [23,24]. The palm oil solidified and drifted up the channel and some landed on the French coastline. Much of the product, estimated at 97%, disappeared and was presumed dispersed or sunk. Figures 4.7 and 4.8 show pictures of palm kernel oil, and Figures 4.9 and 4.10 show pictures of palm oil, which is reddish due to the high β -carotene content.

In the latter part of October 1997, 400 birds including grebes, gulls, and loons were oiled from a mystery vegetable oil slick in Monterey Bay off Santa Cruz, CA [25]. Wildlife officials were able to clean and release some of these birds.

A 4000 L spill of canola was reported in Vancouver (Ross, P., private communication, April, 2001). The spill impacted birds near Stanley Park. More than 240 dead birds were

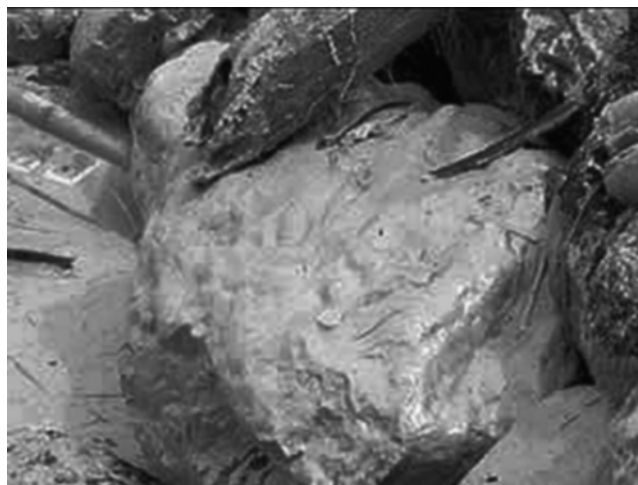


FIGURE 4.7 This photograph shows palm kernel oil coating a rock (Courtesy of the International Tanker Owners Pollution Federation).



FIGURE 4.8 Palm kernel oil near shore (Courtesy of the International Tanker Owners Pollution Federation).



FIGURE 4.9 Palm oil being recovered using oil spill equipment (Courtesy of the International Tanker Owners Pollution Federation).

recovered, 214 live birds were collected, and 126 of the live birds were successfully released. On November 24, 1999, slicks of canola were reported on the western reaches of Burrard Inlet, near Vancouver (Ross, P., private communication, April, 2001). Over the course of a few days, about 188 barrels of oil were recovered along with 110 bags of oiled

debris. The spill may have been as much as 223 tons. The spill was later traced to a loss between a shore-based loading facility and a tank ship. A total of 223 birds were recovered, of which 73 were cleaned and released.

Four small spills of canola oil occurred in Vancouver Harbour in the latter part of 1999 and 2000 (Ross, P., private



FIGURE 4.10 Palm oil contained by booms behind a tanker (Courtesy of the International Tanker Owners Pollution Federation).

communication, April, 2001). A spill of 20 tons of canola oil occurred on February 11, 2000, in Vancouver Harbour (Ross, P., private communication, April, 2001) [3]. Twenty-five birds were recovered, of which nine were released. Much of the oil was subsequently recovered using conventional oil spill recovery equipment.

A spill of 250 tons of sunflower oil occurred into a freshwater marsh [31]. About 70% of the spill was cleaned up using oil spill booms and skimmers. The spill altered the algae population in the marsh. Tolerant species increased and intolerant species decreased.

4.4 AQUATIC TOXICITY

Takeuchi and Watanabe studied the effects of excess fatty acids on the growth of rainbow trout [32]. Feeding of up to four times the amount of essential fatty acids for 10 weeks resulted in lower growth rates and poor food conversion. Effects appeared to be similar for poorly fed fish. There were also long-term liver effects noted. Stickney and Andrews noted similar effects on channel catfish [33]. Salgado studied the sublethal effects of vegetable oils on mussels and found that the excess oils caused a significant decrease in mussel growth [34].

Substitution of canola oils for fish oils in rearing fish showed no effect on Atlantic salmon in two separate studies [35,36]. In another study, this feed substitution was shown to affect swimming behavior [37].

Acute toxicity studies on canola oil showed no effect ($>10,000$ mg/l) to the rainbow trout in 96 h [38].

Mattson et al. studied the acute toxicity of several fatty acids and found that oleic acids showed a small increase with time [39]. The LC_{50} for oleic acid was greater than 1000 mg/l at 1 h, 285 after 24 h, and 205 at 96 h.

Li et al. studied the toxicity of the sediment on which canola oil was degraded [40]. The toxicity using *Microtox* showed an increase for 2 weeks after incubation and then a decrease to 8 weeks after the end of the experiment. The toxicity using an assay of the amphipod *Hyalella azteca* showed a decrease in toxicity throughout the degradation experiment.

Experience in actual spills has shown that there are two other forms of deleterious effects on aquatic organisms from vegetable oil, oxygen depletion and asphyxiation [18]. After a spill, the degradation of the vegetable oil, particularly in a confined and shallow area, will deplete the oxygen, and this in turn can result in the death of aquatic organisms. The spillage of a vegetable oil can smother or asphyxiate intertidal organisms and result in their death as surely as though it were from a petroleum oil.

4.5 PROPERTIES OF THE OILS

The physical properties of the oils vary widely. Table 4.4 lists some of the literature values [41]. The density and viscosity of several oils were measured in the laboratory using procedures outlined in the literature [42]. The values are shown in Table 4.5. There is variation in the properties of the oils, depending on the particular cropping and subsequent oil processing.

TABLE 4.4 Literature values for some properties (after Firestone [41])

Parameter	Units	Oil types						
		Canola	Soybean	Corn	Sunflower	Peanut	Palm	Olive
Density	g/ml at 15°C	0.914–0.92	1.466–1.47	0.917–0.925	0.918–0.923	0.914–0.917	0.891–0.899	0.91–0.916
Refractive index	at 15°C	1.466	1.468	1.471	1.474	1.462	1.455	1.47
Melting point	°C					–2	33–40	–3 to 0

TABLE 4.5 Measured values of vegetable oil properties

Temperature	Canola (degummed)	Canola (refined)	Castor	Olive	Soybean	Soybean (dyed)
Viscosity, mPa·s						
0	182	189	5359	219	153	154
15	83	86	1430	96	73	73
25	54	56	608	62	47	48
Density, g/ml						
0	0.9304	0.9306	0.9737	0.9255	0.9335	0.9337
15	0.9205	0.9205	0.9635	0.9087	0.9232	0.9232
25	0.9136	0.9135	0.9565	0.9157	0.9161	0.9163

4.6 BEHAVIOR IN THE ENVIRONMENT

Sunflower oil polymerized extensively after a spill on a marsh [21,22]. A subsequent test on a marsh of both sunflower and linseed oil resulted in polymerization of the sunflower oil, but not the linseed oil [43,44]. The linseed oil penetrated quickly. The polymerization of the sunflower oil caused the formation of an impermeable cap, which significantly slowed degradation. Another test of sunflower oil on a similar marsh showed no polymerization [44,45]. During this same test, the biodegradation of both linseed and sunflower oils was investigated. The number of aerobic and anaerobic bacteria was quantified. The degradation of both oils proceeded with a concomitant increase in the numbers of both aerobic and anaerobic bacteria. There was preferential degradation of the principal fatty acid components of the oils. Mudge noted that the original spill in a marsh and nearshore may last indefinitely because of polymerization and slow degradation [46]. Aggelis and Sourdis developed a model for the degradation of vegetable oils, noting that most oils degrade with similar kinetics [47]. Li and coworkers studied the degradation of vegetable oils and the formation of oil–mineral aggregates and found that degradation both aerobically and anaerobically proceeds to near completion [48].

Le Goff and Marchand studied the behavior and fate of a palm oil spill [23]. They noted that much of the palm oil solidified immediately into balls of up to 50 cm in diameter. These balls were white on the outside and yellow on the inside and contained many holes filled with seawater. Tests in a small flume showed that much of the oil would break up into small particles and disperse through the water column. Tests of the oxidation of the oil showed that the outer layers were oxidized to an extent, but only linoleic acid was subject

to this process. Bucas and Saliot studied the chemistry of the weathering and noted that only 5 mm of the outer coating was highly subject to oxidation [24]. Linoleic acid disappeared in the outer crust, but its content was unaffected on the interior of the large masses that occurred after the spill. Compositional analysis on the exterior and interior was carried out. These masses were as large as one meter but typically were of the order of about 10 cm.

The oils noted in Table 4.6 were studied in the Environment Canada Laboratory using standard protocols as described in the literature [42]. The oils were subjected to an evaporation test, chemical dispersion test, and emulsification test. The results were similar for all oils. The oils did not evaporate significantly over a month period—only about 1% of the product was lost through evaporation. The oils did not form any type of stable emulsion. All the vegetable oils entrained water but lost this water within a few hours. This only occurred at high energy. The oils did not chemically disperse with Corexit 9500.

DeMello et al. examined the potential effect of fatty acid methyl esters (FAMES) on the evaporation of biodiesels and noted that the presence of the fatty acids did not affect the evaporation [49].

4.7 OXIDATION, BIODEGRADATION, AND POLYMERIZATION

An important part of the behavior and fate of vegetable oils in the environment is the oxidative behavior. Although most vegetable oils biodegrade to a certain extent, this is variable depending on the oil [50]. Salam et al. noted that oils that oxidize to a large extent also polymerize [13]. These oils

TABLE 4.6 Behavior tests on some vegetable oils

Vegetable oil	Water content of oil	Emulsion formation			
		G ^a (mPa)	Water (%)	Visual	Dispersibility ^a
Canola raw and unrefined (RBWD)	<0.1	3400	21.2	Unstable	<10
Canola degummed	0.1	4200	10.2	Unstable	<10
Castor (CEDRE)	0.6	10,000	13.2	Unstable	<10
Olive (M. Sigouin)	<0.1	4400	12.3	Unstable	<10
Soybean (CEDRE)		4200	21.3	Unstable	<10

^aNote: Determined by visual estimation only—did not generate fine dispersion even in upper level of water column.

then biodegrade poorly if they polymerize. An experiment was carried out with antioxidant in varying concentrations (BHT) on an oil (glyceryl trilinoleate). As the amount of BHT added increased, biodegradation increased. Polymerization increased as oxidation increased. Campo et al. studied the biodegradation of five triacylglycerols and three oil liquids and some other oils [51,52]. These were pure oil components such as might be noted in Table 4.1. In most cases, the biodegradation was very limited because of the nonpolar nature of the oils. Sometimes, the oils would form clumps with water rather than mixing to any extent. In most cases, after 30 days, complete mineralization was not achieved. The remnants of the biodegradation tests were examined for Microtox toxicity. Only the solid samples showed some toxicity. The liquid samples did not.

Pereira et al. carried out an experimental spill on a marsh using linseed oil [43]. The linseed oil penetrated rapidly (rate of $10^{-7} \text{ cm}^2 \text{ s}^{-1}$). The surface vegetation including macrofauna and vascular plants died. The biodegradation of the linseed oil led to oxygen depletion in the sediments. The degradation of the linseed oil was a sequential process in terms of degradation products, although aerobic and anaerobic zones coexisted in the sediments. The prime degradation was by aerobic processes and was carried out by indigenous bacteria in the sediments. After 2 months, about 60% of the oil disappeared from the top 30 cm of soil.

Pereira et al. subsequently carried out an experimental spill on a marsh using sunflower and linseed oils [44]. The two oils penetrated the sediments at the same rate but showed different adsorption behaviors to the sediments. The differences in adsorption resulted in anaerobic conditions for the linseed oil at shallower depths than with the sunflower oil. The sunflower oil-contaminated sediments remained almost stable for about 6 months, showing low biodegradation. The linseed oil of sediments showed a biodegradation of about 40% after about 2 months. Bacterial numbers increased more slowly for the sunflower oil. Biodegradation patterns were similar for the two oils; however, that of the sunflower oil was very much slower.

Mudge and Pereira studied the use of biodiesels to enhance the biodegradation of crude oils [53]. Preliminary results showed that there was potential for this technique. Pereira and Mudge studied the use of biodiesels to clean

oiled shorelines [54]. They found that the biodiesels could dissolve crude oils quite well.

DeMello et al. carried out a preliminary study of the biodegradation of biodiesel mixtures [49]. They found that the presence of the FAME components in the mineral petroleum constituents increased the biodegradation rate.

4.8 SPILL COUNTERMEASURES

Several tests of vegetable oil recovery have taken place. Cooper and Obenauf studied canola oil recovery using skimmers and sorbents [55]. The data showed that canola was recovered by both sorbents and skimmers at rates similar to their petroleum equivalents. Further, the rate of coincidental water recovery was lower with the canola oil than with petroleum oils. The same group tested canola biodiesel (100%) and canola vegetable oil against regular diesel fuel using three types of skimmers [56]. The biodiesel was recovered at about the same rate as the petroleum diesel.

Several parties have published procedures for dealing with vegetable oil spills [57,58]. The presumption is that the vegetable oils are less toxic and as easy to clean up as the other oils. This presumption is not necessarily true.

Wincele et al. [59] and Li et al. [60] proposed the use of clay to sediment vegetable oils. The concept was to sediment the oil to the bottom where it might be biodegraded anaerobically. They tested canola oil with high-surface-area clay to show that sedimentation was readily possible. Wrenn et al. studied the effect of energy on the clay sedimentation rate [61].

Wilson studied the natural emulsification of oils, concluding that most vegetable oils do not form oil-in-water emulsions to a large extent [62].

4.9 BIOFUELS

Many biofuels will behave and have properties similar to their nonbiological counterparts as they are often diluted with them. Gasolines diluted with alcohol overall behave similarly to gasoline. Biodiesel, however, can consist largely of biological products. Biodiesels consist primarily of mono-alkyl esters of fatty acids derived from vegetable oils or animal fats [63]. In Canada, the biodiesels are largely derived

from canola and in the United States from soy. Recently, more used animal fat oils are finding their way into biodiesel. Vegetable oils are reacted with either methanol or ethanol to produce the fatty acid esters. Reactions with methanol produce FAME and reactions with ethanol produce fatty acid ethyl ester. In both cases, glycerine is a reaction by-product.

Biodiesels are often blended with petroleum diesel. The nomenclature of these blends lists the amount of biodiesel in the mixture. For example, B20 would indicate that 20% of the mixture is biodiesel, the remainder being petroleum diesel.

The toxicity of biodiesel itself is variable but may be about 5 or 10 times less than that of petroleum diesel [64–66]. As many blends of fuel have only about 10–20% of biodiesel, their toxicity is basically the same as petroleum diesel fuel.

The biodegradability of biodiesels has been investigated by several workers. The consensus is that biodiesels will degrade faster than petroleum diesel [62,65]. Further, the petroleum diesels will degrade faster when mixed with biodiesel. Degradabilities of 60–98% in 28 days have been measured in the laboratory.

The evaporation of biodiesel blends has been studied [66]. The findings are that the evaporation of the biodiesel portion is negligible and the petroleum component evaporates as it would without the biodiesel portion.

4.10 CONCLUSIONS

Spills of vegetable oils can have very negative effects on birds and shoreline life. In the case of birds, the vegetable oils coat feathers resulting in hypothermia in a manner similar to petroleum oils. Shoreline life can be smothered by vegetable oils.

Vegetable oils behave differently than petroleum oils: they do not evaporate, disperse, or dissolve, nor do they emulsify like petroleum oils. On shorelines, they can polymerize, effectively capping the local area. Their fate is to slowly degrade, to sink, or to be distributed widely without significant degradation. The effect on fish is not well studied, but because there is little dissolution of vegetable oils, it is expected that there will be little deleterious effect except where smothering can occur or where oxygen levels are lowered.

REFERENCES

- [1] Mudge, S.M., Deleterious Effects from Accidental Spillages of Vegetable Oils, *Spill Sci. Technol. Bull.*, 2, 187, 1995.
- [2] Mudge, S.M., Vegetable Oil Spills—Pollution or Over-Cautiousness, *Chem. Ecol.*, 14, 259, 1998.
- [3] ABC News, Canada Races to Clean Oil Spill Near Vancouver, http://www.greenspun.com/bboard/q-and-a-fetch-msg.tcl?msg_id=002YRU, 2000 (accessed August 14, 2014).
- [4] CFR part 112, Oil Pollution Prevention: Non-Transportation Related Onshore Facilities: Rule, 40 CFR part 112, EPA, Washington, D.C., 1997.
- [5] Allen, A., Canola Oil as a Substitute for Crude Oil in Cold Water Spill Tests, *Spill Techn. News.*, 4, 1983.
- [6] Mudge, S.M. and N. Miller, Removing Mineral Oil Residue from Beaches with Vegetable Oils, in *Oil and Hydrocarbon Spills, Modelling, Analysis and Control*, R. Garcia-Martinez and C.A. Brebbia, Editors, Computational Mechanics Publications, Southampton, UK, 1998.
- [7] Canola, Canola Oil Processing Background, <http://www.canolainfo.org/canola/index.php?page=6>, 2012 (accessed August 14, 2014).
- [8] Missouri, Canola: A Promising Oilseed, <http://extension.missouri.edu/p/G4280>, 2012 (accessed August 14, 2014).
- [9] O'Brien, R.D., Fats and Oils: An Overview, in *Introduction to Fats and Oils Technology*, R.D. O'Brien, W.E. Farr, and P.J. Wan, Editors, AOCS Press, Champaign, 1, 2000.
- [10] About, Erucic Acid and Erucamide, About Chemistry, <http://chemistry.about.com/>, 2012 (accessed August 14, 2014).
- [11] Cargill, Canola Oil, <http://www.techoils.cargill.com/products/canola.html/>, 2012 (accessed August 14, 2014).
- [12] Wan, P.J., Fats and Oils: An Overview, in *Introduction to Fats and Oils Technology*, R.D. O'Brien, W.E. Farr, and P.J. Wan, Editors, AOCS Press, Champaign, 1, 2000.
- [13] Salam, D.A., M.T. Suidan, and A.D. Venosa, Effect of Antioxidants on the Fate and Impact of Spilled Vegetable Oils in Aquatic Environments, *Proceedings of the 34th AMOP Technical Seminar on Environmental Contamination and Response*, Banff, AB, 786, 2011.
- [14] Rigger, D., Edible Oils: Are They Really That Different? *IOSC*, New Orleans, LA, 59, 1977.
- [15] Newman, G.G. and D.E. Pollock, Organic Pollution of the Marine Environment by Pelagic Fish Factories in the Western Cape, *S. Afr. J. Sci.*, 69, 27–29, 1973.
- [16] Percy-FitzPatrick Institute of African Ornithology, Fish Oil Kills Sea Birds, *Afr. Wildl.*, 28 (4), 24–25, 1974.
- [17] McKelvey, R.W., I. Robertson, and P.E. Whitehead, Effect of Non-petroleum Oil Spills on Wintering Birds Near Vancouver, *Mar. Pollut. Bull.*, 11, 169, 1980.
- [18] Russell, D.J. and B.A. Carlson, Edible-Oil Pollution on Fanning Island, *Pac. Sci.*, 32, 1, 1978.
- [19] Zoun, P.E.F., A.J. Baars, and R.S. Boshulzen, A Case of Seabird Mortality in the Netherlands During the Winter of 1988/1989 Caused by a Spillage of Nonylphenol and Vegetable Oils, *Sula*, 5, 47, 1991.
- [20] Smith, D.W. and S.M. Herunter, Birds Affected by a Canola Oil Spill in Vancouver Harbour, February, 1989, *Spill Techn. News.*, 14, 3, 1983.
- [21] Mudge, S.M., M.A. Salgado, and J. East, Preliminary Investigations into Sunflower Oil Contamination Following the Wreck of the M.V. Kimya, *Mar. Pollut. Bull.*, 26, 40, 1993.
- [22] Mudge, S.M., I.D. Goodchild, and M. Wheeler, Vegetable Oil Spills on Salt Marshes, *Chem. Ecol.*, 10, 127, 1995.
- [23] Le Goff, G. and M. Marchand, Observations of a Palm Kernel Oil Spillage in the English Channel, *AMOP*, Calgary, AB, 75, 1999.
- [24] Bucas, G. and A. Salot, Sea Transport of Animal and Vegetable Oils and Its Environmental Consequences, *Mar. Pollut. Bull.*, 44, 1388, 2002.

- [25] GOPB, World Spill Briefs, *Golub's Oil Pollution Bulletin*, p. 7, 31 October, 1997.
- [26] OSIR 1997, Mystery Goo in Monterey Bay Oils Migrating Water Fowl, *Oil Spill Intelligence Report*, XX (42), 2, 1997.
- [27] GOPB 1998, Cypriot Tanker Suffers Storm-Related Damage and Spills Vegetable Oil in Gulf of Mexico, *Golub's Oil Pollution Bulletin* X (4), 4, 1998.
- [28] OSIR 1998, Collision Spills Canola Oil, *Oil Spill Intelligence Report*, XXI (16), 3–4, 1998.
- [29] OSIR 1998, Tanker Blast Kills One, Spills Fuel and Palm Oil in Mississippi, *Oil Spill Intelligence Report*, XXI (43), 1, 1998.
- [30] GOPB 1998, Panamanian Tanker Spills Palm Oil in Deadly Explosion on the Mississippi River, *Golub's Oil Pollution Bulletin*, X (24), 6, 1998.
- [31] Oberholster, P.J., C. Blaise, and A.M. Botha, Phytobenthos and Phytoplankton Community Changes Upon Exposure to a Sunflower Oil Spill in a South African Protected Freshwater Wetland, *Ecotoxicology*, 19, 1426, 2010.
- [32] Takeuchi, T. and T. Watanabe, Effects of Excess Amounts of Essential Fatty Acids on Growth of Rainbow Trout, *B. Jpn. Soc. Sci. Fish.*, 45 (12), 1517, 1979.
- [33] Stickney, R.R. and J.W. Andrews, Effects of Dietary Lipids on Growth, Food Conversion, Lipid and Fatty Acid Composition of Channel Catfish, *J. Nutr.*, 102, 249, 1972.
- [34] Salgado, M.A., The Effects of Vegetable Oil Contamination on Mussels, Ph.D. Thesis, University of Wales, Bangor, 1995.
- [35] Tocher, D.R., J.G. Bell, J.R. Dick, R.J. Henderson, F. McGhee, D. Michell, and P.C. Morris, Polyunsaturated Fatty Acid Metabolism in Atlantic Salmon (*Salmo salar*) Undergoing Parr-Smolt Transformation and the Effects of Dietary Linseed and Rapeseed Oils, *Fish Physiol. Biochem.*, 23, 59, 2000.
- [36] Dosanjh, B.S., D.A. Higgs, D.J. McKenzie, D.J. Randall, J.G. Eales, N. Rowshandeli, M. Rowshandeli, and G. Deacon, Influence of Dietary Blends of Menhaden Oil and Canola Oil on Growth, Muscle Lipid Consumption, and Thyroidal Status of Atlantic Salmon (*Salmo salar*) in Sea Water, *Fish Physiol. Biochem.*, 19, 123, 1998.
- [37] McKenzie, D.J., D.A. Higgs, B.S. Dosanjh, G. Deacon, and D.J. Randall, Dietary Fatty Acid Composition Influences Swimming Performance, *Fish Physiol. Biochem.*, 19, 111, 1998.
- [38] Parsons, M., N. Russo, and R. Watts, The Acute Toxicity of Vegetable-Based Hydraulic Oils, to Rainbow Trout Underyearlings, *Oncorhynchus mykiss*, *Internal Environment Canada Report*, 1995.
- [39] Mattson, F.H., R.A. Volpenhein, and B.A. Erickson, Effect of Plant Sterol Esters on the Absorption of Dietary Cholesterol, *J. Nutr.*, 107, 1139, 1977.
- [40] Li, Z., K. Lee, S.E. Cobanli, T. King, B.A. Wrenn, K.G. Doe, P.M. Jackman, and A.D. Venosa, Assessment of Sediment Toxicity During Anaerobic Biodegradation of Vegetable Oil Using Microtox and *Hyalella azteca* Bioassays, *Environ. Toxicol.*, 22, 1, 2007.
- [41] Firestone, D., Editor, *Physical and Chemical Characteristics of Oils, Fats and Waxes*, AOCS Press, Washington, D.C., 1999.
- [42] Jokuty, P., S. Whitar, Z. Wang, M.F. Fingas, B. Fieldhouse, P. Lambert, and J. Mullin, *Properties of Crude Oils and Oil Products* (Volume 1, A-K; Volume 2, L-Z), Environment Canada Manuscript Report Number EE-165, Ottawa, Ontario, 1999.
- [43] Pereira, M.G., S.M. Mudge, and J. Latchford, Consequences of Linseed Oil Spills in Salt Marsh Sediments, *Mar. Pollut. Bull.*, 44, 520–533, 2002.
- [44] Pereira, M.G., S.M. Mudge, and J. Latchford, Vegetable Oil Spills on Salt Marsh Sediments: Comparison Between Sunflower and Linseed Oils, *Mar. Environ. Res.*, 56, 367, 2003.
- [45] Pereira, M.G., S.M. Mudge, and J. Latchford, Bacterial Degradation of Vegetable Oils, *Chem. Ecol.*, 14, 291, 1998.
- [46] Mudge, S.M., Can Vegetable Oils Outlast Mineral Oils in the Marine Environment, *Mar. Pollut. Bull.*, 34, 213, 1997.
- [47] Aggelis, G. and J. Sourdis, Prediction of Lipid Accumulation-Degradation in Oleaginous Micro-organisms Growing on Vegetable Oils, *Antonie van Leeuwenhoek*, 72, 1595, 1997.
- [48] Li, Z., D.E. Wincele, and B.A. Wrenn, Anaerobic Biodegradation of Vegetable Oil Spills, *IOSC*, Tampa, FL, 315, 2001.
- [49] DeMello, J.A., C.A. Carmichael, E.E. Peacock, R.K. Nelson, J.S. Arey, and C.M. Reddy, Biodegradation and Environmental Behaviour of Biodiesel Mixtures at Sea: An Initial Study, *Mar. Pollut. Bull.*, 54, 894, 2007.
- [50] Aluyor, E.O., K.O. Obahiagbon, and M. Ori-Jesu, Biodegradation of Vegetable Oils: A Review, *Scient. Res. Ess.*, 543, 2009.
- [51] Campo, P., Y. Zhao, M.T. Suidan, and G.A. Sorial, Biodegradation Patterns of the Constituents of Canola Oil, *Proceedings of the 8th International In Situ and On-Site Bioremediation Symposium*, Miami, FL, 286, 2005.
- [52] Campo, P., Y. Zhao, M.T. Suidan, A.D. Venosa, and G.A. Sorial, Biodegradation Kinetics and Toxicity of Vegetable Oil Triacylglycerols Under Aerobic Conditions, *Chemosphere*, 68, 2054, 2007.
- [53] Mudge, S.M. and G. Pereira, Stimulating the Biodegradation of Crude Oil with Biodiesel Preliminary Results, *Spill Sci. Technol. Bull.*, 5, 353, 1999.
- [54] Pereira, M.G. and S.M. Mudge, Cleaning Oiled Shores: Laboratory Experiments Testing the Potential Use of Vegetable Oil Biodiesels, *Chemosphere*, 54, 297, 2004.
- [55] Cooper, D. and A. Obenauf, Canola Oil—Pick It Up, *AMOP*, Calgary, AB, 351, 2002.
- [56] Cooper, D., D. Velicogna, A. Obenauf, and C. Brown, Biodiesel Spill Response, *AMOP*, Calgary, AB, 351, 2008.
- [57] Cooper, D. and B. Hollebone, Manual for Spills of Hazardous Materials: A Biofuels Update, *AMOP*, Banff, AB, 511, 2011.
- [58] ITOPF, *About Vegetable Oil Spills*, International Tanker Owners Pollution Federation, London, UK, 2010.
- [59] Wincele, D.E., B.A. Wrenn, and A.D. Venosa, Sedimentation of Oil-Mineral Aggregates for Remediation of Vegetable Oil Spills, *J. Environ. Eng.*, 130, 50, 2004.
- [60] Li, Z., R.J. Downer, and B.A. Wrenn, Remediation of Floating Vegetable Oil Spills by Sedimentation Followed by Anaerobic Biodegradation, *IOSC*, Vancouver, BC, 2003.

- [61] Wrenn, B.A., R.J. Downer, and A.D. Venosa, Effects of Mixing Energy on the Sedimentation of Vegetable Oil Spills by Clay, *Environ. Techn.*, 31, 1301, 2010.
- [62] Wilson, G., *Consideration of Characteristics Influencing the Emulsification Factors for Vegetable Oil Spills*, University of Cincinnati Internal Report, Cincinnati, 2005.
- [63] Hollebone, B.P. and Z. Yang, Biofuels in the Environment: A Review of Behaviours, Fates, Effects and Possible Remediation Techniques, *AMOP*, Vancouver, BC, 127, 2009.
- [64] Hollebone, B.P., N. Ho, S. Harrison, M. Landriault, K. Doe, and P. Jackman, Acute Aqueous Toxicities of Diesel-Biodiesel Blends, *AMOP*, Calgary, AB, 297, 2008.
- [65] Kahn, N., M.A. Warith, and G. Luk, A Comparison of Acute Toxicity of Biodiesel, Biodiesel Blends and Diesel on Aquatic Organisms, *J. Air Waste Manag. Assoc.*, 57, 286, 2007.
- [66] Yang, Z., B.P. Hollebone, Z. Wang, C. Yang, and M. Landriault, Evaporation and Stability of Biodiesel and Blends with Diesel in Ambient Conditions, *AMOP*, Banff, AB, 520, 2011.

PART IV

OIL ANALYSIS

CHROMATOGRAPHIC FINGERPRINTING ANALYSIS OF CRUDE OILS AND PETROLEUM PRODUCTS

CHUN YANG, ZHENDI WANG, BRUCE P. HOLLEBONE, CARL E. BROWN, ZEYU YANG,
AND MIKE LANDRIAULT

Emergencies Science and Technology Section (ESTS), Environment Canada, Ottawa, Ontario, Canada

5.1	Introduction	95
5.1.1	Crude Oils and Refined Petroleum Products	96
5.1.2	Chemical Components of Petroleum	97
5.2	Introduction to Oil Analysis Techniques	100
5.2.1	GC	100
5.2.2	GC with Mass Spectrometry	103
5.2.3	Ancillary Oil Fingerprinting Techniques	104
5.3	Methodology of Oil Fingerprinting Analysis	105
5.3.1	Oil Sample Preparation and Separation	105
5.3.2	Identification and Quantitation of Target Petroleum Hydrocarbons	110
5.3.3	Oil Type Screening by GC–FID	113
5.3.4	Aliphatic Hydrocarbons in Petroleum	117
5.3.5	Aromatic Hydrocarbons in Petroleum	130
5.4	Weathering Effect on Oil Chemical Composition	141
5.4.1	Evaporation Weathering	141
5.4.2	Biodegradation Weathering	141
5.4.3	Photodegradation Weathering	146
5.4.4	Assessment of Mass Loss during Weathering	147
5.5	Diagnostic Ratios of Target Hydrocarbons	148
5.5.1	Molecular Diagnostic Ratios for Oil Identification	148
5.5.2	Selection of Diagnostic Ratios	150
5.6	Forensic Oil Spill Identification: A Case Study	151
5.6.1	Product Type Screening and Determination of Hydrocarbon Groups	152
5.6.2	Determination of Oil-Characteristic Alkylated PAHs and Biomarkers	154
5.6.3	Comparison of Diagnostic Ratios	157
5.6.4	Weathering Check	157
5.6.5	Results of Match between Spilled Oils and Candidate Sources	157

5.1 INTRODUCTION

Nonrenewable fossil fuels including crude oil, natural gas, and coal are by far the most commonly used sources of energy, especially petroleum as the source of liquid fuels. Although sustainable and renewable technologies

to generate more power for the future are being explored, petroleum is expected to remain a dominant fuel for many decades although oil demand is increasing but oil reserves are rapidly depleted.

Petroleum has been benefiting mankind for thousands of years; however, it is also blamed for pollution to our environment. There is no other topic that has so widely attracted attention as oil contamination. Oil spills occur in a variety of oil facilities, including oil production, oil refineries, and bulk oil storage in aboveground and belowground storage tanks. Additionally, inland oil spills may come from oil pipeline ruptures, tank spills, and road transportation. Oil spills often result in severe environmental costs and pose significant threats to wildlife, human beings, and the natural environmental system.

The composition of crude oil is very complex, and it is also highly variable from field to field, and even within a given field it is possible to exhibit differences. Physical and chemical characterization of this complex mixture is further complicated by the fact that crude oils are not pure solutions, but commonly include colloiddally suspended components, dispersed solids, and emulsified water [1].

Oil fingerprinting is essential for the prevention, preparedness, and response to oil spills. The aim of forensic oil fingerprinting is to identify the spill sources if suspected sources are available, to at least identify the oil type if not, and to allocate the liability of spills if a spill is contributed by multispillers. The fingerprinting of oil spills can be a challenge to analytical chemists due to the complex nature of crude oils and the low concentrations of many constituents of interest. Once released into the environment, the oil is immediately subjected to a series of weathering processes, and subsequently, it is difficult to recognize its source. In addition, real environmental samples often contain a mixture of more than one oil and are mixed with background

matrices, which makes it even more difficult to have unambiguous identification [2].

Currently, there are a number of publications on the environmental fate and biological effects of spilled oil [3–5]. The purpose of this chapter is to describe the principle and methodology of oil fingerprinting analysis.

5.1.1 Crude Oils and Refined Petroleum Products

5.1.1.1 Crude Oils Crude oil is a fossil fuel. It is widely accepted that crude oil originates mainly from the remains of prehistoric natural organic substance such as microscopic, photosynthetic organisms known as phytoplankton, buried in the primeval mud of swamps, lakes, and oceans. Petroleum-saturated rock was formed from deposited layers of mud and organic debris under enormous pressure and high temperature, and oil and gas were subsequently formed and mobilized into reservoirs. The original chemistry of the organic matter, the environment of deposition, and the time and heat imposed on the organic matter dictate the type of crude oil formed [6]. Every crude oil exhibits a unique chemical fingerprint due to the variety of geological conditions and ages under which it was formed. Oil composition may be altered to various extents by postgeneration processes such as thermal alteration, migration, or biodegradation, consequently generating light, medium, or heavy crude oils.

To classify petroleum, properties such as viscosity, American Petroleum Institute (API) gravity, and sulfur content are usually used. The oil industry uses the API gravity scale, devised by the API and the U.S. National Bureau of Standards. The relationship between API gravity and specific gravity is an arbitrary one shown by the formula

$$\text{API gravity} = \frac{141.5}{\text{Specific gravity at } 15.6^{\circ}\text{C}} - 131.5 \quad (5.1)$$

Thus, an oil with a specific gravity of 1.000 at 15.6°C would have an API gravity of 10.00. Since the specific gravity appears in the denominator of the equation, the heavier the oil, the lower the API gravity, and vice versa. Based on density, crude oils can be roughly classified into light, medium, heavy, and extra heavy oils. Heavy oils have a less than 25° API, and extra heavy oils have a gravity below 10.0° API. The medium oils are defined as having an API gravity between 25° and 35°, and light commercial valuable oils have an API in the range of 35–45°.

Spills of crude oil occur frequently in small to large scales during their exploration, production, and transportation. Most massive accidental oil spills are usually related to crude oil releases on the oceans from drilling rigs, offshore platforms, and supertankers. For example, the Exxon Valdez tanker spilled 11 million gallons of oil into the ecologically sensitive Prince William Sound in 1989; on December 7, 2007, a collision of the *Hebei Spirit* resulted in a leak of

around 10,800 tonnes of crude oil into the Yellow Sea coast of South Korea; the catastrophic explosion that caused an oil spill from a BP offshore drilling rig in the Gulf of Mexico continually released more than about 40,000 barrels of oil per day from April until August 2010. The particular operational conditions and severe weather often make it more difficult to control an ocean oil spillage than an on-land incident. Although oil spills on the open ocean are unlikely to cause an immediate health threat to humans, they often impact the local economy and cause widespread damage to the ecosystem, and the long-term negative effect could last decades. The analysis of spilled oil is essential to monitor the contamination and to evaluate the damage and the recovery of the environment.

Conventional crude oil reserves on land are rapidly being depleted, and heavy oils including oil sands bitumen are currently attracting increased investment interest. In recent years, particularly in Alberta, Canada, a new environmental issue associated with crude oils is the mining, extraction, and production of oil sands bitumen. Canadian Alberta oil sands are known to contain the world's largest reserves of bitumen. According to the Alberta Energy and Utilities Board, the initial volume in place is estimated at 1.7 trillion barrels of bitumen based on current technologies, and three main oil sands deposits in the province of Alberta have 173 billion barrels of recoverable bitumen. The oil sands industry has left significant footprints such as consumption of a large volume of water, emissions of greenhouse gases, and the creation of a large number of tailing ponds. The oil sands tailings waste including residual bitumen, naphthenic acids, and asphaltenes creosols, a variety of hazardous compounds in tailings pond water, pose an enduring threat to the environment. This is different from a typical oil spill incident, in which oil as a whole enters into the environment and causes negative impact.

5.1.1.2 Refined Petroleum Products Although crude oil may be utilized directly as an energy source, the full benefit of the different properties of the constituent hydrocarbons may be realized only when the constituents are separated. According to the U.S. Energy Information Administration, U.S. refineries produce between 19 and 21 gallons of motor gasoline from one barrel (42 gallons) of crude oil [7]. The remainder of the barrel yields distillate and residual fuel oils, jet fuel, and many other products.

Petroleum products are created from crude oil by a variety of refining processes. Distillation is the principal method for separating crude oil into valuable products such as gasoline, kerosene, fuel oil, and lubricating oil (or lube oil). Petroleum fuel mixtures are also produced from crude oil through a variety of refining and blending processes according to requirement for desired end uses. Based on the distillation point, petroleum products can be generally classified into light distillates, medium fuels, and heavy residuals. Each product is composed of different constituents.

Gasoline is the combination of mainly lower-boiling-range compounds including C₄ to C₁₂ alkanes, C₄ to C₇

alkenes, benzene, and alkylbenzenes. Middle distillate products generally include mineral spirits and Stoddard solvent, kerosene, most of the jet fuels, diesel, and light fuel oils. No. 1 fuel oil, No. 2 fuel oil, and No. 3 fuel oil are variously referred to as distillate fuel oils, diesel fuel oils, light fuel oils, gas oils, or just distillates. These products are characterized by a predominance of C_{10} – C_{24} alkanes and polycyclic aromatics with no or little olefins. Fuels 1 and 2 possess moderate to high acute toxicity to biota with product-specific toxicity related to the type and concentration of aromatic compounds, while fuels 5 and 6 are considered to be less acutely toxic relative to other oil types. Fuel 4 has variable acute toxicity, depending on the amount of the light fraction [8].

Heavy fuel oils (HFOs) are fuels used in off-road engines, boilers, furnaces, and other combustion equipments. They are the heavy residual part of the distillation and cracking processes. These oils are often blended with lighter oils for the convenience of transportation and operation. Their composition is complex and varies with the feedstock of the crude oil. In general, these oils contain a mixture of saturated, aromatic, and olefinic hydrocarbons with carbon numbers predominantly in the C_9 to C_{50} range. Their polycyclic aromatic hydrocarbons (PAHs) are dominated by 3-ring homologues, but some cracked 4- to 6-ring species are also present. As residual distillates, these oils often contain relatively high concentrations of sulfur, oxygen, and nitrogen compounds and heavy metals (vanadium, nickel, and others). Relative to other types of refined oil products, spills of HFOs potentially cause the most significant environmental impact with respect to their physical and chemical properties.

Lubricating oils consist of largely base oils and small amount of chemical additives. The base oil used to originate from petroleum mass products; however, over many years, some high-performance lubricants no longer contain petroleum base oils [9]. Hydrogenation and hydrocracking in the manufacture of lubricant base oils significantly influence the chemical structures of mineral oil molecules. On one hand, unstable molecules are chemically stabilized by the removal of the heteroatoms (sulfur, oxygen, and nitrogen). Severe hydrogenation can convert aromatics into saturated naphthenic and paraffinic structures. In addition to the hydrogenation process, hydrocracking breaks down or cracks large molecules into smaller ones. Since commercially valuable lubricating oil is often produced in relatively small amounts, spills of large amounts of lubricating oil are rare.

Massive spills of refined petroleum products rarely occur on land like crude oil spills such as Exxon Valdez and Deep Water Horizon spills. However, most of the crude oil is refined on land, and refined petroleum products are for the most part consumed on the land. Spillages of refined oils frequently occur around oil development and production facilities. Frequent small chronic spillages of refined oils may pose greater environmental problem than the rare accidental spillages of crude oil. According to the Emergency

Response Notification System of the U.S. Coast Guard (USCG) (1993), fuel oils are among the top most spilled petroleum products in U.S. waters, both by volume and by the number of notifications [10].

Spillages of petroleum products on open water often involve mystery illegal discharges of marine vessels and their bilges. The waste from the cleaning of engine chambers is sometimes accidentally or deliberately released from vessels. The presence of lubricating oil in bilges provides a valuable clue to trace the spill source. Accurate analysis and unambiguous results are critical in order to identify the spill source and to allocate the legal liability.

5.1.2 Chemical Components of Petroleum

Petroleum is an extremely complex combination of widely varying constituents and proportions of hydrocarbons; heterocyclic compounds of nitrogen, oxygen, and sulfur; organometallic compounds; inorganic sediments; and water. Although the total number of compounds in crude oil is still unknown, it is recognized that crude oil is likely composed of thousands of compounds [11]. These petroleum hydrocarbons naturally exist in gas, liquid, or solid state. The distribution pattern and profiles of components are, in general, different from oil to oil and from oil to refined products. Despite wide variations in the chemical composition of crudes, their elemental compositions generally fall within the following narrow ranges: carbon (84–87%), hydrogen (10–14%), nitrogen (0.1–2.0%), oxygen (0.05–1.5%), and sulfur (0.05–6.0%) [12]. Metals are encountered in petroleum in the form of salts of carboxylic acids or as porphyrin chelates. Vanadium (V) and nickel (Ni) are predominant, occurring at highest concentrations in crude oil and residual fuel oils.

Crude oils can be characterized compositionally by a number of established methods. An oil sample can be largely separated into saturate (paraffins), aromatic, resin, and asphaltene (SARA) fractions. The SARA fractions are typically determined using gravimetric methods, but nowadays, thin-layer chromatography coupled with flame ionization detection (TLC–FID) is becoming the major quantitative tool [13]. TLC–FID technique separates solvent-extractable petroleum organics on silica-coated quartz rods (Chromarods) into saturates, aromatics, and polar components and detects each hydrocarbon group as a whole using a flame ionization detector [13,14]. However, SARA analysis is not accurate for the component analysis of light oils.

5.1.2.1 Paraffins Paraffins are one of the major constituents of crude oil and are found in refined petroleum products such as gasoline, kerosene, diesel fuel, heating oil, etc. Molecular structures of selected petroleum paraffins are displayed in Figure 5.1. Overall, there are three major classes of paraffins, that is, normal alkanes (straight chain), branched alkanes, and naphthenes (cycloalkanes, especially cyclopentane, cyclohexane, and their alkyl derivatives). The

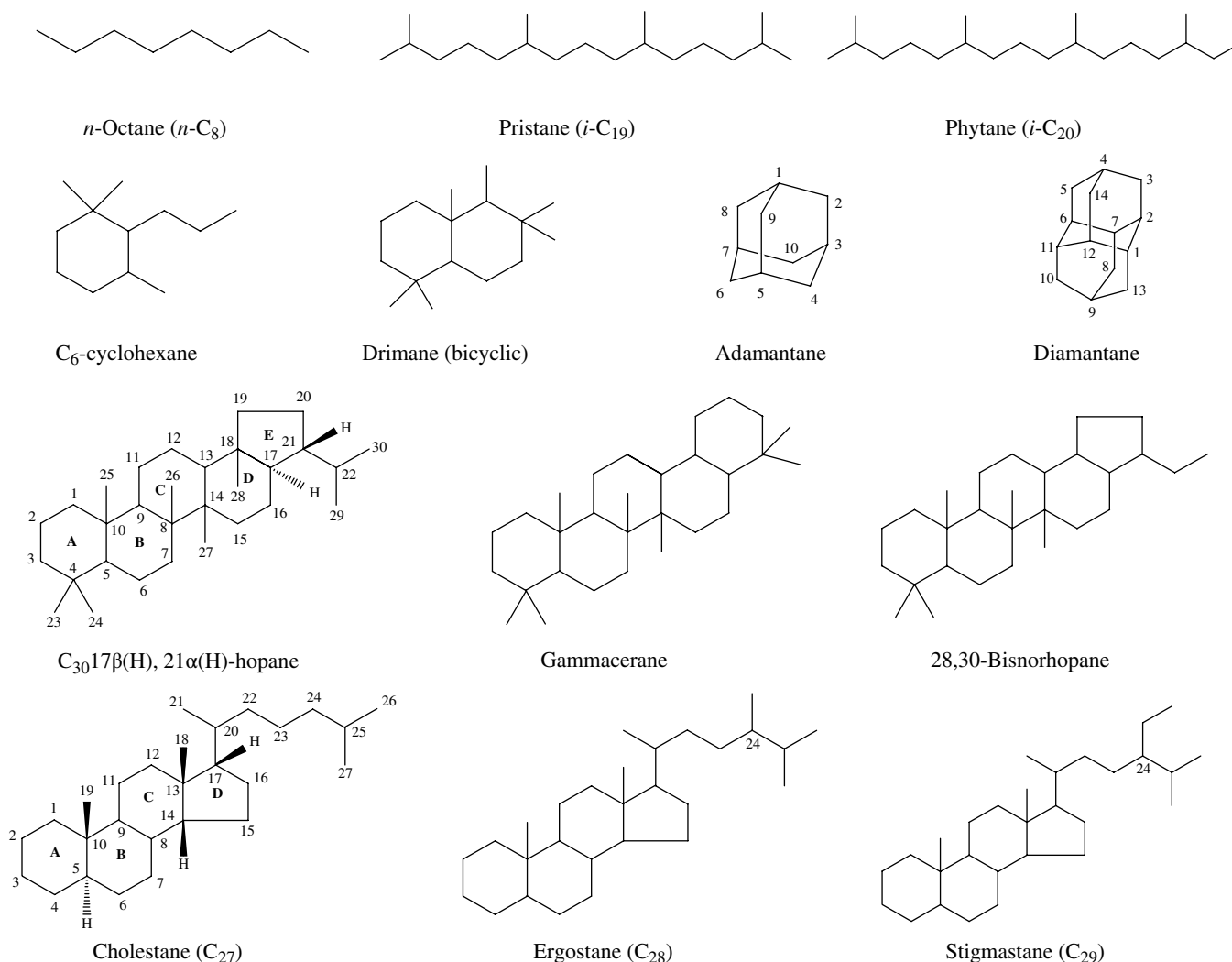


FIGURE 5.1 Molecular structures of representative petroleum paraffins.

normal alkanes have carbon atoms arranged in a line, and there are only two ends to these molecules. Branched alkanes have the carbon atoms arranged similar to the *n*-alkanes, however, some of the carbon atoms are branched, thus creating many different configurations. Paraffins (mainly straight-chain alkanes) ranging from C₁₆ to C₄₀, which occur in solid state at room temperature, are often referred as crude wax. Naphthenes are saturated hydrocarbons containing one or more rings, each of which may have attached paraffin side chains.

Molecules based on isoprenoid units (isoprene, C₅H₈–) have a variable composition. The following types may be distinguished: (i) monoterpanes (C₁₀), both aliphatic and monocyclic; (ii) sesquiterpanes (C₁₅), aliphatic, monocyclic, and bicyclic; (iii) diterpanes (C₂₀), aliphatic, bicyclic, tricyclic, and possibly tetracyclic; and (iv) triterpanes (C₃₀), aliphatic, as well as tricyclic, tetracyclic, and pentacyclic. Among these terpenoids, tetra- and pentacyclic terpanes and steranes are the most important compounds for petroleum chemistry and forensic oil analysis.

5.1.2.2 Olefins These unsaturated hydrocarbons have a double bond and two less hydrogen atoms than their corresponding alkanes. Olefins occur in many crude oils and condensates from numerous basins worldwide. Various types of olefins have been identified in the oils and condensates of North America, Africa, Europe, and Asia [15]. These compounds are found in large quantities in some refined products, produced primarily from larger molecules in cracking processes. Olefins are not present in large amounts in crude oils or straight-run distillates such as kerosene, gas oil, or fuels [16].

5.1.2.3 Aromatics Aromatics contain one or more benzene rings as structural components (Fig. 5.2). A monoaromatic compound has one benzene ring with either six hydrogen groups or a combination of alkyl and hydrogen groups attached to the six-carbon aromatic ring. Polycyclic aromatic compounds have multiple-ring aromatic nuclei of benzenes such as naphthalene, phenanthrene, dibenzothiophene, pyrene, and many more.

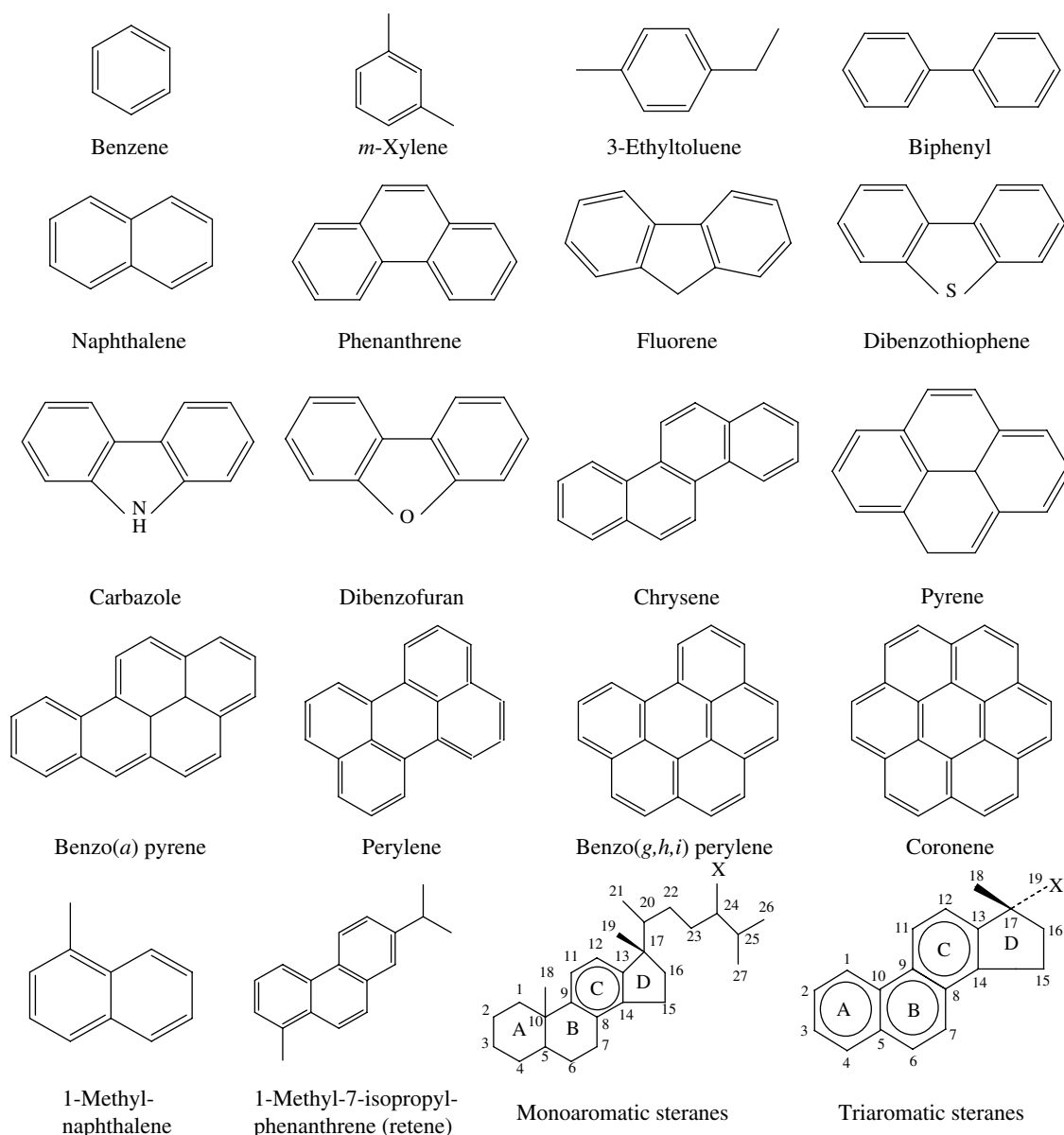


FIGURE 5.2 Molecular structures of selected aromatic hydrocarbons and heterocyclic aromatic compounds in petroleum.

5.1.2.4 Resins Resins include a large group of polar compounds in oil. These include heterosubstituted aromatics (Fig. 5.2), acids, ketones, alcohols, and monoaromatic steroids. Resins are assumed to be insoluble in liquid propane but soluble in *n*-pentane. Because of their polarity, these compounds are more soluble in polar solvents, including water, than the nonpolar compounds, such as waxes and aromatics, of similar molecular weight. They are largely responsible for oil adhesion.

5.1.2.5 Asphaltenes Asphaltenes make up the largest percentage of the asphalt used to pave roads. Asphaltene constituents are the highest molecular weight and most polar constituents in crude oil. During petroleum refining, the asphaltene constituents are nondistillable and remain in the

residual fuels as the distillable fractions are removed [17]. Asphaltene is defined as the part of petroleum, coal, or oil shale that is precipitated by addition of a low-boiling paraffin solvent such as *n*-pentane but soluble in benzene. The color of crude oils and residues is due to the combined effect of neutral resins and asphaltenes. The black color of some crude oils and residues is related to the presence of asphaltenes that are not properly peptized. The neutral asphaltenes and resins are the most important asphaltic compounds of petroleum. On heating above 300–400°C, asphaltenes are not melted but decompose, forming carbon and volatile products. As asphaltenes are determined as a whole, this provides little information to distinguish an oil, and asphaltenes are not often listed as target analytes for forensic oil analysis. However, its content can reflect the oil type.

5.1.2.6 Other Components Other than the main fraction of hydrocarbons, crude oil also contains other compounds consisting of oxygen, sulfur, nitrogen, and trace amounts of phosphorus. Crude oil also contains a small quantity of heavy metals such as vanadium and nickel and trace amount of water. Refined petroleum products contain variable contents of these components due to their removal or enrichment during refining processes.

In this chapter, we will focus on the fingerprinting analysis of selected paraffins and aromatics. Table 5.1 summarizes the overall distribution of these chemical components in various oils. For each petroleum fuel mixture, the table displays the approximate carbon number range of predominant hydrocarbons and relative abundance of common target petroleum hydrocarbons in these oils. Their chemical fingerprints will be described in more detail later in this chapter.

5.2 INTRODUCTION TO OIL ANALYSIS TECHNIQUES

The chemical fingerprints of crudes are altered during manufacture of refined petroleum products in the refining process. Once oil is released into the environment, the fingerprint of an oil will be affected by weathering and mixing with background substances. However, the refined oil petroleum partially inherits its unique fingerprint from the parent crude oil, and weathered oil could retain the unique characteristics of the source oil, which enables a potential to trace its origin.

In recent decades, the technologies of oil analysis have continually progressed due to advanced and automated instrumental techniques. This chapter does not intend to provide an exhaustive list of analytical methods rather it discusses some well-established methods. Because petroleum is a mixture of a large number of hydrocarbons and other substances, it is impractical and unnecessary to analyze petroleum as a whole. The methods most commonly used approach the major hydrocarbon components using gas chromatography (GC) and other techniques [18–22].

5.2.1 GC

Capillary GC is in routine use in environmental laboratories today to provide a detailed analysis of most of the individual organic compounds. The characterizations of individual aliphatic and aromatic compounds in petroleum were mainly based on gas chromatography/flame ionization detection (GC–FID) and gas chromatography/mass spectrometry (GC–MS) analyses. In principle, GC analysis involves a liquid solution being vaporized and introduced into a chromatographic column where separation of a mixture is achieved. The typical capillary column is coated with a fluid onto an inert support material, the stationary phase on the inner wall. An inert gas (i.e., hydrogen, helium, or nitrogen), also called the mobile phase, flows through the column.

Upon introduction into the column, solute molecules distribute between the stationary and the mobile phases. Depending on the phase equilibrium between the stationary and the mobile phase, compounds travel with different velocities through the column. The mixture becomes separated, and as a result, individual compounds reach the detector at different times. The rate at which each sample band moves through the column depends upon the physico-chemical nature of the compound, the chemical structure of the stationary phase, and the column temperature. The width of the sample band depends on the operating conditions and the dimension of the column. By choosing a proper column considering the column length, column internal diameter (ID), stationary phase, film thickness, carrier gas, and linear velocity, a wide range of petroleum hydrocarbons can be well separated under optimal instrumental parameters.

Retention time is the time taken for an analyte moving through the column to reach the detector. If the column and all operating conditions remain constant, in theory, a given compound will always take same time to travel through the column and have the same retention time on a chromatogram. The detection response linearly corresponds to the mass introduced into the detector within certain range. The most commonly used columns for the separation of petroleum hydrocarbons are 30m nonpolar inert capillary columns such as DB-5, DB-5ms, HP-5, and HP-5ms, filmed inside with 5% phenylmethylpolysiloxane. A conventional fused silica capillary column (30m, 0.25 mm ID, and 0.25 μ m film thickness) is used for most oil analyses.

5.2.1.1 Fast GC Analysis Satisfactory separations of complex petroleum samples usually take a long time. To meet the request for high daily sample throughput and/or need for quick results, a fast GC or ultrafast GC can be used in oil analysis. Compared to conventional GC, fast GC provides up to ten times faster analysis and meanwhile maintains sufficient resolving power and comparable accuracy. The prerequisites for a fast GC analysis are the instrument equipped with a fast automatic injection, a narrow-bore capillary column, a high-speed detector, and fast data acquisition and processing software. It is typically performed using a short (typically 15m or shorter in length), narrow-bore (0.10 or 0.18 mm ID) capillary column with hydrogen as carrier gas and rapid oven temperature ramp rates. Munari and Cadoppi studied the reliability and performance of an ultrafast GC technique for total hydrocarbons ranging from n -C₇ to n -C₄₀ in water samples [23]. The results demonstrate that this method can readily fulfill the requirements, but most importantly, it also increases productivity by 10 times when compared with conventional GC. Quicker results allow more timely decisions, less product waste, more higher-value products, and a shorter time to market. Although there are still few approaches using fast GC for oil fingerprinting, it is expected that fast GC technique will receive wide application in petroleum analysis, particularly for fast

TABLE 5.1 Relative abundance of chemical components in various oils

Petroleum types	Approximate carbon number range	Paraffins				Aromatics			
		<i>n</i> -Alkanes	Branched alkanes	Bicyclic sesquiterpanes	Diamondoids	Tri- to pentacyclic terpanes	BTEX	PAHs	Aromatic steranes
Crude oils									
Light or medium crude oil	C ₁ -C ₄₀	High	High	Variable	Variable	Variable	Variable	Variable	Variable
Heavy crude/oil sands bitumen	C ₁₀ -C ₄₀	Low or trace	Low	Low	Variable	High	No or trace	Low in naphthalenes	High
Refined products									
Gasoline	C ₄ -C ₁₂	Low	High	Trace	Trace	Trace	High	Low	No or trace
Kerosene	C ₆ -C ₁₆	High	Lower	Low	Low	Trace	Low	Low	Low
Jet A	C ₈ -C ₁₆	High	Low	High	High	Trace	Low	Low	No or trace
Diesel No. 2	C ₈ -C ₂₁	High	Low	High	High	Low	Low	High	Low
Fuel No. 5/Bunker B	C ₈ -C ₄₀	High	Medium	High	Medium	High	Low	High	Variable
Fuel No. 6/Bunker C	C ₁₂ -C ₃₄	High	High	Low	Low	High	Low	High	Variable
Lubricating oil	C ₁₈ -C ₃₄	Low	Low	Low	Low	High	No or trace	Low	Low

oil type screening and the determination of total petroleum hydrocarbons (TPHs).

5.2.1.2 Comprehensive Two-Dimensional GC It is understood that even when using GC–MS, the high complexity of petroleum hydrocarbon mixtures and the lack of specificity of the mass spectra of certain hydrocarbon types (e.g., alkenes and cycloalkanes) often hamper their identification [24,25]. Comprehensive two-dimensional GC (GC×GC) is a relatively new technique that was introduced by Phillips and coworkers in the early 1990s for the separation of highly complex mixtures using a conventional GC combined with a fast GC [26,27]. GC×GC applies two columns with orthogonal selectivities. Generally, the stationary phase of the first-dimension column is nonpolar (e.g., 30m, 0.25 mm ID, 0.25 μ m DB-5, 5% phenylmethylpolysiloxane), while that of the second-dimension column is more polar (e.g., 2.0m, 0.1 mm ID, 0.1 μ m 14% OV-170, 14% cyanopropyl-phenyl in dimethylpolysiloxane) [28]. There is a jet-type cryogenic modulator between the two chromatographic columns to trap the component in the first column eluate. The analytes eluted from the second column have very narrow bands, that is, 50–150 ms.

In order to perform accurate compound identification and quantitative analysis of petroleum, the GC×GC system requires a very fast data acquisition detector. Typical capable detectors used with GC×GC in most applications include FID [29–31] and fast acquisition time-of-flight mass spectrometry (TOF-MS) [28,32]. Although GC×GC–FID can offer significant advantages in quantitative analysis of oil contamination in environmental samples, it fails to give a clear and full separation of the major hydrocarbon groups, that is, alkanes, cycloalkanes, alkenes, and aromatics [25]. The key features of GC×GC/TOF-MS are its large peak capacity, ability to separate substances into classes, and improved speed [28]. This technique allows not only assignment of a large number of compounds but also resolution of many coeluting components, such as tricyclic and pentacyclic terpanes [33].

Gaines et al. [24] and Cortes et al. [34] reviewed the advances, developments, and applications in GC×GC technique. This technique demonstrated advantage in separation and identification of petroleum hydrocarbons for forensic oil fingerprinting. von Muhlen et al. [35] used GC×GC to characterize petroleum and petroleum derivatives, through group type analysis, such as benzene, toluene, ethylbenzene, and *o*-, *m*-, and *p*-xylenes (BTEX); total aromatic hydrocarbons; polyaromatic hydrocarbons; and heteroatomic sulfur-, oxygen-, and nitrogen-containing compounds.

5.2.1.3 Programmable Temperature Vaporization-Large Volume Injection-Gas Chromatography (PTV-LVI-GC). Forensic oil spill identification relies largely upon the analysis of the chemical fingerprints of a series of petroleum hydrocarbons of the spilled oil and the suspected source. The most time-consuming part of the established oil analysis

methods is the sample preparation. A chromatographic column packed with activated silica gel is widely used to fractionate the petroleum hydrocarbons into the aliphatic and aromatic fractions, which are subsequently subjected to chromatographic analysis by GC–FID and GC–MS. The typical GC analysis generally has specifying 1–2 μ l injections at a splitless injection mode at high temperature (commonly 250–300°C). To improve the method detection limits, further concentration of the fractions is necessary, however this is time-consuming and tedious; in addition, the loss of light components in this preparatory procedure will lead to low accuracy and a low precision of analysis.

In practice, to achieve highly sensitive detection and to save time, more samples can be introduced into the GC column so that more mass consequently reaches the detector instead of further concentration. A large volume of sample, for example, 100 μ l or higher, is injected through a programmable temperature vaporization (PTV) inlet, thereby greatly enhancing the signal intensity of analytes at low concentrations. An additional benefit of this practice is the ability to reduce the amount of sample originally processed. Large-volume injection (LVI) technique was first introduced by Vogt et al. [36], and over the decades, it was continually explored and improved by a number of researchers. In principle, (i) the sample is introduced at a relatively low temperature (below solvent boiling point) to ensure maximum retention of the analytes in the liner by cold trapping and solvent trapping; (ii) then the majority of the solvent in the sample is vented via the split exit with a high flow rate of carrier gas while the higher-boiling analytes are retained in the liner; (iii) the split exit is closed and the injector temperature is rapidly increased to transfer the concentrated sample to the GC column in splitless mode. Meanwhile, the oven temperature is kept below the solvent boiling temperature to refocus the analytes at the front of the column; and (iv) after the splitless transfer, the split exit is reopened to remove residual solvent vapor and low-volatile matrix compounds from the inlet [37,38].

Hoh and Mastovska [37] reviewed the currently available LVI techniques, including basic approaches to their optimization and important real-world applications. To date, only a few simple studies reported using PTV-LVI system for petroleum-related analysis. Yang et al. [39] applied a PTV-LVI system coupled with GC–MS technique for oil fingerprinting analysis. The aliphatic (12 ml of elute) and aromatic (15 ml of elute) fractions of oil samples without nitrogen-blowing concentration were injected at a large volume of up to 25 μ l at the cold inlet temperature, rather than a conventional hot splitless injection of 1 μ l of 1.0 ml concentrated fractions for GC analysis. The target compounds including *n*-alkanes, PAHs, sesquiterpanes, diamondoids, and biomarker terpanes and steranes in crude oil and refined petroleum products were determined and compared using PTV-LVI-GC-MS and conventional GC–MS. Their results demonstrated PTV-LVI method to be efficient and suitable

for the quantitative characterization of target petroleum hydrocarbons. Results obtained from optimization of PTV-LVI parameters were compared with those from conventional hot split/splitless analysis. The detection limits of chromatographic analysis were improved between 1 and 2 orders of magnitude for *n*-alkanes and PAHs by increasing conventional injection volume of 1.0 μ l to a larger injection volume of 20 μ l.

For oil fingerprinting analysis by gas chromatographic instrument, the PTV-LVI technique has many advantages over the conventional hot split/splitless injection. Tedious sample pretreatment procedures may be simplified by eliminating or shortening the solvent evaporation step, which is not only time-consuming but also subject to chemical loss. In addition, a smaller amount of sample is necessary for sample preparation since the detection limits are enhanced greatly for the target compounds. However, the PTV-LVI injection is operated in a more complicated way than conventional hot split/splitless injection. Optimization of many operation factors such as inlet temperature, inlet vent time and speed, injection speed and injection volume, etc. is particularly critical to develop a reliable method.

5.2.2 GC with Mass Spectrometry

5.2.2.1 GC-MS The analytes eluted from a capillary column enter into a detector, where an electronic signal is generated based on the interaction of the solute with the detector. One of the early detection techniques for GC is FID. GC-FID is a robust, reliable, and universal technique for the detection of all species of hydrocarbons. However, this technique only produces two-dimensional data (i.e., retention time and abundance), but it is unable to provide the characteristics of individual molecules. Therefore, using GC-FID alone, it is difficult or impossible to identify or quantify the petroleum biomarkers and PAHs, which are at relatively low concentrations but of interest to forensic oil analysis. MS detection is a relatively recent technique. It has already occupied an outstanding position among analytical methods due to its unparalleled selectivity, detection limits, speed, and diversity of applications [40]. With the progressive development of instrumental analysis, GC-MS instrument has become an analytical tool for routine analysis in the environmental laboratories around the world. GC-MS instrument can provide accurate quantitation for volatile and semivolatile organic compounds in petroleum; moreover, the large mass spectrum library allows to conveniently identify an unknown peak in an instant.

Compounds from a GC capillary column subsequently enter the ion source and are ionized and fragmented. Many ionization techniques are available for different applications and for different target compounds; however, for petroleum analysis, electron impact ionization

(EI) is mostly used and followed by chemical ionization. If an EI source is applied, the analytes in the ion source are bombarded by high-energy (commonly ~70 eV) electrons emitted from the charged filament. The quadrupole mass spectrometer is an MS analyzer that has various applications. The ions travel through the quadrupole mass analyzer with four parallel metal rods. The ions are selectively guided into the mass analyzer by applying specific direct current and radio frequency voltages and electric fields, and as a result, only ions with a certain mass-to-charge ratio (m/z values) can reach the electron multiplier. The fragmentation pattern for each molecule is characteristic, making identification possible. To obtain the best sensitivity for quantitative measurement, the single quadrupole is usually operated in selected ion monitoring mode (SIM). A full-scan MS is still a useful mode of operation because it shows all the ions that are being formed in the ion source. This alerts analysts to other compounds coeluting with compounds of interest and is a helpful information for developing SIM acquisitions [41].

5.2.2.2 GC-MS/MS GC-MS is the preferred analytical technique for determining hydrocarbons in crude oil and petroleum products. However, in chemically complex samples, these compounds sometimes occur at low concentrations, and their distribution patterns are often difficult to distinguish due to environmental alterations; in addition, coeluted interfering substances, particularly unresolved complex mixture (UCM), hinder their accurate identification and quantitation using GC-MS techniques alone. Taking advantage of the selectivity provided by triple quadrupole MS (GC-MS/MS), it is possible to minimize or remove the interference and improve detection levels. In a triple quadrupole MS, ions are formed in the ion source and directed into the first quadrupole (Q1), which is tuned to allow a single precursor ion to pass through the quadrupole field. The isolated target ion enters the second quadrupole (Q2), and the target ions collide with argon atoms and dissociate into smaller product ions. The daughter ions produced by collision-induced dissociation subsequently enter the third-stage quadrupole (Q3), where the selected characteristic ions are separated into a mass spectrum. Through selection of proper precursor ions and product ions, GC-MS/MS undoubtedly provides higher degree of certainty in analyte identification and accuracy in quantitation compared with using any single-stage MS technique.

There are a few reports using this technique for oil analysis. Philp et al. [42] applied triple-stage quadrupole mass spectrometers to determine the complex mixtures of isomers that occur within many classes of biomarkers. MS/MS greatly enhanced the resolution of individual series of compounds and subsequently greatly increased the accuracy of the determinations of certain oil maturity measurements, such as those based on individual sterane isomers

or on the relative proportions of tricyclic and pentacyclic terpanes. Fernández-González et al. [43] developed a method using programmed temperature vaporization gas chromatography tandem mass spectrometry (PTV-GC-MS/MS) for the analysis of 27 unsubstituted and alkylated PAHs. They reported that the method significantly improved the detection and quantification limits, since PTV-GC-MS/MS can detect compounds at low-ppb levels in complex matrices.

To date, the applications of GC-MS/MS are still limited to the analysis of certain individual hydrocarbons. The understandable reasons include the complex nature of petroleum and the difficulty for method development using a sophisticated GC-MS/MS apparatus.

5.2.3 Ancillary Oil Fingerprinting Techniques

5.2.3.1 High-Performance Liquid Chromatography High-performance liquid chromatography (HPLC) is especially well suited when the separation is to be achieved in a short time frame. HPLC has been considered as the indispensable technique for bulk hydrocarbon analysis of the petroleum heavy ends and has been successfully utilized for quantitative analysis of saturates, monoaromatics, diaromatics, and polyaromatics in straight-run and processed fractions by various investigators [44,45].

As an example, an early approach is using HPLC for the separation of aromatic compounds from the saturated hydrocarbons in lubricating oil base stocks and the further separation of PAHs into fractions based on the number of fused rings [45]. Aromatic compounds were separated from the saturated hydrocarbons by HPLC using a silica column. The aromatic compounds were then backflushed onto an amine-derivatized silica column using a six-port two-position switching valve. The PAHs were separated according to the number of fused rings.

HPLC is used much less in oil fingerprinting analysis in comparison to GC techniques. Presently, the major drawback of HPLC applications for quantitation is the lack of availability of a universal detector that produces the same response for all classes of chemical compounds [44]. MS is more powerful than other normal detectors such as ultraviolet/visible (UV-Vis) detectors, fluorescence detectors, or refractive index detectors. However, LC-MS is more difficult to operate than GC-MS because the solvent needs to be removed before the eluate can be processed by the mass spectrometer. So far, it has rarely been used for general petroleum hydrocarbon analysis but could be particularly suitable for the analysis of some specific petroleum component such as naphthenic acids in heavy oils. The presence of naphthenic acids in heavy oils such as Alberta oil sands bitumen is of concern in the petroleum industry due to their corrosivity to refinery units. The characterization of naphthenic acids is also of interest to geochemical studies, particularly migration and biodegradation, and to refinery wastewater treatment for

environmental compliance [46]. MS is well suited for characterizing these acidic components at the molecular level. Hsu et al. [46] evaluated chemical ionization, liquid secondary ion MS (fast ion bombardment), atmospheric pressure chemical ionization (APCI), and electrospray ionization in both positive and negative ion modes for the determination of molecular distribution of acids without derivatization. The selectivity of negative-ion APCI for a whole range of acidic components in a crude oil has also been demonstrated. APCI also holds a great potential for online LC-MS to separate acids by HPLC followed by mass spectrometric characterization of acids.

5.2.3.2 Spectroscopic Techniques Besides the principal chromatographic techniques, many other techniques have been attempted in the application of oil fingerprinting analysis. These methods are mainly based on spectroscopic techniques such as UV-Vis, fluorescence, infrared (IR), and near-infrared (NIR) spectroscopy. These spectrometers have been widely equipped in the modern laboratory due to their simplicity, versatility, speed, accuracy, and cost-effectiveness for the determination of different chemicals.

Among the spectroscopic techniques, synchronous scanning fluorescence spectroscopy is relatively widely used for fingerprinting many petroleum contamination situations [47–51]. This technique simultaneously acquires both the excitation and emission spectra during sample scanning for the identification of fluorescent compounds in complex mixtures. This method allows for the classification and identification of aromatic-containing products such as gasoline, diesel oil, various grades of fuel oil, and asphalt. Used together with multivariate data analysis (e.g., principal component analysis, PCA), it provides a convenient tool to discriminate petrochemical samples.

Gugel and Siegel [52] and Bugden et al. [53] used excitation-emission matrix, also known as the 3D fluorescence spectra, in forensic oil investigations. Von der Dick and Kalkreuth [54] reported that 3D fluorescence can be used as a means of fingerprinting the maturation of coals and oils by detecting differences in the distribution of ring systems. Hegazi et al. [49] expanded on this approach, using remote sensing and time-resolved 3D fluorescence spectra to fingerprint crude oils, as an extension of the earlier work. Liu et al. [50] analyzed nine commercial oil samples of five types (heavy diesel, crude oil, diesel, gasoline, and lubricant) via 3D fluorescence spectroscopy and GC-MS. The 3D fluorescence spectra enabled classification of the nine oil samples into the five oil types, but the spectra were not applicable in distinguishing oils of the same type.

Spectroscopic techniques do not resolve the components in a sample. The chemical information about components is embedded in multiple bands in the spectra. Spectroscopic instruments alone provide very limited information for the unambiguous identification of unknown mixture, in

particular, for petroleum due to its extreme complexity and variety. For example, when applying the Fourier transform infrared (FT-IR) spectroscopy in oil analysis, the same functional groups generate the same frequency of IR absorption bands regardless of the structure of the rest of the molecule. The absorption bands of aliphatic C–H bonds, with additional bands originating from groups containing aromatics, oxygen, sulfur, and nitrogen, usually dominate the spectra of crude oils [55]. FT-IR spectrometer alone could only disclose the presence or absence for petroleum source through identification of strong spectra of C–H bonds and C=C double bonds, but not differentiate the oil type and weathering level.

Spectroscopic techniques could offer more useful information for oil analysis when coupled with chromatographic techniques, for instance, GC–IR and LC–UV. The extraction of information is possible by the use of multivariate techniques. Aske et al. [56] applied HPLC coupled with IR and NIR spectroscopy to characterize a number of oil samples ranging from light condensates to heavy crude oils. They applied HPLC to separate the oil samples into four SARA chemical groups for analysis with IR and NIR spectroscopy.

5.3 METHODOLOGY OF OIL FINGERPRINTING ANALYSIS

Some established chromatographic methods such as U.S. EPA SW-846 method 8270D and ASTM method D3328 provide a valuable basis for many analytical laboratories around the world to develop their own oil analysis methods [21,57]. SW-846 method 8270D, titled *Semivolatile Organic Compounds by Gas Chromatography/Mass Spectrometry (GC/MS)*, is designed to determine semivolatile organic compounds in extracts prepared from many types of solid waste matrices, soils, air sampling media, and water samples by GC/MS [57]. ASTM method D3328, titled *Standard Test Methods for Comparison of Waterborne Petroleum Oils by Gas Chromatography*, describes the comparison of petroleum oils recovered from water or beaches with oils from suspect sources by means of GC [21]. Many oil analytical methods are similar with only subtle differences between the actual experimental procedures, while some methods differ considerably. Thus, the compositional difference of the same oil determined by different laboratories is anticipated. In the last three decades, the Oil Research Laboratory of Environment Canada has been continually developing reliable analytical methods to determine a variety of petroleum hydrocarbons. This laboratory also has established a comprehensive database of physical properties and chemical fingerprints of over 500 crude oils and petroleum products from around the world. Table 5.2 summarizes the target petroleum compounds frequently used for forensic oil fingerprinting analysis by Environment Canada and other oil research

laboratories. These compounds include *n*-alkanes, BTEX and alkylbenzenes, alkylated PAH series, aromatic steranes, petroleum biomarkers, diamondoids, bicyclic sesquiterpanes, and so on.

As stated previously, the chemical composition of crude oil and refined petroleum products is extremely complex. Petroleum contains a huge number of different types of hydrocarbons and isomers. Analysis of the whole composition of petroleum can be endlessly complex, therefore the information to be collected should be dictated by those critical data. The analysis scheme widely applied is to separate a great number of petroleum compounds into largely saturate and aromatic fractions. The saturate fraction consists of nonpolar material including normal alkanes, branched alkanes, and cyclic saturated hydrocarbons including alkylcyclohexanes and polycyclic terpenoids. Aromatics contain one or more aromatic rings including unsubstituted and alkylated PAHs. Among them, *n*-alkanes, unsubstituted PAHs and alkylated PAHs, and biomarkers are commonly of most interest for oil analysis and have been well investigated. Normal alkanes and branched alkanes are typically the major resolved peaks in gas chromatograms of crude oils and light petroleum products. The commonly used biomarkers that occur within the residual range include pentacyclic triterpanes, regular and rearranged steranes, and mono- and triaromatic steranes. In recent years, smaller cyclic hydrocarbons such as diamondoids and bicyclic sesquiterpanes have attracted increasing attention due to their potential forensic applications especially for lighter oils and products [58–63]. These compounds were detected in most crude oils and in a variety of distilled petroleum products, which makes them useful for forensic oil identification particularly for lighter refined products such as jet and diesel fuels. In these lighter refined products, the high-molecular-weight biomarkers have been removed during the refining processes.

It is unnecessary to analyze all target compounds in Table 5.2 in an oil analysis. The selection of appropriate target oil analytes is dependent mainly on the type of oil spilled, the particular environmental compartments being assessed, and the expected needs for current and future data comparison.

5.3.1 Oil Sample Preparation and Separation

The determination of concentrations and relative distributions of target petroleum hydrocarbons are both essential to unambiguous oil spill identification because in some cases a source might have a similar distribution profile of analytes but significantly different actual amounts of these compounds [64]. Due to the complex nature of petroleum, however, proper sample preparation is essential in order to achieve accurate quantification of individual components and unbiased identification of the spill source. Various procedures for the fractionation of

TABLE 5.2 Target analytes frequently used for forensic oil fingerprinting analysis

Compounds	Code	Empirical formula	Molecular weight	Target ions
Internal standards				
5 α -Androstane (for TPH analysis by GC/FID)	IS	C ₁₉ H ₃₂	260	
C ₃₀ 17 β (H),21 β (H)-hopane (for terpane and sterane analysis)	IS	C ₃₀ H ₅₂	412	191
d ₁₈ -Decahydronaphthalene (<i>cis</i> -) (for bicyclic sesquiterpane analysis)	IS	C ₁₀ D ₁₈	156	156
d ₁₆ -Adamantane (for diamondoid analysis)	IS	C ₁₀ D ₁₆	152	152
d ₁₄ -Terphenyl (for PAH analysis)	IS	C ₁₈ D ₁₄	244	244
Surrogates				
<i>o</i> -Terphenyl (for TPH analysis by GC/FID)	Sur	C ₁₈ H ₁₄	230	—
d ₈ -Naphthalene	Sur	C ₁₀ D ₈	136	136
d ₁₀ -Acenaphthene	Sur	C ₁₂ D ₁₀	164	164
d ₁₀ -Phenanthrene	Sur	C ₁₄ D ₁₀	188	188
d ₁₂ -Benz(<i>a</i>)anthracene	Sur	C ₁₈ D ₁₂	240	240
d ₁₂ -Perylene	Sur	C ₂₀ D ₁₂	264	264
Saturated fractions				
Alkanes				
<i>n</i> -Alkanes (<i>n</i> -C ₈ to <i>n</i> -C ₄₄)	<i>n</i> -C _{<i>n</i>}	C _{<i>n</i>} H _{2<i>n</i>+2}	14 <i>n</i> + 2	85, 71, 57
Pristane	Pri	C ₁₉ H ₄₀	268	85, 113
Phytane	Phy	C ₂₀ H ₄₂	282	85, 183
Alkylated cyclopentanes				
		C _{<i>n</i>} H _{2<i>n</i>}	14 <i>n</i>	69, 83
Alkylated cyclohexanes				
		C _{<i>n</i>} H _{2<i>n</i>}	14 <i>n</i>	83, 97
Biomarker terpanes				
C ₁₉ tricyclic terpane	TR19	C ₁₉ H ₃₄	262	191
C ₂₀ tricyclic terpane	TR20	C ₂₀ H ₃₆	276	191
C ₂₁ tricyclic terpane	TR21	C ₂₁ H ₃₈	290	191
C ₂₂ tricyclic terpane	TR22	C ₂₂ H ₄₀	304	191
C ₂₃ tricyclic terpane	TR23	C ₂₃ H ₄₂	318	191
C ₂₄ tricyclic terpane	TR24	C ₂₄ H ₄₄	332	191
C ₂₅ tricyclic terpane (a)	TR25A	C ₂₅ H ₄₆	346	191
C ₂₅ tricyclic terpane (b)	TR25B	C ₂₅ H ₄₆	360	191
Triplet: C ₂₄ tetracyclic terpane + C ₂₆ (S + R) tricyclic terpanes	TET24 + TR26(A + B)	C ₂₄ H ₄₂ + C ₂₆ H ₄₈	330, 374	191
C ₂₈ tricyclic terpane (a)	TR28A	C ₂₈ H ₅₂	388	191
C ₂₈ tricyclic terpane (b)	TR28B	C ₂₈ H ₅₂	388	191
C ₂₉ tricyclic terpane (a)	TR29A	C ₂₉ H ₅₄	402	191
C ₂₉ tricyclic terpane (b)	TR29B	C ₂₉ H ₅₄	402	191
18 α (H)-22,29,30-trisnorhopane	Ts	C ₂₇ H ₄₆	370	191
17 α (H),18 α (H),21 β (H)-25,28,30-trisnorhopane	TH27	C ₂₇ H ₄₆	370	191, 177
17 α (H)-22,29,30-trisnorhopane	Tm	C ₂₇ H ₄₆	370	191
C ₃₀ tricyclic terpane 1	TR30A	C ₃₀ H ₅₂	412	191
C ₃₀ tricyclic terpane 2	TR30B	C ₃₀ H ₅₂	412	191
17 α (H),18 α (H),21 β (H)-28,30-bisnorhopane	H28	C ₂₈ H ₄₈	384	191
17 α (H),21 β (H)-25-norhopane	NOR25H	C ₂₉ H ₅₀	398	191, 177
17 α (H),21 β (H)-30-norhopane	H29	C ₂₉ H ₅₀	398	191
18 α (H),21 β (H)-30-norhopane	C29Ts	C ₂₉ H ₅₀	398	191
17 α (H)-diahopane	DH30	C ₃₀ H ₅₂	412	191
17 β (H),21 α (H)-30-norhopane (normoretane)	M29	C ₂₉ H ₅₀	398	191
18 α (H) and 18 β (H)-oleanane	OL	C ₃₀ H ₅₂	412	191, 412
17 α (H),21 β (H)-hopane	H30	C ₃₀ H ₅₂	412	191
17 α (H)-30-nor-29-homohopane	NOR30H	C ₃₀ H ₅₂	412	191
17 β (H),21 α (H)-hopane (moretane)	M30	C ₃₀ H ₅₂	412	191
22S-17 α (H),21 β (H)-30-homohopane	H31S	C ₃₁ H ₅₄	426	191
22R-17 α (H),21 β (H)-30-homohopane	H31R	C ₃₁ H ₅₄	426	191
Gammacerane				
	G	C ₃₀ H ₅₂	412	191, 412
22S-17 α (H),21 β (H)-30,31-bishomohopane	H32S	C ₃₂ H ₅₆	440	191
22R-17 α (H),21 β (H)-30,31-bishomohopane	H32R	C ₃₂ H ₅₆	440	191
22S-17 α (H),21 β (H)-30,31,32-trishomohopane	H33S	C ₃₃ H ₅₈	454	191
22R-17 α (H),21 β (H)-30,31,32-trishomohopane	H33R	C ₃₃ H ₅₈	454	191
22S-17 α (H),21 β (H)-30,31,32,33-tetrakishomohopane	H34S	C ₃₄ H ₆₀	468	191
22R-17 α (H),21 β (H)-30,31,32,33-tetrakishomohopane	H34R	C ₃₄ H ₆₀	468	191
22S-17 α (H),21 β (H)-30,31,32,33,34-pentakishomohopane	H35S	C ₃₅ H ₆₂	482	191
22R-17 α (H),21 β (H)-30,31,32,33,34-pentakishomohopane	H35R	C ₃₅ H ₆₂	482	191
Biomarker steranes				
C ₂₀ 5 α (H),14 α (H),17 α (H)-sterane	S20	C ₂₀ H ₃₄	274	217, 218
C ₂₁ 5 α (H),14 β (H),17 β (H)-sterane	S21	C ₂₁ H ₃₆	288	217
C ₂₂ 5 α (H),14 β (H),17 β (H)-sterane	S22	C ₂₂ H ₃₈	302	217
C ₂₇ 20S-13 β (H),17 α (H)-diasterane	DIA27S	C ₂₇ H ₄₈	372	217

TABLE 5.2 (Continued)

Compounds	Code	Empirical formula	Molecular weight	Target ions
C ₂₇ 20R-13β(H),17α(H)-diasterane	DIA27R	C ₂₇ H ₄₈	372	217
C ₂₇ 20S-13α(H),17β(H)-diasterane	DIA27S2	C ₂₇ H ₄₈	372	217
C ₂₇ 20R-13α(H),17β(H)-diasterane	DIA27R2	C ₂₇ H ₄₈	372	217
C ₂₈ 20S-13β(H),17α(H)-diasterane	DIA28S	C ₂₈ H ₅₀	386	217
C ₂₈ 20R-13β(H),17α(H)-diasterane	DIA28R	C ₂₈ H ₅₀	386	217
C ₂₉ 20S-13β(H),17α(H)-diasterane	DIA29S	C ₂₉ H ₅₂	400	217
C ₂₉ 20R-13α(H),17β(H)-diasterane	DIA29R	C ₂₉ H ₅₂	400	217
C ₂₇ 20S-5α(H),14α(H),17α(H)-cholestane	C27ααS	C ₂₇ H ₄₈	372	217
C ₂₇ 20R-5α(H),14β(H),17β(H)-cholestane	C27ββR	C ₂₇ H ₄₈	372	217, 218
C ₂₇ 20S-5α(H),14β(H),17β(H)-cholestane	C27ββS	C ₂₇ H ₄₈	372	217, 218
C ₂₇ 20R-5α(H),14α(H),17α(H)-cholestane	C27ααR	C ₂₇ H ₄₈	372	217
C ₂₈ 20S-5α(H),14α(H),17α(H)-ergostane	C28ααS	C ₂₈ H ₅₀	386	217
C ₂₈ 20R-5α(H),14β(H),17β(H)-ergostane	C28ββR	C ₂₈ H ₅₀	386	217, 218
C ₂₈ 20S-5α(H),14β(H),17β(H)-ergostane	C28ββS	C ₂₈ H ₅₀	386	217, 218
C ₂₈ 20R-5α(H),14α(H),17α(H)-ergostane	C28ααR	C ₂₈ H ₅₀	386	217
C ₂₉ 20S-5α(H),14α(H),17α(H)-stigmastane	C29ααS	C ₂₉ H ₅₂	400	217
C ₂₉ 20R-5α(H),14β(H),17β(H)-stigmastane	C29ββR	C ₂₉ H ₅₂	400	217, 218
C ₂₉ 20S-5α(H),14β(H),17β(H)-stigmastane	C29ββS	C ₂₉ H ₅₂	400	217, 218
C ₂₉ 20R-5α(H),14α(H),17α(H)-stigmastane	C29ααR	C ₂₉ H ₅₂	400	217
C ₃₀ steranes	C30ααS	C ₃₀ H ₅₄	412	217
Bicyclic sesquiterpanes				
C ₄ -decalin	BS1	C ₁₄ H ₂₆	194	123, 179
C ₁₄ sesquiterpane	BS2	C ₁₄ H ₂₆	194	123, 179
C ₁₅ sesquiterpane	BS3	C ₁₅ H ₂₈	208	123, 193
C ₁₅ sesquiterpane	BS4	C ₁₅ H ₂₈	208	123, 193
8β(H)-drimane	BS5	C ₁₅ H ₂₈	208	123
C ₁₅ sesquiterpane	BS6	C ₁₅ H ₂₈	208	123
C ₁₆ sesquiterpane	BS7	C ₁₆ H ₃₀	222	123
C ₁₆ sesquiterpane	BS8	C ₁₆ H ₃₀	222	123, 193
C ₁₆ sesquiterpane	BS9	C ₁₆ H ₃₀	222	123, 193
8β(H)-homodrimane	BS10	C ₁₆ H ₃₀	222	123, 207
Adamantanes				
Adamantane	A	C ₁₀ H ₁₆	136	136
1-Methyladamantane	1-MA	C ₁₁ H ₁₈	150	135
1,3-Dimethyladamantane	1,3-DMA	C ₁₂ H ₂₀	164	149
1,3,5-Trimethyladamantane	1,3,5-TMA	C ₁₃ H ₂₂	178	163
1,3,5,7-Tetramethyladamantane	1,3,5,7-TeMA	C ₁₄ H ₂₄	192	177
2-Methyladamantane	2-MA	C ₁₁ H ₁₈	150	135
1,4-Dimethyladamantane, <i>cis</i>	1,4-DMA, <i>cis</i>	C ₁₂ H ₂₀	164	149
1,4-Dimethyladamantane, <i>trans</i>	1,4-DMA, <i>trans</i>	C ₁₂ H ₂₀	164	149
1,3,6-Trimethyladamantane	1,3,6-TMA	C ₁₃ H ₂₂	178	163
1,2-Dimethyladamantane	1,2-DMA	C ₁₂ H ₂₀	164	149
1,3,4-Trimethyladamantane, <i>cis</i>	1,3,4-TMA, <i>cis</i>	C ₁₃ H ₂₂	178	163
1,3,4-Trimethyladamantane, <i>trans</i>	1,3,4-TMA, <i>trans</i>	C ₁₃ H ₂₂	178	163
1,2,5,7-Tetramethyladamantane	1,2,5,7-TeMA	C ₁₄ H ₂₄	192	177
1-Ethyladamantane	1-EA	C ₁₂ H ₂₀	164	135
1-Ethyl-3-methyladamantane	1-E-3-MA	C ₁₃ H ₂₂	178	149
1-Ethyl-3,5-dimethyladamantane	1-E-3,5-DMA	C ₁₄ H ₂₄	192	163
2-Ethyladamantane	2-EA	C ₁₂ H ₂₀	164	135
Diamantanes				
Diamantane	D	C ₁₄ H ₂₀	188	188
4-Methyldiamantane	4-MD	C ₁₅ H ₂₂	202	187
4,9-Dimethyldiamantane	4,9-DMD	C ₁₆ H ₂₄	216	201
1-Methyldiamantane	1-MD	C ₁₅ H ₂₂	202	187
1,4 & 2,4-dimethyldiamantane	1,4 & 2,4-DMD	C ₁₆ H ₂₄	216	201
4,8-Dimethyldiamantane	4,8-DMD	C ₁₆ H ₂₄	216	201
Trimethyldiamantane	TMD	C ₁₇ H ₂₆	230	215
3-Methyldiamantane	3-MD	C ₁₅ H ₂₂	202	187
3,4-Dimethyldiamantane	3,4-DMD	C ₁₆ H ₂₄	216	201
Aromatic fraction				
Alkylated PAHs				
C ₀ -Naphthalene	C0N	C ₁₀ H ₈	128	128
C ₁ -Naphthalenes	C1N	C ₁₁ H ₁₀	142	142
C ₂ -Naphthalenes	C2N	C ₁₂ H ₁₂	156	156
C ₃ -Naphthalenes	C3N	C ₁₃ H ₁₄	170	170

(Continued)

TABLE 5.2 (Continued)

Compounds		Code	Empirical formula	Molecular weight	Target ions
C ₄ -Naphthalenes		C4N	C ₁₄ H ₁₆	184	184
C ₀ -Phenanthrenes/anthracene		C0P	C ₁₄ H ₁₀	178	178
C ₁ -Phenanthrenes/anthracenes		C1P	C ₁₅ H ₁₂	192	192
C ₂ -Phenanthrenes/anthracenes		C2P	C ₁₆ H ₁₄	206	206
C ₃ -Phenanthrenes/anthracenes		C3P	C ₁₇ H ₁₆	220	220
C ₄ -Phenanthrenes/anthracenes		C4P	C ₁₈ H ₁₈	234	234
C ₀ -Dibenzothiophene		C0D	C ₁₂ H ₈ S	184	184
C ₁ -Dibenzothiophenes		C1D	C ₁₃ H ₁₀ S	198	198
C ₂ -Dibenzothiophenes		C2D	C ₁₄ H ₁₂ S	212	212
C ₃ -Dibenzothiophenes		C3D	C ₁₅ H ₁₄ S	226	226
C ₀ -Fluorene		C0F	C ₁₃ H ₁₀	166	166
C ₁ -Fluorenes		C1F	C ₁₄ H ₁₂	180	180
C ₂ -Fluorenes		C2F	C ₁₅ H ₁₄	194	194
C ₃ -Fluorenes		C3F	C ₁₆ H ₁₆	208	208
C ₀ -Chrysene		C0C	C ₁₈ H ₁₂	228	228
C ₁ -Chrysenes		C1C	C ₁₉ H ₁₄	242	242
C ₂ -Chrysenes		C2C	C ₂₀ H ₁₆	256	256
C ₃ -Chrysenes		C3C	C ₂₁ H ₁₈	270	270
C ₀ -Pyrene/fluoranthene		C0Py	C ₁₆ H ₁₀	202	202
C ₁ -Pyrene/fluoranthenes		C1Py	C ₁₇ H ₁₂	216	216
C ₂ -Pyrene/fluoranthenes		C2Py	C ₁₈ H ₁₄	230	230
C ₃ -Pyrene/fluoranthenes		C3Py	C ₁₉ H ₁₆	244	244
Other U.S. EPA priority PAHs (Aromatic ring number)					
Biphenyl	(2-ring)	Bph	C ₁₂ H ₁₀	154	154
Acenaphthylene	(3-ring)	Acl	C ₁₂ H ₈	152	152
Acenaphthene	(3-ring)	Ace	C ₁₂ H ₁₀	154	153
Anthracene	(3-ring)	An	C ₁₄ H ₁₀	178	178
Fluoranthene	(4-ring)	Fl	C ₁₆ H ₁₀	202	202
Pyrene	(4-ring)	Py	C ₁₆ H ₁₀	202	202
Benz(a)anthracene	(4-ring)	BaA	C ₁₈ H ₁₂	228	228
Benzo(b)fluoranthene	(5-ring)	BbF	C ₂₀ H ₁₂	252	252
Benzo(k)fluoranthene	(5-ring)	BkF	C ₂₀ H ₁₂	252	252
Benzo(e)pyrene	(5-ring)	BeP	C ₂₀ H ₁₂	252	252
Benzo(a)pyrene	(5-ring)	BaP	C ₂₀ H ₁₂	252	252
Perylene	(5-ring)	Pe	C ₂₀ H ₁₂	252	252
Indeno(1,2,3- <i>cd</i>)pyrene	(6-ring)	IP	C ₂₂ H ₁₂	276	276
Dibenz(a,h)anthracene	(5-ring)	DA	C ₂₂ H ₁₄	278	278
Dibenzo(g,h,i)perylene	(6-ring)	BP	C ₂₂ H ₁₂	276	276
Triaromatic steranes (TA-steranes, m/z 231)					
C ₂₀ TA-sterane (X=ethyl)		C20TA	C ₂₀ H ₂₀	260	231
C ₂₁ TA-sterane (X=2-propyl)		C21TA	C ₂₁ H ₂₂	274	231
C ₂₂ TA-sterane (X=2-butyl) (a and b are epimers at C-19)		C22TA	C ₂₂ H ₂₄	288	231
C ₂₆ TA-cholestane (20S)		SC26TA	C ₂₆ H ₃₂	344	231
C ₂₆ TA-cholestane (20R) + C ₂₇ TA-ergostane (20S)		RC26TA + SC27TA	C ₂₆ H ₃₂ , C ₂₇ H ₃₄	344, 358	231
C ₂₈ TA-stigmastane (20S)		SC28TA	C ₂₈ H ₃₆	372	231
C ₂₇ TA-ergostane (20R)		RC27TA	C ₂₇ H ₃₄	358	231
C ₂₈ TA-stigmastane (20R)		RC28TA	C ₂₈ H ₃₆	372	231
Monoaromatic steranes (MA-steranes, m/z 253)					
C ₂₁ MA-sterane (X=ethyl)		C21MA	C ₂₁ H ₃₀	282	253
C ₂₂ MA-sterane (X=2-propyl)		C22MA	C ₂₂ H ₃₂	396	253
C ₂₃ MA-sterane (X=2-butyl) (a and b are epimers at C-20)		C23MA	C ₂₃ H ₃₄	410	253
C ₂₇ 5β(H) MA-cholestane (20S)			C ₂₇ H ₄₂	366	253
C ₂₇ MA-diacholestane (20S)			C ₂₇ H ₄₂	366	253
C ₂₇ 5β(H) MA-cholestane (20R) + C ₂₇ MA-diacholestane (20R)			C ₂₇ H ₄₂	366	253
C ₂₇ 5α(H) MA-cholestane (20S)		SC27MA	C ₂₇ H ₄₂	366	253
C ₂₈ 5β(H) MA-ergostane (20S) + C ₂₈ MA-diaergostane (20S)			C ₂₈ H ₄₄	380	253
C ₂₇ 5α(H) MA-cholestane (20R)			C ₂₇ H ₄₂	366	253
C ₂₈ 5α(H) MA-ergostane (20S)			C ₂₈ H ₄₄	380	253
C ₂₈ 5β(H) MA-ergostane (20R) + C ₂₈ MA-diaergostane (20R)			C ₂₈ H ₄₄	380	253
C ₂₉ 5β(H) MA-stigmastane (20S) + C ₂₉ MA-diaestigmastane (20S)			C ₂₉ H ₄₆	394	253
C ₂₉ 5α(H) MA-stigmastane (20S)		SC29MA	C ₂₉ H ₄₆	394	253
C ₂₈ 5α(H) MA-ergostane (20R)		RC28MA	C ₂₈ H ₄₄	380	253
C ₂₉ 5β(H) MA-stigmastane (20R)		RC29MA	C ₂₉ H ₄₆	394	253
C ₂₉ 5α(H) MA-stigmastane (20R)		RC29MA	C ₂₉ H ₄₆	394	253
C ₃₀ 5β(H) MA-sterane (20S)		C30MA	C ₃₀ H ₄₈	408	253

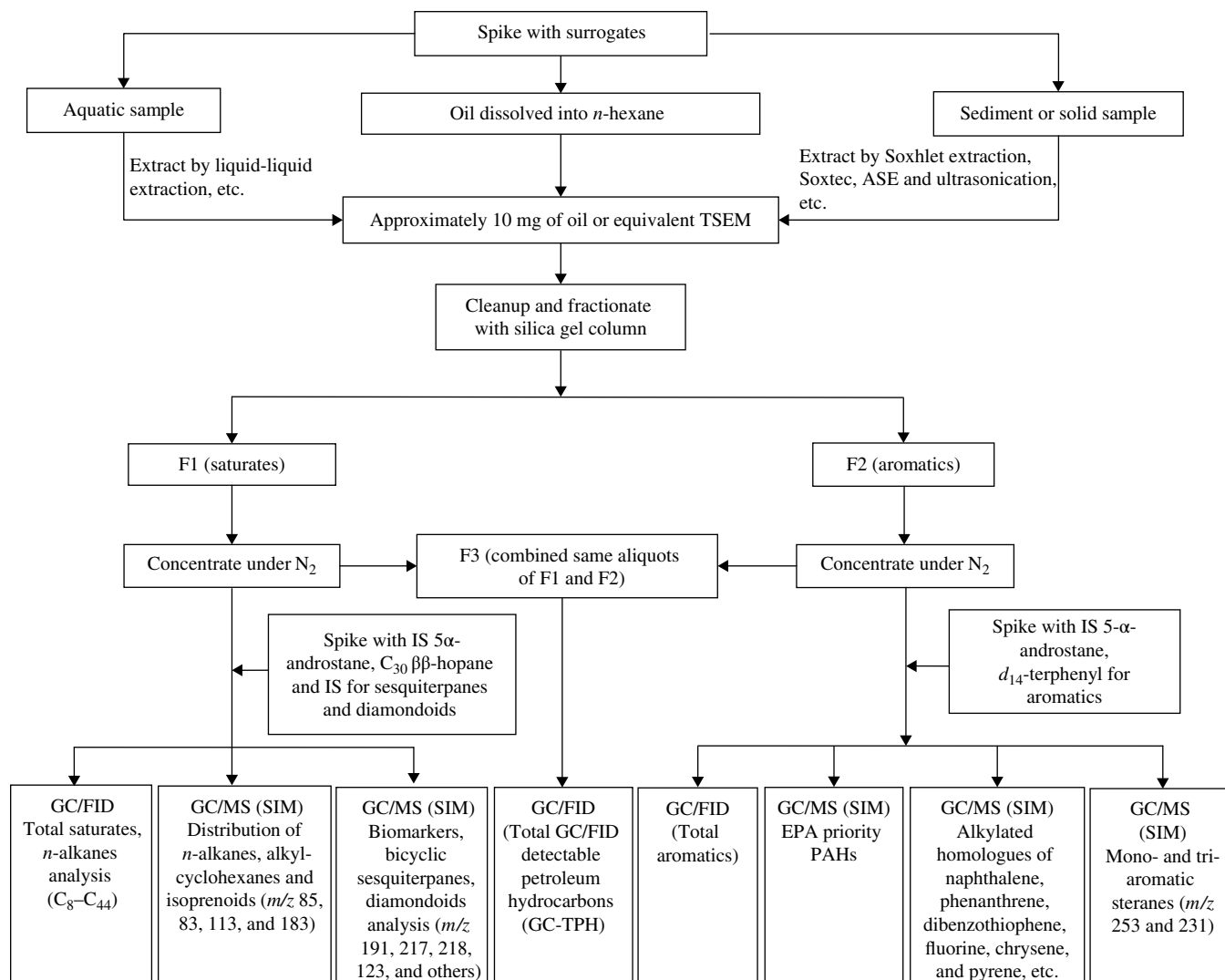


FIGURE 5.3 Schematic of oil analysis procedure.

petroleum into aliphatic, aromatic, and other hydrocarbon groups have been reported in previous studies. The most commonly used methods for forensic oil fingerprinting were developed by the Oil Research Laboratory of Environment Canada [18,60,65,66] and European institutes [19,20,22,67], while other methods have been suggested. These GC-based analytical methods have demonstrated to be efficient and suitable for the quantitative characterization of petroleum hydrocarbons in both crude oils and refined products.

Collection and preparation of representative oil or environmental samples are not discussed in this chapter, but they are crucial to successful forensic approach. Figure 5.3 depicts the procedure of an oil fingerprinting analysis used in the Oil Research Laboratory of Environment Canada. An aliquot of oil solution or equivalent extract of environmental samples is spiked with appropriate

deuterated surrogates. Pure oil samples can be directly weighed and dissolved into proper solvents for analysis. Hexane and dichloromethane (DCM) are often used, but DCM needs to be exchanged into hexane if silica gel column is used for cleanup. The analysis of oil-contaminated environmental samples involves first the recovery of extractable organic materials from their matrices such as water and soil. It is necessary to determine the total solvent-extractable materials (TSEMs) for real environmental samples with a matrix of water and soil in order to reflect the contamination level, to calculate the proper aliquot of the extract to load on the chromatographic column, and to facilitate a comparison of abundance of target compounds in samples. The techniques for extraction of solid samples such as soil and sediments include conventional Soxhlet extraction and ultrasonication, more recent automatic Soxtec extraction, supercritical fluid extraction,

microwave-assisted extraction, and accelerated solvent extraction, which have been promulgated by the U.S. EPA as soil extraction methods [68,69]. For the aqueous samples, the traditional liquid–liquid extraction is most reliable and still used widely although other techniques including solid-phase extraction (SPE), solid-phase microextraction, membrane-assisted solvent extraction, rod extraction, and stir bar sorptive extraction have been developed. To select the proper extraction technique, one should consider the complex nature of petroleum. Some advanced techniques may be unable to process such “dirty” samples. Traditional liquid–solid and liquid–liquid extractions are still used as the first choice in many laboratories due to their simplicity, relatively low cost, and proved high extraction efficiency, although these techniques are very time-consuming.

To achieve reliable and accurate oil analysis results and to protect the instrument from contamination, proper sample cleanup and further fractionation are necessary prior to instrumental analysis although direct injection of diluted oil solution or extracts into an instrument may be applied for fast screening. Oil solution or extract is transferred to the top of an activated silica gel microchromatographic column for sample cleanup and fractionation. The column had been preconditioned using *n*-hexane. Saturated and aromatic hydrocarbons are effectively eluted with *n*-hexane and *n*-hexane/DCM (1:1, v/v), respectively [66].

The saturated hydrocarbon fraction (F_1) is used for analysis of diamondoid hydrocarbons, sesquiterpanes, biomarker terpanes and sterane compounds as well as *n*-alkanes. The aromatic hydrocarbon fraction (F_2) was used for analysis of alkylated homologous polycyclic aromatic hydrocarbons (APAHs) and other U.S. EPA priority unsubstituted PAHs. These two fractions (F_1 and F_2) are carefully concentrated under a stream of nitrogen to appropriate volumes, spiked with internal standards (such as d_{16} -adamantane, d_{18} -*cis*-decahydronaphthalene, C_{30} $\beta\beta$ -hopane, and 5α -androstane into F_1 for analyses of diamondoids, sesquiterpanes, biomarker terpanes and steranes, and *n*-alkanes, respectively, and d_{14} -*p*-terphenyl into F_2 for PAH analysis), and finally adjusted to accurate preinjection volumes for GC–MS (SIM) and GC–FID analyses.

Silica gel column methods have been proven to be effective and reliable; however, they are often complicated and time-consuming because they generally require pretreatment, cleaning, preparation, and activation of adsorbent packing materials. In addition, large volumes of high-purity solvents are necessary for each chromatographic or partitioning step. To meet the need for rapid oil fingerprinting analysis, particularly in emergency spill incidents, commercial SPE cartridges might be a possible alternative for developing a rapid and reproducible method. SPE cartridges remain the most popular means of extraction and concentration for most emerging contaminants. They are used to

capture a broader range of analytes within a single extraction [70].

Recently, commercially available SPE cartridges were applied for accurate determination of aliphatic hydrocarbon and PAH in petroleum residues and further application in chemical fingerprinting of oil spills by GC–MS [71,72]. A series of commercially available Florisil cartridges, normal-phase SPE cartridges, and silica gel/cyanopropyl (SiO_2/C_3 -CN) SPE cartridges were used for the fractionation of oil into aliphatic and aromatic hydrocarbons in various crude oils, refined petroleum products, and environmental sediment samples [72]. It was reported that the Florisil cartridges and normal-phase SPE cartridges could clean up the oil samples but were unable to efficiently separate the oils into two fractions. The SiO_2/C_3 -CN (1.0/0.5 g) SPE cartridge successfully separates oil samples into aliphatic and aromatic fractions by eluting with 4 ml of hexane and 4 ml of DCM/hexane (3:1, v/v), respectively. The SPE fractionation procedure can be compared with the conventional silica gel adsorption chromatography, showing similar results but practical advantages in terms of reproducibility, analysis time, solvent reduction, and cost.

5.3.2 Identification and Quantitation of Target Petroleum Hydrocarbons

The analysis of specific petroleum hydrocarbons is of particular importance in oil forensic studies since they can provide valuable information toward achieving a better characterization and identification of a petroleum sample. The identification of target petroleum hydrocarbons usually relies on the application of reference oils since it is impractical to apply authentic standards for a large number of target compounds. Reference oils processed as a normal sample also provide the quality control for an oil study. For different case studies, different reference oils can be applied. The Oil Research Laboratory of the Emergencies Science and Technology Section established a reference oil (13.1% weathered Prudhoe Bay crude oil), which consists of most of the common target compounds and at appropriate abundance.

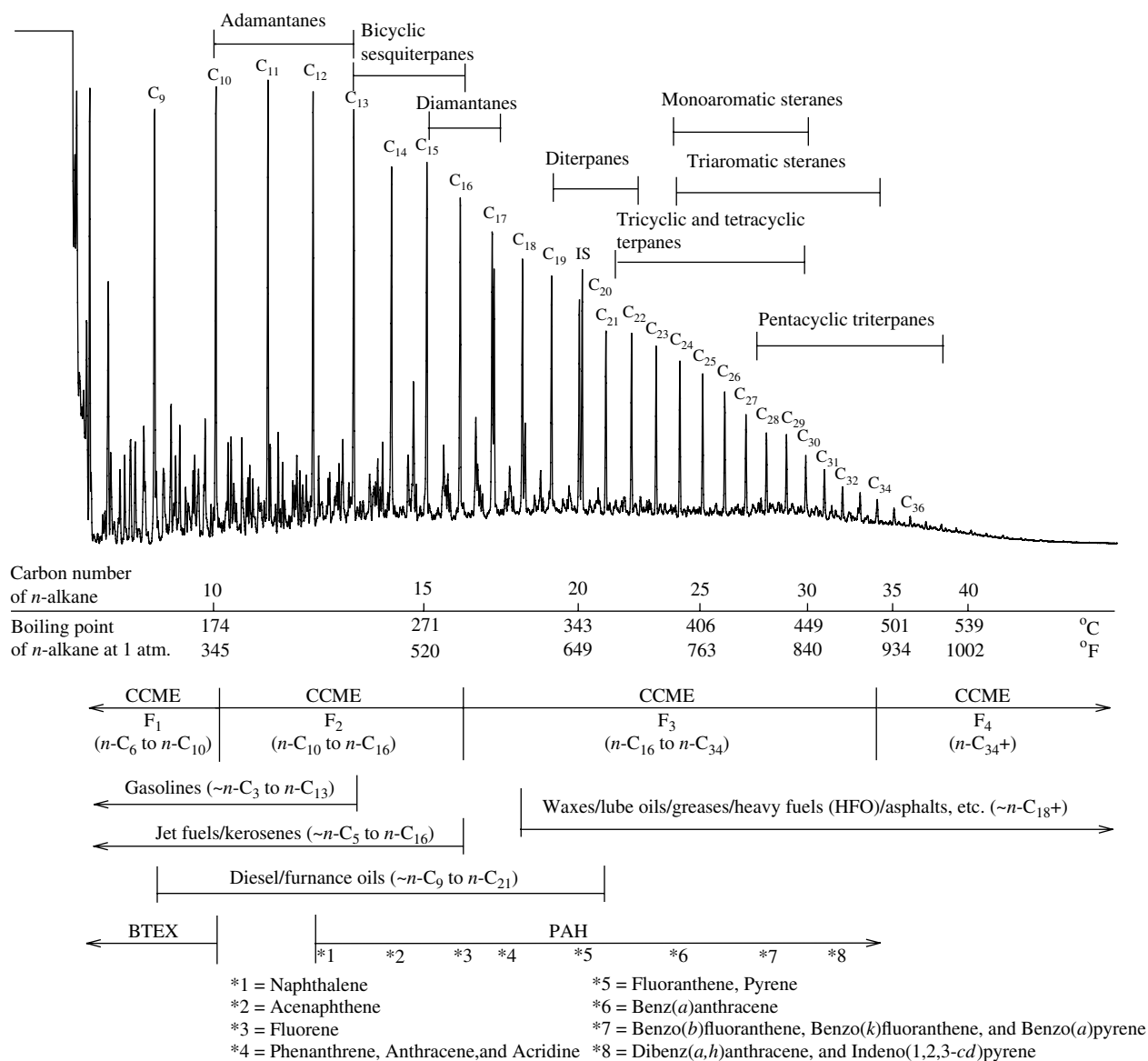
Target compounds frequently used in oil fingerprinting analysis are summarized in Table 5.2, including internal and surrogate standards and aliphatic and aromatic petroleum hydrocarbons. Figure 5.4 depicts the distribution of each hydrocarbon group in chromatographic analysis. The fingerprinting analysis of each hydrocarbon group will be separately discussed in more detail in the following sections. In brief, the commonly used fragment ions are m/z 191 for tri- to pentacyclic terpanes and m/z 217 and 218 for steranes. Bicyclic sesquiterpanes are determined at m/z 123 and confirmed by ions of m/z 179, 193, and 207. The ions for diamondoid analysis include m/z 135, 136, 149, 163, and 177 for adamantanes and m/z 187, 188, 201, and 215 for diamantanes. PAH series can be determined by GC–MS with a suit of parent molecular ions, for

TABLE 5.3 Concentration of GC/FID-detectable petroleum hydrocarbons in representative crude oils and refined petroleum products

	Crude oils					Refined petroleum products						
	Scotia Light (ScL) (API=53.2, Nova Scotia, Canada)	South Louisiana (SoL) (API=37.2, Louisiana, USA)	Cook Inlet (CI) (API=34.1, Southern Alaska)	Troll (API=28.4, North Sea)	Platform Elly (PIE) (API=15.8, U.S. West Coast)	Alberta oil sands bitumen (AOS) ^{iv} (Alberta, Canada)	Jet A (CV-580, Ottawa)	Diesel No. 2 (Ottawa, Canada)	IFO-180 (Canada, 2004)	Bunker B (Fuel No. 5) (USA, 2002)	Bunker C (Fuel No. 6) (Canada, 2002)	Lubricating oil 10W-30 (Motor oil, Ottawa, 2004)
Oil samples												
TPH (mg/g)	577	688	601	723	436	302	914	957	463	476	370	808
≤ <i>n</i> -C ₈ to <i>n</i> -C ₁₀ (%)	9.8	9.9	11.3	6.9	5.3	0.1	13.4	6.3	1.2	0.92	1.85	0.0
<i>n</i> -C ₁₀ to <i>n</i> -C ₁₆ (%)	59.5	28.5	28.5	25.0	18.1	9.5	84.2	54.5	21.8	12.8	13.3	0.1
<i>n</i> -C ₁₆ to <i>n</i> -C ₃₄ (%)	30.1	53.6	50.3	59.3	57.9	65.9	2.4	39.1	71.3	67.5	63.8	84.7
≥ <i>n</i> -C ₃₄ (%)	0.6	8.0	10.0	8.8	18.7	24.4	0.0	0.0	5.7	18.8	21.1	15.2
TSH/TPH (%)	95.3	82.5	73.5	71.6	51.8	57.4	86.6	89.8	52.7	63.1	47.6	94.9
TAH/TPH (%)	4.7	17.5	26.5	28.4	48.2	42.5	13.4	10.2	47.3	36.9	52.4	5.1
Resolved peaks/ GC-TPHs (%)	47.7	20.8	24.8	15.6	13.0	2.5	29.5	22.3	19.4	25.3	27.7	4.1
GC-UCM/GC-TPH (%)	52.3	79.2	75.2	84.4	87.0	97.5	70.5	77.7	80.6	74.7	72.3	95.9
Total <i>n</i> -alkanes (mg/g)	172	73.8	79.0	35.6	21.5	ND	121	128	42.3	46.4	29.1	ND

^aRaw sands extract. Concentration: mg/g of TSEM of Alberta oil sands. This Alberta oil sands sample contains 0.13 g/g of TSEM (DCM as solvent).
ND, nondetectable; TAH, total aromatic hydrocarbons.

Petrogenic hydrocarbons



Note: The carbon ranges of the four fractions, F₁–F₄, are defined in the Tier 1 TPH analytical method by the Canadian Council of Ministers of the Environment (CCME).

Biogenic organic matter (BOM)

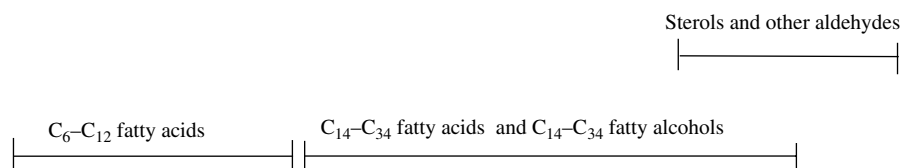


FIGURE 5.4 Distribution of target compounds for forensic oil fingerprinting analysis.

example, m/z 128, 142, 156, 170, and 184 for C₀- to C₄-naphthalenes; m/z 178, 192, 206, 220, and 234 for C₀- to C₄-phenanthrenes; and so on. Aromatic steroids are determined at m/z 231 for triaromatic steranes (TASs) and at m/z 253 for monoaromatic steranes (MASs).

Quantitative analysis requires standard compounds, either external or internal. The relative response factor (RRF) for each hydrocarbon component in the standard solution is calculated relative to the internal standard using the following equation:

$$\text{RRF}_A = \left(\frac{A_A}{C_A} \right) / \left(\frac{A_{IS}}{C_{IS}} \right) \quad (5.2)$$

where A_A and A_{IS} are the response area for a target analyte and the internal standard in the standard solution to be measured, respectively, and C_A and C_{IS} represent the concentration of the target analyte and the internal standard in the standard solution, respectively.

The concentration of target compounds can be obtained by

$$C_A = \frac{A_{A-S} \times C_{IS-S}}{A_{IS-S} \times \text{RRF}_A \times W_S} \quad (5.3)$$

where A_{A-S} is the response for the target analyte in sample solution, A_{IS-S} is the response for the internal standard spiked in the final sample solution, C_{IS-S} is the concentration of internal standard spiked in the final sample solution, and W_S is the sample weight used for the analysis.

For environmental samples such as water and sediment, the final resulting target analytes can be expressed in terms of TSEMs or TPHs instead of units per whole sample. This kind of expression can truly reflect the types of oil in environmental samples and facilitate convenient study on the weathering effect.

The quantitative analysis of many target petroleum hydrocarbons, for example, some APAHs, biomarker terpanes and steranes, and bicyclic sesquiterpanes, is usually based on the RRFs of their corresponding alternatives rather than on authentic standards relative to the internal standards [65]. Discrepancy could result in their quantitation if different quantitative standards are used. In theory, the discrepancy could be avoided or reduced by using authentic standards; however, most alkylated PAHs and biomarkers are not commercially available or very costly, even if available. Nevertheless, for forensic oil fingerprinting analysis, the relative distribution of target compounds is somewhat more important than their real-world concentration; therefore, the quantitation using alternative standards is still meaningful to oil characterization and identification.

5.3.3 Oil Type Screening by GC-FID

The first step of forensic oil fingerprinting is usually to screen the petroleum hydrocarbons in the sample to identify the oil type and evaluate its weathering [4,20,22,67]. Incorrect identification of oil type could misdirect subsequent tiered analysis, eventually leading to incorrect results. The physical appearance such as color and odor are helpful to preliminarily identify the type of oil samples. However, in order to unambiguously identify the oil, dedicated instrumental analysis is important, particularly to those samples may lead to legal issues.

As a universal and nonspecific analytical technique, GC-FID analysis is often first used in a tiered approach. Rather than to determine individual components, it aims to determine the types of oil samples and to investigate if the oil is weathered through the overall distribution of hydrocarbons. These methods do not give access to detailed information of individual target compounds; only the TPH concentration or carbon number fractions can be obtained. In addition to measuring TPH and other hydrocarbon groups (including the total saturates, the total aromatics, the total resolved peaks, and UCM) in oil samples, GC-FID chromatograms provide a distribution pattern of petroleum hydrocarbons (e.g., carbon range and profile of UCM). Generally, preliminary identification of the oil type and weathering can be readily achieved from their GC-FID traces, especially when the spilled oil or petroleum product is at high level, while background levels are low in an impacted environment.

To address the diversity of petroleum contamination types, the GC-detectable petroleum hydrocarbon is divided into four broad physicochemical subfractions according to the Canadian Council of Ministers of the Environment (CCME) method [73]. Fraction 1 (C_6 to C_{10}) represents the volatile fraction of most hydrocarbon mixtures and consists of the aliphatic and aromatic subfractions. Fractions 2 (CCME-F₂) and 3 (CCME-F₃) represent the semivolatile fraction and comprise aromatic and aliphatic subfractions in the ranges $>C_{10}$ to C_{16} and $>C_{16}$ to C_{34} , respectively. As seen in Table 5.3, these two fractions make up most proportion of GC-detectable petroleum hydrocarbons in crude oils and petroleum products. Fraction 4 (CCME-F₄) encompasses compounds of $>C_{34}$ up to C_{50+} , having a low mobility (volatility and solubility). Petroleum hydrocarbons within this range often make up a significant proportion of heavy crude oils such as Alberta oil sands bitumen (24.4%) and refined products such as lubricating oil 10W-30 (15.2%).

The GC-FID chromatograms of petroleum hydrocarbons in representative crude oils are shown in Figure 5.5a, illustrating the difference of these crudes in the chromatographic profiles, carbon range, and UCM distribution patterns. The gross chemical composition of crude oils varies greatly, not only among geological sources but also among samples from a single deposit. Scotia Light crude (API=53.2) contains a large proportion of light components with nearly half of resolved peaks, in which $<C_{16}$ hydrocarbons account for about 70% of TPHs, while $>C_{34}$ account for only 0.6%. In addition, total saturated hydrocarbons (TSH) in Scotia Light crude make up 95.3% of TPH value, obviously higher than in any other oil presented in Table 5.3. The heavy crude oil Platform Elly (API=15.8, from U.S. West Coast) contains about 87% of UCM contents, and $>C_{16}$ fractions contribute to over 75% of GC-detectable TPHs. As the heaviest form of petroleum, oil sands bitumen has a pronounced chromatographic UCM hump eluting between $n-C_{10}$ and $n-C_{40}$, indicating a significant biodegradation of its original crudes. A small UCM hump eluting between $n-C_{27}$ and $n-C_{31}$ is seen on the shoulder of the main UCM hump. This shoulder UCM hump is likely

contributed by polycyclic biomarkers that are relatively highly resistant to biodegradation. Normal alkanes and isoprenoid alkanes have been steadily depleted by biodegradation and/or water washing in this bitumen. Albian Heavy Synthetic (AHS) is a blend of sweet Premium Albian Synthetic (API~34) upgraded from oil sands bitumen with the ebullated-bed

hydrocracking residue. It is understandable that the abundance and distribution of TPHs in AHS are significantly different from those of bitumen extracts. Since Premium Albian Synthetic consists mostly of light hydrocarbons and is absent of vacuum residue, all UCM contents are constituted by the heavier portion of hydrocracking residues.

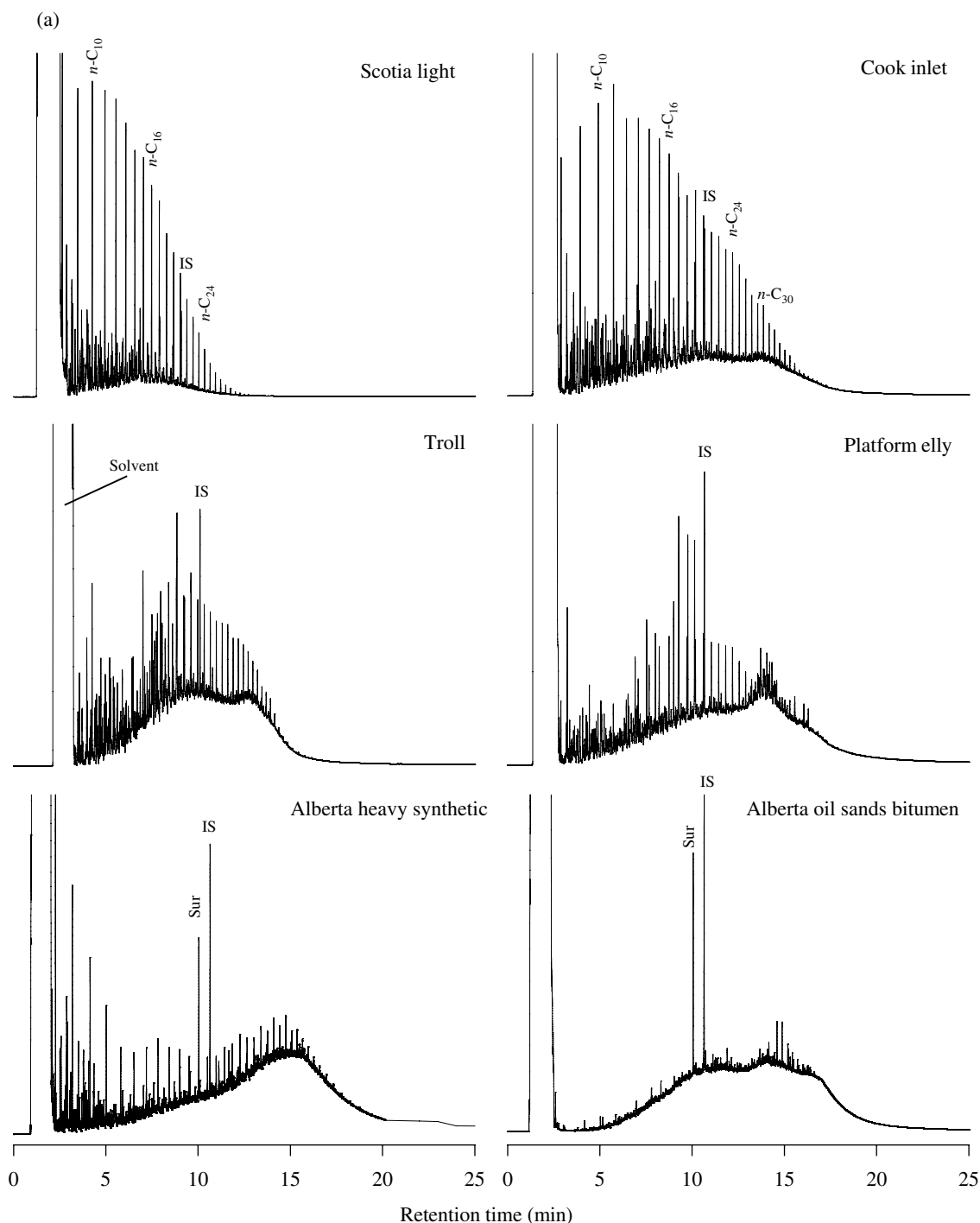


FIGURE 5.5 (a) GC/FID chromatograms of petroleum hydrocarbons in crude oils, including light crude Scotia Light to heavy crude Alberta oil sands bitumen.

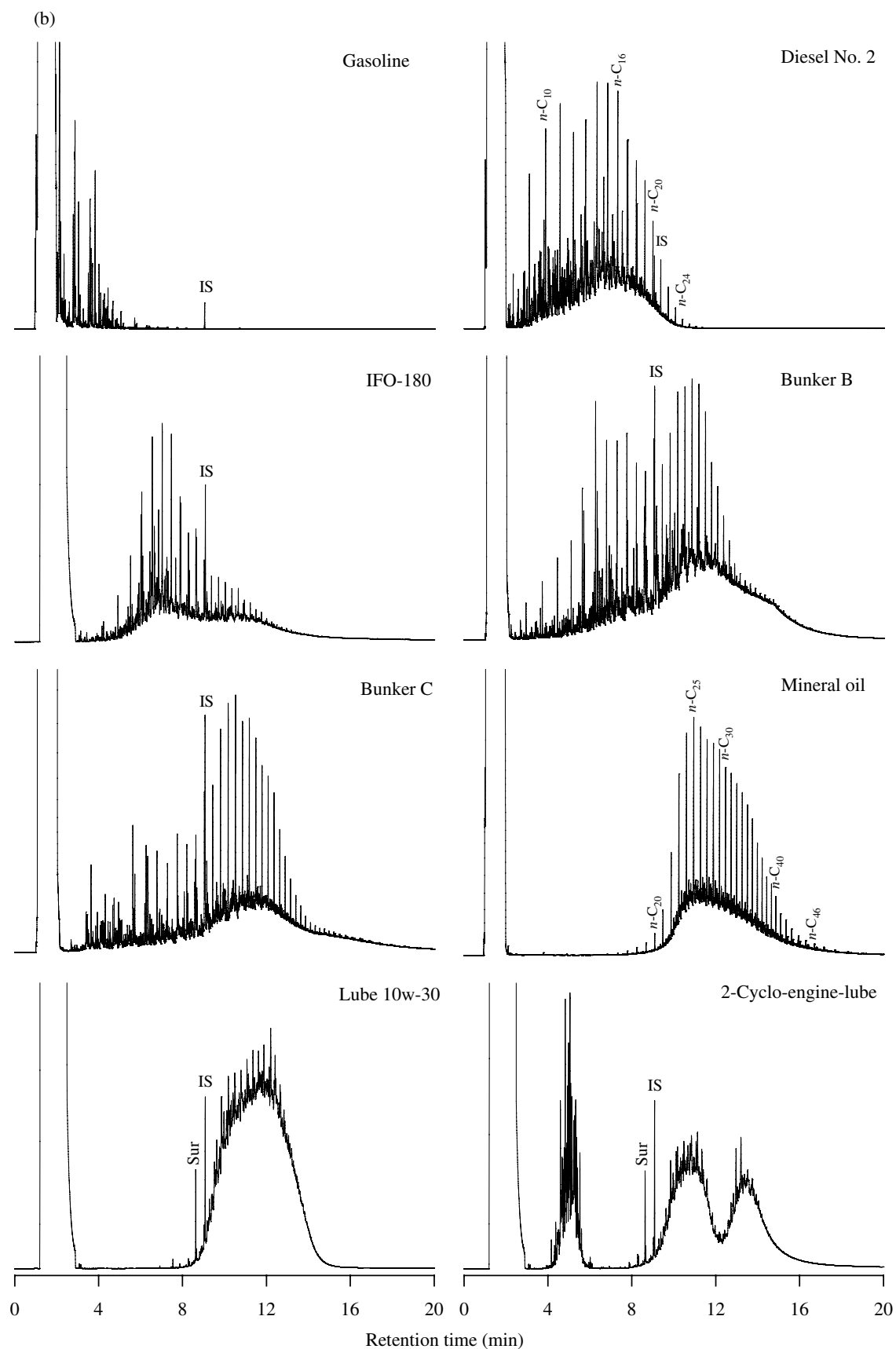


FIGURE 5.5 (Continued) (b) GC/FID chromatograms of petroleum hydrocarbons in refined oil products.

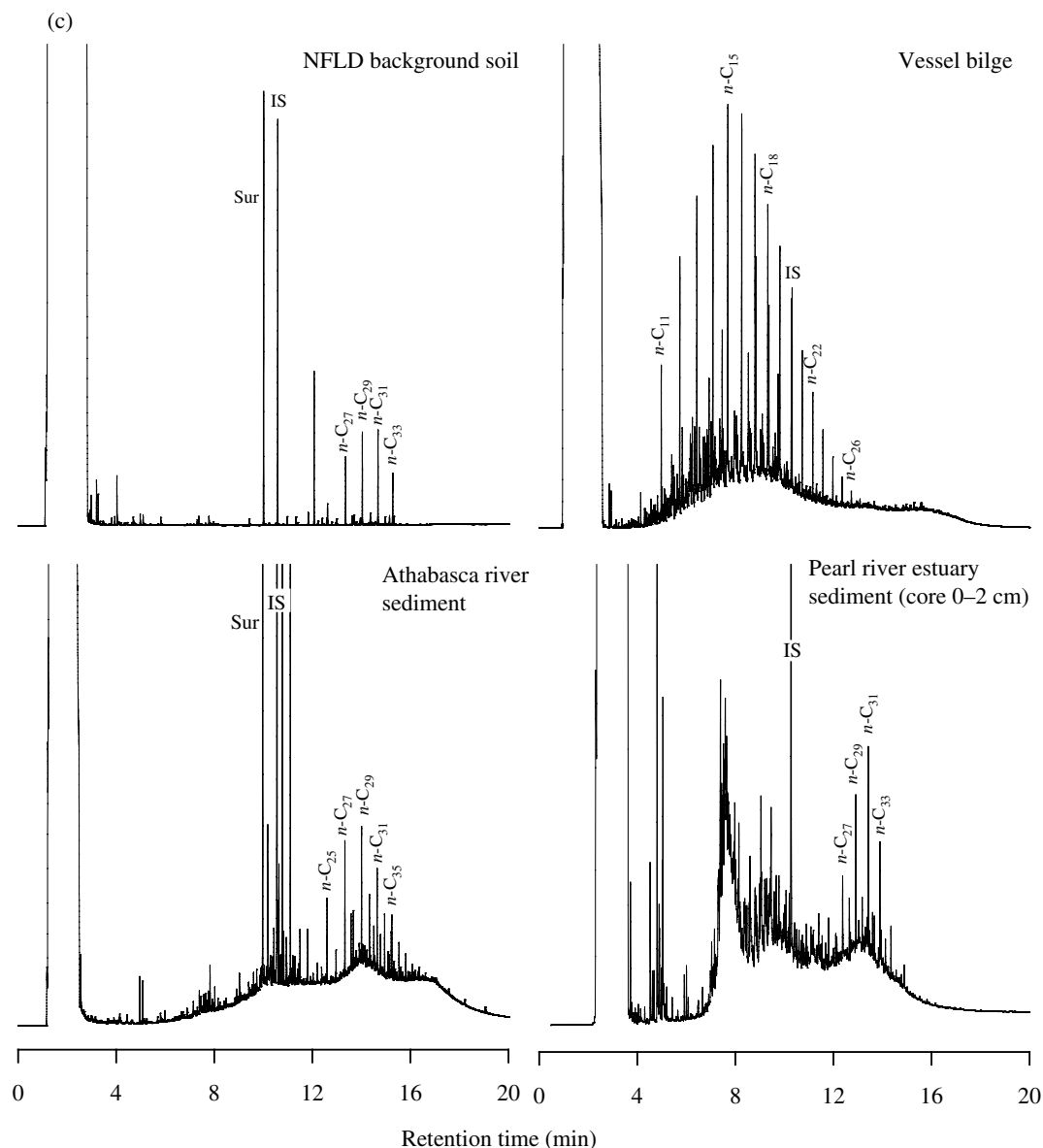


FIGURE 5.5 (Continued) (c) GC/FID chromatograms of hydrocarbons in environmental samples.

Refined petroleum products vary significantly from type to type and oil to oil in the carbon range, hydrocarbon distribution pattern, and UCM profiles (Fig. 5.5b and Table 5.3). The distinguishable characteristics for various types of products are attributed to parent crude oil feedstocks, refining processes, and the materials added in the products for specific purposes.

Light distillates such as gasoline are generally products of light-end resolved hydrocarbons with very little UCM content. The chemical composition of light distillate is relatively simple and has been well characterized. The composition of gasoline generally includes a majority of Paraffins, Isoparaffins, Aromatics (BTEX and alkylbenzenes), Naphthenes, and Olefins (PIANO) and a small amount of additives (such as alcohols). In practice, in some regions, gasoline or diesel is often blended with lighter components in the winter.

As seen in the GC–FID chromatograms of petroleum hydrocarbons in Figure 5.5b, diesel fuel, a midrange distillate, has a carbon range from C_6 to C_{28} . Its GC–FID chromatogram presents a single bell-shaped UCM hump, and normal alkanes are prominent in the GC-resolved peaks.

Typical residual fuels include lighter Fuel No. 5 (Bunker B) and heavier Fuel No. 6 (Bunker C). These residual fuels are often burned in furnaces to generate heat or in maritime or industrial appliances to generate power. These fuels are mixtures of heavy distillate residue and lighter distillates, therefore these oils are characterized by two or more obvious chromatographic UCM humps and particular *n*-alkane distribution. HFO could have a wide carbon range, and some HFOs have similar chromatographic features with weathered crude oils. Their identification and differentiation needs to rely on comparison of their fingerprint details.

Commercial lubricating oil is either mineral-based or synthetic, and the mineral-based lube oils are most commonly used. The applications of lube oil are very diverse. Lube oil can be classified into various categories such as motor oil and transmission oil according to specific applications. Lubricating oil is distinguishable from other refined products by its unique chromatographic profile. It generally consists of high-boiling-point hydrocarbons ranging from $n\text{-C}_{20}$ to $n\text{-C}_{50}$ eluted as a characteristic UCM hump. GC-resolved peaks only account for a very small portion of TPHs in lubricating oil; for example, lubricating 10W-30 motor oil contains about 96% of UCM content (Table 5.3).

Once released into the environment, the oil is immediately subjected to various weathering processes and mixed with background substances. The characteristics of petroleum become difficult to identify. Figure 5.5c shows GC-FID chromatogram of petroleum hydrocarbons in a petroleum-free background soil, a vessel bilge, and petroleum-contaminated sediments. The background soil consists of very little UCM content, although nonpetroleum UCM content is detectable if not properly removed from a silica gel column cleanup [74]. The petroleum hydrocarbons in the vessel bilge clearly consist of primarily a diesel-range fuel and to a lesser extent a lubricating oil. More than two UCM humps are noticeable in the river and marine sediment, indicating multiple sources of the contamination.

5.3.4 Aliphatic Hydrocarbons in Petroleum

The GC-MS analysis provides data on the “source-specific” marker compounds including the target alkylated PAH homologues and other U.S. EPA priority PAHs and biomarker terpane and sterane compounds. These analyses provide detailed information from each class of petroleum hydrocarbons to support the GC-FID analysis.

The saturate fraction consists of nonpolar material including linear, branched, and cyclic saturated hydrocarbons, among which the cyclic biomarker compounds including bicyclic sesquiterpanes, diamondoids, biomarker terpanes, and steranes are most important to forensic oil fingerprinting. In order to better understand the distribution of target hydrocarbons in various petroleum products, the Alaska North Slope (ANS) and Federated crude oils were distilled into four fractions using the vacuum distillation technique. Four distillation fractions correspond to the nominal n -alkane ranges of $n\text{-C}_6$ to $n\text{-C}_{10}$ (initial boiling point of 173°C), $n\text{-C}_{10}$ to $n\text{-C}_{16}$ ($174\text{--}287^\circ\text{C}$), $n\text{-C}_{17}$ to $n\text{-C}_{34}$ ($288\text{--}481^\circ\text{C}$), and $>n\text{-C}_{34}$ ($>481^\circ\text{C}$), respectively. Fraction 1 contains the lightest components, and fraction 4 is in heavy residual oil range. The middle distillation fractions 2 and 3 are roughly equivalent to diesel fuels, together making up 46.8% (w/w) of ANS and 54.0% (w/w) of Federated crude oil, respectively.

It is not surprising that conventional biomarker terpanes and steranes were found almost entirely in heavier fractions 3 and 4 due to their high boiling points, while sesquiterpanes

were found in lighter fractions 2 and 3. Fraction 2 accounted for over 93% of all the adamantanes. Diamantanes were found mainly in the fractions 2 and 3, accounting for about 90% of their total, and were rarely found in the lightest fraction 1 (initial boiling point 180°C). These temperature ranges for diamondoid partitioning are consistent with the observations based on GC chromatograms of n -alkanes and diamondoids (Fig. 5.1). During the distillation of crude oils, the adamantanes in fraction 2 and diamantanes in fractions 2 and 3 were both concentrated approximately sixfold compared to the native crude oils.

5.3.4.1 Normal Alkanes and Isoprenoid Hydrocarbons Normal alkanes and branched alkanes comprise the majority of petroleum hydrocarbons, which enables them to be quantitatively analyzed by GC-FID. However, if their concentrations are too low or subject to interferences to obtain accurate analysis, GC-MS analysis (at m/z 85) can be an alternative fingerprinting technique.

Normal alkanes in crude oils often vary significantly in their concentrations and distributions (Table 5.3 and Fig. 5.5a). Total n -alkanes in Scotia Light crude oil are as high as 172 mg/g, whereas only 21.5 mg/g in Platform Elly crude oil and almost no n -alkanes are detected in Alberta oil sands bitumen. Moreover, it was discovered that crudes with the same geological origin have similar pristane/phytane ratios and similar naphthenic fingerprints. Compared to alkanes, naphthenic hydrocarbons are characterized by their structural stability and preservation of genetic features, which are inherited from peculiarities of the original organic matter and the conditions of its transformation into petroleum hydrocarbons.

Refined petroleum products generally have their distinctive abundance and carbon range in their normal alkane profiles (Fig. 5.5b and Table 5.3). Diesels consist of high levels of C_8 to C_{28} n -alkanes and alkylcyclohexanes. The properties of a given diesel are largely a fraction of the crude oil feedstock. Diesel No. 2 has a high concentration of normal alkanes of 128 mg/g, and its GC chromatogram has a nearly normal distribution with maxima around $n\text{-C}_{11}$ to $n\text{-C}_{14}$. The GC-TPHs are obviously dominated by central UCM hump, totally accounting for 77.7%. Bunker B and Bunker C and marine intermediate fuel oils (IFOs) generally contain less normal alkanes, whereas lubricating oils generally contain very trace amounts of long-chain straight alkanes.

Normal $\text{C}_{10}\text{--}\text{C}_{40}$ alkanes, with a marked predominance of odd-numbered hydrocarbons in the span of $n\text{-C}_{23}$ to $n\text{-C}_{35}$, are identified in higher plants (concentrations of $n\text{-C}_{27}$, $n\text{-C}_{29}$, and $n\text{-C}_{31}$ hydrocarbons are especially high) and soil, river, and marine sediments (see Fig. 5.5c). This characteristic is particularly useful to distinguish biogenic sources from petrogenic sources in environmental samples.

The branched alkanes in petroleum are genetically related to isoprenoid alkanes. These isoprenoids are composed exclusively of “head-to-tail” links of isoprene units,

whereas irregular isoprenoids have a “tail-to-tail” link. Saturated cyclic hydrocarbons (naphthenes) comprise the most useful petroleum hydrocarbons for oil fingerprinting, including bicyclic sesquiterpanes, diamondoids, polycyclic terpanes, and polycyclic steranes (Table 5.2 and Fig. 5.1). These hydrocarbons determine the special place of crude oils among natural organic compounds, as well as among fossil fuels. The acyclic isoprenoids of pristane and phytane were widely assumed to be diagenetic products of the phytyl side chain of chlorophyll, although alternative sources of precursors have been suggested [75–78]. Pristane and phytane are eluted closely with n -C₁₇ and n -C₁₈. They are often investigated together with n -alkane analysis.

5.3.4.2 Biomarker Terpanes and Steranes Analyses of petrochemical biomarkers are of special importance in petrochemistry. These compounds retain all or part of the molecular structures from their original biological molecules produced by living organisms. The origin and formation of petroleum biomarkers have been extensively investigated and reported [78–83]. For example, pentacyclic hopanes are triterpenoids derived from cell membranes of prokaryotes (heterotrophic bacteria and also phototrophic cyanobacteria) [80,82]. Cyclic aliphatic terpenoid biomarkers, in particular the ubiquitous hopanes and steranes, are more resistant to biodegradation relative to other hydrocarbons. These traditional biomarker compounds are eluted after n -C₂₁, indicating they have high boiling points (Fig. 5.4). These hydrocarbons have played an important role to explore the depositional environment of crude oil and to track the genesis, maturation, migration, and biodegradation of petroleum. The information from biomarker analysis is also used to investigate the source and history of the petroleum in the determination of petroleum-derived environmental contaminations.

Biomarker abundances differ greatly from oil to oil and from oil type to type. The biomarker concentrations in crude oils largely depend on the geological source of the oils,

while their concentrations in refined petroleum products vary with the feedstocks and the oil types.

Biomarker Terpanes Crude oils usually have a wide distribution of triterpanes from C₁₉ tricyclic to C₃₅ pentacyclic homohopanes. Pentacyclic hopane series include C₃₀ hopane (C₃₀H₅₂) and its homologues ranging from C₂₇ trinorhopane to C₃₅ homohopanes. These biomarker terpanes have 21 carbon atoms in five rings and six methyl substituents on the ring system, of which four methyls are positioned at the ring junction of C-25, C-26, C-27, and C-28, respectively. In theory, each biomarker terpane has many isomers and epimers due to the chiral center (*R*- or *S*-configuration) at C-22 and two asymmetric carbons (α or β configuration) at C-17 and C-21 in the molecular structure (see Fig. 5.6 and Table 5.2). C₃₀ hopane has four isomers, that is, 17 α (H),21 α (H)-, 17 α (H),21 β (H)- (in petroleum), 17 β (H),21 β (H)- (the biological configuration), and 17 β (H),21 α (H)-hopane (moretane). C₃₀ 17 α (H),21 β (H)-hopane widely occurs in crude oil at high abundance, whereas 17 β (H),21 α (H)-hopane frequently occurs in relatively low concentration. It was found that C₃₀ 17 α (H),21 α (H)-hopane occurs in low concentration in a ratio of typically 0.02–0.04 relative to C₃₀ 17 α (H),21 β (H)-hopane in crude oils and mature sediments [84]. C₃₀ 17 β (H),21 β (H)-hopane is thermodynamically unstable and naturally absent in petroleum, making it a desirable internal standard for quantitative biomarker analysis. C-22 position in the molecular structure is a chiral center resulting in *R*- and *S*-configuration epimers for C₃₁–C₃₅ homohopane series. The 22*S* epimers exist at slightly higher concentration than their 22*R* epimers due to their higher stability. 25-norhopanes are a series of C₂₆–C₃₄ compounds that are structurally equivalent to the regular hopanes, except for the absence of the methyl group at the A/B ring junction.

These saturated biomarker terpanes are determined at their characteristic base ions at m/z 191 (C₁₄H₂₃⁺), which is derived from the cleavage of carbon bonds 9–11 and 8–14 in

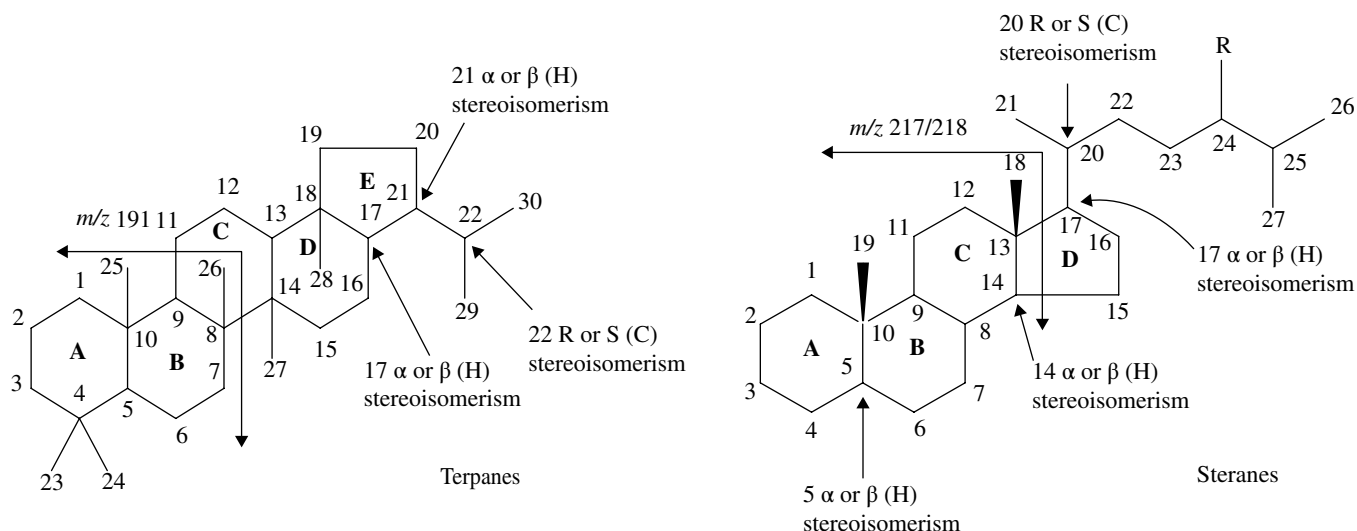


FIGURE 5.6 Stereoisomerism and mass fragmentation of biomarker terpanes and steranes.

ring C of the molecule to form (A+B) ring or (D+E) fragment, respectively. The most intensive ion in the mass spectra of norhopanes such as 17 α (H),21 β (H)-25-norhopane is m/z 177 due to one less methyl group (CH₃-, 15 amu) in their molecular structures.

Biomarker Steranes Steranes have tetracyclic androstane skeleton with a side chain at C-17. These saturated petroleum hydrocarbons represent an important group of biological marker compounds. In a nomenclature that is more familiar to petroleum chemists, α -cholestane has *trans*-connections of all rings (A/B, B/C, and C/D) and a relative *cis*-orientation of carbon bonds 17–20 and 13–18. Steranes and sterenes are believed to be principally derived from C_{27–30} sterol precursors of cell membranes of eukaryotes, mainly algae and higher plants [85,86]. These sterols generate a series of sterane homologues during diagenesis, which inherit the carbon skeletons in the biological precursors and only differ by the addition of a sequence of CH₂- units to a certain place in the molecule. Similar to terpanes, steranes have a chiral center at C-20 position in the molecular structure, resulting in *R*- and *S*-configuration epimers for C₂₇–C₂₉ sterane series (Fig. 5.6).

The distribution profile of C₂₇–C₂₉ sterane is of interest for oil exploration and oil forensic study, although it is more or less the same in most crude oils. C₂₇–C₂₉ steranes are referred to as cholestane, ergostane (24-methylcholestane), and sitostane (or stigmastane, 24-ethylcholestane), respectively (Fig. 5.1). C₂₁ $\beta\beta$ - and C₂₂ $\beta\beta$ -pregnanes are strongly present in the m/z 217 fragmentogram because pregnanes are highly resistant to biodegradation. The typical ions for biomarker steranes are m/z 217 (C₁₆H₂₅⁺) and 218 (C₁₆H₂₆⁺) for GC–MS analysis, which are products of (A+B+C) ring due to the cleavage at junction carbon bonds 13–17 and 14–15 of the C/D ring under electron impact. For all epimers with *cis*-C/D-connection, the intensity of the m/z 218 ion is greater than that of the m/z 217 ion.

Distribution of Biomarker Compounds in Petroleum Petroleum biomarkers have been extensively investigated and reported by geochemists and environmental chemists. Different oils often have varying concentrations and distribution patterns in their biomarkers (Fig. 5.7 and Table 5.4). Figure 5.7a illustrates biomarker terpanes (m/z 191) and steranes (m/z 217 and 218) chromatograms in six crude oils. C₂₇ $\beta\beta$ -, C₂₈ $\beta\beta$ -, and C₂₉ $\beta\beta$ -steranes in most crude oils consistently have a relative abundance in an overall “V-shaped” distribution pattern. As observed from Table 5.4, different from other crude oils, the Scotia Light crude oil contains very low biomarker compounds with a total concentration of 29.0 $\mu\text{g/g}$. In contrast, Platform Elly, a California heavy oil, particularly contains a high concentration of biomarker steranes, which account roughly for 70% of total 2695 $\mu\text{g/g}$ of biomarkers. In addition, unlike most of other crudes studied, the Platform Elly crude oil has a reverse V-shaped steranes distribution with a particular abundant C₂₈ $\beta\beta$.

In fresh crude oils, C₂₃ and C₂₄ tricyclic terpanes and C₂₉ $\alpha\beta$ - and C₃₀ $\alpha\beta$ -hopanes are the most abundant (Fig. 5.7a). C₃₀ $\alpha\beta$ -hopane is usually found at higher concentrations than C₂₉ $\alpha\beta$ -norhopane in most crude oils; however, a reverse feature was observed for some crude oils such as Arabian Light (a Middle East crude oil). The Platform Elly crude has abundant C₂₈-bisanorhopane (H28). In California Sockeye crude oil, H28 is even more abundant than C₂₉ and C₃₀ $\alpha\beta$ -hopanes [87].

Some biomarkers including several geologically rare acyclic alkanes (i.e., C₃₀ 17 α (H)-diahopane, C₃₀ 18 α (H)-hopane, gammacerane, and 4-methylsteranes) are found only in certain oils and can, therefore, be used as unique markers for oil spill identification. As shown in Figure 5.7a, the presence of C₂₈-bisanorhopane and gammacerane is evident in oil sands bitumen and AHS. The occurrence of gammacerane may suggest a saline depositional environment of the original oil in the Alberta Oil Sands. The abundance of homohopanes generally decreases with the increase of carbon numbers, that is, H31>H32>H33>H34>H35, and the *S*-configuration epimer is higher than its *R*-epimer. One specific feature of H34S<H35S and H34R<H35R is noticed for homohopanes in some crude oils such as Alberta oil sands bitumen, which suggests that these oils were derived from source rocks deposited under anoxic conditions [88].

Distribution of Biomarker Compounds in Refined Petroleum Products Biomarker terpanes and steranes all come from their feedstock crude oil as they are unlikely to be produced in distillation and refining process. Figure 5.7b presents the GC–MS chromatograms of biomarkers in six representative refined petroleum products from light Diesel No. 2 to lubricating oil. It can clearly be seen that the biomarker abundances and distribution vary greatly from oil to oil and from type to type (Table 5.4). The biomarker fingerprint of a refined oil may be totally or partially different from that of its original feedstock crude. For lighter petroleum products, refining processes have removed most high-molecular-weight biomarkers from the corresponding crude oil feedstocks. In general, biomarker compounds are undetectable in light fuels such as gasoline and Jet A, and only smaller biomarker compounds occur in trace amounts in the middle distillate fuels. Most of these compounds remain in the residual fraction during distillation. Therefore, they are detected in heavy residual fuels in equivalent or higher concentrations than their feedstock crude oil. Lubricating oils are rich in terpanes and steranes but contain relatively low lighter tricyclic terpanes (C₂₁–C₂₄). The target biomarker terpanes and steranes in 10W-30 motor oil are as high as 3652 and 1666 $\mu\text{g/g}$, respectively.

5.3.4.3 Diamondoids Recently, environmental scientists have applied the multiple-criteria approach with characterization of more than one suite of analytes, including fingerprinting the diamondoid hydrocarbons for oil spill correlation and identifications [58,61,89]. The naturally occurring

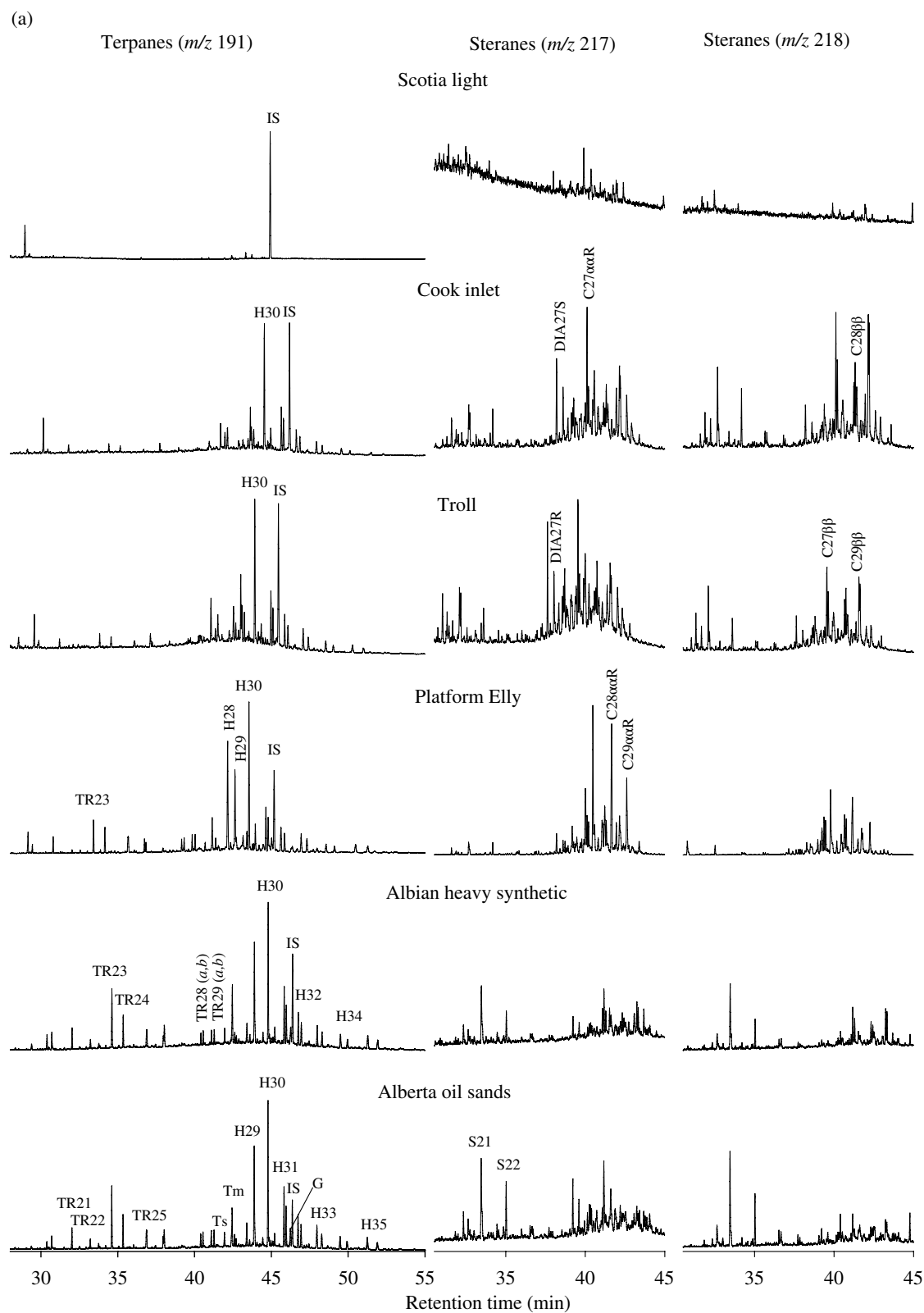


FIGURE 5.7 (a) GC/MS chromatograms of biomarker terpanes (m/z 191) and steranes (m/z 217 and 218) in crude oils.

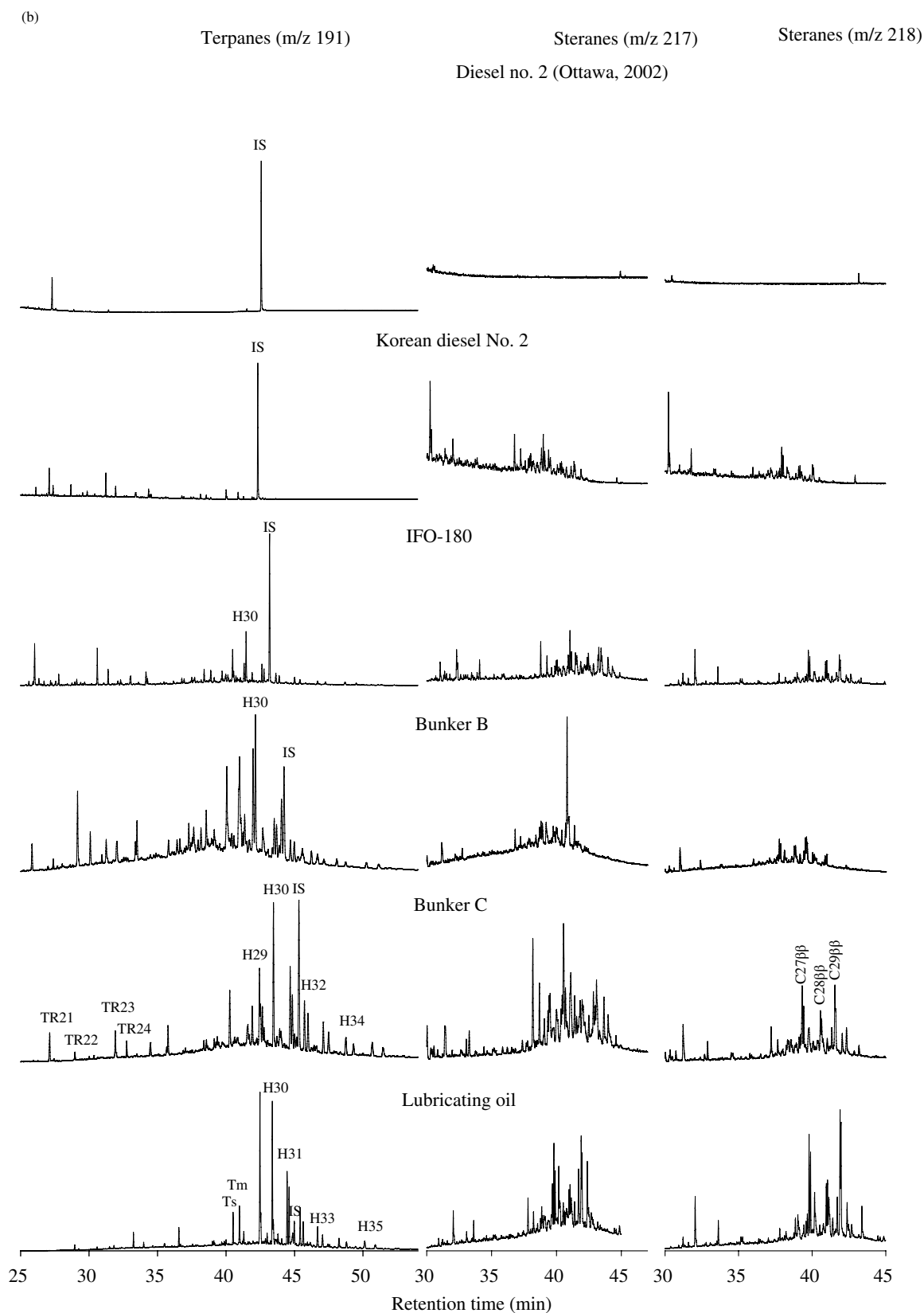


FIGURE 5.7 (Continued) (b) GC/MS chromatograms of biomarker terpanes (m/z 191) and steranes (m/z 217 and 218) in refined oil products.

TABLE 5.4 Concentrations of target biomarker terpanes and steranes in crude oils and refined petroleum products

Oil samples	Crude oils						Refined petroleum products					
	ScL	SoL	CI	Troll	PIE	AOS ^a	Jet A	Diesel No. 2	IFO-180	Bunker B	Bunker C	Lube oil 10W-30
Biomarker terpanes												
TR21	0.00	9.43	7.12	7.81	20.1	36.2	0.00	3.11	9.07	16.1	3.10	11.6
TR22	0.00	3.53	2.77	2.96	4.32	16.9	0.00	1.42	4.39	5.87	1.38	15.2
TR23	0.87	14.8	9.88	11.1	41.3	109	0.00	3.85	30.5	49.6	11.0	68.2
TR24	0.61	10.7	6.16	9.14	33.9	56.7	0.00	1.39	11.5	20.8	5.97	25.5
Ts	1.40	20.3	22.7	34.1	13.2	27.2	0.00	0.00	10.6	25.4	26.1	148
Tm	1.66	29.6	23.4	23.3	55.9	91.7	0.00	0.00	12.0	9.07	2.46	215
H29	3.32	74.6	45.0	56.6	107	219	0.00	0.00	29.7	93.4	31.9	864
H30	5.79	100	125	126	216	256	0.00	0.00	40.2	90.9	59.0	718
H31S	1.74	26.4	45.0	44.3	64.6	114	0.00	0.00	14.8	28.5	36.4	385
H31R	1.24	21.5	35.6	34.5	52.5	83.5	0.00	0.00	11.7	24.7	25.2	305
H32S	0.95	15.2	29.0	30.4	43.0	72.6	0.00	0.00	9.93	16.7	24.8	238
H32R	0.79	9.94	20.1	22.0	32.2	53.2	0.00	0.00	7.55	17.1	19.6	164
H33S	0.00	8.96	16.6	26.7	35.2	54.5	0.00	0.00	8.26	12.6	17.3	140
H33R	0.00	5.48	12.3	16.3	28.5	36.3	0.00	0.00	5.77	11.5	12.9	91.7
H34S	0.00	4.65	10.5	16.4	20.0	36.7	0.00	0.00	4.87	7.03	10.9	77.6
H34R	0.00	2.78	7.48	9.54	15.1	23.4	0.00	0.00	3.33	4.70	6.68	51.6
H35S	0.00	3.33	5.98	12.4	22.1	39.0	0.00	0.00	4.49	6.52	9.94	85.7
H35R	0.00	2.27	4.29	8.73	20.9	36.2	0.00	0.00	3.15	7.15	7.75	47.6
Biomarker steranes												
C27 $\beta\beta$	2.84	89.3	184	172	649	25.4	0.00	0.00	58.8	44.2	87.8	525
C28 $\beta\beta$	2.77	67.4	113	125	754	62.6	0.00	0.00	46.9	39.9	58.8	363
C29 $\beta\beta$	5.20	89.8	232	179	466	45.8	0.00	0.00	55.5	46.6	82.9	778
Total ($\mu\text{g/g}$)	29.0	610	958	968	2695	1519	0.00	9.77	383	578	542	5318

^aConcentration: $\mu\text{g/g}$ of TSEM of Alberta oil sands.

diamondoid compounds are thermodynamically stable [90–92], and therefore, they are particularly useful in oil–source correlation and differentiation for those cases where the traditional tri- to pentacyclic biomarker terpanes and steranes are absent due to removal during the refining processes.

Diamondoids are common in reservoir fluids and have been considered as a problem due to their deposition during production and transportation of natural gas, gas condensates, and light crude oils [93]. Diamondoids, having the general molecular formula $\text{C}_{4n+6}\text{H}_{4n+12}$, are a class of saturated hydrocarbons. These compounds consist of three-dimensionally fused cyclohexane rings, which results in a diamond-like structure. The simplest diamondoid is adamantane (A) ($\text{C}_{10}\text{H}_{16}$), followed by its homologues diamantane (D) ($\text{C}_{14}\text{H}_{20}$), triamantane, tetramantane, pentamantane, and hexamantane. Adamantane and diamantane and their various substituents are widely found in crude oils, intermediate petroleum distillates, and finished petroleum products [60,62,90,94–96]. A suite of petroleum polyman- tanes, including tetramantane, pentamantane, and hexaman- tane, were determined in a gas condensate produced from a very deep petroleum reservoir located in the U.S. Gulf Coast [97]. Dahl et al. [98] reported successful separation of a wide variety of the higher diamondoids containing 4–11 (undecamantane) diamond-crystal cages from petroleum. Diamondoid compounds in petroleum are believed to be the result of carbonium ion rearrangements of suitable cyclic precursors (such as multiringed terpene hydrocarbons) on

clay superacids in the source rock during oil generation [96,99,100]. The higher homologues of diamondoids are considered to be formed from lower homologues under extreme temperature and pressure conditions [90].

As seen in Figure 5.8, adamantane and its 16 alkylated substituents are eluted between $n\text{-C}_{10}$ and $n\text{-C}_{13}$ (boiling point range: 180–230°C), while diamantane series are eluted between $n\text{-C}_{15}$ and $n\text{-C}_{17}$ (boiling point range: 270–300°C) at given chromatographic conditions. Adamantane and its alkylated homologues are determined at m/z 136 (for adamantane), 135 (for methyladamantanes), 149 (for C_2 -adamantanes), 163 (for C_3 -adamantanes), and 177 (for C_4 -adamantanes). Diamantane series are measured at m/z 188 (for diamantane), 187 (for methyladamantanes), 201 (for C_2 -diamantanes), and 215 (for C_3 -diamantanes), respectively (Fig. 5.8 and Table 5.2). The hydrocarbons having at least one substituent at the bridgehead have a wider occurrence [78]. All bridgehead-substituted methyladamantanes have much lower boiling points than those with at least one of the substituents not situated at the bridgehead (2-methyladamantanes, 1,2- and 1,4-dimethyladamantanes, etc.). The difference in the boiling points of these adamantanes is so large that 2-methyladamantane elutes later than 1,3,5,7-tetramethyladamantane [62,78].

Distribution of Diamondoids in Crude Oils GC/MS chromatograms of adamantanes and diamantanes in representative crude oils from South Louisiana oil to

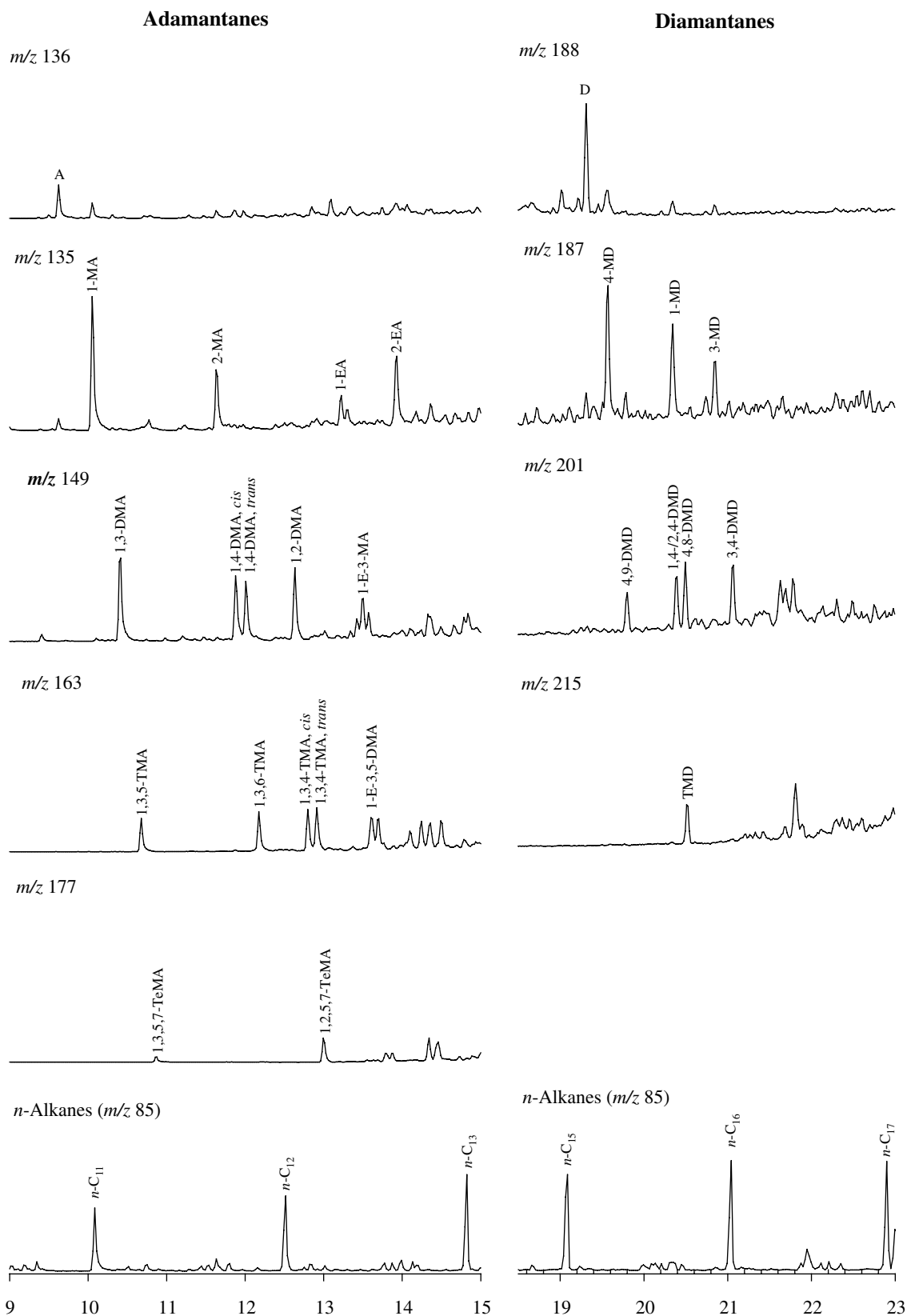


FIGURE 5.8 Identification of adamantanes (at m/z 136, 149, 163, and 207) and diamantanes (at m/z 188, 187, 201, and 215).

Alberta oil sands bitumen are displayed in Figure 5.9a. The concentrations of adamantane, diamantane, and their homologues in these crude oils are shown in Table 5.5. On the whole, the one-cage adamantanes are much more abundant than two-cage diamantanes.

As seen from Table 5.5, the concentrations of individual adamantane and its alkylated derivatives are in the range of approximately 1–30 µg/g for most oils with the exception of approximately 1–300 µg/g for the corresponding individual diamondoids in Troll and South Louisiana crude oils. Among the detected adamantanes, the principal dominant adamantanes are A, 2-MA, 1-MA, 2-EA, 1,2-DMA, and 1,3-DMA, together accounting for about 50% of all detected adamantanes. Either 1-MA (bridgehead substituted) or 2-MA is the most abundant homologue in all oil samples. Tri- and tetramethylated diamondoids have much lower relative abundance compared with methyl and dimethyl homologues. Among the adamantane series, 1,3,5,7-tetramethyladamantane has the lowest concentration probably due to its relatively poor thermal stability. It has four methyl groups, which could spatially interfere with each other and cause the molecular structure to be strained.

The dominant diamantane compounds in petroleum are D, 4-MD, 1-MD, 3-MD, and 3,4-DMD. The concentrations of individual diamantanes range from undetected levels to 10 µg/g for most crude oil samples and up to 10–53 µg/g for South Louisiana oil. The California Platform Elly heavy oil has the lowest concentration of adamantanes among the surveyed oils. Cook Inlet crude oil has a low concentration of diamantanes (9.10 µg/g), although its adamantanes are at a quite high concentration of 209 µg/g.

The concentrations of diamondoids do not appear to be dependent on the densities (or derived API gravities) of the crude oils. Diamondoids in oils from different sources have different signatures of both the absolute concentrations and relative distribution patterns [61,62]. These diamondoid “fingerprints” as well as their molecular ratios (discussed in detail later), particularly that of adamantanes, may be useful for oil source identification.

Distributions of Diamondoids in Refined Products The concentrations of diamondoids in refined products are significantly influenced by the crude oil feedstocks used in production and the distillation cut point of the petroleum products. Figure 5.9b compares the GC/MS chromatograms of adamantanes and diamantanes for six representative refined products including gasoline, diesel fuel, IFO-180, Bunker B, Bunker C, and a lubricating oil. The absolute concentrations and distribution patterns of diamondoids differ widely in the petroleum products. These differences are attributed to the differences in the crude oil feedstocks used in production and the distillation cut point of the petroleum products. From Table 5.5, it can be seen that adamantanes were found in all fuel oil samples. As expected, little or no diamantanes were detected in light fuel and heavy-end lubricating oils. Generally, the overall

distribution pattern of individual diamondoid compounds in petroleum products is comparable to that in crude oils, in which 1-MA and 2-MA and D and 4-MD dominated the adamantanes and diamantanes, respectively.

5.3.4.4 Bicyclic Sesquiterpanes These bicyclic sesquiterpanes with the drimane skeletons are ubiquitous components of ancient sediments, coal, and crude oils. They consist of two fused cyclohexane rings in their molecule structures. These compounds all have a decahydronaphthalene skeleton with various methyl, dimethyl, ethyl, or longer side chains [59,101–103]. These bicyclic terpenoids probably have a microbiological source and are produced from the biodegradation of bigger terpanes or are formed directly from bicyclic compounds of the same carbon framework.

Dimmler et al. [103] found a major series of C_{15} – C_{24} bicyclic terpenoids in the Athabasca oil sands bitumen saturates. Ten small bicyclic sesquiterpanes (C_{14} – C_{16}) commonly analyzed in petroleum fingerprinting elute between n - C_{13} and n - C_{16} (boiling points: 235–287°C), while conventional polycyclic terpanes and steranes elute between n - C_{21} and n - C_{37} (boiling points: 345–500°C) (see Fig. 5.4). These terpenoids are identified as C_{14} (BS1 and BS2), C_{15} (BS3 to BS6), and C_{16} (BS7 to BS10) sesquiterpanes with molecular weights being 194, 208, and 222 atomic mass units, respectively (Table 5.2). These compounds are determined at their characteristic ions at m/z 123 ($C_9H_{15}^+$), and confirmation can be conducted using other prominent ions such as m/z 179, 193, and 207 [63].

Due to commercial unavailability of sesquiterpane standards, Yang et al. [63] used two hydrocarbons with a bicyclic molecular structure, *cis*-decalin and 1-methyldecalin, as alternative standards for the quantitation of sesquiterpanes. The response factor for *cis*-decalin (at m/z 138) and 1-methyldecalin (at m/z 152) is determined relative to the internal standard of decalin- d_{18} (at m/z 156). The average RRF of *cis*-decalin and 1-methyldecalin is then used to determine the concentrations of each target sesquiterpane compound (at m/z 123). This method offers a means for quantitative comparison of bicyclic sesquiterpanes in various oils although it cannot give their real-world concentrations.

Bicyclic sesquiterpanes are resistant to slight to medium weathering, particularly from biodegradation [59,60,63,83]. Recently, sesquiterpane analysis was applied in oil spill correlation and identification [60,104]. Analysis of bicyclic sesquiterpanes provides another criterion to fingerprint oils in addition to PAHs and traditional biomarkers. However, it is recommended that the absence of bicyclic terpanes should be used cautiously as an indicator of biodegradation rank because there is a high potential for their alteration by water washing [83].

Distribution of Sesquiterpanes in Crude Oils Bicyclic sesquiterpanes are widely found in crude oils, intermediate petroleum distillates, and finished petroleum products. Their relative concentrations vary considerably from oil to oil

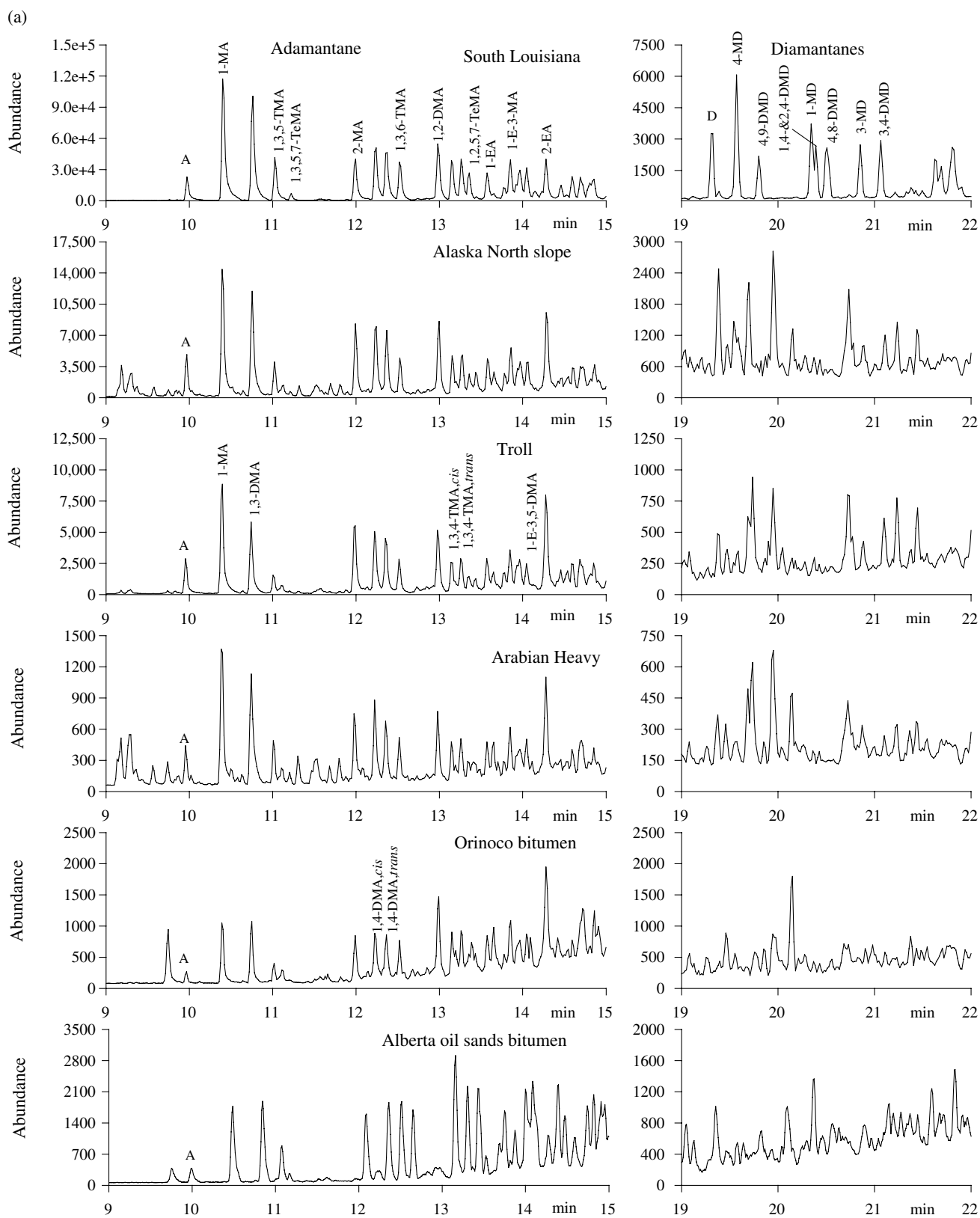


FIGURE 5.9 (a) GC/MS chromatograms of adamantanes (left panel: m/z 136, 135, 149, 163, and 177) and diamantanes (right panel: m/z 188, 187, 201, and 215) in crude oils.

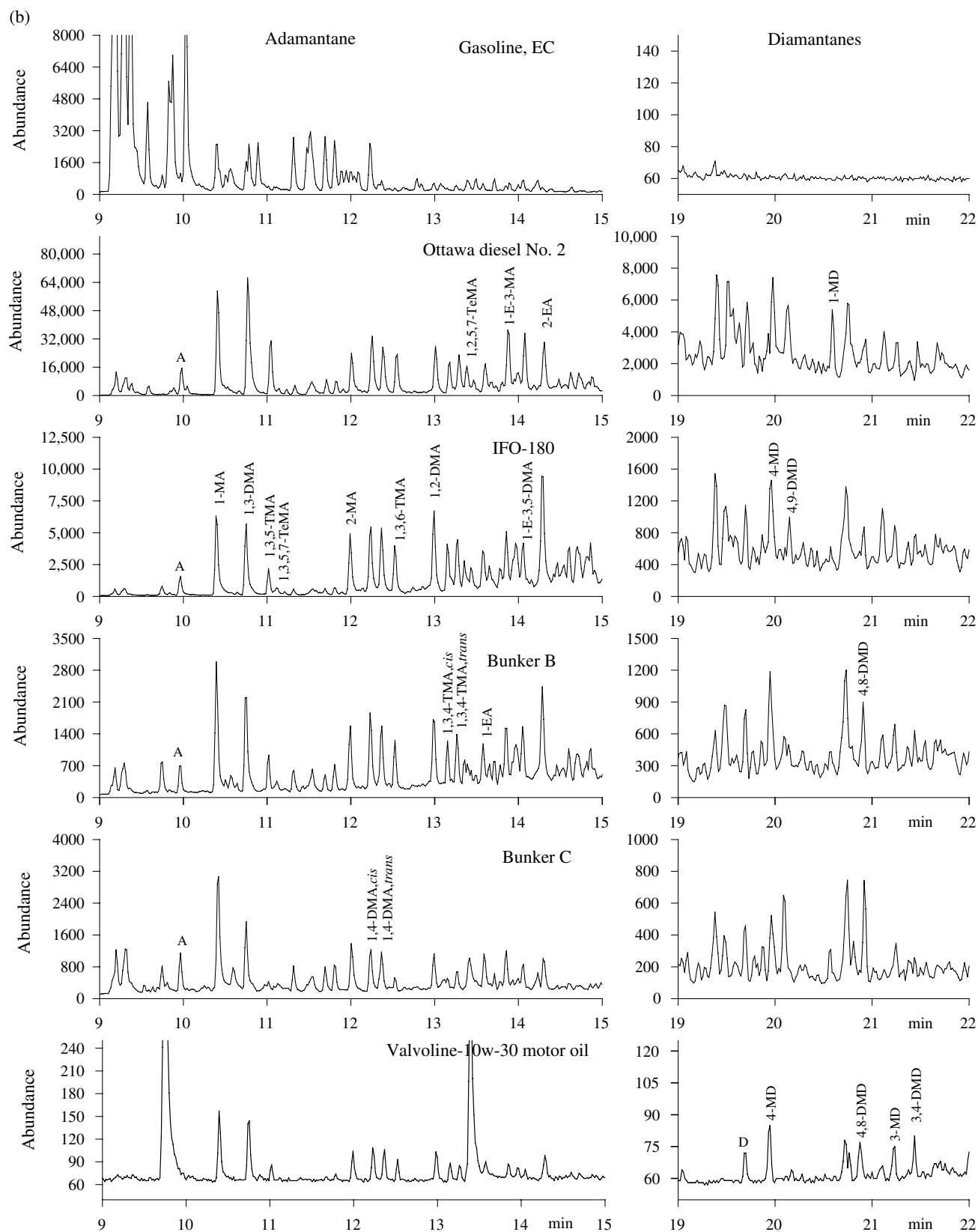


FIGURE 5.9 (Continued) (b) GC/MS total ion chromatograms of adamantanes (left panel: m/z 136, 135, 149, 163, and 177) and diamantanes (right panel: m/z 188, 187, 201, and 215) in refined oil products.

TABLE 5.5 Concentrations of adamantanes and diamantanes in crude oils and refined petroleum products

Concentrations	Crude oils							Refined petroleum products						
	SoL	CoI	ANS	Troll	ArH	PIE	Oil sands	AG100	Jet A	Diesel No. 2	IFO-180	Fuel5	BkC	10W-30
A	126	8.76	19.3	48.6	6.80	0.77	3.16	0.48	181	63.3	3.02	3.46	5.19	0.08
1-MA	288	11.9	33.9	68.0	12.0	2.04	7.46	1.08	222	118	6.45	6.57	7.53	0.19
1,3-DMA	226	13.7	26.2	38.0	9.34	4.23	6.00	1.08	174	144	5.96	6.02	4.40	0.21
1,3,5-TMA	84.3	3.22	7.82	10.3	3.19	0.98	2.59	0.34	49.8	60.3	3.01	2.10	0.90	0.06
1,3,5,7-TeMA	13.7	0.56	1.28	1.50	0.90	0.19	0.52	0.03	7.44	5.85	0.33	0.33	0.03	0.01
2-MA	190	13.3	32.5	81.5	9.96	1.45	9.16	0.69	264	85.4	9.68	6.74	6.53	0.18
1,4-DMA, <i>cis</i>	109	17.9	17.1	32.2	5.97	1.81	4.84	0.50	140	54.3	5.43	3.98	2.61	0.12
1,4-DMA, <i>trans</i>	110	29.0	15.8	32.7	4.80	5.05	4.76	0.43	112	54.3	5.09	3.66	2.39	0.10
1,3,6-TMA	79.3	9.76	9.25	18.0	3.15	2.20	3.64	0.30	64.2	42.7	3.31	2.85	1.05	0.07
1,2-DMA	112	28.3	18.1	34.8	5.01	7.35	6.77	0.41	127	49.2	5.93	4.06	2.27	0.09
1,3,4-TMA, <i>cis</i>	76.7	8.76	9.36	17.5	2.69	1.33	4.99	0.27	52.5	32.0	3.33	2.65	0.92	0.06
1,3,4-TMA, <i>trans</i>	82.6	10.3	10.6	20.6	3.30	3.24	4.54	0.35	70.2	40.0	4.19	3.12	1.60	0.07
1,2,5,7-TeMA	55.5	4.19	5.28	9.50	1.88	1.65	3.33	0.18	31.5	32.3	2.11	1.85	0.47	0.05
1-EA	56.2	10.2	8.38	16.1	2.54	2.26	3.63	0.25	63.3	30.5	3.66	2.41	2.47	0.05
1-E-3-MA	94.1	5.38	14.1	20.7	4.91	3.30	6.87	0.58	75.0	71.4	5.46	4.04	2.75	0.07
1-E-3,5-DMA	89.5	6.72	10.9	21.5	2.67	1.34	7.97	0.33	76.4	31.9	4.84	4.10	1.28	0.07
2-EA	88.3	27.0	23.3	56.2	8.76	2.88	4.33	0.60	193	61.3	10.4	6.03	2.22	0.09
ΣAdamantanes (µg/g oil) ^a	1880	209	263	528	87.8	42.1	84.6	7.90	1904	977	80.2	64.0	44.6	1.58
D	53.3	1.50	9.00	9.31	6.28	1.06	2.43	0.13	10.6	14.0	2.79	3.27	1.66	0.09
4-MD	36.5	1.25	5.19	4.46	5.22	4.38	1.87	0.08	4.50	9.43	2.18	2.32	1.05	0.06
4,9-DMD	11.7	0.26	1.17	0.98	1.02	0.09	0.00	0.02	1.52	2.94	0.48	0.48	0.13	0.02
1-MD	22.8	1.78	3.82	5.06	2.99	0.69	0.00	0.07	2.34	9.96	3.06	3.06	1.92	0.06
1,4- & 2,4-DMD	13.8	0.88	1.78	2.34	1.59	1.02	0.65	0.03	1.29	4.04	1.01	0.85	0.34	0.03
4,8-DMD	14.5	0.75	1.47	1.70	1.41	1.59	0.52	0.01	0.38	2.65	0.65	0.64	0.21	0.04
TMD	10.6	0.01	0.83	0.89	1.05	ND	0.46	0.01	0.12	2.37	0.36	0.34	0.07	0.04
3-MD	15.4	0.85	2.13	3.53	1.44	1.08	1.22	0.04	1.14	4.43	1.15	1.07	0.59	0.04
3,4-DMD	16.3	1.88	2.13	3.38	1.65	0.46	1.85	0.04	1.14	3.78	1.11	1.05	0.39	0.04
ΣDiamantanes (µg/g oil) ^a	195	9.14	27.5	31.6	22.8	10.4	8.99	0.44	23.0	53.6	12.8	13.1	6.36	0.41

^aConcentration: $\mu\text{g/g}$ of TSEM of Alberta oil sands.

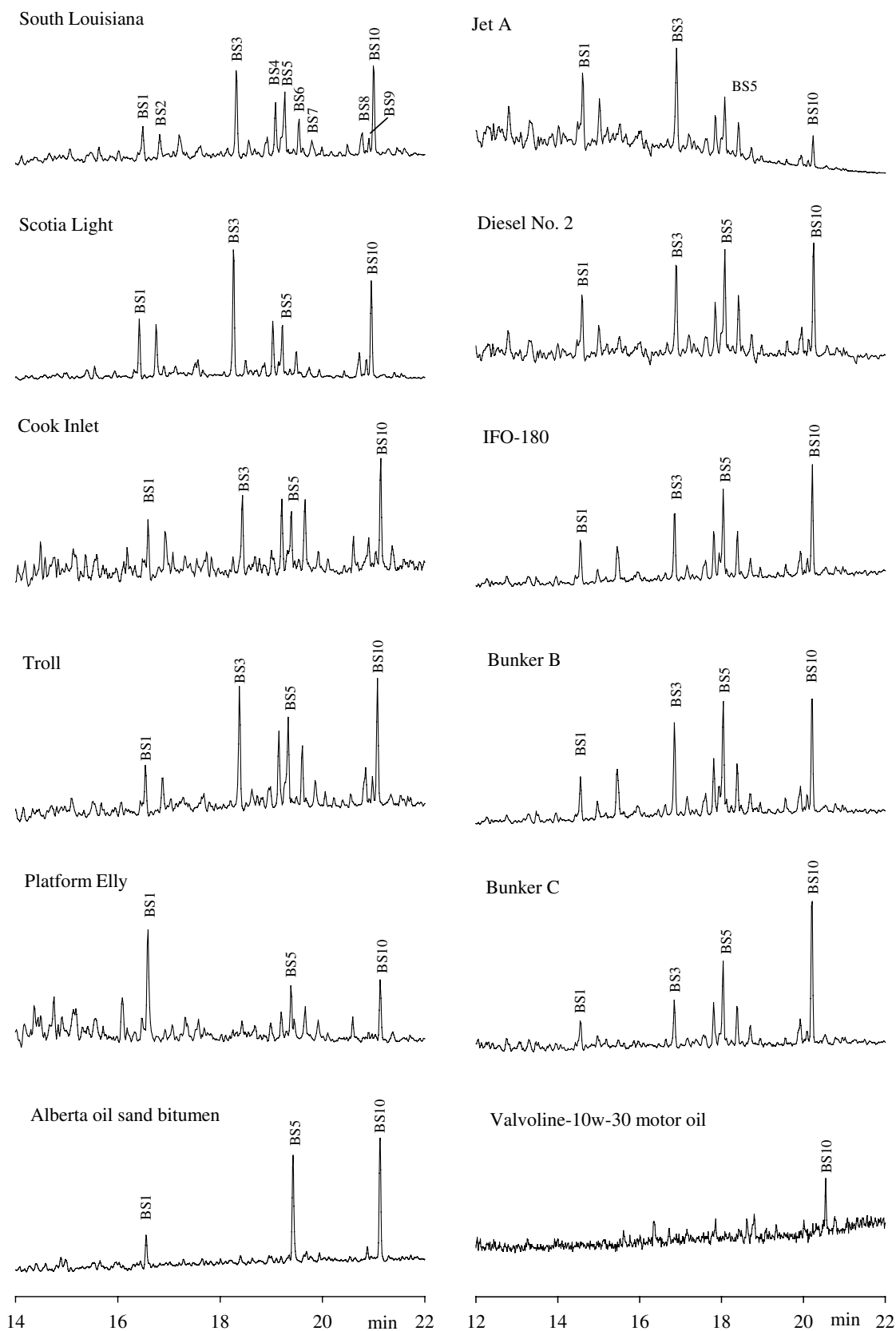


FIGURE 5.10 GC/MS chromatograms of bicyclic sesquiterpanes (m/z 123) in crude oils and refined petroleum products.

TABLE 5.6 Abundance of bicyclic sesquiterpanes in crude oils and refined petroleum products

Oil samples	Total	BS1 (%)	BS3 (%)	BS5 (%)	BS10 (%)
Crude oils ($\mu\text{g/g}$)					
Alberta oil sands bitumen	1988	9.6	6.0	21.3	28.0
Orinoco bitumen	1302	16.4	4.7	25.6	26.9
Cold Lake bitumen	2124	11.7	8.2	24.6	24.3
Federated	3670	8.2	14.7	21.2	14.4
Platform Elly	1129	36.6	4.1	13.2	15.2
Maya	969	10.2	10.1	24.0	26.6
Prudhoe Bay	2551	9.9	12.3	20.7	20.9
Mars TLP	976	12.8	12.5	14.1	26.6
Arabian Heavy	1904	7.8	11.1	19.1	30.1
Mississippi Canyon	917	9.7	14.1	14.3	24.8
Troll	5119	8.1	19.5	13.8	17.3
West Delta Canyon	1010	9.6	13.8	13.5	25.5
Alaska North Slope	2179	10.1	13.3	20.4	20.8
Cook Inlet	2211	8.9	14.1	11.6	17.4
South Louisiana	5155	9.2	20.0	14.6	18.0
Petroleum products ($\mu\text{g/g}$)					
Gasoline	0.0	NA	NA	NA	NA
Kerosene	0.7	100	0.0	0.0	0.0
Aviation gasoline	30.6	15.7	18.8	14.2	11.3
Jet A	6770	18.4	25.0	12.9	6.4
Diesel (Pioneer gas station)	7628	10.3	20.9	15.4	15.0
Diesel (Shell gas station)	8703	9.1	18.3	15.4	17.3
Diesel (Stinson gas station)	8447	8.5	18.7	15.7	17.4
Diesel (Ottawa)	6028	11.9	16.7	16.7	17.2
Korea diesel #1	7658	6.3	15.4	16.1	19.3
Korea diesel #2	5819	6.4	15.4	18.0	24.1
Korea diesel #3	6129	6.4	16.8	17.1	21.9
Fuel No. 4	4221	9.6	19.9	17.4	14.7
IFO-180	2033	10.5	15.4	17.6	19.7
Bunker B (Fuel No. 5)	1449	8.8	16.0	19.7	20.0
Bunker C (Fuel No. 6)	255	8.1	10.9	17.6	29.9
Lube oil 10W-30	10.1	3.3	7.0	14.2	46.4
Synthetic lube oil 10W-30	15.3	1.4	8.3	20.7	34.8
Extreme pressure gear oil	15.6	8.1	15.1	15.1	30.2

[60,63]. Yang et al. [63] reported a quantitation of bicyclic sesquiterpanes in numerous crude oils and refined petroleum products collected from various sources. GC–MS chromatograms of sesquiterpanes for six representative crude oils are compared in Figure 5.10. Table 5.6 summarizes the total concentrations of ten target sesquiterpanes and normalized percentages of major sesquiterpanes in 15 crude oils.

Bicyclic sesquiterpanes occur in all of the crude oils studied. The abundance of sesquiterpanes is unlikely dependent on the densities of the crude oils, similar to the results observed for diamondoid compounds [62]. In general, the GC–MS chromatograms of sesquiterpanes at m/z 123 are often characterized by the dominance of BS1, BS3, BS5, and BS10 with BS5 or BS10 being the most abundant. BS2, BS7, BS8, and BS9 have much lower relative abundance. As seen in Table 5.6, the dominant sesquiterpanes BS1, BS3, BS5, and BS10 together account for about 50–75% of the sum of ten target sesquiterpanes. Bicyclic sesquiterpanes were also detected in extremely heavy oils such as Alberta oil sands bitumen despite the depletion of n -alkanes by biodegradation [103,104]. The bulk concentrations of target sesquiterpanes in oil sands bitumen are at the

same level as many other crude oils. The selected ion chromatograms at m/z 123 show distribution patterns of BS10>BS5>BS1 for Alberta oil sands bitumen. It is evident that bicyclic sesquiterpanes have been partially biodegraded in these heavy oil samples. $8\beta(H)$ -homodrimane is likely the most abundant homologue in oil sands bitumen, which suggests that this compound has the least degradability among all ten sesquiterpanes.

Distribution of Sesquiterpanes in Refined Products The quantitation results of sesquiterpanes in various petroleum products including aviation gasoline, kerosene, jet fuel, diesel, Bunker B, Bunker C, and lubricating oil are also shown in Table 5.6. It can be seen that sesquiterpanes were found in all fuel oil samples except gasoline. The total concentrations of ten sesquiterpanes are in the range of approximately 4000–8700 $\mu\text{g/g}$ in most midrange fuels and in the range of 255–2000 $\mu\text{g/g}$ in heavy residual fuels. As understandable, only traces of sesquiterpanes are detected in gasoline, light kerosene, and lubricating oils. The abundances and distribution patterns of sesquiterpanes differ widely in the petroleum products, which is attributed to the

differences in the crude oil feedstocks and the refining processes. Overall, the distribution pattern of individual sesquiterpane compounds in midrange fuels is similar to that in crude oils. BS3, BS5, and BS10 are the most dominant, while BS8 and BS9 often show the lowest abundances. It is also noted that the dominance of $\delta\beta(H)$ -homodrimane (BS10) is obvious for midrange distillates and heavy residual fuels; particularly among ten common bicyclic sesquiterpanes, only this compound is clearly detected in 10W-30 motor oil.

Obviously, crude oils from different sources and different petroleum products have varied signatures of both the absolute concentrations and relative distribution patterns of sesquiterpanes. In addition, the naturally occurring sesquiterpanes are relatively stable during biodegradation. These fingerprints of sesquiterpanes as well as their diagnostic ratios may find their forensic applications for oil source identification. Early studies on sesquiterpanes mainly focused on geological application in the maturity, depositional environment, and origin of oils. In recent years, they are of special interest in oil-source correlation and differentiation for those refined products in which the high ring number biomarkers were removed during refining processes. Stout et al. reported a successful forensic fingerprinting study of middle distillate fuels in the environment using sesquiterpanes [59]. Wang et al. [60] presented two real-world spill case studies using unique sesquiterpanes for fingerprinting and identifying mystery diesel spills.

5.3.5 Aromatic Hydrocarbons in Petroleum

Although aromatic hydrocarbons make up a smaller proportion of crude oils in comparison with aliphatic hydrocarbons, their concentrations are still considerable. In some heavy crudes and residual fuels, PAHs could reach a large percentage. For example, the refined product pole-treating oil, which is designed for the preservation of wood products such as utility poles, crossarms, and railway ties, could possess as high as 80% aromatic content. Aromatic hydrocarbons in petroleum may be basically classified into three main groups according to their molecular structures, including monoaromatic hydrocarbons, PAHs and their aliphatic substituents, as well as naphthenoaromatic hydrocarbons, which consist of mixed structures of aromatic and saturated cyclic rings.

5.3.5.1 BTEX and Alkylbenzenes BTEX are hazardous carcinogenic and neurotoxic compounds. They are classified as priority pollutants regulated by many environmental organizations around the world. These monoaromatic compounds are highly water soluble and more volatile compared with their aliphatic counterparts. Small aromatics frequently enter air, soil, sediments, and groundwater due to accidental oil spills and leakage of gasoline and other petroleum fuels from underground storage tanks and pipelines and improper oil-related waste disposal practices [105]. With respect to forensic oil spill analysis, these volatile aromatics are of little importance or interest. However, because of their

potential acute toxicity health hazard to humans and aquatic life in the water column, these volatile aromatic hydrocarbons are often required to be analyzed as one group whenever a hydrocarbon fuel is suspected to have been spilled (especially in relatively confined areas).

Wang et al. [105] developed a rapid, reliable, and effective method for direct determination of BTEX and alkyl-substituted benzenes in petroleum using GC/MS in SIM. To avoid the loss of light boiling BTEX in sample preparation, the oil sample was dissolved in *n*-pentane for direct GC analysis. The use of *n*-pentane as a solvent also reduces the column contamination caused by heavy asphaltenes content. Accordingly, mass spectra of alkylated benzenes are characterized by the presence of m/z 91 for methylbenzene, m/z 105 for C_2 -benzenes, and m/z 119 for C_3 -benzene; similarly, the isomers with larger alkylation can be determined using the characteristic $(M-15)^+$ ion.

Benzene and its C_7 - C_{10} homologues have been thoroughly investigated in many crude oils. Wang et al. [105] identified 58 alkyl-substituted benzene components in a light crude oil, Alberta Sweet Mixed Blend (ASMB). They also reported a quantitative analysis of the individual BTEX compounds and C_3 -benzene isomers in over 200 different crude and weathered oils. The plots of the concentrations of BTEX plus C_n -benzenes versus weathering percentages were used to estimate the weathering extent of weathered oil samples, especially for those short-term weathered oils in which the loss of BTEX and C_n -benzenes is significant.

The concentrations of BTEX and alkylbenzenes in different crude oils and refined products are presented in Table 5.7. The total concentration of monoaromatics studied in crude oil is at the mg/g level, while its values vary from oil to oil. Overall, BTEX and C_3 -benzenes make up most of determined monoaromatics. In general, 1,2,3-trimethylbenzene is the most abundant C_3 -benzene isomer followed by 1,3,5-trimethylbenzene. Unlike in conventional crude oils, these light aromatics are barely detectable in Alberta oil sands bitumen.

Gasoline usually consists of high amounts of BTEX and small monoaromatic compounds; for example, in Table 5.7, the fresh gasoline sample has 375 mg/g of monoaromatics. On the contrary, the residual fuels such as Bunker C contain very low concentrations of these components; these compounds are barely detected in lubricating oils such as 10W-30 lube oil.

5.3.5.2 U.S. EPA Individual Priority PAHs PAHs have two or more fused benzene rings as a structural characteristic, and their structural stability results from the concomitant electron pair delocalization. PAHs can have various alkylated groups to form various isomers, and in general these alkylated substituents predominate in petroleum. PAHs are relatively persistent in the environment, and some of them are toxic, carcinogenic, and mutagenic. Although a number of unsubstituted PAHs occur naturally, only a selection of 2- to 6-ring PAHs are monitored in priority due to their

TABLE 5.7 BTEX and alkylbenzenes in crude oils and refined petroleum products

Oil samples	Crude oils					Petroleum products			
	ScL	SoL	Troll	PIE	Alberta oil sands ^a	Gasoline #87	Diesel No. 2	Bunker C	Lube 10W-30
Benzene	0.00	2.65	0.70	0.16	0.000	5.62	0.07	0.03	0.005
Toluene	0.24	6.33	2.53	0.82	0.012	140	1.03	0.19	0.009
Ethylbenzene	0.32	1.32	1.43	0.50	0.001	18.8	0.57	0.12	0.001
<i>m</i> - and <i>p</i> -Xylene	2.05	5.76	5.03	0.74	0.006	63.4	2.38	0.50	0.003
<i>o</i> -Xylene	0.66	2.31	1.30	0.55	0.002	23.3	1.13	0.24	0.001
ΣBTEX	3.03	18.4	11.0	2.77	0.022	251	5.19	1.08	0.019
Isopropylbenzene	0.28	0.34	0.43	0.18	0.000	2.85	0.38	0.03	0.000
Propylbenzene	0.45	0.40	0.61	0.39	0.001	7.28	0.62	0.18	0.000
3- and 4-Ethyltoluene	2.06	1.73	1.97	0.56	0.005	35.4	2.17	1.12	0.001
1,3,5-Trimethylbenzene	1.12	1.49	1.22	0.19	0.003	12.6	1.02	0.45	0.002
2-Ethyltoluene	0.40	0.51	0.67	0.35	0.002	9.52	0.82	0.31	0.000
1,2,4-Trimethylbenzene	2.00	2.12	2.09	0.53	0.008	49.1	4.13	1.99	0.002
1,2,3-Trimethylbenzene	0.30	0.17	0.37	0.14	0.001	0.46	0.72	0.04	0.000
ΣC₃-alkylbenzenes	6.62	6.76	7.36	2.34	0.020	117	9.87	4.12	0.005
Isobutylbenzene	0.28	0.11	0.11	0.02	0.001	0.37	0.22	0.03	0.000
1-Methyl-2-isopropylbenzene	0.12	0.05	0.07	0.02	0.001	0.24	0.08	0.03	0.000
1,2-Dimethyl-4-ethylbenzene	0.56	0.38	0.46	0.17	0.002	4.69	1.42	0.58	0.000
Amylbenzene	0.12	0.04	0.06	0.08	0.005	1.04	1.31	0.26	0.000
<i>n</i> -Hexylbenzene	0.21	0.03	0.05	0.06	0.006	0.06	0.45	0.09	0.000
ΣC₄-C₆ alkyl benzenes	1.23	0.61	0.75	0.35	0.014	6.39	3.48	0.99	0.000
Total (mg/g)	11.2	25.7	19.1	5.46	0.056	375	18.5	6.18	0.02

^aConcentration: mg/g of TSEM of Alberta oil sands.

relatively high toxicity and high concentration in the environment. As shown in Table 5.8, naphthalene, phenanthrene, fluorene, and chrysene are grouped together with their alkylated homologues for the convenience of comparison.

PAHs are ubiquitous in the environment and generally originated from three main sources, that is, petrogenic, pyrogenic, and biogenic. Petrogenic PAHs are related to crude oils or refined products, which are generated from geochemical alteration of organic matter. Pyrogenic PAHs, particularly higher-molecular-weight PAHs ranging from benzo(*a*)anthracene to coronene, are prevalent contaminants resulting from heavy anthropogenic and industrial activities such as the incomplete combustion of fuel, industrial petrochemical practices, residential wood burning, vehicular emissions, and power plant emissions.

At high temperatures, the more reactive alkylated PAHs tend to be destroyed. This explains why homologue groups in pyrogenic assemblages are dominated by nonalkylated, parent compounds, with subsequently less alkyl members as the degree of alkylation increases [89,106]. Biogenic PAHs are produced by organisms or formed during early stage of diagenesis in sediments. Unlike petrogenic and pyrogenic PAHs, biogenic PAHs generally are found individually or in very simple mixtures.

Unsubstituted (or parent) PAHs have a very stable fused hexagonal ring structure. These compounds are normally determined using their prominent parent ions although other less-intensive fragmentograms can be used for confirmation. Crude oils contain high concentrations of 2- and 3-ring

PAHs (i.e., biphenyl, acenaphthylene, and acenaphthene) but only trace amounts of high-molecular-weight 5- and 6-ring PAHs (Fig. 5.11 and Table 5.8). As seen in Table 5.8, the total concentration of 15 unsubstituted PAHs in crude oils spans from tens to hundreds of ppm.

It is noted that Platform Elly heavy crude contains 30.2 µg/g of perylene, significantly more abundant than other 4- to 6-ring PAHs. The PAHs determined in heavily biodegraded Alberta oil sands bitumen are composed of relatively higher 3- to 5-ring compounds than conventional crudes, particularly those light crude oils. In the market, some synthetic crude oils such as AHS (Alberta, Canada) are blended with hydrocracking residues, in which extremely high contents of unsubstituted PAHs were detected with a total concentration of 624 µg/g [104]. It was reported that the PAHs found in tire pyrolysis oil consists largely of alkylated naphthalenes, fluorenes, and phenanthrenes; meanwhile, the concentrations of individual 5-ring benzo(*a*)pyrene ranged from less than 10 to 600 ppm [107].

As seen in Table 5.9, compared with crude oils, refined oil products generally contain much higher concentrations of unsubstituted PAHs with an exception of lubricating oil only having trace amounts of them. In general, PAHs in light distillate fuels are only limited to small 2- and 3-ring compounds; however, obvious increments of 4- to 6-ring PAHs attributed to refining processes are found in residual fuels. For instance, 4- to 6-ring PAHs in total comprise nearly 90% of parent PAHs in Bunker B and Bunker C while only less than 5% in Diesel No. 2 and undetectable levels in gasoline (Table 5.9).

TABLE 5.8 PAH concentration in representative crude oils

Samples	ScL	SoL	CI	Troll	ArH	PIE	AOS ^a
C ₀ -Naphthalene	30.3	806	579	967	140	85.8	0.00
C ₁ -Naphthalenes	230	2,026	1,944	2,900	616	377	0.00
C ₂ -Naphthalenes	734	2,920	2,869	3,646	1,262	744	11.5
C ₃ -Naphthalenes	1,077	2,563	2,151	2,837	1,625	882	103
C ₄ -Naphthalenes	621	1,544	1,066	1,677	1,096	820	240
ΣNaphthalenes	2691	9,858	8,610	12,027	4738	2909	355
C ₀ -Phenanthrene	36.3	145	296	269	55.8	27.3	10.1
C ₁ -Phenanthrenes	77.3	396	618	585	169	91.4	95.5
C ₂ -Phenanthrenes	107	460	604	640	280	137	214
C ₃ -Phenanthrenes	86.5	371	343	543	224	109	274
C ₄ -Phenanthrenes	43.4	229	208	410	140	95.6	198
ΣPhenanthrenes	350	1,601	2,069	2,448	868	460	791
C ₀ -Dibenzothiophene	1.61	35.0	14.1	39.2	89.7	47.4	1.21
C ₁ -Dibenzothiophenes	2.56	85.0	46.5	125	368	115	59.2
C ₂ -Dibenzothiophenes	9.33	201	63.1	182	819	212	265
C ₃ -Dibenzothiophenes	2.77	170	45.7	153	955	187	387
ΣDibenzothiophenes	16.3	491	169	499	2232	561	712
C ₀ -Fluorene	28.7	58.9	106	161	29.2	10.2	1.55
C ₁ -Fluorenes	85.8	178	245	347	80.5	38.5	23.7
C ₂ -Fluorenes	123	300	266	484	169	80.5	77.7
C ₃ -Fluorenes	120	273	202	396	277	78.7	128
ΣFluorenes	357	809	819	1,388	555	208	231
C ₀ -Chrysene	2.88	8.07	55.7	40.3	10.3	10.5	15.9
C ₁ -Chrysenes	6.90	23.3	133	77.3	21.9	19.7	40.3
C ₂ -Chrysenes	6.21	31.1	135	119	39.1	33.0	84.6
C ₃ -Chrysenes	1.88	24.0	97.2	71.8	33.9	24.4	75.9
ΣChrysenes	17.9	86.6	421	309	105	87.6	217
ΣAlkylated PAHs (μg/g)	3433	12,844	12,088	16,670	8498	4226	2305
Biphenyl	25.9	153	60.7	288	23.1	5.77	0.00
Acenaphthylene	3.91	15.9	12.5	16.4	7.65	8.56	0.00
Acenaphthene	24.2	13.6	18.6	53.7	4.42	6.01	2.94
Anthracene	1.57	3.64	10.6	2.96	1.75	0.60	0.00
Fluoranthene	2.93	3.27	4.93	12.6	1.89	1.57	3.02
Pyrene	2.55	4.83	13.9	16.3	4.01	3.81	10.4
Benz(<i>a</i>)anthracene	1.41	2.67	13.7	7.75	2.11	2.43	2.03
Benzo(<i>b</i> + <i>k</i>)fluoranthene	1.59	2.17	8.68	10.6	2.33	2.87	4.31
Benzo(<i>e</i>)pyrene	1.33	1.45	14.3	11.1	2.70	3.55	5.93
Benzo(<i>a</i>)pyrene	0.74	0.59	3.71	3.15	1.33	1.32	2.22
Perylene	1.10	21.2	2.93	4.70	0.97	30.2	4.83
Indeno(1,2,3- <i>cd</i>)pyrene	0.38	0.00	0.63	1.40	0.31	0.00	1.30
Dibenzo(<i>a,h</i>)anthracene	0.30	0.23	2.46	1.50	0.37	0.00	1.53
Benzo(<i>g,h,i</i>)perylene	1.29	0.70	4.27	3.61	1.42	1.48	2.61
ΣEPA priority PAHs (μg/g)	69.2	223	172	434	54.4	68.1	41.1
Total PAHs (μg/g)	3502	13,067	12,259	17,104	8553	4294	2347

^aConcentration in μg/g of TSEM.

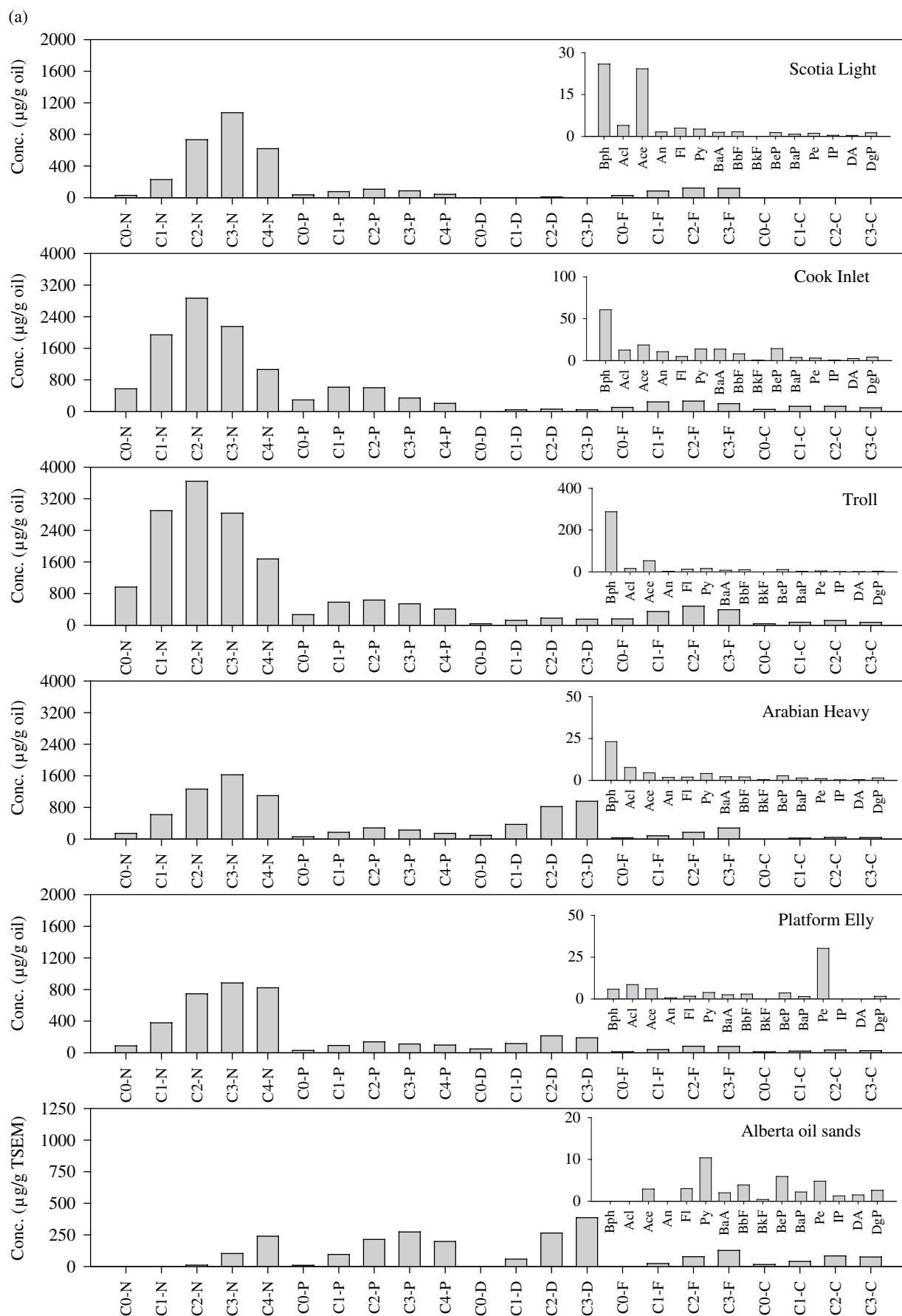


FIGURE 5.11 (a) Distribution PAHs in representative crude oils.

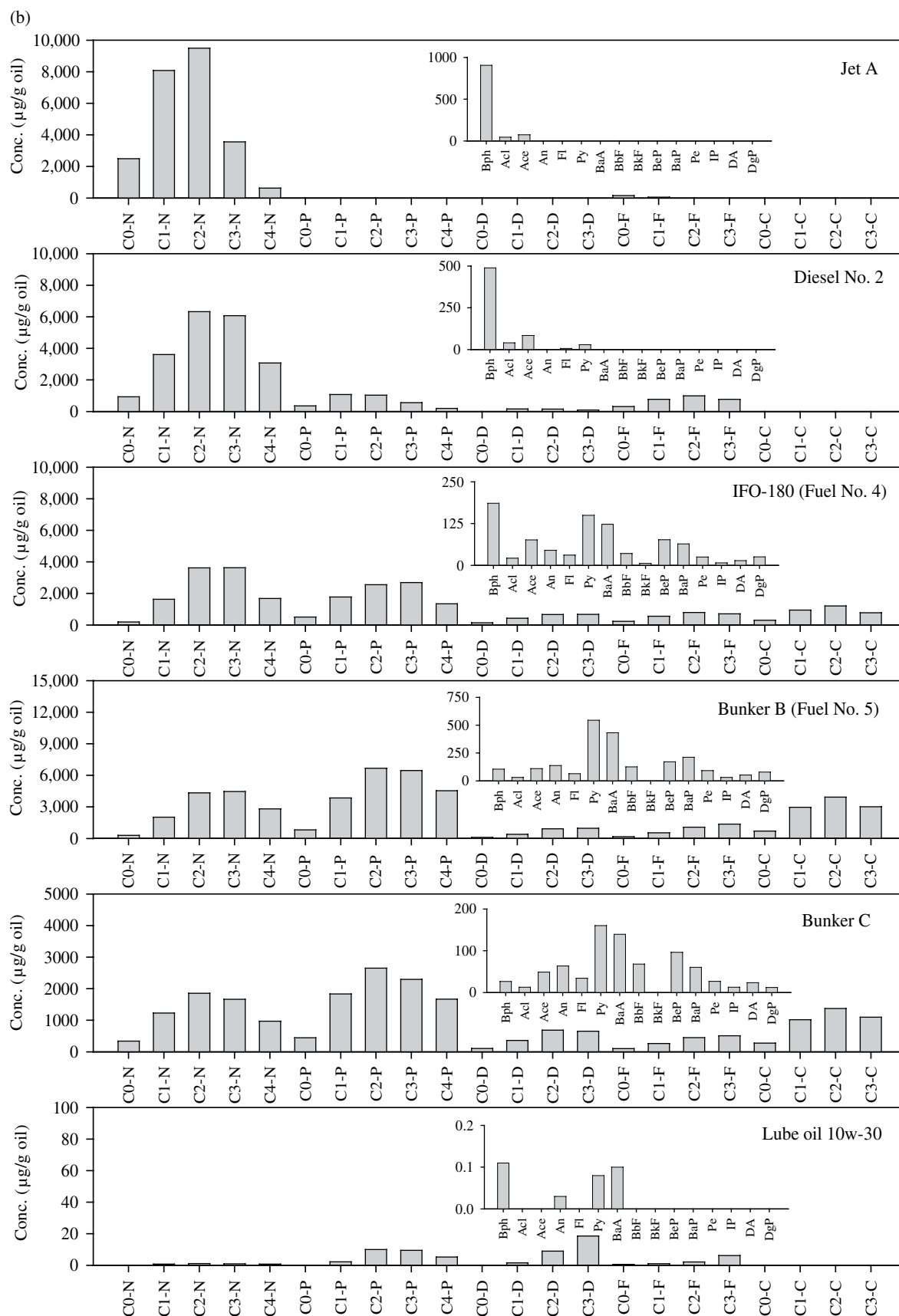


FIGURE 5.11 (Continued) (b) Distribution PAHs in representative refined petroleum products.

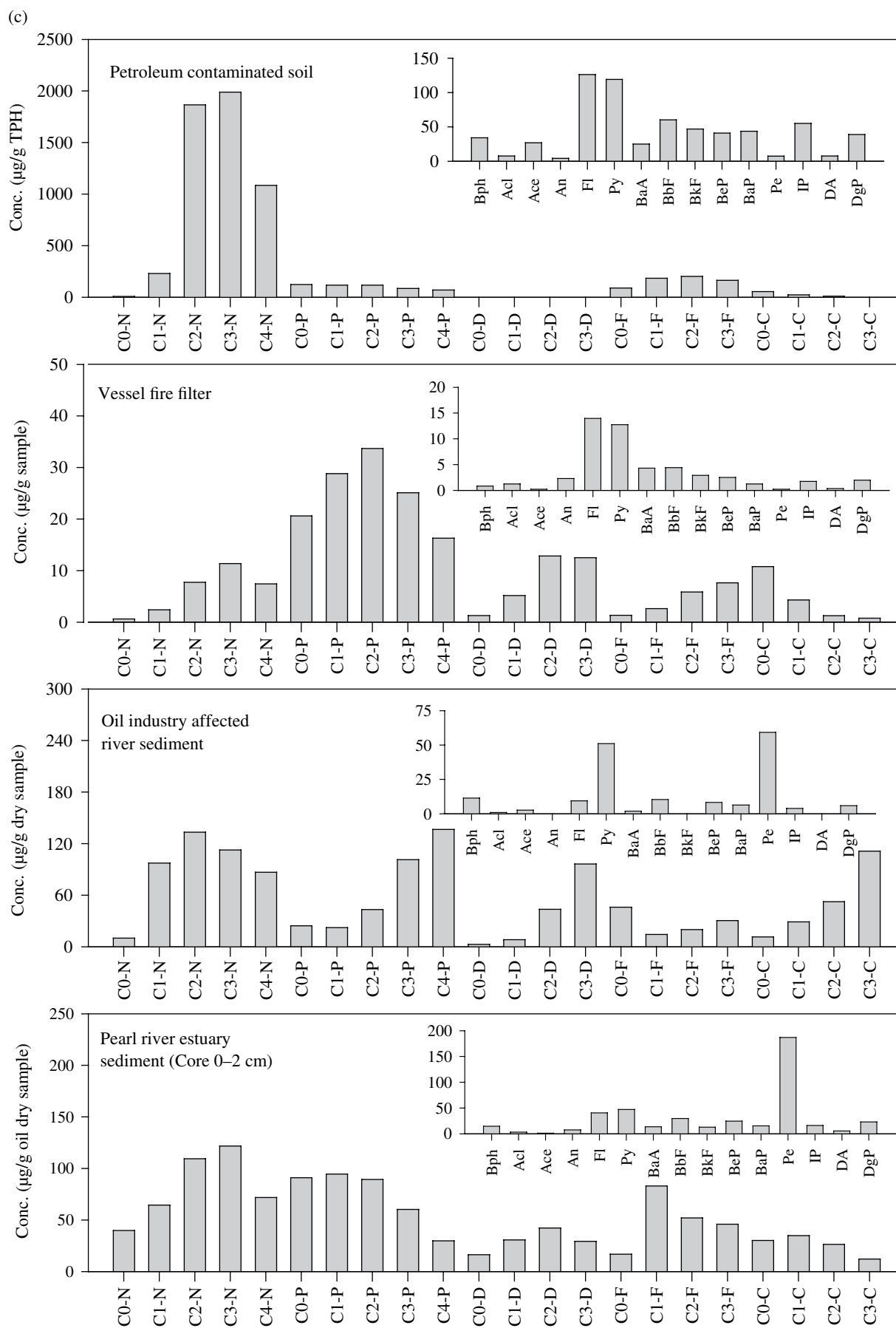


FIGURE 5.11 (Continued) (c) Distribution PAHs in representative environmental samples.

TABLE 5.9 PAH concentration in representative refined petroleum products

Samples	Jet A	Diesel No. 2	IFO-180	Bunker B (Fuel No. 5)	Bunker C (Fuel No. 6)	Lube10W-30
C ₀ -Naphthalene	2,497	933	182	281	342	0.39
C ₁ -Naphthalenes	8,085	3,614	1,624	2,010	1,231	0.78
C ₂ -Naphthalenes	9,497	6,328	3,611	4,325	1,857	1.17
C ₃ -Naphthalenes	3,562	6,077	3,620	4,450	1,665	1.01
C ₄ -Naphthalenes	633	3,078	1,669	2,801	970	0.79
ΣNaphthalenes	24,274	20,030	10,707	13,868	6,064	4.14
C ₀ -Phenanthrene	9.63	359	498	811	445	0.22
C ₁ -Phenanthrenes	7.03	1,081	1,762	3,836	1,837	2.27
C ₂ -Phenanthrenes	8.11	1,041	2,547	6,668	2,653	10.0
C ₃ -Phenanthrenes	0.00	564	2,676	6,444	2,297	9.51
C ₄ -Phenanthrenes	0.00	203	1,335	4,533	1,672	5.27
ΣPhenanthrenes	24.8	3,248	8,817	22,292	8,903	27.2
C ₀ -Dibenzothiophene	2.41	34.0	134	90.4	110	0.15
C ₁ -Dibenzothiophenes	0.00	163	416	387	362	1.54
C ₂ -Dibenzothiophenes	0.00	160	656	907	686	9.03
C ₃ -Dibenzothiophenes	0.00	96.2	664	961	656	18.6
ΣDibenzothiophenes	2.41	454	1,870	2,346	1,814	29.3
C ₀ -Fluorene	160	316	221	160	104	0.65
C ₁ -Fluorenes	55.4	775	543	525	265	1.04
C ₂ -Fluorenes	14.9	992	785	1,058	451	2.13
C ₃ -Fluorenes	0.00	775	699	1,349	510	6.19
ΣFluorenes	230	2,858	2,249	3,092	1,330	10.0
C ₀ -Chrysene	0.00	2.58	290	690	277	0.13
C ₁ -Chrysenes	0.00	5.65	932	2,955	1,017	0.00
C ₂ -Chrysenes	0.00	4.72	1,195	3,912	1,372	0.00
C ₃ -Chrysenes	0.00	0.00	765	3,003	1,097	0.00
ΣChrysenes	0.00	13.0	3,182	10,560	3,763	0.13
ΣAlkylated PAHs (μg/g)	24,531	26,602	26,824	52,157	21,875	70.8
Biphenyl	907	489	186	104	26.1	0.11
Acenaphthylene	44.9	40.1	21.5	30.0	12.3	0.00
Acenaphthene	74.8	84.4	76.4	109	48.4	0.00
Anthracene	0.15	0.00	45.2	136	63.1	0.03
Fluoranthene	0.10	7.05	30.5	62.8	33.8	0.00
Pyrene	0.00	29.1	150	543	160	0.08
Benz(a)anthracene	0.00	0.45	123	430	139	0.10
Benzo(b+k)fluoranthene	0.00	0.00	41.3	124	67.8	0.00
Benzo(e)pyrene	0.00	0.00	76.8	170	95.7	0.00
Benzo(a)pyrene	0.00	0.00	64.4	211	59.9	0.00
Perylene	0.00	0.00	24.9	90.2	26.5	0.00
Indeno(1,2,3-cd)pyrene	0.00	0.00	7.56	30.0	12.2	0.00
Dibenzo(a,h)anthracene	0.00	0.00	14.4	51.2	23.2	0.00
Benzo(g,h,i)perylene	0.00	0.00	25.5	77.5	11.8	0.00
ΣEPA priority PAHs (μg/g)	1,027	650	888	2,169	780	0.32
Total PAHs (μg/g)	25,558	27,251	27,712	54,339	23,029	71.2

Figure 5.11c shows the PAH distributions in some representative environmental samples including a petroleum-contaminated soil, a filter collected from a vessel after a fire incident, a sediment from oil industry-affected river, and a marine sediment from the Pearl River estuary (PRE). Besides the high concentration of naphthalenes, a high amount of 4- to 6-ring parent PAHs suggests other contribution sources to the petroleum-contaminated soil sample. In the filter of a vessel that suffered a fire incident, a high percentage of 4- to 6-ring parent PAHs predominates the total determined PAHs. Among these unsubstituted PAHs in sediments, 4- to 6-ring PAHs are often predominant over those

lower-molecular-weight 2- and 3-ring PAHs (Fig. 5.11c). This typical PAH distribution pattern indicates a contribution from pyrogenic sources, such as run-off from high levels of automobile emissions, which are known to contain high levels of larger molecular PAHs relative to others. PAHs tend to deposit in sediments, soils, and biota, resulting in long-term hazards to the environment. Anthropogenic input is one of the major sources causing significant accumulation of sedimentary PAHs in the river and marine beds.

Biogenic PAHs synthesized by organisms can be easily differentiated from those occurring in petroleum. One of the most abundant biogenic PAHs is perylene, which is believed

to be formed during the bacteriological breakdown of organic matter in marine sediments by a process called early diagenesis [74,108]. In Figure 5.11c, perylene is the most abundant among target unsubstituted PAHs, accounting for a large fraction of the total individual PAHs in oil sands industry-affected river sediment and the PRE sediment. Therefore, the contribution of biogenic sources to the measured hydrocarbons in these sediments is evident.

5.3.5.3 Alkylated PAHs Crude oils and refined products generally contain significant amounts of PAHs, in particular the alkylated homologues (APAHs) of naphthalene, phenanthrene, dibenzothiophene, fluorene, and chrysene [109]. The concentrations of five groups of alkylated homologues are roughly two orders of magnitude higher than the total concentration of the unalkylated PAHs. These alkylated PAHs are particularly useful for source identification because they occur in all crude oils and most refined petroleum products at considerable concentrations. Their relative concentrations also vary significantly between different oils making them source specific [110].

Similar to unsubstituted PAH analysis, APAHs are generally determined using their prominent parent ions. Other fragmentograms such as (M-1)⁺, (M-15)⁺, and (M-29)⁺ can be applied for confirmation. Tables 5.8 and 5.9 summarize the quantitative analytical results of five petroleum-characteristic alkylated PAHs homologous series (naphthalenes, phenanthrenes, dibenzothiophenes, fluorenes, and chrysenes) and 15 individual unsubstituted PAHs in representative light to heavy oil samples.

APAH concentrations in seven crude oils vary widely from 2,300 µg/g for Alberta oil sands bitumen to 16,670 µg/g for Troll crude. Light crude oil does not necessarily contain high concentrations of APAH; as an example, Scotia Light crude only has 3433 µg/g of alkylated PAHs in total. In fresh crude oils, total APAHs are largely contributed by naphthalene and phenanthrene series. Therefore, it is understandable that the presence of 2- to 3-ring PAHs including naphthalenes and phenanthrenes generally implies fresh petroleum pollution. Some crude oils contain particularly high amounts of hetero-PAHs (N, S, O), as seen in Table 5.8; Arabian heavy oil shows 2232 µg/g of dibenzothiophenes, or roughly a quarter of total 8498 µg/g APAHs.

The distribution of alkylated PAHs (generally refer to C₀- to C₄-) in fresh crudes and refined products is usually in characteristic bell-shaped profile due to the different degrees of alkylation (Fig. 5.11). C₁- to C₃-naphthalenes are often the most abundant in many fresh crude oils, but distinctively, they were readily removed in the formation of heavy oils with a very low concentration. A distribution profile of C₀-<C₁-<C₂-<C₃- in nearly all five oil-characteristic alkylated PAH series of Alberta oil sands bitumen is very apparent. This can be explained by the fact that the susceptibility to microbial degradation decreases as the alkylation level increases in each alkylated PAH family. Sometimes, heavy crude like bitumen is mixed with diluent to facilitate easy transportation; therefore, it is not surprising that C₀- to

C₃-naphthalene isomers can be detected in appreciable concentrations [104].

The abundance and distribution profile of APAHs in refined products are often altered by the distillation and refining process. Table 5.9 lists PAH concentrations in selected refined petroleum products ranging from light Jet A to residual fuel Bunker C and lubricating oil. Compared to conventional crudes, many refined oil products except lubricating oil have higher contents of alkylated PAHs with the predominance of naphthalene and phenanthrene series. For example, the concentrations of total APAHs in Jet A, diesel fuel, and Bunker B are as high as 24,531, 26,602, and 52,157 µg/g, respectively. The alkylated PAHs are partially derived from feedstock crude oil and partially from the manufacturing processes. The two-ring naphthalenes are extremely high in Jet A and Diesel No. 2 (24,274 and 20,030 µg/g, respectively), but alkylated dibenzothiophene and chrysene series are hardly detectable. In contrast, the residual fuels such as Bunker C usually contain relatively high contents of alkylated dibenzothiophenes and alkylated chrysenes; meanwhile, naphthalene and phenanthrene are often determined in great concentrations. The small PAH compounds usually come from the blended light products.

Alkylated PAHs together with unsubstituted PAHs are widely used in environmental investigations [111–114]. The distribution of PAHs is very important to decode the contamination sources. The APAH distribution profiles in Figure 5.11c strongly suggest petrogenic contamination in all these environmental samples. The bell-shaped distribution of predominant naphthalene and fluorene series further points to a relatively fresh light fuel to be the main contamination source in the soil sample. All five alkylated PAHs were detected in the vessel filter with a distribution different from that of petroleum, which can be explained by contribution from vessel fuel and pyrogenic PAHs generated in the fire incident that was involved in this case. APAHs in the sediment from an oil sands industry-affected river present an increasing profile of C₀-<C₁-<C₂-<C₃- for phenanthrene, dibenzothiophene, fluorene, and chrysene series, which is a typical feature of oil sands bitumen due to preferential biodegradation. However, the bell-shaped naphthalene series discloses light fuel contamination besides the oil sands bitumen. Of the five PAH series in the PRE sediment core, the alkylated naphthalenes and phenanthrenes are the most predominant, together making up over 70% of total alkylated PAHs. The loss of lower-molecular-weight naphthalene due to weathering was apparent, resulting in the development of the increasing distribution of C₀-N<C₁-N<C₂-N<C₃-N.

Among the five APAH series, C₁- to C₄-alkylated phenanthrenes are frequently applied for forensic oil analysis. Two pairs of methylphenanthrenes (2- and 1- and 4-/9- and 3-) are detected in considerable abundance in the GC/MS chromatogram at *m/z* 192 of both crude oil and many refined products. These compounds remain relatively stable under weathering and therefore are widely applied to distinguish oils and to investigate weathering. 2-Methylanthracene (2-MAn) is eluted between two pairs of methylphenanthrene isomers in

variable concentrations in different types of oils. Methylanthracenes (m/z 192) are generally absent in most conventional crude oils or are present only in low concentrations relative to methylphenanthrenes [115]. Relatively high presence of 2-MAN in an oil sample generally indicates the evidence of cracking process. Based on our experience in analyzing a large number of crude oils and petroleum products, the ratio of 2-MAN relative to the total of methylphenanthrenes (including 3-, 2-, 4-/9-, and 1-methylphenanthrene) ranges from 0 to 0.03 for most of the crude oils, diesels, and lube oils studied, while this ratio is generally greater than 0.03 for heavier refined petroleum products such as Bunker C. In addition, another aromatic cluster at m/z 216 (methylfluoranthene and methylpyrene) has proved to be relatively stable and especially suitable for comparing light fuel oil samples.

Among the heterocyclic PAHs, polycyclic aromatic sulfur heterocycles (PASHs) are the most widely used in forensic oil analysis. PASHs are useful in oil spill source identification even in a wide variety of weathering conditions. The presence or absence of PASHs provides important information to oil identification, particularly to the oil type recognition. Mossner and Wise [116] described an analytical method for the separation, identification, and quantification of a number of PASHs in three fossil fuel-related samples. The compounds measured included three possible naphtha(*b*) thiophenes; dibenzothiophene and selected methyl-, ethyl-, dimethyl-, and trimethyl-substituted isomers; three possible benzo(*b*)naphthothiophenes; and 30 methylbenzo(*b*)naphthothiophene isomers. Among the PASH markers, it has been established that the ratios of the C_1 -dibenzothiophenes (C_1 -DBTs) vary strongly with the source of petroleum and can therefore be used as one parameter in the source identification and differentiation of crude and weathered oils [2,111]. For instance, bunker-type fuels have a ratio of 2-/3- to 4-methyldibenzothiophene (MDBT) around 1.0, which is unusually high compared to most crude oils [112]. The presence of a clear V-pattern (4-methyl > 2- + 3-methyl < 1-methyl) for the MDBTs is generally associated with oils from predominantly carbonate source rocks, while a stair-step pattern (4-methyl > 2- + 3-methyl > 1-methyl) is associated with predominantly siliciclastic source rocks or advanced maturity (late to post oil window) oils from carbonate sources [2]. The MDBTs are also used as biodegradation indicators. 2- and 3-MDBT biodegrade at a higher rate, as shown by the strong decrease in their ratio to 4-MDBT, while 1-MDBT is slightly more resistant to biodegradation than 4-MDBT, indicated by an increase in the ratio of 1-MDBT/4-MDBT [117].

5.3.5.4 Aromatic Steranes Tetracyclic aromatic steroids are a series of naphthenoaromatic hydrocarbons that consist of mixed structures of aromatic and saturated hexyl or pentyl rings. MASs are composed of two cyclohexane rings (A + B) and one cyclopentane ring (D ring) fused with an aromatic ring (C ring) in their molecular structure (see Fig. 5.2). Triaromatic steranes (TAS) have similar molecular structure,

and the main difference is that their cyclohexane rings A and B are replaced by aromatic rings. These aromatic steroids widely occur in various crude oils and shales and are of utmost importance for petroleum chemistry and geochemistry [118]. Although aromatic steranes are in relatively low concentrations in oils, their specific fingerprints and high weathering resistance make them desirable biomarkers for forensic investigation. In the process of catagenesis, monoaromatic steroids undergo degradation of the aliphatic side chains and are transformed into triaromatic hydrocarbons. The aromatization of B ring in MASs (aromatic C ring) occurs at a slow pace, but once completed, subsequent A-ring aromatization proceeds with considerable speed. This results in low concentrations of diaromatic steroids (B and C rings) in crude oil [78]. The abundance of MASs relative to triaromatic steranes is used in various geochemical correlations, particularly in evaluating crude oil maturity [118].

Aromatic steranes in the aromatic fraction have very similar skeletons with saturated biomarker steranes. Due to the aromatization of C ring in monoaromatic and (A + B + C) rings in triaromatic steroids, these compounds have less methyl groups on the ring skeleton and have much less constitutional isomers and stereoisomers than their biomarker sterane analogs. The same reasons can explain why less triaromatic steranes are found in crude oils than MASs (see Table 5.2).

The aromatic steranes have 17 carbons to form a skeleton consisting of four fused rings. The aromatic steranes frequently detected in crude oils range from C_{20} to C_{30} homologues. Besides a methyl group, a substituent such as ethyl or isopropyl positions at C-17 in aromatic steroids. Aromatic sterane isomers have a characteristic configuration of C-17 and C-20 chiral centers. Each aromatic sterane is usually represented by two epimers (20R and 20S) with different concentrations. In a GC/MS analysis, the base peak of triaromatic steroids is m/z 217 ($C_{17}H_{13}^+$) for the nucleus alone and m/z 231 ($C_{18}H_{15}^+$) if with a single methyl group. MASs can be identified by their characteristic fragmentograms at m/z 253 ($C_{19}H_{25}^+$) due to the loss of the alkyl group X on C-17.

Different crude oils and petroleum products have varied chemical fingerprints of aromatic steranes. Figure 5.12 illustrates the GC/MS chromatograms of mono- and triaromatic hydrocarbons isolated in crudes and refined petroleum products. Monoaromatic steroids elute between $n-C_{23}$ and $n-C_{30}$, while triaromatic steroids elute slightly later between $n-C_{24}$ and $n-C_{34}$, similar to the elution range for biomarker terpanes in GC/MS analysis. These steroids are normally found in crude oils. A cluster of TA-cholestanes (C_{26}), TA-ergostanes (C_{27}), and TA-stigmastanes (C_{28}) are the most distinguishable aromatic steranes in most oil samples. C_{26} TA-cholestane (20R) and C_{27} TA-ergostane (20S) are coeluted and present as the highest peaks in m/z 231 chromatograms. As illustrated in Figure 5.12a, MASs are only determined at low abundance in most of the crude oils studied except for the considerable concentration in Platform Elly crude.

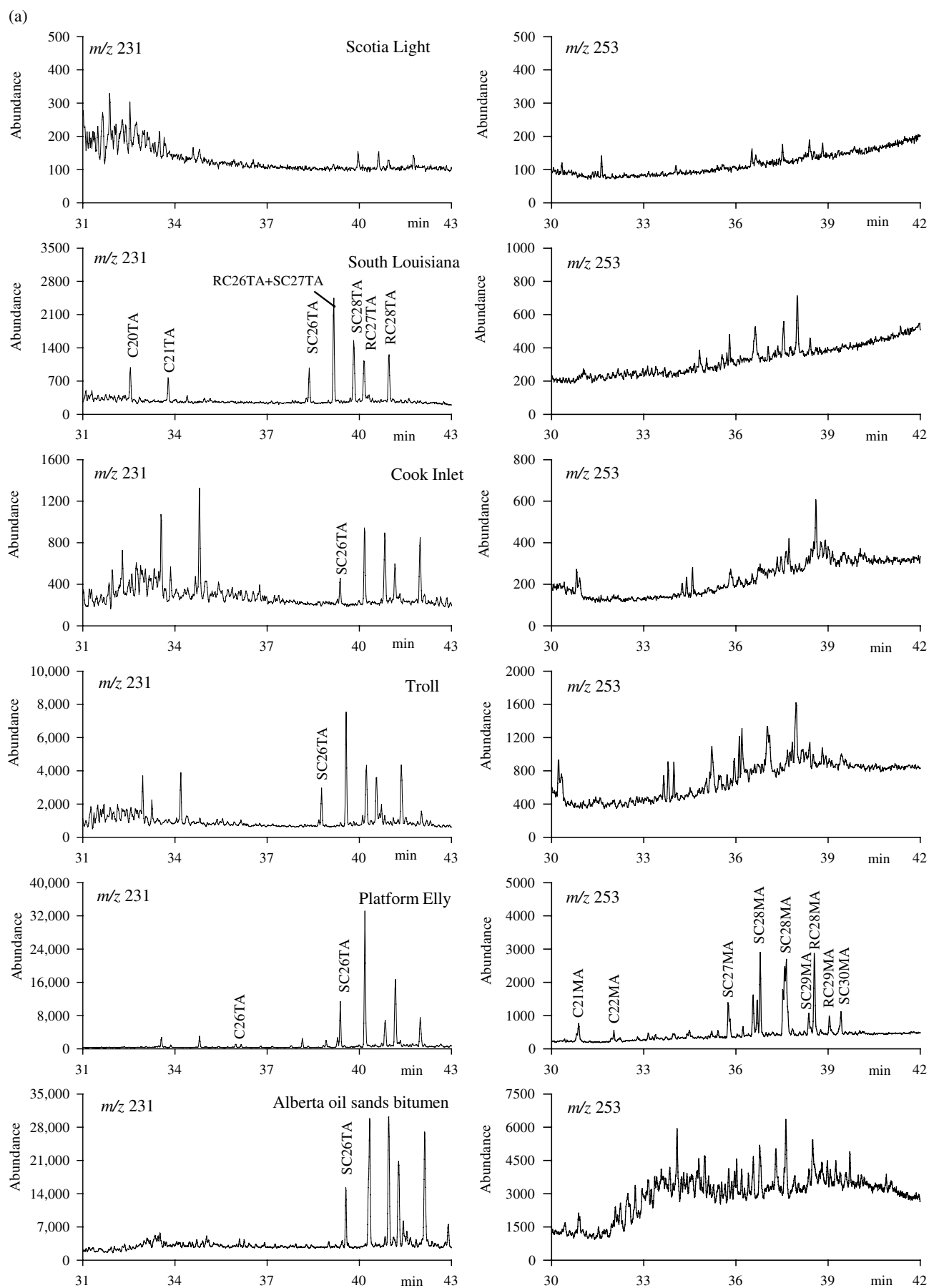


FIGURE 5.12 (a) GC/MS chromatograms of triaromatic (m/z 231) and monoaromatic (m/z 253) steranes in crude oils.

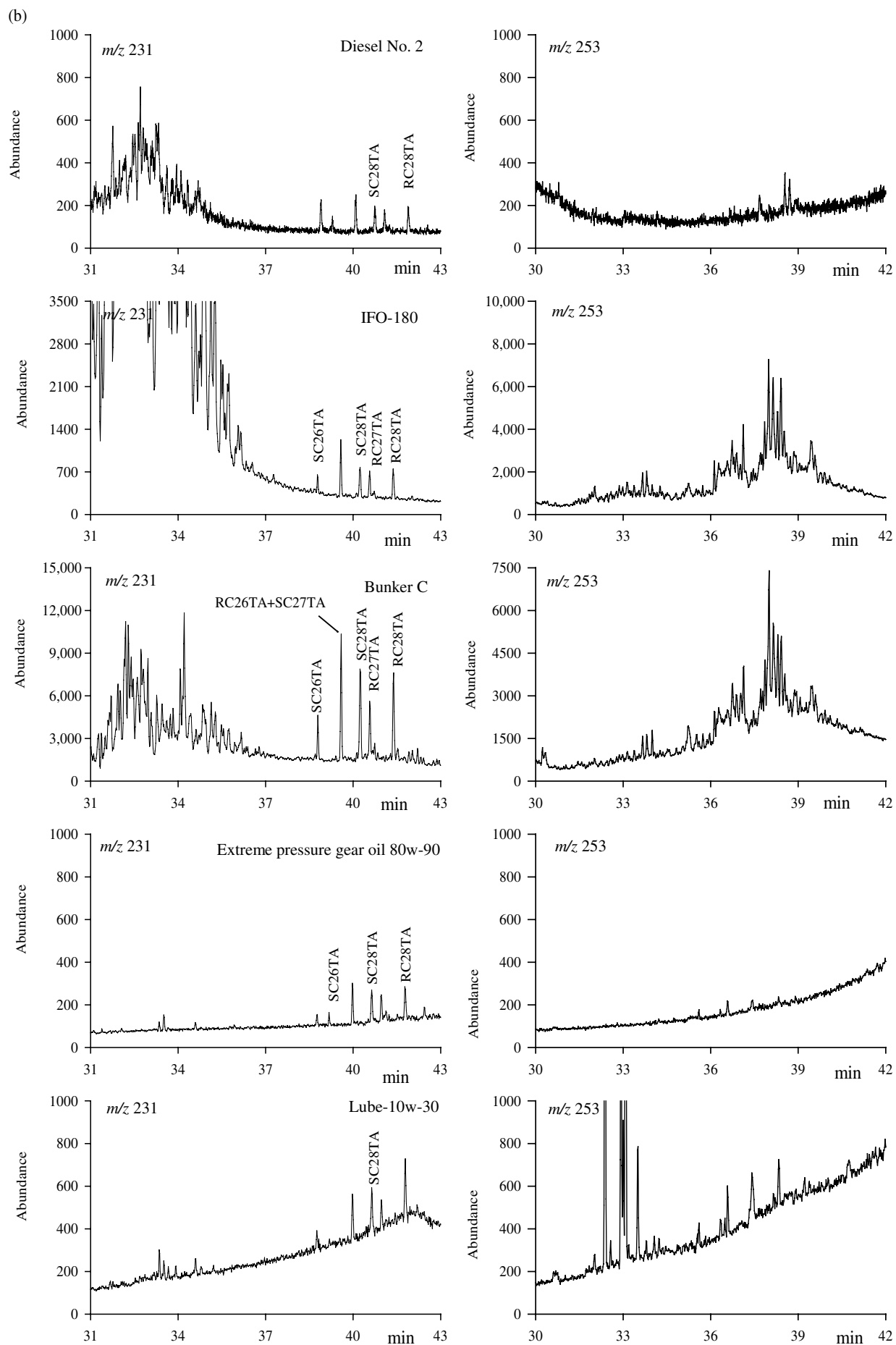


FIGURE 5.12 (Continued) (b) GC/MS chromatograms of triaromatic (m/z 231) and monoaromatic (m/z 253) steranes in refined petroleum products.

Those aromatic steroids having relatively high boiling points are barely found in light and middle distillate fuels such as gasoline and Diesel No. 2. Aromatic steroids occur only in residual oils such as Bunker C at relatively high concentrations. The hydrogenation and hydrocracking in the production of lube oils during the refining process remove most of the aromatic hydrocarbons including those steroids in the base oil. Therefore, lubricating oils generally contain very little of these aromatic steroid compounds (Figure 5.12b).

Barakat et al. [119] used MASs and triaromatic steranes to assess the composition changes during the degradation of the released oil residues in a terrestrial environment. The results of triaromatic distribution are in good agreement with weathering classification based on the analysis of saturated and aromatic hydrocarbons and the ratios of *n*-alkanes, PAHs, and saturated biomarker compounds. Most of parent PAHs and alkylated PAHs are susceptible to microbial degradation; however, aromatic steroids are highly resistant to physical weathering and biodegradation. These features enable them to be suitable candidates for forensic oil analysis, particularly when the oils involved are heavily weathered.

5.4 WEATHERING EFFECT ON OIL CHEMICAL COMPOSITION

Once oil enters into the environment, it is immediately subject to a series of natural processes including evaporation, dissolution, dispersion, oil–sediment aggregation, emulsification, photooxidation, sedimentation, etc. Weathering is termed as the combination of those processes that affect the composition of spilled oil in the environment [3,87,111]. Oil weathering processes have an extensive influence on the behavior, effects, and ultimate fate of an oil spill and have therefore been the topic of much research to inform spill response activities [3]. These processes highly depend on the nature of the oil spilled and the weather conditions during and after the spill (e.g., temperature, wave movement, wind speed, and sun incidence). Numerous studies have been conducted to study the effects of weathering on *n*-alkanes, PAHs and biomarkers [5,64,65,110,120,121], and diamondoids and sesquiterpanes [60–63].

5.4.1 Evaporation Weathering

In the short term after an oil spill, among the potential chemical, physical, and biological weathering processes, evaporation is usually the dominant weathering process [3]. The evaporation effect is particularly significant on the oil remaining on land or water after a spill. The evaporation extent of a specific oil mainly depends on its composition and the weathering conditions [122]. Gasoline evaporates completely in a few hours, while diesel-range oils evaporate more gradually. Since heavy oils generally have been severely weathered in their formation, evaporation has little effect on their chemical composition. Fingas [3] indicated

that, on the land, an ongoing oil evaporation could be considerably slowed down due to the “crust” on the oil surface formed by resin and waxes.

Investigation of evaporation weathering can be simulated in a laboratory under controlled conditions. In order to study the effect of evaporation on oils’ physical and chemical properties, Wang et al. [65,121] used a laboratory oil weathering technique by rotary evaporation to artificially weather oils to varying weathering degrees. This weathering technique allows for the precise control of evaporative weight loss of the oil and can be directly correlated to chemical composition changes of the oil.

Figure 5.13 displays the chromatographic change of selected petroleum hydrocarbons in Troll crude oil and Diesel No. 2 affected by evaporation. Table 5.10 summarizes the chemical composition change of selected hydrocarbon groups in Troll crude oil and Diesel No. 2 at four different evaporative weathering degrees. Evaporation simply transports part of the or all oil mass from its bulk to the surrounding air. It in sequence removes components from an oil basically according to their boiling points, but in fact the molecular interaction of the complex hydrocarbon mixtures could affect their evaporation. In theory, the oil loses lighter compounds with low boiling points first. For lightly evaporated petroleum, most mass loss is attributable to low-boiling-point compounds such as BTEX, alkylated benzene, and alkanes.

The distributions of target hydrocarbons, particularly biomarker terpanes and steranes, high PAH compounds and triaromatic steranes, remain consistent through the evaporation process. In addition, evaporation does not remove significant UCM content, resulting in an increased UCM proportion for evaporated oils.

Clearly, as shown in Table 5.10 and Figure 5.13, evaporative weathering, up to approximately 22% mass loss, has little effect on distribution patterns of most target petroleum hydrocarbons. No apparent depletion was observed; in contrast, most target hydrocarbons were concentrated in proportion to the increase in the weathered percentages. However, if evaporation continues and affects the *n*-alkanes beyond *n*-C₁₃, then a relative depletion of the lower-boiling C₁₄H₂₆ sesquiterpanes would be expected [59]. It was reported that heavier weathering could lead to significant reduction in abundances of light normal alkanes, all adamantanes, and light sesquiterpanes in some oils [123]. In forensic investigation, the concentration reduction of the low-boiling components and the buildup of the high-boiling components relative to the smaller *n*-alkanes could indicate that the oil has been significantly weathered, even though its *n*-alkanes are not completely lost [124].

5.4.2 Biodegradation Weathering

It has been well established that biodegradation can considerably affect the hydrocarbon distributions in petroleum released into the environment. When disasters like Exxon

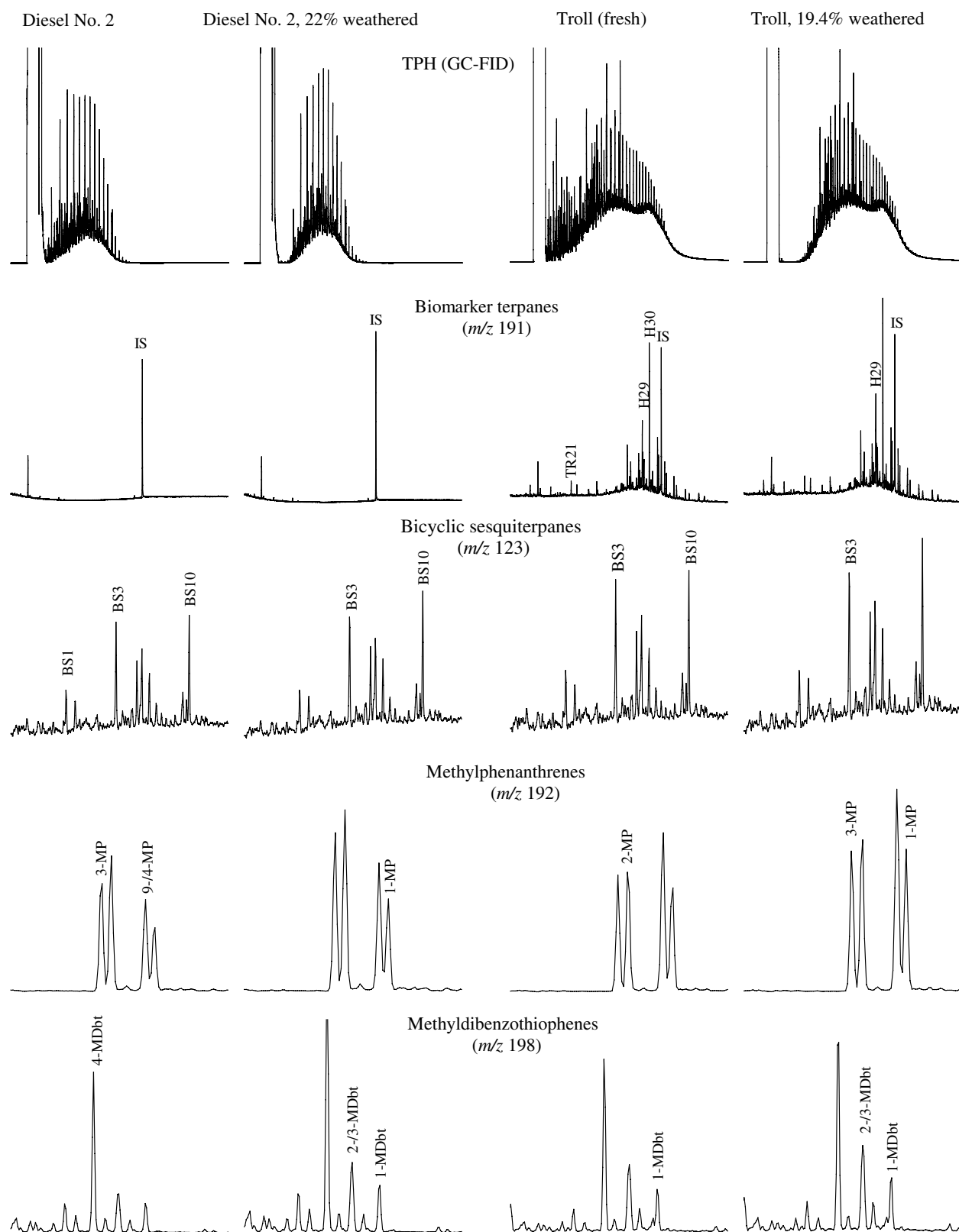


FIGURE 5.13 Effect of evaporation on petroleum hydrocarbons in crude oil and diesel oil.

TABLE 5.10 Effect of evaporation on petroleum hydrocarbons in crude oil and diesel oil

Oil samples	Troll				Diesel No. 2			
	Fresh	6.3	13.1	19.4	Fresh	7.2	14.2	22.0
Weathering (%)								
TPH (mg/g)	723	709	703	699	925	881	900	921
TSH/TPH (%)	71.6	70.9	70.1	68.5	84.2	84.9	80.3	79.0
UCM/TPH (%)	84.6	85.8	86.8	88.5	53.3	54.5	57.4	57.9
<i>n</i> -Alkanes (mg/g)	35.6	37.7	38.3	38.7	150	144	147	145
<i>n</i> -C ₁₀	1.05	1.13	0.73	0.05	13.7	11.5	8.59	3.93
<i>n</i> -C ₁₆	1.57	1.71	1.85	1.98	10.9	11.4	12.1	13.1
<i>n</i> -C ₂₀	1.39	1.48	1.57	1.71	3.20	3.47	3.67	3.93
<i>n</i> -C ₃₀	0.61	0.66	0.72	0.80	0.01	0.01	0.01	0.02
ΣAlkylated PAHs (μg/g)	16,670	16,673	18,127	18,449	25,971	26,454	35,701	39,287
ΣNaphthalenes	12,027	11,861	13,005	12,733	20,860	21,039	29,476	32,482
ΣPhenanthrenes	2,448	2,514	2,678	3,028	2,201	2,347	2,679	2,925
ΣFluorenes	1,388	1,450	1,545	1,680	2,542	2,672	3,094	3,310
ΣDibenzothiophenes	499	515	547	620	363	390	445	563
ΣChrysenes	309	332	352	388	5.76	5.60	6.59	6.06
ΣEPA priority PAHs (μg/g)	434	451	483	499	27.1	27.8	37.4	40.9
Biomarkers (μg/g)	968	1,008	1,080	1,158	9.77	10.5	11.5	12.6
TR23	11.1	11.8	12.4	13.6	3.85	3.47	3.72	4.00
H29	56.6	59.5	64.7	68.2	0.00	0.00	0.00	0.00
H30	126	132	143	150	0.00	0.00	0.00	0.00
C27ββ	172	177	185	199	0.00	0.00	0.00	0.00
C29ββ	179	184	197	213	0.00	0.00	0.00	0.00
Diamondoids (μg/g)	559	565	552	387	1,106	1,228	1,237	1,260
Adamantanes	528	536	515	346	1,042	1,152	1,150	1,162
Diamantanes	31.6	28.6	37.4	41.7	64.3	75.6	87.3	97.8
Sesquiterpanes (μg/g)	5,119	5,461	5,920	6,163	6,028	6,732	7,174	7,768
BS1	415	431	453	473	715	794	872	972
BS3	996	1,059	1,152	1,196	1,005	1,126	1,216	1,327
BS5	707	755	689	735	1,008	1,129	1,149	1,361
BS10	885	935	1,049	1,064	1,034	1,210	1,241	1,417

Valdez oil spill in Alaska and Deepwater Horizon oil spill in the Gulf of Mexico occur, the cleanup of spilled oil and the ecosystem recovery probably relied on a series of natural processes, among them degradation by microorganisms is an important process, despite spilled oil being often recovered or burned on site. Natural biodegradation is generally a long-term weathering process and can be affected by many factors.

Oil biodegradation occurs during the formation of crude oils under geological conditions and when they enter into the environment. It is believed that besides the physical and chemical properties of the oils, many other environmental factors including the nature of the environmental media, the content of nutrient and hazardous contaminants, the characteristics of the microbial population, etc. could affect the rate and extent of oil biodegradation. Many oil spill incidents around the world have offered scientists great opportunities to study oil biodegradation. The biodegradation of petroleum can also be simulated in the laboratory under controllable conditions, while the process in a laboratory environment could be significantly different from a spill site.

Table 5.11 summarizes the concentration of individual or bulk hydrocarbons in ASMB and a Bunker C biodegraded in a laboratory incubator. Figure 5.14 compares the GC/MS chromatograms of petroleum hydrocarbons in ASMB sterile control (left panel) and ASMB oil biodegraded (right panel)

for 4 weeks at 22°C. As seen in Table 5.11, light *n*-alkanes were readily removed under 8 weeks at 4°C enrichment culture and 4 weeks at 22°C culture. Significant degradation was demonstrated for the ASMB oil and Bunker C. The TPH value decreased to 250 and 152 mg/g in 8 weeks at 4°C enrichment culture and 4 weeks at 22°C culture, respectively, from 415 mg/g in ASMB sterile control. Compared with the ASMB crude oil, the TPH in Bunker C is less reduced by biodegradation due to its lesser light components, dropping from 239 mg/g the Bunker C sterile control to 161 and 131 mg/g in 8 weeks at 4°C enrichment culture and 4 weeks at 22°C culture, respectively. As for the specific hydrocarbons, the effect of biodegradation largely depends on the hydrocarbon classes. It is apparent in Figure 5.14 and Table 5.11 that *n*-alkanes including isoprenoids pristane and phytane, C₁-phenanthrenes, and C₁-dibenzothiophenes are considerably removed, whereas UCMs, biomarkers, bicyclic sesquiterpanes, and aromatic steranes remain fairly consistent.

A large number of approaches to oil biodegradation have been reported [63,90,95,117,125–130]. The effects of microbial degradation on the oil composition are different from those of physical weathering processes [87]. Different classes of petroleum hydrocarbons have different susceptibilities to biodegradation. There are many discussions in the literature about the biodegradation order of petroleum hydrocarbons [64,83,127,130]. Overall, this process affects

TABLE 5.11 Effect of biodegradation on petroleum hydrocarbons in Alberta Sweet Mixed Blend (ASMB) crude oil and Bunker C

Oil samples	ASMB			Bunker C		
	Sterile control	Enrichment culture, 8 weeks at 4°C	4 weeks at 22°C	Sterile control	Enrichment culture, 8 weeks at 4°C	4 weeks at 22°C
Weathering						
TPH (mg/g)	415	250	152	239	161	131
TSH/TPH (%)	66.0	70.0	71.7	55.6	67.1	61.6
UCM/TPH (%)	58.8	93.6	88.2	59.1	84.5	82.5
<i>n</i> -Alkanes (mg/g)	46.8	1.08	0.00	8.18	0.65	0.13
<i>n</i> -C ₁₀	0.09	0.00	0.00	0.00	0.00	0.00
<i>n</i> -C ₁₆	3.35	0.00	0.00	0.81	0.04	0.00
<i>n</i> -C ₂₀	2.42	0.05	0.00	0.97	0.06	0.00
<i>n</i> -C ₃₀	0.68	0.05	0.00	0.02	0.01	0.01
ΣAlkylated PAHs (μg/g)	10,588	2482	298	32,327	11,684	3625
ΣNaphthalenes	5,794	443	79.2	15,990	4,763	1370
ΣPhenanthrenes	2,062	1009	74.5	8,263	2,844	1056
ΣFluorenes	1,077	235	34.9	4,882	2,530	658
ΣDibenzothiophenes	1,400	498	34.0	3,094	1,451	446
ΣChrysenes	256	299	75.1	96.6	96.7	94.5
ΣEPA priority PAHs (μg/g)	82.3	34.2	11.2	243	55.6	35.8
Biomarkers (μg/g)	1,213	986	1911	110	140	136
TR23	98.3	79.7	153	40.6	52.0	49.9
H29	106	91.0	193	2.27	2.87	3.16
H30	153	116	256	2.91	3.20	3.60
C27ββ	169	137	166	3.66	4.46	4.72
C29ββ	188	146	309	2.96	3.10	3.74
Diamondoids (μg/g)	13.3	20.4	41.5	86.8	55.6	47.9
Adamantanes	0.64	0.87	0.00	60.5	28.8	16.4
Diamantanes	12.7	19.5	0.00	26.1	26.8	31.5
Sesquiterpanes (μg/g)	5,207	4198	5854	1,380	1,882	1930
BS1	295	203	156	27.7	35.8	38.0
BS3	533	422	519	84.7	113	115
BS5	1,652	1305	1865	365	487	517
BS10	1,122	980	1587	503	724	711

straight-chain *n*-alkanes more than branched alkanes, alkanes more than other hydrocarbon groups, the GC-resolved compounds more than the GC-unresolved complex materials, and small aromatics more than large aromatic compounds. Some researchers tried to rank oil biodegradation based on the depletion of petroleum hydrocarbon classes [83,127,130]. Initial or mild biodegradation readily removes low-molecular-weight *n*-alkanes, which can be easily observed on whole-oil gas chromatograms. Moderate biodegradation is marked by a nearly total loss of *n*-paraffins and the reduction of alkylcyclohexanes, alkylbenzenes, and acyclic isoprenoid alkanes. Biodegradation is evident in the formation of Alberta oil sands bitumen based upon the absence of *n*-alkanes and pristane and phytane in this heavy oil (see GC/FID chromatogram in Fig. 5.5a).

5.4.2.1 Biodegradation of Biomarkers Steranes and triterpanes, which are relatively resistant to biodegradation, have been used extensively for the correlation of biodegraded crudes [125]. Although terpanes and steranes are highly resistant to

biodegradation, several studies have shown that they can be degraded to a certain degree under severe weathering conditions (i.e., extensive microbial degradation) [127,131]. Studies on the Arrow oil spill [124] and the Baffin Island Oil Spill (BIOS) experiment [111] have demonstrated degradation of C₂₃ and C₂₄ tricyclic terpanes. Microbial alteration and removal of the regular steranes and 4α-methylsteranes from petroleum occur after the complete removal of C₁₅–C₂₀ isoprenoids and before or after the hopanes depending on the circumstance.

One of the significant differences between biodegradation and evaporation is that the former selectively reduces an individual compound or a group of petroleum compounds. As is known, terpanes and steranes have many constitutional isomers and stereoisomers. Certain molecular configurations could obstruct microbial degradation. Wang et al. [124] found that 17α(H),21β(H)-22,29,30-trisnorhopane (Tm) is degraded faster relative to 18α(H),21β(H)-22,29,30-trisnorhopane (Ts) even though Ts chromatographically elutes out earlier than Tm, resulting in an increase of the Ts/Tm ratio for heavily degraded oil samples. In general,

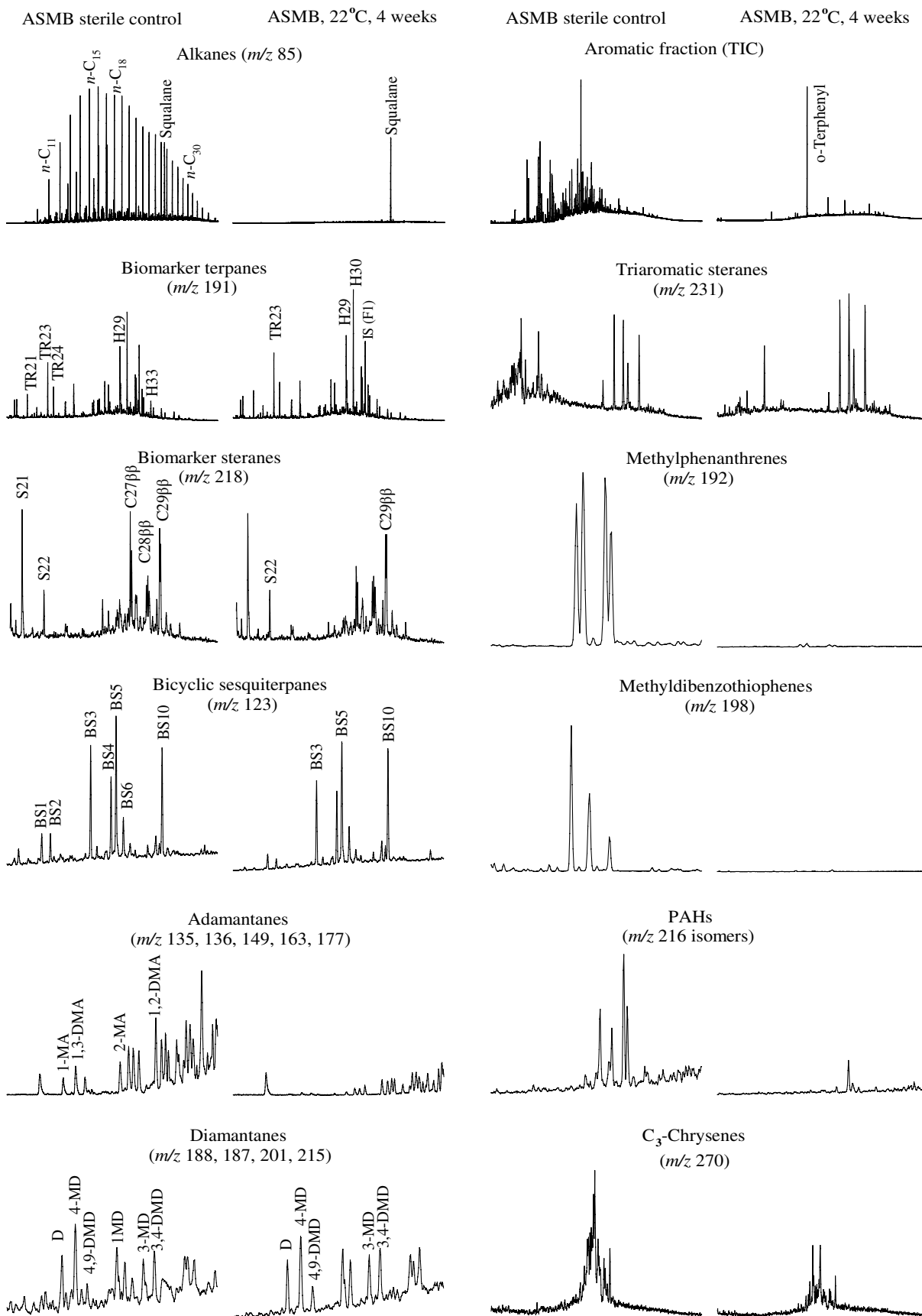


FIGURE 5.14 Effect of biodegradation on selected petroleum hydrocarbons in ASMB crude oil.

sterane susceptibility to microbial degradation is as follows: $\alpha\alpha\alpha\ 20R > \alpha\beta\beta\ 20R > \alpha\beta\beta\ 20S > \alpha\alpha\alpha\ 20S > \text{diasteranes}$. The susceptibility of steranes to biodegradation typically decreases with increasing carbon number for each isomeric configuration $C_{27} > C_{28} > C_{29} > C_{30}$. Diasteranes (C_{26} – C_{30}), a family of rearranged steranes, are most likely formed during diagenesis and catagenesis of biological precursors. Diasteranes are particularly resistant to biodegradation. Evidence suggests that the C_{27} – C_{29} steranes are destroyed completely before diasterane alteration. Pregnane and homopregnane have high resistance to biodegradation, comparable to diasteranes [83].

Bicyclic sesquiterpanes are resistant to slight to medium weathering, particularly from biodegradation [6,60,83]. A series of bicyclic terpenoids were determined in Athabasca oil sands bitumen despite the depletion of *n*-alkanes by biodegradation [103,104,132]. Similar results can be observed in the *m/z* 123 chromatograms of biodegraded ASMB oil in Figure 5.14. Bicyclic sesquiterpanes can be partially biodegraded in laboratory-controlled processes or during formation of heavy oils. Yang et al. [104] found that $\delta\beta(H)$ -homodrimane is likely the most abundant homologue in oil sands bitumen and other crude oils, which suggests that this bicyclic sesquiterpane has the least degradability among the ten common bicyclic sesquiterpanes.

Yang et al. [104] found cage-like diamondoids in significant abundance in Alberta oil sands bitumen. Williams et al. [95] found that a series of diamondoid compounds demonstrated resistance to biodegradation in a severely degraded crude oil, in which pentacyclic triterpanes were almost completely demethylated. The degradation resistance of adamantanes is at least as strong as that of tricyclic terpanes, and the adamantane series should therefore be useful for correlating severely biodegraded oils. Grice et al. [90] investigated the effect of biodegradation on diamondoid distribution in a series of crude oil reservoirs in two Australian sedimentary basins. They reported variable susceptibility to microbial degradation for different diamondoids. Wei et al. [129] reported that the concentration of total diamondoids tends to decrease as the biodegradation rank of oil deposits increases. Figure 5.14 compares the total ion chromatograms of adamantanes and diamantanes in biodegraded ASMB and its sterile control. It is obvious that adamantanes are more susceptible to biodegradation than diamantane analogs.

5.4.2.2 Biodegradation of Aromatics Aromatic hydrocarbons comprise a large percentage of crude oil and refined oil products. Many studies have been conducted to investigate their biodegradation. George et al. [126] studied the biodegradation of a suite of oils. The breakdown of aromatic compounds by ring cleavage is an essential biochemical step in natural carbon cycle and is performed by several kinds of microorganisms. There are three main controls on the susceptibility to biodegradation of cyclic, branched, and aromatic low-molecular-weight hydrocarbons: carbon skeleton, degree of alkylation, and position of alkylation. The biodegradation

of alkylated PAHs varies with the number of aromatic rings of these compounds. The rate of degradation of PAHs decreases with the increase of the number of rings in the PAH molecule. In addition, within each class of APAH, the degradation rate follows a general trend of $C_1 \gtrsim C_2 > C_3 > C_n$, where *n* represents the total number of carbon atoms in the alkyl substituents [117,125]. Among the five target alkylated PAH homologues, the 2-ring alkylated naphthalene homologues were the most susceptible to biodegradation, while the alkyl homologues of 4-ring chrysene were the most resistant to biodegradation.

The positions of the alkyl substituents can strongly affect the rate of biodegradation. The biodegradation of methylphenanthrenes (*m/z* 192) is in the decreasing order of 3-MP or 2-MP > 1-MP \gg 9-/4-MP [104,117]. 2-/3-methyl dibenzothiophene (*m/z* 198) biodegrades at the fastest rate within its isomeric series. In heavy oil sands bitumen, the most refractory isomers in the *m/z* 216 cluster appear to be 4-methyl-pyrene (4-MPy) and 1-methyl-pyrene (1-MPy), while other isomers were degraded in different degrees. The C_{26-28} isomers of triaromatic steranes (TASs) are very resistant to biodegradation and only degraded under extreme conditions [127]. These steroids changed slightly in their abundance and distribution pattern in the *m/z* 231 fragmentogram, even though most of the aromatics including methylphenanthrenes and methyl-dibenzothiophenes were nearly depleted (Fig. 5.14). Preferential depletion of C_{20} – C_{22} triaromatic sterane isomers is found for the severely biodegraded oils.

In general, the biodegradation effects on the oil composition can be summarized in the following patterns [117,133]: (i) smaller hydrocarbons are degraded faster than larger hydrocarbons; (ii) straight-chain *n*-alkanes degrade faster than branched alkanes; (iii) GC-resolved compounds are degraded more than GC-unresolved complex hydrocarbons; (iv) small aromatics are degraded faster than high-molecular-weight aromatics; (v) increase in alkylation level within their alkylated homologous families significantly decreases susceptibility to microbial attack; and (vi) microbial degradation is often isomer specific. Degradation of specific petroleum hydrocarbons generally follows an overall declining order of *n*-alkanes > benzene > toluene > isoalkanes and anteisoalkanes > cyclohexyl alkanes and/or methylcyclopentyl alkanes > acyclic isoprenoids \gg naphthalene > phenanthrene \gg PAHs > C_{27-29} steranes > C_{30-35} hopanes > diasteranes > C_{27-29} hopanes > C_{21-22} steranes > tricyclic terpanes [64,83,125,127]. However, this sequence does not imply complete removal of one class before another is degraded and does not necessarily always apply to all oil biodegradation.

5.4.3 Photodegradation Weathering

Besides long-term biodegradation, oil spilled on the surface of water or land is also subjected to other natural destructive weatherings such as photooxidation [134,135]. Photolysis is generally not considered as an important process for the degradation of oils in soils or deepwater sediments. It is

established that solar irradiation is an important effect for the alteration or removal of petroleum from water and land, especially in tropical and subtropical latitudes under conditions of intensive solar radiation and in oligotrophic waters when nutrients needed for biodegradation may be limited [136–140]. Photooxidation is dependent on the thickness of the oil slick as well as sun exposure. Sunlight (particularly <300 nm spectrum) oxidizes photochemically the aliphatic and aromatic fractions of petroleum into more polar ketones, aldehydes, carboxylic acids, esters, etc. [134]. Moreover, photochemical processes are probably also important to the subsequent biological consumption of oil [136].

Oil photodegradation was not thoroughly studied and therefore less understood by environmental scientists in comparison with oil evaporation and biodegradation. The studies on photodegradation of petroleum mainly focused on polycyclic compounds in petroleum due to their high concentrations and potential high environmental impact. Nicodem et al. [137] reported the photochemical weathering of a crude as a film over seawater by sunlight. The fluorescence emission intensity of the crude decreases rapidly and is only two-fifths of its initial intensity after 100 h of irradiation. It is believed that the reduction of fluorescence intensity is due to the formation of oxygenated derivatives, which are less fluorescent. Ali et al. [139] used a laboratory photodegradation apparatus, incorporating a calibrated xenon lamp, controlled temperature unit, and quartz reaction cells to simulate natural irradiation by sunlight. They reported a pseudo-first-order photodegradation constant (k) of phenanthrene in seawater at 25°C. Andersson [138] reported lower losses of sulfur heterocycles than phenanthrene series when oil was exposed to sunlight irradiation. Their photodegradation follows a declining order of phenanthrene > 1-methylphenanthrene = DBT > 2-methylphenanthrene > 4-methyl-DBT > 1-methyl-DBT > 2- + 3-methyl-DBT > 3,4-dimethyl-DBT > 1,7-dimethyl-DBT > 3,7-dimethyl-DBT. Jacquot et al. [134] studied the photooxidation of petroleum spilled in the marine environment and found that naphthalene and its alkylated homologues were severely altered by photooxidation, whereas phenanthrenes, dibenzothiophenes, and their alkylated homologues were rather recalcitrant. Furthermore, methyl derivatives were more degraded than their parent molecules and the degradation of methylated phenanthrenes (MP) follows a decreasing order of 2-MP < 1-MP < 3-MP < 9-MP.

A preferential alternation of branched alkanes rather than straight alkanes has been reported [134]. The distribution of biomarkers such as drimanes, hopanes, and steranes remains stable in photodegradation. Therefore, the diagnostic ratios of these biomarker compounds are still applied to oil identification when oil is exposed to photodegradation.

5.4.4 Assessment of Mass Loss during Weathering

Quantitative information on the weathering of spilled oil is essential to better understand their environmental fate and behavior. It is also important to examine the quantity of oils

still residing in spilled site for the evaluation of the environmental damage and the recovery of impacted area. Different classes of petroleum compounds are often affected to various extents by natural weathering, making quantitative assessment even more difficult. Environmental scientists attempted to find a conserved internal marker within the oil to act as a standard for a quantitative means of monitoring degradation of spilled oil [60,63,110].

5.4.4.1 Assessment of Mass Loss during Weathering Using Biomarkers The triterpane hopane has been identified as one of the most resistant petroleum hydrocarbons. As biodegradation proceeds, the hopane concentration in the remaining oil increases due to the removal of other components. These weathering-resistant biomarker terpanes such as C_{29} 17 α (H),21 β (H)-norhopane and C_{30} 17 α (H),21 β (H)-hopane have been widely used as an internal reference to estimate the depletion of crude oils in oil-contaminated samples [131]. The concentration of hopane in the weathered oil (H_1), measured on an oil weight basis, relative to its concentration in the initial source oil (H_0) is a function of the amount of oil degraded [110]:

$$\text{Oil depletion (\%)} = \left(1 - \frac{H_0}{H_1}\right) \times 100 \quad (5.4)$$

Individual analyte depletion, corrected for oil loss, is then determined by

$$\text{Analyte depletion (\%)} = \left[1 - \left(\frac{C_1}{C_0}\right) \times \left(\frac{H_0}{H_1}\right)\right] \times 100 \quad (5.5)$$

where C_1 is the analyte concentration in the degraded oil and C_0 is the analyte concentration in the source oil. H_0 is the concentration of hopane in the initial source oil, and H_1 is the concentration of hopane in the weathering oil sample. This equation provides a direct way to estimate the weathering degree of oil-contaminated environmental samples. Because hopane does degrade very slowly under some environmental conditions, the calculations of total oil and individual analyte depletion are conservative and provide a minimum estimate of oil disappearance.

5.4.4.2 Assessment of Mass Loss during Weathering Using Bicyclic Sesquiterpanes Because lighter petroleum products generally contain none or only traces of the high-molecular-weight hopanes, Equations 5.4 and 5.5 are of little use to spilled light fuels. The facts of uniqueness, abundance in petroleum, and chemical stability of bicyclic sesquiterpanes enable them to be useful as marker compounds for oil spill studies, particularly in cases where the tri- to pentacyclic biomarkers are absent. Wang et al. [60] proposed a method using highly abundant C_{15} and C_{16} sesquiterpanes as

internal reference compounds to estimate the depletion degree of lighter diesel-type fuels as the following:

$$P(\%) = \left(1 - \frac{C_s}{C_w}\right) \times 100 \quad (5.6)$$

where $P(\%)$ is the weathered percentage of the weathered oil and C_s and C_w are the concentrations of selected C_{15} or C_{16} sesquiterpanes with high abundance in the source and weathered petroleum samples, respectively.

Yang et al. [63] used dominant sesquiterpanes as the references to access the mass loss of a diesel and three crude oils at varying evaporation degrees. The calculated mass loss of total oil was in good agreement with the real weathering percentages of oil samples studied. For example, corresponding to 6.3, 13.1, and 19.7% evaporated Prudhoe Bay crude oil, the calculated mass losses are 9.3, 14.7, and 17.8% using $8\beta(H)$ -drimane and 8.7, 14.7, and 21.5% using $8\beta(H)$ -homodrimane, respectively. The results are consistent with those obtained using C_{30} $\alpha\beta$ -hopane as the reference (Eq. 5.4), by which the mass depletions were determined to be 10.0, 14.0, and 17.8% at three weathered levels. It appears that the method particularly applies to moderately weathered oils. Further studies are needed to investigate how this method is applicable to biodegraded oil samples.

5.5 DIAGNOSTIC RATIOS OF TARGET HYDROCARBONS

Forensic oil–oil correlations are based on the concept that the target components investigated in spill oils do not significantly differ from those in the candidate source oils. Some of the petroleum compounds in spill samples and source oils, in particular those homologous isomers of biomarkers with similar structure, show little or no changes in their relative abundance. The abundance ratios between these target analytes serve as important criteria for many aspects of oil studies. Diagnostic ratios have been widely applied by geochemists for oil–source rock correlation and oil–oil correlation, determination of organic input and depositional environment, assessment of thermal maturity, and evaluation of oil biodegradation. Environmental chemists frequently use them for the identification, correlation, differentiation of spilled oil, and investigation of its spill history. An important benefit of comparing diagnostic ratios of spilled oil and suspected source oils is that concentration effects are minimized. In addition, the use of ratios tends to induce a self-normalizing effect on the data since variations due to the fluctuation of day-to-day instrument operating conditions, operator, and matrix effects are minimized. Therefore, comparison of diagnostic ratios reflects more directly differences in the target biomarker distribution between samples [87].

5.5.1 Molecular Diagnostic Ratios for Oil Identification

Numerous diagnostic ratios from petroleum compounds have been proposed as molecular markers to identify the source of oil spills [5,87,141]. The diagnostic ratios in Table 5.12 are derived from the target petroleum compounds of alkanes, terpanes, steranes, sesquiterpanes, diamondoids, and PAHs. Ratios are expressed as A/B for simplicity but can be readily redefined using the equation of $A/(A+B)$. It is

TABLE 5.12 Diagnostic ratios of petroleum hydrocarbons frequently used for environmental forensic studies

Isoprenoid ratios	Adamantane ratios
$n-C_{17}/\text{Pri}$	1-MA/(1-MA + 2-MA) (MAI)
$n-C_{18}/\text{Phy}$	1-MA/2-EA
Pri/Phy	1-MA/(1-MA + 2-MA + 2-EA)
$n-C_{17}/n-C_{31}$	1-MA/1,3-DMA
$\Sigma\text{Odd } n\text{-alkanes}/\Sigma\text{Even } n\text{-alkanes}$ (CPI)	1-MA/1,2-DMA
$(n-C_{27} + n-C_{29} + n-C_{31} + n-C_{33})/$ $(n-C_{28} + n-C_{30} + n-C_{32} + n-C_{34})$	1-MA/1,3,5-TMA
Biomarker terpane ratios	Diamantane ratios
TR21/TR22	1-MA/1,3,4-TMA
TR21/TR23	1-MA/1,2,5,7-TeMA
TR23/TR24	1,3-DMA/1,4-DMA
TR21/H30	1,3-DMA/1,2,5,7-TeMA
TR24/H30	1,4-DMA/1,2,5,7-TeMA
NOR25H/H30	Diamantane ratios
H28/H30	4-MD/(1-MD + 3-MD + 4-MD)
H29/H30	4-MD/3,4-DMD
(TR23 + TR24)/(H29 + H30)	4,9-DMD/1,4,9-TMD
OL/H30	PAH ratios
M30/H30	Ph/An
G/H30	Fl/Py
H31S/H31R	BaA/CHR
H32S/H32R	Pe/ $\Sigma 5$ -ring PAHs
H33S/H33R	IP/(IP + BgP)
Ts/Tm	2-MN/1-MN
Ts/H30	(3- + 2-)mP/(9/4- + 1-)mP
H31S/H30	(2/3DBT)/4DBT
$\Sigma(H31 \text{ to } H35)/H30$	$\Sigma 15$ EPA priority PAHs/ $\Sigma 5$ series
Biomarker sterane ratios	APAHs (PI)
S21/S22	C1P/C0P
$C27\beta\beta/C29\beta\beta$	1-DBT/4-DBT
$C28\beta\beta/C29\beta\beta$	C2D/C2P
$C27\beta\beta/(C27\beta\beta + C28\beta\beta + C29\beta\beta)$	C3D/C3C
$C28\beta\beta/(C27\beta\beta + C28\beta\beta + C29\beta\beta)$	C3D/C3P
$C29\beta\beta/(C27\beta\beta + C28\beta\beta + C29\beta\beta)$	C1P/C2P
$C27\alpha\alpha/C27\beta\beta$	C1C/C2C
$C28\alpha\alpha/C28\beta\beta$	C2C/C3C
$C29\alpha\alpha/C29\beta\beta$	$\Sigma N:\Sigma P:\Sigma DBT:\Sigma F:\Sigma C$
$C27(20S)/C27(20R)$	Triaromatic sterane ratios
$C28(20S)/C28(20R)$	C20TA/C21TA
$C29(20S)/C29(20R)$	RC27TA/SC28TA
$C30/(C27-C30)$ steranes	SC28TA/(SC26TA + SC28TA)
Sesquiterpane ratios	RC28TA/SC28TA
BS1/BS2	RC27TA/RC28TA
BS3/BS5	SC28TA/(RC26TA + SC27TA)
BS4/BS5	Ion 216 ratios
BS1/BS5	BaF/4-MPy
BS3/BS10	1-MPy/4-MPy
BS5/BS10	Retene ratios
	t-m-Phen/retene
	Retene/C4P

important to realize that the suite of diagnostic ratios as listed here is neither inclusive nor appropriate for all oil spill identification cases. These ratios should be used in combination to avoid erroneous conclusions. However, it is impossible and unnecessary to include ratios from all target analytes. It is essential to select source-specific representative and weathering-resistant diagnostic ratios for a forensic oil analysis. Herein, we only select some diagnostic ratios frequently used for detailed discussion.

5.5.1.1 *n*-Alkane and Isoprenoid Ratios These ratios are generally based on results from GC/FID analysis or selected ion of GC/MS analysis if these compounds are in very low concentrations in weathered environmental samples. The diagnostic ratios often used from *n*-alkane analysis include $n\text{-C}_{17}$ /pristane, $n\text{-C}_{18}$ /phytane, and pristane/phytane and carbon preference index (CPI).

As mentioned previously, $n\text{-C}_{17}$ -pristane and $n\text{-C}_{18}$ -phytane are eluted closely into two pairs of characteristic peaks in chromatographic analysis. These *n*-alkane and isoprenoid indices are source specific. In addition, the ratios of $n\text{-C}_{17}$ /pristane and $n\text{-C}_{18}$ /phytane remain constant in evaporation, but their values decrease remarkably in biodegraded oil. The ratio of pristane/phytane is relatively stable when oil is subject to certain degree of evaporation and biodegradation:

$$\text{CPI} = \frac{(C_{27} + C_{29} + C_{31} + C_{33})}{(C_{26} + C_{28} + C_{30} + C_{32})} \quad (5.7)$$

CPI is the ratio of odd- versus even-carbon-numbered *n*-alkanes (Eq. 5.7). The ratio of $n\text{-C}_{17}/n\text{-C}_{31}$ is a simplified parameter indicating relative contributions from aquatic/marine and terrestrial sources. This ratio is used to estimate the thermal maturity of crude oil and to identify the source of hydrocarbons in an environmental sample. High-maturity petroleum generally has equally abundant total even and odd number of *n*-alkanes and has a CPI of 1.0. CPI values significantly above (odd preference) or below (even preference) 1.0 indicate low thermal maturity. A CPI value below 1.0 for low-maturity oils or bitumens suggests a typical carbonate or hypersaline environment [83].

CPI is a key diagnostic parameter to determine the relative importance of biogenic and anthropogenic alkane sources to the ambient environment [142]. For the practice of environmental oil analysis, *n*-alkanes are examined within their full span (generally from $n\text{-C}_8$ up to $n\text{-C}_{44}$). CPI obtained from Equation 5.7 is particularly useful in an environmental approach involving biogenic contribution. C_{23-33} normal alkanes, and especially those from $n\text{-C}_{27}$ to $n\text{-C}_{33}$, originate from waxes typical of terrestrial higher plants, whereas anthropogenic sources, including fossil fuel combustion, show no enrichment of the odd carbon alkanes [143]. A strong odd-to-even predominance with a CPI value $\gg 1$ discloses predominant biogenic contribution from terrestrially

derived components in an environmental sample (e.g., soil and sediment). When petroleum is the main contaminant, CPI can be simply calculated from the sum of odd-carbon-numbered *n*-alkanes divided by the sum of even-carbon-numbered *n*-alkanes. A CPI value of near 1.0 suggests a mainly petrogenic source of hydrocarbons.

5.5.1.2 *Biomarker Ratios* Biomarker diagnostic parameters have been long established and are widely used by geochemists for oil correlation (oil–source rock correlation and oil–oil correlation); determination of organic input, precursors, and depositional environment; assessment of thermal maturity; and evaluation of oil in-reservoir biodegradation. Many diagnostic biomarker ratios currently used in oil spill studies and environmental forensics originate from geochemistry.

Table 5.12 lists some of the primary diagnostic ratios of traditional biomarker terpanes and steranes including TR21/TR22, TR23/TR24, H29/H30, Ts/Tm, H31S/H31, H32S/H32R, C27 $\beta\beta$ /C29 $\beta\beta$, C28 $\beta\beta$ /C29 $\beta\beta$, etc. These ratios are regarded as source ratios for oil identification, among which the ratios TR21/TR22, H29/H30, Ts/Tm, and C27 $\beta\beta$ /C29 $\beta\beta$ are the most commonly used as source tracers [124]. The ratios between lighter C_{21-24} tricyclic terpanes and C_{30} 17 α (H),21 β (H)-hopane can provide a useful tool to distinguish refined oil type and to investigate weathering level. Ratios of certain unique biomarker compounds (i.e., C_{30} 17 α (H)-diahopane, C_{30} 18 α (H)-hopane, gammacerane, 4-methylsteranes, etc.) relative to C_{30} 17 α (H),21 β (H)-hopane can furthermore provide exceptional diagnostic information in oil analysis.

Cross-plots (i.e., plot of one diagnostic biomarker ratio vs. another ratio) are frequently used in oil geochemistry for oil–oil correlation and determination of oil source and depositional environment [124,144]. C_{29} 17 α (H),21 β (H)-norhopane and C_{31-35} homohopanes, especially C_{35} homohopanes, are depleted in Southeast Asian crude oils, whereas these compounds are abundant in Middle East crude oils. Based on these chemical evidences, Zakaria et al. [144] used the cross-plots of H29/H30 ratio versus the homohopane index $\Sigma(\text{H31} \sim \text{H35})/\text{H30}$ as key biomarker indicators and successfully distinguished large number of tar ball samples that originated from Southeast Asian crude oil sources from those of Middle East sources.

Furthermore, the ratios of biomarkers with other classes of hydrocarbons can be proposed as weathering ratios. The ratios of full-range targeted compounds versus C_{30} 17 α (H),21 β (H)-hopane are plotted against boiling points, providing a criterion where a spilled oil is weathered compared with source oil [145].

5.5.1.3 *PAH Ratios* PAHs in oils have been thoroughly investigated and their indices are widely used for forensic oil analysis. Certain diagnostic ratios have been widely used in identifying sources of PAHs. To reduce the influence of weathering processes, diagnostic ratios are traditionally

restricted to parent PAHs with the same molecular weight and similar properties or to ratios of alkylated versus parent PAHs [146,147].

Excluding perylene and dibenz(*a,h*)anthracene, nine 4- to 6-ring higher-molecular-weight PAHs (refer to Table 5.2) were classified as combustion PAHs [148,149]. The ratios derived from less stable versus thermodynamically stable PAH isomers, such as fluoranthene to pyrene (Fl/Py), phenanthrene to anthracene (Ph/An), and methylphenanthrenes to phenanthrene (C1P/C0P), are often used to investigate petrogenic contamination against pyrogenic input in environmental samples [4,114,146,150–152]. In contrast to pyrogenic sources, petrogenic sources are characterized by high ratios of Ph/An > 15 and C1P/C0P > 2 in association with lower ratios of fluoranthene/pyrene (Fl/Py < 1) and benzo(*a*)anthracene/chrysene (BaA/CHR < 0.4) [153]. Yunker et al. [146,149] reported that the ratio of IP/(IP + BgP) < 0.20 likely implies petroleum, between 0.20 and 0.50 implies liquid fossil fuel (vehicle and crude oil) combustion, and over 0.50 implies grass, wood, and coal combustion.

Perylene comes primarily from diagenesis of biogenic precursors but partially from petroleum or pyrolytic processes [4,108]. The ratio of perylene to total 5-ring PAHs is found to be effective in differentiating and characterizing biogenic sources from others in environmental samples.

Ratios derived from alkylated PAHs are of special use for forensic oil identification. Methylated PAHs are present in crude oils and refined products in high concentrations. These C1-PAHs are well separated in chromatographic analysis due to their small number of isomers. The ratios among their isomers are often employed for oil analysis, including 2-naphthalene and 1-naphthalene at *m/z* 142; 4-, 2-/3-, and 1-methyl dibenzothiophene at *m/z* 198; and (3- + 2-methylphenanthrene) to (4-/9- + 1-methylphenanthrene) at *m/z* 192. Relative abundance of five alkylated PAHs, $\Sigma N:\Sigma P:\Sigma D:\Sigma F:\Sigma C$, is an important ratio to distinguish oil from oil and type from type. The relative distribution profile $C_0^- : C_1^- : C_2^- : C_3^- : C_4^-$ of each alkylated PAH family is often used to differentiate petrogenic source from other sources and to investigate weathering effect. Wang et al. [4] proposed the “pyrogenic index,” which is defined as the sum of 15 unsubstituted PAHs over the sum of the 5 alkylated PAH homologues ($\Sigma 15$ EPA priority PAHs/ $\Sigma 5$ series APAHs). This ratio is a robust quantitative indicator for the identification of pyrogenic PAHs and for differentiating pyrogenic and petrogenic PAHs. Lighter petroleum products and most crude oils show ratios smaller than 0.01, while heavy oils and heavy fuels show significantly higher ratios in the range of 0.01–0.05. The ratios for the oil–burn soot can be as high as 2.0 [4].

5.5.1.4 Other Ratios Other diagnostic ratios are used less frequently but can be particularly important in some specific oil studies. For example, diamondoid and bicyclic sesquiterpane ratios are of special importance for the analysis of light petroleum. Like traditional biomarker ratios,

these ratios originated from geochemical investigation. Diamondoid hydrocarbon ratios, such as methyladamantane index and methylidamantane index, were developed to evaluate the maturation and evolution of crude oils and to determine the thermal maturity of thermogenic gas and condensate [91,94,154]. The ratio of methyladamantanes to adamantanes rises with increasing biodegradation. The ratio changes significantly at extreme levels, showing that diamondoids can be indicators of petroleum biodegradation especially when most other hydrocarbons have been removed. Wang et al. [5] studied more than 60 possible diagnostic ratios and found that many diamondoids ratios, such as 1-MA/2-EA; 1-MA/1,2-DMA; 1-MA/1,3,4-TMA; 1-MA/1,2,5,7-TeMA; etc., are likely more sensitive and reliable parameters for correlation and differentiation of oils and petroleum products. Diamantane isomers generally occur in crude oils only in relatively low abundance. High measurement uncertainty could be evident in oil analysis; therefore, diagnostic ratios associated with diamantanes should be used cautiously as criteria [62,123].

Diagnostic ratios of selected paired sesquiterpanes were developed and calculated from a large number of oils and petroleum products [58,60,63]. Diagnostic ratios vary greatly between oils from different regions. Obviously, most of these diagnostic ratios are robust for correlation and differentiation of lightly to moderately weathered oil samples. However, for heavily weathered samples, the early-eluted lower-molecular-weight C_{14} sesquiterpanes (BS1 and BS2) could be preferentially depleted to certain degrees, resulting in some changes in their corresponding diagnostic ratios such as BS1/BS5. This implies that the sesquiterpane ratios, in combination with other fingerprinting data, may be used to discriminate different oils and to identify the sources of spill samples.

5.5.2 Selection of Diagnostic Ratios

Diagnostic ratios are calculated based on the concentration of target compounds to eliminate variation due to instrumental variation or on the semiquantitative data (peak area or height) of selected ions if concentrations were not available. All responses of target analytes must be obtained from reliable instrumental analysis and by careful manual integration. Ratios should be ruled out if the related target compounds are not detected or unable to be accurately quantitatively determined. Good practice requires all analyzed peaks to have a signal-to-noise (S/N) greater than 10 in all oil samples. If the relative standard deviation (RSD) of a ratio from triplicate analysis exceeds 10% (the normal 95% level of uncertainty of GC analysis), it should be ruled out for further analysis [123].

In principle, a large number of molecular ratios can be produced on the basis of quantitative analysis of target analytes. However, some ratios are more significantly affected by measurement errors and oil weathering. Thus, a proper selection of diagnostic ratios is important in order to

minimize uncertainties and yield the reliable indices. The diagnostic power (DP) provides a means for the selection of source-sensitive diagnostic ratios [123,155]. DP is defined as the relative standard deviation (RSD_V) of a diagnostic ratio from oils of different origins divided by the relative standard deviation (RSD_A) of the same ratio calculated from reliable replicate measurements. Yang et al. [123] used the Prudhoe Bay crude oil (13.1% weathered) as a reference oil to investigate the source-specific diagnostic ratios in various crude oils collected from various oil sources. Three isoprenoid ratios of $n\text{-C}_{17}/\text{pri}$, $n\text{-C}_{18}/\text{phy}$, and pri/phy are all source specific with high DP values. The most source-sensitive biomarker ratios are $\text{C27}\beta\beta/\text{C29}\beta\beta$, $\text{TR21}/\text{TR22}$, $\text{TR23}/\text{TR30}$, and $(\text{TR23} + \text{TR24})/(\text{H29} + \text{H30})$ with DP values above 10.0. The sesquiterpane ratios of $\text{BS3}/\text{BS5}$, $\text{BS1}/\text{BS2}$, $\text{BS1}/\text{BS5}$, and $\text{BS3}/\text{BS10}$ all have high DP. As to the diamondoid ratios, 1,3-DMA/1,2-DMA; 4,9-DMD/1,4,9-TMD; 1,4-DMA/1,3,4-TMA; 1-MA/2-EA; and 2-EA/1,2-DMA are suggested as the most source specific.

A high DP indicates the high variability of a ratio among the oil samples and then demonstrates the high potential to differentiate or correlate oil samples and oil source(s) in environmental forensic investigations. In principle, the less source-specific ratios with low DP values are inappropriate for oil fingerprinting analysis, although they are probably meaningful in oil weathering studies. Otherwise, the high analytical uncertainties of these low-power indices may lead to erroneous conclusions for spill source identification. The DP values were often obtained from a limited number of oil samples; therefore, it would not be surprising to obtain a different set of DP values for a particular ratio with another set of source oils [123]. It is impossible, however, to measure a “universal” DP value for a diagnostic ratio, and this concept aims to provide guidance for diagnostic ratio selection for oil identification even with a limited set of source oils.

To correctly apply diagnostic ratios in forensic oil studies, there are, therefore, a few critical questions that need to be addressed:

- (i) It is wise to employ backbone source-specific diagnostic ratios in oil spills. In some spill cases, it may be prudent to include some particularly characteristic ratios. In certain situations, the abundances of some analytes may be too low to obtain reliable diagnostic ratios.
- (ii) Other than the usual biomarker terpanes and steranes, triaromatic steranes were found to be highly resistant to evaporation and biodegradation. The relevant diagnostic ratios are robust for oil-to-oil correlation and oil source tracking.
- (iii) In most cases, no matching of biomarker distribution is a strong evidence for the lack of correlation between spill sample(s) and suspected source(s). Matching may be an indication of correlation of a spill sample to a suspected source

but is not necessarily a “proof” that samples are from the same source.

- (iv) Finally, it is extremely important to maintain flexibility when selecting diagnostic ratios for specific cases. Some non-backbone ratios may be helpful for oil identification in specific cases, but were picked using a widely varying set of source oils. The judgment of the analysts remains the most valuable tool in each specific forensic investigation.

5.6 FORENSIC OIL SPILL IDENTIFICATION: A CASE STUDY

Tiered analytical approaches [4,89,141,155] have been increasingly applied for oil spill identification and hydrocarbon forensic analysis in recent years. An integrated methodology for forensic oil spill identification consists of GC/MS analysis, chromatographic data processing, variable-outlier detection, multivariate data analysis, estimation of uncertainties, and statistical evaluation [89,155]. Depending on the needs of specific spilled oil characterization, the analytical approaches may vary from case to case. In general, the tiered approach involves all or part of the following procedures [22,89,109,141,155]:

- Step 1:* Product screening and determination of hydrocarbon groups using GC/FID. This step characterizes the overall carbon range of oil samples and establishes a “weathering check.”
- Step 2:* Fingerprinting and distribution pattern recognition of volatile hydrocarbon (including BTEX and alkylbenzenes), target PAH, and biomarker components.
- Step 3:* Determination and comparison of diagnostic ratios of the “source-specific marker” compounds with the potential source oil and with the corresponding data from database.
- Step 4:* Assessment of the weathered impact to the oil samples.
- Step 5:* Based on results from the aforementioned steps and other information to make a conclusion, whether a spilled sample and a suspected source are a positive match, probable match, inconclusive, or nonmatch.

It is worthy to address here that each spill is different, and it is important to integrate all evidence, including both from analytical results and from other sources, to conduct a comprehensive investigation in order to obtain unbiased results. This case study here briefly describes how to perform a forensic oil analysis using information from oil fingerprinting analysis. In the artificial oil spill scenario, samples 1 and 2 (So 1 and So 2) were collected from two suspected sources and oil samples 3–6 (Sp 3 to Sp 6) were collected

from different spill sites in an oil spill incident [156]. This study applied the methodology described earlier to analyze the suspected and spilled oil samples and to identify the spill source by comparing the fingerprints of these oils.

5.6.1 Product Type Screening and Determination of Hydrocarbon Groups

As the first step of the forensic study, both samples of spills and suspected sources were initially characterized by GC/FID screening. This generally renders a characterization of the oil type and a description of the dominating petroleum hydrocarbons in the oil sample (e.g., the overall boiling range and prominence of individual *n*-alkanes). Table 5.13

shows the results of the hydrocarbon group analysis of the spill samples.

According to Figure 5.15 and Table 5.13, the major chemical composition features of the samples are summarized as follows:

Source sample 1: The resolved hydrocarbons mainly in the carbon range of *n*-C₉ to *n*-C₃₈ with maximum at *n*-C₂₀ to *n*-C₂₄, two GC/FID UCM humps, and relatively high UCM content (68%)

Source sample 2: The resolved hydrocarbons in the carbon range of *n*-C₉ to *n*-C₄₀ with maximum at *n*-C₁₄ to *n*-C₂₄, two UCM humps, and high UCM content (74%)

TABLE 5.13 Concentrations of selected hydrocarbon groups and diagnostic ratios of target compounds in the oil samples of the case study

Oil samples	Source 1	Source 2	Spill 3	Spill 4	Spill 5	Spill 6
TPH (mg/g oil)	199	107	132	51.4	126	82.0
Total resolved peaks (%)	31.7	26.3	17.8	25.0	15.2	12.2
UCM (%)	68.3	73.7	82.2	75.0	84.8	87.8
Alkylated PAH (μg/g)						
ΣNaphthalenes	29,935	13,819	5,440	6,858	758	ND
ΣPhenanthrenes	10,427	4,626	6,817	2,399	8,345	2,438
ΣDibenzothiophenes	2,511	1,086	2,897	498	1,915	420
ΣFluorenes	2,414	1,848	976	625	1,021	69.3
ΣChrysenes	1,814	282	1,697	72.7	2,065	1,568
Total alkylated PAHs	47,102	21,662	17,826	10,453	14,104	4,495
Total EPA priority PAHs (μg/g)	1,149	316	416	147	507	255
Diagnostic ratios (%)						
<i>n</i> -C ₁₇ /Pri	322	324	241	300	334	NA
<i>n</i> -C ₁₈ /Phy	219	247	154	223	215	227
Pri/Phy	63.4	77.8	58.1	76.0	24.4	31.7
C28(22R)/H30	6.71	6.86	14.3	3.26	6.39	5.56
C28(22S)/H30	8.44	8.46	14.1	9.37	10.1	8.64
C29(22R)/H30	5.08	4.51	9.74	4.44	5.33	5.25
C29(22S)/H30	5.66	6.41	11.4	3.74	7.16	5.67
Ts/H30	14.3	10.9	14.1	8.10	15.5	14.6
Tm/H30	44.3	46.6	40.7	50.9	43.9	42.2
H29/H30	121	70.2	71.5	74.4	122	120
M29/H30	8.22	5.81	5.14	6.27	10.7	7.79
H31S/H30	42.3	38.0	49.0	37.8	48.1	44.8
G/H30	20.8	8.08	10.6	9.50	20.7	21.2
C28ββ(R+S)/C27ββ(R+S)	80.5	75.2	70.5	80.9	79.9	80.9
C29ββ(R+S)/C27ββ(R+S)	103	109	102	106	114	109
C27ββ(R+S)/[C28ββ(R+S)+C29ββ(R+S)]	54.6	54.3	58.0	53.4	51.5	52.6
C28ββ(R+S)/[C27ββ(R+S)+C29ββ(R+S)]	39.7	36.0	34.9	39.2	37.3	38.7
SC26TA/SC28TA	33.2	32.0	40.0	29.9	35.4	32.7
(RC26TA+SC27TA)/H30	48.6	50.2	107	42.8	51.2	48.8
RC27TA/RC28TA	116	91.1	90.5	93.6	108	113
2-MF/4-MPy	31.0	30.9	22.4	35.4	29.7	27.9
BaF/4-MPy	67.2	57.8	44.7	63.0	63.4	61.7
B(b+c)F/4-MPy	34.2	24.0	18.4	28.5	32.5	30.3
2-MPy/4-MPy	92.9	96.3	91.9	104	92.1	91.3
4-MPy/H30	6.68	2.85	5.92	2.42	6.34	4.99
1-MPy/4-MPy	83.3	85.5	84.9	88.2	84.3	84.9
t-m-Phen/BNT (benzonaphthothiophene)	132	158	95.4	226	136	126
C2P/C4P	252	355	137	431	216	96.7
C2D/C2P	42.1	38.6	75.3	33.3	39.0	29.4
C3D/C3C	238	524	324	850	196	69.1

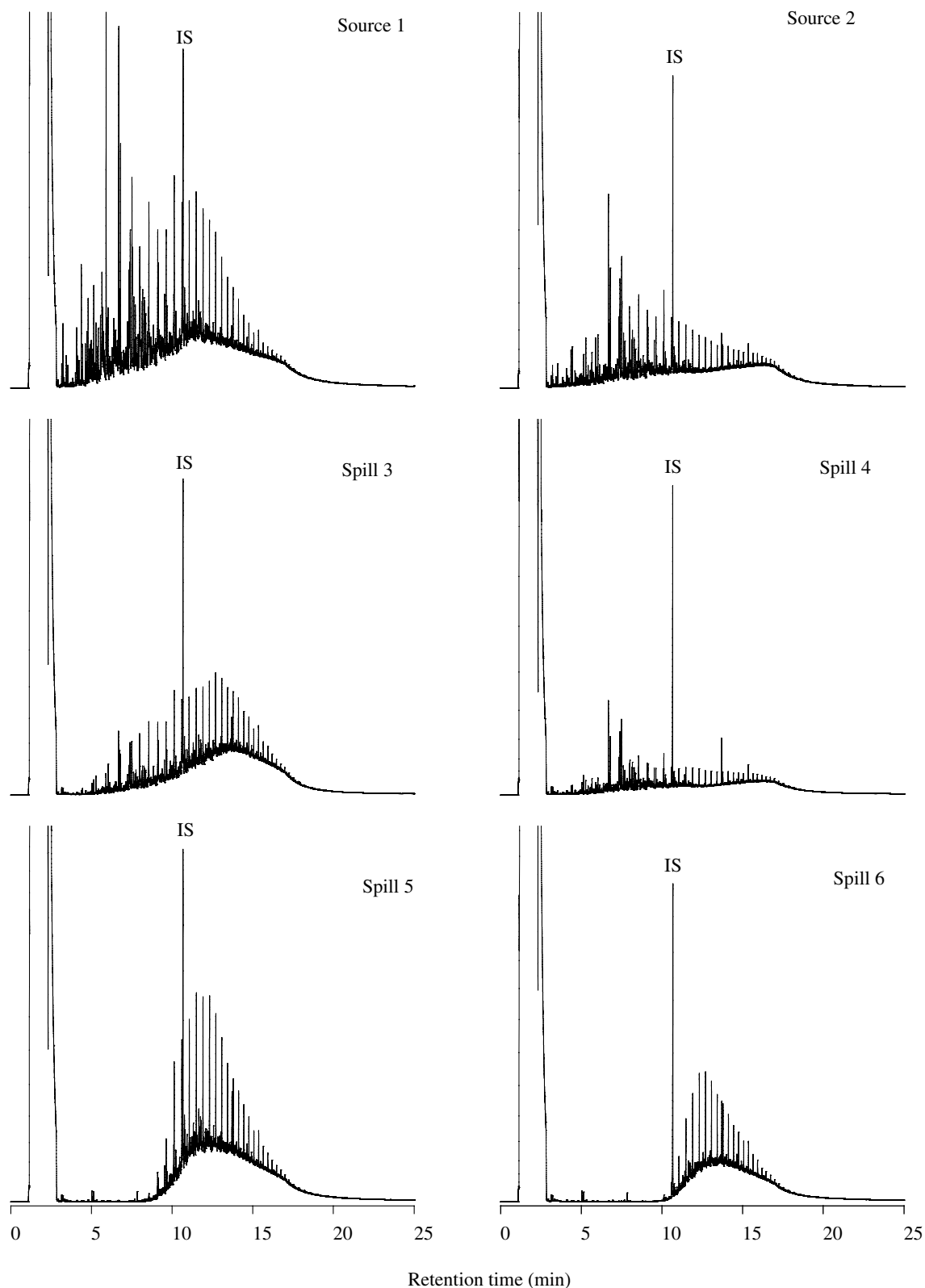


FIGURE 5.15 GC/FID chromatograms of candidate sources and spill samples.

Spill sample 3: The resolved hydrocarbons mainly in the carbon range of $n\text{-C}_{10}$ to $n\text{-C}_{38}$ with maximum at $n\text{-C}_{22}$ to $n\text{-C}_{26}$, one UCM hump, and high UCM content (82%)

Spill sample 4: The resolved hydrocarbons mainly in the carbon range of $n\text{-C}_9$ to $n\text{-C}_{40}$ with maximum at $n\text{-C}_{14}$ to $n\text{-C}_{24}$, two GC/FID UCM humps, and high UCM content (75%)

Spill sample 5: The resolved hydrocarbons mainly in the carbon range of $n\text{-C}_{17}$ to $n\text{-C}_{36}$, one UCM hump, and high UCM content (85%)

Spill sample 6: The resolved hydrocarbons mainly in the carbon range of $n\text{-C}_{19}$ to $n\text{-C}_{38}$, one UCM hump, and high UCM content (88%)

The GC/FID chromatograms in Figure 5.15 show that apart from a predominance of n -alkanes ranging from $n\text{-C}_{19}$ to $n\text{-C}_{38}$ in each oil, various other low-boiling-point compounds were also observed in two source oils, spill samples 3 and 4. The chromatographic features indicate that these peaks are largely attributed to alkylated naphthalenes and phenanthrenes. These chromatographic evidences imply that source samples 1 and 2 and spill samples 3 and 4 all exhibited typical n -alkane distribution pattern of HFOs, that is, Bunker C. HFOs are generally produced by blending light petroleum distillates with various refined residual oils to achieve a specific viscosity for different applications. Normal alkanes lower than $n\text{-C}_{18}$ were not detected in spill samples 5 and 6. Compared with two source oils, spill samples 5 and 6 contain lower resolved peaks (15.2 and 12.2%, respectively) and higher UCM contents. GC/FID analysis reveals that spill samples 5 and 6 appear to be severely weathered HFOs or heavy crude oils.

By simply overlaying chromatograms at m/z 85 for each source and each spill, a notable difference was found in either n -alkane range or abundance between source sample 1 and spill samples 3 and 4 and between source sample 2 and spill samples 3, 5, and 6. The chromatograms of spill samples 5 and 6 are partially similar to that of source sample 1 in relation to the long-chain n -alkane range. The differences in the front portion of the chromatograms were further investigated by a weathering check. The GC/FID chromatographic profile, percentages of UCM, and resolved peaks of spill sample 4 are similar to source sample 2 (Fig. 5.15 and Table 5.13), but its GC-detectable TPHs were determined to be only 51.4 mg/g of sample compared with 107 mg/g for source sample 2. It is excluded that the difference was a result of weathering because spill sample 4 still contained high amounts of very-low-boiling-point compounds. At this point, further tests such as comparison of diagnostic ratios and weathering check are required to investigate this pair of samples.

5.6.2 Determination of Oil-Characteristic Alkylated PAHs and Biomarkers

To defensibly determine the source of spilled oils, the subsequent steps involved the GC/MS fingerprinting of source-specific compounds including PAHs and biomarkers in candidate source samples and spill samples. While numerous ions were used for this work, only a few were selected for discussion.

5.6.2.1 Alkylated PAHs The PAH quantitation results indicate the following:

- (i) The five oil-characteristic alkylated PAH series in two source sample oils and four spill samples all demonstrate the typical characteristic “bell-shaped” distribution profiles.
- (ii) The total concentration of five alkylated PAH homologues in Table 5.13 varied significantly from the highest concentration of 47,102 $\mu\text{g/g}$ for source sample 1 to the lowest concentration of 4,495 $\mu\text{g/g}$ for spill sample 6.
- (iii) Two-ring alkylated naphthalenes were the most predominant series at 63.6, 63.8, and 65.6% of the total APAHs in source sample 1, source sample 2, and spill sample 4, respectively; while the 4-ring alkylated chrysenes were the least abundant series, at only 5.3, 1.3, and 0.7% in these oils, respectively. Distinctively, the most abundant naphthalene series was severely depleted in spill samples 5 and 6. Alkylated chrysenes accounted for relatively higher proportions of the total target APAHs, at 14.6 and 34.9% for spill samples 5 and 6, respectively.

As illustrated in Figure 5.16, distribution patterns of selected PAH isomers (including m/z 192, 216, 231, and 234) in source sample 2 match with those of spill sample 4, but obviously these PAHs in source sample 2 are more abundant. This finding is consistent with those from GC/FID analysis.

The presence of 2-MAN is an indicator for the presence of a cracked gas oil blending stock since 2-MAN is generally absent in most crude oils or only in low concentrations relative to phenanthrenes. It was determined that the ratio of 2-MAN/C1-P is as high as 0.081 and 0.072 for source samples 1 and 2 and 0.072, 0.073, 0.085, and 0.105 for spill samples 3, 4, 5, and 6, respectively, which is significantly higher than the corresponding values for crude oils. The presence of abundant 2-MAN between the four methylphenanthrenes provides further evidence that the two source samples and four spill samples were actually HFOs and not crude oils.

As seen from Figure 5.16, no two samples have identical fingerprints for all ions of m/z 192, 216, 231, and 234. It is likely that all six samples have very similar fingerprints of ions m/z 216 and m/z 234, but source sample 2 and spill sample 4 apparently contain less abundance of these isomers. A series of triaromatic steranes (m/z 231) were found in all six oils. Source sample 1 and spill samples 5 and 6 have a distribution pattern of SC28TA < RC27TA, whereas source sample 2 and spill samples 3 and 4 have an opposite pattern of SC28TA > RC27TA.

5.6.2.2 Biomarker Analysis The biomarker terpanes (m/z 191) and steranes (m/z 218) were detected in all six oil samples (Fig. 5.17). Similar to the characteristic results for triaromatic steranes (m/z 231), source sample 1 and spill samples 5 and 6 show a distribution pattern of biomarker terpanes of H29 > H30; in contrast, source sample 2 and spill

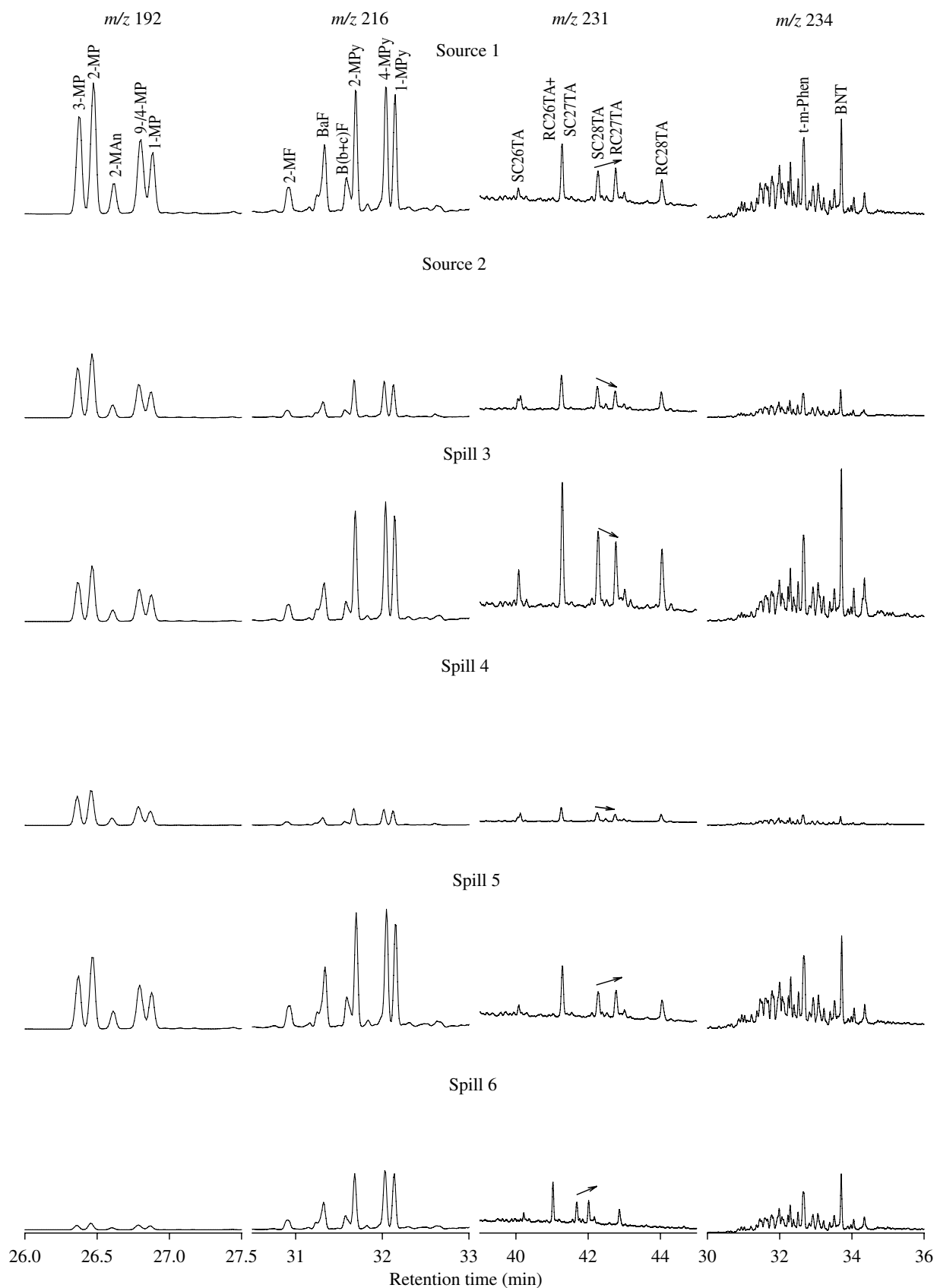


FIGURE 5.16 GC/MS chromatograms of selected aromatic clusters: methylphenanthrenes (m/z 192), m/z 216 isomers, triaromatic steranes (m/z 231), and C_4 -phenanthrenes (m/z 234) in oil samples.

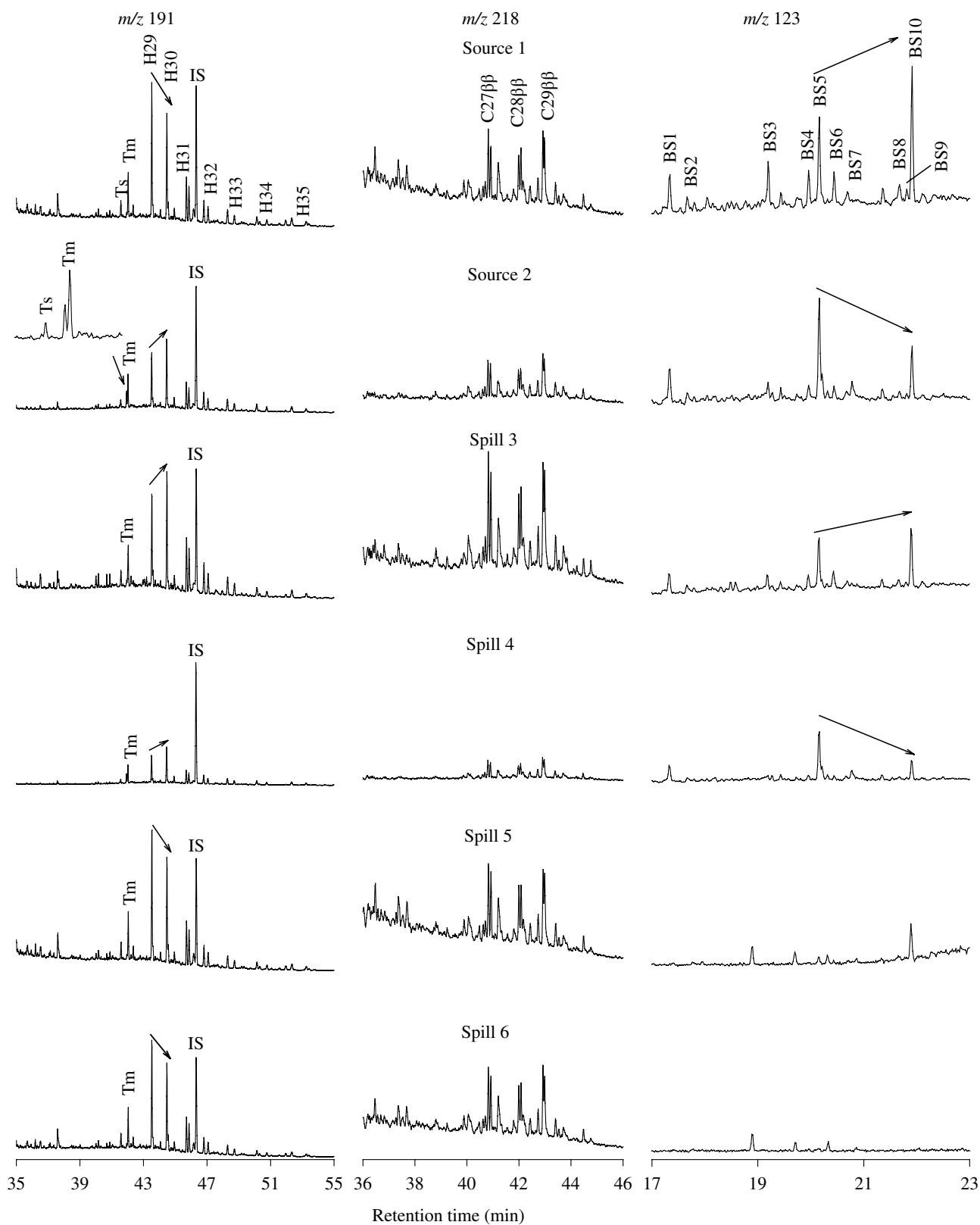


FIGURE 5.17 GC/MS chromatograms of biomarker terpanes (m/z 191), biomarker steranes (m/z 218), and bicyclic sesquiterpanes (m/z 123) in candidate sources and spill samples.

samples 3 and 4 have an opposite distribution pattern of $H_{29} < H_{30}$. Because C_{29} -norhopane (H_{29}) and C_{30} -hopane (H_{30}) are stable in evaporative weathering and resistant to biodegradation, this difference is unlikely caused by weathering. As seen from the chromatograms of biomarker terpanes in Figure 5.17, source sample 2 and spill sample 4 have relatively lower $18\alpha(H), 21\beta(H)$ -22,29,30-trisnorhopane (Ts) in comparison to other four samples. In addition, it is noted that $17\alpha(H), 21\beta(H)$ -22,29,30-trisnorhopane (Tm) in oil samples 2 and 4 have a high left-shoulder peak (a trisnorhopane isomer).

To provide additional supporting information, bicyclic sesquiterpanes were analyzed for this study. As displayed in Figure 5.17, all 10 commonly recognized C_{14} – C_{16} bicyclic sesquiterpanes were detected in source samples 1 and 2 and spill samples 3 and 4. The selected ion chromatograms at m/z 123 showed distribution patterns of $BS_{10} > BS_5 > BS_3 > BS_1$ for source sample 1, $BS_5 > BS_{10} > BS_1$ for source sample 2 and spill sample 4, and $BS_{10} > BS_7 > BS_1 > BS_3$ for spill sample 3. Sesquiterpane compounds were in low concentrations in spill sample 5 and absent in spill 6, but this could be due to severe weathering.

5.6.3 Comparison of Diagnostic Ratios

A number of diagnostic molecular parameters were calculated from the peak areas of target compounds at selected ions, m/z 85 for n -alkanes, m/z 191 and 218 for biomarkers, and m/z 231, 216, 234, 206, 226, and 270 for alkylated PAHs (Table 5.13). The calculated difference in a compound ratio was “flagged” when its value exceeds 14%, where the repeatability limit of 14% based on an RSD of 5% was used as a match criterion [20,22,156]. Most of backbone diagnostic ratios of spill sample 3 are significantly different from those of source samples 1 and 2. Eleven and seven flagged ratios were determined for sample pairs 1–4 and 2–4, respectively. On the other hand, the difference was unlikely to be attributed to weathering or instrumental variation. Therefore, neither of the two candidates are the potential source of spill sample 4. With the exception of three ratios of isoprenoids that are not applicable to severely weathered oils, spill samples 5 and 6 have 2 and 6 flagged ratios compared with source sample 1 and 8 and 13 flagged ratios compared with source sample 2, respectively.

5.6.4 Weathering Check

The comparison of chromatographic and quantitative information has demonstrated pronounced differences among the chromatograms of source sample 1 and spill samples 5 and 6. As seen in Table 5.13, however, these oils have many very similar diagnostic ratios such as H_{29}/H_{30} , $29\beta\beta(R+S)/27\beta\beta(R+S)$, and $SC_{26}TA/SC_{28}TA$, which are highly weathering resistant. This suggests a positive match between spill sample 1 and source samples 5 and 6.

A “weathering check” was therefore conducted to determine whether the difference between the samples could have been caused by weathering.

The peak integration from selected ion monitoring of targeted compounds was normalized to C_{30} $17\alpha(H), 21\beta(H)$ -hopane (H_{30}) [22,145]. The corresponding quantities of target compound X are calculated as follows:

$$R_X = \left[\left(\frac{X_{Sp}}{H_{30}_{Sp}} \right) \right] / \left[\left(\frac{X_{So}}{H_{30}_{So}} \right) \right] \times 100 \quad (5.8)$$

where R_X refers to the corresponding quantities; X_{Sp} and X_{So} are the area or height of targeted compound X acquired by selected ion monitoring for a spill and a source, respectively; and H_{30}_{Sp} and H_{30}_{So} are the area or height of C_{30} $17\alpha(H), 21\beta(H)$ -hopane acquired for a spill and a source, respectively. When the corresponding quantities of selected target compounds for a spill relative to a candidate source are plotted against the retention time (indicating the boiling points), in principle, if these two samples have exactly the same composition, all R_X values should be close to 100% and a straight line will be obtained. When a weathered spilled oil, particularly when the weathering is due to natural evaporation, has an identical source as a source oil, the R_X values increase gradually with increasing boiling points of target compounds, producing a smooth S-shaped trend line. An obvious S-shaped weathering check curve was obtained for source sample 1 against spill sample 5 and source sample 1 against sample spill 6, and only a few ratios are slightly out of the curves due to the low abundance of target compounds. The best-fit curve strongly suggested that the differences in the ratios between source sample 1 and spill samples 5 and 6 are caused by evaporation weathering. Although source sample 2 and spill sample 4 have close values for many diagnostic ratios (Table 5.13), the weathering plot between two oils shows only a cloud of points, not a best-fit curve. Thus, the measured differences in the ratios between samples 2 and 4 are “true” differences rather than a weathering result of corresponding compounds in these samples, leading to a nonmatch for source sample 2 and spill sample 4.

5.6.5 Results of Match between Spilled Oils and Candidate Sources

The following conclusions are based on the overall chemical fingerprinting evidences and data interpretation results: (i) source sample 1 does not match with spill samples 3 and 4. (ii) Spill samples 5 and 6 are obviously weathered and are probably from the same source as source sample 1. With respect to the particular chromatographic shape and distribution of n -alkanes, it is unlikely that such weathering takes place naturally in real oil spills. (iii) It is unlikely that source sample 2 matches with any of the spill samples 3, 4, 5, and

6, although it has many chromatographic similarities with spill sample 4. However, it is worth noting that it is impossible to draw a definite conclusion due to the lack of oil background information, which is particularly essential for oil spill identification.

REFERENCES

- [1] Lubeck, A.J., Analysis of Crude Oils, in *Manual on Hydrocarbon Analysis* (6th ed.), A.W. Drews (ed.), American Society for Testing Materials, West Conshohocken, PA, 34, 1998.
- [2] Hegazi, A.H. and J.T. Andersson, Limitations to GC-MS Determination of Sulfur-Containing Polycyclic Aromatic Compounds in Geochemical, Petroleum, and Environmental Investigations, *Energy Fuel.*, 21, 3375, 2007.
- [3] Fingas, M., *The Basics of Oil Spill Cleanup* (3rd ed.), CRC Press, Taylor and Francis Publishers, Boca Raton, FL, 2012.
- [4] Wang, Z.D., M. Fingas, and D.S. Page, Oil Spill Identification, *J. Chromatogr. A*, 843, 369, 1999.
- [5] Wang, Z.D., M. Fingas, C. Yang, and H.J. Christensen, Crude Oils and Refined Products Fingerprinting: Principles, in *Environmental Forensics: Contaminant Specific Guide*, R.D. Morrison and B.L. Murphy (eds.), Elsevier, New York, NY, 339, 2006.
- [6] DPRA, Formation of Crude Oil and Natural Gas, in *The Origin and Chemistry of Petroleum*, <http://www.dpra.com/index.cfm/m/158>, accessed on May 16, 2011.
- [7] US Energy Information Administration (EIA), *How Many Gallons of Gasoline Does one Barrel of Oil Make*, http://www.eia.doe.gov/ask/crudeoil_faqs.asp, accessed on December 7, 2010.
- [8] National Oceanic and Atmospheric Administration (NOAA), *Options for Minimizing Environmental Impacts of Freshwater Spill Response*, Hazardous Materials Response and Assessment Division (HMRAD), American Petroleum Institute (API), 126, 1994.
- [9] Mang, T. and G. Lingg, Base Oils, in *Lubricants and Lubrication*, T. Mang and W.A. Dresel (eds.), Wiley-VCH Verlag GmbH & Co., KGaA, Weinheim, 45, 2007.
- [10] Irwin, R.J., M. van Mouwerik, L. Stevens, M.D. Seese, and W. Basham, *Environmental Contaminants Encyclopedia: Fuel Oil Number 4 Entry*, National Park Service, Water Resources Division, Fort Collins, CO, 1997.
- [11] Ancheyta, J. and J.G. Speight, *Hydroprocessing of Heavy Oils and Residua*, CRC Press, Boca Raton, FL, 2007.
- [12] Speight, J.G., *The Chemistry and Technology of Petroleum* (4th ed.), CRC Press, Boca Raton, FL, 2007.
- [13] Dunn, K., G.V. Chilingarian, H. Lian, Y.Y. Wang, and T.F. Yen, Analysis of Asphalt and its Components by Thin-layer Chromatography, in *Asphaltenes and Asphalts*, 2, T.F. Yen and G.V. Chilingarian (eds.), Elsevier Science B.V., Amsterdam, 305, 2000.
- [14] Fan T., J. Wang, and J.S. Buckley, Rapid and Accurate SARA Analysis of Medium Gravity Crude Oils, *Energy Fuel.*, 16, 1571, 2002.
- [15] Curiale, J.A. and E.B. Frolov, Occurrence and Origin of Olefins in Crude Oils. A Critical Review, *Org. Geochem.*, 29, 397, 1998.
- [16] Schmidt, P.F., *Fuel Oil Manual* (4th ed.), Industrial Press Inc., New York, NY, 1986.
- [17] Speight, J.G., Petroleum Asphaltenes. Part I: Asphaltenes, Resins and the Structure of Petroleum, *Oil Gas Sci. Technol. Rev. IFP*, 59, 467, 2004.
- [18] Wang, Z.D., M. Fingas, and K. Li, Fractionation of ASMB Oil, Identification and Quantitation of Aliphatic, Aromatic and Biomarker Compounds by GC/FID and GC/MSD, *J. Chromatogr. Sci.*, 32, 361 (Part I) and 367 (Part II), 1994.
- [19] Daling, P.S., L.G. Faksness, A.B. Hansen, and S.A. Stout, Improved and Standardized Methodology for Oil Spill Fingerprinting, *Environ. Forensics*, 3, 263, 2002.
- [20] Faksness, L.G., M.W. Hermann, and P.S. Daling, Revision of the Nordtest Methodology for Oil Spill Identification, *SINTEF Report STF66 A02028*, Nordtest, Trondheim, 2002.
- [21] ASTM, Standard Test Methods for Comparison of Waterborne Petroleum Oils by Gas Chromatography, *ASTM Method D3328-06*, ASTM International, West Conshohocken, PA, 2006.
- [22] CEN (European Committee for Standardization), *Oil Spill Identification-Waterborne Petroleum and Petroleum Products. Part 2: Analytical Methodology and Interpretation of Results*, CEN/TC BT120, the British Standards Institution (BSI), London, 2010.
- [23] Munari, F. and A. Cadoppi, Ultra Fast GC Method for the Analysis of Total Hydrocarbons in Water in Compliance with ISO 9377-2 (Mod.), *The Application Notebook*, 11, 2006.
- [24] Gaines, R.B., G.S. Frysiner, C.M. Reddy, and R.K. Nelson, Oil Spill Source Identification by Comprehensive Two-dimensional Gas Chromatography (GC \times GC), in *Oil Spill Environmental Forensics: Fingerprinting and Source Identification*, Z.D. Wang and S.A. Stout (eds.), Academic Press, Burlington, MA, 169, 2007.
- [25] Mao, D.B., R. Lookman, H. van de Weghe, R. Weltens, G. Vanermen *et al.*, Combining HPLC-GC \times GC, GC \times GC/ToF-MS, and Selected Ecotoxicity Assays for Detailed Monitoring of Petroleum Hydrocarbon Degradation in Soil and Leaching Water, *Environ. Sci. Technol.*, 43, 7651, 2009.
- [26] Liu, Z. and J.B. Phillips, Comprehensive Two-dimensional Gas Chromatography using an On-column Thermal Modulator Interface, *J. Chromatogr. Sci.*, 29, 227, 1991.
- [27] Phillips, J.B. and J. Beens, Comprehensive Two-dimensional Gas Chromatography: A Hyphenated Method with Strong Coupling between the Two Dimensions, *J. Chromatogr. A*, 856, 331, 1999.
- [28] Dimandja, J.D., A New Tool for the Optimized Analysis of Complex Volatile Mixtures: Comprehensive Two-dimensional Gas Chromatography/Time-of-Flight Mass Spectrometry, *Am. Lab.*, 35, 42, 2003.
- [29] Gaines, R.B. and G.S. Frysiner, Oil Spill Source Identification by Comprehensive Two-dimensional Gas Chromatography, *Environ. Sci. Technol.*, 33, 2106, 1999.

- [30] Arey, J.S., R.K. Nelson, and C.M. Reddy, Disentangling Oil Weathering using GC \times GC. 1. Chromatogram Analysis, *Environ. Sci. Technol.*, 41, 5738, 2007.
- [31] Wang, F.C. and C.C. Walters, Pyrolysis Comprehensive Two-dimensional Gas Chromatography Study of Petroleum Source Rock, *Anal. Chem.*, 79, 5642, 2007.
- [32] Tran, T.C., G.A. Logan, E. Grosjean, D. Ryan, and P.J. Marriott, Use of Comprehensive Two-dimensional Gas Chromatography/Time-of-Flight Mass Spectrometry for the Characterization of Biodegradation and Unresolved Complex Mixtures in Petroleum, *Geochim. Cosmochim. Acta*, 15, 6468, 2010.
- [33] Ávila, B.M.F., A. Aguirar, A.O. Gomes, and D.A. Azevedo, Characterization of Extra Heavy Gas Oil Biomarkers using Comprehensive Two-dimensional Gas Chromatography Coupled to Time-of-Flight Mass Spectrometry, *Org. Geochem.*, 41, 863, 2010.
- [34] Cortes, H.J., B. Winniford, J. Luong, and M. Pursch, Comprehensive Two Dimensional Gas Chromatography Review, *J. Sep. Sci.*, 32, 883, 2009.
- [35] von Muhlen, C., C.A. Zini, E.B. Caramao, and P.J. Marriott, Applications of Comprehensive Two-dimensional Gas Chromatography to the Characterization of Petrochemical and Related Samples, *J. Chromatogr. A*, 1105, 39, 2006.
- [36] Vogt, W., K. Jacob, and H.W. Obwexer, Sampling Method in Capillary Column Gas-Liquid Chromatography Allowing Injections of up to 250 μ L, *J. Chromatogr. A*, 174, 437, 1979.
- [37] Hoh, E. and K. Mastovska, Large Volume Injection Techniques in Capillary Gas Chromatography (Review), *J. Chromatogr. A*, 1186, 2, 2008.
- [38] Agilent Technologies, *Agilent Multimode Inlet*, Manual No. G3510-90020, Wilmington, DE, 2009.
- [39] Yang, C., Z.Y. Yang, Z.D. Wang, K. Li, B. Hollebone *et al.*, Application of Programmable Temperature Vaporization Large Volume Injection (PTV-LVI) Coupled to Gas Chromatography-mass Spectrometry (GC-MS) for Oil Fingerprinting Analysis, *Proceedings of the 34th AMOP Technical Seminar*, Environment Canada, Calgary, AB, 2011.
- [40] de Hoffmann, E. and V. Stroobant, *Mass Spectrometry: Principles and Applications* (3rd ed.), John Wiley & Sons, Ltd, Chichester, 2007.
- [41] Agilent Technologies, *Agilent 7000A Triple Quadrupole GC/MS System: Concepts Guide*, Manual Part Number: G7000-90031 (1st ed.), Santa Clara, CA, 2009.
- [42] Philp, R.P., J. Oung, and C.A. Lewis, Biomarker Determination in Crude Oils using a Triple Stage Quadrupole Mass Spectrometer, *J. Chromatogr. A*, 446, 3, 1988.
- [43] Fernández-González, V., S. Muniategui-Lorenzo, P. López-Mahía, and D. Prada-Rodríguez, Development of a Programmed Temperature Vaporization-Gas Chromatography-Tandem Mass Spectrometry Method for Polycyclic Aromatic Hydrocarbons Analysis in Biota Samples at Ultratrace Levels, *J. Chromatogr. A*, 1207, 136, 2008.
- [44] Sarowha, S.L.S., B.K. Sharma, C.D. Sharma, and S.D. Bhagat, Characterization of Petroleum Heavy Distillates using HPLC and Spectroscopic Methods, *Energy Fuel.*, 11, 566, 1997.
- [45] Palmentier, J.P.F., A.J. Britten, G.M. Charbonneau, and F.W. Karasek, Determination of Polycyclic Aromatic Hydrocarbons in Lubricating Oil Base Stocks using High-Performance Liquid Chromatography and Gas Chromatography-Mass Spectrometry, *J. Chromatogr.*, 469, 241, 1989.
- [46] Hsu, C.S., G.J. Dechert, W.K. Robbins, and E.K. Fukuda, Naphthenic Acids in Crude Oils Characterized by Mass Spectrometry, *Energy Fuel.*, 14, 217, 2000.
- [47] Pharr, D.Y., J.K. McKenzie, and A.B. Hickman, Fingerprinting Petroleum Contamination Using Synchronous Scanning Fluorescence Spectroscopy, *Ground Water*, 30, 484, 1992.
- [48] Patra, D. and A.K., Mishra, Study of Diesel Fuel Contamination by Excitation Emission Matrix Spectral Subtraction Fluorescence, *Anal. Chim. Acta*, 454, 209, 2002.
- [49] Hegazi, E., A. Hamdan, and J. Mastromarino, Remote Fingerprinting of Crude Oil using Time Resolved Fluorescence Spectra, *Arab. J. Sci. Eng.*, 30, 3, 2005.
- [50] Liu, Y., J. He, C. Song, Y. Li, S. Wang *et al.*, Oil Fingerprinting by Three-dimensional (3D) Fluorescence Spectroscopy and Gas Chromatography-mass Spectrometry (GC-MS), *Environ. Forensics*, 10, 324, 2009.
- [51] Wang, C.Y., W.D. Li, X.N. Luan, Q.Q. Liu, J.L. Zhang *et al.*, Species Identification and Concentration Quantification of Crude Oil Samples in Petroleum Exploration using the Concentration-Synchronous-Matrix-Fluorescence Spectroscopy, *Talanta*, 81, 684, 2010.
- [52] Gugel, J. and J.A. Siegel, Fluorescence of Petroleum Products III. Three-dimensional Fluorescence Plots of Petroleum-based Products, *J. Forensic Sci.*, 33, 1405, 1988.
- [53] Bugden, J.B.C., C.W. Yeung, P.E. Kepkay, and K. Lee, Application of Ultraviolet Fluorometry and Excitation-Emission Matrix Spectroscopy (EEMS) to Fingerprint Oil and Chemically Dispersed Oil in Seawater, *Mar. Pollut. Bull.*, 56, 677, 2008.
- [54] Von der Dick, H. and W. Kalkreuth, Synchronous Excitation and Three-dimensional Fluorescence Spectroscopy Applied to Organic Geochemistry, *Adv. Org. Geochem.*, 10, 633, 1985.
- [55] Castro, L.V. and F. Vazquez, Fractionation and Characterization of Mexican Crude Oils, *Energy Fuel.*, 23, 1603, 2009.
- [56] Aske, N., H. Kallevik, and J. Sjöblom, Determination of Saturate, Aromatic, Resin, and Asphaltene (SARA) Components in Crude Oils by Means of Infrared and Near-Infrared Spectroscopy, *Energy Fuel.*, 15, 1304, 2001.
- [57] US EPA, Semivolatile Organic Compounds by Gas Chromatography/Mass Spectrometry (GC/MS), Method 8270D Revision 4. *SW-846 Method 8270D*. The U.S. Environmental Protection Agency's Office of Solid Waste, February 2007, <http://www.epa.gov/osw/hazard/testmethods/sw846/pdfs/8270d.pdf>, accessed on August 6, 2014.
- [58] Stout, S.A. and G.S. Douglas, Diamondoid Hydrocarbons Application in the Chemical Fingerprinting of Natural Gas Condensate and Gasoline, *Environ. Forensics*, 5, 225, 2004.
- [59] Stout, S.A., A.D. Uhler, and K.J. McCarthy, Middle Distillate Fuel Fingerprinting using Drimane-based Bicyclic Sesquiterpanes, *Environ. Forensics*, 6, 241, 2005.
- [60] Wang, Z.D., C. Yang, M. Fingas, B.P. Hollebone, M. Landriault *et al.*, Characterization, Weathering, and

- Application of Sesquiterpanes to Source Identification of Spilled Petroleum Products, *Environ. Sci. Technol.*, 39, 8700, 2005.
- [61] Wang, Z.D., C. Yang, B. Hollebone, and M. Fingas, Forensic Fingerprinting of Diamondoids for Correlation and Differentiation of Spilled Oil and Petroleum Products, *Environ. Sci. Technol.*, 40, 5636, 2006.
- [62] Yang, C., Z.D. Wang, B. Hollebone, X. Peng, M. Fingas *et al.*, GC/MS Quantitation Analysis of Diamondoid Compounds in Crude Oils and Petroleum Products, *Environ. Forensics*, 7, 292, 2006.
- [63] Yang, C., Z.D. Wang, B. Hollebone, C. Brown, and M. Landriault, Characteristics of Bicyclic Sesquiterpanes in Crude Oils and Petroleum Products, *J. Chromatogr. A*, 1216, 4475, 2009.
- [64] Wang, Z.D., M. Fingas, E.H. Owen, L. Sigouin, and C. Brown, Long-Term Fate and Persistence of the Spilled Metula Oil in a Marine Salt Marsh Environment Degradation of Petroleum Biomarkers, *J. Chromatogr. A*, 926, 275, 2001.
- [65] Wang, Z.D., M. Fingas, and L. Sigouin, Using Multiple Criteria for Fingerprinting Unknown Oil Samples Having Very Similar Chemical Composition, *Environ. Forensics*, 3, 251, 2002.
- [66] ESTS Oil Research Lab, *Determination of Total Petroleum Hydrocarbons, n-Alkanes, Polycyclic Aromatic Hydrocarbons, and Selected Biomarkers in Oil and Petroleum Products*, ESTS Method No.: ESTD-OR-20, Ottawa, ON, 2006.
- [67] Hansen, A.B., P.S. Daling, L.G. Faksness, K.R. Sorheim, P.Kienhuis *et al.*, Emerging CEN Methodology for Oil Spill Identification, in *Oil Spill Environmental Forensics: Fingerprinting and Source Identification*, Z.D. Wang and S.A. Stout (eds.), Academic Press, Burlington, MA, 229, 2007.
- [68] Sporring, S., S. Bøwadt, B. Svensmark, and E. Bjorklund, Comprehensive Comparison of Classic Soxhlet Extraction with Soxtec Extraction, Ultrasonication Extraction, Supercritical Fluid Extraction, Microwave Assisted Extraction and Accelerated Solvent Extraction for the Determination of Polychlorinated Biphenyls in Soil, *J. Chromatogr. A*, 1090, 1, 2005.
- [69] Majors, R.E., Modern Techniques for the Extraction of Solid Materials: An Update, *LC-GC Asia Pac.*, 9, 8, 2006.
- [70] Richardson, S.D., Environmental Mass Spectrometry: Emerging Contaminants and Current Issues, *Anal. Chem.*, 82, 4742, 2010.
- [71] Alzaga, R., P. Montuori, L. Ortiz, J.M. Bayona, and J. Albaigés, Fast Solid-Phase Extraction-Gas Chromatography-Mass Spectrometry Procedure for Oil Fingerprinting-Application to the Prestige Oil Spill, *J. Chromatogr. A*, 1025, 133, 2004.
- [72] Yang, Z.Y., C. Yang, Z.D. Wang, B. Hollebone, M. Landriault *et al.*, Oil Fingerprinting Analysis using Commercial Solid Phase Extraction (SPE) Cartridge and Gas Chromatography-Mass Spectrometry (GC-MS), *Anal. Methods*, 3, 628, 2011.
- [73] CCME (Canadian Council of Ministers of the Environment), *Reference Method for the Canada-Wide Standard for Petroleum Hydrocarbons in Soil—Tier 1 Method*, Canadian Council of Ministers of the Environment Inc., Winnipeg, Manitoba, 2001.
- [74] Wang, Z.D., C. Yang, F. Kelly-Hooper, B. Hollebone, X. Peng *et al.*, Forensic Differentiation of Biogenic Organic Compounds from Petroleum Hydrocarbons in Biogenic and Petrogenic Compounds Cross-contaminated Soils and Sediments, *J. Chromatogr. A*, 1216, 1174, 2009.
- [75] Volkman, J.K. and J.R. Maxwell, Acyclic Isoprenoids as Biological Markers, in *Biological Markers in the Sedimentary Record*, R.B. Johns (ed.), Elsevier, New York, NY, 1, 1986.
- [76] ten Haven, H.L., J.W. de Leeuw, J. Rullkotter, and J.S. Sinninghe Damste, Restricted Utility of the Pristane/Phytane Ratio as a Palaeoenvironmental Indicator, *Nature*, 330, 641, 1987.
- [77] Forster, A., H. Sturt, P.A. Meyers, and Shipboard Scientific Party, Molecular Biogeochemistry of Cretaceous Black Shales from the Demerara Rise: Preliminary Shipboard Results from Sites 1257 and 1258, Leg 207, in *Proceedings of the Ocean Drilling Program, Initial Reports* (Vol. 207), J. Erbacher, D.C. Mosher, and M.J. Malone (eds.), College Station, TX (Ocean Drilling Program), 2004, pp. 1–22.
- [78] Petrov, A.A., *Petroleum Hydrocarbons*, Springer-Verlag, Berlin/New York, NY, 1987.
- [79] Philp, R.P. and C.A. Lewis, Organic Geochemistry of Biomarkers, *Ann. Rev. Earth Planet. Sci.*, 15, 363, 1987.
- [80] Ourisson, G., M. Rohmer, and K. Poralla, Prokaryotic Hopanoids and Other Polyterpenoid Sterol Surrogates, *Ann. Rev. Microbiol.*, 41, 301, 1987.
- [81] Requjo, A.G., G.B. Hieshima, C.S. Hsu, T.J. McDonald, and R. Sassen, Short-Chain (C_{21} and C_{22}) Diasteranes in Petroleum and Source Rocks as Indicators of Maturity and Depositional Environment, *Geochim. Cosmochim. Acta*, 61, 2653, 1997.
- [82] Prah, F.G., J. Dymond, and M.A. Sparrow, Annual Biomarker Record for Export Production in the Central Arabian Sea, *Deep-Sea Res. II*, 47, 1581, 2000.
- [83] Peters, K.E., C.C. Walters, and J.M. Moldowan, *The Biomarker Guide* (2nd ed.), Cambridge University Press, Cambridge, 2005.
- [84] Nytoft, H.P. and J.A. Bojesen-Koefoed, $17\alpha(H), 21\alpha(H)$ -hopanes: Natural and Synthetic, *Org. Geochem.*, 32, 841, 2001.
- [85] Volkman, J.K., A Review of Sterol Markers for Marine and Terrigenous Organic Matter, *Org. Geochem.*, 9, 83, 1986.
- [86] Volkman, J.K., S.M. Barrett, S.I. Blackburn, M.P. Mansour, E.L. Silkes *et al.*, Microalgal Biomarkers: A Review of Recent Research Developments, *Org. Geochem.*, 29, 1163, 1998.
- [87] Wang, Z.D. and J.H. Christensen, Petroleum Biomarker Fingerprinting for Environmental Forensics (II): Application, in *Environmental Forensics: Contaminant Specific Guide*, R.D. Morrison and B.L. Murphy (eds.), Elsevier, New York, NY, 409, 2006.
- [88] Peters, K.E. and J.M. Moldowan, Effects of Source, Thermal Maturity, and Biodegradation on the Distribution and Isomerization of Homohopanes in Petroleum, *Org. Geochem.*, 17, 47, 1991.

- [89] Stout, S.A., A.D. Uhler, and K.J. McCarthy, A Strategy and Methodology for Defensibly Correlating Spilled Oil to Source Candidates, *Environ. Forensics*, 2, 87, 2001.
- [90] Grice, K.R., R. Alexander, and R.I. Kagi, Diamondoid Hydrocarbons as Indicators of Biodegradation in Australian Crude Oils, *Org. Geochem.*, 31, 67, 2000.
- [91] Schulz, L.K., A. Wilhelms, E. Rein, and A.S. Steen, Application of Diamondoids to Distinguish Source Rock Facies, *Org. Geochem.*, 32, 365, 2001.
- [92] Wei, Z.B., J.M. Moldowan, and A. Paytan, Diamondoids and Molecular Biomarkers Generated from Modern Sediments in the Absence and Presence of Minerals During Hydrous Pyrolysis, *Org. Geochem.*, 37, 891, 2006.
- [93] Vasquez, D. and G.A. Mansoori, Identification and Measurement of Petroleum Precipitates, *J. Petrol. Sci. Eng.*, 26, 49, 2000.
- [94] Bender, A.O., E.Z. Said, and A.K. Abdulsada, Gas Chromatographic Identification of Adamantanes in Some Iraqi Crude Oils, *Analyst*, 111, 575, 1986.
- [95] Williams, J.A., M. Bjoroy, D.L. Dolcater, and J.C. Winters, Biodegradation in South Texas Eocene Oils-Effects on Aromatics and Biomarkers, *Org. Geochem.*, 10, 451, 1986.
- [96] Wingert, W.S., GC-MS Analysis of Diamondoid Hydrocarbons in Smackover Petroleum, *Fuel*, 71, 37, 1992.
- [97] Lin, R. and Z.A. Wilk, Natural Occurrence of Tetramantane ($C_{22}H_{28}$), Pentamantane ($C_{26}H_{32}$) and Hexamantane ($C_{30}H_{36}$) in a Deep Petroleum Reservoir, *Fuel*, 74, 1512, 1995.
- [98] Dahl, J.E., S.G. Liu, and R.M.K. Carlson, Isolation and Structure of Higher Diamondoids, Nanometer-Sized Diamond Molecules, *Science*, 299, 96, 2003.
- [99] Chen, J., J. Fu, G. Sheng, D. Liu, and J. Zhang, Diamondoid Hydrocarbon Ratios: Novel Maturity Indices for Highly Mature Crude Oils, *Org. Geochem.*, 25, 179, 1996.
- [100] Dahl, J.E., J.M. Moldowan, K.E. Peters, G.E. Claypool, M.A. Rooney *et al.*, Diamondoid Hydrocarbons as Indicators of Natural Oil Cracking, *Nature*, 399, 54, 1999.
- [101] Alexander, R., R. Kagi, and R.A. Noble, Identification of Bicyclic Sesquiterpanes Drimane and Eudesmane in Petroleum, *J. Chem. Soc. Chem. Commun.*, 5, 226, 1983.
- [102] Alexander, R., R. Kagi, R.A. Noble, and J.K. Volkman, Identification of Some Bicyclic Alkanes in Petroleum, *Org. Geochem.*, 6, 63, 1984.
- [103] Dimmler, A., T.D. Cyr, and O.P. Strausz, Identification of Bicyclic Terpenoid Hydrocarbons in the Saturate Fraction of Athabasca Oil Sand Bitumen, *Org. Geochem.*, 7, 231, 1984.
- [104] Yang, C., Z.D. Wang, Z.Y. Yang, B. Hollebone, C. Brown *et al.*, Chemical Fingerprints of Alberta Oil Sands Bitumen and Related Petroleum Products, *Environ. Forensics*, 12, 173, 2011.
- [105] Wang, Z.D., M. Fingas, M. Landriault, L. Sigouin, and N. Xu, Identification of Alkylbenzenes and Direct Determination of BTEX and (BTEX + C_3 -Benzenes) in Oils by GC/MS, *Anal. Chem.*, 67, 3491, 1995.
- [106] Boehm, P.D., W.A. Burns, D.S. Page, A.E. Bence, P.J. Mankiewicz *et al.*, Total Organic Carbon, an Important Tool in Holistic Approach to Hydrocarbon Source Fingerprinting, *Environ. Forensics*, 3, 243, 2002.
- [107] Williams, P.T. and D.T. Taylor, Aromatization of Tire Pyrolysis Oil to Yield Polycyclic Aromatic Hydrocarbons, *Fuel*, 72, 1469, 1993.
- [108] Venkatesan, M.I., Occurrence and Possible Sources of Perylene in Marine Sediments—A Review, *Mar. Chem.*, 25, 1, 1988.
- [109] Wang, Z.D. and M. Fingas, Development of Oil Hydrocarbon Fingerprinting and Identification Techniques, *Mar. Pollut. Bull.*, 47, 423, 2003.
- [110] Douglas, G.S., A.E. Bence, R.C. Prince, S.J. McMillen, and E.L. Butler, Environmental Stability of Selected Petroleum Hydrocarbon Source and Weathering Ratios, *Environ. Sci. Technol.*, 30, 2332, 1996.
- [111] Wang, Z.D. and M. Fingas, Use of Methylthiophenes as Markers for Differentiation and Source Identification of Crude and Weathered Oils, *Environ. Sci. Technol.*, 29, 2842, 1995.
- [112] Wang, Z.D. and M. Fingas, Developments in the Analysis of Petroleum Hydrocarbons in Oils, Petroleum Products and Oil-Spill-Related Environmental Samples by Gas Chromatography, *J. Chromatogr. A*, 774, 51, 1997.
- [113] Zakaria, M.P., T. Okuda, and H. Takada, PAHs and Hopanes in Stranded Tar-Balls on the Coast of Peninsular Malaysia: Applications of Biomarkers for Identifying Source of Oil Pollution, *Mar. Pollut. Bull.*, 12, 1357, 2001.
- [114] Yang, C., X. Peng, Z.D. Wang, B. Hollebone, C. Brown *et al.*, Fingerprinting Analysis and Characterization of Hydrocarbons in Sediment Cores from the Pearl River Estuary, China, *Environ. Forensics*, 12, 49, 2011.
- [115] Uhler, A.D., S.A. Stout, and G.S. Douglas, Chemical Heterogeneity in Modern Marine Residual Oils, in *Oil Spill Environmental Forensics: Fingerprinting and Source Identification*, Z.D. Wang and S.A. Stout (eds.), Academic Press, Burlington, MA, 327, 2007.
- [116] Mossner, S.G. and S.A. Wise, Determination of Polycyclic Aromatic Sulfur Heterocycles in Fossil Fuel-related Samples, *Anal. Chem.*, 71, 58, 1999.
- [117] Wang, Z.D., M. Fingas, S. Blenkinsopp, G. Sergy, M. Landriault *et al.*, Comparison of Oil Composition Changes Due to Biodegradation and Physical Weathering in Different Oils, *J. Chromatogr. A*, 809, 89, 1998.
- [118] Seifert, W.K. and J.M. Moldowan, Application of Steranes Terpanes and Monoaromatics to Maturation, Migration and Source of Crude Oils, *Geochim. Cosmochim. Acta*, 42, 77, 1978.
- [119] Barakat, A.O., Y. Qian, M. Kim, and M.C. Kennicutt, Compositional Changes of Aromatic Steroid Hydrocarbons in Naturally Weathered Oil Residues in Egyptian Western Desert, *Environ. Forensics*, 3, 219, 2002.
- [120] Short, J.W. and R.A. Heintz, Identification of Exxon Valdez Oil in Sediments and Tissues from Prince William Sound and the Northwestern Gulf of Alaska based on a

- PAH Weathering Model, *Environ. Sci. Technol.*, 31, 2375, 1997.
- [121] Wang, Z.D., B. Hollebone, C. Yang, B. Fieldhouse, M. Fingas *et al.*, *Oil Composition and Properties for Oil Spill Modelling*, US EPA Order No.: 3D-6152-NAFX, Environment Canada, Ottawa, ON, 2004.
- [122] Fingas, M., A Literature Review of the Physics and Predictive Modeling of Oil Spill Evaporation, *J. Hazard. Mater.*, 42, 157, 1995.
- [123] Yang, C., Z.D. Wang, B. Hollebone, C. Brown, and M. Landriault, Application of Statistical Analysis in the Selection of Diagnostic Ratios for Forensic Identification of an Oil Spill Source, in *Proceeding of the International Oil Spill Conference 2008*, Savannah, GA, 297, 2008.
- [124] Wang, Z.D., M. Fingas, and G. Sergy, Study of 22-year-old Arrow Oil Samples using Biomarker Compounds by GC/MS, *Environ. Sci. Technol.*, 28, 1733, 1994.
- [125] Connan, J., Biodegradation of Crude Oils in Reservoirs, in *Advances in Petroleum Geochemistry* (Vol. 1), J. Brooks and D.H. Welte (eds.), Academic Press, New York, NY, 1983, pp. 299–335.
- [126] George, S.C., C.J. Boreham, S.A. Minifie, and S.C. Teerman, The Effect of Minor to Moderate Biodegradation on C₅ to C₉ Hydrocarbons in Crude Oils, *Org. Geochem.*, 33, 1293, 2002.
- [127] Volkman, J.K., R. Alexander, and R.I. Kagi, Biodegradation of Aromatic Hydrocarbons in Crude Oils from the Barrow Sub-basin of Western Australia, *Org. Geochem.*, 6, 619, 1984.
- [128] Wang, Z.D., M. Fingas, S. Blenkinsopp, G. Sergy, M. Landriault *et al.*, Study of the 25-Year-old Nipisi Oil Spill: Persistence of Oil Residues and Comparisons between Surface and Subsurface Sediments, *Environ. Sci. Technol.*, 32, 2222, 1998.
- [129] Wei, Z.B., J.M. Moldowan, K.E. Peters, Y. Wang, and W. Xiang, The Abundance and Distribution of Diamondoids in Biodegraded Oils from the San Joaquin Valley: Implications for Biodegradation of Diamondoids in Petroleum Reservoirs, *Org. Geochem.*, 38, 1910, 2007.
- [130] Wenger, L.M. and G.H. Isaksen, Control of Hydrocarbon Seepage Intensity on Level of Biodegradation in Sea Bottom Sediments, *Org. Geochem.*, 33, 1277, 2002.
- [131] Prince, R.C., D.L. Elmendorf, J.R. Lute, C.S. Hsu, C.E. Haith *et al.*, 17 α (H),21 β (H)-Hopane as a Conserved Internal Marker for Estimating the Biodegradation of Crude Oil, *Environ. Sci. Technol.*, 28, 142, 1994.
- [132] Strausz, O.P., A. Morales-Izquierdo, N. Kazmi, D.S. Montgomery, J.D. Payzant *et al.*, Chemical Composition of Athabasca Bitumen: The Saturate Fraction, *Energy Fuel.*, 24, 5053, 2010.
- [133] Leahy, J.G. and R.R. Colwell, Microbial Degradation of Hydrocarbons in the Environment, *Microbiol. Rev.*, 53, 305, 1990.
- [134] Jacquot, F., M. Guiliano, P. Doumenq, D. Munoz, and G. Mille, In vitro Photooxidation of Crude Oil Maltenic Fractions: Evolution of Fossil Biomarkers and Polycyclic Aromatic Hydrocarbons, *Chemosphere*, 33, 671, 1996.
- [135] Garrett, P.M., I.J. Pickering, C.E. Haith, and R.C. Prince, Photooxidation of Crude Oils, *Environ. Sci. Technol.*, 32, 3719, 1998.
- [136] Nicodem, D.E., M.C.Z. Fernandes, C.L.B. Guedes, and R.J. Correa, Photochemical Processes and the Environmental Impact of Petroleum Spills, *Biogeochemistry*, 39, 121, 1997.
- [137] Nicodem, D.E., C. Guedes, and R.J. Correa, Photochemistry of Petroleum I. Systematic Study of a Brazilian Intermediate Crude Oil, *Mar. Chem.*, 63, 93, 1998.
- [138] Andersson, J.T., Polycyclic Aromatic Sulfur Heterocyclic III. Photochemical Stability of the Potential Oil Pollution Markers Phenanthrenes and Dibenzothiophenes, *Chemosphere*, 27, 2097, 1993.
- [139] Ali, L.N., R.F. Mantourab, and S.J. Rowland, The Dissolution and Photodegradation of Kuwaiti Crude Oil in Seawater. Part 2: A Laboratory Photodegradation Apparatus and Photodegradation Kinetics of a Model Seawater Soluble Hydrocarbon (Phenanthrene), *Mar. Environ. Res.*, 40, 319, 1995.
- [140] Stepnowski, P., E.M. Siedlecka, P. Behrend, and B. Jastorff, Enhanced Photodegradation of Contaminants in Petroleum Refinery Wastewater, *Water Res.*, 36, 2167, 2002.
- [141] Faksness, L.G., P.S. Daling, and A.B. Hansen, Round Robin Study-Oil Spill Identification, *Environ. Forensics*, 3, 279, 2002.
- [142] Yue, Z.W. and M.P. Fraser, Polar Organic Compounds Measured in Fine Particulate Matter During TexAQS 2000, *Atmos. Environ.*, 38, 3253, 2004.
- [143] Simoneit, B.R.T., Organic Matter of the Troposphere-III. Characterization and Sources of Petroleum and Pyrogenic Residues in Aerosols over the Western United States, *Atmos. Environ.*, 18, 51, 1984.
- [144] Zakaria, M.P., A. Horinouchi, S. Tsutsumi, H. Takada, S. Tanabe *et al.*, Oil Pollution in the Straits of Malacca, Malaysia: Application of Molecular Markers for Source Identification, *Environ. Sci. Technol.*, 34, 1189, 2000.
- [145] Nordtest, *Oil Spill Identification*, Method NT CHEM 001 (2nd ed.), Nordtest, Finland, 1, 1991.
- [146] Yunker, M.B., R.W. Macdonald, R. Brewer, R. Vingarzan, R.H. Mitchell *et al.*, PAHs in the Fraser River Basin: A Critical Appraisal of PAH Ratios as Indicators of PAH Source and Composition, *Org. Geochem.*, 33, 489, 2002.
- [147] Christensen, J.H., G. Tomasi, A. de Lemos Scofield, and M. de Fatima Gudalipe Meniconi, A Novel Approach for Characterization of Polycyclic Aromatic Hydrocarbon (PAH) Pollution Patterns in Sediments from Guanabara Bay, Rio de Janeiro, Brazil, *Environ. Pollut.*, 158, 3290, 2010.
- [148] Barrick, R.C. and F.G. Prahl, Hydrocarbon Geochemistry of the Puget Sound Region-III. Polycyclic Aromatic Hydrocarbons in Sediments, *Estuar. Coast. Shelf Sci.*, 25, 175, 1987.
- [149] Yunker, M.B., R.W. Macdonald, D. Goyette, D.W. Paton, B.R. Fowler *et al.*, Natural and Anthropogenic Inputs of Hydrocarbons to the Strait of Georgia, *Sci. Total Environ.*, 225, 181, 1999.

- [150] Meniconi, M.F.G., I.T. Gabardo, M.E.R. Carneiro, S.M. Barbanti, G.C. Silva *et al.*, Brazilian Oil Spill Chemical Identification-case Studies, *Environ. Forensics*, 3, 303, 2002.
- [151] Fang, M.D., C.L. Lee, and C.S. Yu, Distribution and Source Recognition of Polycyclic Aromatic Hydrocarbons in the Sediments of Hsin-ta Harbour and Adjacent Coastal Areas, Taiwan, *Mar. Pollut. Bull.*, 46, 941, 2003.
- [152] Grimalt, J.O., N.L. van Drooge, A. Ribes, P. Fernandez, and P. Appleby, Polycyclic Aromatic Hydrocarbon Composition in Soils and Sediments of High Altitude Lakes, *Environ. Pollut.*, 131,13, 2004.
- [153] Benlahcen, K.T., A. Chaoui, H. Budzinski, J. Bellocq, and P. Garrigues, Distribution and Sources of Polycyclic Aromatic Hydrocarbons in Some Mediterranean Coastal Sediments, *Mar. Pollut. Bull.*, 34, 298, 1997.
- [154] Li, J.G., P. Philip, and M.Z. Cui, Methyl Diamantane Index (MDI) as a Maturity Parameter for Lower Palaeozoic Carbonate Rocks at High Maturity and Overmaturity, *Org. Geochem.*, 31, 267, 2000.
- [155] Christensen, J.H., A.B. Hansen, J. Mortensen, G. Tomasi, and O. Andersen. Integrated Methodology for Forensic Oil Spill Identification, *Environ. Sci. Technol.*, 38, 2912, 2004.
- [156] Kienhuis, P.G.M. and G. Dahmann, Second Intercalibration Round in the Framework in of Bonn-OSINET-Round Robin 2007, *The Comparison of Six HFO Samples: The Results of Nineteen International Laboratories*, File No. 2007.WIL23x, Bonn-OSINET, London, 1, 2008.

OIL SPILL IDENTIFICATION

JOAN ALBAIGÉS,¹ PAUL G.M. KIENHUIS,² AND GERHARD DAHLMANN³

¹*Department of Environmental Chemistry, IDAEA-CSIC, Barcelona, Spain*

²*Rijkswaterstaat Center for Water Management (RWS-WD), Lelystad, The Netherlands*

³*Bundesamt für Seeschifffahrt und Hydrographie (BSH), Hamburg, Germany*

6.1	Introduction	165
6.2	Sampling	167
6.2.1	Thick Oil Layers and Tar Balls	167
6.2.2	Sampling of Thin Oil Films (Sheens or Slicks)	167
6.2.3	Taking Oil Samples on Beaches and from Oiled Animals	169
6.2.4	Sampling on Board Vessels	170
6.3	Sample Handling in the Laboratory	170
6.4	Analysis	171
6.4.1	Characterization by GC–FID: Level 1	172
6.4.2	Characterization by GC–MS: Level 2	176
6.5	Conclusions	198

6.1 INTRODUCTION

The development of methods for fingerprinting petroleum hydrocarbons in the marine environment, to identify the source of accidental or intentional oil spills, has been an issue of major interest over the last 30 years. The need for these methods has arisen by the significant quantities of crude and refined oils entering the sea through different ways, which have caused extensive damage to marine life, coastal life, and recreational beaches. Efficient and unambiguous analytical methods for the characterization of these spillages are also needed from the standpoint of the enforcement of pollution control laws, designed to protect the public health and the environment. Chemical analytical results are thus used to attach responsibilities, assess penalties, and help recover cleanup costs incurred during an incident.

In this respect, Adlard (1972) stated that “nearly every known analytical technique has been used or suggested for oil pollutants identification, but, certainly, no one has emerged of such superiority that all the others can be considered as redundant” [1]. Therefore, earlier attempts of oil characterization were performed by a

multimethod approach, the particular combination of analytical techniques depending on the facilities and the experience existing in a laboratory and the expenditure that was justified to identify an unknown source.

Representative examples of these early multimethod approaches are reported in Table 6.1. They include analytical determinations such as the IR spectra, asphaltene and paraffin contents, etc., which provided a general classification of the pollutants (crude oils, fuel oils, oil sludges, etc.), and others such as the Ni/V ratio, sulfur content, chromatographic profiles, etc., which permitted, by comparison with reference samples, their unique identification—more or less.

However, another approach involving only one analytical technique but increasing the number of parameters considered was also adopted, particularly with the improvement of resolution of most analytical techniques. This is exemplified in Table 6.2 for trace analysis, IR spectroscopy, and gas chromatography (GC). In these cases, a multiparametric profile was used for identification, instead of a combination of different analytical determinations, and pattern recognition techniques were often applied to improve the diagnostic performance.

The main requirement that these fingerprinting parameters should fulfill, besides their specificity, is that they must remain unaltered during the weathering processes of oil at sea, namely, evaporation, dissolution, photooxidation, and biodegradation. In consequence, both conditions, specificity and stability, need to be investigated in order to evaluate the reliability and the usefulness of any proposed method.

This multiparametric approach received definite support with the advances in the geochemical characterization of crude oils, with the identification of a multitude of components derived from living organisms and specifically related to their geothermal history (“molecular

TABLE 6.1 Overall approaches for identification of oil pollutants

Method	Analytical techniques
IP Method [2]	Specific gravity Asphaltenes S, Ni, and V contents TLC/UV GLC
DGMK Method [3]	IR spectroscopy S, Ni, and V (Ca, Ra, and Zn) Column chromatography GLC
U.S. Coast Guard [4]	IR spectroscopy Fluorescence spectroscopy TLC/UV GLC

TABLE 6.2 Multiparametric methods for fingerprinting oil pollutants

Analytical methods	No. of parameters	References
Trace elements	3	Brunnock et al. [5]
	22	Duewer and Kowalski [6]
IR spectroscopy	3	Kawahara and Ballinger [7]
	18	Lynch and Brown [8]
	23	Mattson et al. [9]
Gas chromatography	3	Ehrhardt and Blumer [10]
	19	Clark and Jurs [11]
	36	Rasmussen [12]

markers"). Molecular markers have extensively been used in oil exploration for fingerprinting oils, the most commonly used being the acyclic isoprenoids and the polycyclic steranes and terpanes [13]. Their characterization has been definitely made practical by the possibilities offered by computerized GC–mass spectrometry (MS) to provide unique compositional profiles for different petroleum products [14].

The large expansion of this knowledge during the 1980s also opened the possibility of obtaining more measurable, objective, and defensible means in oil spill identification. Parameters based on these compounds have been included in several forensic methodologies recently developed and reviewed [15,16]. In 1991, the European Nordic countries supported the development of a specific methodology for oil spill identification (Nordtest method NT CHEM 001). The underlying basis for this method is the widely variable nature of oils with respect to their specific chemical compositions, which allows oils from different sources to be readily distinguished using appropriate compositional characteristics. The method relies upon detailed chemical characterization and numerical comparison between samples (i.e., a spilled oil and a suspected source) to determine if they “match” or not.

During the last decade, the original Nordtest method was extensively revised to include numerical comparisons of diagnostic ratios (DRs) between samples [15,17] and has

been validated through round robin tests [18,19] in order to improve the diagnostic reliability and eliminate qualitative judgments by the analyst. In 2002, the European Committee for Standardization (CEN) established a working group aiming at further refining the revised Nordtest Methodology into two CEN guidelines:

Part I: Oil spill identification – Waterborne petroleum and petroleum products – Sampling (CEN/TR 15522-1; 2006)

Part II: Oil spill identification – Waterborne petroleum and petroleum products – Analytical methodology and interpretation of results (CEN/TR 15522-2; 2012)

with the final objective of establishing a national oil spill identification protocol in each of the European countries, as well as being the norms for further international use. The method has been further assessed and improved through annual round robin tests carried out in the framework of the Bonn Agreement Oil Spill Identification Network Group.¹

Oil fingerprinting methods based on GC and GC–MS profiling have also been developed in the United States. The first attempts relied upon the U.S. EPA standard analytical methods such as (i) method 8015B, *Nonhalogenated Organics Using GC/FID*, and (ii) method 8270, *Semivolatile Organic Compounds by Gas Chromatography/Mass Spectrometry (GC/MS)*. However, because these methods were developed with the intention of measuring specific chemicals of concern (i.e., the so-called priority pollutant chemicals) for regulatory purposes, their usefulness in forensic oil spill investigations was limited [20]. Therefore, further modifications were incorporated in multiple protocols developed specifically by the American Society for Testing and Materials (ASTM) for oil spill characterization. In 1991, the method ASTM D3328, *Standard Test Methods for Comparison of Waterborne Petroleum Oils by Gas Chromatography*, was introduced. This method was based upon GC–FID analysis of spilled oils and their qualitative comparison to potential sources and/or impacted samples. ASTM D3328 has been repeatedly modified, the most current version being updated in 2000 [21]. The GC–MS fingerprinting component was introduced in the 1995 method ASTM D5739, *Oil Spill Identification by Gas Chromatography and Positive Ion Electron Impact Low-Resolution Mass Spectrometry*. This method was updated in 2000 [22].

This chapter will focus on these analytical approaches, with special reference to the CEN method, now implemented by many forensic laboratories and largely used in connection with recent major oil spills in Europe, for example, the *Tricolor* (British Channel, December 14, 2002) [23] and the *Prestige* (off the coast of Galicia, Spain,

¹<http://www.bonnagreement.org>.

November 20, 2002) [24,25]. These include both the sampling techniques and the handling of oil samples prior to their arrival at the laboratory and the diagnostic target compounds methodology for oil spill identification.

6.2 SAMPLING

Sampling is the first step in the process of defensibly determining the source or impact of an oil spill. Designing a comprehensive oil source sampling plan is fundamental in the investigative efforts of an oil spill, and collection of oil from both the spill and the suspected source(s) is crucial to any forensic program. If the sampling is not done in a proper way, the results of the analysis will not provide the adequate information that responders will need to take action.

Oil samples are collected from the water surface or the shoreline and from suspected sources. If the source is a ship, samples from as many segregated tanks in that ship, including possible lube oil, slop, and fuel oil tanks, as well as oil–water separators, should be collected. However, the size and appearance of the spill may give already some information on where to find a possible source.

All spills encountered and all potential sources should be sampled. Even if there is no suspected polluter when an oil spill is observed, sampling of the spilled oil is important because a possible source can be identified at a later stage, for example, by backtracking of vessel routes. If the spill is large, it is important to take samples from several positions within the spill to get a representative sample selection.

Petroleum products, when spilled into the marine environment, undergo rapid physical and chemical alterations (weathering), the greatest rate of changes occurs in most cases during the first few hours to the first day after a spill. This underscores the importance of initiating sampling as early as possible, adjusting the frequency of sampling to be greatest during the initial hours after a release, and the need to prioritize sampling based upon a rapidly changing time-scale. If the spill response operation continues for more than 1 day, samples should be taken every day to make it possible to determine the degree of weathering of the oil as well as a possible contamination by other oils. Together with the samples, all relevant information should be recorded, for example, the sampling conditions and the sample location (e.g., latitude–longitude–depth), the potential spill transport pathways, etc.

During sampling, every action should be taken to prevent sample manipulation, mixing up, or contamination of the samples by other substances. Particular attention should be paid to prevent deterioration of the samples. Therefore, they should be sent as soon as possible to the laboratory. If the transmission is delayed, the samples should be kept in the dark and at a temperature below 4°C.

Samples should be taken with sampling devices of glass, Teflon®, or stainless steel. The most adequate sample containers are 100–250 ml thick-walled wide-neck (30 mm) borosilicate glass bottles, provided with screw caps with Teflon® inlay. Disposable nitrile gloves should be used for protection, and clean gloves should be used between samples to prevent contamination of a sample with the remains of the previous ones.

The oil at sea can be present in thick layers or tar balls to microlayer sheens. Oil stranded on the coast may affect sediments, sandy beaches, or rocky shores as well as flora and fauna. Specific sampling techniques and provisions are required for each one of these compartments, which are described in the following sections.

6.2.1 Thick Oil Layers and Tar Balls

6.2.1.1 Use of a Clean Bucket or a Bottle Directly Globules, balls, and thick oil patches can be sampled with a bucket with small holes at the bottom allowing much of the water to drain away from the oil. After drainage of water, the skimming technique may be repeated several times to increase the amount of oil in the bucket. Finally, the oil may be transferred to the sample container by means of a stainless steel or Teflon® scraper used to scrape the sides of the bucket.

Alternatively, samples can be collected directly with a glass bottle, filling the bottle with as many balls as possible or skimming oil from the surface by repeated sweeps with the bottle and removing the water that has entered. One method of doing this is to close the lid and hold the bottle upside down for a minute to let the oil float upward to the bottom of the bottle so that the water can be drained by careful opening of the lid.

6.2.1.2 Polyethylene Cornet or Conical Teflon® Bag Floating oil on the water surface can often be sampled with a polyethylene cornet following the steps shown in Figure 6.1. The device is swept through the spill so as to skim as much oil as possible. The water in the cornet is slowly let out and the drainage is stopped when the last drop of water has escaped. Then, the oil in the cornet is filled into a 100 ml wide-neck sample bottle.

6.2.2 Sampling of Thin Oil Films (Sheens or Slicks)

6.2.2.1 Teflon® Pad A special pad, woven from Teflon® threads with a diameter of 32–39 µm, can be used if the oil film on the water surface is very thin. The oil is collected in the small openings of the hydrophobic net material. Outside the water, the oil slowly drops from the net as shown in Figure 6.2.

The use of a Teflon® pad can dramatically increase the amount of oil sampled. The pad material should be Teflon®

²An example is a Tefzel® net manufactured by SEFAR (www.sefar.com) (SEFAR Floutex Products ref. 09-150/36 or 9-250/39).

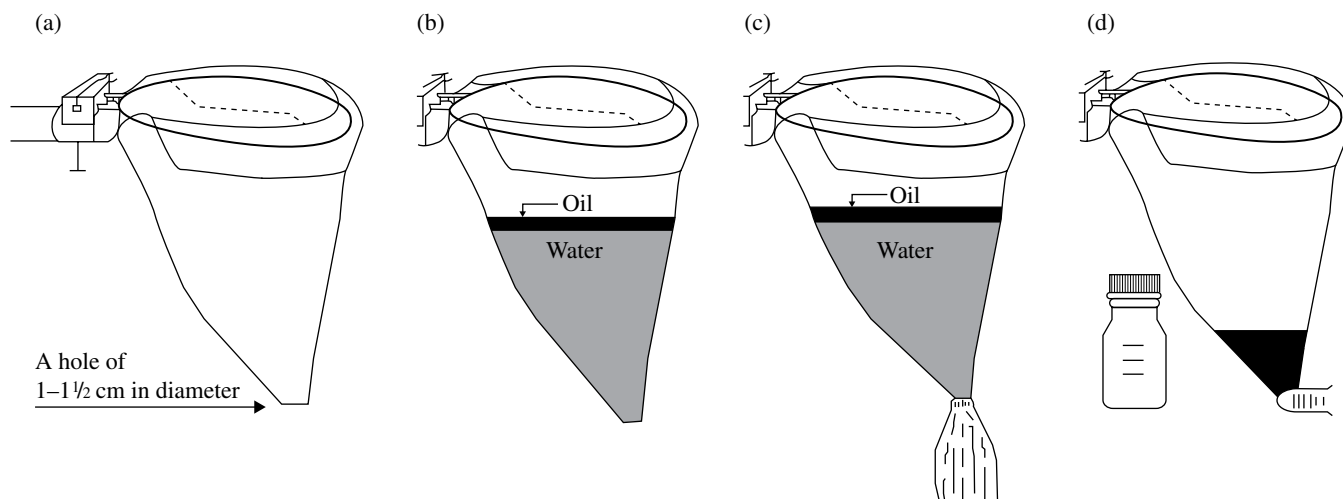


FIGURE 6.1 Sampling surface oil with a polyethylene cornet.

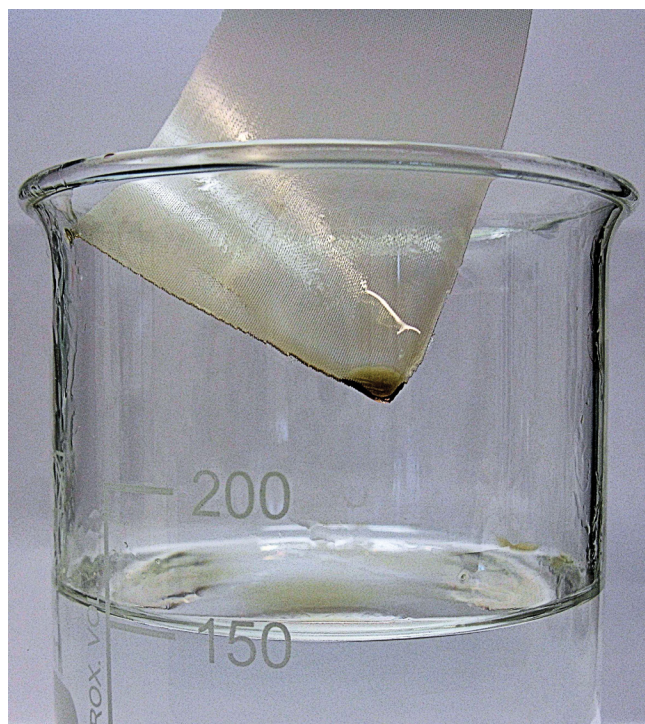


FIGURE 6.2 Five hundred microliters of gas oil on water. After a few immersions of a small piece of Teflon® net, the gas oil drops from the net.

(or a similar inert polyfluoropolymer) because other materials may interfere with the subsequent analytical processes in the chemical laboratory.² However, even the commercially available Teflon pads should be precleaned by solvent extraction prior to their use in the field to avoid potential precontamination.

A practical arrangement for handling a pad is shown in Figure 6.3. Great care must be taken during sampling to

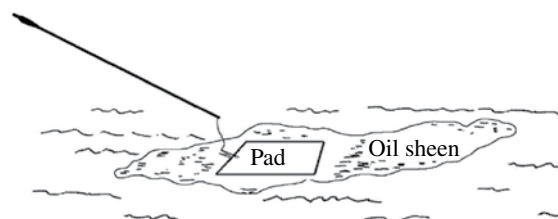


FIGURE 6.3 Teflon® pad on water surface.

avoid contamination of the sheen by traces of oil from the sampling vessel or other sources. The pad should be swept in the spill preferably until it is colored by the oil. However, it should be emphasized that the pad may have absorbed a sufficient amount of oil even if it has no sign of brown color.

After a sufficient number of sweeps, the Teflon® pad is carefully put into a sample bottle. The peg can be used to push the pad into the bottle. Another clean wooden peg of any kind can, if necessary, be used to assist in the procedure. It is important to avoid contact with fingers or any item that might contain traces of other oils. The samples should be kept in the dark, below a temperature of +4°C, and immediately transported to the laboratory.

6.2.2.2 Surface Slick Sampler Oil slicks, particularly in harbors, can be sampled with the device shown in Figure 6.4.

The sampler, developed by BSH, Germany, consists of two closed polyethylene flasks and one open glass bottle assembled in a polyethylene block. Due to the buoyancy of the three empty bottles, initially, the apparatus floats horizontally on the water surface so that water and surface layer film can flow into the sampling bottle. After filling, this bottle sinks down and thereby directs the opening

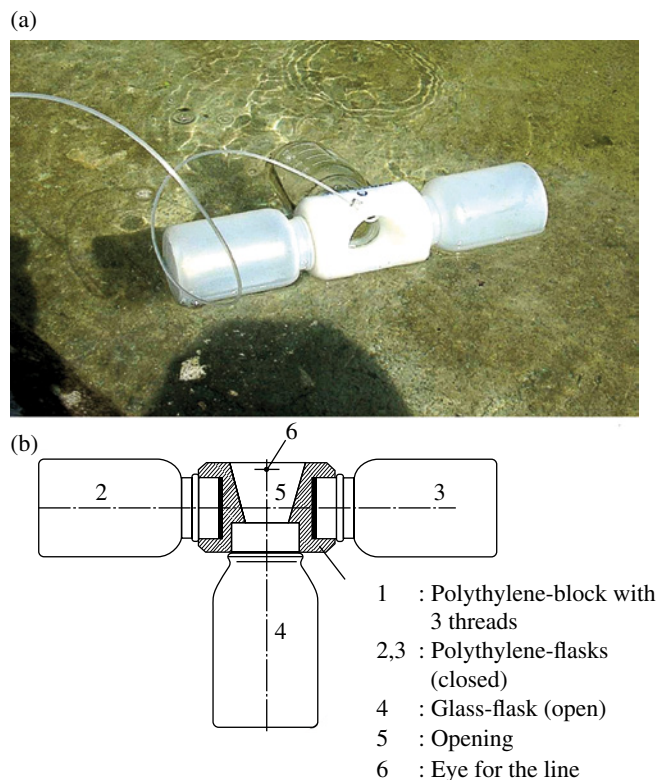


FIGURE 6.4 Surface slick sampler.

upward so that water can no longer flow into or out of the bottle. The bottle is disassembled, closed, and sent to the laboratory.

Under adverse conditions, a small stripe of Teflon® net may be attached to the sampler (kept in place by two plastic screws) (Fig. 6.5). When the sampler is lowered to the sea surface, this Teflon® net is laid upon the oil film. After sampling, the Teflon® net is put into the glass bottle. This sampler can be used not only from a vessel but also from a helicopter during surveillance.

6.2.3 Taking Oil Samples on Beaches and from Oiled Animals

The sampling of oiled sediments or soils can be accomplished by surface grab samples. In the case of a spill that is scattered over a long coastline, many samples should be taken to enable a mapping of the oil distribution on the shores. The oil should be scraped off oiled items and transferred into sample bottles. In cases where it is difficult to obtain clean oil samples, small oiled items (pebbles, small pieces of wood, etc.) can be placed in the bottles.

Any remaining traces on the shore from earlier oil spills must be carefully avoided during sampling a specific new spill. Samples of other possible sources should also



FIGURE 6.5 Teflon® net attached to the surface slick sampler for recovery of surface oil (top) and collected in the sampling jar (bottom).

be collected for identification, whenever anything unusual or suspicious is observed in the polluted area. In case of high viscous or solid samples, analyzing and comparing two aliquots of each sample give information about the heterogeneity of the oil. When heterogeneity has been concluded, the individual aliquots should be treated as different samples in the rest of the comparison.

In the case of oiled animals, it is recommended to cut off small parts of oiled feathers, fur, etc., and put them directly into a sample bottle rather than taking whole animal samples, body tissues, etc., which may become

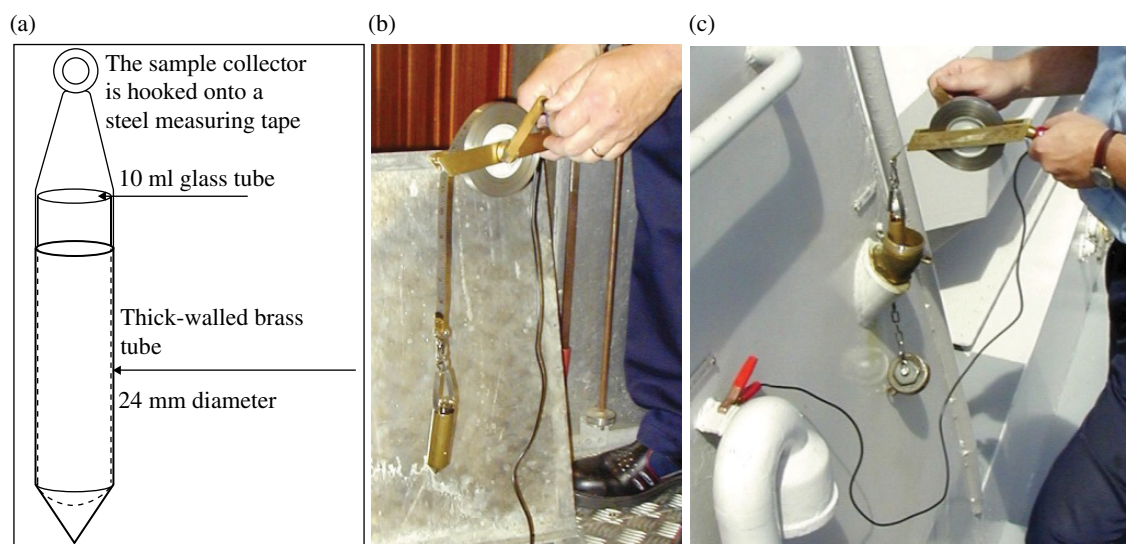


FIGURE 6.6 (a–c) Sample collector for oil on board vessels.

rotten during shipment. Samples with large amounts of organic materials should be frozen before sending to the laboratory to avoid biological decomposition. Alternatively, oil can also be wiped off using a piece of Teflon® net, which can be more easily stored and transported to the laboratory.

6.2.4 Sampling on Board Vessels

Sampling on board vessels is of utmost importance in order to obtain relevant oil samples of suspected sources. Large differences may exist between the fuel oils from different tanks, which results in different compositions of oil samples from the water and the beaches. Therefore, it is important to have a thorough sampling on board vessels. However, it may be difficult to obtain samples from tanks without opening manhole covers or drawing off pipes or pumps. In this case, it is often possible to use sounding pipes with a sample collector and glass tubes as shown in Figure 6.6.

A clean, unused 10 ml glass tube is put into the sample collector that is hooked onto a steel measuring tape that must be grounded before starting the sampling. The oil sample is collected through a sounding pipe and transferred to the sample bottle. The glass tube is discarded, and the sample collector must be thoroughly cleaned.

The bottom of the sample collector has the shape of a cone, which makes it lie down horizontally on the bottom of a tank. This makes it possible to get samples even from very shallow oil layers in a tank.

Samples must be taken on board ships by trained, experienced, and authorized persons, observing appropriate caution in accordance with current safety regulations.

6.3 SAMPLE HANDLING IN THE LABORATORY

Sample handling involves the extraction of the oil residues and their preparation for GC–FID and GC–MS analysis. If samples consist of water, the water is transferred to a separating funnel and repeatedly extracted using dichloromethane (DCM). The combined extracts are dried with sodium sulfate, concentrated using a gentle evaporation technique, and diluted or concentrated to a suitable injection concentration.

Teflon® pad or net samples are thoroughly extracted with DCM. After drying with sodium sulfate, the extract should also be diluted or concentrated to a suitable injection concentration.

Samples consisting primarily of thick oil or emulsified oil should be allowed to equilibrate at room temperature before sample preparation. Any free water should be decanted and the oil/emulsion fraction gently homogenized before an aliquot is dissolved with DCM and dried with sodium sulfate.

As high-boiling compounds are not eluted from the GC column and may strongly influence the performance of the injector, column, and detector, the extracts should also be cleaned in order to remove asphaltenes, resins, and extraneous particles.

A variety of procedures have been described for this purpose, the most common including the separation of hydrocarbon fractions by column chromatography. However, a low variability/high precision in the analytical results is essential for the numerical comparison of samples and proper assessment of differences or coincidences among them. Therefore, minimizing the handling of the samples prior to analysis minimizes any variability potentially introduced by the sample preparation. Consequently, a cleanup procedure instead of a fractionation into aliphatic and aromatic fractions is generally preferred for the preparation of extracts for the analysis by GC–FID and GC–MS. This can



FIGURE 6.7 Cleanup of oil extracts.

be done with commercial solid-phase extraction (SPE) columns and a vacuum manifold column processor. A good alternative is the use of glass Pasteur pipettes (typical volume 2.5 ml), as shown in Figure 6.7, using a mixture of hexane/DCM (50:50) as an eluent. Each Pasteur pipette is filled with a plug of glass wool, a layer of silica or Florisil, and a layer of dry sodium sulfate. A shortened plastic pipette tip can be used to fill the Pasteur pipette and a pipette pump to increase the elution flow rate when needed.

Visible oil in samples of sediments/rocks, vegetation, and wildlife should be wiped off using a piece of Teflon® net. The net should be rinsed with DCM, and the extract should be filtered through a glass fiber filter to take away extraneous particles. If the oil cannot be wiped off, the samples may be rinsed or extracted with DCM or hexane/DCM (50:50). A cleanup of the extracts, as described previously for oil residues, should be performed before the GC analysis.

6.4 ANALYSIS

The analysis of the oil sample extracts is aimed at comparing their detailed chemical composition by chemical fingerprinting. For making the conclusions more provable and reliable, a suite of generic and diagnostic petroleum components are measured. Most frequently, these include *n*-alkanes, acyclic isoprenoids, sterane and triterpane molecular markers, polycyclic aromatic hydrocarbons (PAHs), alkylated PAHs, and sulfur- and nitrogen-containing aromatic compounds [15,16,20,26,27].

These analytes can be measured using GC coupled to different detectors, ranging from nonspecific detectors such as flame ionization detectors (GC-FID) to highly selective mass spectrometers (GC-MS). Other compound-specific detectors such as flame photometric detectors,

chemiluminescence detectors, atomic emission detectors, and isotope ratio mass spectrometry for isotopic composition of individual components have also been used but less frequently and mainly as a confirmation [28].

In general, the complete characterization and identification of the samples is conducted using a tiered analytical approach [26,29] that, depending on the needs of the specific spill site investigation, may vary but broadly encompasses the following steps:

- *Tier 1*—determination of hydrocarbon groups and product type screening
- *Tier 2*—determination and comparison of compound ratios of the source-specific marker compounds (e.g., target biomarkers and PAHs) with the spill and suspected source oil samples
- *Tier 3*—determination of the influence of weathering on the samples
- *Tier 4*—data treatment and conclusions

A protocol/decision chart based on the CEN methodology *Oil spill identification – Waterborne petroleum and petroleum products – Analytical methodology and interpretation of results* (CEN/TR 15522-2) (2012) is shown in Figure 6.8. The chart includes two “tiers” or “levels” of analyses that include the visual characterization and qualitative comparison of the GC-FID and GC-MS profiles of the samples, the calculation and quantitative comparison of selected compound DRs,³ and the weathering checks. Any differences in compound ratios, not influenced by weathering, are only relevant if a difference is larger than the variability of the method itself. Therefore, good analytical performance and strict quality assurance are essential. Laboratories having contributed to CEN/TR 15522-2 adopted a value of 5% relative standard deviation (RSD) for compound ratios, representing the upper limit of the acceptable performance of the method (see page 28).

By using this analytical scheme, sufficient information about the samples to be compared can be gathered, and it can be concluded that the samples “match” or “nonmatch.” But depending on the amount of oil in the sample, the degree of weathering, and/or the contamination of the samples, sometimes, a definitive “match” or “nonmatch” conclusion is not possible. In these cases, conclusions such as “probable match” or even “inconclusive” must be chosen.

A detailed presentation of the two levels is given in the following sections. In the past few years, comprehensive two-dimensional GC (GC×GC) has been assessed for oil fingerprinting purposes [30]. In this technique, two capillary GC columns are connected serially by a thermal modulator—the interface between the two separation

³Ratios between the peak height or peak area of single compounds or groups of compounds selected for their diversity in the chemical composition in petroleum products and their reported response to weathering and degradation processes.

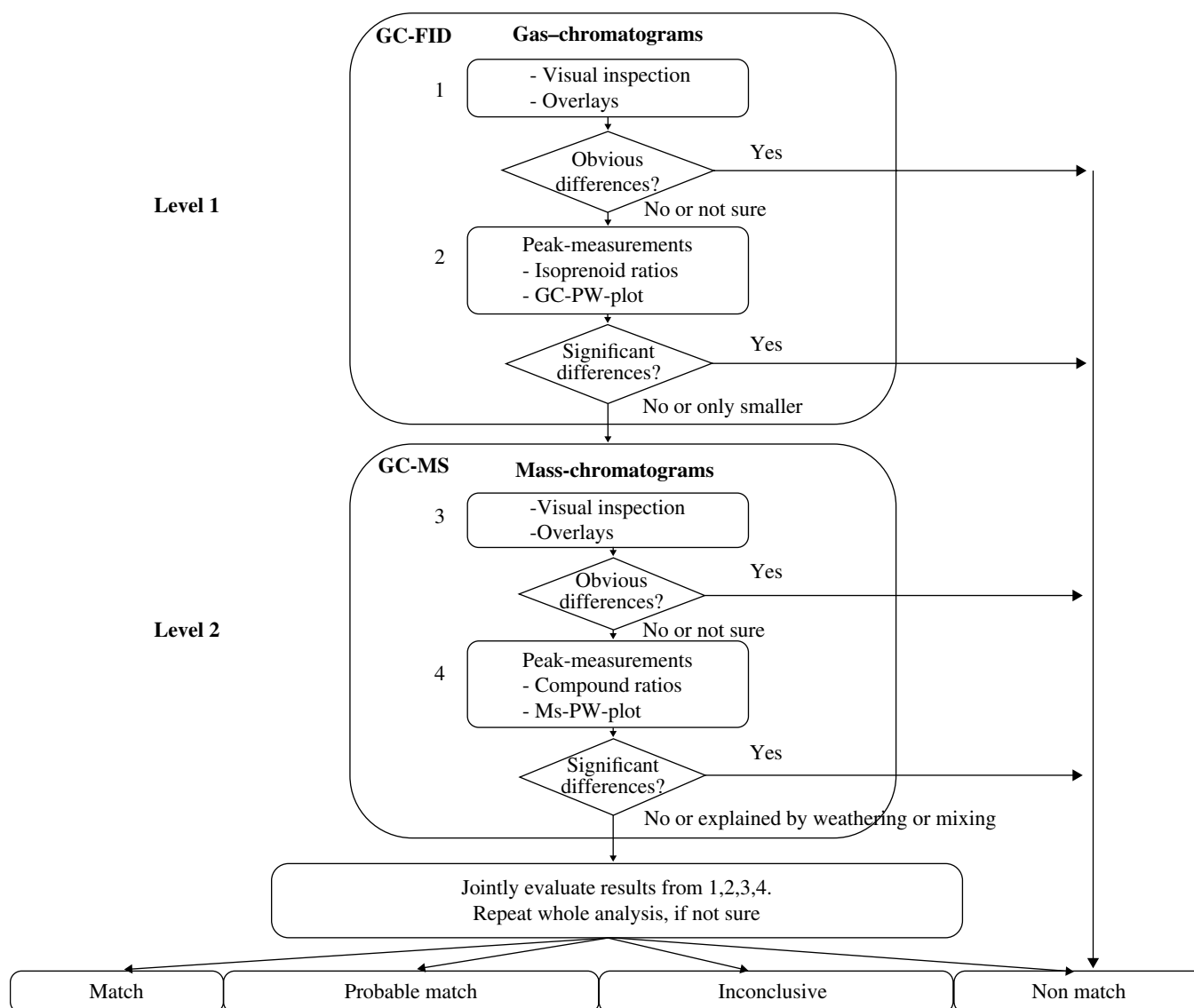


FIGURE 6.8 Protocol/decision chart for the oil spill identification methodology.

dimensions. The first-dimension sample effluent is thus continuously transferred in smaller portions to the second-dimension column throughout the chromatographic run, and each transferred pulse generates a high-speed secondary gas chromatogram. The first-dimension separation uses a non-polar phase to separate analytes by volatility difference, and the second dimension uses a more polar phase to separate first-dimension coelutes by polarity difference. The coupling of the system with high-speed response mass detectors, such as a time-of-flight (ToF) mass spectrometer, enables obtaining as many plots as ions one may intend to look for. The resulting two-dimensional chromatograms can be viewed in several formats, including surface, contour, and peak apex plots. However, despite this very appealing and innovative setup, this technique does not provide any significant information that cannot be obtained with the conventional

GC-MS techniques, although it is still under development and could have advantages for handling and comparing the complex composition of oil samples in the future.

6.4.1 Characterization by GC-FID: Level 1

6.4.1.1 Overall Characterization A screening characterization of the oil samples is carried out by GC-FID [29,31], which provides, besides the oil concentration in the extract, a descriptive “picture” of the hydrocarbon distribution in the samples, based normally on the appearance of resolved individual *n*-alkanes (Fig. 6.9), some isoprenoids, and an envelope of unresolved compounds (unresolved complex mixture, UCM).

The most appropriate capillary columns for oil spill investigations are 15–30 m (0.25 mm i.d.) fused silica coated with 100% methyl- or 5%-(phenyl)-methylpolysiloxane

cross-linked stationary phase. Typically, initial temperatures of 30–35°C and oven ramp rates of 6°C/min are used, which involve running times of about 40–60 min. However, it is possible to use narrower columns (20 m × 0.18 mm i.d.) that give shorter run times (around 30 min) without any loss of resolution, as shown in Figure 6.9, although these columns are more easily overloaded.

The *n*-alkanes, up to C40, are normally the predominant peaks distributed regularly over the entire retention interval of the chromatogram and provide a first indication of the type of product (e.g., crude oil, diesel oil, fuel oil), as illustrated in the examples in Figure 6.10. However, highly biodegraded crude oils (e.g., Dalia crude oil, Figure 6.10) and special refined products (e.g., lubricating and hydraulic oils) are devoid of *n*-alkanes, and the chromatograms are dominated by the UCM.

A large UCM is normally also a dominant component in bilge oils and can give indication of this residue in an oil spill (Fig. 6.11a). Another characteristic profile of oil residues from tank washings is shown in Figure 6.11b. In this case, a large predominance of high-molecular-weight *n*-alkanes overlying a very small hump is observed. This profile results from the waxy residues accumulating on the walls of the oil tanks in oil tankers.

The ratios of *n*-alkanes and acyclic isoprenoids like *n*-C17/pristane, *n*-C18/phytane, and pristane/phytane can be

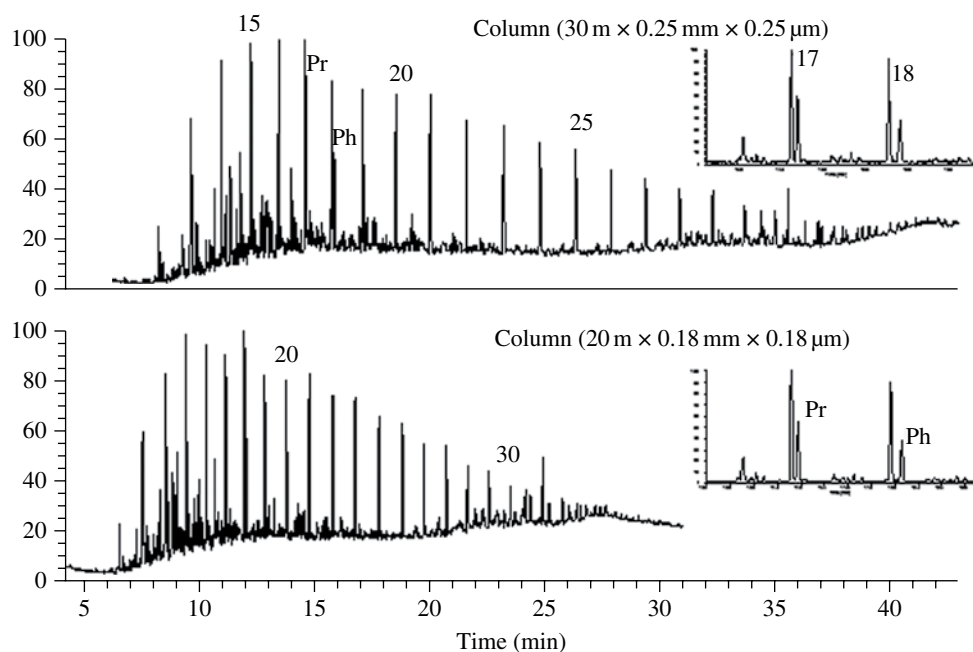
used as source indicators [32]. However, these ratios are sometimes influenced not only by evaporation but also by biodegradation. A thorough weathering check, as discussed later, will provide the basis to determine if these ratios may be affected by weathering of a spilled oil.

At this level of the investigation, the spill samples can be qualitatively and (using the aforementioned ratios) quantitatively compared to the suspected sources, and obviously “nonmatch” samples can be ruled out and eliminated from additional levels of analysis. If, however, the chromatograms of a spill and candidate source oil are different but the observed differences could possibly be caused by weathering, a “weathering check” is recommended.

6.4.1.2 Effect of Weathering on the GC-FID Profiles

When petroleum products are released into the marine environment, they are immediately subject to a wide variety of changes in physical and chemical properties that are termed as “weathering.” The most important weathering processes include evaporation, dissolution, dispersion, and microbial degradation. In the short term, evaporation is the most important and dominant weathering process.

Several tools can be used to estimate the weathering extent of the samples from the data of the GC-FID analysis.



Ratio name	Definition
C17/Pr	<i>n</i> -Heptadecane/pristane
C18/Ph	<i>n</i> -Octadecane/phytane
Pr/Ph	Pristane/phytane

FIGURE 6.9 Gas chromatograms of a crude oil with two different columns. Numbers over the peaks indicate the carbon atoms of the *n*-alkane series. The insert shows the expanded pristane (Pr)/phytane (Ph) section.

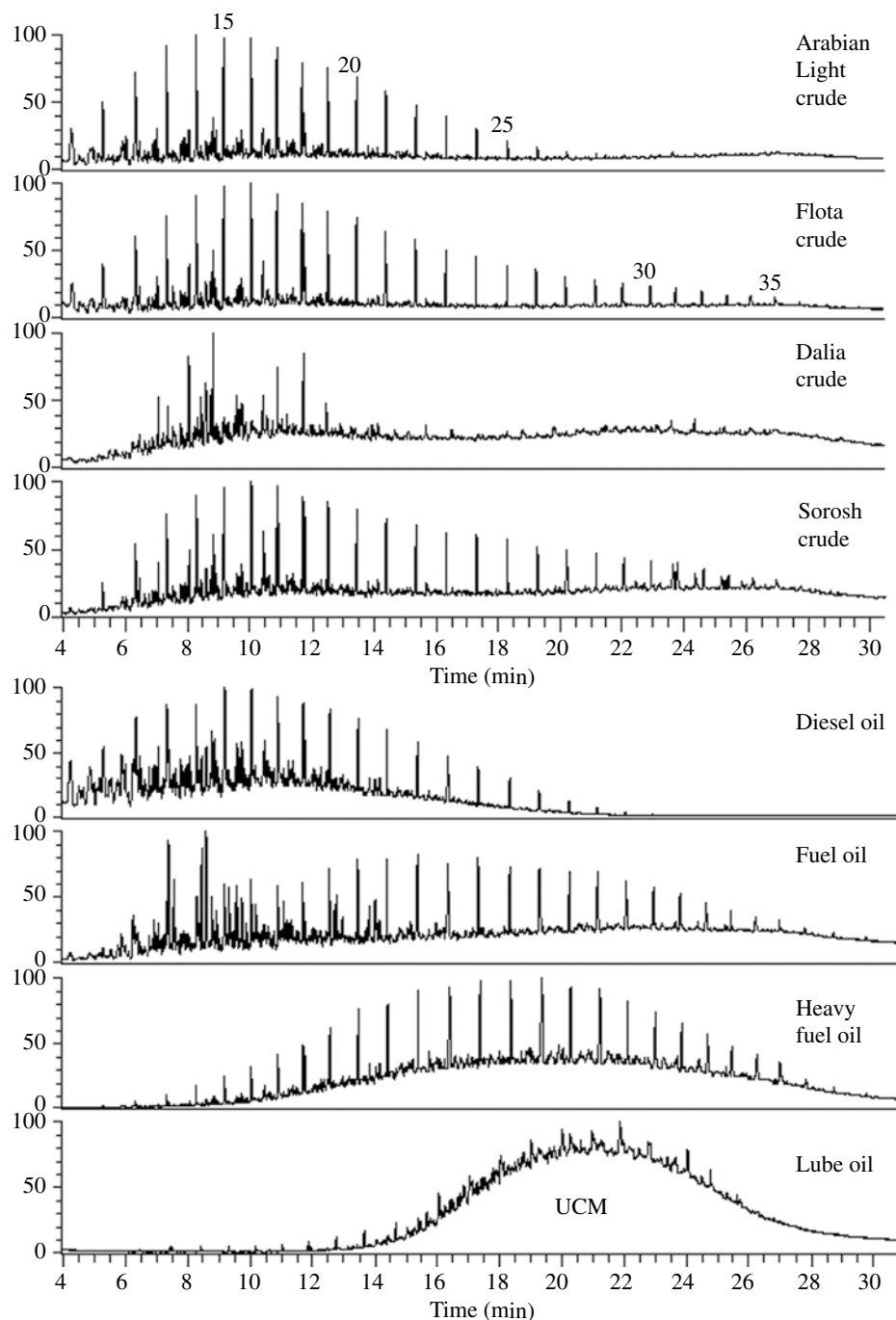


FIGURE 6.10 Examples of GC-FID chromatograms of different crude oils and products. Numbers over the peaks indicate the carbon atoms of the *n*-alkane series.

Figure 6.12 gives examples of the main modifications produced in the GC profiles as a result of two weathering processes. In both cases, the processes have been simulated in the laboratory to enhance the effect. In the first case (a), evaporation gives rise to the loss of the more volatile fraction ($<C_{15}$), whereas in the second (b), biodegradation leads to the loss of the *n*-alkanes.

A strong sign of evaporative loss is the steady decrease of the *n*-alkanes with decreasing carbon number. Figure 6.12a illustrates this process, and it can be concluded that the

difference is caused by evaporative weathering up to C_{18} . As such, DRs relying upon compounds boiling below C_{18} are likely altered by weathering. This must be taken into account when the unweathered source sample is compared to the weathered spill sample.

A “weathering check” can be carried out by a simple overlay of chromatograms of a spill sample and a suspected source. The normalization/manipulation of chromatograms to a comparable attenuation of the nonweathered part in the chromatogram can easily be done, for example, in

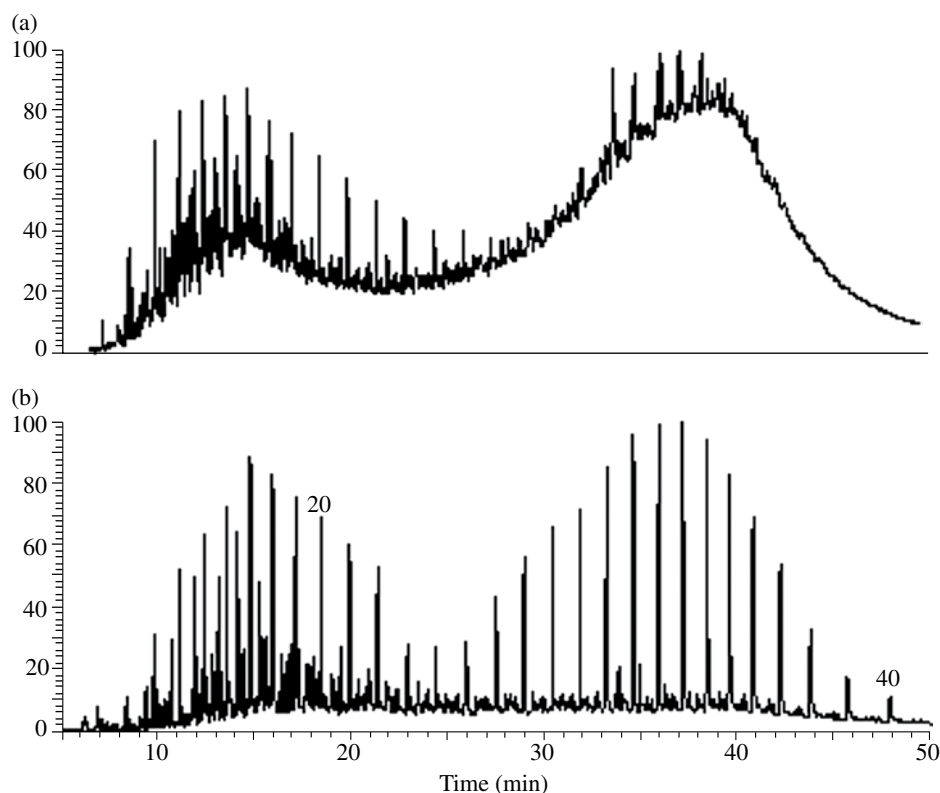


FIGURE 6.11 Examples of GC-FID chromatograms of (a) bilge oil and (b) tanker washing.

PowerPoint™ by expanding one of the chromatograms vertically until the peaks in the range C20–C24 are of the same height (Fig. 6.13). A simple “weathering check” can also be done by measuring peak heights or integrating areas of the homologous series of *n*-alkanes in the GC-FID chromatogram and displaying the sample comparison in bar charts normalized to nonweathered compounds (e.g., the mean of *n*-C20–*n*-C24). Figure 6.14a gives the result of such a bar chart obtained from the example shown in Figure 6.13.

Another way of presenting the data in Figure 6.14a is shown in Figure 6.14b (percentage weathering (PW) plot). In this case, the results are normalized to a compound present in both samples, either the mean of *n*-C20–C24 or 17 α (H),21 β (H)-hopane, and compared as follows:

$$\%C_{N_{\text{spill}}} = \frac{C_{N_{\text{spill}}} / C_{\text{Hopane spill}}}{C_{N_{\text{source}}} / C_{\text{Hopane source}}} \times 100\%$$

After this calculation, the percentage remaining of an alkane, or any other compound in the spill sample, can be calculated when compared to the source sample. For example, C20 in the spill sample is still at the same peak height as in the source sample, so that it is shown as 100% (or 0% loss). Conversely, C15 appears to be 35% with respect to the source, indicating a loss of 65%. The results for the higher alkanes are less accurate because they represent small peaks with a higher variance in analysis and peak integration.

The acyclic isoprenoid ratios *n*-C17/pristane, *n*-C18/phytane, and pristane/phytane are also important source DRs that can be determined in the GC-FID chromatograms. However, if the spill sample is too weathered (as in the examples shown in Figure 6.11) or if the concentrations of these compounds in a sample are low relative to the UCM, for example, as in many lubricating oils or heavy fuel oils (HFOs), these ratios are less reliable. C17 and pristane and also C18 and phytane are in the normal way influenced by evaporation, whereas biodegradation preferentially affects C17 and C18 compared to pristane and phytane.

If the comparison of the GC-FID chromatograms of the spill samples with the candidate source samples reveals differences in the hydrocarbon distributions not caused by analytical inaccuracy (i.e., above the RSD) or by weathering, the analysis may be concluded at this point, since nonmatch has been established. If, however, there are any doubts about the conclusions, the samples should still be considered as potential sources and analyzed in accordance with Level 2 of the flowchart (Fig. 6.8).

In order to test whether a difference in two measured values is significant or not, the analytical error of the method used is needed. Performing a validation test with a reference oil sample, a good system, and careful integration can easily lead to RSDs of 3% or lower for some of the DRs. However, based on the experience of several labs and the results of several intercomparison tests [18,19], a default value of 5% RSD has been adopted. Laboratories should therefore ensure that an RSD of 5% for all relevant normative ratios of the duplicate analyses within an oil case is not exceeded.

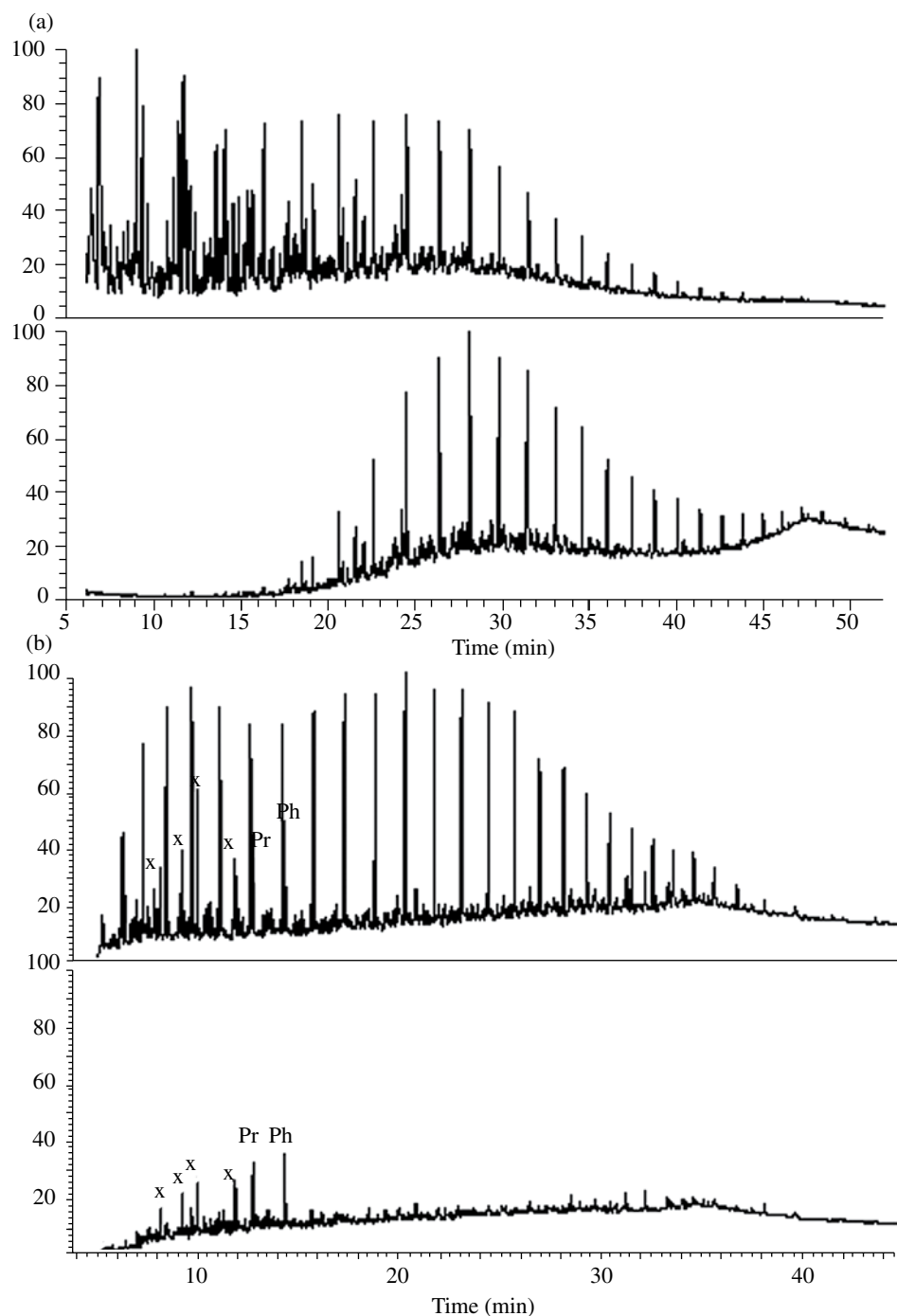


FIGURE 6.12 Effect of (a) evaporation and (b) biodegradation on the GC profiles of oil products. X, acyclic isoprenoids; Pr, pristane; Ph, phytane.

6.4.2 Characterization by GC-MS: Level 2

At Level 2, the spill and candidate source samples are analyzed using computerized GC-MS. This GC-MS analysis enables the separation, identification, and quantitation of a suite of diagnostic petroleum molecular markers and target PAH analytes that are usually undetectable by GC-FID. The utility of these series of compounds for oil characterization lies on the combination of their source specificity and their lower susceptibility to weathering.

6.4.2.1 Overall Characterization By using selected ion monitoring, distributions of specific groups of components can be retrieved from a single GC-MS run of an oil sample and used for comparison purposes. Besides *n*-alkanes and acyclic isoprenoids (m/z 85), molecular markers are easily identified using characteristic fragment ions. These include *n*-alkylcyclohexanes (m/z 82), bicyclic sesquiterpanes (m/z 123), triterpanes (m/z 191), steranes (m/z 217/218), and their mono- and triaromatic counterparts (m/z 253 and 231, respectively).

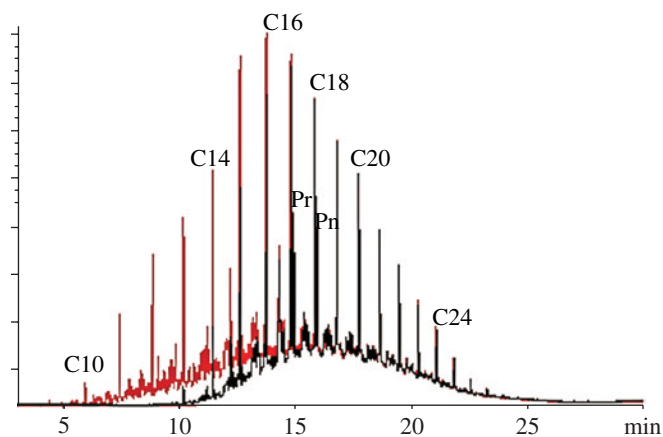


FIGURE 6.13 Overlays of chromatograms from an investigation dealing with gas oil. In black is the spill sample showing a gradual loss of lighter compounds.

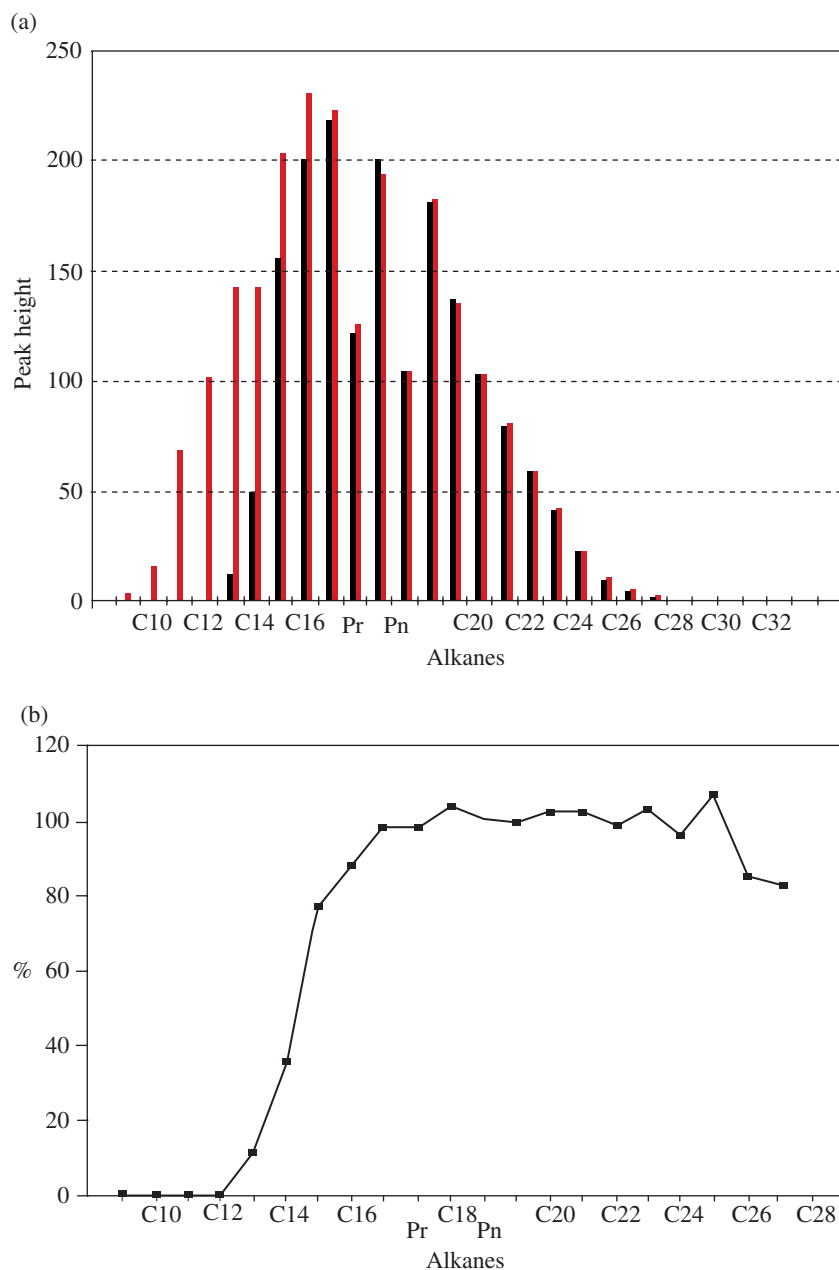


FIGURE 6.14 (a) Bar graph of the alkane peak areas of Figure 6.13 normalized relative to the mean of *n*-C20–C24. (b) PW plot: relative intensity in % of the *n*-alkanes of the spill sample compared to the *n*-alkanes of the source sample after normalization relative to the mean areas of *n*-C20–C24.

On the other hand, a series of homo- and heteroatomic aromatic hydrocarbons can also be used, including *n*-alkylbenzenes (m/z 92) and toluenes (m/z 106), alkylated naphthalenes (m/z $128 + 14n$), phenanthrenes (m/z $178 + 14n$), pyrenes (m/z $202 + 14n$), and chrysenes (m/z $228 + 14n$), as well as sulfur and nitrogen derivatives like dibenzothiophenes (m/z $184 + 14n$) and carbazoles (m/z $167 + 14n$), where n represents the carbon number of the alkyl group.

Comprehensive descriptions of the origin and geochemical significance of these chemical markers can be found elsewhere [13] and will not be reported here. Examples of ion chromatograms with peak identity of these compounds are given in Figures 6.15, 6.16, and 6.17.

In principle, the analysis of the results may begin with a visual inspection of the extracted ion chromatograms of the *n*-alkanes and *n*-alkylcyclohexanes and alkylbenzenes to characterize the boiling range of the spilled oil and the possible presence of mixtures of different petroleum products. The utility of the alkyl derivatives lies in their greater resistance to biodegradation, so they may provide similar information of *n*-alkanes when the samples are moderately weathered. Moreover, in most oils, the profile of the *n*-alkyltoluenes (m/z 106) exhibits a prominent peak, corresponding to an isoprenoid derivative [33,34], that can be compared with the C30-hopane as a complementary DR for source recognition.

Then, the profiles of biomarkers (at least the ions m/z 191, 217, and 231) and the PAHs (at least the methylphenanthrenes (MPs), m/z 192; methylfluoranthenes/pyrenes, m/z 216; and C4-phenanthrenes and benzonaphthothiophene, m/z 234) may serve to identify any obvious nonmatching samples and to determine if the oil spill exhibits any particularly diagnostic features that could be useful in its comparison with candidate sources.

For any of the candidate source samples that cannot be clearly ruled out as possible sources, a more in-depth characterization is necessary, based on the quantitative assessment of the biomarkers and PAHs and the calculation of compound ratios.

If two oil samples are identical, their chemical composition will be the same, apart from those changes experienced by the spilled oil as a result of weathering or contamination (mixing). Thus, measured ratios between any pair of compounds unaffected by weathering or contamination should ideally be the same, up to a certain statistical analysis-related confidence level as discussed in the following.

DRs Calculation and Match Criterion DRs between two different peaks (*A* and *B*) can be based on the formula

$$DR = A/B; \quad \text{or}$$

$$DR = A/(A + B) \text{ (or in \% : } 100 \times A/(A + B) \text{)}$$

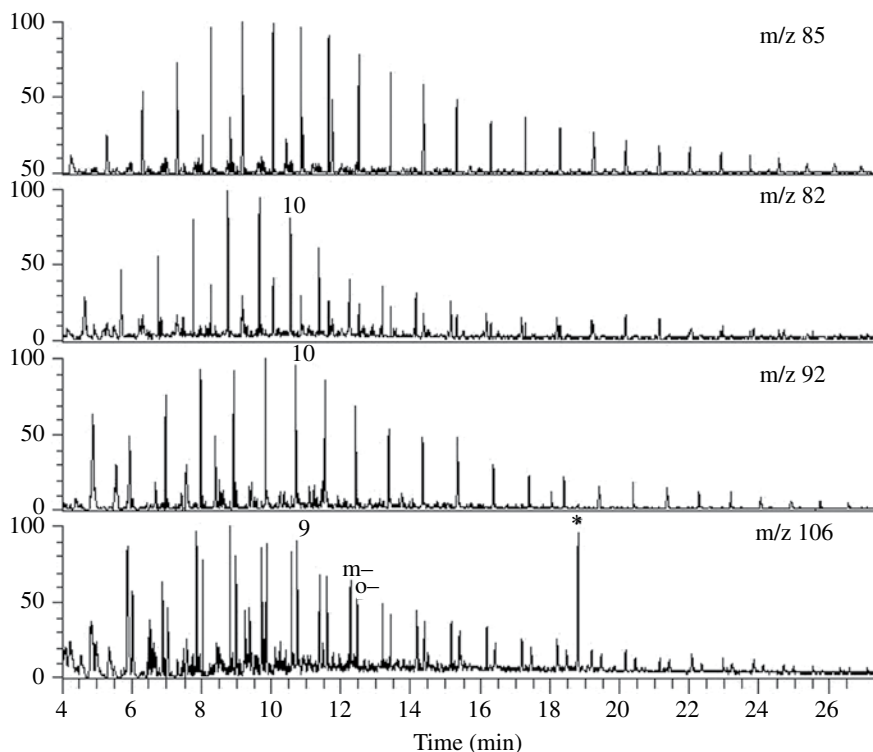


FIGURE 6.15 Ion chromatograms of *n*-alkanes (m/z 85), *n*-alkylcyclohexanes (m/z 82), *n*-alkylbenzenes (m/z 92), and *n*-alkyltoluenes (m/z 106). Numbers over the peaks indicate the number of carbon atoms of the alkyl chain. The *m*- and *o*-methyl isomers are also identified as well as the isoprenoid derivative, 1-methyl-3-phytylbenzene (*). The fragments at even m/z number are selected for their higher specificity for the *n*-alkyl-substituted derivatives.

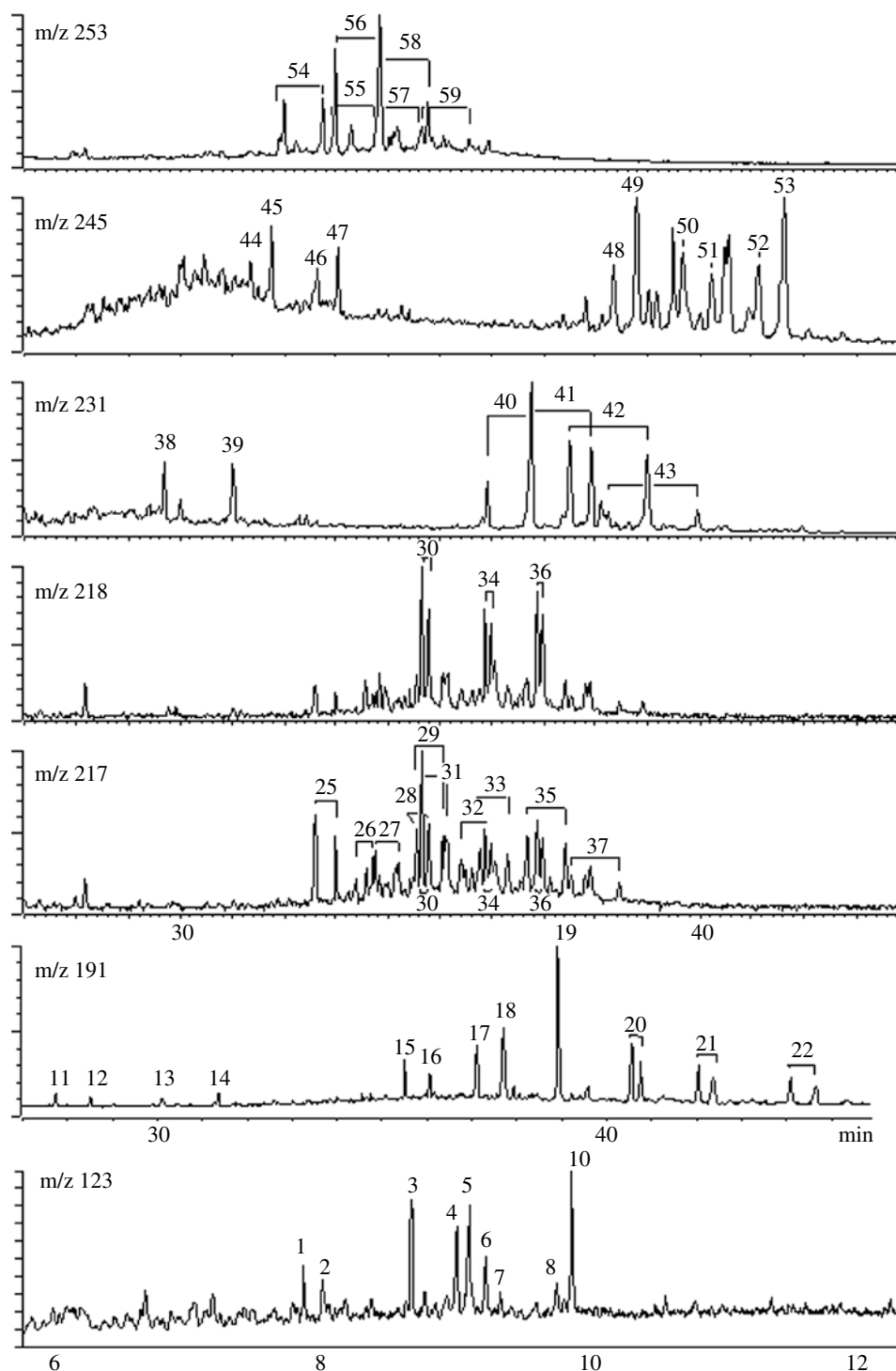


FIGURE 6.16 Ion chromatograms of the diagnostic molecular markers of an oil. Numbers correspond to the structures listed in Table 6.3.

In principle, the use of these types of ratio calculations poses no problem if the RSD is known, but for general comparisons it is more convenient to rely upon a fixed RSD as a standard. In this respect, the result of the ratio formula A/B has a fixed RSD, independently of the individual values of A and B , whereas the $A/(A+B)$ formate yields a ratio-dependent RSD, although it has the benefit of normalizing values

between 0 and 1 (or 0 and 100). Hence, the use of the ratio A/B is recommended.

The maximum RSD of a DR for which the involved peaks are clearly above detection limit ($S/N > 3$) has been defined as 5% by the CEN working group and has been tested in a range of round robin tests (e.g., 18, 19) and real cases. Measured higher values during a validation test with

TABLE 6.3 Identification of individual components of mass fragmentograms in Figure 6.16

GC-MS	Peak label	Compound ^a	Carbon number	Structure ^b
m/z 123	1–2	Nor-drimane	C14	Ia , R=H
	3–6	Drimane	C15	Ia , R=CH ₃
	7–10	Homodrimane	C16	Ia , R=C ₂ H ₅
m/z 191	11.	Tricyclic terpane (13 β , 4 α)	C23	Ib , R=i-C ₄ H ₉
	12.	Tricyclic terpane (13 β , 4 α)	C24	Ib , R=i-C ₅ H ₁₁
	13.	Tricyclic terpane (13 β , 4 α)	C25	Ib , R=i-C ₆ H ₁₃
	14.	17,21-Secohopane (TT)	C24	II
	15.	18 α (H)-22, 29, 30-trisnorneohopane (Ts)	C27	III
	16.	17 α (H)-22, 29, 30-trinorhopane (Tm)	C27	IV , R=H
	17.	17 α (H), 18 α (H), 21 β (H)-28, 30-bisnorhopane	C28	V
	18.	17 α (H), 21 β (H)-30-norhopane	C29	IV , R=C ₂ H ₅
	19.	17 α (H), 21 β (H)-30-hopane	C30	IV , R=i-C ₃ H ₇
	20. S, R	17 α (H), 21 β (H)-homohopane (22S and 22R)	C31	IV , R=i-C ₄ H ₉
	21. S, R	17 α (H), 21 β (H)-bishomohopane (22S and 22R)	C32	IV , R=i-C ₅ H ₁₁
	22. S, R	17 α (H), 21 β (H)-trishomohopane (22S and 22R)	C33	IV , R=i-C ₆ H ₁₃
	23. S, R	17 α (H), 21 β (H)-tetrakishomohopane (22S and 22R)	C34	IV , R=i-C ₇ H ₁₅
	24. S, R	17 α (H), 21 β (H)-pentakishomohopane (22S and 22R)	C35	IV , R=i-C ₈ H ₁₇
m/z 217	25. S, R	13 β , 17 α (H)-diacholestane (20S and 20R)	C27	VI , R=H
	26. S, R	13 α , 17 β (H)-cholestane (20S and 20R)	C27	VII , R=H
	27. S, R	24-Methyl-13 β , 17 α (H)-diacholestane (20S and 20R)	C28	VI , R=CH ₃
	28. S, R	24-Methyl-13 α , 17 β (H)-diacholestane (20S and 20R)	C28	VII , R=CH ₃
	29. S, R	14 α , 17 α (H)-cholestane (20S and 20R)	C27	VIII , R=H
	30. S, R	14 β , 17 β (H)-cholestane (20S and 20R)	C27	IX , R=H
	31. S, R	24-Ethyl-13 β , 17 α (H)-diacholestane (20S and 20R)	C29	VI , R=C ₂ H ₅
	32. S, R	24-Ethyl-13 α , 17 β (H)-diacholestane (20S and 20R)	C29	VII , R=C ₂ H ₅
	33. S, R	24-Methyl-14 α , 17 α (H)-cholestane (20S and 20R)	C28	VIII , R=CH ₃
	34. S, R	24-Methyl-14 β , 17 β (H)-cholestane (20S and 20R)	C28	IX , R=CH ₃
	35. S, R	24-Ethyl-14 α , 17 α (H)-cholestane (20S and 20R)	C29	VIII , R=C ₂ H ₅
	36. S, R	24-Ethyl-14 β , 17 β (H)-cholestane (20S and 20R)	C29	IX , R=C ₂ H ₅
	37. S, R	24-Propyl-14 α , 17 α (H)-cholestane (20S and 20R)	C30	IX , R=C ₃ H ₇
m/z 231	11.	Pregnane	C20	X , R=H
	12.	20-Methyl pregnane	C21	X , R=CH ₃
	13. S, R	Cholestane (20S and 20R)	C26	XI , R=H
	14. S, R	24-Methylcholestane (20S and 20R)	C27	XI , R=CH ₃
	15. S, R	24-Ethylcholestane (20S and 20R)	C28	XI , R=C ₂ H ₅
	16. S, R	24-Propylcholestane (20S and 20R)	C29	XI , R=C ₃ H ₇
m/z 245	17.	1-Methylpregnane	C21	XII , R=H
	18.	4-Methylpregnane	C21	XIII , R=H
	19.	1,20-Dimethylpregnane	C22	XII , R=CH ₃
	20.	4,20-Dimethylpregnane	C22	XIII , R=CH ₃
	21.	1-Methylcholestane (20R)	C27	XIV , R=H
	22.	4-Methylcholestane (20R)	C27	XV , R=H
	23.	1,24-Dimethylcholestane (20R)	C28	XIV , R=CH ₃
	24.	4,24-Dimethylcholestane (20R)	C28	XV , R=CH ₃
	25.	1-Methyl-24-ethylcholestane (20R)	C29	XIV , R=C ₂ H ₅
	26.	4-Methyl-24-ethylcholestane (20R)	C29	XV , R=C ₂ H ₅
m/z 253	27. S, R	5 β (H)-Cholestane (20S and 20R)	C27	XVI , R=H
	28. S, R	5 α (H)-Cholestane (20S and 20R)	C27	XVI , R=H
	29. S, R	5 β (H)-Methylcholestane (20S and 20R)	C28	XVI , R=CH ₃
	30. S, R	5 α (H)-Methylcholestane (20S and 20R)	C28	XVI , R=CH ₃
	31. S, R	5 β (H)-Ethylcholestane (20S and 20R)	C29	XVI , R=C ₂ H ₅
	32. S, R	5 α (H)-Ethylcholestane (20S and 20R)	C29	XVI , R=C ₂ H ₅

^aBasic structures corresponding to aromatic steranes.^bThe description of the structures is shown in Annex I.

GC-MS, gas chromatography-mass spectrometry.

a reference oil sample, involving at least a duplicate analysis, indicate a poor analytical precision and can lead to false-positive results. In this case, the precision must be improved before oil spill identification analyses can be performed.

The repeatability at 95% of confidence level ($r_{95\%}$) is calculated by multiplying r by 2.8 (ISO 5725, part 6 clause 4.1.2). For $r=5\%$, the repeatability will be $2.8 \times 5\% = 14\%$. So when two samples are analyzed under the defined conditions, the ratios with a r of 5% may not differ more than 14% relative

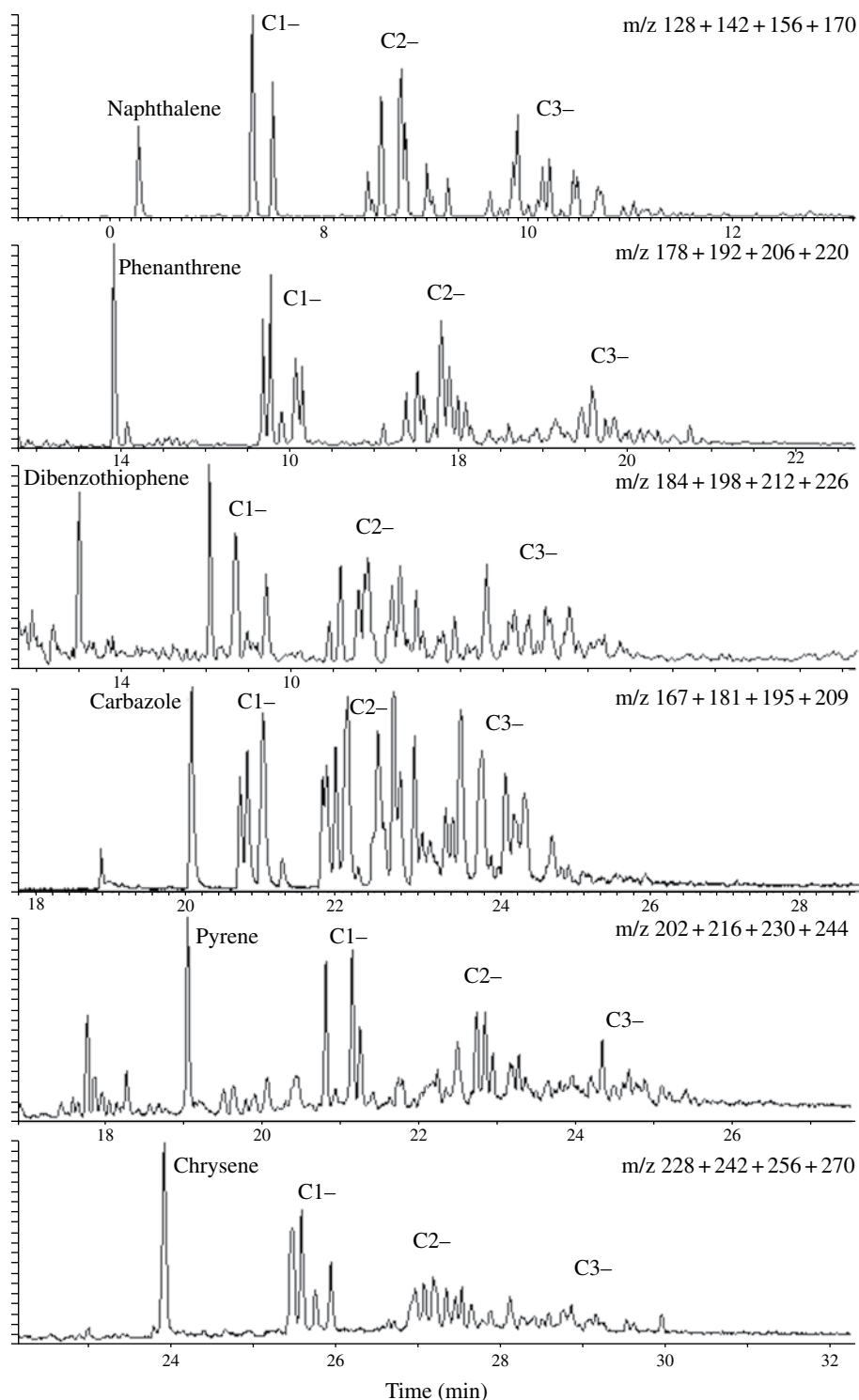


FIGURE 6.17 Ion chromatograms of the diagnostic distributions of alkylated PAHs. Fragment ions correspond to the structures listed in Table 6.4. C1-, C2-, and C3- indicate the alkyl substitution.

[35]. Consequently, any measured difference of two ratios (i.e., the absolute difference in % based on the mean of the two ratios) higher than 14% should be regarded as significant. An example of a ratio comparison is given in Table 6.5.

The ratio comparison is applied to make the method more robust than the qualitative visual comparison of

chromatograms and to make it more independent from the experience of the “oil specialist.” It does, however, not implicate that this comparison is all conclusive. After the mathematical comparison, it is important to compare all chromatograms and ion chromatograms and to jointly use all analytical information for coming to the final conclusion.

TABLE 6.4 Identification of PAH components of mass fragmentograms in Figure 6.17

Rings		m/z	Carbon number	Structure ^a
2	Naphthalene	128	C10	XVII
2	C1-Naphthalenes	142	C11	
2	C2-Naphthalenes	156	C12	
2	C3-Naphthalenes	170	C13	
3	Fluorene	166	C13	XVIII
3	C1-Fluorenes	180	C14	
3	C2-Fluorenes	194	C15	
3	C3-Fluorenes	208	C16	
3	Phenanthrene	178	C14	XIXa
3	Anthracene	178	C14	XIXb
3	C1-Phenanthrenes/anthracenes	192	C15	XX
3	C2-Phenanthrenes/anthracenes	206	C16	
3	C3-Phenanthrenes/anthracenes	220	C17	
3	Retene	234	C18	
3	Dibenzothiophene	184	C12S	XXI
3	C1-Dibenzothiophenes	198	C13S	
3	C2-Dibenzothiophenes	212	C14S	
3	C3-Dibenzothiophenes	226	C15S	
3	Carbazole	167	C12N	XXII
3	C1-Carbazole	181	C13N	
3	C2-Carbazole	195	C14N	
3	C3-Carbazole	209	C15N	
4	Fluoranthene	202	C16	XXIIIa
4	Pyrene	202	C16	
4	C1-Fluoranthenes/pyrenes	216	C17	
4	C2-Fluoranthenes/pyrenes	230	C18	
4	C3-Fluoranthenes/pyrenes	244	C19	XXIVa
4	Benzo[a]fluorene	216	C17	
4	Benzo[b]fluorene	216	C17	
4	Benzo[c]fluorene	216	C17	
4	Benzo[a]anthracene	228	C18	XXVa
4	Chrysene	228	C18	XXVb
4	C1-Chrysenes	242	C19	XXVIa
4	C2-Chrysenes	256	C20	
4	C3-Chrysenes	270	C21	
5	Benzo[b]fluoranthene	252	C20	
5	Benzo[k]fluoranthene	252	C20	XXVIb
5	Benzo[a]pyrene	252	C20	XXVIIa
5	Benzo[e]pyrene	252	C20	XXVIIb
5	Perylene	252	C20	XXVIII
5	Dibenz[ah]anthracene	278	C22	XXIX
6	Indeno[1,2,3-cd]pyrene	276	C22	XXX
6	Benzo[ghi]perylene	276	C22	XXXI

PAH, polycyclic aromatic hydrocarbon.

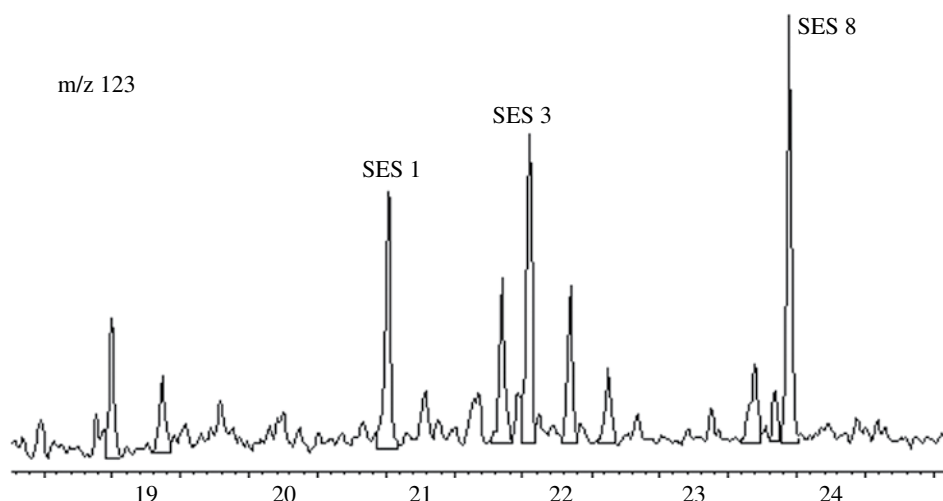
^aThe description of the structures is shown in Annex II.**TABLE 6.5 Example of a ratio comparison based on the repeatability limit**

Ratios to be compared in %		Mean	Absolute difference	Critical difference	Conclusion
Ratio sample 1	Ratio sample 2				
48	52	50	52 – 48 = 4	50 × 14/100 = 7	4 < 7 => No difference
46	54	50	46 – 54 = 8	50 × 14/100 = 7	8 > 7 => Different

The final conclusion of an oil spill investigation should be based on a total evaluation of all analytical results.

DRs of Molecular Markers By making use of the experience gained by petroleum exploration and production geochemi-

stry, combined with the results of an extensive analysis of a large number of oils, several DRs have been selected as technically defensible indices to differentiate among qualitatively similar oils from spills and available sources [15,26,29].



Abbreviation	Name	Ratio name	Definition
SES 0	C ₁₄ H ₂₆ -Sesquiterpanes	DR-SES1/3	SES1/SES3
SES 1	C ₁₅ H ₂₈ -Sesquiterpane	DR-SES2/3	SES2/SES3
SES 2	C ₁₅ H ₂₈ -Sesquiterpane	DR-SES4/3	SES4/SES3
SES 3	C ₁₅ H ₂₈ -8β(H)-Drimane	DR-SES8/3	SES8/SES3
SES 4	C ₁₅ H ₂₈ -Sesquiterpane		
SES 5	C ₁₆ H ₃₀ -Sesquiterpane		
SES 6	C ₁₆ H ₃₀ -Sesquiterpane		
SES 7	C ₁₆ H ₃₀ -Sesquiterpane		
SES 8	C ₁₆ H ₃₀ -8β(H)-Homodrimane		

FIGURE 6.18 Ion chromatogram and recommended diagnostic ratios of sesquiterpanes (m/z 123) (Adapted from CEN/TR 15522-2, reproduced with permission).

In 2005, SINTEF (Norway) composed an oil mixture to give guidance in the recognition of individual compounds and compound groups. The mixture is a combination of three crude oils (from Russia, Sicily, and the North Sea) and a heavy bunker oil (IFO-180). In the following figures (Figs. 6.18, 6.19, 6.20, and 6.21), illustrative profiles of the SINTEF reference oil are shown, together with the identification of the relevant components and the indication of the suggested DRs.

The sesquiterpanes (m/z 123) (Fig. 6.18), eluting at the lower part of the chromatogram, are of particular diagnostic value for the distillate fuels (e.g., diesel oil). Moreover, they dissolve less easily in water compared to the first-eluting PAHs and are rather stable against biodegradation, at least through the complete removal of *n*-alkanes [36], although they can be very easily lost by evaporation.

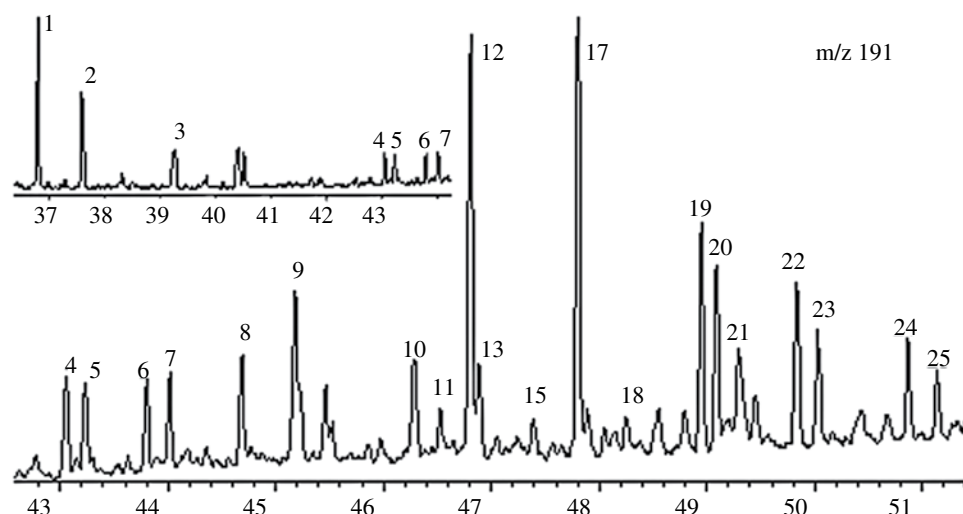
The triterpanes (m/z 191) and steranes (m/z 217/218) have been the first chemical markers proposed by GC-MS fingerprinting of oils [14] as they exhibit high source specificity and resistance to degradation. Moreover, being eluted at the end of the chromatogram, they are hardly affected by evaporation. The most significant component is C30-hopane, which has been proposed as a reference for all DRs because it is highly refractory to weathering [37], although it is almost absent in light refined oil products such as gasoline or diesel oil.

The triterpane profile (Fig. 6.19) exhibits at the lower retention range a number of tri- and tetracyclic terpanes that are unrelated to the pentacyclic terpanes and can provide complementary information for source recognition. Of particular interest are the C23–C25 tricyclic terpanes (peak nos. 1–3), C28–C29 tricyclic terpanes (peak nos. 4–7), and C27-trisnorhopanes (peak nos. 8–9), which are also highly resistant to degradation. Terpanes were found to be of diagnostic value in assessing the *Exxon Valdez* oil spill [38].

The C27–C28–C29 αββ steranes (m/z 218) usually display a characteristic V-shaped profile (Fig. 6.20). A high predominance of the C29 component may indicate a highly weathered residue or the character of a specific oil. In general, marine sediments chronically polluted by oil shows this type of profile [39].

Finally, the triaromatic steroids (m/z 231) (Fig. 6.21) are, in general, much more abundant than the monoaromatic components (m/z 253) and clearly defined. This implies that they are more valuable for oil fingerprinting. Moreover, they are hardly present in lubricating oils as they are devoid of aromatic compounds, so their absence or near absence can be anticipated in bilge oil spills.

However, it is important to realize that this list of analytes and suite of DRs are neither all inclusive nor appropriate for all oil spill identification cases. In some spill cases, it may be

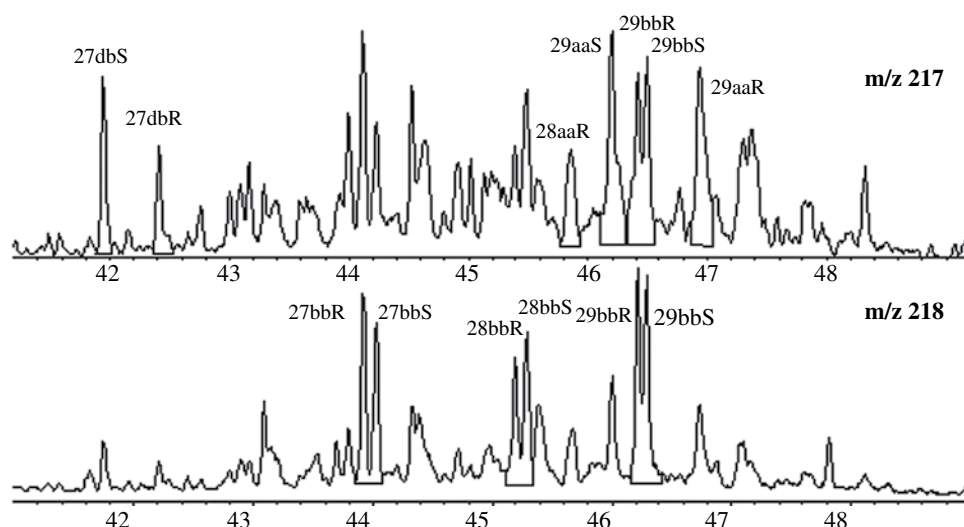


No.	Abbreviation	Name
1	C23Tr	C23 tricyclic diterpane
2	C23Tr	C24 tricyclic diterpane
3	C25Trab	C25 tricyclic diterpane (a + b)
4	C28 (22R)	C28 tricyclic terpene
5	C28 (22S)	C28 tricyclic terpene
6	C29 (22R)	C29 tricyclic terpene
7	C29 (22S)	C29 tricyclic terpene
8	27Ts	18 α (H)-22,29,30-Trisnorhopane
9	27Tm	17 α (H)-22,29,30-Trisnorhopane
10	28ab	17 α (H),21 β (H)-28,30-Bisnorhopane
11	25nor30ab	17 α (H),21 β (H)-25-Norhopane
12	29ab	17 α (H),21 β (H)-30-Norhopane
13	29Ts	18 α (H)-30-Norneohopane
14	30d	15 α -Methyl-17 α (H)-27-norhopane (diahopane) ^a
15	29ba	17 β (H),21 α (H)-30-Norhopane (normoretane)
16	30O	18 α (H)-Oleanane ^a
17	30ab	17 α (H),21 β (H)-Hopane
18	30ba	17 β (H),21 α (H)-Hopane (moretane)
19	31abS	17 α (H),21 β (H), 22S-homohopane
20	31abR	17 α (H),21 β (H), 22R-homohopane
21	30G	Gammacerane
22	32abS	17 α (H),21 β (H), 22S-bishomohopane
23	32abR	17 α (H),21 β (H), 22R-bishomohopane
24	33abS	17 α (H),21 β (H), 22S-trishomohopane
25	33abR	17 α (H),21 β (H), 22R-trishomohopane

Ratio name	Definition	Ratio name	Definition
DR-C28	C28(22S)/30ab	DR-29Ts	29Ts/30ab
DR-27Ts	27Ts/30ab	DR-30d	30d/30ab
DR-27Tm	27Tm/30ab	DR-30O	30O/30ab
DR-28ab	28ab/30ab	DR-30ba	30ba/30ab
DR-5nor30ab	25nor30ab/30ab	DR-31abS	31abS/30ab
DR-29ab	29ab/30ab	DR-30G	30G/30ab

^a Absent in this oil.

FIGURE 6.19 Ion chromatogram and recommended diagnostic ratios of triterpanes (m/z 191) (Adapted from CEN/TR 15522-2, reproduced with permission).



Abbreviation	Name
27dbS	13 β (H),17 α (H), 20S-cholestane (diasterane)
27dbR	13 β (H),17 α (H), 20R-cholestane (diasterane)
28aaR	24-Methyl-5 α (H),14 α (H),17 α (H), 20R-cholestane
29aaS	24-Ethyl-5 α (H),14 α (H),17 α (H), 20S-cholestane
29bbR	24-Ethyl-5 α (H),14 β (H),17 β (H), 20R-cholestane
29bbS	24-Ethyl-5 α (H),14 β (H),17 β (H), 20S-cholestane
29aaR	24-Ethyl-5 α (H),14 α (H),17 α (H), 20R-cholestane
27bbR	5 α (H),14 β (H),17 β (H), 20R-cholestane
27bbS	5 α (H),14 β (H),17 β (H), 20S-cholestane
28bbR	24-Methyl-5 α (H),14 β (H),17 β (H), 20R-cholestane
28bbS	24-Methyl-5 α (H),14 β (H),17 β (H), 20S-cholestane
29bbR	24-Ethyl-5 α (H),14 β (H),17 β (H), 20R-cholestane
29bbS	24-Ethyl-5 α (H),14 β (H),17 β (H), 20S-cholestane

Ratio name	Definition
DR-27dbR	27dbR/27dbS
DR-29aaS	29aaS/29aaR
DR-29bb	29bb(S + R)/29aa(S + R)
DR-27bb	27bb(S + R)/29bb(S + R)

FIGURE 6.20 Ion chromatograms and recommended diagnostic ratios of regular steranes and diasteranes (m/z 217 and 218) (Adapted from CEN/TR 15522-2, reproduced with permission).

practical to include a certain characteristic feature of the spilled oil that is recognized as being particularly diagnostic.

For example, certain oils may contain some **specific biomarker compounds** that can provide additional diagnostic information on the types of original organic matter of the crude oil. For example, the geologically rare acyclic alkane botryococcane ($C_{34}H_{70}$), originated from specific algal remains, was used to identify a new class of Australian non-marine crude oils [40]. The oils from the fields of northern North Sea platforms, including Statfjord, Gullfaks, Brent, Oseberg, etc., seem to be characterized by relative high abundances of C28-bisnorhopane. The presence of this triterpane was of diagnostic value in the case of the *Aegean Sea*

oil spill that involved a Brent crude oil [41]. It was also regarded as a specific source parameter in the case of the *Exxon Valdez* oil spill for differentiating the spilled oil from preexisting oil residues in the area [38].

Oils from the Niger Delta (e.g., Forcados) and from Angola (e.g., Nemba), Congo, and Brazilian marginal basins are characterized by the presence of high abundant oleanane and gammacerane, respectively [42,43]. Gammacerane has been tentatively suggested as a marker for hypersaline episodes of source rock deposition, whereas oleanane is a good indicator of terrestrial input into the oil-prone source rocks deposited in a deltaic environment. The presence of 18 α (H)-oleanane in benthic sediments in Prince William Sound

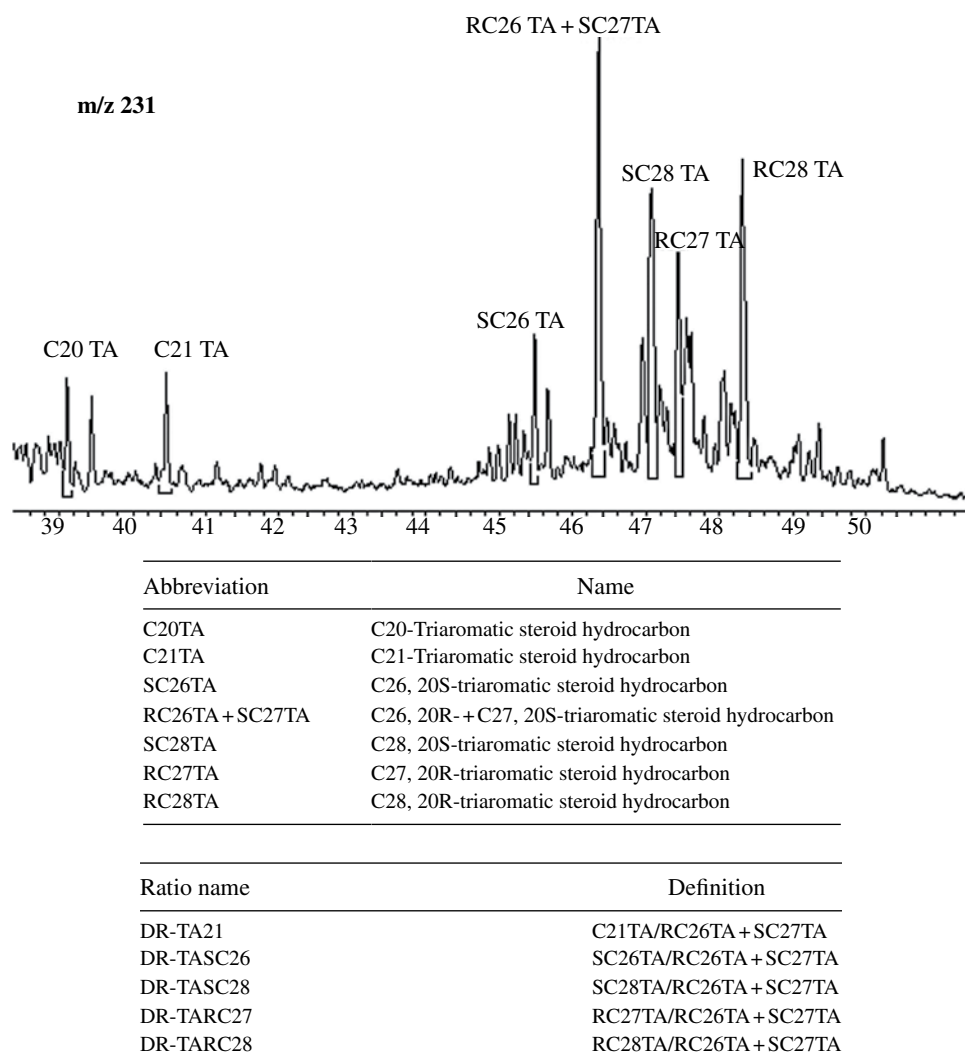


FIGURE 6.21 Ion chromatogram and recommended diagnostic ratios of triaromatic steranes (m/z 231) (Adapted from CEN/TR 15522-2, reproduced with permission).

(PWS), coupled with its absence in Alaska North Slope crude and specifically in *Exxon Valdez* oil and its residues, confirmed another petrogenic source in the region [38]. The pentacyclic triterpanes oleanane, ursane, and lupane are also particularly abundant in some crude oils of continental origin from New Zealand, Taiwan, and Indonesia [44]. Examples of particular distributions of triterpanes are given in Figure 6.22.

Other specific pentacyclic terpanes include C30 17 α (H)-diahopane (potentially related to bacterial hopanoid precursors that have undergone oxidation and rearrangement by clay-mediated acidic catalysis), β -carotane (C₄₀H₇₈, highly abundant in Green River shale), and bicadinanes (believed to indicate inputs from higher plants). Bicadinanes are specific constituents of crude oils from Malaysia, Bangladesh, and Indonesia [45].

Some oils are characterized by unusual abundances of certain markers. Thus, oils from evaporitic source rocks contain higher concentrations of C35 triterpanes [13]. In turn, several California oils contain high concentrations of

steranes with a predominance of the C28 components, and almost all oils from the South China Sea (Pearl River Mouth Basin) contain significant amounts of 4-methylsteranes [46].

DRs of PAHs Crude oils originating from different oil fields may have very different PAH distributions. The most common diagnostic PAH families are the dibenzothiophenes (DBTs) and the phenanthrenes (P), which can be found in all sample types [47]. Additional ratios have also been suggested among the methylpyrenes and methylfluoranthenes/benzofluorenes because the compounds within this group show a lot of variation between oils. Representative ion chromatograms are shown in Figures 6.23, 6.24, 6.25, and 6.26 as well as the recommended DRs.

The profile of MPs (m/z 192) may be used to differentiate between crude oils and refined products containing residues from cracking processes, such as the commonly used HFO. Cracking is conducted at higher temperatures, and Radke et al. [48] demonstrated that with increased thermal stress

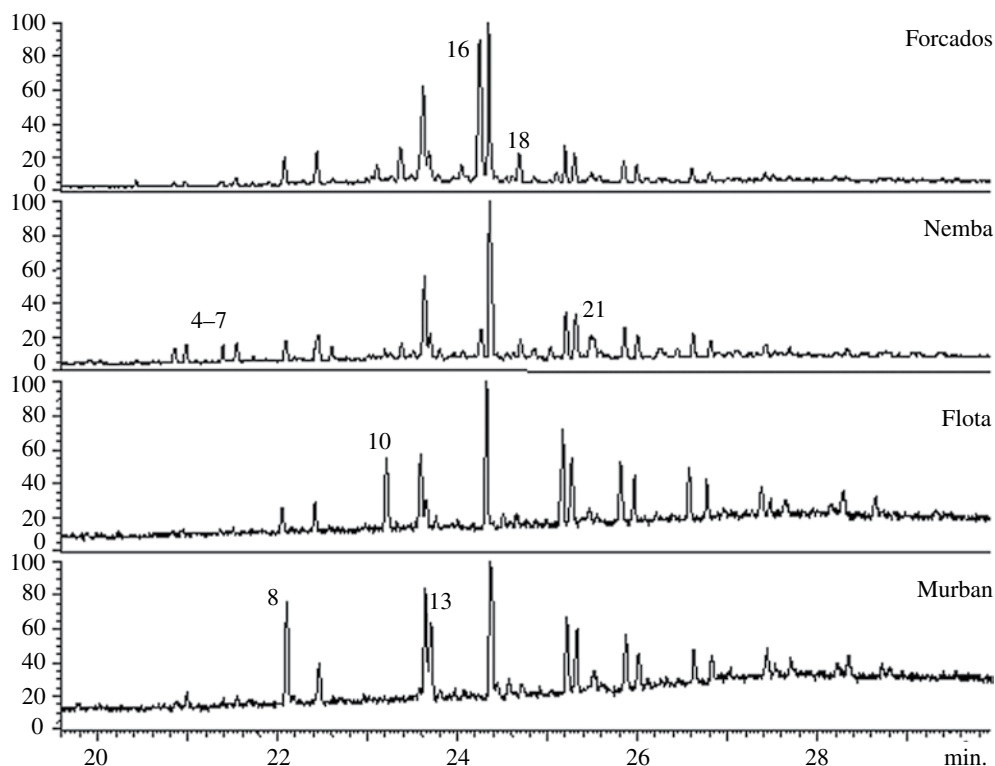


FIGURE 6.22 Triterpane distributions of Forcados (Nigeria), Nemba (Angola), Flota (North Sea), and Murban (Emirates) crude oils. Numbers correspond to the identifications given in Figure 6.19.

there is a shift of methyl substituents from α - to β -positions. Thus, modern heavy bunker fuel oils blended to contain cracked intermediates are relatively enriched in the 2- and 3-methyl isomers, as shown in Figure 6.23. These also exhibit a higher content of methylanthracene (MA). However, some caution is necessary when applying these ratios for oil spill identification because the 2- and 3-methyl isomers are also more easily affected by environmental conditions (see Section 6.4.2.2).

The aromatic compound cluster given by mass 216 (methylpyrenes, fluoranthenes, and benzofluorenes) may also give valuable diagnostic characteristic features, which has shown to be especially suitable, as in the case of MPs, for comparing crude oils and HFOs, the latter being particularly enriched in methylfluoranthenes and benzofluorenes (Fig. 6.24). This cluster is also useful for characterizing middle distillates (e.g., diesel oil or cutter stock oil), which are usually mixed with heavier fractions for adjusting their physicochemical properties.

The DR BNT/T-M-P informs about the sulfur content of the spill (Fig. 6.25). Many labs routinely determine the concentrations of dibenzothiophenes for this purpose and calculate the ratios C2-DBT/C2-P and C3-DBT/C3-P for oil source recognition (Fig. 6.26) [47].

PAHs are common not only in petroleum but also in other products, like coal tar and creosote, and in most environmental matrices as they are widespread contaminants. Therefore, this should be taken into consideration when

using PAHs in source recognition studies. They can be easily distinguished on the basis of their alkyl group distributions. The petrogenic profiles (Fig. 6.17) present in crude oils form a characteristic pattern with a relatively high abundance of alkylated species (C1-, C2-, etc.), whereas pyrogenic sources are highly dominated by the parent compounds.

Several DRs have been proposed to differentiate petrogenic from other hydrocarbon sources, by exploiting the aforementioned differences in the degree of alkylation. Wang et al. [49] proposed a “pyrogenic index” (PI), defined as the ratio of the total concentration of EPA priority 3- to 6-ring PAHs to the total concentration of five alkylated PAH homologues:

$$PI = \Sigma(3\text{- to }6\text{- ring EPA PAHs}) / \Sigma(5\text{ alkylated PAHs})$$

The PI versus Ph/A values for over 100 oils and refined products have been reported [45]. It was found that lighter refined products and most crude oils show PI ratios lower than 0.01, whereas heavy oils and HFOs show higher PI ratios (e.g., 0.01–0.05). In turn, ratios in the range of 0.8–2 are found for pyrogenic products. The usefulness of this index has been shown in several spill case studies [50,51].

To identify any potential source samples as “nonmatches” with the spill sample(s), a distinct chromatographic pattern or just one distinct DR (unaffected by weathering or mixing) can be sufficient. However, in order to prove identity or “positive match,” all chromatographic patterns and ratios (unaffected by weathering or mixing) should be the same,

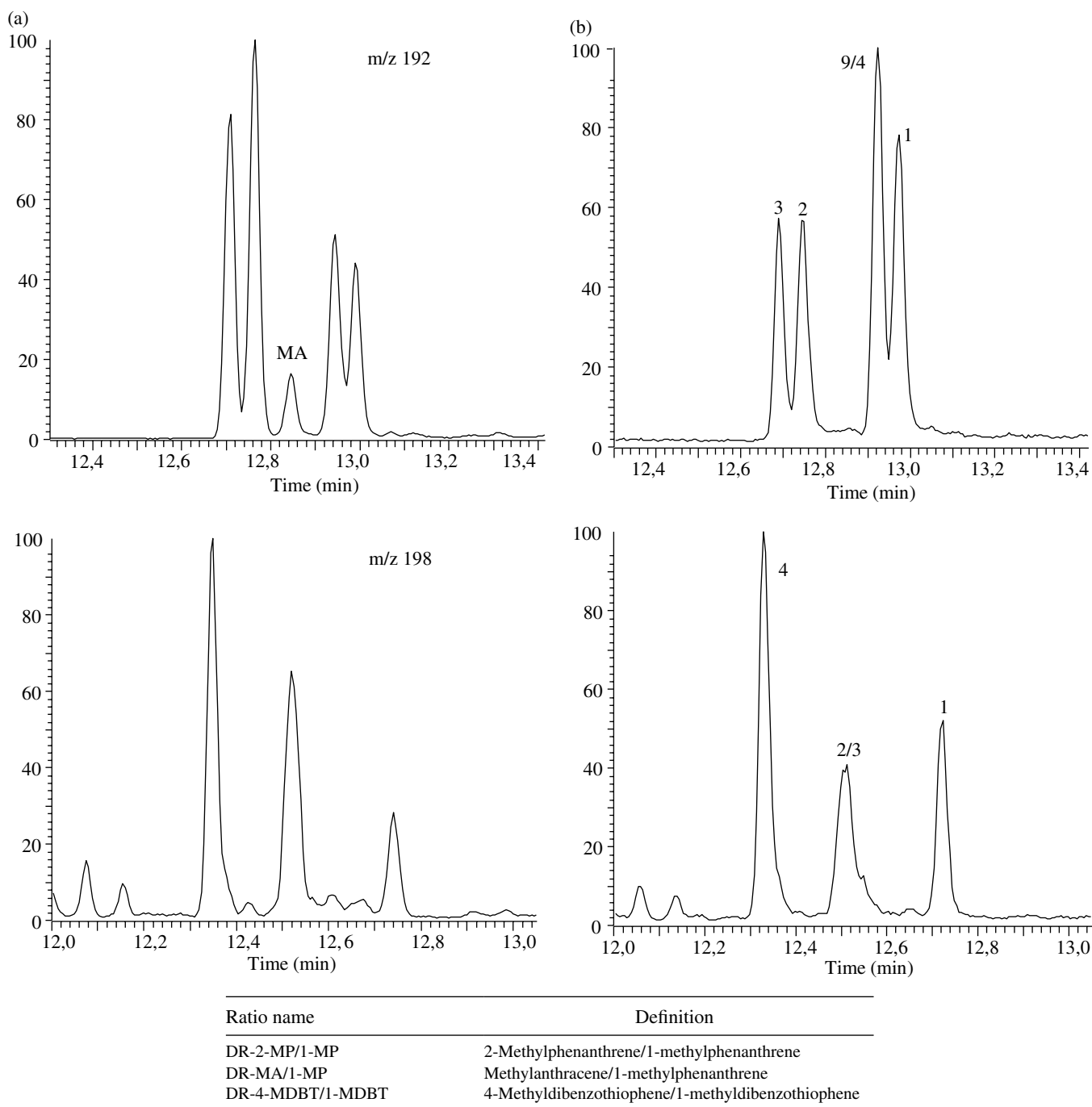


FIGURE 6.23 Ion chromatograms and recommended diagnostic ratios of methylphenanthrenes (m/z 192) and methyldibenzothiophenes (m/z 198) from a heavy fuel oil (a) and a crude oil (b).

which is within the statistical variability of the method, as discussed earlier. To make the mathematical comparison test useful, a set of DRs are needed to represent the different “aspects” of the particular type of oil spilled.

A summary of a set of oil type-specific recommended DRs is shown in Table 6.6. The selection in Table 6.6 should be treated as a minimum—normative—list, which can be extended with appropriate ratios or from the peer-reviewed literature according to the available information. In this respect, if the spill exhibits any particular features not represented by existing

ratios, like the specific molecular markers present in some oils, it is possible to introduce new DR(s) that reflect those features.

Cross-Plots of DRs for Spill Source Identification In particular cases, when a large number of samples need to be compared with a specific source, cross-plots of two DRs may be of primary assistance. Gürgey [52] analyzed 56 rock and 28 crude oil samples from the subsalt and suprasalt section of the southern pre-Caspian Basin. Based on plots of C24/C26T (C24 tetracyclic/C25 tricyclic terpanes) versus C29/C30

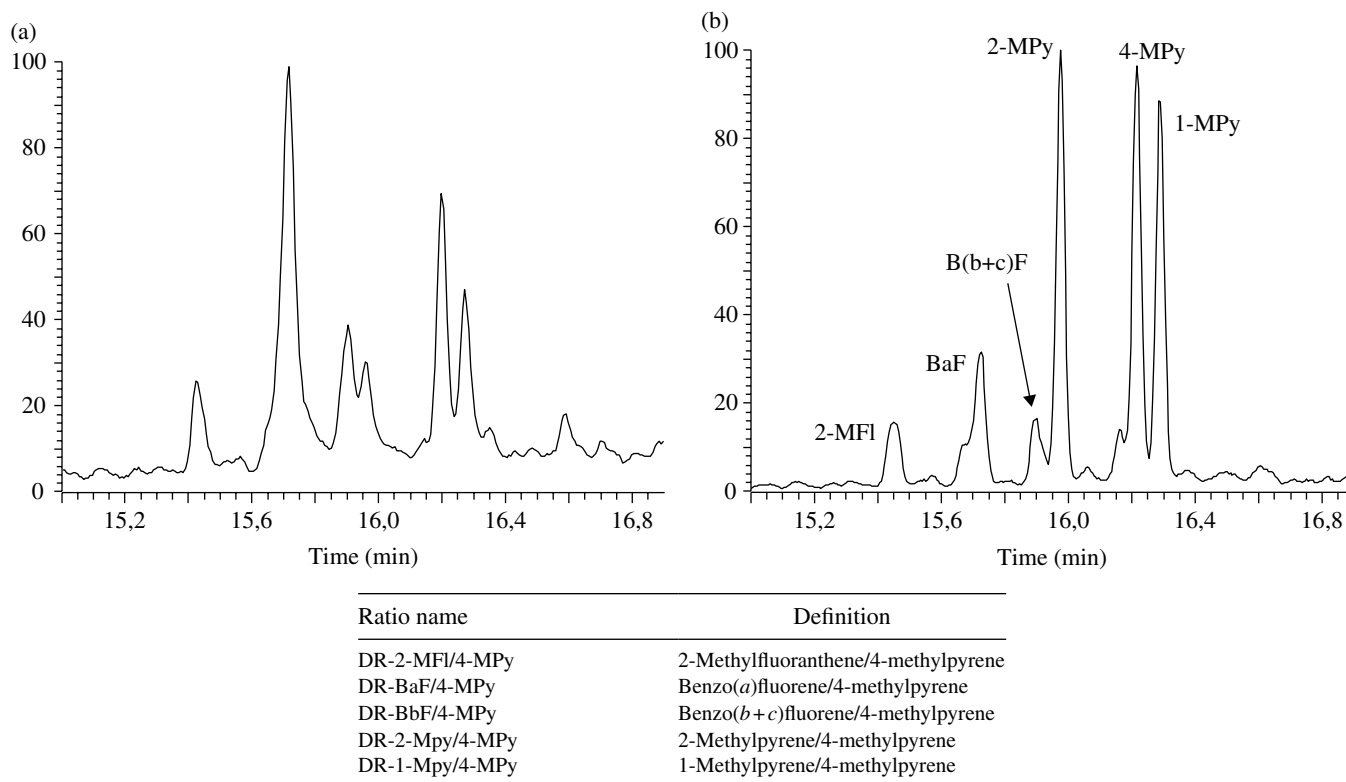


FIGURE 6.24 Ion chromatograms and recommended diagnostic ratios of C1-fluoranthenes/pyrenes (m/z 216) from a heavy fuel oil (a) and a crude oil (b).

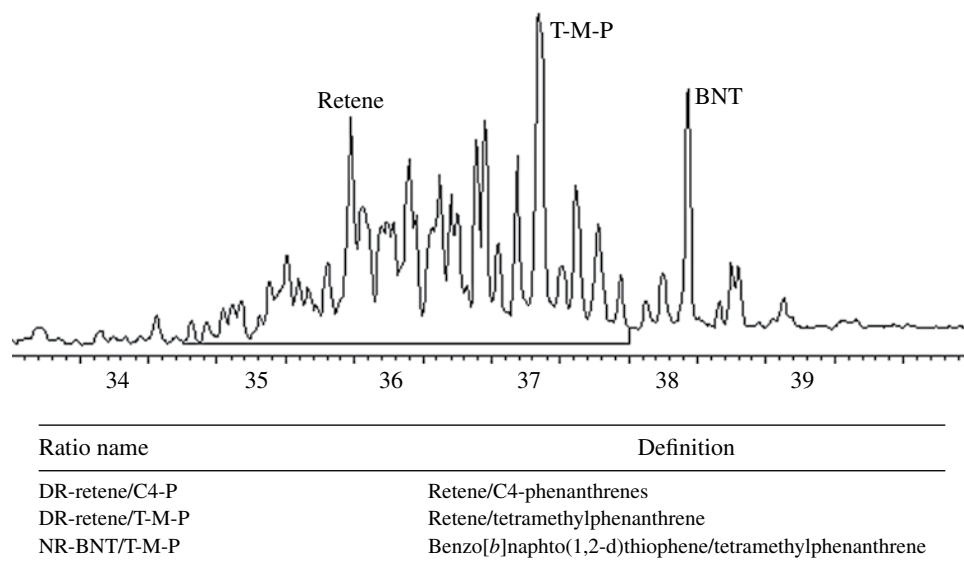


FIGURE 6.25 Ion chromatogram and recommended diagnostic ratios of C4-phenanthrenes, benzo[b]naphtho(1,2-d)thiophene, and retene (m/z 234).

hopane, the author illustrates a clear separation between the two populations.

Based on chemical evidence that Middle East crude oils were characterized by C29 $17\alpha,21\beta$ -norhopane and C31–C35 homohopanes, whereas these compounds were depleted in Southeast Asian crude oils, Zakaria et al. [53,54] proposed the utility of the cross-plots of C29 $\alpha\beta$ /C30 $\alpha\beta$ hopane ratio versus

the homohopane index $\Sigma(C31-C35)/C30$ hopane as key biomarker indicators and successfully distinguished a large number of tar ball samples that originated from Southeast Asian crude oil sources from those of Middle East sources.

Zhang et al. [46] classified crude oils from the eastern Pearl River Mouth Basin into groups based on cross-plots of relative abundances of various isomeric sesquiterpanes (at m/z 123)

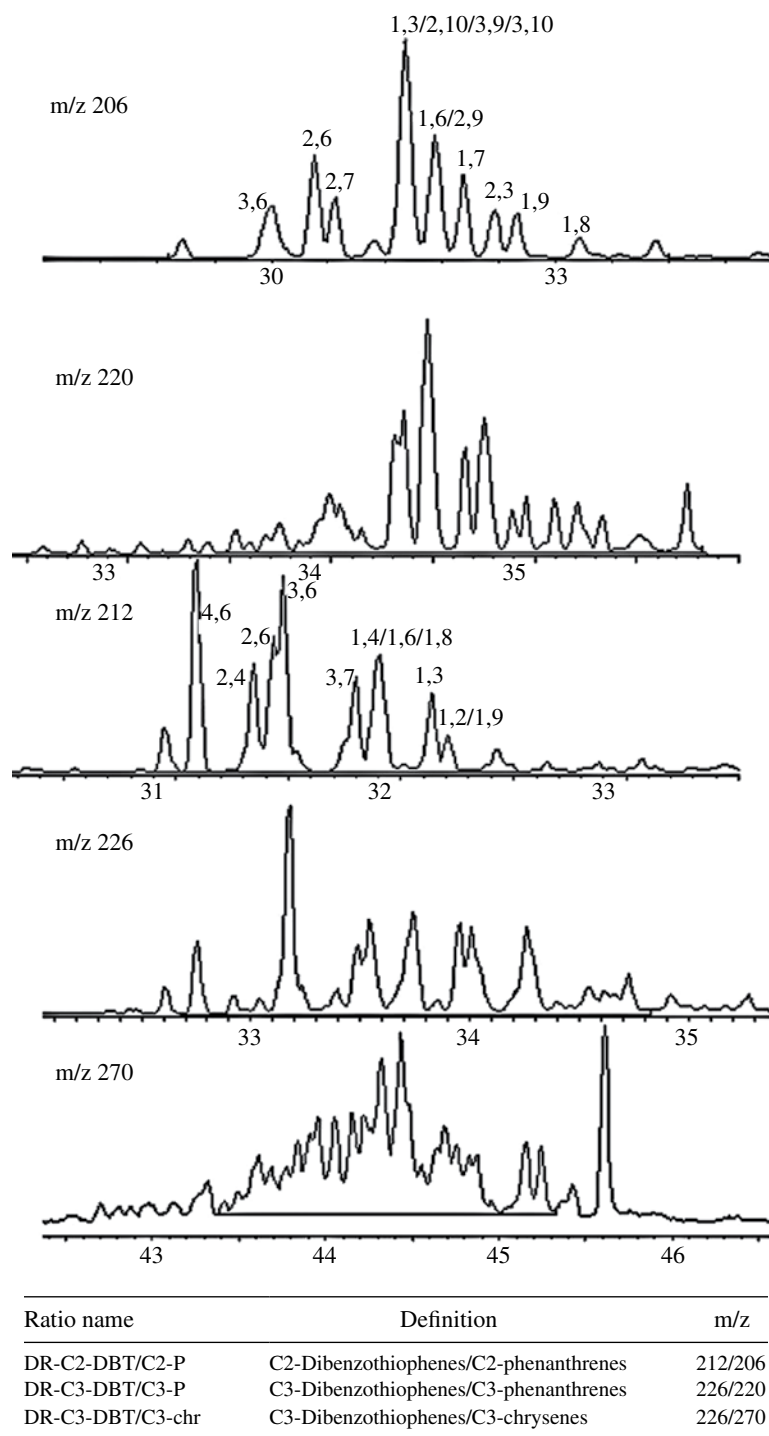


FIGURE 6.26 Ion chromatograms and recommended diagnostic ratios of C2- and C3-phenanthrenes (m/z 206 and 220), C2- and C3-dibenzothiophenes (m/z 212 and 226), and C3-chrysenes (m/z 270).

versus relative abundances of bicadinanes to C30 hopane on the m/z 412 mass chromatogram (bicadinane-T/C30-hopane). On the other hand, using the cross-plots of the sesquiterpane ratios peak 4/peak 5 versus peak 3/peak 5 (Fig. 6.18), Wang et al. [55] were able to separate a large number of crude and weathered oils and refined products (Fig. 6.27a), each weathering oil series producing a tight cluster.

As indicated earlier, the ratios C3-DBT/C3-P and C2-DBT/C2-P, which are rather conservative, have been proposed for oil source recognition [47]. In Figure 6.27b, the cross-plot of these ratios has been used for differentiating oil samples collected after the *Prestige* oil spill along the Galicia coast (chapter 22 of this book). The figure also shows that besides the cluster of samples attributed to the spill, another cluster of

TABLE 6.6 Normative diagnostic ratios for the CEN/Tr method

Ratio	Light fuel (LF)	Lube oil (Lub)	Bilge (LF+Lub)	HFO	Sludge (HFO+Lub)	Crude oil
GC-FID						
C17/Pr	×		×		×	×
C18/Ph	×		×		×	×
Pr/Ph	×		×		×	×
GC-MS						
m/z 85						
C17/Pr	×		×	×	×	×
C18/Ph	×		×	×	×	×
Pr/Ph	×		×	×	×	×
m/z 192/198						
2-MP/1-MP	×		×	×	×	×
4-MDBT/1-MDBT	×		×	×	×	×
m/z 216						
2-MFl/4-MPy	×		×	×	×	×
BaF/4-MPy	×		×	×	×	×
BbF/4-MPy	×		×	×	×	×
2-Mpy/4-MPy	×		×	×	×	×
1-Mpy/4-MPy	×		×	×	×	×
m/z 234						
Retene/T-M-P	×		×		×	×
BNT/T-M-P	×		×	×	×	×
m/z 191						
27Ts/27Tm		×	×	×	×	×
27Ts/30ab		×	×	×	×	×
27Tm/30ab		×	×	×	×	×
28ab/30ab		×	×	×	×	×
29ab/30ab		×	×	×	×	×
30O/30ab		×	×	×	×	×
30G/30ab		×	×	×	×	×
31abS/30ab		×	×	×	×	×
m/z 217/218						
27dbR/27dbS		×	×	×	×	×
27bb/29bb		×	×	×	×	×
m/z 231						
SC26TA/RC26TA + SC27TA				×	×	×
SC28TA/RC26TA + SC27TA				×	×	×
RC27TA/RC26TA + SC27TA				×	×	×
RC28TA/RC26TA + SC27TA				×	×	×

CEN, European Committee for Standardization; GC-FID, gas chromatography-flame ionization detection; GC-MS, gas chromatography-mass spectrometry;

HFO, heavy fuel oil.

samples collected close to an urban-industrial area appeared, suggesting a chronic source.

The ratios of the methyldibenzothiophenes (Fig. 6.23) have also been used to successfully discriminate different oil samples [56]. Wang et al. [26] established a database of the ratios of the C1-DBT isomers for several hundred crude, weathered, and biodegraded oils and petroleum products and used the cross-plots 2-/3-methyldibenzothiophene versus 1-methyldibenzothiophene (both isomers normalized relative to 4-methyldibenzothiophene) for differentiating 49 oils and oil products. The plot shows how scattered the data points representing the various oils were and how related oils produced tight clusters on the plot.

Recently, Albaigés et al. [57] have proposed the use of long-chain alkyltoluenes (m/z 106) (Fig. 6.15) for

fingerprinting marine oil wastes. Using the cross-plots of m-/o-C10 toluenes with m-C10/i-C20 toluenes and i-C20 toluene/ $\alpha\beta$ -hopane, they have been able to differentiate a large number of crude oils.

Comparison of DRs Using Multivariate Statistics Multivariate statistical methods like principal component analysis (PCA) may also assist the univariate method described in previous sections in comparing DRs between multiple samples (e.g., [29,58]). Multivariate statistical methods may facilitate the comparison of relationships between multiple samples and variables (e.g., DRs) by visualizing the so-called factor scores and loading plots. Additional advantages include noise reduction, obtained by multiple measurements of the same phenomenon (i.e., interrelated variables), and their ability to detect outliers.

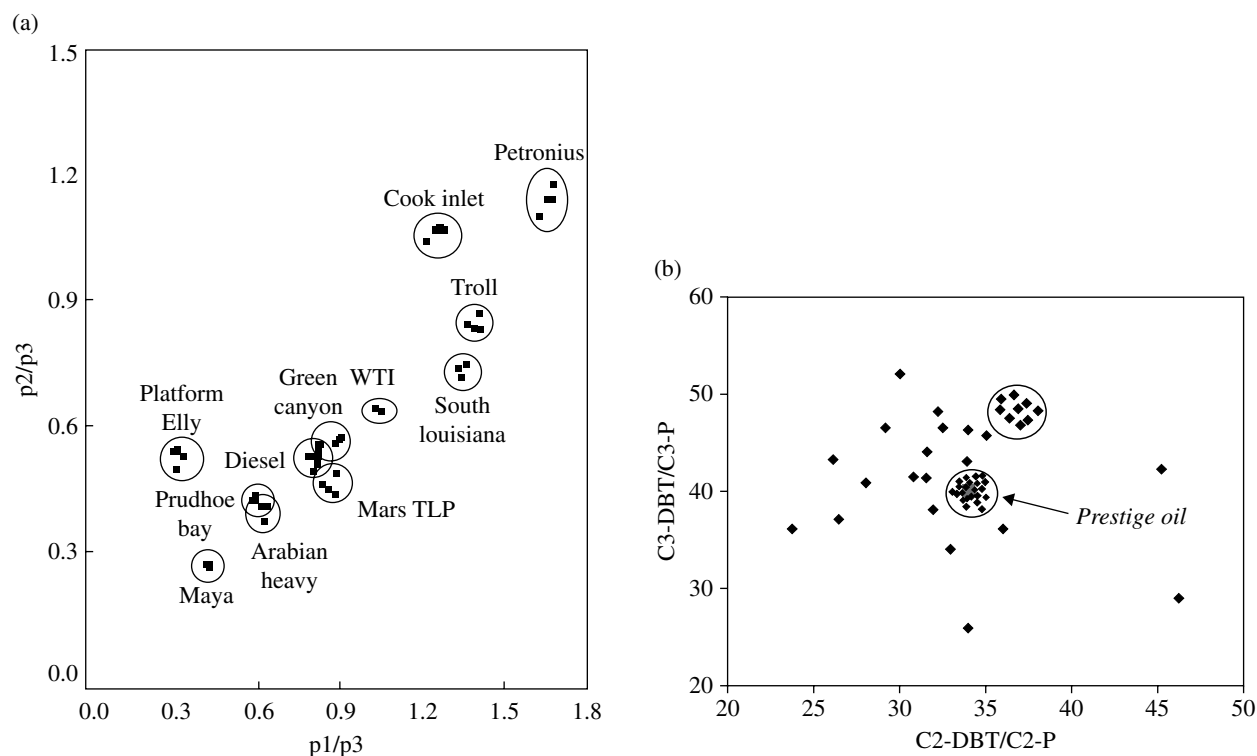


FIGURE 6.27 (a) Cross-plots of the double ratios of sesquiterpane peak 2/peak 3 versus peak 1/peak 3 for 11 weathering oil series and 1 diesel weathering series. (b) Plot of the relative ratios of C2 and C3 alkyl phenanthrenes (P) and dibenzothiophenes (DBT) in stranded oil samples collected after the *Prestige* oil spill.

The fundamentals of PCA as a data treatment tool in chemical fingerprinting are that it summarizes the information in many correlated DRs into a few so-called principal components that are weighted sums of these ratios. Hence, oil samples with similar chemical composition will plot closely in score plots, whereas the opposite is the case for dissimilar oils.

PCA is particularly useful in combination with a database in the prediction of the uniqueness of the samples in a case study. An example of the application of PCA to oil spill characterization is shown by the score plot in Figure 6.28, taken from the COSI database⁴ and analyses conducted at BSH. The data set consisting of 29 DRs of 361 crude oil samples illustrates the large spread of the oil samples, and the excerpt corresponds to a group of very similar Middle East crude oils listed in the table.

The comparison of oil samples by PCA can be further refined by taking into account the uncertainty of the individual DRs. This ensures an objective matching of oil spill samples and suspected sources based on all the available information. In any case, a careful inspection of all the ion chromatograms of a spill/source sample combination is needed before a match can be concluded.

Evaluation of Weathering The loss of *n*-alkanes in the GC profiles, either by evaporation and/or by biodegradation after extensive weathering (Fig. 6.12), has also its complement in the distributions of molecular markers and PAHs. The low-molecular-weight components are primarily lost by evaporation (e.g., sesquiterpanes) or dissolution (e.g., alkyl-naphthalenes). In turn, biodegradation is more dependent on the compounds' structures. Because of their differential resistance to biodegradation, comparisons of their relative ratios can be used to rank oils as to the extent of biodegradation. Similar to this occurs with photodegradation, although the process is less extensive, affecting primarily the PAHs.

Composition Changes of Molecular Markers Literature evidence suggests that pentacyclic triterpanes (*m/z* 191) are relatively conservative molecular markers [13] and *C*₃₀-hopane has been proposed as an internal standard to assess oil weathering in the field [37]. Moreover, the hopane and sterane molecular distributions encompass a number of 22S/R and 20S/R epimeric isomers, respectively, whose ratios usually reach a thermodynamic equilibrium in mature crude oils, being around 0.6 for hopanes and 0.5 for steranes. Therefore, they are in general of limited interest for fingerprinting spilled oils, although they may afford information on the extent of oil biodegradation because of the selective degradation of the natural R configurations over the geochemically formed S isomers [59].

⁴COSI database: computerized oil spill identification database. http://www.bsh.de/en/Marine_data/Environmental_protection/Oil_identification_system/index.jsp.

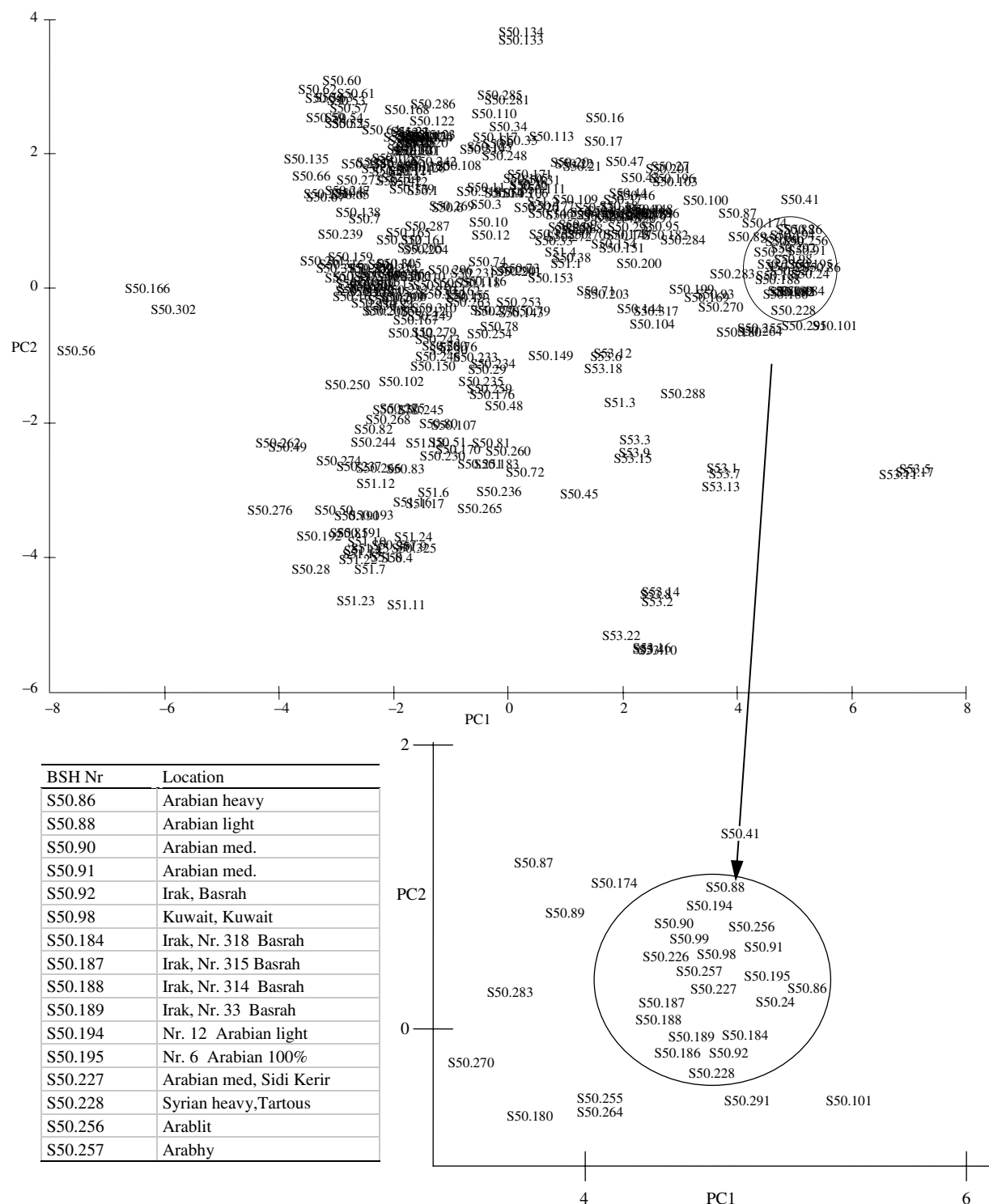


FIGURE 6.28 Score plot of 29 diagnostic ratios of 361 crude oil samples. The oil references in the excerpt are explained in the table.

The sterane and triterpane DRs proposed for oil–source correlation given in Figures 6.19 and 6.20 exhibit no significant differences in the composition of the original and moderately biodegraded samples, thus providing reliable signatures for tracking the oil sources. However,

under certain aerobic conditions, these compounds may undergo different biodegradation patterns, involving preferential degradation of the higher or lower homologues of the homohopane series, with or without the formation of C-10 demethylated hopanes (25-norhopanes) and

possible subsequent biodegradation of steranes [60,61], as well as preferential depletion of R over S isomers. Moreover, 14 α (H),17 α (H) sterane isomers are removed faster than the 14 β (H),17 β (H) isomers, and within the series, the trend is C-27>C-28>C-29 [13,62]. Therefore, the ratios particularly indicative of advanced degradation of a certain oil sample will be the C-29 β /C-29 α and the C-29 β /C-27 β .

In addition, it has been found that tricyclic terpanes degrade more rapidly than tetra- and pentacyclic terpanes. Under severe weathering conditions, the pentacyclic terpane ratio Ts/Tm may suffer changes due to the relatively faster biodegradation rate of Tm [13,63]. A strong depletion of the C-27 sterane components is also observed. At the same time, decreases in the 14 α (H),17 α (H) steranes versus the 14 β (H),17 β (H) isomers and in the 20R versus the 20S isomers may occur.

Less definite trends are observed among the lower terpanes, namely, the C23–C25 tricyclic, C24 tetracyclic (TT), and C27-trisnorhopanes (Ts and Tm). Only the tetracyclic C24 terpane appears to be relatively more prone to degradation. A summary of these trends is shown in Table 6.7 [25,64].

Of alternative use for source recognition are the series of triaromatic steroid hydrocarbons (Fig. 6.21), which are more resistant to biodegradation than steranes and triterpanes (m/z 231) [13]. However, field and laboratory studies have shown that a depletion of C27 components over the others may also

occur, although it is difficult to rationalize such a biodegradation pathway [59,65].

In summary, it appears that the tricyclic terpanes, C27 trisnorhopanes, and C29/C30 hopanes can be used as source indicators, whereas the oil degradation trend can be drawn as follows: acyclic isoprenoids>C27-steranes> β -steranes>pentacyclic triterpanes (homohopanes)>diasteranes>monoaromatic steranes>triaromatic steranes. Although field studies have shown that the relative rates of biodegradation are not as intensive as those shown here and they may change according to the environmental conditions, these observations may provide useful guidelines for interpreting changes in the profiles in tracking oil sources and weathering.

Composition Changes of the Alkylaromatic Hydrocarbons The general biodegradation pattern of the aromatic hydrocarbons indicates that susceptibility to biodegradation decreases with the increase of the PAH alkylation level [63]. However, microbial degradation was demonstrated to be isomeric specific [66,67], so that when partial biodegradation of alkyl PAHs occurs, the relative losses of specific isomers may provide useful indicators of the extent of the oil biodegradation.

Early indicators of biodegradation have been reported within MPs and dibenzothiophenes (MDBT), where 9-MP and 4-MDBT appeared to be more resistant than the others [66]. The relative biodegradation of positional isomers of C2- and C3-naphthalenes has also been reported [59,67–69].

The complexity of the profiles, with many overlapping peaks due to the number of possible isomers (Fig. 6.26), does not always allow determining individual compound's biodegradation, although several studies have pointed out that isomers with β -substituents (e.g., 2- and 3-methyl) or with $\alpha\beta$ -positions unoccupied are more easily co-oxidized than those with adjacent methyl groups [59,67,68].

The profiles of the C2-phenanthrenes (m/z 206; Figure 6.26), which may include 25 dimethyl and 5 ethyl isomers, exhibit 10 prominent peaks. The 1,7- and 2,7-dimethylphenanthrenes seem to be the most refractory isomers to biodegradation, whereas the major peak possibly containing 1,3-, 2,10-, 3,9-, and 3,10-isomers [70] exhibit a significant depletion, and the 3,6-, 2,6-, and 2,3-dimethylphenanthrenes are almost absent in highly degraded samples [69,71]. This confirms the prevalence of the β -methyl substitution in determining the biodegradation of alkylaromatic components.

The profile of the C2-dibenzothiophenes (m/z 212; Figure 6.26) shows three groups of isomers more resistant to biodegradation, namely, 4,6-, 3,6-, and 1,4- + 1,6- + 1,8-dimethyl components, while the 2,4-, 2,6-, 3,7-, and 1,3-dimethyl isomers are significantly depleted. Less evident are the changes observed within the C3-phenanthrenes and dibenzothiophene profiles, where the evolution of the corresponding ratios is more conservative as they encompass higher alkylated species.

TABLE 6.7 Variation of the source diagnostic ratios during extensive oil biodegradation and photooxidation (*in italics*)

Ratio	Variation ^a
m/z 85	
C17/Pr	–
C18/Ph	–
m/z 192	
2-MP/1-MP	–
<i>MA/1-MP</i>	–
m/z 216	
<i>2-MF/4-MPy</i>	–
<i>BaF/4-MPy</i>	–
<i>BbF/4-MPy</i>	–
<i>2-MPy/4-MPy</i>	–
<i>1-MPy/4-MPy</i>	–
m/z 191	
27Ts/27Tm	–
28ab/30ab	–
29ab/30ab	–
m/z 217/218	
27dbR/27dbS	–
29aaS / 29aaR	+
29bb(S + R) / 29aa(S + R)	+
27bb/29bb	–
m/z 231	
<i>SC26TA/RC26TA + SC27TA</i>	–
m/z 234	
<i>BNT/C4-P</i>	+

^aIncrease (+) or decrease (–) of the ratios.

The biodegradation of the methylpyrenes (m/z 216) and methylchrysenes (m/z 242) also exhibits isomer selectivity [65,66]. It is interesting to notice that again the β -substituted (2-methyl) isomers are those more easily degraded, whereas 4-methylpyrene and 3-methylchrysene were the most refractory. Moreover, it is difficult to visualize any major changes in the profiles of the higher homologues, namely, the C2-pyrenes and chrysenes, so they can also be used for source recognition as discussed previously.

The m/z 216 profile may also be altered by the effect of photooxidation. According to our experience, methylpyrenes exhibit the following photochemical degradation trend: 1-MPy > 4-MPy > 2-MPy. The results of a gas oil sun exposure experiment in the field are shown in Figure 6.29a. It appears that 4-methylpyrene has been reduced relative to 2-methylpyrene but the strongest reduction effect is shown for 1-methylpyrene, in agreement with that pattern. A similar trend was observed when a HFO was submitted to photooxidation in the laboratory with a Xe lamp that emits radiation similar to the solar light (Fig. 6.29b). Very recently, Radović et al. [72] have carried out an extensive assessment of photochemical processes in oil spill fingerprinting and observed that the photosensitivity increases with increasing aromaticity and alkylation of PAH compounds. At the

molecular level, besides the previous observation regarding MPys, other significant changes were observed such as the preferential degradation of MA over MPs and the isomeric preferential photooxidation within the methylchrysenes, the 2-methyl isomer being the more resistant, conversely to what is observed during biodegradation. The higher resistance of the S-compounds to photodegradation is reflected in the compositional changes of the C4-phenanthrenes (C4-Ps) and benzo[*b*]naphto[1,2-*d*]thiophene (BNT) profile (Fig. 6.25), where the latter is more conservative. Changes in ratios of TAS biomarkers (Fig. 6.21), which are traditionally considered to be robust at medium- to long-term environmental exposure, were also observed. Consequently, changes in MA/1-MP, 2-MPy/4-MPy, 1-MPy/4-MPy, BNT/T-M-P, and C26S/C26R + C27S ratios, among others, could serve as early indicators of sunlight exposure of samples in the field. Therefore, these changes should be taken into account when largely exposed spill samples are analyzed (Table 6.7).

6.4.2.2 Case Study As an application of the concepts and methods described in the previous sections, a simple case study is presented corresponding to an “emergency” situation at an oil platform that receives and stores crude oil from several production platforms. The emergency resulted

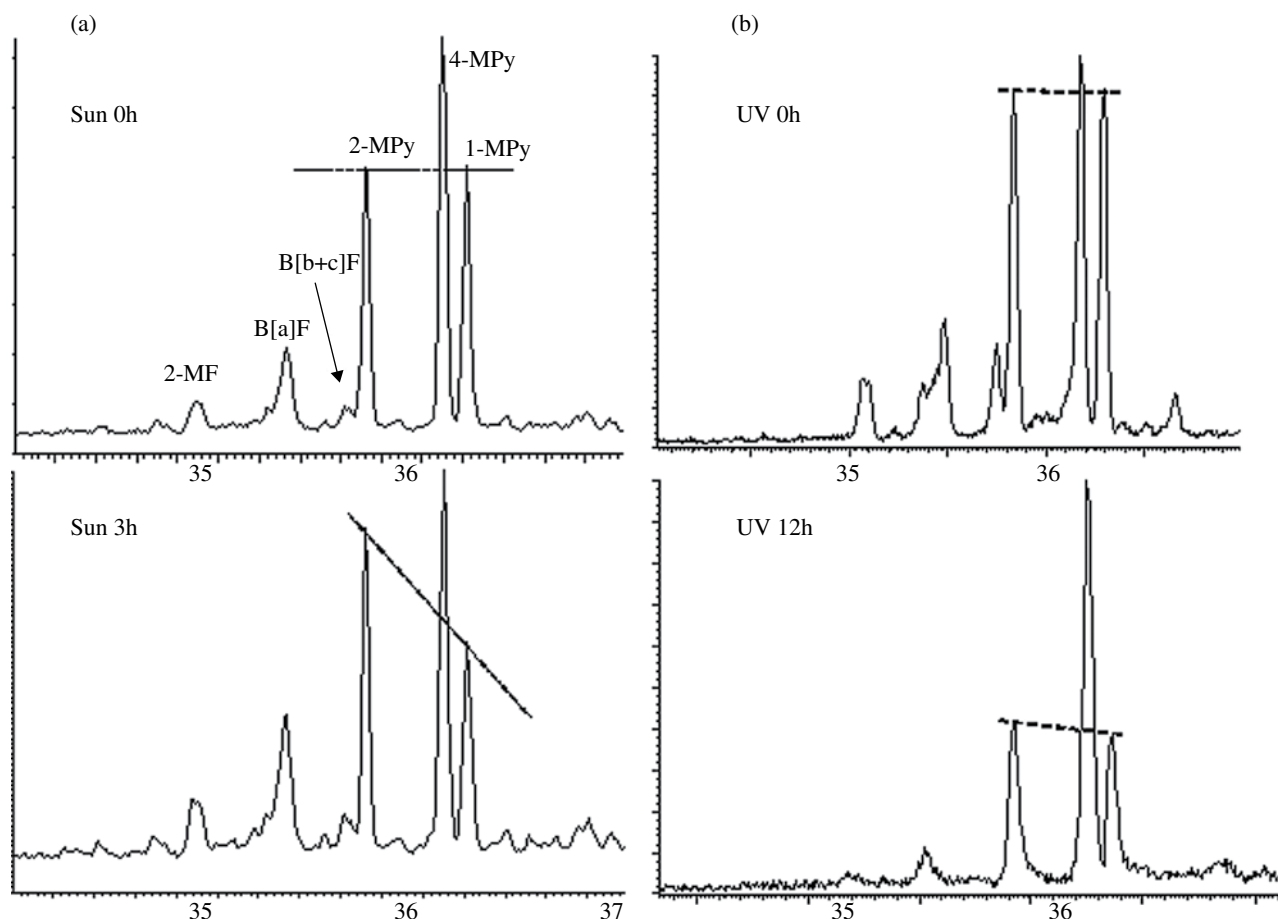


FIGURE 6.29 Variation of the ion chromatogram of m/z 216 after (a) sun exposure of a gas oil and (b) UV radiation exposure of a fuel oil.

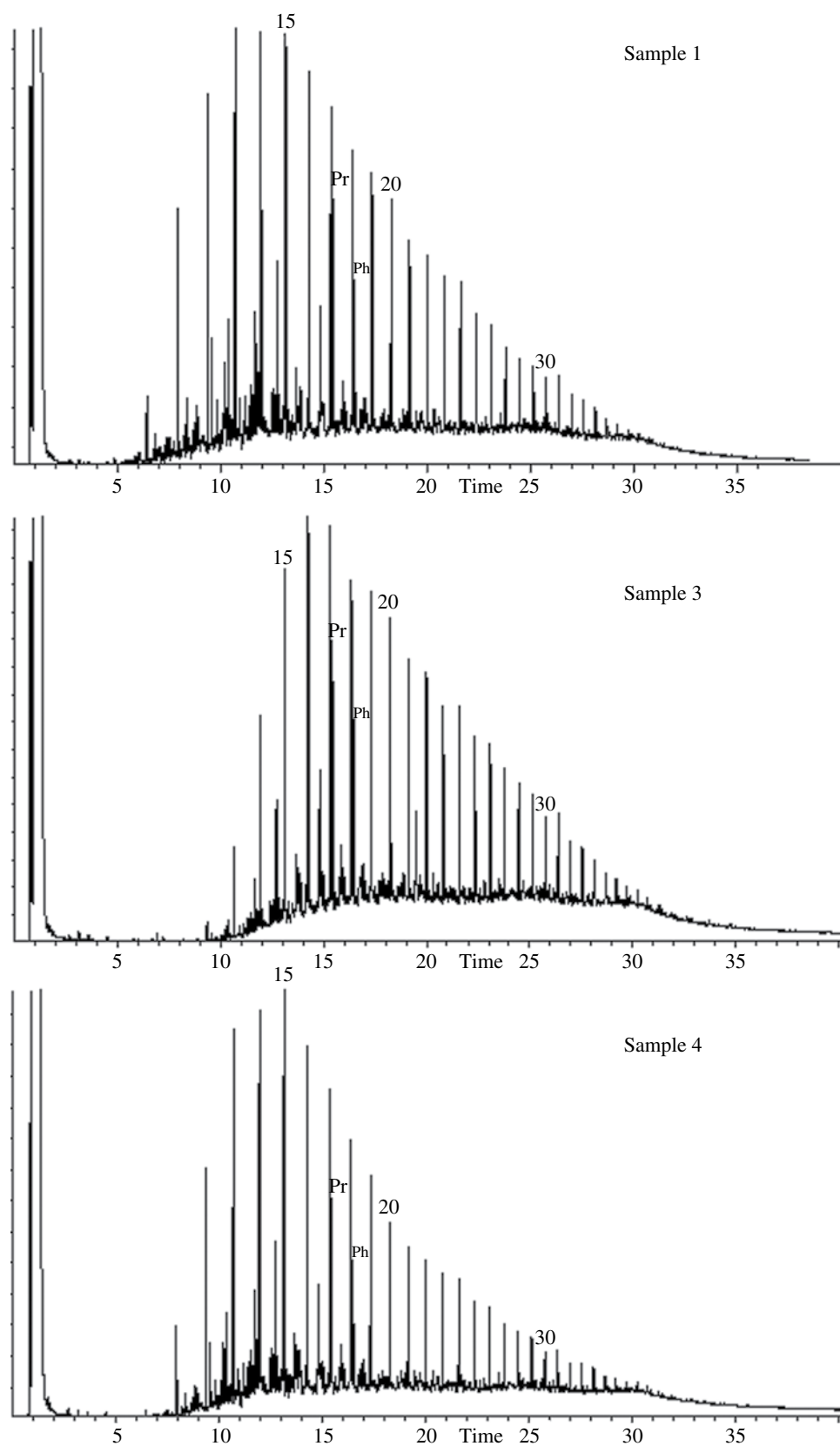


FIGURE 6.30 Gas chromatograms of samples 1, 3, and 4. Sample 2 is not shown because it exhibits a similar profile as sample 1 (see Figure 6.31).

in a “controlled” release of crude oil stored in one of the platform legs (sample 1). Much of the oil was recovered during a response operation close to the platform the same day within 2–5 h (sample 2). However, a part of the slick was not recovered during the first day, and during the night, the slick had drifted several miles and into another oil field. When the recovery operation started the next day, two separate slicks were found there (samples 3 and 4). The question was to determine if all samples were from the same source.

The gas chromatograms of the samples are shown in Figure 6.30. Sample 2 is not shown as it was almost identical to sample 1. In turn, samples 3 and 4 were different, the former exhibiting a loss of the more volatile fraction. The plot of *n*-alkanes, normalized to the mean of *n*-C20–C22 (Fig. 6.31), showed that their relative concentrations in the region C13–C16 were effectively much lower in sample 3 and about 25% higher in spill 4 than in source 1. The difference in the first case can be explained by weathering as sample 3 was at sea 1 day longer than sample 1, but this cannot account for sample 4. It could of course be possible that sample 3 may have been from a thin slick/sheen, whereas sample 4 may have been a sample of a thick slick, where oil protected within an outer layer is more resistant to weathering. But if so, the fact that the concentration of C12, for example, was found to be identical in both samples would then be a contradiction to this hypothesis. Generally, differences of about 25% in some major components of the two oils would justify that the analysis of spill sample 4 could have been stopped at Level 1, Step 1, of the CEN analysis (Fig. 6.8). However, for this case study, we included sample 4 for demonstration purposes. The comparison of source sample 1 with spill samples 2 and 3 still reveals a possible match following Level 1, Step 2, of

the CEN analysis, which warranted these samples’ analysis by GC–MS.

The analysis by GC–MS provided the series of DRs that were compared and represented in the plots of Figures 6.32 and 6.33. The PW plots and column diagrams are simple but effective tools for finding similarities and significant differences between pairs of samples.

A range of PAH and biomarker compounds were integrated, normalized to C30-hopane (30 $\alpha\beta$), and compared. Figure 6.32 (top) shows that samples 1 and 2 are comparably unweathered as all compounds in the spill oil remain at around 100%, relative to the source oil, within the variance of the analysis. A statistical comparison among the DRs in samples 1 and 2 (Figure 6.33, left) shows that all values vary by less than the 14% threshold employed by the CEN method (see preceding text). Therefore, the conclusion is that samples 1 and 2 are a match.

On the other hand, when source sample 1 was compared to spill sample 3, an “S”-shaped weathering curve could be found in the PW plot (Fig. 6.32b), indicating that there is a reduction of the abundance for several of the first-eluting PAH compounds in the spill sample. Thus, evaporation is likely to have affected any DRs based upon lower boiling compounds. A statistical comparison among the DRs in samples 1 and 3 (Fig. 6.33b) shows that all DRs, except those associated with the evaporation-prone sesquiterpanes, are below the 14% threshold. Therefore, despite weathering differences, samples 1 and 3 are concluded to be a match.

Finally, Figure 6.32c shows a great dispersion of normalized abundances of PAHs and biomarkers between the source sample 1 and spill sample 4. These differences, together with the findings from GC screening, could lead to the conclusion that these samples do not match. This conclusion is further justified when the DRs for these two

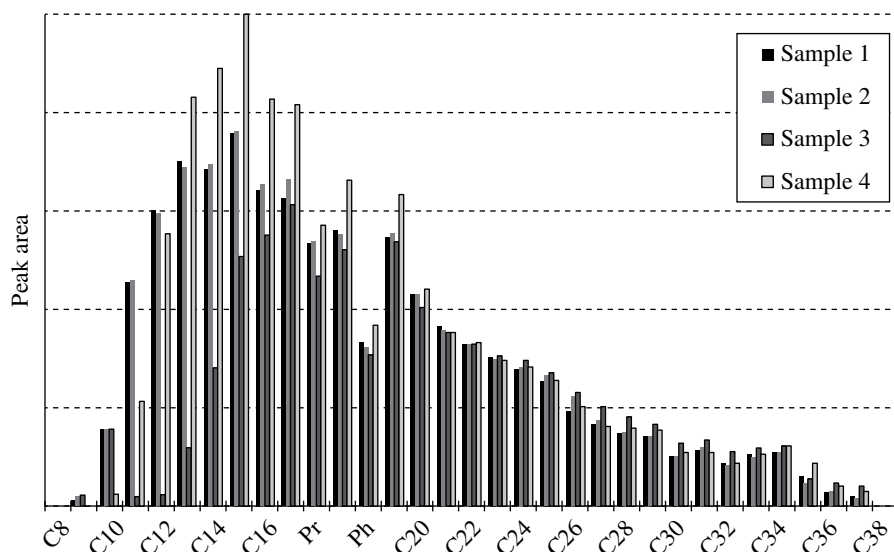


FIGURE 6.31 Distribution of alkanes (peak areas) of samples 1–4, normalized relative to the mean of *n*-C20–C24.

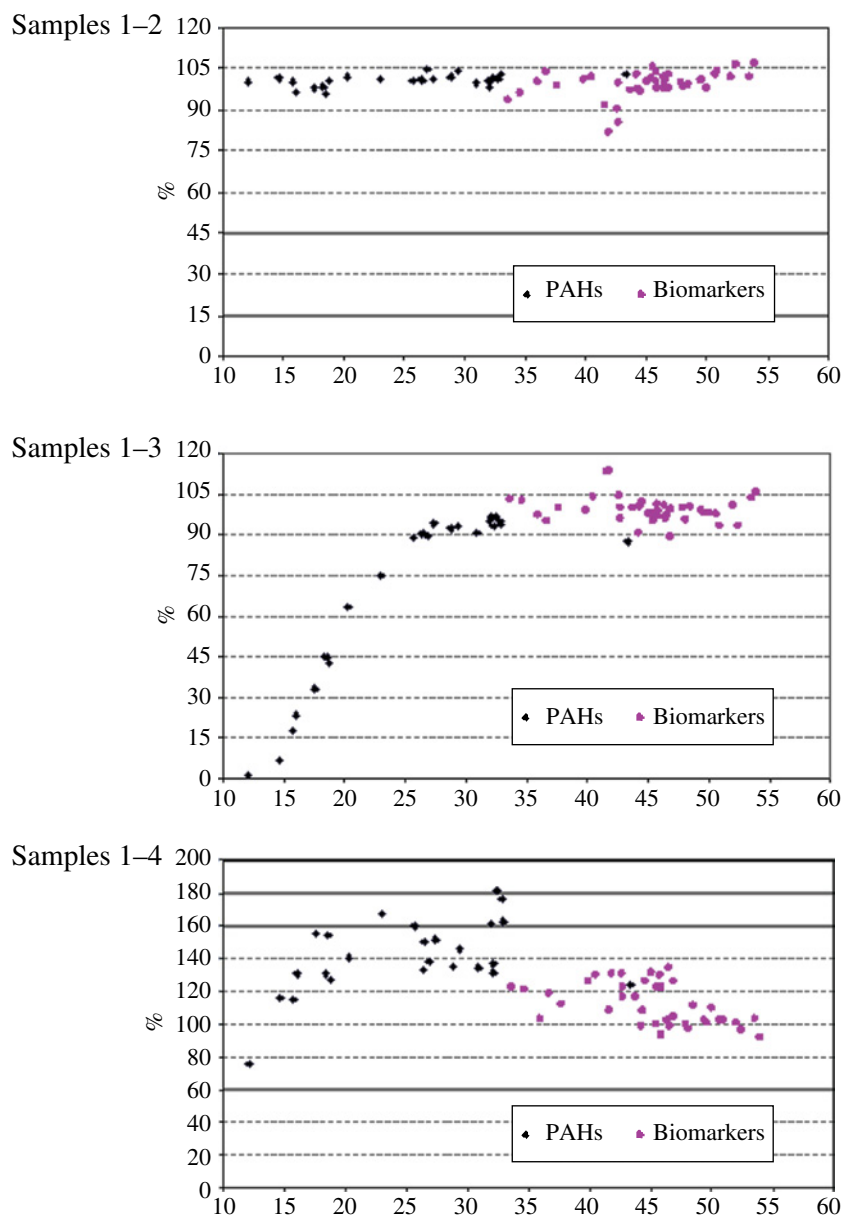


FIGURE 6.32 PW plots: relative intensity in % remaining of the PAHs (diamonds) and biomarkers (circles) of the spill sample compared to those of the source sample after normalization relative to the area of hopane.

samples are statistically compared whereupon multiple DRs are found to exceed the 14% threshold of the CEN method (Fig. 6.33c). Therefore, source sample 1 and spill sample 4 are considered to be nonmatches.

6.5 CONCLUSIONS

The CEN methodology for oil spill identification presented in this chapter is based on a GC–FID screening of all involved samples (Level 1) and a GC–MS fingerprinting of spill and candidate source samples (Level 2), from which a series of molecular markers and PAHs are measured,

selected on the basis of their diversity in oils and their predictable changes due to weathering. From these target analytes, DRs are calculated and compared. Differences due to weathering of the spilled oil are clearly elaborated by means of PW plots.

The comparison of the compound ratios is an important part of the evaluation of the data, however not all conclusive. The final conclusion should be based on a total evaluation using all available data. It is important to visually inspect all the chromatograms and identify possible characteristic features, and not only to evaluate the measured ratios, before final conclusions are made.

By mathematical treatment of the ratios and an overall assessment of results from all analytical levels, the oil spill

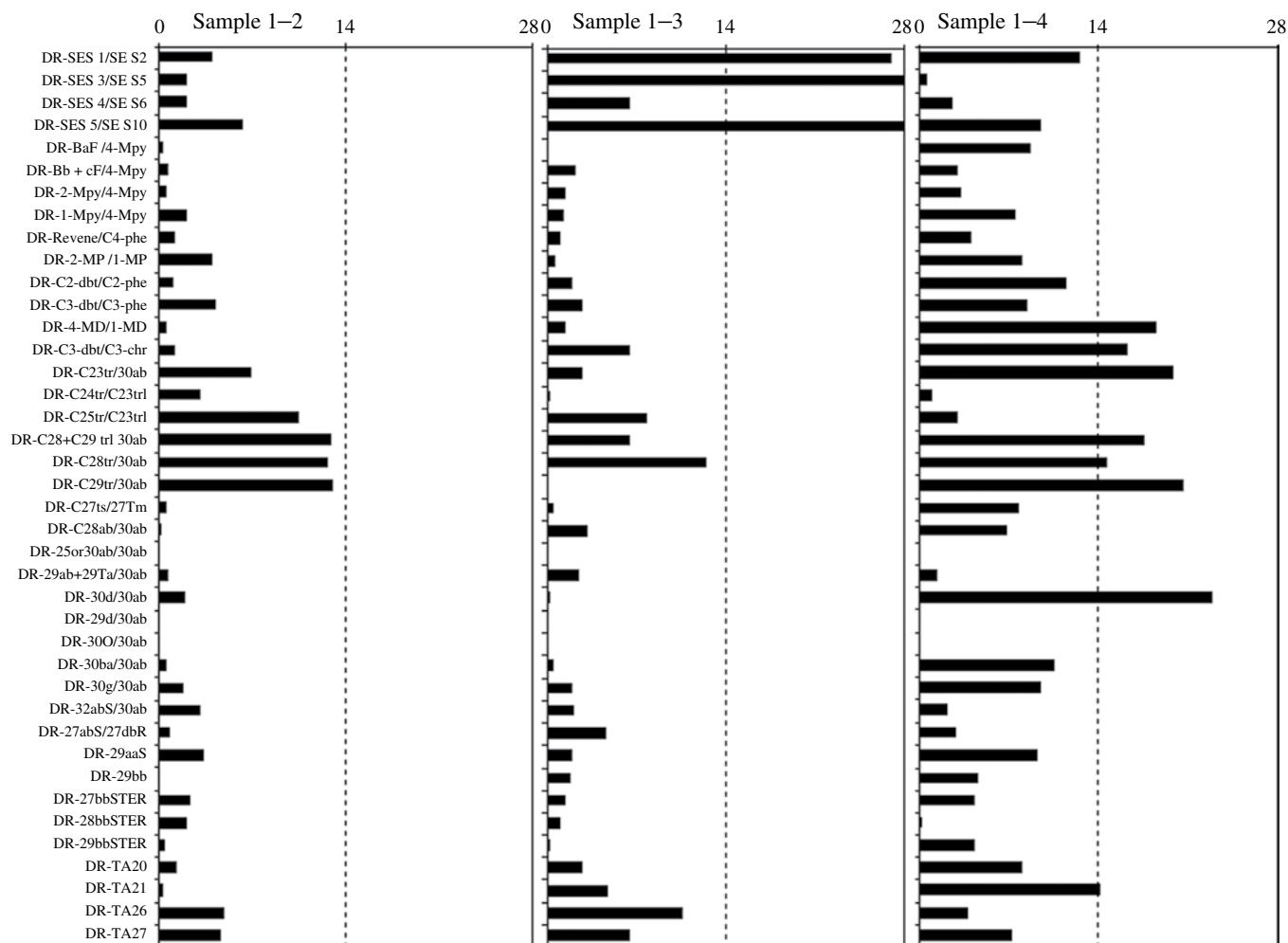


FIGURE 6.33 Relative differences of diagnostic ratios between samples with indication of the threshold value of 14% (see Table 6.5).

identification can be concluded in terms of four operational and technically defensible identification terms:

1. *Match*: The samples are considered to match to a high degree of scientific certainty when the differences in the chromatographic patterns and DRs of samples submitted for comparison are lower than the variability of the method or can be explained unequivocally, for example, by weathering.
2. *Probable match*: The samples are considered to match to a reasonable degree of scientific certainty when differences in chromatographic patterns and DRs do not permit an unequivocal positive match, but they can be explained reasonably by external factors, for example, weathering in combination with mixing, or by nonrepresentative or heterogeneous properties of the available samples.
3. *Inconclusive*: The result will be inconclusive when the differences in the chromatographic patterns and DRs of the samples submitted for comparison do not

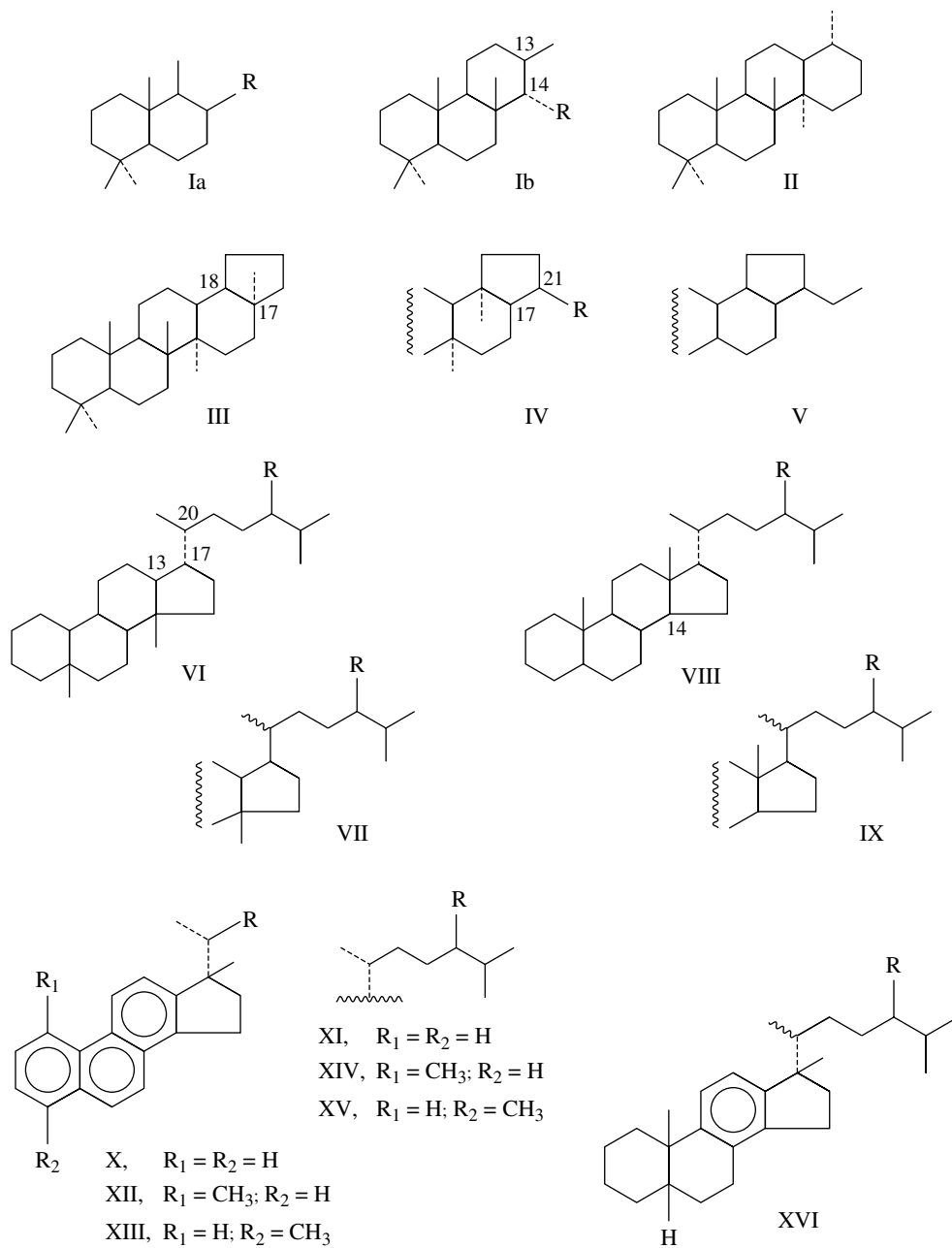
permit a probable match or nonmatch conclusion, for example, in case the concentration of the contaminant in a sample is too low.

4. *Nonmatch*: This applies when differences between the chromatograms and DRs of the samples submitted for comparison are pronounced and cannot be explained by any external factors such as weathering and/or mixing.

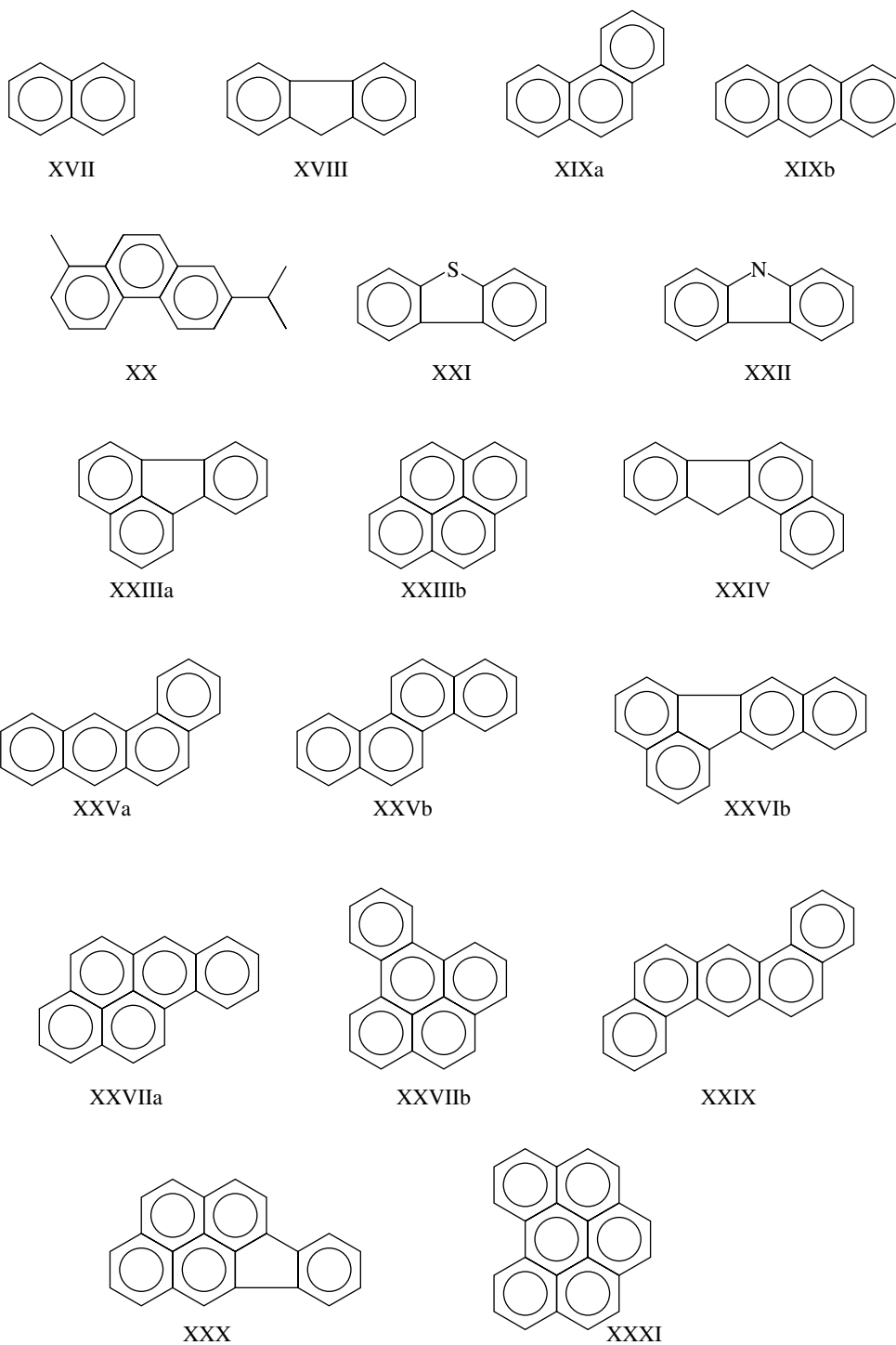
The revised methodology has now been implemented by most of the forensic laboratories and has been used in the last years in connection with several oil spill identification cases, for example, in Denmark [73] and Spain [24]. It has been also intensively used for several years especially in the Netherlands and Germany, where the number of oil spill cases per year is high because of high shipping traffic.

In conclusion, the methodology has been demonstrated to be a strong technically defensible tool to differentiate among qualitatively similar oils from a spill and any available candidate sources.

Annex I



Annex II



REFERENCES

- [1] Adlard, E.R., Creaser, L.F., Matthews, P.H. Identification of hydrocarbon pollutants on seas and beaches by gas chromatography. *Anal. Chem.*, 44, 64, 1972.
- [2] Institute of Petroleum (Ed.), *Marine Pollution by Oil*, Applied Science, Essex, 1974.
- [3] Berthold, B.I., M. Erhardt, M., Hellmann, H., Menzel, H., Prahm, G., Wagnitz, D., Analysen-schema zur charakterisierung und identifizierung von ölverschmutzungen auf dem wasser. DGMK-Projekt 4599, Deutsche Gesellschaft für Mineralölwissenschaft und Kohlechemie, Hamburg, 1973.
- [4] Bentz, A.P. Oil spill identification. *Anal. Chem.*, 48, 454A, 1976.
- [5] Brunnock, J.V., Duckwort, D.F. Stephens, G.G. Analysis of beach pollutants. *J. Inst. Petrol.*, 54, 310, 1968.
- [6] Duewer, D.L., Kowalski, B.R. Forensic data analysis by pattern recognition. *Anal. Chem.*, 47, 526, 1975.
- [7] Kawahara, F.K., Ballinger, D.G. Characterization of oil slicks on surface waters. *Ind. Eng. Chem. Prod. Res. Dev.*, 9, 553, 1970.
- [8] Lynch, P.F., Brown, C.W. Identifying source of petroleum by infrared spectroscopy. *Environ. Sci. Technol.*, 7, 1123, 1973.
- [9] Mattson, J.S., Mattson, C.S., Spencer, M.J., Starks, S.A. Multivariate statistical approach to the fingerprinting of oils by infrared spectrometry. *Anal. Chem.*, 49, 297, 1977.
- [10] Ehrhardt, M., Blumer, M. The source identification of marine hydrocarbons by gas chromatography. *Environ. Pollut.*, 3, 179, 1972.
- [11] Clark, H.A., Jurs, P.C. Qualitative determination of petroleum sample type from gas chromatograms using pattern recognition techniques. *Anal. Chem.*, 47, 374, 1975.
- [12] Rasmussen, D.V. Characterization of oil spills by capillary column gas chromatography. *Anal. Chem.*, 48, 1562, 1976.
- [13] Peters, K.E., Moldowan, J.M. *The Biomarker Guide. Interpreting Molecular Fossils in Petroleum and Ancient Sediments*, 363 pp., Englewood Cliffs, Prentice Hall, 1993.
- [14] Albaigés, J., Albrecht, P. Identification of marine hydrocarbons by computerized gas chromatography-mass spectrometry. *Int. J. Environ. Anal. Chem.*, 6, 171, 1979.
- [15] Daling, P.S., Faksness, L.G., Hansen, A.B., Stout, S.A. Improved and standardized methodology for oil spill fingerprinting. *Environ. Forensics*, 3, 263, 2002.
- [16] Wang, Z.D., Fingas, M.F. Development of oil hydrocarbon fingerprinting and identification techniques. *Mar. Pollut. Bull.*, 47, 423, 2003.
- [17] Faksness, L.-G., Weiss, H., Daling, P.S. *Revision of the Nordtest Methodology for Oil Spill Identification – Technical Report*, SINTEF Report STF66 A01028, Trondheim, Norway, 2002.
- [18] Faksness, L.-G., Daling, P.S., Hansen, A.B. Round Robin Study – oil spill identification. *Environ. Forensics*, 3, 279, 2002.
- [19] Dahlmann, G., Kienhuis, P. *Oil Spill Identification – Round Robin 2005, The Comparison of Four Bilge Samples*, RIZA Report No. 2006.043X, Lelystad, the Netherlands, 2006, <http://www.bonnagreement.org>.
- [20] Douglas, G.S., Uhler, A.D. Optimizing EPA methods for petroleum-contaminated site assessments. *Environ. Testing Anal.*, 5, 46, 1993.
- [21] American Society for Testing and Materials (ASTM). Standard Test Methods for Comparison of Waterborne Petroleum Oils by Gas Chromatography. *ASTM 3328D-00*, ASTM International, W. Conshohocken, PA, 2000.
- [22] American Society for Testing and Materials (ASTM). Oil Spill Identification by Gas Chromatography and Positive Ion Electron Impact Low Resolution Mass Spectrometry. *ASTM D5739-00*, ASTM International, W. Conshohocken, PA, 2000.
- [23] Kerckhof, F., Roose, P., Haelters, J. The Tricolor incident: from collision to environmental disaster. *Atlantic Seabirds*, 6, 85, 2004.
- [24] Diez S., Jover, E., Bayona, J.M., Albaigés, J. Prestige oil spill. III. Fate of a heavy oil in the marine environment. *Environ. Sci. Technol.*, 41, 3075, 2007.
- [25] Jimenez, N., Viñas, M., Sabate, J., Diez, S., Bayona, J.M., Solanas, A.M., Albaiges, J. The Prestige oil spill. II. Enhanced biodegradation of a heavy fuel oil under field conditions by the use of an oleophilic fertilizer. *Environ. Sci. Technol.*, 40, 2578, 2006.
- [26] Wang, Z., Fingas, M., Page, D.S. Oil spill identification. *J. Chromatogr. A*, 843, 369, 1999.
- [27] Stout, S.A., Uhler, A.D., McCarthy, K.J. A strategy and methodology for defensibly correlating spilled oil to source candidates. *Environ. Forensics*, 2, 87, 2001.
- [28] Kienhuis, P., Breidenbach, R., Bakker, I. *Oil Analysis Study. Methods Using GC-AED, ICP-MS and High Temperature GC-FID*, RIZA Internal Report 2006.051X, Lelystad, the Netherlands, 40 pp, 2006.
- [29] Stout, S.A., Uhler, A.D., McCarthy, K.J., Emsbo-Mattingly, S. Chemical fingerprinting of hydrocarbons, in *Introduction to Environmental Forensics*, B. Murphy, Morrison, R.D. editors, Academic Press, San Diego, pp. 137–260, 2002.
- [30] Gaines, R.B., Frysinger, G.S., Reddy, C.M., Nelson, R.K. Oil Spill Source Identification by Comprehensive Two-Dimensional Gas Chromatography (GC x GC), in *Oil spill environmental forensics*, Wang, Z., Stout, S.A. editors, Academic Press, pp. 169–206, 2007.
- [31] Wang, Z., Fingas, M. Developments in the analysis of petroleum hydrocarbons in oils, petroleum products and oil spill-related environmental samples by gas chromatography. *J. Chromatogr.*, 774, 51, 1997.
- [32] Whittaker, M., Pollard, S.J.T. A performance assessment of source correlation and weathering indices for petroleum hydrocarbons in the environment. *Environ. Toxicol. Chem.*, 16, 1149, 1997.
- [33] Sinninghe Damsté, J.S., Kock-van Dalen, A.C., de Leeuw, J.W. Identification of long-chain isoprenoid alkylbenzenes in sediments and crude oils. *Geochim. Cosmochim. Acta*, 52, 2671, 1988.
- [34] Grimalt J.O., Grifoll M., Solanas A.M., Albaiges J. Microbial-degradation of marine evaporitic crude oils. *Geochim. Cosmochim. Acta*, 55, 1903, 1991.
- [35] Hansen, A.B., Daling, P.S., Faksness, L.-G., Sørheim, K.R., Kienhuis, P., Duus, R. Emerging CEN methodology for oil

- spill identification, in *Oil Spill Environmental Forensics*, Wang, Z., Stout, S.A., editors, Academic Press, San Diego, pp. 229–256, 2007.
- [36] Williams, J.A., Bjoroy, M., Dolcater, D.L., Winters, J.C. Biodegradation in South Texas Eocene oils – effects on aromatics and biomarkers. *Org. Geochem.*, 10, 451, 1986.
- [37] Prince, R.C., Elmendorf, D.L., Lute, J.R., Hsu, C.S., Haith, C.E., Senius, J.D., Dechert, G.J., Douglas, G.S., Butler, E.L. 17- α (H),21- β (H)-Hopane as a conserved internal marker for estimating the biodegradation of crude-oil. *Environ. Sci. Technol.*, 28, 142, 1994.
- [38] Bence, A.E., Kvenvolden, K.A., Kennicutt II, M.C. Organic geochemistry applied to environmental assessments of Prince William Sound, Alaska, after the Exxon Valdez oil spill – a review. *Org. Geochem.*, 24, 7, 1996.
- [39] Franco, M.A., Viñas, L., Soriano, J.A., de Armas, D., González, J.J., Beiras, R., Salas, N., Bayona, J.M., Albaigés, J. Spatial distribution and ecotoxicity of petroleum hydrocarbons in sediments from the Galicia continental shelf (NW Spain) after the Prestige oil spill. *Mar. Pollut. Bull.*, 53, 260, 2006.
- [40] McKirdy, D.M., Cox, R.E., Volkman, J.K., Howell, V.J. Botryococcane in a new class of Australian nonmarine crude oils. *Nature*, 320, 57, 1986.
- [41] Pastor, D., Sánchez, J., Porte, C., Albaigés, J. The Aegean Sea oil spill in the Galicia Coast (NW Spain). I. Distribution and fate of crude oil and combustion products in subtidal sediments. *Mar. Pollut. Bull.*, 42, 895, 2001.
- [42] Samuel, O.J., Cornford, C., Jones, M., Adekeye, O.A., Akande, S.O. Improved understanding of the petroleum systems of the Niger Delta Basin, Nigeria. *Org. Geochem.*, 40, 461, 2009.
- [43] Mello, M.R., Telnaes, N., Gaglianone, P.C., Chicarelli, M.I., Brassell, S.C., Maxwell, J.R. Organic geochemical characterisation of depositional palaeoenvironments of source rocks and oils in Brazilian marginal basins. *Org. Geochem.*, 13, 31, 1988.
- [44] Woodhouse, A.D., Oung, J.-N., Philp, R.P., Weston, R.J. Triterpanes and ring-A degraded triterpanes as biomarkers characteristic of Tertiary oils derived from predominantly higher plant sources. *Org. Geochem.*, 18, 23, 1992.
- [45] Currie, T.J., Alexander, R., Kagi, R.I. Coastal bitumens from Western Australia—long distance transport by ocean currents. *Org. Geochem.*, 18, 595, 1992.
- [46] Zhang, S., Liang, D., Gong, Z., Wu, K., Li, M., Song, F., Song, Z., Zhang, D., Wang, P. Geochemistry of petroleum systems in the eastern Pearl River Mouth Basin: evidence for mixed oils. *Org. Geochem.*, 34, 971, 2003.
- [47] Douglas, G.S., Bence, A.E., Prince, R.C., McMillen, S.J., Butler, E.L. Environmental stability of selected petroleum hydrocarbon source and weathering ratios. *Environ. Sci. Technol.*, 30, 2332, 1996.
- [48] Radke, M., Welte, D.H., Willsch, H. Maturity parameters based on aromatic hydrocarbons: influence of the organic matter type. *Org. Geochem.*, 10, 51, 1986.
- [49] Wang, Z.D., Fingas, M., Shu, Y.Y., Sigouin, L., Landriault, M., Lambert, P. Quantitative characterization of PAHs in burn residue and soot samples and differentiation of pyrogenic PAHs from petrogenic PAHs – the 1994 mobile burn study. *Environ. Sci. Technol.*, 33, 3100, 1999.
- [50] Tolosa, I., de Mora, S., Sheikholeslami, M., Villeneuve, J., Bartocci, J., Cattini, C. Aliphatic and aromatic hydrocarbons in coastal Caspian Sea sediments. *Mar. Pollut. Bull.*, 48, 44, 2004.
- [51] Wang, Z.D., Fingas, M., Lambert, P., Zeng, G., Yang, C., Hollebone, B. Characterization and identification of the Detroit River mystery oil spill (2002). *J. Chromatogr.*, 1038, 201, 2004.
- [52] Gürgey, K. An attempt to recognize oil populations and potential source rock types in Paleozoic suband Mesozoic-Cenozoic supra-salt strata in southern margin of the pre-Caspian basin, Kazakhstan republic. *Org. Geochem.*, 33, 723, 2002.
- [53] Zakaria, M.P., Horinouchi, A., Tsutsumi, S., Takada, H., Tanabe, S., Ismail A. Oil pollution in the Straits of Malacca, Malaysia: application of molecular markers for source identification. *Environ. Sci. Technol.*, 34, 1189, 2000.
- [54] Zakaria, M.P., Okuda, T., Takada, H. PAHs and hopanes in stranded tar-balls on the coast of Peninsular Malaysia: applications of biomarkers for identifying source of oil pollution. *Mar. Pollut. Bull.*, 12, 1357, 2001.
- [55] Wang, Z.D., Yang, C., Fingas, M., Hollebone, B., Peng, X., Hansen, A., Christensen, J.H. Characterization, weathering, and application of sesquiterpanes to source identification of spilled petroleum products. *Environ. Sci. Technol.*, 39, 8700, 2005.
- [56] Wang, Z.D., Fingas, M., Use of methylidibenzothiophenes as markers for differentiation and source identification of crude and weathered oils. *Environ. Sci. Technol.*, 29, 2842, 1995.
- [57] Albaigés, J., Jimenez, N., Arcos, A., Dominguez, C., Bayona, J.M. The use of long-chain alkylbenzenes and alkyltoluenes for fingerprinting marine oil wastes. *Chemosphere*, 91, 336, 2013.
- [58] Christensen, J.H., Hansen, A.B., Tomasi, G., Mortensen, J., Andersen, O. Integrated methodology for forensic oil spill identification. *Environ. Sci. Technol.*, 38, 2912, 2004.
- [59] Volkman, J.K., Alexander, R., Kagi, R.I., Rowland, S.J., Sheppard, P.N. Biodegradation of aromatic hydrocarbons in crude oils from the Barrow Sub-basin of Western Australia. *Org. Geochem.*, 6, 619, 1984.
- [60] Bost, F.D., Frontera-Suau, R., McDonald, T.J., Peters, K.E., Morris, P.J. Aerobic biodegradation of hopanes and norhopanes in Venezuelan crude oils. *Org. Geochem.*, 32, 105, 2001.
- [61] Brooks, P.W., Fowler, M.G., Macqueen, R.W. Biological marker and conventional organic geochemistry of oil sands heavy oils, Western Canada Basin. *Org. Geochem.*, 12, 519, 1988.
- [62] Chosson, P., Connan, J., Dessort, D., Lanau, C. In vitro biodegradation of steranes and terpanes: a clue to understanding geological situations, in *Biological Markers in Sediments and Petroleum*, Moldowan, J.M., Albrecht, P., Philp, R.P., editors, Prentice Hall, Englewood Cliffs, pp. 320–349, 1992.

- [63] Wang, Z.D., Fingas, M., Blenkinsopp, S., Sergy, G., Landriault, M., Sigouin, L., Foght, J., Semple, K., Westlake, D.W.S. Comparison of oil composition changes due to biodegradation and physical weathering in different oils. *J. Chromatogr. A*, 809, 89, 1998.
- [64] Díez, S., Sabaté, J., Viñas, M., Bayona, J.M., Solanas, A.M., Albaigés, J. The Prestige oil spill. I. Biodegradation of a heavy fuel oil under simulated conditions. *Environ. Toxicol. Chem.*, 24, 2203, 2005.
- [65] Wardroper, A.M.K., Hoffmann, C.F., Maxwell, J.R., Barwise, A.J.G., Goodwin, N.S., Park, P.J.D. Crude oil biodegradation under simulated and natural conditions. II. Aromatic steroid hydrocarbons. *Org. Geochem.*, 6, 605, 1984.
- [66] Bayona, J.M., Albaiges, J., Solanas, A.M., Pares, R., Garrigues, P., Ewald, M. Selective aerobic degradation of methyl-substituted polycyclic aromatic-hydrocarbons in petroleum by pure microbial cultures. *Int. J. Environ. Anal. Chem.*, 23, 289, 1986.
- [67] Rowland, S.J., Alexander, R., Kagi, R.I., Jones, D.M., Douglas, A.G. Microbial-degradation of aromatic components of crude oils – a comparison of laboratory and field observations. *Org. Geochem.*, 9, 153, 1986.
- [68] Solanas, A.M., Pares, R., Bayona, J.M., Albaiges, J. Degradation of aromatic petroleum-hydrocarbons by pure microbial cultures. *Chemosphere*, 13, 593, 1984.
- [69] Budzinski, H., Raymond, N., Nadalig, T., Gilewicz, M., Garrigues, P., Bertrand, J.C., Caumette, P. Aerobic biodegradation of alkylated aromatic hydrocarbons by a bacterial community. *Org. Geochem.*, 28, 337, 1998.
- [70] Radke, M., Garrigues, P., Willsch, H. Methylated dicyclic and tricyclic aromatic-hydrocarbons in crude oils from the Handil Field, Indonesia. *Org. Geochem.*, 5, 7, 1990.
- [71] Hostettler, F.D., Kvenvolden, K.A. Geochemical changes in crude-oil spilled from the Exxon-Valdez supertanker into Prince-William-Sound, Alaska. *Org. Geochem.*, 21, 927, 1994.
- [72] Radović, J.R., Aeppli, C., Nelson, R.K., Jimenez, N., Reddy, C.M., Bayona, J.M., Albaigés, J. Assessment of photochemical processes in marine oil spill fingerprinting. *Mar. Pollut. Bull.*, 79, 268, 2014.
- [73] Hansen, A.B., Avniskjold, J., Rasmussen, C.A. Application of PAH and biomarker diagnostic ratios in forensic oil spill identification by the revised Nordtest methodology. *Water Studies*, 11, 59, 2002.

PART V

OIL BEHAVIOR

OIL AND PETROLEUM EVAPORATION

MERV FINGAS

Spill Science, Edmonton, Alberta, Canada

7.1	Introduction	207
7.2	Review of Historical Concepts	209
7.3	Development of New Diffusion-Regulated Models	213
7.3.1	Wind Experiments	213
7.3.2	Variation with Area	214
7.3.3	Variation with Mass	215
7.3.4	Evaporation of Pure Hydrocarbons	215
7.3.5	Saturation Concentration	216
7.3.6	Development of Generic Equations Using Distillation Data	216
7.4	Complexities to the Diffusion-Regulated Model	218
7.4.1	Oil Thickness	218
7.4.2	The Bottle Effect	219
7.4.3	Skinning	220
7.4.4	Jumps from the 0-Wind Values	220
7.5	Use of Evaporation Equations in Spill Models	220
7.6	Volatilization	221
7.7	Measurement of Evaporation	221
7.8	Summary	221

7.1 INTRODUCTION

Evaporation is an important process for most oil spills. In a few days, typical crude oils can lose up to 45% of their volume [1]. Most oil spill models include evaporation as a process and output of the model. Despite the importance of the process, only little work has been conducted on the basic physics and chemistry of oil spill evaporation [2]. The difficulty with studying oil evaporation is that oil is a mixture of hundreds of compounds and this mixture varies from source to source and even over time. Much of the work described in the literature focuses on “calibrating” equations developed for water evaporation [2].

Evaporation plays a strong role in the fate of most oils. Almost all oils must undergo evaporation before they form water-in-oil emulsions [1]. Light oils will change very dramatically from fluid to viscous. Heavy oils will become

solid-like. Many oils after long evaporative exposure form tar balls such as illustrated in Figure 7.1.

An important step to understanding evaporation is to understand the mechanisms that regulate evaporation [3]. If there were no regulation, evaporation would proceed nearly instantly. Figure 7.2 shows a schematic of the air-boundary-layer regulation mechanism. The liquid could evaporate at a very high rate if it was not for the regulation caused by the slow transfer of vapor into the air boundary layer. The most common example of this type of regulation is applicable to water. Evaporation of water can be increased by spreading it out or by increasing the wind speed. The wind speed increases the transfer of water across the air boundary layer.

Many liquids are not air-boundary-layer regulated primarily because they evaporate too slowly to have the vapors saturate the air boundary layer above them [1]. Many mixtures are regulated by the diffusion of molecules inside the liquid to the surface of the liquid. This regulatory mechanism is illustrated in Figure 7.3. Such a mechanism is true for many slowly evaporating mixtures of compounds such as oils and fuels. Some of the outcomes of this mechanism may seem counterintuitive to some people such as that increasing area may not increase evaporation rate. More importantly, increasing wind speed does not increase evaporation.

It is possible to have combinations of the two regulation mechanisms. For example, if a mixture has volatile components, these may evaporate via an air-boundary-layer-regulated mechanism, and then the remaining components evaporate via a diffusion-regulated mechanism.

Scientific work on water evaporation is decades old and forms the basis for early oil evaporation work [1,3,4]. There are several fundamental differences between the evaporation of a pure liquid such as water and that of a multicomponent system such as crude oil. The evaporation rate for a single liquid such as water is a constant with respect to time [3,4]. Evaporative loss, either by weight or



FIGURE 7.1 Photograph of tar balls on a beach on Louisiana after the 2010 Deep Water Horizon spill. Oil on the seas often ends up on beaches in the form of tar balls, a highly evaporated residual of oil.

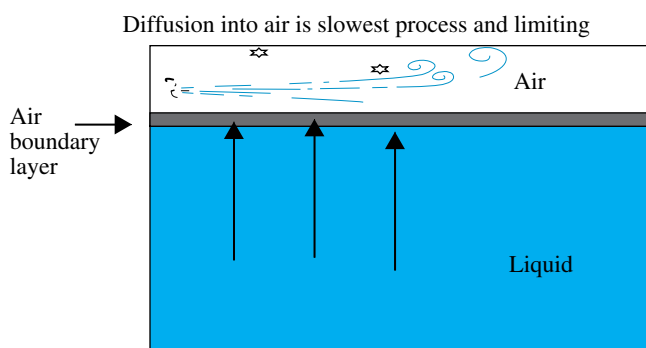


FIGURE 7.2 The diffusion into the air layer is the limiting factor in this case and serves to regulate the evaporation rate. This is called air-boundary-layer regulation. The evaporation rate is affected by turbulence in the air which will increase the transfer of the molecules across the boundary layer. This regulatory mechanism is true for pure liquids that have a high evaporation rate. Water is an example of such a liquid and is the most common concept held for evaporation.

volume, is not linear with time for crude oils and other multicomponent fuel mixtures [5].

Evaporation of a liquid can be considered as the movement of molecules from the surface into the vapor phase above it. The immediate layer of air above the evaporation surface is known as the boundary layer [6]. This boundary layer is the intermediate phase between the air and the liquid and might be viewed as very thin such as less than 1 mm. The characteristics of this air boundary layer can influence evaporation. In the case of water, the boundary layer regulates the evaporation rate. Air can hold a variable amount of water, depending on temperature, as expressed by the relative humidity. Under conditions where the boundary layer is not moving (no wind) or has low turbulence, the air immediately above the water quickly becomes saturated and evaporation slows.

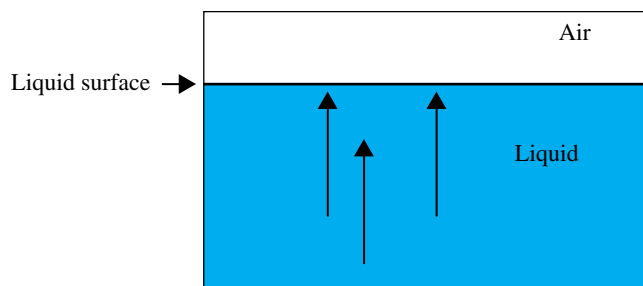


FIGURE 7.3 Diffusion-controlled regulation mechanism where the diffusion rate through the evaporating liquid is the limiting factor and thus the regulation mechanism. This mechanism is generally applicable to oils, fuels, and many other mixtures of liquids that both evaporate more slowly than water and are mixtures.

In actuality, the actual evaporation of water proceeds at a small fraction of the possible evaporation rate because of the saturation of the boundary layer [6]. The air-boundary-layer physics is then said to regulate the evaporation of water. This regulation manifests as the increase of evaporation with wind or turbulence. When turbulence is weak, evaporation can slow down by orders of magnitude. The molecular diffusion of water molecules through air is at least 10^3 times slower than turbulent diffusion [6].

The rate of molecular diffusion for water is about 10^5 slower than the maximum rate of evaporation, purely from thermodynamic considerations [6]. The rate for turbulent diffusion, the combination of molecular diffusion and movement with turbulent air, is in the order of 10^2 slower than that for maximum evaporation. For air-boundary-layer-regulated liquids, one can write the mass transfer rate in semiempirical form (also in generic and unitless form) as [4]

$$E \approx K C T_u S \quad (7.1)$$

where E is the evaporation rate in mass per unit area; K is the mass transfer rate of the evaporating liquid, presumed constant for a given set of physical conditions, sometimes denoted as k_g (gas-phase mass transfer coefficient, which may incorporate some of the other parameters noted here); C is the concentration (mass) of the evaporating fluid as a mass per volume; T_u is a factor characterizing the relative intensity of turbulence; and S is a factor that relates to the saturation of the boundary layer above the evaporating liquid. The saturation parameter, S , represents the effects of local advection on saturation dynamics. If the air is already saturated with the compound in question, the evaporation rate approaches zero. This also relates to the scale length of an evaporating pool. If one views a large pool over which a wind is blowing, there is a high probability that the air is saturated downwind and the evaporation rate per unit area is lower than that for a smaller pool. It is noted that there are many equivalent ways of expressing this fundamental evaporation equation.

Much of the pioneering work for water evaporation was performed by Sutton, who proposed the following equation based on empirical work [7]:

$$E = K C_s U^{7/9} d^{-1/9} Sc^{-r} \quad (7.2)$$

where E is the evaporation rate, C_s is the concentration of the evaporating fluid (mass/volume), U is the wind speed, d is the area of the pool, Sc is the Schmidt number, and r is the empirical exponent assigned values from 0 to 2/3. Other parameters are defined as above. The terms in this equation are analogous to the very generic equation, (7.1), proposed above. The turbulence is expressed by a combination of the wind speed, U , and the Schmidt number, Sc . The Schmidt number is the ratio of kinematic viscosity of air (ν) to the molecular diffusivity (D) of the diffusing gas in air, that is, a dimensionless expression of the molecular diffusivity of the evaporating substance in air [7]. The coefficient of the wind power typifies the turbulence level. The value of 0.78 (7/9), as chosen by Sutton, represents a turbulent wind, whereas a coefficient of 0.5 would represent a wind flow that was more laminar. The scale length is represented by d and has been given an empirical exponent of $-1/9$. This represents for water a weak dependence on size. The exponent of the Schmidt number, r , represents the effect of the diffusivity of the particular chemical and historically was assigned values between 0 and 2/3 [7].

Subsequently, boundary-layer regulation was also assumed to be the primary regulation mechanism for oil and petroleum evaporation. This assumption was never well tested by experimentation [2]. The implications of these assumptions are that evaporation rate for a given oil is increased by:

- Increasing turbulence
- Increasing wind speed
- Increasing the surface area of a given mass of oil

These factors can be verified experimentally to test whether oil is boundary-layer regulated or not [1].

7.2 REVIEW OF HISTORICAL CONCEPTS

The basis for most of the earlier evaporative work is the extensive studies on the evaporation of water [3,4]. In fact, some of the currently used equations still employ portions of these equations. The pioneering work in the development of evaporation equations was carried out by Sutton [7]. Sutton proposed the following equation:

$$E = Ms C_s U^{7/9} d^{1/9} Sc^{-r} \quad (7.3)$$

where E is the mean evaporation rate per unit area, Ms is the mass transfer coefficient, C_s is the concentration of the evaporating fluid (mass/volume), U is the wind speed, d is the

area of the square or circular pool, Sc is the Schmidt number, and r is an empirical exponent assigned values from 0 to 2/3.

Blokker was the first to develop oil evaporation equations for oil evaporation at sea. His starting basis was theoretical [8]. Oil was presumed to be a one-component liquid. The distillation data and the average boiling points of successive fractions were used as the starting point to predict an overall vapor pressure. The average vapor pressure of these fractions was then calculated from the Clausius–Clapeyron equation to yield

$$\log \frac{p_s}{p} = \frac{qM}{4.57} \left(\frac{1}{T} - \frac{1}{T_s} \right) \quad (7.4)$$

where p is the vapor pressure at the absolute temperature, T ; p_s is the vapor pressure at the boiling point, T_s (for p_s , 760 mm Hg was used); q is the heat of evaporation in cal/g; and M is the molecular weight.

The term $qM/(4.57 T_s)$ was taken to be nearly constant for hydrocarbons ($=5.0 \pm 0.2$), and thus, the expression was simplified to

$$\log p_s / p = 5.0 [(T_s - T) / T] \quad (7.5)$$

From the empirical data and Equation (7.5), the weathering curve was calculated, assuming that Raoult's law is valid for this situation giving qM as a function of the percentage evaporated. Pasquill's equation was applied stepwise, and the total evaporation time obtained by summation:

$$t = \frac{\Delta h D^\beta}{K_{ev} U^\alpha} \sum \frac{1}{PM} \quad (7.6)$$

where t is the total evaporation time in hours; Δh is the decrease in layer thickness in m; D is the diameter of the oil spill; β is a meteorological constant (assigned a value of 0.11); K_{ev} is a constant for atmospheric stability (taken to be 1.2×10^{-8}); α is a meteorological constant (assigned a value of 0.78); P is the vapor pressure at the absolute temperature, T ; and M is the molecular weight of the component or oil mass [8].

Blokker constructed a small wind tunnel and tested this equation against the evaporation of gasoline and a medium crude oil [8]. The observed gasoline evaporation rate was much higher than was predicted and the crude oil rate was much lower than predicted. The times of evaporation, however, were relatively close and Equation (7.6) was accepted. The aforementioned equations were then incorporated into spreading equations to yield equations to predict the simultaneous spreading and evaporation of oil and petroleum products.

Mackay and Matsugu approached the problem by using the classical water evaporation and experimental work [9]. The water evaporation equation was corrected to hydrocarbons

using the evaporation rate of cumene. It was noted that the difference in constants was related to the enthalpy differences between water and cumene. Data on the evaporation of water and cumene have been used to correlate the gas-phase mass transfer coefficient as a function of wind speed and pool size by the equation

$$K_m = 0.0292 U^{0.78} X^{-0.11} Sc^{-0.67} \quad (7.7)$$

where K_m is the mass transfer coefficient in units of mass per unit time and X is the pool diameter or the scale size of the evaporating area. Note that the exponent of the wind speed, U , is 0.78, which is equal to the classical water evaporation-derived coefficient. Mackay and Matsugu noted that for hydrocarbon mixtures the evaporation process is more complex, being dependent on the liquid diffusion resistance being present. Experimental data on gasoline evaporation were compared with computed rates. The computed rates showed fair agreement and suggested the presence of a liquid-phase mass transfer resistance.

This work was subsequently extended by the same group to show that the evaporative loss of a mass of oil spilled can be estimated using a mass transfer coefficient, K_m , as shown earlier [10]. This approach was investigated with some laboratory data and tested against some known mass transfer conditions on the sea. The conclusion was that this mass transfer approach could result in predictions of evaporation at sea.

Butler developed a model to examine evaporation of specific hydrocarbon components [11]. The weathering rate was taken as proportional to the equilibrium vapor pressure, P , of the compound and to the fraction remaining:

$$dx/dt = -kP(x/x_o) \quad (7.8)$$

where x is the amount of a particular component of a crude oil at time, t ; x_o is the amount of that same component present at the beginning of weathering ($t=0$); k is an empirical rate coefficient; and P is the vapor pressure of the chosen oil component.

Butler assumed that petroleum is a complicated mixture of compounds; therefore, P is not equal to the vapor pressure of the pure compound, but neither would there be large variation in the activity coefficient as the weathering process occurs [11]. For this reason, the activity coefficients were subsumed in the empirical rate coefficient k . P and k were taken as independent of the amount, x , for a fairly wide range of oils. The equation was then directly integrated to give the fraction of the original compound remaining after weathering as

$$x/x_o = \exp(-ktP/x_o) \quad (7.9)$$

The vapor pressure of individual components was fit using a regression line to yield a predictor equation for vapor pressure [11]:

$$P = \exp(10.94 - 1.06N) \quad (7.10)$$

where P is the vapor pressure in Torr and N is the carbon number of the compound in question.

This combined with Equation (7.9) yielded the following expression:

$$x/x_o = \exp[-(kt/x_o) \exp(10.94 - 1.06N)] \quad (7.11)$$

where x/x_o is the fraction of the component left after weathering, k is an empirical constant, x_o is the original quantity of the component, and N is the carbon number of the component in question [1].

Equation (7.11) predicts that the fraction weathered is a function of the carbon number and decreases at a rate that is faster than predicted from simple exponential decay [11]. If the initial distribution of compounds is essentially uniform (x_o independent of N), then the aforementioned equation predicts that the carbon number where a constant fraction (e.g., half) of the initial amount has been lost ($x=0.5 x_o$) is a logarithmic function of the time of weathering:

$$N_{1/2} = 10.66 + 2.17 \log(kt/x_o) \quad (7.12)$$

where $N_{1/2}$ is half the volume fraction of the oil.

The equation was tested using evaporation data from some patches of oil on shoreline, whose age was known [11]. The equation was able to predict the age of the samples relatively well. It was suggested that the equation was applicable to open water spills; however, this was never subsequently applied in models.

Yang and Wang developed an equation using the Mackay and Matsugu molecular diffusion process [12]. The vapor-phase mass transfer process was expressed by

$$D_{ie} = k_m (p_i - p_{i\infty}) / [RT_s] \quad (7.13)$$

where D_{ie} is the vapor-phase mass transfer rate, k_m is a coefficient that lumps all the unknown factors that affect the value of D_{ie} , p_i is the hydrocarbon vapor pressure of fraction I at the interface, $p_{i\infty}$ is the hydrocarbon vapor pressure of fraction I at infinite altitude of the atmosphere, R is the universal gas constant, and T_s is the absolute temperature of the oil slick.

The following functional relationship was proposed [12]:

$$k_m = \alpha A^\gamma e^{qU} \quad (7.14)$$

where A is the slick area; U is the overwater wind speed; and α , q , and γ are empirical coefficients. This relationship was based on the results of past studies, including, for instance, those of MacKay and Matsugu who suggested the value of γ to be in the range from -0.025 to -0.055 [9]. Further experiments were performed by Yang and Wang to determine the

values of “ a ” and “ q .” The results were found to be twofold. Experiments showed that a film formed on evaporating oils and that this film severely retarded evaporation. Before the surface film developed ($\rho_t/\rho_o < 1.0078$),

$$K_{mb} = 69A^{-0.0055} e^{0.42U} \quad (7.15)$$

where K_{mb} is the coefficient that groups all factors affecting evaporation before the surface film has formed and A is the area.

After the surface film developed ($\rho_t/\rho_o > 1.0078$),

$$K_{ma} = 1/5 k_{mb} \quad (7.16)$$

where ρ_o is the initial oil density, ρ_t is the weathered oil density at time t , and K_{ma} is the coefficient that groups all factors affecting evaporation after the surface film has formed [12]. The evaporation rate was found to be reduced fivefold after the formation of the surface film.

Drivas compared the Mackay and Matsugu equation with data found in the literature and noted that the equations yielded predictions that were close to the experimental data [13]. Reijnhart and Rose developed a simple predictor model for the evaporation of oil at sea [14]. They proposed the following simple relationship:

$$Q_{ei} = \alpha C_o \quad (7.17)$$

where Q_{ei} is the evaporation rate of the component of interest, α is a constant incorporating wind velocity and other factors (taken as 0.0009 m/s), and C_o is the equilibrium concentration of the vapor at the oil surface. Several pan experiments were run to simulate evaporation at sea and the data used to test the equation [13]. No method was given for calculating the essential value, C_o .

Brighton proposed that the standard formulation used by many workers required refining [15]. His starting point for water evaporation was similar to that proposed by Sutton:

$$E = K_m C_s U^{7/9} d^{-1/9} Sc^{-r} \quad (7.18)$$

where E is the mean evaporation rate per unit area; K_m is an empirically determined constant, presumably related to the foregoing mass transfer constant; C_s is the concentration of the evaporation fluid (mass/volume); d is the area of the pool; and r is an empirical exponent assigned values from 0 to 2/3.

Brighton suggested that this equation should conform to the basic dimensionless form involving the parameters U and z_0 (wind speed and roughness length, respectively), which define the boundary-layer conditions [15]. The key factor in Brighton’s analysis was to use a linear eddy diffusivity profile. This feature implied that concentration profiles become logarithmic near the surface, which is suspected

to be more realistic compared with the more finite values previously used. Using a power profile to provide an estimation of the turbulence, Brighton was able to substitute the following identities into the classical relationship:

$$U = \frac{u^*}{k} n \quad (7.19)$$

$$n = \left(\ln \frac{z_1}{z_0} \right) \quad (7.20)$$

where u^* is the friction velocity, z_1 is the reference height above the surface, z_0 is the roughness length, and n is the power law dimensionless term.

The evaporation equation now became

$$U \left(\frac{z}{z_1} \right) \frac{\delta X}{\delta x} = \frac{\delta}{\delta z} \left(\frac{ku^*}{\sigma} \frac{z \delta X}{\delta z} \right) \quad (7.21)$$

where z is the height above the surface, X is the concentration of the evaporating compounds, x is the dimension of the evaporating pool, k is given by K/u^*z and is the von Karman constant, and σ is the turbulent Schmidt number (taken as 0.85).

Brighton subsequently compared his model with experimental evaporation data in the field and in the laboratory, which included laboratory oil evaporation data [16]. The model only correlated well with laboratory water evaporation data, and the reason given was that other data sets were “noisy.”

Tkalin proposed a series of equations to predict evaporation at sea [17]:

$$E_i = \frac{K_a M_i P_{oi} x_i}{RT} \quad (7.22)$$

where E_i is the evaporation rate of component i (or the sum of all components) ($\text{kg/m}^2\text{-s}$),

K_a is the mass transfer coefficient (m/s), M_i is the molecular weight, P_{oi} is the vapor pressure of the component i , and x_i is the amount of component i at time t .

Using empirical data, relationships were developed for some of the factors in the equation

$$P_{oi} = 10^3 e^A \quad (7.23)$$

where

$$A = -(4.4 + \log T_b)[1.803\{T_b/T - 1\} - 0.803 \ln(T_b/T)] \quad (7.24)$$

where T_b is the boiling point of the hydrocarbon, given as

$$K_a = 1.25 U 10^{-3} \quad (7.25)$$

The equations were verified using empirical data from the literature [17].

The most frequently used work in older spill modeling is that of Stiver and Mackay [18]. It is based on some of the earlier work by Mackay and Matsugu [9]. Additional information is given in a thesis by Stiver [19]. The formulation was initiated with assumptions about the evaporation of a liquid. If a liquid is spilled, the rate of evaporation is given by

$$N = KAP/(RT) \quad (7.26)$$

where N is the evaporative molar flux (mol/s), K is the mass transfer coefficient under the prevailing wind (m/s), A is the area (m²), and P is the vapor pressure of the bulk liquid.

This equation was arranged to give

$$dF_v/dt = KAPv/(V_o RT) \quad (7.27)$$

where F_v is the volume fraction evaporated, v is the liquid's molar volume (m³/mol), and V_o is the initial volume of the spilled liquid (m³).

By rearranging, we obtain

$$dF_v = [Pv/(RT)](KAdt/V_o) \quad (7.28)$$

$$\text{or } dF_v = Hd\theta \quad (7.29)$$

where H is Henry's law constant and θ is the evaporative exposure (defined in the following).

The right-hand side of the second last equation has been separated into two dimensionless groups. The group, $KAdt/V_o$, represents the time rate of what has been termed the "evaporative exposure" and was denoted as $d\theta$. The evaporative exposure is a function of the time, the spill area and volume (or thickness), and the mass transfer coefficient (which is dependent on the wind speed). The evaporative exposure can be viewed as the ratio of exposed vapor volume to the initial liquid volume [18].

The group $Pv/(RT)$ or H is a dimensionless Henry's law constant or ratio of the equilibrium concentration of the substance in the vapor phase $[P/(RT)]$ to that in the liquid (l/v) . H is a function of temperature. The product θH is thus the ratio of the amount that has evaporated (oil concentration in vapor times vapor volume) to the amount originally present. For a pure liquid, H is independent of F_v and Equation 7.29 was integrated directly to give

$$F_v = H\theta \quad (7.30)$$

If K , A , and temperature are constant, the evaporation rate is constant and evaporation is complete (F_v is unity) when θ achieves a value of $1/H$ [18].

If the liquid is a mixture, H depends on F_v and the basic equation can only be integrated if H is expressed as a function

of F_v ; that is, the principal variable of vapor pressure is expressed as a function of composition. The evaporation rate slows as evaporation proceeds in such cases.

Equation (7.28) was replaced with a new equation developed using laboratory empirical data:

$$F_v = (T/K_1) \ln(1 + K_1\theta/T) \exp(K_2 - K_3/T) \quad (7.31)$$

where F_v is the volume fraction evaporated and $K_{1,2,3}$ are empirical constants [18].

A value for K_1 was obtained from the slope of the F_v versus $\log \theta$ curve from pan or bubble evaporation experiments. For θ greater than 10^4 , K_1 was found to be approximately $2.3T$ divided by the slope. The expression $\exp(K_2 - K_3/T)$ was then calculated, and K_2 and K_3 determined individually from evaporation curves at two different temperatures.

Hamoda and coworkers performed theoretical and experimental work on evaporation [20]. An equation was developed to express the effects of American Petroleum Institute gravity (API°—a unit of density) of the crude oil, temperature, and salinity on the mass transfer coefficient K :

$$K = 1.68 \times 10^{-5} (\text{API}^\circ)^{1.253} (T)^{1.80} e^{0.1441} \quad (7.32)$$

where K is the mass transfer coefficient, cm/h; API° is the density in API units, unitless; and e is the water salinity in degrees salinity or parts per thousand. The exponents of the equation were determined by multiple linear regression on experimental data.

Quin and coworkers weathered oils in a controlled environment and correlated the data with equations developed starting with Fick's diffusion law and the Clausius–Clapeyron equation [21]. Crude oil was divided into a series of pseudofractions by boiling point. Each fraction was taken to be equivalent to an n -paraffin. The n -paraffin distributions of a number of naturally weathered crude oils were determined by capillary gas–liquid chromatography. The actual measured evaporation was compared with those generated by computer simulation of weathering. Good agreement was obtained for oil film thicknesses between 10 μm and 1 mm, weathered for periods of up to 4 weeks.

Brown and Nicholson studied the weathering of a heavy oil, bitumen [22]. They compared experimental data using a large-scale weathering tank with two spill model outputs. In the Fate Of Oil Spills model, the evaporative exposure concept is used in which the fraction of oil evaporated is given by a variant of the Mackay equation:

$$F = [\ln(P) + \ln(CE) + 1/P]/C \quad (7.33)$$

where F is the fraction evaporated, C is an empirical constant, and E is a measure of the evaporative exposure, defined as

$$E = (K_m Avt)/(RTV_o) \quad (7.34)$$

where

$$K_m = 0.0048 U^{0.78} Z^{-0.11} Sc^{0.67} \quad (7.35)$$

and where K_m is the mass transfer coefficient, A is the slick area, v is the oil molar volume, V_0 is the initial slick volume, Z is the pool size scale factor, and Sc is the Schmidt number (taken as 2.7) [22].

Brown and Nicholson compared the measured evaporation for a 5 m/s wind at an ambient temperature of 20°C, and evaluation was done with the equation earlier. A spill volume of 100 m³ was assumed. A value of about 10⁻⁵ m³/mol was used for the average molar volume. The model generally described the observed evaporation quite well, particularly during the first few hours. Later however, it was found that the model consistently overpredicted the evaporation rate. A simple method of correcting the equation was implemented by assuming that the vapor-phase Schmidt number decreases slightly as the skin on the oil thickens. Subsequently, the evaporative exposure was modified to

$$K_m = (0.0025 - 0.000021t) U^{0.78} \quad (7.36)$$

The predicted evaporation then compared favorably with the measured values.

A commercial model was also compared with the experimental data [22]. This model assumed that the oil consists of a series of components each with a distinct boiling point, API gravity, and molecular weight. A mass transfer rate from the slick was then written for each component as

$$dm/dt = K_m P_i A F_i \text{Mass}_i / RT \quad (7.37)$$

where dm/dt is the mass transfer rate, K_m is the mass transfer coefficient of Mackay, P_i is the vapor pressure of each component, F_i is the fraction of each component remaining, and Mass_i is the mass of each component.

For this simulation, boiling points, volume percents, and API gravities were input for 13 boiling ranges. The general shape of the model curve agreed well with the measured data but the model predicts a higher overall evaporation rate.

Bobra conducted laboratory studies on the evaporation of crude oils [23]. The evaporation curves for several crude oils and petroleum products were measured under several different environmental conditions. These data were compared to the equation developed by Stiver and Mackay [19]. The equation used was

$$F_v = \ln[1 + B(T_G/T)\theta \exp(A - BT_0/T)]\{T/BT_G\} \quad (7.38)$$

where F_v is the fraction evaporated, T_G is the gradient of the modified distillation curve, A and B are dimensionless constants, T_0 is the initial boiling point of the oil, and θ is the evaporative exposure as previously defined.

The results from several comparison runs were carried out to evaluate evaporation models [23]. The agreement between

the experimental data and the equation results were good in a few cases, but poor in most. This comparison showed that the Stiver and Mackay equation predicts the evaporation of most oils relatively well until time approaches 8 h, after which it overpredicted the evaporation. The “overshoot” could be as much as 10% evaporative loss at the 24 h mark. This is especially true for very light oils. The Stiver and Mackay equation was also found to underpredict or overpredict the evaporation of oils in the initial phases. Bobra also noted that most oil evaporation follows a logarithmic curve with time and that a simple approach to this was much more accurate than using Equation (7.38) [23].

In summary, it is difficult to develop a theoretical approach to oil evaporation for several reasons. First, oil consists of many components, and thus, there is no constant boiling point, vapor pressure, or other essential properties used in typical evaporation models. Further, oil evaporation proceeds by diffusion regulation and not by air-boundary-layer regulation. Water evaporation models cannot be accurately modified to oil evaporation for these reasons.

7.3 DEVELOPMENT OF NEW DIFFUSION-REGULATED MODELS

A review of the predictive and theoretical work in Section 7.2 reveals that air-boundary-layer concepts are limited and cannot accurately explain long-term evaporation. Fingas conducted a series of experiments over several years to examine the concepts further [1,24].

The results of the boundary-layer regulation experiments are presented in the order of the experimental series.

7.3.1 Wind Experiments

A simple experiment to determine whether or not oil evaporation is air-boundary-layer regulated is to measure if the evaporation rate increases with wind as would be predicted by Equations (7.2 and 7.7) [24]. Experiments on the evaporation of oil with and without winds were conducted with Alberta Sweet Mixed Blend (ASMB), gasoline, and water. Water formed a baseline data set since this is the substance being compared [3]. Regressions on the data were performed and the equation parameters calculated. Curve coefficients are the constants from the best-fit equation [$\text{Evap} = a \ln(t)$], t = time in minutes, for logarithmic equations or $\text{Evap} = a\sqrt{t}$, for square root equations. Oils such as diesel fuel with few subcomponents evaporating at one time have a tendency to fit square root curves [5,25]. While data were calculated separately for percentage of weight lost and absolute weight, the latter is usually used because it is more convenient. The plots of wind speed versus the evaporation rate (as a percentage of weight lost) for each oil type are shown in Figures 7.4, 7.5, and 7.6. These figures show that the evaporation rates for oils and even the light product, gasoline, are not increased with increasing wind speed. In most cases, there is a small rise from the

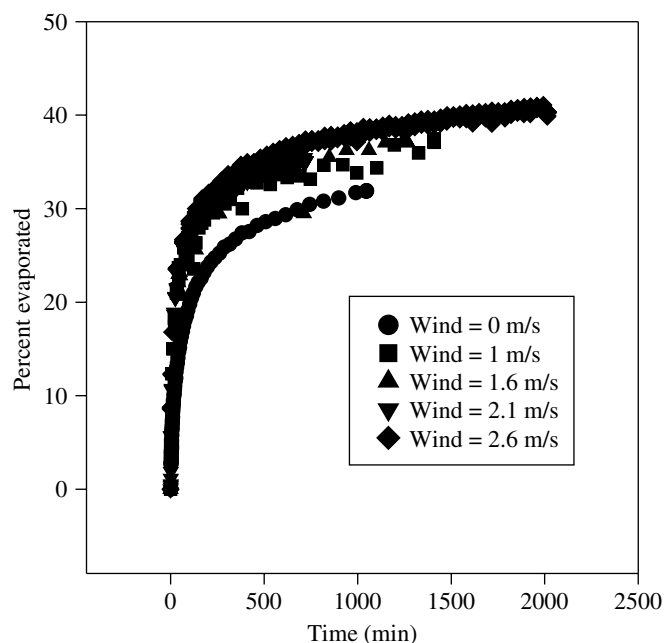


FIGURE 7.4 Evaporation of a crude oil with varying wind velocities. This figure shows that there is little variation with wind velocity except in going from the 0-wind level up to high wind levels. This is due to the stirring effect of wind and not air-boundary-layer regulation.

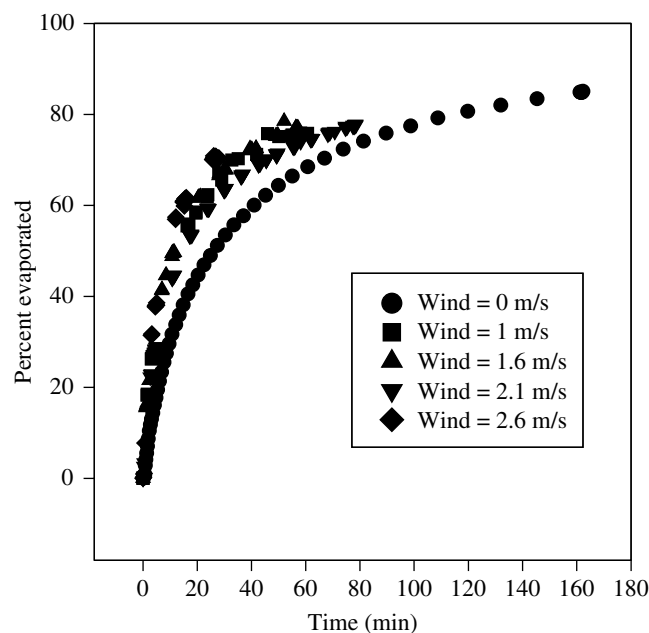


FIGURE 7.5 Evaporation of gasoline subjected to varying wind velocities. This figure also shows that there is little variation with wind velocity except in going from the 0-wind level up to the higher wind levels. This again is because of the stirring effect of wind and not air-boundary-layer regulation.

0-wind level to the 1-m/s level, but after that, the rate remains relatively constant. The evaporation rate after the 0-wind value is nearly identical for all oils. This is due to the stirring effect on the oil, which increases the diffusion rate to the

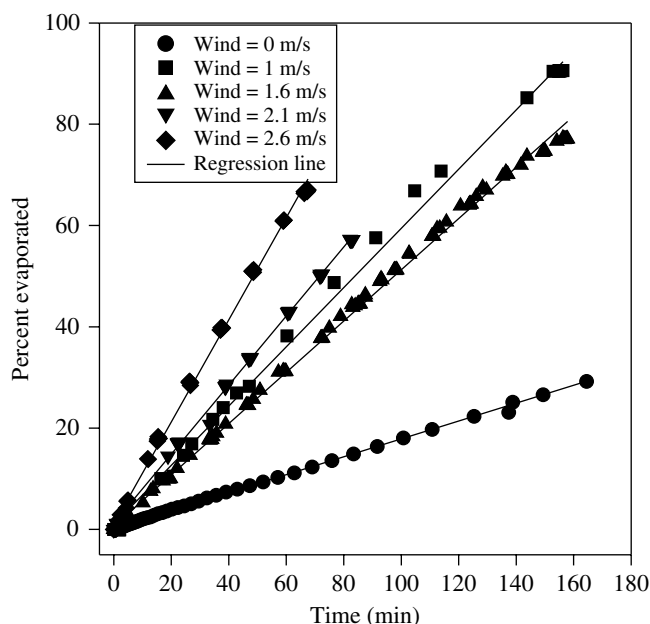


FIGURE 7.6 Evaporation of water with varying wind velocities. This figure shows the large differences in the evaporation rate of water with wind velocity. This is typical of air-boundary-layer regulation. Compare Figure 7.6 with oil evaporation in Figures 7.4 and 7.5 which do not show this trend of variance with wind velocity.

surface. The oil evaporation data can be compared to the evaporation of water, as illustrated in Figure 7.6. These data show the classical relationship of the water evaporation rate with the wind speed (evaporation varies as $U^{0.78}$, where U is the wind speed). This correlation shows that the oils studied here not boundary-layer regulated.

Figure 7.7 shows the rates of evaporation compared to the wind speed for all the liquids used in this study. This figure shows the evaporation rates of all test liquids versus wind speed. The lines shown are those calculated by linear regression. This clearly shows that water evaporation rate increased, as expected, with increasing wind velocity. The oils, ASMB and gasoline, do not show increases with increasing wind speed.

All the aforementioned data show that oil is not air-boundary-layer regulated.

7.3.2 Variation with Area

Air-boundary-layer-regulated liquids evaporate much faster if one increases the area [24]. A small spill of water on the kitchen floor can be evaporated quickly by spreading it out. A test of this tendency will also give confirmation on the proposition that oil is diffusion regulated. ASMB was also used to conduct a series of experiments with varying evaporation area. The mass of the oil was kept constant so that the thickness of the oil would also vary. However, the greater the area, the lesser the thickness and both factors would increase oil evaporation if it were boundary-layer regulated. The experiments showed no correlation between area and evaporation rate. One can conclude that evaporation rate is not highly correlated with area and thus the evaporation of oil is not air-boundary-layer regulated.

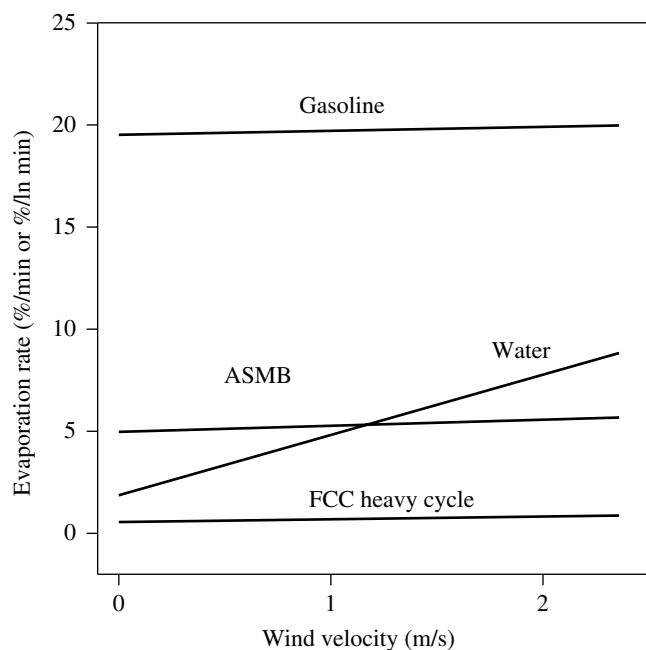


FIGURE 7.7 Correlation of evaporation rates and wind velocity. The lines are drawn through the data points from experimental values. This clearly shows no correlation of oil evaporation rates with wind velocity and the strong and expected high correlation of water with wind velocity. The water evaporation line has been moved to fit on the vertical scale. ASMB is Alberta Sweet Mixed Blend crude oil.

7.3.3 Variation with Mass

Air-boundary-layer liquids showed no correlation between the mass of oil evaporated and the evaporation rate; however, diffusion-regulated liquids do [24]. ASMB oil was again used to conduct a series of experiments with volume as the major variant. Alternatively, thickness and area were held constant to ensure that the strict relationship between these two variables did not affect the final regression results. Figure 7.8 illustrates the relationship between evaporation rate and volume of evaporation material (also equivalent to mass of evaporating material). This figure shows the strong correlation between oil mass (or volume) and evaporation rate. This again proves that there is no boundary-layer regulation.

7.3.4 Evaporation of Pure Hydrocarbons

A study of the evaporation rate of pure hydrocarbons was conducted to test the classic boundary-layer evaporation theory as applied to the hydrocarbon constituents of oils [24]. The evaporation rate data are illustrated in Figure 7.9. This figure shows that the evaporation rates of the pure hydrocarbons have a variable response to wind. Heptane (hydrocarbon number 7) shows a large difference between evaporation rate in wind and no wind conditions, indicating boundary-layer regulation. Decane (carbon number 10) shows a lesser effect, and dodecane (carbon number 12) shows a negligible difference between the two experimental conditions. This experiment shows the extent of boundary-layer regulation

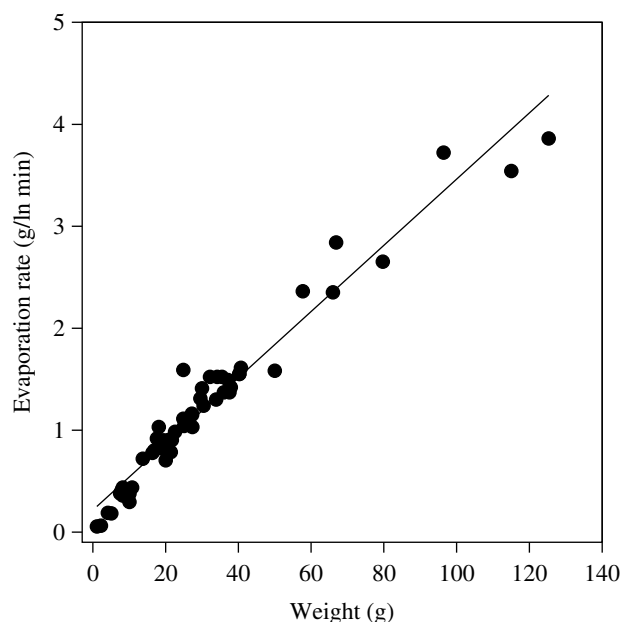


FIGURE 7.8 Correlation of oil mass with evaporation rate. The plots are the equation factors from the evaporation equation which is approximately equivalent to evaporation rate. This shows a direct relationship between evaporation rate of oil and mass of oil. This indicates that oil is diffusion regulated.

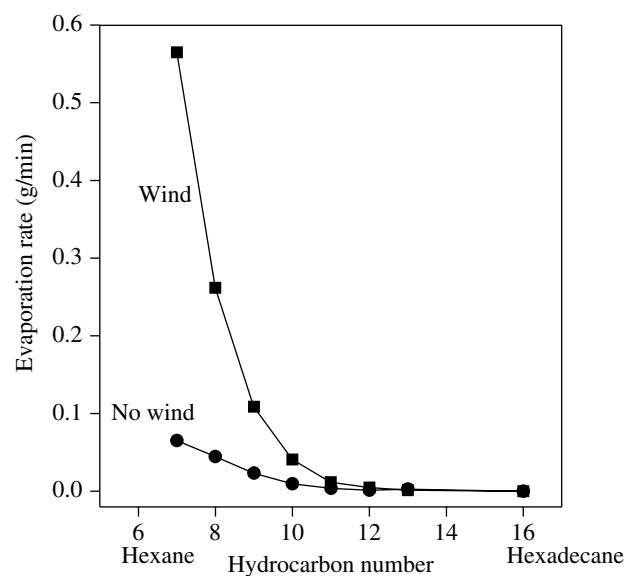


FIGURE 7.9 Evaporation rate of pure hydrocarbons. This shows that hydrocarbons up to about C12 (dodecane) show some air-boundary-regulated behavior whereas those above C12 show no air-boundary-regulated behavior. As most compounds in oil are higher than dodecane, the bulk oil would not show air-boundary-regulated behavior.

and the reason for the small or negligible degree of boundary-layer regulation shown by crude oils and petroleum products. Crude oil contains very little material with carbon numbers less than dodecane, often less than 3% of its composition. Even the more volatile petroleum products, gasoline

TABLE 7.1 Saturation concentration of water and hydrocarbons

Substance	Saturation concentration ^a in g/m ³ at 25°C
Water	20
<i>n</i> -Pentane	1689
Hexane	564
Cyclohexane	357
Benzene	319
<i>n</i> -Heptane	196
Methylcyclohexane	192
Toluene	110
Ethylbenzene	40
<i>p</i> -Xylene	38
<i>m</i> -Xylene	35
<i>o</i> -Xylene	29

^aValues taken from Ullmann's Encyclopedia [26].

and diesel fuel, only have limited amounts of compounds more volatile than decane and thus are also not strongly boundary-layer regulated if at all.

7.3.5 Saturation Concentration

Another evaluation of evaporation regulation is that of saturation concentration, the maximum concentration soluble in air. The saturation concentrations of water and several oil components are listed in Table 7.1 [26]. This table shows that saturation concentration of water is less than that of common oil components. The saturation concentration of water is in fact about two orders of magnitude less than the saturation concentration of volatile oil components such as pentane. This further explains why even light oil components have little boundary-layer limitation. Further, the saturation concentration of water is so regulating that with a high relative humidity, there is little that can be added to the air.

7.3.6 Development of Generic Equations Using Distillation Data

The evaporation equations for oils show unique differences for oils under the same conditions. This implies that unique equations may be needed for each oil and this fact is a significant disadvantage to practical end use. A method to accurately predict evaporation using other readily available data is necessary [27]. Findings show that distillation data can be used to predict evaporation. Distillation data are very common and are often the only data used to characterize oils. This is because the data are crucial in operating refineries. Crude oils are sometimes priced on the basis of their distillation data.

It was noted that oils and fuels evaporated as two distinct types, those that evaporated as a logarithm of time and those that evaporated as a square root of time [5]. Most oils typically evaporated as a logarithm (natural) of time. Diesel fuel and similar oils, such as jet fuel, kerosene, and the like, evaporate as a square root of time [1,25]. The reasons for this are

simply that diesel fuel and such like have a narrower range of compounds that evaporate at similar yield rates, which sum as a square root [5].

The empirically measured parameters at 15°C were correlated with both the slopes and the intercepts of the temperature equations. Full details of this correlation are given in the literature [28–30]. For the variation with temperature, the resulting equation is

$$\text{Percentage evaporated} = [B + 0.045 (T - 15)] \ln(t) \quad (7.39)$$

where B is the equation parameter at 15°C, T is the temperature in degree Celsius, and t is the time in minutes.

Distillation data were correlated to the evaporation rates determined by experimentation. The optimal point was found to be 180°C by using peak functions. The percent mass distilled at 180° was used to calculate the relationship between the distillation values and the equation parameters. The equations used were derived from correlations of the data.

The data from those oils that were better fitted with square root equations—diesel, Bunker C light, and FCC heavy cycle—were calculated separately.

The equations derived from the regressions are as follows:

For oils that follow a logarithmic equation,

$$\text{Percentage evaporated} = 0.165(\%D) \ln(t) \quad (7.40)$$

For oils that follow a square root equation,

$$\text{Percentage evaporated} = 0.0254(\%D) \sqrt{t} \quad (7.41)$$

where $\%D$ is the percentage (by weight) distilled at 180°C.

These equations can be combined with the equations generated in previous work as shown in Equation (7.39) to account for the temperature variations:

For oils that follow a logarithmic equation,

$$\text{Percentage evaporated} = [0.165(\%D) + 0.045(T - 15)] \ln(t) \quad (7.42)$$

For oils that follow a square root equation,

$$\text{Percentage evaporated} = [0.0254(\%D) + 0.01(T - 15)] \sqrt{t} \quad (7.43)$$

where $\%D$ is the percentage (by weight) distilled at 180°C.

A large number of experiments were performed on oils to directly measure their evaporation curves. The empirical equations that result are given in Table 7.2.

Since the equations described earlier require only time and temperature (or at the very worst, the percentage of oil distilled at 180°C), it is relatively simple to apply these forms of equations. They can also be applied in models as increments where t , the time, becomes the total time and the previous evaporation is subtracted, for example, if one was modeling the evaporation of ASMB oil in the time step from 12 to 15 h. The equation is (from Table 7.2)

$$\text{Percentage evaporation} = (3.24 + 0.054T) \ln(t) \quad (7.44)$$

TABLE 7.2 Equations for predicting evaporation

Oil type	Equation	Oil type	Equation
Adgo, Beaufort Sea	$\%Ev = (0.11 + 0.013T) \sqrt{t}$	Jet 40 Fuel	$\%Ev = (8.96 + 0.045T) \ln(t)$
Adgo—long term	$\%Ev = (0.68 + 0.045T) \ln(t)$	Jet A1	$\%Ev = (0.59 + 0.013T) \sqrt{t}$
Alaminos Canyon Block 25	$\%Ev = (2.01 + 0.045T) \ln(t)$	Jet Fuel (Anch)	$\%Ev = (7.19 + 0.045T) \ln(t)$
Alaska North Slope (2002)	$\%Ev = (2.86 + 0.045T) \ln(t)$	Jet Fuel (Anch) short term	$\%Ev = (1.06 + 0.013T) \sqrt{t}$
Alberta Sweet Mixed Blend	$\%Ev = (3.24 + 0.054T) \ln(t)$	Komineft, Russia	$\%Ev = (2.73 + 0.045T) \ln(t)$
Amauligak, Beaufort Sea	$\%Ev = (1.63 + 0.045T) \ln(t)$	Lago, Angola	$\%Ev = (1.13 + 0.045T) \ln(t)$
Amauligak—f24	$\%Ev = (1.91 + 0.045T) \ln(t)$	Lago Treco, Venezuela	$\%Ev = (1.12 + 0.045T) \ln(t)$
Anadarko H1A-376	$\%Ev = (2.66 + 0.013T) \sqrt{t}$	Lucula, Angola	$\%Ev = (2.17 + 0.045T) \ln(t)$
Arabian Medium	$\%Ev = (1.89 + 0.045T) \ln(t)$	Main Pass Block 306	$\%Ev = (2.86 + 0.045T) \ln(t)$
Arabian Heavy	$\%Ev = (1.31 + 0.045T) \ln(t)$	Main Pass Block 37	$\%Ev = (3.04 + 0.045T) \ln(t)$
Arabian Heavy	$\%Ev = (2.71 + 0.045T) \ln(t)$	Malongo, Angola	$\%Ev = (1.67 + 0.045T) \ln(t)$
Arabian Light	$\%Ev = (2.52 + 0.037T) \ln(t)$	Marinus Turbine Oil	$\%Ev = (-0.68 + 0.045T) \ln(t)$
Arabian Light	$\%Ev = (3.41 + 0.045T) \ln(t)$	Marinus Valve Oil	$\%Ev = (-0.68 + 0.045T) \ln(t)$
Arabian Light (2001)	$\%Ev = (2.4 + 0.045T) \ln(t)$	Mars TLP, GOM, USA	$\%Ev = (2.18 + 0.045T) \ln(t)$
ASMB—standard #5	$\%Ev = (3.35 + 0.045T) \ln(t)$	Maui, New Zealand	$\%Ev = (-0.14 + 0.013T) \sqrt{t}$
ASMB (offshore)	$\%Ev = (2.2 + 0.045T) \ln(t)$	Maya, Mexico	$\%Ev = (1.38 + 0.045T) \ln(t)$
Av Gas 80	$\%Ev = (15.4 + 0.045T) \ln(t)$	Mayan crude	$\%Ev = (1.45 + 0.045T) \ln(t)$
Avalon, NL, Canada	$\%Ev = (1.41 + 0.045T) \ln(t)$	Mississippi Canyon Block 807	$\%Ev = (2.28 + 0.045T) \ln(t)$
Avalon J-34	$\%Ev = (1.58 + 0.045T) \ln(t)$	Mississippi Canyon Block 72	$\%Ev = (2.15 + 0.045T) \ln(t)$
Aviation Gasoline 100 LL	$\ln(\%Ev) = (0.5 + 0.045T) \ln(t)$	Mississippi Canyon Block 194	$\%Ev = (2.62 + 0.045T) \ln(t)$
Azeri—long term, Azerbaijan	$\%Ev = (1.3 + 0.045T) \ln(t)$	Mississippi Canyon Block 807	$\%Ev = (2.05 + 0.045T) \ln(t)$
Azeri—short term	$\%Ev = (-0.09 + 0.013T) \sqrt{t}$	Morpeth, LA, USA	$\%Ev = (1.58 + 0.013T) \sqrt{t}$
Barrow Island, Australia	$\%Ev = (4.67 + 0.045T) \ln(t)$	Nektoralik, Beaufort Sea	$\%Ev = (0.62 + 0.045T) \ln(t)$
BCF-24, Venezuela	$\%Ev = (1.08 + 0.045T) \ln(t)$	Neptune Spar (Viosca Knoll 826)	$\%Ev = (3.75 + 0.045T) \ln(t)$
Belridge Crude, CA, USA	$\%Ev = (0.01 + 0.013T) \sqrt{t}$	Nerlerk, Beaufort Sea	$\%Ev = (2.01 + 0.045T) \ln(t)$
Bent Horn A-02, NS, Canada	$\%Ev = (3.19 + 0.045T) \ln(t)$	Ninian, UK	$\%Ev = (2.65 + 0.045T) \ln(t)$
Beta, CA, USA	$\%Ev = (-0.08 + 0.013T) \sqrt{t}$	Norman Wells, Canada	$\%Ev = (3.11 + 0.045T) \ln(t)$
Beta—long term	$\%Ev = (0.29 + 0.045T) \ln(t)$	North Slope—middle pipeline	$\%Ev = (2.64 + 0.045T) \ln(t)$
Boscan, Venezuela	$\%Ev = (-0.15 + 0.013T) \sqrt{t}$	North Slope—northern pipeline	$\%Ev = (2.64 + 0.045T) \ln(t)$
Brent, UK	$\%Ev = (3.39 + 0.048T) \ln(t)$	North Slope—southern pipeline	$\%Ev = (2.47 + 0.045T) \ln(t)$
Bunker C—light (IFO~250)	$\%Ev = (0.0035 + 0.0026T) \sqrt{t}$	Nugini, New Guinea	$\%Ev = (1.64 + 0.045T) \ln(t)$
Bunker C—long term	$\%Ev = (-0.21 + 0.045T) \ln(t)$	Odoptu, Russia	$\%Ev = (4.27 + 0.045T) \ln(t)$
Bunker C (2002)	$\%Ev = (-0.16 + 0.013T) \sqrt{t}$	Olive oil	Litte
Bunker C (short term)	$\%Ev = (0.35 + 0.013T) \sqrt{t}$	Oriente, Ecuador	$\%Ev = (1.32 + 0.045T) \ln(t)$
Bunker C anchorage	$\%Ev = (-0.13 + 0.013T) \sqrt{t}$	Oriente	$\%Ev = (1.57 + 0.045T) \ln(t)$
Bunker C anchorage (long term)	$\%Ev = (0.31 + 0.045T) \ln(t)$	Orimulsion 400—dewater	$\%Ev = (3.6) \ln(t)$ (at 15°C)
California API 11	$\%Ev = (-0.13 + 0.013T) \sqrt{t}$	Orimulsion plus water	$\%Ev = (3 + 0.045T) \ln(t)$
California API 15	$\%Ev = (-0.14 + 0.013T) \sqrt{t}$	Oseberg, Norway	$\%Ev = (2.68 + 0.045T) \ln(t)$
Cano Limon, Colombia	$\%Ev = (1.71 + 0.045T) \ln(t)$	Panuke, NS, Canada	$\%Ev = (7.12 + 0.045T) \ln(t)$
Canola oil	Litte	Petronius VK981A	$\%Ev = (2.27 + 0.013T) \sqrt{t}$
Carpinteria, CA, USA	$\%Ev = (1.68 + 0.045T) \ln(t)$	Pitas Point, CA, USA	$\%Ev = (7.04 + 0.045T) \ln(t)$
Cat Cracking Feed	$\%Ev = (-0.18 + 0.013T) \sqrt{t}$	Platform Gail (Sockeye)	$\%Ev = (1.68 + 0.045T) \ln(t)$
Chayvo, Russia	$\%Ev = (3.52 + 0.045T) \ln(t)$	Platform Holly, CA, USA	$\%Ev = (1.09 + 0.045T) \ln(t)$
Cold Lake Bitumen, AB, Canada	$\%Ev = (-0.16 + 0.013T) \sqrt{t}$	Platform Irene—long term	$\%Ev = (0.74 + 0.045T) \ln(t)$
Combined oil/gas	$\%Ev = (-0.08 + 0.013T) \sqrt{t}$	Platform Irene—short term	$\%Ev = (-0.05 + 0.013T) \sqrt{t}$
Compressor lube oil—new	$\%Ev = (-0.68 + 0.045T) \ln(t)$	Point Arguello—comingled	$\%Ev = (1.43 + 0.045T) \ln(t)$
Cook Inlet—Granite Point	$\%Ev = (4.54 + 0.045T) \ln(t)$	Point Arguello heavy	$\%Ev = (0.94 + 0.045T) \ln(t)$
Cook Inlet—Swanson River	$\%Ev = (3.58 + 0.045T) \ln(t)$	Point Arguello light	$\%Ev = (2.44 + 0.045T) \ln(t)$
Cook Inlet New Batch	$\%Ev = (3.1 + 0.045T) \ln(t)$	Point Arguello light—b	$\%Ev = (2.3 + 0.045T) \ln(t)$
Cook Inlet Trading Bay	$\%Ev = (3.15 + 0.045T) \ln(t)$	Polypropylene Tetramer	$\%Ev = (0.25)(t)$ (at 15°C)
Corrosion Inhibitor Solvent	$\%Ev = (-0.02 + 0.013T) \sqrt{t}$	Port Hueneme, CA, USA	$\%Ev = (0.3 + 0.045T) \ln(t)$
Crude Castor oil	Litte	Prudhoe Bay—old stock	$\%Ev = (1.69 + 0.045T) \ln(t)$
Cusiana, Colombia	$\%Ev = (3.39 + 0.045T) \ln(t)$	Prudhoe Bay (new stock)	$\%Ev = (2.37 + 0.045T) \ln(t)$
Delta West Block 97, USA	$\%Ev = (6.57 + 0.045T) \ln(t)$	Prudhoe stock b	$\%Ev = (1.4 + 0.045T) \ln(t)$
Diesel—anchorage—long	$\%Ev = (4.54 + 0.045T) \ln(t)$	Rangely, CO, USA	$\%Ev = (1.89 + 0.045T) \ln(t)$
Diesel—anchorage—short	$\%Ev = (0.51 + 0.013T) \sqrt{t}$	Sahara Blend, Algeria	$\%Ev = (0.001 + 0.013T) \sqrt{t}$
Diesel—long term	$\%Ev = (5.8 + 0.045T) \ln(t)$	Sahara Blend (long term)	$\%Ev = (1.09 + 0.045T) \ln(t)$
Diesel Mobile 1997	$\%Ev = (0.03 + 0.013T) \sqrt{t}$	Sakhalin, Russia	$\%Ev = (4.16 + 0.045T) \ln(t)$
Diesel (2002)	$\%Ev = (0.02 + 0.013T) \sqrt{t}$	Santa Clara, CA, USA	$\%Ev = (1.63 + 0.045T) \ln(t)$
Diesel (regular stock)	$\%Ev = (0.31 + 0.018T) \sqrt{t}$	Scotia light	$\%Ev = (6.87 + 0.045T) \ln(t)$
Diesel fuel—Southern—long term	$\%Ev = (2.18 + 0.045T) \ln(t)$	Scotia light	$\%Ev = (6.92 + 0.045T) \ln(t)$
Diesel fuel—Southern—short term	$\%Ev = (-0.02 + 0.013T) \sqrt{t}$	Ship Shoal Block 239	$\%Ev = (2.71 + 0.045T) \ln(t)$
Diesel Fuel 2002	$\%Ev = (5.91 + 0.045T) \ln(t)$	Ship Shoal Block 269	$\%Ev = (3.37 + 0.045T) \ln(t)$

(Continued)

TABLE 7.2 (Continued)

Oil type	Equation	Oil type	Equation
Diesel Fuel 2002 short	$\%Ev = (0.39 + 0.013T) \sqrt{t}$	Sockeye, CA, USA	$\%Ev = (2.14 + 0.045T) \ln(t)$
Diesel Mobile 1997 long-term	$\%Ev = (-0.02 + 0.013T) \sqrt{t}$	Sockeye (2001)	$\%Ev = (1.52 + 0.045T) \ln(t)$
Dos Cuadras, CA, USA	$\%Ev = (1.88 + 0.045T) \ln(t)$	Sockeye comingled	$\%Ev = (1.38 + 0.045T) \ln(t)$
Ekofisk, Norway	$\%Ev = (4.92 + 0.045T) \ln(t)$	Sockeye sour	$\%Ev = (1.32 + 0.045T) \ln(t)$
Empire Crude, LA, USA	$\%Ev = (2.21 + 0.045T) \ln(t)$	Sockeye sweet	$\%Ev = (2.39 + 0.045T) \ln(t)$
Endicott, AK, USA	$\%Ev = (0.9 + 0.045T) \ln(t)$	South Louisiana	$\%Ev = (2.39 + 0.045T) \ln(t)$
Esso Spartan EP-680 industrial oil	$\%Ev = (-0.66 + 0.045T) \ln(t)$	South Louisiana (2001)	$\%Ev = (2.74 + 0.045T) \ln(t)$
Eugene Island 224—condensate	$\%Ev = (9.53 + 0.045T) \ln(t)$	South Pass Block 60	$\%Ev = (2.91 + 0.045T) \ln(t)$
Eugene Island Block 32	$\%Ev = (0.77 + 0.045T) \ln(t)$	South Pass Block 67	$\%Ev = (2.17 + 0.045T) \ln(t)$
Eugene Island Block 43	$\%Ev = (1.57 + 0.045T) \ln(t)$	South Pass Block 93	$\%Ev = (1.5 + 0.045T) \ln(t)$
Everdell, AB, Canada	$\%Ev = (3.38 + 0.045T) \ln(t)$	South Timbalier Block 130	$\%Ev = (2.77 + 0.045T) \ln(t)$
FCC heavy cycle	$\%Ev = (0.17 + 0.013T) \sqrt{t}$	Soybean oil	Litte
FCC light	$\%Ev = (-0.17 + 0.013T) \sqrt{t}$	Statfjord, Norway	$\%Ev = (2.67 + 0.06T) \ln(t)$
FCC medium cycle	$\%Ev = (-0.16 + 0.013T) \sqrt{t}$	Sumatran Heavy, Indonesia	$\%Ev = (-0.11 + 0.013T) \sqrt{t}$
FCC-VGO	$\%Ev = (2.5 + 0.013T) \sqrt{t}$	Sumatran Light	$\%Ev = (0.96 + 0.045T) \ln(t)$
Federated, AB, Canada	$\%Ev = (3.47 + 0.045T) \ln(t)$	Taching, China	$\%Ev = (-0.11 + 0.013T) \sqrt{t}$
Federated (new—1999)	$\%Ev = (3.45 + 0.045T) \ln(t)$	Takula, Angola	$\%Ev = (1.95 + 0.045T) \ln(t)$
Fuel oil #5	$\%Ev = (-0.14 + 0.013T) \sqrt{t}$	Tapis, Malaysia	$\%Ev = (3.04 + 0.045T) \ln(t)$
Garden Banks 387, GOM, USA	$\%Ev = (1.84 + 0.045T) \ln(t)$	Tchatamba Crude, Gabon	$\%Ev = (3.8 + 0.045T) \ln(t)$
Garden Banks 426	$\%Ev = (3.44 + 0.045T) \ln(t)$	Terra Nova, NL, Canada	$\%Ev = (1.36 + 0.045T) \ln(t)$
Gasoline	$\%Ev = (13.2 + 0.21T) \ln(t)$	Terresso 150	$\%Ev = (-0.68 + 0.045T) \ln(t)$
Genesis, GOM, USA	$\%Ev = (2.12 + 0.045T) \ln(t)$	Terresso 220	$\%Ev = (-0.66 + 0.045T) \ln(t)$
Green Canyon Block 109	$\%Ev = (1.58 + 0.045T) \ln(t)$	Terresso 46 industrial oil	$\%Ev = (-0.67 + 0.045T) \ln(t)$
Green Canyon Block 184	$\%Ev = (3.55 + 0.045T) \ln(t)$	Thevenard Island, Australia	$\%Ev = (5.74 + 0.045T) \ln(t)$
Green Canyon Block 200	$\%Ev = (3.11 + 0.045T) \ln(t)$	Troll, Norway	$\%Ev = (2.26 + 0.045T) \ln(t)$
Green Canyon Block 65	$\%Ev = (1.56 + 0.045T) \ln(t)$	Turbine oil STO 90	$\%Ev = (-0.68 + 0.045T) \ln(t)$
Greenplus hydraulic oil	$\%Ev = (-0.68 + 0.045T) \ln(t)$	Turbine oil STO 120	$\%Ev = (-0.68 + 0.045T) \ln(t)$
Greenplus hydraulic oil	$\%Ev = (-0.68 + 0.045T) \ln(t)$	Udang, Indonesia	$\%Ev = (-0.14 + 0.013T) \sqrt{t}$
Gullfaks, Norway	$\%Ev = (2.29 + 0.034T) \ln(t)$	Udang (long term)	$\%Ev = (0.06 + 0.045T) \ln(t)$
Heavy reformate	$\%Ev = (-0.17 + 0.013T) \sqrt{t}$	Vasconia, Colombia	$\%Ev = (0.84 + 0.045T) \ln(t)$
Hebron MD-4, NL, Canada	$\%Ev = (1.01 + 0.045T) \ln(t)$	Viosca Knoll Block 826	$\%Ev = (2.04 + 0.045T) \ln(t)$
Heidrun, Norway	$\%Ev = (1.95 + 0.045T) \ln(t)$	Viosca Knoll Block 990	$\%Ev = (3.16 + 0.045T) \ln(t)$
Hibernia, NL, Canada	$\%Ev = (2.18 + 0.045T) \ln(t)$	Voltesso 35	$\%Ev = (-0.18 + 0.013T) \sqrt{t}$
High-viscosity fuel oil	$\%Ev = (-0.12 + 0.013T) \sqrt{t}$	Waxy Light and Heavy	$\%Ev = (1.52 + 0.045T) \ln(t)$
Hondo, CA, USA	$\%Ev = (1.49 + 0.045T) \ln(t)$	West Delta Block 143	$\%Ev = (2.18 + 0.045T) \ln(t)$
Hout, Kuwait	$\%Ev = (2.29 + 0.045T) \ln(t)$	West Delta Block 30 w/water	$\%Ev = (-0.04 + 0.013T) \sqrt{t}$
IFO-180	$\%Ev = (-0.12 + 0.013T) \sqrt{t}$	West Texas Intermediate	$\%Ev = (2.77 + 0.045T) \ln(t)$
IFO-30 (Svalbard)	$\%Ev = (-0.04 + 0.045T) \ln(t)$	West Texas Intermediate	$\%Ev = (3.08 + 0.045T) \ln(t)$
IFO-300 (old Bunker C)	$\%Ev = (-0.15 + 0.013T) \sqrt{t}$	West Texas Sour	$\%Ev = (2.57 + 0.045T) \ln(t)$
Iranian Heavy	$\%Ev = (2.27 + 0.045T) \ln(t)$	White Rose, NL, Canada	$\%Ev = (1.44 + 0.045T) \ln(t)$
Issungnak, Beaufort Sea	$\%Ev = (1.56 + 0.045T) \ln(t)$	Zaire	$\%Ev = (1.36 + 0.045T) \ln(t)$
Isthmus, Mexico	$\%Ev = (2.48 + 0.045T) \ln(t)$		

Substituting for the temperature of 15°C and with a time of 12 h or 720 min, we get a percentage of 26.65. With 18 h, we get a percentage of 27.72 with a difference of 1.07%, the amount evaporated in the interval between 15 and 18 h.

The variation of evaporation is illustrated in Figure 7.10, which shows the evaporation of two oils, diesel fuel and North Slope Crude, at two temperatures [1].

7.4 COMPLEXITIES TO THE DIFFUSION-REGULATED MODEL

7.4.1 Oil Thickness

Studies show that under diffusion regulation very thick slicks (much more than 4 mm) evaporate slower than other slicks [1]. This is due to the increased path length that volatile components must diffuse in a thicker slick. This can certainly be

confused with air-boundary-layer regulation. Figure 7.11 shows the evaporation rate of various thicknesses of oil by the volume-to-thickness ratio. As can be seen, there is very little difference in this standard presentation. Figure 7.12 shows the concept of slower evaporation with increased path length, that is, increased oil thickness. As noted, there are insufficient data to fully evaluate this at this time; however, most slicks at sea do not reach this thickness. Earlier experiments by the present author studied the effect of thickness on the evaporation of a light crude oil, ASMB. The equations noted in Table 7.2 were all measured at a slick thickness of 1.5 mm, which is typical of sea values. The results of this are shown in Figure 7.13. The best curve fit from these is a square root function from which a correction can be given for thickness:

$$\text{Corrected equation factor} = \text{equation factor} + 1 - 0.78 \times \sqrt{t} \quad (7.45)$$

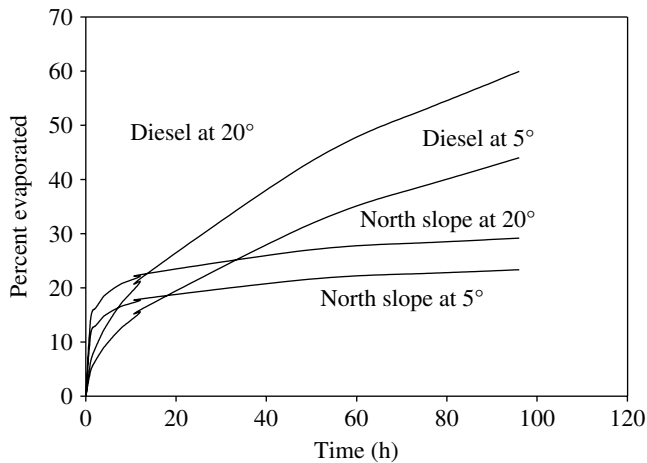


FIGURE 7.10 Comparison of evaporation curves for diesel and a crude oil, Alaska North Slope oils at two different temperatures.

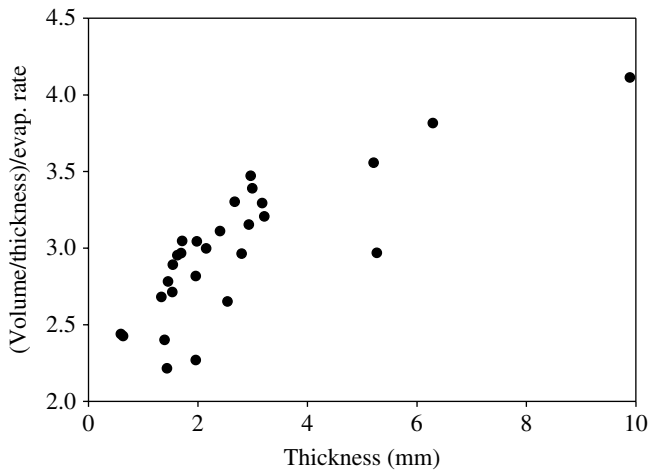


FIGURE 7.11 The relationship of volume over thickness (area) to evaporation rate (given as the equation parameter) for one light crude oil. This shows that there is little relationship up to about 4 mm. Volume largely dictates the evaporation rate; however, for thick slicks of thickness more than about 4 mm, the evaporation rate slows due to the increased diffusion distance through the liquid.

where the corrected equation factor is the factor corrected for the appropriate slick thickness, the equation factors are noted in Table 7.2, and the t is the slick thickness in mm. This equation is true for values above 1.5 mm at which the original equations were measured.

7.4.2 The Bottle Effect

Another confusing phenomenon to understanding evaporation is the bottle effect. This is illustrated in Figure 7.14. If all the evaporating oil mass is not exposed, such as in a bottle, more oil vapors than can readily diffuse through the air layer at the bottle mouth may yield a partial air-boundary-layer regulation effect. This air-boundary-layer regulatory effect may end when the evaporation rate of the oil mass is lower

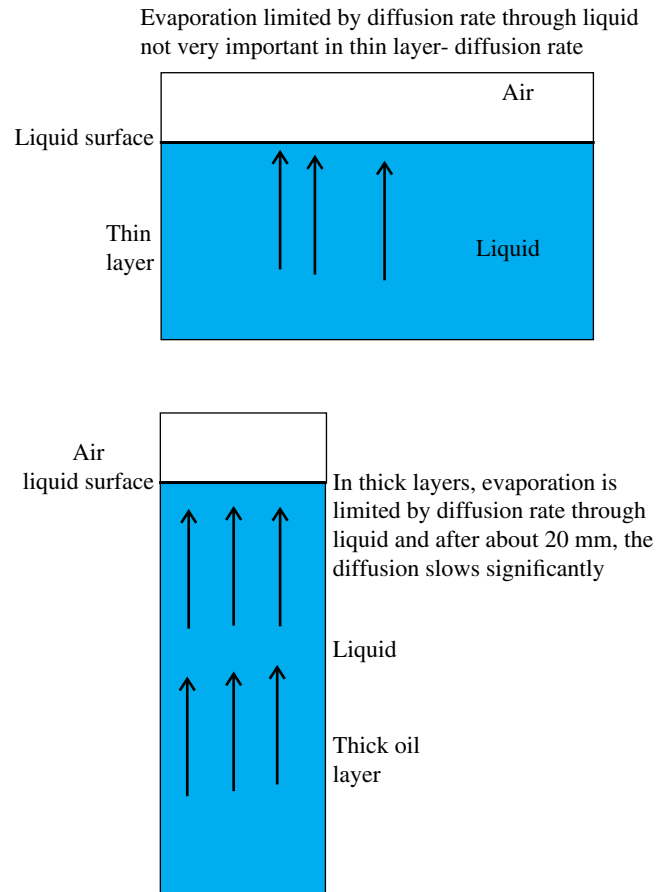


FIGURE 7.12 The effect of great thicknesses of oil. The evaporation rate is slower because of the longer diffusion distance. The difference becomes measurable after about 4 mm of oil thickness. This is greater than typical slicks at sea.

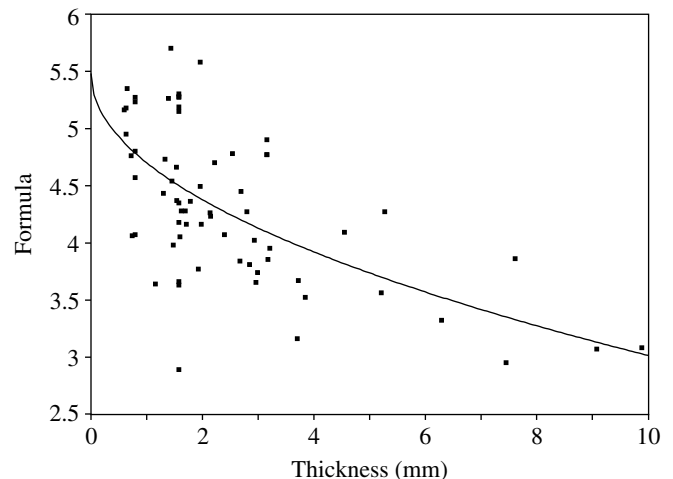


FIGURE 7.13 The difference in evaporation formulas for ASMB oil evaporated at different thicknesses. The data show scatter, because these early measurements lacked good temperature control.

than the rate at which the vapors can readily diffuse through the opening. Such effects could occur in reality in situations such as oil under ice, partially exposed to air, or when a thick skin forms over parts of the oil, blocking evaporation.

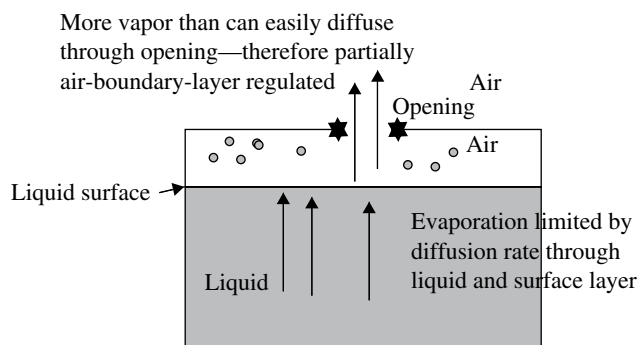


FIGURE 7.14 An illustration of the bottle effect. If all the evaporating oil mass is not exposed, more oil vapors than can readily diffuse through the air layer at the bottle mouth may yield a partial air-boundary-layer regulation effect. This regulatory effect may end when the evaporation of the oil mass lowers past the rate at which the vapors can readily diffuse through the opening.

During a recent experiment in ice, decreasing evaporation rate in smaller test pools was observed [31]. This phenomenon was probably caused by a combination of the bottle effect and partially as a result of the increased thickness in the more confined ice situations.

7.4.3 Skinning

Several workers have noted that some crude oil and petroleum products form “skins” on their surfaces [32,33]. These are largely due to the accumulation of compounds like resins on the surface, some possibly created by photooxidation. These can retard the evaporation of the compounds to a great extent. Figure 7.15 shows the results of some evaporation experiments carried out on two oils, Terra Nova crude and

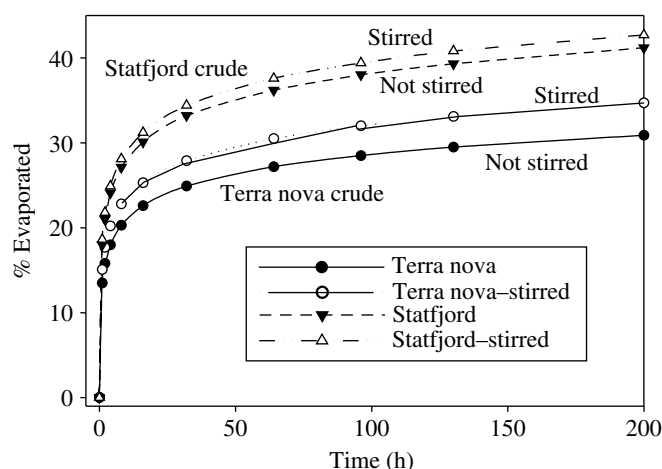


FIGURE 7.15 Results of an experiment to show the effect of “skinning” on oil evaporation. The upper curves in each case is the evaporation of the oil shown with stirring, thus preventing or retarding skin formation. The lower curve is the evaporation without stirring. The effect of skinning for these two oils amounts to several percent differential in evaporation over 200 h. At sea, wind and waves may mix the oil sufficiently to minimize the skinning effect.

Statfjord crude. Simultaneous experiments were carried out on the oils; one was stirred and the other not [1]. As can be seen in Figure 7.15, the stirred oils evaporated to a greater extent than the unstirred oils. The relevance of this at sea may not be great as wind and waves may accomplish the stirring and skin formation may thus be slowed or prevented. During the experiments shown in Figure 7.15, one could see the skin formation on the unstirred oil and this skin was much more evident closer to the end of the 200-h experiments.

Grose used the Mackay and Matsugu equations with some modification to account for the skinning factor [34]:

$$L = (CU^{0.78}D_o^{-0.11}) / (RK) P_i Sk M_i \quad (7.46)$$

where L is the mass of oil evaporated with time (kg/s), C is the environmental transfer constant, U is the wind speed at the surface (m/h), D_o is the diameter of the oiled area (m), K is the oil temperature in Kelvin, P_i is the vapor pressure of the particular component, Sk is the skin factor, and M_i is the molecular weight equivalent of the particular oil fraction.

The skin factor, Sk , ranges from 0.1 to 8 and accounts for the effect of skinning (the formation of a semipermeable surface layer). Yang and Wang suggested a value of $Sk=0.2$ after the density of their test oils had increased by 0.78% [12]. A value of 1.0 was used in testing the model. In addition, mass loss rate depends on the vapor pressure, P_i , and the molecular weight, MW_i , of each fraction. C is a dimensionless environmental transfer constant whose magnitude depends on the units used. The value used by Yang and Wang for C (0.00024) includes the constant 0.015 after Mackay and Matsugu [9].

7.4.4 Jumps from the 0-Wind Values

Experimentation shows that studies of oil evaporation at no turbulence or airflow show a slight decrease in evaporation rate from those experiments carried out with slight air movement such as found in an ordinary room [24]. This is due to the slight stirring of the oil mass, which increases the diffusion rate somewhat. Tests of this phenomenon show that further increases in evaporation rate do not occur with increased air movement or turbulence, thus confirming that this is a phenomenon only at 0-wind or turbulence conditions. These are seen only during capped vessel experiments, and the “jump” in evaporation rate is seen when the conditions are removed.

7.5 USE OF EVAPORATION EQUATIONS IN SPILL MODELS

Evaporation equations are the prime physical change equations used in spill models. A review of the use of evaporation algorithms in oil spill models is given in Fingas (2011) [1]. This is because evaporation is often the most significant change that occurs in an oil’s composition. Many models in the decade after 1984 use the Stiver and Mackay approach

[18]. Currently, more models are moving to equations such as found in Table 7.2.

There are three major errors resulting from the use of air-boundary-layer-regulated models: first and most important is that they cannot accurately deal with long-term evaporation; second, the wind factor results in unrealistic values; and finally, they have not been adjusted for the different curvature for diesel-like evaporation. Some modelers have adjusted their air-boundary-layer models to avoid very high values at long evaporation times by setting a maximum evaporation value. This does avoid very unrealistic high values after a point in time, but does so artificially. Most models of any type will require that one sets a maximum rate to avoid overprediction or values more than 100% for example. This can be best illustrated using a long-term example. A spill in northern Alberta of Pembina oil was sampled 30 years after its spill. Chemical analysis shows that this was weathered to the extent of 58% [35,36]. An air-boundary-layer-regulated predicted value overshoots the estimate by over 60%, despite using only two low wind values of 2 and 7 m/s [1]. Use of higher wind values increases the evaporation to well over 100%. These high evaporation values are physically impossible.

7.6 VOLATILIZATION

There is another phenomenon that has not been investigated thoroughly. It is the volatilization of light components of oils when submerged, dispersed, or released under water. It is known that dispersed oils, rapidly lose their volatile components, in fact, much more rapidly than the same oil evaporated on the surface [37]. This accelerated weathering has been studied somewhat for dispersants, but not much otherwise.

The recent Deep Water Horizon spill involved the high-pressure injection of oil into water, and much of the oil arrived on the surface as emulsion and having been weathered to 40–50% [38]. A similar situation was observed during the Ixtoc spill, and the oil was found to emulsify directly at the wellhead [39]. In both cases, most of the volatile components were lost at the wellhead or in very close proximity. It appears that most of the volatile compounds rose to the surface in the form of small bubbles and in the case of the Ixtoc blowout were burned [39]. This involves a loss of 40–50% in a very short time, not exceeding a few seconds.

7.7 MEASUREMENT OF EVAPORATION

Laboratory evaporation measurement has been carried out over many years. Comparison of field methodologies and laboratory experiments indicated that pan evaporation studies are probably the best methodology, although very few quantitative studies were carried out. Recently, Fieldhouse and Hollebone carried out a study comparing the rotary evaporator to pan evaporation. They found that

the rotary evaporator cannot be used to measure the rate of evaporation, as would be expected [40]. They found that the percent by volume extent of evaporation matched very closely between pan and rotary evaporator with respect to oil composition. Composition was analyzed by gas chromatography.

The percentage of evaporation of an actual sample can be determined using gas chromatographic–mass spectrometric methods [41]. The current method is to measure the content of the starting oil's biomarker terpanes that are weather resistant. Common substances used are C_{29} and C_{30} $\alpha\beta$ -hopanes. Application of this measurement in both the starting oil and the weathered oil can yield the following equation [41]:

$$\text{Oil evaporation \%} = \left[1 - \frac{H_0}{H_1} \right] \times 100 \quad (7.47)$$

where H_0 is the hopane concentration in the original oil and H_1 is the hopane concentration in the weathered oil.

Researchers in the past tried to use ratios of the oil's alkanes such as

$$\text{Evap \%} = \frac{C_{12} + C_{14} + C_{16} + C_{18}}{C_{20} + C_{22} + C_{24} + C_{26}} \times 100 \quad (7.48)$$

This approach does not function well as the alkanes in the subscript of Equation (7.42) also evaporate to a certain degree.

Modern analysis is also capable of differentiating between evaporation and biodegradation [42].

7.8 SUMMARY

A review of the physics of oil evaporation shows that oil evaporation is not air-boundary-layer regulated. The results of the following experimental series have shown the lack of boundary-layer regulation.

1. A study of the evaporation rate of several oils with increasing wind speed shows that the evaporation rate does not change past the 0-level wind. Water, known to be boundary-layer regulated, does show the predicted increase with wind speed, U (U^x , where x varies from 0.5 to 0.78, depending on the turbulence level).
2. Increasing the area does not change the oil evaporation rate. This is contrary to the prediction resulting from boundary-layer regulation.
3. The volume or mass of oil evaporating correlates with the evaporation rate. This is a strong indicator of the lack of boundary-layer regulation because with water, volume (rather than area) and rate do not correlate.

The fact that oil evaporation is not strictly boundary-layer regulated implies that a simplistic evaporation equation will

suffice to describe the process. The following factors do not require consideration: wind velocity, turbulence level, area, and scale size. The factors important to evaporation include time and temperature.

A comparison of the various models used for oil spill evaporation shows that air-boundary-layer models result in erroneous predictions. There are three issues: first, air-boundary-layer models cannot accurately deal with long-term evaporation; second, the wind factor results in unrealistic values; and finally, they have not been adjusted for the different curvature for diesel-like evaporation. There has been some effort on the part of modelers to adjust air-boundary-layer models to be more realistic for longer-term evaporation, but these may be artificial and result in other errors such as underestimation for long-term prediction.

A diffusion-regulated model has been presented along with many empirically developed equations for many oils. The equations are found to be of the following form:

$$\text{Percentage evaporated} = [B + 0.045(T - 15)] \ln t \quad (7.49)$$

where B is the equation parameter at 15°C , T is the temperature in degree Celsius, and t is the time in minutes.

It is also noted that in diesel fuel and similar oils, the curve is different and follows a generic curve such as

$$\text{Percentage evaporated} = [B + 0.01(T - 15)] \sqrt{t} \quad (7.50)$$

The most accurate predictions are carried out using the empirical equations as noted in Table 7.2. If these are not available, the parameters can be estimated using distillation data as follows:

For oils that follow a logarithmic equation,

$$\text{Percentage evaporated} = [0.165(\%D) + 0.045(T - 15)] \ln(t) \quad (7.51)$$

For oils that follow a square root equation,

$$\text{Percentage evaporated} = [0.0254(\%D) + 0.01(T - 15)] \sqrt{t} \quad (7.52)$$

where D is the percentage distilled at 180°C , T is the temperature in Celsius, and t is the time in minutes. Equations are also given that allow estimation of evaporation from density, viscosity, or SARA data; however, these are much less accurate again.

In addition, an estimator for the variation in evaporation for thick slicks was developed and given in Equation (7.45.)

REFERENCES

- [1] Fingas, M., Evaporation Modeling, Chapter 9, in *Oil Spill Science and Technology*, Elsevier, New York, 2011.
- [2] Fingas, M.F., A Literature Review of the Physics and Predictive Modelling of Oil Spill Evaporation, *J. Hazard. Mater.*, 42, 157, 1995.
- [3] Jones, F.E., *Evaporation of Water*, Lewis Publishers, Chelsea, 1992.
- [4] Brutsaert, W., *Evaporation into the Atmosphere*, Reidel Publishing Company, Dordrecht, 1982.
- [5] Fingas, M.F., Studies on the Evaporation of Crude Oil and Petroleum Products: I. The Relationship Between Evaporation Rate and Time, *J. Hazard. Mater.*, 56, 227, 1997.
- [6] Monteith, J.L. and M.H. Unsworth, *Principles of Environmental Physics*, Hodder and Stoughton, London, 1990.
- [7] Sutton, O.G., Wind Structure and Evaporation in a Turbulent Atmosphere, *P. R. Soc. Lond. A*, 146, 701, 1934.
- [8] Blokker, P.C., Spreading and Evaporation of Petroleum Products on Water, *Proceedings of the Fourth International Harbour Conference*, Antwerp, Belgium, 911, 1964.
- [9] Mackay, D. and R.S. Matsugu, Evaporation Rates of Liquid Hydrocarbon Spills on Land and Water, *Can. J. Chem. Eng.*, 51, 434, 1973.
- [10] Goodwin, S.R., D. Mackay, and W.Y. Shiu, Characterization of the Evaporation Rates of Complex Hydrocarbon Mixtures Under Environmental Conditions, *Can. J. Chem. Eng.*, 54, 290, 1976.
- [11] Butler, J.N., Transfer of Petroleum Residues from Sea to Air: Evaporative Weathering, *Marine Pollutant Transfer*, Ed. H.L. Windom and R.A. Duce, Lexington Books, Lexington, 201, 1976.
- [12] Yang, W.C. and H. Wang, Modelling of Oil Evaporation in Aqueous Environments, *Water Res.*, 11, 879, 1977.
- [13] Drivas, P.J., Calculation of Evaporative Emissions from Multi-Component Liquid Spills, *Environ. Sci. Technol.*, 16, 726, 1982.
- [14] Reijnhart, R. and R. Rose, Evaporation of Crude Oil at Sea, *Water Res.*, 16, 1319, 1982.
- [15] Brighton, P.W.M., Evaporation from a Plane Liquid Surface into a Turbulent Boundary Layer, *J. Fluid Mech.*, 159, 323, 1995.
- [16] Brighton, P.W.M., Further Verification of a Theory for Mass and Heat Transfer from Evaporating Pools, *J. Hazard. Mater.*, 23, 215, 1990.
- [17] Tkalin, A.V., Evaporation of Petroleum Hydrocarbons from Films on a Smooth Sea Surface, *Oceanology of the Academy of Sciences of the USSR*, 26, 473, 1986.
- [18] Stiver, W. and D. Mackay, Evaporation Rate of Spills of Hydrocarbons and Petroleum Mixtures. *Environ. Sci. Technol.*, 18, 834, 1984.
- [19] Stiver, W., *Weathering Properties of Crude Oils When Spilled on Water*, Master of Applied Science Thesis, Department of Chemical Engineering and Applied Chemistry, University of Toronto, 4, 110, 132, 1984.
- [20] Hamoda, M.F., S.E.M. Hamam, and H.I. Shaban, Volatilization of Crude Oil from Saline Water, *Oil Chem. Pollut.*, 5, 321, 1989.
- [21] Quin, M.F., K. Marron, B. Patel, R. Abu-Tabanja, and H. Al-Bahani, Modelling of the Ageing of Crude Oils, *Oil Chem. Pollut.*, 7 (4), 119, 1990.
- [22] Brown, H.M. and P. Nicholson, The Physical-Chemical Properties of Bitumen, *AMOP*, Seattle, 107, 1991.
- [23] Bobra, M., *A Study of the Evaporation of Petroleum Oils*, Manuscript Report Number EE-135, Environment Canada, Ontario, 1992.

- [24] Fingas, M.F., Studies on the Evaporation of Crude Oil and Petroleum Products: II. Boundary Layer Regulation, *J. Hazard. Mater.*, 57, 41, 1998.
- [25] Li, Y.Y., X.L. Zheng, B. Li, Y.X. Ma, and J.H. Cao, Volatilization Behaviors of Diesel Oil from the Soils, *J. Environ. Sci. (China)*, 16, 1033, 2004.
- [26] *Ullmann Encyclopedia*, Ullmann Publishing, Hamburg, 1989–2005.
- [27] Fingas, M.F., The Evaporation of Oil Spills: Development and Implementation of New Prediction Methodology, *IOSC*, Seattle, 281, 1999.
- [28] Fingas, M.F., The Evaporation of Oil Spills: Prediction of Equations Using Distillation Data, *AMOP*, Vancouver, 1, 1997.
- [29] Fingas, M.F., Estimation of Oil Spill Behaviour Parameters from Readily-Available Oil Properties, *AMOP*, 1, 2007.
- [30] Fingas, M., Modeling Evaporation Using Models That Are Not Boundary-Layer Regulated, *J. Hazard. Mater.*, 107, 27, 2004.
- [31] Brandvik, P.J. and L.-G. Faksness, Weathering Processes in Arctic Oil Spills: Meso-scale Experiments with Different Ice Conditions, *Cold Reg. Sci. Technol.*, 55, 160, 2009.
- [32] Bobra, M. and E.J. Tennyson, Photooxidation of Petroleum, *AMOP*, Edmonton, 129, 1989.
- [33] Garrett, R.M., I.J. Pickering, C.E. Haith, and R.C. Prince, Photooxidation of Crude Oils, *Environ. Sci. Technol.*, 32, 3719, 1998.
- [34] Grose, P.L., A Preliminary Model to Predict the Thickness Distribution of Spilled Oil, *Proceedings of a Workshop on the Physical Behaviour of Oil in the Marine Environment*, Princeton University, Princeton, 1979.
- [35] Wang, Z., M. Fingas, C. Yang, B. Hollebone, and X. Peng, Biomarker Fingerprinting: Applications and Limitations for Source Identification and Correlation of Oils and Petroleum Products, *AMOP*, Edmonton, 103, 2004.
- [36] McIntyre, C.P., P. M. Harvey, S. Ferguson, A.M. Wressnig, I. Snape, and S.C. George, Determining the Extent of Weathering of Spilled Fuel in Contaminated Soil Using the Diastereomers of Pristane and Phytane, *Org. Geochem.*, 38, 2131, 2007.
- [37] Fingas, M.F., L. Sigouin, Z. Wang, and G. Thouin, Resurfacing of Oil with Time in the Swirling Flask, *AMOP*, Calgary, 773, 2002.
- [38] *The Oil Budget Calculator for the Deep Water Horizon Spill*, NOAA, Washington, DC, 2010.
- [39] Patton, J.S., M.W. Rigler, P.D. Boehm, and D.L. Fiest, Ixtoc 1 Oil Spill: Flaking of Surface Mousse in the Gulf of Mexico, *Nature*, 290, 235, 1981.
- [40] Fieldhouse, B. and B.P. Hollebone, Artificial Weathering of Oils by Rotary Evaporator, *AMOP*, Halifax, 159, 2010.
- [41] Yang, C., Z. Wang, B.P. Hollebone, C.E. Brown, and M. Landriault, Characteristics of Bicyclic Sesquiterpanes in Crude Oils and Petroleum Products, *J. Chromatogr. A.*, 15, 4475, 2009.
- [42] Snape, I., P.M. Harvey, S.H. Ferguson, J.L. Rayner, and A.T. Revill, Investigation of Evaporation and Biodegradation of Fuel Spills in Antarctica I. A Chemical Approach Using GC-FID, *Chemosphere*, 61, 1485, 2005.

WATER-IN-OIL EMULSIONS: FORMATION AND PREDICTION

MERV FINGAS¹ AND BEN FIELDHOUSE²

¹*Spill Science, Edmonton, Alberta, Canada*

²*Emergencies Science and Technology (ESTS), Environment Canada, Ottawa, Ontario, Canada*

8.1	Introduction	225
8.2	Types of Emulsions	225
8.3	Stability Indices	226
8.4	Formation of Emulsions	230
8.4.1	The Role of Asphaltenes	230
8.4.2	The Role of Resins and Other Components	231
8.4.3	Methods to Study Emulsions	232
8.4.4	The Overall Theory of Emulsion Formation	233
8.4.5	The Role of Weathering	235
8.5	Modeling the Formation of Water-in-Oil Emulsions	235
8.5.1	Older Models	235
8.5.2	New Models	236
8.5.3	Development of an Emulsion Kinetics Estimator	250
8.5.4	Model Certainty	250
8.6	Conclusions	251

8.1 INTRODUCTION

Water-in-oil emulsions sometimes form after oil products are spilled. These emulsions, often called “chocolate mousse” or “mousse” by oil spill workers, can make the cleanup of oil spills very difficult [1]. When water-in-oil emulsions form, the physical properties of oil changes dramatically. As an example, stable emulsions contain from 60 to 80% water, thus expanding the spilled material from two to five times the original volume. Most importantly, the viscosity of the oil typically changes from a few hundred mPa·s to about 100,000 mPa·s, an increase by a factor of 500–1000. A liquid product is changed into a heavy, semisolid material. These emulsions are difficult to recover with ordinary spill recovery equipment.

8.2 TYPES OF EMULSIONS

Fingas and Fieldhouse found that four clearly defined water-in-oil types are formed by crude oil when mixed with water

[2]. This was shown by water resolution over time, by a number of rheological measurements, and by the water-in-oil product’s visual appearance, both on the day of formation and 1 week later. Some emulsions were observed for over a year, with the same results. The types are named stable water-in-oil emulsions, mesostable water-in-oil emulsions, entrained water, and unstable water-in-oil types. The differences among the four types are quite large and are based on at least two water content measurements and five rheological measurements. More than 400 oils or petroleum products were studied.

The four water-in-oil types formed by crude oils and petroleum products are stable, mesostable, entrained, and unstable [2,3]. Data on the oils tested and the emulsions formed are in Table 8.A1, Table 8.A2, and Table 8.A3. Table 8.A1 gives the data on oils tested; the visual stability; and the properties of the oils before mixing, upon mixing, and 1 week after mixing. Table 8.A2 gives the data on the emulsions over 1 year after mixing. Table 8.A3 gives the statistical summary data from the foregoing two tables.

Stable emulsions are reddish-brown semisolid substances with an average water content of about 70–80% on the day of formation and about the same 1 week later [2]. Stable emulsions remain stable for at least 4 weeks under laboratory conditions. All of the stable emulsions studied remained so for at least 1 year. The viscosity increase following formation averages 400 times the original viscosity and 1 week later averages 850 times the original viscosity. The average properties of the starting oil required to form a stable emulsion are as follows: density, 0.9 g/ml; viscosity, 300 mPa·s; resin content, 9%; asphaltene content, 5%; and asphaltene-to-resin ratio, 0.6.

Mesostable water-in-oil emulsions are reddish-brown viscous liquids with an average water content of 60–65% on the first day of formation and less than 30% 1 week later [2]. Mesostable emulsions generally break down to about 20% water content within 1 week. The viscosity increase over the

initial viscosity on the day of formation averages a factor of 7 and 1 week later averages 5. The average properties of the starting oil required to form a mesostable emulsion are as follows: density, 0.9 g/ml; viscosity, 1300 mPa-s; resin content, 16%; asphaltene content, 8%; and asphaltene-to-resin ratio, 0.5. The greatest differences between the starting oils for stable and mesostable emulsions are the ratio of viscosity increases (stable 400 on the first day and 850 in 1 week, mesostable 7 on the first day and 5 in 1 week) and resin content (stable, 9%; mesostable, 16%).

Entrained water-in-oil types are black viscous liquids with an average water content of 40–50% on the first day of formation and less than 28% 1 week later [2]. The viscosity increase over the day of formation averages a multiple of 2 and 1 week later still averages two. The average properties of the starting oil required to form entrained water are as follows: density, 0.97 g/ml; viscosity, 60,000 mPa-s; resin content, 18%; asphaltene content, 12%; and asphaltene-to-resin ratio, 0.75. The greatest differences between the starting oils for entrained water-in-oil compared to stable and mesostable emulsions are the viscosity of the starting oil (entrained starting oil averages 60,000 mPa-s compared to 200 mPa-s for stable emulsions and 1300 mPa-s for mesostable emulsions) and the ratio of viscosity increases (entrained = 2 on the first day and 2 in 1 week, stable 400 on the first day and 850 in 1 week, mesostable 7 on the first day and 5 in 1 week). Entrained water-in-oil types appear to be applicable to viscous oils and petroleum products, but not extremely viscous products.

Unstable water-in-oil emulsion types or those oils that do not form any of the other three types are characterized by the fact that the oil does not hold significant amounts of water following mixing with water [2]. There is a much broader range of properties in the starting oil than for the other three water-in-oil states. For example, viscosities are very low or very high. Included in this group are light fuels such as diesel fuel and very heavy, viscous oil products such as heavy residual oils.

The differences between some of the basic properties of emulsions and water-in-oil types are shown in Figure 8.1. Figure 8.1 uses “umbrella” or “spider” graphs to show the relationship of the 10 average properties of each water-in-oil state compared to another water-in-oil state. Moving around the graph, the relative water content on the first day is plotted, then the water content after 1 week, then the starting oil density, then the starting oil viscosity, and then the saturate, aromatic, resin, and asphaltene contents. After this, the graph shows the asphaltene/resin (A/R) content, then the wax content. Each of these parameters is scaled on this graph from 1 to 10 based on the distribution from the lowest to highest relative value. As can be seen from these figures, there are significant differences between the various water-in-oil types. Table 8.1 highlights the two largest differences between the pairs of water-in-oil emulsions compared. Table 8.1 shows that the differences between the starting oils of the water-in-oil pairs are almost always the amount of

asphaltenes and the amount of resins. This indicates that asphaltenes and resins are very important factors in emulsion formation.

The differences between emulsions are further highlighted in Figure 8.2. This shows a picture of stable emulsion and a mesostable emulsion after 1 week. The mesostable emulsion, Figure 8.2B, has obviously broken and only remnants remain. This mesostable emulsion looked similar to the stable emulsion on the day that it was created.

The viscosity and water content differences among the four water-in-oil types are shown in Figure 8.3. Figure 8.3A shows the water content change over 1 year. Stable emulsions, on average, begin at a high level (about 78%) and lose little water over 1 year. Mesostable emulsions, on the other hand, begin at about 65% and lose most of this water within a few days. Entrained water-in-oil types pick up only about 40% water and only slowly lose this over 1 year. Unstable water-in-oil types pick up only a few percent of water and this does not change much over 1 year. Figure 8.3B shows the apparent viscosity over 1 year. This graph shows that the apparent viscosity of stable emulsion increases over the period of 1 year and that of the others generally declines or only increases a small amount. Thus, after a few months, the stable emulsion will have the greatest viscosity. Figure 8.3C shows the change in tan delta, a rheological parameter derived from forced oscillation tests, showing the relative viscous and elastic contributions to overall resistance to flow over the year. This shows that the unstable type changes, becoming more viscous than elastic. The stable emulsion has about the same viscous and elastic components over the year. All other water-in-oil types show a much greater viscous component than the elastic component. Figure 8.3D shows the change in viscosity modulus alone. One can see that the rise in viscosity modulus alone is about the same for the water-in-oil types. This also indicates that only the stable emulsions show a slight rise in their elastic modulus because in Figure 8.3C we noted that the tan delta (ratio of viscous to elastic components) remains about the same for stable emulsions.

8.3 STABILITY INDICES

Fingas and Fieldhouse carried out tests of several indices of stability, a single value that could provide good discrimination between water-in-oil types even on the first day [2]. This was felt to be necessary as the water content alone was not entirely discriminating because some of the water loss occurs within hours or days, especially for mesostable emulsions. It was found that all of these indices could be used to some extent to differentiate the four water-in-oil types. One index of stability was the ratio of the complex modulus of the product on the first day divided by the starting oil viscosity. This index was named stability A. Stability B was the elastic modulus on the first day divided by the starting oil viscosity. Stability C was the combination of these two indices, the log of the cross product of stability

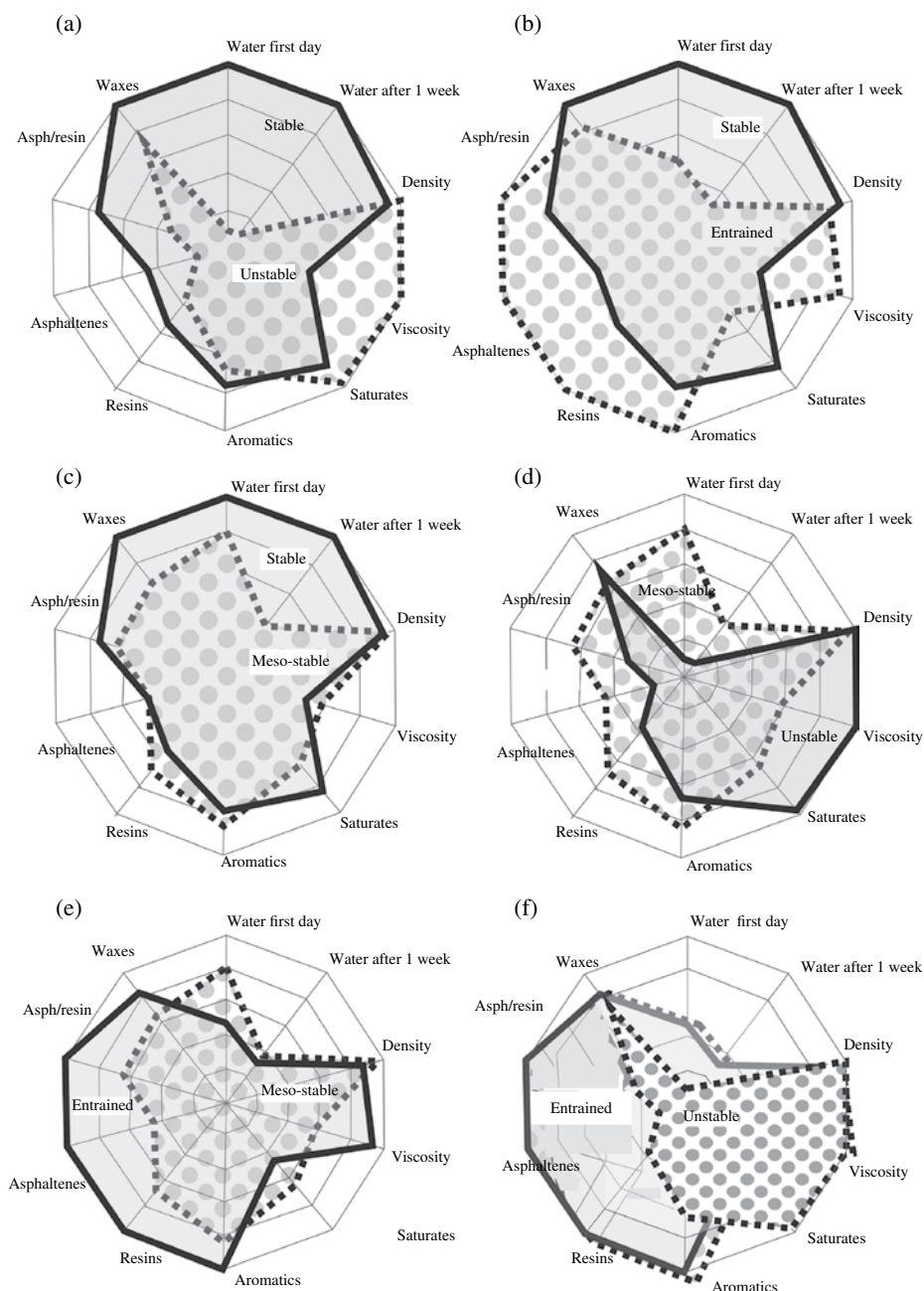


FIGURE 8.1 The relationships between oil properties and the four types of water-in-oil types. (a) The differences between stable emulsions (line around shaded area) and the unstable types or oils that do not form other types (line around patterned area). Note the lines indicate the typical boundaries and the areas are only shown to distinguish the lines. (b) The relationship between stable emulsions (line around shaded area) and the entrained type (line around patterned area). (c) The relationships between stable (line around shaded area) and mesostable emulsions (line around patterned area). (d) The relationships between mesostable emulsions (line around patterned area) and the unstable type or oils that do not form other types (line around shaded area). (e) The property differences between mesostable emulsions (line around patterned area) and the entrained type (line around shaded area). (f) The relationship between the unstable (line around patterned area) and entrained types (line around shaded area).

TABLE 8.1 Differences between water-in-oil states (two largest starting oil property differences named)

Water-in-oil state		Water-in-oil state	
	Unstable (not one of the others)	Entrained	Mesostable
	Stable	Mesostable	Entrained
Stable	Asphaltenes, A/R ratio	Asphaltenes, resins	Resins, saturates
Mesostable	Asphaltenes, resins	Asphaltenes, A/R ratio	
Entrained	Asphaltenes, resins		

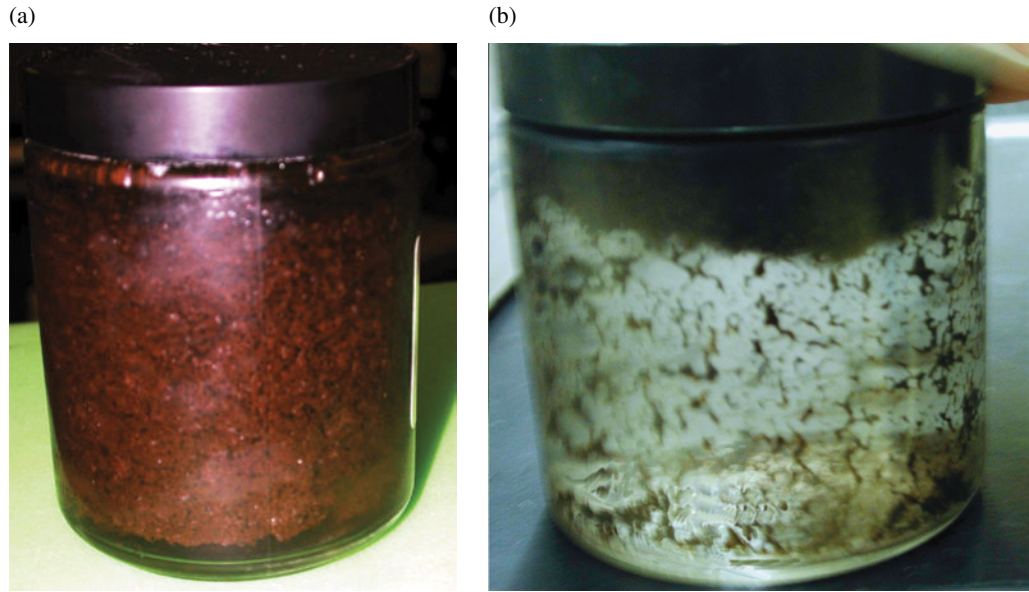


FIGURE 8.2 Photographs of emulsions after 1 week. (a) A stable emulsion 1 week after formation. (b) A mesostable emulsion after 1 week. This latter emulsion was similar in appearance to A upon formation and obviously has broken in 1 week.

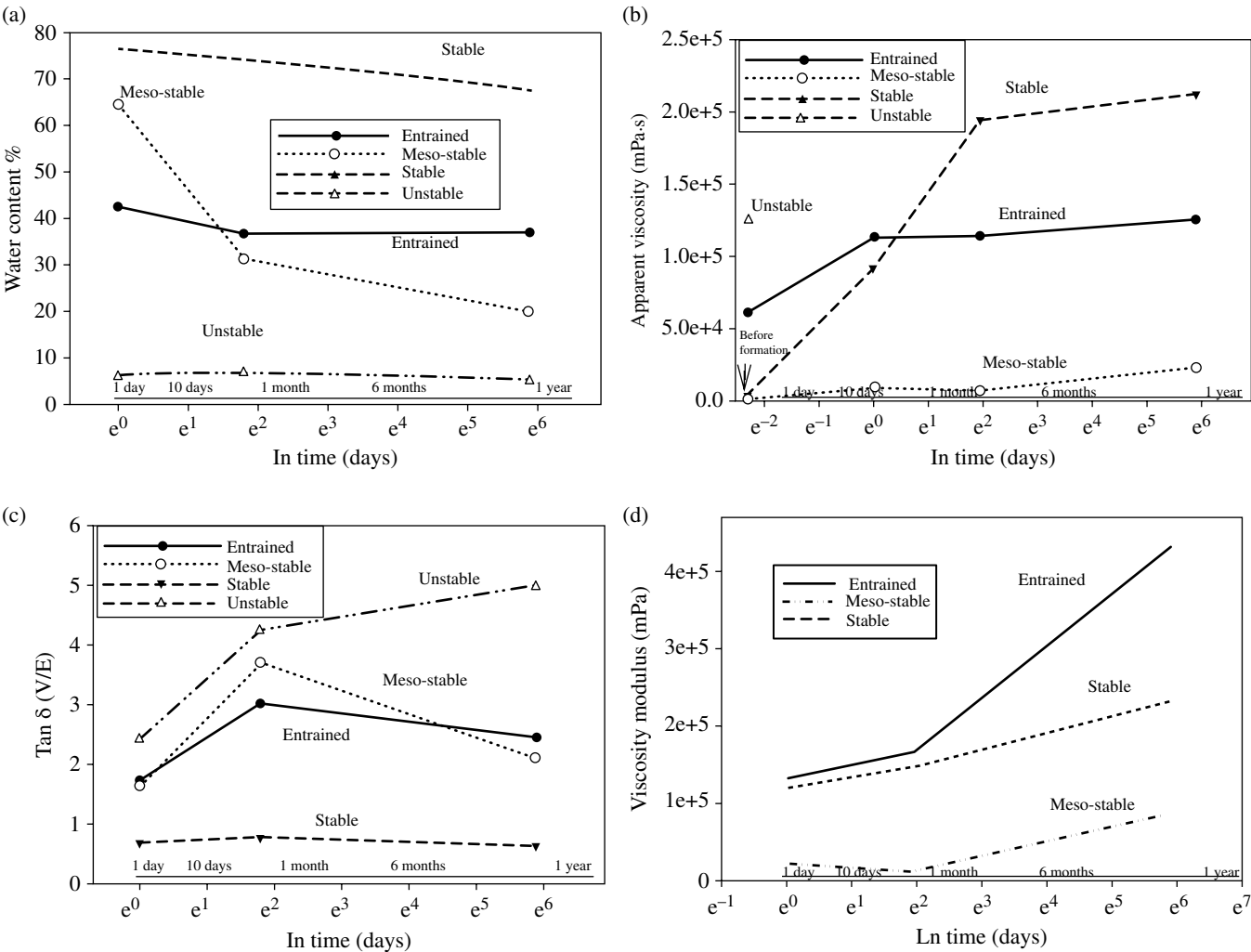


FIGURE 8.3 Comparison of average properties of water-in-oil types over 1 year. (a) Comparison of water content; (b) Comparison of apparent viscosity; (c) Comparison of tan delta; and (d) Comparison of viscosity modulus.

A and B. Another index, the viscosity increase, the ratio of the oil viscosity after mixing divided by the starting oil viscosity was also evaluated. Another test, first-day water times stability A was a simple composite of the first-day water content times stability A. The last two parameters evaluated

were the tan delta on the day of formation and the change in tan delta over 1 week.

The stability indices are graphed in Figure 8.4 using similar umbrella graphs as in the preceding text but with the different stability indices [2]. The index called stability C

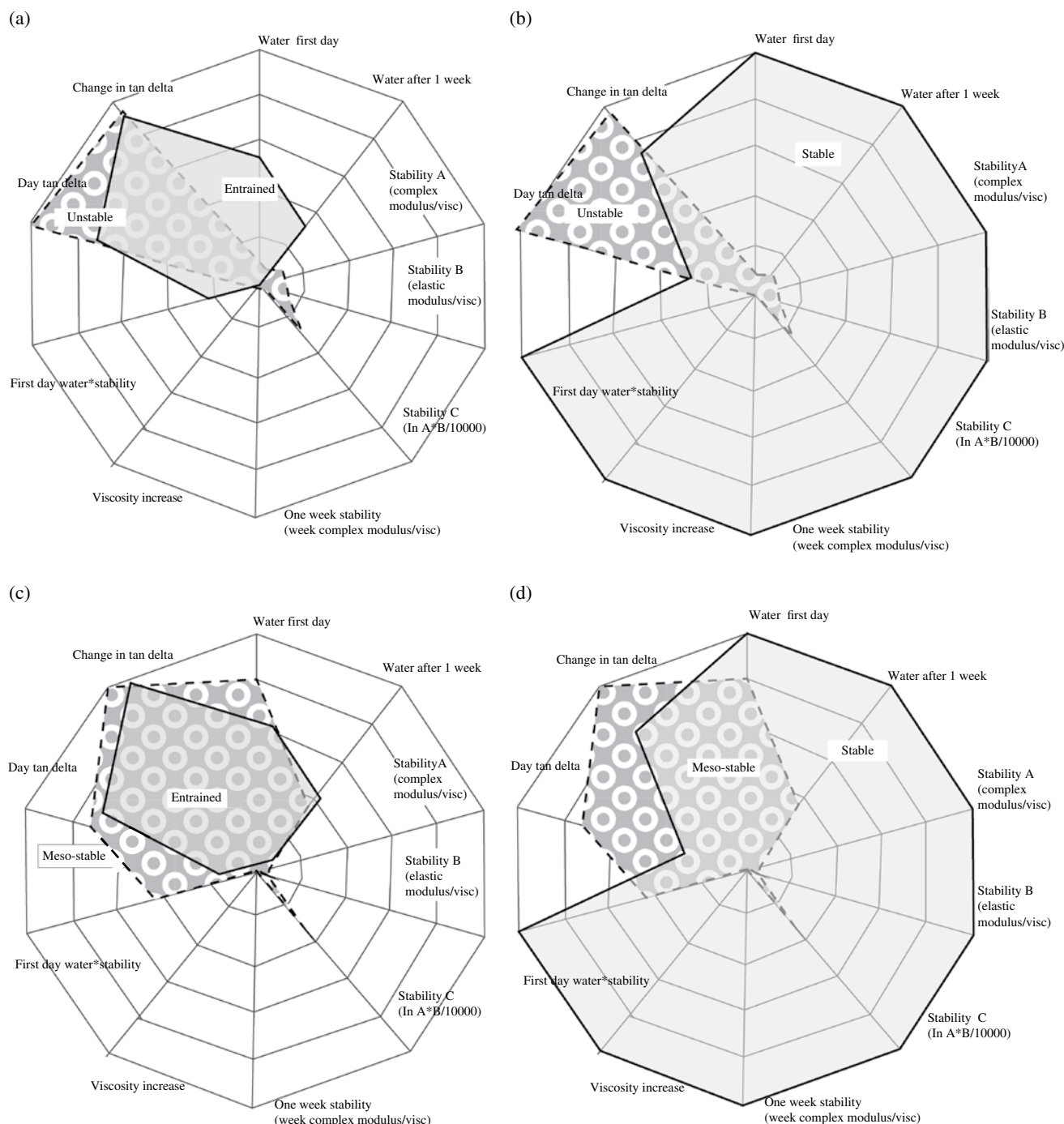


FIGURE 8.4 Comparison of stability indices for the four water-in-oil types. (a) A comparison between unstable (line around patterned area) and entrained (line around shaded area) types; note the lines indicate the typical boundaries and the areas are only shown to distinguish the lines. (b) A comparison between the unstable or oils that do not form other types (line around patterned area) and stable (line around shaded area) types and (c) Between mesostable (line around patterned area) and entrained (line around shaded area) types, and Figure 8.4d between mesostable (line around patterned area) and stable (line around shaded area) types. The “day tan delta” is the tan delta after 1 day. The change is tan delta is the absolute change in tan delta.

proved to be the index that best differentiated all four water-in-oil types on the day of formation and afterward. The baseline used was the water content 1 week after formation. This parameter shows the greatest difference between the four water-in-oil types.

Another analysis of the stability index is shown in Figure 8.5. This shows that stability index C shows little overlap between the various water-in-oil types. Furthermore, there is an upward progression in values between unstable (those that do not form any of the other three types), entrained, mesostable, and stable emulsions. This was an end goal of the project, that is, to provide a single index that can be used on the first or any day after formation to provide information on the stability of the water-in-oil type formed.

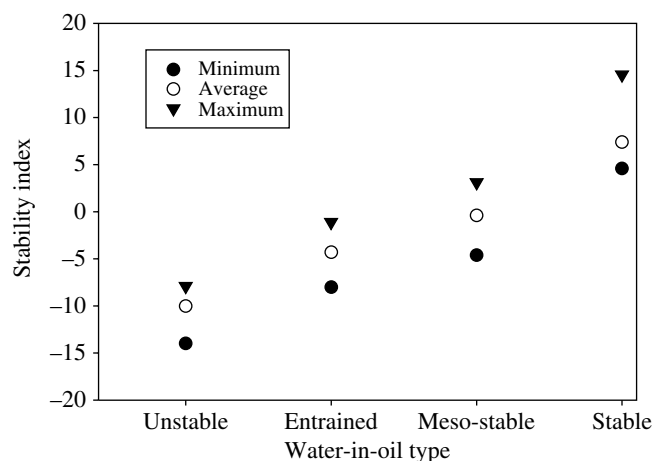


FIGURE 8.5 A plot of the minimum, average, and maximum stability index C values for each water-in-oil type. The figure shows that the averages are different and there is minimum overlap between minimum and maximum values.

The calculation of stability index C, hereafter referred to as the stability index, is shown in Table 8.2. This shows that the stability index can be simply calculated from rheological data and that it can be used, along with some basic property data such as density and viscosity, to classify the water-in-oil types.

8.4 FORMATION OF EMULSIONS

8.4.1 The Role of Asphaltenes

Some researchers reported that asphaltenes were a major factor in water-in-oil emulsions more than 40 years ago [4]. The specific roles of asphaltenes in emulsions were not defined until recently [3]. Currently, the basics of water-in-oil emulsification are now understood to a much better degree [3–7]. The fundamental process is that water-in-oil emulsions are stabilized by the formation of high-strength viscoelastic asphaltene films around water droplets in oil. Resins could also form emulsions, but resins do not form stable emulsions, and actually aid in asphaltene emulsion stability by acting as asphaltene solvents and by providing temporary stability during the time of the slow asphaltene migration. Overall, a wide spectrum of scientists have found that oil composition is the key factor in water-in-oil emulsion formation including the amounts and types of asphaltene, resin, and saturate contents.

Asphaltenes represent a very broad category of substances [8]. Graham et al. separated resins and asphaltenes into two classes of binding and nonbinding [9]. They found that the binding component formed emulsions, whereas the nonbinding did not. Czarnecki analyzed several fractions and found that there were differences in the oxygen and sulfur contents of the different fractions he was studying [8]. Further, he noted that the composition of rag, a persistent emulsion often left behind after an emulsion is broken, consisted of multiple emulsion droplets, a number of water

TABLE 8.2 Calculation of a stability value

Step				
1	Carry out rheological studies on the water-in-oil product measuring complex modulus and elastic modulus			
2	Calculate the cross product (Xpr) of the complex modulus and elastic modulus divided by the starting oil viscosity			
	$X_{pr} = \frac{\text{Complex modulus}}{\text{Starting oil viscosity}} \times \frac{\text{Elastic modulus}}{\text{Starting oil viscosity}}$			
3	Correct the cross product (Xpr) to yield stability (sometimes referred to as stability C)			
	Stability =ln((Xpr/10,000)×(Xpr/10,000))			
Relation of stabilities to water-in-oil type				
Calculated stability		Starting oil properties	Water-in-oil type	Calculated
Minimum	Maximum			Average stability
4	29	Density>0.94 Viscosity>6000	Stable	13
−10	5		Mesostable	−2
−20	3		Entrained	−7
−4	−18	Density<0.85 or >1.0 Viscosity<100 or >800,000 Asphaltenes or resins<1%	Unstable	−15

droplets unable to break through the interface and flocculated fine solids. Varadaraj and Brons found that rag, the residual of a broken emulsion, contains high proportions of asphaltenes [10]. They noted that water-in-oil emulsions, solids-in-oil dispersions, oil-in-oil dispersions, and oil-in-water-in-oil multiple emulsions coexist in the rag.

One group of scientists, McLean and Kilpatrick and coworkers, studied asphaltene aggregation in model emulsions made from heptane and toluene [11]. The asphaltenes were precipitated using heptane and the resins separated using open-column silica columns, as is the typical procedure. They found that, although some emulsions could be generated using resins, they were much less stable than those generated by asphaltenes. McLean and Kilpatrick also found that the concentration of asphaltenes and the availability of solvating resins were important [11]. McLean and Kilpatrick proposed that asphaltenes were most effective in stabilizing emulsions when they are near the point of precipitation [12]. McLean and Kilpatrick noted that there are specific resin-asphaltene interactions because differing combinations yielded different results in the model emulsions. The most effective emulsion stabilizers were found to be the most polar and the most condensed resins and asphaltenes. McLean and Kilpatrick concluded that the most significant factor in emulsion formation is the solubility state of asphaltenes [12].

Several scientists reviewed emulsions and concluded that the asphaltene content is the most important factor in the formation of emulsions [13–15]. Even in the absence of any other possibly synergistic compounds such as resins, asphaltenes were found to be capable of forming rigid, elastic films, which are the primary agents in stabilizing water-in-crude oil emulsions. The exact conformations by which asphaltenes organize at oil–water interfaces, and the corresponding intermolecular interactions have not been elucidated. McLean and colleagues suggest that the intermolecular interactions must be π -bonds between fused aromatic sheets; H bonds; or electron donor–acceptor interactions mediated by porphyrin rings, heavy metals, or heteroatomic functional groups [13]. Workers studying only crude oil emulsions concluded that water-in-oil emulsions are exclusively stabilized by asphaltenes, although the specific stability was not measured [16]. Even though the emulsions contain inorganic solids, waxes, and other organic solids, the main stabilization comes from asphaltenes. Other workers have noted that solid particles, such as clays, when present, can stabilize or enhance the stability of emulsions [17]. This is true of emulsions formed by clay-containing bitumens. These clay-stabilized emulsions may have differences from the crude oil and petroleum product emulsions noted in this chapter.

Asphaltenes are a class of substances defined only by their precipitation from oil in pentane, hexane, or heptane. The specific structure of asphaltenes is unknown; however, the molecular weight averages about 750 daltons or more, and there is a planar aromatic structure surrounded by alkane groups, some with heteroatoms S, N, and O [18]. Studies of

the time dependency of film strength by viscosity measurements showed that the complex modulus increased by about twofold between 2 and 4 h. This indicates increased film strength, probably due to asphaltene aggregation and cross-linking. The mechanism by which emulsions form begins when asphaltenes migrate to the oil–water interface, a process that is regulated by the diffusion of the soluble asphaltenes. At the interface, the asphaltenes self-assemble to produce an elastic, rigid, stable film [6,19,20]. This is the source of stability for water-in-oil emulsions.

Recent work on asphaltenes has shown that separation of asphaltenes into fractions results in more information on the fraction that forms emulsions. Arla and coworkers noted that the acid fractions of the asphaltenes formed more stable water-in-oil emulsions than some other compounds [21].

The absorption of asphaltenes at the water-oil interface proceeds for a long time and may still proceed after a year [22]. This implies that the absorption at the interface lowers the net energy of the system and thus is favored thermodynamically. The bulk concentration of asphaltenes is important and drives the amount that is absorbed at the interface. Asphaltenes have their greatest tendency to absorb and make the strongest interfacial film at their limit of solubility, otherwise they would stay in solution [22]. Several workers noted that there were differences in the stability of emulsions, depending on the fractions of asphaltenes taken and also by the amount of asphaltene aggregation present [23,24]. Asphaltene aggregation may be an important topic in emulsion stability. Asphaltenes may self-associate in a manner that is oligomerization rather than simple stacking. This is to imply that some form of bonding takes place. Chandra et al. proposed that once asphaltenes were on the surface they would form discoid nanoaggregates at the interface [25]. Solovyev et al. studied adsorption of various oil components at the oil-water interface using a Langmuir trough [26]. It was found that asphaltenes adsorbed irreversibly at the oil/water interface. This adsorption was proposed to be largely responsible for the stability of emulsions.

8.4.2 The Role of Resins and Other Components

Several researchers studied the role of resins in water-in-oil emulsion formation [2,16]. They noted that the main role appears to be solvation of the asphaltenes in the oil solution. Research was conducted in experiments that showed that the addition of resins at ratios of 2:1 (resins/asphaltenes) could increase the stability of the water-in-oil emulsions by as much as twice as that without the resins [16]. Others have noted that resins and asphaltenes are somehow correlated in emulsion stability. Some researchers note that with increasing asphaltene/resin ratio, the emulsions in wellheads were more stable [27]. The interfacial properties of asphaltenes in several Norwegian offshore crude oils were studied [28]. Asphaltenes were shown to be the agent responsible for stabilizing the crude oils tested; however, the resins were also noted as being important. Pereira et al. noted that resins can determine

whether asphaltenes stabilize or destabilize emulsions depending on the type of resins and asphaltenes [29]. Resin adsorption experiments were carried out on different substrates including silica substrates and asphaltenes. Some resins were found to adsorb much more on the same surface areas. The experiments showed a high self-interaction, which was suggested as being the key factor in determining whether the resins would stabilize asphaltenes against aggregation or not.

Sjöblom and coworkers noted that many of the stability differences in emulsions can be explained by the interactions between asphaltenes and resins [30,31]. The authors noted that asphaltenes are believed to be suspended as colloids in the oil with stabilization by resins. Each particle is believed to consist of one or more sheets of asphaltene monomers and absorbed resins to stabilize the suspension. Under certain conditions, the resins can desorb from the asphaltenes leading to increased asphaltene aggregation and precipitation of the larger asphaltene aggregates. Several workers note that there is significant interplay between asphaltenes and resins and that resins solvate the asphaltenes [32,33]. However, Sedghi and Goual found that resins do not coat asphaltenes when present at 10–1000 ppm [34]. Recently, Yang et al. proposed that resin-solvated aggregates are able to diffuse and adsorb to the interface stronger than pure asphaltene aggregates [35]. They propose that the resins rearrange and displace the asphaltenes, reducing the emulsion stability compared to the asphaltene stabilization.

Some effect from naphthenic acids was also noted [30]. Gao and coworkers studied the role of naphthenic acids in emulsion formation using model emulsions [36]. The molecular weight of these naphthenic acids ranged from about 166 to 450 g/mol. In the case of Athabasca bitumen, most of the acid consisted of C21–C24 tricyclic terpenoid acids. Other components of oil, especially aromatics, may actually interfere with this process [37].

Waxes have not been found to stabilize water-in-oil emulsions but have been found to play a role in other types of emulsions, such as food formulations, but only if they are molten or deformed [38].

The effects of various chemical conditions have been noted. Aguilera et al. noted that the most stable emulsions were formed in alkaline aqueous conditions [39]. Rondon et al. noted that there is a “critical” concentration of asphaltenes, about 1000 ppm, after which increasing stability is not achieved [40]. They proposed that once the interface is covered, further asphaltenes do not contribute to stability. Borges et al. found that the stability of emulsions was found to depend on salinity and water–oil ratio. The higher the salinity, the lesser the stability [41].

8.4.3 Methods to Study Emulsions

The availability of methodologies to study emulsions is very important. In the past 15 years, dielectric methods and rheological methods and many other methods have been used to study formation mechanisms and stability of emulsions [6,20]. Standard chemical techniques, including nuclear

magnetic resonance (NMR), chemical analysis techniques, near-infrared (NIR) spectroscopy, microscopy, interfacial pressure, and interfacial tension, are also being applied to emulsions. These techniques have largely confirmed findings noted in the dielectric and rheological mechanisms.

Most researchers studied the stability of emulsions by measuring the amount of water resolved with time [7,13,20,42–46]. This certainly is the baseline method. Some researchers also subjected the emulsions to centrifugation to assess stability.

High-pressure NIR spectroscopy has been used by one group to study asphaltene aggregation of live crude oils [31,43,44]. Further NIR spectroscopy information on the amount of asphaltenes and resins was tied to the emulsion stability [44]. Araujo et al. and others studied the use of NIR spectroscopy and found that NIR spectroscopy was sensitive to both the water content and the droplet size, and models were proposed to estimate both water content and droplet size from NIR spectroscopy data [42,47–49]. Many of the measurements can now be intercorrelated. NMR provides the best method of measuring water droplet size in emulsions [50]. Standard optical techniques suffer from the fact that the continuous medium, oil, is not transparent. Therefore, only the surface droplets are measured using optical techniques.

The NMR method is known as pulsed field gradient with diffusion editing NMR [50]. Results from recent measurements of a water-in-oil emulsion show a change in droplet size from the revolution rate of the mixing vessel. The average water droplet size in one experiment varied from about 12 to 30 μm with mixing energy.

Dielectric spectroscopy has been used to study emulsions. The electrical permittivity of the emulsion can be used to characterize an emulsion and assign stability [6,30,33,51,52]. The Sjöblom group has measured the dielectric spectra using the time-domain spectroscopy technique. A sample is placed at the end of a coaxial line to measure total reflection. Reflected pulses are observed in time windows of 20 ns and Fourier transformed in the frequency range from 50 MHz to 2 GHz. Mostowfi et al. developed a new microcell with measurement using a DC potential [53]. A thin film is created at the intersection of two microchannels and the current applied to this film. At a certain potential, the film will rupture. The potential at which this occurs is related to the strength of the film.

Many studies on the rheology of emulsions have been performed [54–56]. Emulsions stabilized by surfactant films (such as resins and asphaltenes) behave like hard-sphere dispersions and display viscoelastic behavior. Relaxation time can be determined for the system, which increases with the volume fraction of the discontinuous phase. It has been noted that the emulsion stability is highly dependent on the rheological properties of the water–oil interface and that a high elasticity will increase the level of stability [7].

Several workers in the field have used the interface forces on single droplets to study emulsions. One group used an oscillating pendant drop apparatus and correlated this to asphaltene solubility as measured by NIR spectroscopy [57].

Yarranton et al. report on the use of interfacial rheology to study emulsion coalescence [58]. Asphaltenes from Athabasca Bitumen were mixed with a solvent and injected into an optical cuvette and the droplet monitored by camera. Interfacial tension was measured from static measurements on the droplet. Elasticity was measured by manipulating the droplet so that sinusoidal oscillations occurred and using Fourier analysis. The findings were that the interfacial modulus was a function of asphaltene content and reached a maximum at an asphaltene concentration of about 1 kg/m^3 . The modulus increased as the interface aged. The data were found to be consistent with the gradual formation of a cross-linked asphaltene network on the interface. Moran et al. studied emulsions using a micropipette technique in which individual emulsion drops are elongated into a cantilever for force measurements [59]. The stress-strain measurements are converted to interfacial rheological behavior. Gao et al. used the micropipette technique to show that the asphaltene components resulted in more surface effect than did the maltenes [60]. This then would confirm the asphaltene stability model. Khristov et al. studied emulsions as a film with toluene dilution and the thin liquid film pressure balance technique [61].

Ridi et al. studied emulsions using differential scanning calorimetry [62].

Many researchers studied emulsification by using model oils or modified crude oils. Other researchers studied emulsions as thin layers or by droplets [11,63]. Hemmingston et al. studied the water-in-oil emulsions formed from 27 crude oils of different origins [64]. They found that there is an increase in stability as viscosity increases. Viscosity also correlated with the saturates, aromatics, resins, and asphaltenes (SARA) data taken on the crude oil. Sjöblom et al. studied 16 crudes from the North Sea and 5 from North Africa [52]. Stability was measured using the results from an electric field cell. A voltage was applied to the cell until coalescence was observed using a microscope. The value of the voltage at the critical point was taken as a measure of stability [52]. Fingas and Fieldhouse studied more than 400 oils at various weathering stages [3].

8.4.4 The Overall Theory of Emulsion Formation

The data suggest that the water-in-oil types are stabilized by both asphaltenes and resins, but for greater stability, resin content should exceed the asphaltene content slightly [2]. However, excess resin content ($A/R > \text{about } 0.6$) apparently destabilizes the emulsion. This does not consider the question of different types of asphaltenes or resins. A high asphaltene content (typically $>10\%$) increases the viscosity of the oil such that a stable emulsion will not form. Viscous oils will only uptake water as entrained water and will slowly lose much of this water over a period of about 1 week. Viscous oils (typically $>1000 \text{ mPa}\cdot\text{s}$) will not form stable or mesostable emulsions. Oils of low viscosity or without significant amounts of asphaltenes and resins will not form any water-in-oil type and will retain less than about 6% water. Oils of very high viscosity (typically $>10,000 \text{ mPa}\cdot\text{s}$)

will also not form any of these water-in-oil types and thus are classified as unstable. This is probably due to the inability of water droplets to penetrate the oil mass.

The discussion in Sections 8.4.1 and 8.4.2 certainly shows that asphaltenes and resins combine to stabilize water droplets in emulsions. This can be seen in Figure 8.6. Figure 8.6 shows a simplified plot of oil composition and viscosity and the types of emulsions that result from this combination. This figure shows that even a very simplified presentation can highlight the importance of the starting oil viscosity and resin and asphaltene contents.

The information given in Section 8.4 highlights the formation process. The scheme for this is shown in Figure 8.7. This describes the current knowledge of water-in-oil emulsion formation. The start of the process is the injection of water droplets into the oil mass. This would typically occur as the result of turbulence or wave action. This also could occur as the result of oil injection into water, such as from an underwater blowout. Once in the oil mass, the water droplets may coalesce and sink to the bottom unless these water droplets are somehow stabilized. Asphaltenes probably reside in the oil in the form of

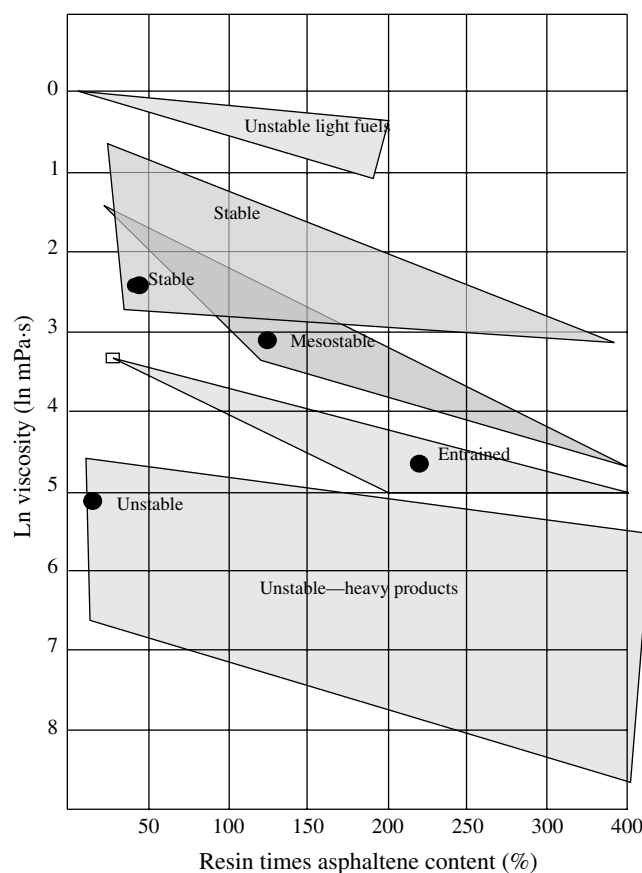


FIGURE 8.6 A plot of the starting oil viscosity versus the asphaltene times the resin content of the starting oil. The shaded regions show all areas where the particular water-in-oil type exists. This simple comparison shows that there are approximate regions of stability with only these three factors. Another important factor is the asphaltene/resin ratio, and this factor may separate any overlaps.

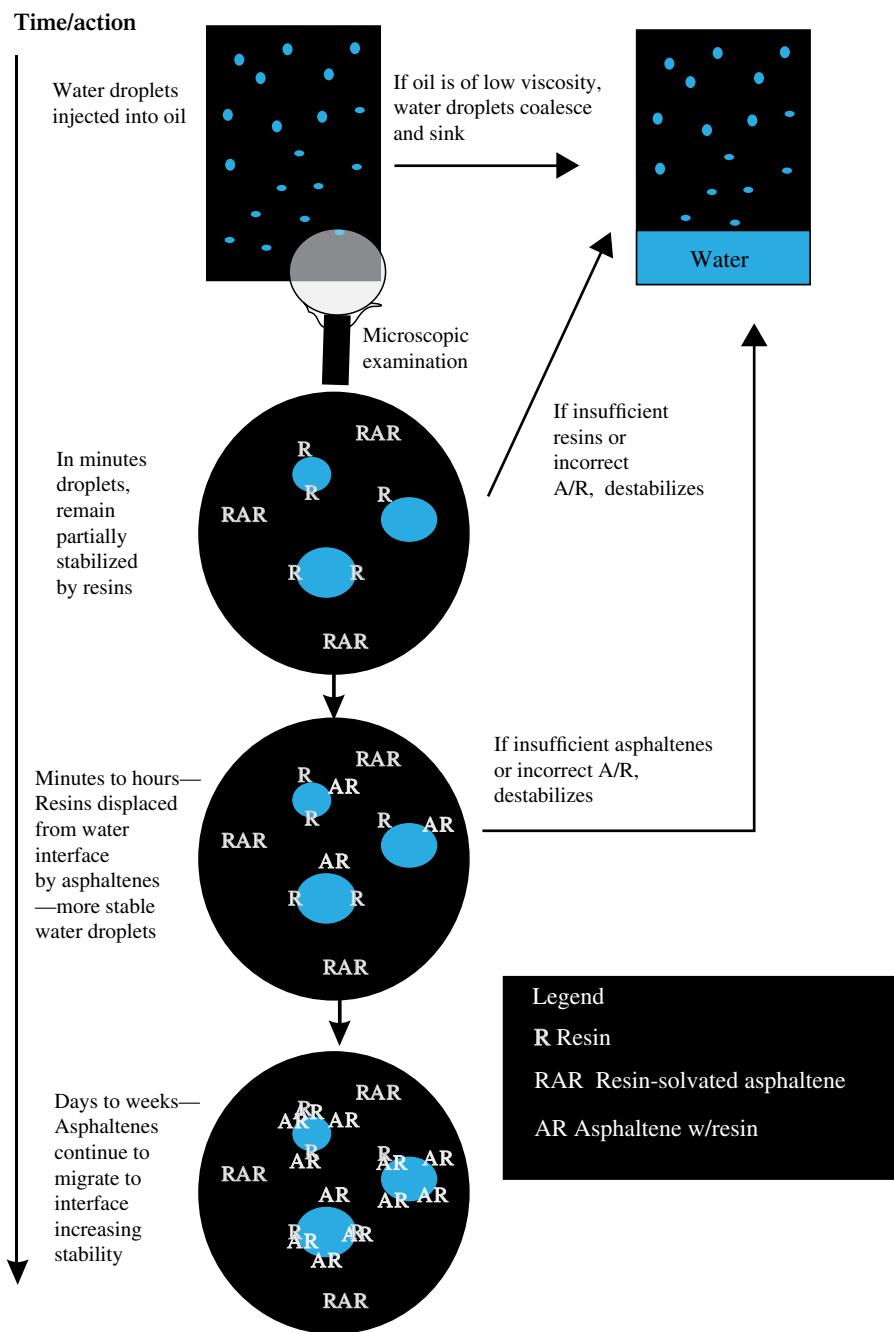


FIGURE 8.7 A scheme to describe the formation of water-in-oil emulsions.

resin-solvated agglomerates. They are not likely to stabilize the water droplets immediately as the large asphaltene/resin agglomerates migrate too slowly. If, however, the oil has a viscosity between about 50 and 5000 mPa-s, the water droplets will move slowly, allowing time for some chemical stabilization. It is thought that resins weakly stabilize the water droplets initially. Resins are also polar compounds and can become associated with polar water. Once stabilized by resins, the large asphaltenes will move toward the water droplets and will form elastic films around the water droplets. The ratio of asphaltenes to resins can affect this process. If the quantity of resins is too high, they will solvate the

asphaltenes to the extent that their migration is affected and will also create a barrier between the asphaltenes and the water droplets. Thus, in the case of too high resin content, destabilization will also occur. It is thought that this destabilization is the origin of mesostable emulsions.

If the viscosity of the oil is too high, water droplets cannot penetrate the oil mass to a great extent and thus emulsions are not formed. At moderate oil viscosities, about 1000–10,000 mPa-s, the water droplets may be retained by viscosity alone. This is felt to be the origin of the entrained water-in-oil type. This type of viscosity and resin/asphaltene effect at high values is also illustrated in Figure 8.8.

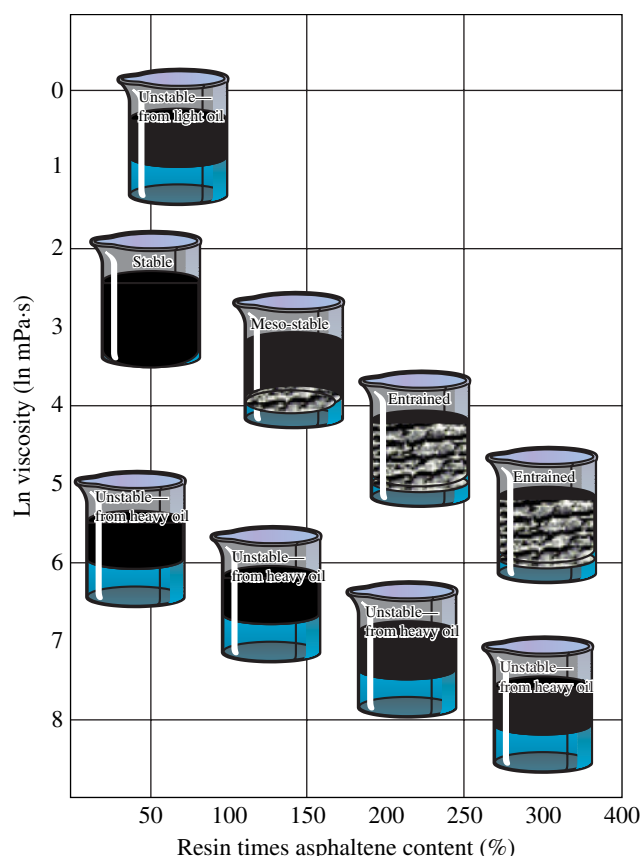


FIGURE 8.8 An illustration of how the starting oil viscosity and asphaltene/resin content can influence the water-in-oil type.

8.4.5 The Role of Weathering

Most crude oils and petroleum products require weathering (evaporation) before they will form emulsions [3]. This can be seen in Table 8.A4, which shows pairs or triplets of oils that when weathered will form a water-in-oil type upon mixing with water. Table 8.A4 shows that many oils require weathering to enable formation of a water-in-oil type. Some heavy oils will make transitions from stable to entrained and further on to being unable to form a water-in-oil mixture (unstable—heavy oil type) upon weathering. Most typical crude oils require weathering to make the transition from the basic crude to a mesostable or stable emulsion. The weathering is necessary to increase the viscosity and the asphaltene/resin content to the point where the next water-in-oil type is possible. Figure 8.9 shows that weathering causes certain transitions. The five transitions shown here are the only ones observed to date. The transitions are always from a fresh crude to an end state. It is also important to note that transitions cannot occur after a water-in-oil state is created. Figure 8.10 illustrates the effect weathering has on the viscosity and relative asphaltene/resin content and where the average water-in-oil types lie.

It should be noted that once a water-in-oil type is formed, it cannot make a transition to another type even if extensive weathering or mixing takes place. This is felt to be a result of the exacting conditions for each type. Further, asphaltene

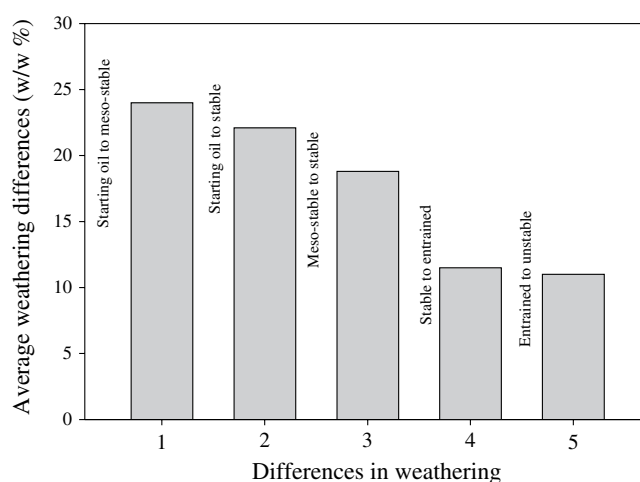


FIGURE 8.9 Illustration of the average difference in weathering between one water-in-oil type and another. It should be noted that after a water-in-oil type is formed, transitions between types do not occur.

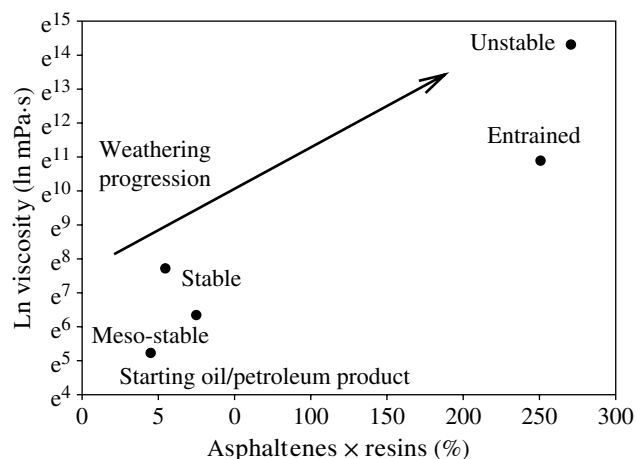


FIGURE 8.10 Illustration of the relative viscosity and asphaltene/resin amounts associated with the weathering process and where the average properties of the various water-in-oil types belong. Again, it is noted that transitions between types do not occur.

appear to be tied up in the form of “rag” in broken mesostable emulsions. This “rag” formation appears to prohibit the formation of other types of emulsions.

8.5 MODELING THE FORMATION OF WATER-IN-OIL EMULSIONS

8.5.1 Older Models

The emulsification processes described earlier were not apparent until about 15 years ago and have since been translated into modeling equations [3]. The different water-in-oil states dictate that one simple equation is not adequate to predict formation. Information on the kinetics of formation at sea and other modeling data was less abundant in the past. It is now known that emulsion formation is a result of surfactant-like action of the polar asphaltene and resin compounds. While

these are similar compounds that both behave like surfactants when they are not in solution, asphaltenes form much more stable emulsions. Emulsions begin to form when the required chemical and viscosity conditions are met and when there is sufficient sea energy. Further, as pointed out earlier, three different water-in-oil types are formed, depending on the oil type and its composition. Some oils do not form any water-in-oil types, and this fact is stated to be a fourth type.

In the distant past, the rate of emulsion formation was assumed to be the first order with time. This was approximated with a logarithmic (or exponential) curve. The physical assumption was that all oils take up water on a first-order basis. Although not consistent with the knowledge of how emulsions form, this assumption was used extensively in oil spill models. As was shown in comparisons, this does not yield correct results [3]. Most models that incorporate the phenomenon use the estimation technique of Mackay and coworkers or a variation of this technique [65–73].

The old models and comparison with newer models are described in the literature [3]. This comparison shows that most of the older approaches are not reliable and can result in inaccurate predictions.

8.5.2 New Models

Several new models for the prediction of water-in-oil emulsions were recently developed by the present author [65–69]. These models used empirical data to predict the formation of emulsions using a continuous function and employing the physical and chemical properties of oil. The emulsification properties of more oils were measured, and the properties of some of the oils in the existing oil set have been remeasured. This enables the models to be recalculated with sound data on over 400 discrete oil samples.

The basis of these models is the result of the knowledge demonstrated earlier—that is, that models are stabilized by asphaltenes, with the participation of resins. Findings of this group and other groups show that the entire SARA distribution effects the formation of emulsions as the prime stabilizers, asphaltenes and secondarily resins, are only available for emulsion formation when the concentration of the saturates and aromatics are at a certain level and when the density and viscosity are correct [2].

The approaches to model development were implemented and are detailed in the literature [65–69]. One approach was to curve fit the physical and content data to an earlier “stability” index, which was at that time the complex modulus of the water-in-oil product divided by the starting oil viscosity. Then this stability factor was used in turn to predict a class (stable, mesostable, entrained, or unstable). Another approach was to predict the class directly from the data, an approach that was later used in an “improved” model. It is important to note that the class was assigned an arbitrary numerical value, which was later adjusted to optimize the fit. This contrasts with the new approach described in this paper, which uses a newly developed “stability index.”

The empirical data including oil content data, viscosity, density, and the resulting water-in-oil-type stability were used to develop mathematical correlation [69]. The value for each parameter was correlated in a series of models using DataFit (Oakdale Engineering), which calculates linear models. A two-step process is necessary as DataFit is not able to calculate the specific mathematical function with more than two variables, due to the large number of possibilities. Thus, the functions (e.g., linear, square, log) were calculated using a two-way regression (TableCurve), and these functions were in turn used in developing a predictor model for emulsification.

It should be noted that there are some problems with the fundamental process of categorizing water-in-oil states at the onset. Some crude oils are treated with emulsion preventers (also called asphaltene suspenders) directly at the wellhead; this is because they are very emulsion prone. Thus, some emulsion-prone oils may not form emulsions during the laboratory or field tests because of the addition of these emulsion-preventing materials. Although attempts are made to receive oils that do not contain these emulsion-preventing materials, it is impossible to know this fact in every case.

The steps to produce the first models are summarized in earlier papers [65–69]. First, the parameters available were correlated one at a time. The latest model used the new stability index as the target of the correlation [3,65–69]. This new approach used a multiregression program directly, using various multifunctional transformations of the input oil property data. This allowed the regression software to assign portions of the functions necessary to achieve the highest correlation factor.

A transformation is needed to adjust the data to a singular increasing or decreasing function. Regression methods will not respond correctly to a function that varies both directly and inversely with the target parameter. Most parameters have an optimal value with respect to class, that is, the values have a peak function with respect to stability or class. This is illustrated in Figures 8.11 and 8.12. The resin content without any adjustment is plotted against stability in Figure 8.11. The stability as shown in these figures is stability C, as described earlier. As can be seen in Figure 8.11, the values of stability peak at about 5% resins. After this correction is made to the values, the regression coefficient increases. The modified distribution is shown in Figure 8.12. The arithmetic converts values in front of the peak to values behind the peak, thus yielding a simple declining function. The optimal value of this manipulation is found by using a peak function as shown by the line in Figure 8.11. This peak function fit is available from TableCurve software.

It is important to note that the scatters observed in Figures 8.11 and 8.12 are typical of scatter observed for a single parameter when a large number of parameters are operative. If one plotted the total number of parameters simultaneously (e.g., in multidimensions), then an individual or single-value function would appear with much less scatter.

The arithmetic to perform the transformation is as follows: (i) if the initial value is less than the peak value,

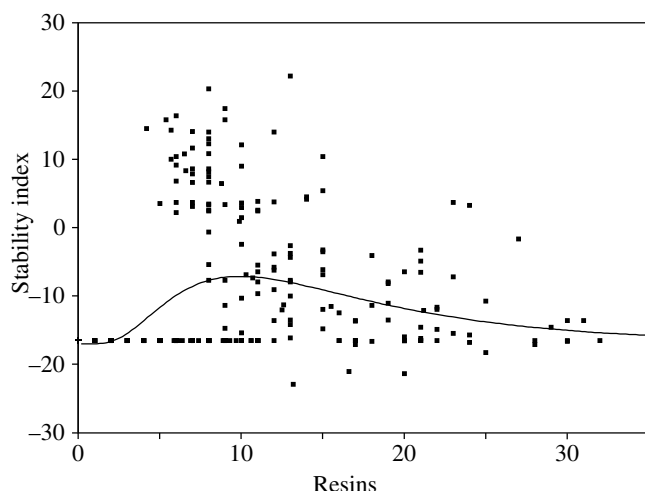


FIGURE 8.11 Graph of resin content (uncorrected) versus stability index C . The curve fit is the calculated peak. This is typical of the scatter associated with multiple-parameter fits, where each parameter accounts for a small amount of the variance.

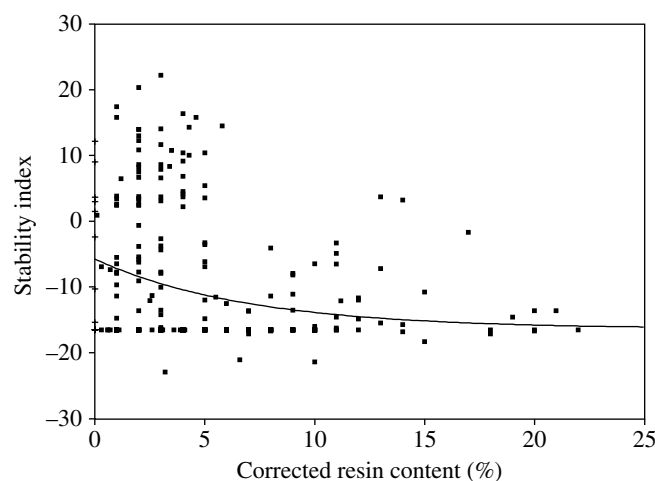


FIGURE 8.12 Graph of corrected resin content versus stability parameter C . The curve fit is the best fit. The scatter is typical of a multiple-parameter fit; however, the correction to the resin results in a simple declining function.

then the adjusted value is the peak value less the initial value; (ii) and if the initial value is more than the peak value, the adjusted value is the initial value less the peak value. The values found for the transformations are listed in Table 8.3. It should be noted that the exponential of density was used and the natural log of the viscosity. Previous modeling work had shown that these mathematical changes are necessary to achieve higher correlations [3].

Having the transformed values, the new model proceeds by fitting a multiple linear equation to the data. The choice of functions was achieved by correlating the stability function directly with the data and taking the best of the functions (e.g., square, log, etc.) into the regression process. The functionalities of square, logarithmic, or exponential curves are achieved by correlating the straight value of the input properties plus

TABLE 8.3 Values used to correct oil property input parameters for Model I

Parameter	Form	Correction value
Density	Exponential	2.5
Viscosity	Natural logarithm	5.8
Saturates	Standard %	45
Resins	Standard %	10
Asphaltenes	Standard %	4
Asphaltene/resin ratio	Standard	0.6

their expanded values, taken here as the cube of the starting parameter as well as the square of the exponential of the starting value, and their companded values, the natural log (\ln) and the logarithm (base 10) of the parameter divided by the square of the value. Each parameter is correlated with the stability index C in five sets of mathematical statements. This is similar to the standard Gaussian expansion regression technique [54]. In this method, the regression is expanded to functionalities above and below linear until the entire entity is optimized. For example, a linear function would be included and then a square, then a square root, and so on until tests of the complete regression show that there are no more gains in increased expansions. Using this technique, six input parameters, namely, exponential of density, \ln of viscosity, saturate content, resin content, asphaltene content, and the asphaltene/resin ratio (A/R), were found to be optimal. Thus, with four transformations and the original values of these input parameters, there are six times five or 30 input combinations.

Using DataFit, a multiple regression software, a maximum of 20 of these could be taken at a time to test the goodness of fit. Values that yield $\text{Prob}(t)$ factors of greater than 0.9 were dropped until all remaining factors could be calculated at once. $\text{Prob}(t)$ is the probability that input can be dropped without affecting the regression or goodness of fit. Over 20 regressions were carried out until the resulting model was optimal. The regression coefficient, r^2 , was 0.75, which is quite high considering the many potential sources of error. The statistics on the new model are shown in Table 8.4, along with the parameters to create the model. Table 8.4 shows that the 14 remaining parameters all contribute to the accuracy of the final result and that none of them can be cut without affecting the outcome of the model. The procedures for using Model I are given in the following and summarized in Table 8.5.

8.5.2.1 Model I The first step is to transform the input data so that it forms a continuous declining or increasing function. It should be noted that the “greater than” can also be read as greater or equal to.

Density: Take the exponential of the density. If it is less than 2.5, then the density parameter is 2.5 less the density and if it is greater than 2.5, it becomes the density less 2.5. The value used in the equation is this transformed value.

(8.1)

TABLE 8.4 Regression results for Model I

Variable	Regression variable results				Input variable	Math applied
	Value	Standard error	<i>t</i> ratio	Prob(<i>t</i>)		
<i>a</i>	0.0126	0.09	0.14	0.88694	Saturates	
<i>b</i>	-1.49	0.48	-3.11	0.00239	Resins	
<i>c</i>	-12.6	12.34	-1.02	0.30914	A/R	
<i>d</i>	-0.073	0.02	-3.97	0.00013	In viscosity	Cubed
<i>e</i>	0.00193	0.00	2.08	0.0402	Resins	
<i>f</i>	0.00016	0.00	0.22	0.82677	Asphaltenes	
<i>g</i>	-4.23	14.21	-0.30	0.76648	A/R	
<i>h</i>	-0.59	0.77	-0.77	0.44215	In viscosity	ln
<i>i</i>	1.59	1.03	1.55	0.12359	Resins	
<i>j</i>	4.03	2.53	1.59	0.11479	A/R	
<i>k</i>	3.73E-26	0.00	1.28	0.20272	In viscosity	Exp squared
<i>l</i>	1.21	7.02	0.17	0.8639	A/R	
<i>m</i>	0.022	0.01	1.59	0.11463	Exp density	Log/square x
<i>n</i>	0.11	0.13	0.83	0.40933	A/R	
<i>o</i>	17.8	8.60	2.07	0.04066	Constant	

Gray shade groups the different functions which have the same mathematical function as that first listed.

TABLE 8.5 Summary of calculations for Model I

Basic inputs	Symbol	Units
Density	D	g/ml
Viscosity	V	mPa·s
Saturate content	S	%
Resin content	R	%
Asphaltene content	A	%
First transformation		Description
Density	expD	Take exponential of density
Viscosity	lnV	Take natural logarithm of viscosity
Asphaltene/resin ratio	A/R	Divide asphaltene content by resin content
Second step—rationalization (converts units to simple declining or increasing functions)		
Density	Dst	If (expD<2.5, 2.5-expD, expD-2.5) ^a
Viscosity	Vst	If (lnV<5.8, 5.8-lnV, lnV-5.8)
Saturate content	Sst	If (S<45, 45-S, S-45)
Resin content	Rst	If (R<10, 10-R, R-10)
Asphaltene content	Ast	If (A<4, 4-A, A-4)
Asphaltene/resin ratio	A/Rst	If (A/R<0.6, 0.6-A/R, A/R-0.6)
Third step—parsing zeros from SARA numbers ^b		
Resin content	Rst	Replace zeros at rationalization stage with “20.1”
Asphaltene content	Ast	Replace zeros at rationalization stage with “20.1”
Asphaltene/resin ratio	A/Rst	Replace zeros at rationalization stage with “0.01”
Fourth step—calculate Gaussian expansion steps		
Viscosity cubed	Vst ³	Cube the rationalized viscosity
Resin content cubed	Rst ³	Cube the rationalized resin content
Asphaltene content cubed	Ast ³	Cube the rationalized asphaltene content
Asphaltene/resin ratio cubed	A/Rst ³	Cube the rationalized asphaltene content
Natural log of viscosity	lnVst	Natural logarithm of rationalized viscosity
Natural log of resin content	lnRst	Natural logarithm of rationalized viscosity
Natural log of asphaltene/resin ratio	lnA/Rst	Natural logarithm of rationalized asphaltene/resin ratio
Exponential of viscosity squared	Exp ² Vst	(Exp(Vst)×Exp(Vst))
Exponential of A/Rst ratio squared	Exp ² A/Rst	(Exp(A/Rst)×Exp(A/Rst))
Log over square of density	LogDst ²	(Log(Exp(Dst))/(Dst ²))
Log over square of A/R ratio	LogA/Rst ²	(Log(Exp(A/Rst))/(A/Rst ²))

^aThis is an Excel-like statement that in this case reads as follows: if the exponential of density is less than 2.5, the standardized density becomes 2.5 less the exponential of density, if not the standardized density is the exponential of density less 2.5.

^bZeros must be purged from numbers as they cause problems in division and with logarithmic expressions.

SARA saturates, aromatics, resins, and asphaltenes.

Viscosity: Take the natural logarithm (ln) of the viscosity. If it is less than 5.8, then the viscosity parameter is 5.8 less the viscosity natural log and if it is greater than 5.8, it becomes the natural log of viscosity less 5.8. The value used in the equation is this transformed value.

(8.2)

Saturate Content: If the saturate content is less than 45, then the saturate content parameter is 45 less the saturate content and if it is greater than 45, it becomes the saturate becomes the saturate content less 45. The value used in the equation is this transformed-

(8.3)

Resin Content: If the resin content is less than 10, then the resin content parameter is 10 less the resin content and if it is greater than 10, it becomes the resin content less 10. The value used in the equation is this transformed value. If the value of the resins is zero, then set this value to 20.

(8.4)

Asphaltene Content: If the asphaltene content is less than 4, then the asphaltene content parameter is four less the asphaltene content and if it is greater than 4, it becomes the asphaltene content less 4. The value used in the equation is this transformed value. If the value of the asphaltene content is zero, then set the value to 20.

(8.5)

A / R or Asphaltene / Resin Ratio: The A / R is taken as the direct value of the asphaltene content in percent (untransformed) divided by the resin content in percent (again untransformed). If A / R is less than 0.6, then the A / R parameter is 0.6 less the A / R and if it is greater than 0.6, it becomes the A / R less 0.6. The value used in the equation is this transformed value.

(8.6)

The class of the resulting emulsion is then calculated as follows:

$$\begin{aligned} \text{Stability} = & 17.8 + 0.013 \times \text{Sst} - 1.49 \times \text{Rst} - 12.6 \\ & \times \text{A} / \text{Rst} - 0.073 \times \text{Vst}^3 + 0.0019 \times \text{Rst}^3 \\ & + 0.00016 \times \text{Ast}^3 - 4.23 \times \text{A} / \text{Rst}^3 - 0.59 \\ & \times \ln(\text{Vst}) + 1.59 \times \ln(\text{Rst}) + 4.028 \times \ln(\text{A} / \text{Rst}) \\ & + 3.72 \times 10^{-26} \times \text{Exp}(\text{Vst})^2 + 1.207 \times \text{Exp}(\text{A} / \text{Rst})^2 \\ & + 0.022 \times (\text{LogDst} / \text{Dst}^2) + 0.11 \\ & \times (\text{LogA} / \text{Rst} / \text{A} / \text{Rst}^2) \end{aligned} \quad (8.7)$$

where stability is the stability of the resulting water-in-oil type; Sst is the transformed saturate content as calculated in

Equation (8.3), abbreviated A here; Rst is the transformed resin content as calculated in Equation (8.4), abbreviated B; A/Rst is the transformed asphaltene/resin ratio as calculated in Equation (8.6), abbreviated C; Vst³ is the cube of the transformed ln viscosity as calculated in Equation (8.2), abbreviated D; Rst³ is the cube of the transformed resin content as calculated in Equation (8.4), abbreviated E; Ast³ is the cube of the transformed asphaltene content as calculated in Equation (8.5), abbreviated F; A/Rst³ is the cube of the transformed A/R ratio as calculated in Equation (8.6), abbreviated G; ln Vst is the natural logarithm (ln) of the transformed viscosity as calculated in Equation (8.2), abbreviated H; ln Rst is the natural logarithm (ln) of the transformed resin content as calculated in Equation (8.4), abbreviated I; ln A/Rst is the natural logarithm (ln) of transformed asphaltene/resin ratio as calculated in Equation (8.6), abbreviated J; Exp(Vst)² is the exponential of the square of the transformed viscosity Vst as calculated in Equation (8.2), abbreviated K; Exp(A/Rst)² is the exponential of the square of the A/R ratio as calculated in Equation (8.6), abbreviated L; LogDst/Dst² is the logarithm (base 10) of the exponential of the density divided by the square of the transformed density, the transformed density as calculated in Equation (8.1), abbreviated M; and LogA/Rst/A/Rst² is the logarithm (base 10) of the exponential of the A/R ratio divided by the square of the A/R ratio, the transformed A/R ratio as calculated in Equation (8.6), abbreviated N.

A simplified version of the equation is then

$$\begin{aligned} \text{Stability} = & 17.8 + 0.013A - 1.49B - 12.6C - 0.073D \\ & + 0.0019E + 0.00016F - 4.23G - 0.59H + 1.59I \\ & + 4.028J + 3.72 \times 10^{-26}K + 1.207L + 0.022M \\ & + 0.11N \end{aligned} \quad (8.8)$$

where the parameters A to N are defined as earlier.

The stability of the resulting product is calculated using the rheological measurements of the water-in-oil product formed.

The basic uncorrected *Stability* or cross product is

$$\text{Xpr} = \frac{\text{Complex modulus}}{\text{Starting oil viscosity}} \times \frac{\text{Elastic modulus}}{\text{Starting oil viscosity}} \quad (8.9)$$

(Old stability A) (Old stability B)

The corrected stability is

$$\text{Stability} = \ln((\text{Xpr} / 10,000) \times (\text{Xpr} / 10,000)) \quad (8.10)$$

where Xpr is the value from Equation (8.9).

Or equivalently, stability C can be calculated from

$$\text{Stability C} = \ln((\text{Stab A} \times \text{Stab B})^2 / 10^{11}) \quad (8.11)$$

The values of stability C that are assigned to each class are given in Table 8.2. The viscosity of the resulting product can be taken as the average of the types at a given time as shown in Table 8.6.

TABLE 8.6 Viscosity increases from starting oil and typical water content

	Viscosity increase on		
	First day	Week	Year
Entrained	1.9	1.9	2.1
Mesostable	7.2	11	32
Stable	405	1054	991
Unstable	0.99	1.0	1.0

	Typical water content		
	First day	Week	Year
Entrained	44.5	27.5	6
Mesostable	64.3	30	6
Stable	81	78	70
Unstable	6.1	6	5

8.5.2.2 Model II More recently, renewed efforts have been placed on developing more accurate and more simplified equations. One of these will be presented in the following. The differences between the equation shown above and that below include the following:

1. The Gaussian expansion is simplified to one term expansion and one term compression.
2. Three terms are not rationalized in the same manner as in the preceding text, which include density, viscosity, and asphaltene/resin ratio. These are felt to be continuous functions as they are and thus can be used as such.
3. The input values are also used directly as well as the Gaussian expansion.

The first step to procedure 2 is to transform the input data so that it forms a continuous declining or increasing function. It should be noted that the "greater than" can also be read as greater or equal to.

Density: *not transformed—just take the exponential, abbreviated Den.*

Viscosity: *not transformed—just take the natural log, abbreviated Visc.*

Saturate Content: *If the saturate content is less than 45, then the saturate content parameter is 45 less the saturate content and if it is greater than 45, it becomes the saturate content less 45. The value used in the equation is this transformed value.*

Resin Content: *If the resin content is less than 10, then the resin content parameter is 10 less the resin content and if it is greater than 10, it becomes the resin content less 10. The value used in the equation is this transformed value. If the value of the resins is zero, then set this value to 20.*

(8.13)

Asphaltene Content: *If the asphaltene content is less than 4, then the asphaltene content parameter is four less the asphaltene content and if it is greater than 4, it becomes the asphaltene content less 4. The value used in the equation is this transformed value. If the value of the asphaltene content is zero, then set the value to 20.*

(8.14)

A/R Ratio: *not transformed*

For procedure 2, the class of the resulting emulsion is then calculated as follows:

$$\begin{aligned}
 \text{Stability} = & 5667 - 9520 \times \text{Den} - 3.99 \times \text{Visc} \\
 & + 0.138 \times \text{Sst} + 2.16 \times \text{Rst} - 0.395 \times \text{Ast} \\
 & + 17.9 \times A/R + 224 \times \exp(\text{den}) + 2.88E^{-10} \\
 & \times \exp(\text{Rst}) - 4.35 \times \exp(A/R) \\
 & + 16,823 \times \ln(\text{den}) + 10.5 \times \ln(\text{Visc}) \\
 & - 0.671 \times \ln(\text{Sst}) + 0.147 \times \ln(\text{Rst}) + 0.107 \\
 & \times \ln(\text{Ast}) + 1.62 \times \ln(A/R)
 \end{aligned}
 \quad (8.15)$$

where stability is the stability of the resulting water-in-oil type; Den is the untransformed exponential of the density, abbreviated *A* here; Visc is the untransformed natural logarithm (ln) of the viscosity, abbreviated *B* here; Sst is the transformed saturate content as calculated in Equation (8.12), abbreviated *C* here; Rst is the transformed resin content as calculated in Equation (8.13), abbreviated *D*; Ast is the transformed asphaltene content as calculated in Equation (8.14), abbreviated *E*; A/R is the (untransformed) asphaltene/resin ratio, abbreviated *F*; Exponential den is the exponential of the exponential of density, abbreviated *G*; Exponential Rst is the exponential of the transformed resins, calculated in Equation (8.13), abbreviated *H*; Exponential of A/R, abbreviated *I*; ln (natural logarithm) of the exponential of density, abbreviated *J*; ln (natural logarithm) of the natural logarithm of viscosity, abbreviated *K*; ln (natural logarithm) of the transformed saturates as calculated in Equation (8.12), abbreviated *L*; ln (natural logarithm) of the transformed resins as calculated in Equation (8.13), abbreviated *M*; ln (natural logarithm) of the transformed asphaltenes as calculated in Equation (8.14), abbreviated *N*; and ln (natural logarithm) of the (untransformed) (A/R) ratio, abbreviated *O*. A simplified version of the equation is then

$$\begin{aligned}
 \text{Stability} = & 5667 - 9520A - 3.99B + 0.138C \\
 & + 2.16D - 0.395E + 17.9F + 224G \\
 & + 2.88E^{-10}H - 4.35 \times I + 16,823J + 10.5K \\
 & - 0.671L + 0.147M + 0.107N + 1.62O
 \end{aligned}
 \quad (8.16)$$

where the parameters A to O are defined as in the preceding text.

As with Model I, the values of stability C that are assigned to each class are given in Table 8.2. The viscosities and water contents of the resulting products can be taken as the average of the types at a given time as shown in Table 8.6.

The regression table for Model II is given in Table 8.7. The calculations for Model II are summarized in Table 8.8. A comparison of models is given in Table 8.9. This shows advantages for Model II in terms of accuracy; however, this

TABLE 8.7 Regression results for the emulsification Model II

Regression variable results						
Variable	Value	Standard error	t ratio	Prob(t)	Input variable	Math applied
a	-9520	7200	-1.32	0.189	Density	Exp
b	-3.99	1.789	-2.23	0.028	Viscosity	Ln
c	0.138	0.128	1.07	0.285	Saturates	Adjusted
d	0.216	0.224	0.966	0.336	Resins	Adjusted
e	-0.395	0.269	-1.47	0.145	Asphaltenes	Adjusted
f	17.9	13	1.37	0.172	A/R	
g	224	158	1.42	0.159	Exp density	Exp
h	2.883E-10	0.000	0.323	0.747	Exp resins	
i	-4.35	3.64	-1.20	0.235	A/R	
j	16.830	13.200	1.28	0.205	Exp density	Ln
k	10.5	12.1	0.867	0.388	ln viscosity	
l	-0.671	1.100	-0.610	0.543	Saturates _{t}	
m	0.147	0.706	0.208	0.835	Resins _{t}	
n	0.107	0.889	0.120	0.905	Asphaltenes _{t}	
o	1.622	2.95	0.549	0.584	A/R	
p	5667	4006	1.42	0.160	Constant	

Gray shade groups the different functions which have the same mathematical function as that first listed.
 t subscript indicates adjusted value.

TABLE 8.8 Summary of calculations for Model II

Basic inputs	Symbol	Units
Density	D	g/ml
Viscosity	V	mPa-s
Saturate content	S	%
Resin content	R	%
Asphaltene content	A	%
First calculation		Description
Density	Den	Take exponential of density
Viscosity	Visc	Take natural logarithm of viscosity
Asphaltene/resin ratio	A/R	Divide asphaltene content by resin content
Second step—rationalization (converts units to simple declining or increasing functions)		
Saturate content	Sst	If ($S < 45$, $45 - S$, $S - 45$)
Resin content	Rst	If ($R < 10$, $10 - R$, $R - 10$)
Asphaltene content	Ast	If ($A < 4$, $4 - A$, $A - 4$)
Third step—parsing zeros from SARA numbers ^a		
Resin content	Rst	Replace zeros at rationalization stage with “20.1”
Asphaltene content	Ast	Replace zeros at rationalization stage with “20.1”
Fourth step—calculate Gaussian expansion steps		
Exponential of density	exp(Den)	Exponential of the exponential of density
Exponential of resin content	exp(Rst)	Exponential of rationalized resin content
Exponential of A/R ratio	exp(A/R)	Exponential of A/R ratio
Natural logarithm of density	ln(Den)	Natural logarithm (ln) of the exponential of density
Natural logarithm of viscosity	ln(Visc)	Natural logarithm (ln) of the natural logarithm of viscosity
Natural logarithm of saturates	ln(Sst)	Natural logarithm (ln) of the rationalized saturate content
Natural logarithm of resins	ln(Rst)	Natural logarithm (ln) of the rationalized resin content
Natural logarithm of asphaltenes	ln(Ast)	Natural logarithm (ln) of the rationalized asphaltene content
Natural logarithm of A/R ratio	ln(A/R)	Natural logarithm (ln) of the A/R ratio

^aZeros must be purged from numbers as they cause problems in division and with logarithmic expressions.
 SARA, saturates, aromatics, resins, and asphaltenes.

TABLE 8.9 Comparison of model predictions (gray shading indicates classification error)

Oil	Oil evaporation %	Actual stability	Model I prediction	Model II prediction	Density (at 15°C)	Viscosity mPa.s	Resins %	Asphaltenes %	Actual stability	Model I	Model II
Albian Heavy Synthetic	0	Stable	Meso	Stable	0.9372	156	26	6	19.0	-0.8	3.5
Arabian Light	0	Stable	Meso	Stable	0.8658	14	6	3	23.3	2.5	17.6
Arabian Medium	0	Stable	Stable	Stable	0.8783	29	7	6	21.0	6.5	19.9
Canolimon	0	Stable	Stable	Stable	0.8817	46	8	8	27.2	7.8	19.8
Canolimon	6.97	Stable	Stable	Stable	0.8961	103	8	9	19.9	8.0	16.9
Canolimon	13.5	Stable	Stable	Stable	0.9077	254	8	10	15.1	8.2	13.7
Canolimon	21.0	Stable	Stable	Stable	0.9200	1,350	10	11	9.9	6.8	5.6
Cook Inlet—Swanson River	39.7	Stable	Stable	Stable	0.9143	152	7	7	14.8	9.8	13.6
Fuel Oil #5 (2000)	0	Stable	Stable	Stable	0.9883	1410	8	8	10.2	7.9	2.6
Fuel Oil #5 (2000)	7.25	Stable	Meso	Stable	1.0032	4530	8	13	7.0	1.8	0.7
Garden Banks 426	37.7	Stable	Stable	Stable	0.8993	136	10	3	6.7	7.1	7.0
Hebron M-04	8.8	Stable	Stable	Stable	0.9344	676	9	13	4.0	6.1	6.5
Hebron M-04	16.4	Stable	Stable	Stable	0.9423	1,442	12	14	5.2	7.4	2.4
Hondo	0	Stable	Stable	Stable	0.9356	735	24	12	10.1	-2.0	2.4
Hondo	16.7	Stable	Unstable	Meso	0.9674	9,583	29	12	0.9	-3.6	-7.0
Lago Treco	0	Stable	Stable	Stable	0.9230	272	14	11	11.4	8.2	7.6
Lucula	0	Stable	Meso	Stable	0.8574	43	8	4	20.9	6.4	18.3
Lucula	15.4	Stable	Stable	Stable	0.8904	6,118	9	4	3.6	6.3	2.7
Malongo	11.8	Stable	Stable	Stable	0.8970	6,359	10	3	0.6	4.6	-1.6
Mississippi Canyon 72	26.2	Stable	Stable	Stable	0.9095	195	11	3	9.5	10.1	4.7
Neptune [2009]	0	Stable	Meso	Stable	0.9244	402	19	10	4.0	1.0	5.5
Neptune Spar (Viosca Knoll 826)	22.6	Stable	Stable	Stable	0.8986	187	8	2	15.6	9.4	6.6
Platform Gail (Sockeye)	0	Stable	Meso	Stable	0.9297	406	21	12	3.6	-2.7	4.5
Point Arguello Comingled	0	Stable	Meso	Stable	0.9248	533	23	16	10.6	-1.0	5.2
Point Arguello Comingled	9.05	Stable	Meso	Meso	0.9528	4,988	19	17	2.0	0.6	-3.0
Point Arguello Heavy	0	Stable	Meso	Stable	0.9447	3,250	17	19	1.4	2.5	-0.6
Point Arguello Light	0	Stable	Stable	Stable	0.8739	22	9	7	22.7	6.7	19.1
Point Arguello Light	10.2	Stable	Stable	Stable	0.8979	76	9	8	24.3	8.8	15.3
Point Arguello Light	19	Stable	Stable	Stable	0.9132	183	12	9	20.9	9.5	9.8
Point Arguello Light	28.3	Stable	Stable	Stable	0.9289	671	12	11	10.7	9.2	7.3
Prudhoe Bay (1995)	9.32	Stable	Meso	Stable	0.9048	55	10	3	19.0	6.4	7.4
Sockeye	0	Stable	Meso	Stable	0.8965	45	13	8	29.1	1.7	13.7
Sockeye	12.5	Stable	Meso	Stable	0.9166	163	15	9	17.3	16.9	9.0
Sockeye	22.1	Stable	Stable	Stable	0.9264	628	15	11	12.3	5.7	4.9
Sockeye Comingled	0	Stable	Meso	Stable	0.9350	550	21	13	2.0	-3.9	3.5
Sockeye Sour	0	Stable	Meso	Stable	0.9409	821	20	13	0.5	-1.7	1.7
Sockeye Sweet	26.9	Stable	Stable	Stable	0.9229	321	14	6	11.0	9.1	4.6
Takula	0	Stable	Stable	Stable	0.8637	110	8	2	17.8	8.8	11.9

Takula	11	Stable	Stable	Stable	0.8860	844	10	4	10.5	6.8	7.2
Takula	18	Stable	Stable	Stable	0.8961	3,148	11	4	5.1	8.0	2.3
Viosca Knoll 826	24	Stable	Stable	Stable	0.9067	325	8	3	9.3	11.6	6.5
Viosca Knoll 990	35.2	Stable	Stable	Stable	0.8905	91	8	2	9.5	8.7	9.2
Carpenteria	10.3	Meso	Meso	Meso	0.9299	755	19	11	-1.0	-2.6	3.0
Carpenteria	14.9	Meso	Meso	Meso	0.9482	3,426	22	11	-4.8	-2.8	-3.1
Dos Cuadras	11.2	Meso	Meso	Meso	0.9270	187	20	7	-9.1	1.9	5.0
Dos Cuadras	20.3	Meso	Meso	Entrain	0.9359	741	19	9	-4.2	1.3	1.5
Gail E019	24.4	Meso	Stable	Meso	0.9346	1,357	12	8	6.8	5.2	1.5
Garden Banks 387	23.3	Meso	Stable	Meso	0.9287	579	13	2	-9.3	8.1	-2.3
Genesis	23.1	Meso	Meso	Meso	0.9364	543	21	3	-5.2	0.6	-1.3
Green Canyon 184	38.2	Meso	Stable	Meso	0.9043	117	11	1	1.5	8.6	1.8
Green Canyon 200	30.7	Meso	Stable	Meso	0.9071	121	9	1	3.9	9.2	4.2
Green Canyon 65	7.7	Meso	Stable	Meso	0.9509	457	15	5	3.3	6.7	-0.9
Green Canyon 65	13.1	Meso	Stable	Meso	0.9559	800	15	4	0.0	6.1	-3.6
Green Canyon 65	22.9	Meso	Meso	Meso	0.9716	4,250	16	8	-5.6	1.8	-5.6
Gulfaks	29.8	Meso	Stable	Meso	0.9129	202	12	1	2.1	9.4	-0.2
Hibernia [2000]	22.8	Meso	Stable	Meso	0.8893	99	8	2	10.4	8.7	9.1
Hibernia [2000]	33.5	Meso	Stable	Meso	0.9075	773	11	4	9.4	9.6	3.8
Lucula	10.7	Meso	Stable	Stable	0.8821	5,214	8	4	-0.8	5.3	5.4
MARS—TLP	8.42	Meso	Stable	Meso	0.9122	93	11	6	-0.4	4.6	9.9
MARS—TLP	17.2	Meso	Stable	Meso	0.9331	404	13	7	-4.4	5.5	3.7
MARS—TLP	26.2	Meso	Stable	Stable	0.9520	2,237	13	10	-5.2	7.1	-1.3
Mississippi Canyon 72	18	Meso	Stable	Stable	0.8966	76	9	2	-0.8	8.8	7.4
Mississippi Canyon 807	0	Meso	Stable	Stable	0.8894	41	12	6	3.1	6.2	13.8
Mississippi Canyon 807	8.67	Meso	Stable	Stable	0.9187	127	13	7	-0.8	6.7	8.1
Mississippi Canyon Block 807	11.8	Meso	Stable	Stable	0.9202	165	8	6	1.5	9.4	11.6
Mississippi Canyon Block 807	22.4	Meso	Stable	Meso	0.9562	396	10	7	-0.6	6.5	3.0
Mississippi Canyon Block 807	35.9	Meso	Stable	Meso	0.9693	1472	11	10	-2.8	8.9	0.3
Mississippi Canyon Block 807	15.2	Meso	Stable	Meso	0.9426	551	10	6	-0.3	6.0	2.8
Morpeth EW921	24.0	Meso	Meso	Meso	0.9619	3,697	13	8	-3.2	1.2	-3.9
Morpeth EW921	30.5	Meso	Meso	Meso	0.9418	900	12	7	0.7	3.4	0.8
North Slope (Middle Pipeline)	31.1	Meso	Meso	Meso	0.9402	748	12	7	1.2	3.6	1.9
North Slope (Northern Pipeline)	29.6	Meso	Meso	Meso	0.9431	961	13	7	2.5	5.2	0.2
North Slope (Southern Pipeline)	0	Meso	Stable	Stable	0.8837	22	10	4	4.5	4.6	13.1
Prudhoe Bay (1995)	27.3	Meso	Stable	Meso	0.9352	623	15	5	3.6	6.3	0.5
Prudhoe Bay (1995)	42.0	Meso	Stable	Meso	0.9201	52	10	2	8.4	6.8	3.2
Sakhalin	0	Meso	Meso	Meso	0.9202	304	29	13	-7.7	1.9	6.5
Santa Clara	11.4	Meso	Meso	Meso	0.9479	1,859	27	13	5.3	-2.4	-1.4
Santa Clara	21.6	Meso	Meso	Meso	0.9672	22,760	23	17	-8.5	-7.2	-8.7
Sockeye (2000)	0	Meso	Meso	Meso	0.9354	761	18	15	2.9	3.3	3.3

(continued)

TABLE 8.9 (Cont'd)

Oil	Oil evaporation %	Actual stability	Model I prediction	Model II prediction	Density (at 15°C)	Viscosity mPa.s	Resins %	Asphaltenes %	Actual stability	Model I	Model II
Sockeye (2000)	7	Meso	Meso	Meso	0.9537	2,720	19	16	-1.3	1.2	-1.9
Sockeye Sweet	17.5	Meso	Stable	Stable	0.9089	103	13	5	4.3	8.1	8.3
Waxy Light Heavy Blend	12	Meso	Meso	Meso	0.9582	2,002	24	6	-9.9	-1.5	-4.4
Waxy Light Heavy Blend	19.6	Meso	Meso	Entrain	0.9749	17,280	28	6	-10.2	-5.8	-10.7
West Texas (2000)	21	Meso	Stable	Stable	0.8827	38	8	1	6.3	7.5	10.2
West Texas (2000)	31	Meso	Stable	Meso	0.8973	112	10	2	7.9	6.8	6.5
Belridge Heavy	0	Entrn	Entrain	Entrain	0.9746	12,610	30	3	-6.7	-4.0	-33.8
Beta	0	Entrn	Entrain	Entrain	0.9738	13,380	31	7		-2.5	-30.5
Bunker C (1987)	0	Entrn	Entrain	Entrain	0.9830	45,030	15	7	-7.9	-4.4	-34.5
Bunker C (Anchorage)	0	Entrn	Entrain	Entrain	0.9891	8,706	17	11	-10.2	-2.5	-28.1
California API 11.0	0	Entrn	Entrain	Entrain	0.9882	34,000		16			
California API 15.0	0	Entrn	Entrain	Entrain	0.9770	6,400	23	22	-0.3	-1.9	-26.6
Cold Lake Bitumen	0	Entrn	Entrain	Entrain	1.0166	825,000	13	17	-16.0	-16.2	-35.6
Ellen A038	0	Entrn	Entrain	Entrain	0.9587	3,098	24	14	-11.7	-6.5	-25.9
Ellen A040	0	Entrn	Entrain	Entrain	0.9790	19,680	25	14	-19.5	-12.0	-32.1
Gail E010	0	Entrn	Entrain	Entrain	0.9709	11,560	25	23	-8.1	-3.9	-30.1
Heavy Fuel Oil 6303	0	Entrn	Entrain	Entrain	0.9888	22,800	16	13	-4.6	-0.9	-31.0
Heavy Fuel Oil 6303	2.5	Entrn	Entrain	Entrain	0.9988	149,000	17	18	-14.2	-13.5	-35.4
High Viscosity Fuel Oil	0	Entrn	Entrain	Entrain	1.0140	13,460	13	26	-7.3	-6.6	-29.1
IFO—180	0	Entrn	Meso	Entrain	0.9670	2,324	11	10	-1.1	8.4	-23.2
IFO—180	7.77	Entrn	Entrain	Entrain	0.9840	27,280	17	15	-6.8	-2.8	-31.0
IFO—300	0	Entrn	Entrain	Entrain	0.9859	14,470	12	10	-6.7	4.2	-28.7
Irene [2009]	0	Entrn	Entrain	Entrain	0.9591	8,514	33	19	-5.1	-3.8	-26.7
Irene Comingled	0	Entrn	Entrain	Entrain	0.9787	57,347	23	16	-9.6	-12.4	-35.0
Lago Treco	16	Entrn	Entrain	Entrain	0.9661	16,160	15	15	-5.1	1.0	-28.9
Lucula	26.9	Entrn	Entrain	Entrain	0.9050	32,590	12	4	-2.2	1.2	-26.9
Malongo	15.5	Entrn	Entrain	Entrain	0.9026	10,950	13	3	3.2	4.3	-25.2
Malongo	21.7	Entrn	Entrain	Entrain	0.9141	25,600	15	4	0.8	0.8	
Maya	15	Entrn	Entrain	Entrain	0.9657	8,670	10	17	-3.4	-3.7	-28.0
Oriente	21	Entrn	Meso	Entrain	0.9426	6,124	11	15	0.4	3.9	-23.2
Petronius Block VK786A	0	Entrn	Meso	Meso	0.8713	28	6	2	9.1	5.8	-2.7
Petronius Block VK786A	8.0	Entrn	Meso	Meso	0.8858	55	6	2	16.1	6.7	-5.5
Petronius Block VK786A	15.8	Entrn	Entrain	Entrain	0.8978	146	7	2	13.5	8.6	-10.3
Petronius Block VK786A	23.6	Entrn	Entrain	Entrain	0.9096	327	8	3	13.6	12.3	-12.7
Platform Gail (Sockeye)	20.6	Entrn	Entrain	Entrain	0.9810	161,500	25	19	-11.4	-19.3	-37.3
Platform Irene	0	Entrn	Entrain	Entrain	0.9907	76,000	22	22	-8.0	-11.8	-34.1
Point Arguello Comingled	15.2	Entrn	Entrain	Entrain	0.9688	41,860	21	19	-9.3	-7.9	-32.4
Point Arguello Heavy	8.88	Entrn	Entrain	Entrain	0.9706	59,390	18	20	-9.8	-8.1	-32.9

Port Hueneme	0	Enm	Entrain	0.9662	4,131	20	12	-9.7	-1.7	-26.1
Port Hueneme	3.14	Enm	Entrain	0.9745	7,833	21	14	-7.7	-4.6	-27.8
Port Hueneme	6.37	Enm	Entrain	0.9787	20,990	28	13	-9.6	-7.1	-31.4
Sockeye (2000)	13	Enm	Entrain	0.9692	15,100	19	18	-6.6	-2.4	
Sockeye (2000)	20	Enm	Entrain	0.9839	274,000	20	20	-14.4	-21.5	-39.1
Udang	0	Enm	Entrain	0.9701	10,700	24	3	-8.8	-5.0	-34.3
Zaire	0	Enm	Entrain	0.8720	15,100	9	5	-4.5	1.0	-16.2
Zaire	6	Enm	Entrain	0.8872	52,800	9	5	-7.8	-4.7	-22.3
Zaire	14	Enm	Entrain	0.9015	94,560	10	5	-8.5	-8.7	-27.8

Anadarko	0	DNF		0.8507	11	3	0	little		
Atwater Valley Block 37	0	DNF		0.9148	13	4.6	0.0	little		
Atwater Valley Block 37	22.1	DNF		0.937	40	5.2	0.0	little		
Barrow Island	0	DNF		0.8410	2	4	0	little		
Brent	0	DNF		0.8351	6	4	1	little		
Cook Inlet – Granite Point	0	DNF		0.8293	4	5	1	little		
Cusiana	0	DNF		0.8328	7	3	1	little		
Cusiana	12.6	DNF		0.8598	10	5	1	little		
Cusiana	24.0	DNF		0.8773	31	5	2	little		
Diesel (Anchorage)	0	DNF		0.8300	2	1	0	little		
Diesel (Anchorage)	37.4	DNF		0.8515	5	1	0	little		
Diesel (Mobile Burn #3)	0	DNF		0.8389	5	2	0	little		
Diesel (Mobile Burn #3)	8.21	DNF		0.8427	5	2	0	little		
Diesel (Mobile Burn #3)	16.3	DNF		0.8447	6	2	0	little		
Eugene Island Block 32	0	DNF		0.8399	10	2	1	little		
Eugene Island Block 32	6	DNF		0.8418	9	2	1	little		
Eugene Island Block 32	13	DNF		0.8453	16	2	1	little		
Eugene Island Block 32	20	DNF		0.8481	21	3	1	little		
Eugene Island Block 43	0	DNF		0.8404	13	3	1	little		
Eugene Island Block 43	7	DNF		0.8518	21	4	1	little		
Eugene Island Block 43	16	DNF		0.8594	36	7	1	little		
Eugene Island Block 43	24	DNF		0.9665	65	5	1	little		
Everdell	0	DNF		0.8064	4	2	0	little		
Everdell	15	DNF		0.8355	9	2	0	little		
Everdell	29	DNF		0.8520	25	2	0	little		
Everdell	42	DNF		0.8670	113	2	0	little		
Gail E019	0	DNF		0.8996	52	11.4	5.8	little		
Garden Banks 387	0	DNF		0.8782	29	10	1	little		
Garden Banks 387	7.07	DNF		0.8979	64	11	1	little		
Garden Banks 387	15.1	DNF		0.9144	181	11	1	little		

(continued)

TABLE 8.9 (Cont'd)

Oil	Oil evaporation %	Actual stability	Model I prediction	Model II prediction	Density (at 15°C)	Viscosity mPa.s	Resins %	Asphaltenes %	Actual stability	Model I	Model II
Garden Banks 426	0	DNF			0.8285	6	5	1	little		
Garden Banks 426	12.3	DNF			0.8561	13	8	1	little		
Garden Banks 426	24.8	DNF			0.8779	34	8	2	little		
Genesis	0	DNF			0.8841	26	10	2	little		
Genesis	8.11	DNF			0.9074	66	9	2	little		
Genesis	15.1	DNF			0.9223	157	11	2	little		
Green Canyon 109	0	DNF			0.8921	39	9	1	little		
Green Canyon 109	8	DNF			0.9101	98	10	1	little		
Green Canyon 109	14	DNF			0.9218	225	11	1	little		
Green Canyon 184	0	DNF			0.8314	5	6	1	little		
Green Canyon 184	12.1	DNF			0.8575	11	8	1	little		
Green Canyon 184	26	DNF			0.8824	31	8	1	little		
Green Canyon 200	0	DNF			0.8501	11	7	1	little		
Green Canyon 200	12.0	DNF			0.8758	22	8	1	little		
Green Canyon 200	19.1	DNF			0.8876	39	8	1	little		
Gulfaks	0	DNF			0.8701	13	5	1	little		
Gulfaks	10.2	DNF			0.8891	31	6	1	little		
Gulfaks	19.4	DNF			0.9017	91	11	1	little		
Heidrun	0	DNF			0.8835	18	9	1	little		
Heidrun	7.7	DNF			0.9013	38	9	1	little		
Heidrun	14.9	DNF			0.9128	76	9	1	little		
Heidrun	22.6	DNF			0.9222	152	10	1	little		
Jet A1	0	DNF			0.8159	2	0	0	little		
Jet A1	12	DNF			0.8193	2	0	0	little		
Jet A1	23.2	DNF			0.8216	2	1	0	little		
Jet A1	37.1	DNF			0.8244	2	0	0	little		
Jet Fuel (Anchorage)	0	DNF			0.8111	2	0	0	little		
Jet Fuel (Anchorage)	52.7	DNF			0.8354	3	0	0	little		
Lago	0	DNF			0.8907	153	11	3	little		
Main Pass Block 306	0	DNF			0.8606	9	5	1	little		
Main Pass Block 306	12	DNF			0.8849	19	8	1	little		
Main Pass Block 306	24	DNF			0.9034	54	10	1	little		
Main Pass Block 306	37	DNF			0.9203	219	11	1	little		
Main Pass Block 37	0	DNF			0.8311	7	5	1	little		
Main Pass Block 37	16	DNF			0.8543	16	5	1	little		
Main Pass Block 37	30	DNF			0.8689	36	6	1	little		
Maui	0	DNF			0.8081	15	2	2	little		
Maui	14.2	DNF			0.8340	212	3	2	little		

Mississippi Canyon 194	0	DNF	0.8483	7	4	0	little
Mississippi Canyon 194	10	DNF	0.8655	11	6	0	little
Mississippi Canyon 194	21	DNF	0.8762	21	6	0	little
Mississippi Canyon 194	35	DNF	0.8874	51	7	0	little
Mississippi Canyon 72	0	DNF	0.8649	16	7	2	little
Mississippi Canyon 72	9.41	DNF	0.8827	34	8	2	little
Neptune Spar (Viosca Knoll 826)	0	DNF	0.8687	17	6	1	little
Neptune Spar (Viosca Knoll 826)	7.92	DNF	0.8826	42	6	2	little
Pitas Point	0	DNF	0.8341	2	3	0	little
Pitas Point	23.6	DNF	0.8537	2	0	0	little
Sahara Blend	0	DNF	0.8078	4	3	1	little
Sahara Blend	13.7	DNF	0.8336	7	3	1	little
Sakhalin	0	DNF	0.8632	4	6	1	little
Scotian Light	0	DNF	0.7655	1	1	0	little
Scotian Light	25	DNF	0.7949	2	1	0	little
Scotian Light	44	DNF	0.8139	2	1	0	little
Scotian Light	64	DNF	0.8356	5	1	0	little
Ship Shoal Block 239	0	DNF	0.8972	34	7	2	little
Ship Shoal Block 239	43	DNF	0.8977	74	8	2	little
Ship Shoal Block 269	0	DNF	0.8309	5	6	0	little
Ship Shoal Block 269	13	DNF	0.8517	7	5	0	little
Ship Shoal Block 269	26	DNF	0.8657	18	6	1	little
Ship Shoal Block 269	39	DNF	0.8796	44	6	1	little
South Louisiana	0	DNF	0.8518	8	4	1	little
South Louisiana	10.3	DNF	0.8696	16	5	0	little
South Louisiana	20.1	DNF	0.8831	36	6	0	little
South Louisiana	30.8	DNF	0.8953	80	7	0	little
South Louisiana (2001)	0	DNF	0.8562	10	6	1	little
South Louisiana (2001)	11	DNF	0.8770	24	6	1	little
South Louisiana (2001)	20	DNF	0.8906	49	8	1	little
South Louisiana (2001)	28	DNF	0.9018	141	8	2	little
South Pass Block 60	0	DNF	0.8453	9	8	1	little
South Pass Block 60	17	DNF	0.8709	22	7	1	little
South Pass Block 60	25	DNF	0.8809	41	8	1	little
South Pass Block 93	0	DNF	0.8574	19	4	3	little
South Pass Block 93	11	DNF	0.8637	23	4	2	little
South Pass Block 93	21	DNF	0.8698	32	4	2	little
South Timbalier Block 130	0	DNF	0.8487	7	5	0	little
South Timbalier Block 130	11	DNF	0.8632	10	5	0	little
South Timbalier Block 130	22	DNF	0.8748	19	6	0	little

(continued)

TABLE 8.9 (Cont'd)

Oil	Oil evaporation %	Actual stability	Model I prediction	Density (at 15°C)	Viscosity mPa.s	Resins %	Asphaltenes %	Actual stability	Model I	Model II
South Timbalier Block 130	35	DNF		0.8877	48	8	1	little		
Tapis	0	DNF		0.8020	8	2	2	16		
Thevenard Island	0	DNF		0.7855	1	2	0	little		
Thevenard Island	22.7	DNF		0.8301	3	2	0	little		
Thevenard Island	43.9	DNF		0.8352	5	2	0	little		
Thevenard Island	59	DNF		0.8498	9	3	0	little		
Troll	0	DNF		0.8852	24	6	1	little		
Troll	6.3	DNF		0.8972	44	6	1	little		
Troll	13.1	DNF		0.9060	80	7	1	little		
Troll	19.4	DNF		0.9134	175	8	1	little		
Viosca Knoll 826	0	DNF		0.8668	16	6	2	2		
Viosca Knoll 826	8.14	DNF		0.8842	43	7	3	little		
Viosca Knoll 826	16.9	DNF		0.8970	132	6	3	little		
Viosca Knoll 990	0	DNF		0.8337	7	4	1	0		
Viosca Knoll 990	12.3	DNF		0.8585	12	6	1	little		
Viosca Knoll 990	24.4	DNF		0.8752	31	6	1	little		
West Delta Block 97	0	DNF		0.7783	1	1	0	little		
West Delta Block 97	23	DNF		0.8020	1	1	0	little		
West Delta Block 97	48	DNF		0.8191	3	3	0	little		
West Delta Block 97	74	DNF		0.8388	7	2	0	little		
West Texas (2000)	0	DNF		0.8474	9	6	1	little		
West Texas (2000)	10	DNF		0.8665	16	7	1	little		
Group 2 – Highly viscous oils that do not form water-in-oil types										
Ellen A038	15.9	DNF		0.9987	1.09E+06	40.8	21.6	little		
Ellen A040	14.6	DNF		1.0064	1.74E+06	35.7	17.6	little		
Gail E010	16.9	DNF		1.0086	3.25E+06	33.9	24.1	little		
Heritage HE 05	0	DNF		0.9928	3.59E+05	33.5	10.2	little		
Heritage HE 05	16.3	DNF		1.0178	3.80E+07	50.8	14.4	little		
Heritage HE 26	0	DNF		0.9865	1.86E+05	28.5	10.7	little		
Heritage HE 26	14.5	DNF		1.0129	2.74E+07	31.0	10.8	little		
Hondo	32.3	DNF		0.9881	4.50E+05	32	13	5		
IFO—300	5.33	DNF		0.9996	2.20E+05	30	17	11		
Irene [2009]	17.4	DNF		1.0073	8.34E+06	37.7	26.4	little		
Irene Comingled	20.3	DNF		1.0107	2.21E+07	44.3	37.5	little		
Maui	29.8	DNF		0.8421	1.08E+03	7	2	little		
Maui	43.5	DNF		0.8640	2.00E+03	4	3	little		

Maya	22	DNF	0.9868	4.05E+05	11	22	2
Orinoco	0	DNF	1.0166	1.02E+07	17	21	8
Point Arguello Comingled	22.1	DNF	0.9853	2.27E+06	21	22	2
Point Arguello Heavy	17.8	DNF	0.9914	4.95E+06	21	22	little
Sockeye Sour	18.5	DNF	0.9838	4.75E+05	22	24	10
Sumatran Heavy	5.26	DNF	0.9374	1.29E+04	16	8	2
Sumatran Light	0	DNF	0.8600	4.15E+04	6	8	13
Taching	0	DNF	0.8700	5.14E+06	9	6	4
Tapis	28.6	DNF	0.8396	8.00E+02	3	2	9
Tapis	43.4	DNF	0.8552	1.44E+03	4	3	8
Wabiska Bitumen	0	DNF	0.9572	1.28E+05	26.4	8.1	little
Wabiska Bitumen	10.7	DNF	1.0069	2.79E+05	38.3	8.4	little
Zaire	23	DNF	0.9020	5.33E+05	16	5	5

DNF, did not form.

TABLE 8.10 Comparison of Models I and II

Point	Model I	Model II	
R^2 —correlation coefficient	0.46	0.69	
Number of parameters	14	15	Total numbers of
Number of Gaussian sets	4	2	data points
Errors on stable emulsions	40%	5%	42
Errors on mesostable emulsions	63%	26%	43
Errors on entrained type	10%	5%	41
Errors on all types	35%	12%	126
Advantages	Low coefficients	Accurate, simpler math	
Disadvantages	Lower accuracy	High coefficients	

model has high coefficients, which may cause problems in certain circumstances. Table 8.10 shows the values of the input model set and compares the stabilities and the predicted emulsion type. This shows the details of prediction by Models I and II.

8.5.3 Development of an Emulsion Kinetics Estimator

The kinetics of emulsion formation has been studied, and data are available to compute the time to formation [74, 75]. This study has shown the time to formation for stable emulsions is particularly rapid and that of entrainment is also rapid—both in a matter of minutes. The past study yielded data in terms of relative formation time and energy (rpm) of the mixing apparatus. A study in a large test tank has also yielded data on the formation time of the various water-in-oil states [74,75]. The data of the relative formation times and the wave height are available. The average data over 25 runs were used to calculate the formation time, which was taken as that time at which 75% of the maximum stability measured occurs. The conditions under which these tests took place and the measurements taken are described in the literature [74,75]. The wave height for each experiment was measured and used to indicate relative sea energy, taken for a fully developed sea. The laboratory data were converted from rotational energy to wave height by equating formation times and then using this multiplier to calculate the equivalent wave height. Formulae were fitted to each of the three categories, and the common formula among all three relevant classes was found to be $1/x^{1.5}$ (12), as shown in Table 8.11. The regression coefficients for this formula are also given. Application of the equations in Table 8.11 will then provide a user with a time to formation of a particular water-in-oil state, given the wave height.

8.5.4 Model Certainty

It is noted that there is little error for more stable types but more error for the unstable types or those that do not form any of the other three types [3]. This was noted in past

TABLE 8.11 Wave height prediction

Resulting equation			
Predictor	Equation	$y = a + b/x^{1.5}$	(8.16)
	a	b	R^2
Stable	27.1	7520	0.51
Mesostable	47	49,100	0.95
Entrained	30.8	18,300	0.94

x is wave height in cm; y = time to formation in minutes

modeling as well [67,69]. It is suspected that the reasons for this are as follows:

- Unstable types or those oils that do not form any of the other three types generally consist of three widely separate classes of oils or fuels, namely, very light oils such as the fuels that have little or no resins or asphaltenes, those very heavy oils that are so viscous that they will not take up water, and those oils that have the incorrect ratio or amounts of resins or asphaltenes. It is difficult to mathematically incorporate all three of these variances into one grouping.
- Some of the oils may be able to form different water-in-oil types, but emulsion inhibitors or asphaltene suspenders have been added to the products. These types of oils make prediction very difficult.
- There are many different asphaltenes some of which make much more stable emulsions than others. Recent work has shown that there are hundreds of asphaltene subcomponents varying very much in composition and molecular size [18]. Thus, the percent of asphaltenes (or resins) certainly does not tell the whole story about the emulsion stabilizers.

It is important to recognize that the properties and behaviors of the four water-in-oil types are very different from each other. Table 8.A3 shows the different average properties of



FIGURE 8.13 A photograph of an emulsion formed in the Deep Water Horizon spill (Photo from US Coast Guard website—<http://www.pbs.org/newshour/tag/gulf-coast-oil-spill/>).

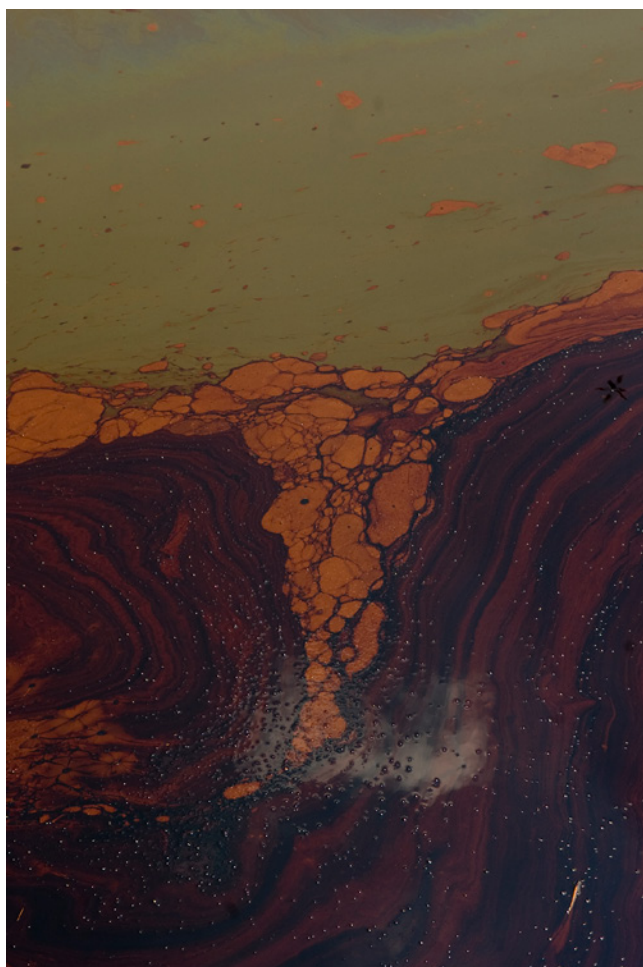


FIGURE 8.14 Another photograph of an emulsion formed during the Deep Water Horizon spill. Emulsions shown in Figures 8.13 and 8.14 were stable (Photo from US Coast Guard website—<http://www.pbs.org/newshour/tag/gulf-coast-oil-spill/>).

the four water-in-oil types. It should be noted that on the day of formation, only mesostable and stable emulsions may be somewhat similar; this similarity disappears after 1 week when the mesostable emulsions break down. The change in water content with time is portrayed in Figure 8.3a. As can be seen in this figure, the unstable type loses the most water in the first few days. The water content of the four types is very different at the start and especially after 1 week. The other significant point in these figures is that the change in water content of the entrained types is the slowest of all.

Another comparison of the viscosities of the four water-in-oil types is shown in Figure 8.3b and d. The rate of change in viscosity is quite different for the four types as seen in Figure 8.3b. The rise of viscosity for the mesostable types is more than expected and is due to the weathering of the oil, which proceeds more rapidly without water content. The apparent viscosity of the four water-in-oil types is shown in Figure 8.3b. As the viscosity axis is logarithmic, the differences are very significant among the four types. In summary, the four water-in-oil types differ by as much as orders of magnitude in viscosity and water content at 1 day, 1 week, and 1 year.

Figures 8.13 and 8.14 show typical emulsions at sea as a result of the 2010 Deep Water Horizon Spill. Emulsion formation is important to actions to deal with spills. Therefore, it is important to correctly predict their formation.

8.6 CONCLUSIONS

Water-in-oil emulsions are formed as a result of asphaltene and resin surfactant characteristics in oil of moderate viscosity (50–2000 mPa·s). Four types of water-in-oil products are formed: stable and mesostable emulsions, entrained water-in-oil type, and unstable (or those that do not form any of the other three types) types. Each of these types has unique characteristics and is thought to be nonconvertible to other types once formed.

The knowledge that water-in-oil types exist and that a new scheme to classify their stability, herein called stability C or simply stability, enables the development of new and much more accurate emulsion formation models. The density, viscosity, and asphaltene and resin contents are used to develop a regression equation to stability C, which in turn predicts either an unstable or an entrained water-in-oil state or a mesostable or a stable emulsion. The new model can provide accurate prediction of class about 90% of the time. The major inaccuracy lies with the unstable types and this because of the fact that there are three distinct types of oils or fuels in this class, each very different, and because of the possible presence of emulsion breakers or asphaltene suspenders in the oils.

TABLE 8.A1 Summary of Oil and Emulsion properties

Oil	Oil evaporation	Stability	H ₂ O content	Density	Viscosity	Saturates	Aromatics	Resins	Asphaltenes	Waxes
	%	visual	(%w/w)	at 15°C	mPa.s	%	%	%	%	%
Alaska North Slope [2002]	0	Unstable	<0.1	0.8663	12	75	15	6	4	3
Anadarko	0	Unstable	0.20	0.8507	11	89	8	3	0	
Arabian Light	0	Stable	<0.1	0.8658	14	51	39	6	3	5
Arabian Light [2002]	0	Meso	<0.1	0.8641	13	76	15	6	4	3
Arabian Medium	0	Stable	<0.1	0.8783	29	54	32	7	6	6
ASMB (std.#5)	0	Meso	<0.1	0.8404	6	77	17	4	2	4
Aviation Gasoline 100LL	0	Unstable	<0.1	0.7143	1					0
Barrow Island	0	Unstable	<0.1	0.8410	2	64	32	4	0	0
Belridge Heavy	0	Entrained	2.4	0.9746	12,610	28	39	30	3	1
Beta	0	Entrained	1.7	0.9738	13,380	21	39	31	7	3
Brent	0	Unstable	0.2	0.8351	6	72	23	4	1	
Bunker C (1987)	0	Entrained	0.1	0.9830	45,030	24	55	15	7	12
Bunker C (Anchorage)	0	Entrained	0.2	0.9891	8,706	25	47	17	11	2
California API 11.0	0	Entrained	<0.1	0.9882	34,000				16	1
California API 15.0	0	Entrained	<0.1	0.9770	6,400	19	35	23	22	1
Canolimon	0	Stable	0.4	0.8817	46	60	24	8	8	
Canolimon	6.97	Stable	<0.1	0.8961	103	57	25	8	9	
Canolimon	13.5	Stable	<0.1	0.9077	254	56	25	8	10	
Canolimon	21.0	Stable	<0.1	0.9200	1,350	51	28	10	11	
Carpenteria	0	Unstable	<0.1	0.9155	164	44	30	17	9	7
Carpenteria	10.3	Meso	<0.1	0.9299	755	40	30	19	11	5
Carpenteria	14.9	Meso	<0.1	0.9482	3,426	31	36	22	11	4
Coal Oil Point Seep Sample	0	with water	33.3	0.9872	165,750	21	35	24	21	1
Cold Lake Bitumen	0	Entrained	<0.1	1.0166	825,000	46	24	13	17	
Cook Inlet—Granite Point	0	Unstable	<0.1	0.8293	4	72	22	5	1	
Cook Inlet—Granite Point	45.3	Meso	<0.1	0.9028	75	62	28	7	3	
Cook Inlet—Swanson River	0	Meso	0.2	0.8420	6	65	25	6	5	
Cook Inlet—Swanson River	39.7	Stable	<0.1	0.9143	152	56	29	7	7	
Cook Inlet—Swanson River										
Cook Inlet—Trading Bay	0	Unstable	0.1	0.8602	10	62	26	7	5	
Cook Inlet—Trading Bay	33.3	Meso	<0.1	0.9242	278	51	32	9	8	
Crude Castor oil										
Cusiana	0	Unstable	<0.1	0.8328	7	76	20	3	1	
Cusiana	12.6	Unstable	<0.1	0.8598	10	71	23	5	1	
Cusiana	24.0	Unstable	<0.1	0.8773	31	70	23	5	2	
Cusiana	38.3	Meso	<0.1	0.8965	326	71	22	5	2	
Diesel (Anchorage)	0	Unstable	<0.1	0.8300	2	74	24	1	0	
Diesel (Anchorage)	37.4	Unstable	<0.1	0.8515	5	75	23	1	0	
Diesel (Mobile Burn #3)	0	Unstable	<0.1	0.8389	5	76	22	2	0	10
Diesel (Mobile Burn #3)	8.21	Unstable	<0.1	0.8427	5	78	20	2	0	11
Diesel (Mobile Burn #3)	16.3	Unstable	<0.1	0.8447	6	78	20	2	0	11
Dos Cuadras	0	Unstable	<0.1	0.9000	51	48	30	17	6	6
Dos Cuadras	11.2	Meso	<0.1	0.9270	187	42	31	20	7	4

Oil	Oil evaporation	Emulsion properties											
		On day of formation						One week after formation					
		Complex		Elasticity	Viscosity	tan	Water	Complex		Elasticity	Viscosity	tan	Water
		Viscosity	Modulus	Modulus	Modulus	delta	Content	Viscosity	Modulus	Modulus	Modulus	delta	Content
		(mPa.s)	(mPa)	(mPa)	(mPa)	(V/E)	(%w/w)	(mPa.s)	(mPa)	(mPa)	(mPa)	(V/E)	(%w/w)
	%												
Arabian Light	0	2.3E+04	4.70E+05	4.70E+05	5.00E+04	0.11	87.4	2.3E+04	4.6E+05	4.6E+05	4.0E+04	0.09	86.9
Arabian Light [2002]	0		9.27E+04	8.62E+04	3.42E+04	0.39	91.1						
Arabian Medium	0	4.1E+04	5.48E+05	5.44E+05	5.10E+04	0.09	84.7	5.5E+04	6.8E+05	6.7E+05	7.2E+04	0.11	84.4
ASMB (std.#5)	0		1.33E+05	1.27E+05	4.01E+04	0.32	89.6						
Belridge Heavy	0	4.2E+04	2.96E+05	1.88E+05	2.29E+05	1.2	57.9	5.4E+04	1.6E+05	8.1E+04	1.4E+05	1.68	44.4
Bunker C (1987)	0	1.1E+05	8.11E+05	4.80E+05	6.60E+05	1.3	26.4	1.4E+05	8.0E+05	5.7E+05	5.6E+05	1.01	24.0
Bunker C (Anchorage)	0	2.8E+04	1.26E+05	3.67E+04	1.20E+05	3.3	34.7	1.5E+05	1.3E+05	1.5E+04	1.2E+05	8.00	31.0
California API 15.0	0		8.31E+05	4.29E+05	7.10E+05	1.7	39.0						
Canolimon	0		4.2E+06	4.1E+06	3.2E+05	0.08	91.8		4.3E+06	4.2E+06	3.5E+05	0.08	88.3
Canolimon	6.97		1.5E+06	1.5E+06	1.9E+05	0.13	86.5		1.3E+06	1.3E+06	1.8E+05	0.14	86.5
Canolimon	13.5		1.1E+06	1.1E+06	2.1E+05	0.20	83.3		1.5E+06	1.5E+06	2.9E+05	0.20	83.8
Canolimon	21.0		1.6E+06	1.6E+06	5.1E+05	0.33	75.1		1.3E+06	1.2E+06	4.8E+05	0.38	74.0
Carpenteria	10.31	2.1E+04	7.30E+04	4.70E+04	5.60E+04	1.2	71.8	2.3E+04	3.6E+04	3.2E+03	3.6E+04	11.25	28.2
Carpenteria	14.87	2.9E+04	1.30E+05	8.20E+04	9.90E+04	1.2	54.3	2.1E+04	2.9E+05	2.6E+05	1.5E+05	0.57	30.9
Coal Oil Point Seep Sample	0	2.8E+05	1.18E+06	5.31E+05	1.05E+06	2.0	32.2	4.0E+05	1.5E+06	6.7E+05	1.4E+06	2.01	39.2
Cold Lake Bitumen	0		2.82E+06	8.01E+05	2.71E+06	3.4	17.1		3.0E+06	8.0E+05	2.9E+06	3.58	14.8
Cook Inlet—Granite Point	45.32	1.6E+04	3.65E+05	3.61E+05	1.04E+05	0.29	83.1	8.5E+03	2.7E+05	2.6E+05	7.5E+04	0.29	57.6
Cook Inlet—Swanson River	0	2.9E+03	1.03E+04	6.91E+03	7.62E+03	1.10	76.0	1.9E+03	2.7E+04	2.2E+04	1.6E+04	0.76	57.5
Cook Inlet—Swanson River	39.69	2.9E+04	6.19E+05	5.97E+05	1.64E+05	0.28	81.5	1.8E+05	1.1E+06	1.1E+06	3.4E+05	0.34	80.8
Cook Inlet—Trading Bay	33.3	2.4E+04	3.71E+05	3.61E+05	1.20E+05	0.33	76.2	4.3E+04	6.7E+05	6.5E+05	1.9E+05	0.29	61.4
Cusiana	38.3		4.6E+05	4.4E+05	1.5E+05	0.35	71.5		2.2E+05	2.0E+05	8.8E+04	0.44	65.3
Dos Cuadras	11.17	8.0E+02	3.45E+03	1.08E+03	3.29E+03	3.0	47.6	5.3E+02	4.5E+03	7.4E+02	4.3E+03	5.82	29.5
Dos Cuadras	20.3	9.8E+03	3.28E+04	2.05E+04	2.56E+04	1.3	68.6	1.9E+03	1.3E+04	3.1E+03	1.3E+04	4.16	28.7
Fuel Oil #5 (2000)	0		1.85E+06	1.79E+06	4.63E+05	0.27	76.3		2.1E+06	2.0E+06	5.6E+05	0.28	74.9
Fuel Oil #5 (2000)	7.25		2.67E+06	2.51E+06	9.04E+05	0.36	77.4		3.3E+06	3.0E+06	1.2E+06	0.41	74.6
Garden Banks 387	23.3	6.8E+03	8.15E+03	3.98E+03	7.11E+03	1.80	36.5						
Garden Banks 426	37.72	9.2E+03	8.00E+04	6.47E+04	3.43E+04	0.53	64.7						
Genesis	23.06	1.1E+04	2.65E+04	8.14E+03	2.53E+04	3.10	61.5						
Green Canyon 184	38.21	8.3E+03	2.18E+04	1.30E+04	1.73E+04	1.34	69.5						
Green Canyon 200	30.7		3.9E+04	2.6E+04	2.4E+05	1.14	78.2		2.1E+04	1.4E+04	1.6E+04	1.38	71.4
Green Canyon 65	7.7		1.38E+05	8.02E+04	1.12E+05	1.40	78.3						
Green Canyon 65	13.13		1.14E+05	5.67E+04	9.89E+04	1.75	73.5						
Green Canyon 65	22.91		1.56E+05	6.99E+04	1.40E+05	2.00	57.2						
Gulfaks	29.8		4.1E+04	2.8E+04	3.0E+04	1.09	75.7		3.5E+04	2.3E+04	2.7E+04	1.19	76.6
Heavy Fuel Oil 6303	0		9.06E+05	5.66E+05	7.07E+05	1.26	57.3		1.2E+06	7.0E+05	1.0E+06	1.43	57.7
Heavy Fuel Oil 6303	2.5		8.65E+05	2.16E+05	8.37E+05	3.99	21.1		1.0E+06	2.4E+05	1.0E+06	4.24	20.7
Hebron M-04	8.8		2.25E+05	1.52E+05	1.65E+05	1.13	75.0						
Hebron M-04	16.44		5.89E+05	4.76E+05	3.40E+05	0.89	71.6						
Hebron M-04	22.6		5.47E+05	3.49E+05	4.19E+05	1.26	56.5						
Hibernia [2000]	0		1.4E+05	1.3E+05	3.9E+04	0.30	74.7		1.2E+05	1.2E+05	3.6E+04	0.38	71.5
Hibernia [2000]	11.8		1.3E+05	1.3E+05	4.1E+04	0.34	72.0		1.4E+04	1.1E+04	7.5E+03	0.68	68.9
Hibernia [2000]	22.8		1.4E+05	1.3E+05	5.0E+04	0.39	72.4		9.1E+04	8.3E+04	3.9E+04	0.47	72.5
Hibernia [2000]	33.5		8.2E+05	7.8E+05	2.4E+05	0.32	74.7		4.5E+05	4.2E+05	1.7E+05	0.41	74.1

(continued)

TABLE 8.A1 (Cont'd)

Oil	Oil evaporation	Stability	H ₂ O content	Density	Viscosity	Saturates	Aromatics	Resins	Asphaltenes	Waxes
	%	visual	(%w/w)	at 15°C	mPa.s	%	%	%	%	%
Dos Cuadras	20.3	Meso	<0.1	0.9359	741	41	31	19	9	6
Eugene Island Block 32	0	Unstable	<0.1	0.8399	10	84	14	2	1	2
Eugene Island Block 32	6	Unstable	<0.1	0.8418	9	83	14	2	1	
Eugene Island Block 32	13	Unstable	<0.1	0.8453	16	82	15	2	1	
Eugene Island Block 32	20	Unstable	<0.1	0.8481	21	81	16	3	1	
Eugene Island Block 43	0	Unstable	0.20	0.8404	13	81	16	3	1	2
Eugene Island Block 43	7	Unstable	<0.1	0.8518	21	78	17	4	1	
Eugene Island Block 43	16	Unstable	<0.1	0.8594	36	77	15	7	1	
Eugene Island Block 43	24	Unstable	<0.1	0.9665	65	78	16	5	1	
Everdell	0	Unstable	<0.1	0.8064	4	79	19	2	0	
Everdell	15	Unstable	<0.1	0.8355	9	77	21	2	0	
Everdell	29	Unstable	<0.1	0.8520	25	77	21	2	0	
Everdell	42	Unstable	<0.1	0.8670	113	75	23	2	0	
Fuel Oil #5 (2000)	0	Stable	3.1	0.9883	1,410	44	40	8	8	2
Fuel Oil #5 (2000)	7.25	Stable	<0.1	1.0032	4,530	40	39	8	13	3
Garden Banks 387	0	Unstable	1.0	0.8782	29	53	36	10	1	
Garden Banks 387	7.07	Unstable	<0.1	0.8979	64	51	38	11	1	
Garden Banks 387	15.1	Unstable	<0.1	0.9144	181	51	37	11	1	
Garden Banks 387	23.3	Meso	<0.1	0.9287	579	46	40	13	2	
Garden Banks 426	0	Unstable	0.8	0.8285	6	70	24	5	1	
Garden Banks 426	12.3	Unstable	<0.1	0.8561	13	61	30	8	1	
Garden Banks 426	24.8	Unstable	<0.1	0.8779	34	62	28	8	2	
Garden Banks 426	37.7	Stable	<0.1	0.8993	136	56	32	10	3	
Genesis	0	Unstable	<0.1	0.8841	26	59	30	10	2	1
Genesis	8.11	Unstable	<0.1	0.9074	66	57	32	9	2	1
Genesis	15.1	Unstable	<0.1	0.9223	157	57	30	11	2	1
Genesis	23.1	Meso	<0.1	0.9364	543	48	28	21	3	1
Green Canyon 109	0	Unstable	0.4	0.8921	39	51	39	9	1	2
Green Canyon 109	8	Unstable	<0.1	0.9101	98	46	43	10	1	
Green Canyon 109	14	Unstable	<0.1	0.9218	225	44	44	11	1	
Green Canyon 109	22		<0.1	0.9341	690	42	43	14	1	
Green Canyon 184	0	Unstable	1.2	0.8314	5	69	24	6	1	
Green Canyon 184	12.1	Unstable	<0.1	0.8575	11	61	30	8	1	
Green Canyon 184	26	Unstable	<0.1	0.8824	31	58	33	8	1	
Green Canyon 184	38.2	Meso	<0.1	0.9043	117	54	34	11	1	
Green Canyon 200	0	Unstable	<0.1	0.8501	11	82	10	7	1	
Green Canyon 200	12.0	Unstable	<0.1	0.8758	22	81	11	8	1	
Green Canyon 200	19.1	Unstable	<0.1	0.8876	39	80	12	8	1	
Green Canyon 200	30.7	Meso	<0.1	0.9071	121	77	13	9	1	
Green Canyon 65	0		7.40	0.9365	177	38	40	14	8	2

Oil	Oil evaporation	Emulsion properties											
		On day of formation				One week after formation							
		Complex		Elasticity	Viscosity	tan	Water	Complex		Elasticity	Viscosity	tan	Water
		Viscosity	Modulus	Modulus	Modulus	delta	Content	Viscosity	Modulus	Modulus	Modulus	delta	Content
		(mPa.s)	(mPa)	(mPa)	(mPa)	(V/E)	(%w/w)	(mPa.s)	(mPa)	(mPa)	(mPa)	(V/E)	(%w/w)
	%												
High Viscosity Fuel Oil	0	7.4E+04	3.18E+05	1.50E+05	2.80E+05	1.87	47.6	8.3E+04	3.7E+05	1.8E+05	3.3E+05	1.84	49.8
Hondo	0	1.1E+05	9.39E+05	9.07E+05	2.41E+05	0.27	80.9	1.7E+05	8.8E+05	8.3E+05	2.9E+05	0.35	80.0
Hondo	16.67	1.9E+05	1.27E+06	1.16E+06	5.36E+05	0.46	66.2	2.8E+05	8.7E+05	6.2E+05	6.1E+05	0.99	64.2
IFO - 180	0	5.3E+04	2.41E+05	1.31E+05	2.03E+05	1.56	69.4	5.9E+04	2.4E+05	1.2E+05	2.1E+05	1.72	68.4
IFO - 180	7.77	1.5E+05	6.06E+05	4.11E+05	4.46E+05	1.09	58.4	1.5E+05	5.8E+05	3.78E+05	4.4E+05	1.16	58.8
IFO - 300	0	9.7E+04	3.93E+05	1.87E+05	3.45E+05	1.85	52.3	9.7E+04	4.2E+05	1.95E+05	3.7E+05	1.90	52.2
Lago	10.54		1.76E+05	1.13E+05	1.33E+05	1.18	70.8						
Lago	16.68		5.08E+05	2.89E+05	4.17E+05	1.47	60.7						
Lago Treco	0		4.80E+05	4.64E+05	1.25E+05	0.27	83.2						
Lago Treco	16		5.35E+05	3.82E+05	3.75E+05	0.98	62.6						
Lucula	0		7.97E+05	7.88E+05	1.24E+05	0.16	84.6						
Lucula	10.69		4.41E+05	4.07E+05	1.65E+05	0.47	70.4						
Lucula	15.41		1.52E+06	1.48E+06	3.09E+05	0.21	77.6						
Lucula	26.93		2.07E+06	1.75E+06	1.09E+06	0.66	13.4						
Malongo	11.83		7.41E+05	7.25E+05	1.53E+05	0.21	70.5						
Malongo	15.54		2.50E+06	2.34E+06	8.62E+05	0.37	50.6						
Malongo	21.74		3.18E+06	3.02E+06	9.90E+05	0.33	46.0						
MARS—TLP	8.42	5.8E+03	1.30E+04	5.36E+03	8.99E+03	1.70	63.4						
MARS—TLP	17.21	1.1E+04	3.10E+04	5.74E+03	2.63E+04	5.50	64.9						
MARS—TLP	26.15	3.1E+04	9.45E+04	4.01E+04	8.56E+04	2.15	62.2						
Maya	15		4.53E+05	3.04E+05	3.36E+05	1.11	54.9						
Maya	22		2.05E+03	6.86E+05	1.93E+06	2.82	2.0						
Mississippi Canyon 72	18.01	4.9E+03	7.00E+03	5.49E+03	5.05E+03	0.92	51.9						
Mississippi Canyon 72	26.15	3.3E+04	2.20E+05	2.00E+05	1.01E+05	0.51	74.4						
Mississippi Canyon 807	0	6.2E+03	1.02E+04	7.65E+03	5.55E+03	0.73	60.0						
Mississippi Canyon 807	8.67	1.0E+04	1.95E+04	5.50E+03	1.86E+04	3.65	68.4						
Mississippi Canyon 807	16.44	1.8E+04	5.45E+04	2.65E+04	4.62E+04	1.90	67.5						
Mississippi Canyon 807	25.51	3.4E+04	1.60E+05	8.03E+04	1.36E+05	1.65	65.4						
Mississippi Canyon Block 807	0		2.6E+04	9.4E+03	2.4E+04	2.84	79.7		2.5E+04	7.9E+03	2.4E+04	3.68	78.3
Mississippi Canyon Block 807	11.8		4.4E+04	1.3E+04	4.2E+04	3.36	79.7		4.8E+04	1.4E+04	4.6E+04	3.29	78.1
Mississippi Canyon Block 807	22.4		6.1E+04	1.9E+04	5.8E+04	3.27	76.2		6.7E+04	1.8E+04	6.4E+04	3.76	75.0
Mississippi Canyon Block 807	35.9		1.4E+05	3.8E+04	1.4E+05	3.65	72.1		1.5E+05	3.8E+04	1.4E+05	3.73	70.8
Morpeth EW921	15.2		9.4E+04	2.8E+04	9.0E+04	3.56	73.6		1.0E+05	3.4E+04	9.4E+04	2.98	72.6
Morpeth EW921	24.0		2.3E+05	1.2E+05	2.0E+05	1.64	69.4		2.4E+05	1.2E+05	2.1E+05	1.67	69.5
Neptune Spar (Viosca Knoll 826)	15.41	1.4E+04	5.45E+05	5.35E+05	1.05E+05	0.19	47.9						
Neptune Spar (Viosca Knoll 826)	22.62	3.1E+04	9.25E+05	9.05E+05	2.12E+05	0.23	62.5						
North Slope (Middle Pipeline)	30.54	2.6E+03	1.12E+05	1.01E+05	4.80E+04	0.48	61.9	1.8E+03	1.1E+04	3.3E+03	1.1E+04	3.26	21.8
North Slope (Northern Pipeline)	31.14	1.4E+03	1.06E+05	9.43E+04	4.74E+04	0.50	69.8	1.7E+03	9.4E+03	2.7E+03	9.0E+03	3.35	15.0
North Slope (Southern Pipeline)	29.62	1.9E+03	1.89E+05	1.74E+05	7.49E+04	0.43	53.5	2.2E+03	2.0E+04	7.7E+03	1.8E+04	2.20	21.1
Oriente	21		7.60E+05	6.12E+05	4.50E+05	0.75	55.7						

(continued)

TABLE 8.A1 (Cont'd)

Oil	Oil evaporation	Stability	H ₂ O content	Density	Viscosity	Saturates	Aromatics	Resins	Asphaltenes	Waxes
	%	visual	(%w/w)	at 15°C	mPa.s	%	%	%	%	%
Green Canyon 65	7.7	Meso	4.4	0.9509	457	38	42	15	5	
Green Canyon 65	13.1	Meso	1.5	0.9559	800	36	44	15	4	
Green Canyon 65	22.9	Meso	0.2	0.9716	4,250	32	45	16	8	
Gulfaks	0	Unstable	0.5	0.8701	13	60	35	5	1	
Gulfaks	10.2	Unstable	<0.1	0.8891	31	59	34	6	1	
Gulfaks	19.4	Unstable	<0.1	0.9017	91	50	38	11	1	
Gulfaks	29.8	Meso	<0.1	0.9129	202	46	42	12	1	
Heavy Fuel Oil 6303	0	Entrained	0.1	0.9888	22,800	43	29	16	13	3
Heavy Fuel Oil 6303	2.5	Entrained	<0.1	0.9988	149,000	39	27	17	18	3
Hebron M-04	0			0.9189	154					5
Hebron M-04	8.8	Stable	<0.1	0.9344	676	46	32	9	13	6
Hebron M-04	16.4	Stable	<0.1	0.9423	1,442	40	35	12	14	6
Hebron M-04	22.6	Stable	<0.1	0.9564	7,369	38	32	13	17	6
Heidrun	0	Unstable		0.8835	18	55	35	9	1	
Heidrun	7.7	Unstable		0.9013	38	57	33	9	1	
Heidrun	14.9	Unstable		0.9128	76	52	38	9	1	
Heidrun	22.6	Unstable		0.9222	152	52	36	10	1	
Hibernia [2000]	0	Meso	0.3	0.8504	13	73	18	7	2	
Hibernia [2000]	11.8	Meso	<0.1	0.8753	35	71	19	8	2	
Hibernia [2000]	22.8	Meso	<0.1	0.8893	99	61	29	8	2	
Hibernia [2000]	33.5	Meso	<0.1	0.9075	773	56	29	11	4	
High Viscosity Fuel Oil	0	Entrained	0.2	1.0140	13,460	18	43	13	26	2
Hondo	0	Stable	1.5	0.9356	735	33	31	24	12	4
Hondo	16.7	Stable	<0.1	0.9674	9,583	27	33	29	12	4
Hondo	32.3	No	<0.1	0.9881	449,700	27	28	32	13	4
IFO - 180	0	Entrained	0.1	0.9670	2,324	29	51	11	10	2
IFO - 180	7.77	Entrained	<0.1	0.9840	27,280	28	39	17	15	2
IFO - 300	0	Entrained	<0.1	0.9859	14,470	26	52	12	10	2
IFO - 300	5.33	No	<0.1	0.9996	220,000	24	28	30	17	2
Jet A1	0	Unstable	<0.1	0.8159	2	94	6	0	0	
Jet A1	12	Unstable	<0.1	0.8193	2	98	2	0	0	
Jet A1	23.2	Unstable	<0.1	0.8216	2	96	3	1	0	
Jet A1	37.1	Unstable	<0.1	0.8244	2	98	2	0	0	
Jet Fuel (Anchorage)	0	Unstable	<0.1	0.8111	2	81	19	0	0	
Jet Fuel (Anchorage)	52.7	Unstable	<0.1	0.8354	3	80	19	0	0	
Lago	0	Unstable	<0.1	0.8907	153	56	31	11	3	10
Lago	10.5	Stable	<0.1	0.9128	7,819	51	33	14	2	8
Lago	16.7	Stable	<0.1	0.9230	39,320	53	30	14	3	8
Lago Treco	0	Stable		0.9230	272	38	38	14	11	
Lago Treco	16	Entrained		0.9661	16,160	32	38	15	15	
Lucula	0	Stable	<0.1	0.8574	43	67	22	8	4	13
Lucula	10.7	Meso	<0.1	0.8821	5,214	64	23	8	4	10
Lucula	15.4	Stable	<0.1	0.8904	6,118	62	26	9	4	11

Oil	Oil evaporation	Emulsion Properties											
		On day of formation						One week after formation					
			Complex	Elasticity	Viscosity	tan	Water		Complex	Elasticity	Viscosity	tan	Water
		Viscosity	Modulus	Modulus	Modulus	delta	Content	Viscosity	Modulus	Modulus	Modulus	delta	Content
		(mPa.s)	(mPa)	(mPa)	(mPa)	(V/E)	(%w/w)	(mPa.s)	(mPa)	(mPa)	(mPa)	(V/E)	(%w/w)
	%												
Orinoco	0		3.55E+07	7.82E+06	3.47E+07	4.43	8.2		4.2E+07	9.6E+06	4.1E+07	4.23	5.2
Petronius Block VK786A	0		3.1E+04	2.4E+04	1.8E+04	0.79	74.4		1.3E+04	8.5E+03	8.7E+03	1.39	63.4
Petronius Block VK786A	8.0		3.1E+05	3.0E+05	8.1E+04	0.39	78.3		3.6E+04	2.6E+04	2.5E+04	1.06	76.4
Petronius Block VK786A	15.8		4.4E+05	4.1E+05	1.3E+05	0.39	78.9		1.2E+05	9.9E+04	6.5E+04	0.78	77.3
Petronius Block VK786A	23.6		9.9E+05	9.6E+05	2.5E+05	0.27	78.4		3.4E+05	3.1E+05	1.4E+05	0.59	76.8
Platform Gail (Sockeye)	0	3.6E+04	1.20E+05	8.34E+04	8.76E+04	1.06	75.8						
Platform Gail (Sockeye)	7.34	7.0E+04	2.02E+05	1.24E+05	1.60E+05	1.25	75.1						
Platform Gail (Sockeye)	13.33	1.1E+05	3.38E+05	2.15E+05	2.56E+05	1.20	67.1						
Platform Gail (Sockeye)	20.63	4.0E+05	1.21E+06	7.25E+05	9.61E+05	1.34	44.4						
Platform Holly	0	1.5E+05	4.4E+05	2.91E+05	3.32E+05	1.14	77.1	1.8E+05	5.3E+05	3.7E+05	3.8E+05	1.05	75.6
Platform Holly	24.24	3.6E+05	1.6E+06	1.15E+06	1.16E+06	1.01	59.6	3.8E+05	1.7E+06	1.2E+06	1.2E+06	1.01	59.3
Platform Holly	53.87	6.7E+05	3.5E+06	2.16E+06	2.74E+06	1.27	48.6	7.1E+05	4.0E+06	2.5E+06	3.2E+06	1.28	46.8
Platform Holly	78.47	8.0E+05	3.4E+06	2.19E+06	2.53E+06	1.16	34.5	8.9E+05	3.3E+06	2.2E+06	2.5E+06	1.14	33.9
Platform Irene	0	3.9E+05	1.39E+06	7.58E+05	1.17E+06	1.54	62.2	5.4E+05	3.0E+06	1.9E+06	2.3E+06	1.18	34.9
Point Arguello Comingled	0	1.8E+05	7.86E+05	7.21E+05	3.12E+05	0.43	82.3	1.8E+05	1.1E+06	1.1E+06	3.9E+05	0.37	82.2
Point Arguello Comingled	9.05	1.5E+05	8.53E+05	7.94E+05	3.11E+05	0.39	67.9	1.5E+05	6.6E+05	4.7E+05	4.6E+05	0.96	69.4
Point Arguello Comingled	15.19	1.4E+05	6.16E+05	2.72E+05	5.53E+05	2.04	30.2	1.6E+05	8.0E+05	3.5E+05	7.2E+05	2.09	28.4
Point Arguello Comingled	22.12		6.12E+06	3.15E+06	5.23E+06	1.66	2.2						
Point Arguello Heavy	0	1.5E+05	5.12E+05	4.16E+05	2.98E+05	0.72	73.0	1.8E+05	7.2E+05	5.9E+05	4.3E+05	0.73	75.0
Point Arguello Heavy	8.88		8.49E+05	3.12E+05	7.90E+05	2.53	16.8		9.2E+05	3.1E+05	8.6E+05	2.78	16.7
Point Arguello Heavy	17.78												
Point Arguello Light	0	6.7E+04	6.45E+05	6.42E+05	6.11E+04	0.10	93.1	9.6E+04	8.3E+05	8.2E+05	1.4E+05	0.17	93.8
Point Arguello Light	10.19	2.8E+05	3.35E+06	3.34E+06	1.70E+05	0.05	88.8	2.5E+05	2.9E+06	2.9E+06	3.3E+05	0.12	87.8
Point Arguello Light	19.04	2.7E+05	3.43E+06	3.42E+06	2.50E+05	0.07	85.5	3.1E+05	3.7E+06	3.6E+06	4.9E+05	0.14	85.6
Point Arguello Light	28.33	1.4E+05	9.85E+05	9.53E+05	2.49E+05	0.26	79.8	1.6E+05	1.5E+06	1.5E+06	4.2E+05	0.29	75.9
Port Hueneme	0	1.6E+04	6.32E+04	2.11E+04	5.96E+04	2.83	38.0	8.8E+03	4.4E+04	4.6E+03	4.4E+04	9.41	20.1
Port Hueneme	3.14	4.6E+04	1.67E+05	7.94E+04	1.47E+05	1.85	45.3	2.7E+04	1.3E+05	2.1E+04	1.3E+05	5.95	29.2
Port Hueneme	6.37	7.1E+04	2.68E+05	1.36E+05	2.30E+05	1.69	43.4	5.4E+04	2.6E+05	6.4E+04	2.5E+05	3.95	26.4
Prudhoe Bay (1995)	0	5.0E+02	6.81E+03	6.80E+03	2.20E+02	0.03	43.1	529.62	5.2E+03	5.1E+03	8.3E+02	0.16	39.4
Prudhoe Bay (1995)	9.32	4.6E+04	6.44E+05	6.40E+05	6.63E+04	0.10	85.1	31973	3.5E+05	3.4E+05	5.7E+04	0.17	85.1
Prudhoe Bay (1995)	27.25	1.6E+03	1.58E+05	1.52E+05	4.31E+04	0.28	20.4		2.3E+05	2.3E+05	4.9E+04	0.22	18.8
Sakhalin	42.0		4.4E+04	4.0E+04	1.7E+04	0.45	45.9						Broken
Santa Clara	0	2.7E+03	1.65E+04	1.21E+03	1.65E+04	13.7	60.6	2.6E+03	1.7E+04	3.0E+03	1.6E+04	5.42	12.8
Santa Clara	11.4	2.0E+04	6.98E+05	6.87E+05	1.26E+05	0.18	50.4	1.5E+04	7.5E+04	1.9E+04	7.3E+04	3.78	38.7
Santa Clara	21.63	1.0E+05	3.56E+05	2.03E+05	2.92E+05	1.44	39.0	9.2E+04	3.8E+05	2.0E+05	3.3E+05	1.67	40.2
Scotian Light	0												
Sockeye	0	6.9E+05	6.50E+06	6.45E+06	4.09E+05	0.07	86.5	2.8E+06	4.8E+06	4.7E+06	4.7E+05	0.10	87.0
Sockeye	12.5	2.0E+05	1.27E+06	1.20E+06	2.80E+05	0.24	80.7	2.5E+05	1.2E+06	1.1E+06	3.4E+05	0.31	76.8
Sockeye	22.1	2.5E+05	1.40E+06	1.35E+06	3.54E+05	0.25	79.1	3.1E+05	1.4E+06	1.3E+06	2.5E+05	0.19	74.8
Sockeye (2000)	0		1.83E+05	1.32E+05	1.28E+05	0.99	75.6						
Sockeye (2000)	7		2.51E+05	1.54E+05	1.98E+05	1.29	73.3						
Sockeye (2000)	13		3.91E+05	2.11E+05	3.30E+05	1.57	53.4						
Sockeye (2000)	20		1.30E+06	4.23E+05	1.23E+06	2.91	17.7						

(continued)

TABLE 8.A1 (Cont'd)

Oil	Oil evaporation	Stability	H ₂ O content	Density	Viscosity	Saturates	Aromatics	Resins	Asphaltenes	Waxes
	%	visual	(%w/w)	at 15°C	mPa.s	%	%	%	%	%
Lucula	26.9	Entrained	<0.1	0.9050	32,590	59	26	12	4	12
Main Pass Block 306	0	Unstable	0.3	0.8606	9	65	29	5	1	1
Main Pass Block 306	12	Unstable	<0.1	0.8849	19	63	29	8	1	
Main Pass Block 306	24	Unstable	<0.1	0.9034	54	58	32	10	1	
Main Pass Block 306	37	Unstable	<0.1	0.9203	219	55	33	11	1	
Main Pass Block 37	0	Unstable	7.0	0.8311	7	73	21	5	1	9
Main Pass Block 37	16	Unstable		0.8543	16	73	21	5	1	
Main Pass Block 37	30	Unstable		0.8689	36	70	23	6	1	
Main Pass Block 37	50			0.8855	115	66	24	8	2	
Malongo	0	Unstable	<0.1	0.8701	63	62	25	9	4	10
Malongo	11.8	Stable	<0.1	0.8970	6,359	60	28	10	3	9
Malongo	15.5	Entrained	<0.1	0.9026	10,950	55	29	13	3	9
Malongo	21.7	Entrained	<0.1	0.9141	25,600	54	28	15	4	5
MARS—TLP	0	Unstable	0.6	0.8883	33	60	24	11	6	2
MARS—TLP	8.42	Meso	0.1	0.9122	93	55	28	11	6	1
MARS—TLP	17.2	Meso	<0.1	0.9331	404	50	30	13	7	2
MARS—TLP	26.2	Meso	<0.1	0.9520	2,237	49	29	13	10	2
Maui	0	Unstable	0.8	0.8081	15	76	21	2	2	
Maui	14.2	Unstable	0.1	0.8340	212	69	27	3	2	
Maui	29.8	Unstable	<0.1	0.8421	1,084	61	31	7	2	
Maui	43.5	Unstable	<0.1	0.8640	2,000	67	26	4	3	
Maya	0			0.9255	280	38	39	8	16	7
Maya	9			0.9515	1,980	33	41	8	17	3
Maya	15	Entrained	<0.1	0.9657	8,670	31	41	10	17	4
Maya	22	No	<0.1	0.9868	405,000	28	39	11	22	4
Mississippi Canyon 194	0	Unstable	0.1	0.8483	7	71	25	4	0	1
Mississippi Canyon 194	10	Unstable	<0.1	0.8655	11	71	23	6	0	
Mississippi Canyon 194	21	Unstable	<0.1	0.8762	21	69	24	6	0	
Mississippi Canyon 194	35	Unstable	<0.1	0.8874	51	67	26	7	0	
Mississippi Canyon 72	0	Unstable	1.0	0.8649	16	64	27	7	2	
Mississippi Canyon 72	9.41	Unstable	<0.1	0.8827	34	57	33	8	2	
Mississippi Canyon 72	18	Meso	<0.1	0.8966	76	58	32	9	2	
Mississippi Canyon 72	26.2	Stable	<0.1	0.9095	195	52	34	11	3	
Mississippi Canyon 807	0	Meso	0.2	0.8894	41	47	35	12	6	
Mississippi Canyon 807	8.67	Meso	<0.1	0.9187	127	39	41	13	7	
Mississippi Canyon 807	16.4	Stable	<0.1	0.9375	491	39	41	13	7	
Mississippi Canyon 807	25.5	Stable	<0.1	0.9582	3,454	31	43	18	8	
Mississippi Canyon Block 807	0	Meso	11.9	0.9461	5	73	15	6	5	
Mississippi Canyon Block 807	11.8	Meso	10.8	0.9202	165	70	16	8	6	
Mississippi Canyon Block 807	22.4	Meso	4.8	0.9562	396	66	17	10	7	
Mississippi Canyon Block 807	35.9	Meso	0.4	0.9693	1,472	63	16	11	10	
Morpeth EW921	0	Unstable	0.3	0.8996	45	71	17	8	4	
Morpeth EW921	9.3	Unstable	0.2	0.9282	195	69	17	9	5	

Oil	Oil evaporation	Emulsion Properties											
		On day of formation				One week after formation							
		Complex		Elasticity	Viscosity	tan	Water	Complex		Elasticity	Viscosity	tan	Water
		Viscosity	Modulus	Modulus	Modulus	delta	Content	Viscosity	Modulus	Modulus	Modulus	delta	Content
		(mPa.s)	(mPa)	(mPa)	(mPa)	(V/E)	(%w/w)	(mPa.s)	(mPa)	(mPa)	(mPa)	(V/E)	(%w/w)
%													
Sockeye Comingled	0	3.9E+04	1.13E+05	7.29E+04	8.60E+04	1.18	73.6	24259	8.5E+04	3.3E+04	7.8E+04	2.41	66.2
Sockeye Sour	0	3.2E+04	1.19E+05	7.10E+04	9.51E+04	1.34	73.6	25252	1.1E+05	5.3E+04	9.4E+04	1.76	53.1
Sockeye Sour	9.6	7.9E+04	3.12E+05	1.93E+05	2.45E+05	1.27	59.9	84937	3.3E+05	2.0E+05	2.6E+05	1.33	60.2
Sockeye Sweet	17.46	8.2E+03	3.15E+04	2.87E+04	1.28E+04	0.45	81.8	4.3E+03	2.1E+04	1.8E+04	9.0E+03	0.49	76.8
Sockeye Sweet	26.91	4.8E+04	5.13E+05	4.97E+05	1.29E+05	0.26	75.5	36271	1.3E+05	1.2E+05	6.7E+04	0.58	72.3
Takula	0	4.5E+04	9.45E+05	9.35E+05	1.65E+05	0.17	84.8	8.7E+04	8.9E+05	8.8E+05	1.6E+05	0.18	83.8
Takula	11	8.3E+04	1.20E+06	1.15E+06	1.85E+05	0.21	81.3	1.1E+05	1.2E+06	1.1E+06	2.4E+05	0.20	81.4
Takula	18	1.1E+05	1.15E+06	1.10E+06	3.18E+05	0.27	75.0	1.5E+05	1.2E+06	1.2E+06	3.6E+05	0.31	73.9
Udang	0		1.91E+05	7.35E+04	1.76E+05	2.44	38.8		2.0E+05	5.9E+04	1.9E+05	3.22	36.2
Viosca Knoll 826	23.97	1.4E+04	3.40E+05	3.30E+05	8.84E+04	0.27	64.1						
Viosca Knoll 990	35.15	9.3E+03	9.8E+04	9.60E+04	3.38E+04	0.38	63.9						
Waxy Light Heavy Blend	12	6.2E+03	3.05E+04	9.31E+03	2.90E+04	3.12	49.7		1.5E+04	2.4E+03	1.5E+04	6.14	14.4
Waxy Light Heavy Blend	19.6	4.4E+04	1.90E+05	9.50E+04	1.65E+05	1.74	54.6	3.3E+04	1.2E+05	5.1E+04	1.1E+05	2.08	59.2
West Texas (2000)	21		1.91E+04	1.68E+04	9.60E+03	0.61	82.7						
West Texas (2000)	31		8.19E+04	7.82E+04	2.93E+04	0.38	83.6						
Zaire	0		5.10E+05	4.82E+05	1.64E+05	0.34	76.2						
Zaire	6		7.53E+05	7.33E+05	1.62E+05	0.24	65.5		4.7E+05	4.3E+05	1.8E+05	0.42	56.6
Zaire	14		1.15E+06	1.10E+06	3.37E+05	0.31	61.0		4.4E+05	3.5E+05	2.6E+05	0.81	58.6
Zaire	23		2.27E+06	1.81E+06	1.36E+06	0.77	5.3						

(continued)

TABLE 8.A1 (Cont'd)

Oil	Oil evaporation	Stability	H ₂ O content	Density	Viscosity	Saturates	Aromatics	Resins	Asphaltenes	Waxes
	%	visual	(%w/w)	at 15°C	mPa.s	%	%	%	%	%
Morpeth EW921	15.2	Meso	0.2	0.9426	551	66	18	10	6	
Morpeth EW921	24.0	Meso	0.1	0.9619	3,697	60	19	13	8	
Neptune Spar (Viosca Knoll 826)	0	Unstable	0.1	0.8687	17	65	28	6	1	4
Neptune Spar (Viosca Knoll 826)	7.92	Unstable	<0.1	0.8826	42	63	29	6	2	4
Neptune Spar (Viosca Knoll 826)	15.4	Meso	<0.1	0.8925	84	62	29	7	2	5
Neptune Spar (Viosca Knoll 826)	22.6	Stable	<0.1	0.8986	187	61	29	8	2	5
North Slope (Middle Pipeline)	0	Unstable	0.2	0.8761	16	52	35	9	5	
North Slope (Middle Pipeline)	30.5	Meso	<0.1	0.9418	900	42	38	12	7	
North Slope (Northern Pipeline)	0	Unstable	0.1	0.8719	14	51	34	9	5	
North Slope (Northern Pipeline)	31.1	Meso	<0.1	0.9402	748	44	37	12	7	
North Slope (Southern Pipeline)	0	Unstable	0.2	0.8766	18	54	32	8	6	
North Slope (Southern Pipeline)	29.6	Meso	<0.1	0.9431	961	42	39	13	7	
Oriente	0			0.8981	85	48	32	9	12	2
Oriente	21	Entrained		0.9426	6,124	41	33	11	15	
Orinoco	0	No	<0.1	1.0166	10,200,000	41	22	17	21	
Petronius Block VK786A	0	Entrained		0.8713	28	84	9	6	2	
Petronius Block VK786A	8.0	Entrained		0.8858	55	83	9	6	2	
Petronius Block VK786A	15.8	Entrained		0.8978	146	81	10	7	2	
Petronius Block VK786A	23.6	Entrained	<0.1	0.9096	327	79	10	8	3	
Pitas Point	0	Unstable	<0.1	0.8341	2	80	18	3	0	0
Pitas Point	23.6	Unstable	<0.1	0.8537	2	62	35	0	0	0
Platform Gail (Sockeye)	0	Stable	1.3	0.9297	406	39	28	21	12	2
Platform Gail (Sockeye)	7.34	Stable	0.3	0.9489	1,450	35	31	21	13	2
Platform Gail (Sockeye)	13.3	Stable	0.1	0.9645	7,092	32	28	25	15	2
Platform Gail (Sockeye)	20.6	Entrained	<0.1	0.9810	161,500	27	29	25	19	2
Platform Holly	0	Stable*	75.7	0.9928	3,314	54	14	15	17	2
Platform Holly	24.2	Stable*	61.7	1.0003	150,200	29	30	19	24	
Platform Holly	53.9	Stable*	50.1	1.0066	399,700	36	25	17	22	
Platform Holly	78.5	Stable*	25.5	1.0705	304,550	19	26	19	36	
Platform Irene	0	Entrained	57.3	0.9907	76,000	26	29	22	22	2
Point Arguello Comingled	0	Stable	1.2	0.9248	533	36	25	23	16	8
Point Arguello Comingled	9.05	Stable	<0.1	0.9528	4,988	31	33	19	17	4
Point Arguello Comingled	15.2	Entrained	<0.1	0.9688	41,860	27	33	21	19	4
Point Arguello Comingled	22.1	No	0.1	0.9853	2,266,000	24	33	21	22	5
Point Arguello Heavy	0	Stable	<0.1	0.9447	3,250	32	32	17	19	6
Point Arguello Heavy	8.88	Entrained	<0.1	0.9706	5,9390	26	35	18	20	4
Point Arguello Heavy	17.8	No	<0.1	0.9914	4,953,000	25	34	21	22	4
Point Arguello Light	0	Stable	<0.1	0.8739	22	57	27	9	7	6
Point Arguello Light	10.2	Stable	<0.1	0.8979	76	54	30	9	8	6
Point Arguello Light	19	Stable	<0.1	0.9132	183	48	31	12	9	7
Point Arguello Light	28.3	Stable	<0.1	0.9289	671	45	32	12	11	8
Port Hueneme	0	Entrained	0.9	0.9662	4,131	24	43	20	12	5
Port Hueneme	3.14	Entrained	0.1	0.9745	7,833	23	41	21	14	3

TABLE 8.A1 (Cont'd)

Oil	Oil evaporation	Stability	H ₂ O content	Density	Viscosity	Saturates	Aromatics	Resins	Asphaltenes	Waxes
	%	visual	(%w/w)	(@15C)	mPa.s	%	%	%	%	%
Port Hueneme	6.37	Entrained	<0.1	0.9787	20,990	23	37	28	13	3
Prudhoe Bay (1995)	0	Meso	0.3	0.8837	22	53	34	10	4	4
Prudhoe Bay (1995)	9.32	Stable	<0.1	0.9048	55	51	35	10	3	5
Prudhoe Bay (1995)	18.1	Unstable	<0.1	0.9204	148	52	32	12	4	5
Prudhoe Bay (1995)	27.3	Meso	<0.1	0.9352	623	43	38	15	5	5
Sahara Blend	0	Unstable		0.8078	4	76	21	3	1	
Sahara Blend	13.7	Unstable		0.8336	7	77	20	3	1	
Sahara Blend				0.8528	19	72	23	4	1	
Sahara Blend				0.8678	53	69	24	6	1	
Sakhalin	0	Unstable	<0.1	0.8632	4	61	32	6	1	
Sakhalin	42.0	Meso	<0.1	0.9201	52	56	32	10	2	
Santa Clara	0	Meso	1.8	0.9202	304	36	22	29	13	6
Santa Clara	11.4	Meso	0.5	0.9479	1,859	32	28	27	13	4
Santa Clara	21.6	Meso	0.1	0.9672	22,760	28	32	23	17	5
Scotian Light	0	Unstable	0.3	0.7655	1	92	8	1	0	9
Scotian Light	25	Unstable	0.2	0.7949	2	89	10	1	0	4
Scotian Light	44	Unstable	0.1	0.8139	2	85	14	1	0	5
Scotian Light	64	Unstable	<0.1	0.8356	5	60	38	1	0	10
Ship Shoal Block 239	0	Unstable	30.5	0.8972	34	68	23	7	2	4
Ship Shoal Block 239	17	Unstable	27.4	0.9103	70					
Ship Shoal Block 239	43	Unstable	4.9	0.8977	74	64	26	8	2	
Ship Shoal Block 239	53		0.1	0.9076	194	60	28	9	4	
Ship Shoal Block 269	0	Unstable	0.3	0.8309	5	79	15	6	0	1
Ship Shoal Block 269	13	Unstable	<0.1	0.8517	7	71	23	5	0	
Ship Shoal Block 269	26	Unstable	<0.1	0.8657	18	69	24	6	1	
Ship Shoal Block 269	39	Unstable	<0.1	0.8796	44	67	26	6	1	
Sockeye	0	Stable	0.1	0.8965	45	48	31	13	8	6
Sockeye	12.5	Stable	<0.1	0.9166	163	44	32	15	9	5
Sockeye	22.1	Stable	<0.1	0.9264	628	39	34	15	11	5
Sockeye (2000)	0	Meso	0.8	0.9354	761	50	18	18	15	2
Sockeye (2000)	7	Meso	0.1	0.9537	2,720	47	17	19	16	2
Sockeye (2000)	13	Entrained	0.1	0.9692	15,100	45	18	19	18	2
Sockeye (2000)	20	Entrained	<0.1	0.9839	274,000	42	18	20	20	2
Sockeye Comingled	0	Stable	0.6	0.9350	550	34	32	21	13	
Sockeye Sour	0	Stable	0.6	0.9409	821	38	29	20	13	
Sockeye Sour	9.6	Stable	0.1	0.9682	8,708	29	31	22	17	
Sockeye Sour	18.5	No	<0.1	0.9838	475,200	26	30	22	24	
Sockeye Sweet	0	Unstable	0.3	0.8792	20	55	31	10	4	
Sockeye Sweet	8.1	Unstable	<0.1	0.8945	39	56	30	10	4	
Sockeye Sweet	17.5	Mesostable	<0.1	0.9089	103	50	32	13	5	
Sockeye Sweet	26.9	Stable	<0.1	0.9229	321	48	33	14	6	
South Louisiana	0	Unstable	0.5	0.8518	8	73	21	4	1	4

(continued)

TABLE 8.A1 (Cont'd)

Oil	Oil evaporation	Stability	H ₂ O content	Density	Viscosity	Saturates	Aromatics	Resins	Asphaltenes	Waxes
	%	visual	(%w/w)	at 15°C	mPa.s	%	%	%	%	%
South Louisiana	10.3	Unstable	0.1	0.8696	16	69	25	5	0	3
South Louisiana	20.1	Unstable	<0.1	0.8831	36	66	27	6	0	4
South Louisiana	30.8	Unstable	<0.1	0.8953	80	64	29	7	0	4
South Louisiana (2001)	0	Unstable	<0.1	0.8562	10	81	13	6	1	2
South Louisiana (2001)	11	Unstable	<0.1	0.8770	24	80	12	6	1	2
South Louisiana (2001)	20	Unstable	<0.1	0.8906	49	78	13	8	1	2
South Louisiana (2001)	28	Unstable	<0.1	0.9018	141	77	13	8	2	2
South Pass Block 60	0	Unstable	0.1	0.8453	9	71	20	8	1	1
South Pass Block 60	17	Unstable	<0.1	0.8709	22	67	26	7	1	
South Pass Block 60	25	Unstable	<0.1	0.8809	41	64	27	8	1	
South Pass Block 60	38		<0.1	0.8979	161	61	28	9	2	
South Pass Block 67	0	Unstable	44.2	0.9564	39	NM	High sand/water content			NM
South Pass Block 67	22	Unstable	41.0	0.9928	110	NM	NM	NM	NM	NM
South Pass Block 67	45		24.2	0.9510	108	NM	NM	NM	NM	NM
South Pass Block 67	64		0.3	0.9306	236	NM	NM	NM	NM	NM
South Pass Block 93	0	Unstable	9.0	0.8574	19	73	20	4	3	4
South Pass Block 93	11	Unstable		0.8637	23	74	20	4	2	
South Pass Block 93	21	Unstable		0.8698	32	73	20	4	2	
South Pass Block 93				0.8832	80	71	22	5	3	
South Timbalier Block 130	0	Unstable	0.1	0.8487	7	78	16	5	0	1
South Timbalier Block 130	11	Unstable	<0.1	0.8632	10	72	22	5	0	
South Timbalier Block 130	22	Unstable	<0.1	0.8748	19	71	23	6	0	
South Timbalier Block 130	35	Unstable	<0.1	0.8877	48	68	23	8	1	
Sumatran Heavy	0	Entrained	0.8	0.9312	13,300	46	30	13	10	1
Sumatran Heavy	5.26	No	0.2	0.9374	12,900	45	32	16	8	4
Sumatran Light	0	No	0.2	0.8600	41,480	70	15	6	8	11
Taching	0	No	0.1	0.8700	5,138,000	74	12	9	6	23
Takula	0	Stable	0.1	0.8637	110	65	22	8	2	8
Takula	11	Stable	<0.1	0.8860	844	62	24	10	4	8
Takula	18	Stable	<0.1	0.8961	3,148	60	25	11	4	9
Tapis	0	Unstable	<0.1	0.8020	8	81	15	2	2	
Tapis	13.9	Entrained	<0.1	0.8237	57	77	19	3	1	
Tapis	28.6	Unstable	<0.1	0.8396	800	80	16	3	2	
Tapis	43.4	Unstable	<0.1	0.8552	1,440	79	14	4	3	
Thevenard Island	0	Unstable	<0.1	0.7855	1	85	13	2	0	1
Thevenard Island	22.7	Unstable	<0.1	0.8301	3	79	19	2	0	5
Thevenard Island	43.9	Unstable	<0.1	0.8352	5	79	19	2	0	7
Thevenard Island	59	Unstable	<0.1	0.8498	9	75	22	3	0	9
Troll	0	Unstable		0.8852	24	67	27	6	1	
Troll	6.3	Unstable		0.8972	44	66	27	6	1	
Troll	13.1	Unstable		0.9060	80	65	28	7	1	
Troll	19.4	Unstable		0.9134	175	62	29	8	1	
Udang	0	Entrained	1.0	0.9701	10,700	32	41	24	3	1
Viosca Knoll 826	0	Unstable	0.2	0.8668	16	66	26	6	2	

TABLE 8.A1 (Cont'd)

Oil	Oil evaporation	Stability	H ₂ O content	Density	Viscosity	Saturates	Aromatics	Resins	Asphaltenes	Waxes
	%	visual	(%w/w)	at 15°C	mPa.s	%	%	%	%	%
Viosca Knoll 826	8.14	Unstable	<0.1	0.8842	43	61	29	7	3	
Viosca Knoll 826	16.9	Unstable	<0.1	0.8970	132	62	29	6	3	
Viosca Knoll 826	24	Stable	<0.1	0.9067	325	59	29	8	3	
Viosca Knoll 990	0	Unstable	0.2	0.8337	7	73	22	4	1	2
Viosca Knoll 990	12.3	Unstable	<0.1	0.8585	12	69	25	6	1	3
Viosca Knoll 990	24.4	Unstable	<0.1	0.8752	31	66	26	6	1	3
Viosca Knoll 990	35.2	Stable	<0.1	0.8905	91	62	28	8	2	3
Waxy Light Heavy Blend	0	Unstable	0.1	0.9311	184	39	35	21	5	4
Waxy Light Heavy Blend	12	Meso	<0.1	0.9582	2,002	32	38	24	6	1
Waxy Light Heavy Blend	19.6	Meso	<0.1	0.9749	17,280	30	35	28	6	1
West Delta Block 30	0	Unstable	65.4	0.9894	1,180	NM	High water content			NM
West Delta Block 30	24		58.6	0.9562	1,350	NM	NM	NM	NM	NM
West Delta Block 30	42		34.9	0.9594	1,560	NM	NM	NM	NM	NM
West Delta Block 30	61		0.1	0.9598	4,970	NM	NM	NM	NM	NM
West Delta Block 97	0	Unstable	0.1	0.7783	1	92	7	1	0	0
West Delta Block 97	23	Unstable	<0.1	0.8020	1	81	18	1	0	
West Delta Block 97	48	Unstable	<0.1	0.8191	3	87	10	3	0	
West Delta Block 97	74	Unstable	<0.1	0.8388	7	85	14	2	0	
West Texas (2000)	0	Unstable	<0.1	0.8474	9	79	15	6	1	3
West Texas (2000)	10	Unstable	<0.1	0.8665	16	79	14	7	1	3
West Texas (2000)	21	Meso	<0.1	0.8827	38	76	15	8	1	3
West Texas (2000)	31	Meso	<0.1	0.8973	112	75	14	10	2	4
Zaire	0	Entrained	<0.1	0.8720	15,100	64	22	9	5	20
Zaire	6	Entrained	<0.1	0.8872	52,800	61	24	9	5	11
Zaire	14	Entrained	<0.1	0.9015	94,560	59	26	10	5	12
Zaire	23	No	<0.1	0.9020	533,100	53	28	16	5	13

TABLE 8.A2 Long-term data on the emulsions produced from the oils

Oil name	Evaporation (%w/w)	Day Water Content (%w/w)	Week Water Content (%w/w)	>1 year after formation					
				Viscosity (mPa·s)	Complex Modulus (mPa)	Elasticity Modulus (mPa)	Viscosity Modulus (mPa)	tan delta (V/E)	Water Content (%w/w)
Arabian Light	0	87.4	86.9	1.0E+04	8.6E+04	7.8E+04	3.7E+04	0.48	76
Arabian Light	12.04	88.9	85.8	4.9E+03	1.4E+04	8.5E+03	1.1E+04	1.24	59
Arabian Light	24.2	84.7	83.6	4.5E+03	2.2E+04	1.4E+04	1.7E+04	1.23	48
Arabian Medium	0	84.7	84.4	4.3E+04	2.9E+05	2.9E+05	6.2E+04	0.22	84
Arabian Medium	13.15	76.5	77.1	5.6E+04	4.4E+05	4.3E+05	1.1E+05	0.27	77
Belridge Heavy	0	57.9	44.4	6.1E+04	1.6E+05	7.0E+04	1.4E+05	2.01	35
Belridge Heavy	2.74	59.6	45.2	7.1E+04	2.1E+05	8.8E+04	1.9E+05	2.18	33
Bunker C (1987)	0	26.4	24.0	3.9E+05	3.5E+06	1.8E+06	3.0E+06	1.63	23
Bunker C (Anchorage)	0	34.7	31.0	3.9E+04	4.2E+05	3.7E+05	1.9E+05	0.52	18
California API 15.0	0	39.0	22.0		2.3E+06	1.3E+06	1.9E+06	1.49	44
Carpenteria	10.31	71.8	28.2	NM	2.4E+05	1.4E+05	2.0E+05	1.46	23
Carpenteria	14.87	54.3	30.9	3.6E+04	7.5E+05	6.6E+05	3.5E+05	0.53	18
Cook Inlet—Granite Point	45.32	83.1	57.6	5.6E+03	4.3E+05	3.9E+05	1.4E+05	0.35	21
Cook Inlet—Swanson River	0	76.0	57.5	1.1E+04	4.5E+05			0.37	61
Cook Inlet—Swanson River	39.69	81.5	80.8	3.5E+05	2.8E+06	2.7E+06	8.1E+05	0.30	79
Cook Inlet—Trading Bay	33.3	76.2	61.4	6.7E+04	1.8E+06	1.7E+06	5.8E+05	0.33	53
Dos Cuadras	11.17	47.6	29.5	NM	5.3E+04	3.0E+04	4.3E+04	1.43	7
Dos Cuadras	20.3	68.6	28.7	1.3E+04	3.1E+04	5.8E+03	3.0E+04	5.22	20
High Viscosity Fuel Oil	0	47.6	42.2	2.0E+05	6.6E+05	3.7E+05	5.4E+05	1.46	48
Hondo	0	80.9	80.0	1.9E+05	9.5E+05	8.9E+05	3.2E+05	0.36	77
IFO—180	0	69.4	22.0	1.4E+05	3.9E+05	2.3E+05	3.2E+05	1.41	66
IFO—80	7.77	58.4	37.0	2.7E+05	6.7E+05	4.4E+05	5.1E+05	1.14	58
IFO—300	0	52.3	32.0	1.8E+05	5.8E+05	3.1E+05	4.9E+05	1.58	45
Lago Treco	16	62.6	32.0		8.1E+05	5.4E+05	6.0E+05	1.11	63
Lucula	10.69	70.4			3.6E+06	3.4E+06	1.2E+06	0.36	44
Lucula	26.93	13.4	13.0		3.0E+07	2.8E+07	1.0E+07	0.37	8
Maya	15	54.9	25.0		7.7E+05	4.8E+05	6.0E+05	1.26	57
Mississippi Canyon 807	0	60.0			1.2E+04	4.9E+03	1.1E+04	2.21	44
North Slope (Middle Pipeline)	30.54	61.9	21.8						10
North Slope (Northern Pipeline)	31.14	69.8	15.0						6
North Slope (Southern Pipeline)	29.62	53.5	21.1						10
Oriente	21	55.7	16.0		6.4E+05	4.5E+05	4.6E+05	1.02	56
Platform Irene	0	62.2	34.9		9.8E+06	7.5E+06	6.4E+06	0.85	53
Point Arguello Comingled	0	82.3	82.2	3.9E+05	1.7E+06	1.6E+06	5.1E+05	0.32	82
Point Arguello Comingled	15.19	30.2	28.4		1.7E+06	1.2E+06	2.3E+05	1.30	30
Point Arguello Light	0	93.1	93.8	1.6E+05	1.1E+06	1.1E+06	2.3E+05	0.21	90
Point Arguello Light	10.19	88.8	87.8	5.2E+05	2.7E+06	2.7E+06	4.3E+05	0.16	86
Point Arguello Light	19.04	85.5	85.6	7.9E+05	3.7E+06	3.7E+06	6.8E+05	0.19	88
Point Arguello Light	28.33	79.8	75.9	3.7E+05	2.3E+06	2.2E+06	6.5E+05	0.29	78
Port Hueneme	0	38.0	20.1	1.5E+04	4.8E+04	4.8E+03	4.8E+04	9.93	10
Port Hueneme	3.14	45.3	29.2	3.6E+04	2.6E+05	7.4E+04	2.5E+05	3.38	23
Port Hueneme	6.37	43.4	26.4	6.4E+04	1.3E+05	3.0E+04	1.3E+05	4.30	24
Prudhoe Bay (1995)	0	43.1	39.4	3.9E+03	9.1E+03	5.7E+03	7.1E+03	1.24	38
Prudhoe Bay (1995)	9.32	85.1	85.1	1.7E+04	5.1E+04	3.7E+04	3.5E+04	0.95	71
Prudhoe Bay (1995)	27.25	20.4	18.8		3.3E+04	1.5E+04	2.9E+04	1.98	12
Santa Clara	0	60.6	12.8						7
Santa Clara	11.4	50.4	38.7	3.9E+04	1.3E+05	2.9E+04	1.3E+05	4.45	19
Santa Clara	21.63	39.0	40.2	1.6E+05	1.2E+06	1.0E+06	6.0E+05	0.59	33
Sockeye	0	86.5	87.0	8.1E+05	3.7E+06	3.6E+06	8.4E+05	0.24	83
Sockeye	12.5	80.7	76.8	3.1E+05	1.8E+06	1.7E+06	6.6E+05	0.40	69
Sockeye	22.1	79.1	74.8	3.9E+05	2.2E+06	2.0E+06	8.6E+05	0.43	66
Sockeye Comingled	0	73.6	46.2	5.2E+04	1.3E+05	4.7E+04	1.2E+05	2.49	71
Sockeye Sour	0	73.6	53.1	5.2E+04	1.5E+05	5.6E+04	1.4E+05	2.48	49
Sockeye Sour	9.6	59.9	30.2	1.3E+05	3.9E+05	2.1E+05	3.2E+05	1.49	54
Sockeye Sweet	17.46	81.8		4.8E+03	8.6E+04	7.2E+04	4.7E+04	0.66	34
Sockeye Sweet	26.91	75.5	72.3	3.1E+04	2.7E+05	2.2E+05	1.6E+05	0.73	59
Takula	0	84.8	83.8	1.5E+05	3.1E+06	3.1E+06	5.8E+05	0.19	81
Takula	11	81.3	81.4	2.5E+05	1.9E+06	1.8E+06	4.1E+05	0.22	78
Waxy Light Heavy Blend	19.6	54.6	39.2	6.9E+03	9.7E+04	8.4E+03	9.7E+04	11.50	59

NM, not measured.

TABLE 8.A3 Average, minimum, and maximum water-in-oil-type composition and rheological properties

Rheological properties																	
Day of formation																	
	Day	Week	Density (at 15°C)	Viscosity	Log Viscosity	Saturates	Aromatics	Resins	Asphaltenes	A/R	Waxes	Viscosity (mPa·s)	Complex Modulus (mPa)	Elasticity Modulus (mPa)	Viscosity Modulus (mPa)	tan delta (V/E)	Water Content (%w/w)
Averages	Entrained	44.5	27.5 ^a	0.9697	60,530	4.8	35	35	18.0	12.4	0.75	4.3	1.1E+05	8.30E+05	5.14E+05	5.87E+05	1.73
	Mesostable	64.3	29.6 ^a	0.9328	1,300	3.1	46	31	15.6	7.8	0.49	3.4	9.3E+03	1.33E+05	1.07E+05	6.20E+04	1.7
	Stable	80.7	77.4	0.9000	226	2.4	59	26	9.0	5.4	0.58	5.3	9.2E+04	7.50E+05	7.10E+05	1.78E+05	0.7
	Unstable	6.1	6.85 ^a	0.8700	143,600	5.2	68	23	6.7	2.3	0.3	4.1	1.10E+07	3.37E+06	3.37E+06	1.08E+07	2.4
Entrained	Maximum	76.2	45.2	1.0166	825,000	5.9	64.0	55.0	31.0	26.0	2.0	20.0	4.0E+05	3.18E+06	3.02E+06	2.71E+06	4.0
Entrained	Minimum	13.4	12.7 ^a	0.9015	2,324	3.4	18.0	18.0	9.0	3.0	0.1	1.0	1.6E+04	6.32E+04	2.11E+04	5.96E+04	0.2
Mesostable	Maximum	83.6	53.1	0.9716	8,708	3.9	76.3	45.0	29.0	17.0	0.9	10.0	1.1E+05	6.98E+05	6.87E+05	2.56E+05	13.7
Mesostable	Minimum	20.4	10 ^a	0.8821	22	1.3	29.0	13.8	8.0	1.0	0.1	1.0	5.0E+02	3.45E+03	1.08E+03	2.20E+02	0.0
Stable	Maximum	93.1	93.8	0.9883	1,410	3.1	84.0	44.0	24.0	16.0	1.3	13.0	6.9E+05	6.50E+06	6.45E+06	5.10E+05	2.8
Stable	Minimum	62.5	57.5	0.8404	5.0	0.7	33.0	9.0	4.2	2.0	0.2	2.3	2.9E+03	1.03E+04	6.91E+03	7.62E+03	0.1
Unstable	Maximum	15.9	11.2	1.0166	1.02E+07	7.0	98.0	44.0	32.0	24.0	2.0	23.0	0.0	3.55E+07	7.82E+06	3.47E+07	4.4
Unstable	Minimum	0.2	1.9 ^a	0.7143	1.00E+00	0.0	23.0	2.0	0.0	0.0	0.0	0.0	0.0	2.05E+03	6.86E+05	1.36E+06	0.8
Rheological properties																	
One week after formation																	
	Viscosity (mPa·s)	Complex Modulus (mPa)	Elasticity Modulus (mPa)	Viscosity Modulus (mPa)	tan delta (V/E)			Viscosity (mPa·s)	Complex Modulus (mPa)	Elasticity Modulus (mPa)	Viscosity Modulus (mPa)	tan delta (V/E)	Complex Viscosity (mPa·s)	Water Content (%w/w)			
Averages	Entrained	1.1E+05	7.0E+05	3.2E+05	6.0E+05	3.02		125,430	2.7E+06	2.2E+06	1.3E+06	2.45	4.3E+05	39.33			
	Mesostable	7.0E+03	8.0E+04	5.0E+04	5.3E+04	3.70		2.3E+04	5.4E+05	4.8E+05	2.2E+05	2.10	8.6E+04	19.80			
	Stable	1.9E+05	8.1E+05	7.6E+05	2.1E+05	0.77		2.1E+05	1.4E+06	1.4E+06	4.3E+05	0.63	2.3E+05	67.83			
	Unstable	5.40E+05	4.2E+07	9.6E+06	4.1E+07	4.23		3.91E+05	2.99E+07	2.82E+07	9.99E+06	11.5	4.76E+06	65.7			
Entrained	Maximum	8800.0	4.37E+04	4.62E+03	4.35E+04	0.4		6.88E+03	4.81E+04	4.82E+03	4.78E+04	0.4	7.65E+03	7.7			
Entrained	Minimum	8.49E+04	3.25E+05	2.60E+05	2.59E+05	11.3		1.31E+05	3.62E+06	3.41E+06	1.20E+06	5.2	5.76E+05	70.8			
Mesostable	Maximum	529.6	4.48E+03	7.40E+02	8.30E+02	0.2		3.92E+03	9.11E+03	4.94E+03	7.09E+03	0.4	1.45E+03	5.7			
Mesostable	Minimum	2.84E+06	4.76E+06	4.74E+06	5.61E+05	3.7		8.07E+05	3.74E+06	3.68E+06	8.55E+05	1.2	5.95E+05	90.2			
Stable	Maximum	1900.0	7.19E+03	6.00E+03	3.93E+03	0.1		4.47E+03	1.35E+04	8.50E+03	1.05E+04	0.2	2.15E+03	21.2			
Stable	Minimum	0.0	4.17E+07	9.62E+06	4.06E+07	4.2		0.00E+00	0.00E+00	0.00E+00	0.00E+00	0.0	0.00E+00	0.0			
Unstable	Maximum	0.0	4.17E+07	9.62E+06	4.06E+07	4.2		0.00E+00	0.00E+00	0.00E+00	0.00E+00	0.0	0.00E+00	0.0			
Unstable	Minimum	0.0	4.17E+07	9.62E+06	4.06E+07	4.2		0.00E+00	0.00E+00	0.00E+00	0.00E+00	0.0	0.00E+00	0.0			

^aThese water content values are high as most were not measured as they appeared to be very low.

TABLE 8.A4 Effects of weathering on pairs or triplets of oils that form water-in-oil types

Oil	% Evaporation	Visual Stability	H ₂ O content (%w/w)	Density g/ml (15°C)	Viscosity mPa·s	Saturates %	Aromatics %	Resins %	Asphaltenes %	A/R	A×R
Alaska North Slope [2002]	0	Starting oil	<0.1	0.8663	12	75	15	6	4	0.66	24.4
Alaska North Slope [2002]	30.5	Meso	<0.1	0.9340	625	65	19	10	6	0.62	65.92
Arabian Light [2002]	0	Meso	<0.1	0.8641	13	76	15	6	4	0.63	20.52
Arabian Light [2002]	17	Stable	<0.1	0.9028	60	72	17	7	4	0.65	28.38
ASMB (std. #5)	0	Meso	<0.1	0.8404	6	77	17	4	2	0.48	8.4
ASMB (std. #5)	24	Stable	<0.1	0.8852	32	77	15	6	2	0.42	13.68
Carpenteria	0	Starting oil	<0.1	0.9155	164	44	30	17	9	0.53	153
Carpenteria	10.3	Meso	<0.1	0.9299	755	40	30	19	11	0.58	209
Cook Inlet—Swanson River	0	Meso	0.2	0.8420	6	65	25	6	5	0.83	30
Cook Inlet—Swanson River	39.7	Stable	<0.1	0.9143	152	56	29	7	7	1	49
Cook Inlet—Trading Bay	0	Starting oil	0.1	0.8602	10	62	26	7	5	0.71	35
Cook Inlet—Trading Bay	33.3	Meso	<0.1	0.9242	278	51	32	9	8	0.89	72
Cusiana	0	Starting oil	<0.1	0.8328	7	76	20	3	1	0.33	3
Cusiana	38.3	Meso	<0.1	0.8965	326	71	22	5	2	0.4	10
Dos Cuadras	0	Starting oil	<0.1	0.9000	51	48	30	17	6	0.35	102
Dos Cuadras	11.2	Meso	<0.1	0.9270	187	42	31	20	7	0.35	140
Garden Banks 387	0	Starting oil	1.0	0.8782	29	53	36	10	1	0.1	10
Garden Banks 387	23.3	Meso	<0.1	0.9287	579	46	40	13	2	0.15	26
Garden Banks 426	0	Starting oil	0.8	0.8285	6	70	24	5	1	0.2	5
Garden Banks 426	37.7	Stable	<0.1	0.8993	136	56	32	10	3	0.3	30
Genesis	0	Starting oil	<0.1	0.8841	26	59	30	10	2	0.16	15.52
Genesis	23.1	Meso	<0.1	0.9364	543	48	28	21	3	0.16	69.96
Green Canyon 184	0	Starting oil	1.2	0.8314	5	69	24	6	1	0.17	6
Green Canyon 184	38.2	Meso	<0.1	0.9043	117	54	34	11	1	0.09	11
Green Canyon 200	0	Starting oil	<0.1	0.8501	11	82	10	7	1	0.14	7
Green Canyon 200	30.7	Meso	<0.1	0.9071	121	77	13	9	1	0.11	9
Green Canyon 65	0	Starting oil	7.40	0.9365	177	38	40	14	8	0.57	112
Green Canyon 65	7.7	Meso	4.4	0.9509	457	38	42	15	5	0.33	75
Gulfaks	0	Starting oil	0.5	0.8701	13	60	35	5	1	0.2	5
Gulfaks	29.8	Meso	<0.1	0.9129	202	46	42	12	1	0.08	12
Hebron M-04	0	Starting oil		0.9189	154						0
Hebron M-04	8.8	Stable	<0.1	0.9344	676	46	32	9	13	1.4	115.57
Lago	0	Starting oil	<0.1	0.8907	153	56	31	11	3	0.27	33
Lago	10.5	Stable	<0.1	0.9128	7819	51	33	14	2	0.14	28
Lago Treco	0	Stable		0.9230	272	38	38	14	11	0.79	154
Lago Treco	16	Entrained		0.9661	16,160	32	38	15	15	1	225
Lucula	0	Stable	<0.1	0.8574	43	67	22	8	4	0.5	32
Lucula	26.9	Entrained	<0.1	0.9050	32,590	59	26	12	4	0.33	48
Malongo	0	Starting oil	<0.1	0.8701	63	62	25	9	4	0.44	36
Malongo	11.8	Stable	<0.1	0.8970	6359	60	28	10	3	0.3	30
Malongo	15.5	Entrained	<0.1	0.9026	1,0950	55	29	13	3	0.23	39
MARS—TLP	0	Starting oil	0.6	0.8883	33	60	24	11	6	0.52	58.3
MARS—TLP	8.42	Meso	0.1	0.9122	93	55	28	11	6	0.58	66.34
Maya	0	Starting oil		0.9255	280	38	39	8	16	2	128
Maya	15	Entrained	<0.1	0.9657	8670	31	41	10	17	1.7	170
Maya	22	Unstable	<0.1	0.9868	405,000	28	39	11	22	2	242
Mississippi Canyon 72	0	Starting oil	1.0	0.8649	16	64	27	7	2	0.29	14
Mississippi Canyon 72	18	Meso	<0.1	0.8966	76	58	32	9	2	0.22	18
Mississippi Canyon 72	26.2	Stable	<0.1	0.9095	195	52	34	11	3	0.27	33
Mississippi Canyon 807	0	Meso	0.2	0.8894	41	47	35	12	6	0.5	72
Mississippi Canyon 807	16.4	Stable	<0.1	0.9375	491	39	41	13	7	0.54	91
Morpeth EW921	0	Starting oil	0.3	0.8996	45	71	17	8	4	0.5	32
Morpeth EW921	15.2	Meso	0.2	0.9426	551	66	18	10	6	0.6	60
Neptune Spar (Viosca Knoll 826)	0	Starting oil	0.1	0.8687	17	65	28	6	1	0.17	6
Neptune Spar (Viosca Knoll 826)	15.4	Meso	<0.1	0.8925	84	62	29	7	2	0.29	14

TABLE 8.A4 (Cont'd)

Oil	% Evaporation	Visual Stability	H ₂ O content (%w/w)	Density g/ml (15°C)	Viscosity mPa·s	Saturates %	Aromatics %	Resins %	Asphaltenes %	A/R	A×R
Neptune Spar (Viosca Knoll 826)	22.6	Stable	<0.1	0.8986	187	61	29	8	2	0.25	16
North Slope (Middle Pipeline)	0	Starting oil	0.2	0.8761	16	52	35	9	5	0.56	45
North Slope (Middle Pipeline)	30.5	Meso	<0.1	0.9418	900	42	38	12	7	0.58	84
North Slope (Northern Pipeline)	0	Starting oil	0.1	0.8719	14	51	34	9	5	0.56	45
North Slope (Northern Pipeline)	31.1	Meso	<0.1	0.9402	748	44	37	12	7	0.58	84
North Slope (Southern Pipeline)	0	Starting oil	0.2	0.8766	18	54	32	8	6	0.75	48
North Slope (Southern Pipeline)	29.6	Meso	<0.1	0.9431	961	42	39	13	7	0.54	91
Oriente	0	Starting oil		0.8981	85	48	32	9	12	1.33	108
Oriente	21	Entrained		0.9426	6124	41	33	11	15	1.36	165
Platform Gail (Sockeye)	13.3	Stable	0.1	0.9645	7092	32	28	25	15	0.6	375
Platform Gail (Sockeye)	20.6	Entrained	<0.1	0.9810	161,500	27	29	25	19	0.76	475
Point Arguello	9.05	Stable	<0.1	0.9528	4988	31	33	19	17	0.89	323
Point Arguello Comingled											
Point Arguello Comingled	15.2	Entrained	<0.1	0.9688	41,860	27	33	21	19	0.9	399
Point Arguello Comingled	22.1	Unstable	0.1	0.9853	2,266,000	24	33	21	22	1.05	462
Point Arguello Heavy	0	Stable	<0.1	0.9447	3250	32	32	17	19	1.12	323
Point Arguello Heavy	8.88	Entrained	<0.1	0.9706	59,390	26	35	18	20	1.11	360
Point Arguello Heavy	17.8	Unstable	<0.1	0.9914	4,953,000	25	34	21	22	1.05	462
Sakhalin	0	Starting oil	<0.1	0.8632	4	61	32	6	1	0.17	6
Sakhalin	42.0	Meso	<0.1	0.9201	52	56	32	10	2	0.2	20
Sockeye Sweet	0	Starting oil	0.3	0.8792	20	55	31	10	4	0.4	40
Sockeye Sweet	26.9	Stable	<0.1	0.9229	321	48	33	14	6	0.43	84
Sumatran Heavy	0	Entrained	0.8	0.9312	13,300	46	30	13	10	0.77	130
Sumatran Heavy	5.26	Unstable	0.2	0.9374	12,900	45	32	16	8	0.5	128
Tapis	0	Starting oil	<0.1	0.8020	8	81	15	2	2	1	4
Tapis	13.9	Entrained	<0.1	0.8237	57	77	19	3	1	0.33	3
Tapis	28.6	Unstable	<0.1	0.8396	800	80	16	3	2	0.67	6
Viosca Knoll 826	0	Starting oil	0.2	0.8668	16	66	26	6	2	0.33	12
Viosca Knoll 826	24	Stable	<0.1	0.9067	325	59	29	8	3	0.38	24
Viosca Knoll 990	0	Starting oil	0.2	0.8337	7	73	22	4	1	0.25	4
Viosca Knoll 990	35.2	Stable	<0.1	0.8905	91	62	28	8	2	0.25	16
Waxy Light Heavy Blend	0	Starting oil	0.1	0.9311	184	39	35	21	5	0.24	105
Waxy Light Heavy Blend	12	Meso	<0.1	0.9582	2002	32	38	24	6	0.25	144
West Texas (2000)	0	Starting oil	<0.1	0.8474	9	79	15	6	1	0.12	4.2
West Texas (2000)	21	Meso	<0.1	0.8827	38	76	15	8	1	0.14	8.8
Zaire	0	Entrained	<0.1	0.8720	15,100	64	22	9	5	0.56	45
Zaire	23	Unstable	<0.1	0.9020	533,100	53	28	16	5	0.31	80

REFERENCES

- [1] NAS, *Oil in the Sea III, Inputs, Fates and Effects*, National Research Council, National Academies Press, Washington, D.C., 2002.
- [2] Fingas, M. and B. Fieldhouse, Studies on Crude Oil and Petroleum Product Emulsions: Water Resolution and Rheology, *Colloids Surf. A*, 333, 67, 2009.
- [3] Fingas, M., Models for Water-in-Oil Emulsion Formation, Chapter 10, in *Oil Spill Science and Technology*, M. Fingas, Editor, Elsevier Publishers, New York, 243–273, 2011.
- [4] Berridge, S.A., R.A. Dean, R.G. Fallows, and A. Fish, The Properties of Persistent Oils at Sea, *J. Instit. Petr.*, 54, 300, 1968.
- [5] McLean, J.D., P.M. Spiecker, A.P. Sullivan, and P.K. Kilpatrick, The Role of Petroleum Asphaltenes in the Stabilization of Water-in-Oil Emulsions, *Structure and Dynamics of Asphaltenes*, O.C. Mullins and E.Y. Sheu, Editors, Plenum Press, New York, 377, 1998.
- [6] Sjöblom, J., N. Aske, I.H. Auflem, O. Brandal, T.E. Havre, O. Saether, A. Westvik, E.E. Jonsen, and H. Kallevik, Our Current Understanding of Water-in-Crude Oil Emulsions: Recent Characterization Techniques and High Pressure Performance, *Adv. Colloid Interface Sci.*, 100–102, 399, 2003.
- [7] Sjöblom, J., P.V. Hemmingsen, and H. Kallevik, The Role of Asphaltenes in Stabilizing Water-in-Crude Oil Emulsions, *Asphaltenes, Heavy Oils and Petroleomics*, O.C. Mullins, E.Y. Sheu, A. Hammami, and A.G. Marshall, Editors, Springer Publications, Amsterdam, 549, 2007.
- [8] Czarnecki, J., Stabilization of Water in Crude Oil Emulsions. Part 2, *Energy Fuels*, 23, 1253, 2009.
- [9] Graham, B.F., E.F. May, and R.D. Trengove, Emulsion Inhibiting Components in Crude Oil, *Energy Fuels*, 22, 1093, 2008.
- [10] Varadaraj, R. and C. Brons, Molecular Origins of Crude Oil Interfacial Activity Part 3: Characterization of the Complex Fluid Rag Layer Formed at Crude Oil-water Interfaces, *Energy Fuels*, 21, 1617, 2007.
- [11] McLean, J.D. and P.K. Kilpatrick, Effects of Asphaltene Solvency on Stability of Water-in-Oil Emulsions, *J. Colloid Interface Sci.*, 189, 242, 1997.
- [12] McLean, J.D. and P.K. Kilpatrick, Effects of Asphaltene Aggregation in Model Heptane-Toluene Mixtures on Stability of Water-in-Oil Emulsions, *J. Colloid Interface Sci.*, 196, 23, 1997.
- [13] McLean, J.D., P.M. Spiecker, A.P. Sullivan, and P.K. Kilpatrick, The Role of Petroleum Asphaltenes in the Stabilization of Water-in-Oil Emulsion, *Structure and Dynamics of Asphaltenes*, O.C. Mullins and E.Y. Sheu, Editors, Plenum Press, New York, 377, 1998.
- [14] Gu, G., Z. Xu, K. Nandakumar, and J.H. Masliyah, Influence of Water-Soluble and Water-Insoluble Natural Surface Active Components on the Stability of Water-in-Toluene-Diluted Bitumen Emulsion, *Fuel*, 81, 1859, 2002.
- [15] Yarranton, H.W., H. Hussein, and J.H. Masliyah, Water-in-Hydrocarbon Emulsions Stabilized by Asphaltenes at Low Concentrations, *J. Colloid Interface Sci.*, 228, 52, 2000.
- [16] Kilpatrick, P.E. and P.M. Spiecker, Asphaltene Emulsions, *Encyclopedic Handbook of Emulsion Technology*, J. Sjöblom, Editor, Marcel Dekker, New York, 707, 2001.
- [17] Sztukowski, D.M. and H.W. Yarranton, Characterization and Interfacial Behaviour of Oil Sands Solids Implicated in Emulsion Stability, *J. Disp. Sci. Technol.*, 21, 299, 2004.
- [18] Groenzin, H. and O.C. Mullins, Asphaltene Molecular Size and Weight by Time-Resolved Fluorescence Depolarization, *Asphaltenes, Heavy Oils and Petroleomics*, O.C. Mullins, E.Y. Sheu, A. Hammami, and A.G. Marshall, Editors, Springer Publications, Amsterdam, 17, 2007.
- [19] Lobato, M.D., J.M. Pedrosa, A.R. Hortal, B. Martinez-Haya, R. Lebron-Aguilar, and S. Lago, Characterization and Langmuir Film Properties of Asphaltenes Extracted from Arabian Light Crude Oil, *Colloids Surf. A*, 298, 72, 2007.
- [20] Zhang, L.Y., R. Lopetinsky, Z. Xu, and J.H. Masliyah, Asphaltene Monolayers at a Toluene/Water Interface, *Energy Fuels*, 19, 1330, 2005.
- [21] Arla, D., A. Singuin, T. Palermo, C. Hurtevent, A. Graciaa, and C. Dicharry, Influence of pH and Water Content on the Type and Stability of Acidic Crude Oil Emulsions, *Energy Fuels*, 21, 1332, 2007.
- [22] Fingas, M.F. and B. Fieldhouse, A Review of Knowledge on Water-in-Oil Emulsions, *AMOP*, Vancouver, 1, 2006.
- [23] Spiecker, P.M., K.L. Gawrys, and P.K. Kilpatrick, Aggregation and Solubility Behavior of Asphaltenes and Their Subfractions, *J. Colloid Interface Sci.*, 267, 178, 2003.
- [24] Yang, X., H. Hamza, and J. Czarnecki, Investigation of Subfractions of Athabasca Asphaltenes and Their Role in Emulsion Stability, *Energy Fuels*, 18, 770, 2004.
- [25] Chandra, M.S., Z. Xu, and J.H. Masliyah, Interfacial Films Absorbed from Bitumen in Toluene Solution at a Toluene-Water Interface: A Langmuir and Langmuir-Blodgett Film Approach, *Energy Fuels*, 22, 1784, 2008.
- [26] Solovyev, A., L.Y. Zhang, Z. Xu, and J.H. Masliyah, Langmuir Films of Bitumen at Oil/Water Interfaces, *Energy Fuels*, 20, 1572, 2006.
- [27] Ali, M.F. and M.H. Alqam, The Role of Asphaltenes, Resins and Other Solids in the Stabilization of Water in Oil Emulsions and Its Effects on Oil Production in Saudi Oil Fields, *Fuel*, 79, 1309, 2000.
- [28] Nordli, K.G., J. Sjöblom, and P. Stenius, Water-in-Crude Oil Emulsions from the Norwegian Continental Shelf: 4. Monolayer Properties of the Interfacially Active Crude Oil Fraction, *Colloids Surf. A*, 57, 83, 1991.
- [29] Pereira, J.C., I. Lopez, R. Salas, F. Silva, C. Fernandez, C. Urbina, and J.C. Lopez, Resins: The Molecules Responsible for the Stability/Instability Phenomena of Asphaltenes, *Energy Fuels*, 21, 1317, 2007.
- [30] Havre, T.E. and J. Sjöblom, Emulsion Stabilization by Means of Combined Surfactant Multilayer (D-phase) and Asphaltene Particles, *Colloids Surf. A*, 228, 131, 2003.
- [31] Silset, A., A. Hannisdal, P. Hemmingsen, and J. Sjöblom, Emulsions of Heavy Crude Oils. II. Viscous Responses and Their Influence on Emulsion Stability Measurements, *J. Disp. Sci. Technol.*, 31, 1432, 2010.
- [32] Spiecker, P.M., K.L. Gawrys, C.B. Trail, and P.K. Kilpatrick, Effects of Petroleum Resins on Asphaltene Aggregation and

- Water-in-Oil Emulsion Formation, *Colloids Surf. A*, 220, 9, 2003.
- [33] Sjöblom, J., T. Skodvin, T. Jakobsen, and S.S. Dukhin, Dielectric Spectroscopy and Emulsions: A Theoretical and Experimental Approach, *J. Disp. Sci. Technol.*, 15, 401, 1994.
- [34] Sedghi, M. and L. Goual, Role of Resins on Asphaltene Stability, *Energy Fuels*, 24, 2275, 2010.
- [35] Yang, X., V.J. Vernito, and P.K. Kilpatrick, Dynamic Asphaltene-Resin Exchange at the Oil/Water Interface: Time-Dependent W/O Emulsion Stability for Asphaltene/Resin Model Oils, *Energy Fuels*, 21, 1343, 2007.
- [36] Gao, S., K. Moran, Z. Xu, and J. Masliyah, Role of Bitumen Components in Stabilizing Water-in-Diluted Model Oil Emulsions, *Energy Fuels*, 23, 2606, 2009.
- [37] Al-Sahhaf, T., A. Elsharkawy, and M. Fahim, Stability of Water-in-Crude Oil Emulsions: Effect of Oil Aromaticity, Resin to Asphaltene Ratio and pH of Water, *Pet. Sci. Technol.*, 26, 2009, 2008.
- [38] Binks, B.P. and A. Rocher, Effects of Temperature on Water-in-Oil Emulsions Stabilized Solely by Wax Microparticles, *J. Colloid Interface Sci.*, 335, 94, 2009.
- [39] Aguilera, B.M., J.G. Delgado, and A.L. Cardenas, Water-in-Oil Emulsions Stabilized by Asphaltenes Obtained from Venezuelan Crude Oils, *J. Disp. Sci. Technol.*, 31, 359, 2010.
- [40] Rondon, M., J.C. Pereira, P. Bouriat, A. Graciaa, J. Lachaise, and J-L. Salagar, Breaking of Water-in-Crude-Oil Emulsions. 2. Influence of Asphaltene Concentration and Diluent Nature on Demulsifier Action, *Energy Fuels*, 22, 702, 2008.
- [41] Borges, B., M. Rondon, O. Sereno, and J. Asuaje, Breaking of Water-in-Crude-Oil Emulsions. #. Influence of Salinity and Water-Oil Ratio on Demulsifier Action, *Energy Fuels*, 23, 1568, 2009.
- [42] Araujo, A.M., L.M. Santos, M. Fortuny, R.L.F.V. Melo, R.C.C. Coutinho, and A.F. Santos, Evaluation of Water Content and Average Droplet Size in Water-in-Crude Oil Emulsions by Means of Near-Infrared Spectroscopy, *Energy Fuels*, 22, 3450, 2008.
- [43] Kallevik, H., O.M. Kvalheim, and J. Sjöblom, Qualitative Determination of Asphaltenes and Resins in Solution by Means of Near-Infrared Spectroscopy: Correlations to Emulsion Stability, *J. Colloid Interface Sci.*, 225, 494, 2000.
- [44] Kallevik, H., S.B. Hansen, Ø. Saether, O.M. Kvalheim, and J. Sjöblom, Crude Oil Model Emulsion Characterized by Means of Near Infrared Spectroscopy and Multivariate Techniques, *J. Disp. Sci. Technol.*, 21, 245, 2000.
- [45] Song, M.-G., S.-H. Jho, J.-Y. Kim, and J.-D. Kim, Rapid Evaluation of Water-in-Oil (W/O) Emulsion Stability by Turbidity Ratio Measurements, *J. Colloid Interface Sci.*, 230, 213, 2000.
- [46] Dicharry, C., D. Arla, A. Siquin, A. Graciaa, and P. Bouriat, Stability of Water/Crude Oil Emulsions Based in Interfacial Dilational Rheology, *J. Colloid Interface Sci.*, 297, 785, 2006.
- [47] Xia, L., S. Lu, and G. Cao, Stability and Demulsification of Emulsions Stabilized by Asphaltenes or Resins, *J. Colloid Interface Sci.*, 271, 504, 2004.
- [48] Sztukowski, D.M. and H.W. Yarranton, Oilfield Solids and Water-in-Oil Emulsion Stability, *J. Colloid Interface Sci.*, 285, 821, 2005.
- [49] Yarranton, H.W., P. Urrutia, and D.M. Sztukowski, Effect of Interfacial Rheology on Model Emulsion Coalescence: II Emulsion Coalescence, *J. Colloid Interface Sci.*, 310, 253, 2007.
- [50] Aichele, C.P., W.G. Chapman, L.D. Rhyne, H.J. Subramani, and W.V. House, Analysis of the Formation of Water-in-Oil Emulsion, *Energy Fuels*, 23, 3674, 2009.
- [51] Midttun, Ø., H. Kallevik, J. Sjöblom, and O.M. Kvalheim, Multivariate Screening Analysis of Water-in-Oil Emulsions in High External Electric Fields as Studied by Means of Dielectric Time Domain Spectroscopy, *J. Colloid Interface Sci.*, 227, 262, 2000.
- [52] Aske, N., H. Kallevik, and J. Sjöblom, Water-in-Crude Oil Emulsion Stability Studied by Critical Electric Field Measurement: Correlation to Physico-Chemical Parameters and Near-Infrared Spectroscopy, *J. Petr. Sci. Eng.*, 36, 1, 2002.
- [53] Mostowfi, F., J. Czarnecki, J. Masliyah, and S. Bhattacharjee, A Microfluidic Electrochemical Detection Technique for Assessing Stability of Thin Films and Emulsions, *J. Colloid Interface Sci.*, 317, 593, 2008.
- [54] Tadros, Th.F., Fundamental Principles of Emulsion Rheology and Their Applications, *Colloids Surf. A*, 91, 39, 1994.
- [55] Johnsen, E.E. and H.P. Rønningsen, Viscosity of 'Live' Water-in-Crude-Oil Emulsions: Experimental Work and Validation of Correlations, *J. Petr. Sci. Eng.*, 38, 23, 2003.
- [56] Spiecker, P.M. and P.K. Kilpatrick, Interfacial Rheology of Petroleum Asphaltenes at the Oil-Water Interface, *Langmuir*, 20, 4022, 2004.
- [57] Aske, N., H.R. Orr, and J. Sjöblom, Interfacial Properties of Water-Crude Oil Systems Using the Oscillating Pendant Drop. Correlations to Asphaltene Solubility by Near Infrared Spectroscopy, *J. Disp. Sci. Technol.*, 25, 263, 2004.
- [58] Yarranton, H.W., D.M. Sztukowski, and P. Urrutia, Effect of Interfacial Rheology on Model Emulsion Coalescence: I Interfacial Rheology, *J. Colloid Interface Sci.*, 310, 246, 2007.
- [59] Moran, K., A. Yeung, and J. Masliyah, The Viscoplastic Properties of Crude Oil-Water Interfaces, *Chem. Eng. Sci.*, 61, 6016, 2006.
- [60] Gao, S., K. Moran, Z. Xu, and J. Masliyah, Role of Naphthenic Acids in Stabilizing Water-in-Diluted Model Oil Emulsions, *J. Phys. Chem.*, 114, 7710, 2010.
- [61] Khristov, K., S.D. Taylor, J. Czarnecki, and J. Masliyah, Thin Liquid Film Technique: Application to Water-Oil-Water Bitumen Emulsion Films, *Colloids Surf. A*, 174, 183, 2000.
- [62] Ridi, F., N. Verdal, P. Balioni, and E.Y. Sheu, Phase Separation Kinetics of Maya Asphaltene Emulsion and Free-to-Bound Water Transformation, *Fuel*, 88, 319, 2009.
- [63] Yang, X. and J. Czarnecki, The Effect of Naphtha to Bitumen Ratio on Properties of Water in Diluted Bitumen Emulsions, *Colloids Surf. A*, 211, 213, 2002.
- [64] Hemmington, P.V., A. Silset, A. Hannisdal, and J. Sjöblom, Emulsions of Heavy Crude Oils. I: Influence of Viscosity, Temperature and Dilution, *J. Disp. Sci. Technol.*, 26, 615, 2005.
- [65] Fingas, M.F. and B. Fieldhouse, Formation of Water-in-Oil Emulsions and Application to Oil Spill Modelling, *J. Hazard. Mater.*, 107, 37, 2004.

- [66] Fingas, M.F. and B. Fieldhouse, Modelling of Water-in-Oil Emulsions, *AMOP*, Edmonton, 335, 2004.
- [67] Fingas, M.F. and B. Fieldhouse, An Update to the Modelling of Water-in-Oil Emulsions, *AMOP*, Calgary, 923, 2005.
- [68] Fingas, M.F. and B. Fieldhouse, A Review of Knowledge on Water-in-Oil Emulsions, *AMOP*, Vancouver, 1, 2006.
- [69] Fingas, M., A New Generation of Models for Water-in-Oil Emulsion Formation, *AMOP*, Vancouver, 577, 2009.
- [70] Yetilmezsoy, K., M. Fingas, and B. Fieldhouse, Modeling Water-in-Oil Emulsion Formation Using Fuzzy Logic, *J. Multiple-Valued Logic Soft Comput.*, 18, 1, 2011.
- [71] Mackay, D., I.A. Buist, R. Mascarenhas, and S. Paterson, *Oil Spill Processes and Models*, Environment Canada Manuscript Report EE-8, Environment Canada, Ottawa, 1980.
- [72] Mackay, D., *A Mathematical Model of Oil Spill Behaviour*, Environment Canada Manuscript Report EE-7, Environment Canada, Ottawa, 1980.
- [73] Mackay, D. and W. Zagorski, *Studies of Water-in-Oil Emulsions*, Environment Canada Manuscript Report EE-34, Environment Canada, Ottawa, 1982.
- [74] Fingas, M.F., B. Fieldhouse, J. Noonan, P. Lambert, J. Lane, and J. Mullin, Studies of Water-in-Oil Emulsions: Testing of Emulsion Formation in OHMSETT, Year II, *AMOP*, Calgary, 29, 2002.
- [75] Fingas, M. and B. Fieldhouse, Water-in-Oil Emulsions and Application to Oil Spill Modelling, *Proceedings of the Fifth International Marine Environmental Modelling Seminar*, Sintef, Trondheim, Norway, 339, 2001.

OIL BEHAVIOR IN ICE-INFESTED WATERS

MERV FINGAS¹ AND BRUCE P. HOLLEBONE²

¹*Spill Science, Edmonton, Alberta, Canada*

²*Emergencies Science and Technology Section (ESTS), Environment Canada, Ottawa, Ontario, Canada*

9.1	Introduction	271
9.2	Spreading on Ice	271
9.3	Spreading on or in Snow	273
9.4	Spreading under Ice	273
9.4.1	Water Stripping Velocity under Ice	274
9.5	Spreading on Water with Ice Present	274
9.6	The Effect of Gas on Oil-under-Ice Spreading	275
9.7	Movement through Ice	276
9.8	Oil in Leads	277
9.9	Absorption to Snow and Ice	280
9.10	Containment on Ice	280
9.11	Heating Effect of Oil on the Surface of Ice	280
9.12	Oil under Multiyear Ice	280
9.13	Oil in Pack Ice	281
9.14	Growth of Ice on Shorelines and Effect on Oil Retention	281
9.15	Effect of Oil on Ice Properties	281
9.16	Concluding Remarks	283

9.1 INTRODUCTION

Extensive research efforts (including field tests and observations, laboratory tests, and numerical studies) have been expended to understand the interactions that occur when oil and oil and gas mixtures are discharged in cold waters or where ice is present. Research has been conducted using test tanks, and there have been several large field experiments. Much has been learned from accidental spills in ice-infested environments.

This chapter will focus on summarizing the knowledge gained from more than 40 years of study and also on the specific mathematical relationships that might be used to predict the behavior of oil in ice environments. A specialized study was conducted to combine existing knowledge into one report [1]. This study summarized key papers related to oil behavior in ice-infested environments and formed the foundation of earlier summaries of this type. Several studies since this time have been included. There have also been

some reviews on certain facets of this issue [2]. Recently, there have been a series of experiments to reexamine some of the earlier concepts [3,4].

This chapter summarizes the studies on oil behavior in ice environments under headings of the specific ice situation or behavioral mechanism. This section uses standard ice notation as described in the appendix of this book. The behavioral mechanisms will then be summarized. This chapter does not cover weathering processes such as evaporation or emulsification as these are covered in other sections of this book. Readers may also examine some of the papers specifically on this topic [5].

9.2 SPREADING ON ICE

Many of the oil spreading models on ice are based on the semi-empirical model of oil spreading on open water of Fay and Hoult [6]. The dynamics of spreading was divided into three successive regimes or phases characterized by opposing forces that dominated each phase. The phases are gravity–inertia, gravity–viscosity, and interfacial tension–viscosity. These results will be discussed in more detail later in this paper.

Glaeser and Vance studied the spreading of hot oil on ice using releases onto ice from openings of two sizes [7]. The ice was a crystalline mass about 5 cm thick. The ice surface absorbed the oil to a saturation level of about 25%. They calculated spreading as

$$L = 2.75 V^{1/4} t^{3/4} \quad (9.1)^1$$

where L is the length parameter (or D), V is the volume spilled, and t is the spreading time.

¹*Equations in this chapter are presented as in the original papers. No corrections were made unless the author was contacted. Some equations may not be unit consistent.*

Chen conducted studies in the field using small spills [8]. He found that there was no spreading below -19°C . He also found that warm oil spread rapidly.

McMinn developed spreading equations based on Fay and some empirical work [9]. The final radius was given by

$$\text{radius} = \sqrt[3]{[Qt/\pi z_0]} \quad (9.2)^1$$

where Q is the average flow rate, t is the time of flow (and therefore Qt would be the amount spilled), and z_0 is the average ice surface roughness ($\sim 3\text{ cm}$ fits the data best).

McMinn also concluded that gravity is the only important spreading force and thus radius can be given as a function of time:

$$\text{Radius} = [g \times Q/\pi]^{1/4} t^{3/4} \quad (9.3)$$

where Q is the average flow rate, g is the acceleration due to gravity, and t is the time of flow.

But experimental evidence yielded the following equation:

$$\text{Radius} = 1.3 (Q^3 g)^{0.1} t^{1/2} \quad (9.4)$$

where Q is the average flow rate, g is the acceleration due to gravity, and t is the time of flow.

McMinn and Golden later revised this equation to read [10]

$$\text{Radius} = 0.756 (Qg)^{1/4} t^{3/4} \quad (9.5)$$

where Q is the average flow rate, g is the acceleration due to gravity, and t is the time of flow.

While these were based on further theoretical considerations, the second round of field work results were consistent with Equation (9.4).

Buist et al. used the work of McMinn to compare test results. The axisymmetric forms of the equation were as follows [11]:

$$\text{Gravity-inertia regime: } r = k (gV)^{1/4} t^{1/2} \quad (9.6)$$

where r is the radius in cm, k is a constant (~ 1), g is the gravity constant in $\text{cm/g}\cdot\text{s}^2$ (6.67×10^{-8}), V is the volume of the oil in ml, and t is the time in seconds.

$$\text{Gravity-viscous regime: } r = k \left[\frac{gV^3 \rho_0}{\pi^3 \mu} \right]^{1/8} t^{1/8} \quad (9.7)$$

where all are the same as in (9.6) and ρ_0 is the density of the oil in g/cm^3 and

μ is the viscosity of the oil in $\text{g/cm}\cdot\text{s}$.

Chen et al. conducted laboratory experiments on spreading and developed a quasiempirical equation based partially on Fay [12]:

$$r/V^{1/3} = 0.24 [t\rho g V^{1/3}/\mu]^{1/5} + 0.35 \quad (9.8)$$

where r is the slick radius as a function of time, V is the volume spilled, t is the time after spillage, ρ is the oil density, and μ is the oil viscosity.

Equation (9.8) was found to reproduce laboratory-scale spreading on smooth ice surfaces. From this result, Chen concluded that oil-on-ice spreading in the absence of surface roughness effects is dominated by gravity and oil viscosity. Furthermore, over a temperature range of -3 to -14°C , the effect of temperature was accounted for by the change in viscosity with temperature.

Kawamura et al. conducted extensive laboratory experiments and some small-scale field experiments on the spreading of oil on ice [13]. Considering all the forces on a slick, Kawamura and coworkers concluded that the final size of the slick must have the form

$$A = V/h_f \left[1 - e^{-(t/\gamma)x} \right] \quad (9.9)$$

where A is the final area, V is the volume spilled, h_f is the final spill thickness, t is the spreading time, γ is an empirical spreading constant, and x is a slope term from experimental data.

Fitting experimental data for h_f , the final extent of spreading was determined to be

$$\frac{A_f}{V^{2/3}} = 6.0 \frac{V^{0.18} \rho_c^{0.33} g^{0.21}}{\mu^{0.24} \sigma^{0.09}} \quad (9.10)$$

where A is the final area, V is the volume spilled, ρ is the oil density, g is the gravity, μ is the viscosity, and σ is the interfacial tension with water.

Noting that σ and ρ are not greatly variable between oils, Kawamura et al. simplified Equation (9.10) to directly yield the slick thickness [13]:

$$h_f = 0.08 V^{0.15} \mu^{0.24} \quad (9.11)$$

Buist et al. used a variant of this equation to compare to experiments on ice [11]:

$$h_f = 0.04 V^{0.15} \mu^{0.24} \quad (9.12)$$

where h_f is the final spill thickness in cm, V is the volume of oil in ml, and μ is the dynamic viscosity of the oil in $\text{g/cm}\cdot\text{s}$.

Comparison of these forms of spreading has never been done on a rigorous basis. It is obvious that these equations will not show identical results because even simple quantities, such as spill amount, have quite different relationships in the different equations. In particular, Chen et al. concluded that gravity and viscosity were the dominant forces [12]. However, the work by Kamamura et al. showed that oil-ice interfacial tension was also important [13]. Tests showed that the Kawamura work as given in Equations (9.10 and 9.11) did correspond to field results to some degree [11].

Recently, Bellino et al. carried out experiments on spreading in a small ice channel [14]. These experimenters found that none of the spreading equations in the literature

worked well and overpredicted the spreading of an artificial oil by a very large amount.

9.3 SPREADING ON OR IN SNOW

Kawamura et al. extended the oil-on-ice equations to predict the spreading of oil on snow [13]:

$$\frac{A_f}{V^{2/3}} = 4.5 \frac{V^{0.2} d^{0.2} \rho_0^{0.8675} g^{0.4125} \mu^{0.05}}{(\zeta \rho_s)^{0.48} \sigma^{0.4375}} \quad (9.13)$$

where A_f is the final area; V is the volume spilled; d is the depth of the snow cover; ρ is the oil density; g is the gravity; μ is the viscosity; ζ is the snow type, 1 for fresh, 0.5 for crusty, and 0.1 for hard; ρ_s is the density of the snow; and σ is the interfacial tension with snow.

Similar to the ice equation, an expression for spill depth was also given:

$$h_f = 5.3 \times 10^{-4} V^{0.13} d^{-0.2} \mu^{-0.05} (\zeta \rho_s)^{0.48} \quad (9.14)$$

where symbol definitions are as in the preceding text.

Ross and Dickins and Buist et al. developed and tested an equation to predict the spread of oil in snow [11,15]:

$$r = \left[\frac{2K \rho_o g V}{\pi E^2 \mu} \right]^{1/4} t^{1/4} \quad (9.15)$$

where r is the radius in cm, ρ_o is the oil density in g/cm³, V is the spill volume in ml, g is the gravitational constant in cm/g·s² (6.67×10^{-8}), E is the porosity of the snow $= (1 - \rho_s/\rho_i)$ where in turn, ρ_s is the density of snow in g/cm³ and ρ_i is the density of ice in g/cm³, and μ is the viscosity of the oil in g/cm·s.

K is the specific permeability of snow (cm²), which is given by

$$K = 7.7 \times 10^{-2} d_0^2 e^{(-7.8\rho_s/\rho_i)} \quad (9.16)$$

where d_0 is the mean snow grain size (cm) and the other values are as in the preceding text.

9.4 SPREADING UNDER ICE

Glaeser and Vance studied the spreading of oil under ice using several small releases [7]. They found that the oil remained near the site with little spreading but filled nearby undulations under the ice. Keevil and Ramseier studied the subice behavior of oil by releasing hot crude oil under ice [16]. They found that the oil separated into droplets 0.1–0.2 cm in diameter. Upon contact with the ice sheet above, these droplets spread concentrically at about 1 cm/s and formed an oil lens about 1 cm thick, which then became trapped into the growing ice sheet.

NORCOR Engineering studied the behavior of oil released under a first-year ice sheet in the Beaufort Sea [17]. Upon release, the oil formed small droplets less than 1 cm in diameter and spread to form a thickness of no less than 0.8 cm and up to 20 cm in deep depressions under the ice. A lip of ice formed around the oil lenses within hours, and within days, the oil was completely encapsulated.

Chen et al. observed the spreading of oil under a freshwater ice sheet in a small test tank [18]. In the absence of currents, the spreading rate was proportional to the 1/4 power of the elapsed time. In the presence of a strong current, the droplets traveled a distance before rising and many droplets did not adhere to the ice surface.

Greene et al. studied the spreading and behavior of oil using an experimental spill of warm crude oil under the ice of a freshwater pond [19]. The oil spread to thicknesses of about 0.5–2 cm. Spreading lasted only a few hours.

Dome Petroleum studied the behavior of oil and gas releases (simulated by compressed air) under first-year ice in the Beaufort Sea [20]. The release rate was equivalent to 400 m³/day of oil (2500 barrels/day) at a gas-to-oil ratio of 200:1. The particle size of droplets under the ice varied with distance from the centre of the rise point. This factor can be given by

$$D = \sqrt{\frac{18\mu V_c Z}{gx(\rho_w - \rho_p)}} \quad (9.17)$$

where D is the droplet size, μ is the oil viscosity, V_c is the drift current under the ice (here, it was 0.04 m/s), g is the acceleration due to gravity, Z is the vertical distance from the discharge to the ice sheet (here, it was 5 m), x is the lateral drift distance, ρ_w is the density of the water, and ρ_p is the density of the oil.

Goodman and coworkers developed a technique using molding to copy under-ice surface contours and then measure the volume of the under-ice surface [21]. This was carried out at several locations. Literature values of storage volume fractions were reported to range from 0.01 to 0.06 (m³/m²).

Uzuner and coworkers studied the movement of oil under a smooth ice sheet in a test flume [22]. They found that the velocity of crude oil could be approximated as

$$U_s = 8.6 \times 10^{-6} U_w^{4.29} \quad (9.18)$$

where U_s is the velocity of the oil and U_w is the water velocity.

The aforementioned equation was applicable for water velocities up to 28 cm/s. For velocities of 28–36 cm/s, the following equation was developed:

$$U_s = 1.1 U_w - 16.6 \quad (9.19)$$

where U_w is in cm/s.

A separate equation was also developed for diesel fuel that showed significantly different behavior.

Puskas and McBean studied the movement of oil under ice and developed a theoretical model that was calibrated using a small-scale laboratory flume [23,24]. The following equation resulted:

$$U_s = 0.0185 \frac{h \rho_w}{\mu_o} R_t^{-1/5} (U_w - 2U_s)^2 \quad (9.20)$$

where U_s is the velocity of the oil, h is the thickness of the oil, ρ is the density of the water, R_t is the Reynolds number, μ_o is the viscosity of the oil, and U_w is the water velocity.

Puskas and coworkers developed the aforementioned equation further and developed equations for slick thickness based on static fluid equations [23].

Yapa and Chowdhury tested an empirical equation of the following form [25]:

$$R = K \left[\frac{\Delta \rho g Q^3}{\mu_o} \right]^{1/8} t^{1/2} \quad (9.21)$$

where R is the radius of the oil slick, K is a constant, $\Delta \rho$ is the density difference between water and the oil, g is the acceleration due to gravity, Q is the discharge rate, μ_o is the viscosity of the oil, and t is the time after the spill started.

Yapa and Chowdhury also developed the following expression for the final radius of the oil spreading under ice [25]:

$$R_F = \left(\frac{1}{2\pi^2} \right)^{1/4} \left(\frac{\Delta \rho g}{\sigma_n} \right)^{1/4} V^{1/2} \quad (9.22)$$

where R is the final radius of the oil slick, $\Delta \rho$ is the density difference between water and the oil, g is the acceleration due to gravity, σ is the interfacial tension of the oil and water, and V is the total volume discharged.

Izumiyama and Konno studied the spreading of oil under ice surfaces in a test tank and correlated the data with the values in Equation (9.22) [26,27].

Peishi et al. studied the profiles of ice movement using flume test results and mathematical modeling techniques based on physical profiles of the oil [28]. They found that under ice oil did not move until the water velocity reached 6 cm/s.

In summary, under quiescent conditions (low currents), the oil will spread upon reaching the under-ice surface under the combined actions of buoyancy, viscous, and surface tension forces. A number of force-balance models have been developed to predict spreading under a smooth ice bottom. However, in practice, sea ice is characterized by significant under-ice roughness. Field observations have shown that the final under-ice configuration is dominated by the under-ice topography. The oil has been observed to spread systematically, filling the nearest under-ice depressions first before overflowing into the next depression.

Local ice conditions are much more important to the final oil disposition than microscale spreading behavior. A volumetric analysis is considered to be the most effective approach for predicting the spread of large oil and gas

discharges under an ice sheet, and several general spreading models have utilized this method. The key parameters are oil and gas volumes, under-ice storage capacity, and potential for gas venting through the ice. Some field studies have been carried out to measure typical under-ice storage capacities. All of the volumetric models developed to date have used an empirical approach to predict the under-ice storage capacity. This is a reliable approach, considering that a relatively extensive base of field data is available.

Comparison of the numerical under-ice spreading models has shown that the results are not comparable. The reason for this is likely that factors such as the under-ice roughness were not considered in formulation.

9.4.1 Water Stripping Velocity under Ice

When oil is under ice, the droplets of oil will be driven to the upper ice surface by buoyancy and will move after a certain water velocity is attained. This water velocity is sometimes called the stripping velocity or critical velocity. The presence of currents will affect the movement of the oil under ice. At relatively high currents (i.e., >20 cm/s as observed in laboratory tests), oil and gas may be stripped from the under-ice depressions. At lower currents, field tests have shown that the oil rising through the water column will be carried downstream until it reaches the under-ice surface, after which it will remain adhered to the rough skeletal layer of growing ice.

Buist et al. employed the earlier equation of Cox and Schultz to predict the water stripping velocity [11,29]:

$$U_{th} = C_i \left[\frac{305.79}{88.68 - \mu_o} \right] \quad (9.23)$$

where U_{th} is the threshold (stripping or critical) water velocity (cm/s); C_i is the under-ice roughness factor, 1 for smooth freshwater ice, 2 for saline ice, 3 for undulating freshwater ice, 4 for undulating sea ice, and 6 for rubble ice; and μ_o is the oil viscosity in poise.

9.5 SPREADING ON WATER WITH ICE PRESENT

Spreading on water with ice present has been the subject of modeling for many years. Historically, there were two rules of thumb—if the ice coverage was less than 30%, the oil movement and spreading would not include the ice and if the ice coverage was greater than 60–70%, the oil would drift with the ice [4,5,30]. The spreading of oil is very much reduced in the presence of ice, often resulting in thicknesses as great as centimeters [31].

Khelifa summarized the modeling work carried out on oil spreading and transport when ice was present [32]. This paper focuses on the transport of oil on water with ice and the modeling of these facets. An extensive review is given of the Johansen approach in which correction factors are applied to various current components and states in which



FIGURE 9.1 Oil spreading among pack ice floes. Here, the presence of much frazil ice prevents spreading and adsorbs much of the oil.

the oil is found such as trapped under ice, etc. [33,34]. Further, a transition matrix is created to apply between the various states in which oil is found.

Sayed and Løset studied the spreading of oil on water and among brash ice. They found that the following equation could describe their data [35]:

$$\frac{2.5 \times 10^6 \mu R^3 R'}{\gamma V} + \frac{2.5 \times 10^4 \sigma R}{\gamma \sqrt{V}} = 1 \quad (9.24)$$

where μ is the oil viscosity, R is the final radius, R' is the time derivative of the radius, σ is the oil surface tension, and γ is the oil density.

Laboratory testing of oil spreading in brash ice (5–8 tenths concentration) has shown that the ice effectively confines the oil, but as the conditions are not comparable to actual ice environments, the equations developed are likely inadequate to describe the situation in the field. A modified Fay equation for spreading based on the results of small field spills represents the most suitable analysis to date but requires more verification to be used with confidence.

Gjøsteen developed a model for spreading in cold waters. The following generalized equation was proposed [36]:

$$(\rho_o h U)_t + (h \rho_o U^2)_x + (h \rho_o U V)_y + P_x + S_x + M_{oil} + M_{water} = 0 \quad (9.25)$$

where ρ_o is the density of the oil, h is the thickness (depth) of the oil, U is the mean velocity in the x direction, V is the mean velocity in the y direction, P_x is the pressure integrated over thickness, S_x is the surface tension, M_{oil} is the stress from oil viscosity, and M_{water} is the stress from water drag.

Analytical expressions are developed for each of the aforementioned expressions and the results compared to experimental data from the author's own data [37]. The

comparison between the calculated spreading rates and the experimental rates was reported to be favorable.

Oil can be seen spreading among pack ice in Figure 9.1. In this case, much of the oil adsorbs to the frazil ice present.

9.6 THE EFFECT OF GAS ON OIL-UNDER-ICE SPREADING

Purves studied the spread and behavior of oil released under saline ice in a test tank along with a 60:1 ratio of gas to oil [38]. The oil spread to thicknesses of about 0.2 cm and spread more rapidly and more thinly in the presence of gas. While the oil appeared to coat the gas bubbles, at the 60:1 ratio used in this experiment, there was insufficient oil to coat all the gas. Furthermore, it was found that the presence of the gas did not change the release rate of the oil when the ice melted. Gas was released quickly upon melting.

Dome Petroleum used compressed air to simulate a gas and oil well blowout under ice [20]. Release of gas only resulted in ice fractures and ice heaving. Discharges under ice in April and May resulted in less fractures and heaving because gas was able to penetrate the ice more readily. When oil was released with the air, it coated the air bubbles under the ice. Most of the bubbles were a few millimeters in diameter. The gas-to-oil ratio was 200:1.

As gas is likely to be released in much greater quantities than oil during a blowout, the area of contamination will be affected significantly if the gas is vented (which can occur if the ice sheet is cracked by the buoyant force of the trapped gas bubble). One of the available spreading models analyzes venting by determining, at each time step, if the ice has failed, while the others utilize an empirical treatment. The former approach is preferable as it treats ice failure and gas venting as a separate event impacting the spread of the oil and gas.

9.7 MOVEMENT THROUGH ICE

NORCOR Engineering studied the behavior of oil released under a first-year ice sheet in the Beaufort Sea [17]. The oil rapidly became encapsulated and remained in place until February and March when it began to migrate through former brine channels to the surface. About 20 cm of vertical movement had taken place by March. This rate increased until April when a lens of oil under 150 cm of ice appeared on the surface in less than an hour. Figure 9.2 shows the oil resurfaced in spring from this experiment.

Martin studied brine channel formation in the field [39]. When sea ice forms, the surface ice has a saline layer. When the

ice warms in spring, the surface salt layer liquefies and drains through the ice, preferentially through column interstitial spaces, leading to the formation of top-to-bottom brine channels.

Dome Petroleum studied the release of oil and air (to simulate gas) under first-year ice in the Beaufort Sea [20]. Several releases were made from December to May. The December spill started appearing on the surface in early June. The April and May spills started appearing in mid-June. Oil was released to the surface by both migration through brine channels and simple ice ablation (melting of the ice). The oil surfaced slowly in all cases. Figure 9.3 shows some of the ice removed for testing after this experiment. The oil was encapsulated several days after the experiment.



FIGURE 9.2 Oil on the surface of the ice in the Beaufort Sea. This oil rose through the first-year ice in the spring.



FIGURE 9.3 A large piece of ice removed with encapsulated oil after an experiment in the Beaufort Sea. This oil was encapsulated only several days after release under the ice.

Buist et al. conducted experiments in which oil and water-in-oil emulsion were placed under first-year ice in the southern Beaufort Sea [40]. Both the oil and emulsion were encapsulated within 48 h. The oil migrated to the surface through the brine channels, and the emulsion remained as emulsion and appeared on the surface only by ice ablation.

Payne et al. conducted a series of indoor and outdoor experiments to evaluate the fate and behavior of oil spills with and under ice [41]. They presented the rise rate velocity of oil through an ice sheet as

$$\mu_z = \frac{(\rho_w - \rho_o)g\delta d^2}{32L\mu} \quad (9.26)$$

where μ_z is the rise rate in mm/s; ρ_o and ρ_w are the densities of the oil and water, respectively; g is the gravitational constant (980 cm/s²); δ is the brine channel diameter (taken here as 0.36 cm); L is the ice thickness; and μ is the oil viscosity (here 5.5 g cm/s).

Payne et al. found a rise rate of 0.35 mm/s for the experiment they conducted [41]. They noted that Martin had found a rise rate of double this amount [38]. However, it was noted that different oil viscosities and ice conditions can change the rise rate by a large amount.

Payne et al. also attempted to calculate a volume flow rate of oil to the surface as [41]

$$V = \frac{\pi d^2}{4} \mu_z N' A \quad (9.27)$$

where V is the volume rate in ml/h, δ is the brine channel diameter (taken here as 0.36 cm), μ_z is the rise rate in mm/s, N' is the number of brine channels per area (here 0.01 cm⁻²), and A is the area of the spill (cm²).

Payne et al. calculated a volumetric flow rate of about 27 ml/h for their experiment, which was higher than experimental values [41]. Several possible reasons were given for this difference.

When the oil and gas are discharged under a growing ice sheet, the oil and gas will be encapsulated in the ice by subsequent growth beneath it. Two aspects of this process need to be considered: (i) the time required for encapsulation to occur and (ii) the effect of the encapsulated oil and gas on subsequent ice growth. Some studies of this encapsulation have been conducted [42–44].

The time required for encapsulation to occur depends on many factors, including the air–ice–water temperature gradient, the under-ice topography, and the volume and properties of the spilled oil and gas. During all of the field tests to date, the oil and gas have been encapsulated relatively quickly (i.e., within about 24 h, sometimes partially within 4 h). The encapsulation time has not been analyzed numerically to date. An empirical approach is recommended at present as this is simple and a relatively large database of field experience is available to document the effect of the encapsulated oil and gas on subsequent ice growth. Numerical models based on heat flow across the oil

and gas lens generally predict that the ice growth beneath the lens will be reduced (as the thermal conductivity of the oil is less than that of the ice for most field situations). However, no measurable difference in thickness between oiled and unoiled ice has been observed at field spills. This can be attributed to the presence of a snow cover (and its natural variations in thickness), which produces natural variations in ice thickness that are greater than those induced by the oil and gas. Unless very thick pools are involved, the effect of encapsulated oil on subsequent ice growth will probably be minimal.

The available field and laboratory test data show that the encapsulated oil will be released in the spring as the ice sheet deteriorates. Oil escapes from the ice sheet by a combination of two general processes: (i) vertical rise of the oil through the brine channels in the ice and (ii) ablation of the ice surface down to the oil lens in the ice. For a combined oil and gas spill, the gas will be released in advance of the oil. Both release processes are important and have been observed to occur in the field. The relative quantities of oil released depend on several factors including the depth of the oil lens in the ice, the rate of brine channel opening, and the configuration of the oil in the ice, for example, discrete droplets versus pools of oil. No theoretical models are available to describe the release of oil by surface ablation. Two simple models have been developed to predict release by vertical migration, and these models have been compared to laboratory test results. However, the combination of vertical migration and surface ablation has not been analyzed. As proven models are not available, an empirical approach is considered to be the most reliable method at present for modeling oil release from the ice sheet.

During all of the field spills conducted to date under first-year sea ice, the encapsulated oil was released in the next melt season. The only information relating to the release from under multiyear ice comes from one series of small-scale field spills. These data indicate that the oil will rise quickly to the surface through cracks but persist for at least two melt seasons and possibly five on the surface of the ice (as multiyear ice is thicker and the brine channels may be discontinuous).

9.8 OIL IN LEADS

Cammaert conducted preliminary tank tests on the movement of oil out of leads [45]. It was found that a current of 44 cm/s was required to force oil out of an undulation 1.5 cm deep and a current of 25 cm/s was required to force oil out of an undulation 0.5 cm deep.

Buist and coworkers studied the behavior of oil in leads using a test tank [46]. Experiments showed that only a fraction of oil was incorporated into newly formed ice. A formula for wind herding was developed:

$$T_h = 1.01h_0 + 0.72U \quad (9.28)$$

where T_h is the thickness of the wind-herded slick, h_0 is the original thickness (mm), and U is the wind speed (m/s).

MacNeill and Goodman studied the effect of lead closure rates on the movement of oil up or down under the ice surface [47]. Tests were conducted in an outdoor basin. It was found that at low lead closure rates most of the oil was forced under the ice when the lead closed. At lead closure rates of 12 cm/s or above, most of the oil was forced up to the top of the ice.

The phenomenon known as “lead pumping” has been postulated as a mechanism to redistribute oil from the water to the ice surface under dynamic conditions. Lead pumping

is the movement of oil to the surface of the ice as a result of the pumping action of rapid lead closure. An analysis of lead closure rates in the Beaufort Sea and Lancaster Sound revealed that typical rates were much lower than those required for lead pumping. Except for the case of ice closing behind ships’ tracks, lead closure is unlikely to serve as a mechanism for distributing oil onto ice surfaces.

Figures 9.4, 9.5, 9.6, 9.7, and 9.8 show oil in narrow leads. The specific fate of this oil, if left alone, is not exactly known.



FIGURE 9.4 Oil trapped in a narrow lead. The oil in this case is several centimeters thick.



FIGURE 9.5 Oil in a lead before much spreading or adsorption has taken place.

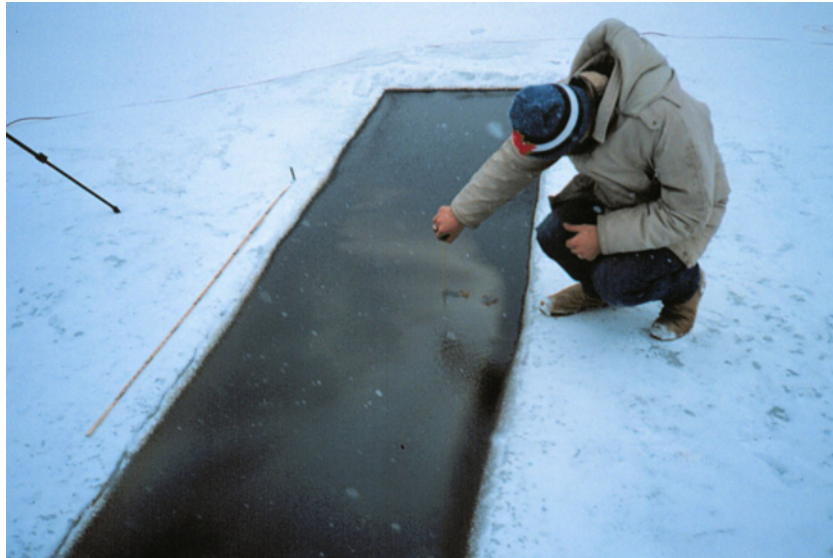


FIGURE 9.6 Sampling of oil in a man-made lead.

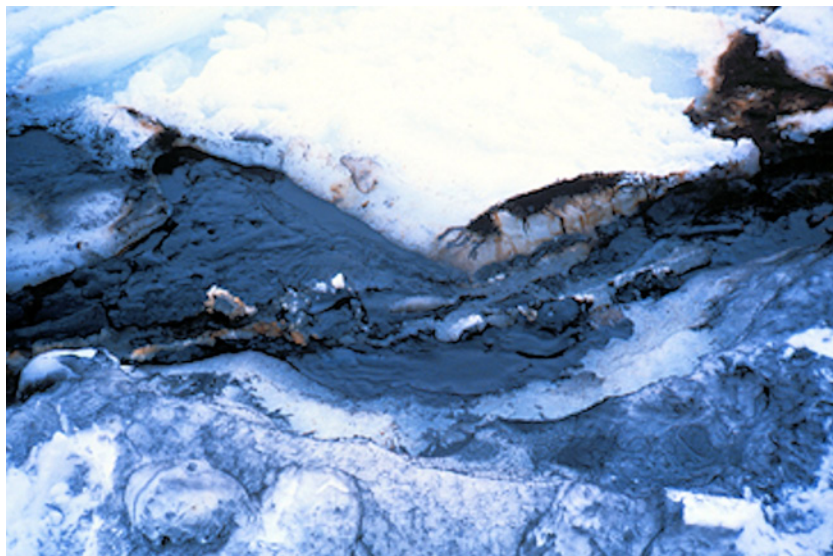


FIGURE 9.7 Oiled lead in pack ice.

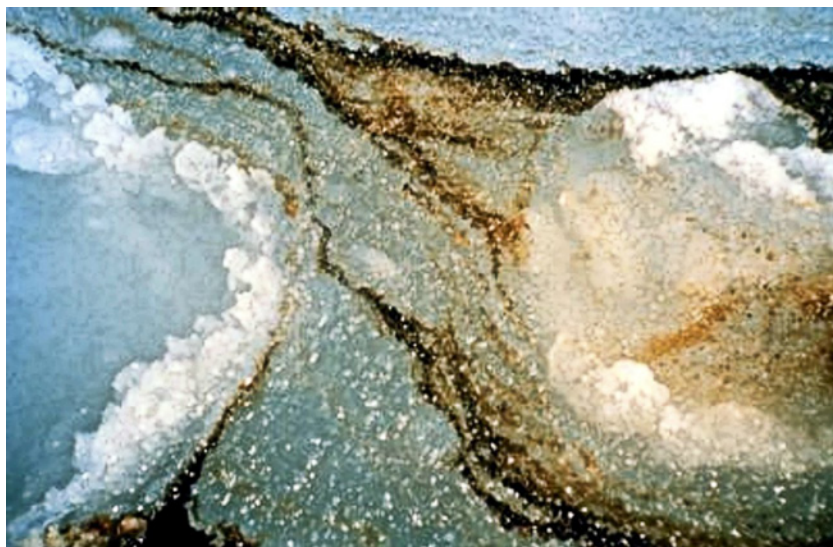


FIGURE 9.8 A close-up of oil adsorbed to frazil ice in pack ice. This picture covers about 1 m² area. This type of behavior has not been studied extensively.



FIGURE 9.9 A close-up of oil on top of ice. This oil did not adsorb to the frazil ice around the pack ice and is stationary on top of the pack ice.

9.9 ABSORPTION TO SNOW AND ICE

McMinn found that snow absorbed 20% oil by volume to yield a mulch that was fairly stable [9]. Buist et al. report a value of 25% [46]. Owens et al. report on earlier experiments that show an initial absorption of Prudhoe Bay crude of 70% declining exponentially over 6 days to about 40% [48]. Owens also noted that diesel fuel showed an initial adsorption of 40% declining to slightly less than 20% over 6 days. These test results are for fresh snow and would be different for other types. Owens et al. note that few tests have been carried out and little has been done to characterize the snow in any tests carried out [48].

Adsorption of oil to ice is a topic not well studied. Figure 9.8 shows oil adsorption to frazil ice, and Figure 9.9 shows oil that was pumped to the surface of a lead. In these cases, the oil did not adsorb to frazil ice or ice crystals.

9.10 CONTAINMENT ON ICE

Deslauriers and coworkers studied the fate and behavior of an oil spill incident in Buzzards Bay [49]. Rafted ice led to the formation and containment of oil pools of up to 0.15 m in depth. These pools held approximately 30% of the spilled oil. The ice prevented oil from reaching nearshore areas. After ice breakup, oiled floes distributed oil over a wide area. Oil was not contained by the

ice edge and oil moved under ice with strong tidal currents of about 0.5 m/s.

9.11 HEATING EFFECT OF OIL ON THE SURFACE OF ICE

Glaeser and Vance studied the heating of oil on ice using releases onto ice [7]. They found that there were large variances, but overall, oil absorbed 30% more heat from the sun than did normal ice. Chen measured the temperature of oil under snow and found that the oil temperature was 3–6°C higher than the air temperature [8]. NORCOR measured the effect of albedo on the surface and found that the presence of oil may have accelerated the melting of the ice by as much as 1–3 weeks [17]. The albedo of the oil test area was as low as half of the surrounding unoiled area. The albedo of the oil was similar to that of melt water pools on the surface. Subsequent field studies did not detect any increase in breakup caused by simulated oiling [20].

9.12 OIL UNDER MULTIYEAR ICE

Comfort and Purves report on a study of an experimental crude oil spill under multiyear ice in the Canadian high Arctic [50]. Oil was placed under the ice and, when the site was revisited for the first time, most of the oil had migrated to the surface. A revisit to the site 5 years later showed no oil left, even on the surface. The oil had presumably been absorbed by the snow and carried away by winds.

9.13 OIL IN PACK ICE

The movement of oil in pack-ice conditions is similar to that on open water given that the ice is less than about 50% or 5/10 [32]. In closer pack ice, however, this changes. Ross and Dickins report on three experimental spills in pack ice off the eastern coast of Canada [15]. Conditions for each spill varied and ranged from relatively open to closed conditions. The spreading of oil was measured and then compared to an adjusted Fay model and the adjusted empirical model of Kawamura. The adjusted Fay model was able to predict the spreading to a large degree, and the Kawamura model was less successful. The adjusted Fay model is as follows:

$$\text{Gravity-inertia: } A = 4.1(\Delta g V t^2)^{1/2} \quad (9.29)$$

$$\text{Gravity-viscous: } A = 6.6 \left[\frac{\Delta g V^2 t^{3/2} \rho^{1/2}}{\mu^{1/2}} \right]^{1/3} \quad (9.30)$$

$$\text{Surface tension-viscous: } A = 16.6 \left(\frac{\sigma^2 t^3}{\rho \mu} \right)^{1/2} \quad (9.31)$$

For spreading in pack ice, the authors recommend using

$$A_{\mu 1} = \left[\frac{\mu_o}{\mu} \right]^{-0.15} (1 - f_i)^A \quad (9.32)$$

where A is the area, $A_{\mu 1}$ is the corrected area for spreading in pack ice, Δ is the fractional buoyancy of the oil, g is the acceleration due to gravity, V is the slick volume, t is the time, ρ is the oil density, μ is the viscosity of the water, μ_o is the viscosity of the oil, σ is the spreading coefficient, and f_i is the fraction of ice cover.

9.14 GROWTH OF ICE ON SHORELINES AND EFFECT ON OIL RETENTION

Oil fate and behavior on shorelines can be affected very much by the growth of ice structures on shorelines. If the oil arrives before these structures form, then the oil is trapped until the melting season. If the oil arrives at the shoreline after these structures form, then the oil may be kept off the shoreline. Øksenvåg et al. studied the formation of ice on shorelines in northern Norway noting that the most common types observed were frozen swash and ice foot [51]. Frozen spray and grounded floes were also common. Freshwater flowing over the backshore areas froze in the supratidal and sometimes upper intertidal areas. Models for frozen spray

on ships were adapted to the shoreline situation and found fit reasonably well. Inputs included temperature, wind speed, and wave height.

9.15 EFFECT OF OIL ON ICE PROPERTIES

NORCOR measured the effect of five large, oiled under-ice surfaces on the growth rate of ice compared to surrounding areas [17]. They found no measurable effect on ice growth. Chen et al. studied oil under freshwater ice in a small basin and found that the ice above an oil lens was 2–6°C cooler [18]. This was attributed to the insulating effect of the oil. Greene and coworkers studied the behavior of a warm oil release under ice in a freshwater pond [19]. The heat transfer to the water and ice occurred rapidly and did not affect ice growth after a few hours.

Martin and coworkers studied the growth of grease and pancake ice in a test tank [52]. It was found that oil released to the water surface quickly surfaced to the top of the grease ice. The presence of the oil did not affect the ice growth. Oil spilled under pancake ice rose to the surface around the edges of the individual pancake formations. Once the oil was on the surface of the pancake ice, the rims of the pancake formation served to contain it.

Wilson and Mackay studied the incorporation of oil into grease ice during formation using a small laboratory test tank [53]. It was shown that large amounts of oil are incorporated into the ice as grease ice is formed. Increasing turbulence increased the amount of oil incorporated.

Li et al. studied the effects of oil on slush ice, noting that the waves and temperature were important factors influencing the properties of the slush ice and the absorption of oil [53].

Oil in developing and brash ice has been observed to behave in many ways during various spills of opportunity, including the following [54–56]:

- Trapped in the ice slurries at the ice edges and incorporated into the ice crystalline structure (*Arrow* spill of Bunker C)
- Held in the crystalline structure of grease ice (Matane, Quebec, spill of No. 6 oil)
- Transported under ice for large distances, dispersed under the ice as leads opened, and incorporated into deformed ice as the leads closed (Buzzards Bay, MA, spill of No. 2 oil)
- Carried beneath water and ice, mixing in brash ice, and trapped on floe surfaces (*Kurdistan* spill of Bunker C)

Field and laboratory tests of oil behavior in developing ice (frazil, grease, slush, and pancake ice) are inconclusive. Oil

has been observed to surface easily through slush if some agitation is present, but too much agitation can result in incorporation of oil into the ice. Horizontal spreading of oil seems to be hindered by slush, resulting in equilibrium thicknesses greater than that of open water spreading. Wave action has been observed to distribute oil onto the surfaces of

pancake ice during two laboratory tests and during the *Kurdistan* spill. Figures 9.10 and 9.11 show oil after the *Kurdistan* spill. Figure 9.12 shows ice sandwiched between oil layers. This spill in Siberian Russia was studied during several seasons, and several interesting oil-ice interactions were observed.

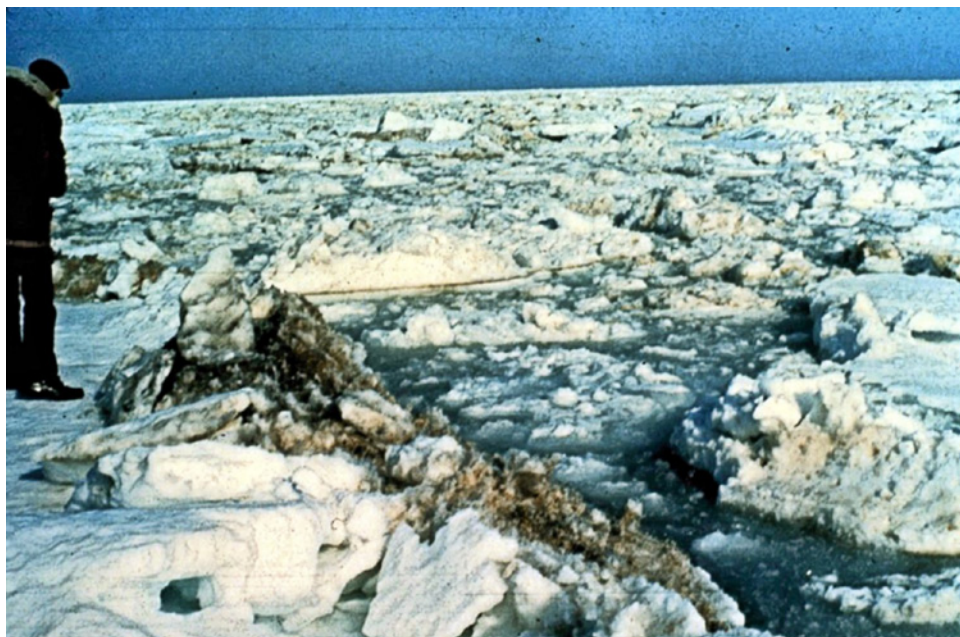


FIGURE 9.10 A view of oiled ice about 1 month after the *Kurdistan* spill off the east coast of Canada. Much of the oil resided in such oiled ice margins. Most of this oil was released to the water during the spring melt.



FIGURE 9.11 A close-up of some of the oiled ice during the *Kurdistan* spill. In this case, the oil is adsorbed to the granular ice.

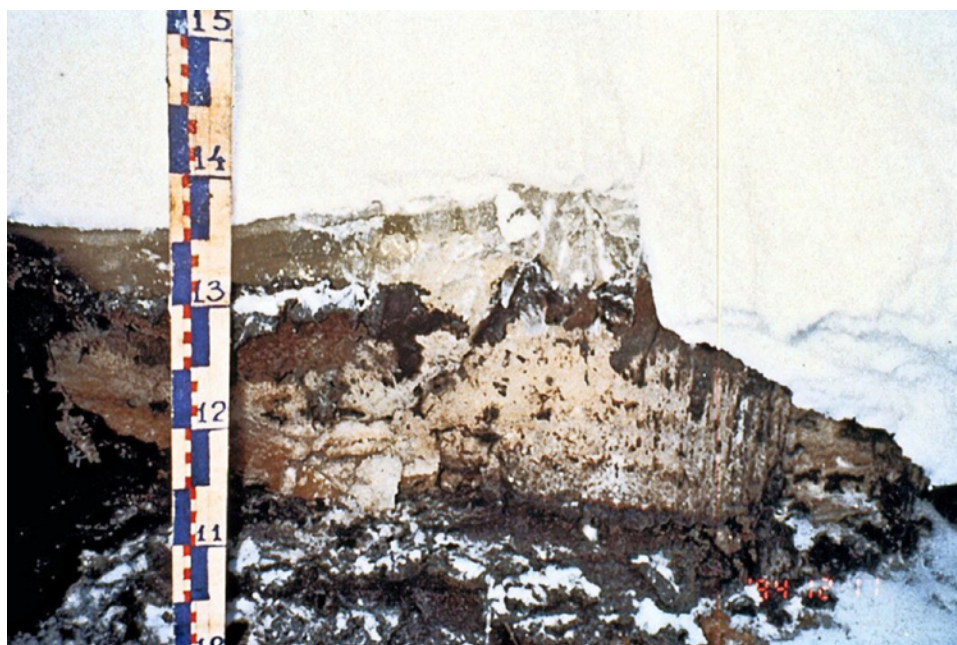


FIGURE 9.12 A view of oil sandwiched between layers of ice. This occurred in a creek where two separate oil releases impacted the area and in one case the oil was encapsulated under the ice and in another flowed over the ice. This spill occurred in Siberian Russia and was studied through various seasons.

9.16 CONCLUDING REMARKS

Oil spills in ice-infested waters undergo complex behavior and fate processes. There is some understanding of the processes involved in oil interaction with ice. Modeling of this behavior can be carried out at present using many of the concepts presented earlier. There are gaps and uncertainties in some of the algorithms. Some of the equations are unit inconsistent and appear to have inconsistencies. More research, especially quantitative, is needed before there is a full capability to predict oil behavior and fate in ice-infested environments. In addition, much of the work is now 30 years or more old and some measurement methods have improved to the extent that older results may be significantly updated.

REFERENCES

- [1] Hollebone, B.P., M.F. Fingas, and D. Permann, *The Fate and Behaviour of Oil in Freezing Environments*, Unpublished Report, Environment Canada, Ottawa, 2000.
- [2] Yapa, P.D. and L.K. Dasanayaka, State-of-the-Art Review of Modelling Oil Transport and Spreading in Ice Covered Waters, *AMOP*, Vancouver, 893, 2006.
- [3] Sørstrøm, S.E., P.J. Brandvik, I. Buist, P. Daling, D. Dickins, L.-G. Faksness, S. Potter, J.F. Rasmussen, and I. Singaas, *Joint Industry Program on Oil Spill Contingency for Arctic and Ice-Covered Waters*, Sintef Report A 14181, Trondheim, Norway, 2010.
- [4] Faksness, L.-G., R.L. Daae, P.J. Brandvik, F. Leivik, and J.F. Borseth, *Oil Distribution and Bioavailability Field Experiment—FEX 2009*, Sintef Report A 16584, Trondheim, Norway, 2010.
- [5] Brandvik, P.J. and L.-V. Faksness, Weathering Processes in Arctic Oil Spills: Meso-Scale Experiments with Different Ice Conditions, *Cold Regions Sci. Technol.*, 55, 160, 2009.
- [6] Fay, J.A. and D.P. Hoult, *Physical Processes in the Spread of Oil on a Water Surface*, AD-726 281, United States Coast Guard, Washington, D.C., 1971.
- [7] Glaeser, J.L. and G. Vance, *A Study of the Behaviour of Oil Spills in the Arctic*, Report Number 714/08/A/001,002, United States Coast Guard, Washington, D.C., 1971.
- [8] Chen, E.C., *Arctic Winter Oil Spill Test*, Technical Bulletin No. 68, Environment Canada, Ottawa, ON, 1972.
- [9] McMin, T.J., *Crude Oil Behaviour on Arctic Winter Ice*, Project 734108, United States Coast Guard, Washington, D.C., 1972.
- [10] McMin, T.J. and P.C. Golden, Behavioral Characteristics and Cleanup Techniques of North Slope Crude Oil in an Arctic Environment, *IOSC*, Washington, D.C., 263, 1973.
- [11] Buist, I.A., R. Belore, A. Guarino, D. Hackenberg, Z. Wang, and D.F. Dickins, Empirical Weathering Properties of Oil in Ice and Snow, *AMOP*, Vancouver, 67, 2009.
- [12] Chen, E.C., C.K. Overall, and C.R. Phillips, Spreading of Crude Oil on an Ice Surface, *Can. J. Chem. Eng.*, 52, 71, 1974.
- [13] Kawamura, P., D. Mackay, and M. Goral, *Spreading of Chemicals on Ice and Snow*, Manuscript Report EE-79, Environment Canada, Ottawa, ON, 1986.
- [14] Bellino, P.W., M.R. Flynn, and A.S. Rangwala, A Study of Spreading of Crude Oil in an Ice Channel, *J. Loss Prev. Proc.*, 26 (3), 558, 2012.
- [15] S.L. Ross Environmental Research Ltd. and D.F. Dickins Associates Ltd., *Field Research Spills to Investigate the Physical and Chemical Fate of Oil in Pack Ice*, Environmental Studies Research Fund, Report No. 062, National Energy Board, Calgary, 1987.
- [16] Keevil, B.E. and R. Ramseier, Behaviour of Oil Spilled Under Floating Ice, *IOSC*, San Francisco, 497, 1975.
- [17] NORCOR Engineering and Research Ltd., *The Interaction of Crude Oil with Arctic Sea Ice*, Beaufort Sea Technical Report,

- No. 27, Beaufort Sea Project, Department of the Environment, Victoria, BC, 1975.
- [18] Chen, E.C., B.E. Keevil, and R.O. Ramseier, *Behaviour of Oil Spilled in Ice-Covered Rivers*, Scientific Series No. 61, Environment Canada, Ottawa, ON, 1976.
- [19] Greene, G.D., P.J. Leinonen, and D. Mackay, An Exploratory Study of the Behaviour of Crude Oil Spills Under Ice, *Can. J. Chem. Eng.*, 55, 696, 1977.
- [20] Dome Petroleum Ltd., *Oil and Gas Under Sea Ice*, Report CV-1, Canadian Offshore Oil Spill Research Association (COOSRA), Vols. I and II, Calgary, AB, 1981.
- [21] Goodman, R.H., A.G. Holoboff, T.W. Daley, P. Waddell, L.D. Murdock, and M. Fingas, A Technique for the Measurement of Under-Ice Roughness to Determine Oil Storage Volumes, *IOSC*, Baltimore, 395, 1987.
- [22] Uzuner, M.S., F.B. Weiskopf, J.C. Cox, and L.A. Schultz, *Transport of Oil Under Smooth Ice*, EPA-600/3-79-041, Environmental Protection Agency, Corvallis, OR, 1979.
- [23] Puskas, J., E. McBean, and N. Kouwen, Behaviour and Transport of Oil Under Smooth Ice, *Can. J. Civil Eng.*, 14, 510–518, 1987.
- [24] Puskas, J.K. and E.A. McBean, The Transport of Crude Oil Under Saline Ice, in *Proceedings of the Fourth International Conference on Cold Region Engineering*, American Society of Civil Engineers, New York, NY, 670, 1986.
- [25] Yapa, P.D. and T. Chowdhury, *Spreading of Oil Spilled Under Ice*, Report No. 89-10, Clarkson University, Potsdam, New York, 1989.
- [26] Izumiyama, K. and A. Konno, Experimental Study on the Spreading of Oil Under Ice Covers, in *Proceedings of the International Offshore and Polar Conference*, Kitakyushu, Japan, Vol. 1, 821, 2002.
- [27] Izumiyama, K., S. Uto, S. Kanada, S. Kioka, and S. Sakai, Estimation of Oil Area Spill Under an Ice Cover, in *Proceedings of the 15th ISOPE*, Seoul, Korea, Vol. 1., 910, 2004.
- [28] Peishi, Q., S. Zhiguo, and L. Yunzhi, Mathematical Simulation on the Oil Slick Spreading and Dispersion in Nonuniform Flow Fields, *Int. J. Environ. Sci. Tech.*, 8, 339, 2011.
- [29] Cox, J.C. and L.A. Schultz, The Transport and Behaviour of Oil Spilled Under Ice, *AMOP*, Edmonton, 45, 1980.
- [30] Vefsnmo, S. and B.O. Johannessen, Experimental Oil Spill in the Barents Sea—Draft and Spread of Oil in Broken Ice, *AMOP*, Vancouver, 1331, 1994.
- [31] Singaas, I., P.J. Brandvik, P.S. Daling, M. Reed, and A. Lewis, Fate and Behaviour of Oils Spilled in the Presence of Ice—A Comparison of the Results from Recent Laboratory, Meso-Scale Flume and Field Tests, *AMOP*, Vancouver, 355, 1994.
- [32] Khelifa, A., A Summary Review of Modelling Oil in Ice, *AMOP*, Halifax, 587, 2010.
- [33] Johansen, O., Oil Spill in Ice Simulation Model Development, in *Proceedings of PCAC'89: Ports and Ocean Engineering Under Arctic Conditions*, Lulea, Sweden, 1131, 1989.
- [34] Johansen, O., K. Skognes and V. Sveen, *Oil Drift in Ice Model*, OCEANOR Report No. OCN 95026, 1995.
- [35] Sayed, M. and S. Løset, Laboratory Experiments of Oil Spreading in Brash Ice, in *Proceedings of the Third International Offshore and Polar Engineering Conference*, International Society of Offshore and Polar Engineers, Golden, CO, pp. 224–231, 1993.
- [36] Cjøsteen, J.K.O., A Model for Oil Spreading in Cold Waters, *Cold Reg. Sci. Technol.*, 39, 117, 2004.
- [37] Cjøsteen, J.K.O. and S. Løset, Laboratory Experiments on Oil Spreading in Broken Ice, *Cold Reg. Sci. Technol.*, 38, 103, 2004.
- [38] Purves, F., *The Interaction of Crude Oil and Natural Gas with Laboratory-Grown Saline Ice*, EPS-4-EC-78-9, Environment Canada, Ottawa, ON, 1978.
- [39] Martin, S., A Field Study of Brine Drainage and Oil Entrainment in First-Year Sea Ice, *J. Glaciol.*, 22, 473, 1979.
- [40] Buist, I.A., S.G. Potter, and D.F. Dickins, Fate and Behaviour of Water-in-Oil-Emulsions in Ice, *AMOP*, Edmonton, 263, 1983.
- [41] Payne, J.R., G.D. McNabb, and J.R. Clayton, Oil-Weathering Behavior in Arctic Environments, *Polar Res.*, 10, 631, 1990.
- [42] Izumiyama, K., S. Uto, and S. Sakai, Prediction of Oil-Ice Sandwich Formation, *Int. J. Offshore Polar Eng.*, 14, 169, 2004.
- [43] Izumiyama, K., S. Uto, and S. Sakai, Prediction of Oil-Ice Sandwich Formation, in *Proceedings of the International Offshore and Polar Engineering Conference*, Honolulu, 815, 2003.
- [44] Otsuka, N., H. Kondo, and H. Saeki, Experimental Study on the Characteristics of Oil Ice Sandwich, in *Ocean '04—MTS/IEEE Techno-Ocean '04: Bridges Across the Oceans—Conference Proceedings*, Piscataway, 3, 1470, 2004.
- [45] Cammaert, A.B., *Oil and Gas Under Ice Laboratory Study*, Beaufort Environmental Impact Statement RWC17, Environment Canada, Ottawa, ON, 38 p, 1980.
- [46] Buist, I., S. Joyce, and D.F. Dickins, *Oil Spills in Leads: Tank Tests and Modelling*, Manuscript Report EE-95, Environment Canada, Ottawa, ON, 1987.
- [47] MacNeill, M.R. and R.H. Goodman, *Oil Monitoring During Lead Closure*, Environmental Studies Research Fund, Report No. 053, National Energy Board, Calgary, AB, 1987.
- [48] Owens, E.H., D.F. Dickins, and G.A. Sergy, The Behavior and Documentation of Oil Spilled on Snow- and Ice-Covered Shorelines, *IOSC*, Miami, 2005.
- [49] Deslauriers, P.C., S. Martin, B. Morson, and B. Baxter, *The Physical and Chemical Behaviour of the Bouchard No. 65 Oil Spill in the Ice-Covered Waters of Buzzards Bay*, National Oceanic and Atmospheric Administration (NOAA), Environmental Research Laboratory, Boulder, CO, 1977.
- [50] Comfort, G. and W. Purves, *The Behaviour of Crude Oil Spilled Under Multi-Year Ice*, EPS 4-EC-82-4, Environment Canada, Ottawa, ON, 1982.
- [51] Øksenvåg, J.H.C., B. Brørs, and E. Owens, Ice Formation on Shorelines—Observation Study and Modelling, *AMOP*, Vancouver, 141, 2009.
- [52] Martin, S., P. Kauffman, and P.E. Welander, A Laboratory Study of the Dispersion of Crude Oil Within Sea Ice Grown in a Wave Field, in *Proceedings of the Twenty-Seventh Alaska Science Conference*, Vol. II, American Association for the Advancement of Science, Fairbanks, AK, 261, 1977.
- [53] Wilson, D.G. and D. Mackay, *The Behaviour of Oil in Freezing Situations*, Manuscript Report EE-92, Environment Canada, Ottawa, ON, 1987.
- [54] Li, Z.-J., B. Hollebone, M. Fingas, and B. Fieldhouse, Physical Model Technique on the Behaviour of Oil Spills in Grease Ice Under Wave Actions, *Dalian Haishi Daxue Xuebao/J. Dalian Maritime University*, 33, 91, 2007.
- [55] Brandvik, P.J., K.R. Sørheim, I. Singaas, and M. Reed, *Short State-of-the-Art Report on Oil Spills in Ice-Infested Waters*. Final, Sintef Report A 06148, Trondheim, Norway, 2006.
- [56] Fingas, M.F., The Behaviour of Oil in Ice, in *Combating Marine Oil Spills in Ice and Cold Conditions*, National Board of Waters and the Environment, Helsinki, Finland, 5, 1993.

PART VI

MODELING

INTRODUCTION TO SPILL MODELING

MERV FINGAS

Spill Science, Edmonton, Alberta, Canada

10.1	Introduction	287
10.2	An Overview of Weathering	287
10.3	Evaporation	288
10.4	Water Uptake and Emulsification	290
	10.4.1 Regression Model Calculation	291
10.5	Natural Dispersion	293
10.6	Summary of Natural Dispersion	295
10.7	Other Processes	295
	10.7.1 Dissolution	295
	10.7.2 Photooxidation	295
	10.7.3 Sedimentation, Adhesion to Surfaces, and Oil-Fines Interaction	295
	10.7.4 Biodegradation	296
	10.7.5 Sinking and Overwashing	296
	10.7.6 Formation of Tar Balls	297
10.8	Movement of Oil and Oil Spill Modeling	297
	10.8.1 Spreading	297
	10.8.2 Movement of Oil Slicks	298
10.9	Spill Modeling	299

10.1 INTRODUCTION

When oil is spilled, whether on water or land, a number of transformation processes occur; many of these processes are referred to as the behavior of the oil. The first process is weathering, a series of processes whereby the physical and chemical properties of the oil change after the spill, of which the most important are evaporation and emulsification [1–4]. A second group of processes is related to the movement of oil in the environment. Spill modeling combines the knowledge of both these sets of processes and provides the user with information on future locations of the oil as well as information on the state of the oil [5–8]. Weathering and movement processes can overlap, with weathering strongly influencing how oil is moved in the environment and vice versa. All processes depend very much on the type of oil spilled and the weather conditions during and after the spill.

10.2 AN OVERVIEW OF WEATHERING

The specific behavior processes that occur after an oil spill determine how the oil should be cleaned up and its effect on the environment. For example, if an oil evaporates rapidly, less oil is required to be cleaned up, but the hydrocarbons in the oil enter the atmosphere. An oil slick could be carried by surface currents or winds to the vicinity of a bird colony or to a shore where seals or sea lions are breeding and severely affect wildlife and their habitat. On the other hand, a slick could be carried out to sea where it has less immediate effect on the environment.

The fate and effects of a particular spill are determined by the behavior processes that are in turn almost entirely determined by the type of oil and the environmental conditions at the time of the spill. Spill responders need to know the ultimate fate of the oil in order to take measures to minimize the overall impact of the spill.

Oil spilled on water undergoes a series of changes in physical and chemical properties that in combination are termed “weathering.” Weathering processes occur at very different rates but begin immediately after oil is spilled into the environment. Weathering rates are not consistent throughout the duration of an oil spill and are usually highest immediately after the spill. Both weathering processes and the rates at which they occur depend more on the type of oil than on environmental conditions. Most weathering processes are highly temperature dependent, however, and will often slow to insignificant rates as temperatures approach zero degrees.

The processes included in weathering are evaporation, emulsification, natural dispersion, dissolution, photooxidation, sedimentation, adhesion to materials, interaction with mineral fines, biodegradation, and formation of tar balls. These processes are listed in order of importance in terms of their effect on the percentage of total mass balance, that is, the greatest loss from the slick in terms of percentage, and what is known about the process.

10.3 EVAPORATION

Evaporation is usually the most important weathering process [9]. It has the greatest effect on the amount of oil remaining on water or land after a spill, especially that of a light oil. Over a period of several days, a light fuel such as gasoline evaporates completely at typical ambient temperatures, whereas only a small percentage of a heavier Bunker C oil evaporates. The rate at which an oil evaporates depends primarily on the oil's composition. Figure 10.1 shows the differential evaporation of several typical oils. The more volatile components an oil or fuel contains, the greater the extent and rate of its evaporation. Many components of heavier oils will not evaporate at all, even over long periods of time and at high temperatures.

Oil and petroleum products evaporate in a slightly different manner than water, and the process is much less dependent on wind speed and surface area. Oil evaporation can be considerably slowed down, however, by the formation of a "crust" or "skin" on top of the oil. This happens primarily on land or in calm areas where the oil layer does not get mixed. The skin or crust is formed when the smaller compounds in the oil are removed leaving the larger

compounds, such as waxes and resins, at the surface. This crust then seals off the remainder of the oil and slows evaporation. Stranded oil from old spills has been reexamined over many years, and it has been found that when this crust has formed, there is no significant evaporation in the oil underneath. When this crust has not formed, a similar oil could be weathered to the hardness of wood over the same amount of years.

The rate of evaporation is very rapid immediately after a spill and then slows considerably. About 80% of evaporation that will take place occurs in the first 2 days after a spill. The evaporation of most oils follows a logarithmic curve with time. Some oils such as diesel fuel, however, evaporate as the square root of time, at least for the first few days. This means that the evaporation rate slows very rapidly in both cases, after a few days. This can be seen in Figure 10.1.

The properties of an oil can change significantly with the extent of evaporation. If about 40% (by weight) of an oil evaporates, its viscosity could increase by as much as a 1000-fold. Its density could rise by as much as 10% and its flash point by as much as 400%. The extent of evaporation can be the most important factor in determining properties of an oil at a given time after the spill and in changing the behavior of the oil.

The basis for most of the earlier oil evaporative work is the extensive studies on the evaporation of water [10,11]. In fact, some of the model equations still employ portions of these equations. The pioneering work in the development of water evaporation equations was carried out by Sutton [12]. Sutton proposed the following equation:

$$E = Ms C_s U^{7/9} d^{1/9} Sc^{-r} \quad (10.1)$$

where E is the mean evaporation rate per unit area, Ms is the mass transfer coefficient, C_s is the concentration of the evaporating fluid (mass/volume), U is the wind speed, d is the area of the square or circular pool, Sc is the Schmidt number, and r is an empirical exponent assigned values from 0 to 2/3.

The most frequently used work in older spill modeling is that of Stiver and Mackay [13,14]. It is based on some of the earlier work by Mackay and Matsugu [15]. The formulation was initiated with assumptions about the evaporation of aliquid. If a liquid is spilled, the rate of evaporation is given by

$$N = KAP/(RT) \quad (10.2)$$

where N is the evaporative molar flux (mol/s), K is the mass transfer coefficient under the prevailing wind (m/s), A is the area (m²), and P is the vapor pressure of the bulk liquid. This equation was arranged to give

$$dF_v/dt = KAPv/(V_o RT) \quad (10.3)$$

where F_v is the volume fraction evaporated, v is the liquid's molar volume (m³/mol), and V_o is the initial volume of spilled liquid (m³).

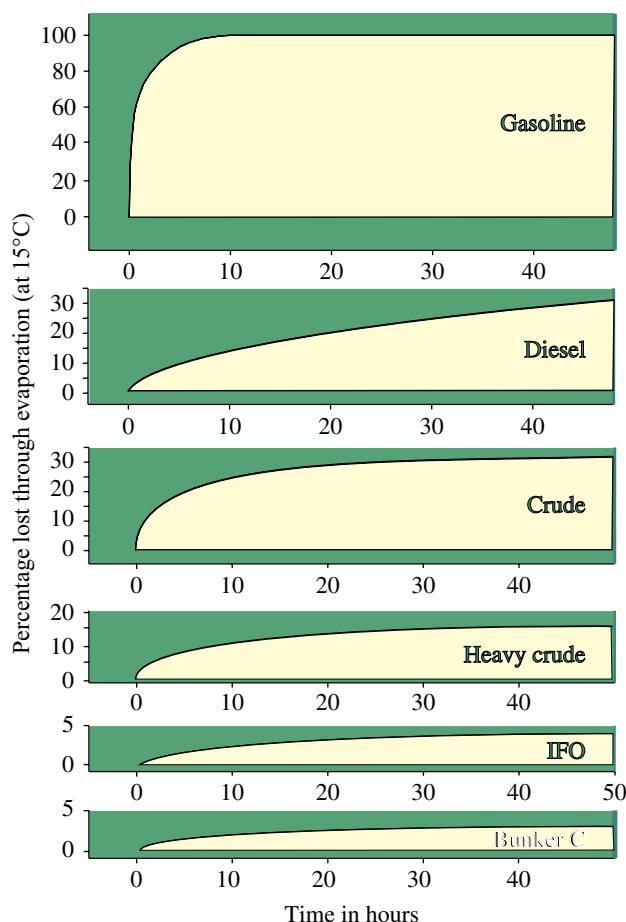


FIGURE 10.1 Oil evaporation curves for several typical oils—data from experiments.

By rearranging, we obtain

$$dF_v = [Pv/(RT)](KA dt/V_o) \quad (10.4)$$

$$\text{or} \quad dF_v = Hd\theta \quad (10.5)$$

where H is Henry's law constant and θ is the evaporative exposure (defined in the following).

The right-hand side of the second last equation has been separated into two dimensionless groups. The group $KA dt/V_o$ represents the time rate of what has been termed the "evaporative exposure" and was denoted as $d\theta$. The evaporative exposure is a function of time, the spill area and volume (or thickness), and the mass transfer coefficient (which is dependent on the wind speed).

The group $Pv/(RT)$ or H is a dimensionless Henry's law constant or ratio of the equilibrium concentration of the substance in the vapor phase $[P/(RT)]$ to that in the liquid (l/v) . H is a function of temperature. The product θH is then the ratio of the amount that has evaporated (oil concentration in vapor times vapor volume) to the amount originally present. For a pure liquid, H is independent of F_v and Equation (10.5) was integrated directly to give

$$F_v = H\theta \quad (10.6)$$

If K , A , and temperature are constant, the evaporation rate is constant and evaporation is complete (F_v is unity) when θ achieves a value of $1/H$.

If the liquid is a mixture, H depends on F_v and the basic equation can only be integrated if H is expressed as a function of F_v , that is, the principal variable of vapor pressure is expressed as a function of composition. The evaporation rate slows as evaporation proceeds in such cases.

Equation (10.6) could not be directly related to oil data and was replaced with a new equation developed using laboratory empirical data:

$$F_v = (T/K_1) \ln(1 + K_1\theta/T) \exp(K_2 - K_3/T) \quad (10.7)$$

where F_v is the volume fraction evaporated and $K_{1,2,3}$ are empirical constants [13].

A value for K_1 was obtained from the slope of the F_v versus $\log \theta$ curve from pan or bubble evaporation experiments. For θ greater than 10^4 , K_1 was found to be approximately $2.3T$ divided by the slope. The expression $\exp(K_2 - K_3/T)$ was then calculated, and K_2 and K_3 determined individually from evaporation curves at two different temperatures.

Fingas studied oil evaporation and found that oil did not evaporate in the same manner as water [9,16]. Instead of being air boundary layer regulated, it was found that oil was regulated by diffusion through the oil mass. This allowed for a simplified oil prediction of the following type:

$$\text{Percentage oil evaporated} = c \ln(t) \quad (10.8)$$

where c is an empirical constant at a given temperature and t is the time in minutes.

This was further expanded to provide a relationship with temperature for a variety of oils to yield

$$\text{Percentage evaporated} = [C + 0.045(T - 15)] \ln(t) \quad (10.9)$$

where C is a constant for each type of oil or petroleum product, T is the temperature in Celsius, and t is the time in minutes.

A large number of experiments were performed on oils to directly measure their evaporation curves. The empirical equations that result are given in another paper in this book [9].

It was found that oils and fuels evaporated as two distinct types: those that evaporated as a logarithm of time and those that evaporated as a square root of time [9]. Most oils typically evaporated as a logarithm (natural) of time. Diesel fuel and similar oils, such as jet fuel, kerosene, and the like, evaporate as a square root of time [9]. The reasons for this are simply that diesel fuel and such like have a narrower range of compounds that evaporate at similar yield rates, which sum as a square root.

For those oils such as diesel fuel, which evaporate as a square root of time, the equation is

$$\text{Percentage evaporated} = [C + 0.01(T - 15)] \sqrt{t} \quad (10.10)$$

where the parameters are as in Equation (10.9). Again, many experimental constants are in a table in another paper in this book [9].

The question then becomes, what does one do if you do not have the empirical constant, which takes days to measure? A procedure to use only distillation data provides a simple estimation method:

For oils that follow a logarithmic equation,

$$\text{Percentage evaporated} = [0.165(\%D) + 0.045(T - 15)] \ln(t) \quad (10.11)$$

For oils that follow a square root equation,

$$\text{Percentage evaporated} = [0.0254(\%D) + 0.01(T - 15)] \sqrt{t} \quad (10.12)$$

where $\%D$ is the percentage (by weight) distilled at 180°C .

The equations noted previously were all measured at a slick thickness of 1.5 mm, which is typical of sea values. This has been studied and a correction factor for thickness can be applied as

$$\text{Corrected equation factor } (C') = \text{equation factor} \\ (C) + 1 - 0.78 \times \sqrt{t} \quad (10.13)$$

where C' is the thickness-corrected factor for application in Equation (10.9), C is the empirical equation factor as noted in the table in the evaporation paper in this volume [9], and t is the thickness of the slick in mm. It should be noted that this thickness adjustment is typically not needed for many situations in which oils spread quickly below 1.5 mm.

10.4 WATER UPTAKE AND EMULSIFICATION

Emulsification is the process by which one liquid is dispersed into another one in the form of small droplets [17]. Water droplets can remain in an oil layer in a stable form, and the resulting material is completely different. These water-in-oil emulsions are sometimes called “mousse” or “chocolate mousse.”

The mechanism of emulsion formation is not yet fully understood, but it probably starts with sea energy forcing the entry of small water droplets, about 10–25 μm (or 0.010–0.025 mm) in size, into the oil. If the oil is only slightly viscous, these small droplets will not leave the oil quickly. On the other hand, if the oil is too viscous, droplets will not enter the oil to any significant extent. Once in the oil, the droplets slowly gravitate to the bottom of the oil layer. Asphaltenes and resins in the oil will interact with the water droplets to stabilize them. Depending on the quantity of asphaltenes and resins, as well as other conditions, an emulsion may be formed. The conditions required for emulsions of any stability to form may only be reached after a period of evaporation. Evaporation increases the viscosity to the critical value and increases the resin and asphaltene percentage in the oil. Further discussion on emulsion formation is found in a separate chapter [17].

Water can be present in oil in five ways. First, some oils contain about 1% water as soluble water. This water does not significantly change the physical or chemical properties of the oil. The second way is called “entrainment,” whereby water droplets are simply held in the oil by its viscosity to form an unstable mixture. These are formed when water droplets are incorporated into oil by the sea’s wave action and there are not enough asphaltenes and resins in the oil. The third way is that of unstable emulsions or those oils that simply do not form water-in-oil types. Unstable emulsions break down into water and oil within minutes or a few hours, at most, once the sea energy diminishes. The properties and appearance of the unstable emulsion are almost the same as those of the starting oil, although the water droplets may be large enough to be seen with the naked eye.

Mesostable emulsions represent the fourth way water can be present in oil. These are formed when the small droplets of water are stabilized to a certain extent by a combination of the viscosity of the oil and the interfacial action of asphaltenes and resins. These emulsions generally break down into oil and water or sometimes into water, oil, and a stable residue within a few days. Mesostable emulsions are viscous liquids that are reddish brown in color.

The fifth way that water exists in oil is in the form of stable emulsions. These form in a way similar to mesostable emulsions except that the oil contains a sufficient amount of resins and asphaltenes to stabilize the water droplets. The viscosity of stable emulsions is 800–1000 times higher than that of the starting oil, and the emulsion will remain stable for weeks and even months after formation. Stable emulsions are reddish brown in color and appear to be nearly solid. Because of their high viscosity and near solidity, these

emulsions do not spread and tend to remain in lumps or mats on the sea or shore.

The formation of emulsions is an important event in an oil spill. First, and most importantly, emulsification substantially increases the actual volume of the spill. Emulsions that contain about 70% water triple the volume of the oil spill. Even more significantly, the viscosity of the oil increases by as much as 1000 times, depending on the type of emulsion formed. For example, an oil that has the viscosity of motor oil can triple in volume and become almost solid through the process of emulsification.

These increases in volume and viscosity make cleanup operations more difficult. Emulsified oil is difficult or impossible to disperse or to recover with skimmers. Emulsions can be broken down with special chemicals in order to recover the oil with skimmers. It is thought that emulsions break down into oil and water by further weathering, oxidation, mixing with unemulsified oil, and freeze–thaw action. Meso- or semistable emulsions are relatively easy to break down, whereas stable emulsions may take months or years to break down naturally, if they ever do break down.

Emulsion formation also changes the fate of the oil. It has been noted that when oil forms stable or mesostable emulsions, evaporation slows considerably. Biodegradation also appears to slow down. The dissolution of soluble components from oil may also cease once emulsification has occurred.

The various types form “regions” when the natural logarithm of viscosity is plotted against the asphaltene times the resin content. As there are other factors involved such as the asphaltene/resin ratio, the total saturate content and the density, there is some overlap between regions. A simplified version of this is shown in Figure 10.2. Correlation of water-in-oil types shows that the most important factors are the starting oil viscosity and the asphaltene and resin contents. Even a simple graphical presentation of these three oil properties shows that the resulting water-in-oil type can be predicted with relative accuracy. Correlation of these factors alone shows distinct regions where the four kinds of water-in-oil types exist. The data show that the water-in-oil types are physically stabilized by the oil viscosity and chemically stabilized by both asphaltenes and resins. For greater stability, resin content should exceed the asphaltene content slightly. Excess resin content ($A/R < \text{about } 0.6$) apparently destabilizes the emulsion. A high asphaltene content (typically $>10\%$) increases the viscosity of the oil such that a stable emulsion will not form. Viscous oils will only take up water as entrained water and will slowly lose much of this water over a period ranging up to months. Oils of low viscosity or without significant amounts of asphaltenes and resins will not form any water-in-oil type and will retain less than about 6% water. Oils of very high viscosity (typically $>10,000 \text{ mPa}\cdot\text{s}$) will not form any of these water-in-oil types.

The modeling of emulsion formation is somewhat complex but can be carried out by several different means. Table 10.1 shows the input parameters needed. There are three approaches now available.

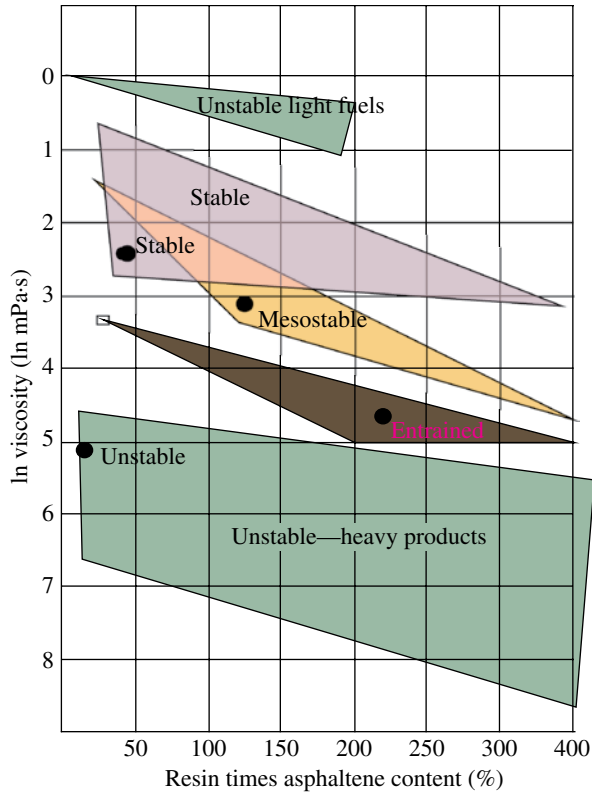


FIGURE 10.2 A simplified drawing of the regions of formation for various water-in-oil types.

TABLE 10.1 Inputs for modeling emulsion formation

Variable	Computational units	Range (min, max)
Wind or wave	m/s or m	(0, 20) or (0, 1)
Oil density	kg/m ³	(0.4, 1.1)
Oil viscosity	mPa·s	(1–10 ¹⁰)
Asphaltene content	%	(1–90)
Saturate content	%	(1–90)
Resin content	%	(1–90)
Asphaltene/resin ratio	Unitless ratio	(0.1–0.99)

1. Empirical (compare requested oil to the database of oils) [18]

Benefits—highly accurate

Disadvantages—requires a big database (~430 oils at different weathering percentages) and needs another method for oil input however

2. Fuzzy logic (use Yetilmezsoy model) [19,20]

Benefits—fairly accurate

Disadvantages—difficulty in having to deal with a “black box” model and may have difficulty in obtaining and integrating

3. Calculate using regression model (use Fingas regression model) [21]

Benefits—somewhat accurate and has control over inputs and outputs

Disadvantages—less accurate than the above two approaches

10.4.1 Regression Model Calculation

The regression model is the second easiest model to implement, after the empirical approach [21]. The first step is to transform the input data so that it forms a continuous declining or increasing function. It should be noted that the “greater than” can also be read as greater or equal to.

Density: *not transformed—just take the exponential, abbreviated Den*

(10.14)

Viscosity: *not transformed—just take the natural log, abbreviated Visc*

(10.15)

Saturate content: *If the saturate content is less than 45, then the saturate content parameter is 45 less the saturate content, and if it is greater than 45, it becomes the saturate content less 45. The value used in the equation is this transformed value.*

(10.16)

Resin content: *If the resin content is less than 10, then the resin content parameter is 10 less the resin content, and if it is greater than 10, it becomes the resin content less 10. The value used in the equation is this transformed value. If the value of the resins is zero, then set this value to 20.*

(10.17)

Asphaltene content: *If the asphaltene content is less than 4, then the asphaltene content parameter is four less the asphaltene content, and if it is greater than 4, it becomes the asphaltene content less 4. The value used in the equation is this transformed value. If the value of the asphaltene content is zero, then set the value to 20.*

(10.18)

Asphaltene/resin (A/R) ratio: *not transformed*

(10.19)

The class of the resulting emulsion is then calculated as follows:

$$\begin{aligned} \text{Stability} = & -15.3 + 1010 \times \text{Den} - 3.66 \times \text{Visc} + 0.174 \\ & \times \text{Rst} - 0.579 \times \text{Ast} + 34.4 \times \text{A/R} + 1.02 \times \exp(\text{Den}) \\ & - 7.91 \times \exp(\text{A/R}) - 2740 \times \ln(\text{Den}) + 12.2 \times \ln(\text{Visc}) \\ & - 0.334 \times \ln(\text{Sst}) - 3.17 \times \ln(\text{Rst}) + 0.99 \times \ln(\text{Ast}) \\ & - 2.29 \times \ln(\text{A/R}) \end{aligned}$$

(10.20)

where Den is the untransformed exponential of the density, abbreviated A here; Visc is the untransformed natural logarithm (ln) of the viscosity, abbreviated B here; Rst is the transformed resin content as calculated in Equation (10.18), abbreviated C; Ast is the transformed asphaltene

TABLE 10.2 Stability and the four oil types

Step				
1	Carry out rheological studies on the water-in-oil product measuring complex modulus and elastic modulus			
2	Calculate the cross product (Xpr) of the complex modulus and elastic modulus divided by the starting oil viscosity			
	$Xpr = \frac{\text{Complex modulus}}{\text{Starting oil viscosity}} \times \frac{\text{Elastic modulus}}{\text{Starting oil viscosity}}$			
3	Correct the cross product (Xpr) to yield stability (sometimes referred to as Stability C)			
	Stability = ln((Xpr/10, 000) × (Xpr/10, 000))			
	Relation of stabilities to water-in-oil type			
Calculated stability				Calculated
Minimum	Maximum	Starting oil properties	Water-in-oil type	Average stability
−20	3	Density >0.94 Viscosity >6000	Entrained	−7
−4	−18	Density <0.85 or >1.0 Viscosity <100 or >800,000 Asphaltenes or resins <1%	Unstable	−15
		If density or viscosity is other than those above		
4	29		Stable	13
−10	5		Mesostable	−2

content as calculated in Equation (10.19), abbreviated D ; A/R is the (untransformed) asphaltene/resin ratio, abbreviated E ; Exponential den is the exponential of the exponential of density, abbreviated F ; exponential (A/R) is the exponential of the asphaltene/resin ratio, abbreviated G ; \ln (natural logarithm) of the exponential of density, abbreviated H ; \ln (natural logarithm) of the natural logarithm of viscosity, abbreviated I ; \ln (natural logarithm) of the transformed saturates as calculated in Equation (10.17), abbreviated J ; \ln (natural logarithm) of the transformed resins as calculated in Equation (10.18), abbreviated K ; \ln (natural logarithm) of the transformed asphaltenes as calculated in Equation (10.14), abbreviated L ; and \ln (natural logarithm) of the untransformed A/R ratio, abbreviated M .

A simplified version of the equation is then

$$\begin{aligned} \text{Stability} = & -15.3 + 1010 \times A - 3.66 \times B + 0.174 \times C - 0.579 \\ & \times D + 34.4 \times E + 1.02 \times F - 7.91 \times G + 2740 \times H + 12.2 \\ & \times I - 0.334 \times J - 3.17 \times K + 0.99 \times L - 2.29 \times M \end{aligned} \quad (10.21)$$

where the parameters A – M are defined as above.

The stability of the resulting product is calculated using the rheological measurements of the water-in-oil product formed (see Table 10.2).

The basic uncorrected stability or cross product is

$$Xpr = \frac{\text{Complex modulus}}{\text{Starting oil viscosity}} \times \frac{\text{Elastic modulus}}{\text{Starting oil viscosity}} \quad (10.22)$$

The corrected stability is

$$\text{Stability} = \ln(Xpr^2 / 10,000) \quad (10.23)$$

where Xpr is the value from Equation (10.22).

TABLE 10.3 Viscosity increases from starting oil

	Viscosity increase on		
	First day	Week	Year
Entrained	1.9	1.9	2.1
Mesostable	7.2	11	32
Stable	405	1054	991
Unstable	0.99	1	1

TABLE 10.4 Time to formation prediction

Resulting equation

$$\text{Equation: } y = a + b/x^{1.5} \quad (10.24)$$

x is wave height in cm, y is time to formation in minutes

Predictor	a	b	R ²
Stable	27.1	7,520	0.51
Mesostable	47	49,100	0.95
Entrained	30.8	18,300	0.94

The values of stability that are assigned to each class are given in Table 10.2. The viscosity of the resulting product can be taken as the average of the types at a given time as shown in Table 10.3.

The kinetics of emulsion formation has been studied, and data are available to compute the time to formation [21]. Empirical data on the formation time of the various water-in-oil states was studied. The data of the relative formation times and the wave height are available. Formulas were fitted to each of the three categories, and the common formula among all three relevant classes was found to be $1/x^{1.5}$ (10.24), as shown in Table 10.4. The regression coefficients for this formula are also given. Application of the equations in Table 10.4 provides the time to formation of a particular water-in-oil state, given the wave height.

10.5 NATURAL DISPERSION

Natural dispersion occurs when fine droplets of oil are transferred into the water column by wave action or turbulence. Small oil droplets ($<20\mu\text{m}$ or 0.020mm) are somewhat stable in water and will remain so for short periods of time. Large droplets tend to rise, and larger droplets (more than $50\mu\text{m}$) will not stay in the water column for more than a few seconds. Depending on oil conditions and the amount of sea energy available, natural dispersion can be insignificant or it can remove the bulk of the oil. In 1993, the oil from a stricken ship, the Braer, dispersed and sedimented almost entirely as a result of high seas off Scotland at the time of the spill and the dispersible nature of the oil cargo [22]. It should be noted that natural dispersion may just be an intermediary in the oil–sediment reaction and subsequent sedimentation. The Braer spill is more likely a good example of oil sedimentation as a result of oil–particle interaction rather than natural dispersion.

Natural dispersion is dependent on both the oil properties and the amount of sea energy [23]. Heavy oils such as Bunker C or a heavy crude will not disperse naturally to any significant extent, whereas diesel fuel and even light crudes can disperse significantly if the saturate content is high and the asphaltene and resin contents are low. In addition, significant wave action is needed to disperse oil. In 40 years of monitoring spills on the oceans, those spills where oil has dispersed naturally have all occurred in very energetic seas—up to Beaufort 7.

The long-term fate of dispersed oil is not known, although it may degrade to some extent as it consists primarily of saturate components. Some of the dispersed oil may rise and form another surface slick or it may become associated with sediment and be precipitated to the bottom.

Delvigne and associates studied the natural dispersion of oil in a series of wave tanks and a series of smaller apparatuses [24–29]. The turbulence energy was related to the creation of naturally dispersed droplets. Of prime importance to oil spill modeling, the following empirical equation was created:

$$Q_{(d)} = C_o D^{0.57} d^{0.7} \Delta d S_{\text{cov}} F_{\text{wc}} \quad (10.25)$$

where $Q_{(d)}$ is the entrained mass rate of droplet sizes in the interval around d per unit surface area and per unit time—given in $\text{kg/m}^2\text{s}$; D is the energy dissipation of the breaking wave per unit surface area (J/m^2); C_o is a constant for a given oil, where a light oil is about 1000–1800, a medium oil about 500–1000, and a heavier oil <500 ; d and Δd are the droplet size and range of droplet size (interval) in m, respectively; S_{cov} is the fraction of the sea covered by oil (0–1); and F_{wc} is the fraction of sea surface affected by breaking waves per unit time (s^{-1}).

This was developed further by defining portions of the above equation [29]:

$$F_{\text{wc}} = C_b (U - U_i) / T_w \quad (10.26)$$

where F_{wc} is the fraction of sea surface affected by breaking waves per unit time (s^{-1}) as in the equation above, C_b is a constant $\sim 0.032\text{ s/m}$, U is the wind speed (m/s), U_i is the wind speed at the initiation of breaking waves ($\sim 5\text{ m/s}$), and T_w is the wave period (s).

So the equation above can be rewritten as

$$F_{\text{wc}} = 0.032 (U - 5) / T_w \quad (10.27)$$

Also, the energy dissipation (D) has been proposed as [29]

$$D = 0.0034 \rho_w g H_{\text{rms}}^2 \quad (10.28)$$

where D is the energy dissipation of the breaking wave per unit surface area (J/m^2); ρ_w is the density of water (kg/m^3), which is 1030 for typical seawater; g is the acceleration due to gravity (m/s^2), which is 9.81 ; and H_{rms} is the r.m.s. value of the wave height (m).

This then becomes

$$D = 34.4 H_{\text{rms}}^2 \quad (10.29)$$

Substituting both of these in Equation (10.5), we get

$$Q_{(d)} = C_o (34.4 H_{\text{rms}}^2)^{0.57} d^{0.7} \Delta d S_{\text{cov}} (0.032 (U - 5) / T_w) \quad (10.30)$$

where $Q_{(d)}$ is the entrained mass rate of droplet sizes in the interval around d per unit surface area and per unit time—given in $\text{kg/m}^2\text{s}$.

An analysis of this equation using typical values shows that the most important factor is the wave height. This is shown in Figure 10.3. This is obvious as wave height is a square function in the equation and the 0.57 power factor does not remove the effect. The values in Figure 10.3 are plotted with the baselines fixed as wind is 10 m/s , wave height is 0.5 m , droplet size is $50\mu\text{m}$, sea coverage is 0.3 ,

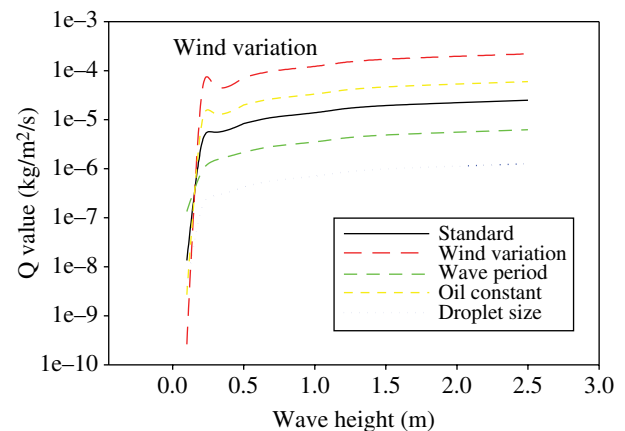


FIGURE 10.3 The sensitivity of parameters in Delvigne's formulation.

wave period is 10, and oil constant is 500. The parameters in the model were varied as follows: wind from 5 to 50 m/s, wave period from 1 to 40 s, oil constant from 100 to 1200, and droplet size from 10 to 300 μm .

Several issues have been noted about the formation developed previously [30]. These are as follows:

1. The natural dispersion predicted was measured as a temporary phenomenon—that is, the instantaneous droplets in the water column. Their persistence was not measured. The equation was designed to yield only the temporary transport in the water. Later workers assumed that this amount was permanently dispersed.
2. The equation overpredicts natural dispersion in most cases, especially in cases of low sea states.
3. The given Q is a rate with no input factor; thus, mass on the ocean is not input or defined. Further, it was stated that this is independent of the oil on the surface, also stated to be independent of oil thickness, an obvious difficulty.
4. The oil constants appear to be arbitrary, and the rules that they are $1/\text{viscosity}$ does not work for cSt.
5. The wave periods in the wave tank experiments were very short.
6. The initiation wind should be greater than 5 m/s—perhaps 10–20 m/s.

These can be partially solved in terms of the Delvigne tank experiments. First, the experiments were mostly conducted with a thickness of 0.6 mm; this constitutes an oil density of 0.6 kg/m². Dividing Equation (10.25) times this factor, we get

$$F_{(d)} = 1.67 C_o (34.4 H_{\text{rms}}^2)^{0.57} d^{0.7} \Delta d S_{\text{cov}} (0.032 (U - 5) / T_w) \quad (10.31)$$

where $F_{(d)}$ is the fraction of entrained mass rate of droplet sizes in the interval around d per unit surface area and per unit time—given in /s, C_o is a constant for a given oil, where a light oil is about 1000–1800, a medium oil about 500–1000, and a heavier oil <500; H_{rms} is the r.m.s. value of the wave height (m); d and Δd are the droplet size and range of droplet size (interval) in m, respectively; S_{cov} is the fraction of the sea covered by oil (0–1); U is the wind speed in m/s; and T_w is the wave period in s.

The droplet size is an issue. Delvigne had suggested a diameter of 300 μm ; however, examination by a number of parties shows that only about 20 μm is relatively stable for several hours [30]. This can be seen in Figure 10.4. This shows that a diameter of 300 μm has a half-life in the water column less than a second or two. Thus, substituting 20 μm with a width of 10 μm into

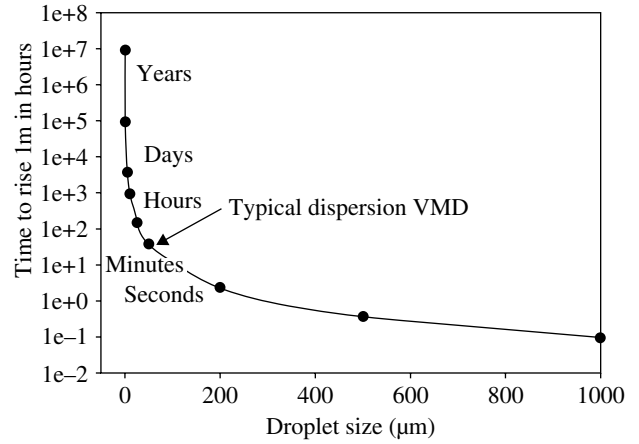


FIGURE 10.4 Droplet sizes and rise times.

Equation (10.31) and assuming that 1/2 of the sea surface is covered in oil,

$$F_{(d)} = 1.75 \times 10^{-8} C_o (34.4 H_{\text{rms}}^2)^{0.57} (0.032 (U - 5) / T_w) \quad (10.32)$$

where $F_{(d)}$ is the fraction of entrained mass rate of droplet sizes in the interval around from 10 to 30 μm —given in /s; C_o is a constant for a given oil, where a light oil is about 1000–1800, a medium oil about 500–1000, and a heavier oil <500; H_{rms} is the r.m.s. value of the wave height (m); U is the wind speed in m/s; and T_w is the wave period in s.

The oil constant (C_o) can be corrected by multiplying the viscosity value in cSt or mPa-s by 10^{-6} . Then the reciprocal becomes the constant noted in Delvigne's work. An example of this is if we have a medium crude with a viscosity of 120 mPa-s, then the oil constant becomes

$$1/100 \times 10^{-6} \text{ or } 0.83$$

It should be noted that the rule of thumb given in the Delvigne papers does not come out to the constant he used [24,9]. This follows the Delvigne papers' verbal description but not the mathematical examples. Further, the units need to be converted correctly. So converting Equation (10.8) to include the viscosity of the oil rather than the constant and changing the time to hours, we get

$$F_{(d)} = 6.3 \times 10^{-4} / \rho^{1.5} (34.4 H_{\text{rms}}^2)^{0.57} (0.032 (U - 5) / T_w) \quad (10.33)$$

where $F_{(d)}$ is the fraction of entrained mass rate of droplet sizes in the interval around from 10 to 30 μm —given in /hour; ρ is the viscosity of the oil in cSt or mPa-s; H_{rms} is the r.m.s. value of the wave height (m); U is the wind speed in m/s; and T_w is the wave period in s.

A test of this is shown in Figure 10.5, which shows the hours until the slick is completely dissipated with the new

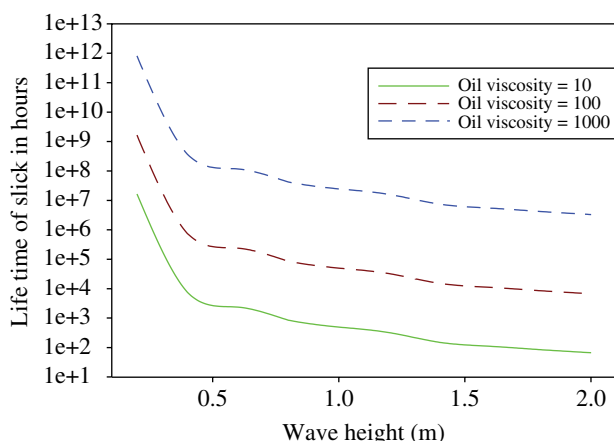


FIGURE 10.5 The dissipation oils of various viscosities as predicted by the modified natural dispersion formula.

formulation. The wave height is coupled to the wind and the period so that only one axis is plotted. This figure shows a reasonable pattern where the lightest oil would be completely dissipated in about 60 h under energetic conditions and the heavier oils are little affected under light conditions. So this now seems reasonable compared to earlier formulations that showed even heavy oils being dissipated in a few hours.

10.6 SUMMARY OF NATURAL DISPERSION

The natural dispersion of oil as formulated by Delvigne and coworkers has been reformulated not only to conform to the studies carried out in the test tanks but also to yield reasonable results and solve some of the issues surrounding the topic.

The ending formulation is

$$F_{(d)} = 6.3 \times 10^{-4} / \rho^{1.5} (34.4 H_{rms}^2)^{0.57} (0.032 (U - 15) / T_w) \quad (10.34)$$

where $F_{(d)}$ is the fraction of entrained mass rate of droplet sizes in the interval around from 10 to 30 μm —given in/hour—this should be noted as a temporary entrainment; fate of the droplets was not determined; ρ is the viscosity of the oil in cSt or mPa·s; H_{rms} is the r.m.s. value of the wave height (m); U is the wind speed in m/s; and T_w is the wave period in s.

10.7 OTHER PROCESSES

10.7.1 Dissolution

Through the process of dissolution, some of the soluble components of the oil are lost to the water under the slick [30–32]. These include some of the lower-molecular-weight

aromatics. As only a small amount, usually much less than a fraction of a percent of the oil, actually enters the water column, dissolution does not measurably change the mass balance of the oil. The significance of dissolution is that the soluble aromatic compounds are particularly toxic to fish and other aquatic life. If a spill of oil containing a large amount of soluble aromatic components occurs in shallow water and creates a high localized concentration of compounds, then significant numbers of aquatic organisms can be killed.

Gasoline, diesel fuel, and light crude oils are the most likely to cause aquatic toxicity. A highly weathered oil is unlikely to dissolve into the water. On open water, the concentrations of hydrocarbons in the water column are unlikely to kill aquatic organisms.

Dissolution occurs immediately after the spill occurs and the rate of dissolution decreases rapidly after the spill as soluble substances are quickly depleted. Some of the soluble compounds also evaporate rapidly.

There are a variety of estimation techniques for dissolution; however, there is no good continuous model at this time [31].

10.7.2 Photooxidation

Photooxidation can change the composition of an oil [33–36]. It occurs when the sun's action on an oil slick causes oxygen and carbons to combine and form new products, which may be resins. The resins may be somewhat soluble and dissolve into the water or they may cause water-in-oil emulsions to form. It is not well understood how photooxidation specifically affects oils, although certain oils are susceptible to the process, while others are not. For most oils, photooxidation is not an important process in terms of changing their immediate fate or mass balance after a spill.

10.7.3 Sedimentation, Adhesion to Surfaces, and Oil-Fines Interaction

Sedimentation is the process by which oil is deposited on the bottom of the sea or other water bodies. While the process itself is not well understood, certain facts about it are. Most sedimentation noted in the past has occurred when oil droplets reached a higher density than water after interacting with mineral matter in the water column. This interaction sometimes occurs on the shoreline or very close to the shore. Once oil is on the bottom, it is usually covered by other sediments and degrades very slowly. In a few well-studied spills, a significant amount (about 10%) of the oil was sedimented on the seafloor. Such amounts can be very harmful to biota that inevitably come in contact with the oil on the sea bottom. Because of the difficulty in studying sedimentation, data are limited.

Oil is very adhesive, especially when it is moderately weathered, and binds to shoreline materials or other mineral materials with which it comes in contact. A significant

amount of oil can be left in the environment after a spill in the form of residual amounts adhering to shorelines and man-made structures such as piers and artificial shorelines. As this oil usually contains a high percentage of aromatics and asphaltenes with high molecular weight, it does not degrade significantly and can remain in the environment for decades.

Oil slicks and oil on shorelines sometimes interact with mineral fines suspended in the water column, and the oil is thereby transferred to the water column [37]. Particles of mineral with oil attached may be heavier than water and sink to the bottom as sediment or the oil may detach and refloat. Oil-fines interaction does not generally play a significant role in the fate of most oil spills in their early stages but can have an impact on the rejuvenation of an oiled shoreline over the long term.

10.7.4 Biodegradation

A large number of microorganisms are capable of degrading petroleum hydrocarbons. Many species of bacteria, fungi, and yeasts metabolize petroleum hydrocarbons as a food energy source [38,39]. Bacteria and other degrading organisms are most abundant on land in areas where there have been petroleum seeps, although these microorganisms are found everywhere in the environment. As each species can utilize only a few related compounds at most, however, broad-spectrum degradation does not occur. Hydrocarbons metabolized by microorganisms are generally converted to an oxidized compound, which may be further degraded, may be soluble, or may accumulate in the remaining oil. The aquatic toxicity of the biodegradation products is sometimes greater than that of the parent compounds.

The rate of biodegradation depends primarily on the nature of the hydrocarbons and then on the temperature. Generally, rates of degradation tend to increase as the temperature rises. Some groupings of bacteria, however, function better at lower temperatures and others function better at higher temperatures. Indigenous bacteria and other microorganisms are often the best adapted and most effective at degrading oil as they are acclimatized to the temperatures and other conditions of the area. Adding “superbugs” to the oil does not necessarily improve the degradation rate.

The rate of biodegradation is greatest on saturates, particularly those containing approximately 12–20 carbons. Aromatics and asphaltenes, which have a high molecular weight, biodegrade very slowly, if at all. This explains the durability of roof shingles containing tar and roads made of asphalt, as both tar and asphalt consist primarily of aromatics and asphaltenes. On the other hand, diesel fuel is a highly degradable product as it is largely composed of degradable saturates and lower aromatics. Light crudes are also degradable to a degree. While gasoline contains degradable components, it also contains some compounds that are toxic to some microorganisms. These compounds generally evaporate more rapidly, but in almost all cases, most of the gasoline

will evaporate before it can degrade. Heavy crudes contain little material that is readily degradable, and Bunker C contains almost none.

The rate of biodegradation is also highly dependent on the availability of oxygen. On land, oils such as diesel can degrade rapidly at the surface but very slowly if at all only a few centimeters below the surface, depending on oxygen availability. In water, oxygen levels can be so low that degradation is limited. It is estimated that it would take all the dissolved oxygen in approximately 400,000 L of seawater to completely degrade 1 L of oil. The rate of degradation also depends on the availability of nutrients such as nitrogen and phosphorus, which are most likely to be available on shorelines or on land. Finally, the rate of biodegradation also depends on the availability of the oil to the bacteria or other microorganisms. Oil degrades significantly at the oil–water interface at sea and, on land, mostly at the interface between the soil and the oil.

Biodegradation can be a very slow process for some oils. It may take weeks for 50% of a diesel fuel to biodegrade under optimal conditions and years for 10% of a crude oil to biodegrade under similar conditions. For this reason, biodegradation is not considered an important weathering process in the short term.

10.7.5 Sinking and Overwashing

If oil is more dense than the surface water, it may sometimes actually sink. Some rare types of heavy crudes and Bunker C can reach these densities and sink. When this occurs, the oil may sink to a denser layer of water rather than to the bottom. Less dense layers of water may override these denser layers of water. This occurs, for example, when seas are not high and warmer freshwater from land overrides dense seawater. Freshwater has a density of about 1.00 g/ml and the seawater a density of about 1.03 g/ml. An oil with a density greater than 1.00 but less than 1.03 would sink through the layer of freshwater and ride on the layer of salt water. The layer of freshwater usually varies in depth from about 1 to 10 m. If the sea energy increases, the oil may actually reappear on the surface, as the density of the water increases from 1.00 to about 1.03.

It is important to note that sinking of any form, whether to the bottom or to the top of a layer of dense seawater, is rare. When oil does sink, it complicates cleanup operations as the oil can be recovered only with underwater suction devices or special dredges.

Overwashing is another phenomenon that occurs quite frequently and can hamper cleanup efforts. At moderate sea states, a dense slick can be overwashed with water. When this occurs, the oil can disappear from view, especially if the spill is being observed from an oblique angle, as would occur if someone is observing a slick from a ship. Overwashing causes confusion about the fate of an oil spill as it can give the impression that the oil has sunk and then resurfaced.

A summary of the modeling formulations for sinking and submergence is given in the literature [40].

10.7.6 Formation of Tar Balls

Tar balls are agglomerations of thick oil less than about 10 cm in diameter. Larger accumulations of the same material ranging from about 10 cm to 1 m in diameter are called tar mats. Tar mats are pancake shaped, rather than round. Their formation is still not completely understood, but it is known that they are formed from the residuals of heavy crudes and Bunker C. After these oils weather at sea and slicks are broken up, the residuals remain in tar balls or tar mats. The reformation of droplets into tar balls and tar mats has also been observed, with the binding force being simply adhesion.

The formation of tar balls is the ultimate fate of many oils [37]. These tar balls are then deposited on shorelines around the world. The oil may come from spills, but it is also residual oil from natural oil seeps or from deliberate operational releases such as from ships. Tar balls are regularly recovered by machine or by hand from recreational beaches.

10.8 MOVEMENT OF OIL AND OIL SPILL MODELING

10.8.1 Spreading

Oil spreads to a lesser extent and more slowly on land than on water. Oil spilled on or under ice spreads relatively rapidly but does not spread to as thin a slick as on water [39]. On any surface other than water, such as ice or land, a large amount of oil is retained in depressions, cracks, and other surface irregularities.

After an oil spill on water, the oil tends to spread into a slick over the water surface. This is especially true of the lighter products such as gasoline, diesel fuel, and light crude oils, which form very thin slicks. Heavier crudes and Bunker C initially spread to slicks several millimeters thick. Heavy oils may also form tar balls and tar mats and thus may not go through progressive stages of thinning. The area of spreading for different types of oil is illustrated in Figure 10.6.

Oil spreads horizontally over the water surface even in the complete absence of wind and water currents. This spreading is caused by the force of gravity and the interfacial tension between oil and water. The viscosity of the oil opposes these forces. As time passes, the effect of gravity on the oil diminishes, but the force of the interfacial tension continues to spread the oil. The transition between these forces takes place in the first few hours after the spill occurs.

As a general rule, an oil slick on water spreads relatively quickly immediately after a spill. The outer edges of a typical slick are usually thinner than the inside of the slick at this stage so that the slick may resemble a “fried egg.” After a day or so of spreading, this effect diminishes.

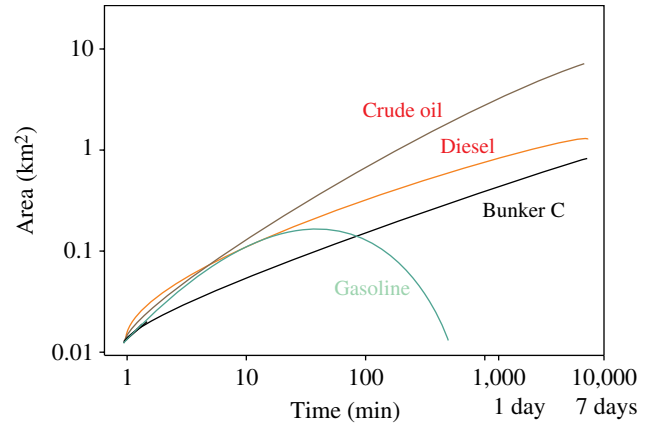


FIGURE 10.6 The spreading of several oils on the sea (10 tons each) less the amount evaporated. This is taken over a time period of 1 week. Gasoline initially spreads rapidly and then its area shrinks because of rapid evaporation.

Winds and currents also spread the oil out and speed up the process. Oil slicks will elongate in the direction of the wind and currents and, as spreading progresses, take on many shapes depending on the driving forces. Oil sheens often precede heavier or thicker oil concentrations. If the winds are high (more than 20 km/h), the sheen may separate from thicker slicks and move downwind.

A slick often breaks into “windrows” on the sea under the influence of either waves or zones of convergence or divergence. Oil tends to concentrate between the crests of waves simply due to the force of gravity. There are often vertical circulation cells in the top 20 m of the sea. When two circulation cells meet, a zone of convergence is formed. When two currents diverge, it forms a zone of divergence. Oil moving along these zones is alternately concentrated and spread out by the circulation currents to form ribbons or windrows of oil rather than continuous slicks. In some locations close to shore, zones of convergence and divergence often occur in similar locations so that oil spills may appear to have similar trajectories and spreading behavior in these areas.

The most common formulation of spreading is algorithms proposed by Fay. Formulation by Fay for gravity-viscous spreading is as follows [41,42]:

Initial area

$$A_0 = \pi \frac{k_1^4}{k_2^2} \left(\frac{V_o^5 g \Delta \rho}{\nu_w^2} \right)^{1/6} \quad (10.35)$$

where

$$\Delta \rho = \frac{\rho_w - \rho_o}{\rho_w}$$

where ρ_w is the density of the water, ρ_o is the density of the oil, k_1 and k_2 are spreading constants (typically 1.52 and 1.21, respectively), g is the gravitational acceleration, V_o is the volume of the oil spilled, and ν_w is the viscosity of the water.

As a function of time,

$$A_t = \pi k_2^2 \left(\frac{V_0^2 g \Delta \rho t^{1.5}}{v_w^{0.5}} \right)^{1/3} \quad (10.36)$$

where all is as before and t is the time since oil spilled in hours.

10.8.2 Movement of Oil Slicks

In addition to their natural tendency to spread, oil slicks on water are moved along the water surface, primarily by surface currents and winds. If the oil slick is close to land and the wind speed is less than 10 km/h, the slick generally moves at a rate that is 100% of the surface current and approximately 3% of the wind speed. In this case, wind does not generally play an important role.

If the wind speed is more than about 20 km/h, however, and the slick is on the open sea, wind predominates in

determining the slick's movement. Both the wind and surface current must be considered for most situations. The movement resulting from both wind and current inputs is illustrated in Figure 10.7.

When attempting to determine the movement of an oil slick, two factors affect accuracy. The more significant factor is the inability to obtain accurate wind and current speeds at the time of a spill. The other, very minor factor is a phenomenon commonly known as the Coriolis effect, whereby the earth's rotation deflects a moving object slightly

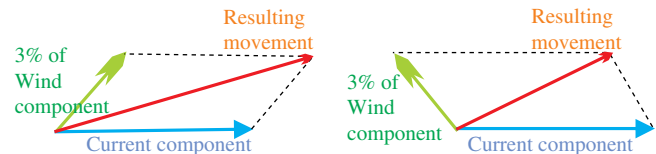


FIGURE 10.7 The effect of different wind and current directions on the resulting movement of an oil slick.

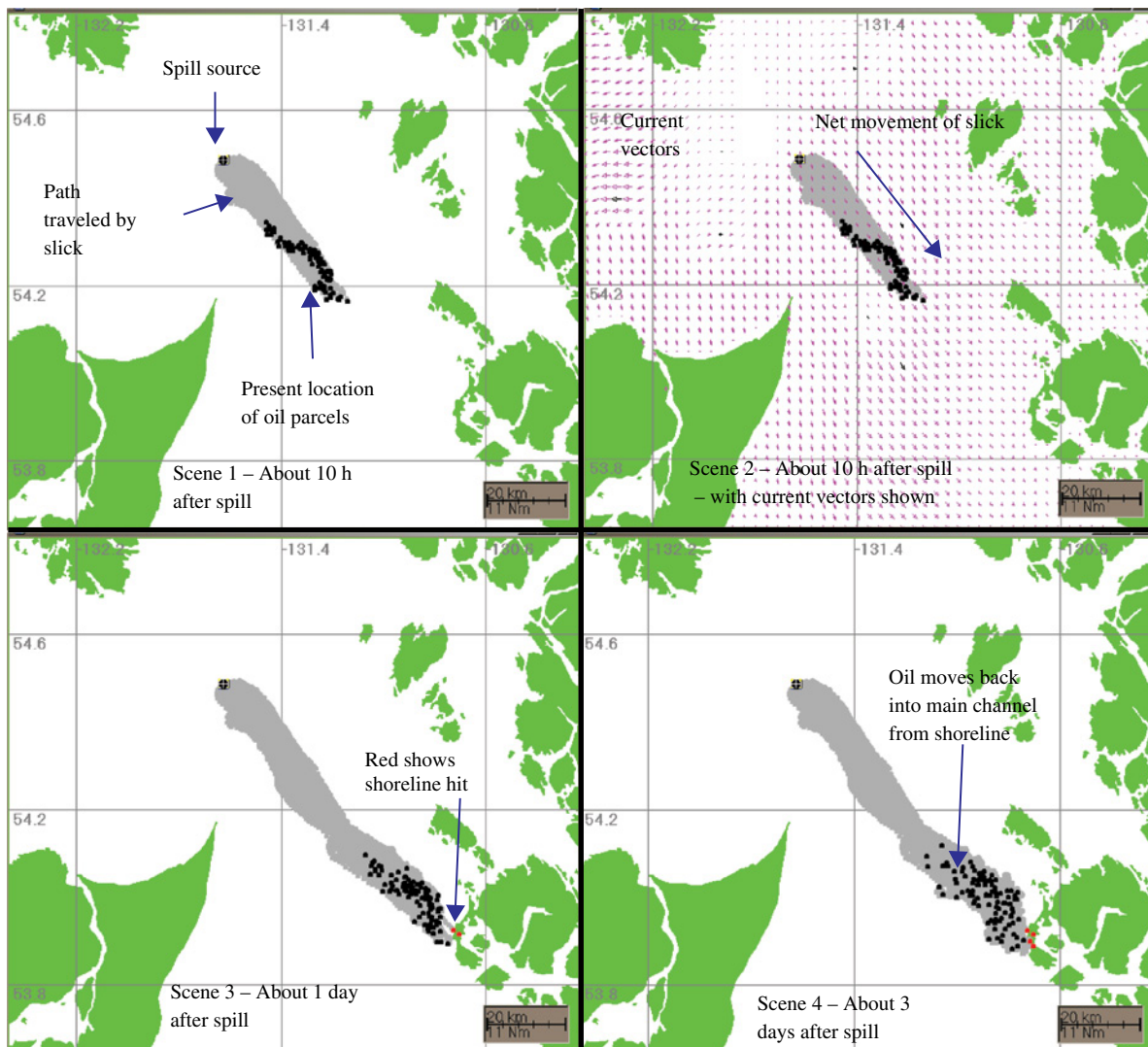


FIGURE 10.8 Illustration of the outputs of a spill trajectory model.

to the right in the northern hemisphere and to the left in the southern hemisphere.

10.9 SPILL MODELING

Spill response personnel need to know the direction in which an oil spill is moving in order to protect sensitive resources and coastline. To assist them with this, computerized mathematical models have been developed to predict the trajectory or pathway and fate of oil. Outputs of one such spill model are shown in Figure 10.8.

Today's sophisticated spill models combine the latest information on oil fate and behavior with computer technology to predict where the oil will go and what state it will be in when it gets there. Their major limitation to accurately predicting an oil slick's movement is the lack of accurate estimates of water current and wind speeds along the predicted path. This is likely to remain a major limitation in the future.

In addition to predicting the trajectory, these models can estimate the amount of evaporation, the possibility of emulsification, the amount of dissolution and the trajectory of the dissolved component, the amount and trajectory of the portion that is naturally dispersed, and the amount of oil deposited and remaining on shorelines. Accurate spill modeling is now a very important part of both contingency planning and actual spill response.

Spill models operate in a variety of modes. The most typical is the trajectory mode, which predicts the trajectory and weathering of the oil. The stochastic mode uses available data to predict a variety of scenarios for the oil spill, which includes the direction, fate, and property changes in the oil slick. In another mode, often called the receptor mode, a site on the shore or water is chosen and the trajectory from the source of the oil is calculated. Increasingly, statistically generated estimates are added to oil spill models to compensate for the lack of accurate knowledge of winds and currents.

REFERENCES

- [1] Boehm, P.D., D.S. Page, J.S. Brown, J.M. Neff, J.R. Bragg, and R.M. Atlas, Distribution and Weathering of Crude Oil Residues on Shorelines 18 Years After the Exxon Valdez Spill, *Environ. Sci. Technol.*, 42, 9210, 2008.
- [2] Wardlaw, G.D., J.S. Arey, C.M. Reddy, R.K. Nelson, G.T. Ventura, and D.L. Valentine, Disentangling Oil Weathering at a Marine Seep Using GCxGC: Broad Metabolic Specificity Accompanies Subsurface Petroleum Biodegradation, *Environ. Sci. Technol.*, 42, 7166, 2008.
- [3] Díez, S., E. Jover, J.M. Bayona, and J. Albaigés, Prestige Oil Spill. III. Fate of a Heavy Oil in the Marine Environment, *Environ. Sci. Technol.*, 41, 3075, 2007.
- [4] Short, J.W., G.V. Irvine, D.H. Mann, J.M. Maselko, J.J. Pella, et al., Slightly Weathered Exxon Valdez Oil Persists in Gulf of Alaska Beach Sediments After 16 Years, *Environ. Sci. Technol.*, 41, 1245, 2007.
- [5] French McCay, D.P., Modeling Impacts of Oil and Chemical Releases, *Sea Technol.*, 47, 21, 2006.
- [6] French-McCay, D., Modeling as a Scientific Tool in NRDA for Oil and Chemical Spills, *IOSC*, Savannah, GA, 2008.
- [7] Etkin, D.S., J. Michel, D.F. McCay, M. Boufadel, and H. Li, Development of a Practical Methodology for Integrating Shoreline Oil-Holding Capacity into Spill Modeling, *AMOP*, Calgary, AB, 564, 2008.
- [8] French-McCay, D., J. Rowe, and D.S. Etkin, Transport and Impacts of Oil Spills in San Francisco Bay—Implications for Response, *AMOP*, Calgary, AB, 159, 2008.
- [9] Fingas, M., Oil and Petroleum Evaporation, Chapter 7, in *Handbook of Oil Spill Science and Technology*, M. Fingas, Editor, John Wiley & Sons Inc., Hoboken, , 2014.
- [10] Jones, F.E., *Evaporation of Water*, Lewis Publishers, Chelsea, 1992.
- [11] Brutsaert, W., *Evaporation into the Atmosphere*, Reidel Publishing Company, Dordrecht, 1982.
- [12] Sutton, O.G., Wind Structure and Evaporation in a Turbulent Atmosphere, *P. R. Soc. Lond.*, 146, 701, 1934.
- [13] Stiver, W. and D. Mackay, Evaporation Rate of Spills of Hydrocarbons and Petroleum Mixtures, *Environ. Sci. Technol.*, 18, 834, 1984.
- [14] Stiver, W., *Weathering Properties of Crude Oils When Spilled on Water*, Master of Applied Science Thesis, Department of Chemical Engineering and Applied Chemistry, University of Toronto, 4, 110, 132, 1984.
- [15] Mackay, D. and R.S. Matsugu, Evaporation Rates of Liquid Hydrocarbon Spills on Land and Water, *Can. J. Chem. Eng.*, 51, 434, 1973.
- [16] Fingas, M., Studies on the Evaporation Regulation Mechanisms of Crude Oil and Petroleum Products, *Adv. Chem. Eng. Sci.*, 2, 246–256, 2012.
- [17] Fingas, M. and B. Fieldhouse, Water-in-Oil Emulsions: Formation and Prediction, Chapter 8, in *Handbook of Oil Spill Science and Technology*, M. Fingas, Editor, John Wiley & Sons Inc., Hoboken, 2014.
- [18] Environment Canada Oil Catalogue, http://www.etc-cte.ec.gc.ca/databases/Oilproperties/oil_prop_e.html, 2013 (accessed August 26, 2014).
- [19] Yetilmezsoy, K., M. Fingas, and B. Fieldhouse, Modeling Water-in-Oil Emulsion Formation Using Fuzzy Logic, *J. Multiple-Valued Logic Soft Comput.*, 1, 2011, 2012.
- [20] Yetilmezsoy, K., M. Fingas, and B. Fieldhouse, An Adaptive Neuro-Fuzzy Approach for Modeling of Water-in-Oil Emulsion Formation, *Colloids Surf. A*, 389, 50, 2011.
- [21] Fingas, M., Water-in-Oil Emulsions: Formation and Prediction, *AMOP*, Banff, AB, 460, 2011.
- [22] Lunel, T., The Braer Spill: Oil Fate Governed by Dispersion, *IOSC*, Long Beach, CA, 790, 1995.
- [23] Farwell, C., C.M. Reddy, E. Peacock, R.K. Nelson, L. Washburn, and D.L. Valentine, Weathering and the Fallout Plume of Heavy Oil from Strong Petroleum Seeps Near Coal Oil Point, CA, *Environ. Sci. Technol.*, 43, 3542, 2009.
- [24] Delvigne, G.A.L., *Experiments on Natural and Chemical Dispersion of Oil in Laboratory and Field Circumstances*,

- Publication No. 327, Delft Hydraulic Laboratory, Delft, The Netherlands, 1984.
- [25] Delvigne, G.A.L. and L.J.M. Hulsen, Simplified Laboratory Measurement of Oil Dispersion Coefficient: Application in Computations of Natural Oil Dispersion, *AMOP*, Vancouver, BC, 173, 1994.
 - [26] Delvigne, G.A.L. and C.E. Sweeney, Natural Dispersion of Oil, *Oil Che. Pollut.*, 4, 281, 1988.
 - [27] Delvigne, G.A.L. and C.E. Sweeney, *Natural Dispersion of Oil*, Publication No. 399, Delft Hydraulic Laboratory, Delft, The Netherlands, 1989.
 - [28] Delvigne, G.A.L., J.A. van der Stel, and C.E. Sweeney, *Measurement of Vertical Turbulent Dispersion and Diffusion of Oil Droplets and Oiled Particles*, Report No. Z 75-2, Delft Hydraulic Laboratory, Delft, The Netherlands, 1987.
 - [29] Delvigne, G.A.L., Natural and Chemical Dispersion of Oil, *J. Adv. Mar. Technol. Conf.*, 11, 23, 1994.
 - [30] Fingas, M., Introduction to Oil Spill Modeling, Chapter 8, in *Oil Spill Science and Technology*, M. Fingas, Editor, Gulf Publishing Company, New York, 187, 2011.
 - [31] Danchuk, S. and C.S. Willson, Numerical Modeling of Oil Spills in the Inland Waterways of the Lower Mississippi River Delta, *IOSC*, Savannah, GA, 887, 2008.
 - [32] Faksness, L.-G. and P.J. Brandvik, Distribution of Water Soluble Components from Arctic Marine Oil Spills—A Combined Laboratory and Field Study, *Cold Regions Sci. Technol.*, 54, 97, 2008.
 - [33] Taghvaei Ganjali, S., B. Nahri Niknafs, and M. Khosravi, Photooxidation of Crude Petroleum Maltenic Fraction in Natural Simulated Conditions and Structural Elucidation of Photoproducts, *Iran. J. Environ. Health Sci. Eng.*, 4, 37, 2007.
 - [34] Fernandez-Varela, R., M.P. Gomez-Carracedo, P. Fresco-Rivera, J.M. Andrade, S. Muniategui, and D. Prada, Monitoring Photooxidation of the Prestige's Oil Spill by Attenuated Total Reflectance Infrared Spectroscopy, *Talanta*, 69, 409, 2006.
 - [35] Plata, D.L., C.M. Sharpless, and C.M. Reddy, Photochemical Degradation of Polycyclic Aromatic Hydrocarbons in Oil Films, *Environ. Sci. Technol.*, 42, 2432, 2008.
 - [36] Plata, D. and C.M. Reddy, Photochemical Degradation of Select Polycyclic Aromatic Hydrocarbons: First-Order Disappearance Rates and Primary Degradation Mechanisms in Oil-Contaminated Coastal Zones, *ACS Nat. Meet. Book Abstr.*, 230, 2005.
 - [37] Khelifa, A., and L. Gamble, Prediction of Tar Ball Formation, *AMOP*, Vancouver, BC, 79, 2006.
 - [38] Lepo, J.E., C.R. Cripe, J.L. Kavanaugh, S. Zhang, and G.P. Norton, The Effect of Amount of Crude Oil on Extent of Its Biodegradation in Open Water- and Sandy Beach-Laboratory Simulations, *Environ. Technol.*, 24, 1291, 2003.
 - [39] Spaulding, M.L., A State-of-the-Art Review of Oil Spill Trajectory and Fate Modeling, *Oil Chem. Pollut.*, 4, 39, 1988.
 - [40] Fingas, M.F., B. Hollebone, and B. Fieldhouse, The Density Behaviour of Heavy Oils, in Water, *AMOP*, Vancouver, 57, 2006.
 - [41] Elliot, A., N. Hurford, and C. Penn, Shear Diffusion and the Spreading of Slicks, *Mar. Pollut. Bull.*, 17, 308, 1996.
 - [42] Fay, J.A., The Spread of Oil Slicks on a Calm Sea, in *Oil on the Sea*, D.P. Hoult, Editor, Plenum Press, New York, 53, 1969.

OCEANOGRAPHIC AND METEOROLOGICAL EFFECTS ON SPILLED OIL

C.J. BEEGLE-KRAUSE¹ AND WILLIAM J. LEHR²

¹*SINTEF, Trondheim, Norway*

²*Emergency Response Division, National Oceanic and Atmospheric Administration, Seattle, WA, USA*

List of Symbols	301	P	Pressure
11.1 Introduction	301	ρ_w	Water density
11.2 Chapter Scope	302	D_E	Ekman depth
11.3 Atmospheric Boundary Layer	302	H	Wave height
11.4 Water Currents	303	c	Wave speed
11.5 Waves	304	B	Beaufort number
11.6 Sea Spray	306	H_s	Significant wave height
11.7 Langmuir Cells	306	H_{rms}	Root mean square wave height
11.8 Oil Transport	307	f_{bw}	Wave-breaking fraction
11.9 Areas of Active Research	308	T_M	Monahan time constant
11.9.1 Ice	308	f_{aero}	Aerosol volume fraction
11.9.2 Lagrangian Coherent Structures	308	X_f	Fetch
11.9.3 Subsurface Well Blowouts	308	D_x, D_y	Horizontal diffusion coefficients

LIST OF SYMBOLS

K_m	Eddy viscosity
k_a	von Karman constant
u^*	Friction velocity
z_0	Roughness length
τ	Wave period
U	Surface wind speed
ρ_a	Air density
z_{ref}	Reference height
U_{ref}	Reference wind speed
U_{10}	Wind at 10 m elevation
C_D	Drag coefficient
f	Planetary vorticity
h	Water depth
Π	Potential vorticity
λ	Wave length
τ_s	Surface stress
ED	Excursion distance
U_s	Water surface current
U_c	Water current

11.1 INTRODUCTION

Most oil spills occur at the interface of two other large fluid bodies: the body of water that floats the oil (usually coastal) and the atmosphere, with winds that also move the oil. The interactions between these three fluids can be highly complex. Often, the key to predicting the transport and fate of an oil spill is to understand air–sea interaction. Where there is no wind, there would be no waves and no wind-driven transport of the oil, so most oils would float on the surface, not reaching the shoreline and the sensitive natural resources, such as bird rookeries, or valuable tourist resources, such as beaches. With wind, there can be waves, and the oil can be pushed onto the shoreline. Waves can be energetic enough to break the oil into small droplets, dispersing the oil into tiny droplets that submerge, the smallest droplets never to refloat. Thus, we need to understand both the ocean and the atmosphere in order to understand what happens to the oil.

11.2 CHAPTER SCOPE

While both kinetic energy and thermal energy are transferred between water and air, it is mostly a one-sided process. Ocean bodies can have a definite thermal effect on the atmosphere. The different climates of Labrador and England, roughly sharing the same latitude, amply demonstrate this point. The reverse is less the case because of the smaller heat capacity of air compared to that of water. Surface winds, however, do transfer momentum to the water surface by creating gravity waves and inducing surface currents. These waves and currents can greatly change the fate of floating oil.

As this is a book on oil spills, only a cursory summary of this complex subject can be given here. Emphasis is on air-sea phenomena that are required to calculate movement and fate of spilled oil. Many important topics are ignored or greatly simplified. The interested reader should consult an introductory oceanographic textbook for more in-depth coverage. Reed et al. touch on aspects of this chapter with more details regarding modeling the oil itself [1].

Some readers may find this chapter frustrating as we do not offer a comprehensive unified theory to describe oceanographic and atmospheric effects on oil spills. A full treatment of the topic would be a full volume in itself! Instead, the scope of this chapter reflects the author's preferences, through experience in operational spill response, in citing those studies and methods that have generally proven their use in the field, as opposed to those reflecting the latest fashion in academic research. Operational modeling is different than academic research. Publishing a paper is much easier than providing an accurate and useful trajectory in a real event, and the authors have worked on hundreds of spills between them.

11.3 ATMOSPHERIC BOUNDARY LAYER

The atmosphere makes up a very thin coating on the surface of this planet. The Kaman line of 100 km is often taken as the somewhat arbitrary atmospheric outer limit, but approximately three-fourths of the atmospheric mass lies within the first 10 km above the surface. This compares to the diameter of the earth of about 12,700 km. If the earth were shrunk to a standard desktop globe of 20 cm diameter, the outer limit of the atmosphere would be 1.5 mm with most of the gas being within the first 0.15 mm, about the thickness of a couple coats of paint. However, the part of the atmosphere important to oil spillage is often thinner. This is the planetary boundary layer, the lowest part of the atmosphere that is directly affected by (and affects) the surface of the earth [2]. The planetary boundary layer over marine areas is characterized by its interface with the ocean, a body with a very large heat capacity and that is typically turbulent. The exact depth of the boundary layer is determined by wind speed and surface roughness but usually exhibits close to neutral stratification over open waters due to the absence of the significant

differential surface heating often found over land. This is not necessarily the case for coastal areas where the air may be either stable (resists mixing) or unstable (rapid mixing). For the latter cases, mixing of the air is a function of both temperature stratification and mechanical turbulence with the former either increasing or dampening the latter. Meteorologists use a function with the dimension of length, called the Monin–Obukhov length after the inventors, to measure atmospheric stability. A negative Monin–Obukhov length applies to unstable conditions, while a positive length designates stable atmospheres. The value is zero for neutral conditions where the air density is nearly hydrostatically neutral. For neutral conditions, atmospheric turbulence is a purely mechanical phenomenon. A common situation over ocean waters, neutral stability greatly simplifies subsequent process formulation and will henceforth be assumed.

Because of its chaotic nature, it is not possible to predict exactly the turbulent wind patterns in the boundary layer. One simple averaging scheme is to treat turbulent mixing similar to molecular mixing, defining an eddy viscosity in analogy to the molecular term of the same name. This eddy viscosity, K_m , is the exchange coefficient for momentum and has the dimensions of kinematic viscosity, length squared divided by time. K-theory, also called first-order closure, approximates K_m as a constant (second-order closure models do not make this assumption and result in much more complex solutions for the boundary layer). K_m at the air-sea interface can be shown (Eq. 11.1) to be proportional to a product of local eddy velocity and surface eddy size or roughness length, z_0 . Average surface wind effectively vanishes at this height. For open water, z_0 is quite small, on the order of 0.1 mm.

$$K_m = k_a u^* z_0 \quad (11.1)$$

The friction velocity, u^* , is related to the average surface eddy velocity. The proportionality constant, k_a , is the von Karman constant, empirically measured to be approximately 0.4.

Stress, τ_s , at the interface is given by

$$\tau_s = K_m \rho_a \frac{\partial U}{\partial z} \quad (11.2)$$

where U is the surface wind speed at height z and ρ_a is the air density. The vertical wind speed is usually modeled by the use of a logarithmic profile. Then wind speed U at height z above the sea surface is approximated by

$$U = \frac{u^*}{0.4} \ln \left(\frac{z}{z_0} \right) \quad (11.3)$$

The roughness length, z_0 , is often mistakenly equated to obstacle heights but more properly depends on wind eddy size at the surface. For coastal waters, z_0 may range from a millimeter to a tenth of that for calm conditions. The term,

u^* , is called the friction velocity. While it has the dimensionality of a velocity, it actually represents the square root of the surface stress, τ_s , divided by the air density, ρ_a

$$u^* = \sqrt{\frac{\tau}{\rho_a}} \quad (11.4)$$

As neither surface stress nor friction velocity is easily measurable by the spill responder, they are usually estimated by inverting Equation 11.1 and solving for u^* , based upon a known wind measurement at a known height (for an alternative approach [3]). For example, most oil spill models are based upon the meteorological “surface wind,” which is actually the wind velocity at 10 m height. Direct measurement from a small vessel or from a pier might be at 3 m height. Using this measurement in Equation 11.1 to calculate u^* , the same equation can subsequently be employed to estimate wind speed at 10 m elevation, U_{10} .

A common alternative to the logarithmic profile is a power law expression

$$U = U_{\text{ref}} \left(\frac{z}{z_{\text{ref}}} \right)^p \quad (11.5)$$

In order to be consistent with Equation 11.1 at the reference height, z_{ref} , the exponent, p , must be chosen so that the numerical values of the two equations are the same. If 10 m is the reference height, then a typical value for p over open water is 0.11. Equations 11.1 and 11.3 will differ if used to estimate winds at heights significantly different from the reference height.

Another parameterization for surface friction that is commonly used is

$$u^* = \sqrt{C_D} U_{10} \quad (11.6)$$

where C_D is a dimensionless drag coefficient. Typical estimated values of C_D are ≈ 0.002 although the actual value varies somewhat with wind speed. However, in using this formula, investigators have discovered greater wind stress in developing wave fields compared to more developed seas [4].

11.4 WATER CURRENTS

A complete description of the phenomena creating water currents is beyond the scope of this chapter. There are certain common features to currents, particularly nearshore currents, that are important for oil spill transport. For example, the obvious observation that water cannot flow through solid barriers provides guidance to the spill forecaster predicting oil movement in coastal areas. Currents will flow parallel to the shoreline, carrying floating oil downstream along the shoreline. Other forces, usually wind stress, are required to cause beaching. One case is an onshore wind with water

currents, such that the wind moves the oil across the water onto the shoreline. Another is called “pinning” the oil, where oil has moved into an area on the rising tide and a light wind keeps the oil in place as the tide recedes. The oil is then stranded on the low-tide areas as the water recedes from under the oil.

For rivers and simple tidal estuaries, first-order flow is along streamlines. In these cases, the spill thickness changes as the water column changes in diameter: as water deepens and the water column decreases in diameter, the oil becomes thicker, while as the water shallows, the water column diameter becomes wider, and the oil thickness decreases as it spreads out. In more complex estuaries, flow may be three-dimensional and include surface convergence areas as the tide ebbs (conversely surface divergence areas as the tide floods). Oil, buoyant at the surface, collects in convergence zones. These collection areas can result in the reappearance of surface oil slicks.

Other processes can cause or destroy surface convergences. Particularly in tidal basins and estuaries, the ebb and flow of the tide significantly changes the volume of water. Convergence can also occur where two water masses of very different densities meet, such as a freshwater plume spreading out over salt water. In tidal areas, as water flows outward on with the ebbing tide, the water level drops. As the water comes together to flow out through the outlet, convergence lines can form in the surface water, with the water sinking below the line. As water flows inward on the incoming tide, the water rises and spreads over a wider area, leading to surface divergence.

Tide tables are a standard tool for the spill forecaster. While tides are principally the result of the interplay of gravitational attraction by the sun and the moon, the specific tides in a region may vary greatly. Most areas are dominated by the lunar component, with a periodicity of 12.42 h, but some regions will be mostly diurnal with a single major high tide with a period just short of a day.

About every 15 days, the phases of the major semidiurnal and diurnal component align, producing “spring tides” that are larger than normal. Smaller tides resulting from the two components being 90° out of phase are called neap tides. Oil that beaches on a spring tide is likely to remain high on the shoreline surface for an extended time. As mentioned earlier, tides in estuaries can cause surface oil convergence. Tide heights themselves may also increase as the wave front moves up the narrowing estuary. For closed bays of the right length and depth, amplification of wave height can be dramatic. Resonance between the incoming wave and the reflected wave can occur if the wave period satisfies Merian’s formula

$$\tau = \frac{2L}{\sqrt{gh}} \quad (11.7)$$

where L is the length of the bay. The Bay of Fundy in Canada is a classic example of such resonance.

Oil spill responders often use an approximate rule of thumb to estimate movement of a slick during a tidal cycle. Assuming that the surface water flow is predominantly semi-diurnal tidal current, the net excursion distance, ED, is approximately

$$ED = \int_0^{\pi/2} U_s \sin(2\pi/\tau) dt \approx 4U_s \quad (11.8)$$

where U_s is the surface current.

The movement of water, air, and floating oil is calculated with regard to the earth's surface, but the surface itself is rotating, giving rise to an apparent force characterized by f , the planetary vorticity or Coriolis parameter. This parameter varies from zero to twice the earth's angular velocity at the North Pole.

Horizontal flow in the coastal ocean flow can be estimated by assuming that Π , the potential vorticity, is conserved where [5]

$$\Pi = \frac{\nabla \times U_s + f}{h} \quad (11.9)$$

This generality translates as flow following bathymetric contours. In essence, the water columns of the flow become somewhat stiff in the larger scale. These columns tend to follow bathymetric contours as the currents move rather than the water column height changing. The water columns may move inshore or offshore as the bathymetric contours change inshore or offshore. This may cause the water columns to accelerate or decelerate as bathymetric contours become more steep or more gradual, in order to keep the water column height constant and the water currents moving.

In the deep ocean, the surface flow is wind and wave driven. Overall, the flow is geostrophic, driven by Ekman flow in the wind-driven surface layer. The geostrophic equation is

$$fz \times U_c = \frac{1}{\rho_w} \left(\nabla P + \frac{\partial \tau_s}{\partial z} \right) \quad (11.10)$$

where ρ_o is the mean density of the surface layer, P is the pressure, and τ is the wind stress. This results in the classic Ekman spiral, to the right in the Northern Hemisphere (NH) and to the left in the Southern Hemisphere (SH). The surface water moves at 45° to the right (NH; left SH) of the wind direction.

Ekman calculated the vertical change in this surface current by balancing frictional and Coriolis forces [6]. The currents decrease in strength but increase in rotational angle as one moves into the water column. The depth at which the subsurface flow is the reverse direction of the surface is called the Ekman layer depth, D_E . A typical value of D_E in the open ocean might be around 50–100m with the depth decreasing at higher latitudes. The Ekman layer is sometimes

equated to the wind mixed layer, the top layer of the ocean where temperature and salinity are fairly uniform, although the latter is a more complicated phenomenon. While Ekman spiral (rotation of current with depth) has been verified over a wide range of timescales, interaction with the mixed layer affects it. Vertical integration of the Ekman layer indicated an overall transport to the right of the wind (NH). Stratification of the underlying water flattens the spiral but does not prevent the wind-driven momentum from penetrating this layer.

Currents caused by wind stress have direct relevance to spilled oil transport. In most oil spill models, the wind drift is usually calculated based on some version of the “three percent rule” [7]. This rule states that the surface speed of the slick over the water surface is given by the value of

$$\sqrt{\frac{\rho_{oil}}{\rho_w}} U_{10} \approx 0.03 U_{10} \quad (11.11)$$

A surface water flow is also created with a rotation to the right (NH) due to Coriolis forces.

11.5 WAVES

Wave action has a profound effect on surface oil. Breaking waves disperse oil into the water columns, encourage formation of water-in-oil emulsions, and can impede efforts to contain or remove the spilled oil. Wave conditions are a commonly sought data requirement by the on-scene command. Waves can be caused by different events. The most catastrophic are probably tsunamis, caused by geological events or major storm surges that accompany hurricanes. However, most spill responses work in wave fields produced by normal wind stress.

Surface waves are characterized by their amplitudes, equal to half the wave height, H ; wavelengths, λ , defined as the distance between two successive peaks; and periods, τ , given as the time period between two peaks at the same location. Ocean surface waves are chiefly transverse waves. A cork floating on the water surface will bob up or down with little horizontal motion. However, the wave impulse will travel with a speed, c , given by

$$c = \frac{\lambda}{\tau} \text{ for deepwater waves} \quad (11.12)$$

and

$$c = \sqrt{\frac{g\lambda}{2\pi} \tanh\left(\frac{2\pi \times h}{\lambda}\right)} \text{ for shallow – water waves} \quad (11.13)$$

The latter are defined by water shallow enough to allow bottom affects to influence the wave speed. For very shallow

waters, wave speed is a function of depth alone, being proportional to the square root of the water depth. Displacing water above or below this static level takes energy. The total energy per unit area of wave is given by

$$E = 1/8 \rho_w g H^2 \quad (11.14)$$

where ρ_w is the water density. Four major factors influence the development of wind waves on the ocean: wind speed, fetch, duration, and water depth. Mariners and ocean engineers have developed empirical, practical formulas to estimate and characterize these waves. Wind speed usually refers to surface wind, that is, wind at 10 m elevation although some formulas use correction factors. Waves will form at the air–sea interface when the wind speed is approximately 1 m/s or greater. Fetch refers to the length of water over which a given wind has blown. The longer the fetch, the larger the expected wave height. Duration refers to the time extent of the given wind strength and direction. Water depth becomes important in shallow areas where bottom friction will have an effect. For over two centuries, mariners have used an empirical scale, called the Beaufort scale, to estimate surface winds on the open ocean from observed sea conditions. Traditionally, a Beaufort number was assigned to the number of sails that had to be furled because of wind strength. The Beaufort number, B , can be roughly related to wind speed in m/s by the formula

$$U = 0.836 B^{1.5} \quad (11.15)$$

Of course, a real ocean wave field is a mixture of values for all three of these terms. The smallest waves have both gravity and surface tension as restoring forces, while larger waves are affected by gravity alone. The former, called capillary waves, are important in oil spill detection because surface oil tends to dampen these waves, causing a noticeable drop in surface roughness. Radar-equipped satellites and aircraft can observe this smoother surface. Normal, locally generated, wind waves have wavelengths up to roughly a hundred meters and periods of a few seconds. Swells, which are long-wavelength waves generated by significant storms long distances away, have deeper penetration into the ocean.

There are several methods to describe the strength of surface waves. The most common is to specify the average height of the largest one-third of the waves, called the significant wave height, H_s . This is used for sea-state reporting and wave forecasting because significant height tends to be statistically stable, a feature not true for simply the largest observed height. For spill response, guidelines to estimate effectiveness of boom deployments often use significant wave height as one of the determining parameters. Another common height is the root mean square, H_{rms} . Since the two are approximately related by a constant, $H_s \approx 1.4 H_{rms}$, specifying one defines the other.

Sverdrup and Munk, later modified by Bretschneider [8,9], using dimensional analysis, produced a simple set (the SMB model for the three developers) of empirical formulas to estimate significant wave heights and periods for fully developed seas in deep water that have been widely applied for coastal engineering and are part of common oil spill fate and behavior models [10]:

$$\begin{aligned} \frac{g H_s}{U_{cor}^2} &= 0.283 \tan h \left(0.0125 \left(\frac{g X_f}{U_{cor}^2} \right)^{0.42} \right) \\ \frac{g T_s}{2\pi U_{cor}} &= 1.2 \tan h \left(0.077 \left(\frac{g X_f}{U_{cor}^2} \right)^{0.25} \right) \end{aligned} \quad (11.16)$$

Here, X_f is the fetch and U_{cor} is the corrected wind speed to adjust for factors such as air–sea temperature differences and shortness in wind measurement duration. Alternative formulas exist for unlimited fetch and shallow water conditions.

Other researchers developed similar formulas that also account for other factors such as peak wave frequency and angle between wave field and wind direction [11]. This assumes some choice of wave spectrum. Based upon actual observation and computational convenience, a common distribution choice for maximum wave height is the Rayleigh distribution, given by the formula

$$p(H) = \frac{H}{\sigma(H)} \exp\left(\frac{-H^2}{2\sigma^2}\right) \quad (11.17)$$

where $p(H)$ is the probability of height H and σ is the standard deviation in heights.

The Rayleigh distribution is commonly used for many environmental applications. For open water waves, the assumptions that justify this choice are that the individual horizontal wave velocity components are independent and normally distributed. The various moments of the distribution can be related to physical quantities, for example, the significant wave height $H_s = 4\sigma$.

With the advent of powerful computers, numerical models have been developed. These are sometimes referred to as third-generation wave models, with the SMB models being the first and spectral models being the second generation. One of the most widely used is the WAM model produced for the U.S. National Oceanic and Atmospheric Administration (NOAA) [12]. WAM estimates the evolution of the wave energy spectrum by solving the wave transport equation explicitly without any assumption on the wave spectrum, as was the case with most of the earlier models. Another popular model is the Simulated Waves Nearshore model developed by the Delft University of Technology, which computes random, short-crested waves from wind fields in areas of inland and coastal waters [13].

An important sea surface phenomenon in calculating dispersion of oil into the water column is breaking waves. In fact, most spill behavior models require breaking wave conditions for dispersion to happen. While waves that have small amplitude (height), H , compared to their wavelength, λ , can be accurately approximated by a sine function, these waves become more peaked as the ratio increases, with wave breaking occurring at $H/\lambda \approx 0.08$. Waves of any wavelength will break in shallow waters when the wave height is greater than 80% of the water depth wave parameters are illustrated in Figure 11.1.

A significant challenge for oil spill modelers is accurately estimating breaking wave fraction, f_{bw} , for a given wind strength [14,15]. Lehr and Simecek-Beatty, utilizing the studies of Monahan, suggest [16,17]

$$f_{bw} = \frac{0.025(U-3)}{T_M} \quad 0 \leq U \leq 4 \quad (11.18)$$

$$f_{bw} = \frac{0.01U + 0.01}{T_M} \quad U > 4$$

where T_M is the Monahan's time constant in seconds. Several studies suggest that breaking waves should be modeled using higher-order function of wind than the linear function in the preceding text [18,19]. However, Ding and Farmer argue that these studies include both active whitecaps and foam, thus resulting in a much more rapid increase with wind speed for effective f_{bw} than actually present [14].

The experimental results of Delvigne and Sweeney indicate that the maximum intrusion depth due to breaking waves is about one and half the height of the breaking wave [20]. Oil droplets caught in the breaking waves are driven into the water column as the breaking wave energy is dissipated. Delvigne and Sweeney estimate that the dissipated wave energy per unit surface area is approximately related to the root mean square wave height H_{rms} . The turbulent energy dissipates into finer length scales, finally reaching the Kolmogorov microscale of about a millimeter.

11.6 SEA SPRAY

Wind will also create surface spray above the water [21]. If oil is present, it will be entrained in the water droplets. Presumably, this should increase the volatilization rate of the slick, but few spill evaporation models take this process into account. Exton et al. used field data from the Outer Hebrides to fit an empirical formula for f_{aero} , the aerosol volume fraction in the surface marine atmospheric layer [22]:

$$\ln(f_{aero}) = aU_{10} + b \quad (11.19)$$

Typical values for the constants are $a \approx 0.2$ s/m and $b \approx -23$. They point out that the aerosol droplet size distribution can

be separated into droplets smaller than $0.3 \mu\text{m}$, which remain for longer periods in the atmosphere, and bigger droplets, which are locally produced from sea foam (whitecaps) bubbles bursting that return back to the water surface.

There are actually two mechanisms for droplet formation from whitecaps [23]. As the air bubbles that form a whitecap burst, the film breaks into droplets over various sizes that peak in number around a few microns in diameter. The pressure released from the collapsing bubble creates a second set of larger droplets that can reach a few hundred microns in diameter. A third set of droplets are formed from direct wind removal (spume), which can produce even larger droplets.

Several authors have developed semiempirical formulas for droplet formation per unit droplet size [24,25]. Unfortunately, there is little standardization even in the terminology applied. A popular model [26] uses the whitecap calculation of Monahan and O'Muircheartaigh [19] multiplied by a droplet production spectrum term that is interpolated from field measurements. Andreas suggests wide discrepancy in different model results, indicating that this is an area for further study [21].

11.7 LANGMUIR CELLS

An important consideration for oil spill cleanup options is the tendency of surface water to form windrows or Langmuir cells, vortices in the surface water with axis along the direction of the wind. Oil collects in the valleys of these cells, while the peaks are relatively oil-free. Skimmers align with these windrows to greatly increase their oil collection efficiency.

In the open ocean, these cells form at a continuum of scales ranging from a few millimeters to a hundred meters across. Langmuir circulations reside in, and are partly responsible for maintaining the surface mixed layer. Smith et al. showed that the maximum spacing between any two windrows is about two to three times the mixed layer depth

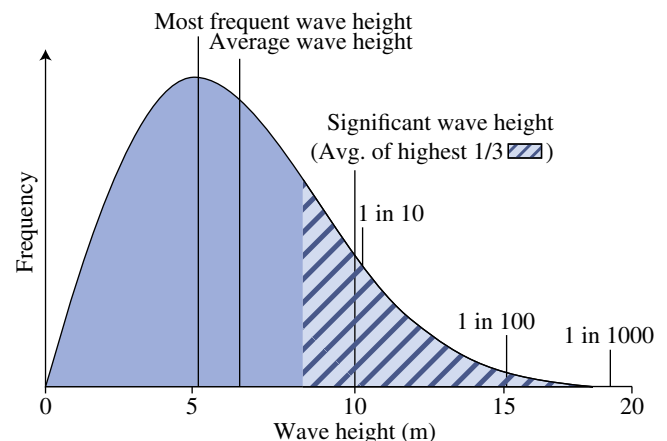


FIGURE 11.1 Rayleigh distribution of wave heights (NOAA).

[27]. This fact is sometimes used by oil spill observers to give a rough estimate of the mixed layer in estimating dispersed oil penetration.

Leibovich and Lumley claimed that the phenomenon was a product of the interaction of wave orbital motions with slowly varying, wind-induced surface currents [28]. Variations of their original formulation have been used to develop modified oil dispersion models [29–31]. These models have only recently been included in industry oil behavior software [32]. If these models are correct, then spilled oil will spread and move proportionally faster along the direction of the wind than standard spill models predict. Also, for dispersed oil droplets large enough that buoyancy forces cannot be neglected, there are subsurface locations on the Langmuir vortices where positive buoyancy is matched by downward vertical velocity. These Stommel retention zones would then partly trap the droplets, resulting in higher oil concentrations in these zones. However, Langmuir cells are quite transitory. Thorpe et al. suggest that most Langmuir cells under variable wind conditions have lifetimes measured in minutes, so observing this effect in typical spill conditions would be difficult [30]. A more general theory about the variation in scales of these cells is wave–current interaction modifying the turbulence regime and special variance in the Langmuir cells and spill windrows [33].

11.8 OIL TRANSPORT

Spilled oil that is buoyant adds a new fluid and two new interfaces (oil–air and oil–water) to the situation. Other sections in this text discuss in detail the change in oil properties that occur at these interfaces. This section will concentrate on the movement of the oil, either by spreading or transport. The former refers to the oil surface area expanding by gravitational forces acting on the slick or through the interaction of the oil–water interface. The latter examines the net movement of the oil either through wind stress or surface current.

An operationally reliable surface oil spreading model does not yet exist except under very specialized conditions. Realistic initial information available in a spill incident is insufficient to predict spreading with any certainty, providing at best probability estimates of spill coverage.

Oil begins to spread as soon as it is spilled, but it does not spread uniformly. Any shear in the surface current will cause stretching, and even a slight wind will cause a thickening of the slick in the downwind direction. Most spills quickly form a comet shape where a small black region is trailed by a much larger sheen that can be of varying colors. Figure 11.2 demonstrates this phenomenon for an experimental spill of 50 bbl of Arabian crude oil. Figure 11.3 shows a generalized oil transport concept.

Fay developed a formula for oil spreading that envisioned three spreading regimes due to internal forces and neglecting surface water turbulence [34]. This formula has fared poorly for describing actual spills [35]. Alternative approaches have

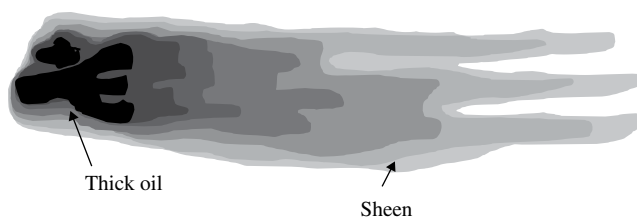


FIGURE 11.2 Uneven surface spreading of 50 bbl crude oil spill (lehr).

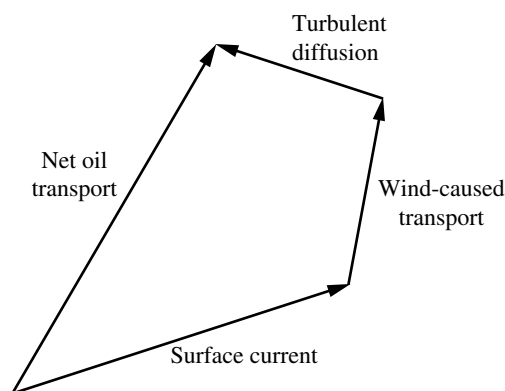


FIGURE 11.3 Oil transport diagram.

treated the oil as a passive component of the surface water and looked at spreading as a non-Fickian dispersion phenomenon [36,37].

Wind stress plays a role not only in slick transport but also in spreading. Roughly two-thirds of slick movement represents Stokes drift of the surface waves. One of the recent advances is the vertical Stokes drift in coastal waters [38]. The remaining one-third represents the movement of the slick along the water surface. Also, oil is driven into the water column by breaking waves and broken into droplets of different size [20]. The larger droplets quickly resurface, while the smaller droplets remain subsurface for longer time periods and trail the moving main slick. This is likely the cause for the “comet” shape.

The simplest trajectory model for oil slick transport is a vector sum of the distance as a result of each action upon the oil:

Wind-caused transport is, as discussed earlier, approximately 3% of the wind speed at 10m height. The turbulent diffusion component recognizes that the surface currents are approximate averages over the resolution scale of our forecast model or surface measurement. Smaller, unresolved eddies will cause a net random diffusion approximated by defining constant horizontal diffusion coefficients D_x and D_y [38].

Some models use a parameterization of the Stokes drift for oil movement due to wind waves rather than a 3% windage factor. Research areas are in wave current interaction and the resulting modification of the surface turbulence fields [33].

Spills are challenging because of the lack of information available both on the oil itself and, particularly, the local environmental conditions. This is called an “under-determined system,” where there is not enough information to provide an exact answer or prediction. Numerical models are used both to fill in information based on field observations and to assist the user in making predictions. The model requires individual information about each physical process (e.g., winds, currents, turbulence), each with associated errors. Even the best oil spill model does poorly when provided inaccurate or incomplete information. Error estimates can be used to constrain the model results or, at least, advise the user of potential inaccuracies.

Most oil spill trajectory models are “particle-tracking models” also known as “Eulerian–Lagrangian” models. The oil is simulated as particles (or “Lagrangian Elements”) moving within continuous fields of winds, currents, and turbulence (or “Eulerian” fields). These particle models may be two- or three-dimensional, depending on the user’s interest. These models use a variety of spill information (time, location, volume, and oil types) to move the oil within the environmental fields. The environment may be a custom forecast, a model prediction, a historical climatology, or other environmental information related to the situation at hand. For planning purposes, many trajectories may be run over a long (decadal) time period to develop statistics of where spills could go. During a response, a predictive model or custom forecast may be used to estimate where the spill will be over the next operational period of the spill response. The accuracy of the input fields determines the value of the results.

11.9 AREAS OF ACTIVE RESEARCH

11.9.1 Ice

As yet, a comprehensive model of oil and ice interaction has not been developed, though work is advancing [39]. With the potential of arctic development and increased vessel traffic due to climate change, many groups are looking at development of oil and ice interaction modeling. A recent review by Drozdowski et al. [40] describes some of the oil–ice challenges. Modeling oil interaction with ice is difficult because the oil can be on top of the ice, within the ice in brine channels, and under the ice. When floating oil and ice interact, some portion of the spilled oil will move with the ice, which does not necessarily follow surface currents the way traditional slicks would. Current simplistic rules of thumb move oil independently to the ice at ice concentrations below 60%, while the ice is viewed to control the oil at ice concentrations above 60%. If the oil is completely encapsulated in the ice, tracking oil transport becomes chiefly one of tracking ice movement. However, oil trapped in the ice

may also migrate through the ice and detection of oil in and under ice is very difficult. Current proposed technologies, involving such tools as nuclear magnetic resonance, while often exotic, are problematic at best. Even if the ice and oil remain separate, the presence of ice cover affects local current and wave patterns.

Weathering behavior for oil in ice-covered waters is different as well. Evaporation is usually slower, and dispersion and emulsification can be retarded—although brash ice may increase oil scavenging. Hopefully, the large research effort in this area will develop new, more accurate, arctic weathering models to handle such conditions.

11.9.2 Lagrangian Coherent Structures

Application of chaos theory to Lagrangian problems is an active area of research, including for oil spills [41]. These Lagrangian coherent structures (LCS) form the underlying skeleton of fluid flow and so control the overall path and shape of an oil spill [42] and can be used for early detection of areas of rapid change in the surface expression of the spill [43]. One advantage of these calculations is that they are independent of any trajectory model. Transport barriers from LCS provide information on where the oil spill cannot travel, which can provide additional information to traditional trajectory forecasting. With advances in braid theory for use in calculating transport barriers, there is potential to advance this technique for use in ice modeling and thus in future ice–oil interaction models [44].

11.9.3 Subsurface Well Blowouts

Two high-volume subsurface blowouts have shaped our understanding of well blowouts that start beneath the surface of the water. The first was the IXTOC I exploratory well in 1979, which lasted approximately nine months, and the next was the Deepwater Horizon oil spill (also known as “Mississippi Canyon 252 oil spill” or “Macondo oil spill”) in 2010, which lasted approximately 3 months. The high pressures of the seabed and other factors make response to these events very challenging. Droplet size distribution is a key issue because the smallest droplets may rise so slowly as to not reach the surface or not in significant amount to cause a sheen, while the largest droplets rise quickly enough for the oil to reach the surface. Hence, droplet size distribution controls the mass balance between the recoverable and the nonrecoverable oil.

Books have and will be written on the Deepwater Horizon oil spill. For a preliminary look on modeling efforts, see the American Geophysical Union (AGU) volume *Monitoring and Modeling the Deepwater Horizon Oil Spill: A Record Breaking Enterprise* [45]. All the federal data and modeling results are available through the web portal to the Emergency Response Mapping Application on the U.S. National Oceanic and Atmospheric Administration website. A variety of analysis reports are also available, such as the Deepwater Horizon Study Group final report [45].

REFERENCES

- [1] Reed, M., Ø. Johansen, P.J. Brandvik, P. Daling, A. Lewis, R. Fiocco, D. Mackay, and R. Prentik, Oil Spill Modeling Towards the Close of the 20th Century: Overview of the State of the Art, *Spill Sci. Technol. Bull.*, 5 (1), 3–16, 1999.
- [2] Lettau, H., *Atmosphärische Turbulenz*, Akademische Verlagsgesellschaft, Leipzig, 283, 1939.
- [3] Hara, T. and S.E. Belcher, Wind Profile and Drag, Coefficient over Mature Ocean Surface Wave Spectra, *J. Phys. Oceanogr.*, 34, 2345, 2004.
- [4] Vickers, D. and L. Mahrt, Fetch Limited Drag Coefficients, *Boundary Layer Meteorol.*, 85, 53, 1997.
- [5] Pedlosky, J., *Geophysical Fluid Dynamics*, 2nd ed., Springer-Verlag, New York, 710, 1987.
- [6] Ekman, V.W., On the Influence of the Earth's Rotation on Ocean Currents, *Ark. Mat. Astron. Fys.*, 2, 1, 1905.
- [7] Stolzenbach, K.D., O.S. Madsen, E.E. Adams, A.M. Pollack, and C. Cooper, *A Review and Evaluation of Basic Techniques for Predicting the Behavior of Surface Oil Slicks*, Prepared for the National Oceanic and Atmospheric Administration, Seattle, WA, 1977.
- [8] Bretschneider, C.L., The Generation and Decay of Wind Waves in Deep Water, *Trans. Am. Geophys. Union*, 33, 381, 1952.
- [9] Bretschneider, C.L., *Wave Variability and Wave Spectra for Wind Generated Gravity Waves*, Tech. Memo No. 118, Beach Erosion Board, U.S. Army Corps of Engineers, Washington, DC, 1959.
- [10] Lehr, W., R. Jones, M. Evans, D. Simecek-Beatty, and R. Overstreet, Revisions of the ADIOS Oil Spill Model, *Environ. Model. Softw.*, 17, 191, 2002.
- [11] Hasselmann, K., T. Barnett, E. Buwos, H. Carlson, D. Cartwright, K. Enke, J. Ewing, H. Gienapp, D. Hasselmann, P. Kruseman, A. Merrburg, P. Muller, D. Olbers, K. Richter, W. Sell, and H. Waldon, Measurements of Wind-Wave Growth and Swell Decay during the Joint North Sea Wave Project (JONSWAP), *Dtsch. Hydrogr. Z.*, A12, 95, 1973.
- [12] Komen, G., L. Cavaleri, M. Donelan, K. Hasselmann, and P. Janssen (Eds), *Dynamics and Modelling of Ocean Waves*, Cambridge University Press, Cambridge, 1994.
- [13] Delft University of Technology, "The Official SWAN Home Page," <http://swanmodel.sourceforge.net/>, accessed January 10, 2013.
- [14] Ding, L. and D. Farmer, Observations of Breaking Wave Statistics, *J. Phys. Oceanogr.*, 24, 1368, 1994.
- [15] Thorpe, S.A. and P.N. Humphries, Bubbles and Breaking Waves, *Nature*, 283, 463, 1980.
- [16] Lehr, W. and D. Simecek-Beatty, The Relation of Langmuir Circulation Processes to the Standard Oil Spill Spreading, Dispersion, and Transport Algorithms, *Spill Sci. Technol. Bull.*, 6, 247, 2000.
- [17] Monahan, E.C., Oceanic Whitecaps, *J. Phys. Oceanogr.*, 1, 139, 1971.
- [18] Wu, C., Oceanic Whitecaps and Sea State, *J. Phys. Oceanogr.*, 9, 1064, 1979.
- [19] Monahan, E. and I. O'Muircheartaigh, Optimal Power-law Description of Oceanic Whitecap Coverage, Dependence on Wind Speed, *J. Phys. Oceanogr.*, 10, 2094, 1980.
- [20] Delvigne, G.A.L. and C.E. Sweeney, Natural Dispersion of Oil, *Oil Chem. Pollut.*, 4, 281, 1988.
- [21] Andreas, E.L., A New Sea Spray Generation Function for the Wind Speeds up to 32 m/sec, *J. Phys. Oceanogr.*, 28, 2175, 1998.
- [22] Exton, H., J. Latham, P. Park, S. Perry, M. Smith, and R. Allen, The Production and Dispersal of Marine Aerosol, *Q.J.R. Meteorol. Soc.*, 111, 817, 1985.
- [23] Kientzler, C., C. Arons, D. Blanchard, and A. Woodcock, Photographic Investigations of the Projection of Droplets by Bubbles Bursting at a Water Surface, *Tellus*, 6, 1, 1954.
- [24] Ling, S., T. Kao, and A. Saad, Microdroplets and Transport of Moisture from Ocean, *Proc. ASCE J. Eng. Mech. Div.*, 106, 1327, 1980.
- [25] Pattison, M. and S. Belcher, Production Rates of Sea-Spray Droplets, *J. Geophys. Res.*, 104, 18397, 1999.
- [26] Fairall, C., J. Kepert, and G. Holland, The Effects of Sea-Spray on Surface Energy Transports Over the Ocean, *Global Atmos. Ocean Syst.*, 2, 121, 1994.
- [27] Smith, J., R. Pinkel, and R. Weller, Vertical Structure in the Mixed Layer During Mildex, *J. Phys. Oceanogr.*, 17, 425, 1987.
- [28] Leibovich, S. and J.L. Lumley, *A Theoretical Appraisal of the Joint Effects of Turbulence and of Langmuir Circulations on the Dispersion of Oil Spilled in the Sea*, U.S. Coast Guard Office of Research and Development Report CG-D-26-82, Washington, DC, 119, 1981.
- [29] Leibovich, S., *Surface and Near-Surface Motion of Oil in the Sea*, Report to U.S. Minerals Management Service, Herndon, VA, Contract 14-35-0001-30612, 1997.
- [30] Thorpe, S.A., M.S. Cure, A. Graham, and A.J. Hall, Sonar Observations of Langmuir Circulation and Estimation of Dispersion of Floating Particles, *J. Atmos. Oceanic Technol.*, 11, 1273–1294, 1994.
- [31] Li, M., Estimating Horizontal Dispersion of Floating Particles in Wind-Driven Upper Ocean, *Spill Sci. Technol. Bull.*, 6 (3), 255–261, 2000.
- [32] Galt, J. and R. Overstreet, *Development of Spreading Algorithms for the ROC*, Genwest Systems, Inc. Technical Note, Seattle, 68, 2009.
- [33] Sullivan, P.P. and J.C. McWilliams, Dynamics of Winds and Currents Coupled to Surface Waves, *Annu. Rev. Fluid Mech.*, 42, 19–42, 2010.
- [34] Fay, J.A., Physical Processes in the Spread of Oil on a Water Surface, in *Proceedings of the Joint Conference on Prevention and Control of Oil Spills*, American Petroleum Institute, Washington, DC, 463–467, 1971.
- [35] Lehr, W.J., H.M. Cekirge, R.J. Fraga, and M.S. Belen, Empirical Studies of the Spreading of Oil Spills, *Oil Petrochem. Pollut.*, 2, 7–12, 1984.
- [36] Elliot, A.J., N. Hurford, and C.J. Penn, Shear Diffusion and the Spreading of Oil Slicks, *Mar. Pollut. Bull.*, 17, 308–313, 1986.
- [37] McWilliams, J.C., J.M. Restrepo, and E.M. Lane, An Asymptotic Theory for the Interaction of Waves and Currents in Coastal Waters, *J. Fluid Mech.*, 511, 135–178, 2004.
- [38] Barker, C.H. and J.A. Galt, Analysis of methods used in spill response planning: Trajectory Analysis Planner TAP II. In *Proceedings of the 1999 International Marine Environmental Modeling Seminar*, Lillehammer, Norway. SINTEF Applied Chemistry, Trondheim, Norway, 1999.

- [39] Yapa, P.D. and S.A. Weerasuriya, Spreading of Oil Spilled Under Floating Ice, *J. Hydraul. Eng.*, 123, 676–683, 1997.
- [40] Drozdowski, A., S. Nudds, C.G. Hannah, H. Niu, I. Peterson, and W. Perrie, *Review of Oil Spill Trajectory Modeling in the Presence of Ice*, Canadian Technical Report of Hydrographic and Ocean Sciences. Ocean Sciences Division, Maritimes Region, Fisheries and Oceans Canada, Volume 274, 89, 2011.
- [41] Peacock, T. and G. Haller, Lagrangian Coherent Structures: The Hidden Skeleton of Fluid Flows, *Phys. Today*, 66, 41, 2013.
- [42] Beegle-Krause, C.J., T. Peacock, and M. Allshouse, Exploiting Lagrangian Coherent Structures (LCS) for the Calculations of Oil Spill and Search and Rescue Drift Patterns in the Ocean, in *Proceedings of the 34th AMOP Technical Seminar*, Banff Environment Canada, Ottawa, ON, pp. 169–176, 2011.
- [43] Olascoaga, M.J. and G. Haller, Forecasting Sudden Changes in Environmental Contamination Patterns, *Proc. Natl. Acad. Sci.*, 109, 4738–4743, 2012.
- [44] Allshouse, M.R. and J.-L. Thiffeault, Detecting Coherent Structures Using Braids, *Physica D*, 241 (2), 95–105, 2011.
- [45] Deepwater Horizon Study Group (DHSG), *Final Report on the Investigation of the Macondo Well Blowout*, Deepwater Horizon Study Group, Washington, DC, 124, 2011.

PART VII

DETECTION, TRACKING, AND REMOTE SENSING

OIL SPILL REMOTE SENSING

MERV FINGAS¹ AND CARL E. BROWN²

¹*Spill Science, Edmonton, Alberta, Canada*

²*Emergencies Science and Technology Section (ESTS), Environment Canada, Ottawa, Ontario, Canada*

12.1	Introduction	313
12.2	Atmospheric Properties	314
12.3	Oil Interaction with Light and Electronic Waves	314
12.4	Visible Indications of Oil	316
12.5	Optical Sensors	317
12.5.1	Visible	317
12.5.2	IR	323
12.5.3	Near IR	323
12.5.4	UV	325
12.6	Laser Fluorosensors	325
12.7	Microwave Sensors	326
12.7.1	Radiometers	326
12.7.2	Radar	327
12.7.3	Microwave Scatterometers	331
12.7.4	Surface-Wave Radars	331
12.7.5	Interferometric Radar	331
12.8	Slick Thickness Determination	331
12.8.1	Visual Thickness Indications	331
12.8.2	Slick Thickness Relationships in Remote Sensors	332
12.8.3	Specific Thickness Sensors	332
12.9	Integrated Airborne Sensor Systems	333
12.10	Satellite Remote Sensing	334
12.10.1	Optical	334
12.10.2	Radar	335
12.11	Oil-Under-Ice Detection	340
12.12	Underwater Detection and Tracking	340
12.13	Small Remote-Controlled Aircraft	344
12.14	Real-Time Displays and Printers	345
12.15	Routine Surveillance	345
12.16	Future Trends	346
12.17	Recommendations	347

12.1 INTRODUCTION

Large spills of oil and related petroleum products in the marine environment may have substantial environmental impacts [1]. Remote sensing plays an increasingly important role in oil spill response efforts. Public and media scrutiny is usually intense following a spill, with demands that the location and extent of the oil spill be accurately determined. Through the use of modern remote sensing instrumentation, oil can be monitored on the open ocean on a 24 h basis [2]. With a knowledge of slick locations, response personnel can more effectively plan countermeasures. A strong role for remote sensing has been the detection of illegal discharges, especially in view of the large seabird mortality associated with such discharges [3].

The operational use of remote sensing equipment lags behind the technology, even though sensor design and electronics are becoming increasingly sophisticated and much less expensive. The most common forms of oil spill surveillance and mapping are still sometimes carried out with simple still or video photography. Remote sensing from aircraft is still the most common form of oil spill tracking. Remote sensing from satellites using radar sensors is now an increasingly common technique. Attempts to use visual satellite remote sensing for oil spills are increasing, although success is generally limited to identifying features at sites where known oil spills have occurred or for mapping known discharges or known spills.

It is important to divide the uses of remote sensing into the end use or objective, as the utility of the sensor is best

defined that way. Oil spill remote sensing systems used for routine surveillance certainly differ from those used to detect oil on shorelines or land. One tool does not serve for all functions. For a given function, many types of systems may, in fact, be needed. Further, it is necessary to consider the end use of the data. The end use of the data, be it location of the spill, enforcement, or support to cleanup, may also dictate the resolution or character of the data needed.

There are several broad uses of remote sensing, which are as follows:

1. Enforcement of ship discharge laws
2. Surveillance and general slick detection
3. Provision of evidence for prosecution
4. Mapping of spills for various reasons
5. Direction of oil spill countermeasures
6. Determination of slick trajectories

There are several generic problems in oil spill remote sensing including the following:

1. There are no cheap commercial off-the-shelf sensors that provide ready, remote sensing capability for oil.
2. Thickness information is not present in sensors currently used, nor is useful information available in the visible. Only very thin slicks show a few visible indications of oil, but this is not useful.
3. Many of the sensors and sensor outputs require extensive processing to make the data useful for the many purposes or uses described earlier.
4. All of the highly useful sensors require extensive aircraft modifications, which are both costly and time-consuming.

Several general reviews of oil spill remote sensing have been published [4–9]. These reviews show that there is progress in oil spill remote sensing; however, that progress is not necessarily moving at the speed that technology itself moves. These reviews show that specialized sensors offer advantages compared to off-the-shelf sensors.

12.2 ATMOSPHERIC PROPERTIES

The atmosphere has certain transmission/adsorption windows that affect the way that one can carry out remote sensing. Figures 12.1, 12.2, and 12.3 show the atmospheric attenuation at different electromagnetic wavelengths. These figures show that the commonly used wavelengths in the visible, long-wave infrared (IR) and radar bands are relatively free of atmospheric adsorption. One must consider rain, fog, and snow, which limit operations in both the visible and the IR regions. This leaves radar as the only all-weather and day and night sensor. Radar, as noted in the following, has many limitations in that it does not actually detect oil but only detects the dampening of sea capillary waves at a certain range of wind speeds.

12.3 OIL INTERACTION WITH LIGHT AND ELECTRONIC WAVES

Oil interacts with light and electromagnetic waves in certain specific ways; this can yield detectability of oil.

Several researchers have measured oil optical properties [10–14]. Weathering of oil increases the light absorption of the oil along with an increase in light scattering. An

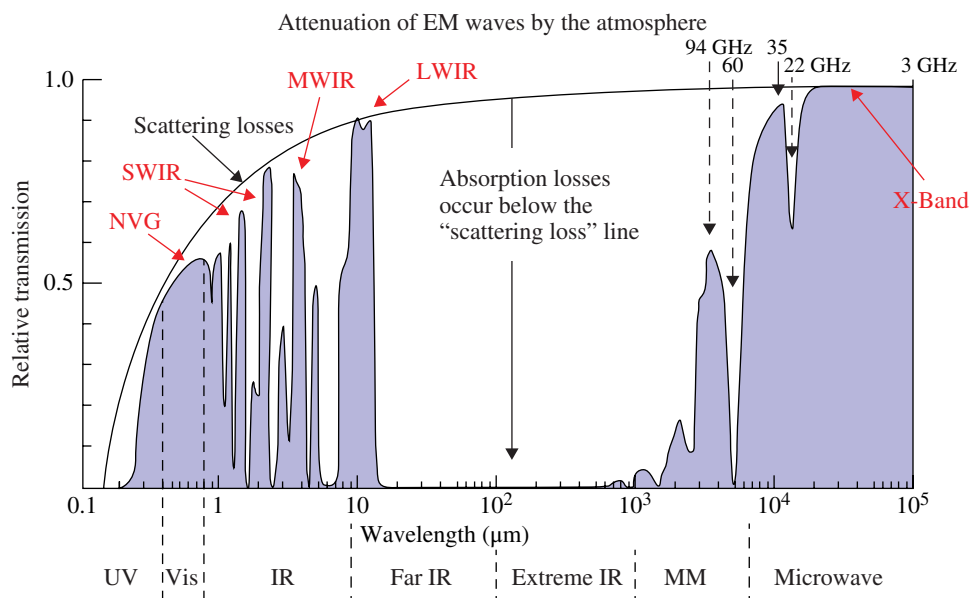


FIGURE 12.1 Atmospheric attenuation in the electromagnetic spectrum. EM, electromagnetic; IR, infrared; LWIR, long-wave infrared; MM, millimeter; MWIR, medium-wave infrared; NVG, night-vision goggles; SWIR, short-wave infrared; UV, ultraviolet; Vis, visible.

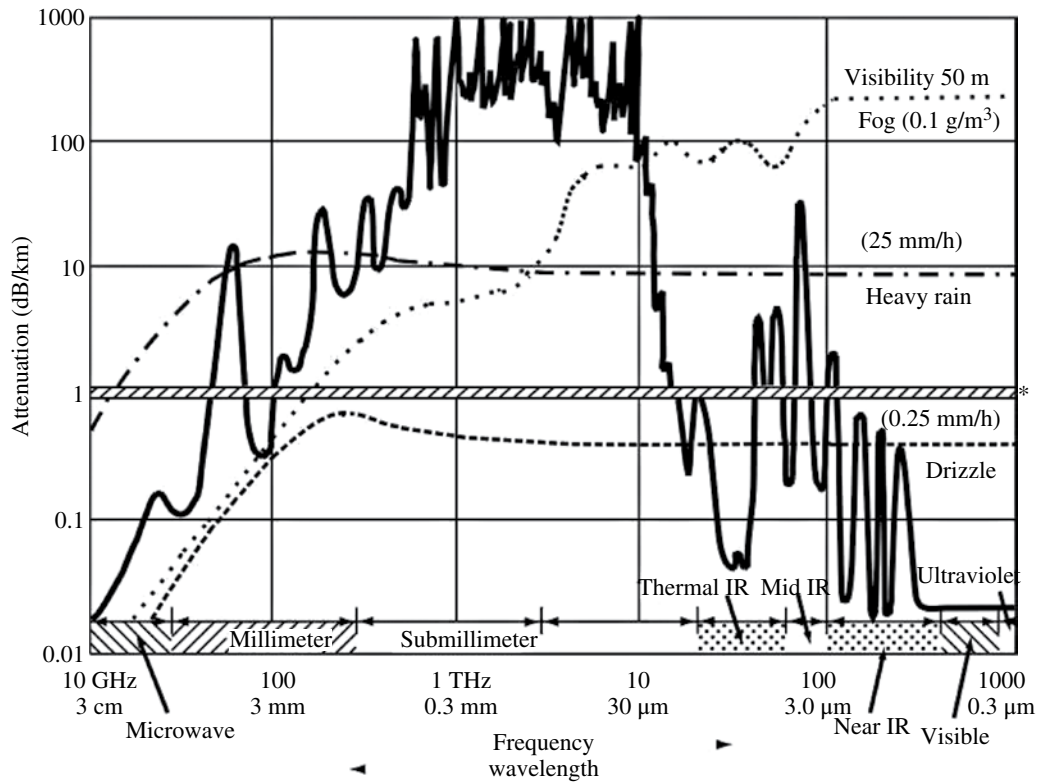


FIGURE 12.2 Another view of atmospheric attenuation. *In many cases, region below band represents atmospheric windows for airbase sensing. Figure courtesy of Ron Goodman.

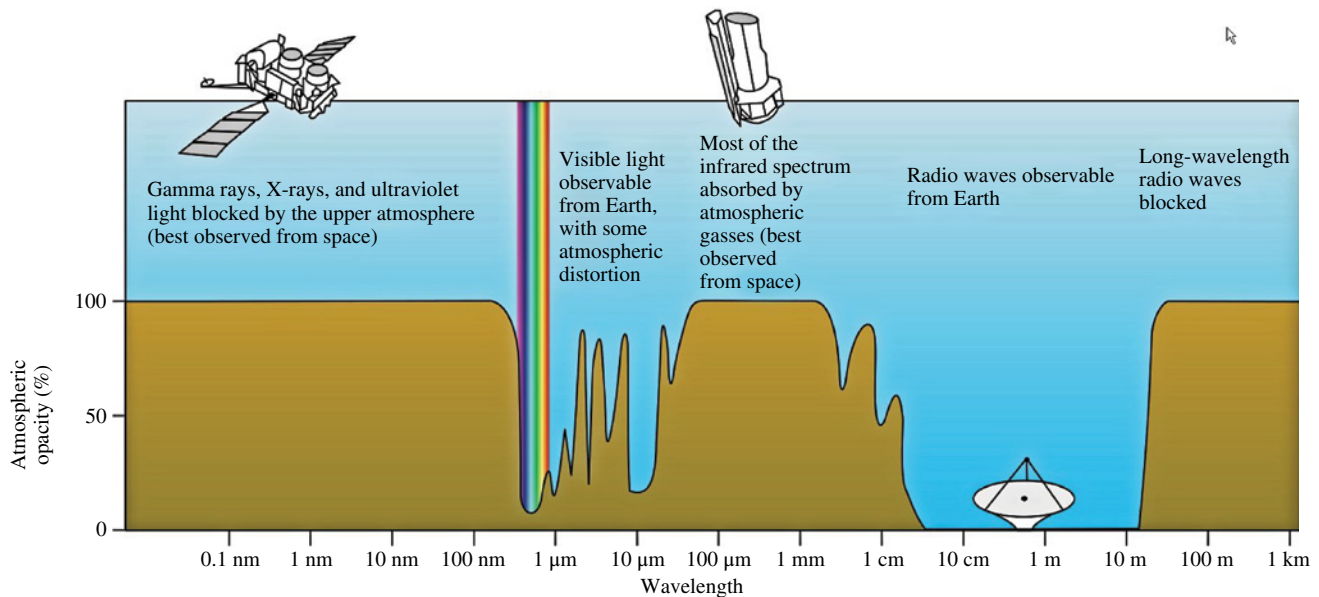


FIGURE 12.3 Atmospheric attenuation from a remote sensing point of view.

emulsion also absorbs more light and attenuates the light in the water column. Some researchers studied the ultraviolet (UV) and visible absorption of oils for analytical purposes, noting that crude oils were opaque and thus had to be diluted. The implication for remote sensing is that UV and visible signatures of oil are insufficient for characterization. The

light reflectance of crude oils floating on water does not contain spectral information [12–14].

Hong and Shin proposed that IR images be used to detect oil spills at sea at night [15]. Instead of using the IR image, they suggest that the images be used to calculate the difference in refractive indices. Seawater has a refractive

index of 1.227 and oil 1.53 at an IR wavelength of $10\mu\text{m}$. The refractive index can be calculated from the IR data (in this case Moderate Resolution Imaging Spectroradiometer (MODIS)), thus enabling a plot of surface oil or water. The technique has not been subsequently demonstrated.

The reflectance of oil is greater than seawater and increases with decreasing wavelength, that is, greater in the blue-green region. Figure 12.4 shows typical reflectance curves between oil and water. Several researchers have tried to use this reflectance difference to discriminate oils; however, the best application is to use it as an indicator of oil on the surface [16]. Ma et al. noted that the spectral bands between 400 and 500nm were particularly useful for visible

detection of oil from the MODIS satellite [17]. Lammoglia and de Souza Filho studied the spectra of oil compared to that of water and noted that in the visible there was little difference and the spectra were basically flat [18]. However, in the IR, both the very near infrared (VNIR) and the short-wave infrared (SWIR) showed significant differences in spectra between the oils and water. Further, they proposed that there were sufficient spectral differences to distinguish different oils in the VNIR and SWIR regions.

In summary, there are few very distinct characteristics that oil exhibits in the visible, IR, or shorter wavelengths. Oil remote sensing depends on secondary effects for oil detection and mapping.

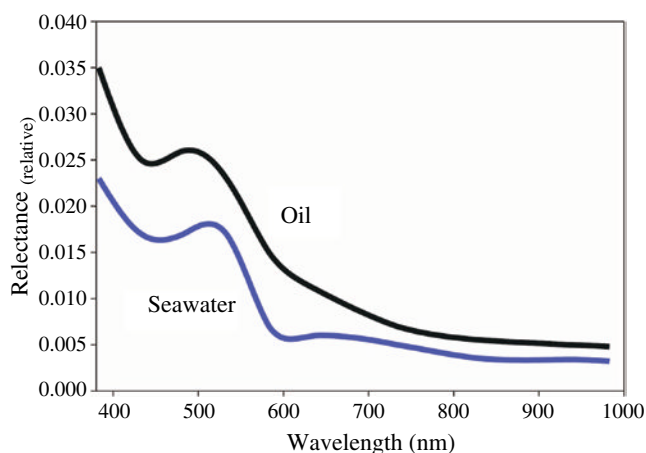


FIGURE 12.4 The differential reflection of water and oil. This is not sufficient difference to enable optical detection.

12.4 VISIBLE INDICATIONS OF OIL

Under many circumstances, oil is not visible to the eye on the water surface [8]. Other than the obvious situations of nighttime and fog, there exist many situations where oil cannot be seen. A very common situation is that of thin oil such as from ship discharges or the presence of materials such as seaweed, ice, and debris, which mask oil presence. Often, there are conditions on the sea that may appear like oil, when there is indeed no oil. These include wind shadows from land forms, surface wind patterns on the sea, surface dampening by submerged objects or weed beds, natural oils or biogenic material, and oceanic fronts. In the case of large spills, the area may be too great to be mapped visually. Several cases of confusion of oil slick appearance and other phenomena are illustrated in Figures 12.5, 12.6, 12.7, 12.8,

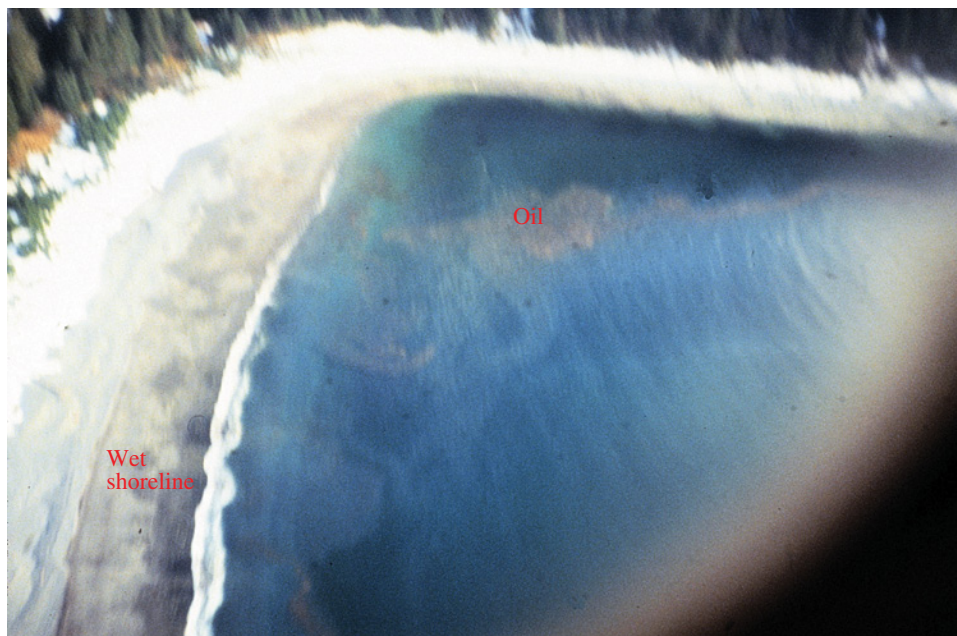


FIGURE 12.5 A photographic view of a shoreline. While it may appear that oil is on this shoreline, further investigation showed that it was actually wet sand. There is oil, however, near to the shore. Photograph from Environment Canada.



FIGURE 12.6 A photograph of an inlet that shows a particular coloration. This blue coloration is due to mineral matter called “glacial flour.” There is no oil in this picture. Photograph from Environment Canada.

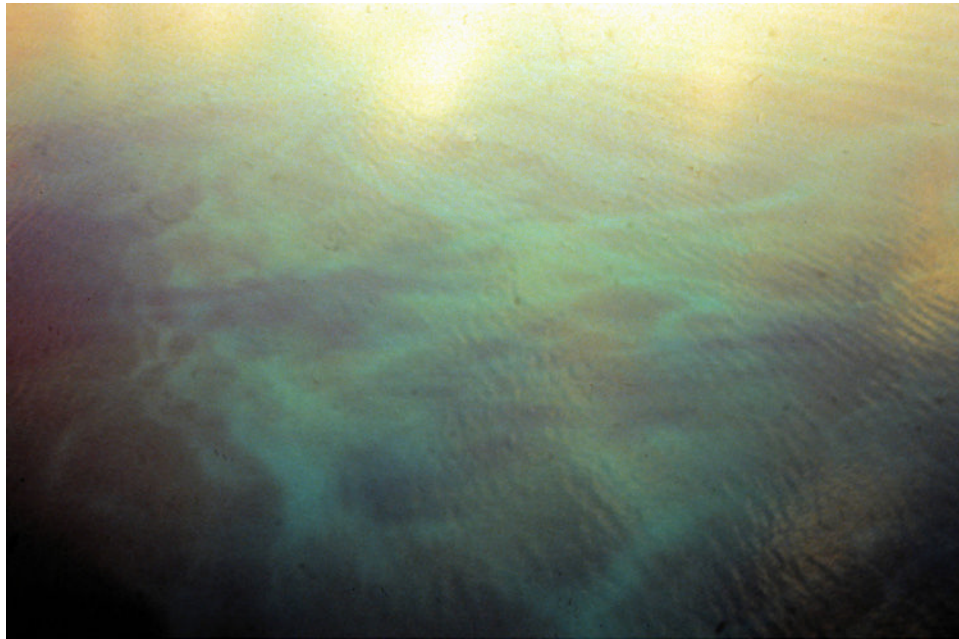


FIGURE 12.7 This is a photograph taken under poor lighting conditions and with heavy fog. What appears to be oil is simply an artifact of lighting. Photograph from Environment Canada.

12.9, 12.10, 12.11, 12.12, and 12.13. All these factors dictate that remote sensing systems be used to assist in the task of mapping and identifying oil. In many cases, aerial observation and remote sensing are necessary to direct cleanup crews to slicks. Figure 12.14 shows a case where no aerial direction was given and thus a skimmer crew misses the slick by about 0.5 km.

12.5 OPTICAL SENSORS

12.5.1 Visible

The use of human vision alone is not considered remote sensing; however, it still forms the most common technique for oil spill surveillance. In the past, major campaigns using only human vision were mounted with varying



FIGURE 12.8 Various slicks that are barely visible under the poor lighting conditions. Photograph from Environment Canada.

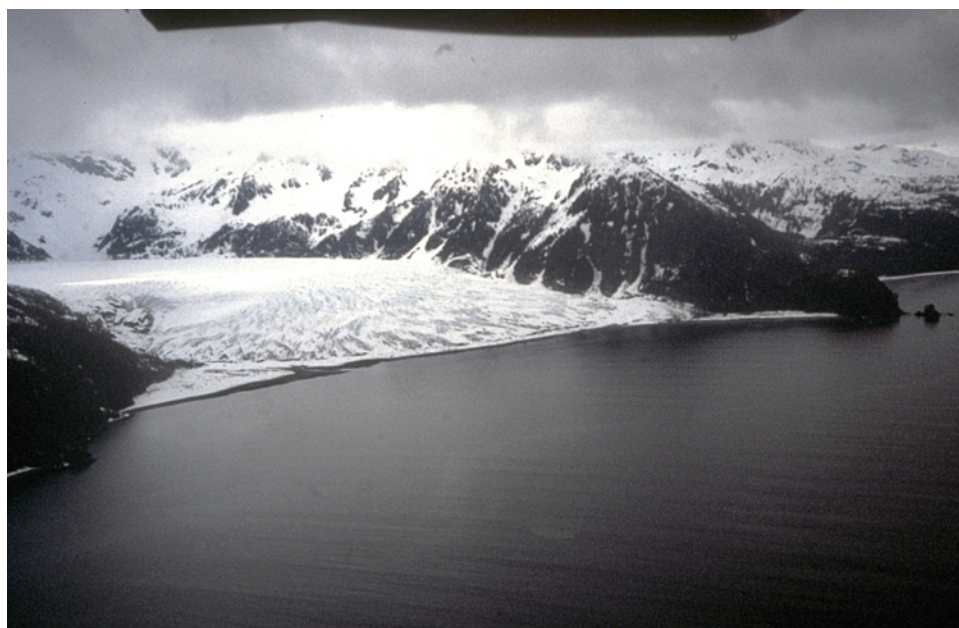


FIGURE 12.9 Calms near this glacier were mistaken for oil. There is no oil in this picture. Photograph from Environment Canada.

degrees of success [4]. Optical techniques, using the same range of the visible spectrum detection, are the most common means of remote sensing. Cameras, both still and video, are common because of their low price and commercial availability. Systems are now available to directly map remote sensing data onto base maps [4]. The limitations of visible means should always be borne in mind.

In the visible region of the electromagnetic spectrum ($\sim 400\text{--}700\text{ nm}$), oil has a higher surface reflectance than water but shows limited nonspecific absorption/reflection

tendencies as shown in Figure 12.4. This was reviewed in Section 12.3. Oil generally manifests throughout the entire visible spectrum. Sheen shows up silvery and reflects light over a wide spectral region down to the blue. As there is no strong information in the $500\text{--}600\text{ nm}$ region, this region is often filtered out to improve contrast [19]. Overall, however, oil has no specific characteristics that distinguish it from the background [20]. A specific study of oil spectra in the laboratory and the field observed flat spectra with no useable features distinguishing it from the background [21]. Therefore, techniques that separate specific spectral regions



FIGURE 12.10 This is a front between two slightly different bodies of water. There is no oil in this picture. Photograph from Environment Canada.



FIGURE 12.11 This photograph shows some oil in the foreground. Upon investigation, it turns out that the surface features further up the inlet are not oil.

do not increase detection capability. Some researchers noted that while the oil spectra are flat, the presence of oil may slightly alter water spectra [22]. It has been suggested that the water peaks are raised slightly at 570–590, 710–780, and 710–800 nm. At the same time, there are depressions or troughs at 650–680 and 740–760 nm. It has been found that high contrast in visible imagery can be achieved by setting the camera at the Brewster angle (53° from vertical) and using a horizontally aligned polarizing filter that passes

only that light reflected from the water surface [23]. This is the component that contains the information on surface oil [19]. It has been reported that this technique increases contrast by up to 100%. Filters with band-pass below 450 nm can be used to improve contrast. View angle is important, and some researchers have noted that the thickness changes the optimal view angle [24]. Some researchers claim that hyperspectral data from space was useful in distinguishing oil spills [25].



FIGURE 12.12 The white material on the water is herring “milk” or sperm. There is no oil in this picture.

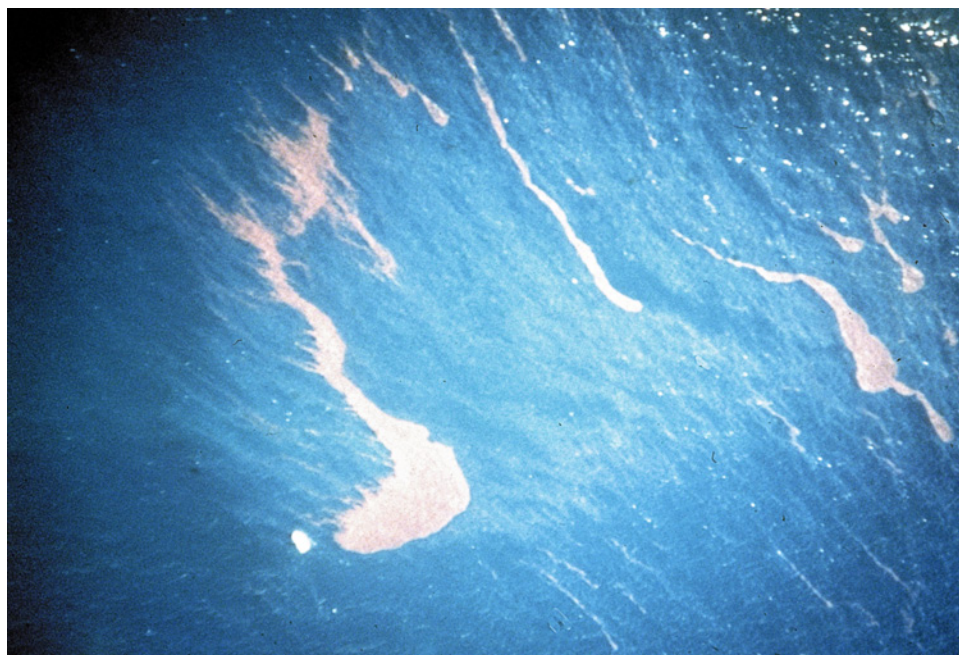


FIGURE 12.13 This picture shows oil emulsion (reddish material) and sheen. This can be clearly found on the water as little else has this appearance.

On land, hyperspectral data (use of multiple bands, typically 10–100) has been used to delineate the extent of an oil well blowout [26]. The technique used was spectral reflectance in the various channels as well as the usual oil black coloration.

Sun glitter is a particular problem in visible remote sensing. Sun glitter can sometimes be confused for oil sheens. Zhan et al. removed sun glitter from visible airborne hyperspectral imagery by using the ratio of longer versus shorter

wavelengths [27]. Images can then be “corrected” using this ratio. The premise is that glitter is more pronounced at shorter wavelengths. Figures 12.15, 12.16, and 12.17 show the effects of sun glitter on slick photography.

Video cameras are often used in conjunction with filters to improve the contrast in a manner similar to that noted for still cameras. This technique has had limited success for oil spill remote sensing because of poor contrast and lack of positive discrimination. Despite this, video systems have



FIGURE 12.14 A cleanup crew missing the slick by a wide margin as no aerial direction was given. The oil slick, in this case, is hard to see from the water. Photograph from Environment Canada.



FIGURE 12.15 Sun glitter appears to show that there is oil behind this tanker. There is no oil in this scene.

been proposed as remote sensing systems [28]. With new light-enhancement technology (low lux), video cameras can be operated even in darkness. Tests of a generation III night-vision camera show that this technology is capable of providing imagery in very dark night conditions [29,30].

Scanners were used in the past as sensors in the visible region of the spectrum. A rotating mirror or prism swept the

field of view (FOV) and directed the light toward a detector. Before the advent of charge-coupled device (CCD) detectors, this sensor provided much more sensitivity and selectivity than video cameras. Another advantage of scanners was that signals were digitized and processed before display. Recently, newer technology has evolved and similar digitization can be achieved without scanning by using a CCD



FIGURE 12.16 A picture of thin oil sheens stretching far into the horizon. Sun glitter makes it appear as though this span is endless.

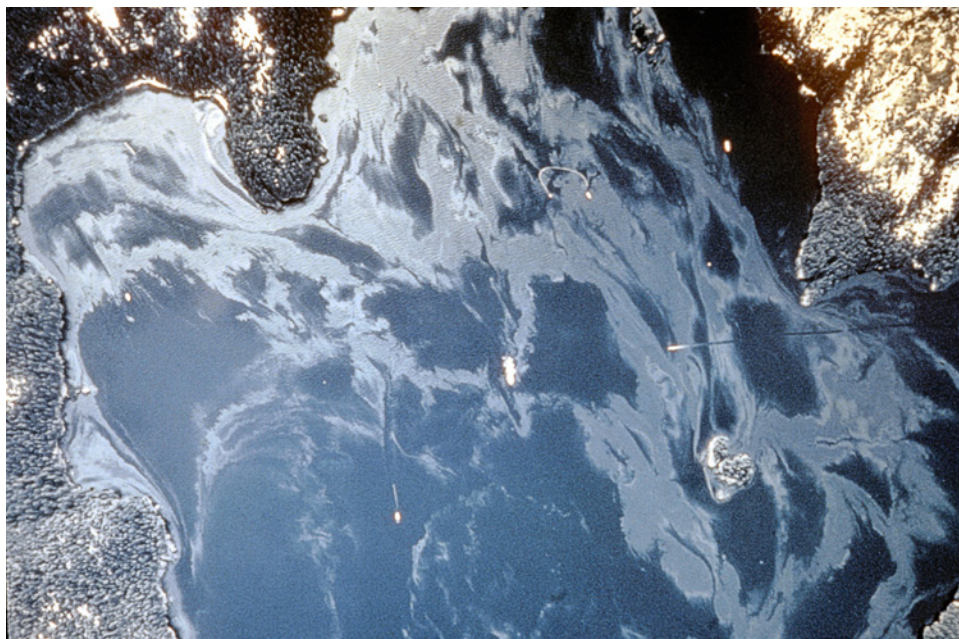


FIGURE 12.17 A down-looking (nadir) view of a major oil of a coastal area. Sun glitter does not interfere with this image of oil. Photograph from Environment Canada.

imager and continually recording all elements, each of which is directed to a different FOV on the ground. This type of sensor, known as a push-broom scanner, has many advantages over the older scanning types. It can overcome several types of aberrations and errors, the units are more reliable than mechanical ones, and all data are collected simultaneously for a given line perpendicular to the direction of the aircraft's flight. Several types of scanners were developed. In Canada, the multidetector electro-optical imaging scanner

and the compact airborne spectrographic imager have been developed, and in the Netherlands, the Caesar system was developed [19,31,32]. In China, the MAMS and AISA systems have been developed [33].

Digital photography has enabled the combination of photographs and the processing of images. Locke et al. used digital photography from vertical images to form a mosaic of an area impacted by an oil spill [34]. It was then possible to form a singular image and to classify oil

types by color within the image. The area impacted by the spill was also determined.

The detection or measurement of oil in water has never been successfully accomplished using visible remote sensing technology. There may be potential for light-scattering technology. Stelmaszewski and coworkers measured the light scattering of crude oil in water emulsions and noted that scattering increases with wavelength in the UV range and decreases slightly with the wavelength of visible light [35].

The use of visible techniques in oil spill remote sensing is largely restricted to documentation of the spill because there is no mechanism for positive oil detection. Furthermore, there are many interferences or false alarms. Sun glint and wind sheens can be mistaken for oil sheens. Biogenic material such as surface seaweeds or sunken kelp beds can be mistaken for oil. Oil on shorelines is difficult to identify positively because seaweeds look similar to oil and oil cannot be detected on darker shorelines. In summary, the usefulness of the visible spectrum for oil detection is limited. It is an economical way to document spills and provide baseline data on shorelines or relative positions.

12.5.2 IR

Oil, which is optically thick, absorbs solar radiation and reemits a portion of this radiation as thermal energy, primarily in the 8–14 μm region. Thus, IR is a case where one is measuring the emissions from the oil [36]. In IR images, thick oil appears hot, oils of intermediate thicknesses appear cool, and thin oil or sheens are not detected. The thicknesses at which these transitions occur are poorly understood, but evidence indicates that the transition between the hot and cold layer lies between 50 and 150 μm and the minimum detectable layer is between 10 and 70 μm [36–40]. The reason for the appearance of the “cool” slick is not fully understood. A likely theory is that a moderately thin layer of oil on the water surface causes destructive interference of the thermal radiation waves emitted by the water, thereby reducing the amount of thermal radiation emitted by the water [8]. This is analogous to the appearance of the rainbow sheen, which is explained in Section 12.8. The cool slick would correspond to the thicknesses as observed earlier because the minimum destructive thickness would be about two times the wavelength, which is between 8 and 10 μm . This would yield a destructive interference onset of about 16–20 μm to about four wavelengths or about 32–40 μm . The destructive or “cool” area is usually only seen with test slicks, which is explained by the fact that the more rapidly spreading oil is of the correct thickness to show this phenomenon. Slicks that have been on the water for a longer period of time usually are thicker or thinner (i.e., sheen) than 16–40 μm . The onset of the hot thermal layer would in theory then be at thicknesses greater than this or at about 50 μm .

IR sensors cannot detect emulsions (water-in-oil emulsions) under most circumstances [41]. This is probably a result of the high thermal conductivity of emulsions as they



FIGURE 12.18 A test slick shown only in the visible spectrum. The slick is poorly discriminated.

typically contain 50–70% water and thus do not show temperature differences from water.

Most IR sensing of oil spills takes place in the thermal IR at wavelengths of 8–14 μm . Specific studies in the thermal IR (8–14 μm) show that there is no spectral structure in this region [42]. Tests of a number of IR systems show that spatial resolution is extremely important when the oil is distributed in windrows and patches. Emulsions are not always visible in the IR. Cameras operating in the 3–5 μm range are only marginally useful [43,44]. Nighttime tests of IR sensors show that there is detection of oil (oil appears cold on a warmer ocean); however, the contrast is not as good as during daytime [45]. Further, on many nights, no difference is seen.

The relative thickness information in the thermal IR can be used to direct skimmers and other countermeasures equipment to thicker portions of the slick. Figures 12.18, 12.19, 12.20, and 12.21 illustrate the utility of IR oil imaging compared to that of visible imaging. Oil detection in the IR is not positive, however, as several false targets can interfere, including seaweeds, sediment, organic matter, shoreline, and oceanic fronts [46]. IR sensors are reasonably inexpensive, however, and are currently the prime tool used by the spill remote sensor operator. IR cameras are now very common, and commercial units are available from several manufacturers.

12.5.3 Near IR

Clark et al. and Leifer et al. proposed that color composite images assembled from both visible and near-IR wavelengths could be used to make images of thick oil, but such images also show strong reflections from clouds and the glint from the ocean surface [47,48]. Clark et al. proposed that spectroscopic analysis of the reflectance



FIGURE 12.19 The same slick as shown in Figure 12.18 but with infrared added. The addition of the IR adds a little thickness information as the thicker oil is shown in the orange coloration. The sheen is in various shades of blue. The outer pale blue fringes are from the ultraviolet, which highlights very thin sheen.



FIGURE 12.20 A view of a test slick in the visible. The sunglint makes it difficult to find the edges of the slick.

spectra within remote sensing imagery could resolve the absorptions due to the organic compounds in oil and can better discriminate the spectral shape of oil [47]. A method to analyze absorptions due to specific materials is called absorption-band depth mapping. Clark and others showed that simple three-point band depth mapping will show the location of absorption features but cannot

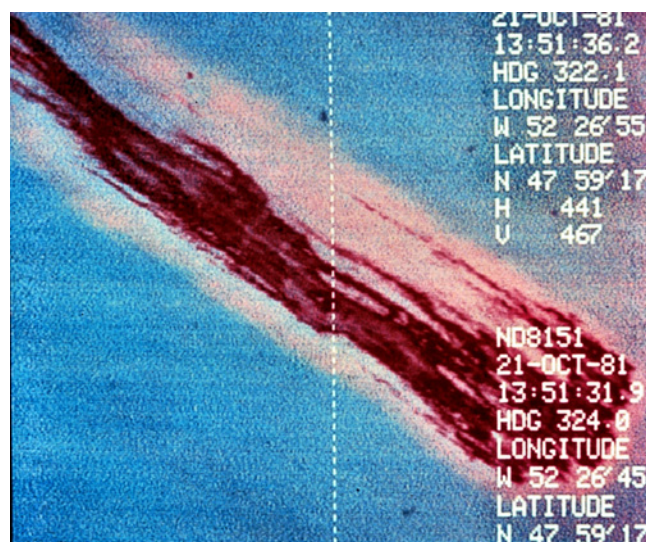


FIGURE 12.21 A view of the same test slick as in Figure 12.20 but with the addition of infrared. The infrared adds much contrast between the water and the slick and removes the effect of the sun glitter.

identify specific compositions of compounds causing these features when compound mixtures have absorptions near the same wavelength [47]. In the case of open ocean images, composed of pixels containing water, oil–water mixtures, and clouds, the organic compounds in the oil and oil–water mixtures have absorption features that are distinct from those of water and clouds. These spectral differences allow one to map qualitative variations in oil abundance. Other than the Gulf oil spill, this system has not been proven.

The researchers used the NASA Airborne Visible/Infrared Imaging Spectrometer (AVIRIS). AVIRIS provides data on the spectrum of the surface at each pixel from 0.35 to 2.5 μm (the visible spectrum is blue, 0.4 μm ; green, 0.53 μm ; and deep red, 0.7 μm) in 224 channels. AVIRIS data from oil overflights are used to produce a three-point band depth map, indicating potential locations of thick oil, by the following methods: (i) Radiance data are converted to surface reflectance using a two-step process [47]. (ii) Three-point band depth images are computed using continuum-removed reflectance spectra using the equation [47]

$$\text{Depth of waveband} = 1 - 2 R_b / (R_l + R_r) \quad (12.1)$$

where R_b is the reflectance around the absorption maximum (minimum reflectance), R_l is the reflectance of the left continuum end point, and R_r is the reflectance of the right continuum end point.

The proposed adsorption scheme is shown in Figure 12.22 [48].

For AVIRIS, the following wavelength intervals were used in three-point band depth computations [47]:

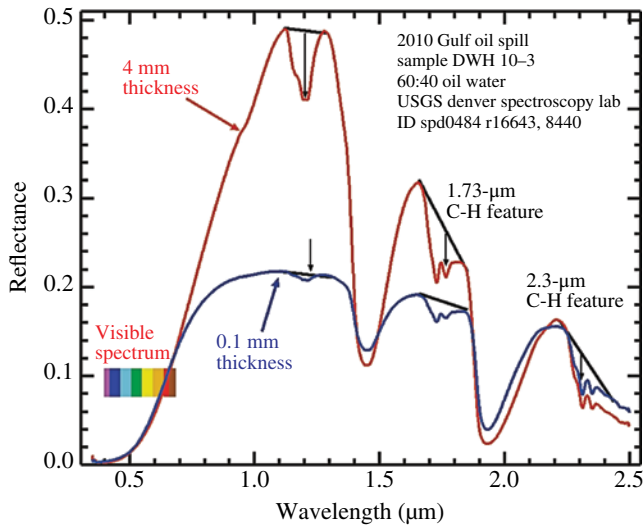


FIGURE 12.22 Wavelength versus reflectance in the near infrared. This shows the wavelength proposed by Clark et al. [47] to map slick thicknesses.

1.2 μm feature:

Rb = average of the channels in the interval from 1.197 to 1.216 μm

Rl = average of the channels in the interval from 1.073 to 1.102 μm

Rr = average of the channels in the interval from 1.273 to 1.293 μm

1.7 μm feature:

Rb = average of the channels in the interval from 1.712 to 1.732 μm

Rl = average of the channels in the interval from 1.622 to 1.642 μm

Rr = average of the channels in the interval from 1.782 to 1.802 μm

2.3 μm feature:

Rb = average of the channels in the interval from 2.287 to 2.327 μm

Rl = average of the channels in the interval from 2.198 to 2.238 μm

Rr = average of the channels in the interval from 2.407 to 2.447 μm

The band depth images produced from these three calculations are combined into a color composite image as follows: the 2.3 μm feature in the red channel, the 1.73 μm feature in the green channel, and the 1.2 μm feature in the blue channel. The thicker oil then shows up in the green-blue regions of the image.

The Gulf oil spill was mapped using the AVIRIS sensor in the ER aircraft, and thickness maps were plotted [47]. This method appeared to work for the Gulf oil spill; however, confirmation on other spills awaits.

12.5.4 UV

Oil shows a high reflectance of sunlight in the UV range. UV sensors can be used to map sheens of oil as oil slicks display high reflectivity of UV radiation even at thin layers ($<0.1 \mu\text{m}$). Overlaid UV and IR images are often used to produce a relative thickness map of oil spills. This is illustrated in Figure 12.19. UV cameras, although inexpensive, are not often used in this process, however, as it is difficult to overlay camera images [49]. Data from IR scanners and that derived from push-broom scanners can be easily superimposed to produce these IR/UV overlay maps. UV data are also subject to many interferences or false images such as wind slicks, sunglints, and biogenic material. Since these interferences are often different than those for IR sensing, combining IR and UV can provide a more positive indication of oil than using either technique alone.

Yin et al. developed a new push-broom UV detector (340–370 nm, 512 pixels) and incorporated it into a push-broom sensor along with two visible sensors, one in the red region and another in the green region [50]. Testing showed that the UV sensor was able to discriminate oil from water while the other red and green sensors were not able to. In recent years, UV has not been used much in oil spill remote sensing as the sheen information by itself is not useful to countermeasures.

12.6 LASER FLUOROSENSORS

Laser fluorosensors are sensors that use the phenomenon that aromatic compounds in petroleum oils absorb UV light and become electronically excited. This excitation is rapidly removed through the process of fluorescence emission, primarily in the visible region of the spectrum. Since very few other compounds show this tendency, fluorescence is a strong indication of the presence of oil. Natural fluorescing substances, such as chlorophyll, fluoresce at sufficiently different wavelengths than oil to avoid confusion. As different types of oil yield slightly different fluorescent intensities and spectral signatures, it is possible to differentiate between classes of oil under ideal conditions [51–60].

Most laser fluorosensors used for oil spill detection employ a laser operating in the UV region of 308–355 nm [51,61,62]. With this wavelength of activation, there exists a broad range of fluorescent response for organic matter, centered at 420 nm. This is referred to as Gelbstoff or yellow matter, which can be easily annulled. Chlorophyll yields a sharp peak at 685 nm. The fluorescent response of crude oil ranges from 400 to 650 nm with peak centers in the 480 nm region. The use of laser fluorosensors for chlorophyll and other applications has been well documented [51].

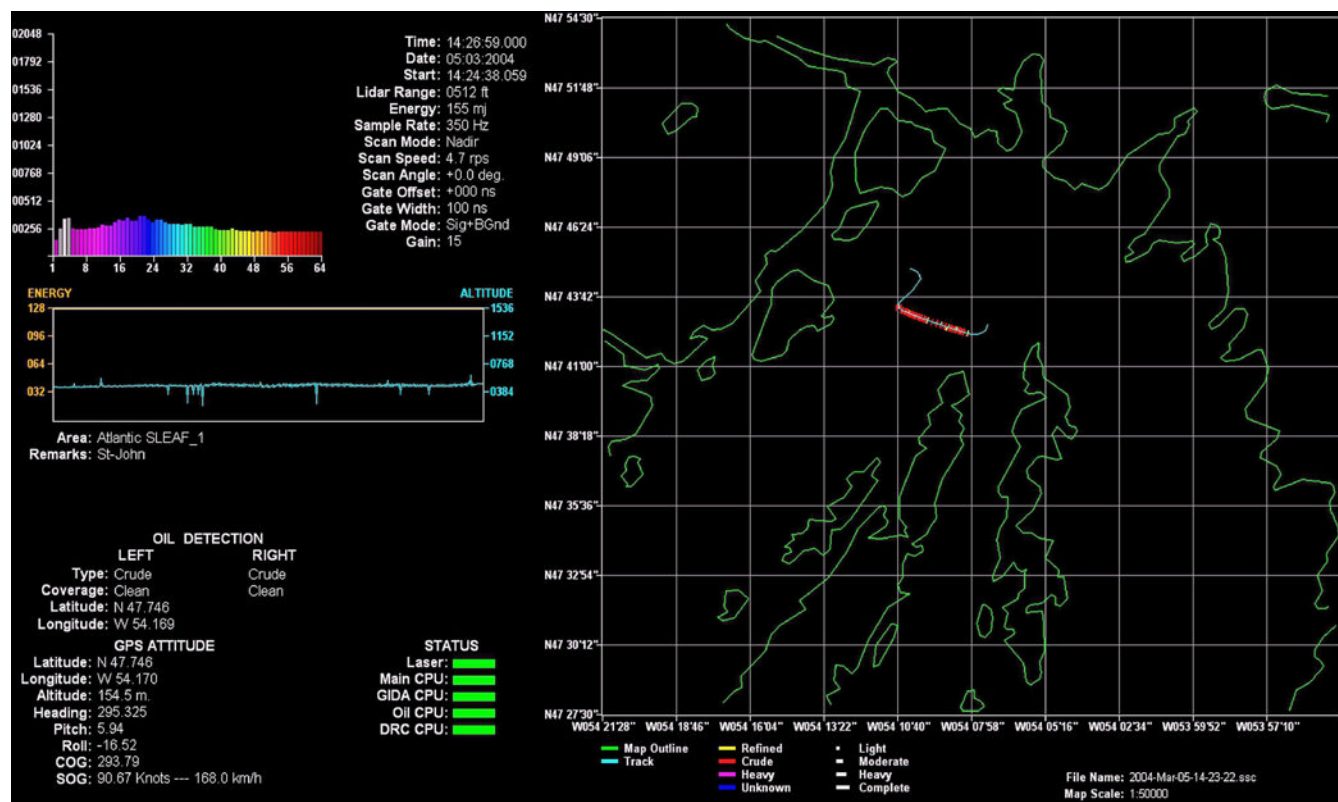


FIGURE 12.23 An illustration of a fluorosensor display. On the left, instrument and detection criteria are given. On the right, the flight track is annotated with oil detection “hits” shown as gray bars. The map on the right is a real-time actual map. Image from Environment Canada.

Another phenomenon, known as Raman scattering, involves energy transfer between the incident light and the water molecules. When the incident UV light interacts with the water molecules, Raman scattering occurs. This involves an energy transfer between the incident light and water molecules. The water molecules absorb some of the energy as rotational–vibrational energy and emit light at a wavelength that is the difference between the incident radiation and the rotational–vibrational energy of the molecule. The Raman signal for water occurs at 344 nm when the incident wavelength is 308 nm (XeCl laser). With an excitation at 460 nm (tunable dye laser), the Raman signal occurs at about 540 nm [63]. The water Raman signal is useful for maintaining wavelength calibration of the fluorosensor in operation but has also been used in a limited way to estimate oil thickness, because the strong absorption by oil on the surface will suppress the water Raman signal in proportion to thickness [63–65]. The point at which the Raman signal is entirely suppressed depends on the type of oil, since each oil has a different absorption coefficient. The Raman signal suppression has led to estimates of sensor detection limits of about 0.05–0.1 μm [66]. It should be noted that this thickness is well below that of interest for oil spill countermeasures.

Laser fluorosensors have significant potential as they may be the only means to discriminate between oiled and unoled seaweeds and to detect oil on different types of

shorelines. Tests on shorelines show that this technique has been very successful [67]. Algorithms for the detection of oil on shorelines have been developed [68]. Work has been conducted on detecting oil in the water column such as that occurs with the product Orimulsion [69–73]. The fluorosensor is also the only reliable means of detecting oil in certain ice and snow situations. Operational use shows that the laser fluorosensor is a powerful tool for oil spill remote sensing [51]. Currently, one company makes two commercial models of the instrument (Optimare).

Laser fluorosensors have shown high utility in practice and are now becoming essential sensors in many remote sensing packages. The information in the output is unique, and the technique provides a unique method of oil identification. The method is analogous to performing chemistry in flight. Figure 12.23 shows a display of a laser fluorosensor. The typical fluorosensor can provide an abundance of information to the user.

12.7 MICROWAVE SENSORS

12.7.1 Radiometers

Microwave radiometers detect the presence of an oil film on water by measuring the reflective interference pattern excited by the radiation from free space. The apparent emissivity

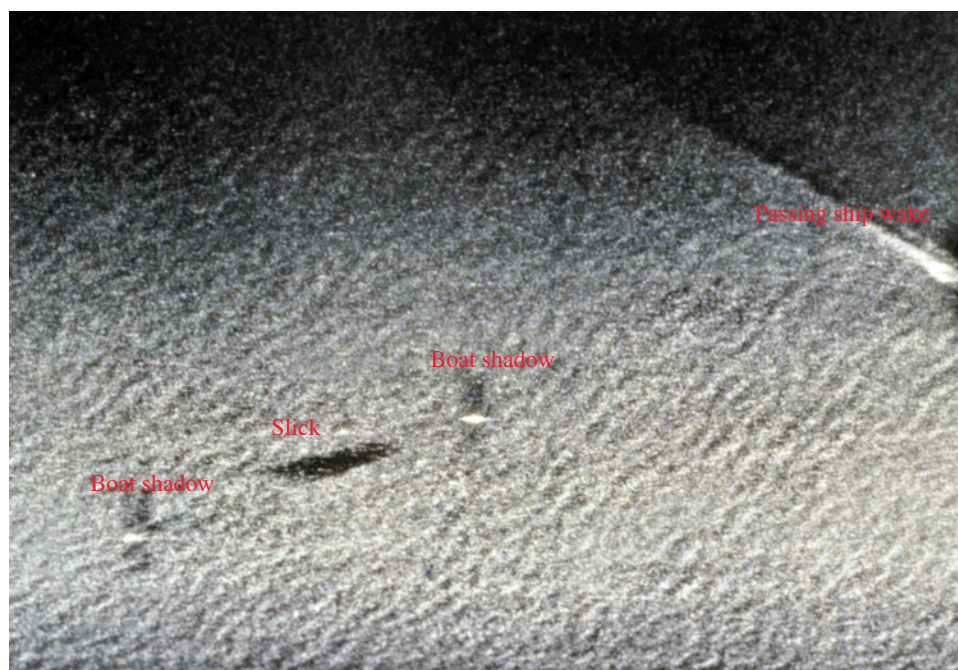


FIGURE 12.24 An old airborne radar image showing some typical features of radar imagery, including shadows from boats and ships.

factor of water is 0.4 compared to 0.8 for oil [74]. A passive microwave radiometer can detect this difference in emissivity and could therefore be used to detect oil. In addition, as the signal changes with thickness, in theory, the device could be used to measure thickness. This detection method has not been very successful in the field, however, as several environmental and oil-specific parameters must be known. In addition, the signal return is dependent on oil thickness but in a cyclical fashion. A given signal strength can imply any one of the several film thicknesses within a given slick. Microwave energy emission is greatest when the effective thickness of the oil equals an odd multiple of one-quarter of the wavelength of the observed energy. Biogenic materials also interfere and the signal-to-noise ratio is low. In addition, it is difficult to achieve high spatial resolution (might need resolution in meters rather than the typical tens of meters for a radiometer) [75].

The Swedish Space Corporation has carried out work with different systems, including a dual band 22.4 and 31 GHz device and a single band 37 GHz device [76]. Skou, Sorensen, and Poulson describe a 2-channel device operating at 37.5 and 10.7 GHz [77]. Mussetto and coworkers at TRW described the tests of 44–94 GHz and 94–154 GHz 2-channel devices over oil slicks [78]. TRW showed that correlation with slick thickness is poor and suggests that factors other than thickness also change surface brightness. They suggest that a single-channel device might be useful as an all-weather, relative thickness instrument. Tests of single-channel devices over oil slicks have also been described in the literature, specifically a 36 GHz and a 90 GHz device [79,80]. A recent method of microwave radiometry has been developed in which the polarization contrasts at two orthogonal polarizations are measured in an attempt to measure oil

slick thickness [81,82]. A series of frequency-scanning radiometers have been built and appear to have overcome the difficulties with the cyclical behavior [83,84].

In summary, passive microwave radiometers may have potential as all-weather oil sensors. Their potential as a reliable device for measuring slick thickness, however, is uncertain at this time.

12.7.2 Radar

Capillary waves on the ocean reflect radar energy, producing a “bright” image known as sea clutter. Since oil on the sea surface dampens capillary waves, the presence of an oil slick might be detected as a “dark” sea or one with an absence of this sea clutter [85]. Unfortunately, oil slicks are not the only phenomena that are detected in this way. There are many interferences or false targets, including freshwater slicks, wind slicks (calms), wave shadows behind land or structures, shallow seaweed beds that calm the water just above them, glacial flour, biogenic oils, and whale and fish sperm [86–91]. As a result, radar can be marginally effective in locations such as Prince William Sound, Alaska, where dozens of islands, freshwater inflows, ice, and other features produce hundreds of such false targets. Liu et al. showed that even with extensive processing, false hits on synthetic aperture radar (SAR) imagery were 20%, that is, 20% of the images reported as oil were still look-alikes [92]. Figures 12.24, 12.25, 12.26, 12.27, 12.28, 12.29, and 12.30 illustrate some of the many slick look-alikes that appear in radar displays. Despite these limitations, radar is an important tool for oil spill remote sensing because it is the only sensor that can be used for searches of large areas and it is



FIGURE 12.25 An ERS-2 satellite radar image of the coast of Belgium. The streak through the top portion of the image is the wake of a vessel. The oil look-alikes near the coastline and in the estuaries are calm areas resulting from wind protection from the land.

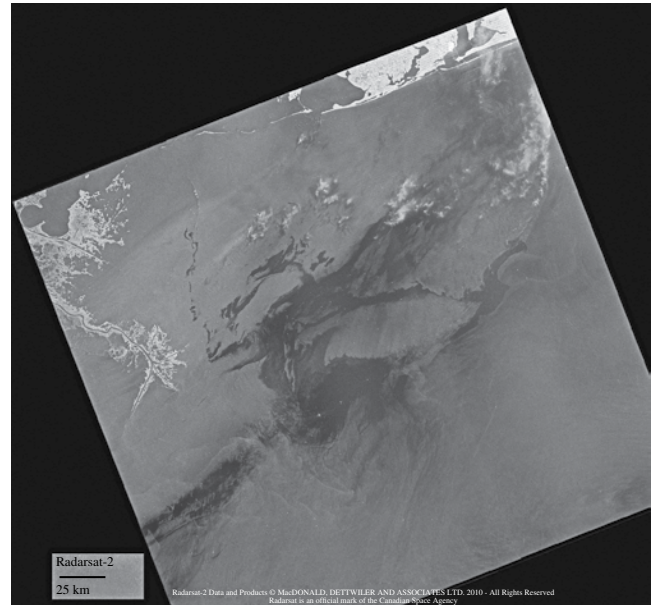


FIGURE 12.27 A Radarsat image of the Gulf oil spill. The spill can be clearly seen as can the cliff shadows and calm areas near the shore. What appears to be clouds on the left-hand side of the images are high-water-current areas. Clouds are not seen on radar images. Photo from Canadian Space Agency website <http://www.asc-csa.gc.ca/images>

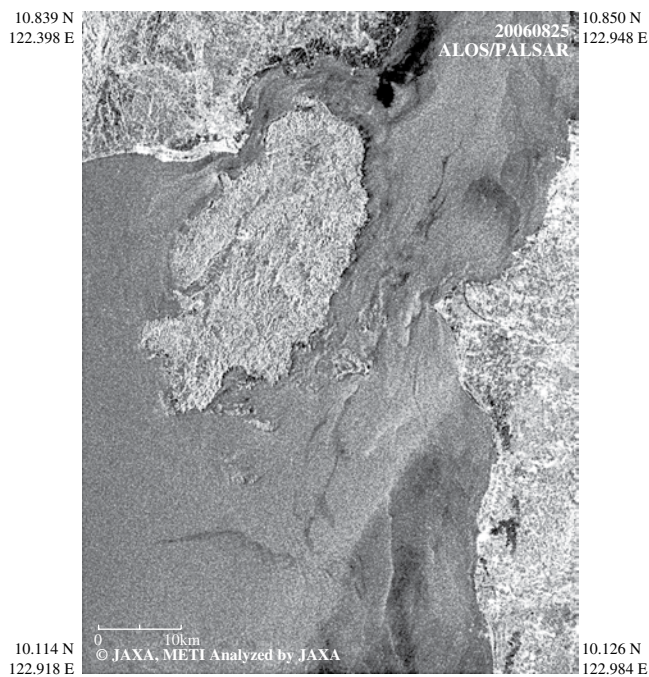


FIGURE 12.26 A PALSAR image of an oil spill near the Philippines. PALSAR operates in the L-band. This image shows the many interferences possible in a radar image. Only a small percentage of the dark matter depicted here is actually oil. Photo from Japan website http://www.eorc.jaxa.jp/ALOS/en/img_up/pal_oil200608.htm

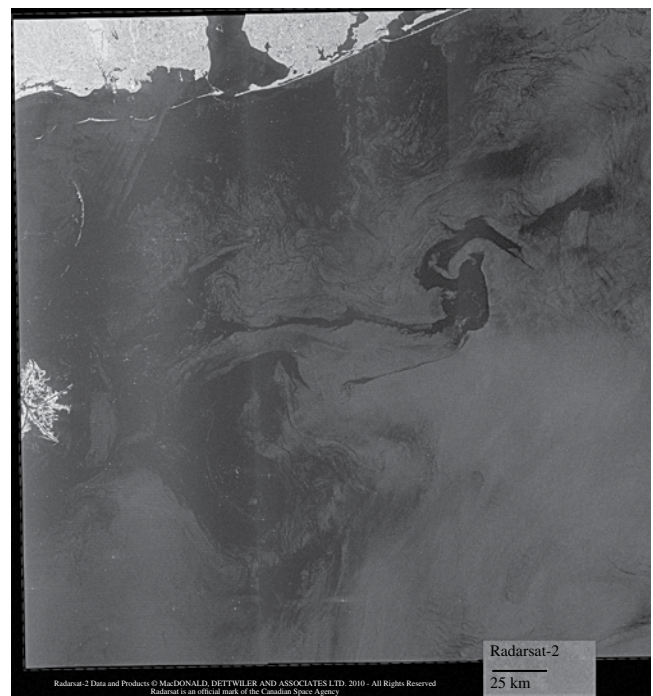


FIGURE 12.28 A Radarsat image of the Gulf oil spill. The spill can be clearly seen as can the cliff shadows and calm areas near the shore. The small white dots near the shore are boats and ships. Photo from Canadian Space Agency website <http://www.asc-csa.gc.ca/images>

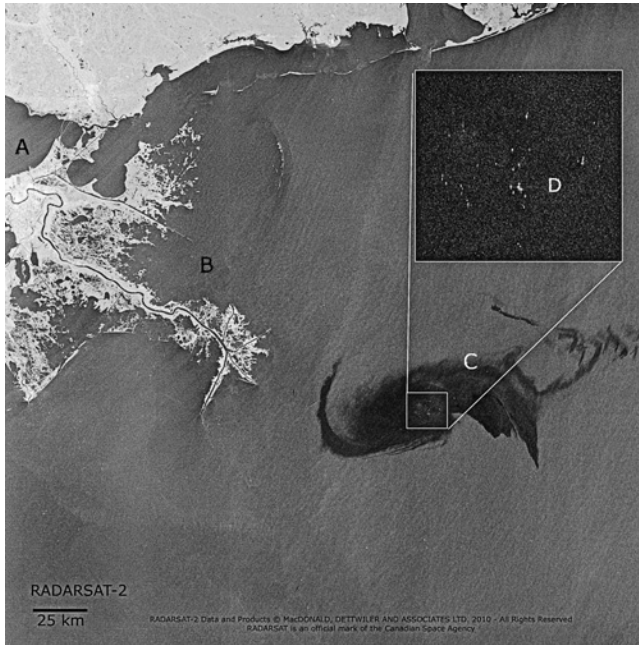


FIGURE 12.29 A Radarsat image of the Gulf oil spill. The spill can be clearly seen as can the cliff shadows and calm areas near the shore. Figure (c) is the main slick and (d) is an expansion of part of the slick area. Figure (a and b) show targets that might appear to be oil but are not. The small white dots in the blowout area (d) are boats and ships working on well capping and spill response. Photo from Canadian Space Agency website <http://www.asc-csa.gc.ca/images>

one of the few sensors that can detect anomalies at night and through clouds or fog.

The two basic types of imaging radar that can be used to detect oil spills and for environmental remote sensing in general are SAR and side-looking airborne radar (SLAR). The latter is an older, but less expensive technology, which uses a long antenna to achieve spatial resolution. SAR uses the forward motion of the aircraft to synthesize a long antenna, thereby achieving very good spatial resolution, which is independent of range, with the disadvantage of requiring sophisticated electronic processing. While inherently more expensive, the SAR has greater range and resolution than the SLAR. Comparative tests show that SAR is vastly superior [93–95]. Search radar systems, such as those frequently used by the military, cannot be used for oil spills as they usually remove the clutter signal, which is the primary signal of interest for oil spill detection. Furthermore, the signal processing of this type of radar is optimized to pinpoint small, hard objects, such as periscopes. This signal processing is very detrimental to oil spill detection.

SLAR has predominated airborne oil spill remote sensing, primarily because of the lower price [96,97]. There is some recognition among the operators that SLAR is very subject to false hits, but solutions are not offered. Experimental work on oil spills has shown that X-band radar yields better data than L- or C-band radar [98–101]. Several different polarizations exist based on vertical (V) and horizontal (H)

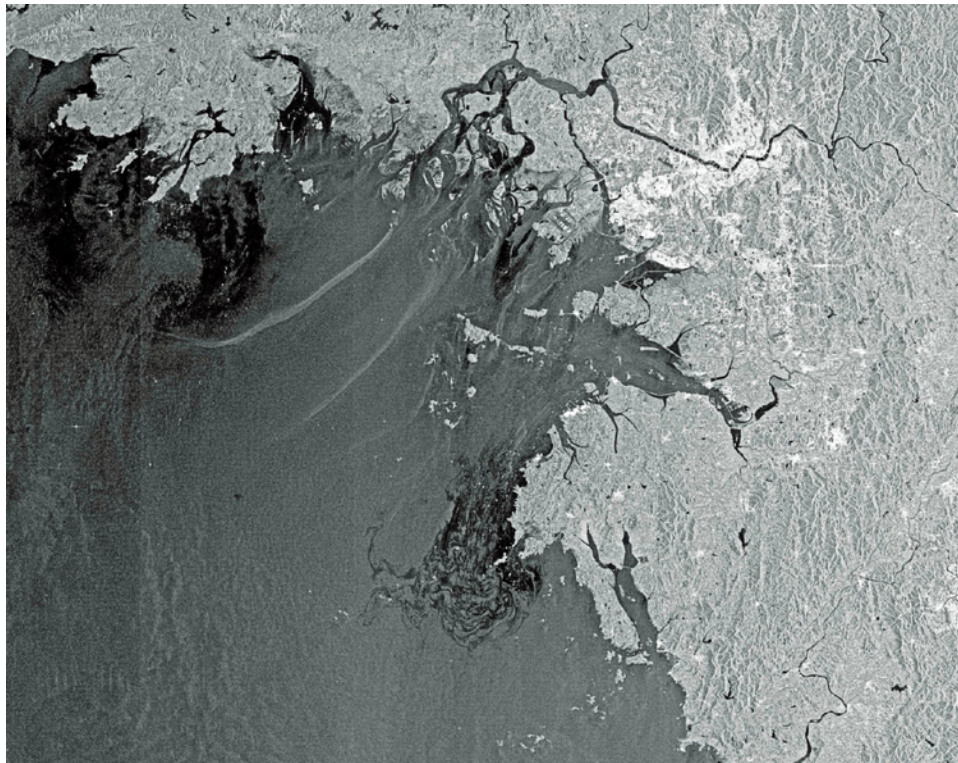


FIGURE 12.30 A Radarsat image of the Hebei Spirit oil spill off Korea. Oil slicks are largely black except near the coast where the black is calm areas and also the black areas inside the estuaries and rivers are also calm areas. Photo from Canadian Space Agency website <http://www.asc-csa.gc.ca/images>

electromagnetic wave propagation. Typically, transmission and reception are in the same polarity, that is, VV or HH. But, there are actually four poles available: HH, VV, HV, and VH. The use of all four of these is designated as quadrupole. It has also been shown that vertical antenna polarizations for both transmission and reception (VV) yield better results than other configurations [93,102–104]. Several researchers have shown that VV is best for oil spill detection and discrimination [105–108]. Some workers noted that VV polarization tends to be more suitable for oil pollution detection when winds are strong and HH when winds are light although this was observational [109,110]. However, the dependency of HH polarization on the incidence angle is greater than that of VV polarization. This means that if the incidence angle is small, the difference in intensity between HH and VV polarization is small, but if the incidence angle is large, the VV image on the sea is brighter than the HH image. This suggests that generally the VV image is better for detecting oil spills.

A larger standard deviation for the slick compared to the sea typically indicates that it is oil. Several workers have noted that polarimetric SAR can provide powerful discrimination between slicks and look-alikes [111]. Additionally, phase differences can be used to detect oil. Migliaccio et al. calculated that the copolarized phase difference (CPD) would yield a larger signal for oil compared to that for the sea [106]. Migliaccio et al. showed that the CPD—for example, the difference between the HH and VV phases—can be used to discriminate oil slicks from biogenic slicks [107]. Velotto et al. studied the use of copolarized radar data for oil spill detection [112]. They used the TerraSAR-X dual-polarized HH and VV bands and calculated the CPD between these bands. They claimed that this approach is able to better discriminate oil spills from weak-damping look-alikes.

Figure 12.31 illustrates the difference between a VV and HH polarization. The ability of radar to detect oil is limited by sea state. Sea states that are too low will not produce enough sea clutter in the surrounding sea to contrast to the oil and very high seas will scatter radar sufficiently to block detection inside the wave troughs. Indications are that minimum wind speeds of 1.5 m/s (~3 knots) are required to allow detectability and a maximum wind speed of 6 m/s (~12 knots) will again remove the effect [113–116]. The most accepted limits are 1.5 m/s (~3 knots) to 10 m/s (~20 knots). This limits the environmental window of application of radar for detecting oil slicks. Gade et al. studied the difference between extensive systems from a space-borne mission and a helicopter-borne system [117]. They found that at high winds, it was not possible to discriminate biogenic slicks from oil. At low wind speeds, it was found that images in the L-band showed discrimination. Under these conditions, the biogenic material showed greater damping behavior in the L-band. Okamoto et al. studied the use of ERS-1 (Earth and Space Research) using an artificial oil (oleyl alcohol) and found that an image was detected at a wind speed of 11 m/s, but not at 13.7 m/s [118].

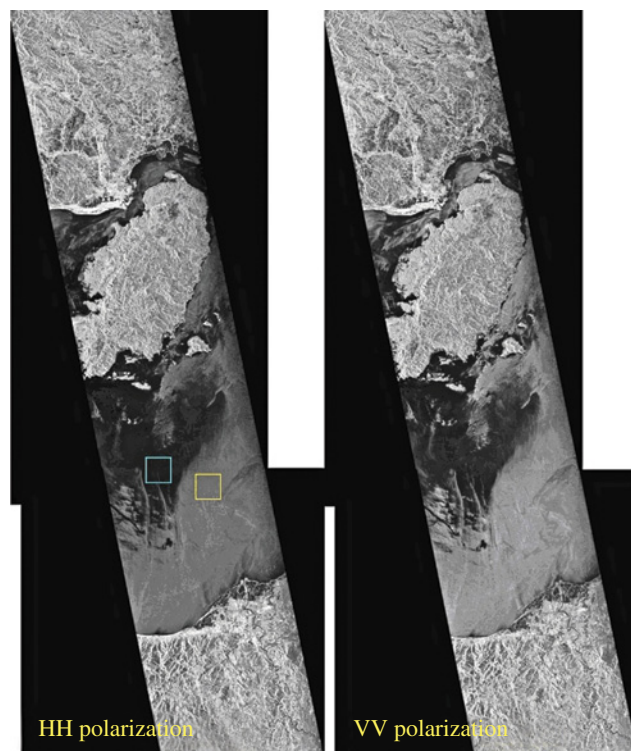


FIGURE 12.31 A PALSAR image of an oil spill. PALSAR operates in the L-band. This image compares the difference between HH and VV polarization. In this case, there is not much difference; however, in open seas, VV may be slightly better. At more shallow view angles, VV is much better. Photo from Japan website http://www.eorc.jaxa.jp/ALOS/en/img_up/pal_oil200608.htm

Shipborne radar has similar limitations and the additional handicap of low altitude, which restricts its range to between 8 and 30 km, depending on the height of the antenna. Ship radars can be adjusted to reduce the effect of sea clutter de-enhancement. Shipborne radar successfully detected many slicks, and commercial systems are now available. During the *Prestige* spill, a Netherlands vessel successfully used this technique to guide a recovery vessel into slicks [119]. The technique is, however, very limited by sea state and in all cases where it was used, the presence and location of the slick were already known or suspected. Recently, researchers have carried out work on improving the imaging of slicks from shipborne radars [119]. Today, there are some commercial products to enhance the images from shipborne radar to enable some oil imaging.

Gangeskar has proposed an automatic system that could be mounted on oil drilling platforms [120]. This system would use standard X-band ship navigation units and would provide an alert if an oil spill is present. The system includes an extensive postprocessing system to provide both a user-friendly graphical user interface and an automatic detection and alert system. The system has not been fully tested to date.

Radar has also been used to measure currents and predict oil spill movements by observing frontal movements

[121,122]. Work has shown that frontal currents and other features can be detected by SAR [123].

In summary, radar optimized for oil spills is useful in oil spill remote sensing, particularly for searches of large areas and for nighttime or foul weather work. The technique is highly prone to false targets, however, and is limited to a narrow range of wind speeds. Because of the all-weather and day–night capability, radar is now the most common means of oil spill remote sensing.

12.7.2.1 False Detections and No Detections Because radar detection of oil spills is so highly susceptible to false images, much work has taken place on means to differentiate oil slicks and false targets, often called look-alikes. These look-alikes include low-wind areas, areas sheltered by land, rain cells, organic films, grease ice, wind fronts, upwelling zones, oceanic fronts, algae blooms, current shear zones, etc. [124]. Extensive effort has been placed upon removing these look-alikes from imagery and automating the process of slick detection [116,125–165]. This issue is relevant to both satellite and airborne SAR systems.

Anderson et al. noted that false detections and lack of detections on satellite-borne systems can be high [109,125]. In analyzing 775 SAR images over the Baltic Sea with potential oil spills, they classified 94% as low or medium confidence. On the other hand, they noted that of the 69 actual oil pollution incidents in the Latvian Baltic, only about 45% were actually detected by SAR. About 40% of the SAR detections were slick look-alikes or very minor amounts of oil.

12.7.3 Microwave Scatterometers

A microwave scatterometer is a device that measures the scattering of radar energy by a target. One radar scatterometer was flown over several oil slicks and used a low-power transmitter operating in the Ku band (13.3 GHz) [19]. The scatterometer detected the oil, but discrimination was poor. The “Heliscat,” a device with five frequencies, has been used to investigate capillary wave damping [113]. The advantage of a microwave scatterometer is that it has an aerial coverage similar to optical sensors and it can look at several incident angles. The main disadvantages include the lack of discrimination for oil and the lack of imaging capability.

12.7.4 Surface-Wave Radars

It is possible to send radio waves along the sea using high frequency. The conductivity of the sea acts as a wave guide. These radars can be used to detect ships as far out as 500 km [166]. Since these are surface-wave phenomena, only targets above the surface are detected; thus, slicks may not be detected by this technique [167]. Modeling of the technique does not show whether there is potential for oil detection by this method or not [168]. There are several types of these; one type is used to measure ocean surface currents [169,170].

12.7.5 Interferometric Radar

Radars can be used to measure height, currents, and other surface elevation phenomena using interferometric techniques. Some radar systems on aircraft are fitted for this application such as the Government of Canada Convair 580. This can also be carried out in space using two satellites traveling in tandem. One research group employed the tandem satellite pair of ERS-2 and Envisat (Environmental Satellite) to carry out such work, but there are no reports on interferometric use on oil spills [171].

12.8 SLICK THICKNESS DETERMINATION

There is a need to measure oil slick thickness; this need has been expressed both within the oil spill response community and among academics in the field. There are presently no reliable methods, either in the laboratory or in the field, for accurately measuring oil-on-water slick thickness. The ability to do so would significantly increase understanding of the dynamics of oil spreading and behavior. Knowledge of slick thickness would make it possible to determine the effectiveness of certain oil spill countermeasures including dispersant application and in situ burning. Indeed, the effectiveness of individual dispersants could be determined quantitatively if the oil remaining on the water surface following dispersant application could be accurately measured [172,173].

12.8.1 Visual Thickness Indications

A very important tool for working with oil spills has been the relationship between appearance and thickness. Careful study of the literature and comparing with field experience show that there is limited potential to scale thicknesses to visual appearance [8]. The only physics-based appearance occurs at thicknesses of about 0.7–2.5 μm , at which the rainbow colors appear as a result of multiple constructive and destructive interferences by light. Table 12.1 shows the summation of the best knowledge on this phenomenon. Figures 12.32 and 12.33 show typical rainbow sheens for which we can estimate that the thickness is about 1 μm . This is the only color appearance that has a physical slick thickness associated with it.

TABLE 12.1 Relationship of thickness to appearance

	Minimum	Silvery	Rainbow	Visibility thresholds (μm)	Dull colors	Dark
				Darkening colors		
Typical thickness	0.09	0.1	0.6 ^a	0.9	2.7	8.5

^aNote this is the only physics-based appearance factor.

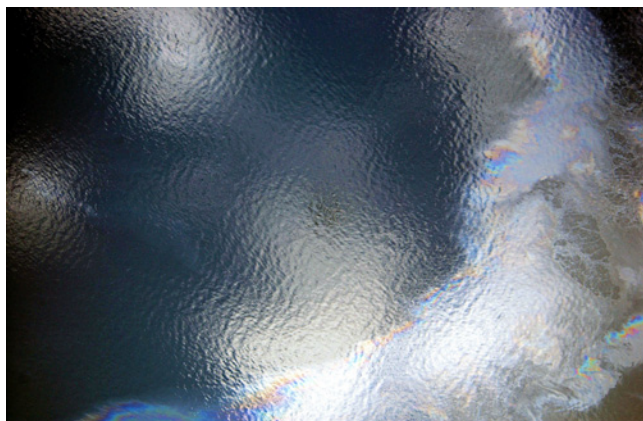


FIGURE 12.32 A picture of a rainbow sheen. This is the only spill thickness that has a physical explanation. Photograph from Environment Canada.

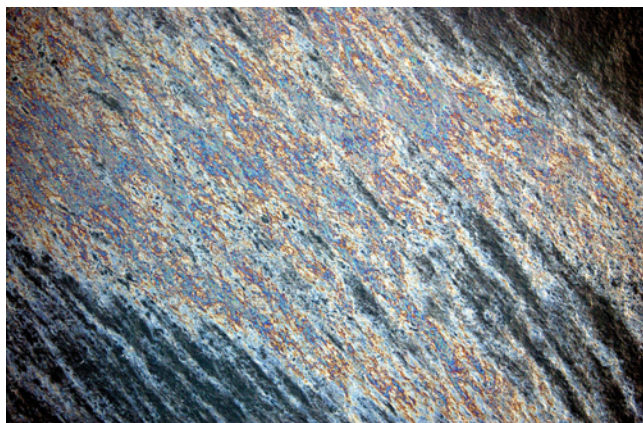


FIGURE 12.33 Another picture of a rainbow sheen. This is from newly discharged oil from behind a vessel. Photograph from Environment Canada.

Lehr argues that the visual indications of slick thickness are so poor as to not allow for any slick thickness estimation [174]. In particular, he notes that the Bonn agreement thickness code provides insufficient proof for greater thicknesses as it purports to. Lehr suggests that the solution to this is simply to use two thickness regimes, sheen and thicker oil, and not to estimate slick volumes from this.

12.8.2 Slick Thickness Relationships in Remote Sensors

A number of investigators tried to correlate slick thickness with appearance in various remote sensing instruments. Hollinger and Mennella conducted a series of eight controlled oil spills off Virginia to investigate the use of microwave radiometry to delineate oil spills [175]. They used 19.4 and 69.8 GHz radiometers on the spills. Measurements using sorbents were used to calibrate the radiometer. It was noted that the sheens typically had a thickness of 2–4 μm . It was found that 90% of the oil was in 10% of the slick area and that the microwave threshold was about 0.1 mm (100 μm).

A series of experiments were carried out in 1979 to evaluate IR and SLAR for oil spill detection [176]. The imagery was correlated against visual and sorbent measurements, which were used to derive a thickness estimate. It was concluded that the IR threshold was between 25 and 50 μm and for SLAR 100 nm. Further, manipulation of data showed that a mass balance could be achieved if the thickness at which the IR showed oil to be colder at the sea occurred at 100 μm and for the heated portion of the oil at 1000 μm . This has not been validated and at this time the thicknesses appear to be rather large.

The United Kingdom conducted Isowake Experiments in 1982 [177–179]. On the basis of estimations and calculations, it was concluded that the lowest detectable slick thickness for IR was between 10 and 50 μm , whereas hot spots in the IR image could be as much as 1000 μm thick.

MacDonald used photography from the space shuttle to define up to 124 slicks in an area of the Gulf of Mexico, off-shore Louisiana [180]. Similarly, a thematic image from Landsat showed at least 66 slicks in one large area. Some of the thickness relationships were based on unpublished experimental data from Duckworth.

Brown et al. conducted experiments to measure the visibility of oil slicks. The observers and a UV and visible camera were mounted in a crane basket 30 m over the slick [181]. It was found that the detection ability decreased by over 50% for most oils and for the cameras when the angle was changed from 90° to 55° from the horizontal (equivalent incidence angle of 0–35°). Detectability degraded to 70% and sometimes to nil as the viewing angle was decreased past 55 through 35°. Brown et al. conducted several experiments to ascertain the relationship between thickness of slicks and the density (or intensity) of the IR image [46]. The thicknesses varied between 1 and 10 mm, and thicknesses were measured using an acoustic system. No relationship between slick thickness and IR brightness was found.

12.8.3 Specific Thickness Sensors

The suppression of the water Raman peak in laser fluorosensor data has not been fully exploited or tested. This technique may work for thin slicks, but not necessarily for thick ones, at least not with a single excitation frequency. Attempts have been made to calibrate the thickness appearance of IR imagery but also without success. It is suspected that the temperatures of the slick as seen in the IR are highly dependent on oil type, sun angle, and weather conditions. If so, it may not be possible to use IR as a calibrated tool for measuring thickness. As accurate ground truth methods do not exist, it is very difficult to calibrate existing equipment [182,183]. The use of sorbent techniques to measure surface thickness yields highly variable results [172]. As noted in the section on microwave radiometers, the signal strength measured by these instruments can imply one of several thicknesses. This methodology does not appear to have potential, other than for measuring relative oil thickness.

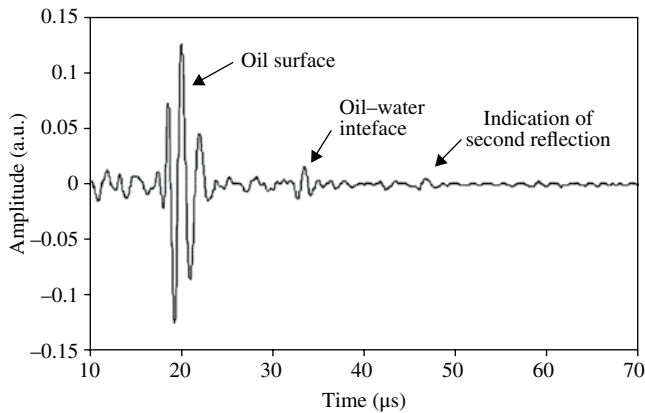


FIGURE 12.34 The signal from a three-laser thickness sensor. The time of the first pulse return corresponds to a thickness of about 6 mm. This was measured by a prototype sensor mounted in an aircraft and flying over containers with various thicknesses of oil on water [190].

A variety of electrical, optical, and acoustic techniques for measuring oil thickness has been investigated [182,183]. Two promising techniques were pursued in a series of laboratory measurements. In the first technique, known as “thermal mapping,” a laser is used to heat a region of oil, and the resultant temperature profiles created over a small region near this heating are examined using an IR camera [183]. The temperature profiles created are dependent on the oil thickness. A more promising technique involves laser acoustics [184–186]. The laser ultrasonic remote sensing of oil thickness sensor consists of three lasers, one of which is coupled to an interferometer to accurately measure oil thickness [186–191]. The sensing process is initiated with a thermal pulse created in the oil layer by the absorption of a powerful CO_2 laser pulse. Rapid thermal expansion of the oil occurs near the surface where the laser beam was absorbed, which causes a steplike rise of the sample surface as well as an acoustic pulse of high frequency and large bandwidth (~ 15 MHz for oil). The acoustic pulse travels down through the oil until it reaches the oil–water interface where it is partially transmitted and partially reflected back toward the oil–air interface, where it slightly displaces the oil’s surface. The time required for the acoustic pulse to travel through the oil and back to the surface again is a function of the thickness and the acoustic velocity of the oil. The displacement of the surface is measured by a second laser probe beam aimed at the surface. Motion of the surface induces a phase or frequency shift (Doppler shift) in the reflected probe beam. This phase or frequency modulation of the probe beam can then be demodulated with an interferometer [191]. The thickness can be determined from the time of propagation of the acoustic wave between the upper and lower surfaces of the oil slick. This is a very reliable means of studying oil thickness and has great potential. Laboratory tests have confirmed the viability of the method, and a test unit has been flown to confirm its operability

[182]. Figure 12.34 shows the first airborne measurement of slick thickness.

Several attempts have been made to measure thickness by using visible spectral imaging. As there is no visual indication other than the rainbow sheen area around $0.8 \mu\text{m}$, these efforts are wasted [192,193]. Others have tried to use laboratory measurements to attempt to establish relationships for remote sensing outputs; such efforts fail because of the complex relationships of light in the atmosphere and on the surface [16]. Similarly, several workers have tried to use the assumption that the oil layer is transparent; therefore, the differences in reflection from the water surface and the top of the oil layer could yield a thickness measurement [194–196]. Unfortunately, this oil is not transparent in the visible ranges, therefore such methods do not work.

12.9 INTEGRATED AIRBORNE SENSOR SYSTEMS

Increasingly, a number of different types of airborne oil spill remote sensors are being consolidated into sensor systems. The reason for this integration is to take advantage of the different information provided by each of the specific sensors and combine the information to provide a more comprehensive information product. Although each of the individual sensors has specific inherent weaknesses such as false detections, these false detections are often different for each sensor type; hence, a consolidation of information can help resolve some of the uncertainties that exist from a single data source. Furthermore, additional information can be deduced from the overlaying of imagery from several sensor types. Although the absolute thickness of an oil slick remains the subject of continued research and scientific opinion, the ability to locate the thicker portions of the slick is essential in terms of operational spill cleanup and response. In addition to the integration of a number of remote sensors into a sensor system, information from other sources such as marine vessel traffic surveillance systems (i.e., automatic identification system, AIS) can be integrated and can play an essential role in identifying the source of the marine pollution.

Two commercially available airborne marine oil spill remote sensing systems are the MEDUSA and the MSS 6000 [197,198]. MEDUSA incorporates a number of sensor technologies such as laser fluorosensors, IR/UV line scanners, forward-looking IR sensors, microwave radiometers, SLAR systems and camera systems, as well as processing software into a flexible real-time data acquisition and processing system. The data from the various sensors are georeferenced and fused with information from AIS and marine surveillance radars into a geographic information system (GIS)-based display output format. The processing software is known as the Oil Spill Scene Analysis System and allows for the extraction of features such as the area of

oil coverage including areas of intermediate and thicker portions of the slick. The MSS 6000 Maritime Surveillance System is composed of a flexible suite of sensors such as SLAR systems, IR/UV line scanners, forward-looking IR sensors, microwave radiometers, and camera systems, along with data processing and mission management software in order to perform the oil spill remote sensing surveillance task. The MSS 6000 also focuses on sensor integration and includes AIS and marine search radar inputs. All sensor data, imagery, slick targets, vessels, etc. are annotated using navigation data from a single source to form an integrated part of a GIS. Both the MEDUSA and MSS 6000 can distribute their data in near real-time via direct downlink or satellite communications to vessels or shore-based communication centers. A large number of maritime nations are now employing integrated airborne sensor systems [199,200].

12.10 SATELLITE REMOTE SENSING

12.10.1 Optical

The use of optical satellite remote sensing for oil spills has been attempted several times. The slick from the Ixtoc I well blowout in Mexico was detected using Geostationary Operational Environmental Satellite and by the Advanced Very High Resolution Radiometer (AVHRR) on the Land Satellite (Landsat) satellite [19]. A blowout in the Persian Gulf was subsequently detected. The large Exxon Valdez slick was detected on Satellite Pour l'Observation de la Terre satellite data [201]. Oiled ice in Gabarus Bay resulting from the Kurdistan spill was detected using LANDSAT data [202,203]. Results of this are shown in Figures 12.35 and 12.36. Several workers were able to detect the Arabian Gulf War Spill in 1991 [204–207]. The Haven spill near Italy was also monitored by satellite [208]. A spill in the Barents Sea was tracked using an IR band on National Oceanic and Atmospheric Administration (NOAA) 10 [209]. There were many uses of visual imagery from satellites during the Deepwater Horizon spill in the United States [210]. It is significant to note that, in all these cases, the position of the oil was known and data had to be processed to actually see the oil, which sometimes took several weeks. Newer findings show that the ability to detect oil may be a complex function of conditions, oil types, and view angles [211–213].

Land spills have been defined by visible satellites on several occasions. Hese and Schmuilius mapped out the oil land contamination in Western Siberia using Landsat and QuickBird data [214].

In the past, there were several problems associated with relying on satellites operating in optical ranges, for oil spill remote sensing. The first is the timing and frequency of overpasses and the absolute need for clear skies to perform optical work [215]. This is particularly true with older satellites with very infrequent overpasses. The chances of the overpass and the clear skies occurring at the same time gave a very low probability of seeing a spill on a satellite image. This point is

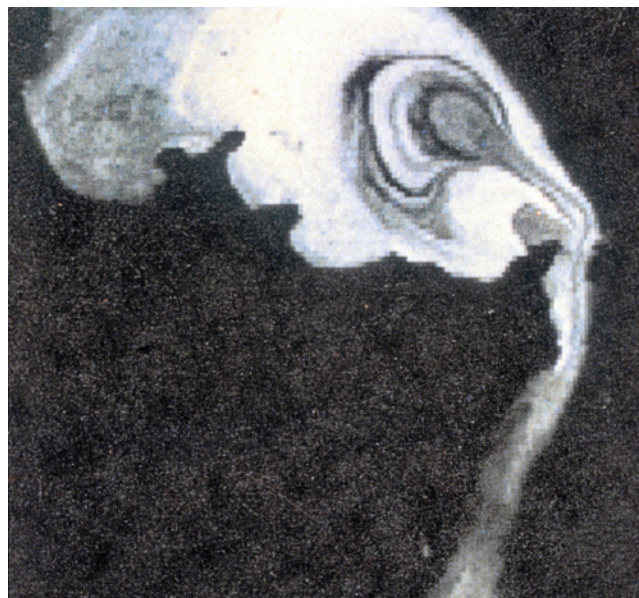


FIGURE 12.35 Landsat imagery of oiled ice off the east coast of Canada. The black lines in the ice are either sediment or oil. The unenhanced image does not easily lend itself to interpretation.

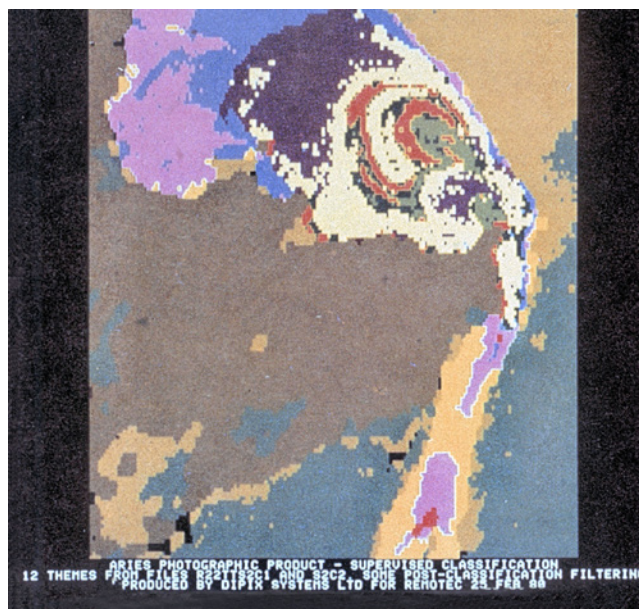


FIGURE 12.36 The same image as in Figure 12.35 but processed to show some of the oil using the more reddish color of oil compared to the sediment. The red indicates oil; however, some other material near the shore also shows this coloration but it is not oil.

well illustrated in the case of the Exxon Valdez spill [215]. Although the spill covered vast amounts of ocean for over a month, there was only one clear day that coincided with a satellite overpass, and that was on April 7, 1989. Another disadvantage of satellite remote sensing is the difficulty in developing algorithms to highlight the oil slicks and the long time required to do so. For the Exxon Valdez spill, it took over 2 months before the first group managed to

“see” the oil slick in the satellite imagery, although its location was precisely known [216]. Fortunately, this has changed with the data availability in modern satellites.

Recently, several workers have attempted to use visible data to detect oil spills [217–219]. These techniques generally rely on ancillary data, such as suspected position or other satellite data, to be successful. Srivastava and Singh used only MODIS to detect known oil spills in Lake Maracaibo, Venezuela [220]. First, the use of L1B data visually did show oil; however, uncorrected features at 469, 555, and 645 nm showed significant indications of oil. Further study showed that the ratio of the difference and sun at 645 and 555 nm normalized by 469 nm provided the best results. More recently, several workers used MODIS and other satellite data to detect the oil during the Macondo spill in the U.S. Gulf of Mexico [210]. Hu demonstrated a technique to remove sunglint from MODIS imagery [221]. This correction was at wavelengths of 469, 555, 645, 959, and 1240 nm.

Cococcioni and Corucci [222] and Corucci et al. [223] used MODIS imagery to locate oil spills. The procedure was to take a multispectral image from MODIS and subject it to a series of corrections and then use a supervised classification system to highlight oil spills. This was tested on small slicks in the Mediterranean Sea. Grimaldi et al. used MODIS and AVIRIS data to locate oil spills. This was tested on the Lebanon oil spill [224,225].

The major interference to optical satellite use is the presence of clouds. Figure 12.37 illustrates cloud blockage of optical satellite sensing. During the Gulf of Mexico spill, extensive efforts were made to use optical satellite data. This had varied success as illustrated in Figures 12.38, 12.39, 12.40, 12.41, 12.42, 12.43, 12.44, 12.45, and 12.46.

There is some information on slicks available from angular information. For example, Chust and Sagarminaga used the multiangle imaging spectroradiometer sensors aboard a satellite to detect oil spills on Lake Maracaibo, Venezuela [226]. These sensors use nine push-broom cameras at fixed angles from nadir to 70.5° to examine particular surfaces. A comparison of this angular sensor shows that better contrast was obtained than a simple nadir camera on another satellite. Data analysis showed that oil spills appear in greater contrast in those view angles affected by sun glitter because of the presence of oil.

IR data from satellite has been used to map the land oil pollution in Kuwait [227]. It was found that the old hydrocarbon-contaminated areas showed as much as 10°C difference from the surrounding land. Ground truthing was used extensively in compiling the data. Casciello also made an attempt to use IR imagery from the thermal IR region of the AVHRR satellite to locate known oil spills [228]. Grimaldi et al. used channels 4 and 5 of the thermal IR channels of AVHRR to calculate the presence of oil spills [225]. This technique relies on the contrast in the IR between clean and oiled water. Li et al. used the sea surface temperature (SST) information in the IR from MODIS to detect oil spills [229].

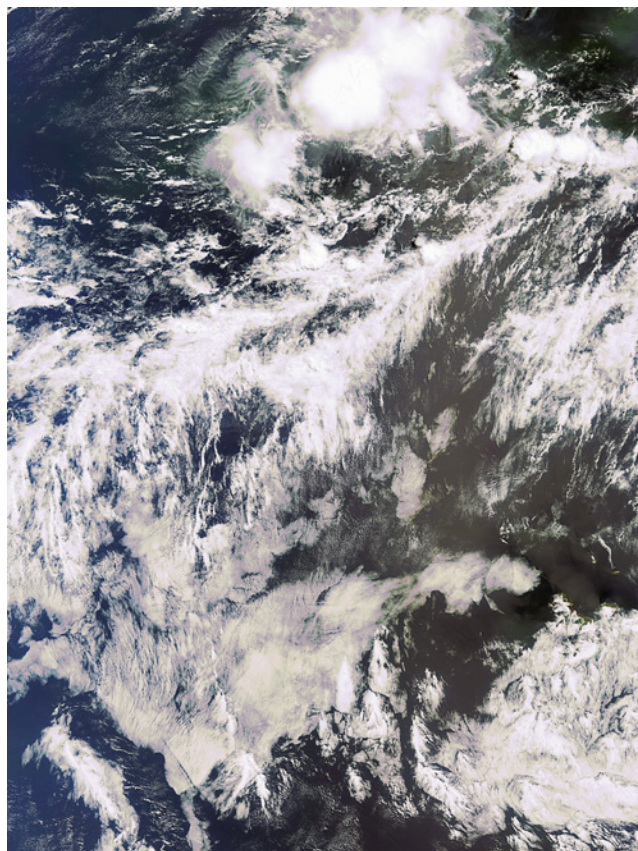


FIGURE 12.37 The medium-resolution imaging spectrometer image of the coast of France. On this particular day, there was so much cloud that even the coastline was obscured. This illustrates that clouds are the major obstacle to satellite optical remote sensing. Photo from European Space Agency website <http://www.esa.int/esaEO/>

12.10.2 Radar

Radar satellites, including ERS-1 and ERS-2, Radarsat-1 and Radarsat-2, and Envisat, have usefulness for detecting large offshore spills and for spotting anomalies [95,230, 231]. Radarsat has been used for detecting oil seeps and smaller spills resulting from an oil barge [232,233]. The relative location of these smaller slicks was known before the detection. A novel application of Radarsat has been the study of oil lakes in the deserts of Kuwait [234]. A depiction of Radarsat is shown in Figure 12.47.

Radar satellites are now used routinely by a number of nations to provide imagery for spills and to give indications of ship discharges. ERS-1 and ERS-2 have been used for mapping of oil spills in the Caspian Sea [235]. Fortuny describes the use of ERS-2 and Envisat to provide imagery during the Prestige incident off Spain [236]. Torres Palenzuela and coworkers used two advanced synthetic aperture radar (ASAR) images from the Envisat satellite to study the same Prestige spill off Spain [237]. Using several techniques that were readily available such as filtering and comparison to GIS data of the areas, several slicks were



FIGURE 12.38 A MODIS image of the Gulf of Mexico (GOM) during the Deep Water Horizon (DWH) spill. The MODIS sensor flies aboard the NASA Aqua satellite. The oil slick is outlined by the box. Photo from NASA website, www.nasa.gov



FIGURE 12.39 A MODIS image of the GOM during the DWH spill. The MODIS sensor flies aboard the NASA Aqua satellite. The oil slick shown in Figure 12.38 is enhanced here. Photo from NASA website, www.nasa.gov

identified. These slicks were confirmed by recorded sightings from helicopters and ships.

Radar satellite data is increasingly being used to monitor oil spills. As there are several satellites active, frequent coverage is now possible. During the 2010 Gulf of Mexico oil spill, there was extensive use of satellite data. Some of this is illustrated in Figures 12.48, 12.49, 12.50, 12.51, 12.52, 12.53, 12.54, and 12.55.

Several countries have instituted satellite monitoring systems for oil pollution [238–240]. Many of these use processing methods as described earlier. Extensive programs are in place in the Baltic Sea, North Sea, and English

Channel [163]. There are now programs in the Black, Caspian, and Azov Seas [240,241]. Canada has had a program in place for several years [242]. The Mediterranean Sea has had such a program for a long time [162,163]. A constellation of monitoring satellites is proposed for the Mediterranean Sea [243].

In recent years, there have been a number of new satellite-borne SAR sensors launched (see Table 12.2). While one of these sensors, Radarsat-2, operates in the traditional C-band, TerraSAR-X and COSMO SkyMed operate in the X-band, and the Phased Array L-band Synthetic Aperture Radar (PALSAR) sensor on Advanced Land Observation

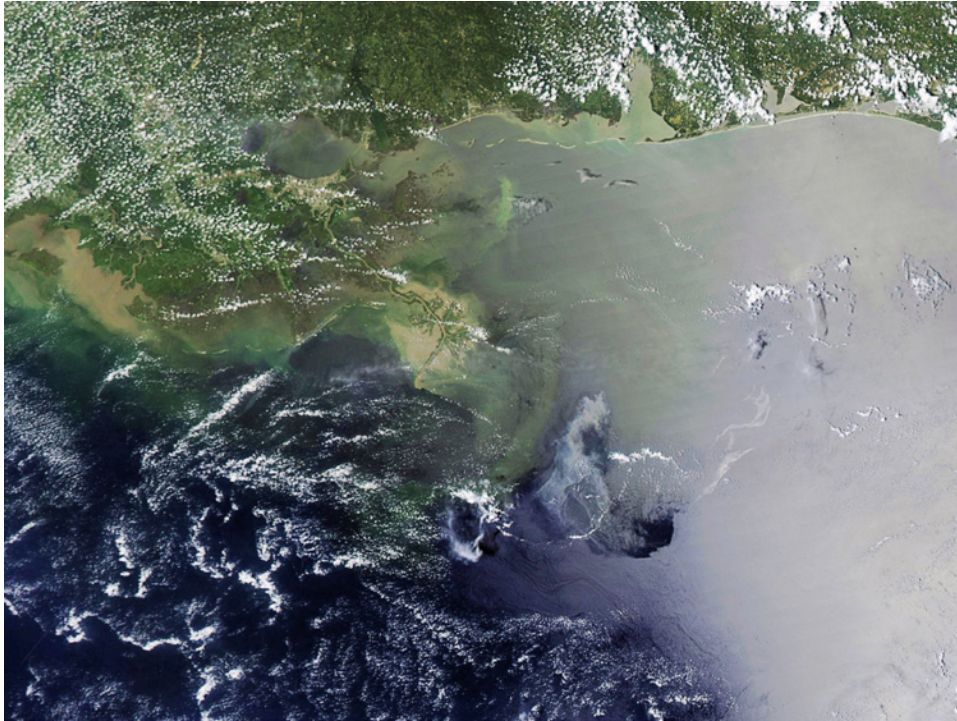


FIGURE 12.40 A MODIS image of the GOM during the DWH spill. The image shows little oil between the clouds and the land—although there are too many clouds to definitively find the oil. The sediment from the Mississippi River is clearly seen south of Louisiana. Much of the other structures on the water are clouds. Photo from NASA website, www.nasa.gov

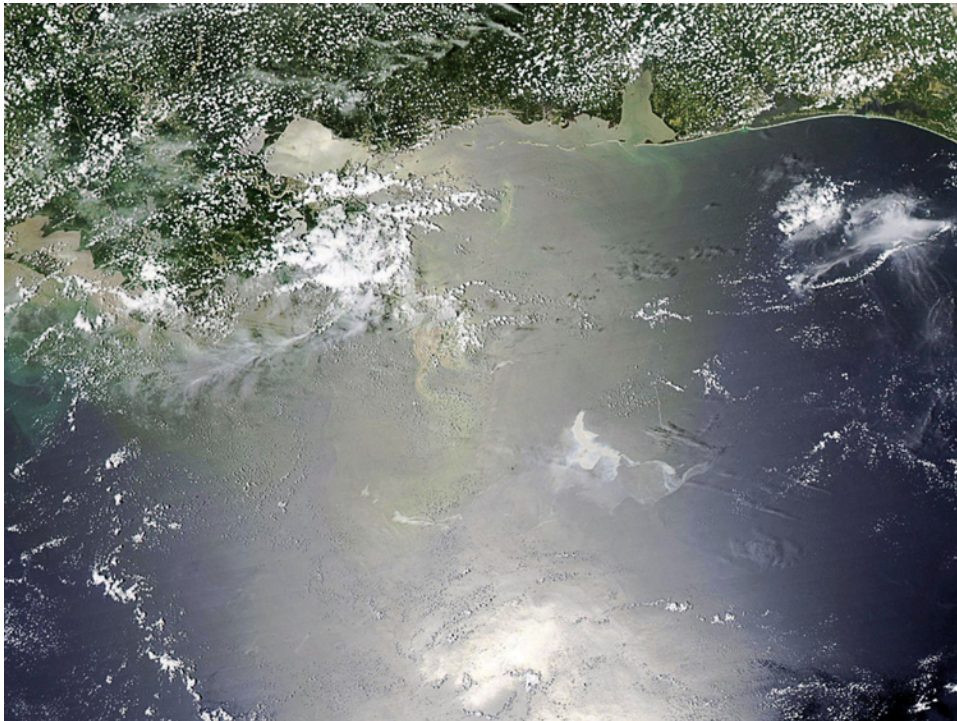


FIGURE 12.41 A MODIS image of the GOM during the DWH spill. The image shows some oil between the clouds and the land—although there are too many clouds to definitively find the oil. Much of the other structures on the water are clouds. Photo from NASA website, www.nasa.gov

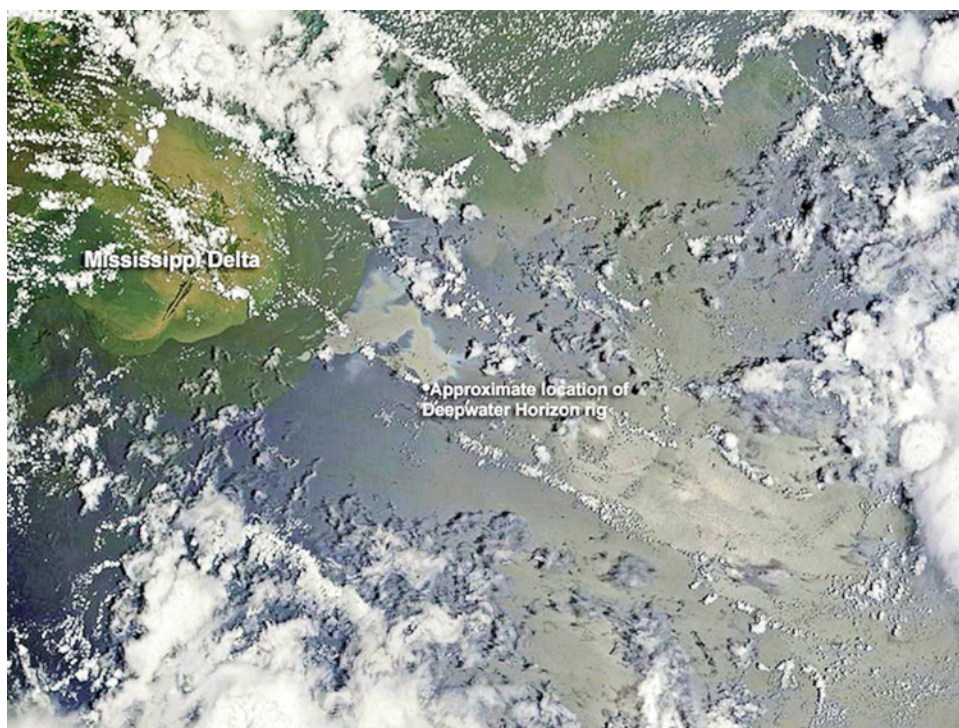


FIGURE 12.42 A MODIS image of the GOM during the DWH spill. The image shows oil between the DWH rig site and the land (to the north) as well as oil directly to the south. Much of the other items on the water are clouds. Photo from NASA website, www.nasa.gov

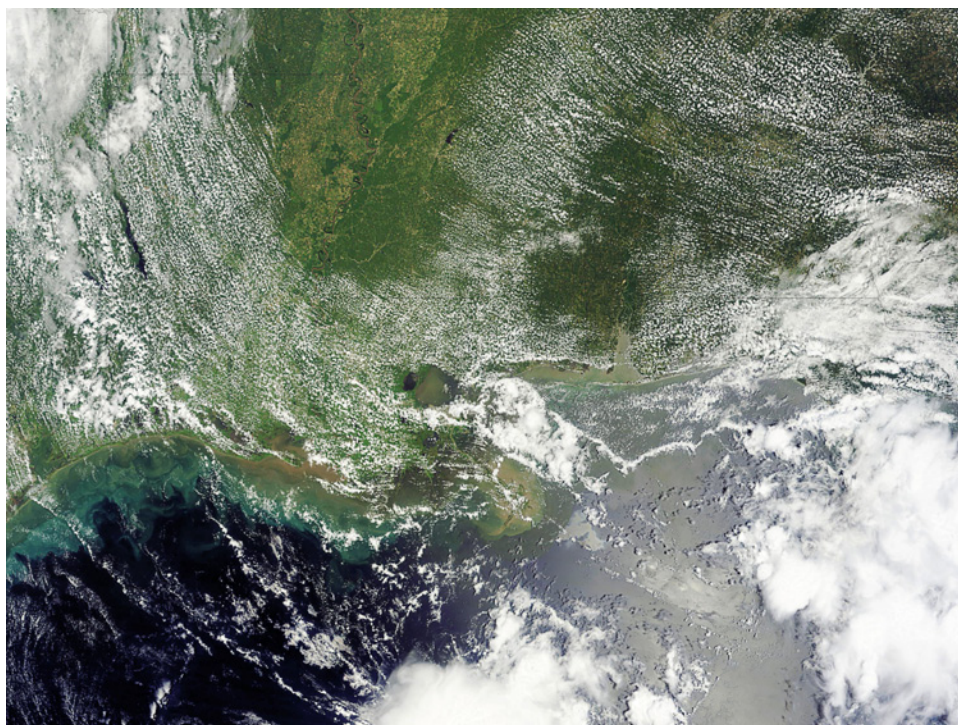


FIGURE 12.43 A MODIS image of the GOM during the DWH spill. The image is almost completely obscured by cloud—a typical situation. Photo from NASA website, www.nasa.gov

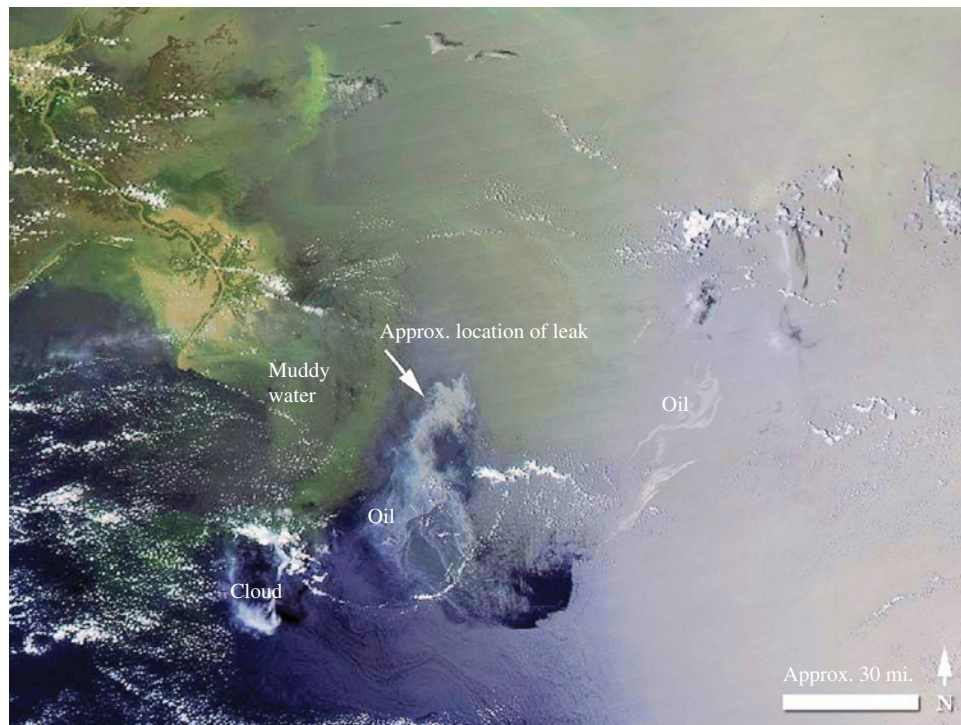


FIGURE 12.44 A MODIS image of the GOM during the DWH spill. The image is annotated as to oil and cloud. Photo from NASA website, www.nasa.gov

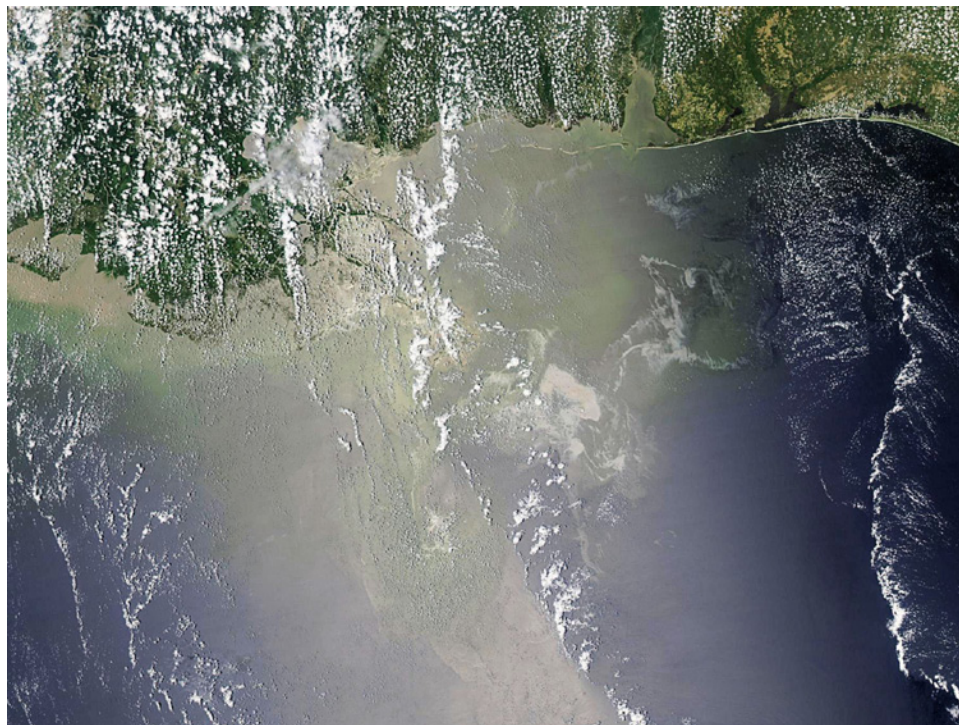


FIGURE 12.45 A MODIS image of the GOM during the DWH spill. Oil can be seen to the right and top of the image. There are clouds in the image that block some views of the land and sea. Photo from NASA website, www.nasa.gov

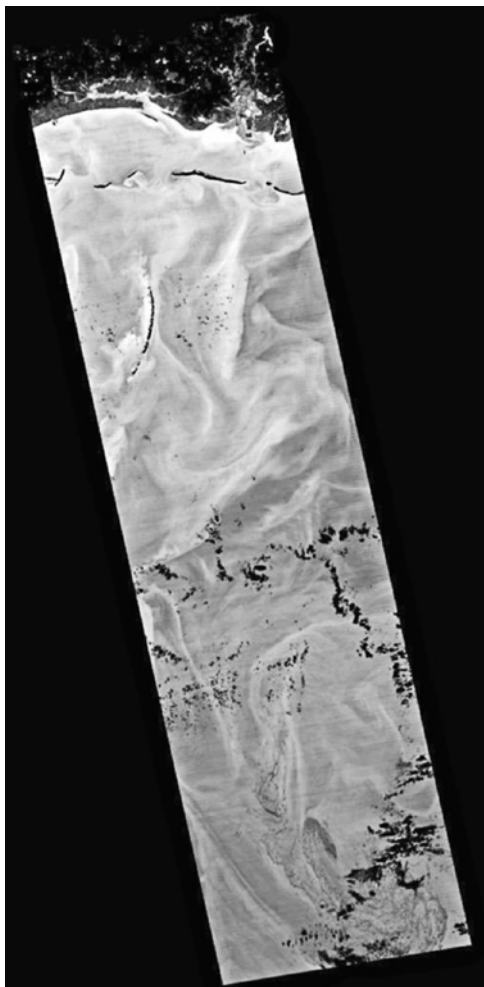


FIGURE 12.46 NASA infrared image shows spill view full size. The advanced space-borne thermal emission and reflection radiometer instrument on NASA's Terra spacecraft captured this image of the oil spill in the Gulf of Mexico on May 7, 2010. The image is a thermal image, with the coldest surfaces appearing dark and the warmest appearing white. The city of Pascagoula, Mississippi, is visible in the upper right corner; at night, the land is colder (darker) than the Gulf waters. Photo from NASA website, www.nasa.gov

Satellite (ALOS) operates in the L-band. As noted earlier, X-band is the preferred band for oil spill remote sensing in terms of Bragg scattering. All four of these new SAR satellites have polarimetric imaging modes (some are experimental vs. operational modes) and much higher spatial resolution (down to 3 m), which may have application for oil spill remote sensing. Radarsat-2, like its predecessor, is an operational commercial satellite that can be tasked to respond to emergency situations like major oil spills. The time required to task Radarsat-2 in emergency mode is now 4 h, which is a large improvement from the 12 h required to task its predecessor. As noted earlier, VV polarization provides a superior clutter-to-noise ratio over HH polarization for oil spill detection [239]. Radarsat-2 is fully polarimetric, and there is interest in investigating whether a dual-polarization ScanSAR mode utilizing VV/VH polarizations will work for oil and

ship detection, respectively, as part of the Integrated Satellite Tracking of Pollution program [242]. The increased number of SAR satellites plus the plans to operate constellations of small satellites like Cosmos (Constellation of Small Satellites for Mediterranean basin Observation) will provide increased temporal coverage with revisit times down to a few hours in some circumstances. The opportunity for increased frequency of image collection should prove useful to the oil spill response community. Figures 12.25, 12.26, 12.27, 12.28, 12.29, and 12.30 show the use of radar satellites and the look-alikes to oil that sometimes appear in the images.

Li et al. highlighted the differences between optical and radar satellites [244]. This research group studied the Montara spill in the Timor Sea using the ALOS PALSAR (L-band radar), the Envisat ASAR (C-band radar), and the MODIS (Aqua—color visible) satellite data. The ALOS PALSAR did function but, as expected from L-band radar, was not clear. The Envisat ASAR data was the clearest and provide useful imagery always. The visible data from MODIS function well only during completely clear skies, but most of the time did not yield useful images. Cloud interference in the latter was cited as a reason, but the lack of specific oil coloration should have also been noted.

12.11 OIL-UNDER-ICE DETECTION

The difficulties in detecting oil in or under ice are numerous. Ice is a heterogeneous material and incorporates air, sediment, salt, and water, many of which may present false oil-in-ice signals to the detection mechanisms. In addition, snow on top of the ice or even incorporated into the ice adds complications. During freeze-up and thaw in the spring, there may not be distinct layers of water and ice. There are many different types of ice and different ice crystalline orientations. This is a separate field and readers may consult the literature [245]. An update on this topic is also in this book.

12.12 UNDERWATER DETECTION AND TRACKING

Many different techniques have been tried for underwater oil detection. First, the division should be made between the oil in the water column or floating on a pycnocline and oil on the bottom. Quite different physics and conditions can apply to these different situations.

Several parties have tried to use standard sonars to detect submerged oil on the bottom. Oil on the bottom can appear as a softer surface than ordinary bottom sediment [246]. The problem arises in that vegetation on the bottom also appears similar and thus many false positives arise. In the water column, sonar can be useful as it can locate intermediate oil on pycnoclines; however, there is no unique signature and there are often weeds and other debris on pycnoclines. Wendelboe et al. report on tests using a 200 and 400 kHz

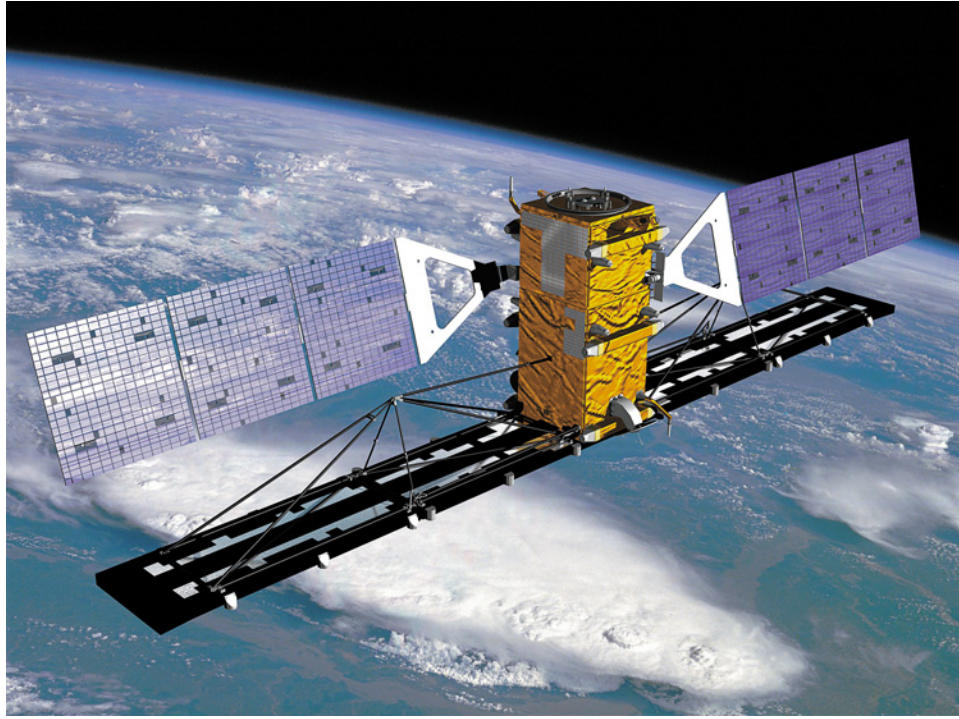


FIGURE 12.47 A depiction of the Radarsat-2 satellite. The directional antennae are on the bottom, and the top shows the solar cells. Photo from Canadian Space Agency website <http://www.asc-csa.gc.ca/images>

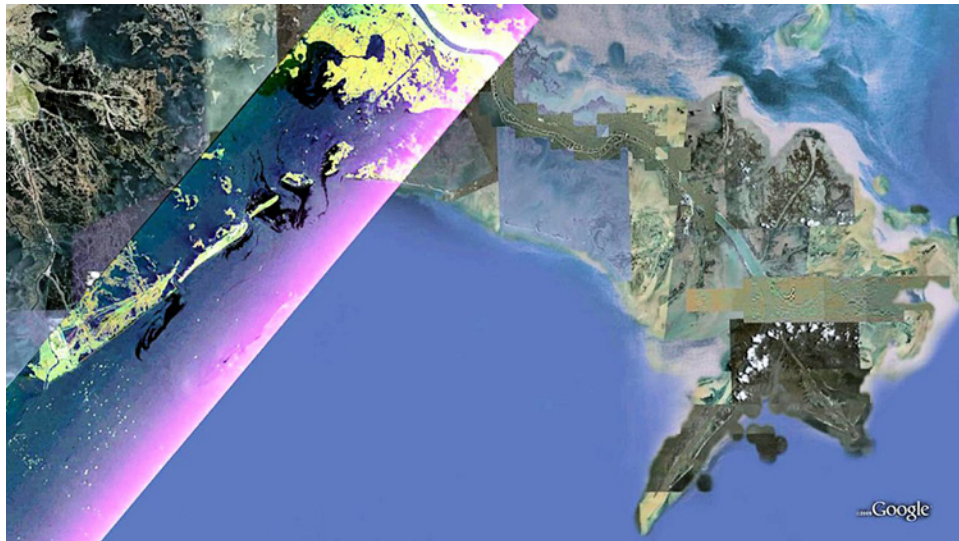


FIGURE 12.48 The Uninhabited Aerial Vehicle Synthetic Aperture Radar (UAVSAR) from the NASA radar mapper shown on top of a MODIS visible image of the Gulf; the black near the shoreline is oil. The UAVSAR is built by NASA and currently flies on a Gulfstream-III aircraft. Photo from NASA website, www.nasa.gov

(dual-frequency) multibeam system [247]. The contributing signal is the lower acoustic reflectivity of the oil than typical bottom geological formation or the better reflection than weed beds. Wendelboe et al. used the backscatter signals from several tests to develop algorithms for oil detection. This was tested in a tank with a 90% success rate and a 23% false detection rate [247]. Hansen reviewed various systems

noting that the narrow-scan sonar systems showed promise [248]. Medialdea et al. studied the use of commercially available multibeam sonars to characterize bottom material [249]. They were able to characterize bottom sediments and suggested that oil on the bottom might be characterized by such a technique. These workers did not actually scan areas where there was known oil.

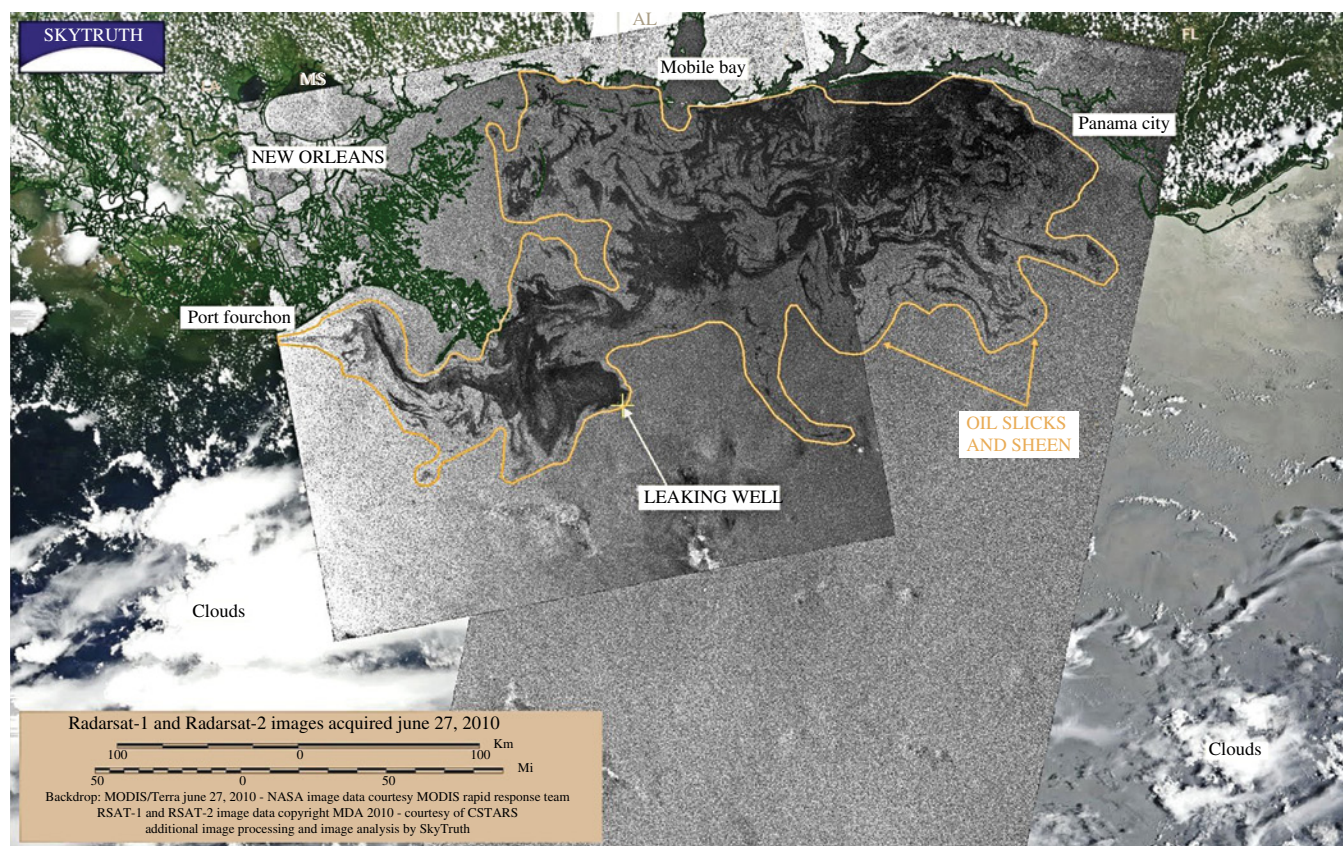


FIGURE 12.49 A Radarsat-1 and Radarsat-2 combined image of the Gulf oil spill. The radar images are laid upon a satellite visible image of the coast. Oil slicks and sheen are outlined in color. Photo from Canadian Space Agency website <http://www.asc-csa.gc.ca/images>

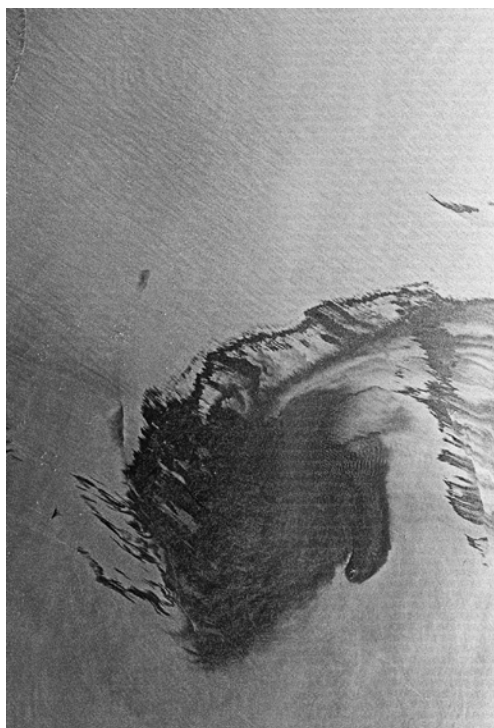


FIGURE 12.50 A Radarsat-2 detailed image of the Gulf oil spill. This image shows that details of the slick can be generated. Photo from Canadian Space Agency website <http://www.asc-csa.gc.ca/images>

Oil on the bottom has successfully been mapped by underwater cameras, often mounted on sleds [250–252]. The problems with this technique are the bottom visibility, often insufficient to discriminate, and the difficulty in towing the camera vehicle as slow as 1 knot, the necessary speed. Pfeifer et al. were successful in employing mosaics of photographs to determine the aerial extent of oil on the seafloor [251,252].

A low-technology approach had been historically employed. Heavy oil, having a density as would cause it to sink, often adheres to oil snares or pom-poms, which are polypropylene strips mounted as a cheerleader's pom-pom. These can be mounted on a beam and towed over the bottom and then raised periodically to see if oil has adhered [250]. Alternatively, they can be mounted on an anchor with a marker buoy. These are then raised periodically to check if the subsurface oil has contacted them.

The use of laser fluorosensors for underwater oil has been suggested [253]. Camilli et al. have successfully applied mass spectrometry to the detection of sunken heavy oil (Fuel Oil #6) [254]. Using the small and enclosed mass spectrometer, TETHYS, the low-molecular-weight hydrocarbons coming from sunken oil masses are monitored. The mass spectrometer is mounted in a submersible that is driven over the seafloor. The exact position of the submersible is monitored closely using an acoustic positioning system on the surface. Signals then can be correlated closely to the position on the seafloor. Three ion peaks of m/z 43, 41, and 27 are

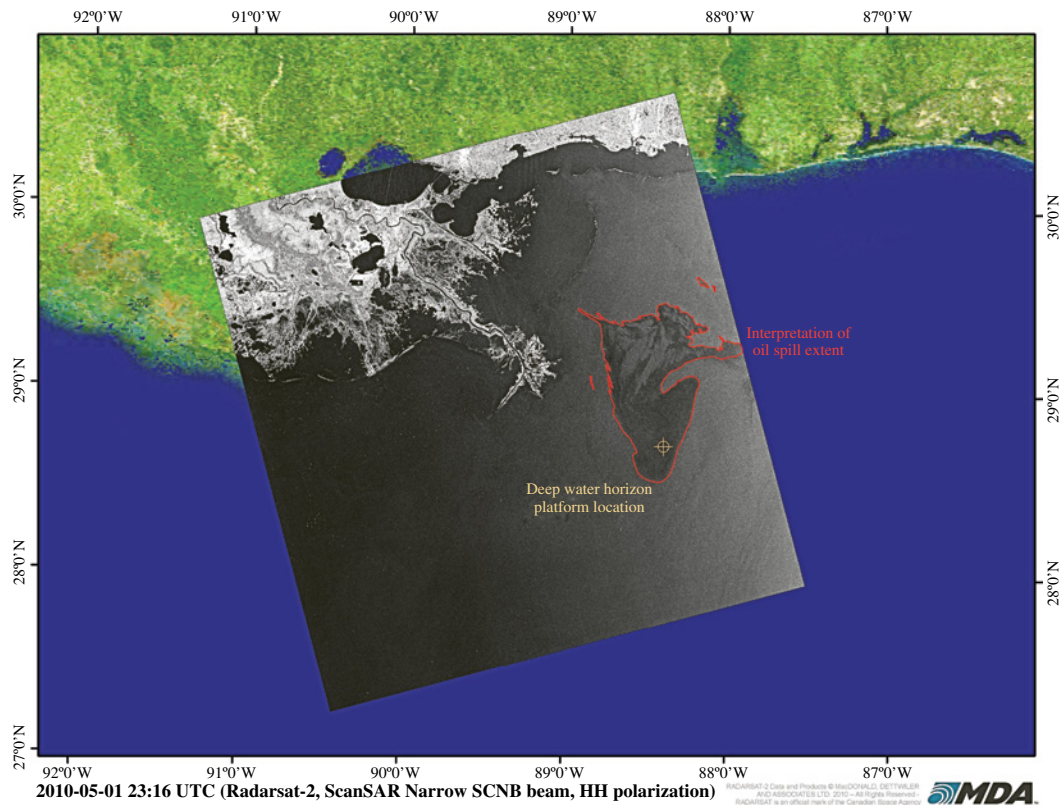


FIGURE 12.51 A Radarsat-2 image of the Gulf oil spill. The spill can be clearly seen and is outlined in gray. The shoreline is in white and the image is set onto a visible satellite image. Photo from Canadian Space Agency website <http://www.asc-csa.gc.ca/images>

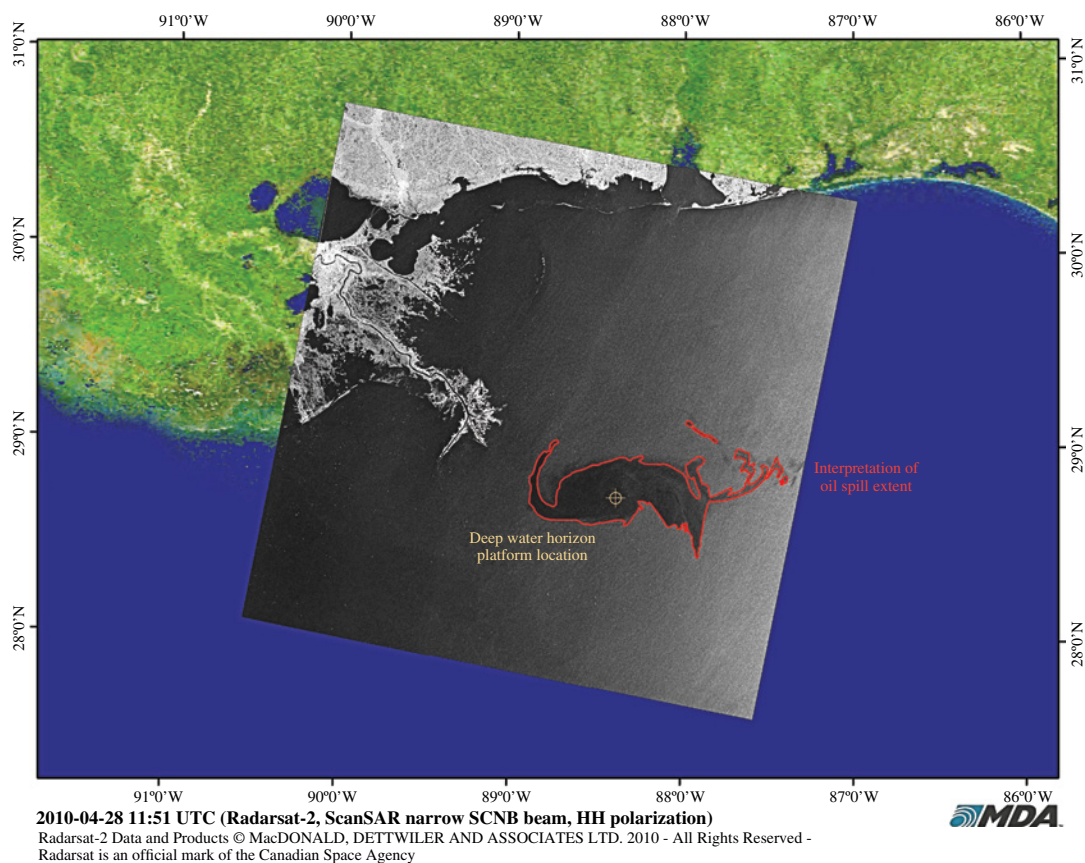


FIGURE 12.52 A Radarsat-2 image of the Gulf oil spill. The spill can be clearly seen and is outlined in gray. Photo from Canadian Space Agency website <http://www.asc-csa.gc.ca/images>



FIGURE 12.53 An Envisat image of the Gulf oil spill. The spill can be clearly seen as can the cliff shadows and calm areas near the shore. Photo from European Space Agency website <http://www.esa.int/esaEO/>

monitored to establish hydrocarbon presence. Tests show that the ion peaks provide sensitivity as low as 0.4 ppb. This is fully sufficient to monitor sunken oil. Tests were conducted in a test tank and later over actual spills in the Gulf of Mexico. The technique was able to find concentrations of sunken oil and place the locations within 1 m. The tests in the Gulf of Mexico were conducted at depths of 200 m and confirmed by using cameras on the submersible.

12.13 SMALL REMOTE-CONTROLLED AIRCRAFT

Several parties have suggested remote-controlled aircraft to provide more economical solutions for response personnel [255–257]. In fact, remote-controlled aircraft have been used by a number of parties for monitoring a variety of pollutants since the 1970s [257].

Belgium employs a UAV of the B-Hunter class to routinely monitor its portion of the North Sea [256]. This is a large Unmanned aerial vehicle (UAV) that has visible and IR camera systems aboard. The unit has a 10 h endurance over the targets.

A variety of commercial platforms are now available that can provide carriage for small sensors such as visible and IR

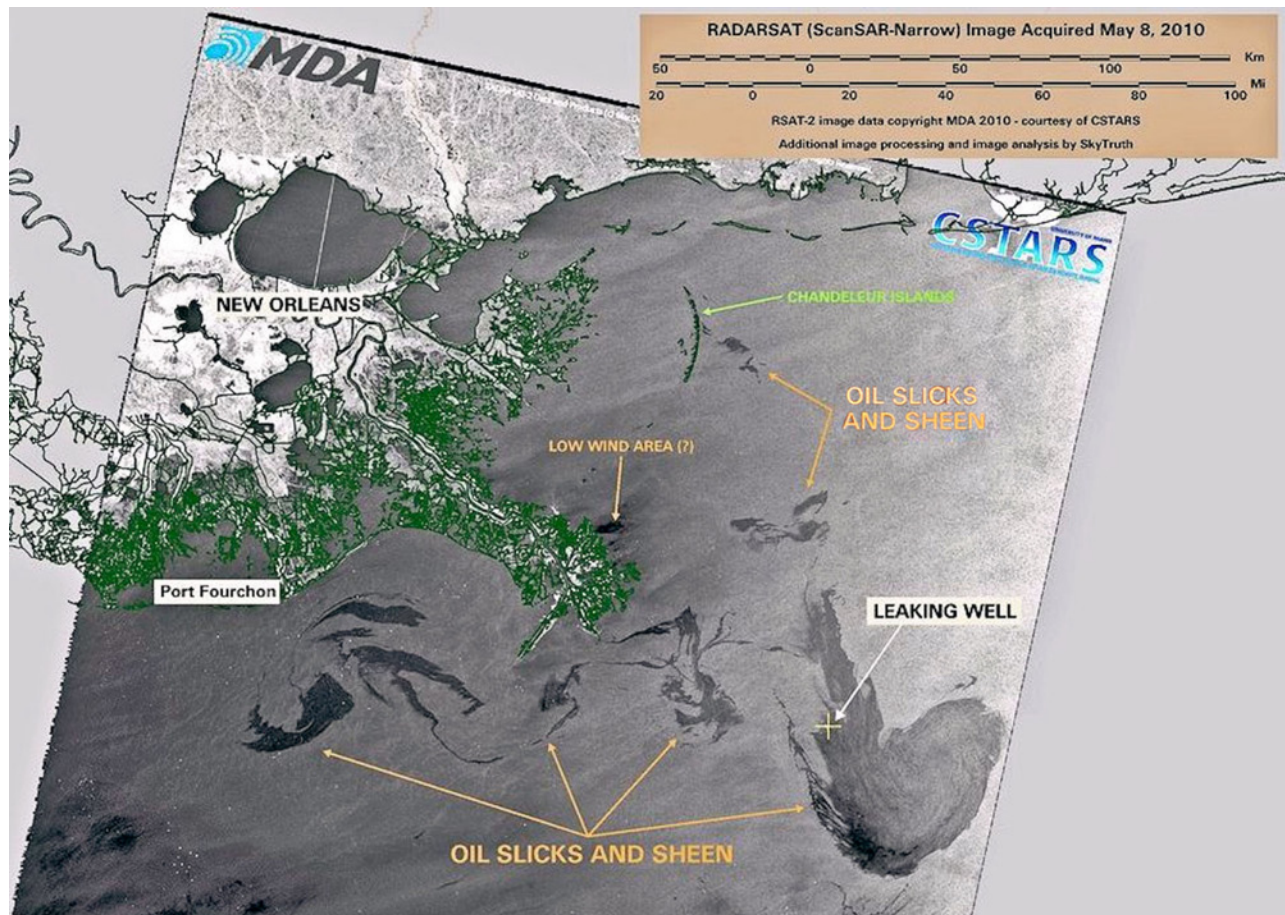


FIGURE 12.54 A Radarsat image of the Gulf oil spill. The annotation on this image provides information on the scenes. The land is imaged by visible satellite. Photo from MDA website <http://sm.mdacorporation.com>

cameras. Further, automatic navigation technology has now made these units, especially helicopters, very much easier to fly than in previous years.

12.14 REAL-TIME DISPLAYS AND PRINTERS

A very important aspect of remote sensing is the production of data so that operations people can quickly and directly use it. Real-time displays are important so that remote sensor

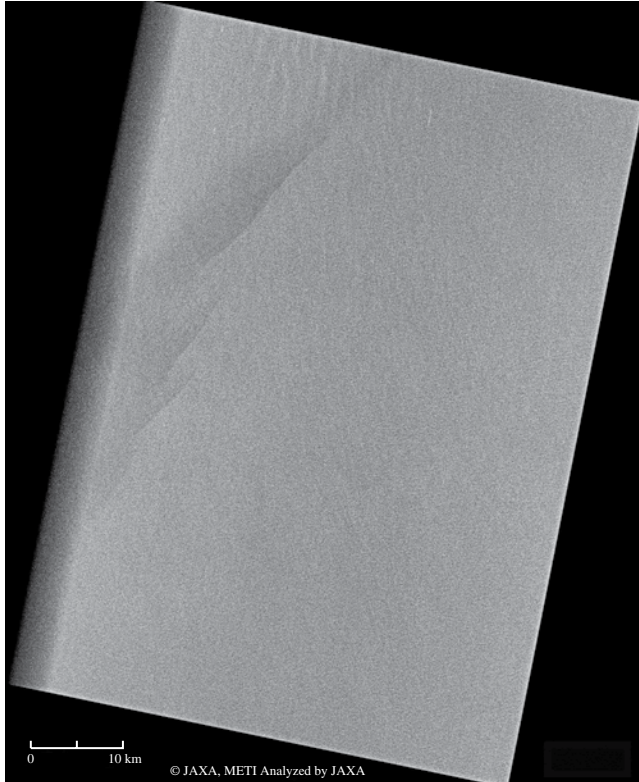


FIGURE 12.55 A PALSAR image of an oil spill (not the Gulf spill). The oil image is rather light because the PALSAR operates in the L-band, which usually results in less contrast for oil spills. Photo from Japan website http://www.eorc.jaxa.jp/ALOS/en/img_up/pal_oil200608.htm

operators can adjust instruments directly in flight and provide information quickly on the location or state of the spill. A major concern of the client is that data be rapidly available [258]. An additional concern is that the data from various sensors be available in a combined or fused form [96]. Further, there is a need to correct this data for aircraft motion and to annotate the data with time and position. At this time, existing hardware and software must be adapted as commercial off-the-shelf equipment for directly outputting and printing sensor data is not yet available. Figure 12.56 shows a typical aircraft used for radar measurements, and Figure 12.57 shows one of the control panels inside the aircraft.

One means to overcome some of these problems is the development of entire packages for oil spill remote sensing. Robbe and Hengstermann describe the MEDUSA system, which consists of an integrated system with IR, UV, SLAR, microwave radiometer, laser fluorosensor, and navigation systems [2].

12.15 ROUTINE SURVEILLANCE

One of the applications of oil spill remote sensing equipment is to detect and map slicks resulting from illegal discharges of oil from ships and offshore platforms. Historically, this has always been performed using visual techniques but in the past decade has increasingly been turned over to aircraft with some instrumentation. Typical instrumentation includes SLAR, IR/UV scanner, and cameras. This sensor package is economical compared to more ideal packages and greatly improves capability beyond just visual observation. Limitations include limited ability to “look into” ship wakes, limited night operations, and inability to positively identify oil slicks. Recent additions such as improved SLAR systems, better display systems, and nighttime cameras have added to the capability, but do not overcome these limitations.

There are many efforts to perform surveillance of illegal discharges. Most existing operative remote systems are dedicated to this function. These systems are estimated to number around 35, most of these around Europe [259,260]. There are intensive programs in some areas, for example, in

TABLE 12.2 Current and future satellite-borne SAR sensors

Satellite	Launch date	Owner/operator	Band	Polarization
ERS-1	1991 (end 2000)	European Space Agency	C	
ERS-2	1995 (end 2011)	European Space Agency	C	VV
Radarsat-1	1995 (end 2013)	Canadian Space Agency	C	HH
Radarsat-2	2007	Canadian Space Agency	C	
Envisat (ASAR)	2002 (end 2012)	European Space Agency	C	HH, VV, Cross pol
ALOS (PALSAR)	2006 (end 2011)	Japan Aerospace Exploration Agency	L	
TerraSAR-X	2007	German Aerospace Centre	X	
Tandem-X	2010	German Aerospace Centre	X	
Cosmos Skymed-1/2	2007, 2010	Italian Space Agency	X	
TecSAR	2008	Israel Aerospace Industries	X	
Kompsat-5	2013	Korean Space Agency	X	
Sentinel-1	2013	European Space Agency	C	
Radarsat-Constellation (3-satellites)	2018	Canadian Space Agency	C	



FIGURE 12.56 A photograph of a remote sensing aircraft. This unit houses twin radars in X and C bands. The main radome is under the rear portion of the aircraft. The antenna on the side is for interferometric radar measurements. Photograph from Environment Canada.



FIGURE 12.57 One of the seven interior control racks in the remote sensing aircraft shown in Figure 12.56. Photograph from Environment Canada.

the North Sea. Carpenter reports on the 18-year program of surveillance in the North Sea [260]. Some interesting statistics are noted. In 2004, 418 unidentified slicks were found, 65 slicks from oil rigs and 57 slicks from ships. In 2004, 3314 h were flown in daylight and 594 in darkness. In the same year, 91 slicks were found in the darkness and 449 in daylight.

Ferraro et al. describe a routine surveillance program using satellite and aircraft data for the Mediterranean Sea [163]. Future work in the Mediterranean Sea proposes a cluster of radar satellites to constantly monitor oil pollution [261].

A word about aircraft is noted here. A variety of aircrafts are deployed as remote sensing aircrafts. Typically different types are deployed for routine surveillance and for remote sensing research. The latter requires flexibility in mounting sensors and in access to the outside of the aircraft. One such airplane is shown in Figure 12.56 with some of the internal controls shown in Figure 12.57.

12.16 FUTURE TRENDS

Advances in sensor technology will continue to drive the use of remote sensors as operational oil spill response tools in the future. Cameras and thermal IR cameras that offer high sensitivity are cheap and plentiful. This improvement reduces not only the size and complexity of the sensor but also the cost. In the next decade, advances in solid-state laser technology, in particular diode-pumped solid-state lasers, will greatly reduce the size and energy consumption of

laser-based remote sensors. This will promote the use of these sensors in smaller, more economical aircraft within the budget of many more regulatory agencies and maritime countries. Rapidly improving computer capabilities will allow for true real-time processing. At the present time and for the foreseeable future, there is no single “Magic Bullet” sensor that will provide all the information required to detect, classify, and quantify oil in the marine and coastal environment. An example of the improvement in recent years is that of the night-vision camera. It is now possible to use this sensor to visualize oil at night under certain circumstances.

It will require the combined advances in sensor technologies and computer capabilities noted earlier to gather, integrate, and merge several sources of data into a real-time format, useable by response crews in the field. If this type of information can be made available to response crews in a short enough time frame following a spill incident, then it can be used to lessen the potentially disastrous effects of a major oil spill on the marine ecosystem.

As technology in remote-controlled systems evolve, it is possible to employ such technology in oil spill remote sensing. First efforts in the deployment of remote-controlled sensing aircraft have posted success and will, no doubt, be expanded in the future [262].

12.17 RECOMMENDATIONS

Recommendations are based on the aforementioned considerations and include economy as a major factor. Tables 12.3 and 12.4 show the considerations related to the development state, cost, and use of the sensor. The laser fluorosensor offers the only potential for discriminating between oiled and unoiled weeds or shoreline and for positively identifying oil pollution on ice, among ice, and in a variety of other situations. This instrument, however, is large and expensive. A cheap sensor recommended for oil spill work is an IR camera. This is the cheapest but indiscriminating device. This is the only piece of equipment that can be purchased off the shelf. All other sensors require special order and, often, development. Radar, although low in priority for purchase, offers the only potential for large-area searches and foul weather remote sensing. Most other sensors are experimental or do not offer good potential for oil detection or mapping. Any sensor package should include a real-time printer and display and a downlink.

In order to respond effectively to major marine oil spills, it is recommended that one employs a combination of airborne and satellite-borne sensor systems. Improvements in the resolution of satellite-based systems, particularly SAR systems, combined with the increased number of such systems and the ability to steer them to image the area of the oil

TABLE 12.3 Attributes for airborne sensor selection

Sensor	State of development	Amount of experience in use	Specific to oil	Immunity to false targets	Typical coverage (km)	Acquisition cost range (\$1000)	Aircraft physical requirements
Still camera	High	High	Poor	Poor	0.25–2	1–5	No
Video	High	High	Poor	Poor	0.25–5	1–10	No
Night time vision camera	Medium	Medium	Poor	Poor	0.25–2	5–20	No
IR camera (8–14 μm)	High	Medium	Medium	Medium	0.25–2	20–50	No
UV camera	Medium	Medium	Poor	Poor	0.25–2	4–20	No
Multi-spectral scanner	Medium	Medium	Poor	Poor	0.25–2	100–200	Yes: minor
Radar	High	High	Medium	Poor	5–50	1200–8000	Yes: dedicated
Microwave radiometer	Medium	Medium	Medium	Medium	1–5	400–1000	Yes: dedicated
Laser fluorosensor	Medium	Limited	Good	Good	0.01–0.1	300–1000	Yes: dedicated

TABLE 12.4 Sensor suitability for various missions

Sensor	Support for cleanup	Night and fog operation	Detection of oil with debris	Oiled shoreline survey	Spill mapping	Ship discharge surveillance	Enforcement and prosecution
Still camera	2	n/a	1	2	2	2	2
Video	2	n/a	1	2	2	2	2
Night time vision camera	3	4	1	n/a	2	2	2
IR camera (8–14 μm)	4	2	1	n/a	3	3	3
UV camera	2	n/a	n/a	n/a	3	2	1
UV/IR scanner	4	2	1	n/a	4	2	2
Multi-spectral scanner	1	n/a	n/a	1	2	1	1
Radar	n/a	4	n/a	n/a	4	3	2
Microwave radiometer	1	3	n/a	n/a	2	2	1
Laser fluorosensor	4	3	5	5	1	5	5

n/a, not applicable.

Numerical values represent a scale from 1 = poorly suited to 5 = ideally suited.

spill will lead to their increased use in a tactical role. Being capable of imaging vast areas of the open ocean will ensure that satellite-borne sensors will also continue to be used in a strategic manner. There are a number of commercially available airborne sensor systems that provide near real-time information on oil slick location and indications of thicker areas of the pollution in an easily interpretable graphical manner. These airborne sensor systems are currently being employed by a large number of maritime nations in conjunction with satellite-based sensor systems.

Prospective buyers should be aware of “new” suppliers. Many oil spill groups have suffered from poor and inoperative equipment. Vendors offering “magic” solutions are abundant. Inevitably such products do not perform as promised, and often, the buyers must return to the marketplace to start over. This scenario recurs too frequently.

There are an increasing number of satellite-borne SAR and optical sensors, some of which currently or soon will operate in constellations to provide increased coverage of the earth’s surface. These enhanced capabilities will allow for the possible use of these sensors in a tactical mode of operation. In spite of these increased capabilities, there remains an essential role for airborne oil spill remote sensing platforms. The ability to collect and deliver real-time oil slick location information will ensure the continued use of airborne systems in spite of their high operational costs.

If this type of real-time oil spill remote sensing information can be made available to response crews in a short enough time frame following a spill incident, the information can be used to mitigate the potentially disastrous effects of a major oil spill on the marine ecosystem.

ACKNOWLEDGMENTS

The authors acknowledge the many parties who contributed to this paper. In particular, they acknowledge Environment Canada for the many photographs in this subsection. Mr. Lloyd Gamble of Environment Canada is acknowledged for gathering some of the references used in this document.

REFERENCES

- [1] NAS, *Oil in the Sea*, National Academy of Sciences, Washington, DC, 2003.
- [2] Robbe, N. and T. Hengstermann, Remote Sensing of Marine Oil Spills from Airborne Platforms Using Multi-Sensor Systems, *Water Pollution VIII: Modelling, Monitoring and Management*, 347, 2006.
- [3] Serra-Sogas, N., P.D. O’Hara, R. Canessa, P. Keller, and R. Pelot, Visualization of Spatial Patterns and Temporal Trends for Aerial Surveillance of Illegal Oil Discharges in Western Canadian Marine Waters, *Mar. Pollut. Bull.*, 56, 815, 2008.
- [4] Fingas, M. and C.E. Brown, Oil Spill Remote Sensing: A Review, in *Oil Spill Science and Technology*, M. Fingas, Editor, Gulf Publishing Company, New York, NY, 111, 2011.
- [5] Fingas, M. and C.E. Brown, Review of Oil Spill Remote Sensing, *Proceedings of the Eighth International Conference on Remote Sensing for Marine and Coastal Environments*, Altarum, Ann Arbor, MI, 2005.
- [6] Hengstermann, T. and N. Robbe, Airborne Oil Spill Remote Sensing, *Hydro International*, 12, 10, 2008.
- [7] Jha, M.N., J. Levy, and Y. Gao, Advances in Remote Sensing for Oil Spill Disaster Management: State-of-the-Art Sensors Technology for Oil Spill Surveillance, *Sensors*, 8, 236, 2008.
- [8] Fingas, M.F., C.E. Brown, and L. Gamble, The Visibility and Detectability of Oil Slicks and Oil Discharges on Water, *AMOP*, Calgary, AB, 865, 1999.
- [9] Brown, C.E. and M.F. Fingas, The Latest Developments in Remote Sensing Technology for Oil Spill Detection, *Interspill*, Marseilles, 2009.
- [10] Krol, T., A. Stelmaszewski, and W. Freda, Variability in the Optical Properties of a Crude Oil-Seawater Emulsion, *Oceanologia*, 48, 203, 2006.
- [11] Evdokimov, I.N. and A.P. Losev, Potential of UV-Visible Absorption Spectroscopy for Characterizing Crude Petroleum Oils, *Oil and Gas Business*, 1, 2007.
- [12] Otremba, Z., J. Piskozub, and T. Król, Modelling the Reflectance of Sea Areas Polluted with Oil Emulsion, *Fresen. Environ. Bull.*, 12, 1109, 2003.
- [13] Otremba, Z. and J. Piskozub, Modelling of the Optical Contrast of an Oil Film on a Sea Surface, *Opt. Express*, 9, 411, 2001.
- [14] Otremba, Z. and J. Piskozub, The Modification of Light Flux Leaving a Wind-Roughened, Oil Covered Sea Surface: Example of Computations for Shallow Seas, *Ocean. Studies*, 29, 117, 2000.
- [15] Hong, S. and I. Shin, *Nighttime Detection of Oil Spills on the Sea Surface Using Spaceborne Infrared Images*, Korea Meteorological Administration, 2010.
- [16] Wettle, M., P.J. Daniel, G.A. Logan, and M. Thankappan, Assessing the Effect of Hydrocarbon Type and Thickness on a Remote Sensing Signal: A Sensitivity Study Based on the Optical Properties of Two Different Oil Types and the HYMAP and Quickbird Sensors, *Remote Sens. Environ.*, 113, 2000, 2009.
- [17] Ma, L., Y. Li, and Y. Liu, Oil Spill Monitoring Based on Its Spectral Characteristics, *Environ. Forensics*, 10, 317, 2009.
- [18] Lammoglia, T. and C.R. de Souza Filho, Spectroscopic Characterization of Oils Yielded from Brazilian Offshore Basins: Potential Applications of Remote Sensing, *Remote Sens. Environ.*, 115, 2525, 2011.
- [19] O’Neil, R.A., R.A. Neville, and V. Thompson, *The Arctic Marine Oilspill Program (AMOP) Remote Sensing Study*, Environment Canada Report EPS 4-EC-83-3, 1983.
- [20] Brown, H.M., J.P. Bittner, and R.H. Goodman, The Limits of Visibility of Spilled Oil Sheens, *Proceedings of the Second Thematic International Airborne Remote Sensing Conference and Exhibition*, ERIM, San Francisco, III 327, 1996.
- [21] Taylor, S., *0.45 to 1.1 μ m Spectra of Prudhoe Crude Oil and of Beach Materials in Prince William Sound, Alaska*, CRREL Special Report No. 92-5, 1992.
- [22] Huang, M., Y. Yu, Y. Zhang, J. Shen, and X. Qi, Analysis of Water Spectral Features of Petroleum Pollution and Estimate Models from Remote Sensing Data, *SPIE*, 712312, 2008.

- [23] Ahmed, S., A. Gilerson, M. Oo, J. Zhou, J. Chowhardy, et al., The Polarization Properties of Reflectance from Coastal Waters and the Ocean-Atmosphere System, *SPIE*, 636003, 2006.
- [24] Carnesecchi, F., V. Byfield, P. Cipollini, G. Corsini, and M. Diani, An Optical Model for the Interpretation of Remotely Sensed Multispectral Images of Oil, *SPIE*, 710504, 2008.
- [25] Zhang, L., B. Zhang, Z. Chen, L. Zheng, and Q. Tong, The Application of Hyperspectral Remote Sensing to Coast Environment Investigation, *Acta Oceanol. Sin.*, 28, 1, 2009.
- [26] Bianchi, R., R.M. Cavalli, C.M. Marino, S. Pignatti, and M. Poscolieri, Use of Airborne Hyperspectral Images to Assess the Spatial Distribution of Oil Spilled during the Trecate Blow-Out (Northern Italy), *SPIE*, 352, 1995.
- [27] Zhan, Y., T. Mao, F. Gong, D. Wang, and J. Chen, An Oil Film Information Retrieval Method Overcoming the Influence of Sun Glitter – Based on AISA+ Airborne Hyperspectral Image, *SPIE*, 7825, 2010.
- [28] Bagheri, S., M. Stein, and C. Zetlin, Utility of Airborne Videography as an Oil Spill-Response Monitoring System, in *Encyclopedia of Environmental Control Technology*, Paul N. Cheremisinoff, Editor, Gulf Publishing Company, Houston, TX, 367, 1995.
- [29] Brown, C.E., M.F. Fingas, and R. Marois, Oil Spill Remote Sensing: Laser Fluorosensor Demonstration Flights off the East Coast of Canada, *AMOP*, Edmonton, 317, 2004.
- [30] Brown, C.E., M.F. Fingas, and R. Marois, Oil Spill Remote Sensing Flights in the Coastal Waters Around Newfoundland, *Proceedings of the Eighth International Conference on Remote Sensing for Marine and Coastal Environments*, Altarum, Ann Arbor, MI, 2005.
- [31] Palmer, D., G.A. Borstad, and S.R. Boxall, Airborne Multi Spectral Remote Sensing of the January 1993 Shetlands Oil Spill, *Proceedings of the Second Thematic Conference on Remote Sensing for Marine and Coastal Environments: Needs, Solutions and Applications*, ERIM, Stasbourg, FR, II-546, 1994.
- [32] Wadsworth, A., W.J. Looyen, R. Reuter, and M. Petit, Aircraft Experiments with Visible and Infrared Sensors, *Int. J. Remote Sens.*, 13, 1175, 1992.
- [33] Wang, D., F. Gong, D. Pan, Z. Hao, and Q. Zhu, Introduction to the Airborne Marine Surveillance Platform and Its Application to Water Quality Monitoring in China, *Acta Oceanol. Sin.*, 29, 33, 2010.
- [34] Locke, C., M. White, J. Michel, C. Henry, J.D. Sellars, and M.L. Aslaksen, Use of Vertical Digital Photography at the Bayou Perot, LA, Spill for Oil Mapping and Volume Estimation, *IOSC*, Savannah, GA, 127, 2008.
- [35] Stelmaszewski, A., T. Krol, and H. Toczek, Light Scattering in Baltic Crude Oil—Seawater Emulsion, *Oceanologia*, 51, 405, 2009.
- [36] Pinel, N. and C. Bourlier, Unpolarized Infrared Emissivity of Oil Films on Sea Surfaces, *IGARSS*, Cape Town, SA, 2009.
- [37] Hurford, N., Review of Remote Sensing Technology, in *The Remote Sensing of Oil Slicks*, A.E. Lodge, Editor, John Wiley & Sons, New York, NY, 7, 1989.
- [38] Goodman, R.H., Application of the Technology in North America, in *The Remote Sensing of Oil Slicks*, A.E. Lodge, Editor, John Wiley & Sons, New York, NY, 39, 1989.
- [39] Belore, R.C., A Device for Measuring Oil Slick Thickness, *Spill Technol. Newsl.*, 7, 44, 1982.
- [40] Neville, R.A., V. Thompson, K. Dagg, and R.A. O'Neil, An Analysis of Multispectral Line Scanner Imagery from Two Test Spills, *Proceedings of First Workshop Sponsored by Working Group I of the Pilot Study on the Use of Remote Sensing for the Control of Marine Pollution*, NATO Challenges of Modern Society, Brussels, BE, 201, 1979.
- [41] Bolus, R.L., Airborne Testing of a Suite of Remote Sensors for Oil Spill Detecting on Water, *Proceedings of the Second Thematic International Airborne Remote Sensing Conference and Exhibition*, ERIM, San Francisco, III 743, 1996.
- [42] Salisbury, J.W., D.M. D'Aria, and F.F. Sabins, Thermal Infrared Remote Sensing of Crude Oil Slicks, *Remote Sens. Environ.*, 45, 225, 1993.
- [43] Hover, G.L., Testing of Infrared Sensors for U.S. Coast Guard Oil Spill Response Applications, *Proceedings of the Second Thematic Conference on Remote Sensing for Marine and Coastal Environments: Needs, Solutions and Applications*, ERIM, Strasbourg, FR, I-47, 1994.
- [44] Grierson, I.T., Use of Airborne Thermal Imagery to Detect and Monitor Inshore Oil Spill Residues During Darkness Hours, *Environ. Manag.*, 22, 905, 1998.
- [45] Shih, W-C. and A.B. Andrews, Infrared Contrast of Crude-Oil-Covered Water Surfaces, *Opt. Lett.*, 33, 3019, 2008.
- [46] Brown, H.M., J.J. Baschuk, and R.H. Goodman, The Limits of Visibility of Spilled Oil Sheens, *AMOP*, Edmonton, 805, 1998.
- [47] Clark, R.N., G.A. Swayze, I. Leifer, K.E. Livo, S. Lundeem, et al., *A Method for Qualitative Mapping of Thick Oil Using Imaging Spectroscopy*, United States Geological Survey, Denver, CO, 2010, <http://pubs.usgs.gov/of/2010/1101/> (accessed August 15, 2010).
- [48] Leifer, I., R. Clark, G. Swayse, D. Roberts, R. Kokaly, et al., *Imaging Spectroscopy of the Deepwater Horizon Spill: A 21st Century Oil Spill Response*, NOAA Report, Seattle, WA, 2011.
- [49] Goodman, R.H., *Simple Remote Sensing System for the Detection of Oil on Water*, Environmental Studies Research Fund Report No. 98, 1988.
- [50] Yin, D., X. Huang, W. Qian, X. Huang, Y. Li, and Q. Feng, Airborne Validation of a New-Style Ultraviolet Push-Broom Camera for Ocean Oil Spill Pollution Surveillance, *SPIE*, 7825, 2010.
- [51] Brown, C.E., Laser Fluorosensors, in *Oil Spill Science and Technology*, M. Fingas, Editor, Gulf Publishing Company, New York, NY, 171–184, 2011.
- [52] Brown, C.E., M.F. Fingas, and J. An, Laser Fluorosensors: A Survey of Applications and Developments of a Versatile Sensor, *AMOP*, Edmonton, 485, 2001.
- [53] Brown, C.E., R. Nelson, M.F. Fingas, and J.V. Mullin, Airborne Laser Fluorosensing: Overflights during Lift Operations of a Sunken Oil Barge, *Proceedings of the Fourth Thematic Conference on Remote Sensing for Marine and Coastal Environments*, ERIM, Copenhagen, I 23, 1997.
- [54] Brown, C.E., R. Marois, M.F. Fingas, M. Choquet, J-P. Monchalain, et al., Airborne Oil Spill Sensor Testing: Progress and Recent Developments, *IOSC*, Tampa, FL, 917, 2001.

- [55] Brown, C.E. and M.F. Fingas, Review of the Development of Laser Fluorosensors for Oil Spill Application, *Mar. Pollut. Bull.*, 47, 477, 2003.
- [56] Hengsternann, T. and R. Reuter, Lidar Fluorosensing of Mineral Oil Spills on the Sea Surface, *Appl. Opt.*, 29, 3218, 1990.
- [57] Balick, L., J.A. DiBenedetto, and S.S. Lutz, Fluorescence Emission Spectral Measurements for the Detection of Oil on Shore, *Proceedings of the Fourth Thematic Conference on Remote Sensing for Marine and Coastal Environments*, ERIM, Copenhagen, I 13, 1997.
- [58] Sarma, A.K. and A.G. Ryder, Comparison of the Fluorescence Behaviour of a Biocrude Oil and Crude Petroleum Oils, *Energy Fuels*, 20, 783, 2006.
- [59] Samberg, A., The State-of-the-Art of Airborne Laser Systems for Oil Mapping, *Can. J. Remote Sens.*, 33, 143, 2007.
- [60] Jha, M.N. and Y. Gao, Oil Spill Contingency Planning Using Laser Fluorosensors and Web-Based GIS, *Proceedings Oceans Marine Technology Society*, 2008.
- [61] Diebel, D., T. Hengsternann, R. Reuter, and R. Willkomm, Laser Fluorosensing of Mineral Oil Spirits, in *The Remote Sensing of Oil Slicks*, A.E. Lodge, Editor, John Wiley & Sons, New York, NY, 127, 1989.
- [62] Geraci, A.L., F. Landolina, L. Pantani, and G. Cecchi, Laser and Infrared Techniques for Water Pollution Control, *IOSC*, Tampa, FL, 525, 1993.
- [63] Vasilescu, J., L. Marmureanu, E. Carstea, and C.P. Cristescu, Oil Spills Detection from Fluorescence Lidar Measurements, *U.P.B. Sci. Bull.*, 72, 149, 2010.
- [64] Hoge, F.E. and R.N. Swift, Oil Film Thickness Measurement Using Airborne Laser-Induced Water Raman Backscatter, *Appl. Opt.*, 19, 3269, 1980.
- [65] Piskozub, J., V. Drozdowska, and V. Varlamov, A Lidar System for Remote Measurement of Oil Film Thickness on Sea Surface, *Proceedings of the Fourth Thematic Conference on Remote Sensing for Marine and Coastal Environments*, ERIM, Copenhagen, I-386, 1997.
- [66] Goodman, R. and C.E. Brown, Oil Detection Limits for a Number of Remote Sensing Systems, *Proceedings of the Eighth International Conference on Remote Sensing for Marine and Coastal Environments*, Alterum, Ann Arbor, MI, 2005.
- [67] Dick, R., M. Fruhwirth, and C. Brown, Laser Fluorosensor Work in Canada, *Proceedings of the First Thematic Conference on Remote Sensing for Marine and Coastal Environments*, ERIM, New Orleans, LA, 223, 1992.
- [68] James, R.T.B. and R. Dick, Design of Algorithms for the Real-Time Airborne Detection of Littoral Oil-Spills by Laser-Induced Fluorescence, *AMOP*, Calgary, AB, 1599, 1996.
- [69] Brown, C.E., M.F. Fingas, R.L. Gamble, and G.E. Myslicki, The Remote Detection of Submerged Oil, *Proceedings of the Third R&D Forum on High-Density Oil Spill Response*, IMO, Brest, FR, 46–54, 2002.
- [70] Brown, C.E., R. Marois, G. Myslicki, and M.F. Fingas, Initial Studies on the Remote Detection of Submerged Oil-mulsion with a Range-Gated Laser Fluorosensor, *AMOP*, Calgary, AB, 773, 2002.
- [71] Brown, C.E., R. Marois, G. Myslicki, M.F. Fingas, and R. MacKay, Remote Detection of Submerged Oil-mulsion with a Range-Gated Laser Fluorosensor, *IOSC*, Vancouver, BC, 779, 2003.
- [72] Brown, C.E., R. Marois, R.L. Gamble, and M.F. Fingas, Further Studies on the Remote Detection of Submerged Oil-mulsion with a Range-Gated Laser Fluorosensor, *AMOP*, Victoria, BC, 279, 2003.
- [73] Brown, C.E., M. Fingas, R. Marois, B. Fieldhouse, and R.L. Gamble, Remote Sensing of Water-in-Oil Emulsions: Initial Laser Fluorosensor Studies, *AMOP*, Edmonton, 295, 2004.
- [74] Ulaby, F.T., R.K. Moore, and A.K. Fung, *Microwave Remote Sensing: Active and Passive*, Artech House, Dedham, MA, 1466, 1989.
- [75] Goodman, R.H., Remote Sensing Resolution and Oil Slick Inhomogeneities, *Proceedings of the Second Thematic Conference on Remote Sensing for Marine and Coastal Environments: Needs, Solutions and Applications*, ERIM, Strasbourg, FR, I-1-17, 1994.
- [76] Fäst, O., Remote Sensing of Oil on Water—Air and Space-Borne Systems, *Proceedings of the DOOS Seminar*, Trondheim, NO, 1986.
- [77] Skou, N., B.M. Sorensen, and A. Poulson, A New Airborne Dual Frequency Microwave Radiometer for Mapping and Quantifying Mineral Oil on the Sea Surface, *Proceedings of the Second Thematic Conference on Remote Sensing for Marine and Coastal Environments*, ERIM, Strasbourg, FR, 1994.
- [78] Mussetto, M.S., L. Yujiri, D.P. Dixon, B.I. Hauss, and C.D. Eberhard, Passive Millimeter Wave Radiometric Sensing of Oil Spills, *Proceedings of the Second Thematic Conference on Remote Sensing for Marine and Coastal Environments: Needs, Solutions and Applications*, ERIM, Strasbourg, FR, I-35, 1994.
- [79] Zhifu, S. and W. Wiesbeck, A Study of Passive Microwave Remote Sensing, *Proceedings of the 1988 International Geoscience and Remote Sensing Symposium*, Edinburgh, UK, 1091, 1988.
- [80] Süß, H., K. Grüner, and W.J. Wilson, Passive Millimeter Wave Imaging: A Tool for Remote Sensing, *Alta Frequenza*, 58, 457, 1989.
- [81] Pelyushenko, S.A., Microwave Radiometer System for the Detection of Oil Slicks, *Spill Sci. Technol. Bull.*, 2, 249, 1995.
- [82] Pelyushenko, S.A., The Use of Microwave Radiometer Scanning System for Detecting and Identification of Oil Spills, *Proceedings of the Fourth Thematic Conference on Remote Sensing for Marine and Coastal Environments*, ERIM, Copenhagen, I-381, 1997.
- [83] McMahon, O.B., E.R. Brown, G.D. Daniels, T.J. Murphy, and G.L. Hover, Oil Thickness Detection Using Wideband Radiometry, *IOSC*, Long Beach, CA, 15, 1995.
- [84] McMahon, O.B., T.J. Murphy, and E.R. Brown, Remote Measurement of Oil Spill Thickness, *Proceedings of the Fourth Thematic Conference on Remote Sensing for Marine and Coastal Environments*, ERIM, Copenhagen, I-353, 1997.
- [85] Nunziata, F., M. Migliaccio, and P. Sobieski, A BPM Two-scale Contrast Model, *IGARSS*, Boston, IV-593, 2008.
- [86] Frysinger, G.S., W.E. Asher, G.M. Korenowski, W.R. Barger, M.A. Klusty, et al., Study of Ocean Slicks by Nonlinear Laser Processes in Second-Harmonic Generation, *J. Geophys. Res.*, 97, 5253, 1992.
- [87] Alpers, W. and H. Hühnerfuss, Radar Signatures of Oil Films Floating on the Sea Surface, *IGARSS*, Ann Arbor, 741, 1987.

- [88] Poitevin, J. and C. Khaif, A Numerical Study of the Backscattered Radar Power in Presence of Oil Slicks on the Sea Surface, *Proceedings of the First Thematic Conference on Remote Sensing for Marine and Coastal Environments*, ERIM, Ann Arbor, 171, 1992.
- [89] Hühnerfuss, H., W. Alpers, and F. Witte, Layers of Different Thicknesses in Mineral Oil Spills Detected by Grey Level Textures of Real Aperture Radar Images, *Int. J. Remote Sens.*, 10, 1093, 1989.
- [90] Gens, R., Oceanographic Applications of SAR Remote Sensing, *GISci. Remote Sens.*, 45, 275, 2008.
- [91] Cheng, Y., X. Li, Q. Xu, O. Garcia-Pineda, O.B. Anderson, and W.C. Pichel, SAR Observation and Model Tracking of an Oil Spill Event in Coastal Waters, *Mar. Pollut. Bull.*, 62, 350, 2011.
- [92] Liu, P., C. Zhao, X. Li, M. He, and W. Pichel, Identification of Ocean Oil Spills in SAR Imagery Based on Fuzzy Logic Algorithm, *Int. J. Remote Sens.*, 31, 4819, 2010.
- [93] Bartsch, N., K. Grüner, W. Keydel, and F. Witte, Contribution to Oil Spill Detection and Analysis with Radar and Microwave Radiometer: Results of the Archimedes II Campaign, *IEEE Trans. Geosci. Remote Sens.*, 25, 677, 1987.
- [94] Mastin, G.A., J.J. Mason, J.D. Bradley, R.M. Axline, and G.L. Hover, A Comparative Evaluation of SAR and SLAR, *Proceedings of the Second Thematic Conference on Remote Sensing for Marine and Coastal Environments: Needs, Solutions and Applications*, ERIM, Strasbourg, FR, I-7, 1994.
- [95] Brown, C.E. and M.F. Fingas, Synthetic Aperture Radar Sensors: Viable for Marine Oil Spill Response? *AMOP*, Victoria, BC, 299, 2003.
- [96] Zielinski, O. and N. Robbe, Past and Future of Airborne Pollution Control, *Interspill*, Trondheim, NO, 2004.
- [97] Dyring, A. and O. Fäst, MSS Puts the Aircraft in the Oil Spill Tracking Network, *Interspill*, Trondheim, NO, 2004.
- [98] Intera Technologies, *Radar Surveillance in Support of the 1983 COATTF Oil Spill Trials*, Environment Canada Report EE-51, 1984.
- [99] C-CORE (Centre for Cold Ocean Resources Engineering), *Microwave Systems for Detecting Oil Slicks in Ice-Infested Waters: Phase I—Literature Review and Feasibility Study*, Environment Canada Report EPS 3-EC-81-3, 1981.
- [100] Yang, C-S., Y-S. Kim, K. Ouchi, and J-H. Na, Comparison with L-, C-, and X-Band Real SAR Images and Simulation SAR Images of Spilled Oil on Sea Surface, *IGARSS*, Cape Town, SA, 673, 2009.
- [101] Kim, D-J., W.M. Moon, and Y-S. Kim, Application of TerraSAR-X for Emergent Oil-Spill Monitoring, *IEEE Trans. Geosci. Remote Sens.*, 48, 852, 2010.
- [102] Macklin, J.T., The Imaging of Oil Slicks by Synthetic Aperture Radar, *GEC J. Res.*, 10, 19, 1992.
- [103] Kozu, T., T. Umehara, T. Ojima, T. Suitsu, H. Masuyko, and H. Inomata, Observation of Oil Slicks on the Ocean by X-Band SLAR, *IGARSS*, Ann Arbor, 735, 1987.
- [104] Madsen, S., N. Skou, and B.M. Sorensen, Comparison of VV and HH Polarized SLAR for Detection of Oil on the Sea Surface, *Proceedings of the Second Thematic Conference on Remote Sensing for Marine and Coastal Environments: Needs, Solutions and Applications*, ERIM, Strasbourg, FR, I-498, 1994.
- [105] Migliaccio, M., A. Gambardella, and A. Tranfaglia, SAR Polarimetry to Observe Oil Spills, *IEEE Trans. Geosci. Remote Sens.*, 45, 506, 2007.
- [106] Migliaccio, M., F. Nunziata, and A. Gambardella, On the Co-Polarized Phase Difference for Oil Spill Observation, *Int. J. Remote Sens.*, 30, 1587, 2009.
- [107] Gambardella, A., M. Migliaccio, and G. De Grandi, Wavelet Polarimetric SAR Signature Analysis of Sea Oil Spills and Look-Alike Features, *IGARSS*, Barcelona, 983, 2007.
- [108] Nunziata, F., A. Gambardella, and M. Migliaccio, On the Use of Dual-Polarized SAR Data for Oil Spill Observation, *IGARSS*, Boston, II-225, 2008.
- [109] Anderson, S., R. Uiboupin, S. Verjovkina, and U. Raudsepp, Sar Imagery and Seatrack Web as Decision Making Tools for Illegal Oil Spill Combating—A Case Study, *2010 IEEE/OES US/EU Baltic International Symposium*, Riga, Latvia, 2010.
- [110] Kuzmanic, I. and I. Vujovic, Oil Spill Detection in SAR Images Using Wavelets and Morphology, *ELMAR 2010 Proceedings*, Zadar, Croatia, 337, 2010.
- [111] Wang, W., F. Lu, P. Wu, and J. Wang, Oil Spill from Polarimetric SAR Image, *ICSP Proceedings*, Beijing, China, 832, 2010.
- [112] Velotto, D., M. Migliaccio, F. Nunziata, and S. Lehner, Oil-Slick Observation Using Single Look Complex Terrasar-X Dual Polarized Data, *IGARSS*, Honolulu, HA, 3684, 2010.
- [113] Hühnerfuss, H., W. Alpers, H. Dannhauer, M. Gade, P.A. Lange, et al., Natural and Man-made Sea Slicks in the North Sea Investigated by a Helicopter-borne 5-frequency Radar Scatterometer, *Int. J. Remote Sens.*, 17, 1567, 1996.
- [114] Hielm, J.H., NIFO Comparative Trials, in *The Remote Sensing of Oil Slicks*, A.E. Lodge, Editor, John Wiley & Sons, New York, NY, 67, 1989.
- [115] Marghany, M., A.P. Cracknell, and M. Hasim, Modification of Fractal Algorithm for Oil Spill Detection from RADARSAT-1 SAR Data, *Int. J. Appl. Earth Obs. Geoinf.*, 11, 96, 2009.
- [116] Akar, S., M.L. Suezzen, and N. Kaymakci, Detection and Object-Based Classification of Offshore Oil Slicks Using ENVISAT-ASAR Images, *Environ. Monit. Assess.*, 183, 1926, 2011.
- [117] Gade, M., W. Alpers, H. Huehnerfuss, and V. Wismann, Radar Signatures of Different Oceanic Surface Films Measured during the SIR-C-X-SAR Missions in Remote Sensing, *16th Symposium of the European Association of Remote Sensing Laboratories (EARSEL)*, Rotterdam, 233–240, 1996.
- [118] Okamoto, K., T. Kobayashi, H. Masuko, S. Ochiai, H. Horie, et al., Results of Experiments Using Synthetic Aperture Radar Onboard the European Remote Sensing Satellite 1–4. Artificial Oil Pollution Detection, *J. Commun. Res. Lab.*, 43, 327, 1996.
- [119] Nøst, E. and C.N. Egset, Oil Spill Detection System—Results from Field Trials, *Proceedings Oceans Marine Technology Society*, Boston, MA, 2006.
- [120] Gangeskar, R., Automatic Oil-Spill Detection by Marine X-Band Radars, *Sea Technol.*, 40, 2004.
- [121] Forget, P. and P. Brochu, Slicks, Waves and Fronts Observed in Sea Coastal Area by an X-band Airborne Synthetic Aperture Radar, *Remote Sens. Environ.*, 57, 1, 1996.

- [122] Abascal, A.J., S. Castanedo, R. Medina, I.J. Losada, and E. Alvarez-Fanjul, Application of HF Radar Currents to Oil Spill Modelling, *Mar. Pollut. Bull.*, 58, 238, 2009.
- [123] Marmorino, G.O., D.R. Thompson, H.C. Graber, and C.L. Trump, Correlation of Oceanographic Signatures Appearing in Synthetic Aperture Radar and Interferometric Synthetic Aperture Radar Imagery with in-situ Measurements, *J. Geophys. Res.*, 102, 723, 1997.
- [124] Topouzelis, K., V. Karathanassi, P. Pavlakis, and D. Rokos, Potentiality of Feed-Forward Neural Networks for Classifying Dark Formation to Oil Spills and Look-Alikes, *Geocarto Int.*, 24, 179, 2009.
- [125] Anderson, S., U. Raudsepp, and R. Uiboupin, Oil Spill Statistics from SAR Images in the North Eastern Baltic Sea Ship Route in 2007–2009, *IGARSS*, Honolulu, HA, 1883, 2010.
- [126] Solberg, R. and N. Theophilopoulos, ENVISYS—A Solution for Automatic Oil Spill Detection in the Mediterranean, *Proceedings of the Fourth Thematic Conference on Remote Sensing for Marine and Coastal Environments*, ERIM, Copenhagen, I-3, 1997.
- [127] Ferraro, G., B. Baschek, G. de Montpellier, O. Njoten, M. Perkovic, and M. Vespe, On the SAR Derived Alert in the Detection of Oil Spills According to the Analysis of the EGEMP, *Mar. Pollut. Bull.*, 60, 91–102, 2010.
- [128] Wahl, T., K. Eldhuset, and Å. Skøelv, Ship Traffic Monitoring and Oil Spill Detection Using ERS-1, *Proceedings of the International Symposium "Operationalization of Remote Sensing"*, Enschede, The Netherlands, ITC, 97, 1993.
- [129] Bern, T.-I., T. Wahl, T. Anderssen, and R. Olsen, Oil Spill Detection Using Satellite Based SAR: Experience from a Field Experiment, *Photogramm. Eng. Remote Sens.*, 59, 423, 1993.
- [130] Yan, X.-H. and P. Clemente-Colon, The Maximum Similarity Share Matching (MSSM) Method Applied to Oil Spill Feature Tracking Observed in SAR Imagery, *Proceedings of the Fourth Thematic Conference on Remote Sensing for Marine and Coastal Environments*, ERIM, Copenhagen, I-43, 1997.
- [131] Bentz, C.M., A.T. Politano, and N.F.F. Ebecken, Automatic Recognition of Coastal and Oceanic Environmental Events with Orbital Radars, *IGARSS*, Barcelona, 914, 2007.
- [132] Trivero, P., W. Biamino, and F. Nirchio, High Resolution COSMO-SkyMed SAR Images for Oil Spills Automatic Detection, *IGARSS*, Barcelona, 2, 2007.
- [133] Tian, W., Y. Shao, and S. Wang, A System for Automatic Identification of Oil Spill in ENVISAT ASAR, *IGARSS*, Boston, MA, III-1394, 2008.
- [134] Shao, Y., W. Tian, S. Wang, and F. Zhang, Oil Spill Monitoring Using Multi-Temporal SAR and Microwave Scatterometer Data, *IGARSS*, Boston, MA, III-1378, 2008.
- [135] Rodriguez, M.H., K. Bannerman, R.G. Caceres, F. Pellon de Miranda, and E.C. Pedroso, Cantarell Natural Seep Modelling Using SAR Derived Ocean Surface Wind and Meteorological Oceanographic Buoy Data, *IGARSS*, Barcelona, 3257, 2007.
- [136] Robson, M., J. Secker, and P.W. Vachon, Evaluation of eCognition for Assisted Target Detection and Recognition in SAR Imagery, *IGARSS*, Denver, CO, 145, 2006.
- [137] Garcia-Pineda, O., I. MacDonald, and B. Zimmer, Synthetic Aperture Radar Image Processing Using the Supervised Textural-neural Network Classification Algorithms, *IGARSS*, Boston, IV-1265, 2008.
- [138] Morales, D.J., M. Moctezuma, and F. Parmiggiani, Detection of Oil Slicks in SAR Images Using Hierarchical MRF, *IGARSS*, Boston, III-1390, 2008.
- [139] Bertacca, M., A FEXP Model Short Range Dependence Analysis for Improving Oil Slicks and Low-wind Areas Discrimination in SAR Imagery, *IGARSS*, Denver, CO, 959, 2006.
- [140] Topouzelis, K.N., Oil Spill Detection by SAR Images: Dark Formation Detection, Feature Extraction and Classification Algorithms, *Sensors*, 8, 6642, 2008.
- [141] Topouzelis, K., V. Karathanassi, P. Pavlakis, and D. Rokos, Dark Formation Detection Using Neural Networks, *Int. J. Remote Sens.*, 29, 4705, 2008.
- [142] Topouzelis, K., D. Stathakis, and V. Karathanassi, Investigation of Genetic Contribution to Feature Selection for Oil Spill Detection, *Int. J. Remote Sens.*, 30, 179, 2009.
- [143] Karathanassi, V., K. Topouzelis, P. Pavlakis, and D. Rokos, An Object-Oriented Methodology to Detect Oil Spills, *Int. J. Remote Sens.*, 27, 5235, 2006.
- [144] Topouzelis, K., V. Karathanassi, P. Pavlakis, and D. Rokos, Detection and Discrimination between Oil Spills and Look-Alike Phenomena through Neural Networks, *ISPRS J. Photogramm. Remote Sens.*, 62, 264, 2007.
- [145] Karantzalos, K. and D. Argialas, Automatic Detection and Tracking of Oil Spills in SAR Imagery with Level Set Segmentation, *IGARSS*, Boston, MA, 6281, 2008.
- [146] Tahvonen, K. and T. Pyhälä, The Use of Environmental Data in Reliability: Assessment of Oil Spill Detection by SAR Imagery, *IGARSS*, 3671, 2006.
- [147] Karvonen, J., I. Heiler, M. Similä, and K. Tahvonen, Oil Spill Detection with RADARSAT-1 in the Baltic Sea, *IGARSS*, Denver, CO, 4075, 2006.
- [148] Shi, L., A.Y. Ivanov, M. He, and C. Zhao, Oil Spill Mapping in the Western Part of the East China Sea Using Synthetic Aperture Radar Imagery, *Int. J. Remote Sens.*, 29, 6315, 2008.
- [149] Muellenhoff, O., B. Bulgarelli, G. Ferraro, and K. Topouzelis, The Use of Ancillary Metocean Data for the Oil Spill Probability Assessment in SAR Images, *Fresen. Environ. Bull.*, 17, 1382, 2008.
- [150] Muellenhoff, O., B. Bulgarelli, G. Ferraro, M. Perkovic, K. Topouzelis, and V. Sammarini, Geospatial Modelling of Metocean and Environmental Ancillary Data for the Oil Probability Assessment in SAR Images, *SPIE*, 71100R, 2008.
- [151] Assilzadeh, H. and Y. Gao, Oil Spill Emergency Response Mapping for Coastal Area Using SAR Imagery and GIS, *Proceedings Oceans Marine Technology Society*, Quebec City, Quebec, 2008.
- [152] Migliaccio, M., A Physical Approach for the Observation of Oil Spills in SAR Images, *IEEE J. Ocean. Eng.*, 30, 496, 2005.
- [153] Shu, Y., J. Li, H. Yousef, and G. Gomes, Dark-Spot Detection from SAR Intensity Imagery with Spatial Density Thresholding for Oil-Spill Monitoring, *Remote Sens. Environ.*, 114, 2026, 2010.
- [154] Migliaccio, M., G. Ferrara, A. Gambardella, F. Nunziata, and A. Sorrentino, A Physically Consistent Stochastic

- Model to Observe Oil Spills and Strong Scatterers on SLC SAR Images, *IGARSS*, Barcelona, 1322, 2007.
- [155] Gambardella, A., G. Giacinto, and M. Migliaccio, On the Mathematical Formulation of the SAR Oil-Spill Observation Problem, *IGARSS*, Boston, MA, III-1382, 2008.
- [156] Marghany, M., A.P. Cracknell, and M. Hasim, Comparison between RADARSAT-1 SAR Different Data Modes for Oil Spill Detection by a Fractal Box Counting Algorithm, *Int. J. Digit. Earth*, 2, 237, 2009.
- [157] Danisi, A., G. Di Martino, A. Iodice, D. Riccio, G. Ruello, et al., SAR Simulation of Ocean Scenes Covered by Oil Slicks with Arbitrary Shapes, *IGARSS*, Barcelona, 1314, 2007.
- [158] Zhang, F., Y. Shao, W. Tian, and S. Wang, Oil Spill Identification Based on Textural Information of SAR Image, *IGARSS*, Boston, MA, IV-1308, 2008.
- [159] Tello, M., R. Bonastre, C. Lopez-Martinez, J.J. Mallorqui, and A. Danisi, Characterization of Local Regularity in SAR Imagery by Means of Multiscale Techniques: Application to Oil Spill Detection, *IGARSS*, Barcelona, 5228, 2007.
- [160] Lounis, B., G. Mercier, and A. Belhadj-Aissa, Statistical Similarity Measure for Oil Slick Detection in SAR Image, *IGARSS*, Boston, MA, I-233, 2008.
- [161] Pelizzari, S. and J. Bioucas-Dias, Oil Spill Segmentation of SAR Images via Graph Cuts, *IGARSS*, Barcelona, 1318, 2007.
- [162] Ferraro, G., A. Bernardini, M. David, S. Meyer-Roux, O. Muellenhoff, et al., Towards an Operational Use of Space Imagery for Oil Pollution Monitoring in the Mediterranean Basin: A Demonstration in the Adriatic Sea, *Mar. Pollut. Bull.*, 54, 403, 2007.
- [163] Ferraro, G., S. Meyer-Roux, O. Muellenhoff, M. Pavilha, J. Svetak, et al., Long-Term Monitoring of Oil Spills in European Seas, *Int. J. Remote Sens.*, 30, 627, 2009.
- [164] Adamo, M., G. De Carolis, V. De Pasquale, and G. Pasquariello, On the Combined Use of Sun Glint MODIS and MERIS Signatures and SAR Data to Detect Oil Slicks, *SPIE*, 63600G, 2006.
- [165] Sipelgas, L. and R. Uiboupin, Elimination of Oil Spill Like Structures from Radar Image Using MODIS Data, *IGARSS*, 2007, 429, 2007.
- [166] Vesecky, J.F., K. Laws, and J.D. Paduan, Monitoring of Coastal Vessels Using Surface Wave HF Radars: Multiple Frequency, Multiple Site and Multiple Antenna Considerations, *IGARSS*, Boston, MA, I405, 2008.
- [167] Pinel, N. and C. Bourlier, Forward Propagation of Thick Oil Spills on Sea Surface for a Coastal Coherent Radar, *IGARSS*, Boston, MA, IV-1125, 2008.
- [168] Demarty, Y., V. Gobin, L. Thirion, R. Guinvarc'h, and M. Lesturgie, Exact Electromagnetic Modeling of the Scattering of Realistic Sea Surfaces for HFSWR Applications, *IGARSS*, Barcelona, 1004, 2007.
- [169] Tinis, S.W., D.O. Hodgins, and M.F. Fingas, Assimilation of Radar Measured Surface Current Fields into a Numerical Model for Oil Spill Modelling, *Spill Sci. Technol. Bull.*, 3, 247, 1996.
- [170] Valentin, M., T. Helzel, V. Mariette, and N. Thomas, Coastal Radar WERA, A Tool for Search and Rescue and Oil Spill Management, *2010 IEEE/OES US/EU Baltic International Symposium*, Riga, Latvia, 2010.
- [171] Schultz-Stellenfleth, J., S. Lehner, T. Koenig, A. Reppucci, and S. Brusch, Use of Tandem Pairs of ERS-2 and ENVISAT SAR Data for the Analysis of Oceanographic and Atmospheric Processes, *IGARSS*, 2007, 3265, 2007.
- [172] Goodman, R.H. and M.F. Fingas, The Use of Remote Sensing for the Determination of Dispersant Effectiveness, *AMOP*, Edmonton, 377, 1988.
- [173] Jensen, H.V., J.H.S. Andersen, P.S. Daling, and E. Noest, Recent Experience from Multiple Remote Sensing and Monitoring to Improve Oil Spill Response Operations, *IOSC*, Savannah, GA, 407, 2008.
- [174] Lehr, W.J., Visual Observations and the Bonn Agreement, *AMOP*, Halifax, NS, 669, 2010.
- [175] Hollinger, J.P. and R.A. Mennella, Oil Spills: Measurements of Their Distributions and Volumes by Multifrequency Microwave Radiometry, *Science*, 181, 54, 1973.
- [176] Horstein, B., The Visibility of Oil-Water Discharges, *IOSC*, Washington, DC, 91, 1973.
- [177] Parker, H.D. and D. Cormack, *Evaluation of Infrared Line Scan (IRLS) and Side-Looking Airborne Radar (SLAR) Over Controlled Oil Spills in the North Sea*, Warren Spring Laboratory Report, 1979.
- [178] Hurford, N. and F.N. Martinelli, *Use of An Infrared Line Scanner and a Side-Looking Airborne Radar to Detect Oil Discharges from Ships*, Warren Spring Laboratory Report, Stevenage, UK, 1982.
- [179] Hurford, N. and F.N. Martinelli, Use of An Infrared Line Scanner and a Side-Looking Airborne Radar to Detect Oil Discharges from Ships, in *Remote Sensing for the Control of Marine Pollution*, J.M. Massin, Editor, Plenum Press, New York, NY, 405, 1984.
- [180] MacDonald, I.R., N.L. Guinasso, Jr., S.G. Ackleson, J.F. Amos, R. Duckworth, et al., Natural Oil Slicks in the Gulf of Mexico Visible from Space, *J. Geophys. Res.*, 98, 351, 1993.
- [181] Brown, H.M., J.P. Bittner, and R.H. Goodman, *Visibility Limits of Spilled Oil Sheens*, Imperial Oil Internal Report, Calgary, AB, 1995.
- [182] Brown, C.E., M.F. Fingas, J-P. Monchalain, C. Neron, and C. Padioleau, Airborne Measurement of Oil Slick Thickness, *AMOP*, Vancouver, BC, 911, 2006.
- [183] Reimer, E.R. and J.R. Rossiter, *Measurement of Oil Thickness on Water from Aircraft; A: Active Microwave Spectroscopy; B: Electromagnetic Thermoelastic Emission*, Environmental Studies Revolving Fund Report No. 078, 1987.
- [184] Goodman, R., H. Brown, and J. Bittner, The Measurement of Thickness of Oil on Water, *Proceedings of the Fourth Thematic Conference on Remote Sensing for Marine and Coastal Environments*, ERIM, Copenhagen, I-31, 1997.
- [185] Aussel, J.D. and J-P. Monchalain, *Laser-Ultrasonic Measurement of Oil Thickness on Water from Aircraft, Feasibility Study*, Industrial Materials Research Institute Report, Québec, 1989.
- [186] Krapez, J.C. and P. Cielo, Optothermal Evaluation of Oil Film Thickness, *J. Appl. Phys.*, 72, 1255, 1992.
- [187] Choquet, M., R. Héon, G. Vaudreuil, J-P. Monchalain, C. Padioleau, and R.H. Goodman, Remote Thickness

- Measurement of Oil Slicks on Water by Laser Ultrasonics, *IOSC*, 1993.
- [188] Brown, C.E., M.F. Fingas, M. Choquet, A. Blouin, D. Drolet, et al., The LURSOT Sensor: Providing Absolute Measurements of Oil Slick Thickness, *Proceedings of the Fourth Thematic Conference on Remote Sensing for Marine and Coastal Environments*, ERIM, Copenhagen, I-393, 1997.
- [189] Brown, C.E. and M.F. Fingas, Development of Airborne Oil Thickness Measurements, *Mar. Pollut. Bull.*, 47, 485, 2003.
- [190] Brown, C.E., M.F. Fingas, J-P. Monchalain, C. Neron, and C. Padioleau, Airborne Oil Slick Thickness Measurements: Realization of a Dream, *Proceedings of the Eighth International Conference on Remote Sensing for Marine and Coastal Environments*, Altarum, Ann Arbor, MI, 2005.
- [191] Monchalain, J.P., Optical Detection of Ultrasound, *IEEE Trans. Ultrason. Ferroelectr. Freq. Con.*, UFFC-33, 485, 1986.
- [192] Svejksky, J., J. Muskat, and J. Mullin, Mapping Oil Spill Thickness with a Portable Multispectral Aerial Imager, *IOSC*, Savannah, GA, 131, 2008.
- [193] Svejksky, J., J. Muskat, and J. Mullin, Adding a Multi-spectral Aerial System to the Oil Spill Response Arsenal, *Sea Technol.*, 50, 17, 2009.
- [194] Lue, L., B. Ge, W. Yao, and Y. Zhang, A Method for Measuring the Thickness of Transparent Oil Film on Water Surface Using Laser Trigonometry, *Opt. Lasers Eng.*, 49, 13, 2011.
- [195] Lu, Y-C., Q-J. Tian, and Z. Li, The Remote Sensing Inversion Theory of Offshore Oil Slick Thickness Based on a Two-Beam Interference Model, *Sci. China Earth Sci.*, 54, 4154, 2011.
- [196] Lu, Q., H. Wu, and D. Wu, Experimental Determination of the System Parameter of Oil Thickness Measurement, *SPIE*, Savannah, GA, 7890, 2010.
- [197] Optimare, <http://www.optimare.de/cms/en/divisions/fek.html> (accessed June 2011).
- [198] Swedish Space Corporation, <http://www.ssc.se/?id=5772> (accessed June 2011).
- [199] Armstrong, L., O. Fäst, H.A. Schneider, and A.H. Abrahamsson, Integration of Airborne AIS Brings a New Dimension to the Detection of Illegal Discharge of Oil Spills, *IOSC*, Savannah, GA, 179, 2008.
- [200] Brown, C.E. and M.F. Fingas, A Review of Current Global Oil Spill Surveillance, Monitoring and Remote Sensing Capabilities, *AMOP*, Calgary, AB, 789, 2005.
- [201] Dean, K.G., W.J. Stringer, J.E. Groves, K. Ahlinas, and T.C. Royer, The Exxon Valdez Oil Spill: Satellite Analyses, in *Oil Spills: Management and Legislative Implications*, M.L. Spaulding and M. Reed, Editors, ASCE, New York, NY, 492, 1990.
- [202] Dawe, B.R., S.K. Parashar, T.P. Ryan, and R.O. Worsfold, *The Use of Satellite Imagery for Tracking the KURDISTAN Oil Spill*, Environment Canada Report EPS 4-EC-81-6, 1981.
- [203] Alfoldi, T.T. and N.A. Prout, *The Use of Satellite Data for Monitoring Oil Spills in Canada*, Environment Canada Report EPS 3-EC-82-5, 1982.
- [204] Cross, A., Monitoring Marine Oil Pollution Using AVHRR Data: Observations off the Coast of Kuwait and Saudi Arabia during January 1991, *Int. J. Remote Sens.*, 13, 781, 1992.
- [205] Rand, R.S., D.A. Davis, M.B. Satterwhite, and J.E. Anderson, *Methods of Monitoring the Persian Gulf Oil Spill Using Digital and Hardcopy Multiband Data*, U.S. Army Corps of Engineers Report TEC-0014, 1992.
- [206] Al-Ghunaim, I., M. Abuzar, and F.S. Al-Qurnas, Delineation and Monitoring of Oil Spill in the Arabian Gulf Using Landsat Thematic Mapper (TM) Data, *Proceedings of the First Thematic Conference on Remote Sensing for Marine and Coastal Environments*, ERIM, New Orleans, LA, 1151, 1992.
- [207] Al-Hinai, K.G., M.A. Khan, A.E. Dabbagh, and T.A. Bader, Analysis of Landsat Thematic Mapper Data for Mapping Oil Slick Concentrations—Arabian Gulf Oil Spill 1991, *Arabian J. Sci. Eng.*, 85, 1993.
- [208] Cecamore, P., A. Ciappa, and V. Perusini, Monitoring the Oil Spill Following the Wreck of the Tanker Haven in the Gulf of Genoa through Satellite Remote Sensing Techniques, *Proceedings of the First Thematic Conference on Remote Sensing for Marine and Coastal Environments*, ERIM, New Orleans, LA, 183, 1992.
- [209] Voloshina, I.P. and O.Y. Sochnev, Observations of Surface Contamination of the Region of the Kol'shii Gulf from IR Measurements, *Soviet J. Remote Sens.*, 9, 996, 1992.
- [210] Leifer, I., B. Lehr, D. Simecek-Beatty, E. Bradley, R. Clark, et al., State of the Art Satellite and Airborne Oil Spill Remote Sensing: Application to the BP Deepwater Horizon Oil Spill, *Remote Sens. Environ.*, 124, 185, 2012.
- [211] Li, Y., S. Yu, L. Ma, M. Liu, and Q. Li, Satellite Image Processing and Analyzing for Marine Oil Spills, *SPIE*, 712311, 2008.
- [212] Alawadi, F., C. Amos, V. Byfield, and P. Petrov, The Application of Hyperspectral Image Techniques on Modis Data for the Detection of Oil Spills in the RSA, *SPIE*, 71100Q, 2008.
- [213] Lotliker, A., R. Mupparthy, S. Kumer, and S. Nayak, Evaluation of Hi-Resolution MODIS-Aqua Data for Oil Spill Monitoring, *SPIE*, 71500S, 2008.
- [214] Hese, S. and C. Schmullius, High Spatial Resolution Image Object Classification for Terrestrial Oil Spill Contamination Mapping in West Siberia, *Int. J. Appl. Earth Obs. Geoinf.*, 11, 130, 2009.
- [215] Clark, C.D., Satellite Remote Sensing for Marine Pollution Investigations, *Mar. Pollut. Bull.*, 26, 92, 1989.
- [216] Noerager, J.A. and R.H. Goodman, Oil Tracking, Containment and Recovery During the Exxon Valdez Response, *IOSC*, San Diego, CA, 193, 1991.
- [217] Li, Y., Y. Liu, L. Ma, and X. Li, Oil Spill Monitoring Using MODIS Data, *SPIE*, 67955G, 2007.
- [218] Li, Y., L. Ma, S. Yu, C. Li, and Q. Li, Remote Sensing of Marine Oil Spills and its Applications, *SPIE*, 71450C, 2008.
- [219] Wang, D., D. Pan, Y. Zhan, and Z. Qiankun, Experiment of Monitoring Oil Spill on the Base of EOS/MODIS Data, *SPIE*, 7831, 2010.
- [220] Shrivastava, H. and T.P. Singh, Assessment and Development of Algorithms to Detection of Oil Spills Using MODIS Data, *J. Indian Soc. Remote Sens.*, 38, 161, 2010.

- [221] Hu, C., An Empirical Approach to Derive MODIS Ocean Color Patterns Under Severe Sun Glint, *Geophys. Res. Lett.*, 38, 2011.
- [222] Cococcioni, M. and L. Corucci, Issues and Preliminary Results in Oil Spill Detection Using Optical Remotely Sensed Images, *IEEE*, Bremen, 2009.
- [223] Corucci, L., F. Nardelli, and M. Cococcioni, Oil Spill Classification from Multi-Spectral Satellite Images: Exploring Different Machine Learning Techniques, *SPIE*, 7825, 2010.
- [224] Grimaldi, C.S.L., I. Coviello, T. Lacava, N. Pergola, and V. Tramutoli, Near Real Time Oil Spill Detection and Monitoring Using Satellite Optical Data, *IGARSS*, Cape Town, SA, 709, 2009.
- [225] Grimaldi, C.S.L., D. Casciello, I. Coviello, T. Lacava, N. Pergola, and V. Tramutoli, Satellite Oil Spill Detection and Monitoring in the Optical Range, *IGARSS*, Honolulu, HA, 4487, 2010.
- [226] Chust, G. and Y. Sagarminaga, The Multi-Angle View of MISR Detects Oil Slicks under Sun Glitter Conditions, *Remote Sens. Environ.*, 107, 232, 2007.
- [227] ud Din, S., A. Al Dousari, and P. Literathy, Evidence of Hydrocarbon Contamination from the Burgan Oil Field, Kuwait—Interpretations from Thermal Remote Sensing Data, *J. Environ. Manag.*, 86, 605, 2008.
- [228] Casciello, D., T. Lacava, N. Pergola, and V. Tramutoli, Robust Satellite Techniques (RST) for Oil Spill Detection and Monitoring, *Proceedings of MultiTemp 2007–2007 International Workshop on the Analysis of Multi-Temporal Remote Sensing Images*, Leuven, Belgium, 2007.
- [229] Li, X., L. Ge, Z. Hu, and H-C. Chang, *The 2009 Montara Oil Spill in the Timor Sea as Observed by Earth Observation Satellites*, University of New South Wales, Sydney, NSW, 2010.
- [230] Brown, C.E. and M.F. Fingas, Upcoming Satellites: Potential Applicability to Oil Spill Remote Sensing, *AMOP*, Edmonton, 495, 2001.
- [231] Brown, C.E., M.F. Fingas, and T.J. Lukowski, Airborne and Space-Borne Synergies: The Old Dog Teaches Tricks to a New Bird, *Proceedings of the Fifth International Airborne Remote Sensing Conference and Exhibition*, San Francisco, Veridien, 8 p., 2002.
- [232] Biegert, E.K., R.N. Baker, J.L. Berry, S. Mott, and S. Scantland, Gulf Offshore Satellite Applications Project Detects Oil Slicks Using RADARSAT, *International Symposium: Geomatics in the Era of RADARSAT*, Ottawa, Canada, 1997.
- [233] Werle, D., B. Tittley, E. Theriault, and B. Whitehouse, Using RADARSAT-1 SAR Imagery to Monitor the Recovery of the Irving Whale Oil Barge, *Proceedings of International Symposium: Geomatics in the Era of RADARSAT*, Ottawa, Canada, 1997.
- [234] Kwarteng, A.Y., V. Singhroy, R. Saint-Jean, and D. Al-Ajmi, RADARSAT SAR Data Assessment of the Oil Lakes in the Greater Burgan Oil Field, Kuwait, *Proceedings of International Symposium: Geomatics in the Era of RADARSAT*, Ottawa, Canada, 1997.
- [235] Ivanov, A.Y. and I.S. Ermoshkin, Mapping of Oil Spills in the Caspian Sea Using the ERS-1, ERS-2 SAR Image Quick-Looks and GIS, *Interspill*, Trondheim, Norway, 2004.
- [236] Fortuny, J., D. Tarchi, G. Ferraro, and A. Sieber, The Use of Satellite Radar Imagery in the Prestige Accident, *Interspill*, Trondheim, Norway, 2004.
- [237] Torres Palenzuela, J.M., L.G. Vilas, and M.S. Cuadrado, *Use of ASAR Images to Study the Evolution of the Prestige Oil Spill off the Galician Coast*, 1931, 2006.
- [238] Gauthier, M-F., L. Weir, Z. Ou, M. Arkett, and R. De Abreu, Integrated Satellite Tracking of Pollution: A New Operational Program, *IGARSS*, Barcelona, 967, 2007.
- [239] Brekke, C. and A.H.S. Solberg, Oil Spill Detection by Satellite Remote Sensing, *Remote Sens. Environ.*, 95, 1, 2005.
- [240] Olga, L., M. Marina, B. Tatiana, K. Andrey, and K. Vladimir, Multisensor Approach to Operational Oil Pollution Monitoring in Coastal Zones, *IGARSS*, Boston, MA, III-1386, 2008.
- [241] Kostianoy, A., O. Lavrova, M. Mityagina, T. Bocharova, K. Litovchenko, et al., Complex Monitoring of Oil Pollution in the Baltic, Black and Caspian Seas, *Proceedings ENVISAT Symposium*, Montreux, Switzerland, 23, 2007.
- [242] DeAbreu, R., M-F. Gauthier, and W. Van Wycken, SAR-Based Oil Pollution Surveillance in Canada: Operational Implementation and Research Priorities, *Proceedings Ocean SAR 2006—Third Workshop on Coastal and Marine Applications of SAR*, St. Johns, Newfoundland, 2006.
- [243] Nirchio, F., G. Pandiscia, G. Ruggieri, R. Santoleri, F. Tataranni, et al., COSMO-SKYMED Contribution in Oil Spill Monitoring of the Mediterranean Sea, *IGARSS*, Cape Town, SA, 781, 2009.
- [244] Li, Y., G-X. Lan, J-J. Li, and L. Long, Potential Analysis of Maritime Oil Spill Monitoring Based on MODIS Infrared Data, *IGARSS*, Cape Town, SA, 2009.
- [245] Fingas, M.F. and C. Brown, Detection of Oil in and Under Ice, *AMOP*, Vancouver, BC, 1994, 2002.
- [246] Redman, R., C. Pfeifer, E. Brzozowski, and R. Markian, A Comparison of Methods for Locating, Tracking and Quantifying Submerged Oil Used During the T/B DBL 152 Incident, *IOSC*, Savannah, GA, 255, 2008.
- [247] Wendelboe, G., L. Fonseca, M. Ericksen, F. Hvidbak, and M. Mutschler, Detection of Heavy Oil on the Seabed by Application of a 400 kHz Multibeam Echo Sounder, *AMOP*, Vancouver, BC, 791, 2009.
- [248] Hansen, K.A., Research Efforts for Detection and Recovery of Submerged Oil, *AMOP*, Halifax, NS, 1055, 2010.
- [249] Medialdea, T., L. Somoza, R. Leon, M. Farran, G. Ercilla, et al., Multibeam Backscatter as a Tool for Sea-Floor Characterization and Identification of Oil Spills in the Galicia Bank, *Mar. Geol.*, 249, 93, 2008.
- [250] Michel, J., Spills of Nonfloating Oil: Evaluation of Response Technologies, *IOSC*, Savannah, GA, 261, 2008.
- [251] Pfeifer, C., E. Brzozowski, R. Markian, and R. Redman, Quantifying Percent Cover of Submerged Oil Using Underwater Video Imagery, *IOSC*, Savannah, GA, 269, 2008.
- [252] Pfeifer, C., E. Brzozowski, R. Markian, and R. Redman, Long-Term Monitoring of Submerged Oil in the Gulf of Mexico Following the T/B DBL 152 Incident, *IOSC*, Savannah, GA, 275, 2008.
- [253] An, J. and Z. Liu, Underwater Detection by Laser Remote Sensing, *SPIE*, 7858, 2010.

- [254] Camilli, R., B. Bingham, C.M. Reddy, R.K. Nelson, and A.N. Duryea, Method for Rapid Localization of Seafloor Petroleum Contamination Using Concurrent Mass Spectrometry and Acoustic Positioning, *Mar. Pollut. Bull.*, 58, 1505, 2009.
- [255] Lehr, W.J., The Potential Use of Small UAS in Spill Response, *IOSC*, Savannah, GA, 431, 2008.
- [256] Donnay, E., Use of Unmanned Aerial Vehicle (UAV) for the Detection and Surveillance of Marine Oil Spills in the Belgian Part of the North Sea, *AMOP*, Vancouver, BC, 771, 2009.
- [257] Li, K., M.F. Fingas, J.R.P. Paré, P. Boileau, P. Beaudry, and E. Dainty. The Use of Remote-Controlled Helicopters for Air Sampling in an Emergency Response Situation, *AMOP*, Vancouver, BC, 139, 1994.
- [258] Goodman, R.H., Overview and Future Trends in Oil Spill Remote Sensing, *Spill Sci. Technol.*, 1, 11, 1994.
- [259] Huisman, J., Use of Surveillance Technology to Support Response Decision Making and Impact Assessment, *Interspill*, London, UK, 2006.
- [260] Carpenter, A., The Bonn Agreement Aerial Surveillance Programme: Trends in North Sea Oil Pollution: 1986–2004, *Mar. Pollut. Bull.*, 54, 149, 2007.
- [261] De Dominicis, M., N. Pinardi, G. Coppini, M. Tonani, A. Guarnieri, et al., Oil Spill Detection and Forecasting Using MOON Real Time Data Interspill, Marseilles, FR, 2009.
- [262] Allen, J. and B. Walsh, Enhanced Oil Spill Surveillance, Detection and Monitoring Through the Applied Technology of Unmanned Air Systems, *IOSC*, Savannah, GA, 113, 2008.

DETECTION, TRACKING, AND REMOTE SENSING: SATELLITES AND IMAGE PROCESSING (SPACEBORNE OIL SPILL DETECTION)

KONSTANTINOS TOPOUZELIS¹, DARIO TARCHI², MICHELE VESPE², MONICA POSADA²,
OLIVER MUELLENHOFF², AND GUIDO FERRARO²

¹*Department of Marine Sciences, University of the Aegean, Mytilene, Greece*

²*Maritime Affairs Unit, Institute for Security and Protection of the Citizen – JRC European Commission, Ispra, Italy*

13.1	Introduction	357
13.2	Oil Spills Detection by Satellite	358
13.2.1	Optical Remote Sensing	358
13.2.2	Microwave Remote Sensing	360
13.3	From Research to Operational Services	366
13.3.1	Historical Attempts	366
13.3.2	Operational Oil Spill Detection	371
13.3.3	Oil Seepage Detection Aspects	374
13.4	Ancillary Data	375
13.4.1	Detection Capability	375
13.4.2	Risk of Pollution	377
13.4.3	Ship Detection (AIS, LRIT, VMS, Satellite AIS)	377
13.5	Summary and Conclusions	378

13.1 INTRODUCTION

A number of remote sensing systems are available for the detection and monitoring of oil slicks in the marine environment [1,2]. Conventional sensors are both passive (i.e., infrared cameras, optical sensors, infrared/ultraviolet systems, microwave radiometers) and active (i.e., laser fluorosensors and radar systems). Their use, combined with an appropriate procedure for data fusion, offers a promising way to improve the reliability of pollution identification and provide additional valuable information, such as identification of the spilled area, analysis of the spatial heterogeneity of the slick, and the determination of the thick and thin parts of the oil slicks. In the case of spaceborne observations, synthetic aperture radar (SAR) is still the best satellite sensor for operational oil spill detection, due to its wide area coverage and day and night all-weather capabilities. The effectiveness of

such a sensor is well known since a long time. During the last two decades, systematic and intensive efforts, in combination with an increasing number of available satellites with augmented capabilities, have constantly increased the ability of detecting oil spills at sea. Moreover, during this time, technology has steadily improved the spatiotemporal coverage of the SAR images, their reliability, and their timeliness. Nevertheless, radar sensors do not have capabilities for oil spill thickness estimation and oil-type recognition and only are applicable for oil spill monitoring in a certain range of wind speeds. Discrimination of oil slicks from other natural phenomena that dampen the short waves and create dark patches on the surface is an aspect that causes false positives and needs further investigations. Ice, internal waves, kelp beds, natural organics, pollen, plankton blooms, jellyfish, algae, guano washing off rocks, threshold wind speed areas (wind speed <3 m/s), wind sheltering by land, rain cells, and shear zones may all appear as oil [1]. These natural dark patches are termed oil spill look-alikes.

Still, from an operational point of view, spaceborne SAR is today a fundamental element, in combination with airborne/shipborne tools and metocean/contextual data, at continental scales, to detect/identify oil spills and identify the responsible vessel [3].

Until recently, satellite optical sensors have not been of much use for oil spill detection due to a number of different reasons, such as revisit time, false positives, sensitivity to scene geometry, lack of coverage, and lack of appropriate data processing algorithms [2]. This situation started changing with new optical sensor technologies, whose derived products may contribute in combination with SAR observations, to improve discrimination between oil spills and other

look-alikes [1]. Some potential direct capability for oil spill monitoring in the marine environment also has been reported [4]. In the future, high potential not only for oil spill detection but also for oil identification and classification may be possible from hyperspectral imaging sensors.

The following section summarizes some theoretical issues on optical and radar (SAR) sensors for the detection of oil spills at sea. Then, we briefly discuss the main results of some studies and activities, including specific projects that were carried out with the aim of validating the use of radar imagery. The next section includes the need of ancillary data, that is, the diverse meteorological and oceanographic phenomena that have an impact on the short-scale sea surface waves and thus over the SAR images. The last section concludes with discussion on the detection, tracking, and remote sensing of the oil spills.

13.2 OIL SPILLS DETECTION BY SATELLITE

13.2.1 Optical Remote Sensing

13.2.1.1 Theory Oil has a characteristic spectral signature, which distinguishes it from the water and from the other in-water optically active components, like humic yellow substances, chlorophyll, and sediments. In comparison with seawater, crude and heavy refined oils are characterized by higher refractive index and absorption coefficient [5]:

- The oil refractive index typically ranges between 1.57 and 1.67 in the UV up to 1.48–1.52 in the visible (while seawater refractive index is in the range 1.33–1.35). As a consequence, oil reflects visible radiance more than a flat seawater surface.
- The oil absorption coefficient is several orders of magnitude greater than that of water in the blue, and decays exponentially with wavelength. The magnitude of the absorption coefficient influences the “limiting thickness” at which all transmitted light is absorbed, which typically ranges between 0.02 mm for heavy crude at 440 nm and approximately 2 mm for light crudes at 750 nm [6].

Oil fluorescence is affected mainly by the natural light in the UV and the blue part of the electromagnetic spectrum. Fluorescence peaks vary in width and wavelength portion according to oil type and decay exponentially toward the red and NIR wavelengths. The phenomenon is more pronounced in light crudes, where the absorption coefficient decays more rapidly [6–8]. As a consequence of these optical properties, when oil is floating on the sea surface, the reflected signal will increase and the signal leaving the water body (the so-called water emission radiance) will decrease. As a net effect, an optical contrast (i.e., a difference in the optical signal) between the oil slick and the surrounding seawater appears.

Many different factors contribute to the appearance of an oil slick and its contrast with the surrounding water: oil type,

oil thickness, oil position in the water column, optical properties of the surrounding seawater, optical properties of the atmosphere, illumination and observation geometry, sea surface state, sea depth, and bottom type. Hence, the impact of the oil film on the optical contrast is a rather complex, multivariable problem. Different attempts have been done to address the problem and isolate the dependence of the signal from the different variables. Otremba and Piskozub performed radiative transfer simulations with a 3D Monte Carlo code to analyze how wavelength, sea surface state, and oil position in the water column influence the oil bidirectional distribution function and hence the contrast of an oil slick [9–11]. For a thin crude oil film floating over a coastal flat sea surface, they showed that the contrast strongly depends on wavelength, showing greater values at short wavelengths and decreasing afterward with the highest gradient between 420 and 550 nm [11]. Under similar conditions (5 μ m crude Romashkino oil), they found that for a flat surface the contrast is always negative, while for a rough sea surface, the contrast ranges from negative to positive. The highest magnitude of positive contrast occurs in correspondence of the sun reflection angle (off the actual sun glitter region), while negative contrasts appear for almost horizontal observations or with the sun behind the observer’s back for very slanted illuminations. Since the contrast continuously varies from positive to negative, even cases of no contrast occur [9]. The optical signal can penetrate through the sea surface inside the water column. Hence, even submerged oil slicks can create an optical contrast, as well as dispersed oil droplets [10].

On the base of a simple analytical model and field data, Byfield and Boxall showed that in spectrum regions where the water emission radiance is low (ultraviolet and NIR for clean open ocean), the contrast likely is positive, while in regions where the water emission radiance is higher, the contrast depends on oil thickness and absorption and may be positive for thin oil and negative for thicker oil [5]. However, when seawater reflectance is sufficiently high (green to red during algal blooms or throughout the visible and NIR spectrum for turbid waters), even very thin slicks may cause a negative contrast. Furthermore, dampening of the sea surface capillary waves due to oil higher viscosity will influence the signal leaving the oil feature and hence the optical contrast with the surrounding seawater.

In summary, it is potentially possible, once all other parameters are known, to retrieve information on oil type and thickness from the optical contrast. Byfield and Boxall, for example, suggest using the peak to NIR radiance ratio L_{550}/L_{750} to classify oil into broad categories (such as light refined, light crude, heavy crude, and heavy refined oil) and determine its relative thickness. Additionally, hyperspectral retrievals could help identifying the spectral characteristics of the observed target, discriminating look-alike phenomena [5]. For example, phytoplankton blooms could be ruled out if no positive contrast occurs at 555 and 645 nm.

Finally, it is essential to remember that, particularly for satellite applications, a correct and accurate removal of the

atmospheric contribution is critical. Top-of-atmosphere (TOA) data include the entire signal coming from the atmosphere, which can be more than 80% of the overall signal and for our purposes represents just noise. Not corrected TOA data are meaningless for geophysical parameters: these data can just allow detecting the location of the possible oil features, but provide no further information because the contrast and the TOA spectral signal are not coming from the sea level.

13.2.1.2 Available Sensors Optical sensors can be classified according to the number of spectral bands. When the sensor has a single channel detector sensitive to radiation within a broad wavelength range, it is called panchromatic imaging system. If the wavelength range coincides with the visible range, then the resulting image resembles a “black-and-white” image taken from space. The physical quantity being measured is the apparent brightness of the targets. The spectral information or “color” of the targets is lost. Examples of panchromatic imaging systems are IKONOS PAN and SPOT HRV-PAN. When the sensor is a multichannel detector with several spectral bands, it is called multispectral imaging system. Each channel is sensitive to radiation within a narrow wavelength band. The resulting image is a “multilayer image,” which contains both the brightness and spectral (color) information of the targets being observed. Examples of multispectral systems with few spectral bands are Landsat MSS, Landsat TM, Landsat OLI SPOT HRV-XS, and IKONOS MS. There are also multispectral systems (sometimes called superspectral imaging sensors) with many more spectral channels (typically >10), characterized by narrower bandwidths in order to capture the finer spectral characteristics of the targets. Examples are Moderate-Resolution Imaging Spectroradiometer (MODIS) and MEdium-Resolution Imaging Spectrometer (MERIS). Finally, we speak of hyperspectral imaging systems (also known as “imaging spectrometers”) when the images are acquired in about a hundred or more contiguous spectral bands (bandwidth between 5 and 10 nm). The detailed spectral information contained in a hyperspectral image enables better characterization and identification of targets. At present, many airborne hyperspectral sensors are available to collect data, but only two civil spaceborne hyperspectral sensors exist as technology demonstrator: the Hyperion sensor on NASA’s EO-1 satellite and the CHRIS sensor on the European Space Agency’s PROBA satellite. Consequently, the opportunity to use spaceborne hyperspectral remote sensing for operational oil spill monitoring is not yet available. Nevertheless, the future of satellite hyperspectral remote sensing for oil pollution in the marine/coastal environment is very promising.

The NASA MODIS shows strong potential for marine oil spill monitoring: two higher-resolution bands (250 m resolution at nadir), two daily acquisitions, near-real-time (NRT) data, and data freely available. MODIS is a key instrument onboard the Terra (EOS AM) and Aqua (EOS PM) satellites (<http://modis.gsfc.nasa.gov/>). Terra’s orbit

around the earth is timed so that it passes from north to south across the equator in the morning, while Aqua passes from south to north over the equator in the afternoon. Terra MODIS and Aqua MODIS view the entire earth’s surface every 1–2 days, acquiring data in 36 spectral bands, or groups of wavelengths spanning from 0.4 to 14.4 μm . MODIS data are provided at different processing stages. Ocean color products are produced by the Ocean Color Data Processing System by the NASA Ocean Biology Processing Group on a NRT basis using the SeaDAS image analysis package and are distributed via a dedicated website (<http://oceancolor.gsfc.nasa.gov/>) [12]. Since late August 2006, the processing code, traditionally applied only to 1 km resolution ocean bands 8–16, also is applicable to higher-resolution land bands 1–7. Finally, it is important to cite the data service provided by the MODIS Rapid Response System. The MODIS Rapid Response System provides true-color, photo-like imagery and false-color imagery within a few hours of being collected. Real-time true-color composite images in jpg format use MODIS bands 1, 4, and 3 of the L1B processing stage (5 min acquisition).

13.2.1.3 Case Study: Lebanon The Lebanon oil pollution in the summer of 2006 was a spill from a terrestrial source. On July 13 and 15, 2006, in the course of conflict in the Middle East, the oil-fueled power plant of Jieh, located directly on the Lebanon coastline, approximately 30 km south of Beirut, was hit by bombs. Part of the power plant storage tanks caught fire and burned for several days. A large part of the fuel spilled into the Mediterranean Sea as a result of the blast. The Lebanese Ministry of Environment estimated that approximately 30,000 tons of heavy fuel oil was released into the sea. Due to strong coastal ocean currents and winds from south westerly directions, in addition to the war situation that prevented the implementation of measures and actions to contain the disaster, the oil spill moved along the Lebanese coast northward and contaminated large part of the coast, reaching Syrian waters. The pollution resulting from this spill was one of the largest man-made disasters in the Mediterranean Sea.

The Lebanon spill represents a large oil slick that, due to long-time source leakage, persisted for a considerable time in a region and at a period of the year with favorable climate conditions. All these circumstances allowed the creation of a large data set of MODIS images where the same oil slick was observed under a wide variety of geometrical and meteorological conditions. Using available SAR data as reference, such data set was analyzed extensively to study under which conditions MODIS can detect oil features on the sea surface and what kind of information can be retrieved.

In total, 45 MODIS Aqua and 47 MODIS Terra L0 images (raw data) have been collected. All images were further processed, displayed, and visually analyzed using the SeaDAS code (<http://oceancolor.gsfc.nasa.gov/seadas/>). Out of the sample, about 20% of the images were discarded because of complete cloud coverage of the area of interest. Each MODIS

image at L1B processing stage was visually analyzed to identify suspected features. Corroboration was from the temporally closest available SAR image [13].

Suspected features were detected in at least one band in more than 40% of the cases. Their visibility was analyzed in detail in terms of (i) meteorological conditions (i.e., wind speed and atmospheric turbidity), (ii) observation geometry, and (iii) illumination geometry.

The last aspect has great influence on suspected feature visibility, since it may cause sun glint contamination. This occurs when solar radiance directly reflects from the sea surface into the sensor field of view. Suspected feature visibility is remarkably different for areas contaminated or not contaminated by sun glint.

In the presence of sun glint, feature detection was possible at any sensor optical band but was at its best at high-resolution band, 859 nm. The sign of the contrast ranged from negative to positive (depending on the sun-sensor geometry), but maintained the same sign throughout sensor's bands. Features detection in the presence of glint depends (as for SAR) on the different surface physical properties of oil spills and water: oil dampens the surface roughness, affecting the sun-reflected light pattern. Because sunlight reflected by the sea surface is so much greater than the sunlight reflected from the subsurface, retrieval of information about in-water constituents is severely compromised. Indeed, analysis of the retrieved products showed that features tend to be misinterpreted as atmospheric phenomena. No spectral properties of the observed feature could be retrieved.

As to oil detectability in the absence of sun glint contamination, no detection is possible from the low-sensitivity NIR high-resolution bands. Suspected features were only visible at medium-/low-resolution bands, particularly in the blue where oil absorption is highest. Retrieval of useful spectral information requires a careful application of the SeaDAS atmospheric correction code, because it does not account for possible oil features and hence easily misinterprets sea surface features as atmospheric ones. It was shown that in the presence of sun glint and for MODIS sensor viewing angle lower than 40° , detected features were similar to those detected by correspondent SAR images but no spectral properties reasonably could be retrieved [13].

Despite this, MODIS images acquired in glint conditions may be used in conjunction with RADAR images to follow slick movement. Indeed, because MODIS does not tilt to avoid looking into the sun glint field, its glint-affected areas tend to be considerably larger than for those sensors that do tilt, such as SeaWiFS. In the considered case, slightly more than 40% of the retained data set was acquired for sun glint conditions.

13.2.2 Microwave Remote Sensing

13.2.2.1 Theory Over the ocean, the radar backscatter comes from the roughness components of the sea surface components that are approximately of similar scale of the radar wavelength. The roughness components are mainly the

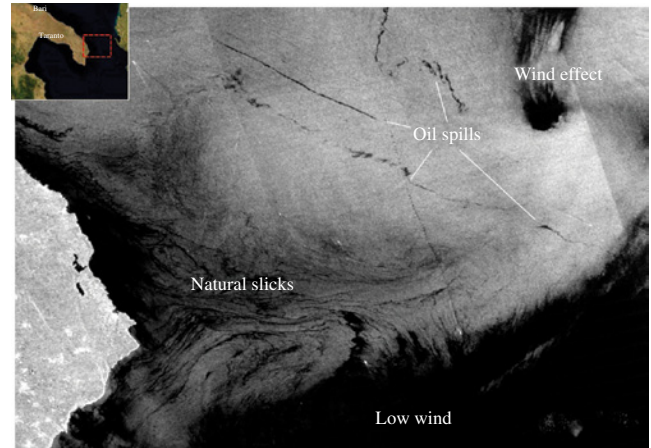


FIGURE 13.1 X-band ScanSAR image acquired over the Adriatic Sea showing oil spills, a number of potential sources of misclassification (look-alikes), and areas below the threshold wind speed, COSMO-SkyMed Product © ASI—Agenzia Spaziale Italiana (2010). All Rights Reserved.

short-scale and wind-generated capillary and short gravity waves. The range of the sea waves have wavelengths of some centimeters and periods less than 1 s. For example, in Envisat's C band of 5.6 cm, the sea roughness components are circa 3 cm. SAR sensors detect spills on the sea surface indirectly, through the modification they cause on the wind-generated short gravity-capillary waves [14]. Oil spills damp these waves, which at oblique incidence angles are the primary backscattering agents of the radar signals. The SAR backscatter from the ocean occurs due to Bragg or resonance scattering. Under Bragg scattering, the radar waves are backscattered by the sea waves λ_B , whose wavelengths are similar to radar frequency λ_r , using the following equation:

$$\lambda_B = \lambda_r / 2 \sin \theta \quad (13.1)$$

where θ is the radar incidence angle. This results in an additional (resonance) of returns from waves that are traveling toward or away from the radar look direction. Slicks show as high contrast on SAR imagery relative to the surrounding clean sea, as dark patches of reduced backscattering (see Fig. 13.1). Therefore, a precondition for detecting oil spills with SAR is the existence of a light wind, sufficient to generate short gravity-capillary waves on the sea surface. The minimum wind speed, referred to as the threshold wind speed, depends on the SAR frequency, the angle of incidence, the oceanographic conditions, and the presence of surface contaminants (natural or anthropogenic).

Different microwave bands probe different spectral regions of the gravity-capillary waves, which in turn require different threshold wind levels. For a C-band SAR, that is, such as those onboard the ERS-1, ERS-2, Radarsat and Sentinel-1 satellites, at least 2–3 m/s wind speed is required [15]. On the other extreme, too high wind speed causes the disappearance of the spill from the SAR image. Considering only wind effects (i.e., assuming that the corresponding sea

state is not yet fully developed, so no rolling wave breaking exists), at a certain wind speed, the short gravity–capillary waves will receive sufficient energy to counterbalance their energy loss caused by the spill. Under such conditions, spills may be detected at wind speeds as high as 14 m/s [16]. As the sea state develops however, the increasing turbulence in the upper sea layer may break up the spill and/or sink it, so its effect on the sea surface will be drastically reduced. Hence, with developed sea state, the upper wind speed limit for spill detection drops to lower levels. Dedicated open sea experiments indicate that for wind speeds higher than 8–10 m/s, the detectability of oil spills becomes rather difficult [17,18]. This depends, however, on the oil type, age, and spill thickness. Extended theoretical and experimental work has been done so far for understanding the effects involved in the damping of the short gravity–capillary waves by mineral oil spills. Central aspect of such investigations is the variation of the wave-damping strength in a spilled sea surface, as a function of the wavelength of the sea waves. According to the Bragg scattering theory, at oblique incidence angles, the microwave backscattered intensity is almost proportional to the amplitude of short sea waves, whose wavelength projection, on the radar look direction equals the half of the radar wavelength [19,20]. Therefore, the wave-damping function between the spilled and clean sea versus wavelength of sea waves (or wave number) can be delineated using multifrequency scatterometers and measuring the backscattering at different angles of incidence [21]. According to early investigations of this type, a possible explanation refers to a resonance-type mechanism, directly related to the elastic properties of the floating film of the spill [22,23]. This resonance-type theory, known also as Marangoni damping, was initially developed for explaining the sea surface smoothness, caused by very thin monomolecular organic films of natural occurrence, that is, the well-known sea slicks [23–25]. Experiments did not allow to come to a clear conclusion and also suggest an alternative interpretation that better accounts for the consistence of mineral oil [23]. According to this, the damping effect of the short gravity–capillary waves is linked, in the case of mineral oil spills, to their much higher viscosity, rather than to the elastic properties of their film. The viscous-damping consideration has an essential practical value, since it explains reasonably the lateral variability of the radar backscattering contrast within a mineral oil spill, as the result of the lateral variability of thickness and/or viscosity. Indeed, the multifrequency scatterometer measurements of Wismann et al. yielded such evidence [24]. In greater detail, higher spilled/clean sea contrast ratios were measured, both over the thicker downwind parts of a mineral oil spill and over spills of higher-viscosity oil, in comparison with spills of lower ones.

13.2.2.2 Sensors: Satellites Several spaceborne SAR systems have been used for oil spill monitoring. They usually are characterized by their frequency (or band). The NASA's SEASAT satellite, launched in 1978, was the first satellite designed to observe the sea surface with an L-band SAR

TABLE 13.1 Main characteristics of satellites with SAR sensors used for oil spills detection^a

Satellite (sensor)	Operative	Owner	Band
SEASAT	1978–1978	NASA	L
ALMAZ	1991–1992	RSA	S
ERS-1	1991–1996	ESA	C
ERS-2	1995–2011	ESA	C
Radarsat-1	1995–2013	CSA	C
Radarsat-2	2007–operating	CSA	C
Envisat (ASAR)	2002–2012	ESA	C
ALOS (PALSAR)	2006–2011	JAXA	L
ALOS-2 (PALSAR)	2014–operating	JAXA	L
TerraSAR-X	2007–operating	DLR	X
TanDEM-X	2010–operating	DLR	X
Cosmos SkyMed	2007–operating	ASI	X
Sentinel-1	2014–operating	ESA	C

^a Adapted from Ref. 26.

Legend: ASI, Italian Space Agency; DLR, German Aerospace Centre; ESA, European Space Agency; JAXA, Japan Aerospace Exploration Agency; NASA, National Aeronautics and Space Administration (United States).

system. Later, SAR systems were launched by the Russian Space Agency (RSA), the European Space Agency (ESA), and the Canadian Space Agency (CSA). The main satellites that were used or are in operational status for monitoring oil spills and their characteristics are presented in Tables 13.1 and 13.2.

An SAR sensor can be described by the frequency band; the polarization, which refers to the orientation of the signal oscillations; the incidence angle, that is, the angular relationship between the radar beam and the ground target; the swath width, that is, width of the imaged scene; and the image resolution. There is a trade-off between the image resolution and the swath coverage. Usually, for oil spill detection, large swath widths are chosen at the expense of lower resolution. Table 13.2 presents the satellite modes that are commonly used for sea monitoring above European waters. It should be noted that none of these satellites were designed primarily for oil spill detection.

13.2.2.3 Detection Methodologies Three main approaches exist for the oil spill detection on SAR images: the manual approach, where operators are trained to analyze images for detecting oil spills; the semiautomatic approach, where some of the operations are made automatically; and fully automatic approach, where all operations are made automatically. Any formation on the image that is darker than the surrounding area is treated as possible oil spill, and further examination is done. Although this process seems to be not very difficult for a trained interpreter, it contains two main difficulties for semiautomated or automated methods. First, look-alike phenomena are presented as dark areas too and further analysis is needed for discriminating them. Second, dark areas can have various contrast values, depending on local sea state, oil spill type, image resolution, and incidence angle.

Manual Inspection Manual inspection is the most popular technique for oil spill detection. Nevertheless, it relies upon human experience, which varies. First, all the possible

TABLE 13.2 Satellite modes commonly used for ocean remote sensing^a

SAR sensor	Mode	Resolution (m)	Swath width (km)	Incidence angle (°)
ERS-2	PRI	30×26.3	100	20–26
Envisat	IM	30×30	100	15–45
Radarsat-1/Radarsat-2	SCN	50×50	300	20–46
Radarsat-1/Radarsat-2	SCW	100×100	450–500	20–49
Envisat	WSM	150×150	400	16–44
TerraSAR-X	SC	Up to 18	100	15–60
COSMO-SkyMed	WR	30×30	100	20–60
COSMO-SkyMed	HR	100×100	200	20–60
Sentinel-1	EWS	100×100	400	19–47

^a Adapted from Ref. 1.

Legend: HR, huge region; IM, image mode; PRI, precision image mode; SC, ScanSAR mode; SCN, ScanSAR narrow; SCW, ScanSAR wide; WR, wide region; WSM, wide swath mode; EWS, extra wide swath.

candidates being oil spills are defined on an SAR image. Then a discrimination process is performed to distinguish oil spills from look-alikes. Some look-alikes are quite easy to classify as they have characteristic shapes and configurations completely different from those of the oil spills, such as dark patches caused by internal wave areas, eddies, or rain cells. However, many spills are complicated. The discrimination is particularly difficult in presence of natural slicks and falls in areas with low wind speeds. In these situations, a more detailed analysis is necessary, where several factors have to be taken into account like shipping lines, distance from platforms, etc. The most important are the wind conditions, the period of the year, the shape analysis, the slick size, and the general morphology of the observed area.

Knowledge of wind conditions is crucial, as low wind speeds of 2–3 m/s result in many false positives while wind speeds above 8–10 m/s prevent oil detection. The period of the year is useful to discriminate natural slicks (i.e., algae bloom) and grease ice on summer, while the slick size is considered to exclude low-wind areas or even large natural slicks. The general morphology is crucial to distinguish dark formations caused by sudden changes of the wind conditions, that is, the passage from a region in which the wind is not present to another in which wind is blowing. In many cases, the dark formations are the result of the sheltering action due to area bathymetry (e.g., areas close to the land, high submarine mountains). More complicated are areas containing fronts, which are boundaries between water masses with dissimilar properties, like two water masses of different densities (due to different temperatures or/and salinities). In these cases, dark formations can contain complex combinations of shapes and sizes.

Shape analysis is very useful for discriminating oil spills from look-alikes, mainly natural phenomena, since the two categories have specific characteristics. Shape analysis takes into consideration the characteristics of the border, the tails, and the roundness of the dark formations. The borders of oil spills are usually very well defined, with a sharp step in the backscattering values between the spilled region and the surrounding region. On the contrary, natural phenomena usually have more structured borders. However, old spills present much more complex border structure than a fresh one. The

tails can be thin, straight, or slightly curved for oil spills, while false positives often have smoother turnings. Look-alikes can be some kilometers in length probably due to wind sheltering action and are usually connected with natural structures like eddies. Nevertheless, this could be the case of artificial spills as a result of a large accident, for example, Deepwater accident at the Gulf of Mexico [27]. Roundness of dark formations, that is, the measure of the sharpness of edges and corners, is essential for identifying fresh spills, elongated with or without curves. Usually, man-made spills have a linear elongated shape, while many natural phenomena have a round shape. Roundness cannot really be measured; therefore, it is in general based on the experience of the photointerpreter. A very good categorization of the oil spills is given by Pavlakis et al., where more than 1600 oil spills are classified in five categories (Fig. 13.2) [28].

In general, it can be assumed that dark formations are usually classified by photointerpreters as potential oil spills according to the following criteria:

- Dark homogeneous spots in a uniform windy area.
- Linear dark areas, not extremely large, with abrupt turns, that is, most likely abrupt turns due to wind directions change or surface current. Natural slicks in these conditions tend to disappear. Man-made slicks are thicker and tend to change their shape.

Dark formations are usually classified by photointerpreters as look-alikes according to the following criteria:

- Low-wind areas
- Coastal zones due to wind sheltering
- Elongated dark areas with smooth turnings in spiral shape, that is, slick's curve emanates from a central point

When oil spill detection service is provided manually, usually an assignment of the possible oil spill is also provided. Mainly three categories are used representing slicks with high, medium, or low probability of being oil. This assignment is mainly based on the experience of the photointerpreters and is under discussion by the research community [1,26]. To this end, the experience of the interpreter becomes a critical

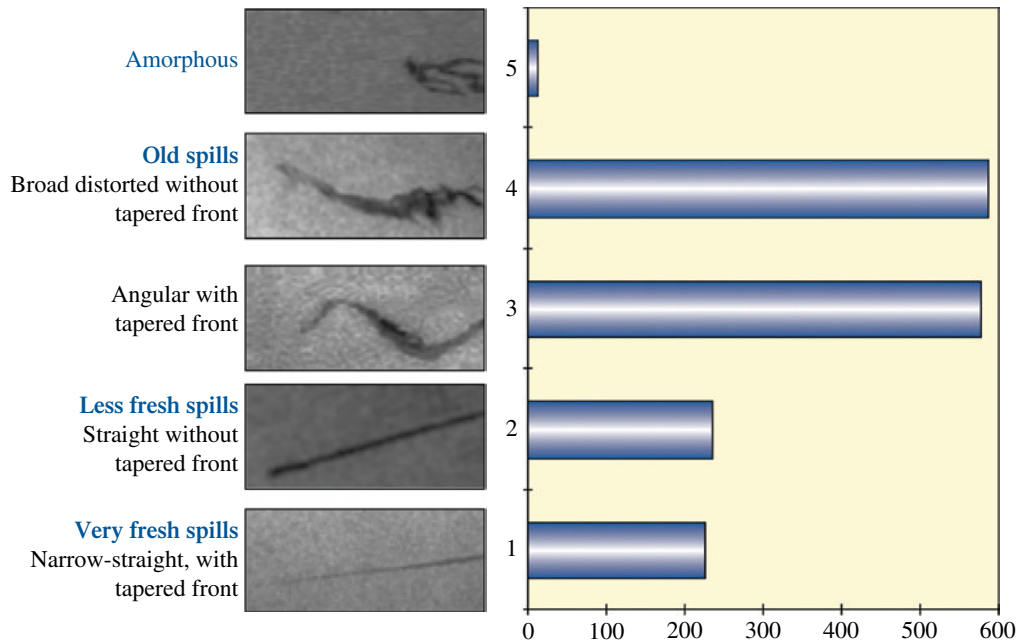


FIGURE 13.2 Classification of 1638 detected oil spills in terms of their shapes. Adapted from Ref. 28.

factor. Because such experience is not widely available, efforts are made to develop systems that will detect and identify dark formations as oil spills in an automatic or in a semi-automatic way.

Semiautomatic and Fully Automatic Methodologies Semi-automatic and fully automatic methodologies are not used very often for oil spill detection mainly because they produce too many false negatives/positives and secondarily because they are complex, they cannot be reproduced easily and require specific knowledge on image understanding, pattern recognition, and classifications theories. The basic idea for such approaches is presented in Figure 13.3 and can be summarized in four steps [28,29]:

1. Detection and isolation of all dark formations presented in the image. Mainly this step is a result of thresholding and segmentation processing.
2. Extraction of statistical parameters of the dark formations, so-called features for each oil spill candidate. These features are related with the geometry of the formation (e.g., area, perimeter), their characteristics (e.g., mean backscatter value), and their context in the image (e.g., distance to ships).
3. Test of the extracted values against predefined statistical values. These values characterize man-made oil spills and look-alike phenomena and are usually determined through phenomenological considerations and statistical assessments.
4. Classification of dark formations as oil spills or look-alikes. Several classification approaches have been used, that is, statistical approach through computation of probabilities, neural networks, fuzzy logic, etc.

Semiautomatic or fully automatic algorithms should operate under all wind conditions, including low winds where high numbers of look-alikes are expected. In these conditions, the false alarm ratio (i.e., look-alikes that categorized as oil spills) is usually extremely high for the automatic algorithms.

Dark Formation Detection Dark formation detection is considered the fundamental step in oil spill detection systems and constitutes the first step in oil spill detection approaches. Once dark formations are detected, classification methods are applied to characterize them as oil spills or look-alikes. If dark formations are not detected in this step, they will never be classified.

Dark formations can be located manually by cropping a broader area containing the dark formation or an image window with fixed size can be used, in which threshold algorithms—adapted or not—can be applied. Threshold represents an appropriate value that determines which pixels will be considered as dark formations and which as clean sea background. Simple thresholds have one value for the whole image, for example, the half of the average normalized radar cross section (NRCS) of the image or NRCS minus the standard deviation [30,31]. In adaptive algorithms, threshold is calculated locally, mainly on areas covered by a moving window. Solberg et al. used an adaptive threshold that was calculated using the mean value of a moving window in different scales of the image [29,32]. In Karathanassi et al., the threshold is fully adaptive to local contrast and brightness of large image segments, therefore the image window does not have a fixed size but it varies according to brightness and contrast values of large areas in the image [33]. This happened using a large image segmentation on the SAR image brightness at the very early stage. Large segments were

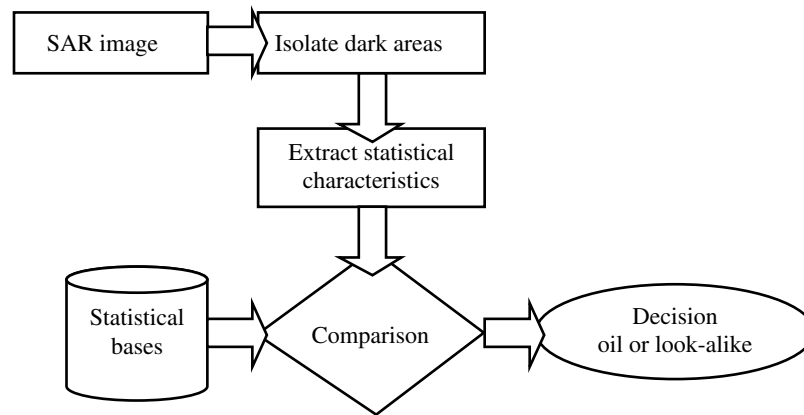


FIGURE 13.3 The basic functions of oil spill detection methodologies. Adapted from Ref. 26.

obtained as image windows, in which a unique threshold was calculated using the mean and standard deviation of the segment's brightness. Del Frate et al. used an edge detection technique based on image histograms that were derived from areas with suspicious dark formations [34]. This method took advantage of the different histograms obtained in dark areas and through histogram comparison calculated a unique threshold. Kanaa et al. [34,35] applied a hysteresis thresholding (Canny [36]) where linear dark formations were successfully detected. Thresholding with hysteresis required two thresholds—high and low. High threshold detected important edges and low threshold was used for fine tuning. Huang et al. applied a partial differential equation (PDE)-based level set technique, which represents the slick surface as in implicit propagation interface [37]. That method can be seen as a numerical technique for tracking interfaces and shapes using unknown multivariable functions and their partial derivatives.

All the aforementioned studies use statistical-based techniques to locate dark formations. A different approach is given by Liu et al., where the use of wavelets for oil spill detection was described [38,39]. This study was performed for ocean feature detection on SAR data including oil spills. In later studies, wavelets were used specific for the oil spill detection problem [40,41]. Moreover, in Benelli and Garzelli, dark formations were detected using a fractal dimension estimation, where a multiresolution algorithm based on fractal geometry for texture analysis was applied [42]. Later, Marghany et al. presented a method for modification of the formula of the fractal box-counting dimension [43]. A different technique, based on texture analysis, was presented by Marghany, where several textures (i.e., entropy, homogeneity, contrast, energy, and correlation) were examined to detect dark formations [44,45]. Finally, Topouzelis proposed a neural network approach to detect dark formations using high-resolution SAR images [26].

All the aforementioned techniques have one common goal: to detect dark formations on SAR images by means of their position and shape. The next step is to extract several

features, which describe the black formation in order to use them as input to the classifier.

Feature Extraction Features are very important for the classification because they are used as inputs to the classifier. Therefore, the combination of features that discriminate better the oil spill from the look-alikes is of very high importance for the classifier and for the method's accuracy. In general, oil spill detection methodologies traditionally use arbitrary selected quantitative and qualitative statistical features for classifying dark objects on SAR images into oil spills or look-alike phenomena.

The features that are usually used for oil spill detection can be generally grouped into three major categories [1,33,46]: features referring to the geometrical characteristics of oil spills (e.g., area, perimeter, complexity), features capturing the physical behavior of oil spills (e.g., mean or max backscatter value, standard deviation of the dark formation or a bigger surrounding area), and features referring to the oil spill context in the image (e.g., number of other dark formations in the image, presence of ships).

The absence of a systematic research on features extracted as well as their contribution to the classification results force researchers to arbitrarily select features as input to their systems. Solberg et al. used 11 features [29]; Fiscella et al. used 14 [30], in general different from the 11 used by Del Frate et al. [34]; Keramitsoglou et al. [47] used 14; and Karathanassi et al. used 13, many of them different from the previous studies [33].

The lack of systematic research can be attributed to the fact that the existing methodologies for searching into a large number of different compilations have not been fully exploited. Stathakis et al. [46] and Topouzelis et al. [48] tried to bridge this chasm and to discover the most useful features of oil spill detection using a combination of genetic algorithms and neural networks.

Several studies try to unify all the features used having similar characteristics [1,49,50]. Table 13.3 presents a grouping of the 25 most commonly used features applied in

TABLE 13.3 Commonly used features^a

No	Feature	Code	No	Feature	Code
1.	Area	A	14.	Mean contrast	ConMe
2.	Perimeter	P	15.	Max contrast	ConMax
3.	Perimeter to area ratio	P/A	16.	Mean contrast ratio	ConRaMe
4.	Complexity	C	17.	Standard deviation contrast ratio	ConRaSd
5.	Shape factor I	SP1	18.	Local area contrast ratio	ConLa
6.	Shape factor II	SP2	19.	Mean border gradient	GMe
7.	Object mean value	OMe	20.	Standard deviation border gradient	GSd
8.	Object standard deviation	OSd	21.	Max border gradient	GMax
9.	Object power to mean ratio	Opm	22.	Mean difference to neighbors	NDm
10.	Background mean value	BMe	23.	Spectral texture	TSp
11.	Background standard deviation	BSd	24.	Shape texture	TSh
12.	Background power to mean ratio	Bpm	25.	Mean Haralick texture	THm
13.	Ratio of the power to mean ratios	Opm/Bpm			

^aAdapted from Refs. 46 and 48.

the majority of research studies. The first six features (1–6) refer to the geometrical characteristics, the next sixteen features (7–22) refer to the physical characteristics, and the last three (23–25) refer to the texture characteristics of the dark formations. Detailed description can be found in Stathakis et al. and Topouzelis et al. [46,48].

Classifiers The purpose of the classifier is to distinguish oil spills from look-alikes. How difficult is the classification task depends on the variability of the oil spill and look-alike examples. Classifiers learn the patterns from examples (training step) and in a later stage are called to take a decision (classification step). The most known are the statistical classifiers, in which the classification decision is based on probability. Statistical classifiers are quite popular as they are rather simple and reliable and can be easily reproduced. Their classification reliability can be measured a priori, according to the database samples of oil spills and look-alikes.

Several classifiers have been proposed in the literature. Solberg et al. proposed a statistical modeling with a rule-based approach [29]. The probabilities assigned using Gaussian density function and derived from a signature database of 7051 dark formations containing 71 oil spills and 6980 look-alikes. In a recent study, an updated version of the method was presented for Radarsat and Envisat images [32]. Their training data set consisted of 56 Envisat WS ASAR images and 71 Radarsat SAR images, while the reported test set consisted of 27 Envisat images containing 37 oil spills and 12,110 look-alikes. A similar statistical classification methodology was presented by Fiscella et al. [30]. They applied a Mahalanobis and a compound probability classifier. Their training set includes 80 oil spills and 43 look-alikes, and they measured the probability p of dark formations to be oil spill (a priori classification probability). They used three classification categories: oil spills, uncertain, and look-alikes. Nirchio et al. presented another statistical approach based on multiregression analysis (or Fisher discrimination approach) [31]. They used 13 features as inputs and tried to set up a relation between the predictor variables and the

dependent variable on a data set containing 153 verified oil spills and 237 look-alikes.

A different classification methodology was presented by Del Frate et al. [34]. They used neural networks to classify the dark formations. Neural network classifiers are not very popular as they are rather complex and they require specific knowledge on the theory of neural systems. Del Frate et al. applied the multilayer perceptron (MLP) network family with a topology of 11 inputs (i.e., the calculated features describing the dark formations), one output and two hidden layers with eight and four neurons, respectively [34]. Their data set was 600 ERS images in low resolution from which they extracted 139 dark formations, 71 oil spills, and 68 look-alikes. Neural networks were used also as classifiers for oil spill detection by Topouzelis et al. [51]. They used a MLP network with topology 10:51:2, that is, 10 features as inputs, 51 neurons in the hidden layer, and 2 output nodes. The topology and the input features were chosen using a genetic algorithm. The genetic algorithm had chosen the selected 10 from a base of 25 inputs and the proper topology after searching 100 generations using 7 bit chromosome. Detailed information regarding the selected topology and the feature selection is given by Stathakis et al. and Topouzelis et al. [46,48]. Their data set consisted of 24 high-resolution SAR images containing 159 dark formations, 90 look-alikes, and 69 oil spills. Recently, a texture-classifying neural network algorithm was proposed by Garcia-Pineda et al., in which SAR data are processed from a wide selection of beam modes [52]. A combination of edge detection filters, descriptors of texture, collection information, and environmental data is processed with a neural network as classifier.

Another classification methodology, based on fuzzy logic, was implemented by Keramitsoglou et al. [47] and Karathanassi et al. [33]. Fuzzy classifiers work with ranges of values, solving problems in a way that more resembles human logic. The input variables in a fuzzy-based methodology are mapped into by sets of membership functions. They require specific knowledge on the theory of fuzzy systems but they are considered reliable classifiers since they try to resemble human logic and they can be reproduced easily. Keramitsoglou

et al. estimated the probability of a dark formation to be oil spill using an artificial intelligence fuzzy modeling system [47]. Their method developed using 9 ERS-1/ERS-2 low-resolution images and was tested on 26 images. Karathanassi et al. also proposed a classification method based on fuzzy classification rules [33]. Their methodology was based on an object-oriented image classification technique, in which on the first step homogeneous image, objects are extracted in any chosen resolution and in later stage are classified by means of fuzzy logic. They used 13 features as inputs on 12 ERS-1/ERS-2 high-resolution images.

Comparison between the different classifiers in terms of classification accuracies is very difficult. Mainly because oil spill detection approaches use different data sets, have different dark formation detection techniques, extract arbitrary number of features, and in the end use different classifiers. Therefore, the reported classification accuracies cannot be directly compared. Another issue with high importance for the detection methodologies is the computational time. Unfortunately, there are no sufficient data in the literature to compare the methodologies in terms of necessary time from image acquisition to final classification report. This comparison should be made under the same data in order to check not only the time frame but also the method's accuracy. Nevertheless, we can point out that as long as the methodologies have been developed, the most time-consuming step for analyzing a new image is the dark formation detection step. Once the dark formations have been detected, the feature calculation step and the classification step need few seconds to complete their actions.

As the quantity of the SAR data increases rapidly, there is a big need for semiautomatic or fully automatic methodologies to detect and identify dark formations as oil spills, fast and accurately. There are several methodologies proposed in the literature but their results are under discussion and they cannot really be compared. The main reason is that each study is using its available data set, which in most of the cases does not contain verified examples. Therefore, there is a need for a common database with verified oil spills and look-alikes, which will be widely available in the scientific community. This database should contain a wide range of verified oil spills (in age, shape, and brightness) and verified look-alikes, in different wind conditions, by several SAR sensors, polarizations, and modes. Also, a categorization is needed for the verification means (e.g., airplane, vessel) and the time gap between the image acquisition and the verification. Only then the different methodologies will be comparable and their improvements measurable. Moreover, under this perspective, the three main parts of the methodologies (i.e., dark formation detection, feature extraction, and classification) can also be examined and compared in terms of accuracy and processing time.

The key issues for an effective oil spill methodology are given by Kubat et al. [53]. They refer to five critical factors that should be taken into account: the scarcity of the data in terms presence of oil spills; the imbalanced training set

(there are more negative examples, i.e., look-alikes, than positive examples, i.e., oil spills); the validity of the data selection (there is no guaranty that the examples used at the development phase are representatives of the examples that will arise after development); the feature selection procedure; and the highly dynamic environment in terms of data set, feature selection, and classification algorithm. Another issue is the accuracy estimator, that is, the performance of a method can be also added as a key factor. These issues have to be very carefully studied before designing a new methodology or applying a new data set to existing methods.

Semiautomatic methods can be very helpful under certain circumstances, but the manual approach will never be eliminated and more work is needed on the comparison between semiautomatic and fully automatic methods. In particular, predefined automatic methods should be compared against photointerpreters with different levels of experience. This test will help to better understand the advantages and the limitations of the automatic methods. Last but not least, current automatic methodologies should put more effort to their weak points especially on detection at low-wind situations and where natural films are present.

13.3 FROM RESEARCH TO OPERATIONAL SERVICES

13.3.1 Historical Attempts

13.3.1.1 JRC Reconnaissance Studies in the Mediterranean Sea At the beginning of the 1990s of the last century, the launch of the first European satellite equipped with SAR, the ERS-1, and later on its successor ERS-2 together with the Canadian Radarsat-1 made the widespread availability of SAR imagery possible. It has also to be noted that over areas where data from regular aerial surveillance were unavailable, such as the Mediterranean Sea, spaceborne observations represented the only possible way to provide an estimation of the dimension of the problem due to operational illegal spilling from vessels. In addition, the availability of a quite large volume of archived SAR images for a time span of several years made also possible to analyze trends for the problem. However, using historical data it is not possible to confirm results with other means so that the detections have to be considered as possible rather than validated oil spills.

This kind of systematic mapping over the Mediterranean has been pioneered by JRC [16,28,54]. The data type used in these studies was mainly calibrated by low-resolution imagery, since this is the most targeted and cheap product for the application. A spatial resolution (pixel) of about 200 m appeared to be sufficient for statistical investigations of marine oil pollution [55]. For determining to the maximum degree possible that the detected spills were due to man-made activities and not to look-alike manifestations, all the images were carefully analyzed using a dedicated semiautomatic

TABLE 13.4 Yearly coverage and possible oil spills detected over the whole Mediterranean Sea in the period 1999–2004

Year	Coverage (km ²)	Possible oil spills
1999	153.402	1.638
2000	404.262	2.297
2001	276.945	1.641
2002	204.240	1.401
2003	254.079	897
2004	431.235	1.425
Total	1724.163	9.299

detection scheme, which includes, as final step, the decision by a skilled operator. Each identified spill then was registered in a database, together with information concerning its geographic position, the date and time of detection, the spilled area, its average contrast strength, and a vector describing its shape. To assess the distribution of detected anomalies, their number has to be referred to the total number of satellite images analyzed. It also is necessary to account precisely for the images that are only partially covering a sea area. To this aim, the coverage is expressed in terms of square degrees observed per year, where only areas corresponding to sea are taken into consideration. A square degree is a square having approximately 60 nautical miles per side, that is, about 110 km. In total, 18,947 SAR images were analyzed for the period 1999–2004; 9299 possible oil spills were detected. Table 13.4 summarizes the results.

The coverage of analyzed images for the same period and the cumulative results as a point-like map are displayed in Figures 13.4 and 13.5, respectively.

With reference to Figure 13.4, it should be noted that a few images were available for Libyan coastal waters, while, by contrast, many images were available for the seas surrounding the Italian peninsula. As a consequence, the results are skewed accordingly. However, the variations of coverage may be considered quite smooth and the problem almost disappears when taking into consideration subareas of limited size. Figure 13.5 presents the detected spills during the period 1999–2004. Each dot is independent, that is, no spill was observed repeatedly in more than one satellite image. The size of the dot is constant for all the detections and does not connect with the actual size of the spill detections. Figure 13.5 targets on the cumulative representation of the detected cases and can be seen as an intermediate product, where most of the spills were detected. Figure 13.6 displays the possible oil spill density as obtained by merging the information from the two previous maps; that is, normalizing the number of observed possible oil slicks in a given area with the total number of observations available for that area. Such a procedure basically removes bias and accounts for uneven coverage of the area. Even if this happens partially, since noise gets worst when coverage is few, this method is very effective in identifying areas with high probability of spill presence. In summary, the map can be employed to understand the spatial distribution of possible oil slicks and to identify hot-spot areas.

As could have been easily supposed, the spill distribution appears to be highly correlated with the major shipping routes. Concentrations appear in the Ionian Sea, the Adriatic Sea, the Messina Straits, the Sicily Channel, the Ligurian Sea, the Gulf of Lion, and East of Corsica. All over the region, however, the possible spills show considerable spatial dispersion. It has to be mentioned that some boat wakes could yield false-positive cases. Also, in some areas, route lines are not uniform or interrupted, that is, area between Sicily and Port Said. This happens because most discharges happen close to the destination port or shortly before.

13.3.1.2 The AESOP Project The AESOP strategy was conceived taking into consideration all the experience previously gained in a number of research projects focused on sea-based oil pollution monitoring, such as RAMSES, GAIANET, VASCO, and CLEOPATRA funded by EC and ESA, but with the clear aim of representing a substantial step forward with the operational use of space imagery. AESOP intended to assess the possibility of setting up an operational system based on the use of NRT spaceborne imagery to support and integrate aerial surveillance in the detection of oil pollution and in the monitoring of main shipping routes in the Mediterranean region. The Adriatic Sea was selected as the study area, and the summer months were selected as the test period. Besides its morphological characteristics, ecological heritage, and the intense maritime traffic characterizing the area, the choice of the study zone was determined by taking into consideration the different forms of cooperation already in place within the basin, such as the subregional contingency plan between Italy, Croatia, and Slovenia and the Adriatic Ionian initiative. Furthermore, the Adriatic Sea well represents an important theater able to involve different countries (Italy, Slovenia, Croatia, Bosnia, Serbia–Montenegro, Albania, and Greece) playing synergistic roles for the implementation of the project and the achievement of its goals. Taking into consideration the ultimate objective of providing the user community with an operational service, able to fulfill user needs for the prevention of and response to oil pollution at sea, the project was aiming at assessing the actual reliability of the radar satellite images detection by comparing them with observations from aerial means. This exercise represented a fundamental preliminary step aiming at cross-validating remote sensing observations. The project developed through the following steps:

- Selection of a number of suitable satellite images
- Planning and execution of patrolling activities by aerial means over the same areas and at the same time
- Analysis of satellite images in terms of oil spill signatures
- Comparison of the results of this analysis with the aerial observations

Within AESOP also, preliminary attempts to reconstruct the spilling scenarios by integrating satellite observations, oil

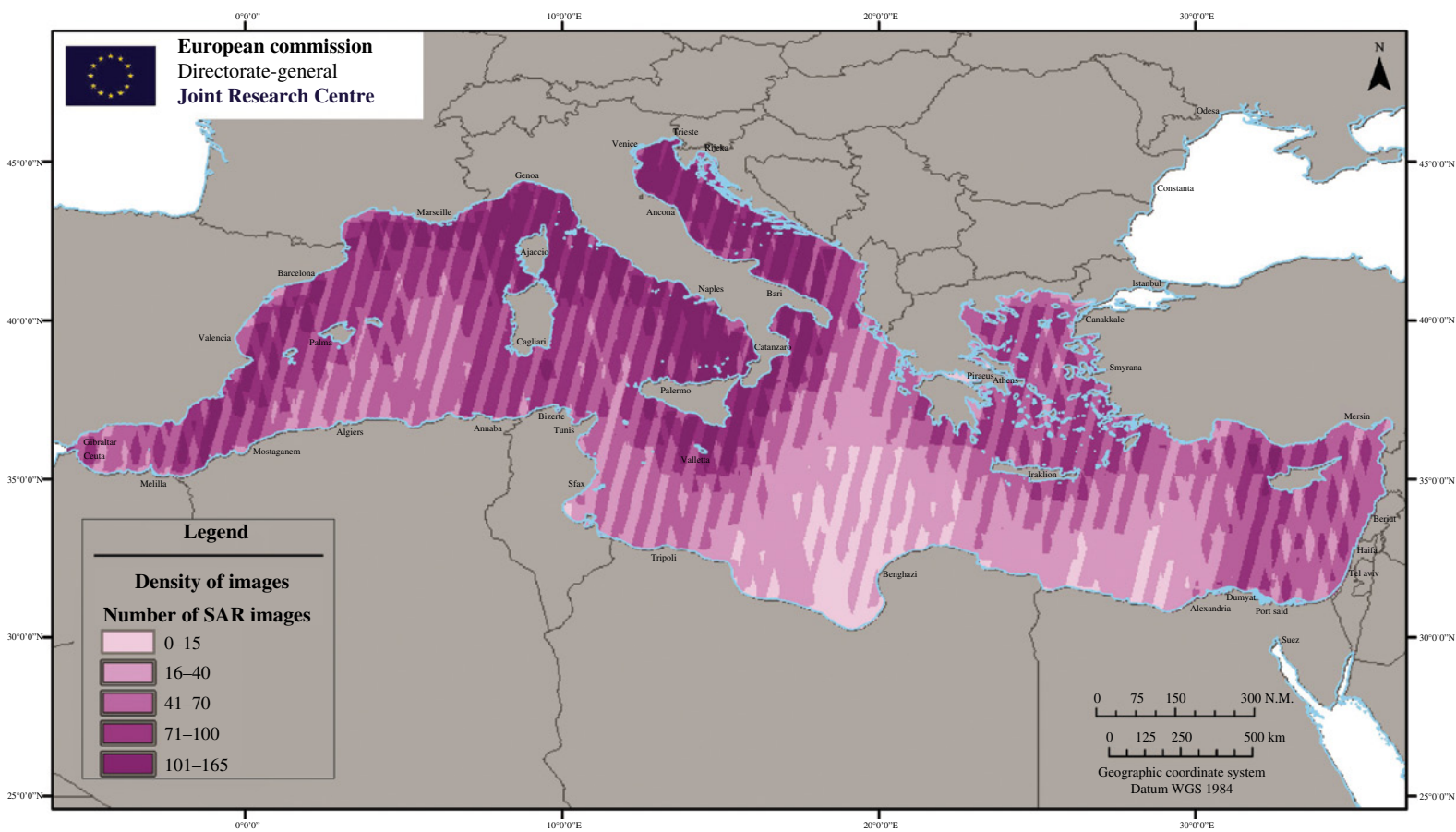


FIGURE 13.4 Coverage of SAR images analyzed for the period 1999–2004.

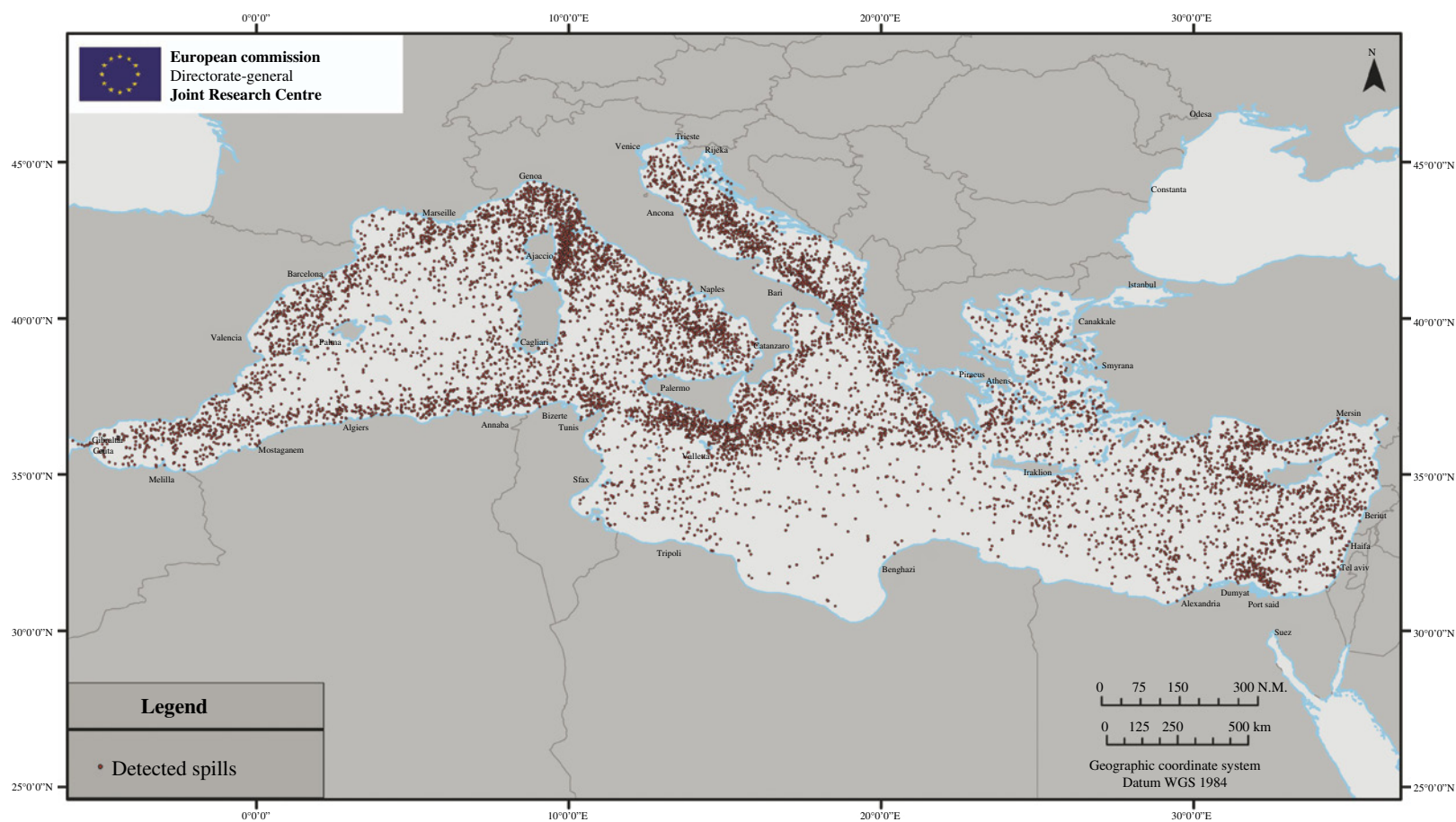


FIGURE 13.5 Possible oil spills detected in the period 1999–2004 in the Mediterranean basin.

dispersion model, automatic identification system (AIS) data, and metocean data have been made. They gave very encouraging results and indicated a promising methodology for identifying the culprit vessel.

In total, 5 Radarsat high-resolution images and 75 medium-resolution images (MRI) from ERS2 have been analyzed. Radarsat images were delivered in NRT mode (few hours after the acquisition), while no such service was available for ERS2 MRI data. The analysis was performed by using a semiautomatic detection scheme with a final inspection by a skilled operator. Despite the excellent quality, no spills were detected in the Radarsat frames, while in the 69 good-quality MRI (out of the 75 delivered), 66 possible oil spills were identified. Six of these 69 images were delivered by the space provider with unexpected rapidity. This opportunity, even if not planned in advance, was used to inform the Italian Coast Guard of the possible oil spills detected in the satellite images. The analysis and the verification of these images by aircraft or vessels of the Italian Coast Guard were particularly interesting. For four of these six images, the pollution was not confirmed by vessels. The results may look at a first glance discouraging, but the following elements must be taken into consideration:

- The time delay, between the acquisition and the verification, was, in all cases, significantly long (longer than 1 day with a maximum of 2 days).
- The verification was done only by vessels.
- Only the position of the possible slick at the time of observation was communicated (not oil volume or oil type).
- No simulation on the possible drift of the slick was made.

In the two remaining cases, the verification took place within a few hours from the image acquisition giving the results detailed in the following.

Possible spills were detected in the satellite image (Fig. 13.7) acquired on August 25, 2005, at 11:28 (local time), offshore from San Cataldo Point in Puglia (South Adriatic), and results were reported to the Italian Coast Guard at 14:48 (local time). The oil detection was verified by vessels, and relevant oil pollution was identified. A response operation to collect the oil at sea, in both little hydrocarbon agglomerates and unbroken wakes of 5/6 mm thickness, was activated and coordinated by the Italian Coast Guard. The operations ended on August 27.

Four possible spills were detected in the satellite image acquired on September 6, 2005, at 11:50 (local time), off Ancona (middle Adriatic), and results were reported to the Italian Coast Guard at 13:32 (local time). Another presumed slick, close to the coast, was also detected in the satellite image. On this day, the Italian Coast Guard was able to verify the pollution reported by aircraft and not only by vessels. The aircraft in three cases out of four confirmed the slicks. The presumed oil slick was verified by the aircraft to be composed by drifts coming out from a river. It was pollution but not oil pollution.

13.3.2 Operational Oil Spill Detection

Differently from research and development activities, operational services have to deal with information timeliness, reliability, and usability. In order to efficiently trigger additional monitoring, response, and control operations by the appointed authorities, the potential oil spill detection has to be delivered in NRT, that is, in the order of tens of minutes from the satellite overpass. The reliability of the delivered information is intended at both input (SAR image quality, expanded in the following) and output (oil spill detection output) levels and has to be factored in the production and delivery of the alert. Ultimately, usability is related to the way that the information is presented and delivered.

The service output is nowadays required to include additional data to the SAR-based oil spill detection alert in order to derive, for instance, the oil spill impact and the potential polluter identification. For instance, currently, operational services also include SAR-based vessel detection, providing indications about the potential position of the pollution culprit, and its identification via correlation to AIS data. Moreover, through the integration of ancillary metocean data and contextual information, it is possible to provide additional indications on the detection capabilities of the system as explained in Section 13.4.

In Europe, oil spill detection based on satellite SAR systems has become an operational service following the European Directive 2005/35/EC. The European Maritime Safety Agency (EMSA) developed the CleanSeaNet service (<http://emsa.europa.eu/operations/cleanseanet.html>), providing assistance to the European Union coastal Member States, Norway and Iceland. The service provides SAR-based oil spill detection NRT alerts (i.e., within 30 min from the satellite acquisition) and is linked to the national oil pollution surveillance and response chains. The service also integrates vessel positioning systems and ancillary data, providing situational awareness and drifting prediction capabilities.

13.3.2.1 Image Quality Aspects SAR oil spill detection process consists of segmentation and classification algorithms based on geometric and radiometric features extraction from the image product. In order to produce a reliable oil spill detection analysis, the SAR image quality is therefore expected to be compliant to certain specifications. Some of them are achieved by instrument calibration and validation procedures operated by the SAR image providers on a routine basis, aiming at correcting errors introduced by the electronics, antenna, or processing subsystem levels. Nevertheless, even for calibrated products, there are aspects that can affect the operational system output leading to either false alarms or missed detections. This is particularly true when the oil spill detection algorithms work in a fully automatic way.

Image quality aspects are strongly application oriented, meaning that a degradation of SAR geometric or radiometric parameters affects with different extents diverse maritime

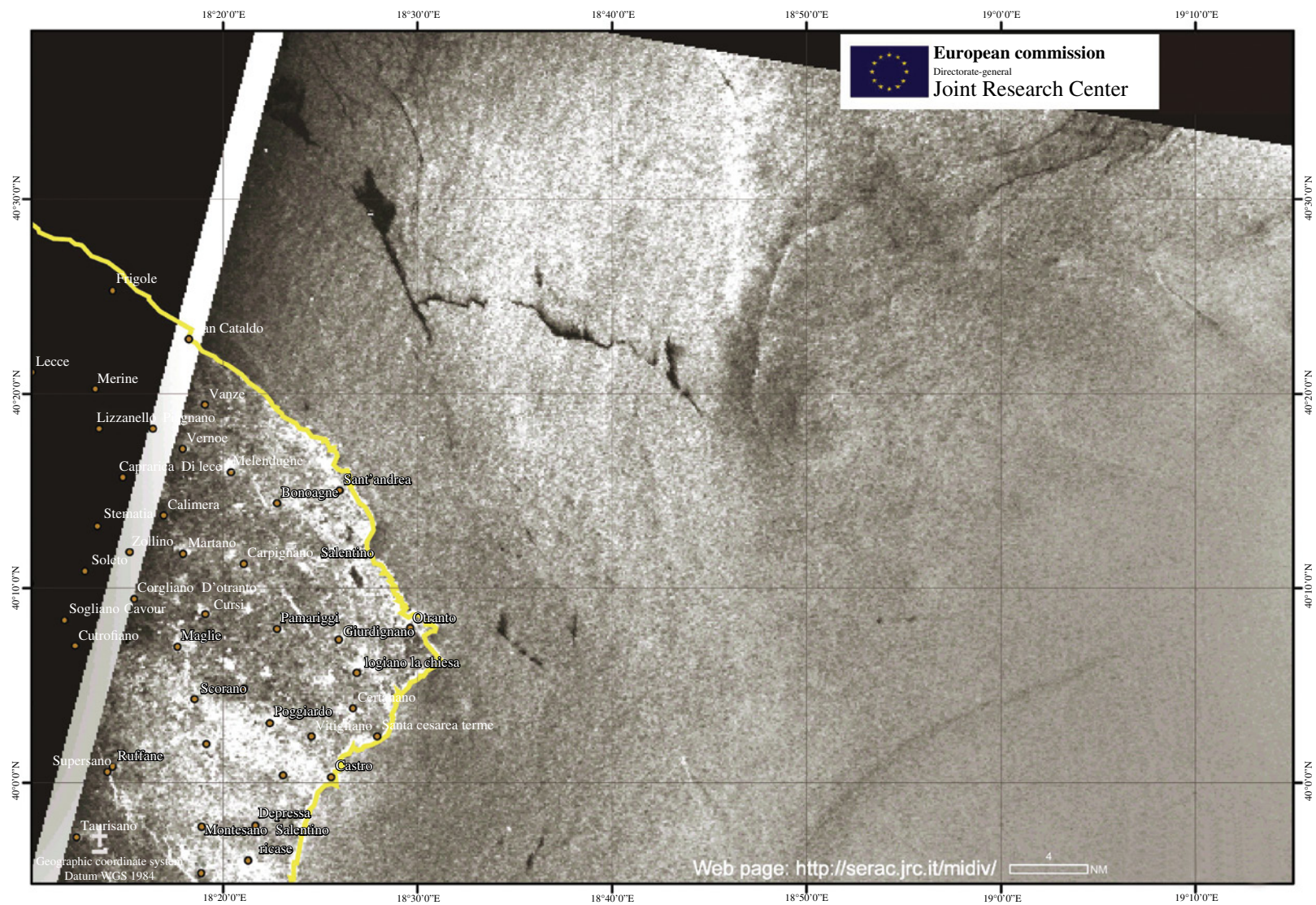


FIGURE 13.7 Oil spill detected in the satellite image of August 25 at 11:28 (local time).

applications [56]. Operational oil spill detection services primarily privilege wide area coverage, usually greater than 100 km swaths. For SAR products, this is achieved at the expense of resolution, for instance, preferring ScanSAR over strip map modes. This is motivated by the size of the dark patches of interest identified by accidental and intentional oil spills. For instance, Envisat ASAR Wide Swath mode, characterized by 150 m resolution and around 400 km coverage, has been widely used in oil spill detection (CleanSeaNet service).

The geolocation accuracy, that is, the ground distance between the SAR measured and ground truth location, can be measured as the distance between land areas within the image and additional shoreline data. Although this quality aspect does not often fulfill the specifications, for oil spill detection, the geolocation quality requirements can be relaxed to hundreds of meters since it is sufficient to locate detections in relatively large areas.

Differently from geometric quality aspects, radiometric resolution, radiometric error, and instrument sensitivity deviations from the specifications may lead to missed oil spill detections. Radiometric error higher than 2 dB may impact oil spill detection algorithms since it can modify the sea and oil backscattering. This can often be observed in ScanSAR modes as residual scalloping or elevation beam mismatch (Figure 13.8).

The *radiometric resolution* is the ability to distinguish objects characterized by different backscatter. It is defined as $\Gamma = [1 + (\text{ENL})^{-1/2}]$, where the equivalent number of looks (ENL), related to the averaging of subapertures and range presumming, can be estimated from the image and checked against the specifications through the computation of mean μ and the standard deviation σ calculated over wide homogeneous sea backscattering: $\text{ENL} = (\mu/\sigma)^2$ [57]. As reported by Pavlakis et al., the vast majority of oil spills detected with the

C-band ERS-2 are characterized by low contrast with the surrounding sea backscatter (e.g., <4 dB) [28]. This suggests a requirement $\Gamma \leq 1.5$ dB for oil spill detection. Such C-band requirement is of use also for X-band instruments (e.g., COSMO-SkyMed and TerraSAR-X) since the ratio between oil-free and oil-covered-sea backscatter is expected to be larger [58]. The SAR instrument *sensitivity* is given by the noise equivalent sigma zero (NES0), which measures the lowest backscatter level that can be detected above the noise level. The NES0 degradation is a general key issue that affects oil spill detection, since a reduced sensitivity performance progressively decreases the backscatter transitions between Bragg scattering and potential oil spills with the result of reducing the detection capabilities. This parameter can be directly calculated from the calibrated image product over homogeneous sea areas in near-zero wind conditions. At C band, the requirements –28 dB for HH-polarized and –23 dB for VV-polarized images indicate the lowest detectable sea backscatter at 45° incidence angle with a wind of 5 m/s cross-wind. Such requirements allow for the detection of oil spills at far range (portion of the image with larger incidence angles) for wind speeds close to the wind threshold. Moreover, this requirement is expected to hold at X-band [59].

Data integrity issues related to artifacts like strong range ambiguities and ground-based emissions at the SAR operating frequency may vary the statistics of the sea backscatter, upsetting segmentation and classification algorithms. Furthermore, such data integrity issues may mask actual spills as shown in Figure 13.9 where, although a human operator easily detects the dark patch, automatic algorithms may fail to do so.

For this reason, they have to be taken into account in the image quality estimation process by identifying nonexploitable areas. For operational purposes, the concept of “application suitability” has been proposed [56].

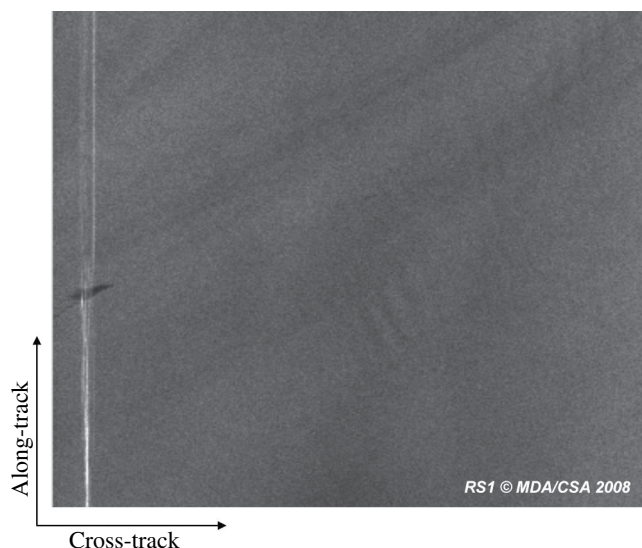


FIGURE 13.8 Radiometric error given by elevation beam mismatch. © ESA—European Space Agency.

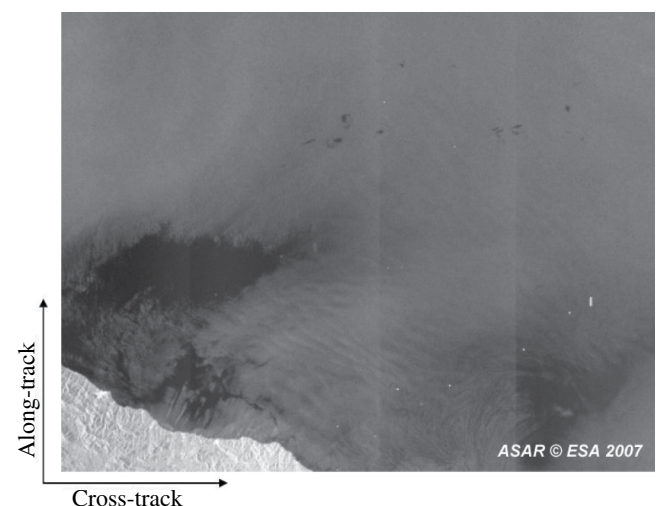


FIGURE 13.9 Nadir ambiguities masking and oil spill. © MDA/CSA—Canadian Space Agency.

All the described quality aspects need to be properly checked and should be assessed and provided to end user over the input SAR image before operating oil spill detection, as a component of the application quality assessment. The potential oil spill detection should also be labeled by a degree of input SAR product reliability to better identify the consistency of the delivered information.

13.3.2.2 Confidence Level and Alert System The detection based on SAR image processing described in Section 13.2.2.3 leads to a set of dark features that can be classified as oil spills with varying confidence. This is generally calculated as the likelihood that the detected dark patch and the extracted features (shape, size, texture, backscatter, etc.) are related to an oil spill. Nevertheless, this process is still considerably affected by false alarms and missed detections, independently of the goodness of the algorithm used. In order to refine the oil spill alert, it is still possible to include additional ancillary relevant data. The extraction of wind fields from the same SAR image, by independent remote sensing data, or through *in situ* measurements, leads to an additional discrimination capability between oil spills and look-alikes (wind or not wind related), with the result of augmenting the reliability of the service. Low-wind areas and their neighboring regions are put outside the useful range of detection. Moreover, the knowledge of the area of interest through the use of ancillary metocean information can further improve the oil spill alert reliability. The confidence level associated to the SAR-based oil spill detection can therefore be progressively improved (e.g., increased if along a tanker traffic lane, decreased if detected in high-natural activity area) as further discussed in Section 13.4. This is often implemented following a decision tree process but recently also using data fusion algorithms [60,61].

In addition to this, the transition from a confidence level-based chain to a more articulate alert system, delivering information of particular interest to the end user, has recently been observed [62]. For instance, AIS-based traffic information is used for the identification of the potential polluter, or the impact of the oil spill is presented in order to better elaborate the alert associated to such detection. It is worth noting that the oil spill detection operational services are not expected to provide or suggest a final decision on the follow-up action to be taken with reference to the specific detection, but a transparent set of information that allows the user to make a decision. The end user's follow-up action can range from the reanalysis of the image and further check of additional information (AIS, nautical and maritime information, local sea state conditions) to the check of the alert by aerial means or patrol vessels. Based on the specific position of the spill, combined to its size, the authorities can decide to ignore the alert, send out pollution response vessels, and/or initiate investigation. If sampling of the oil has been taken, it is also possible to initiate or require port state control inspections of the vessels allegedly originating the oil pollution. As a result, such actions are driven by the combination of the classification

level associated to the detection with criteria linked to the possibility of verification and to the relevant oil spill impact [62,63]. In particular, the latter criterion is deduced from the combination of the oil spill motion over time and the position of environmentally sensitive areas or shoreline. In order to better estimate the specific trajectory of the oil spill, it is necessary to run models based on the evaluation of a time-varying drifting vector primarily computed using surface wind fields, surface current, and tidal and river flows information [64]. It is worth mentioning that the reliability of oil spill models is reduced to a few hours' drift hindcast/forecast from the acquisitions, since affected by the need of information seldom available when integrating SAR-based services, such as volume and chemical properties of the oil, crucial in predicting the weathering process over time [65].

In summary, operational oil spill services are progressively providing information related to not only the position of the detection based on SAR image processing but also additional contextual, vessel traffic, metocean information and models to better assess the impact of the detection.

13.3.3 Oil Seepage Detection Aspects

Many dark patches visible in SAR imagery do not originate from illegal discharges or accidental pollution, but rather from natural oil seeps. The effect of natural oil seeps on the radar backscattering is similar to that for oil originating from ships and rigs (see Section 13.2.2.1). A significant amount of crude oil is discharged naturally to the world's oceans each year and is caused by geological effects. A study of the NRC (National Research Council) in 2003 estimates worldwide natural oil seepage into the marine environment of between 0.02×10^6 and 2.0×10^6 tons yearly, with a best estimate of 600,000 tons. These estimates were made based on Kvenvolden and Harbaugh's reevaluation of the estimates made by Wilson et al. [66,67].

Hydrocarbon migration in marine sediment is a widespread phenomenon throughout the world's oceans. The hydrocarbons move from the source to the trap along permeable pathways, predominantly upward under the effect of buoyancy to the sea surface. The trap is formed by a permeable and porous rock (e.g., sandstone) overlain by an impermeable layer (e.g., shale). For hydrocarbons to accumulate, the sandstone/shale boundary needs to form an inverted basin, which prevents the hydrocarbons from continuing to rise to the surface. Traps are usually formed by tilted fault blocks, where tectonic forces have stretched a basin so that it is breaking it into a series of fault blocks [68].

Although the oil leakage point at the sea bottom is stationary, the surfacing footprint of the oil on the sea surface varies according to the metocean conditions. They appear under calm sea conditions as shining concentric shapes with a diameter usually close to 1 m, also known as oil "pancakes." These small slicks come together and drift with the prevailing wind and current directions to produce the continuous slicks that can be observed from space.

The direct link between surface seepage and subsurface oil and gas accumulations can be assessed. Merely around 5% of the total number of slicks detected results from natural seepage and are of exploration interest [69]. The focus of the offshore oil exploration is moving more and more into ultradeep waters, which is accompanied with a huge increase of exploration costs. Therefore, the seep detection with SAR systems has become a fundamental technique for the oil and gas industry seeking a low-cost, high-coverage, noninvasive, offshore basin screening tool as a routine part of their initial exploration phase. Multitemporal remote sensing data over deepwater hot spots provide the locations for follow-up surface sampling.

Several authors developed a consistent and systematic analysis scheme to discriminate seepage slicks from other slicks [52,69]. Three main categories of slicks are distinguished: seepage slicks, pollution slicks, and natural film slicks. The seep categorization is based on the following criteria [52,69]:

- Environmental factors: Sea surface temperature (SST), sea surface height (SSH), ocean currents, wind conditions at the moment of the SAR snapshot, and wind history.
- Repetition: A repeating emission point is shown on successive images. This is the most compelling parameter but is restricted to the leakiest basin types (episodic seepage is a feature of most seepage and in most offshore basins).
- Size: The minimum size of a resolvable seepage slick depends on sea state and sensor.
- Location: Slicks located in known or predicted sedimentary basins are potentially of interest.
- Morphology: Seeps are generally intermittent and elongated, with high aspect ratios (length to width) and with a recognizable emission point.
- Direction of flows (streaming direction): Seepage slicks will conform to dominant wind and current directions (and/or tidal effects). Pollution slicks, especially from ships, are typically straight and have a distinct feathered edge.
- Context: This is either geological (i.e., location over plausible migration conduits) or geographic (i.e., location within shipping lanes or in areas of oil production).
- Backscatter reduction: Oil slicks (seeps and pollution) generally have a greater contrast and edge enhancement (i.e., sharpness) than natural films, but this property is dependent on wind speed.
- Edge characteristics (i.e., sharpness) and relation to wave facets, current, and wind: These details are very helpful to the analysis because they depend on the slick thickness and material, which correspond to seeps or man-made spills.

Examples of typical seepage slicks visible in SAR and multispectral imagery are shown in Figure 13.10. The fusion of

imagery analysis from SAR and MODIS/Terra, with wind speed and direction from ASCAT and geostrophic current vector layer, is shown in Figure 13.10e.

13.4 ANCILLARY DATA

The SAR imaging technique of ocean–atmosphere interaction interface introduces a high degree of uncertainty in SAR image interpretation. This happens due to all exchanges between the atmosphere and the ocean, that is, heat, momentum, light, water, and gases, which SAR is capturing [70]. Diverse meteorological and oceanographic phenomena have an impact on the short-scale sea surface waves, and thus, their manifestations are reflected over the SAR image. Under specific circumstances, these manifestations yield reduced backscatter patterns therefore adding up misclassification sources to the oil spill identification process. These natural or man-related look-alike phenomena can be grouped into the following categories:

- Man related (e.g., ship wakes, floating production facilities drain emissions)
- Atmospheric (e.g., wind sheltering, rain cells, atmospheric instability areas)
- Oceanographic (e.g., internal waves, coastal upwelling, eddies, current shears, bathymetry/currents interaction, grease ice)
- Natural/biological (e.g., natural seepage, fish oil in cold waters, algae blooms, pollen from plants and trees, coral spawn, natural surfactants)

In order to discriminate some of the look-alikes, there have been attempts to integrate ancillary data into the detection loop [61]. These ancillary data are used to estimate two relevant concepts on oil spill detection, namely, (1) detection capability and (2) risk of pollution. Then, these estimations are fused with the detection output itself aiming at providing a more reliable assessment.

13.4.1 Detection Capability

Given an SAR image, the detection capability refers to an estimation of the appearance of look-alike features based on the analysis of relevant data sets over the imaged area.

To this extent, the challenges are first to find comprehensive data sets that enable to isolate occurrences of specific metocean/contextual circumstances associated to false-positive producers, then to define proper methodologies for their mapping, and finally to integrate these output as variables into the detection system.

The occurrence of the aforementioned phenomena could be inferred with adapted algorithms by using specific combinations of disparate data sources. Nonetheless, time and spatial resolutions of relevant data represent an issue. For instance, spatial resolution of an SAR image ranges from

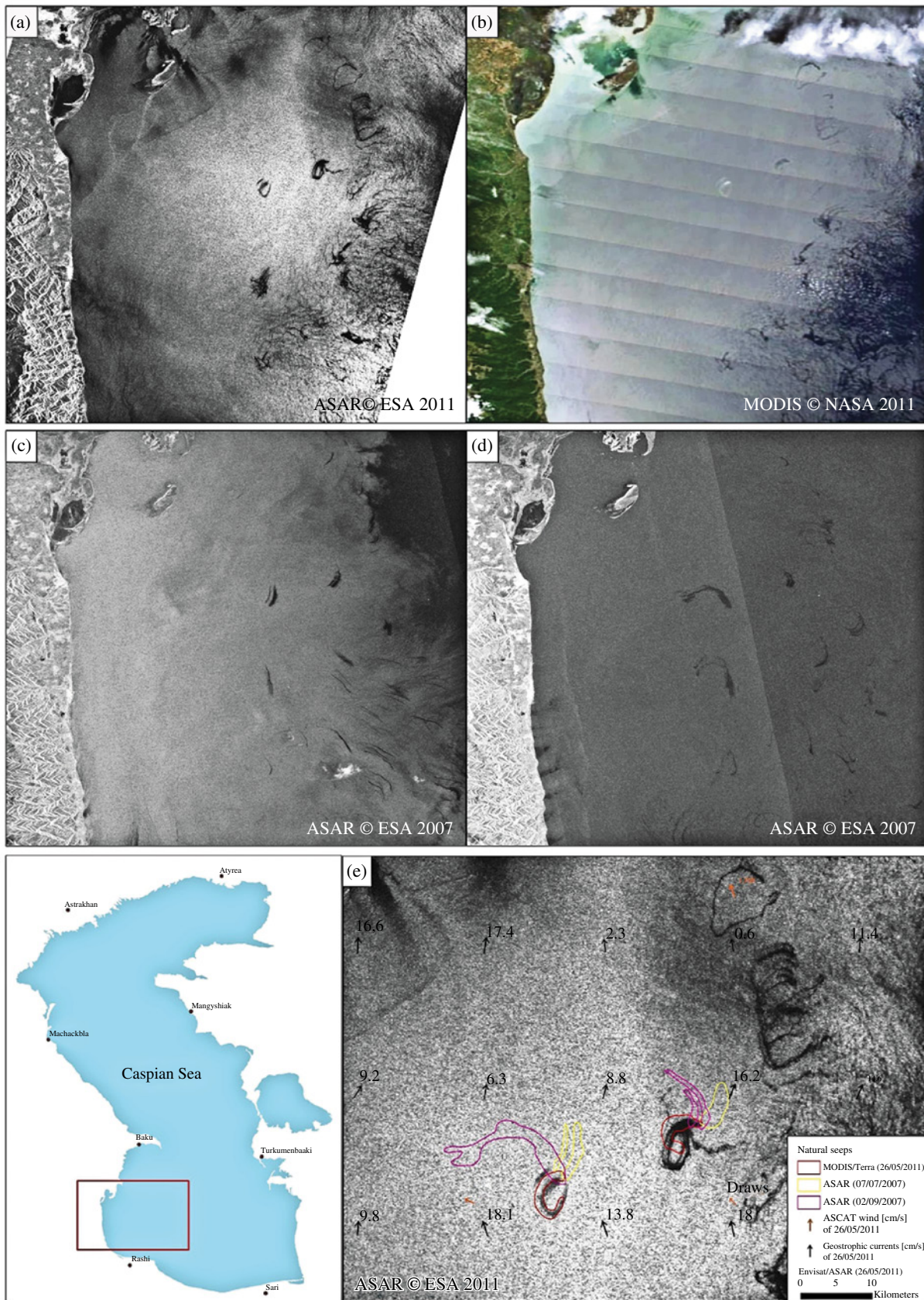


FIGURE 13.10 South Caspian Basin, typical seepage slicks. Multiple seeps are visible in (a) ASAR acquisition, June 25, 2011; (b) MODIS/Terra acquisition, June 25, 2011; (c) ASAR acquisition, July 7, 2007; (d) ASAR acquisition, September 2, 2007; and (e) repeated seeps in different colors.

approximately 10 up to approximately 150 m, whereas met-ocean products normally start on cells of few kilometers. This resolution is far too low to accurately isolate false-positive patterns. Moreover, due to the instant character of the SAR image, only concurrent and in situ met-ocean data can provide the absolute ground truth control for its interpretation. Most often, however, such ground truth control is not available when and where is needed. Model data and met-ocean products could be helpful in decreasing the false detections and therefore increasing the positive oil spill detection cases.

13.4.1.1 Look-Alike Mapping Methodologies In order to increase the reliability of oil spill classification, environmental data have been used as additional help. The available data set includes low-wind conditions, SST-derived cold water fronts, air–sea interactions, current shears, biogenic oil films, etc. The generated maps could be used for cross-checking with the oil spill detection methodologies, in order to effectively assign the corresponding level of the reliability to oil spill candidates. The data are not related to specific time of SAR image acquisition. On the contrary, such maps aim at describing monthly and seasonal trends in the areas of interest. The study was geographically extended to the European seas. Table 13.5 characterizes the data sources used and explains methodologies applied for the identification of look-alike patterns over them. These maps could be considered a potential decision-making support and validation tool that could be easily adapted to stakeholder requirements.

Once all relevant ancillary sources were processed and potential affecting phenomena isolated, the outcome was integrated into a single layer. Given the ocean–atmosphere interface interactions, the complexity, and the interrelation between measurable variables, a weighted sum was approached for the probability of occurrence detection. The more influential undesired phenomena occurring over an area at the same time, the lower is the detection capability. Figure 13.11 depicts the results of mapping detection capability degrees over EU seawaters.

13.4.2 Risk of Pollution

The risk of pollution associated to a specific area can be thought of as a measure of the likelihood of observing oil spill occurrences. Here is a list of data that can be processed to estimate such parameter, with a brief analysis of the reasoning behind their relevance:

Ship traffic density: Main ship lanes appear to be one of the key data source to be included on the risk of pollution analysis, due to heavy traffic leading to high deballasting and bilge discharge activities [71].

Ports: Port information based on port influence area, oil terminal presence, and incoming traffic can also be

selected as relevant factors pointing to high risk of pollution.

Ship wrecks: They can be considered due to the associated long-lasting pollution, although highly influenced by wreckage final environment and general conditions [72].

Offshore platforms: Operational discharges in offshore oil exploration are associated with produced water and systems fail.

Oil pipelines marine runs: Although there is no certain figure of how many miles of offshore pipelines are actually in the world (estimation is about 52,000 km of pipelines [73]), the run of marine pipelines could also be considered as a risk factor in oil spill monitoring.

This information can be estimated through a GIS approach by identifying areas with higher risk of illicit oil spill events on the basis of their proximity to potential polluting sources (see Fig. 13.12). The aim is to integrate this layer into the detection system so as to raise the level of confidence of an oil spill candidate whenever it falls in areas at risk.

13.4.3 Ship Detection (AIS, LRIT, VMS, Satellite AIS)

Nowadays, operational bodies that use SAR technology for regular monitoring of the sea are already in place. A natural qualitative step forward to improve capacities of these bodies would be to provide also with reliable information on the potential polluter. This would help competent authorities to timely apply proper inspections and thus facilitate the prosecution of infractions.

Satellite SAR images are, so far, unable to identify the pollution culprit. At best, satellites can detect the position of a probable polluter. In this sense, the capability of correlating ship detection performed over the SAR imagery with vessel positioning data is considered a key issue in the field.

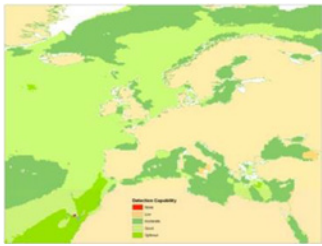
An increasing number of maritime surveillance sensors are providing vessel positioning data, for example, AIS, long-range identification and tracking (LRIT), vessel monitoring system (VMS), satellite AIS, and coastal radar tracks. Fusion techniques for merging these data into comprehensive maritime information layer are currently investigated. Moreover, techniques for backtracking positions of vessels at the time of the SAR image are based on oil spill dispersion and drift models [71]. The degree of confidence of such identification is proportional to the time lag between the relevant information and the sensors' intrinsic uncertainties. Ship detection is sometimes used as additional information to increase the likelihood of the detection being an oil spill, although this does not increase the probability of true positives [29].

Conversely, connected ship and oil spill events shall raise the alert level of the detection since it can be thought of as a relevant factor for follow-up activities concerning the prosecution of potential polluters.

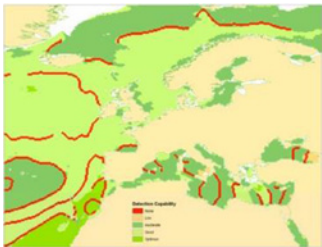
TABLE 13.5 Look-alike patterns layout examples

Wind data: Monthly averaged QuikSCAT wind data products from SeaWinds were utilized. These products contain gridded data of wind speed and direction 10 m above the sea surface. Data was processed and parameterized in two variables:

- (1) Wind speed range for mapping areas according to their suitability for oil spill detection
- (2) Wind current fronts for mapping wind masses interaction associated with potential decrease of wind velocity and thus yielding false positives



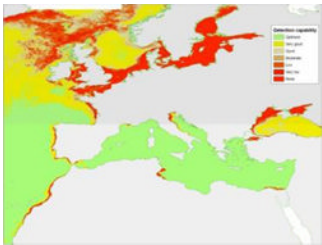
Wind speed range



Wind fronts

Chlorophyll-A: Monthly averaged regional products were used from the JRC MERSEA Project (<http://mersea.jrc.ec.europa.eu/>). This information is injected as an indicator of biogenic activity that, under certain favorable circumstances of quantity of light energy and inorganic nutrients, may produce the release of biogenic oil films, that is, look-alikes

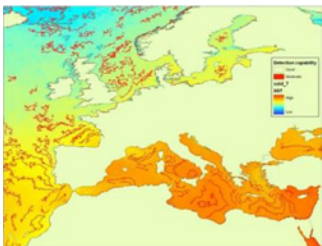
In this case, the look-alike map layout is derived using chlorophyll-A concentration threshold. This threshold is set on the basis of the analysis of Envisat SAR imagery over the Mediterranean basins (oligotrophic environment) with synchronous chlorophyll-A measurements from MERIS sensor



Chlorophyll-A: Areas of potential high biogenic activity

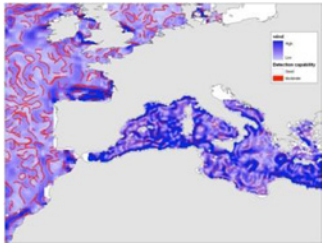
Sea surface temperature (SST): Variations on the SST may affect the stability of the atmosphere above. This effect may have an impact on the wind stress and indirectly modify the sea surface modulation. According to this, water temperature strong gradients were mapped over SST layers as potential sources of ambiguity

Data were retrieved from (i) AVHRR Pathfinder V5 product providing temporal monthly averages as a result of the reanalysis of older AVHRR data and (ii) MODIS/AQUA, derived from the MODIS IR channels using two channels in either the thermal IR (11–12 μm) or the mid-IR region (3.8–4.1 μm)



SST water masses fronts

Geostrophic currents: Geostrophic velocity anomalies derived from AVISO altimeter information were used, specifically absolute dynamic topography products for both Mediterranean region and global extent. Sea currents alter short wave patterns mainly in areas where currents interact (e.g., gyres, current shears, and eddies) by accumulating surfactants on certain areas of the converging/diverging waters. The approach intended to identify sea current fronts where their interaction might yield the generation of dark patches



13.5 SUMMARY AND CONCLUSIONS

In this chapter, the possibility of detecting and tracking oil spills by satellite remote sensing means has been illustrated from both theoretical and technical points of view. We tried to describe the scientific process, which is, still today,

attempting to continuously and progressively enhance the reliability of space imagery in identifying oil spills at sea. The starting point is an in-depth and sound theoretical analysis of the chemical–physical mechanisms governing the effects of an oil film over the sea surface and specifically the “appearance” of the oil film in different regions of the

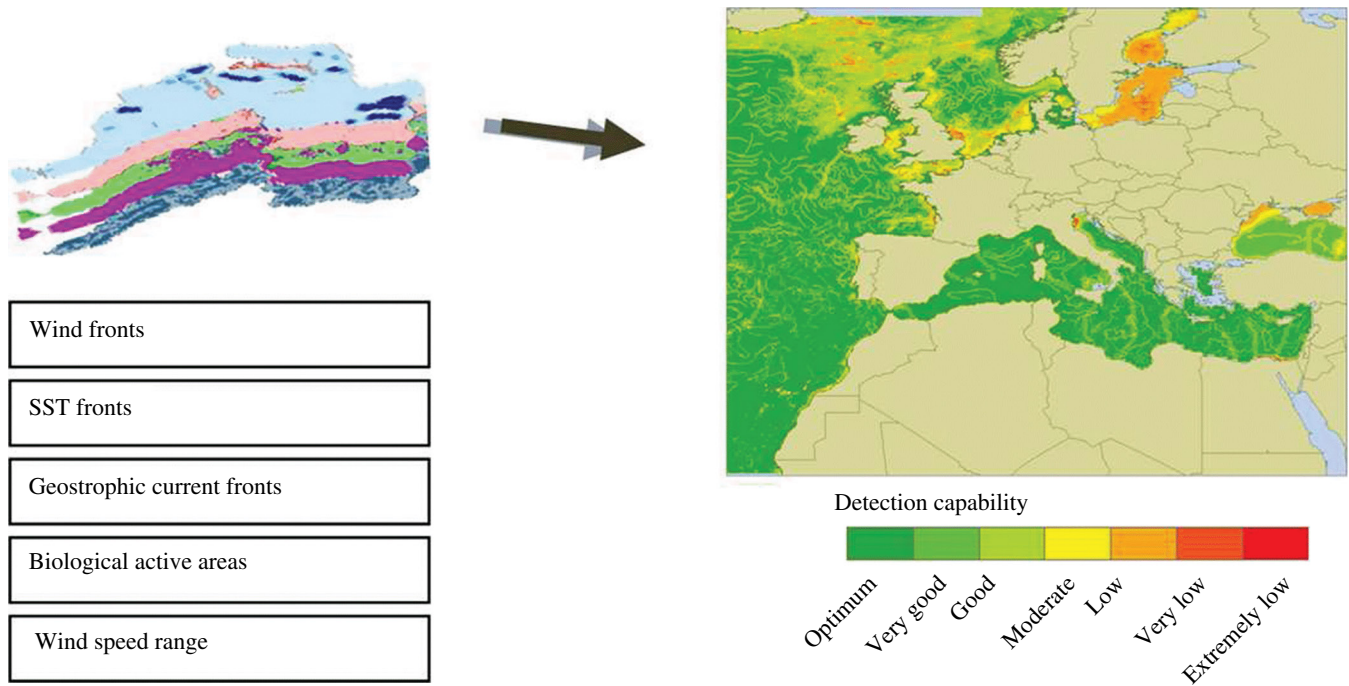


FIGURE 13.11 Integrated detection capability estimations example performed for the month of July.

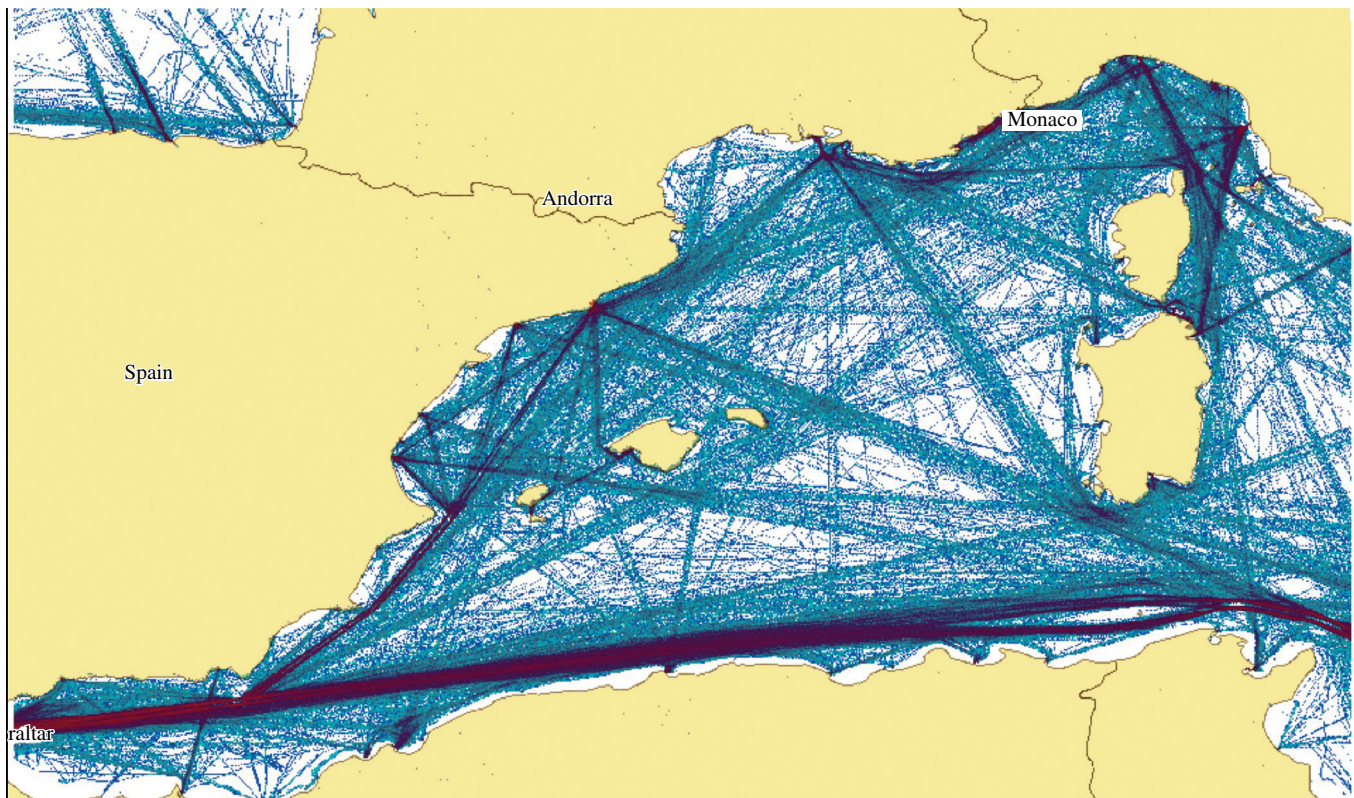


FIGURE 13.12 Risk of pollution estimation layouts and density of vessel traffic.

electromagnetic spectrum. We reported the main results of some studies and activities trying to validate the use of SAR imagery, by searching for those image features that may be the indication of the presence of an oil film. Then the

potential advantages of integrating ancillary data, that is, the diverse meteorological and oceanographic phenomena, which have also an impact on the appearance of the sea surface in SAR images, were discussed. Finally, we made

reference to the integration with cooperative ship reporting systems data, which is a new element to further enhance the value of space imagery for operational use.

In the beginning, optical remote sensing on oil spill detection was also introduced. Oil and its characteristic spectral signature can be detected using optical sensors onboard satellites. Main restrictions are the daylight, the absence of clouds, the desired resolution, and the availability of the observations at the necessary wavelengths. It is important to underline the potentiality to retrieve information on oil type and thickness from the optical contrast. The NASA's MODIS shows strong potential for marine oil spill monitoring providing two 250 m resolution bands, two daily acquisitions, NRT data, and data freely available. The potential of MODIS data was clearly shown by the Lebanon case study. In total, 92 MODIS L0 images (raw data) have been collected, processed, displayed, and visually analyzed. Out of the sample, about 20% of the images were discarded because of complete cloud coverage of the area of interest. Suspected features were detected in at least one band in more than 40% of the cases. The Lebanon successful story has shown the need for using more spectral bands. Therefore, the opportunity to use hyperspectral remote sensing for oil spill detection appears promising. Two civil spaceborne hyperspectral sensors exist, that is, NASA's EO-1 Hyperion sensor and ESA's PROBA CHRIS sensor, and they may provide suitable data for carrying out additional systematic investigations.

The larger part of the chapter is devoted to remote sensing of oil spills through SAR sensors operating in the microwave part of the electromagnetic spectrum. The theory of microwave remote sensing of oil film is described with a direct reference to satellite sensors. This leads to the identification and detailed description of three different detection methodologies, that is, the manual, the semiautomatic, and the fully automatic approach. For the manual approach, the experience of the image analyst to evaluate the shape and size of spills was found to be crucial. For the other two methodologies, their four main steps were clearly described: (1) detection and isolation of all dark patches in the image, (2) extraction of statistical parameters of the detected features, (3) test of the extracted values against predefined statistical values, and (4) classification of dark formations as oil spills or look-alikes. The first step is fundamental in oil spill detection systems since a possible loss in that stage leads directly to misclassification. Features extraction is still an open research area because in the bibliography there is no clearly identified necessary number of features and their contribution to the final classification. The comparison of the extracted features against predefined values in the third step requires databases containing ground truth data. Those data should be based on the analysis of verified oil spills or look-alikes, for example, by airborne and shipborne observations and/or direct sampling. National authorities or international agencies may play a central role by providing standard bulk data for training and testing, as

EMSA has started to do in Europe. Finally, classification systems should be compared with standard databases and a central mechanism should apply on their sustainability at operational stage. Future directions could be the creation of standard databases with verified oil and look-alike cases, as well as, a common procedure check for operational use.

The next sections deal with the historical aspects of oil spill detection, including a specific application to monitor the trend of the problem of illicit discharges on the long term, which lead to the operational services. At the beginning of 1990s, it was noted that over certain areas, such as the Mediterranean Sea, data from regular aerial surveillance were unavailable. Therefore, satellites represented the only possible source of observations to try to estimate the dimension of the problem due to operational illegal spilling from vessels. The availability of a quite large volume of archived SAR images for several years made also possible to analyze trends for the problem. However, using historical data was not possible to confirm results with other means so that the detections have to be considered as possible rather than validated oil spills. The Joint Research Center (JRC) of the European Commission has pioneered this kind of systematic mapping over the Mediterranean Sea. The data type used in these studies was mainly calibrated by low-resolution imagery with a spatial resolution (pixel) of about 200 m. The main products were image coverage maps, point-like maps with the detected possible spills, and possible oil spill density maps derived by merging the information from the two previous maps. Those first studies concluded that the spill distribution appears to be highly correlated with the major shipping routes and hot spots, that is, highly spilling concentrations are the Ionian Sea, the Adriatic Sea, the Messina Straits, the Sicily Channel, the Ligurian Sea, the Gulf of Lion, and the East of Corsica. The next substantial step forward for the operational use of space imagery came with the AESOP project, an operational system based on the use of NRT spaceborne imagery to support and integrate aerial surveillance in the detection of oil pollution and in the monitoring of main shipping routes in the Mediterranean region. The Adriatic Sea was selected as the study area, and the summer months were selected as the test period. In several cases, possible spills were detected from the satellite images, and they were verified by the aerial surveillance. During the AESOP project, pros and cons of synergetic use of airborne coverage and satellite coverage for operational use were for the first time reported.

The last part of the chapter addresses the possible use of ancillary data in the detection loop. In fact, ancillary data could be proven helpful in identifying phenomena, which yield reduced backscatter patterns on SAR imagery. Those phenomena could be man related, atmospheric, oceanographic, or natural/biological. Ancillary data were integrated into the detection loop through two relevant concepts: detection capability and risk of pollution. Detection capability refers to an estimation of the appearance of look-alike features based on the analysis of relevant data sets over the

imaged area, while risk of pollution associated to a specific area can be thought of as a measure of the likelihood of observing oil spill occurrences.

Nowadays, in Europe, oil spill detection based on satellite SAR systems has become an operational service managed by the European Maritime Safety Agency (EMSA). EMSA has developed the CleanSeaNet service (<http://emsa.europa.eu/operations/cleanseanet.html>), which provides NRT alerts of oil spill occurrences based on SAR images. EMSA's service already integrates vessel positioning systems and ancillary data, providing situational awareness and drifting prediction capabilities. Importantly, it is linked to the national oil pollution surveillance and response chains. Responsible national authorities may then use airborne or naval assets to go on the spot, verify the possible slick, and provide a feedback. It can be concluded that operational service is a fact and can be successfully applied to other areas. The actual service may be certainly improved by integrating additional observations as soon as new sensors and platforms will be considered mature enough for operational use, for example, unmanned aerial vehicles (UAV). However, it has to be stressed as the operational system in place may change dramatically the situation by providing a large amount of validated observations to be fed into the detection process as described earlier. In addition, a systematic approach to better define the oil spill validation procedure should be initiated.

The second aspect that will be certainly further developed in the future is the integration of satellite observations and vessel positional data from cooperative reporting systems (e.g., AIS, L-RIT, satellite AIS, and coastal radar tracks). In such a way, it is possible to partially overcome the inability of SAR sensors to identify the pollution culprit. To enhance the capabilities of connecting an identified ship to an oil spill event shall raise the deterrent effect of the detection since it can be thought of as a relevant factor for follow-up activities concerning the prosecution of potential polluters.

Finally, it can be concluded that from an operational point of view, spaceborne SAR is today a fundamental element, in combination with airborne/shipborne tools and metocean/contextual data, at continental scales, to detect/identify oil spills and identify the responsible vessel.

REFERENCES

- [1] Brekke, C. and A.H.S. Solberg, Oil spill detection by satellite remote sensing, *Remote Sens. Environ.*, 95, 1–13, 2005.
- [2] Fingas, M. and C.E. Brown, Review of oil spill remote sensing, *Spill Sci. Technol. Bull.*, 4, 199–208, 1997.
- [3] Vespe, M., M. Posada Sanchez, E.C. Ferraro Di Silvi, B. Bulgarelli, H. Van Wimersma Greidanus, and S. Djavidnia, Oil spill detection based on SAR and Metocean/Contextual Data Fusion. In *Conference Proceedings: 33rd International Symposium on Remote Sensing of Environment*, Stresa, Lago Maggiore, Italy, pp. 862–865, 2009.
- [4] Hu, C., F.E. Mueller-Krager, C.J. Taylor, D. Myhre, B. Murch, A.L. Odriozola, et al., MODIS detects oil spills in Lake Maracaibo, Venezuela, *EOS Trans. Am. Geophys. Union*, 84 (33), 313–319, 2003.
- [5] Byfield, V. and S. Boxall, Thickness estimated and classification of surface oil using passive sensing at visible and near-infrared wavelength. In *Proceedings of the IEEE International Geoscience and Remote Sensing Symposium*, Hamburg, Germany, 1999.
- [6] Mullins, O.C., S. Mitra-Kirtley, and Y. Zhu, The electronic absorption edge of petroleum, *Appl. Spectrosc.*, 46 (9), 1405–1411, 1992.
- [7] Downare, T.D. and O.C. Mullins, Visible and near-infrared fluorescence of crude oils, *Appl. Spectrosc.*, 49 (6), 754–764, 1995.
- [8] Wang, X. and O.C. Mullins, Fluorescence lifetime studies of crude oils, *Appl. Spectrosc.*, 48 (8), 977–984, 1994.
- [9] Otremba, Z. and J. Piskozub, Modeling the optical contrast of an oil on a sea surface, *Opt. Express*, 9 (8), 411–416, 2001.
- [10] Otremba, Z. and J. Piskozub, Modeling the remotely sensed optical contrast caused by oil suspended in the sea water column, *Opt. Express*, 11 (1), 2–6, 2002.
- [11] Otremba, Z. and J. Piskozub, Modeling the bidirectional reflectance distribution function (BRDF) of seawater polluted by an oil film, *Opt. Express*, 12 (8), 1671–1676, 2004.
- [12] Baith, K., R. Lindsay, G. Fu, and C.R. McClain, SeaDAS, a data analysis system for ocean-color satellite sensors, *EOS Trans. Am. Geophys. Union*, 82, 202, 2001.
- [13] Tarchi, D., J. Fortuny, G. Ferraro, S. Meyer-Roux, O. Muellenhoff, K. Topouzelis, et al., The use of satellite imagery during the pollution crisis in Lebanon. In *Workshop on Monitoring Activities Related to the Oil Pollution in Lebanon*, EUR 22531 EN, Ispra, Italy, pp. 37–47, 2006.
- [14] Alpers, W. and H. Huhnerfuss, The damping of ocean waves by surface films: A new look at an old problem, *J. Geophys. Res.*, 94, 6251–6265, 1989.
- [15] Donelan, M.A. and W.J. Pierson, Jr, Radar scattering and equilibrium ranges in wind-generated waves with application to scatterometry, *J. Geophys. Res.*, 92, 4971–5029, 1987.
- [16] Pavlakis, P., Investigation of the potential of ERS-1/2 SAR images for monitoring oil spills on the sea surface, HCM Post Doctoral Fellowship Final Report, Catalogue: CL-NA-16351-EN-C, EUR 16351 EN, pp. 65, 1995.
- [17] Bern, T.-I., T. Wahl, T. Anderssen, and R. Oslen, Oil spill detection using satellite based SAR: Experience from a field experiment. In *Proceedings of the First ERS-1 Symposium—Space at the Service of our Environment*, Cannes, France, pp. 4–6, 1992.
- [18] Wahl, T., A. Skely, and J. Pedersen, Practical use of ERS-1 SAR images in oil pollution monitoring. In *Proceedings of the International Geoscience and Remote Sensing Symposium (IGARSS'94)*, Vol. 4 (IEEE), Piscataway, NJ, pp. 1954–1956, 1994.
- [19] Wright, J.W., A new model for sea clutter, *IEEE Trans. Antennas Propag.*, 16, 217–223, 1968.
- [20] Valenzuela, G.R., Theories for the interaction of electromagnetic and oceanic waves—a review, *Boundary Layer Meteorol.*, 13, 61–85, 1978.

- [21] Wismann, V.R., W. Theis, W. Alpers, and H. Huhnerfuss, The damping of short gravity-capillary waves by experimental sea slicks measured by a multifrequency microwave scatterometer. In *Proceedings of OCEANS 93*, Vol. II (New York, IEEE), Victoria, BC, pp. 342–347, 1993.
- [22] Singh, K.P., A.L. Gray, R.K. Hawkins, and R.A. O’Neil, The influence of surface oil on C-band and K-band ocean backscatter, *IEEE Trans. Geosci. Remote Sens.*, 24, 738–744, 1986.
- [23] Alpers, W. and H. Huhnerfuss, Radar signatures of oil films floating on the sea surface and the Marangoni effect, *J. Geophys. Res.*, 93, 3642–3648, 1988.
- [24] Wismann, V.M., M. Gade, W. Alpers, and H. Huhnerfuss, Radar signatures of marine mineral oil spills measured by an airborne multi-frequency radar, *Int. J. Remote Sens.*, 19 (18), 3607–3623, 1988.
- [25] Gade, M., W. Alpers, H. Huhnerfuss, V.R. Wismann, and P.A. Lange, On the reduction of the radar backscatter by oceanic surface films: Scatterometer measurements and their theoretical interpretation, *Remote Sens. Environ.*, 66, 52–70, 1998.
- [26] Topouzelis, K., Oil spill detection by SAR images: Approaches and algorithms, *Sens. J.*, 8, 6642–6659, 2008.
- [27] MacDonald, I.R., M. Smith, and F.W. Huffer, Community structure comparisons of lower slope hydrocarbon seeps, northern Gulf of Mexico, *Deep Sea Res. Part II: Top. Stud. Oceanogr.*, 57 (21–23), 1904–1915, 2010.
- [28] Pavlakis, P., D. Tarchi, and A. Sieber, On the monitoring of illicit vessel discharges using spaceborne SAR remote sensing—a reconnaissance study in the Mediterranean sea, *Ann. Télécommun.*, 56 (11–12), 700–718, 2001.
- [29] Solberg, A., G. Storvik, R. Solberg, and E. Volden, Automatic detection of oil spills in ERS SAR images, *IEEE Trans. Geosci. Remote Sens.*, 37, 1916–1924, 1999.
- [30] Fiscella, B., A. Giancaspro, F. Nirchio, and P. Trivero, Oil spill detection using marine SAR images, *Int. J. Remote Sens.*, 21, 3561–3566, 2000.
- [31] Nirchio, F., M. Sorgente, A. Giancaspro, W. Biamino, E. Parisato, R. Ravera, et al., Automatic detection of oil spills from SAR images, *Int. J. Remote Sens.*, 26 (6), 1157–1174, 2005.
- [32] Solberg, A., C. Brekke, and P.Q. Husoy, Oil spill detection in Radarsat and Envisat SAR images, *IEEE Trans. Geosci. Remote Sens.*, 45, 746–755, 2007.
- [33] Karathanassi, V., K. Topouzelis, P. Pavlakis, and D. Rokos, An object-oriented methodology to detect oil spills, *Int. J. Remote Sens.*, 27, 5235–5251, 2006.
- [34] Del Frate, F., A. Petrocchi, J. Lichtenegger, and G. Calabresi, Neural networks for oil spill detection using ERS-SAR data, *IEEE Trans. Geosci. Remote Sens.*, 5, 2282–2287, 2000.
- [35] Kanaa, T.F.N., E. Tonye, G. Mercier, V.P. Onana, J.M. Ngono, P.L. Frison, et al., Detection of oil slick signatures in SAR images by fusion of hysteresis thresholding responses. In *Proceedings of the IEEE International Geoscience and Remote Sensing Symposium (IGARSS’03)*, Vol. 4, Toulouse, France, pp. 2750–2752, July 21, 2003.
- [36] Canny, J., A computational approach to edge detection, *IEEE Trans. Pattern Anal. Mach. Intell.*, 8, 679–698, 1986.
- [37] Huang, B., H. Li, and X. Huang, A level set method for oil slick segmentation in SAR images, *Int. J. Remote Sens.*, 26, 1145–1156, 2005.
- [38] Liu, A.K., C.Y. Peng, and S.Y.S. Chang, Wavelet analysis of satellite images for coastal watch, *IEEE J. Ocean. Eng.*, 22, 9–17, 1997.
- [39] Wu, S.Y. and A.K. Liu, Towards an automated ocean feature detection, extraction and classification scheme for SAR imagery, *Int. J. Remote Sens.*, 24, 935–951, 2003.
- [40] Araujo, R., F. De Medeiros, R. Costa, R. Marques, R. Moreira, and J. Silva, Locating oil spill in SAR images using wavelets and region growing, *Lect. Note Comput. Sci.*, 3029, 1184–1193, 2004.
- [41] Derrode, S. and G. Mercier, Unsupervised multiscale oil slick segmentation from SAR images using a vector HMC model, *Pattern Recognit.*, 40, 1135–1147, 2007.
- [42] Benelli, G. and A. Garzelli, Oil-spills detection in SAR images by fractal dimension estimation. In *Proceedings of the IEEE International Geoscience and Remote Sensing Symposium (IGARSS’99)*, Vol. 1, Hamburg, Germany, pp. 218–220, June 28–July 2, 1999.
- [43] Marghany, M., M. Hashim, and A.P. Cracknell, Fractal dimension algorithm for detecting oil spills using RADARSAT-1 SAR. In *International Conference on Computational Science and Its Applications 2007, Lecture Notes in Computer Science*, Vol. 4705, Part I, Gervasi, O. and Gavrilova, M. (Eds.), Springer-Verlag: Berlin/Heidelberg, pp. 1054–1062, 2007.
- [44] Marghany, M., RADARSAT automatic algorithms for detecting coastal oil spill pollution, *Int. J. Appl. Earth Obs. Geoinf.*, 3, 191–196, 2001.
- [45] Marghany, M., RADARSAT for oil spill trajectory model, *Environ. Model. Softw.*, 19, 473–483, 2004.
- [46] Stathakis, D., K. Topouzelis, and V. Karathanassi, Large-scale feature selection using evolved neural networks. In *Proceedings of SPIE, Image and Signal Processing for Remote Sensing XII*, Bruzzone, L. (Ed.), SPIE Bellingham Wash. ETATS-UNIS: Stockholm, Sweden, p. 6365, September 13–14, 2006.
- [47] Keramitsoglou, I., C. Cartalis, and C. Kiranoudis, Automatic identification of oil spills on satellite images, *Environ. Model. Softw.*, 21, 640–652, 2006.
- [48] Topouzelis, K., D. Stathakis, and V. Karathanassi, Investigation of genetic algorithms contribution to feature selection for oil spill detection. *Int. J. Remote Sens.*, 30 (3), 611–625, 2009.
- [49] Migliaccio, M. and M. Tringaglia, Oil spill observation by SAR: A review. In *US-Baltic International Symposium*, Klaipeda, Lithuania, June 14–17, 2004.
- [50] Montali, A., G. Giancinto, M. Migliaccio, and A. Gambardella, Supervised pattern classification techniques for oil spill classification in SAR images: Preliminary results. In *SEASAR2006 Workshop, ESA-ESRIN*, Frascati, Italy, January 23–26, 2006.
- [51] Topouzelis, K., V. Karathanassi, P. Pavlakis, and D. Rokos, Detection and discrimination between oil spills and look-alike phenomena through neural networks, *ISPRS J. Photogramm. Remote Sens.*, 62, 264–270, 2007.
- [52] Garcia-Pineda, O., B. Zimmer, M. Howard, W. Pichel, X. Li, and I. MacDonald, Using SAR images to delineate ocean oil slicks with a texture-classifying neural network algorithm (TCNNA), *Can. J. Remote Sens.*, 35 (5), 1–11, 2009.

- [53] Kubat, M., R.C. Holte, and S. Matwin, Machine learning for the detection of oil spills in satellite radar images. *Mach. Learn.*, 2–3, 195–215, 1998.
- [54] Topouzelis, K., A. Bernardini, G. Ferraro, S. Meyer-Roux, and D. Tarchi, Satellite mapping of oil spills in the Mediterranean Sea, *Fresen. Environ. Bull.*, 15, 10091–100914, 2006.
- [55] Gade, M. and J.M. Redondo, Marine pollution in European coastal waters monitored by the ERS-2 SAR: A comprehensive statistical analysis. In *Proceedings of the IEEE International Geoscience and Remote Sensing Symposium (IGARSS'99)*, Vol. 3, Hamburg, Germany, pp. 1637–1639, 1999.
- [56] Vespe, M. and H. Greidanus, SAR image quality assessment and indicators for vessel and oil spill detection, *IEEE Trans. Geosci. Remote Sens.*, 50 (11), 4726–4734, 2012.
- [57] Brooks, S.R. and P.F. Miller, The influence of radiometric resolution on synthetic aperture radar design parameters. In *ESA ESASAT Workshop*, ESA SP-154, pp.79–85, 1979.
- [58] Kim, D.-J., W.M. Moon, and Y.-S. Kim, Application of TerraSAR-X data for emergent oil-spill monitoring, *IEEE Trans. Geosci. Remote Sens.*, 48 (2), 852–863, 2010.
- [59] Unal, C.M.H., P. Snoeij, and P.J.F. Swart, The polarization-dependent relation between radar backscatter from the ocean surface and surface wind vector at frequencies between 1 and 18 GHz, *IEEE Trans. Geosci. Remote Sens.*, 29 (4), 621–626, 1991.
- [60] Furevik, B., T. Hamre, M. Babiker, K. Kloster, and R. Elisassen, *Operators Manual for Slick Analysis in SAR Images*, NERSC Special Report, NERSC, No. 75, 2005.
- [61] Vespe, M., M. Posada, G. Ferraro, and H. Greidanus, Data fusion of SAR derived features and ancillary information for automatic oil spill detection, *Fresen. Environ. Bull.*, 20 (1), 36–43, 2011.
- [62] Ferraro, G., B. Baschek, G. de Montpellier, O. Njoten, M. Perkovic, and M. Vespe, On the SAR derived alert in the detection of oil spills according to the analysis of the EGEMP, *Mar. Pollut. Bull.*, 60 (1), 91–102, 2010.
- [63] Price, J.M., M. Reed, M.K. Howard, W.R. Johnson, Z. Ji, C.F. Marshall, et al., Preliminary assessment of an oil-spill trajectory model using a satellite-tracked, oil-spill-simulating drifter, *Environ. Model. Softw.*, 21, 258–270, 2006.
- [64] Olita, A., A. Cucco, S. Simeone, A. Ribotti, L. Fazioli, B. Sorgente, et al., Oil spill hazard and risk assessment for the shorelines of a Mediterranean coastal archipelago, *Ocean Coast. Manag.*, 57, 44–52, 2012.
- [65] Sotillo, M.G., E. Alvarez Fanjul, S. Castanedo, A.J. Abascal, J. Menendez, R. Olivella, et al., Towards an operational system for oil spill forecast in the Spanish waters: Initial developments and implementation test, *Mar. Pollut. Bull.*, 56 (4), 686–703, 2008.
- [66] Kvenvolden, K.A. and J.W. Harbaugh, Reassessment of the rates at which oil from natural sources enters the marine environment, *Mar. Environ. Res.*, 10 (4), 223–243, 1983.
- [67] Wilson, R.D., P.H. Monaghan, A. Osanik, L.C. Price, and M.A. Rogers, Natural marine oil seepage, *Science*, 184 (4139), 857–865, 1974.
- [68] Clayton, C.J., M.D. Lines, and S.J. Hay, *Leakage and Seepage, an Explorer's Guide: BP Internal Report*, Robertson Research International, p. 65, 1991.
- [69] Williams, A. and G. Lawrence, The role of satellite seep detection in exploring the South Atlantic's ultradeep water. In *Surface Exploration Case Histories: Applications of Geochemistry, Magnetism and Remote Sensing*, Schumacher, D. and LeSchack, L.A. (Eds.), AAPG Studies in Geology No. 48 and SEG Geophysical References Series No. 11, pp. 327–344, 2002.
- [70] Holt, B., SAR imaging of the ocean surface. In *Synthetic Aperture Radar Marine User's Manual*, Jackson, C. and Apel, J. (Eds.), National Oceanic and Atmospheric Administration/ US Department of Commerce: Washington, DC, pp. 25–79, September 2004.
- [71] Ferraro, G., A. Bernardini, M. David, S. Meyer-Roux, O. Muellenhoff, M. Perkovic, et al., Towards an operational use of space imagery for oil pollution monitoring in the Mediterranean basin: A demonstration in the Adriatic Sea, *Mar. Pollut. Bull.*, 54, 403–422, 2007.
- [72] Amato, E. and F. Cabioch, DEEPP project—database for potentially polluting wrecks within the Mediterranean Cetacean Sanctuary, *D.G. Environment, Civil Protection Unit*. Contract n° 07.030900/2004/395842/SUB/A5, 2007.
- [73] Deluca, M. and L. Leblanc, Offshore forecast—1998, *Offshore Magazine*, December 1997.

DETECTION OF OIL IN, WITH, AND UNDER ICE AND SNOW

MERV FINGAS¹ AND CARL E. BROWN²

¹*Spill Science, Edmonton, Alberta, Canada*

²*Emergencies Science and Technology Section (ESTS), Environment Canada, Ottawa, Ontario, Canada*

14.1	Introduction	385
14.2	Overview of Detection of Oil in or under Ice and Snow	385
14.2.1	Optical Methods	386
14.2.2	Acoustic Methods	386
14.2.3	Radio-Frequency Methods	389
14.2.4	Ground-Penetrating Radar	390
14.2.5	UHF Radiometer	391
14.2.6	Nuclear Techniques	391
14.2.7	Gas Sniffing and Leak Detection	391
14.2.8	Nuclear Magnetic Resonance	392
14.3	Detection of Surface Oil with Ice: Conventional Techniques	392
14.4	Conclusions	392

14.1 INTRODUCTION

Public scrutiny demands that the location and extent of oil spills be identified. Through the use of modern remote sensing instrumentation, oil can be monitored on the open ocean during most times and conditions. With a knowledge of slick locations and movement, response personnel can more effectively plan countermeasures in an effort to lessen the effects of the pollution. In the Arctic, detection is complicated by the presence of ice, and in many situations, there are no technologies to detect oil.

This paper reviews the technology and gives the general state of developments in the field when oil is in or under ice or snow. Of course, the situation is much more difficult when oil is in or under ice, with only a few technologies showing promise for detecting oil in these conditions. It is important to consider the specific types of oil in ice that one is discussing. This book contains a separate section on ice definitions [1].

Several general reviews of oil spill remote sensing in open water situations have been published [2,3]. These

reviews show progress and indicate that oil spill remote sensing is at a relatively good state of the art in open waters or where some ice might be present. This chapter will also review the state of the art of oil-in-ice detection. While some reviews of the detection of oil in and with ice have been published, all point out that the state of the art is significantly behind that for detecting oil on open water [4–9].

14.2 OVERVIEW OF DETECTION OF OIL IN OR UNDER ICE AND SNOW

The difficulties in detecting oil in or under ice or snow are numerous. Ice is always a heterogeneous material and incorporates air, sediment, salt, and water, many of which may present false oil-in-ice signals to the detection mechanisms. In addition, snow on top of the ice or even incorporated into the ice adds complications. During freeze-up and thaw in the spring, there may not be distinct layers of water and ice. There are many different types of ice and different ice crystalline orientations. Snow is also somewhat heterogeneous and may consist of several layers with different densities. Furthermore, oil may penetrate snow easily and thus move to the subsurface of the snow, which may be ice or soil.

The feasibility of various technologies for detecting oil in ice was extensively reviewed by Gill [4]. Based on this feasibility study, some of the technologies were tried on oil under ice in a test tank [10,11]. This led to the pursuit of acoustic technologies, which were taken as far as the field testing of a prototype. Many of the other technologies have not been tried since. Much of the literature on the topic is now three decades old. Lately, reassessments of oil-in-ice technologies have taken place and some of these subjected to both controlled laboratory and field testing [7,8]. With this

arise some new potential technologies; however, most of these will require more research and development before they become field tools.

14.2.1 Optical Methods

Over the years, many researchers have suggested that one might use the transparency of some ices to detect oils. Unfortunately, in reality, ice in the field is rarely transparent because of the incorporation of salt, air, and sediment. Often, snow is on top of ice. The use of most optical methods is highly restricted by the impurities in ice [4].

Rice University studied the detection of oil under ice using fluorescence techniques [12]. This study indicated that fluorescence signals from oil could be distinguished from natural background signals through 22 cm of ice. The tests were performed using perfect samples of ice and would not be applicable to normal sea ice, which would not transmit the UV signal.

Moir and Yetman studied oil fluorescence under artificially grown ice, both freshwater and saltwater [13]. A gated strobe lamp was used as the transmitter. Visual observation through goggles was the prime detection means. The detection limit was about 80 cm for freshwater ice and about 60 cm for sea ice. Laidley used a CO_2 laser operating at $10.6\mu\text{m}$ to heat oil encased in ice [14]. While preliminary results showed that oil might be detectable by this method, it was not pursued. Goncharov and Lyskov performed the theoretical analysis of using a laser at 510 and 578 nm to activate fluorescence in oil under ice [15]. They concluded that a 30 and 22 kW laser would suffice to penetrate the ice and fluoresce the oil.

The end result of all these studies is that actual sea ice is never transparent and there are doubts that any of these optical techniques would work.

14.2.2 Acoustic Methods

Sound or acoustic waves can be viewed as consisting of two types: compressive or longitudinal waves and transverse waves. A transverse wave is a moving wave that consists of oscillations perpendicular to the direction of travel. Longitudinal waves propagate by means of compression and decompression in the direction of travel. Longitudinal waves are waves that have the same direction of vibration as their direction of travel. These two types have different movements in ice as will be described later.

The acoustical properties of ice are variable. Figures 14.1 and 14.2 show the temperature dependencies of the speed of different sound waves through ice (after Gill [4]). It should be noted that compressive waves travel almost three times as rapidly as transverse waves, although the speed varies significantly with the type of ice. The attenuation of acoustic waves is also affected by ice type as shown in Figure 14.2. This shows that the sound is strongly attenuated with increasing salinity and increasing frequency. A frequency of

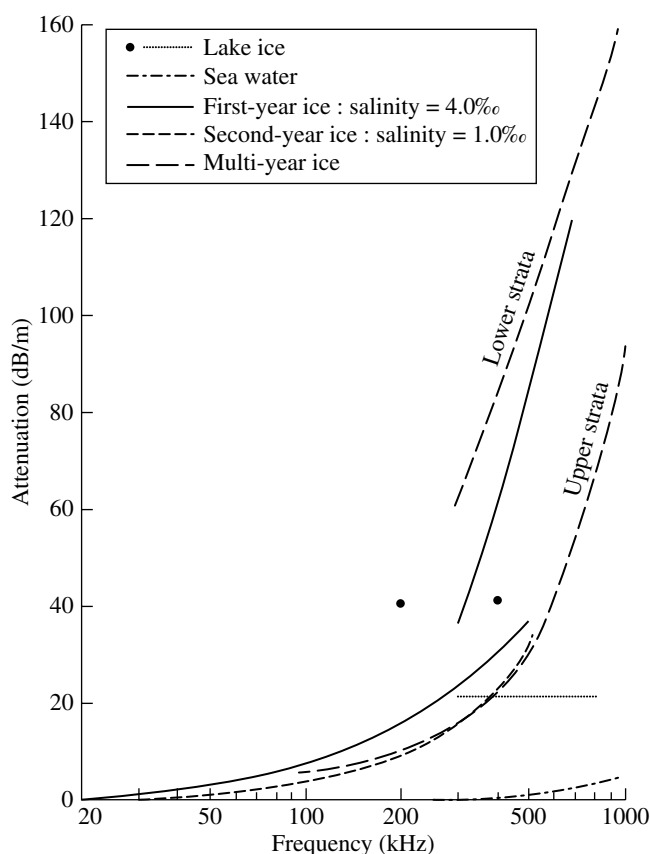


FIGURE 14.1 The attenuation of acoustic compressive waves with temperature. This figure shows that above about 200 kHz, the attenuation is very high and therefore high frequencies cannot be used to penetrate ice. Upper strata salinity = 0.19‰ and lower strata salinity = 3.01‰ (after Gill [4]).

about 200 kHz is about the maximum usable with typical multiyear ice. The salinity of the ice is also a factor. Figure 14.3 shows how the speed of compressive and transverse waves varies with the salinity of the ice [4]. In summary, the speed of the wave is decreased as the salinity rises. The acoustic impedance of air and different types of ice vary and are shown in Table 14.1.

Experimenters quickly found that standard acoustic units designed for metal and concrete inspection could be used for oil-in-ice detection [10,11]. Initially, this was a surprise because the attenuation of ice and the source of the reflected signal for oil were not readily apparent from the data. Figure 14.4 shows a typical return of oil under ice using a standard ultrasound detector. Subsequent studies have shown that the physics of sound/oil interaction is relatively simple. There are two sources of signals from oil in or under ice. First, oil reflects the standard compressive (p) wave and this signal is received by standard acoustic units just like the interfaces in metal or other building materials. But oil behaves acoustically like a non-Newtonian fluid and will also reflect the shear or (s) wave (also called the transverse wave). The s-waves travel at about half to one-third the velocity of the

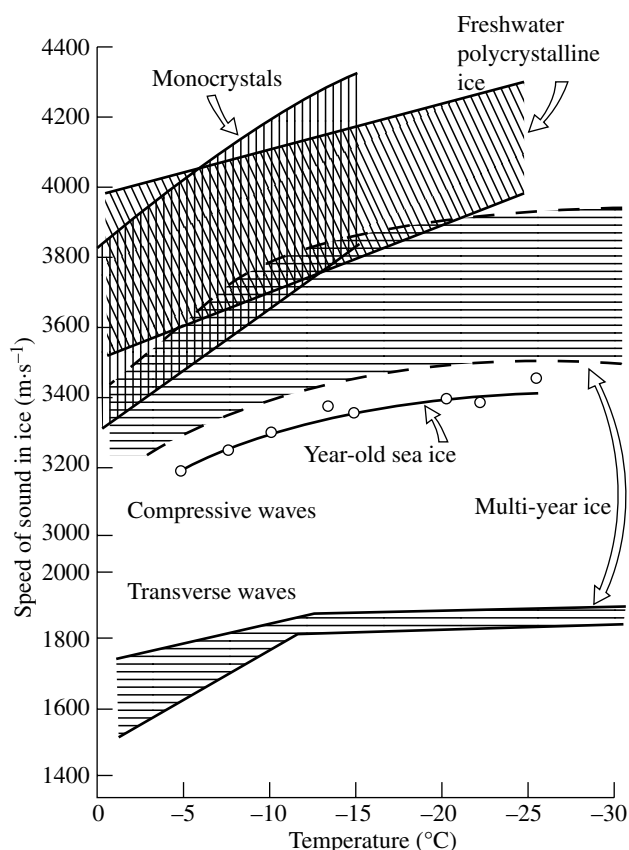


FIGURE 14.2 The temperature dependencies of the propagation of acoustic waves through ice. Note that compressive waves move about three times faster than transverse waves (after Gill [4]).

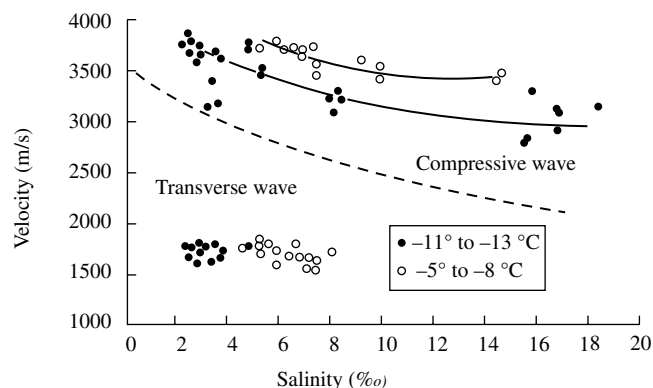


FIGURE 14.3 The variation of acoustic velocity with salinity. As salinity rises, the speed of the acoustic waves slows (after Gill [4]).

TABLE 14.1 Acoustic impedance of materials^a

	Impedance
Air	43
Ice	300,000
Oil	119,000
Water	148,300

^aFrom Ref. 6.

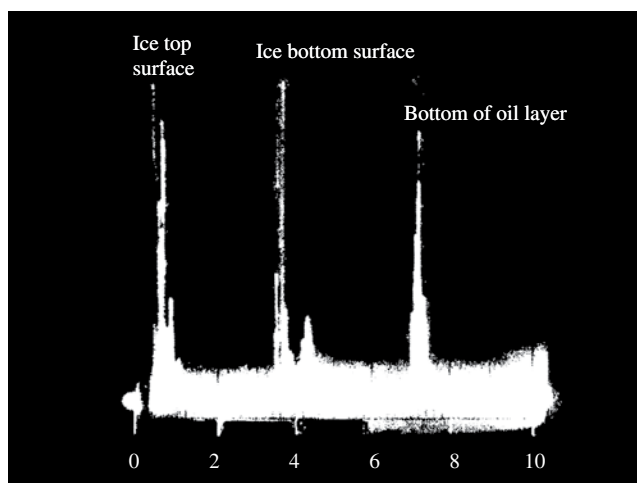


FIGURE 14.4 Photograph of a screen of an ultrasonic detector. The peaks are annotated as to their origin. This method clearly shows the bottom of the ice layer and the bottom of the oil layer. As this was carried out in a test tank, the values could be verified by physical measurement.

compressive waves and can be distinguished by their time delay. One could develop a more discriminating oil-in-ice detector by developing a unit that selectively detected shear waves. In theory, only sediment would propagate similar shear waves.

Jones and Kwan [16,17] and Jones et al. [18,19] studied the problem and developed a detection device consisting of a phased array detector that was capable of detecting transverse or shear waves directly and thus determining whether oil was present, with a high factor of reliability. Jones et al. found that acoustic detection of oil was possible because oil behaves as a solid in acoustic terms and transmits a shear wave [18,19]. Furthermore, there is an angular dependence to these phenomena, and it can be used to distinguish between the many possible interferences in ice, such as air bubbles, and oil. Laboratory tests were conducted and a consortium of Environment Canada with Imperial Oil and the Technical University of Nova Scotia developed the acoustic means to the point of developing a field prototype unit and testing this unit. The prototype was built and tested at Norman Wells and in the Canadian Beaufort Sea. Figures 14.5, 14.6, 14.7, 14.8, 14.9, and 14.10 show facets of this test.

Knudsen studied the acoustic and electric properties of transducers and the coupling to ice [20]. Goodman et al. reviewed the technology and noted the differences in using low and high acoustic frequency, the latter yielding better spatial resolution, but with lower penetration capability [21].

The studies above show that acoustic means of detecting oil under ice show potential. Unfortunately, these technologies were not commercialized or developed further. Part of this may be due to their large logistical requirements in the field.



FIGURE 14.5 The location of the oil-under-ice test in the Beaufort Sea.

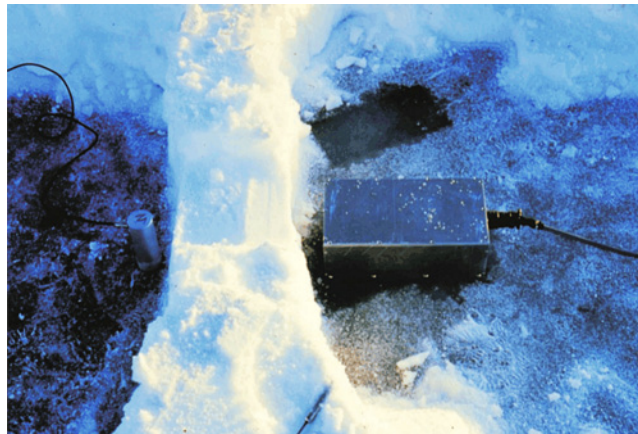


FIGURE 14.8 Another transducer array used to test for the presence of oil under this ice. This array is experimental and provides both angular and directional view of the under-ice surface.



FIGURE 14.6 Divers preparing to place oil under ice during a test of the acoustic oil-under-ice detector in the Beaufort Sea.



FIGURE 14.9 The back of the acoustic oil-under-ice detector. The wires go to the transducers.



FIGURE 14.7 A transducer array used to test for the presence of oil under this ice. This array is experimental and provides an angular and directional view of the under-ice surface.



FIGURE 14.10 The panel of the prototype acoustic oil-under-ice detector showing an oil detection. This is during a test in the Beaufort Sea.

14.2.2.1 Underwater Acoustic Methods Underwater acoustic measurements of the ice/water surface have taken place for many years and are a prime method for determining under-ice roughness [22]. This method may also be useful for oil under ice as it has been suggested that the oil/water and oil/ice interfaces may be detectable and also that the oil would change the underwater ice profile [22–25].

One unusual application of acoustic measurements, that of placing the sensing and detecting arrays in the water under the ice, was conducted by the University of Washington for the United States Coast Guard [26]. The difference in roughness between oil and ice could be detected, including at distances several meters from the site.

14.2.3 Radio-Frequency Methods

A prime effort has been to try radar methods of detection of targets in ice. A radar system has a radio transmitter that emits radio waves. When these come into contact with an object, they are usually reflected and/or scattered in many directions. Radar signals are reflected well by materials of considerable electrical conductivity—especially by most metals, seawater, wet land, and wetlands. It was hoped that the differences in conductivity of oil, ice, and seawater would provide for oil detection.

Ice has variable transparency to radio waves. Freshwater ice is relatively transparent to radio waves, whereas saline first-year ice is highly attenuating. Figure 14.11 shows the attenuation of radio frequency through various types of ice [4]. This figure shows that attenuation increased rapidly with increasing frequency and salinity. Low frequencies (<1 MHz) are best suited to the task of penetrating ice.

Extensive investigations of ice electromagnetic properties were carried out by Kovacs and coworkers [27–29]. Morey et al. studied the *in situ* complex dielectric constant of sea ice using time-domain spectroscopy [27]. It was found that (i) for sea ice with a preferred horizontal crystal c-axis alignment, the anisotropic or polarizing properties of the ice increased with depth; (ii) brine inclusion conductivity increased with decreasing temperature down to about -8°C , at which point the conductivity decreased with decreasing temperature; (iii) the DC conductivity of sea ice increased with increasing brine volume; (iv) the real part of the complex dielectric constant is strongly dependent upon brine volume but less dependent upon the brine inclusion orientation; and (v) the imaginary part of the complex dielectric constant was strongly dependent upon brine inclusion orientation but much less dependent upon brine volume. Because the electromagnetic properties of sea ice are dependent upon the physical state of the ice, which is continually changing, it appears that only trends in the relationships between the electromagnetic properties of natural sea ice and its brine volume and brine inclusion structure can be established. This study was followed up by a study of multiyear ice [28]. Sounding of multiyear sea ice, using impulse radar operating in the 80 to 500 MHz frequency band, revealed that the bottom of this ice

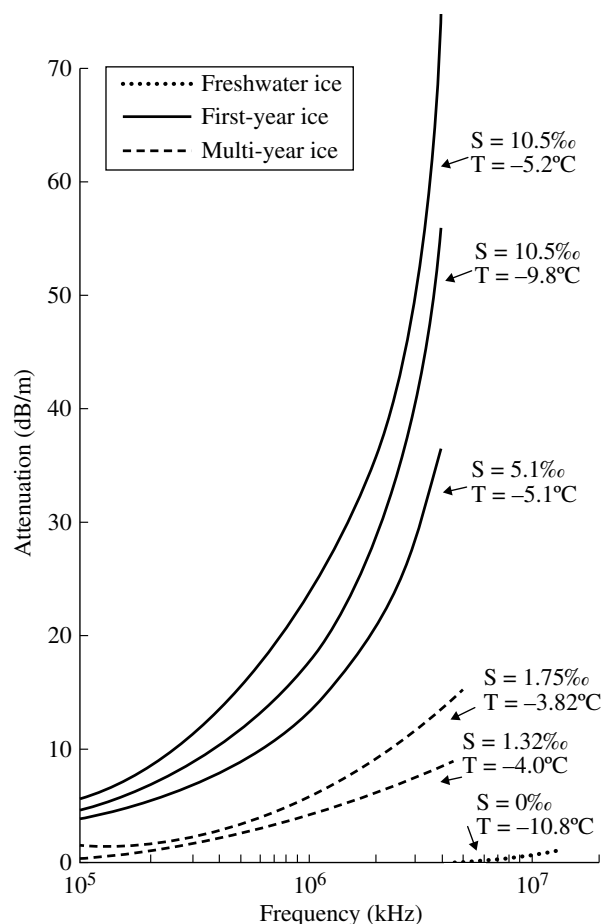


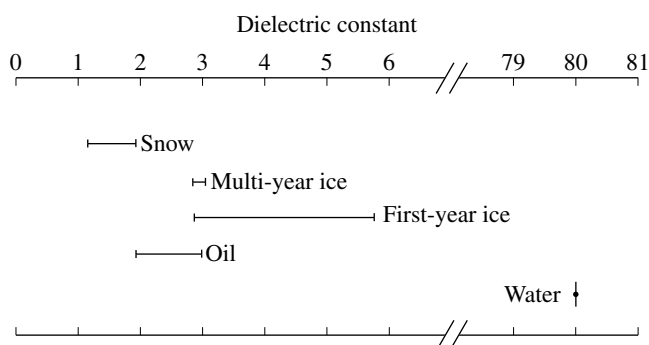
FIGURE 14.11 The attenuation of electromagnetic waves with temperature. The different T and S values indicate the different salinities and temperatures at which the attenuation was measured. This figure shows that above about 200 kHz, the attenuation is very high and therefore high frequencies cannot be used to penetrate ice (after Gill [4]).

could not always be detected. It was found that the bottom of the ice could not be detected when the ice structure had a high brine content. Because of brine's high conductivity, the brine volume dominates the loss mechanism in first-year sea ice, and the same was found true for multiyear sea ice.

The second important facet of radio frequency is the differential dielectric constant of oil, ice, and water. Oil has a dielectric constant of 2–3, snow of 1–2, and seawater of about 80 [4]. Multiyear ice has a dielectric constant of about 3 and first-year ice of 3 to about 5. Table 14.2 lists some of these dielectric values, and Figure 14.12 illustrates the basic differences. This differential in dielectric constants has led many theorists to predict that oil should be detectable in ice because of the phase reversals that should be apparent when a wave passes through a dielectric constant of 2 (oil) and immediately hits the seawater with a dielectric constant of 80. If the oil was not there, the dielectric constant would slowly change from that of ice (2–5) to that of seawater. The rapid change with oil present should produce a return due to the strong reflection caused by the dielectric change.

TABLE 14.2 Dielectric permittivity and conductivity

	Dielectric constant	Conductivity (S/m)
Snow	1.4–2.5	10^{-7}
Oil	2–4	10^{-5}
Freshwater ice	3	
Sea ice	4–7	$>10^{-2}$
Frozen soil	4–5	
Water	80	

**FIGURE 14.12** Illustration of the dielectric differences between ice, seawater, and oil. The “water” in the bottom right is seawater (after Gill [4]).

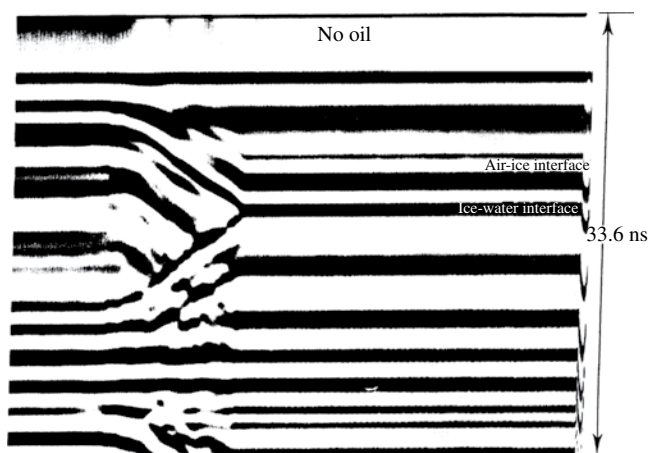
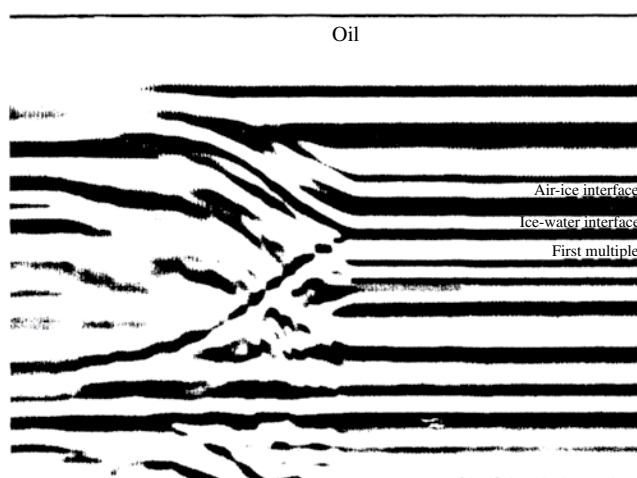
The third facet of radio-frequency possibilities of detecting oil under ice or snow is that of conductivity. Table 14.2 shows that there are major conductivity differences between oil, snow, and sea ice.

Four types of signal return might be used to detect the presence of oil under ice: (1) out-of-phase returns due to the low conductivity of oil; (2) large amplitude returns due to constructive interference effects; (3) spatial dependence of amplitude-of-return signals due to interference effects; and (4) conductivity differences [12].

Resonance scattering theory was proposed as a means of explaining the signals that might be achieved from plane dielectric layers of oil and ice [30,31]. Subsequent analysis by Tunaley and coworkers showed this to be an inappropriate model [32–34]. Moorcroft and Tunaley summarize this in calculations that show there would be essentially no electromagnetic resonance effect in sea ice at frequencies above about 0.2GHz [35]. This is because of the combined effects of absorption in the conducting sea ice and variations in its thickness. Additional effects are present that also serve to eliminate resonances, including scattering of the electromagnetic wave by small-scale surface structures. As a result, there is no possibility of using resonances to detect the presence of oil under sea ice, confirming the findings from the tank experiments.

14.2.4 Ground-Penetrating Radar

Ground-penetrating radar (GPR) reflections will be seen if the targets have different electromagnetic properties (dielectric permittivity and electric conductivity). Some of

**FIGURE 14.13** The output of a test of an old-generation impulse radar on ice with no oil below.**FIGURE 14.14** The output of a test of an impulse radar on ice with oil below. Note that there are few differences between this output and that of Figure 14.13, where there was no oil.

the same constants apply as in Table 14.2. One of the issues is that there are rarely pure targets; for example, sea ice (dielectric permittivity of about 5) often has saltwater intrusions (dielectric permittivity of about 80). This certainly complicates oil under ice or snow detection. Additionally, the processing of GPR is complex but can be sometimes used to delineate targets [36].

Several early workers proposed that the oil–ice boundary should be seen in impulse radar outputs [4]. A field test in the Beaufort Sea showed anomalies in the output when the oil and gas were located under the ice [37]. In another field test, an anomaly was observed where oil was present [38]. The interface was not seen, however, in subsequent tank tests [10].

Figures 14.13 and 14.14 show the testing of impulse radar over oil and no-oil situations, showing that there was no detection. These images were collected with a GSSI impulse radar with a center frequency of 400MHz and a pulse of

5 ns. One of the difficulties is probably the time resolution needed for such detection. Goodman and Fingas calculate that the time resolution required for a 1 cm thick layer of oil is 5 ps (5×10^{-12} s), which is about four orders of magnitude greater than the impulse radar systems then available [12]. Other studies indicate that phase change detection may negate this limit. Dean proposed that impulse radar could be used to measure the presence of oil under ice and subsequently conducted tank experiments showing that oil could not be detected [39].

A study of impulse radar in multiyear ice was carried out [28]. Sounding of multiyear sea ice, using impulse radar operating in the 80 to 500 MHz frequency band, revealed that the bottom of this ice could not always be detected. It was found that the bottom of the ice could not be detected when the ice structure had a high brine content. Because of brine's high conductivity, its volume dominates the loss mechanism in first-year sea ice, and the same was found true for multiyear sea ice. Newer Global Positioning System (GPS) units may be able to detect the phase transitions that occur with oil present because of the strong dielectric constant changes.

Dickins et al. applied GPR to a test oil spill off Svalbard and noted that anomalies were observed where the oil was under the ice [40–43]. There are some differences between the two outputs over oil and no oil; these may be due to phase change.

For snow, there has been some work on impulse radar testing [44,45]. Radar propagates easily through snow, and the dielectric permittivity is also relatively favorable (see Table 14.2). Sea ice, on the other hand, has low conductivity and can possess structure and therefore heterogeneity. Snow, being more consistent, is an easier medium to penetrate. Oil and snow do have somewhat similar electromagnetic properties and thus are harder to distinguish. Oil may be more easily distinguished from snow when oil displaces air in the snow thus creating a higher dielectric target. This anomaly from air-filled snow may be easier to detect using GPR. The depth of an oil layer that can be distinguished is at least one-quarter of the wavelength of the radar wavelength. Since most commercial radars have upper frequency limits of 1–1.5 GHz, one-quarter wavelength in snow is about 4–8 cm. This does not count looking at phase changes. Bradford et al. noted that oil spills could constitute a very complex environment if they drain through a snow pack, rather than form on ice in one consistent layer [44,45]. The penetration of GPR through snow depends on the density of snow and the presence of ice. A mature snow pack with ice and other heterogeneities would constitute a difficult situation for the GPR to discriminate.

A field test in Norway showed that detection was possible by observing phase change [44,45]. This test was conducted with a 1000 MHz GPR system. Bradford et al. concluded that commercial GPR systems could be effectively used to detect crude oil spills under snow. Observation of the reflection amplitude is the indicator of oil. The 2 cm thick oil film trapped between snow and ice (an ideal system) resulted in a 45%

decrease in amplitude. The researchers felt that they could detect oil layers as thin as 1 cm. Thickness of the oil layer might be estimated in some cases. Complications arise from water, in homogeneous snow, mixed layers and ice layers, as well as heterogeneous snow–ice boundaries [44,45].

14.2.5 UHF Radiometer

A Ultra High Frequency (UHF) radiometer was built and used in conjunction with an impulse radar. The intensity of the reflected radiation was measured at several frequencies. If selected regions of the spectrum would be absorbed by the oil under the ice, then such a phenomenon would be observed with this device. Frequencies from 300 to 1000 MHz were monitored [10]. No consistent signal was observed if oil was present or not.

14.2.6 Nuclear Techniques

Several proposals involved using techniques borrowed from downhole oil well logging. Gamma ray technology uses the carbon absorption peaks at 3.42 and 3.93 MeV to detect oil [4]. Similar techniques are available in the X-ray region. The use of these techniques outside of an oil well is very risky, and safety concerns override other issues.

14.2.7 Gas Sniffing and Leak Detection

Many oils have a significant volatile component and may penetrate ice to the surface and could possibly be detected using sensitive gas-sniffing techniques [4]. Tests of this technique in the field have not been successful. There is concern that too little volatile material actually penetrates the ice to yield detection.

Bryce reviewed *in situ* contact methods of oil detection for leaks on pipelines [46]. The Siemens LEOS fiber-optic detection system was recommended. Dickins and Andersen reviewed some tests of gas detection [7]. A test of methane emissions from freshly spilled oil appeared to indicate that this method has potential. However, further discussion resulted in a dismissal of this method because it was felt that methane would be gone too fast (e.g., 10 min) to provide a good detection means.

Hirst and O'Connor tested the evolution of methane from oil spilled under ice in two test series [47]. In the first test, the Shell LightTouch methane detector was used to test if methane could be detected above an artificial ice of 0.4 m. This test was successful. A series of four tests were carried out in Svalbard using a long-path methane detector. Barrel-size amounts of crude oil were spilled four times and the methane monitored. The methane was measured at 2.4–4.4 E⁻⁵ kg/s for these spills. There was extensive discussion on whether such levels would actually be detected in real spills. Consideration of this concept shows that these methane levels were only detected shortly after the spill and that the oil had relatively high amounts of methane. Ethane sensing

has also been conducted in the past to look for geological oil [48]. This technology has not been tested on oil under ice.

A variation on this theme was the use of trained dogs [43]. It was found that trained dogs could find oil under snow under a variety of circumstances. The maximum distance that dogs could locate the oil was 5 km downwind.

14.2.8 Nuclear Magnetic Resonance

The concept of using nuclear magnetic resonance (NMR) to detect oil under snow or ice has been around for years. When placed in a magnetic field, NMR-active nuclei (such as ^1H —protons or ^{13}C —carbon 13) absorb electromagnetic radiation at a frequency characteristic of the isotope. The resonant frequency, energy of the absorption, and the intensity of the signal are proportional to the strength of the magnetic field. For example, in a 21 T magnetic field, protons (^1H) resonate at 900 MHz. It is common to refer to a 21 T magnet as a 900 MHz magnet, although different nuclei resonate at different frequencies at this field strength. In the earth's magnetic field, such as might be used on oil, the same nuclei resonate at audio frequencies. Proton NMR frequencies are about 1.3 kHz near the equator to 2.5 kHz near the poles, around 2 kHz being typical of midlatitudes. These are audio frequencies that vary with the local magnetic field. These earth magnetic field NMR devices are relatively cheap but suffer from a number of limitations—especially in mobile applications as there is an absolute need for a homogeneous magnetic field to operate. As there is water everywhere, with two hydrogens, one must either separate the hydrogens or use ^{13}C to measure the oil; however, the latter signal is relatively weak.

Nedwed studied the use of NMR to detect oil under snow or ice [49]. Preliminary tests were carried out, and the results of these appeared to be promising. Exxon Mobil has initiated a joint project to pursue the modification of another instrument to oil spill purposes [43].

14.3 DETECTION OF SURFACE OIL WITH ICE: CONVENTIONAL TECHNIQUES

The state of the art in technology for the detection of oil with ice is more advanced than that for oil under ice [2,3]. Some of these techniques have proposed to have application to oil in or under ice; however, no potential for this has been shown. Electromagnetic wave penetration of ice, as noted earlier, is highly dependent on frequency and ice properties. Further, as noted in the overview, the presence of snow and other material on the surface blocks the penetration of most electromagnetic radiation [50].

There is an extensive review of the use of remote sensing for open water or that partially infested in ice in this book [2,3]. The best potential for detecting surface oil with ice is the laser fluorosensor [51–53]. Many of the other techniques used for oil on open water suffer when ice is present. This includes infrared, radar, and passive microwave.

14.4 CONCLUSIONS

The technology for detecting oil in or under ice is still evolving. Of the many potential technologies reviewed, acoustic techniques show potential and have been successfully tested in the field. Potential radio-frequency techniques are still awaiting further tests in the field.

Many acoustic techniques were tried in test tank situations, and it was found that acoustic detection of oil was possible because oil behaves as a solid in acoustic terms and transmits a shear wave. Furthermore, there is an angular dependence to these phenomena, and it can be used to distinguish between the many possible interferences in ice, such as air bubbles, and oil. Laboratory tests were conducted, and a prototype was built and tested in the field. This technology has not, however, been pursued or commercialized, possibly because the technique may be impractical in the field.

Radio-frequency methods such as GPR have been tried for both oil under ice and oil under snow. The method appeared to show success in field tests. Other radio-frequency methods have been proposed but at this time are not sufficiently tested or developed.

Several other oil-in-ice detection schemes have been assessed and tried including NMR, gamma ray detection, standard acoustic thickness probes, fluorosensor techniques, and augmented infrared detection. Each of these showed potential in theory and some during tank tests. Further development and testing on these proposed methods are required.

The technology for detecting surface oil with ice is further advanced. There is very limited potential for optical techniques, particularly infrared techniques. Radar and microwave do not show good potential for this application. Laser fluorosensors have been tested on oil with and on ice and function well for that application. As such, laser fluorosensors show the greatest potential for detection of oil when the oil is exposed to the surface.

REFERENCES

- [1] Ice Definitions, *Handbook on Oil Spill Science and Technology*, Wiley Science Publishers, New York, NY, 2014.
- [2] Fingas, M. and C.E. Brown, Oil Spill Remote Sensing: A Review, in *Oil Spill Science and Technology*, M. Fingas, Editor, Gulf Publishing Company, New York, NY, 111, 2011.
- [3] Fingas, M. and C.E. Brown, A Review of Oil Spill Remote Sensing, in *Oil Spills a Scholarly Approach*, M. Fingas, Editor, Wiley Science Publishers, New York, NY, 2014.
- [4] Gill, R., *Feasibility of Surface Detection of Oil Under Ice*, Environment Canada, Environmental Protection Service Report EPS 3-EC-79-11, Ottawa, ON, 1979.
- [5] Dickins, D.F., *Detection and Tracking of Oil Under Ice*, United States Minerals Management Report, Herndon, VA, 2000.
- [6] Goodman, R., Oil Under Ice Detection: What is the State-of-the-Art?, in *Oil Spill Response: A Global Perspective*, W.F. Davidson, K. Lee, and A. Cogswell, Editors, Springer, Dordrecht, 7, 2008.
- [7] Dickins, D.F. and J.H.S. Andersen, *Remote Sensing Technology Review and Screening*, SINTEF Report No. 22, Trondheim, Norway, 2009.

- [8] Dickins, D.F. and J.H.S. Andersen, *Evaluation of Airborne Remote Sensing Systems for Oil in Ice Detection*, SINTEF Report No. 28, Trondheim, Norway, 2010.
- [9] Fingas, M.F. and C.E. Brown, A Review of the Status of Advanced Technologies for the Detection of Oil in and with Ice, *Spill Sci. Technol. Bull.*, 6, 295, 2000.
- [10] Remotec Applications Ltd., *Laboratory Experiments in the Detection of Oil Under Ice*, Environment Canada Manuscript Report EE-26, Ottawa, ON, 1981.
- [11] Stapleton, G.F., S.K. Parashar, J.B. Snellen, and R.D. Worsfold, Detection of Oil Under Ice—A Laboratory Program, *AMOP*, Edmonton, AB, 587, 1981.
- [12] Goodman, R.H. and M.F. Fingas, Detection of Oil-Under-Ice – A Joint Esso/EPS Project, *AMOP*, Edmonton, AB, 207, 1983.
- [13] Moir, M.E. and D.C. Yetman, Detection of Oil under Sea Ice by Pulsed Ultraviolet Fluorescence, *IOSC*, Tampa, FL 521, 1993.
- [14] Laidley, T., Laser Detection of Oil in Ice, *C-CORE News*, 1981.
- [15] Goncharov, V.K. and V.G. Lyskov, Problems of Forecasting of Spreading and Remote Sensing of the Under Ice Oil Spills, in *Proceedings of the Conference on Port and Ocean Engineering under Arctic Conditions*, Helsinki, Finland, 800, 1999.
- [16] Jones, H.W. and H.W. Kwan, The Detection of Oil Spills Under Arctic Ice by Ultrasound, *AMOP*, Edmonton, AB, 391, 1982.
- [17] Jones, H.W. and H.W. Kwan, The Detection of Oil Spills Under Seawater in the Arctic Ocean, *AMOP*, Edmonton, AB, 241, 1983.
- [18] Jones, H.W., H.W. Kwan, and E.M. Yeatman, On the Design of an Apparatus to Detect Oil Trapped Under Sea Ice, *AMOP*, Edmonton, AB, 295, 1984.
- [19] Jones, H.W., H.W. Kwan, T. Hayman, and E.M. Yeatman, The Detection of Oil Under Ice by Ultrasound Using Multiple Element Phased Arrays, *AMOP*, Edmonton, AB, 475, 1986.
- [20] Knudsen Engineering Ltd., *Experiments in the Detection of Oil Under Ice*, Environment Canada Manuscript Report, Ottawa, ON, 1984.
- [21] Goodman, R.H., H. Jones, and M.F. Fingas, The Detection of Oil Under Ice Using Acoustics, in *Proceedings of the Conference on Port and Ocean Engineering Under Arctic Conditions*, Narssarsuaq, Greenland, 903, 1985.
- [22] Dowdeswell, J.A., J. Evans, R. Mugford, G. Griffiths, S. McPhail, N. Millard, P. Stevenson, M.A. Brandon, C. Banks, K.J. Heywood, M.R. Price, P.A. Dodd, A. Jenkins, K.W. Nicholls, D. Hayes, E.P. Abrahamsen, P. Tyler, B. Bett, D. Jones, P. Wadhams, J.P. Wilkinson, K. Stansfield, and S. Ackley, Autonomous Underwater Vehicles (AUVs) and Investigations of the Ice-ocean Interface in Antarctic and Arctic Waters, *J. Glaciol.*, 54, 661, 2008.
- [23] Doble, M.J., A.L. Forrest, P. Wadhams, and B.E. Laval, Through-ice AUV Deployment: Operational and Technical Experience from Two Seasons of Arctic Fieldwork, *Cold Reg. Sci. Technol.*, 56, 90, 2009.
- [24] Doble, M.J., P. Wadhams, A.L. Forrest, and B.E. Laval, Experiences from Two-years' Through-ice AUV Deployments in the High Arctic, in *Proceedings of Autonomous Underwater Vehicles, 2008. AUV 2008. IEEE/OES*, Woods Hole, MA, 1–7, 2008.
- [25] Wadhams, P., J.P. Wilkinson, and S.D. McPhail, A New View of the Underside of Arctic Sea Ice, *Geophys. Res. Lett.*, 33, L04501, 2006.
- [26] Fitzpatrick, M., R.E. Francois, and C.D. McKindra, Oil Spill Detection Under Ice—Status Report, *AMOP*, Edmonton, AB, 391, 1982.
- [27] Morey, R.M., A. Kovacs, and G.F.N. Cox, Electromagnetic Properties of Sea Ice, *Cold Reg. Sci. Technol.*, 9, 53, 1984.
- [28] Rexford, M., M. Morey, and A. Kovacs, Investigation of the Electromagnetic Properties of Multi-year Sea Ice, *Conference on Arctic Matters*, Hanover, New Hampshire, 151, 1985.
- [29] Kovacs, A., R.M. Morey, and G.F.N. Cox, Modeling the Electromagnetic Property Trends in Sea Ice, Part I, *Cold Reg. Sci. Technol.*, 14, 207, 1987.
- [30] Jackins, P.D., G.C. Gaunaurd, and C.D. McKindra, Radar Resonance Reflection from Sets of Plane Dielectric Layers, *AMOP*, Edmonton, 365, 1982.
- [31] Goodman, R.H., A. Dean, and M.F. Fingas, The Detection of Oil Under Ice Using Electromagnetic Radiation, in *Proceedings of the Conference on Port and Ocean Engineering Under Arctic Conditions*, Narssarsuaq, Greenland, 895, 1985.
- [32] Tunaley, J.K.E., The Scattering of Electromagnetic Waves from the Sea-Ice Oil and Sea-Water Interfaces, *AMOP*, Edmonton, 292, 1985.
- [33] Tunaley, J.K.E. and D.R. Moorcroft, Aspects of the Detection of Oil Under Sea Ice Using Radar Methods, *AMOP*, Edmonton, 463, 1986.
- [34] MacDougall, J.W. and J.K.E. Tunaley, The Complex Permittivity of Crude Oil, *AMOP*, Edmonton, 413, 1986.
- [35] Moorcroft, D.R. and J.K.E. Tunaley, Electromagnetic Resonance in Layers of Sea Ice Over Sea Water, *AMOP*, Edmonton, 269, 1985.
- [36] Cassidy, N.J., Cassidy, Processing, Modelling and Analysis, in *Ground Penetrating Radar Theory and Applications*, H. Jol, Editor, Elsevier, Boston, MA, 141–176, 2008.
- [37] Butt, K., P. O'Reilly, and E. Reimer, A Field Evaluation of Impulse Radar for Detecting Oil in and Under Sea Ice, in *Oil and Gas under Sea Ice Experiment*, Dome Petroleum, APOA Contract 169, 1981.
- [38] Goobie, G.I., T.W. Laidley, and E.M. Reimer, C-CORE Oil Spill Research Activities, *AMOP*, Edmonton, 623, 1981.
- [39] Dean, A.M., Investigating the Practical Applications of the Resonant Scattering Theory for the Detection of Oil Under Sea Ice, *AMOP*, Edmonton, 235, 1983.
- [40] Dickins, D., J. Bradford, L. Liberty, B. Hirst, E. Owens, V. Jones, G. Gibson, L. Zabilansky, and J. Lane, Testing Ground Penetrating Radar and Ethane Gas Sensing to Detect Oil in and under Ice, *AMOP*, Edmonton, 799, 2005.
- [41] Dickins, D.F., P.J. Brandvik, J. Bradford, L-G. Fakness, L. Liberty, and R. Daniloff, Svalbard 2006 Experimental Oil Spill under Ice: Remote Sensing, Oil Weathering under Arctic Conditions and Assessment of Oil Removal by in-situ Burning, *IOSC*, Savannah, GA, 681, 2008.
- [42] Bradford, J.H., L.M. Liberty, and D.F. Dickins, Locating Oil Spills under Sea Ice Using Ground-Penetrating Radar, in *Leading Edge*, Tulsa, OK, 1424, 2008.
- [43] Dickins, D.F., *Project P5: Remote Sensing Summary Report*, SINTEF Report No. 30, Trondheim, Norway, 2010.
- [44] Bradford, J.H., D.F. Dickins, and P.J. Brandvik, Assessing the Potential to Detect Oil Spills in and under Snow Using Airborne Ground-Penetrating Radar, *Geophysics*, 75, 2, 2010.
- [45] Bradford, J., D. Dickins, and P.J. Brandvik, *Airborne GPR to Detect Oil under Snow*, SINTEF Report No. 24, Trondheim, Norway, 2010.
- [46] Bryce, P., Design Considerations for Arctic Subsea Leak Detection Systems, in *Proceedings of the International Oil and Ice Workshop*, ACS, Anchorage, AK, 2000.
- [47] Hirst, B. and S. O'Connor, *Measurement of Methane Emissions from Oil Spill Experiments at Svea Test Site. Svalbard, April 2007*, SINTEF Report No. 23, Trondheim, Norway, 2010.
- [48] Hirst, B., G. Gibson, S. Gillespie, I. Archibald, O. Podlaha, K.D. Skeldon, J. Courtial, S. Monk, and M. Padgett, Oil and Gas Prospecting by Ultra-Sensitive Optical Gas Detection with Inverse Gas Dispersion Modelling, *Geophys. Res. Lett.*, 31, L12115 1, 2004.
- [49] Nedwed, T., L. Srnka, and H. Thomann, Remote Detection of Oil Spilled Under Ice and Snow Using Nuclear Magnetic Resonance, *AMOP*, Calgary, 693, 2008.

- [50] Babiker, M., K. Kloster, and S. Sandven, *The Utilization of Satellite Images for the Oil in Ice Experiment in the Barents Sea, May 2009*, SINTEF Report No. 29, Trondheim, Norway, 2010.
- [51] Brown, C.E., Oil Spill Remote Sensing: A Review, in *Oil Spill Science and Technology*, M. Fingas, Editor, Gulf Publishing Company, New York, NY, 171, 2011.
- [52] Brown, C.E. and M.F. Fingas, Review of the Development of Laser Fluorosensors for Oil Spill Application, *Mar. Pollut. Bull.*, 47, 477, 2003.
- [53] Brown, C.E., M.F. Fingas, and J. An, Laser Fluorosensors: A Survey of Applications and Developments of a Versatile Sensor, *AMOP*, Edmonton, 485, 2001.

PART VIII

OIL SPILLS ON LAND

BIOREMEDIATION OF OIL SPILLS ON LAND

LISA D. BROWN AND ANIA C. ULRICH

Department of Civil and Environmental Engineering, University of Alberta, Edmonton, Canada

15.1	Introduction	397
15.2	Brief Overview of Bioremediation Techniques for Land Oil Spills	397
15.2.1	<i>In Situ</i> versus <i>Ex Situ</i>	397
15.2.2	Biostimulation versus Bioaugmentation	398
15.3	Key Organisms Involved in Biodegradation of Oil Spills on Land	398
15.3.1	Communities versus Isolates	399
15.4	Environmental Factors Affecting Bioremediation	399
15.4.1	Temperature	399
15.4.2	pH	399
15.4.3	Salinity	399
15.4.4	Nutrients	399
15.4.5	Moisture	400
15.4.6	Redox Environment	400
15.4.7	Soil Type	400
15.5	<i>In Situ</i> Bioremediation Strategies	400
15.5.1	Bioventing	401
15.5.2	Enhanced Bioremediation	401
15.5.3	Monitored Natural Attenuation	401
15.6	<i>Ex Situ</i> Land Treatment Techniques	402
15.6.1	Landfarming and Land Treatment	402
15.6.2	Biopiles	403
15.6.3	Organic Amendments	403
15.7	Bioaugmentation Strategies	404
15.7.1	Key Bacteria Used in Bioaugmentation	404
15.7.2	Role of Other Organisms	404
15.8	Biostimulation Strategies	404
15.8.1	Biosurfactants	404

15.1 INTRODUCTION

Biodegradation of hydrocarbons by naturally occurring populations of microorganisms is one of the primary mechanisms by which petroleum is removed from the environment [1]. Biodegradation of petroleum hydrocarbons in soil differs greatly from aquatic environments due to the predominantly vertical infiltration of the oil contamination into the

subsurface, where sorption processes may reduce toxicity of oil components but may also serve as a persistent source of contamination [1]. In addition, volatile organic compounds may become trapped in the soil matrix, potentially causing toxic effects on microorganisms [1]. This chapter focuses on treating the solid, or soil, phase in both unsaturated and saturated zones in the subsurface.

15.2 BRIEF OVERVIEW OF BIOREMEDIATION TECHNIQUES FOR LAND OIL SPILLS

Bioremediation is the acceleration or encouragement of the natural biodegradation process via alteration of the contaminated media. Bioremediation of contaminated soils has been used extensively in Europe and the United States [2]. In remote areas, bioremediation may represent the most effective and cost-efficient means of treating soils contaminated with petroleum hydrocarbons [3].

15.2.1 *In Situ* versus *Ex Situ*

Bioremediation technologies may be employed on-site or off-site and *in situ* or *ex situ*. *In situ* bioremediation involves microbial biodegradation of the contamination within the subsurface soil/water matrix. No excavation of the contaminated soil takes place, but groundwater pumping or vacuum aeration may be required to distribute constituents, such as nutrients or oxygen, required for enhanced degradation [2]. *Ex situ* technologies require the excavation of the contaminated soil, which may be treated on- or off-site. Contamination of surface soils may be easily treated by *ex situ* techniques, which are often analogous to agricultural practices, but treatment of deeper contamination is more difficult, and *in situ* techniques are likely to be more appropriate [4].

In situ treatment approaches are typically more cost-effective, but it can be challenging to ensure that the required

amendments are delivered and that the appropriate level of treatment has been achieved. The main advantage of *ex situ* technologies lies in process control, but excavation of soil is disruptive, is costly, and increases exposure to contaminants.

15.2.2 Biostimulation versus Bioaugmentation

On a fundamental level, bioremediation may take two forms: biostimulation and bioaugmentation [2]. Biostimulation involves the alteration of a site's physical or chemical characteristics to enhance the natural biodegradation processes performed by the indigenous microorganisms [2]. Bioaugmentation entails the addition of microorganisms selected for their ability to biodegrade the contaminants of concern in the system.

15.3 KEY ORGANISMS INVOLVED IN BIODEGRADATION OF OIL SPILLS ON LAND

Due to the ubiquitous presence of hydrocarbons in the environment, microorganisms able to biodegrade petroleum hydrocarbons are plentiful in soil. Heterotrophic bacteria and fungi are the predominant microorganisms biodegrading hydrocarbons [1]. Many studies have found that microbial diversity is decreased in contaminated soil, likely due to the selection and subsequent dominance of microorganisms able to degrade petroleum hydrocarbons within the indigenous community [5,6]. These same studies have also shown a significant increase in petroleum hydrocarbon-degrading bacteria in contaminated soils. Table 15.1 highlights a number of identified

TABLE 15.1 Examples of hydrocarbon-degrading microorganisms identified in field and laboratory studies

Microorganism		Redox condition	Carbon source	Reference
Genus	Species			
<i>Pseudomonas</i>	<i>fluorescens</i>	Aerobic	Oil	[7]
	sp. ^a	Aerobic	Diesel	[8]
	sp.	Aerobic	Oil	[5]
	sp.	Aerobic	Crude oil	[9,10]
	ETB 001/2, 005/2	Aerobic	Refinery oil	[11]
	<i>putida</i>	Aerobic	Crude oil	[12,13]
<i>Bacillus</i>	<i>mycoides</i>	Aerobic	Oil	[7]
	sp.	Aerobic	Crude oil	[9,10]
<i>Serratia</i>	<i>marcescens</i>	Aerobic	Oil	[7]
<i>Rhodococcus</i>	<i>rhodochrous</i>	Aerobic	Oil	[14]
	sp.	Aerobic	Oil	[5]
	<i>baikonurensis</i> EN3	Aerobic	Diesel	[15]
	sp.	Aerobic	Refinery oil	[11]
	<i>ruber</i>	Aerobic	Crude oil	[16]
<i>Ralstonia</i>	sp.	Aerobic	Oil	[5]
<i>Cyanobacterium</i>	<i>mastigocladus</i>	Aerobic	Gasoline	[17]
<i>Micrococcus</i>	sp.	Aerobic	Crude oil	[9,10]
<i>Proteus</i>	sp.	Aerobic	Crude oil	[9]
<i>Acinetobacter</i>	sp.	Aerobic	Diesel	[18]
	sp.	Aerobic	Refinery oil	[11]
	sp.	Aerobic	Crude oil	[10]
<i>Mycobacterium</i>	sp.	Aerobic	Refinery oil	[11]
<i>Arthrobacter</i>	sp.	Aerobic	Refinery oil	[11]
	sp.	Aerobic	Crude oil	[10]
<i>Flavobacterium</i>	sp.	Aerobic	Crude oil	[10]
<i>Moraxella</i>	sp.	Aerobic	Crude oil	[10]
<i>Corynebacterium</i>	sp.	Aerobic	Crude oil	[10]
Fungi: <i>Pleurotus</i>	<i>ostreatus</i>	Aerobic	Tar	[19]
		Aerobic	Oil	[20]
Yeast: <i>Candida</i>	<i>tropicalis</i>	Aerobic	Crude oil	[21]
Earthworm: <i>Eisenia</i>	<i>fetida</i>	Aerobic	Crude oil	[22]
Earthworm: <i>Allolobophora</i>	<i>chlorotica</i>	Aerobic	Crude oil	[22]
Earthworm: <i>Lumbricus</i>	<i>terrestris</i>	Aerobic	Crude oil	[22]
Fungi: <i>Phanerochaete</i>	<i>chrysosporium</i>	Aerobic	Oil	[20]
Fungi: <i>Coriolus</i>	<i>versicolor</i>	Aerobic	Oil	[20]
<i>Bacillus</i>	sp.	Anaerobic	Waste oil	[23]
<i>Arthrobacter</i>	sp.	Anaerobic	Waste oil	[23]
<i>Clavibacter</i>	sp.	Anaerobic	Waste oil	[23]
<i>Corynebacterium</i>	sp.	Anaerobic	Waste oil	[23]
<i>Nocardia</i>	sp.	Anaerobic	Waste oil	[23]
<i>Azoarcus</i> (<i>Thauera</i>)	sp.	Anaerobic	BTEX	[24,25]
<i>Geobacter</i>	sp.	Anaerobic	Toluene	[24]
<i>Dechloromonas</i>	sp.	Anaerobic	Benzene	[24]

^aSpecies.

bacteria, fungi, and earthworms able to utilize various hydrocarbons as a carbon source.

15.3.1 Communities versus Isolates

Leahy and Colwell indicate that individual organisms can only metabolize a limited number of hydrocarbon compounds, so mixed populations of microorganisms are required to biodegrade complex mixtures of compounds found in oil [1]. Numerous studies have found that biodegradation of petroleum hydrocarbons is more pronounced with mixed cultures than with isolated microorganisms [5,6]. Benka-Coker and Ekundayo isolated indigenous microorganisms capable of degrading hydrocarbons but found that 20% greater degradation of crude oil was achieved with mixed cultures versus a pure culture of *Micrococcus* sp. after 14 days, as individual microorganisms are specialized to degrade specific compounds [6].

15.4 ENVIRONMENTAL FACTORS AFFECTING BIOREMEDIATION

Two principal sources of rate-limiting factors for field applications of bioremediation technologies are biochemical factors and environmental factors [2]. In some cases, changing the environmental conditions of the site may be required to enhance biodegradation, especially with contaminated sites that have been stagnant for extended periods of time.

15.4.1 Temperature

Temperature is an important environmental factor impacting bioremediation as the physical nature and chemical composition of the oil, microbial metabolism, and composition of the microbial community are all temperature dependent [1]. With decreasing temperature, the viscosity of oil increases, and potentially toxic volatiles are less volatile and more water soluble, delaying the onset of biodegradation [1]. In general, microbial metabolism rates decrease with decreasing temperature. A study of the biodegradation of diesel found that microbial activities peaked in a few days at 20°C versus 3 weeks at 6°C and carbon dioxide production was greater and diesel mineralization was almost five times greater at the higher temperature [3].

Psychrotolerant bacteria have been readily isolated from hydrocarbon-contaminated polar soils, growing at temperatures less than 10°C [26], and biodegradation has been observed in soils as cold as -1 to -3°C [26]. Although mineralization will occur at low temperatures, the rate, and perhaps even the extent, of biodegradation will be higher at elevated temperatures [26].

Thermophilic microorganisms grow optimally at temperatures between 40 and 70°C and are dominant in a number of *ex situ* treatment technologies, including composting and bioventing piles [27]. Although two cases of temperature-sensitive microorganisms are given here, most of the microbial world

in the subsurface flourishes at temperatures between these two extremes, and Mohammed et al. report that optimal petroleum hydrocarbon biodegradation will occur between 10 and 30°C [2].

15.4.2 pH

Most heterotrophic bacteria and fungi prefer neutral pH environments, but terrestrial environments are more variable compared to aquatic ecosystems, where soil pH can vary from 2.5 to 11.0 [1] due to soil chemistry [26]. Optimum hydrocarbon biodegradation occurs around pH 6.5–8.0 [26].

Soil pH may be lowered due to fertilizer application or the production of aliphatic acids during alkane biodegradation [26]. Adjustment to pH can be achieved by the addition of lime or sulfur, for example, for alkaline or acidic correction, respectively.

Margesin and Schinner hypothesize that the persistence of aromatic hydrocarbons in the environment is due to sensitivity of aromatic degraders to pH [27]. Chang et al. observed that the biodegradation rate constants for various polycyclic aromatic hydrocarbons doubled when pH changed from 7.0 or 9.0 to the optimal pH value of 8.0 [28].

15.4.3 Salinity

Although microorganisms exist that require salt for growth (halophiles), it is generally assumed that an inverse relationship exists between salinity and the biodegradation of petroleum hydrocarbons [27]. However, there is little information on the effects of salinity on the bioremediation of petroleum-contaminated soils [27]. One study found that artificial salinity at a level comparable to an oil-field brine inhibited oil degradation by 20–44% [27]. Salt concentrations greater than 1% (w/v) inhibited biodegradation of weathered hydrocarbons from production facilities by increasing lag time and decreasing mineralization rate, even reducing the extent of mineralization in some cases [29]. Ulrich et al. also found that salt concentrations in the range of 0.5–1% (w/v) stimulated microbial activity [29]. Margesin and Schinner hypothesize that microorganisms found in natural saline soil environments may be impacted less by high salt concentrations due to acclimation [27].

15.4.4 Nutrients

Nitrogen and phosphorus are the most important inorganic nutrients required for microbial growth. Some soil environments may be deficient in nitrogen and/or phosphorus, and a number of studies have demonstrated increased biodegradation of hydrocarbons due to macronutrient addition, while few others have shown little change [1]. The success of nutrient addition will depend on the composition of the soil and the presence of nitrogen-fixing bacteria [1]. No consensus has been reached in the literature on optimum

nutrient levels; carbon to nitrogen ratios for enhancing the biodegradation of hydrocarbons in soil range from 200:1 to 9:1 [26]. The U.S. Environmental Protection Agency recommends a carbon to nitrogen to phosphorus ratio ranging from 100:10:1 to 100:1:0.5 for bioremediation technologies [30]. Cumulative carbon dioxide production increased by 76% following the addition of nitrogen fertilizer to diesel-contaminated soil [3].

Nitrogen concentrations in the soil that are either too high or too low will inhibit biodegradation [3]. Care must be taken when utilizing inorganic fertilizers on soils with low water holding capacity, as overfertilization may cause osmotic stress; slow-release fertilizers, such as those used for gardening, are recommended [26].

Micronutrients, namely, trace metals such as calcium, magnesium, sulfur, and zinc, tend to be present in most soil environments in sufficient quantities so that microbial growth is not inhibited.

15.4.5 Moisture

The moisture content of the contaminated soil impacts the dissolution of petroleum hydrocarbon compounds and thus substrate diffusion and availability, microbial transport, and the removal of metabolic by-products [2]. Most studies have indicated that the optimum moisture content is 50–70% of the water holding capacity of the soil [2]. Hydrocarbon biodegradation may be limited in soils where moisture is below 30% [1]. An additional consideration is that soil grains coated in oil can render the soil more hydrophobic, reducing water holding capacity [26].

A study on diesel-contaminated sand indicated that gravimetric moisture contents ranging from 2 to 12% had little impact on biodegradation rates, but cumulative carbon dioxide production did increase with increasing moisture content [3].

15.4.6 Redox Environment

The redox environment biochemically influences what microbial populations exist based on the dominant terminal electron acceptor. The amount of oxygen available in the soil matrix is dependent on microbial oxygen consumption, type of soil, and whether the soil is saturated or unsaturated [1].

Historically, anaerobic biodegradation of petroleum hydrocarbons was thought to occur at negligible rates and thus was considered insignificant [1]. Research in the late 1980s and 1990s provided evidence that aromatic hydrocarbons are degraded under denitrifying, iron-reducing, sulfate-reducing, and fermentative and methanogenic conditions, with iron reduction, fermentation, and methanogenesis dominating the anaerobic processes at several sites [4]. In a soil column study, Boopathy found that total petroleum hydrocarbons were removed by 88% in 310 days from diesel fuel when mixed electron acceptors were provided, versus 61% under sulfate-reducing conditions [31].

The limited solubility of oxygen in water and the rapid consumption of available dissolved oxygen by microorganisms have resulted in new perspectives on enhancing particular anaerobic environments through the addition of alternative electron acceptors, such as nitrate and sulfate [4]. However, consideration must be given to the impacts of injecting these compounds in the subsurface, and authorities may be concerned with the potential accumulation in groundwater, where negative effects on drinking water may occur [4].

15.4.7 Soil Type

Soil type greatly influences permeability, which Mohammed et al. identify as one of the most important factors in *in situ* bioremediation, and they do not recommend this treatment technology for soil with permeability less than 10^{-4} cm/s [2]. As highlighted in Section 15.4.5, water is required to transport nutrients, microorganisms, substrate, and electron acceptors [2]. Fluid movement in the soil matrix is a function of permeability.

Properties of soils that impact sorption, such as organic matter and surface charge, also impact bioavailability and biodegradation of hydrocarbon compounds. Hydrophobic organic compounds, such as polycyclic aromatic hydrocarbons, will partition to those soils with high clay or organic content and be rendered unavailable to microorganisms [32].

A study on diesel-contaminated soil compared the effects of sand and gravel soils on degradation [3]. Cumulative carbon dioxide production for the contaminated sand was double that for the gravel, and this contrast is attributed to the increased surface area and porosity of the sand, increasing bioavailability of the contaminants and oxygen supply to microorganisms.

15.5 *IN SITU* BIOREMEDIATION STRATEGIES

In situ bioremediation techniques focus on generating or enhancing the degradation of the contaminants of concern in the subsurface. According to Brown and Crosbie [33], unsaturated and residually saturated soils contain the most significant contaminant load and provide a continual source of groundwater contamination if left untreated. If contamination has occurred deep enough in the subsurface, as seen with leaking underground storage tanks, or site conditions, such as proximity to structures, render excavation of contaminated soil infeasible, *in situ* bioremediation strategies are an effective means of waste treatment.

A key first step in *in situ* bioremediation is the evaluation of site conditions, particularly the presence of petroleum hydrocarbon degraders among the indigenous microbial population and assessment of limiting factors that may need to be altered during treatment [34].

15.5.1 Bioventing

Bioventing enhances aerobic biodegradation in the subsurface by supplying air or pure oxygen into the unsaturated zone through gas injection or extraction wells installed into the soil and was one of the first *in situ* technologies applied at a large scale in the 1990s [4]. In contrast with soil vapor extraction, a physical remediation technique, bioventing employs very low airflow rates to minimize volatilization of hydrocarbons. Midweight petroleum products, such as diesel and jet fuel, are particularly well suited to bioventing treatment; gasoline, due to rapid volatilization, may be removed more rapidly via soil vapor extraction [30].

The installation and use of soil venting systems is an efficient method for providing oxygen to unsaturated contaminated soils for aerobic biodegradation [33]. Air may be added to the soil by either injection or vacuum withdrawal; Brown and Crosbie highlight that withdrawal is more common because volatile organic compounds will also be removed [33]. However, a requirement to treat volatiles prior to releasing withdrawn air to the atmosphere will potentially significantly increase treatment costs. Despite this, Brown and Crosbie identified bioventing as the most cost-effective means of providing an oxygen source for *in situ* bioremediation [33].

Bioventing also provides the added opportunity to pump warm air into the subsurface to extend the season that bioremediation is effective in colder climates.

Soil permeability is the most significant factor in evaluating the applicability of bioventing at a contaminated site [30]. Cost is driven primarily by the extent of the contamination and soil permeability, as both parameters impact the number of injection/extraction wells that are required [35]. Bioventing is considered ineffective for clays and silts [30].

15.5.2 Enhanced Bioremediation

Enhanced bioremediation refers to any *in situ* bioremediation scheme whereby constituents are provided to promote biodegradation of contamination. Amendments include nutrients, terminal electron acceptors, surfactants, and microorganisms, all intended to improve the existing conditions in the subsurface for enhanced bioremediation.

Injection wells are utilized for contamination deep in the subsurface, but infiltration methods, such as spray irrigation or ditches, may suffice for shallow contamination [35]. Treated groundwater from the site may be utilized for delivery of amendments.

Nitrogen and phosphorus are often required as contaminated soil has been depleted of these major nutrients due to the increased carbon loading provided by petroleum hydrocarbons. Oleophilic fertilizers are widely used as they adhere to hydrocarbons, providing nutrients at the oil–water interface [34].

Menendez-Vega et al. state that aerobic biodegradation is preferred as the most common petroleum hydrocarbon-

biodegrading microorganisms are aerobic [34]. Oxygen may be provided via bioventing, as discussed in Section 15.5.1, or through the injection of chemicals, such as hydrogen peroxide or nitrate [33]. Hydrogen peroxide is most widely used, due to its high oxygen-releasing potential [34], but Brown and Crosbie point out that high operating costs may result if soils contain high levels of iron or manganese, as hydrogen peroxide will decompose due to metal catalysis [33]. Anaerobic biodegradation may be enhanced by the injection of nitrate, but in many jurisdictions, regulations exist for nitrate concentrations in groundwater [33].

Surfactants may be injected into the subsurface, or allowed to infiltrate through the unsaturated zone, to increase bioavailability of contaminants to microorganisms [34]. Bioaugmentation may also be employed to improve biodegradation. Both will be discussed further in Sections 15.8.1 and 15.7, respectively.

Examples of the successful field application of enhanced bioremediation are provided in Table 15.2.

15.5.3 Monitored Natural Attenuation

Monitored natural attenuation is an *in situ* bioremediation strategy, whereby no human intervention occurs, but extensive monitoring of the natural processes in the soil and groundwater is conducted to establish a case for reduction in mass, toxicity, volume, or concentration of contaminants [4]. This technique is not a “do nothing” approach. Typically, monitoring requirements are more extensive than with other remediation technologies, and a case for treatment within a reasonable time frame must be established [30]. Often, monitored natural attenuation is utilized after more active treatment techniques have been employed or in areas of dilute contamination [30].

Natural attenuation will involve both aerobic and anaerobic biodegradation, as microorganisms in the subsurface exhaust the available supply of each terminal electron acceptor. In addition, natural attenuation will not solely involve biodegradation of contaminations, as physical and chemical processes will also occur in the subsurface, such as dilution, sorption, and volatilization.

Monitoring requirements include obtaining direct evidence of the occurrence of biodegradation of contamination. The concentrations of the contaminants of concern are closely monitored, and documented evidence of decreasing concentrations at the site must be provided. Evidence of microbial activity also provides indication of biodegradation occurring. Observing changes in the geochemical conditions within the plume can also provide indirect evidence of biodegradation occurring [4]. Compound stable isotope analysis has emerged as technique for demonstrating that biodegradation or abiotic processes have transformed the contaminant of concern, as the ratio of stable isotopes will change with the extent of degradation [38].

A field example where monitored natural attenuation was utilized is provided in Table 15.2.

TABLE 15.2 Field results from selected *in situ* bioremediation studies

Site description	Contaminant	Treatment technique	% Reduction	Reference
Municipal vehicle maintenance yard	Diesel, motor oil, gasoline, automotive fluids	Enhanced bioremediation—hydrogen peroxide and nitrogen	TPH ^a as gasoline, 99% (GC) TOG ^b , 84% (Infrared)	[36]
Industrial site	Mixture of petroleum hydrocarbons	Enhanced bioremediation—hydrogen peroxide, fertilizer, surfactant	Oil, 100% Lubricant, 99% Gas oil, 100% (GC-FID, GC-MS) (in groundwater)	[34]
Refinery site	Oil hydrocarbons	Enhanced bioremediation—treated groundwater with nutrients, surfactant, microorganisms	Total oil hydrocarbons, 86% in 15 weeks (GC-FID)	[11]
Former waste oil refinery	Oil hydrocarbons	Enhanced bioremediation—nitrogen, phosphorus, oxygen, hydrogen peroxide	Oil, 50–70% in 300 days (GC)	[23]
Alpine skiing area	Diesel oil	Monitored natural attenuation	TPH, 50% in 780 days (Infrared)	[37]

^aTotal petroleum hydrocarbons.^bTotal oil and grease.**TABLE 15.3** Field results from select *ex situ* bioremediation studies

Site description	Contaminant	Treatment technique	% Reduction	Reference
Kuwait desert	Crude oil	Landfarming	TPH, ^a 82.5%	[39]
		Turned piles	TPH, 74.2%	[39]
		Static bioventing piles	TPH, 64.2% (Infrared)	[39]
Kuwait desert	Crude oil	Turned piles	TPH, ~60% (GC-FID)	[40]
Oil-field treatment facility	Oily waste from crude oil production	Landfarming	Organic fraction, 78% (Soxhlet, TLC ^b)	[41]
Agricultural soil contaminated from leaking pipeline	Crude oil	Biopiles (no aeration)	Up to 57% (Gravimetric)	[16]
Contaminated soil at refinery	Hydrocarbons	Landfarming	TPH, 67–75% (Infrared)	[42]
Heavy vehicle maintenance yard	Oily waste	Landfarming	TPH, 74% (GC)	[43]

^aTotal petroleum hydrocarbons.^bThin-layer chromatography.

15.6 EX SITU LAND TREATMENT TECHNIQUES

Ex situ bioremediation technologies require that contaminated soil be excavated, where it can then be treated either on- or off-site. *Ex situ* techniques facilitate greater control on environmental conditions, enabling biodegradation rate optimization [26]. Due to the ability to homogenize contaminated soil, treatment is typically more uniform and requires less time than *in situ* treatment techniques. However, *ex situ* technologies are more costly due to excavation and site preparation and operation. In addition, excavation of soil increases exposure to, and mobility of, contaminants.

Site preparation for most *ex situ* bioremediation technologies requires the construction of a liner system to prevent the movement of contaminants into the subsurface and

surface water runoff control systems to prevent off-site transport. Operational requirements include inputs to maintain optimal environmental conditions, including nutrient and moisture application and aeration, via blower systems or mechanical agitation.

Results from examples of field application of *ex situ* treatment technologies are given in Table 15.3.

15.6.1 Landfarming and Land Treatment

Landfarming, or land treatment, involves land application of a waste stream such as contaminated soil in thin layers, where nutrient and moisture additions, and tillage to increase aeration, stimulate and enhance biodegradation [26]. Landfarming may also refer to the placement of thin lifts of soil in lined beds, versus applying directly to the

land [35]. If contaminated soil is applied directly to the land without a barrier in place, on- and off-site impacts on groundwater and surface water, air, and the food chain must be prevented.

Bleckmann et al. highlight that the petroleum industry has been successfully using land treatment or landfarming for treatment and disposal for decades [41]. Landfarming is well suited for the treatment of continuous waste streams [43]. This method is particularly effective in areas with low rainfall (275 mm), high evaporative climates (annual evaporation of 2700 mm), and large areas of available land [43]. Shallow contamination may be treated with this technique without the need for excavation [30].

A key limitation of land treatment is the loss of volatile organic contaminants to the atmosphere [43]. Legislation may prevent the use of landfarming as a remediation strategy if air emissions of volatile organic compounds are to be controlled.

During a 1-year assessment of three *ex situ* bioremediation technologies, landfarming resulted in the greatest reduction of oil contamination [39]. Ninety-one percent of total alkanes and 82.5% of total petroleum hydrocarbons were degraded, where the soil was amended with nitrogen, phosphorus, and wood chips [39]. Field-scale landfarming successfully reduced soil concentrations of diesel contamination to target levels, but it is unknown to what degree evaporation contributed to these losses [26].

A laboratory study investigating the optimization of environmental conditions for landfarming of oily sludges indicated that the addition of micronutrients supplied via dilution of Hoagland trace element solution and organic supplements (yeast extract and dried domestic sewage sludge) was not beneficial [44]. Optimal conditions include a soil water holding capacity of 30–90%; a pH of 7.5–7.8; C–N and C–P ratios of 60:1 and 800:1, respectively; and a temperature of 20°C or greater. Biodegradation of saturated hydrocarbons was greatest at low application rates, but the opposite was true for aromatic hydrocarbons. Thus, the authors concluded that an application rate of 5% w/w was a good compromise between biodegradation rates of all hydrocarbon compounds and efficient land use.

15.6.2 Biopiles

In general, the biopile technique involves mixing excavated soils with amendments and placing the material on a treatment area that encompasses both a leachate collection system and some form of aeration [35]. Aeration may be achieved by placing soil in either windrows that are turned regularly with heavy equipment or in static piles with aeration pipes placed below or within the pile. In-vessel systems are uncommon due to high costs; windrows are considered to be the most cost-effective biopile method, and mechanical agitation facilitates the addition of moisture or nutrients [35]. Soil biopiles may be covered, enabling more favorable temperature and moisture conditions for effective bioremediation.

Typically, piles are placed on an impermeable liner to prevent seepage of contamination into the subsurface soils. Often, front-end loaders are utilized for periodic turning and windrow construction, but dedicated windrow-turning machinery may be used.

Contaminated soil is often amended with bulking agents, which function to increase air space in the matrix, and organic amendments to ensure the required carbon to nitrogen ratio exists.

Al-Daher et al. evaluated the use of turned windrows at pilot scale following selection as the most appropriate technology for remediation of oil-contaminated soil in the Kuwait desert [39]. On average, 60 and 55% reduction in total petroleum hydrocarbons and total polycyclic aromatic hydrocarbons were observed. Wood chips, dried sewage sludge, and mature compost were assessed as soil amendments, but did not significantly impact hydrocarbon degradation. Covering the windrow during the summer months increased the moisture content from 3 to 12% and resulted in 19.3% increase in total petroleum hydrocarbon degradation over 3 months. Static biopiles were found to reduce total petroleum hydrocarbons less than both windrow piles and landfarming but resulted in significantly lower operation and maintenance costs, smaller operating area, and less water for irrigation [39].

Eszenyiova et al. determined during a pilot-scale experiment that turned windrows reduced the time required to decontaminate soil by two and a half to three times, compared to land treatment [42].

15.6.3 Organic Amendments

Amending excavated contaminated soil with organic amendments is common, especially for biopile treatment technologies. Amendments may serve to increase air space within the soil matrix, ensuring aerobic conditions are maintained, supply nutrients for microbial growth, increase the water holding capacity of the soil, and supply viable microbial populations [45]. Examples of organic amendments include, but are not limited to, agricultural crop residues such as straw, animal manure, wastewater biosolids, and commercial waste products such as sawdust.

Pometto et al. demonstrated in a laboratory study that biodegradation of petroleum hydrocarbons was increased by 20% when soil was mixed with soybean hulls [45]. A comparative study assessed peat or sawdust as a spill adsorbent and subsequent organic nutrient provider and established that peat not only increased alkane degradation by 1.5% over sawdust but also provides a soluble carbon source for sustaining biomass [46]. Although biosolids have been found to stimulate biodegradation of hydrocarbons in soil, Rivera-Espinoza and Dendooven concluded that the addition of biosolids or maize to clayey soil contaminated with polycyclic aromatic hydrocarbons did not accelerate biodegradation [47].

The addition of amendments may be dictated more by what is locally available versus what has been found to be most effective in improving biodegradation from literature studies.

15.7 BIOAUGMENTATION STRATEGIES

Terrestrial environments tend to inhabit a larger number of microorganisms compared to aquatic environments, due to higher concentrations of organic and inorganic matter. Indigenous microbial populations that are adapted to the particular soil environment are expected to negatively impact seeded microorganisms' ability to survive and thrive due to competition [1]. Studies have shown, however, that the addition of microorganisms already acclimated to hydrocarbons to a contaminated soil system enhances the biodegradation rate [2]. If no increase in biodegradation is observed following bioaugmentation, either sufficient indigenous microbial communities capable of biodegrading petroleum hydrocarbons already exist [2] or the additional microorganisms could not compete with existing populations. Jorgensen concluded that few success stories of bioaugmentation exist to date [4]. Since microorganisms capable of biodegrading petroleum hydrocarbons are so numerous in the subsurface and easily stimulated under both aerobic and anaerobic conditions, inoculation with foreign species may provide little advantage [4]. Aislabie et al. concluded that, in general, concentrating efforts on alleviating inhibitory environmental conditions is more beneficial than bioaugmentation, especially in cold climates, since acclimated microorganisms capable of biodegrading petroleum hydrocarbons are prolific in the subsurface [26].

It is essential when selecting strains of microorganisms for bioaugmentation that not only their ability to metabolize the contaminants of concern is considered but also the environment in which the injected microorganisms are to function.

15.7.1 Key Bacteria Used in Bioaugmentation

Nonindigenous *Acinetobacter* sp. increased hydrocarbon biodegradation in Antarctic soil, and an indigenous *Rhodococcus* sp. enhanced biodegradation of diesel fuel [26]. Since few studies of successful bioaugmentation exist, there is little data about specific microbial isolates utilized. Mandal et al. developed a bacterial consortium consisting of four indigenous bacteria isolated from oil-contaminated sites [48]. This consortium degraded more than 90% total petroleum hydrocarbons at a contaminated site, versus only 14% degradation with no treatment.

15.7.2 Role of Other Organisms

Organisms other than microbes, such as earthworms, may improve biodegradation via a number of mechanisms. Earthworms maintain a complex relationship with microorganisms, whereby earthworms fragment organic matter and microorganisms serve as a major source of nutrients for earthworms [22]. The presence of three species of earthworm (*Lumbricus terrestris*, *Allolobophora chlorotica*, and *Eisenia fetida*) significantly improved the biodegradation of total petroleum hydrocarbons, reducing concentrations by

up to 40%, versus 9–17% without worms [22]. Californian red worms contributed to bioremediation of oil-polluted soils in 5 months [49]. An indirect benefit of the presence of earthworms is aeration of the soil due to their movement.

15.8 BIOSTIMULATION STRATEGIES

Biostimulation improves the conditions for biodegradation to occur, either by indigenous microorganisms or inoculants. Aside from improving environmental conditions for microorganisms, via the addition of nutrients or an electron acceptor, additional biostimulation strategies exist to better biodegradation.

15.8.1 Biosurfactants

Biodegradation of petroleum hydrocarbons may be limited by availability to microorganisms in the soil [50]. The addition of synthetic or biogenic biosurfactants has been considered as a means for increasing accessibility of hydrocarbon compounds to microorganisms for biodegradation [2]. Surfactants are surface-active agents that reduce surface tension and stabilize emulsions [10]. Since microorganisms are only able to degrade hydrocarbons at the oil–water interface, increasing the surface area of this interface will greatly increase biodegradation potential.

The release of biosurfactants by bacteria and fungi represents an important process for the uptake of hydrocarbons [1]. Those microorganisms that are able to produce biosurfactants or emulsifiers may have a selective advantage to biodegrade hydrophobic hydrocarbon compounds, especially at lower temperatures where the effects of viscosity and water solubility are more intense [5]. For example, some rhodococci have been found to produce cell-associated biosurfactants for alkanes that are solid at low temperatures [26]. Banat et al. isolated numerous bacterial species that produced biosurfactants [10].

Martins et al. utilized the filamentous fungus *Aspergillus fumigatus* to produce a biosurfactant using solid-state fermentation [51]. A 99% reduction in both aliphatic and polycyclic aromatic hydrocarbons was observed when the biosurfactant was utilized, versus 90% for a chemical disperser. Martienssen and Schirmer emphasize that the use of industrial surfactants for bioremediation purposes is not advisable, as these compounds possess inadequate biocompatibility with microorganisms, sometimes even causing toxic effects [50]. Thus, they conclude that biosurfactants, or close to nature synthetic surfactants, will effectively improve bioavailability of substrates to microorganisms without negative impacts.

Readers are encouraged to refer to the following source for more information, especially with regard to designing engineered bioremediation systems:

Atlas, R. and Philip, J., Bioremediation of contaminated soils and aquifers, *Bioremediation—Applied Microbial Solutions for Real-World Environmental Cleanup*, ASM Press, 139, 2005.

REFERENCES

- [1] Leahy, J.G. and R.R. Colwell, Microbial degradation of hydrocarbons in the environment, *Microbiol. Rev.*, 54, 305, 1990.
- [2] Mohammed, N., R.I. Allayla, G.F. Nakhla, S. Farooq, and T. Husain, State-of-the-art review of bioremediation studies, *J. Environ. Sci. Health*, A31, 1547, 1996.
- [3] Horel, A. and S. Schiewer, Investigation of the physical and chemical parameters affecting biodegradation of diesel and synthetic diesel fuel contaminating Alaskan soils, *Cold Reg. Sci. Technol.*, 58, 113, 2009.
- [4] Jorgensen, K.S., In-situ bioremediation, *Adv. Appl. Microbiol.*, 61, 285, 2007.
- [5] Ahn, J., M. Kim, M. Kim, J. Lim, G. Lee, et al., Analysis of bacterial diversity and community structure in forest soils contaminated with fuel hydrocarbons, *J. Microbiol. Biotechnol.*, 16, 704, 2006.
- [6] Benka-Coker, M.O. and J.A. Ekundayo, Applicability of evaluating the ability of microbes isolated from an oil spill site to degrade oil, *Environ. Monit. Assess.*, 45, 259, 1997.
- [7] Akoachere, J.T.K., T.N. Akenji, F.N. Yongabi, G. Nkwelang, and R.N. Ndip, Lubricating oil-degrading bacteria in soils from filling stations and auto-mechanic workshops in Buea, Cameroon: Occurrence and characteristics of isolates, *Afr. J. Biotechnol.*, 7, 1700, 2008.
- [8] Biswas, D., S. Dutta, and R. Saha, Effect of *Pseudomonas* sp. on diesel and other petroleum fractions, *J. Indian Chem. Soc.*, 83, 1185, 2006.
- [9] Ijah, U.J.J. and S.P. Antai, The potential use of chicken-drop micro-organisms for oil spill remediation, *Environmentalist*, 23, 89, 2003.
- [10] Banat, I.M., K.S.M. Rahman, and J. Thahira-Rahman, Bioremediation of hydrocarbon pollution using biosurfactant producing oil degrading bacteria, in *Oil and Hydrocarbon Spills III: Modelling, Analysis, and Control*, C.A. Brebbia (eds.), Southampton: Wessex Institute of Technology, 2002.
- [11] Ellis, B., M.T. Balba, and P. Theile, Bioremediation of oil contaminated land, *Environ. Technol.*, 11, 443, 1990.
- [12] Nwachukwu, S.U., Bioremediation of sterile agricultural soils polluted with crude petroleum by application of the soil bacterium, *Pseudomonas putida*, with inorganic supplements, *Curr. Microbiol.*, 42, 231, 2001.
- [13] Rughavan, P.U.M. and M. Vivekanandan, Bioremediation of oil-spilled sites through seeding of naturally adapted *Pseudomonas putida*, *Int. Biodeterior. Biodegradation*, 4, 29, 1999.
- [14] Rema, S., M.R. Pandian, S. Sudhakaran, and R. Devi, Petroleum hydrocarbon degradation by native isolate *Rhodococcus*, *Asian J. Microbiol. Biotechnol. Environ. Sci.*, 9, 973, 2007.
- [15] Lee, M., M.K. Kim, I. Singleton, M. Goodfellow, and S.T. Lee, Enhanced biodegradation of diesel oil by a newly identified *Rhodococcus baikourensis* EN3 in the presence of mycolic acid, *J. Appl. Microbiol.*, 100, 325, 2006.
- [16] Christofi, N., I.B. Ivshina, M.S. Kuyukina, and J.C. Philp, Biological treatment of crude oil contaminated soil in Russia, in *Contaminated Land and Groundwater: Future Directions*, D.N. Lerner and N.R.G. Walton (eds.), London: Engineering Geology Special Publications, 1998.
- [17] Banerjee, M. and S. Shrivastava, Sensitivity of cyanobacterium *Mastigocladus* to petrol and its role in bioremediation, *J. Ind. Pollut. Control*, 21, 77, 2005.
- [18] Gallego, J.L.R., J. Loredó, J.F. Llamas, F. Vazquez, and J. Sanchez, Bioremediation of diesel-contaminated soils: Evaluation of potential *in situ* techniques by study of bacterial degradation, *Biodegradation*, 12, 325, 2001.
- [19] Hestbjerg, H., P.A. Willumsen, M. Christensen, O. Andersen, and C.S. Jacobsen, Field scale bioremediation of tar contaminated soil with commercial mushroom *Pleurotus ostreatus* refuse, in *Oil and Hydrocarbon Spills III: Modelling, Analysis, and Control*, C.A. Brebbia (eds.), Southampton: Wessex Institute of Technology, 2002.
- [20] Yateem, A., M.T. Balba, and N. Al-Awadhi, White rot fungi and their role in remediating oil-contaminated soil, *Environ. Int.*, 24, 181, 1998.
- [21] Palittapongampim, M., P. Pokethitiyook, E.S. Upathm, and L. Tangbanluekal, Biodegradation of crude oil by soil microorganisms in the tropic, *Biodegradation*, 9, 83, 1998.
- [22] Schaefer, M., S.O. Peterson, and J. Filser, Effects of *Lumbricus terrestris*, *Allolobophora chlorotica* and *Eisenia fetida* on microbial community dynamics in oil-contaminated soil, *Soil Biol. Biochem.*, 37, 2065, 2005.
- [23] Dott, W., D. Feidieker, M. Steiof, P.M. Becker, and P. Kampfer, Comparison of ex situ and in situ techniques for bioremediation of hydrocarbon-polluted soils, *Int. Biodeterior. Biodegradation*, 35, 301, 1995.
- [24] Foght, J.M., Anaerobic biodegradation of aromatic hydrocarbons: Pathways and prospects, *J. Mol. Microbiol. Biotechnol.*, 15, 93, 2008.
- [25] Widdel, F. and R. Rabus, Anaerobic biodegradation of saturated and aromatic hydrocarbons, *Curr. Opin. Biotechnol.*, 12, 259, 2001.
- [26] Aislabie, J., D.J. Saul, and J.M. Foght, Bioremediation of hydrocarbon-contaminated polar soils, *Extremophiles*, 10, 171, 2006.
- [27] Margesin, R. and F. Schinner, Biodegradation and bioremediation of hydrocarbons in extreme environments, *Appl. Microbiol. Biotechnol.*, 56, 650, 2001.
- [28] Chang, B.V., L.C. Shiung, and S.Y. Yuan, Anaerobic biodegradation of polycyclic aromatic hydrocarbon in soil, *Chemosphere*, 48, 717, 2002.
- [29] Ulrich, A.C., S.E. Guigard, J.M. Foght, K.M. Semple, K. Pooley, et al., Effect of salt on aerobic biodegradation of petroleum hydrocarbons in contaminated groundwater, *Biodegradation*, 20, 27, 2009.
- [30] US EPA, *How To Evaluate Alternative Cleanup Technologies For Underground Storage Tank Sites: A Guide For Corrective Action Plan Reviewers*, Washington, DC: U.S. Environmental Protection Agency, 2004.
- [31] Boopathy, R., Anaerobic biodegradation of no. 2 diesel fuel in soil: A soil column study, *Bioresour. Technol.*, 94, 143, 2004.
- [32] Gogoi, B.K., N.N. Dutta, P. Goswami, and T.R. Krishna Mohan, A case study of bioremediation of petroleum-hydrocarbon contaminated soil at a crude oil spill site, *Adv. Environ. Res.*, 7, 767, 2003.
- [33] Brown, R.A. and J.R. Crosbie, Oxygen sources for bioremediation, in *Bioremediation: Field Experience*, P.E. Flathman, D.E. Jerger, and J.H. Exner (eds.), CRC Press, Inc., Boca Raton, FL, 1994.
- [34] Menendez-Vega, D., J.L.R. Gallego, A.I. Pelaez, F. de Cordoba, J. Moreno, et al., Engineered *in situ* bioremediation of soil and groundwater polluted with weathered hydrocarbons, *Eur. J. Soil Biol.*, 42, 310, 2007.
- [35] Van Deuren, J., T. Lloyd, S. Chhetry, R. Liou, and J. Peck, *Remediation Technologies Screening Matrix and Reference Guide*, Version 4.0, Federal Remediation Technologies Roundtable, Platinum International, Inc., Alexandria, VA, 2002.
- [36] Nelson, C.H., R.J. Hicks, and S.D. Andrews, An integrated approach for in situ bioremediation of petroleum hydrocarbon-contaminated soil and groundwater, in *Bioremediation: Field Experience*, P.E. Flathman, D.E. Jerger, and J.H. Exner (eds.), CRC Press, Inc., Boca Raton, FL, 1994.
- [37] Margesin, R. and F. Schinner, Bioremediation (natural attenuation and biostimulation) of diesel-oil-contaminated soil in an alpine glacier skiing area, *Appl. Environ. Microbiol.*, 67, 3127, 2001.

- [38] Hunkeler, D., R.U. Meckenstock, B.S. Lollar, T.S. Schmidt, and J.T. Wilson, A guide for assessing biodegradation and source identification of organic ground water contaminants using compound specific isotope analysis (CSIA), EPA 600/R-08/148, United States Environmental Protection Agency, 2008.
- [39] Balba, M.T., R. Al-Daher, N. Al-Awadhi, H. Chino, and H. Tsuji, Bioremediation of oil-contaminated desert soil: The Kuwait experience, *Environ. Int.*, 24, 163, 1998.
- [40] Al-Daher, R., N. Al-Awadhi, and A. El-Nawawy, Bioremediation of damaged desert environment using the windrow soil pile system in Kuwait, *Environ. Int.*, 24, 175, 1998.
- [41] Bleckmann, C.A., M.E. Oxley, E.J. Wilson, K.W. Hayes, and N.L. Hercyk, Land treatment of produced oily sand: Field results, *Waste Manag. Res.*, 15, 223, 1997.
- [42] Eszenyiova, A., G. Polakovicova, V. Bilka, and H. Rajnochova, Biological clean-up of hydrocarbon pollution, *PTQ*, Autumn, 133, 2000.
- [43] Guerin, T.F., Long-term performance of a land treatment facility for the bioremediation of non-volatile oily wastes, *Resour. Conserv. Recy.*, 28, 105, 2000.
- [44] Dibble, J.T. and R. Bartha, Effect of environmental parameters on the bioremediation of oil sludge, *Appl. Environ. Microbiol.*, 37, 729, 1979.
- [45] Pometto, A.L., C.S. Oulman, A.A. DiSpirito, K.E. Johnson, and S. Baranow, Potential of agricultural by-products in the bioremediation of fuel spills, *J. Ind. Microbiol. Biotechnol.*, 20, 369, 1998.
- [46] Saez-Navarrete, C., C.A. Gelmi, L. Reyes-Bozo, and A. Godoy-Faundez, An exploratory study of peat and sawdust as enhancers in the (bio)degradation of n-dodecane, *Biodegradation*, 19, 527, 2008.
- [47] Rivera-Espinoza, Y. and L. Dendooven, Dynamics of carbon and nitrogen in a mixture of polycyclic aromatic hydrocarbons contaminated soil amended with organic residues, *Environ. Technol.*, 28, 883, 2007.
- [48] Mandal, A.K., P.M. Sarma, M. Dwivedi, A. Swaleh, B. Lal, et al., Bioremediation of oil contaminated soil at South Santhal CTF, Mehsana, India: A case study, *Asia Pacific Oil & Gas Conference and Exhibition*, Society of Petroleum Engineers, Jakarta, Indonesia, October 30–November 1, 2007.
- [49] Ilarionov, S.A., I.G. Kalachnikova, and V.A. Sergeev, Rehabilitation of oil-polluted soils using products obtained in the process of organic wastes bioconversion, in *Oil and Hydrocarbon Spills III: Modelling, Analysis, and Control*, C.A. Brebbia (eds.), Southampton: Wessex Institute of Technology, 2002.
- [50] Martienssen, M. and M. Schirmer, Use of surfactants to improve the biological degradation of petroleum hydrocarbons in a field site study, *Environ. Technol.*, 28, 573, 2007.
- [51] Martins, V.G., S.J. Kalil, and J.A.V. Costa, In situ bioremediation using biosurfactant produced by solid state fermentation, *World J. Microbiol. Biotechnol.*, 25, 843, 2009.

MICROBE-ASSISTED PHYTOREMEDIATION OF PETROLEUM IMPACTED SOIL: A SCIENTIFICALLY PROVEN GREEN TECHNOLOGY

KAREN E. GERHARDT,^{1,2} PERRY D. GERWING,³ XIAO-DONG HUANG,² AND BRUCE M. GREENBERG^{1,2}

¹Department of Biology, University of Waterloo, Waterloo, Ontario, Canada

²Waterloo Environmental Biotechnology Inc., Hamilton, Ontario, Canada

³Earthmaster Environmental Strategies Inc., Calgary, Alberta, Canada

16.1	Introduction	407
16.1.1	Overview of Phytoremediation	407
16.1.2	Developing Microbe-Assisted Phytoremediation as a Remedial Strategy for PHC	407
16.1.3	Benefits and Challenges of Phytoremediation and Microbe-Assisted Phytoremediation	411
16.1.4	Successful Field Tests of Phytoremediation	413
16.2	PGPR-Enhanced Phytoremediation System(s)	413
16.2.1	Development, Proof, and Full-Scale Application of PEPS	414
16.2.2	Keys to the Success of PEPS	415
16.3	Case Studies of Full-Scale Petroleum Phytoremediation	416
16.3.1	Case Study #1: Edson, Alberta	416
16.3.2	Case Study #2: Peace River, Alberta	418
16.3.3	Case Study #3: Hinton, Alberta	419
16.3.4	Case Study #4: Dawson Creek, British Columbia	420
16.3.5	Overall Conclusions from Case Studies	420
16.4	Achieving Regulatory Criteria	421
16.4.1	Optimizing PHC Analytical Protocols for Removal of BOC	421
16.4.2	Plant Toxicity Testing	422
16.5	Conclusions	422

16.1 INTRODUCTION

16.1.1 Overview of Phytoremediation

Phytoremediation is a strategy whereby plants are used to extract, immobilize, contain, and/or degrade soil contaminants. Although employing plants for remediation was explored in the 1950s to remove radionuclides from

contaminated soil, the term phytoremediation was not used until the 1980s, and rapid expansion in this field only began in the mid-1990s [1]. Phytoremediation has now emerged as a promising remedial technology for *in situ* removal of many contaminants, including petroleum hydrocarbon(s) (PHC) [2–4]. Microbe-assisted phytoremediation, including rhizoremediation, appears to be particularly effective for removal and/or degradation of PHC from impacted soils, especially when used in conjunction with PHC-tolerant plant species and appropriate agronomic techniques [5–15].

Plants have extensive rooting systems that can explore large volumes of soil to allow for effective remediation of various contaminants within different soil types. Using this process, contaminants are either broken down in the soil or stored in plant tissue (typically in the leaves). When phytoremediation and microbe-assisted phytoremediation are used to treat PHC-impacted soil, the PHC do not accumulate in plants; instead, they are metabolized in the soil to nontoxic and biological compounds [2–14]. A variety of PHC-degrading enzymes can be found in plants, fungi, endophytic bacteria, and root-colonizing bacteria; these include peroxidases, dioxygenases, ω -oxygenases, P450 monooxygenases, laccases, and nitrilases [2,3,16–25]. In the soil surrounding plant roots (the rhizosphere), naturally occurring soil bacteria and plants work together or independently to degrade PHC.

16.1.2 Developing Microbe-Assisted Phytoremediation as a Remedial Strategy for PHC

Extensive research has been performed in laboratories and greenhouses to develop phytoremediation systems. Some of this work explored the use of plants for removal of

contaminants from spiked soil and soil excavated from contaminated sites [10–12,26–28]. Many of these experiments provided valuable insight into the mechanisms associated with phytoremediation of organic contaminants, including PHC [2,3,6,14,29–31]. Some organic compounds can be taken up by plant roots and transported across plant cellular membranes. Some of these same water-soluble low-molecular-weight compounds can then be released through leaves during transpiration (loss of water from plants) in a process termed phytovolatilization. Some of the nonvolatile compounds can be degraded or rendered nontoxic via enzymatic modification and sequestration *in planta* (phytodegradation, phytoextraction). Various organic compounds can also be degraded by plant enzymes such as laccases, dehalogenases, nitroreductases, nitrilase, and peroxidases that are released into the soil (e.g., alfalfa root peroxidase may be involved in rhizosphere degradation of phenanthrene) [31–34]. In addition, root growth and death create channels that allow for movement of water and oxygen into and within the soil matrix (i.e., the areas around plant roots generate small conduits through which oxygen can diffuse), which can enhance oxidative degradation of recalcitrant organic compounds that were previously “trapped” in soil [13,23,35,36]. In the case of PHC, some of the low-molecular-weight compounds can be phytovolatilized; however, root uptake is negligible or minimal for most high-molecular-weight compounds, and the majority of PHC are putatively degraded in the rhizosphere [28,31,37,38].

Laboratory and greenhouse experiments had also been conducted with spiked and/or excavated soil to determine how contaminated soils affect plant growth [3,10,12,19,29,36,39–42]. These experiments allowed researchers to explore methods for overcoming contaminant stress, without the confounding effects of field-dependent variables such as weather and nutrient limitation. It has been reported that plants can produce more than 160 million km of roots per acre, which suggests great potential for phytoremediation in natural environments [43]; however, soil PHC tend to inhibit seed germination and plant growth, including root growth, in part due to oxidative stress [10,12,19,40–42,44]. Notably, preferential root growth in uncontaminated soil has been demonstrated, with growth through petroleum-contaminated zones occurring only when no immediate uncontaminated soil is available [39]. Thus, plant root density is often greater in zones with lower PHC levels. When plants are exposed to PHC-impacted soil, volatile hydrocarbons can pass through root cell membranes and adversely affect plant growth, and/or hydrophobicity of the oil-contaminated soil limits seed and root access to water and oxygen [41,44]. The resulting plant stress will limit the rate of phytoremediation *in situ* [10,11,36]. Contaminated soils also tend to be nutrient poor and/or lack microbial diversity, which contributes to suboptimal plant biomass accumulation, as well as impeded rates of remediation [12,36,45,46].

When using spiked soils for remediation experiments in the greenhouse, the focus has often been on the ability of a

given plant to survive and grow in the presence of a specific compound and/or to remediate it. However, soils at contaminated sites generally contain complex mixtures of chemicals that often include both organic and inorganic components. In spiked soils, chemicals tend to be bioavailable, whereas contaminants in naturally weathered soils are often not as readily bioavailable [47–49]. For example, germination and plant growth of seven plant species was assessed in soil spiked with a pure PAH mixture, soil spiked with coal tar, and weathered soil from a former coking plant [50]. Significantly different results in germination and plant growth were observed using these three experimental soils, which highlighted the need to perform greenhouse experiments with soils collected from contaminated sites before implementing a field-level phytoremediation program.

Concomitant with phytoremediation garnering widespread interest, the field of microbial bioremediation has also been extensively explored [51–54]. Contaminant-degrading microbes have been isolated from impacted soils and characterized [13,27,51,55,56], and it is postulated that contaminant-degrading bacteria can be found virtually in all soils [14]. Mechanistic studies using these microbial isolates have been performed on both spiked and field soils [12,53,55,57,58].

The first step in microbial PHC metabolism involves a membrane-bound oxygenase; therefore, the microbes must come in direct contact with the PHC substrate. Oil droplets are often trapped between soil particles, limiting their accessibility to microbes (Fig. 16.1a). Aerobic PHC degradation in soil often occurs at the oil droplet–water interface in aqueous micropores (Fig. 16.1b). At the PHC–water interface, microbes use adhesion methods and/or biosurfactants [13,54,55,59]. The first steps of the degradative pathway incorporate two O atoms into the PHC to form fatty acid analogues (Fig. 16.1c). The PHC-degrading microbes then grow and multiply at the surface of the oil droplet. Because any given microbe can only degrade part of the complex mixture of hydrocarbons in the oil droplet, they desorb from the surface and can be replaced by other microbes that will continue the degradation process [54]. Some microbes can completely degrade a specific petroleum compound (usually a low-molecular-weight PHC); however, individual species generally do not contain entire degradation pathways. As long as there is a microbial species present that contains the enzyme required to catalyze the limiting step in the degradation pathway, microbial consortia in soil can work in tandem to effectively degrade the catabolic intermediates [4,12,13,23,60–62]. In general, alkanes are more biodegradable than aromatics, resins, and asphaltenes. Resins and asphaltenes (polar fraction) can be particularly recalcitrant due to their hydrophobicity and low bioavailability [37,63].

Following isolation and characterization of PHC-degrading microbes, attempts have been made to inoculate contaminated field soils with the isolates; however, this remedial strategy has proven to be largely unsuccessful [2,13,52,53]. There are numerous reasons for this general

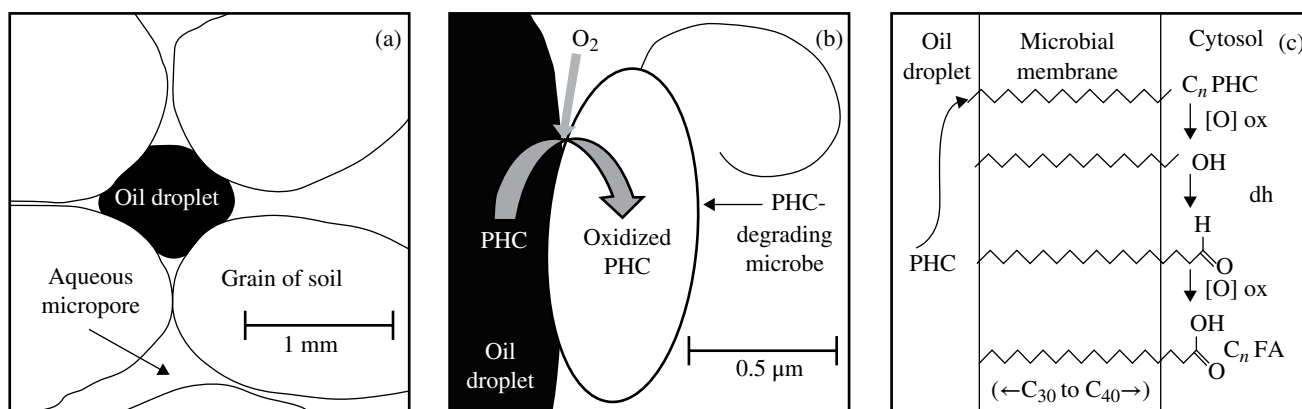


FIGURE 16.1 Microbial PHC degradation in soil. (a) Hydrophobic oil droplet trapped in an aqueous micropore and bound to soil particles. (b) Aerobic PHC degradation in the aqueous micropore by a PHC-degrading microbe at the oil–microbe interface. (c) Potential oxygenation pathway of a PHC to a fatty acid by a PHC-degrading bacterium. In many soil bacteria, oxygenation is catalyzed by ω -oxygenase. dh, dehydrogenase; FA, fatty acid; ox, oxygenase.

lack of success [13,47,49,56]. Lack of bioavailability of some PHC in bulk soil is one key factor. Hydrophobic oil droplets comprised of a complex mixture of PHC compounds are often bound to soil particles or physically trapped in micropores (Fig. 16.1a). Bioavailability depends on complex interactions between chemical, biochemical, physical, and environmental factors in the microenvironment [2,64–66]. Insufficient nutrient levels in PHC-contaminated soils are another key factor: theoretically, it takes 150 mg N and 30 mg P for microbes to convert 1 g PHC to microbial biomass [54]. The importance of nitrogen for efficient degradation of phenol by *Pseudomonas putida* has been demonstrated recently [67]. The elemental composition of crude oil is predominantly carbon (~85%) and hydrogen (~12%), and there is little nitrogen (0.1–2.0%) and no phosphorus present for use in metabolic processes [68]. Other reasons that microbial bioremediation often fails in the field are low soil O_2 concentration, which limits the rate of PHC metabolism; the inability of microbes to grow to sufficient depths to reach subsurface contaminants; the preferential utilization of carbon compounds other than the contaminant of interest; the inability of introduced microbes to compete with existing microflora and microfauna in the soil environment; the presence of other toxicants at the site that inhibit microbial growth; and the difficulty of getting microbes to reach high enough titers (i.e., high microbial biomass) in bulk soil to facilitate rapid rates of remediation.

A convergence of phytoremediation and microbial bioremediation strategies has led to a more successful approach to remediation of organic contaminants. Microbe-assisted phytoremediation has been investigated in the laboratory, greenhouse, and field with the focus on either native soil microbial communities or the introduction of specific microbes via seed inoculation [10–14,28,69,70]. Many organic compounds, including the majority of PHC, can be degraded by microbes in the rhizosphere (rhizoremediation) [23,38,71]. The rhizosphere is a dynamic microhabitat

within the soil that extends 1–2 mm beyond plant roots [60, 72]. This area is densely populated with microbes relative to bulk soil [60]. On a per gram basis, rhizosphere soil has 10–100 times more microbes than non-vegetated soil, and this marked increase in microbial biomass is an attribute of the “rhizosphere effect” [38,73,74]. In soil containing large volumes of roots, microbial populations can reach titers of approximately 10^{12} cells per gram of soil [75]. Notably, in PHC-contaminated soils, the rhizosphere tends to be enriched in PHC degraders, relative to the bulk soil [44,76]. After the Gulf War, plants growing in an oil-contaminated area of the Kuwaiti desert were found to support hundreds of millions of oil-degrading microbes per gram of fresh roots [77]. Microbial populations can thrive in the rhizosphere microenvironment because plants provide substrates for microbial growth and water drawn to the plant roots is available for use in microbial metabolism [72].

Many of the plant–microbe interactions in the rhizosphere are mutually beneficial. Some rhizosphere microbes can enhance plant growth via chelators for delivering key plant nutrients, protection against plant pathogens, degradation of contaminants (including PHC) before they can negatively impact the plants, and synthesis of compounds that stimulate root growth or protect plants by decreasing stress hormone levels [4,12,72,78–81]. Enhanced plant growth results in higher root biomass, which in turn supports more microbial growth, including PHC degraders in the rhizosphere. Rhizoremediation is emerging as one of the most effective means by which plants can be used to significantly enhance PHC remediation, including degradation of large recalcitrant compounds. Complex interactions involving roots, root exudates, rhizosphere soil, and microbes result in degradation of PHC to nontoxic or less toxic compounds. Some of the main processes involved in rhizoremediation of PHC are summarized in Figure 16.2.

PHC degradation using microbe-assisted phytoremediation is achieved primarily by phytostimulation of rhizosphere

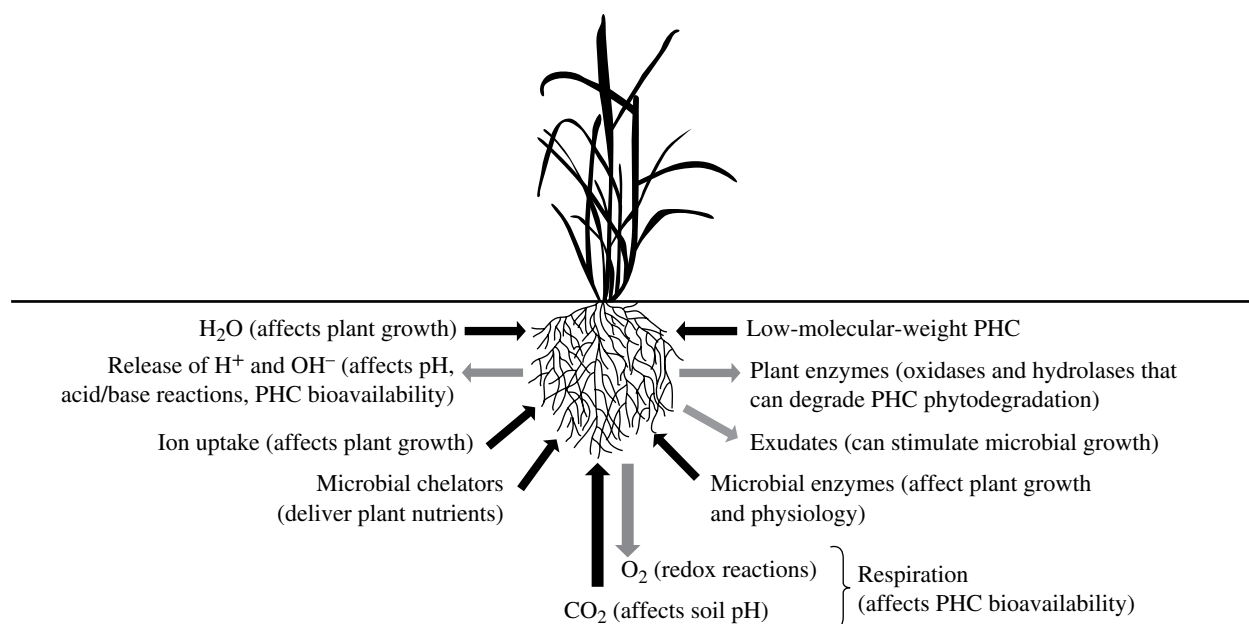


FIGURE 16.2 Rhizosphere processes that play a role in phytoremediation and microbe-assisted phytoremediation.

microbes, including PHC degraders. Roughly 40% of a plant's photosynthate is rapidly deposited in the soil as sugars, organic acids, and other organic compounds (rhizodeposition) [33,82,83]. These compounds are commonly used as energy (oxidation/reduction reactions convert the organics to oxidized end products) and carbon sources (the organic carbon is incorporated into new cellular material) by soil microbes during normal metabolic processes [12,14,35,46,84]. Root exudates containing amino acids and small soluble proteins can also provide available forms of nitrogen (a potentially limiting nutrient in oil-contaminated soils) [34,85–87]. For example, tryptophan is significantly more available to microbes in the rhizosphere of slender oat plants than to those in adjacent bulk soils [86]. In addition to nutrients being released by plant roots, soil water movement driven by plant transpiration can carry other nutrients into the rhizosphere from adjacent bulk soil [88].

The successful application of phytoremediation and rhizoremediation is largely dependent on the capacity of contaminant degraders or plant growth-promoting microbes to efficiently colonize growing roots [89]. Numerous bacterial traits, involving a multitude of genes, are required for effective root colonization [13,60,89–93]. Such traits include the ability to produce thiamine and biotin, synthesize the O-antigen of lipopolysaccharide, synthesize amino acids, and produce isoflavonoid induced efflux pumps.

The importance of microbial motility for rhizoremediation has been demonstrated using aflagellate mutants and rhizobacteria with diminished motility relative to wild-type colonizers [90,94]. Chemotaxis toward specific root exudate compounds is a key factor in efficient root colonization,

although the chemotactic response can be elicited by different compounds depending on the colonizing species [92,93]. Plants can also support PHC-degrading microbes within the root interior (endophytes). For example, Altai wild rye (*Elymus angustus*, a perennial grass) selectively recruits endophytic hexadecane degraders in the presence of high PHC concentrations and maintains them during periods of environmental stress [95].

One important group of plant compounds involved in root colonization processes are complex aromatic exudates such as flavonoids and coumarins. Notably, there is little accumulation of these compounds in soil, because they are consumed by microflora that degrade them and use the reduced carbon and nitrogen [12,14,33,35,46]. It is fortuitous that these aromatic plant compounds are structurally similar to many PHC, including polycyclic aromatic hydrocarbons (PAHs), thereby providing a means to exploit natural processes in the rhizosphere for the remediation of these contaminants [23,30,96–98].

One reason rhizoremediation occurs naturally is because flavonoids and other compounds released by roots can stimulate growth and activity of PHC-degrading bacteria [12,30,35,36,76,99,100]. For example, slender oat root exudates significantly enhanced degradation of phenanthrene in rhizosphere soils by increasing and maintaining PHC degrader populations [76]. Rhizospheric degradation of phenanthrene was shown to be a function of proximity to ryegrass roots, where higher numbers of PAH-degrading bacteria were found [62]. Secondary plant metabolites such as salicylate have been shown to stimulate microbial degradation of other PAHs [30]. In some cases, root compounds may selectively enhance PHC-degrading populations [101]; however, rhizodeposition

can also result in general increases in microbial numbers, thereby leading to nonselective proliferation of PHC-degrading microbes [71]. Notably, some plant species appear to increase the number of degradative microbes in a large volume of soil that extends beyond the rhizosphere [35,46].

Although rhizoremediation of PHC occurs naturally, it can be optimized using suitable plant-microbe pairs [6,23,96,102,103]. Desirable criteria for the plants are PHC tolerance and extensive root systems that can maximize contact between PHC and PHC-degrading microbes in the soil [23,41]. Relative to taproots, the fibrous root systems of grasses have more surface area that can support extensive microbial communities in close proximity to PHC, particularly because the fine roots have access to small pores in the soil where PHC are trapped [6,48,104]. Total measured root lengths of Italian ryegrass, Bermuda grass, and Southern crabgrass grown to maturity in 41 pots (~16 cm × 19 cm) containing 2% (w/w) diesel oil were 185, 858, and 1398 m, respectively [19]. In addition to high root biomass, large amounts of soluble organics are exuded by grass roots (2200 kg C/ha is translocated to the rhizosphere by grasses during one vegetative period) [82]. Grass roots have been shown to positively influence PHC remediation, reportedly to a depth of up to 3 m below the soil surface [62,76,95,105]. In a study of 18 diverse species from eight plant families, the Poaceae (grass) family was the most effective at degrading aged PAHs; perennial ryegrass, a member of the Poaceae family, was the most effective species tested [48]. Very high rates of PHC degradation have also been observed using a PHC-tolerant ornamental plant, *Impatiens balsamina*, which has an extensive fibrous root system [37]. In that study, a strong correlation between root length, total number of rhizosphere microbes, and PHC degradation was shown. Desirable criteria for microbes include plant growth-promoting properties and/or the ability to degrade PHC. Many bacteria and fungi can promote plant growth; *Pseudomonas* and *Bacillus* are the most commonly described genera of plant growth-promoting rhizobacteria (PGPR), and arbuscular mycorrhizal fungi such as *Glomus mosseae* have been shown to promote plant growth in PHC-impacted soils [60,106]. Approximately 70 genera of oil-degrading microorganisms have been identified, including well-studied soil bacteria from the genera *Pseudomonas*, *Bacillus*, *Acinetobacter*, *Rhodococcus*, and *Arthrobacter* and fungi such as basidiomycetes, which include white-rot and litter-decomposing fungi [17,18,56,77,102].

Pairing of plants and microbes for enhanced PHC remediation can range from relatively simple combinations to fairly complex ones. For example, a single suitable plant species can be combined with a single bacterium. Kuiper et al. [93,103] combined a PAH-tolerant grass cultivar with an extensive root system (*Lolium multiflorum* cv. Barmultra) and a naphthalene-degrading microbe with exceptional root-colonizing properties (*P. putida* strain PCL1444). The pseudomonad protected the annual ryegrass against naphthalene phytotoxicity, and the growing roots propelled the naphthalene-degrading

pseudomonad into an area of the soil that was inaccessible to the bacteria alone. The authors suggested that, in soil, the plant roots could deliver the PAH-degrading bacteria to areas such as clumps of clay containing pollutants that would not be accessed by bacteria in the absence of plant growth. Multiple species can be used in plant and/or microbial mixes. Tang et al. [102] showed enhanced remediation of PHC using perennial ryegrass and a microbial mix comprised of PHC degraders. As well, a mix of grass species/pseudomonades (PGPR) combination has been used to effect PHC remediation in the lab and the field [8,10,11,40,69]. It has even been suggested that it may be possible to select or engineer plant-microbe pairs to overcome the problem of lack of competitiveness in inoculated microbes under field conditions by using plants with exudates that are primarily available to a given PHC-degrading bacteria [6]. For more comprehensive discussions of the biological, chemical, biochemical, and physical processes involved in phytoremediation and rhizoremediation, the reader is directed to reviews of these processes [2,6,23,33,54,64,72,85,88,100,107].

16.1.3 Benefits and Challenges of Phytoremediation and Microbe-Assisted Phytoremediation

There are numerous advantages of microbe-assisted phytoremediation that other remedial options do not provide [2,3,12,108]. From a commercial standpoint, the most pronounced advantage is that phytoremediation is highly cost-effective [26]. Conventional *ex situ* methods, such as excavation and incineration/thermal desorption, off-site storage/landfill disposal, soil washing, chemical oxidative procedures, and *in situ* capping for stabilization are generally much more expensive than *in situ* phytoremediation and rhizoremediation. The cost of PGPR-enhanced phytoremediation is \$25–50 per m³ compared to \$75–150 per m³ for other remediation strategies [109]. As fuel costs continue to increase and landfill space becomes scarcer, landfill disposal costs are certain to rise. In addition to being expensive, these remedial strategies also involve high energy consumption, making them environmentally costly. Notably, landfill disposal does not actually eliminate PHC contamination, it merely moves the contamination and associated liability from one location to another, whereas PHC degradation occurs during microbe-assisted phytoremediation, resulting in clean soil that can be reused.

In addition to the cost savings, there are numerous other benefits to using microbe-assisted phytoremediation. Protocols for site preparation and planting are similar to those used in the agricultural industry and equipment requirements are limited to agricultural machinery. Because plant growth is driven by solar energy, maintenance costs after initial site preparation and planting are minimal. There is no size restriction for sites that can be remediated, and microbe-assisted phytoremediation can be used in any geographical area that can support plant growth, including much of the subarctic. Low- and high-molecular-weight

petroleum compounds can be effectively degraded, and in many cases, concomitant removal of multiple contaminants (e.g., PHC, salt, and metals) can be achieved (Greenberg et al., unpublished results). The aforementioned advantages mean that microbe-assisted phytoremediation can be used effectively at remote sites where alternative means of PHC remediation would be cost-prohibitive.

Another benefit of phytoremediation is that the overall soil quality and structure improves at remediated sites due to organic materials, nutrients, and oxygen that are added to soil via plant and microbial metabolic processes (see Section 6.1.2). Plants also provide groundcover, and their roots help to stabilize soil, which mitigates erosion from both wind and water. Plant growth results in net carbon sequestration (greenhouse gas storage): approximately 6 tonnes/hectare annually, which adds more environmental appeal to this already “green” technology (calculations from first principles) [110,111]. Green technologies have high public acceptance, making microbe-assisted phytoremediation an attractive option for industry and regulators.

Despite the numerous advantages to using microbe-assisted phytoremediation, there are also challenges that need to be considered. Large amounts of plant biomass are required for efficient rates of PHC degradation [10–12,40,45,46,104]. As a result, a key component for successful phytoremediation is alleviating plant stress at impacted sites so that they grow quickly on contaminated soils. Growing healthy plants that generate large amounts of biomass is difficult in impacted and/or poor-quality soils [10,12,19,39–42]. For instance, these conditions can result in the production of stress ethylene, a gaseous plant hormone that causes plant growth inhibition and results in decreased accumulation of biomass [9,112,113].

As noted earlier, many microbes, including PGPR, can promote plant growth. This can be achieved via direct (nutrient cycling, phytostimulation) and indirect (mitigating the impact of plant pathogens) mechanisms [60,114,115]. One direct mechanism by which PGPR can promote plant growth involves lowering stress ethylene concentrations via the enzyme 1-aminocyclopropane-1-carboxylic acid (ACC) deaminase [9,80,112–114]. ACC deaminase hydrolyzes ACC, the immediate precursor to ethylene in plants, to ammonia and α -ketobutyrate, providing the PGPR with reduced nitrogen and sugar. Thus, the presence of this enzyme can lower the rate of stress ethylene biosynthesis in plants and lead to increased plant growth and biomass production [9,60,114]. Seeds of contaminant-tolerant plant species can be inoculated with PGPR that have ACC deaminase activity so that upon germination, the PGPR can colonize the roots and/or the rhizosphere. Many PGPR also exude a plant growth hormone (an auxin) that is transferred to roots, which leads to increased plant root and shoot growth [60,115,116]. Notably, some PGPR (e.g., *P. putida*) have been shown to degrade PHC (see preceding text).

Although microbe-assisted phytoremediation is relatively straightforward to implement, there are numerous environmental factors that can positively or negatively influence

this remedial strategy in the field. These include daylight hours, length of growing season, weather, soil structure and composition (organic matter and nutrient content, grain size distribution), natural soil chemistry (high salt, low or high pH), availability of water and oxygen in the soil, and effects of weathering on PHC [6,47–49,117,118]. Each site is unique, and the various influences result in complex and dynamic scenarios, particularly within the rhizosphere. The key to success is to be aware of the variables, their potential effects on the phytoremediation outcome, and the steps that can be taken to mitigate negative influences and maximize positive ones. For example, agronomic analyses of the soil, followed by appropriate amendments and site preparation are essential for preparing a suitable seed bed and microbial environment prior to planting. Researching the climate and weather patterns of the area will help in choosing an appropriate plant species for phytoremediation (e.g., drought tolerant or cold tolerant species) and a planting date (e.g., fall vs. spring planting). Knowledge of soil and contaminant biochemistry plus plant physiology is crucial to assess the likelihood of success at any given site, and to troubleshoot if the expected results are not achieved.

Choosing appropriate plant and bacterial species can also be a challenge. Despite the general advantages of PHC-tolerant and PHC-degrading species, introducing nonnative species to an area poses an ecological risk because introduced species, particularly plants species, can become invasive [2,119]. Native species can also be invasive, as is the case with many weeds: although they can effectively remediate PHC-impacted soil, their invasive nature is of concern to farmers and environmental regulators. For further information on choosing noninvasive and/or native plant species, readers should consult invasive plant species lists and/or native plant species lists for any geographical area of interest (these are generally available from government agency websites and other online databases). The best way to acquire microbial species native to the area being phytoremediated is to isolate them from the soils of that area. As discussed earlier, competition from existing soil microbes tends to prevent introduced microbial species from reaching high titers in bulk soil, so they are rarely invasive; however, caution must be used to ensure that the microbes are non-pathogenic before using them in microbe-assisted phytoremediation. Various microbial pathogen lists are readily available from online microbial databases.

Microbe-assisted phytoremediation primarily occurs within the rooting zone of plants, which is an important consideration when choosing plant species for a remedial system. Some grass species have shallow rooting patterns that form dense mats with large surface areas (per unit volume of soil); other species have taproots that can penetrate soil to significant depths. Impacted soil below the rooting zone can also be excavated and spread to an appropriate depth across the surface of a treatment site, which would allow for desirable shallow-rooted plant species to be used.

Another significant challenge in the demonstration of successful microbe-assisted phytoremediation is the presence of biological organic compounds (BOC) in soil [120,121]. The Canadian Council of Ministers of the Environment (CCME) method, used routinely in most Canadian analytical laboratories, measures soil PHC by molecular weight range. There are four weight ranges or fractions (fraction 1 [F1], C_6-C_{10} ; fraction 2 [F2], $C_{10}-C_{16}$; fraction 3 [F3], $C_{16}-C_{34}$; and fraction 4 [F4], C_{34+}) [122]. Using this method, all compounds extractable by 1:1 hexane/acetone are deemed to be PHC. In actuality, not all extractable materials originate from petroleum sources. A wide variety of organic compounds, many of them biogenic in origin, are coextracted from soil samples with PHC. Using gas chromatography, these compounds mainly elute in the F2 and F3 ranges, although some elute in the F4 range as well. Sources of BOC include animals, plants, and microbes and include compounds such as fatty acids, sterols, and alkanes. During phytoremediation, BOC will accumulate in soil as a result of plant and microbial metabolic processes. For example, during the degradation of plant material (e.g., during root turnover), phenolic compounds are released into soil [71,84]. Levels of BOC can be high enough in soils that they exceed PHC regulatory remediation guideline values. When 180 pristine rural and old urban parkland sites were sampled by the Ontario Ministry of the Environment, of the 218 samples that were analyzed for PHC content, only thirty-six had undetectable levels of F3, and eight of the samples exceeded F3 assessment/remediation criteria [123]. Because the standard Canadian laboratory method for PHC analysis does not accurately differentiate between plant-derived and petroleum-derived hydrocarbon compounds, the positive effects of phytoremediation can be masked. Although there are methods to distinguish between petrogenic material and BOC, their primary use thus far has been in chemical fingerprinting to assess liability after crude oil or refined PHC releases [124]. These analyses are too costly for routine monitoring of phytoremediation.

The CCME recognizes that BOC will interfere with PHC analyses, and can lead to biased results that indicate erroneously high levels of PHC (particularly F3) [122]. They recommend addressing the issue by subtracting background levels of BOC, use of GC-MS analysis, and dilution of extracts/column cleanup. Recently, a cost-effective enhanced BOC method has been developed and validated. This method, which uses two external silica (Si) gel column cleanup steps, removes almost all BOC from soil sample extracts. The enhanced BOC method will be discussed in Section 16.4.1.

16.1.4 Successful Field Tests of Phytoremediation

With the challenges discussed earlier, the successes of laboratory and greenhouse experiments are not often realized to the same extent in the field. However, there have been encouraging results that justify continued application

of phytoremediation. For example, phytoremediation over a 2-year period in the field decreased the total soil PHC concentration by 30%, which was double that of non-vegetated soils at a highly contaminated site [46]. A field study conducted on a site contaminated by a crude oil spill showed a 42% decrease in total PHC concentration using ryegrass (*Lolium annual*), and a 50% decrease using St. Augustine grass (*Stenotaphrum secundatum*), after 21 months [125]. At another site impacted by a crude oil spill, 3 years of phytoremediation with a combination of grasses and fertilizer led to a decrease in PAH concentrations, including some of the recalcitrant components [45]. In soil contaminated with aged creosote, degradation of the PAHs acenaphthene, fluorene, fluoranthene, pyrene, and chrysene occurred in the rhizosphere of tall fescue over a 3-year period [126]. Relative to non-vegetated plots, tall fescue enhanced the degradation of most PAHs tested. In an oil-sludge pit at a petroleum refinery, phytoremediation using rye (*Secale cereale*) plants resulted in a consistent decrease in oil-sludge content over a 3-year period [101]. In Nigeria, carpet grass (*Axonopus compressus*) and nutsedge (*Cyperus rotundus*) were grown in independent plots for 3 months (one growing season) at an oil-impacted site. PHC decreases of 47 and 48% were observed for the carpet grass and nutsedge, respectively. When these plant species were grown together with soil inorganic and organic soil amendments, a 59% decrease in PHC was observed [127]. In all cases, rhizoremediation would have been partly or wholly responsible for PHC degradation in these field experiments. For instance, it has been shown in field experiments that a plant-PGPR system successfully remediated recalcitrant soil PHC [128] (see Section 16.2).

16.2 PGPR-ENHANCED PHYTOREMEDIATION SYSTEM(S)

As described in Section 16.1, to achieve successful phytoremediation will require a skill set beyond being able to plant seeds. A solid understanding of soil and plant science plus contaminant chemistry is necessary. Vigorous plant growth must be achieved to obtain sufficient biomass for remediation within an acceptable time frame. Therefore, seed beds of the highest quality must be prepared, because soils at impacted sites are often in poor condition. Most impacted soils are subsoils with low organic content and poor structure. Proper soil conditioning and amendment additions are essential. Once plants are growing well, one must then be able to monitor and evaluate microbial activity, contaminant chemistry and degradation or uptake of the contaminants from soil. In addition, the various procedures within any specific phytoremediation system must adhere to regulatory guidelines.

To overcome the challenges discussed earlier and to ensure a more reliable microbe-assisted phytoremediation

strategy for field applications, novel PGPR-enhanced phytoremediation system(s) (PEPS) was developed [10,11,128–131]. The basis of this technology is the combined use of contaminant-tolerant plant species and PGPR (including a PHC degrader) at sites that have been specifically prepared to maximize plant growth. By combining different techniques, the remediation process capitalizes on the benefits of each, resulting in complete and rapid rates of rhizoremediation. Using PEPS, acceptable remediation time frames of approximately 2–3 years are typical.

Specifically, there are two key components to PEPS. The first is soil pretreatment. The soil is tilled and mixed to homogenize and mitigate contaminant “hot spots” and to aerate and allow for some photochemical degradation of contaminants. Appropriate levels of fertilizer are added and organic amendments may or may not be necessary at a site to improve soil tilth, seed germination, and plant growth. Whenever possible, the impacted soil treatment zone is kept at a 0.5 m depth so that the bulk of the soil being treated will be in the rooting zone of grasses. The second key component to PEPS is the PGPR, which accelerate plant growth. Inoculation of seeds with PGPR prior to planting increases plant tolerance to PHC, salt and trace metal stress, as well as other environmental stressors [5,9,11,15,80,113,132,133]. This leads to rapid growth of plants, including their roots. The resulting vigorous plant growth leads to greater proliferation of naturally existing microbes in the soil, leading to a very active rhizosphere. This is typical in soils with normal plant growth. The substantial amount of root and microbial biomass that accumulates in the soil provides a sink that allows for rapid partitioning of PHC molecules out of the soil and their subsequent metabolism within the rhizosphere. Further, the PGPR used in PEPS have been shown to have PHC (including PAH)-degrading capacity [55,84,134,135].

The PGPR used in PEPS are all nonpathogenic, nongenetically modified soil bacteria (usually pseudomonades) extracted from, and native to, Canadian soils. These strains are naturally occurring and express ACC deaminase. They also synthesize indoleacetic acid (an auxin), which promotes root cell growth of the host plants [81]. They are sensitive to common antibiotics, do not grow at 37°C (therefore, they cannot proliferate in the human body), and are all classified as biosafety level 1 (the safest possible designation). They are ubiquitous in nature, common to soils around the world, and pose no threat to humans, wildlife or the environment. With PEPS, the PGPR are used only via a seed treatment where the seeds are treated in a controlled environment and only the plant roots of the treated seeds are inoculated with the PGPR as they pass through the seed coat during germination. A mixture of PGPR is used because the right combination of mixed microbial strains can result in higher PHC degradation rates than use of a single strain (Greenberg et al., unpublished results) [102].

Mixtures of grass species, including cereals, are used in PEPS. Specific plant species are utilized because they have been shown to be PHC tolerant and produce a large amount

of root biomass. Using more than one plant species (crocropping) can enhance overall microbe-assisted phytoremediation because the unique characteristics and properties of each plant species may support different microbial communities in the rhizosphere, differentially penetrate the soil matrix, and lead to degradation of different PHC compounds [6]. We note that PEPS will also work with a variety of plant species (e.g., canola, corn, sunflower, and alfalfa).

For PEPS, plant species native to the area in which phytoremediation is being undertaken are used whenever possible, to eliminate ecological risk. This strategy also facilitates native habitat reconstruction/reclamation following remediation. Native PGPR are also used: frequently, PGPR are isolated from the site being remediated. This provides multiple benefits: it eliminates ecological risk; and PGPR isolated from specific PHC-contaminated soils are PHC tolerant and are often PHC degraders, using PHC as their source of carbon in the nutrient-poor soils [136].

The standard PEPS protocol includes preparation of a “control” or unimpacted area on the remediation site whereby a control soil is tilled, planted, and sampled or monitored in similar fashion to the impacted areas being treated. Soil samples taken from the control area are analyzed in the laboratory to establish BOC levels due to plant and microbial growth. Monitoring changes in BOC levels in this soil ultimately allows for adjustments in measured PHC levels from the treated impacted soils, as BOC is similarly generated in the impacted soil due to plant and microbial biomass.

16.2.1 Development, Proof, and Full-Scale Application of PEPS

In the initial stages of PEPS development, laboratory and greenhouse experiments were conducted under controlled conditions [10,11,29,40,80,113,131]. These experiments were followed up with small-scale field trials [5,128]. The process that involved landfarming techniques, plant growth, and PGPR was initially termed the multiprocess phytoremediation system. A brief summary of this research is as follows.

Various grass species (*Festuca arundinacea*, *L. multiflorum*, *S. cereale*, *Pennisetum glaucum*, *Hordeum vulgare*, *Poa pratensis*, and *Elymus canadensis*) were used in the initial experiments. Seeds were treated with various naturally occurring, nonpathogenic *Pseudomonas* strains. Although phytoremediation was observed in the absence of PGPR treatments, the addition of PGPR consistently enhanced remediation rates. Notably, PGPR seed treatments protected the photosynthetic apparatus in plants grown in impacted soil [40].

In the greenhouse, 86% of creosote in spiked soil (2 g/kg soil) and 50% of PAHs from an industrial brownfield soil (500 mg/kg soil) were removed during 8- and 4-month growth periods, respectively [11,131]. The average efficiency for removal of 16 priority PAHs by this remediation system in a

4-month period was twice that of land farming and 1.5 times faster than bioremediation or phytoremediation alone. For highly hydrophobic PHC (C_{10} – C_{34}), it was 1.5–2.0 times faster than land farming or phytoremediation alone [11]. Over 2- and 4-month periods, over 90% of PHC (50 g/kg soil) were removed from weathered soil containing oil sludge using the multiprocess phytoremediation system [10]. Numerous organic compounds were successfully remediated in the greenhouse experiments, including highly toxic and recalcitrant PAHs such as chrysene, benzo(b)fluoranthene, benzo(a)pyrene, dibenzo(ah)pyrene, benzo(ghi)perylene, indo(123-cd)pyrene, and hydrophobic, recalcitrant PHC from CCME F3 (often highly toxic compounds) and F4 fractions [10,11,131]. Notably, PHC, including PAHs, were not stored in plant tissues during phytoremediation so these experiments showed that there would be no need to dispose of the plants after field experiments. These experiments also indicated that the complementary processes accelerated remediation and suggested that complete remediation of sites impacted with highly persistent PHC could be achieved in 2–5 years. After achieving success in the laboratory and greenhouse, PEPS was assessed in several small-scale field trials. Similar results were observed in the field (Table 16.1) [5,8128].

The initial experiments indicated that PHC were not stored in plant tissue and had therefore been degraded, either *in planta* or in the soil. Further experiments definitively showed that the PHC were degraded *in situ* in the rhizosphere and that biodegradation by the microbial community in PHC-impacted soils is a major pathway for PHC removal by PEPS [128,136]. This was shown by three lines of evidence: (1) GC-MS and HPLC analyses showed that the chemicals do not accumulate in the plants and that specific PHC compounds are degraded. (2) Soil microbial analyses during PEPS trials showed that naturally occurring, petroleum-consuming microbe populations increased by two orders of magnitude due to plant growth. (3) Isotope analysis showed that the PHC were metabolized to fatty acids and mineralized to CO_2 . The isotope analyses were performed by measuring ^{14}C in phospholipid fatty acids (PLFA) of soil microbes. While ^{14}C was found in new plant tissue, PHC

molecules contained virtually no ^{14}C . Very low ^{14}C was subsequently detected in the PLFA biomarkers (>80% of the microbial PLFA carbons were derived from PHC), indicating that the carbon came from PHC metabolism and that the microbes in the soil were subsisting primarily on PHC. Microbes in an adjacent uncontaminated control soil had modern ^{14}C signatures in their PLFA, which indicated consumption of the modern plant-derived fraction of soil organic carbon. Further, measurements of ^{13}C and ^{14}C indicated that mineralization of PHC contributed to CO_2 in the contaminated soil.

Following the small-scale field trials and the mechanistic studies, PEPS deployment was initiated for full-scale field-level PHC remediation programs in Canada [8,109,128–130,137]. Between 2006 and 2011, successful field applications of PEPS culminated in meeting generic regulatory targets at four sites in Alberta, one site in British Columbia, one site in Manitoba and one site in Quebec. Site closure was achieved following 1 to 3 years of treatment. See Table 16.2 for some examples of full-scale field PHC remediation using PEPS.

As noted in Section 16.2, one crucial aspect when conducting a full-scale field application using PEPS is to establish an adjacent unimpacted “control” area. These control areas, which are planted as per the impacted area, are used to establish background levels of nonpetrogenic hydrophobic materials in the soil that are naturally occurring or that arise due to plant growth during PEPS. Samples from the control and impacted areas are sent to an accredited analytical laboratory for PHC analyses. Based on gas chromatography with flame ionization detection (GC–FID) data of samples taken from the beginning and end of season, the unresolved complex mixture (UCM; PHC peaks that elute so closely together they are not resolved separately in the chromatograms) in the impacted soil decreases over time, whereas there are peaks in control samples that accumulate over time; these are primarily BOC (Fig. 16.3). Measuring the level of change in BOC in the control area soil establishes the amount of natural or biogenic hydrocarbon that can be subtracted from the measured PHC levels within the impacted soil. When corrections are made for the nonpetrogenic material that accumulates in the impacted soil at a site during phytoremediation, the data reflect actual PHC levels (i.e., petrogenic hydrocarbons) in the soil.

TABLE 16.1 Remediation in small-scale field trials of PEPS

Trials		PHC concentration (%)	Plant species	% remediation
Trial #1: Land farm				
2004	Year 1	15	Rye	44±5
2005	Year 2		Rye/fescue	35±6
2006	Year 3		Rye/fescue/barley	22±3
2007	Year 4		Rye/fescue/barley	16±2
Trial #2: Constructed biopile				
2005	Year 1	1	Rye/fescue	35±2
2006	Year 2		Rye/fescue	26±1
2007	Year 3		Rye/fescue	19±3

Percentage remediation (±SE) represents the decrease in PHC between the beginning and end of the season for a given year.

16.2.2 Keys to the Success of PEPS

Successful transfer of the science of PEPS from the lab to the field has resulted in a working remedial strategy: (i) strategies for aggressive plant growth in impacted and/or poor-quality soils were developed and tested in the lab prior to implementation at full-scale sites. (ii) PEPS are deployed in the field by highly trained scientists. (iii) Phytoremediation progress is monitored at each site by following the environmental chemistry from start

TABLE 16.2 PHC remediation at several full-scale sites in Canada

Sites	Sampling period	PHC analysis	Average (mg/kg)	Remediation (%)	Average remediation per year (%)
Completed sites					
Edson, AB	Spring 2007	CCME F3	1500		
	Fall 2008	CCME F3	1000	33	17
Peace River, AB	Spring 2007	CCME F3	500		
	Fall 2008	CCME F3	200	60	30
Hinton 2, AB	Spring 2007	CCME F3	900		
	Fall 2008	CCME F3	500	44	22
	Spring 2009	EPH(C ₁₀ -C ₁₉)	6600		
	Fall 2011	EPH(C ₁₀ -C ₁₉)	650	90	30
Dawson 1, BC	Spring 2009	EPH(C ₁₉ -C ₃₂)	2500		
	Fall 2011	EPH(C ₁₉ -C ₃₂)	525	79	26
Sites currently undergoing PEPS treatment					
Hinton 1, AB	Spring 2010	CCME F2	1100		
	Fall 2010	CCME F2	250	77	77
	Spring 2010	CCME F3	3200		
	Fall 2010	CCME F3	1400	56	56
	Spring 2009	CCME F2	1400		
	Fall 2010	CCME F2	300	79	40
Swan Hills, AB	Spring 2009	CCME F3	2550		
	Fall 2010	CCME F2	900	65	33
	Spring 2009	EPH(C ₁₀ -C ₁₉)	6500		
	Fall 2011	EPH(C ₁₀ -C ₁₉)	3500	46	15
Dawson 2, BC	Spring 2009	EPH(C ₁₉ -C ₃₂)	700		
	Fall 2011	EPH(C ₁₉ -C ₃₂)	400	43	14
	Spring 2009	EPH(C ₁₀ -C ₁₉)	7000		
	Fall 2011	EPH(C ₁₀ -C ₁₉)	1300	81	27
Dawson 3, BC	Spring 2009	EPH(C ₁₉ -C ₃₂)	3500		
	Fall 2011	EPH(C ₁₉ -C ₃₂)	1500	57	19
Beaver River, BC	Spring 2010	EPH(C ₁₀ -C ₁₉)	1600		
	Fall 2010	EPH(C ₁₀ -C ₁₉)	1200	25	25
	Spring 2010	EPH(C ₁₉ -C ₃₂)	850		
	Fall 2010	EPH(C ₁₉ -C ₃₂)	550	35	35

The PHC fractions requiring remediation at each site are given. The sites are located in British Columbia and Alberta, Canada.

Note: In British Columbia, EPH_{C10-C19} and EPH_{C19-C32} are used instead of F2 and F3, respectively. Average remediation per year for these sites was 31 ± 4%. The error term represents SE.

to finish. (iv) PEPS are continuously improved through ongoing scientific research.

PEPS for PHC remediation are effective for several reasons: (i) the complementary processes build on each other so that remediation is rapidly initiated and is sustained throughout the growing season. (ii) The PGPR alleviate plant stress and promote plant growth. (iii) The large amount of root and microbial biomass produced in the soil allows for effective partitioning of contaminants out of the soil. (iv) The PGPR confer PHC tolerance to the plants and also confer tolerance to cocontaminants such as salt and trace metals. (v) The PGPR also protect plants against other potentially harmful conditions (e.g., salt, cold, drought, poor-quality soil) that result in the production of stress ethylene. (vi) The PGPR have the ability to metabolize PHC. (vii) PEPS result in high levels of PHC-degrading microorganisms in the soil and resultant high PHC degradation rates. (viii) Each PHC-contaminated site has a unique set of features and PEPS are tailored to site-specific conditions.

16.3 CASE STUDIES OF FULL-SCALE PETROLEUM PHYTOREMEDIATION

PEPS have been used successfully to remediate *in situ* PHC-impacted soil at a number of field sites in Canada (Table 16.2) [109,129]. The case studies presented below are a subset of commercial project sites where PEPS have been deployed. A brief synopsis of site features, phytoremediation processes, and results has been recorded for each project. For Case Study #1, a cost analysis is also included.

16.3.1 Case Study #1: Edson, Alberta

16.3.1.1 Site Details The site was located 20 km north of Edson, Alberta, Canada. An area of 10,700 m² was impacted with approximately 2000 mg/kg PHC, of which greater than 90% was F3. The F3 PHC concentration exceeded the applicable Alberta Tier 1 remediation guideline values at several sampling points. The PHC originated from previously land-spread diesel invert drilling mud. The PHC were in the soil

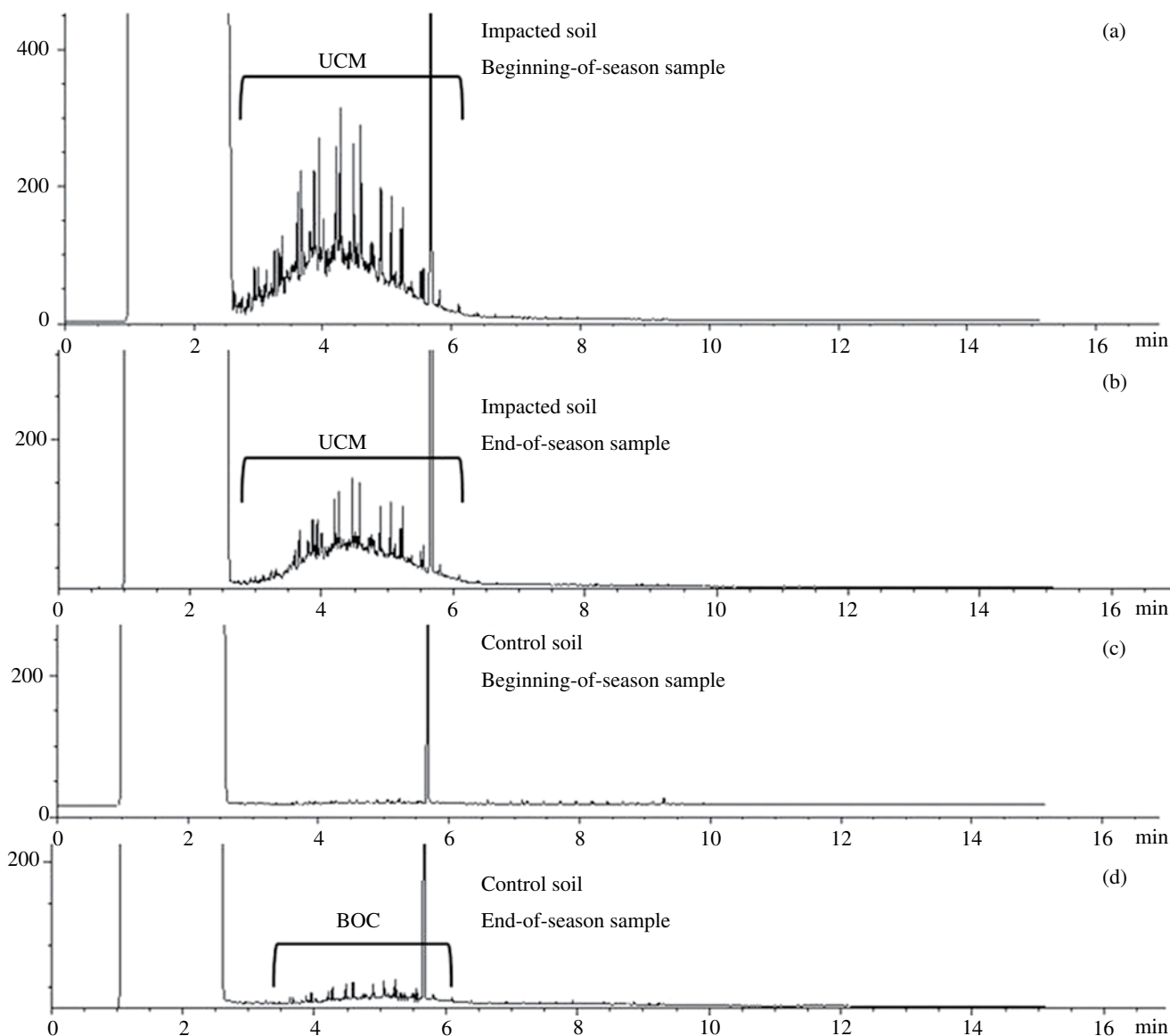


FIGURE 16.3 GC-FID chromatograms of control (c,d) and impacted (a,b) samples from the beginning (a,c) and end (b,d) of the season. The size of the UCM decreased between July and September in the impacted soil. Peaks not apparent at the beginning of the season in the control area are evident in the chromatogram from the end-of-season sample. These are putative BOC arising from plant growth.

for more than a decade prior to PEPS deployment and had previously been treated using conventional land farming techniques and wood chip-induced composting. Prior to PEPS being deployed, all of the PHC impacts were within the top 0.3 m of the soil profile, and vegetation at the site was sparse. The impacted subsoil had a poor structure, was low in organic matter, was nutrient deficient, and contained an abundance of rock.

16.3.1.2 PEPS Deployment In 2006, prior to planting, the soil was tilled and fertilizer was applied based on agronomic analyses. In September, a three-seed mix containing annual ryegrass (*L. multiflorum*), tall fescue (*F. arundinacea*), and fall rye (*S. cereale*) was sown. The seeds were pretreated with two strains of PGPR (*Pseudomonas* spp. [strain UW3] and

P. putida [strain UW4]). All subsequent references to PGPR-treated seeds indicate the application of this UW3+UW4 mix. Fall planting was performed with a broadcast seeder, and the site was harrowed after seeding.

In the Spring of 2007, vegetation from the Fall 2006 seeding event resumed growth. In July 2007, the treatment zone soils were sampled. Bare or sparsely vegetated areas of the site were overseeded with PGPR-treated annual ryegrass and tall fescue. At the end of the growing season, plant growth was assessed and the site was sampled to determine the extent of remediation.

In 2008, 1 week before seeding, fertilizer was applied to the site. The soils were disked and prepared for planting in June. As in 2007, the soils were sampled and the site was overseeded with PGPR-treated annual ryegrass, tall fescue,

and oats (*Avena sativa*). A broadcast seeder was used for planting, followed by harrowing. In October of 2008, plant growth was assessed, and soil samples were obtained to determine the extent of remediation.

16.3.1.3 Results and Site Status After the Fall 2006 planting, vegetation cover was established before the end of the growing season. Growth resumed in the Spring of 2007 and vegetation cover at the site was approximately 50% before overseeding. After the 2007 overseeding, plants grew vigorously to maturity. In less than 3 months (July 11 to October 5), greater than 90% ground vegetation coverage was achieved. In-house gravimetric soil assay results indicated that the average PHC level for this site had decreased by 22% between June 2007 and June 2008 (Fig. 16.4). A field survey conducted after the 2008 growing season (October) showed plant ground coverage to be 100% (Fig. 16.4). The average PHC remediation was 30% in 2008 (a decrease from 1400 mg/kg in June 2008 to 1000 mg/kg in October 2008) (Fig. 16.4). At the end of the 2008 season, 10 of 12 sampling points had F3 levels below the Alberta Tier 1 remediation guidelines for fine-grain soils (1300 mg/kg). By the Spring of 2009, soil at the two sampling points that had exceeded remediation guideline values the previous fall were in compliance. Commercial laboratory CCME analyses confirmed that soil from all sampling points across the site had PHC levels that adhered to Alberta Tier 1 remediation guideline values, which would allow for site closure.

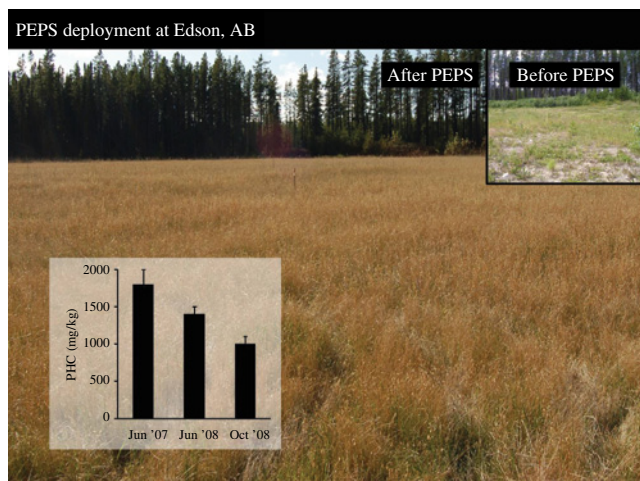


FIGURE 16.4 Plant growth and petroleum hydrocarbon (PHC) remediation at a site near Edson, Alberta. Plant growth before (top inset) and after deployment of a PGPR-enhanced phytoremediation system (PEPS) is shown. Plant species used for PEPS were annual ryegrass (*Lolium multiflorum*), tall fescue (*Festuca arundinacea*), fall rye (*Secale cereale*), and oats (*Avena sativa*). All seeds were treated with PGPR (a mix of two pseudomonades). The graph (bottom inset) shows PHC remediation between June 2007 and October 2008 (two growing seasons). Soil PHC levels were determined using a gravimetric analysis.

16.3.1.4 Costs of Phytoremediation Using PEPS The petroleum impacted soil was spread over 10,700 m² to a depth of 0.3 m. The total volume of treated soil was 3210 m³. The costs for the entire project, including all professional fees, materials, subcontractors, and other third-party costs, was \$104,000 or \$32.50/m³. The unit cost for remediation of this site was comparable to that for other sites, including more remote sites of similar size. Unit costs drop as the volume of impacted soil increases. In comparison, based on a 2 h truck turnaround time, landfill disposal of this same volume of material would have cost at least \$85/m³. At more remote sites, the unit cost of landfill disposal increases dramatically.

16.3.2 Case Study #2: Peace River, Alberta

16.3.2.1 Site Details The site was located near Peace River, Alberta, Canada. An area of 4750 m² was impacted with PHC at approximately 2200 mg/kg (~40% F3, with several sampling points that exceeded the applicable Alberta Tier 1 remediation guideline values). The PHC originated from upstream oil and gas activities and was highly weathered. The PHC-impacted soil, which was excavated from a former earthen (i.e., flare) pit, had a high clay content and poor structure and tilth and was deficient in essential plant nutrients.

16.3.2.2 PEPS Deployment In 2006, the excavated sub-soil was homogenized prior to placement on a prepared treatment pad. The soil was spread to a depth of 0.5 m across a treatment area. Prior to planting, the soil was homogenized and aerated. In late August 2006, after seed bed preparation was complete, a seed mix of tall fescue, fall rye and perennial ryegrass (*Lolium perenne*) was broadcast and harrowed into the treatment zone soil. Prior to sowing, the seeds were treated with PGPR. In 2007, fertilizer was applied and the site was overseeded with PGPR-treated tall fescue, annual ryegrass, and barley seeds. A broadcast seeder was used for planting, followed by harrowing. In 2008, PEPS was deployed as per 2007, except that a four-seed mix containing annual ryegrass, perennial ryegrass, tall fescue, and oats was used.

16.3.2.3 Results and Site Status The late August 2006 planting did not generate a great deal of aboveground vegetative growth due to an early frost. The Spring 2007 overseeding resulted in vigorous plant growth. After 4 months of growth (June to October 2007), the plants reached full maturity, and vegetation ground coverage was 100% (Fig. 16.5). Root penetration was measured to a depth of approximately 0.4 m. Gravimetric assays of PHC in soil samples before and after plant growth indicated that PHC levels decreased from an average of 2200 to 1600 mg/kg (~30% remediation) in less than 4 months of plant growth (Fig. 16.5).

The perennial grasses seeded in 2006 and 2007 overwintered well and covered approximately 85% of the treatment area in the Spring of 2008. The site was overseeded in July

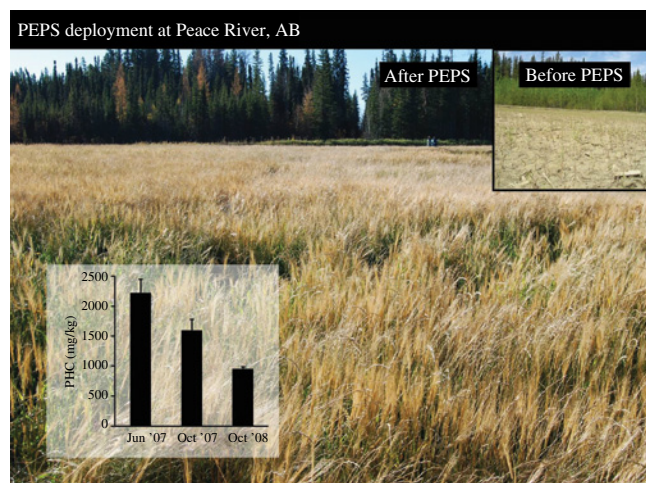


FIGURE 16.5 Plant growth and petroleum hydrocarbon (PHC) remediation at a site near Peace River, Alberta. Plant growth before (top inset) and after deployment of a PGPR-enhanced phytoremediation system (PEPS) is shown. Plant species used for PEPS were tall fescue (*Festuca arundinacea*), fall rye (*Secale cereale*), perennial ryegrass (*Lolium perenne*), annual ryegrass (*Lolium multiflorum*), and oats (*Avena sativa*). All seeds were treated with PGPR (a mix of two pseudomonades). The graph (bottom inset) shows PHC remediation between June 2007 and October 2008 (two growing seasons). Soil PHC levels were determined using a gravimetric analysis.

2008 with a three-species mixture of PGPR-treated seeds, as per 2007. As before, the plants grew well and vegetation ground coverage was approximately 100% after 3 months of plant growth. In the Fall of 2008, soil samples collected from all permanent treatment area assessment points had PHC and F3 levels below applicable Alberta Tier 1 remediation guideline values. In two growing seasons, PEPS resulted in an average total PHC decrease from 2200 to 950 mg/kg (Fig. 16.5). The average F3 level decreased from 500 mg/kg in 2007 to 200 mg/kg in October 2008, an overall 60% decrease. Based on the results of PHC analyses by both in-house gravimetric assays and commercial laboratory CCME analyses, the PHC-impacted soils at this location were completely remediated to Alberta Tier 1 standards.

16.3.3 Case Study #3: Hinton, Alberta

16.3.3.1 Site Details The site was located approximately 20 km north of Hinton, Alberta, Canada. Soil over an area of 3850 m² had been impacted with approximately 1200 mg/kg PHC for more than a decade. The highly weathered PHC had originated from diesel invert drilling mud and was composed of approximately 80% F3. The F3 PHC levels exceeded the applicable remediation guideline value at several sampling points across the site. Prior to PEPS deployment, PHC remediation had been attempted using a wood chip compost treatment and conventional land treatment techniques. It was determined that the wood chips severely inhibited plant growth, and the associated remedial efforts were deemed

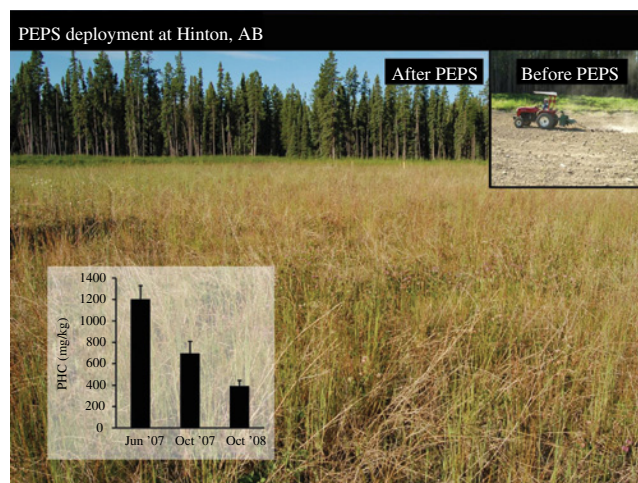


FIGURE 16.6 Plant growth and petroleum hydrocarbon (PHC) remediation at a site near Hinton, Alberta. Plant growth before (top inset) and after deployment of a PGPR-enhanced phytoremediation system (PEPS) is shown. Plant species used for PEPS were annual ryegrass (*Lolium multiflorum*), tall fescue (*Festuca arundinacea*), perennial ryegrass (*Lolium perenne*), and oats (*Avena sativa*). All seeds were treated with PGPR (a mix of two pseudomonades). The graph (bottom inset) shows PHC remediation between June 2007 and October 2008 (two growing seasons). Soil PHC levels were determined using a gravimetric analysis.

unsuccessful. The impacted soil was fine grained and deficient in nutrients and contained a significant proportion of wood chips that produced phytotoxic effects in plants originating from non-PGPR-treated seeds.

16.3.3.2 PEPS Deployment Prior to planting in the Spring of 2007 and 2008, the soil was tilled and fertilized as required. A mix of PGPR-treated tall fescue, annual ryegrass, perennial ryegrass, and oats was planted after site preparation. A broadcast seeder was used for planting, followed by harrowing and roller packing of the soil to achieve good seed-soil contact.

16.3.3.3 Results and Site Status In 2007, seedlings emerged and grew vigorously on the impacted soil. After 3 months of plant growth (July–October), ground coverage was approximately 80% with root penetration measured to a depth of approximately 0.3 m. In-house gravimetric assays of soil samples before and after plant growth indicated that PHC levels had decreased from an average of 1200 to 700 mg/kg, an overall decrease of 42% in 3 months (Fig. 16.6). In 2008, plant growth was also very good with ≥85% ground coverage (Fig. 16.6). Soil samples were taken before planting and at the end of the 2008 growing season. In-house gravimetric assays of soil samples collected from the main area of the site indicated that PHC levels had decreased from an average of 1200 mg/kg in June 2007 to 400 mg/kg in October 2008, an overall decrease of 66% in two growing seasons (Fig. 16.6). Most importantly, soil

samples collected from all permanent assessment points had PHC concentrations below 1000 mg/kg, as measured at a commercial analytical laboratory. All sampling points met the Alberta Tier 1 remediation guideline values for F3 PHC in fine-grain surface soils in natural areas (1300 mg/kg). Thus, this site was completely remediated to Alberta Tier 1 standards in two growing seasons.

16.3.4 Case Study #4: Dawson Creek, British Columbia

16.3.4.1 Site Details The site was located 55 km south of Dawson Creek, British Columbia, Canada. It was a 5800 m² land treatment area that contained approximately 1700 m³ of weathered PHC-impacted soil to a depth of 0.3 m. In addition, there were some elevated PHC concentrations between 0.3 and 0.7 m within the soil treatment area. The average PHC concentration was 4600 mg/kg (~70% EPH_{C10-C19} and ~30% EPH_{C19-C32}). The EPH_{C10-C19} levels ranged from 1700 to 15,300 mg/kg with an average level of 6600 mg/kg. The average EPH_{C19-C32} level was 2500 mg/kg (maximum level of 4000 mg/kg). The soil was nutrient poor and had a high gravel content (between 10 and 20%). There was sparse plant growth at this site prior to PEPS deployment.

16.3.4.2 PEPS Deployment Prior to planting in June 2009 and July 2010, the soil was tilled and fertilized as required. In July 2010, the site was excavated such that impacted soil at a depth of 0.7 m was homogenized with the surface soil. In October 2010, a fall planting was performed. At each planting, a PGPR-treated seed mix of three plant species (annual ryegrass, perennial ryegrass, and tall fescue) was broadcast and harrowed into the impacted soil across the treatment area. In July 2011, the site was overseeded with the same seed mix that was used in the preceding years.

16.3.4.3 Results and Site Status In 2009, plants germinated and grew well on the impacted soil. After 4 months of plant growth (June–October), the ground coverage was approximately 90%. BC EPH assays of soil samples before and after plant growth indicated that the average EPH_{C10-C19} level decreased from 6600 to 3800 mg/kg and the average EPH_{C19-C32} level decreased from 2500 to 2000 mg/kg, overall decreases of 42 and 20%, respectively. In 2010, plant growth was not as good as it was in 2009 due to severe drought conditions in the first half of the growing season. Although vegetation ground coverage was only 90% and plant height was only approximately 3 cm, root growth was good. We also observed good rates of EPH remediation, likely due to healthy roots and an active rhizosphere. In 2010, a fall seeding was performed. The rationale was that this would allow for spring germination with no, or minimal, drought stress, which would lead to abundant plant growth in July and August. In June 2011, ground coverage was 95–100% and plants were healthy and grew to high density. By October 2011, ground coverage was 100% (Fig. 16.7). The annual grasses had reached

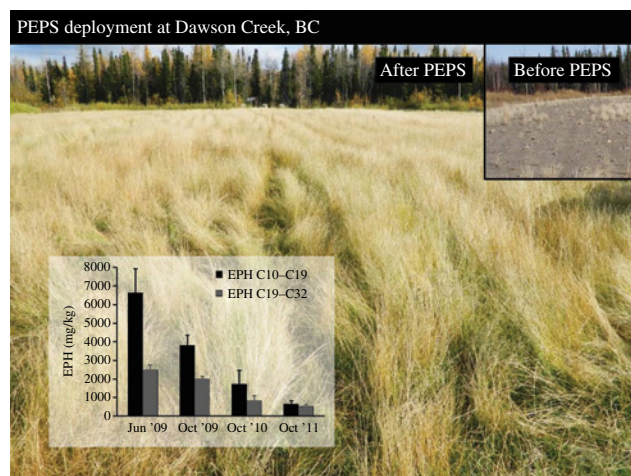


FIGURE 16.7 Plant growth and remediation of extractable petroleum hydrocarbons (EPH) at a site near Dawson Creek, British Columbia. Plant growth before (top inset) and after deployment of a PGPR-enhanced phytoremediation system (PEPS) is shown. Plant species used for PEPS were annual ryegrass (*Lolium multiflorum*), perennial ryegrass (*Lolium perenne*), and tall fescue (*Festuca arundinacea*). All seeds were treated with PGPR (a mix of two pseudomonades). The graph (bottom inset) shows EPH remediation between June 2009 and October 2011 (three growing seasons). Soil EPH levels were determined using BC Method 10.

senescence and were approximately 0.6–1.0 m high, and the perennial grasses were green and approximately 0.2 m high. Root growth was measured to 0.35 m depth. In 2011, in 0.0–0.3 m soil depth, significant decreases were measured in EPH_{C10-C19} and EPH_{C19-C32} levels; by October 2011, the average levels of EPH_{C10-C19} and EPH_{C19-C32} had decreased to 650 and 525 mg/kg, respectively (Fig. 16.7). Soil samples from all but four permanent assessment points had EPH_{C10-C19} levels below the BC Contaminated Sites Regulation (CSR) End Land Use Standards (1000 mg/kg), and all but one sampling point was below the EPH_{C19-C32} criteria of 1000 mg/kg. All sampling points in the 0.0–0.6 m soil sampling interval, except one, had EPH_{C10-C19} and EPH_{C19-C32} levels below, or close to, the criteria of 1000 mg/kg. After spring plant growth in 2012 and soil homogenization, no soil samples from any of the permanent assessment points had PHC levels that exceeded criteria and this site was deemed fully remediated.

16.3.5 Overall Conclusions from Case Studies

PEPS, novel microbe-assisted phytoremediation systems for remediation of PHC, have an outstanding performance record at several sites in Canada. Using PEPS, it took only 2–3 years to remediate the Alberta and British Columbia PHC-impacted sites to levels required for site closure under regulatory criteria. Notably, PEPS are equally effective for remediation of total PHC and CCME F3/BC EPH_{C19-C32} (the most recalcitrant PHC compounds). This cost-effective “green” technology can achieve simultaneous remediation and revegetation of impacted sites.

16.4 ACHIEVING REGULATORY CRITERIA

During the course of full-scale PEPS applications, it became apparent that further research was needed to optimize analytical laboratory PHC quantification methods to ensure accurate measurement of PHC levels in soil. The basis of the research was to examine the composition of the extractable organic material (i.e., BOC vs. PHC) in both impacted and unimpacted soils over time. More complete removal of BOC from soil samples undergoing PHC analyses will result in more accurate measurement of soil PHC levels, which in turn will allow for easier compliance with generic regulatory criteria. Site-specific risk assessment (Alberta Tier 2) toxicity end points, using five plant species, are also being used at a research level to assess when PHC-impacted field soils become nontoxic during PEPS treatments. The toxicity data being generated will ultimately be used to predict at what measured PHC level the soils would be nontoxic according to Tier 2 CCME protocols.

16.4.1 Optimizing PHC Analytical Protocols for Removal of BOC

Although it has been definitively shown that PHC are degraded in soils during PEPS treatment [128,136], accumulation of BOC can confound the results of standard PHC analytical methods. This issue was discussed in Section 16.1.3. For standard soil PHC analyses, hydrocarbons in the CCME F2–F4 range are extracted using hexane/acetone and tumbler

extraction (i.e., aggressive shaking). Samples are back extracted to remove the acetone. Cleanup of soil extracts with Si gel can then be used to remove polar compounds, including BOC. There are two methods typically used in analytical labs to remove BOC: *in situ* treatment with an activated Si gel (standard method) and *ex situ* Si gel column cleanup (enhanced cleanup, such as Method 10 used in British Columbia, Canada) [138]. Sample extracts are then analyzed using GC–FID. The mass of the hydrocarbon fractions is determined by integrating all area counts under the chromatogram curve.

A new extraction method for enhanced BOC removal has been developed [137]. This method, which uses a double *ex situ* Si gel column cleanup (the soil extract is passed through two Si gel columns), removes almost all BOC from PHC-impacted soil extracts without compromising accurate PHC quantification [137]. This method complies with accepted regulatory methods for PHC analyses. By using this more aggressive cleanup method, most of the nonpetrogenic hydrophobic materials can be removed from the impacted soil samples [137].

Analyses of soil samples by GC–FID were conducted following two cleanup methods (*in situ* Si gel and *ex situ* Si gel columns) to remove polar BOC [137]. Both of these methods complied with CCME regulations for use in soil PHC analysis. Cleanup with these Si gel methods resulted in removal of specific chromatographic peaks that fell in the F3 molecular weight range (C_{16} – C_{34}). When no cleanup was performed, the putative BOC were highly prevalent (Fig. 16.8a). About 50% of these compounds were removed by an *in situ* Si gel cleanup (Fig. 16.8b). This has been the

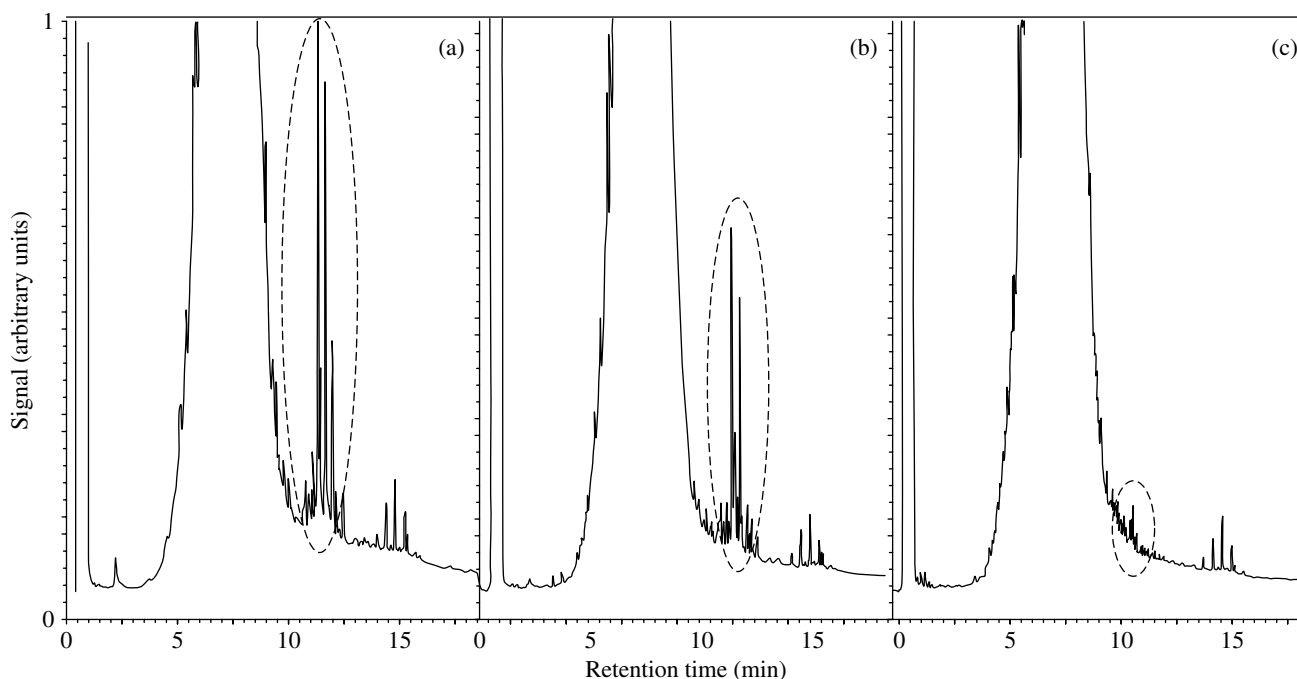


FIGURE 16.8 Analysis of PHC by GC–FID. The standard analytical protocol for PHC analysis (outlined in Section 16.4.1) was followed. After back extraction with acetone, the sample was divided into three aliquots. One aliquot was left untreated (a), one aliquot was subjected to an *in situ* Si gel cleanup (b), and one aliquot was subjected to a double Si gel column cleanup (c). The material removed by the Si gel columns has been identified as BOC. The BOC in the gas chromatograms are circled.

standard PHC analytical method used in most Canadian analytical laboratories. The efficacy of BOC removal when the soil extract is passed a single time through an external Si gel column was also tested: it did not remove all of the BOC (data not shown). Nearly all BOC were quantitatively removed when a double Si gel column cleanup was performed (Fig. 16.8c). Notably, the unresolved complex mixture (UCM), which represents PHC, was unaffected by the double Si gel column cleanup.

GC-MS has been used to examine the compounds removed by the double Si gel column cleanup (i.e., to determine whether they are BOC) [137]. All of the compounds that have been identified to date are plant-derived compounds (phenols, sterols, and terpenoids) that accumulated in the soil during the course of phytoremediation. None have been identified as PHC. The extent to which these plant-derived organic compounds factor into reported PHC levels, and identification of methods by which they can be removed without affecting the petroleum concentration of samples, warrants further studies.

16.4.2 Plant Toxicity Testing

If generic regulatory remediation guideline values are not met, most jurisdictions allow for site-specific risk assessments to demonstrate that soils are no longer harmful to sensitive environmental receptors (e.g., plants, animals). This allows one to set site-specific remediation guideline values. Toxicity testing of PHC-impacted soil using alfalfa, barley, cucumber, northern wheatgrass, and red clover was initiated to determine if Tier 2 risk assessment criteria would be met following phytoremediation. The toxicity tests were based on Environment Canada protocols. Parameters measured for the toxicity tests were cotyledon emergence, root and shoot dry biomass, and root and shoot length. Results for the aforementioned five species indicated that soils reported to have PHC concentrations in excess of 6000 mg/kg (well above the generic remediation guideline values) resulted in very few toxic effects and the toxic effects that were observed did not correlate well with measured PHC levels (Knezevich, Gerwing, and Greenberg, unpublished results) [137]. In the majority of tests conducted with PHC-impacted soils (500–10,000 mg/kg PHC), only very weak correlations were observed between soil PHC levels and soil phytotoxicity.

Plant toxicity test results acquired from several plant species were analyzed as a function of PHC F3 concentration [137]. Test soils came from various PEPS sites as listed in Table 16.2. Based on Environment Canada protocols, values indicating a pass for each measured parameter (cotyledon emergence, root and shoot dry biomass, and root and shoot length) in reference control soils were given a value of one: all data were normalized to this value so they could be plotted on the same scale. The majority of data points were greater than 1, indicating satisfactory plant growth on soils from PHC-impacted sites. This means that the soils would pass their respective toxicity tests, suggesting that they are

not toxic to plants, despite reported F3 concentrations above generic regulatory guideline values. This implies that current soil remediation guideline values for F3 hydrocarbons in Canada may be overly conservative. The current regulatory Tier 1 criteria were developed using fresh PHC spiked soils. It has been shown that weathered PHC are less toxic [139] and the data described herein is consistent with this observation. Given the lack of correlation between plant toxicity and F3 hydrocarbon levels, failed toxicity tests were likely the result of poor soil quality rather than toxic soil PHC levels.

16.5 CONCLUSIONS

Rapid, efficient, and cost-effective remediation technologies for PHC-contaminated soils are in great demand, particularly in the oil and gas industry. Microbial bioremediation and phytoremediation have garnered interest because they are environmentally responsible and cost-effective relative to many other remediation strategies. However, when microbes and plants are used independently, soil toxicity and nutrient restrictions in PHC-impacted soils can severely limit their growth, resulting in unacceptably slow rates of remediation. Microbe-assisted phytoremediation can significantly improve the rates of PHC remediation: the presence of plant roots can greatly enhance microbial growth in impacted soils, and increased microbial activity in the rhizosphere can promote degradation, sequestration, and removal of PHC. A novel, rapid, and effective microbe-assisted phytoremediation technology (PEPS) for *in situ* removal of PHC from oil-contaminated soils has been successfully applied at more than 30 sites in Canada. This innovative technology is based on principles and experimental protocols that have been scientifically proven and that are effective at full-scale field levels when deployed by qualified scientists. One of the key components of PEPS is the use of PGPR to promote vigorous plant growth under stress conditions by influencing levels of plant hormones related to stress and plant growth. For soils with initial PHC levels up to 20,000 mg/kg, PEPS can remediate PHC to generic regulatory remediation guideline values within 2–4 years, particularly if an enhanced BOC removal method is used in association with PHC analyses to assess remediation. Degradation of all PHC fractions, including typically recalcitrant molecules (e.g., CCME F3 PHC), occurs during PEPS treatment, typically at a rate of 20–40% per year. Although PHC are degraded in soils during PEPS treatment, accumulation of BOC can confound the results when using standard PHC analytical methods. A new enhanced BOC cleanup method has been developed that removes most of the nonpetrogenic hydrophobic materials from PHC-contaminated soil sample extracts, resulting in more accurate measurements of soil PHC. This, in turn, allows for compliance with generic regulatory remediation guideline values in a more timely fashion. Based on plant toxicity tests, it is apparent that PHC concentrations are not always

the driving factor in soil toxicity; this suggests that if generic regulatory remediation guideline values are not met, it may be possible to use site-specific guideline values (e.g., Tier 2 toxicity testing) to confirm that acceptable remedial end points have been met and successful remediation has occurred. Microbe-assisted phytoremediation of PHC-contaminated sites, including those in remote locations, can be achieved at a fraction of the cost of other remedial strategies. PEPS is an environmentally responsible “green” technology that has great potential for widespread use on soils impacted by oil spills or other hydrocarbon-based compounds or products.

ACKNOWLEDGMENTS

The work performed in the lab of B.M.G. was supported by grants from the Natural Science and Engineering Research Council of Canada. We also thank our partners (EBA Engineering Consultants, MWH Canada, Seaway Energy Services, Stantec and Maxxam Analytics) for research support and helpful discussions.

REFERENCES

- [1] Willey, N. (ed.), *Methods in Biotechnology*, Vol. 23, *Phytoremediation Methods and Reviews*, Humana Press, Totowa, NJ, 2007, p. v.
- [2] Pilon-Smits, E., Phytoremediation, *Annu. Rev. Plant Biol.* 56, 15, 2005.
- [3] Susarla, S., V.F. Medina and S.C. McCutcheon, Phytoremediation: An Ecological Solution to Organic Chemical Contamination, *Ecol. Eng.* 18, 647, 2002.
- [4] Macek, T., M. Mackova and J. Kas, Exploitation of Plants for the Removal of Organics in Environmental Remediation, *Biotechnol. Adv.* 18, 23, 2000.
- [5] Gerhardt, K.E., X.-D. Huang, B.R. Glick and B.M. Greenberg, Phytoremediation of Organic Soil Contaminants: Potential and Challenges, *Plant Sci.*, 176, 20–30, 2009.
- [6] Wenzel, W.W., Rhizosphere Processes and Management in Plant-Assisted Bioremediation (Phytoremediation) of Soils, *Plant Soil*, 321, 385, 2009.
- [7] Zhuang, X., J. Chen, H. Shim and Z. Bai, New Advances in Plant Growth-Promoting Rhizobacteria for Bioremediation, *Environ. Int.* 33, 406, 2007.
- [8] Greenberg, B.M., X.-D. Huang, Y. Gurska, K.E. Gerhardt, W. Wang et al., Successful Field Tests of a Multi-Process Phytoremediation System for Decontamination of Persistent Petroleum and Organic Contaminants, *Proceedings of the 29th Arctic and Marine Oil Spill Program (AMOP). Technical Seminar Vol. 1*. Environment Canada, Ottawa, 389, 2006.
- [9] Gerhardt, K.E., B.M. Greenberg and B.R. Glick, The Role of ACC Deaminase in Facilitating the Phytoremediation of Organics, Metals and Salt, *Curr. Trends Microbiol.* 2, 61, 2006.
- [10] Huang, X.-D., Y.S. El-Alawi, J. Gurska, B.R. Glick and B.M. Greenberg, A Multi-Process Phytoremediation System for Decontamination of Persistent Total Petroleum Hydrocarbons (TPHs) from Soils, *Microchem. J.* 81, 139, 2005.
- [11] Huang, X.-D., Y.S. El-Alawi, D. Penrose, B.R. Glick and B.M. Greenberg, A Multi-Process Phytoremediation System for Removal of Polycyclic Aromatic Hydrocarbons from Contaminated Soils, *Environ. Poll.* 130, 465, 2004.
- [12] Chaudhry, Q., M. Blom-Zandstra, S. Gupta and E.J. Joner, Utilizing the Synergy Between Plants and Rhizosphere Microorganisms to Enhance Breakdown of Organic Pollutants in the Environment, *Environ. Sci. Pollut. Res.* 12, 34, 2005.
- [13] Kuiper, I., E.L. Lagendijk, G.V. Bloembergen and B.J.J. Lugtenberg, Rhizoremediation: A Beneficial Plant-Microbe Interaction, *Mol. Plant Microbe Interact.* 17, 6, 2004.
- [14] Singer, A.C., I.P. Thompson and M.J. Bailey, The Tritrophic Trinity: A Source of Pollutant-Degrading Enzymes and Its Implications for Phytoremediation, *Curr. Opin. Microbiol.* 7, 239, 2004.
- [15] Glick, B.R., Phytoremediation: Synergistic Use of Plants and Bacteria to Clean Up the Environment, *Biotechnol. Adv.* 21, 383, 2003.
- [16] Phillips, L.A., C.W. Greer, R.E. Farrell and J.J. Germida, Plant Root Exudates Impact the Hydrocarbon Degradation Potential of a Weathered-Hydrocarbon Contaminated Soil, *Appl. Soil Ecol.* 52, 56, 2012.
- [17] Novotný, Č., T. Cajthaml, K. Svobodová, M. Šušla and V. Šašek, *Irpex lacteus*, a White-Rot Fungus with Biotechnological Potential – Review, *Folia Microbiol.* 54, 375, 2009.
- [18] Steffen, K.T., S. Schubert, M. Tuomela, A. Hatakka and M. Hofrichter, Enhancement of Bioconversion of High-Molecular Mass Polycyclic Aromatic Hydrocarbons in Contaminated Non-Sterile Soil by Litter-Decomposing Fungi, *Biodegradation*, 18, 359, 2007.
- [19] Kaimi, E., T. Mukaidani and M. Tamaki, Screening of Twelve Plant Species for Phytoremediation of Petroleum Hydrocarbon-Contaminated Soil, *Plant Prod. Sci.* 10, 211, 2007.
- [20] Kaplan, O., V. Vejvoda, O. Plíhal, P. Pompach, D. Kavan et al., Purification and Characterization of a Nitrilase from *Aspergillus niger* K10, *Appl. Microbiol. Biotechnol.* 73, 567, 2006.
- [21] McLean, K.J., M. Sabri, K.R. Marshall, R.J. Lawson, D.G. Lewis et al., Biodiversity of Cytochrome P450 Redox Systems, *Biochem. Soc. Trans.* 33, 796, 2005.
- [22] Coon, M.J., Omega Oxygenases: Nonheme-Iron Enzymes and P450 Cytochromes, *Biochem. Biophys. Res. Co.* 338, 378, 2005.
- [23] Cohen, M.F., H. Yamasaki and M. Mazzola, Bioremediation of Soils by Plant-Microbe Systems, *Int. J. Green Energy*, 1, 301, 2004.
- [24] Pieper, D.H., V.A.P. Martins dos Santos and P.N. Golyshein, Genomic and Mechanistic Insights into the Biodegradation of Organic Pollutants, *Curr. Opin. Biotechnol.* 15, 215, 2004.
- [25] Urlacher, V.B., S. Lutz-Wahl and R.D. Schmid, Microbial P450 Enzymes in Biotechnology, *Appl. Microbiol. Biotechnol.* 64, 317, 2004.
- [26] Cunningham, S.D., W.R. Berti and J.W. Huang, Phytoremediation of Contaminated Soils, *Trends Biotechnol.*, 13, 393–397, 1995.
- [27] Johnson, D.L., K.L. Maguire, D.R. Anderson and S.P. McGrath, Enhanced Dissipation of Chrysene in Planted Soil: The Impact of a Rhizobial Inoculum, *Soil Biol. Biochem.* 36, 33, 2004.

- [28] Liste, H.-H. and M. Alexander, Accumulation of Phenanthrene and Pyrene in Rhizosphere Soil, *Chemosphere* 40, 11, 2000.
- [29] Reed, M.L.E. and B.R. Glick, Growth of Canola (*Brassica napus*) in the Presence of Plant Growth-Promoting Bacteria and Either Copper or Polycyclic Aromatic Hydrocarbons, *Can. J. Microbiol.* 51, 1061, 2005.
- [30] Singer, A.C., D.E. Crowley and I.P. Thompson, Secondary Plant Metabolites in Phytoremediation and Biotransformation, *Trends Biotechnol.* 21, 123, 2003.
- [31] Alkorta, I. and C. Garbisu, Phytoremediation of Organic Contaminants in Soils, *Bioresource Technol.* 79, 273, 2001.
- [32] Muravova, A. Yu., V.V. Kapitonova, M.P. Chernyshova and O.V. Turkovskaya, Enzymatic Activity of Alfalfa in a Phenanthrene-Contaminated Environment, *World Acad. Sci. Eng. Technol.* 34, 569, 2009.
- [33] Kumar, R., S. Pandey and A. Pandey, Plant Roots and Carbon Sequestration, *Curr. Sci.* 91, 885, 2006.
- [34] Miya, R.K. and M.K. Firestone, Bioremediation and Biodegradation, *J. Environ. Qual.* 30, 1911, 2001.
- [35] Leigh, M.B., J.S. Fletcher, X. Fu and F.J. Schmitz, Root Turnover: An Important Source of Microbial Substrates in Rhizosphere Remediation of Recalcitrant Contaminants, *Environ. Sci. Technol.* 36, 579, 2002.
- [36] Ferro, A.M., S.A. Rock, J. Kennedy, J.J. Herrick and D.L. Turner, Phytoremediation of Soils Contaminated with Wood Preservatives: Greenhouse and Field Evaluations, *Int. J. Phytorem.* 1, 289, 1999.
- [37] Cai, Z., Q. Zhou, S. Peng and K. Li, Promoted Biodegradation and Microbiological Effects of Petroleum Hydrocarbons by *Impatiens balsamina* L. with Strong Endurance, *J. Hazard. Mater.* 183, 731, 2010.
- [38] Anderson, T.A., E.A. Guthrie and B.T. Walton, Bioremediation, *Environ. Sci. Technol.* 27, 2630, 1993.
- [39] Kechavarzi, C., K. Pettersson, P. Leeds-Harrison, L. Ritchie and S. Ledin, Root Establishment of Perennial Ryegrass (*L. perenne*) in Diesel Contaminated Subsurface Soil Layers, *Environ. Pollut.* 145, 68, 2007.
- [40] Huang, X.-D., Y.S. El-Alawi, D. Penrose, B.R. Glick and B.M. Greenberg, Responses of Three Grass Species to Creosote During Phytoremediation, *Environ. Pollut.* 130, 453, 2004.
- [41] Adam G. and H. Duncan, Influence of Diesel Fuel on Seed Germination, *Environ. Pollut.* 120, 363, 2002.
- [42] Harvey, P.J., B.F. Campanella, P.M. Castro, H. Harms, E. Lichtfouse et al., Phytoremediation of Polyaromatic Hydrocarbons, Anilines and Phenols, *Environ. Sci. Pollut. Res. Int.* 9, 29, 2002.
- [43] Boyajian, G.E. and L.H. Carreira, Phytoremediation: A Clean Transition from Laboratory to Marketplace? *Nat. Biotechnol.* 15, 127, 1997.
- [44] Kirk, J.L., J.N. Klironomos, H. Lee and J.T. Trevors, The Effects of Perennial Ryegrass and Alfalfa on Microbial Abundance and Diversity in Petroleum Contaminated Soil, *Environ. Pollut.* 133, 455, 2005.
- [45] White Jr., P.M., D.C. Wolf, G.J. Thoma and C.M. Reynolds, Phytoremediation of Alkylated Polycyclic Aromatic Hydrocarbons in a Crude Oil-Contaminated Soil, *Water Air Soil Pollut.* 169, 207, 2006.
- [46] Siciliano, S.D., J.J. Germida, K. Banks and C.W. Greer, Changes in Microbial Community Composition and Function During a Polyaromatic Hydrocarbon Phytoremediation Field Trial, *Appl. Environ. Microbiol.* 69, 483, 2003.
- [47] Syafruddin, S., G. Wieshammer, M. Puschenreiter, I. Langer, M. Wieshammer-Zivkovic and W.W. Wenzel, Effect of N and P Fertilisation and Aeration on Biodegradation of Crude Oil in Aged Hydrocarbon Contaminated Soils, *Plant Soil Environ.* 56, 149, 2010.
- [48] Olson, P.E., A. Castro, M. Joern, N.M. DuTeau, E.A.H. Pilon-Smits and K.F. Reardon, Comparison of Plant Families in a Greenhouse Phytoremediation Study on an Aged Polycyclic Aromatic Hydrocarbon-Contaminated Soil, *J. Environ. Qual.* 36, 1461, 2007.
- [49] Allard, A.-S., M. Remberger and A.H. Neilson, The Negative Impact of Aging on the Loss of PAH Components in a Creosote-Contaminated Soil, *Int. Biodeterior. Biodegrad.* 46, 43, 2000.
- [50] Smith, M.J., T.H. Flowers, H.J. Duncan and J. Alder, Effects of Polycyclic Aromatic Hydrocarbons on Germination and Subsequent Growth of Grasses and Legumes in Freshly Contaminated Soil and Soil with Aged PAHs Residues, *Environ. Pollut.* 141, 519, 2006.
- [51] Lovley, D.R., Cleaning Up with Genomics: Applying Molecular Biology to Bioremediation, *Nat. Rev.* 1, 35, 2003.
- [52] Dua, M., A. Singh, N. Sethunathan and A. Johri, Biotechnology and Bioremediation: Successes and Limitations, *Appl. Microbiol. Biotechnol.* 59, 143, 2002.
- [53] Harms, H. and T.N.P. Bosma, Mass Transfer Limitation of Microbial Growth and Pollutant Degradation, *J. Ind. Microbiol. Biotechnol.* 18, 97, 1997.
- [54] Rosenberg, E., R. Legmann, A. Kushmaro, R. Taube, E. Adler and E.Z. Ron, Petroleum Bioremediation – A Multiphase Problem, *Biodegradation* 3, 337, 1992.
- [55] Hwang, G., Y.-M. Ban, C.-H. Lee, C.-H. Chung and I.-S. Ahn, Adhesion of *Pseudomonas putida* NCIB 9816-4 to a Naphthalene-Contaminated Soil, *Colloid Surface B* 62, 91, 2008.
- [56] Joo, H.-S., P.M. Ndegwa, M. Shoda and C.-G. Phae, Bioremediation of Oil-Contaminated Soil Using *Candida catenulata* and Food Waste, *Environ. Pollut.* 156, 891, 2008.
- [57] Slater, G.F., R.K. Nelson, B.M. Kile and C.M. Reddy, Intrinsic Bacterial Biodegradation of Petroleum Contamination Demonstrated In Situ Using Natural Abundance, Molecular-Level ¹⁴C Analysis, *Org. Geochem.* 37, 981, 2006.
- [58] Huesemann, M.H., T.S. Hausmann and T.J. Fortman, Biodegradation of Hopane Prevents Use as Conservative Biomarker During Bioremediation of PAHs in Petroleum Contaminated Soils, *Biorem. J.* 7, 111, 2003.
- [59] Song, R., Z. Hua, H. Li and J. Chen, Biodegradation of Petroleum Hydrocarbons by Two *Pseudomonas aeruginosa* Strains with Different Uptake Modes, *J. Environ. Sci. Health Pt. A* 41, 733, 2006.
- [60] Ahemad, M. and M.S. Khan, Functional Aspects of Plant Growth Promoting Rhizobacteria: Recent Advancements, *Insight Microbiol.* 1, 39, 2011.
- [61] Yateem, A., T. Al-Sharrah and A. Bin-Haji, Investigation of Microbes in the Rhizosphere of Selected Grasses for Rhizoremediation of Hydrocarbon-Contaminated Soils, *Soil Sed. Contam.* 16, 269, 2007.

- [62] Corgié, S.C., E.J. Joner and C. Leyval, Rhizospheric Degradation of Phenanthrene is a Function of Proximity to Roots, *Plant Soil* 257, 143, 2003.
- [63] Naveenkumar, S., N. Manoharan, S. Ganesan, S.P. Manivannan and G. Velsamy, Isolation, Screening and In Vitro Mutational Assessment of Indigenous Soil Bacteria for Enhanced Capability in Petroleum Degradation, *Int. J. Environ. Sci.* 1, 498, 2010.
- [64] Doucette, W.J., Quantitative Structure-Activity Relationships for Predicting Soil-Sediment Sorption Coefficients for Organic Chemicals, *Environ. Toxicol. Chem.* 22, 1771, 2003.
- [65] Cunningham, S.D., T.A. Anderson, A.P. Schwab and F.C. Hsu, Phytoremediation of Soils Contaminated with Organic Pollutants, *Advances in Agronomy*, Vol. 56, Chap. 2, D.L. Sparks (ed.), Academic Press, San Diego, CA, 55, 1996.
- [66] Uraizee, F.A., A.D. Venosa and M.T. Suidan, A Model for Diffusion Controlled Bioavailability of Crude Oil Components, *Biodegradation* 8, 287, 1998.
- [67] Sridevi, V., M.V.V.C. Lakshmi, A.V.N. Swamy and M.N. Rao, Implementation of Response Surface Methodology for Phenol Degradation Using *Pseudomonas putida* (NCIM 2102), *J. Bioremed. Biodegrad.* 2, 121, 2011.
- [68] Speight, J.G., The Chemistry and Technology of Petroleum, Fourth Edition, CRC Press, Boca Raton, FL, 2006.
- [69] Greenberg, B.M., Development and Field Tests of a Multi-Process Phytoremediation System for Decontamination of Soils, *Can. Reclamation* Spring/Summer 1, 27, 2006.
- [70] Banks, M.K., H. Mallede and K. Rathbone, Rhizosphere Microbial Characterization in Petroleum-Contaminated Soil, *Soil Sed. Contam.* 12, 371, 2003.
- [71] Da Silva, M.L.B., R. Kamath and P.J.J. Alvarez, Effect of Simulated Rhizodeposition on the Relative Abundance of Polynuclear Aromatic Hydrocarbon Catabolic Genes in a Contaminated Soil, *Environ. Toxicol. Chem.* 25, 386, 2006.
- [72] Hinsinger, P., G.R. Gobran, P.J. Gregory and W.W. Wenzel, Rhizosphere Geometry and Heterogeneity Arising from Root-Mediated Physical and Chemical Processes, *New Phytol.* 168, 293, 2005.
- [73] Warembourg, F.R., The 'Rhizosphere Effect': A Plant Strategy for Plants to Exploit and Colonize Nutrient-Limited Habitats, *Boccone* 7, 187, 1997.
- [74] Lynch, J.M., *The Rhizosphere*, Wiley, New York, 1990.
- [75] Whipps, J.M., Carbon Economy, *The Rhizosphere*, Chapter 3, J.M. Lynch (ed.), Wiley, New York, 59, 1990.
- [76] Miya, R.K. and M.K. Firestone, Phenanthrene-Degrader Community Dynamics in Rhizosphere Soil from a Common Annual Grass, *J. Environ. Qual.* 29, 584, 2000.
- [77] Radwan, S., N. Sorkhoh and I. El-Nemr, Oil Biodegradation Around Roots, *Nature* 376, 302, 1995.
- [78] Dams, R.I., G.I. Paton and K. Killham, Rhizoremediation of Pentachlorophenol by *Sphingobium chlorophenolicum* ATCC 39723, *Chemosphere* 68, 864, 2007.
- [79] Gianfreda, L. and M.A. Rao, Potential of Extra Cellular Enzymes in Remediation of Polluted Soils: A Review, *Enzyme Microb. Technol.* 35, 339, 2004.
- [80] Hontzeas, N., J. Zoidakis and B.R. Glick, Expression and Characterization of 1-Aminocyclopropane-1-Carboxylate Deaminase from the Rhizobacterium *Pseudomonas putida* UW4: A Key Enzyme in Bacterial Plant Growth Promotion, *Biochim. Biophys. Acta* 1703, 11, 2004.
- [81] Patten, C.L. and B.R. Glick, The Role of Bacterial Indoleacetic Acid in the Development of the Host Plant Root System, *Appl. Environ. Microbiol.* 68, 3795, 2002.
- [82] Kuzyakov, Y. and G. Domanski, Carbon Input by Plants into the Soil. Review, *J. Plant Nutr. Soil Sci.* 163, 421, 2000.
- [83] Lynch, J.M. and J.M. Whipps, Substrate Flow in the Rhizosphere, *Plant Soil* 129, 1, 1990.
- [84] Basha, K.M., A. Rajendran and V. Thangavelu, Recent Advances in the Biodegradation of Phenol: A Review, *Asian J. Exp. Biol. Sci.* 1, 219, 2010.
- [85] Jones, D.L., C. Nguyen and R.D. Finlay, Carbon Flow in the Rhizosphere: Carbon Trading at the Soil-Root Interface, *Plant Soil* 321, 5, 2009.
- [86] Jaeger, C.H., S.E. Lindow, W. Miller, E. Clark and M.K. Firestone, Mapping of Sugar and Amino Acid Availability in Soil Around Roots with Bacterial Sensors of Sucrose and Tryptophan, *Appl. Environ. Microb.* 65, 2685, 1999.
- [87] Curl, E.A. and B. Truelove, *The Rhizosphere*, Springer-Verlag, Berlin, 1986.
- [88] Cardon, Z.G. and D.J. Gage, Resource Exchange in the Rhizosphere: Molecular Tools and the Microbial Perspective, *Annu. Rev. Ecol. Evol. Sys.* 37, 459, 2006.
- [89] Lugtenberg, B.J.J., L. Dekkers and G.V. Bloemberg, Molecular Determinants of Rhizosphere Colonization by *Pseudomonas*, *Annu. Rev. Phytopathol.* 39, 461, 2001.
- [90] Capdevila, S., F.M. Martínez-Granero, M. Sánchez-Contreras, R. Rivilla and M. Martín, Analysis of *Pseudomonas fluorescens* F113 Genes Implicated in Flagellar Filament Synthesis and Their Role in Competitive Root Colonization, *Microbiology* 150, 3889, 2004.
- [91] Silby, M.W. and S.B. Levy, Use of In Vivo Expression Technology to Identify Genes Important in Growth and Survival of *Pseudomonas fluorescens* Pf0-1 in Soil: Discovery of Expressed Sequences with Novel Genetic Organization, *J. Bacteriol.* 186, 7411, 2004.
- [92] de Weert, S., H. Vermeiren, I.H.M. Mulders, I. Kuiper, N. Hendrickx et al., Flagella-Driven Chemotaxis Towards Exudates Components is an Important Trait for Tomato Root Colonization by *Pseudomonas fluorescens*, *Mol. Plant Microbe Interact.* 15, 1173, 2002.
- [93] Kuiper, I., L.V. Kravchenko, G.V. Bloemberg and B.J.J. Lugtenberg, *Pseudomonas putida* Strain PCL1444, Selected for Efficient Root Colonization and Naphthalene Degradation, Effectively Utilizes Root Exudates Components, *Mol. Plant Microbe Interact.* 15, 734, 2002.
- [94] Turnbull, G.A., J.A.W. Morgan, J.M. Whipps and J.R. Saunders, The Role of Bacterial Motility in the Survival and Spread of *Pseudomonas fluorescens* in Soil and in the Attachment and Colonisation of Wheat Roots, *FEMS Microbiol. Ecol.* 36, 21, 2001.
- [95] Phillips, L.A., C.W. Greer, R.E. Farrell and J.J. Germida, Field-Scale Assessment of Weathered Hydrocarbon Degradation by Mixed and Single Plant Treatments, *Appl. Soil Ecol.* 42, 9, 2009.
- [96] Siciliano, S.D. and J.J. Germida, BIOLOG Analysis and Fatty Acid Methyl Ester Profiles Indicate that *Pseudomonas* Inoculants that Promote Phytoremediation Alter the

- Root-Associated Microbial Community of *Bromus biebersteinii*, *Soil Biol. Biochem.* 30, 1717, 1998.
- [97] Holden, P.A. and M.K. Firestone, Soil Microorganisms in Soil Cleanup: How Can We Improve Our Understanding? *J. Environ. Qual.* 26, 32, 1997.
- [98] Leahy, J.G. and R.R. Colwell, Microbial Degradation of Hydrocarbons in the Environment, *Microbiol. Rev.* 54, 305, 1990.
- [99] Corgié, S.C., T. Beguiristain and C. Leyval, Spatial Distribution of Bacterial Communities and Phenanthrene Degradation in the Rhizosphere of *Lolium perenne* L., *Appl. Environ. Microbiol.* 70, 3552, 2004.
- [100] Thoma, G.J., T.B. Lam and D.C. Wolf, A Mathematical Model of Phytoremediation for Petroleum Contaminated Soil: Sensitivity Analysis, *Int. J. Phytorem.* 5, 125, 2003.
- [101] Muratova, A.Y., T.V. Dmitrieva, L.V. Panchenko and O.V. Turkovskaya, Phytoremediation of Oil-Sludge-Contaminated Soil, *Int. J. Phytoremediation* 10, 486, 2008.
- [102] Tang, J., R. Wang, X. Niu and Q. Sun, Enhancement of Soil Petroleum Remediation by Using a Combination of Ryegrass (*Lolium perenne*) and Different Microorganisms, *Soil Till. Res.* 110, 87, 2010.
- [103] Kuiper, I., G.V. Bloemberg and B.J.J. Lugtenberg, Selection of a Plant-Bacterium Pair as a Novel Tool for Rhizostimulation of Polycyclic Aromatic Hydrocarbon-Degrading Bacteria, *Mol. Plant Microbe Interact.* 14, 1197, 2001.
- [104] Parrish, Z.D., M.K. Banks and A.P. Schwab, Effectiveness of Phytoremediation as a Secondary Treatment for Polycyclic Aromatic Hydrocarbons (PAH's) in Composted Soil, *Int. J. Phytoremed.* 6, 119, 2004.
- [105] Aprill, W. and R.C. Sims, Evaluation of the Use of Prairie Grasses for Stimulating Polycyclic Aromatic Hydrocarbon Treatment in Soil, *Chemosphere* 20, 253, 1990.
- [106] Binet, P., J.M. Portal and C. Leyval, Fate of Polycyclic Aromatic Hydrocarbons (PAH) in the Rhizosphere and Mycorrhizosphere of Ryegrass, *Plant Soil* 227, 207, 2000.
- [107] Venkata Mohan, S., T. Kisa, T. Ohkuma, R.A. Kanaly and Y. Shimizu, Bioremediation Technologies for Treatment of PAH-Contaminated Soil and Strategies to Enhance Process Efficiency, *Rev. Environ. Sci. Biotechnol.* 5, 347, 2006.
- [108] Pilon-Smits, E.A.H. and J.L. Freeman, Environmental Cleanup Using Plants: Biotechnological Advances and Ecological Considerations, *Front. Ecol. Environ.* 4, 203, 2006.
- [109] Greenberg, B. and P. Gerwing, Phytoremediation, *HazMat Manag.* Fall, 27–31, 2009.
- [110] Pretty, A. and A. Ball, Agricultural Influences on Carbon Emissions and Sequestration: A Review of Evidence and the Emerging Trading Options, Centre for Environment and Society Occasional Paper 2001-03, University of Essex, Colchester, 2001.
- [111] Arnalds, A., Carbon Sequestration – A Powerful Incentive in Combating Land Degradation and Desertification, ISCO Conference, Beijing, 52, 2002.
- [112] Glick, B.R., Z. Cheng, J. Czarny and J. Duan, Promotion of Plant Growth by ACC Deaminase-Producing Soil Bacteria, *Eur. J. Plant Pathol.* 119, 329, 2007.
- [113] Glick, B.R., D.M. Penrose and J. Li, A Model for the Lowering of Plant Ethylene Concentrations by Plant Growth-Promoting Bacteria, *J. Theor. Biol.* 190, 63, 1998.
- [114] Glick, B.R., Modulation of Plant Ethylene Levels by the Enzyme ACC Deaminase, *FEMS Microbiol. Lett.* 251, 1, 2005.
- [115] Glick, B.R., The Enhancement of Plant Growth by Free-Living Bacteria, *Can. J. Microbiol.* 41, 109, 1995.
- [116] Lim, J.-H. and S.-D. Kim, Synergistic Plant Growth Promotion by the Indigenous Auxins-Producing PGPR *Bacillus subtilis* AH18 and *Bacillus licheniformis* K11, *J. Korean Soc. Appl. Biol. Chem.* 52, 531, 2009.
- [117] Njoku, K.L., M.O. Akinola and B.O. Oboh, Phytoremediation of Crude Oil Polluted Soil: Effect of Cow Dung Augmentation on the Remediation of Crude Oil Polluted Soil by Glycine Max, *J. Appl. Sci. Res.* 8, 277, 2012.
- [118] Liu, B., M.K. Banks and P. Schwab, Effects of Soil Water Content on Biodegradation of Phenanthrene in a Mixture of Organic Contaminants, *Soil Sed. Contam.* 10, 633, 2001.
- [119] Gressel, J. and H. Al-Ahmad, Assessing and Managing Biological Risks of Plants Used for Bioremediation, Including Risks of Transgene Flow, *Z. Naturforsch [C]* 60, 154, 2005.
- [120] Wang, Z., C. Yang, Z. Yang, B. Hollebone, C.E. Brown et al., Fingerprinting of Petroleum Hydrocarbons (PHC) and Other Biogenic Organic Compounds (BOC) in Oil-Contaminated and Background Soil Samples, *J. Environ. Monit.* 14 (9), 2367–2381, 2012.
- [121] Wang, Z., C. Yang, F. Kelly-Hooper, B.P. Hollebone, X. Peng et al., Forensic Differentiation of Biogenic Organic Compounds from Petroleum Hydrocarbons in Biogenic and Petrogenic Compounds Cross-Contaminated Soils and Sediments, *J. Chromatogr. A* 1216, 1174, 2009.
- [122] Canadian Council of Ministers of the Environment (CCME), *Reference Method for the Canada-Wide Standard for Petroleum Hydrocarbons in Soil – Tier 1 Method*, ISBN 1-896997-01-5, Publication No. 1310, 44 pp, 2001.
- [123] Doran, J. and A. Takar, *Ontario Typical Range Soil Background Study Project Report*, MOE/OCE, Ontario, Canada, 2010.
- [124] Stout, S.A., V.S. Magar, R.M. Uhler, J. Ickes, J. Abbott and R. Brenner, Characterization of Naturally-Occurring and Anthropogenic PAHs in Urban Sediments – Wycoff/Eagle Harbor Superfund Site, *Environ. Forensics* 2, 287, 2001.
- [125] Nedunuri, K.V., R.S. Govindaraju, M.K. Banks, A.P. Schwab and Z. Chen, Evaluation of Phytoremediation for Field-Scale Degradation of Total Petroleum Hydrocarbons, *J. Environ. Eng.* 126, 483, 2000.
- [126] Robinson, S.L., J.T. Novak, M.A. Widdowson, S.B. Crosswell and G.J. Fetterolf, Field and Laboratory Evaluation of the Impact of Tall Fescue on Polyaromatic Hydrocarbon Degradation in an Aged Creosote-Contaminated Surface Soil, *J. Environ. Eng.* 129, 232, 2003.
- [127] Efe, S.I. and A.E. Okpali, Management of Petroleum Impacted Soil with Phytoremediation and Soil Amendments in Ekpan Delta State, Nigeria, *J. Environ. Protect.* 3, 386, 2012.
- [128] Gurska, J., W. Wang, K.E. Gerhardt, A.M. Khalid, D.M. Isherwood et al., Three Year Field Test of a Plant Growth Promoting Rhizobacteria Enhanced Phytoremediation System at a Land Farm for Treatment of Hydrocarbon Waste, *Environ. Sci. Tech.* 43, 4472, 2009.

- [129] Huang, X.-D., X.-M. Yu, K. Gerhardt, B. Glick and B. Greenberg, A Novel Phytoremediation Technology Shown to Remediate Petroleum Hydrocarbons from Soils In Situ, *Can. Reclamation* 1 Spring/Summer, 46, 2009.
- [130] Greenberg, B.M., X.-D. Huang, P. Gerwing, J. Gurska, K. Gerhardt et al., Use of a Multi-Process Phytoremediation System for Decontamination of Petroleum Impacted Soils: Results of Successful Field Trials, *Proceeding of the 33rd AMOP Technical Seminar*, Environment Canada, Ottawa, 615, 2008.
- [131] Greenberg, B.M., X.-D. Huang, D. G. Dixon and B.R. Glick, An Integrated Multi-Process Phytoremediation System (MPPS) for Removal of Persistent Organic Contaminants from Soil, *Proceedings of the 8th International In Situ and On-Site Bioremediation Symposium*, B. Alleman and M. Kelly (eds.), Batelle Press, Columbus, OH, Paper K-08, 2005.
- [132] Greenberg, B.M., X.-D. Huang, P. Gerwing, X.-M. Yu, P.-C. Chang et al., Phytoremediation of Salt Impacted Soils: Greenhouse and Field Trials Using Plant Growth Promoting Rhizobacteria (PGPR) to Improve Plant Growth and Salt Phytoaccumulation, *Proceedings of the 33rd AMOP Technical Seminar*, Environment Canada, Ottawa, 627, 2008.
- [133] Mayak, S., T. Tirosh and B.R. Glick, Plant Growth-Promoting Bacteria that Confer Resistance in Tomato to Salt Stress, *Plant Physiol. Biochem.* 42, 565, 2004.
- [134] Fang, J., N. Lovanh and P.J.J. Alvarez, The Use of Isotopic and Lipid Analysis Techniques Linking Toluene Degradation to Specific Microorganisms: Applications and Limitations, *Water Res.* 38, 2529, 2004.
- [135] Yuste, L. and F. Rojo, Role of the *crc* Gene in Catabolic Repression of the *Pseudomonas putida* GPo1 Alkane Degradation Pathway, *J. Bacteriol.* 183, 6197, 2001.
- [136] Cowie, B.R., B.M. Greenberg and G.F. Slater, Determination of Microbial Carbon Sources and Cycling During Remediation of Petroleum Hydrocarbon Impacted Soil Using Natural Abundance ¹⁴C Analysis of PLFA, *Environ. Sci. Technol.* 44, 2322, 2010.
- [137] Greenberg, B.M., X.-D. Huang, K. Gerhardt, P. Mosley, X.M. Yu et al., Phytoremediation of Petroleum and Salt Impacted Soils: A Scientifically-Based Innovative Remediation Process, *Proceedings of the 35th AMOP Technical Seminar on Environmental Contamination and Response*, Vancouver, BC, Canada, 420, 2012.
- [138] British Columbia Ministry of Environment, Land and Parks, Silica Gel Cleanup of Extractable Petroleum Hydrocarbons, Version 1.0, CSR - Analytical Method 10, 15 pp, May 2004.
- [139] Canadian Council of Ministers of the Environment (CCME), Five-Year Review of the Canada-Wide Standards for Petroleum Hydrocarbons (PHC CWS): Ecological, Direct Soil Contact Guidance, Report to the Canadian Council of Ministers of Environment (CCME) Soil Quality Guidelines Task Group (SQGTG) by the Ecological Criteria Advisory Subgroup, 93 pp, March 2006.

PART IX

EFFECTS OF OIL

OVERVIEW OF EFFORTS TO DOCUMENT AND REDUCE IMPACTS OF OIL SPILLS ON SEABIRDS

ROGER C. HELM,¹ HARRY R. CARTER,² R. GLENN FORD,³ D. MICHAEL FRY,⁴ ROCÍO L. MORENO,⁵ CAROLINA SANPERA,⁵ AND FLORINA S. TSENG⁶

¹*U.S. Fish and Wildlife Service, Science Applications, Falls Church, VA, USA*

²*Carter Biological Consulting, Victoria, BC, Canada*

³*R.G. Ford Consulting Company, Portland, OR, USA*

⁴*U.S. Fish and Wildlife Service, Environmental Contaminants, Pacific Islands Fish and Wildlife Office, Honolulu, HI, USA*

⁵*Departament de Biologia Animal, Facultat de Biologia, Universitat de Barcelona, Barcelona, Spain*

⁶*Cummings School of Veterinary Medicine, North Grafton, MA, USA*

17.1	Introduction	431
17.2	Vulnerability	433
17.3	Effect of Oiling on Individual Birds	435
17.3.1	External Oil Effects	435
17.3.2	Internal Oil Effects	435
17.3.3	Oil Effects on Reproduction	436
17.4	Rehabilitation and Veterinary Care	436
17.4.1	Key Considerations in Care	436
17.4.2	Release Rates	437
17.4.3	Post-Release Survival and Reproduction	437
17.4.4	Rehabilitation Process	438
17.5	Estimating Mortality	441
17.5.1	Oiled Birds at Sea	441
17.5.2	Oiled Birds on Land	442
17.5.3	Cause of Death and Background Deposition	443
17.6	Long-Term Impacts	444
17.7	Restoration	446
17.7.1	<i>Apex Houston Barge Oil Spill, Central California</i>	446
17.7.2	<i>American Trader Oil Spill, Southern California</i>	448

17.1 INTRODUCTION

The global development, marine transportation, and use of oil since the nineteenth century have led to widespread and regular marine oil spills. Worldwide, many thousands of seabirds

Disclaimer:

The findings and conclusions in this article are those of the authors and do not necessarily represent the views of the U.S. Fish and Wildlife Service.

are killed each year from oil spills from marine vessels, offshore production platforms, and onshore facilities [1–4]. On occasion, very large marine spills (e.g., 1989 *Exxon Valdez* oil spill, Alaska) kill hundreds to thousands of seabirds in a single event [5]. More commonly small to large oil spills kill hundreds to thousands of seabirds, while some small spills kill only a few birds or none at all [6]. In this overview, we cover a variety of topics related to the effects of marine oil spills on seabirds and efforts to document and reduce those impacts. We define seabirds broadly to include true seabirds, shorebirds, many waterbirds, and nearly all other marine-associated bird species. We describe (i) vulnerability of different bird taxa to oil, (ii) various physical and physiological mechanisms by which oil injures or kills individual birds, (iii) the increasingly complex field of oiled bird rehabilitation, including details on various pitfalls and recommended approaches to nurturing some oiled birds back to health, (iv) methodologies for accurately estimating total bird mortality caused by a spill, (v) long-term effects of oil on seabird populations, and (vi) measures taken to restore seabird populations with examples showing different degrees of success. We did not provide an exhaustive examination of any of these topics, but instead focused on the most salient literature and our own observations and experience on each topic. A brief summary of each section follows to provide a basic framework for the more detailed explanations presented in this chapter:

In Section 17.2, we examine oil vulnerability indexes developed for seabird species which exhibit different

susceptibilities to becoming oiled and different effects from being oiled. Those species that dive into or sit on the water surface are most susceptible to becoming moderately to heavily oiled, while those species that spend little time on or in the water typically only become lightly oiled. Some of the factors considered in determining the vulnerability of a species to the effect of oil are at-sea distribution, location of breeding and wintering areas, population size, breeding phenology, demography, and resting and foraging behavior.

In Section 17.3, we discuss how oil impacts the health of individual birds by fouling the feathers, damaging skin and eyes, or creating internal physiological harm following ingestion or inhalation. The most volatile and highly toxic aromatic components, concentrated during the refining process, cause the most severe and immediate injuries to birds. Oil fouled feathers cause loss of homeothermy; impaired flight, diving, feeding, and buoyancy; and death for most species. The adverse effects of ingested oil include acute toxic impacts to the blood, digestive tract, liver, kidney, adrenals, and occasionally lungs. Secondary complications cause immunosuppression, leading to respiratory fungal infections, greater susceptibility to disease, and inflamed joints. For individuals that survive initial impacts, oil effects can negatively impact their reproductive output. Even small amounts of oil on a seabird will significantly suppress sex steroid hormone production, and adult seabirds exposed to oil early in the breeding season exhibit breeding depression from stress or impaired egg formation. Oil applied to eggs also decreases embryo survival and increases malformations.

In Section 17.4, we detail the many variables that must be successfully addressed during rehabilitation for an oiled bird to recover sufficiently to warrant release. For example, most live oiled birds suffer from hypothermia, dehydration, and malnutrition at the time of capture which typically leads to anemia and other potentially life threatening problems. A key variable determining the success of the rehabilitation process is tolerance to stress of capture, handling, and captive care. Generally, those species with higher release rates are the larger, more colonial species that typically roost on land; the smaller, pelagic, solitary, and water roosting species often fair much more poorly. For many species, release rates tend to be higher for those individuals captured and rehabilitated soon after being oiled.

Despite the decades of effort and thousands of birds processed and released after rehabilitation, we know little about the long-term survivorship or the subsequent reproductive output of most rehabilitated birds. The lone exception is penguins, which appear to survive the rehabilitation process well and re-enter the breeding population. It seems likely that public demand for the care of injured wildlife following an oil spill will continue to require governments and spillers to pursue this expensive and time intensive effort despite its limited value at a population level.

Following most large oil spills, local or international non-profit oiled wildlife care organizations and veterinarians are

contacted by governments or spillers to take a leading role in locating, capturing, transporting, cleaning, and providing veterinary care for live oiled birds. In many countries, local wildlife rehabilitation organizations are far less experienced and equipped than in the United States and they are not prepared to address a large influx of oiled birds. Thus, this section also provides a practical experience-based guide for wildlife rehabilitators to enhance their preparedness, knowledge, and success when faced with caring for oiled seabirds, especially when veterinarians are not available.

In Section 17.5, we explain how to accurately assess the impact an oil spill has on seabirds. Historically, the number of seabirds impacted by an oil spill was presented as either a broad estimate (e.g., several thousand or tens of thousands) or a simple tally of the dead oiled birds recovered. Neither of these approaches produced a reasonably accurate accounting. In the mid-1980s, new methods evolved to quantify seabird mortality using beached bird surveys, at-sea determination of oil and seabird distribution, and rehabilitation data. The demand for greater accuracy of seabird mortality estimates has continued to increase since the passage of the Oil Pollution Act of 1990 (OPA 90) as spillers are being held financially responsible for fully restoring seabirds injured from an oil spill and seabird restoration can be expensive [7]. Obtaining more accurate estimates depends upon knowing (i) the amount and type of oil spilled, (ii) the number, type, and on water distribution of birds in the spill zone, (iii) the length and type of coastline impacted, (iv) the ratio of live to dead birds reaching shore, (v) the effort and efficiency of beach searches, and (vi) the dates of collection and persistence of bird carcasses. These data are used in the beached bird model, which has become a standard technique in the United States, to estimate total bird mortality following a marine oil spill.

In Section 17.6, we discuss how oil spills can affect long-term bird population dynamics by lowering population size, densities, reproduction, or altering sex ratios. However, clearly demonstrating a long-term causal relationship between a seabird population decline and a specific oil spill is challenging. Marine ecosystems are complex and affected by many natural and anthropogenic factors. For seabirds, it is clear that not all species are affected equally by an oil spill and some species recover more quickly than others. Long-term studies indicate that nearshore feeding species may be the most susceptible to short-term and long-term habitat disturbance resulting from oil spills. Population impacts appear to be greatest when a spill coincides with other natural or anthropogenic factors that also diminish population size or reproductive rates. These other factors can sometimes mask the significant negative effect an oil spill can have on local populations.

In Section 17.7, we provide a brief review of seabird conservation and the evolution of seabird restoration in the wake of natural resource damage assessment claims in the United States after a spill. Seabird restoration efforts typically focus on (i) acquisition and protection of breeding

habitats, (ii) management of colonies through introduced mammalian predator removal or other breeding habitat improvements, and (iii) promoting public education and regulations to reduce anthropogenic related impacts on land and at sea. Most post-oil spill seabird restoration projects in the United States have been recently initiated, and for the most part, their final outcomes have not been achieved or adequately assessed. Nevertheless, while many restoration efforts are ultimately expected to succeed, certain efforts may fall short of their original goals. The difficulty and risk of restoring seabirds severely impacted by human activities indicates that even relatively small oil spills can contribute to devastating long-term or permanent impacts on local seabird populations, especially without restoration.

17.2 VULNERABILITY

Seabirds and shorebirds are a diverse group of aquatic birds (Tables 17.1 and 17.2) that derive at least part of their food, usually fish, invertebrates, or plankton, from marine waters during all or part of the year [8]. Seabirds use various feeding

methods including wing-propelled and foot-propelled pursuit diving, plunge diving, surface seizing, aerial dipping, kleptoparasitism, and scavenging. Only pursuit divers probe deeper than a few meters into the ocean and only a few species such as penguins and certain alcids dive to depths beyond 100m. Seabirds are often divided into two groups: inshore or coastal species that usually forage within sight of land and offshore species that usually forage well out to sea. Shorebirds use various visual and tactile feeding methods to forage along coastlines and they tend to be particularly abundant in intertidal and estuarine areas. Phalaropes are the only shorebird family that sit on the ocean surface while feeding, often far out to sea. Some individual species of a few other bird families prey upon or scavenge seabirds, shorebirds, and fish or feed along shoreline edges. However, these marine-associated species, such as vultures, ospreys, eagles, hawks, falcons, crows, jays, and ravens, are typically considered terrestrial species. Several families of seabirds (i.e., “true seabirds”) such as penguins, albatrosses, shearwaters, petrels, and alcids live almost entirely at sea and usually only come onshore to breed. Certain other bird families, such as loons, grebes, and sea ducks are also considered seabirds in

TABLE 17.1 Main seabird families^a

Order	Family	English name	No. species
Anseriformes	Anatidae	Ducks, Geese, Swans	164
Sphenisciformes	Spheniscidae	Penguins	19
Gaviiformes	Gaviidae	Loons	5
Procellariiformes	Diomedidae	Albatrosses	21
	Procellariidae	Shearwaters, Fulmars, Gadfly Petrels, Prions	85
	Hydrobatidae	Storm-Petrels	22
	Pelecanoididae	Diving Petrels	4
Podicipediformes	Podicipedidae	Grebes	21
Phaethontiformes	Phaethontidae	Tropicbirds	3
Pelecaniformes	Fregatidae	Frigatebirds	5
	Pelecanidae	Pelicans	8
	Sulidae	Boobies, Gannets	10
	Phalacrocoracidae	Cormorants, Shags	36
Charadriiformes	Laridae	Gulls, Terns, Kittiwakes, Noddies, Skimmers	102
	Stercoracidae	Skuas, Jaegers	7
	Alcidae	Dovekie, Razorbill, Murres, Guillemots, Murrelets, Auklets, Puffins	23

^aFrom Ref. 2.

TABLE 17.2 Main shorebird families^a

Order	Family	English name	No. species
Phoenicopteriformes	Phoenicopteridae	Flamingos	6
Pelecaniformes	Threskiornithidae	Ibises, Spoonbills	34
	Ardeidae	Hérons, Bitterns	67
Gruiiformes	Rallidae	Rails, Crakes, Coots	130
	Gruidae	Cranes	15
Charadriiformes	Haematopodidae	Oystercatchers	11
	Recurvirostridae	Stilts, Avocets	10
	Charadriidae	Plovers, Lapwings, Dotterels,	67
	Scolopacidae	Sandpipers, Woodcocks, Snipes, Dowitchers, Godwits, Curlews, Phalaropes	91

^aFrom Ref. 2.

this chapter, even though they may spend considerable amounts of time roosting, feeding, or breeding on land or in freshwater environments.

Essentially all seabird and shorebird species can be impacted by marine oil spills that occur on or near marine waters. Seabirds that dive into or sit on the surface of marine waters are most susceptible to becoming moderately to heavily coated with oil. Shorebirds and other marine associated birds that spend little time on or in the water often only become lightly oiled, except during very large oil spills. Not all birds in the vicinity of a spill will be oiled to the same extent because (i) birds vary in their tendency to avoid oil, (ii) oil is often distributed in discontinuous patches, even near the origin of the spill, and (iii) depending upon a number of factors (e.g., time since spillage, type of oil, environmental conditions, and use of dispersants), oil will be more or less likely to contact a bird. Birds not obviously coated with oil still may be seriously affected by oil from inhaling petroleum vapors or ingesting oil while feeding or preening. In addition, without close in-hand inspection or chemical testing of feathers, light-colored and semi-transparent oils can be difficult or impossible to detect visually, especially on dark-colored birds. Along with the timing and location of the oil spill, the other primary factors determining the vulnerability of a seabird species to impacts from oil pollution are at-sea distribution, locations of breeding areas, locations of wintering areas, population size, time of breeding, demography, and resting and foraging behavior. All of these factors combine to determine the numbers and types of species likely to be oiled and, along with other factors discussed below, determine the long-term significance of oiling to seabird and shorebird populations at local to global scales.

Oil vulnerability indexes (OVI), which sum the scores of various factors affecting species survival in relation to oil

spill impacts, have been developed for species and families of seabirds in portions of the North Pacific and North Atlantic Oceans (Table 17.3) [9–13]. In both regions, alcids were found to be the most vulnerable group (mean OVI 77–78 out of a maximum of 100) followed by cormorants, loons, gannets, storm-petrels, sea ducks, diving ducks, shearwaters, grebes, and albatrosses (mean OVI 50–66), and terns, gulls, and skuas (mean OVI 41–48). In the Northeast Pacific, the alcids Kittlitz's Murrelet (*Brachyramphus brevirostris*), Whiskered Auklet (*Aethia pygmaea*), Marbled Murrelet (*Brachyramphus marmoratus*), Cassin's Auklet (*Ptychoramphus aleuticus*), and Pigeon Guillemot (*Cephus columba*) were found to be the most vulnerable with OVIs in excess of 80 [11]. Other sea, shore, and terrestrial bird families had lower mean OVI values than alcids, but certain species within these other families were found to be at relatively high risk. For example, Spectacled Eider (*Somateria fischeri*; 78), Black Oystercatcher (*Haematopus bachmani*; 65), Northern Phalarope (*Phalaropus lobatus*; 62), Rock Sandpiper (*Calidris pilocnemis*; 59), and Bald Eagle (*Haliaeetus leucocephalus*; 58) are likely to be impacted if a marine spill occurs within their range [11].

OVI's were not specifically designed to predict which species will be oiled in greatest numbers. For example, in both the Northeast Atlantic and Northwest Pacific Oceans, murrets (*Uria* sp.) have moderately high OVI scores (70–82) but are typically oiled in the highest numbers in coastal and nearshore oil spills because they are abundant and widespread at all times of year in many areas. The OVI of more rare species is higher due to the potential for greater population impacts from a substantial oil spill.

OVI's have not been developed for southern hemisphere and tropical ocean seabird species (such as penguins, albatrosses, shearwaters, petrels, tropicbirds, frigatebirds, boobies, gannets,

TABLE 17.3 Oil Vulnerability Indexes (OVI) for seabird families in the Northeast Pacific Ocean and North Atlantic Ocean^a

Family	Northeast Pacific			North Atlantic		
	Mean	Min	Max	Mean	Min	Max
Alcidae	78	70	88	77	65	86
Phalacrocoracidae	59	52	63	66	59	73
Gaviidae	55	47	65	66	65	68
Sulidae	—	—	—	65	65	65
Hydrobatidae	65	63	67	50	49	54
Anatidae (Sea Ducks)	—	—	—	64	45	75
Procellariidae	52	47	57	59	47	65
Anatidae (Diving Ducks)	—	—	—	58	58	58
Anatidae (All Waterfowl)	53	32	78	—	—	—
Podicipedidae	49	44	56	53	46	58
Diomedidae	51	50	52	—	—	—
Laridae ^b (Terns)	—	—	—	48	46	51
Laridae ^b (Gulls)	—	—	—	45	36	66
Laridae (Skuas)	41	39	43	43	36	58

Families are ordered roughly from highest to lowest mean OVI values from either the North Pacific or North Atlantic.

^aFrom Refs. 3, 4.

^bIn the North Pacific, gulls and terns combined had a mean score of 66.

terns and noddies) nor for marine estuaries (dominated by ducks, geese, swans, cormorants, pelicans, shags, grebes, gulls, terns, skimmers, and many shorebird species). While species that spend more time on or in the water are most likely to be vulnerable to oiling, that does not mean their OVIs will be the highest. A significant aid to the oil spill response communities operating in these areas would be the development of OVIs for these numerous families of seabirds and shorebirds.

17.3 EFFECT OF OILING ON INDIVIDUAL BIRDS

The major adverse effects of direct oil exposure to individual seabirds and shorebirds are physical fouling of the feathers, damage to exposed skin and eyes, and the toxic effects of ingested or inhaled petroleum hydrocarbons. Oil is ingested by birds when preening oiled feathers, feeding in oiled environments, and by consuming oil contaminated prey. Inhalation of the highly volatile aromatic compounds present immediately after a spill can result in severe acute toxicity. All of these effects can result in severe complications to the health, reproductive biology, and survival of birds [14–16]. In general, most moderately to heavily oiled birds and many lightly oiled birds will die from oil exposure without rehabilitation and only some will survive with rehabilitation. Trace to very lightly oiled birds may survive initial exposure without rehabilitation, especially certain shorebirds, but there is little data on the long-term survival and reproductive success of birds in this category.

17.3.1 External Oil Effects

Most oils, whether crude or refined products, have similar fouling effects on the feathers of flying birds. The effect of oils on penguin feathers is less well understood. In most birds, oils adhere tenaciously to the hydrophobic keratin surface of the feather vanes and barbules, damaging insulation qualities and waterproofing. The penetration of oil into the plumage is dependent upon the physical viscosity of the oil and the degree of weathering after a spill. Thin, low viscosity oils penetrate to the skin and quickly result in hypothermia. Highly viscous or weathered oils adhere to the surface of the plumage, but usually do not penetrate deeply [17,18].

Typically, oil fouled feathers rapidly lose their waterproofing and insulating capacity allowing water to penetrate through the plumage reducing buoyancy and wetting the skin. Even slightly oiled birds exposed to cold water quickly become hypothermic, with as little as 12 ml of oil on waterfowl or 3–5 ml on a small alcid such as a Cassin's Auklet [17,19,20]. Lightly oiled birds still may be able to fly, but if the flight feathers are oiled, most seabirds are usually unable to sustain flight and some will try to swim to shore to avoid hypothermia. Fouled plumage likely reduces the foraging range and time, increases preening, and increases metabolism from hypothermic heat loss, causing an oiled bird to consume stored body fat [15,17,19]. Starving birds will

metabolize pectoral muscle tissues and may suffer muscle wasting within a week of exposure to oil [15,21].

Injury to bare skin and eyes is usually greatest with light oils and refined products that contain a high proportion of volatile polyaromatic hydrocarbon (PAHs) solvents like benzene, toluene, xylene, and naphthalene. These toxic chemicals are corrosive to the cornea, quickly damage other sensitive tissues, and require intensive therapeutic efforts for successful bird rehabilitation (Section 17.7) [22].

17.3.2 Internal Oil Effects

Adverse effects of ingested oil include acute toxic effects to the blood, digestive tract, liver, kidney, adrenals, and occasionally lungs. Most crude oils and bunker fuels contain highly toxic chemical components, including the PAHs mentioned earlier, along with sulfur and heavy metals. Bunker fuels and crude oils produce irritation and erosion of the mucosal lining of the mouth, throat, stomach, and intestines, which may cause gastric bleeding. However, care should be taken when interpreting mouth and throat lesions, as most seabirds have incidental traumatic lesions of the throat and stomach caused by injuries from the spiny projections of many prey species [20]. Polyaromatic fractions may adversely affect uptake of nutrients and small volumes of ingested oil have been shown to retard growth of gull, murre, and storm-petrel chicks [23–28]. Gastroenteritis, as a result of chemical irritation from ingested oil, may produce diarrhea resulting in dehydration, leading to death [29].

The liver plays a major role in detoxification and metabolism of hydrocarbons, and ingestion of oil induces the activity of mixed-function oxidases, the enzymes responsible for metabolism of hydrocarbons into hydrophilic products that can be excreted [30,31]. The ability of vertebrates to breakdown and excrete PAHs leads to only a remnant percentage of parent PAH compounds in tissues within a relatively short period after exposure [32,33]. However, chemical injury may cause disassociation of liver cells and functional impairment, reducing the detoxification of hydrocarbons. Liver lesions include disassociation of liver parenchymal cells, mild to severe accumulations of hemosiderin pigment, and urate deposits indicative of dehydration or muscle wasting [20,29,34]. The tissue dissociation may be a precursor of degeneration and fatty infiltration which has been observed with waterfowl exposed to bunker fuels [35]. Hemosiderosis in liver Kupffer's cells and hepatocytes results from liver scavenging red blood cells with damaged hemoglobin caused by aromatic chemicals dissolved in blood [36,37]. Oxidative damage from exposure to PAH metabolites may lead to hemolytic anemia [38].

Abnormal clinical chemistry values in blood associated with oil exposure reflect acute liver and kidney damage with increases in serum levels of diagnostic enzymes such as aspartate aminotransferase, lactic dehydrogenase, and gamma-glutamyl transferase [39,40]. Muscle wasting results in elevated blood levels of the muscle specific enzymes

creatine phosphokinase and lactic dehydrogenase. Serum elevations of brain acetyl cholinesterase have been reported, reflecting neural damage apparently caused by circulating toxic hydrocarbons. Interpretation of hydrocarbon induced clinical chemistry changes is complicated by additional serum protein alterations reflecting generalized stress responses including altered albumin:globulin ratios, abnormal increases in serum alpha- and beta-globulins (interpreted to be stress proteins), and reduction in liver synthesis of serum proteins such as pre-albumin, indicating impaired liver function [41,42].

Impaired kidney function and dehydration have been noted in seabirds exposed to bunker C fuel oil and weathered Santa Barbara crude and by benzene and naphthalene components of both refined oils and light crudes [20,29]. Chemical-induced injury associated with PAHs includes degeneration of kidney tubules that are needed to conserve water and excrete uric acid. Poorly functioning kidney tubules may result in an elevation of uric acid in the blood and deposition in the internal organs, causing visceral gout.

Secondary lesions such as respiratory fungal infections or inflamed joints are associated with oil exposure, and stem from stress in weakened, immunosuppressed individuals. Stress from oil exposure, hypothermia, and captivity results in corticosterone release from adrenal glands and adrenal enlargement to produce additional stress hormones. Stress-induced rises in corticosterone cannot be maintained chronically, and prolonged stress from oiling, rehabilitation, or captivity will lead to adrenal failure, decreases in circulating corticosterone, impaired immune function, and slow or no recovery [43–46].

Intestinal inflammation from ingested oil may cause diarrhea and dehydration, and chemically induced kidney tubule injury will result in electrolyte imbalance. As birds attempt to maintain proper electrolyte levels, they may develop enlarged salt glands as a secondary response. Enlarged salt glands will revert to normal when the electrolyte levels rebalance [13,20,25,29]. Proper hydration during cleaning and rehabilitation of oiled birds may prevent or reverse both electrolyte imbalance and salt gland hypertrophy.

17.3.3 Oil Effects on Reproduction

Small amounts of oil on seabirds can significantly suppress sex steroid hormone production and negatively impact breeding. Oiled Magellanic Penguins (*Spheniscus magellanicus*) showed reduced levels of the sex hormones estradiol, testosterone, and leutenizing hormone, and elevated levels of the stress hormone corticosterone [47]. Similar results were observed when oil was applied to wild Cassin's Auklets, which showed decreases in estradiol in females and testosterone in males, elevations in corticosterone in both sexes, and delayed egg laying [17].

Adult seabirds exposed to oil early in the breeding season, either experimentally or in the wild, exhibit breeding depression from stress and impaired egg formation. Chronic feeding

of Kuwait crude to ducks or single doses of Santa Barbara crude to quail resulted in altered levels of ovarian hormones, decreased intensity of egg laying, delayed egg formation, and decreased eggshell thickness [48–54]. Experimental dosing of Cassin's Auklets and Wedge-tailed Shearwaters (*Puffinus pacificus*) in the field prior to egg laying resulted in abandonment of burrows, delayed egg laying, reduced incubation and hatchability, and mate switching in subsequent years [17,55]. When 2.0 ml of weathered oil was placed on breast feathers of Wedge-tailed Shearwaters approximately four weeks before laying, only 12% of females laid eggs, although none showed a delay in egg formation. Subsequently, all oil exposed birds abandoned their nests during incubation and experienced complete hatching failure, whereas sham dosed controls had 50% hatching success and 65% fledging success [17,55]. Adult Leach's Storm-Petrels (*Oceanodroma leucorhoa*) dosed orally with 0.1 ml of oil during chick rearing exhibited increased chick neglect, reduced chick growth, and reduced fledging success [27].

Oil applied to eggs of Mallards (*Anas platyrhynchos*) caused decreased embryo survival and increased malformations [56–60]. The degree of effect correlated with the PAH fractions of the different crude and weathered oils. Cassin's Auklet eggs dosed with weathered oil during incubation showed reduced hatching success from either direct embryo toxicity or incubation neglect [17]. Other oil feeding experiments with birds have shown behavioral changes such as impaired avoidance [61].

17.4 REHABILITATION AND VETERINARY CARE

Undoubtedly, capture, transportation, and the intake process at a rehabilitation facility are very stressful on a bird that is already sufficiently debilitated by oil that capture is possible. In addition, the cleaning and animal husbandry process is fraught with challenges that depend upon species type, age, body condition when oiling occurred, type of petroleum product, time between oiling and capture, individual response to cleaning and captive care, training and expertise of rehabilitation personnel, and availability and quality of rehabilitation facilities. Following release, a rehabilitated bird faces many additional challenges that combine to determine its survival during the first several months, including the time of year, the physiological manifestations of oil ingestion and captive care, availability of prey, timing of migration, predation pressures, and other potential sources of mortality. Long-term survival and future reproduction are unlikely if the effects of oiling or the rehabilitation process develop after release.

17.4.1 Key Considerations in Care

Different types of petroleum products typically affect birds in different ways and result in variable success in captive care. Highly volatile products, such as gasoline and diesel

fuel, are more likely to result in acute mortality from skin and corneal burns, inhalant pneumonia, and neurotoxicity. Heavier petroleum products, such as crude and bunker oil, usually cause hypothermia and chronic physiological effects.

Captivity-related stress plays a major role in the success of the rehabilitation process. A number of studies have evaluated corticosterone levels and other stress-related blood parameters in different groups of birds following capture, blood sampling and, in some cases, rehabilitation. In captivity, prolonged elevation of corticosterone levels has led to immunosuppression, which increases the likelihood of secondary complications such as infectious diseases. For example, the blood parameters of Rhinoceros Auklets (*Cerorhinca monocerata*) dosed with oil in the laboratory were more profoundly affected by wild capture and captivity than by ingestion of oil, but both oiled and non-oiled birds (control) developed anemia within three weeks of capture [62]. Corticosterone levels in wild caught Scripps's Murrelet (*Synthliboramphus scrippsi*) were elevated to a similar degree an hour after capture regardless of whether the birds were handled extensively, including attaching radio-tags, or were simply kept in a holding box [63].

The time between oiling and the initiation of rehabilitation efforts can profoundly affect the survival rate of oiled wildlife in captive care. For non-moribund birds, the more quickly capture and rehabilitation efforts are initiated, the more likely some oiled wildlife will survive until release. While most heavily oiled seabirds die, a few species (e.g., Brown Pelican, *Pelecanus occidentalis*) are more likely to survive captive care, and these species also tend to be more easily captured following contact with oil. However, most oiled seabirds have to be considerably weakened by hypothermia, physiological effects, and/or malnutrition, before they can be caught.

Over the past two decades, bird rehabilitation organizations and veterinarians have become more timely and effective in responding to spills through advances in pre-spill planning and the development of protocol-driven oiled wildlife care response actions [64,65]. Pre-spill preparations include designating facilities for rehabilitation efforts, training personnel in all aspects of response, establishing a standing volunteer base, and stockpiling supplies for response. Such preparations contribute to increased release rates for some species.

17.4.2 Release Rates

In general, large and/or hardy species, captured soon after being oiled, show the highest release rates. These species tend to withstand greater periods of fasting, exhibit less fear of humans, become hypothermic more slowly, and usually can be captured before they become moribund. In addition, they seem to more easily adjust to the stress of capture, constant handling, and captivity and they more rapidly reach the minimum threshold health criteria necessary for release. Species that withstand the rigors of captivity typically form

groups for breeding, roosting or feeding, and have a broad diet. Penguins, pelicans, cormorants, geese, and ducks typically have high survival rates, while loons, grebes, and many alcids, excluding the relatively large and densely breeding Common Murre (*Uria aalge*), typically have lower rates.

Release rates can vary tremendously from spill to spill. International Bird Rescue (IBR; California, USA) has been capturing and rehabilitating oiled birds since 1971. Most of the rehabilitation and release efforts of this group in the 1970s and 1980s met with limited success [65]. However, with greater experience and other advances in oiled seabird care, release rates have improved. Since 1996, this organization has responded to over 70 oil spills. During this time, release rates for spills involving greater than 100 treated animals have continued to range widely (3 to 96%), but the average rates of release have increased from 40 to 50% (www.bird-rescue.org).

17.4.3 Post-Release Survival and Reproduction

Data on post-release survival and the subsequent reproductive success of oiled seabirds are limited, and for most species and populations, the expense and effort of rehabilitation appears to outweigh the benefits. Band return studies in North America and Great Britain found that oiled and rehabilitated (ORHB) Common Murres had lower survival than control birds [66,67]. However, these studies were based on data from the 1980s and early 1990s when rehabilitation techniques were less developed. Over 20 years of bird banding data compiled along the U.S. east coast found that the annual survival rates of ORHB Mallards and Canada Geese (*Branta canadensis*) were similar to those of free-ranging non-oiled wildlife [68]. After the 1990 *American Trader* oil spill (California), ORHB and control Brown Pelicans were radio-marked, released, and monitored by aircraft. ORHB pelicans were lost to radio-tracking at a higher rate than controls, suggesting lower survival and the ORHB birds did not breed during the two year study [69].

In 1994, the Oiled Wildlife Care Network (OWCN) was established in California to provide improved rehabilitation for oiled wildlife. OWCN has funded several post-release studies to measure survival of ORHB seabirds using radio-telemetry. Following the 1997 *Torch/Platform Irene* oil spill (California), seven ORHB, 10 non-oiled and sham-rehabilitated, and 10 non-oiled control Western Gulls (*Larus occidentalis*) were radio-marked, released, and monitored by aircraft. All gulls survived until the transmitter batteries reached their 4–8 month life spans. No statistically significant differences could be detected in the size of geographical areas used by these different groups of gulls [70]. After the 1999 *Stuyvesant* oil spill (California), 31 ORHB and 25 control Common Murres were radio-marked, released, and monitored by aircraft [71]. ORHB murres were four times more likely to die than control murres, but 21 ORHB murres survived for at least 80 days

and two survived for at least 142 days. Radio failures precluded longer-term survival measurement for most murres. The survival of ORHB and control murres did not differ after day 34 of the study and 80% of the mortalities occurred between 15 and 40 days post-release. The at-sea distribution, mobility, and movements of ORHB murres surviving past day 34 appeared to be similar to the control birds.

After the 1995 Unocal-Metrolink oil spill (California), ORHB and control American Coots (*Fulica americana*) were placed in an enclosure and closely monitored for survival and physical condition. ORHB coots had significantly lower survival over a 120 day period, and at 60–90 days, the coots that would subsequently die were unable to gain weight or maintain body condition. In contrast, at about 105 days, surviving ORHB coots had blood parameters that were similar to control coots [42,72]. Apparently, while lower survival of ORHB coots is likely over the short term, the long-term prognosis of coots that survive the initial recovery phase may be positive.

Rehabilitated penguins have not only shown significantly higher survival rates than other ORHB seabirds, they have also shown post-release reproductive activity. The best documented example is African Penguins (*Spheniscus demersus*) in which 79% of ORHB penguins survived and 87% of survivors subsequently reproduced, similar to controls [73]. The high survival and subsequent reproduction by these penguins likely reflects their large body size, greater average lifespans, dense specialized plumage, thick subcutaneous fat layer, and hardness in captivity. Penguins are not representative of any other seabird or shorebird group.

Post-release monitoring to determine short-term and long-term survival of ORHB birds should become a required component of the rehabilitation process. In part to evaluate their post-release survival, many rehabilitated seabirds in the United States are banded with numbered metal leg bands. Few bands have been found on dead seabirds and because many seabirds breed in dense, difficult to access colonies, there are limited data from reading band numbers on live birds. The limited metal leg band data have not been sufficient to determine if improvements in the rehabilitation process are significantly enhancing the survival of oiled seabirds. Color banding and rigorous follow-up studies may provide sufficient statistical power for specific species with well known and limited breeding sites, but these results may not be representative of other species and locations. Currently, radio-telemetry or satellite-telemetry studies appear to offer the most effective means of determining survival and subsequent reproductive success of ORHB seabirds, especially for those species that range widely. However, so far even radio-telemetry studies have provided limited information on this subject due to the tremendous mobility of seabirds, and the limitations of radio and satellite telemetry methodologies (e.g., limited battery life, limited transmission range, and attachment methods).

17.4.4 Rehabilitation Process

The following brief introduction to the practical care and management of oiled seabirds is provided for guidance to inexperienced seabird rehabilitators involved in a large spill event. These protocols have been developed through time, primarily by Tristate Bird Rescue & Research (Delaware, USA) and IBR. While rehabilitation methods are constantly being improved, much of the basic considerations for care discussed in the following are well established.

17.4.4.1 Initial Stabilization Over the past two decades, most live and dead oiled wildlife have been captured or recovered during search and collection efforts by government agency personnel or experienced wildlife responders from rehabilitation or other private groups. These personnel are trained to accurately record intake data (e.g., date, time, location of capture, species, and names of field personnel involved) which is important for determining overall seabird mortality from a spill (see Section 17.5), tracking individual birds during treatment, and assessing the factors that determine release rates.

After initial capture, personnel should try to immediately address three issues (i) large amounts of oil should be wiped away from the eyes, nares, or throat, and any fractured limbs or obvious wounds should be stabilized, (ii) body temperatures of captured birds should be assessed with a digital thermometer placed carefully in the cloaca, and (iii) hypo- or hyperthermic birds should be treated with instant heating or cooling gel packs wrapped in towels and placed in the transport container. Less critical, but helpful in shortening time to release, is beginning the rehydration process by tube-feeding oral electrolyte solutions (Pedialyte®, Ross Labs, Columbus, OH) at the field stabilization site.

17.4.4.2 Transportation After initial field stabilization, birds should be transported to a rehabilitation facility as quickly as possible. The vehicle and the transport container should allow for free air exchange and permit temperature adjustments to expedite the return of thermoregulation. Visual and auditory stimuli should be minimized to decrease captivity related stress. Birds should be monitored frequently during transport to detect potential problems such as overheating or unnatural positioning.

17.4.4.3 Intake Procedures A standardized intake protocol is highly recommended. In the United States and increasingly elsewhere, intake data can become legal evidence for a criminal or natural resource damage assessment claim. At intake, each bird should be individually identified with a numbered leg band or other means. An oiled feather also should be removed, placed in aluminum foil, and placed inside a plastic bag with the intake number. A photograph of each bird should be taken at the time of intake with the intake number visible. All data should be retained in a manner that provides a chain-of-custody for information on each

individual. The bird will then be given a thorough physical examination, noting especially the extent of oiling and signs of hypothermia, dehydration, and malnutrition. Blood samples will be drawn to provide a baseline for assessing changes in health parameters. Packed cell volume (PCV) can provide an indication of anemia and the total solids indicate blood protein levels that reflect nutritional status. The blood parameters should be recorded on the intake sheet, which will track all subsequent treatment or other information for each individual. At this point in the intake process, oiled seabirds are usually triaged into three groups (i) moribund individuals that can be humanely euthanized, (ii) those directed toward more extensive and individualized veterinary care, and (iii) those that require standard flock care. The latter group are typically housed with other birds, fed a normal diet for that species, and evaluated on a regular basis as they progress through the rehabilitation process.

17.4.4.4 Housing The rehabilitation facility should maximize the efficient flow of people and care of seabirds and minimize the possibility of spreading disease. An ideal facility will have adequate indoor space and capabilities for intake, veterinary services, food preparation, storage, bird cleaning (i.e., washing, rinsing, and drying), necropsies, and other areas for general use (e.g., bathrooms, changing clothes, safe eating, meetings, data entry, and communications) by volunteers, staff, and visitors. To provide sufficient space for the bird holding area within a facility, including walking and aisle space, allow about 0.6 m² per individual for birds weighing less than or equal to 1 kg, with additional space for substantially larger birds [74]. Separate housing should be provided for non-cleaned and cleaned birds, and species-appropriate outdoor pools and aviaries should allow for evaluation of waterproofing, diving capability, and other behaviors prior to potential release.

Oiled birds usually are immunosuppressed, both from exposure to petroleum products and from the stress of capture and rehabilitation. This makes them especially prone to developing infectious diseases such as aspergillosis, avian pox, Newcastle disease, avian tuberculosis, salmonellosis, and chlamydiosis. Any bird suspected of harboring potential pathogens should be quarantined. Good ventilation will help to reduce mucus membrane irritation from petroleum fumes and reduce aspergillosis. For animal holding spaces, 10–15 air changes per hour are recommended. The use of high-efficiency particulate air (HEPA) filters is also highly recommended [74].

Loons, grebes, sea ducks, and certain other species that cannot easily stand on land typically develop pressure sores on the sternum keel and the tarsal joints (“ankles”) if housed in typical bird holding cages. Pressure sores over the keel usually result in feather loss and reduction in waterproofing and thermoregulation. Pressure sores over the ankle often lead to joint infections, which are difficult to treat in birds and prolong the length of time in rehabilitation. These types

of birds should be housed in “net bottomed” cages, with flooring created by shrimp seine netting which allows the ventral surface of the bird to be supported more evenly and for feces and urates to drop through onto easily cleaned or replaceable surfaces below [75].

17.4.4.5 Nutritional Support Many oiled birds are dehydrated and malnourished at intake. Gastrointestinal disturbances can further exacerbate dehydration, through additional fluid losses from regurgitation and diarrhea. Oiled birds with normal PCV and total protein levels should be tube-fed with high calorie nutritional slurries up to four times daily, alternating with rehydrating solutions four times daily. While these multiple daily handlings probably increase stress levels, they are necessary until birds self-feed and gain weight. The amount of fluid or slurry given depends on the species, size, and health status of the bird. For birds with low total protein values (<2.0 g/dl), a more easily digestible product should be substituted for the nutritional slurry. Once the total protein levels have risen and regurgitation has ceased, the birds can be gradually transferred to the slurry diet. Shallow pans with water and small non-spiny fish (i.e., larval/juvenile fish or smelt-like fish) may be provided in daylight hours for piscivorous species. Food pans should be small enough to prevent birds from climbing into them or they will soil and wet their feathers. Cleaned birds can be hand-fed fish while housed in outdoor pools, but fish should not be left in their enclosures to avoid soiling feathers. All birds should be weighed daily during rehabilitation to help track recovery.

17.4.4.6 Medical Considerations Before subjecting a bird to the rigorous and very stressful washing process, it should be treated for typical admission abnormalities such as hypothermia, dehydration, malnourishment, and anemia [76]. A common mistake of inexperienced rehabilitators is to immediately wash oiled birds before they are physiologically stable and meet certain clinical criteria. To assess the birds, blood samples are taken and checked for PCV and total protein levels. Blood should be taken approximately every 2–3 days to determine if the bird is sufficiently stable to undergo cleaning stress. Since many medical problems associated with exposure to volatile, highly refined fuels can be difficult to treat, birds exposed to these products should be given a “quick wash” to remove the bulk of the product and reduce inhalant and contact problems. This quick wash should be 5 min or less to minimize stress and should consist of baths in several tubs of a 1–2% Dawn® (Procter & Gamble, Cincinnati, OH) solution, followed by a rinse to remove the soap. Birds with inhalant pneumonia or emphysema, which exhibit respiratory difficulty, abnormal lung sounds, and characteristic signs of fluid infiltration on radiography, should be treated with antibiotic and antifungal medications, housed in oxygen cages, and monitored closely. Skin burns are a special problem in aquatic birds, as the serous exudate and feather loss in the affected area results in loss of waterproofing and

hypothermia. These burns should be thoroughly cleansed with a dilute chlorhexidine solution (Nolvasan®, Fort Dodge Company, Fort Dodge, IA) and treated with a water-soluble antibiotic product. Use of petroleum-based ointments should be avoided in order to prevent further feather contamination and disruption of waterproofing.

Birds suffering mild to moderate fluid losses (5–8%) can be treated with oral fluids or subcutaneously injected fluids, if they are regurgitating. Subcutaneous fluids are not recommended for pelicans, boobies, and gannets which have subcutaneous air sacs that cushion them during plunge diving. More severe dehydration should be treated with intravenous or intraosseous fluid administration. Dehydrated birds with low protein levels may require intravenous colloid solutions (e.g., Hetastarch®, Abbott Laboratories, North Chicago, IL). During a large oil spill, individual bird treatment may not be possible. In these instances, captive flock health protocols should be followed, which assume that the average oiled bird at intake is approximately 8–10% dehydrated.

Attempts to prevent birds from preening their feathers through the use of collars or materials that cover the body have met with limited success. Many oiled birds treated in this manner are highly stressed with these restrictions and can easily overheat. Instead, keeping room temperatures high enough to prevent hypothermia will reduce the incidence of preening and subsequent ingestion of oil. The use of intestinal protectants (e.g., bismuth subsalicylate Pepto Bismol®, Procter & Gamble, Cincinnati, OH) has been used with some success [77]. Providing appropriate rehydration and nutritional slurries also will help decrease gastrointestinal abnormalities resulting from ingestion of oil.

Anemia from hemolysis of red blood cells is a common toxic effect of oil ingestion and can be exacerbated by stress, chronic disease, or other factors. Treating any compounding factors, such as infectious disease or malnutrition, will aid in reducing anemia, and supporting therapy with B complex vitamins (20 mg/kg based on the thiamine component IM q 5–7 days) also may be helpful.

17.4.4.7 Wash/Rinse/Drying Procedures Birds should be stabilized in captivity for at least 48 h prior to washing. At least two people, a holder and a washer, should work as a team, and with particularly large or aggressive birds, at least three people are recommended. Wash personnel should wear waterproof aprons, gloves, boots, and safety goggles. Dawn dishwashing detergent has proven to be the most effective detergent for oil removal [78]. Birds should be washed in multiple tubs containing a 1–2% Dawn solution in fresh water heated to 40–41°C (104–106°F). Water temperature should never fall below 37°C (99°F). Birds are moved from one bath to the next as each tub becomes oily until the bird no longer has any oil on it and the tub water is clean. The detergent solution is moved through the feathers by partly lifting the contour feathers away from the body with a gentle against-the-grain stroking while simultaneously using caution to prevent breaking the feather shafts. Stiff wing and

tail feathers should be gently worked free of oil by massaging the feathers toward the distal tips of the feather shafts. The head is best cleaned using a Waterpik® (Teledyne, Fort Collins, CO) while taking care not to spray directly into the eyes or ears. Alternatively, a soft toothbrush can be used to gently lift the feathers of the head and allow the soap solution to penetrate. To rinse, gently pour clean water over the area and repeat until all soap is gone. The bill should be pointed slightly downward to keep water from getting into the nares. To reduce stress to the bird, it is best if the wash team works quickly and efficiently, keeping noise levels to a minimum.

Birds should be rinsed with water heated to 40–41°C (104–106°F) using a high-pressure nozzle (1110–1660 g/cm³ or 40–60 psi). This amount of pressure is needed to efficiently and effectively rinse the detergent from the feathers. It also is important to use water of 2–5 grains hardness for the rinse. Softer water is ineffective in rinsing the detergent and the minerals in harder water bind with microscopic amounts of detergent to form calcium carbonate crystals in the feathers which can lead to waterproofing problems [79]. These same crystals also form when birds are placed in outdoor pools containing hard water during the next 24–48 h. A good guide to determine if birds have been adequately rinsed is to note whether the water beads off the feathers in small droplets.

After birds are completely clean, they should be placed in a clean drying pen. For larger birds (>500 g) and those species that typically do not rest out of the water, use net bottomed cages. The ambient air temperature should range from 32 to 35°C (90–95°F) and the top and sides of the pen should be covered with a light colored sheet. Smaller birds can be dried in well-ventilated enclosures with a heat lamp. The drying time will vary by species, with small birds drying in about 30 min and larger birds taking up to 3 h. Birds in drying pens must be checked frequently to prevent overheating.

17.4.4.8 Waterproofing Considerations Move clean and dry birds into outdoor pool enclosures as soon as possible. The diameter and depth of pools should be large enough to allow for an accurate assessment of diving behavior, feeding habits, and waterproofing status. Large offshore species need pools at least 3.5 m wide and 1 m deep. Providing clean flowing water over the pool surface at all times and skimming debris will prevent further soiling of feathers by oily feces and fish. When birds with compromised waterproofing are placed in cold water pools, the water will penetrate to the skin and result in shivering, agitation, excessive preening, or attempts to leave the water. Any bird acting in this manner should be removed from the pool, re-evaluated, and treated appropriately to address the underlying problem.

17.4.4.9 Release Criteria Rehabilitated birds should be released when their probability of survival in the wild appears greater than staying longer in captivity. Release criteria usually include typical feeding, swimming, and

diving behavior; body weights within approximately 10% of the normal range for the species; good waterproofing; normal hematological and serum chemistry values; and resolution of any abnormalities. Before release, the bird should be banded with a permanent metal leg band or other means of individual identification. These bands will identify rehabilitated birds that may again become debilitated and be recaptured and they may provide post-release survival or mortality data.

17.5 ESTIMATING MORTALITY

Until the mid-1980s in the United States, estimates of the numbers of birds affected by oil spills were often limited to counts of oiled birds captured for rehabilitation or found dead on shore [80]. For most spills, these simple tallies greatly underestimated total mortality, as a large proportion of oiled birds never reached shore and most that did were not recovered. In the United States, there has been an increasing interest by federal and state governments to account for the environmental impact of hazardous chemicals and oil on wildlife. In 1980, the Comprehensive Environmental Response, Compensation, and Liability Act (Superfund) established a statutory mandate to evaluate the effect of a hazardous material release, and in 1990, after the *Exxon Valdez* oil spill, the Oil Pollution Act established a similar need for an oil release. Under these and other statutes, government agencies are authorized to utilize scientifically credible methodologies to determine the extent of injuries to natural resources caused by an oil or hazardous chemical spill, and to make a damage claim for restoration to the party responsible for the release. Using techniques first developed in the 1980s, the number of seabirds killed from an oil spill can now be reasonably accurately quantified with data obtained during or soon after a spill.

The science of quantifying seabird mortality resulting from an oil spill began with the 1984 *Puerto Rican* and 1986 *Apex Houston* oil spills in California, were advanced further during studies associated with the 1989 *Exxon Valdez* spill, and have been refined even more during spills and studies in the 1990s and 2000s [81,82]. Factors that typically influence the accuracy of seabird mortality estimates include (i) unsearched or inaccessible portions of the coastline, (ii) loss of dead birds at sea due to sinking or scavenging, (iii) removal of carcasses from beaches by scavengers, (iv) removal of carcasses from beaches by wave action, (v) failure of searchers to find dead birds, and (vi) accounting for birds that die from causes unrelated to the oil spill [83–90]. Fully accounting for these potential factors necessitates obtaining data on (i) the persistence of carcasses at sea and on the beach, (ii) the success rate of searchers, and (iii) the background or non-spill related deposition rate. Accounting for the at-sea loss of birds requires knowledge of the movement and location of oil at sea combined with the at-sea distribution of birds in the spill area (Table 17.4).

TABLE 17.4 Summary of basic information needed for accurately estimating seabird mortality after oil spills

Documentation of beach searches, including time, location, and number of searchers
Numbers, species and conditions of birds recovered on documented searches
Carcass persistence rates in typical shoreline habitats
Searcher efficiency rates in typical shoreline habitats
Time required for carcasses to beach
Carcass persistence rates at sea
Background beach deposition rates for birds unaffected by an oil spill
Representative samples of source oil
Representative sample of oiled feathers recovered during the spill

17.5.1 Oiled Birds at Sea

Many seabirds die or are unable to fly soon after contact with oil and it is common for live and dead oiled birds to begin beaching within hours after a nearshore oil spill. However, some individuals and species are able to fly or swim after relatively light oiling and can move significant distances before becoming impaired. After the relatively localized *Torch/Platform Irene* oil spill, one heavily oiled Brown Pelican was found 65km from the spill site [91]. Similarly, many oiled seabirds were found alive 60–100km from the 2001–2002 release of *Luckenbach* oil (California) [86]. Pochard (*Aythya ferina*) heavily oiled by a spill in the Firth of Forth, Scotland, flew 7km inland to a lake, where they later succumbed [92]. During the 2004 *Selendang Ayu* spill (Alaska), the majority of dead birds were recovered on beaches about 40km outside the leading edge of the spill zone, indicating substantial movements of live oiled birds [93]. It is unclear how frequently movements on this scale occur, but movements of live oiled birds on the order of 5–10km or greater are probably common.

Gulls, pelicans, shorebirds, and many species of waterfowl are frequently observed on land or at traditional roosting sites soon after being oiled [94,95]. In some cases, the first indications that a spill has occurred are observations of oiled birds onshore such as the 1985 *Arco Anchorage* spill (Washington) and the 1998 *Tesoro* spill (Hawaii). Typically, the number of oiled seabirds peaks within days of the initial release, and then declines steadily over a period of weeks [86]. Prevailing winds and local weather conditions often have a strong effect on the rate of onshore carcass deposition, with more birds beaching when winds are blowing onshore. Oiled waterfowl will sometimes remain on or very near shore for days or weeks before succumbing [96]. Generally, species that rarely occur on land except when breeding, such as alcids, loons, grebes, or seaducks, come ashore only when impaired or moribund.

Recoveries of oiled birds in bays and estuaries tend to include higher proportions of live birds than on open ocean beaches. For example, after the 2007 *Cosco Busan* spill (California), 55% of the more than 1500 birds recovered in estuarine habitats were dead, whereas 75% of the nearly

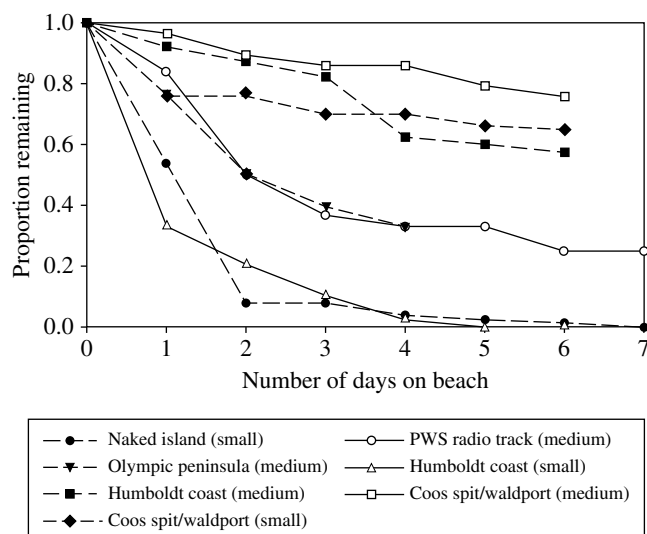


FIGURE 17.1 Proportion of bird carcasses remaining on beach as a function of the number of days since they were set out in five different studies [83,95,97]. Small and medium carcasses weighed less than 500 g and 500–1000 g, respectively.

1300 birds recovered on the outer coast were dead [96]. The ratio of live to dead birds tends to change overtime. Early in a spill, recoveries of live birds often predominate, whereas later in the spill, dead birds usually predominate, suggesting that oiling and mortality for most seabirds is a protracted process [96,97].

Dead and moribund birds tend to drift passively, typically with the surface current plus about 2.5–3.0% of wind speed. Their movement is similar to that of the surface oil, and oil spill trajectory models can effectively be used to predict bird carcass movement patterns [98–101]. Dead seabirds that are not pushed ashore become waterlogged and sink. After the *Exxon Valdez* spill, the carcass sinking process was studied by fitting fresh seabird carcasses and foam dummies built to float like seabird carcasses with radio transmitters [83]. None of the foam dummies disappeared, but carcasses began to disappear after a week. The average persistence time of radio-marked carcasses was about two weeks, with some lasting over three weeks. Although at-sea scavengers may accelerate the rate of carcass loss, there are very few observations of carcasses being scavenged at sea. During the 2010 DeepWater Horizon spill (Gulf of Mexico), shark densities were observed to be quite high in some areas where bird carcasses were found, and examination of a few shark stomachs revealed both feathers and oil (RCH and RGF, personal observations) [102].

17.5.2 Oiled Birds on Land

Along with other floating debris, dead and dying birds are deposited in the wash zone and the wrack line where onshore winds and currents prevail. Studies conducted with Common Murre carcasses show that successive tidal cycles either push carcasses further up the beach or wash them back out to

sea where they sink or again wash onshore some distance away [86,89]. Unless removed by scavengers, carcasses pushed above the wrack line ultimately become skeletons or hollowed out mummies which may appear and disappear multiple times as they are buried and uncovered by drifting sand. When winds are strong, even fresh carcasses can be buried within hours on loose sand beaches [95].

Some beached birds that are not removed by scavengers may never be found, even on regularly searched beaches. Birds can be hidden in small depressions, behind rocks, or blend into wrack lines with other debris; even trained observers working under good field conditions can miss significant numbers of beached carcasses [103]. A study of searcher efficiency on wide sandy beaches in Washington showed that at a distance of 5 m, only 40% of carcasses were found, and at 35 m less than 5% were found (RGF, unpublished data). Searchers looking for King Eiders (*Somateria spectabilis*) killed during the 1996 *Citrus* spill (Alaska) detected from 44 to 94% of these large birds, with higher detection rates occurring on sandy versus rocky beaches [99]. After the 1997 *Kure* spill (California), searcher efficiency ranged from 13 to 55%, with higher carcass detection on sandy and rocky beaches than in marshes, and with larger birds found more easily than smaller birds [95].

The effectiveness of beached bird recovery efforts is usually determined by the amount and type of oil spilled, the number and type of birds in the spill zone, the length and type of coastline impacted, the ratio of live to dead birds, the persistence of beached birds, and the number and effort of search personnel. Even relatively small volume spills can oil hundreds of kilometers of shoreline and, when the shoreline is convoluted or dominated by vegetation, finding oil impacted birds can be particularly challenging [95,96]. In addition, it is not unusual for sick and dead oiled birds to continue to beach after cleanup efforts are considered complete. This likely occurs because carcasses and slowly dying birds can persist longer at sea than oil, especially in small spills or spills involving volatile products like gasoline or Jet A fuel where evaporation, wind and wave action rapidly disperse the slick.

A large array of scavengers readily feed upon or remove beached carcasses, such as gulls, corvids, raptors, vultures, rats, skunks, raccoons, foxes, coyotes, bears, alligators, amphipods, and crabs. On beaches where scavenger activity is high, carcasses can rapidly be reduced to feathers and disarticulated bones, indistinguishable from other beach debris. During some spills, over 90% of the carcasses disappeared within 48 h of arriving on the beach, whereas in other cases, over 90% of carcasses were still present a week after beaching (Fig. 17.1). Some scavengers consume the edible portion of carcasses *in situ*, leaving feathers, bones, and other clear evidence of scavenging that can persist for several days. Many avian scavengers will swallow or fly away with small seabird carcasses (<500 g), and mammals usually remove carcasses completely from the beach, sometimes caching carcasses in upper beach vegetation. Both behaviors leave

little or no evidence that a carcass was ever present. During both the *Kure* and *Luckenbach* spills, smaller birds were removed from the beach at a significantly greater rate than larger birds [84].

In many spills, especially those affecting relatively long lengths of coastline such as the *Exxon Valdez* or the *Luckenbach*, it is not feasible for responders to search all accessible portions of the entire affected coastline regularly [83,89]. When this occurs, the carcass deposition rate along sections of coastline that were infrequently searched can be inferred from comparable sections that were more frequently searched.

17.5.3 Cause of Death and Background Deposition

Seabirds regularly die from natural and anthropogenic causes, and dead non-oiled seabirds often are found on shorelines throughout the world [1]. During an oil spill, this “background” mortality can become mixed with spill-related mortality, and it may be necessary to separate the two sources in order to quantify spill-related effects. Background mortality can affect the spill-related mortality numbers in two ways. First, birds that died and beached before the spill may be collected during early beach survey efforts. On beaches with few scavengers or traffic, the number of these older carcasses may be relatively high. Usually, it is fairly easy to separate out many of these carcasses due to their obvious weathering, but not always [96]. Second, in certain situations, natural die-offs unrelated to a spill can occur. The build-up of bird carcasses prior to a spill can be addressed most effectively by clearing beaches of carcasses at the beginning of the spill, before the wave of oil affected birds begin beaching. This approach requires early mobilization of beach search efforts and an accurate determination of where the slick and the birds will reach landfall [96].

Although the presence of visible oiling on a beached bird is a strong indication that bird was killed or injured by oil, many birds recovered during a spill are not visibly oiled. In most spills, the beaching of both oiled and non-oiled birds is highly synchronous, and the beaching rates of both categories rise and fall in tandem [86]. While it is possible that these visibly unoiled birds were victims of a natural die-off occurring at exactly the same time and place as the spill, the probability of such a coincidence is generally very small. Data compiled from a variety of spills indicates that using visible oiling as the primary criterion for linking the spill to bird injury probably underestimates spill-related injuries by a factor of about 50% (Fig. 17.2).

Conducting necropsies on visibly oiled and unoiled birds is often suggested as a potential method for determining if the cause of death is oil related. Unfortunately, while there are numerous anatomical and histological effects of oil ingestion that can be detected, none of them are unique to oil ingestion. For most oiled seabirds, the proximal cause of death is likely to be hypothermia or starvation, which can be confused with starvation due

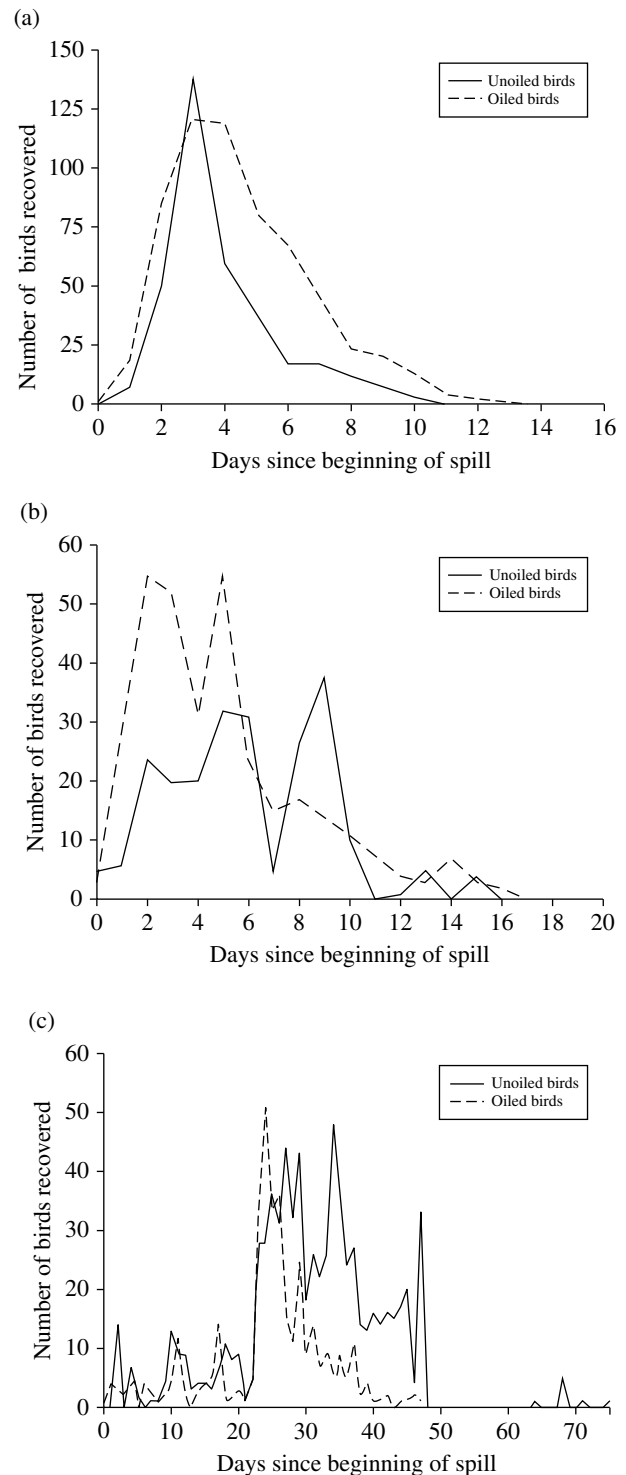


FIGURE 17.2 Recovery of visibly oiled birds (dashed line) and non-visibly oiled birds (solid line) during three oil spills. (a) *Kure* [97], (b) *Stuyvesant* (California Department of Fish and Wildlife, unpublished data), and (c) *New Carissa* [95].

to periodic insufficient food availability, disease, or other factors. Distinguishing between non-spill and spill-related mortality is difficult, and usually requires data on age class, species composition, location of carcasses, and

the timing of deposition. Necropsies or careful carcass inspections may eliminate alternative causes of death such as paralytic shellfish poisoning, gill-net mortality, fishing gear entanglement, or other factors.

It is also regularly proposed that a determination of cause and effect could be obtained by using recently developed analytical chemistry techniques to “fingerprint” the oil [90]. While this approach has merit, it also has limitations. For example, “fingerprinting” is only capable of determining whether a particular oil sample is consistent with a source oil sample, it does not provide certainty. In some spills, numerous oils are released and a source sample of each oil type is not always obtained. As oil weathers (or is changed chemically by dispersants or in situ burning), its composition changes and the fingerprinting technique becomes more problematic. Ingested oil is nearly impossible to fingerprint as oil is rapidly broken down within the digestive system and metabolized into many separate constituents that cannot be reconstructed.

Given the difficulty of determining whether an increase in non-visibly oiled carcasses was caused by a particular oil spill, a different approach was developed during the 1999 *New Carissa* oil spill (Oregon) [97]. This approach involved determining the expected background deposition rates of carcasses (by species, time and area affected by the spill) and subtracting that number from the estimate of non-visibly oiled carcasses. Sometimes background deposition rates for an area are available, as was the case for the *New Carissa* spill, but if none exist, some information can be obtained by (i) response teams surveying beaches before oil and oiled birds begin beaching or (ii) analyzing past data collected by beached bird monitoring programs such as SEANET, COASST, or BeachWatch. However, if data collected by beach bird monitoring groups are used for this purpose, their protocols need to be consistent with spill responder protocols to avoid producing seriously upward biased estimates [86].

17.6 LONG-TERM IMPACTS

Marine oil spills regularly impact seabird populations and marine environments throughout the world [2,104–106]. On occasion, certain populations of seabirds are substantially impacted by large spills such as the 1967 *Torrey Canyon* (England/France), 1978 *Amoco Cadiz* (France), 1989 *Exxon Valdez* (Alaska), and the 2002 *Prestige* spill (Spain) [5,83,103,107–109]. When marine spills are particularly large or occur near areas of dense human populations, such as the Deepwater Horizon oil spill, they usually become highly visible media events that immediately garner substantial public and government attention. In most spills, rapid professional response for collection and clean-up of oil and oiled birds, coupled with the activation of experienced wildlife rehabilitation groups, rapidly removes the negative images of oiled wildlife from the nightly news. When these events fade from the headlines, so does the public pressure on the responsible party and the government to determine the environmental harm. The

impact to the environment remains and understanding the full extent and magnitude of the impact usually requires years of study. Some small spills do not affect many seabirds and have not been shown to have long-lasting impacts on the environment. However, small to large spills that kill many seabirds, impact extensive shoreline reaches, or contact sensitive species, populations, or habitats may have long-lasting effects [82,83,110–120]. Long-term impacts can be particularly severe for isolated populations, small populations, or when other natural or anthropogenic factors act concurrently. For example, a Common Murre breeding colony near San Francisco was extirpated by the *Apex Houston* oil spill after the colony had been substantially impacted from two years of high mortality due to a coastal gill net fishery and reduced productivity from two consecutive El Niño years [82].

Following a spill, most oil is removed from the environment through a combination of response efforts and the natural processes of dispersion, evaporation, and degradation. As the oil progressively becomes less available in the environment, direct impacts on individual wildlife, such as smothering, hypothermia, fouling, contamination of prey, and the physiological harm from ingestion of oil, decrease. Impacts at the population level such as reduced population size, reduced breeding success, and reductions in prey availability may persist for long periods of time. However, unless there is a spatial and strong temporal association between the spill and the observed effects, they can be challenging to link. The difficulty in demonstrating a link is typically the result of insufficient baseline data to compare against the observed effect or any number of factors that can obscure the effect. For instance, natural variation (especially with respect to prey availability and climate), anthropogenic factors (such as fishing, pollution, colony disturbance, and habitat destruction), and compensating factors (such as a significant increase in immigration or recruitment) could all potentially mask small to moderate sized impacts at the population level.

Until recently, most of the effort and resulting knowledge concerning long-term effects of large oil spills on seabird populations have been based on studies following the *Exxon Valdez* spill, which was estimated to have killed at least 375,000 seabirds [83]. The compelling imagery, public outrage, and financial liability resulting from this event led to considerable funding for research to determine the ecological impact of an event of this magnitude and duration, and generated focus on the reliability of the endpoints to be measured, different methodologies applied, and results obtained. After a decade of research, three general conclusions were drawn (i) oil pollution can have long-term impacts at the population level for certain species and habitats, (ii) because effects may be localized, single isolated temporal and spatial studies can provide misleading information about the status and recovery of marine ecosystems more generally, and (iii) both post-spill studies and long-term monitoring data on seabirds and the marine environment are needed to accurately determine certain impacts from a large oil spill [115,121]. However, even this

well-studied example reflects a unique set of circumstances and applying conclusions drawn from it, or any other specific spill incident, to spills in other times and places must be done with caution. Overall, it appears that the measurable detrimental impact of a spill on seabirds can vary widely and is not easily predicted based simply on the volume spilled or the breadth of area oiled. For seabirds, the most important factors determining the number of birds killed seem to be timing, location, and size of the spill combined with the species composition in the spill area. However, the population impact for any one species is not directly proportional to numbers killed and depends on many factors.

Beyond the initial acute mortality, oil spills can affect long-term seabird population dynamics by lowering population densities or altering sex ratios. In the area affected by the *Exxon Valdez* spill, reduced summer population densities of several marine birds were found, including cormorants (*Phalacrocorax* spp.), goldeneyes (*Bucephala* spp.), mergansers (*Mergus* spp.), Common Murres, and Pigeon Guillemots; these populations had not returned to pre-spill levels nine years after the accident [82,83,114,122,123]. Even after considering the shaping effect of other environmental conditions on population dynamics, oil spills can have a wide-scale impact on seabird populations at breeding colonies and at wintering locations and the long-term influence of an oil spill may not be apparent within one year after the spill [124,125]. Following the 1997–1998 release of *Luckenbach* oil, reduced numbers of Common Murres were counted in the small breeding colony complex at Drakes Bay, California; and carcass necropsies revealed that a disproportionately high percentage of male subadults and adults were killed [125]. In contrast, the *Prestige* spill killed more female than male European Shags (*Phalacrocorax aristotelis*) [126]. Disproportionate impacts on populations from oil spills may only be evident after careful examination and further work is necessary to determine its importance at the population level.

Oil from a spill is often deposited on shorelines and intertidal habitats used by many species of seabirds, shorebirds, and sea ducks. In many areas, water movement and response operations decrease the amount of oil on shorelines relatively quickly. However, on islands or in areas with limited access or difficult topography, oil can remain for up to a decade or more after a spill [115,127]. Petroleum hydrocarbons persisted in marsh sediments 30 years after the 1969 *West Falmouth* diesel oil spill (Massachusetts) [128]. Twelve years after the *Exxon Valdez* spill, the largest reservoir of biologically available polycyclic aromatic hydrocarbons were found on beaches impacted during the spill [129,130]. Certain seabird and shorebird species are likely to encounter this persistent oil while foraging or breeding [131]. Remaining oil can reduce the quality of spill-affected habitats and may cause shifts in bird distribution. Although not all seabird species are affected by an oil spill and some recover more quickly than others, inshore-feeding species

appear to be most susceptible to both initial and long-term habitat disturbance resulting from oil spills [114,132,133].

Effects of oil pollution also may cause long-term reductions in populations of the preferred prey of seabirds as a result of prey habitat degradation, prey population declines, cascading trophic interactions, or changes in prey behavior [115,134–136]. Such prey reductions may lead to reduced survivorship or reduced reproductive success, especially for seabirds that are prey specialists not readily capable of switching to other food. At a local level, Harlequin Duck (*Histrionicus histrionicus*) population densities are strongly influenced by the abundance of preferred prey such as limpets, other snails, mussels, and amphipods. As prey abundance declined following the *Exxon Valdez* spill, Harlequin Duck populations also declined [136]. Eight years after the spill, the Harlequin numbers in the oiled area had not appreciably increased, despite similar biomass densities of the preferred prey in oiled and unoled areas. In addition, although ducks from oiled and unoled areas had similar body-mass indices, the oiled area birds also exhibited elevated cytochrome P-450 induction, an immune response biomarker that can be caused by oil ingestion [133]. While it is thought these effects were due to the lingering effects from the spill, they may result from ongoing exposure [136–138]. Long-term impacts on Pigeon Guillemot populations in the area impacted by the *Exxon Valdez* spill also seem to be related to continued exposure to residual oil and reductions in key prey species abundance. Fishes with high-lipid content are important for rapid guillemot chick growth and high fledging success. Nine years after the *Exxon Valdez* spill, high-lipid fishes in the diet of guillemot chicks remained lower than before the spill and the guillemot population had not returned to pre-spill levels [139,140]. The *Prestige* oil spill also had population-level consequences on the European Shag in northwest Spain. Shag population numbers before the incident were similar between colonies that would be oiled and those that would not be impacted. However, six months after the spill started, the colonies located in the spill zone declined by approximately 10% whereas the unoled colonies continued to increase [108]. Changes in prey availability in the year after the oil spill was thought to mostly explain the lower reproductive performance of the shags in the spill zone and a longer-term study determined that the spill changed prey availability and resulted in multi-year effects to the continental shelf ecosystem of northwest Spain [141]. However, additional work also showed that American Mink (*Neovison vison*) had begun raiding colonies and shags were also drowning in fishing nets. It was the combination of all these mortality factors, including the direct and indirect effects of the oil spill, which best explained the observed population decline [142,143].

To accurately assess the full impact of an oil spill on seabird populations, pre-spill knowledge of population dynamics and extended post-spill studies are needed. The effect of a spill often is most apparent when it occurs concurrently with other significant natural and/or anthropogenic

impacts. Sufficient long-term post-spill studies have not been completed to accurately assess the range or average duration of impacts, but for some species or populations effects up to a decade or more seem probable.

17.7 RESTORATION

Seabird conservation has been practiced widely in North America and Europe since the late nineteenth century. The extinction of the flightless Great Auk (*Alca impennis*) in the North Atlantic Ocean in 1844 marked the first well-recognized evidence of the impact of unmanaged human hunting on seabirds [144]. In millennia past, the spread of Polynesian people across island groups in the Pacific Ocean also led to the extirpation of several seabird species, such as certain *Pterodroma* petrels, which were killed for food and feathers [145]. In addition, human introductions of mammalian predators have continued to devastate seabird populations on some islands. As human populations have grown in coastal areas and have increasingly sought to exploit marine resources around the world, much evidence of human impacts on seabirds has accumulated and various conservation strategies have been employed to protect seabird populations and their breeding, roosting, and feeding areas (Table 17.5).

In the United States, Canada, Europe, New Zealand, Australia, and certain other countries, seabird conservation efforts have focused on (i) acquisition and protection of breeding colonies, (ii) management of colonies through removal of introduced predators or control of native predators, and (iii) promoting regulations to reduce anthropogenic impacts on land and at sea. Extensive restoration programs also have developed for certain species on the brink of extinction such as the Short-tailed Albatross (*Phoebastria albatrus*) in Japan and the Cahow (*Pterodroma cahow*) in Bermuda.

Since the passage of the Oil Pollution Act in 1990 (OPA 90), seabird restoration projects have become common place in the United States after a marine oil spill [7]. Under the natural resource damage assessment (NRDA) regulations in OPA 90, dozens of oil spill related NRDA cases have been filed in the U.S. Federal Court and settlements from these cases have resulted in tens of millions of dollars for seabird restoration projects. These NRDA restoration projects have built upon earlier seabird conservation actions by focusing restoration on enhancing or re-establishing breeding colonies of impacted seabirds or preventing the loss of colonies or roosting habitats. Restoration projects are usually developed

by government agencies, in consultation with seabird biologists, to address the most heavily impacted seabirds within the impact area of the spill. For those species, projects also may be implemented at breeding areas outside the impact area (Table 17.6).

17.7.1 Apex Houston Barge Oil Spill, Central California

Most oil spill NRDA seabird restoration projects in the United States have been initiated over the past decade and are still in progress. One case where initial restoration goals have been reached is the *Apex Houston* oil spill. The restoration actions associated with this incident illustrate that difficult-to-conduct projects on heavily impacted species in the impact area can be successfully implemented with sufficient knowledge, funding and support, although consistently achieving successful restoration outcomes is challenging.

In January 1986, approximately 615 barrels (25,900 U.S. gallons) of crude oil spilled from the barge *Apex Houston* into the coastal marine waters off central California between San Francisco and Monterey. Extensive documentation of dead and live oiled seabirds was obtained from beached bird surveys and from rehabilitation center records. These data, combined with at-sea surveys documenting the distribution and abundance of seabirds at risk of being oiled, were used to estimate that approximately 9000 seabirds died as a result of this spill. The seabird species most heavily impacted was the Common Murre with an estimated mortality of 6300. Also of particular significance was the mortality of at least 12, but possibly up to 100, federally threatened Marbled Murrelets [81,82,100]. Following five years of contentious negotiation and litigation, a \$5.4 million (U.S.) settlement was obtained. Most of the money (\$4.9 million) was directed to re-establish a Common Murre breeding colony that disappeared following the spill.

In the early 1980s, approximately 2500 Common Murres were breeding on Devil's Slide Rock, a small island located within the spill zone. By 1986, after two years of mortality from drowning in gill-nets, reduced prey availability from a strong El Niño event, and high mortality from the *Apex Houston* oil spill, this colony was gone. From 1987 to 1995, only small numbers of murres landed on Devil's Slide Rock and breeding did not occur [146]. In 1996, the Common Murre Restoration Project began. This restoration project involved the deployment of numerous murre decoys and mirrors and the broadcasting of murre vocalizations to attract this highly colonial species to the former breeding colony. The initial goal of the restoration effort was to develop a population of at least 100 breeding pairs by 2005. In the first year of deployment, six pairs of murres bred at the site and up to 29 birds were counted at one time [147]. Each year thereafter, the number of breeding pairs increased and by 2005 restoration efforts ended [147]. This colony has continued to grow and by 2007 (most recent estimate available) 394

TABLE 17.5 Conservation actions for seabirds

Prevent or reduce exploitation for food or feathers
Prevent or reduce disturbance at breeding colonies and roosts
Prevent or reduce loss or degradation of breeding and roosting habitats
Remove introduced predators from breeding islands
Reduce at-sea impacts caused by pollution and fisheries

TABLE 17.6 Natural resource damage assessment restoration projects designed to compensate for injuries to seabirds as a result of a marine oil spill in the U.S. from 1986 to 2007, excluding Alaska

Case name	State	Year of spill	Gallons (U.S.)	Est. dead birds	Funding for bird rest	Seabird restoration activities	Source
Apex Houston	CA	1986	25,900	9,856	\$5,400,000	Common Murre recolonization; Purchase old growth forest for Marbled Murrelets; Education on seabirds	http://www.dfg.ca.gov/osp/NRDA/index.aspx
Nestucca	WA	1988	230,000	65,000	\$500,000	Enhance forest structure for nesting Marbled Murrelets; Control/remove exotic vegetation and increase tidal flow in salt marsh; Enhance nesting habitat for Snowy Plovers	http://www.cerc.usgs.gov/orda_docs/Assets/UploadedFiles/CaseDocuments/Restoration_Docs/plans/WA_barge_Nestucca_RP_10-04.pdf http://www.dfg.ca.gov/osp/NRDA/index.aspx http://www.darrp.noaa.gov
American Trader	CA	1990	416,598	3,400	\$2,485,000	Enhance/Protect Brown Pelican roosts; Non-native rat eradication to benefit burrow/crevice nesting seabirds	http://www.dfg.ca.gov/osp/NRDA/index.aspx
Tenyo Maru	WA	1991	173,000	5,040	\$4,760,000	Purchase old growth forest for Marbled Murrelets; Education on seabirds	http://www.darrp.noaa.gov
Luckenbach	CA	1992–2003	Unknown	51,569	\$20,650,949	Nesting colony protection in Alaska, northern California, New Zealand, Baja California; Corvid management; Introduced mammal control at colonies; Nesting habitat enhancement	http://www.dfg.ca.gov/osp/NRDA/index.aspx
Cape Mohican	CA	1996	40,000	593	\$985,500	Shorebird habitat protection; Exotic vegetation and introduced mammal control; Acquisition of breeding habitat; California Least Tern habitat enhancement	http://www.dfg.ca.gov/osp/NRDA/index.aspx
Kure	CA	1997	4,537	3,950	\$2,060,000	Protect grebe nesting colonies in N. California, Brown Pelican roosting sites, and Common Murre colonies; Corvid management; Wetland restoration; Conservation easement of old growth forest to benefit nesting Marbled Murrelets valued at an additional \$2,400,000	http://www.dfg.ca.gov/osp/NRDA/index.aspx
Tesoro	HI	1998	4,914	No estimate	\$500,000	Predator control for Newell's Shearwater; Predator control and nesting habitat enhancement offshore islets and National Wildlife Refuge	http://www.darrp.noaa.gov
Command	CA	1998	3,000	1,900	\$3,200,000	Purchase old growth forest for Marbled Murrelets; Corvid management; Education on seabirds	http://www.dfg.ca.gov/osp/NRDA/index.aspx
New Carissa	OR	1999	70,000	3,137	\$26,870,334	Purchase old growth forest for Marbled Murrelets; Tidal marsh restoration; Education on seabirds	http://www.darrp.noaa.gov
Stuyvesant	CA	1999	2,000	2,405	\$6,098,900	Tidal wetland, dune, rocky shoreline projects; Grebe/loon nesting habitat improvements; Cormorant/pelican nesting/roosting habitat protection; Marbled Murrelet, Snowy Plover projects	http://www.dfg.ca.gov/osp/NRDA/index.aspx
North Cape	RI	1996	828,000	2,292	\$8,349,126	Habitat acquisition for loons and eiders; Education and monitoring; Habitat improvements for seabirds; Salt pond enhancements; Piping Plover colony management	http://www.darrp.noaa.gov
Westchester	LA	2000	550,000	582	not specified	Marsh creation	http://www.darrp.noaa.gov/northeast/athos/pdf/LOSCO%20et%20al%202001.pdf http://www.darrp.noaa.gov
Chalk Point	MD	2000	140,000	696	not specified	Ruddy Duck nesting habitat protection Prairie Pothole Region midwestern U.S.; Intertidal wetlands and shoreline habitat restoration	http://www.darrp.noaa.gov
Bouchard No. 120 Athos I	MA NJ	2003 2004	98,000 256,000	479 3,308	\$715,000 \$1,300,000	Piping Plover management; Shoreline protection Tidal wetlands, marsh, shoreline, pond, and uplands protection and restoration	http://www.darrp.noaa.gov http://www.darrp.noaa.gov
Cosco Busan	CA	2007	58,000	6,849	\$5,000,000	Nesting habitat enhancement for Western/Clark's Grebes, alcids, procellariids, gulls, cormorants, snowy plover; Winter and roosting habitat enhancement for pelicans, small diving ducks and grebes; Grants to benefit surf scoters and large diving ducks; Corvid management to improve Marbled Murrelet nesting	http://www.dfg.ca.gov/osp/NRDA/index.aspx

breeding pairs were present, nearly four times the initial goal [148,149]. In 2009, over 1000 murrees were counted at this site [150]. Most remaining funds from the *Apex Houston* settlement were combined with private conservation funds to purchase 111 acres of coastal old-growth forest in central California. This purchase was expected to directly protect the breeding habitat of the federally threatened tree-nesting Marbled Murrelet and prevent further fragmentation of the coastal old-growth forest ecosystem this seabird species depends upon. Unfortunately, despite this purchase and other conservation and restoration efforts, the Marbled Murrelet population in central California has continued to decline and it may soon be extirpated from this region [151]. The possible failure of this restoration effort highlights the risk of restoring heavily impacted seabirds affected by several anthropogenic factors and it suggests that even relatively small oil spills can contribute to devastating long-term or permanent impacts on some local seabird populations. Although it presently appears unlikely, there remains hope that the restoration and conservation efforts for this genetically distinct small population may allow it to persist long enough to reach more sustainable numbers in the future.

17.7.2 American Trader Oil Spill, Southern California

Restoration efforts following the *American Trader* oil spill provide an example of our incomplete knowledge regarding how some seabirds or populations will respond to restoration actions. In February 1990, about 9900 barrels (416,600 U.S. gallons) of crude oil spilled from the tanker *American Trader* while at anchor off Huntington Beach, southern California. The oil spread south along the California coast between Long Beach and Dana Point impacting about 3400 seabirds, including 185 Brown Pelicans (*P. occidentalis*) that were listed as federally endangered at that time [152]. The NRDA claim was settled for nearly \$3.2 million (U.S.) in 1994, but litigation and other issues held up the implementation of restoration activities for several years. The primary restoration project developed for seabirds was the eradication of the introduced Black Rat (*Rattus rattus*) from nearby Anacapa Island. Anacapa Island is the main breeding island for Brown Pelicans in southern California and contains breeding populations of several other seabird species. Of particular concern to seabird management agencies was the impact the rats were likely having on the island's small populations of burrow and crevice nesting seabirds such as Scripps's Murrelet.

In 2001–2002, the introduced rats on Anacapa Island were exterminated by helicopter-broadcast of the rodenticide brodifacoum during the non-breeding season for seabirds [153]. Follow-up studies indicated that the rodenticide killed relatively few non-target species and that the pre-broadcast removal, captive care, and subsequent reintroduction of hundreds of the endemic Deer Mouse (*Peromyscus maniculatus anacapae*) were successful [154]. It was never certain that the rats were

having a substantial impact on Brown Pelicans, and following the eradication effort, the pelican population remained relatively stable and the species was delisted in 2009. Post-eradication (2003–2010) monitoring of a remnant population on Scripps's Murrelets determined that nest numbers increased by 18% per annum and reproductive success increased from 30% pre-eradication (2001–2002) to 85% post-eradication [155]. Despite these significant improvements, most of the seemingly suitable breeding habitat on the island remained unpopulated by murrelets eight years after the eradication effort. The species was state listed as threatened in 2004, and it remains a candidate for federal listing. Cassin's Auklets, another small seabird likely being affected by the rats, recolonized Anacapa Island in 2003 shortly after eradication and by 2012 there were about 50 breeding pairs on the island [156]. While the removal of introduced predators has become a common management tool to assist seabird population recovery, this well-documented effort demonstrates that some seabird species or populations either may never recover or require long time periods to fully respond. This effort also demonstrates that long-term post-restoration monitoring programs should be required to accurately measure the nature and degree of benefits to seabirds obtained over time.

REFERENCES

- [1] Piatt, J.F., H.R. Carter, and D.N. Nettleship, Effects of oil pollution on marine bird populations, J. White (ed.), Proceedings of the 2nd International Effects of Oil on Wildlife Conference, Herndon, VA, October 16–20, 1990, Hanover, PA, Sheridan Press, 125, 1991.
- [2] Wiese, F.K. and P.C. Ryan, The extent of chronic marine oil pollution in southeastern Newfoundland waters assessed through beached bird survey 1984–1999, *Mar. Pollut. Bull.*, 46, 1090, 2003.
- [3] Russell, R.W., *Interactions between migrating birds and offshore oil and gas platforms in the northern Gulf of Mexico*, New Orleans, LA, U.S. Dept. of the Interior, Minerals Management Service, Gulf of Mexico OCS Region, MMS 2005-009, Unpublished report, 348, 2005.
- [4] Van der laar, F.J.T., *Green light to birds: investigation into the effect of bird-friendly lighting*, Assen, Netherlands, Nederlandse Aardolie Maatschappij BV (NAM), Nam Locatie L-15-FA-1, Unpublished report, joop.marquenie@shell.com-joop.marquenie@shell.com, 2007.
- [5] Piatt, J.F. and R.G. Ford, How many seabirds were killed by the *Exxon Valdez* oil spill? S.D. Rice, R.B. Spies, D.A. Wolfe, and B.A. Wright (eds.), Proceedings of the *Exxon Valdez* Oil Spill Symposium, *Am. Fish. Soc. Symp.*, 18, 712, 1996.
- [6] Munilla, I., J.M. Arcos, D. Oro, D. Alvarez, P.M. Levenda et al., Mass mortality of seabirds in the aftermath of the *Prestige* oil spill, *Ecosphere*, 2, art83, 2011, Doi:10.1890/ES11-00020.1.
- [7] Helm, R.C., R.G. Ford, and H.R. Carter, The Oil Pollution Act of 1990 and natural resource damage assessment, *Mar. Ornith.*, 34, 99, 2006.

- [8] Ashmole, P.N., Seabird ecology and the marine environment, *Avian Biology*, Vol. 1, D.S. Farner, J.K. King, and K.C. Parkes (eds.), New York, Academic Press, 224, 1971.
- [9] Gill, F., M. Wright, and D. Donsker, *IOC World Bird Names (version 4.3)*, <http://www.worldbirdnames.org/> (accessed August 29, 2014).
- [10] Camphuysen, C.J., *Methods for Assessing Seabird Vulnerability to Oil Pollution*, <http://www.docstoc.com/docs/45830287/METHODS-FOR-ASSESSING-SEABIRD-VULNERABILITY-TO-OIL-POLLUTION>, 2006 (accessed August 29, 2014).
- [11] King, J.G. and G.A. Sanger, Oil vulnerability index for marine oriented birds, *Conservation of Marine Birds of Northern North America*, J.C. Bartonek and D.N. Nettleship (eds.), Wildlife Research Report 11, Washington, DC, U.S. Fish and Wildlife Service, 227, 1979.
- [12] Williams, J.M., M.L. Tasker, I.C. Carter, and A. Webb, A method of assessing seabird vulnerability to surface pollutants, *Ibis*, 137, S147, 1995.
- [13] Speich, S.M., D.A. Manuwal, and T.R. Wahl, The bird/habitat oil index—a habitat vulnerability index based on avian utilization, *Wildl. Soc. Bull.*, 19, 216, 1991.
- [14] National Research Council, *Oil in the Sea: Inputs, Fates, and Effects*, Washington, DC, National Academies Press, 1985.
- [15] National Research Council, *Oil in the Sea III: Inputs, Fates, and Effects*, Washington, DC, National Academies Press, 2003.
- [16] Leighton, F.A., The toxicity of petroleum oils to birds: an overview, J. White (ed.), *Proceedings of the 2nd International Effects of Oil on Wildlife Conference*, Herndon, VA, October 16–20, 1990, Hanover, PA, Sheridan Press, 125, 1991.
- [17] Nero and Associates, *Seabird oil toxicity study*, Los Angeles, CA, U.S. Dept. of the Interior, Minerals Management Service, Pacific OCS Region, MMS-87-0005, Unpublished report, 1987.
- [18] Hartung, R. and G.S. Hunt, Toxicity of some oils to waterfowl, *J. Wildl. Manage.*, 30, 564, 1966.
- [19] Hartung, R., Energy metabolism in oil-covered ducks, *J. Wildl. Manage.*, 31, 798, 1967.
- [20] Fry, D.M. and L.J. Lowenstine, Pathology of Common Murres and Cassin's Auklets exposed to oil, *Arch. Environ. Contam. Toxicol.*, 14, 725, 1985.
- [21] Jauniaux, T., L. Brosens, and F. Coignoul, Lesions observed on stranded seabirds along the Belgian coast from 1992 to 1995, *ICES J. Mar. Sci.*, 54, 714, 1997.
- [22] Williams, A.S., J. Burridge, and M. Kane, *Rehabilitating Oiled Sea Birds: A Field Manual*, Washington, DC, American Petroleum Institute, Publication 4407, 1985.
- [23] Peakall, D.B., D.J. Hallett, D.J. Bend, J.L. Foureman, and D.S. Miller, Toxicity of Prudhoe Bay crude oil and its aromatic fractions to nestling Herring Gulls, *Environ. Res.*, 27, 206, 1982.
- [24] Peakall, D.B., D.S. Miller, and W.B. Kinter, Toxicity of crude oils and their fractions to nestling Herring Gulls: physiological and biochemical effects, *Mar. Environ. Res.*, 8, 63, 1983.
- [25] Miller, D.S., D.B. Peakall, and W.B. Kinter, Ingestion of crude oil: sublethal effects in Herring Gull chicks, *Science*, 199, 315, 1978.
- [26] Peakall, D.B., D.S. Hallett, D.S. Miller, R.G. Butler, and W.B. Kintner, Effects of ingested crude oil on Black Guillemots: a combined field and laboratory study, *Ambio*, 9, 28, 1980.
- [27] Trivelpiece, W., R.G. Butler, D.S. Miller, and D.B. Peakall, Reduced survival of chicks of oil-dosed adult Leach's Storm-Petrels, *Condor*, 86, 8, 1984.
- [28] Boersma, P.D., E.M. Davies, and W. Reid, Weathered crude oil effects on chicks of Fork-tailed Storm-Petrels (*Oceanodroma furcata*), *Arch. Environ. Contam. Toxicol.*, 17, 527, 1988.
- [29] Balseiro, A., A. Espí, I. Márquez, V. Pérez, M.C. Ferreras et al., Pathological features in marine birds affected by the Prestige's oil spill in the north of Spain, *J. Wildl. Dis.*, 41, 371, 2005.
- [30] Hall, R.J. and N.C. Coon, Interpreting residues of petroleum hydrocarbons in wildlife tissues, *U.S. Fish Wildl. Serv. Biol. Rep.*, 88(15), 8, 1988.
- [31] Naf, C., D. Broman, and B. Brunstrom, Distribution and metabolism of polycyclic aromatic hydrocarbons (PAHs) injected into eggs of chicken (*Gallus domesticus*) and Common Eider duck (*Somateria mollissima*), *Environ. Toxicol. Chem.*, 11, 1653, 1992.
- [32] Ariese, F., S.J. Kok, M. Verkaik, C. Gooijer, N.H. Velthorst et al., Synchronous fluorescence spectrometry of fish bile: a rapid screening method for the biomonitoring of PAH exposure, *Aqua. Tox.*, 26, 273, 1993.
- [33] Di Giulio, R.T., W.H. Benson, B.M. Sanders, and P.A. van Veld, Biochemical mechanisms: metabolism, adaptation and toxicity, *Fundamentals of Aquatic Toxicology*, G.M. Rand (ed.), Washington, DC, Taylor and Francis, 1995.
- [34] Yamato, O., I. Goto, and Y. Maede, Hemolytic anemia in wild seaducks caused by marine oil pollution, *J. Wildl. Dis.*, 32, 381, 1996.
- [35] Langenberg, J.A. and F.J. Dein, Pathology of Ruddy Ducks (*Oxyura jamaicensis*) contaminated with spilled #6 fuel oil, D. Rosie and S.N. Barnes (eds.), *Proceedings of the 1st International Effects of Oil on Wildlife Conference*, Wilmington, DE, September 17–19, 1982, Newark, DE, Tri-State Bird Rescue and Research, Inc., 139, 1983.
- [36] Leighton, F.A., Y.Z. Lee, A.D. Rahimtula, P.J. O'Brien, and D.B. Peakall, Biochemical and functional disturbances in red blood cells of Herring Gulls ingesting Prudhoe Bay crude oil, *Toxicol. Appl. Pharmacol.*, 81, 25, 1985.
- [37] Fry, D.M. and L.A. Addiego, Hemolytic anemia complicates the cleaning of oiled seabirds, *Wildlife J.*, 10, 3, 1987.
- [38] Troisi, G., L. Borjesson, S. Bexton, and I. Robinson, Biomarkers of polycyclic aromatic hydrocarbon (PAH)-associated hemolytic anemia in oiled wildlife, *Environ. Res.*, 105, 324, 2007.
- [39] Alonso-Alvarez, C., I. Munilla, M. López-Alonso, and A. Velando, Sublethal toxicity of the Prestige oil spill on Yellow-legged Gulls, *Environ. Int.*, 33, 773, 2007.
- [40] Alonso-Alvarez, C., C. Pérez, and A. Velando, Effects of acute exposure to heavy fuel oil from the Prestige spill on a seabird, *Aqua. Toxicol.*, 84, 103, 2007.
- [41] Oropesa, A.L., M. Pérez-López, D. Hernández, J.P. García, L.E. Fidalgo et al., Acetylcholinesterase activity in seabirds affected by the Prestige oil spill on the Galician coast (NW Spain), *Sci. Total Environ.*, 372, 532, 2007.
- [42] Newman, S.H., D.W. Anderson, M.H. Ziccardi, J.G. Trupkiewicz, F.S. Tseng et al., An experimental soft-release of oil-spill rehabilitated American Coots (*Fulica americana*): II. Effects on health and blood parameters, *Environ. Pollut.*, 107, 295, 2000.

- [43] Gorsline, J. and W.N. Holmes, Variations with age in the adrenocortical responses of Mallard ducks (*Anas platyrhynchos*) consuming petroleum-contaminated food, *Bull. Environ. Contam. Toxicol.*, 29, 146, 1982.
- [44] Gorsline, J. and W.N. Holmes, Adrenocortical function and hepatic naphthalene metabolism in Mallard ducks (*Anas platyrhynchos*) consuming petroleum distillates, *Environ. Res.*, 28, 139, 1982.
- [45] Rattner, B.A., V.P. Eroschenko, G.A. Fox, D.M. Fry, and J. Gorsline, Avian endocrine responses to environmental pollutants, *J. Exp. Zool.*, 232, 683, 1984.
- [46] Briggs, K.T., S.H. Yoshida, and M.E. Gershwin, The influence of petrochemicals and stress on the immune system of seabirds, *Regul. Tox. Pharmacol.*, 23, 145, 1996.
- [47] Fowler, G.S., J.C. Wingfield, and P.D. Boersma, Hormonal and reproductive effects of low levels of petroleum fouling in Magellanic Penguins (*Spheniscus magellanicus*), *Auk*, 112, 382, 1995.
- [48] Holmes, W.N., W. Cavanaugh, and J. Cronshaw, The effects of ingested petroleum on oviposition and some aspects of reproduction in experimental colonies of Mallard ducks (*Anas platyrhynchos*), *J. Reprod. Fert.*, 54, 335, 1978.
- [49] Vangilder, L.D. and T.J. Peterle, South Louisiana crude oil and DDE in the diet of Mallard hens: effects on reproduction and duckling survival, *Bull. Environ. Contam. Toxicol.*, 25, 23, 1980.
- [50] Harvey, S., H. Klandorf, and J.G. Phillips, Reproductive performance and endocrine responses to ingested petroleum in domestic ducks (*Anas platyrhynchos*), *Gen. Comp. Endocrinol.*, 45, 372, 1981.
- [51] Cavanaugh, K.P. and W.H. Holmes, Effects of ingested petroleum on plasma levels of ovarian steroid hormones in photo-stimulated Mallard ducks, *Arch. Environ. Contam. Toxicol.*, 11, 503, 1982.
- [52] Cavanaugh, K.P., A.R. Goldsmith, W.H. Holmes, and B.K. Follett, Effects of ingested petroleum on the plasma prolactin levels during incubation and on the breeding success of paired Mallard ducks, *Arch. Environ. Contam. Toxicol.*, 12, 335, 1983.
- [53] Grau, C.R., T. Roudybush, J. Dobbs, and J. Wathen, Altered yolk structure and reduced hatchability of eggs from birds fed single doses of petroleum oils, *Science*, 195, 779, 1977.
- [54] Wootton, T.A., C.R. Grau, T.E. Roudybush, M.E. Hahs, and K.V. Hirsch, Reproductive responses of quail to Bunker C oil fractions, *Arch. Environ. Contam. Toxicol.*, 8, 457, 1979.
- [55] Fry, D.M., J. Swenson, L.A. Addiego, C.R. Grau, and A. Kang, Reduced reproduction of Wedge-tailed Shearwaters exposed to single doses of weathered Santa Barbara crude oil, *Arch. Environ. Contam. Toxicol.*, 15, 453, 1986.
- [56] Hoffman, D.J., Embryotoxic effects of crude oil in Mallard ducks and chicks, *Tox. Appl. Pharm.*, 46, 183, 1978.
- [57] Hoffman, D.J., Embryotoxic and teratogenic effects of crude oil on Mallard embryos on day one of development, *Bull. Environ. Contam. Toxicol.*, 22, 632, 1979.
- [58] Hoffman, D.J. and M.L. Gay, Embryotoxic effects of Bellzo(a)pyrene, chrysene, and 7,12-Dimethylbenz(a)anthracene in petroleum hydrocarbon mixtures in Mallard ducks, *J. Toxicol. Environ. Health*, 7, 775, 1981.
- [59] Hoffman, D.J., W.C. Eastin Jr., and M.L. Gay, Embryotoxic and biochemical effects of waste crankcase oil on birds' eggs, *Toxicol. Appl. Pharm.*, 63, 230, 1982.
- [60] Couillard, C.M. and F.A. Leighton, The toxicopathology of Prudhoe Bay crude oil in chicken embryos, *Fundam. Appl. Toxicol.*, 14, 30, 1990.
- [61] Coon, N.C. and M.P. Dieter, Responses of adult Mallard ducks to ingested South Louisiana crude oil, *Environ. Res.*, 24, 309, 1981.
- [62] Newman, S.H., M.H. Ziccardi, J.K. Mazet, C.L. Leiske, D.A. Fauquier et al., *Hematologic changes and anemia associated with captivity and petroleum exposure in seabirds*, Sacramento, CA, California Department of Fish and Game, Office of Spill Prevention and Response, Unpublished Report, 1998.
- [63] Newman, S.H., H.R. Carter, D.L. Whitworth, and J.G. Zinkl, Health assessments and stress response of Xantus's Murrelets to capture, handling, and radio-marking, *Mar. Ornith.* 33, 147, 2005.
- [64] Mazet, J.K., S.H. Newman, K.V.K. Gilardi, F.S. Tseng, J.B. Holcomb et al., Advances in oiled bird emergency medicine and management, *J. Avian. Med. Surg.*, 16, 146, 2002.
- [65] Newman, S.H., M.H. Ziccardi, A.B. Berkner, J. Holcomb, C. Clumpner et al., A historical account of oiled wildlife care in California, *Mar. Ornithol.*, 31, 59, 2003.
- [66] Sharp, B.E., Post-release survival of oiled, cleaned seabirds in North America, *Ibis*, 138, 222, 1996.
- [67] Wernham, C.V., W.J. Peach, and S.J. Browne, *Survival rates of rehabilitated guillemots*, Thetford, Norfolk, British Trust for Ornithology, Research Report No. 186, 1997.
- [68] Anderson, D.W., F. Gress, and D.M. Fry, Survival and dispersal of oiled Brown Pelicans after rehabilitation and release, *Mar. Pollut. Bull.*, 32, 711, 1996.
- [69] Dunne, R. and E. Miller, Post-release survival of oiled, rehabilitated waterfowl, J.G. Massey (ed.), Proceedings of the 9th International Effects of Oil on Wildlife Conference, Monterey, CA, June 25–29, 2007, Davis, CA, University of California, Wildlife Health Center, 30, 2007.
- [70] Golightly, R.T., S.H. Newman, E.N. Craig, H.R. Carter, and J.A.K. Mazet, Survival and behavior of Western Gulls following exposure to oil and rehabilitation, *Wildlife Soc. Bull.*, 30, 539, 2002.
- [71] Newman, S.H., R.T. Golightly, E.N. Craig, H.R. Carter, and C. Kreuder, *The effects of petroleum exposure and rehabilitation on post-release survival, behavior, and blood health indices: a Common Murre (Uria aalge) case study following the Stuyvesant petroleum spill*, Davis, CA, Oiled Wildlife Care Network, School of Veterinary Medicine, University of California, Unpublished Report, 2004.
- [72] Anderson, D.W., S.H. Newman, P.R. Kelly, S.K. Herzog, and K.P. Lewis, An experimental soft-release of oil-spill rehabilitated American Coots (*Fulica americana*): I. Lingering effects on survival, condition and behavior, *Environ. Pollut.*, 107, 285, 2000.
- [73] Berg, C., *Best Practices for Migratory Bird Care during Oil Spill Response*, Anchorage, AK, U.S. Fish and Wildlife Service, 2003.
- [74] Whittington, P.A., Post-release survival of rehabilitated African Penguins, *Rehabilitation of Oiled African Penguins*:

- A Conservation Success Story*, C.D. Nel and P.A. Whittington (eds.), Cape Town, South Africa, BirdLife and Avian Demography Unit, 8, 2003.
- [75] Holcomb, J.B., Net bottom caging for waterfowl, *Wildl. J.*, 11, 3, 1998.
- [76] Tseng, F.S., Considerations in care for birds affected by oil spills, *Semin. Avian Exotic Practice Med.*, 8, 21, 1999.
- [77] Frink, L. and E.A. Miller, Principles of oiled bird rehabilitation, L. Frink (ed.), Proceedings of the 3rd International Effects of Oil on Wildlife Conference, New Orleans, LA, January 1993, Newark, DE, Tri-State Bird Rescue and Research, Inc., 61, 1995.
- [78] Bryndza, H.E., J.P. Foster, J.H. McCartney, B. Lundberg, and J.C. Lober, Surfactant efficacy in removal of petrochemicals from feathers, J. White (ed.), Proceedings of the 9th International Effects of Oil on Wildlife Conference, Herndon, VA, October 16–20, 1990, Hanover, PA, Sheridan Press, 78, 1991.
- [79] Clumpner, C.J., Water hardness and waterproofing of oiled birds: lessons from the *Nestucca*, *Exxon Valdez* and the *American Trader* spills, J. White (ed.), Proceedings of the 2nd International Effects of Oil on Wildlife Conference, Herndon, VA, October 16–20, 1990, Hanover, PA, Sheridan Press, 101, 1991.
- [80] Carter, H.R., Oil and California's seabirds, *Mar. Ornith.*, 31, 1, 2003.
- [81] Ford, R.G., G.W. Page, and H.R. Carter, Estimating mortality of seabirds from oil spills, Proceedings of the 1987 Oil Spill Conference, Baltimore, MD, April 6–9, 1987, Washington, DC, American Petroleum Institute, 547, 1987.
- [82] Carter, H.R., V.A. Lee, G.W. Page, M.W. Parker, R.G. Ford et al., The 1986 *Apex Houston* oil spill in central California: seabird injury assessments and litigation process, *Mar. Ornith.*, 31, 9, 2003.
- [83] Ford, R.G., M.L. Bonnell, D.H. Varoujean, G.W. Page, H.R. Carter et al., Total direct mortality of seabirds from the *Exxon Valdez* oil spill, S.D. Rice, R.B. Spies, D.A. Wolfe, and B.A. Wright (eds.), Proceedings of the *Exxon Valdez* Oil Spill Symposium, *Am. Fish. Soc. Symp.*, 18, 684, 1996.
- [84] Ford, R.G. and M.A. Zafonte, Scavenging of seabird carcasses at two oil spill sites in California and Oregon, *Mar. Ornith.*, 37, 205, 2009.
- [85] Byrd, G.V., J.H. Reynolds, and P.L. Flint, Persistence rates and detection probabilities of bird carcasses on beaches of Unalaska Island, Alaska, following the wreck of the *M/V Selendang Ayu*, *Mar. Ornith.*, 37, 197, 2009.
- [86] Ford, R.G., Using beached bird monitoring data for seabird damage assessment: the importance of search interval, *Mar. Ornith.*, 34, 91, 2006.
- [87] Fowler, A.C. and P.L. Flint, Persistence rates and detection probabilities of oiled King Eider carcasses on St. Paul Island, Alaska, *Mar. Poll. Bull.*, 34, 522, 1997.
- [88] Flint, P. and A. Fowler, A drift experiment to assess the influence of wind on recovery of oiled seabirds on St. Paul Island, Alaska, *Mar. Poll. Bull.*, 36, 165, 1988.
- [89] Ford, R.G., N.A. Strom, and J.L. Casey, *Acute seabird mortality resulting from the S. S. Luckenbach and associated mystery oil spills, 1990–2003*, Portland, OR, R.G. Ford Consulting Company, Unpublished report, 2006.
- [90] Mauseth, G., Background oiling and incident specific attribution, Proceedings of the 2005 International Oil Spill Conference, Miami, FL, May 15–19, 2005, Washington, DC, American Petroleum Institute, 2005.
- [91] California Department of Fish and Game, *Spills and Events Natural Resource Damage Assessment and Restoration (NRDA) Estimating Bird Mortality*, https://www.dfg.ca.gov/ospr/Science/estimating_bird_mortality.aspx, 2004 (accessed August 7, 2014).
- [92] Campbell, L.H., K.T. Standing, and C.J. Cadbury, Firth of Forth oil pollution incident, February 1978, *Mar. Poll. Bull.*, 9, 335, 1978.
- [93] Ford, R.G., V. Byrd, and J. Reynolds, *Pre-assessment report: M/V Selendang Ayu background beaching and oiling rates for bird carcasses*, Portland, OR, R.G. Ford Consulting Company, Unpublished report, 2007.
- [94] Jaques, D. and R.G. Ford, *Brown Pelicans and the M/V KURE/Humboldt Bay oil spill*, Portland, OR, R.G. Ford Consulting Company, Unpublished report, 2000.
- [95] Ford, R.G., G.K. Himes Boor, B.E. Sharp, and J.L. Casey, *Estimates of bird impacts resulting from the M/V Kure/Humboldt Bay oil spill of November 5, 1997*, Portland, OR, R.G. Ford Consulting Company, Unpublished report, 2002.
- [96] Ford, R.G., J.L. Casey, and W.A. Williams, *Acute seabird and waterfowl mortality resulting from the M/V Cosco Busan oil spill, November 7, 2007*, Portland, OR, R.G. Ford Consulting Company, Unpublished report, 2009.
- [97] Ford, R.G., G.K. Himes Boor, and J.C. Ward, *Seabird mortality resulting from the M/V New Carissa oil spill incident, February and March 1999*, Portland, OR, R.G. Ford Consulting Company, Unpublished report, 2001.
- [98] Dobbin, J.A., H.E. Robertson, R.G. Ford, K.T. Briggs, and E.H. Clark, II, *Resource damage assessment of the T/V Puerto Rican oil spill incident*, Alexandria, VA, James Dobbin Associates, Inc., Unpublished report, 1986.
- [99] Ford, R.G. and J. Piatt, *Estimates of seabird mortality resulting from the M/V Citrus oil spill at St. Paul, Alaska, 1996*, Portland, OR, R.G. Ford Consulting Company, Unpublished report, 2006.
- [100] Page, G.W., H.R. Carter, and R.G. Ford, Numbers of seabirds killed or debilitated in the 1986 *Apex Houston* oil spill in central California, *Auks at Sea*, S.G. Sealy (ed.), *Studies in Avian Biology*, 14, 164, 1990.
- [101] Wiese, F.K. and I.L. Jones, Experimental support for a new drift block design to assess seabird mortality from oil pollution, *Auk*, 118, 1062, 2001.
- [102] Castro, J.I. and D.R. Peebles, *The Sharks of North America*, New York, Oxford University Press, 2011.
- [103] Monnat, J.Y. and Y. Guerneur, *The Amoco Cadiz and the birds*, Brest, France, Society for the Study of Protection of Nature in Brittany and Ministry of Environment and Framework of Life, (in French), 1979.
- [104] Burger, A.E. and D.M. Fry, Effects of oil pollution on seabirds in the Northeast Pacific, *The Status, Ecology and Conservation of Marine Birds in the North Pacific*, K. Vermeer, K.T. Briggs, K.H. Morgan, and D. Siegel-Causey (eds.), Ottawa, ON, Canadian Wildlife Service, Special Publication, 254, 1993.

- [105] Burger, A.E., Estimating the mortality of seabirds following oil spills: effects of spill volume, *Mar. Pollut. Bull.*, 26, 140, 1993.
- [106] Camphuysen, C.J. and M. Heubeck, Marine oil pollution and beached bird surveys: the development of a sensitive monitoring instrument, *Environ. Pollut.*, 112, 443, 2001.
- [107] Bourne, W.R.P., J.D. Parrack, and G.R. Potts, Birds killed in the Torrey Canyon disaster, *Nature*, 215, 1123, 1967.
- [108] Velando, A., D. Álvarez, J. Mouriño, F. Arcos, and A. Barros, Population trends and reproductive success of the European Shag *Phalacrocorax aristotelis* on the Iberian Peninsula following the Prestige oil spill, *J. Ornith.*, 146, 116, 2005.
- [109] Moreno, R., L. Jover, C. Diez, and C. Sanpera, Seabird feathers as monitors of the levels and persistence of heavy metal pollution after the *Prestige* oil spill, *Environ. Poll.*, 159, 2454, 2011.
- [110] Piatt, J.F. and P. Anderson, Response of Common Murres to the Exxon Valdez oil spill and long-term changes in the Gulf of Alaska marine ecosystem, S.D. Rice, R.B. Spies, D.A. Wolfe, and B.A. Wright (eds.), Proceedings of the Exxon Valdez Oil Spill Symposium, *Am. Fish. Soc. Symp.*, 18, 720, 1996.
- [111] Oakley, K.L. and K.J. Kuletz, Population, reproduction, and foraging of Pigeon Guillemots at Naked Island, Alaska, before and after the Exxon Valdez oil spill, S.D. Rice, R.B. Spies, D.A. Wolfe, and B.A. Wright (eds.), Proceedings of the Exxon Valdez Oil Spill Symposium, *Am. Fish. Soc. Symp.*, 18, 759, 1996.
- [112] Rice, S.D., R.E. Thomas, M.G. Carls, R.A. Heintz, A.C. Wertheimer et al., Impacts to Pink Salmon following the Exxon Valdez oil spill: persistence, toxicity, sensitivity, and controversy, *Rev. Fish. Sci.*, 9, 165, 2001.
- [113] Hawkins, S.J., P.E. Gibbs, N.D. Pope, G.R. Burt, B.S. Chesman et al., Recovery of polluted ecosystems: the case for long-term studies, *Mar. Env. Res.*, 54, 215, 2002.
- [114] Irons, D.B., S.J. Kendall, W.P. Erickson, L.L. McDonald, and B.K. Lance, Nine years after the "Exxon Valdez" oil spill: effects on marine bird populations in Prince William Sound, Alaska, *Condor*, 102, 723, 2000.
- [115] Peterson, C.H., S.D. Rice, J.W. Short, D. Esler, J.L. Bodkin et al., Long-term ecosystem response to the Exxon Valdez oil spill, *Science*, 302, 2082, 2003.
- [116] Guterman, L., *Exxon Valdez* turns 20, *Science*, 323, 1558, 2009.
- [117] Clark, R.B., Impact of oil pollution on seabirds, *Environ. Pollut. Ser. A*, 33, 1, 1984.
- [118] Parrish, J.K. and P.D. Boersma, Muddy waters: seabird mortality following the Exxon Valdez oil spill, *Amer. Sci.*, 83, 112, 1995.
- [119] Wiens, J.A., R.H. Day, S.M. Murphy, and K.R. Parker, Changing habitat and habitat use by birds after the Exxon Valdez oil spill, 1989–2001, *Ecol. Appl.*, 14, 1806, 2004.
- [120] Camphuysen, K.C.J., Seabirds and chronic oil pollution: self-cleaning properties of gulls, Laridae, as revealed from colour-ring sightings, *Mar. Pollut. Bull.*, 62, 514, 2011.
- [121] Harwell, M.A. and J.H. Gentile, Ecological significance of residual exposures and effects from the Exxon Valdez oil spill, *Integr. Environ. Assess. Manag.*, 2, 204, 2006.
- [122] Camphuysen, C.J., M. Heubeck, S.L. Cox, R. Bao, D. Humple et al., The Prestige oil spill in Spain, *Atl. Seabirds*, 4, 131, 2002.
- [123] Votier, S.C., B.J. Hatchwell, A. Beckerman, R.H. McCleery, F.M. Hunter et al., Oil pollution and climate have wide-scale impacts on seabird demographics, *Ecol. Lett.*, 8, 1157, 2005.
- [124] Votier, S.C., T.R. Birkhead, D. Oro, M. Trinder, M.J. Grantham et al., Recruitment and survival of immature seabirds in relation to oil spills and climate variability, *J. Anim. Ecol.*, 77, 974, 2008.
- [125] Nevins, H.M. and H.R. Carter, Age and sex of Common Murres *Uria aalge* recovered during the 1997–98 Point Reyes Tarball Incidents in central California, *Mar. Ornith.*, 31, 51, 2003.
- [126] Martínez-Abraín, A., A. Velando, D. Oro, M. Genovart, C. Gerique et al., Sex-specific mortality of European Shags after the Prestige oil spill: demographic implications for the recovery of colonies, *Mar. Ecol. Prog. Ser.*, 318, 271, 2006.
- [127] Irvine, G.V., H.D. Mann, and J.W. Short, Multi-year persistence of oil mousse on high energy beaches distant from the Exxon Valdez spill origin, *Mar. Ecol. Prog. Ser.*, 38, 572, 1999.
- [128] Reddy, C.M., T.L. Eglinton, A. Hounshell, H.K. White, L. Xu et al., The West Falmouth oil spill after thirty years: the persistence of petroleum hydrocarbons in marsh sediments, *Environ. Sci. Technol.*, 36, 4754, 2002.
- [129] Short, J.W., M.R. Lindeberg, P.M. Harris, J.M. Maselko, J.J. Pella et al., Estimate of oil persisting on the beaches of Prince William Sound 12 years after the Exxon Valdez oil spill, *Environ. Sci. Technol.*, 38, 19, 2004.
- [130] Short, J.W., J.M. Maselko, M.R. Lindeberg, P.M. Harris, and S.D. Rice, Vertical distribution and probability of encountering intertidal Exxon Valdez oil on shorelines of three embayments within Prince William Sound, *Environ. Sci. Technol.*, 40, 3723, 2006.
- [131] Day, R.H., S.M. Murphy, J.A. Wiens, G.D. Hayward, E.J. Harner et al., Effects of the Exxon Valdez oil spill on habitat used by birds in Prince William Sound Alaska, *Ecol. Appl.*, 7, 593, 1997.
- [132] Esler, D., T.D. Bowman, K.A. Trust, B.E. Ballachey, T.A. Dean et al., Harlequin duck population recovery following the "Exxon Valdez" oil spill: progress, process and constraints, *Mar. Ecol. Prog. Ser.*, 241, 271, 2002.
- [133] Burns, K.A., S.D. Garrity, and S.C. Levings, How many years until mangrove ecosystems recover from catastrophic oil spills?, *Mar. Pollut. Bull.*, 26, 239, 1993.
- [134] Poggiale, J.C. and J.C. Dauvin, Long-term dynamics of three benthic *Ampelisca* (Crustacea-Amphipoda) populations from the Bay of Morlaix (western English Channel) related to their disappearance after the "Amoco Cadiz" oil spill, *Mar. Ecol. Prog. Ser.*, 214, 201, 2001.
- [135] Hjermann, D.O., A. Melson, G.E. Dingsor, J.M. Durant, A.M. Eikeset et al., Fish and oil in the Lofoten-Barents Sea system: synoptic review of the effect of oil spills on fish populations, *Mar. Ecol. Prog. Ser.*, 339, 283, 2007.
- [136] Esler, D., J.A. Schmutz, R.L. Jarvis, and D.M. Mulcahy, Winter survival of adult female Harlequin Ducks in relation to history of contamination by the Exxon Valdez oil spill, *J. Wildl. Manage.*, 64, 839, 2000.

- [137] Highsmith, R.C., T.L. Rucker, M.S. Stekoll, S.M. Saupe, M.R. Lindeberg et al., Impact of the Exxon Valdez oil spill on intertidal biota, S.D. Rice, R.B. Spies, D.A. Wolfe, and B.A. Wright (eds.), *Proceedings of the Exxon Valdez Oil Spill Symposium, Am. Fish Soc. Symp.*, 18, 212, 1996.
- [138] Jewett, S.C., T.A. Dean, R.O. Smith, and A. Blanchard, The "Exxon Valdez" oil spill: impacts and recovery in the soft-bottom benthic community in and adjacent to eelgrass beds, *Mar. Ecol. Prog. Ser.*, 185, 59, 1999.
- [139] Golet, G.H., P.E. Seiser, A.D. McGuire, D.D. Roby, J.B. Fischer et al., Long-term direct and indirect effects of the "Exxon Valdez" oil spill on Pigeon Guillemots in Prince William Sound, Alaska, *Mar. Ecol. Prog. Ser.*, 241, 287, 2002.
- [140] Golet, G.H., K.J. Kuletz, D.D. Roby, and D.B. Irons, Adult prey choice affects chick growth and reproductive success of Pigeon Guillemots, *Auk*, 117, 82, 2000.
- [141] Velando, A., I. Munilla, and M. Leyenda, Short-term indirect effects of the "Prestige" oil spill on European Shags: changes in availability of prey, *Mar. Ecol. Prog. Ser.*, 302, 263, 2005.
- [142] Moreno, R., L. Jover, C. Diez, A. Velando, X. Ruiz et al., *Monitoring temporal changes in trophic ecology of Phalacrocorax aristotelis after the Prestige oil spill*, Barcelona, Spain, University of Barcelona, Unpublished report (in Spanish), 2007.
- [143] Velando, A. and I. Munilla, *Conservation plan for the European Shag in the Atlantic Islands of Galicia National Park*, Vigo, Spain, University of Vigo, Unpublished report, 2008.
- [144] Gaskell, J., *Who Killed the Great Auk?* Oxford, United Kingdom, Oxford University Press, 2000.
- [145] Steadman, D., Prehistoric extinctions of Pacific Island birds: biodiversity meets zooarchaeology, *Science*, 267, 1123, 1995.
- [146] McShane, C., T. Hamer, H. Carter, G. Swartzman, V. Friesen et al., *Evaluation Report for the 5-year Status Review of the Marbled Murrelet in Washington, Oregon, and California*, Seattle, WA, EDAW Inc., Unpublished report, 2004.
- [147] Carter, H.R., U.W. Wilson, R.W. Lowe, M.S. Rodway, D.A. Manuwal et al., Population trends of the Common Murre (*Uria aalge californica*), *Biology and Conservation of the Common Murre in California, Oregon, Washington, and British Columbia. Volume 1: Natural History and Population Trends*, D.A. Manuwal, H.R. Carter, T.S. Zimmerman, and D.L. Orthmeyer (eds.), Washington, DC, U.S. Geological Survey, Information and Technology Report USGS/BRD/ITR-2000-0012, 33, 2001.
- [148] Parker, M.W., S.W. Kress, R.T. Golightly, H.R. Carter, E.B. Parsons et al., Assessment of social attraction techniques used to restore a Common Murre colony in central California, *Waterbirds*, 30, 17, 2007.
- [149] McChesney, G.J., L.E. Eigner, P.J. Kappes, T.B. Poitras, D.N. Lontoh et al., *Restoration of Common Murre colonies in central California: annual report 2007*, Newark, CA, U.S. Fish and Wildlife Service, Unpublished report, 2008.
- [150] Eigner, L.E., G.J. McChesney, S.J. Rhoades, M.W. Davis, J.A. Shore et al., *Restoration and monitoring of Common Murre colonies in central California: annual report 2010*, Newark, CA, U.S. Fish and Wildlife Service, Unpublished report, 2011.
- [151] Peery, M.Z., S.R. Beissinger, S.H. Newman, E. Burkett, and T.D. Williams, Applying the declining population paradigm: diagnosing causes of poor reproduction in the Marbled Murrelet, *Conserv. Biol.*, 18, 1088, 2004.
- [152] American Trader Trustee Council (ATTC), *Final restoration plan and environmental assessment for seabirds injured by the American Trader oil spill*, Published by American Trader Resource Trustee Council, U.S. Fish and Wildlife Service, California Department of Fish and Game, and National Oceanic and Atmospheric Administration, 2001.
- [153] Howald, G.R., K.R. Faulkner, B. Tershy, B. Keitt, H. Gellerman et al., Eradication of Black Rats from Anacapa Island: biological and social considerations, D.K. Garcelon and C.A. Schwemm (eds.), *Proceedings of the 6th California Islands Symposium*, National Park Service Technical Publication CHIS-05-01, Arcata, CA, Institute for Wildlife Studies, Unpublished report, 299, 2005.
- [154] Gellerman, H., *Conservation of the Anacapa Deer Mouse: impact and recovery from an eradication*, San Luis Obispo, CA, California Polytechnic State University, M.Sc. thesis, 2007.
- [155] Whitworth, D.L., H.R. Carter, and F. Gress, Recovery of a threatened seabird after eradication of an introduced predator: eight years of progress for Scripps's Murrelet at Anacapa Island, *Biol. Conserv.*, 162, 52, 2013.
- [156] Whitworth, D.L., A.L. Harvey, H.R. Carter, R.J. Young, J.S. Koepke. In press. Breeding of Cassin's Auklet (*Ptycoramphus aleuticus*) at Anacapa Island, California, after eradication of Black Rats. *Mar. Ornithol.*

OVERVIEW OF EFFECTS OF OIL SPILLS ON MARINE MAMMALS

ROGER C. HELM,¹ DANIEL P. COSTA,² TERRY D. DEBRUYN,³ THOMAS J. O'SHEA,⁴ RANDALL S. WELLS,⁵ AND TERRIE M. WILLIAMS⁶

¹U.S. Fish and Wildlife Service, Science Applications, Falls Church, VA, USA

²Department of Ecology and Evolutionary Biology, University of California, Santa Cruz, CA, USA

³U.S. Fish and Wildlife Service, Anchorage, AK, USA

⁴U.S. Geological Survey (Retired), Glen Haven, CO, USA

⁵Chicago Zoological Society-Mote Marine Laboratory, Sarasota, FL, USA

⁶Center for Ocean Health, University of California, Santa Cruz, CA, USA

18.1	Introduction	455
18.1.1	Sea Otters	456
18.1.2	Seals and Sea Lions	457
18.1.3	Sea Cows	457
18.1.4	Polar Bears	457
18.1.5	Whales, Dolphins, and Porpoises	457
18.2	Sea Otters	458
18.2.1	External Exposure	458
18.2.2	Internal Exposure	459
18.2.3	Long-Term Effects	461
18.3	Seals and Sea Lions	461
18.3.1	Direct Effects	462
18.3.2	Vulnerability and Risk	462
18.4	Sea Cows	464
18.4.1	Direct Effects	465
18.4.2	Indirect Effects	465
18.5	Polar Bears	465
18.5.1	Direct and Indirect Effects	465
18.5.2	Vulnerability and Risk	466
18.6	Whales, Dolphins, and Porpoises	467
18.6.1	Direct Effects	467
18.6.2	Vulnerability and Risk	468

18.1 INTRODUCTION

The 1989 *Exxon Valdez* oil spill (EVOS) in Alaska killed tens of killer whales (*Orcinus orca*), hundreds of harbor seals (*Phoca vitulina*), thousands of sea otters (*Enhydra lutrius*),

Disclaimer

The findings and conclusions in this article are those of the authors and do not necessarily represent the views of the U.S. Fish and Wildlife Service.

and hundreds of thousands of birds (sea birds, shorebirds, and marine-associated birds) and greatly impacted marine habitats that contain the forage fish and marine invertebrates that fuel higher trophic levels [1–4]. These numbers represent the documented deaths from that spill, which undoubtedly killed many more animals. More than 20 years after the EVOS, long-term individual effects (e.g., impaired health and reproduction) and population impacts, especially in the near-shore ecosystem, are most evident for killer whales, sea otters, and some marine birds. The ongoing effects and slow recovery of some species are attributed to long-term exposure to spilled oil sequestered in nearshore habitats and, in the case of the social killer whale, to the legacy of key pod member mortalities from the oil [5–9]. While apparently not as devastating to marine mammals as the EVOS, there is evidence the massive MC-252 Deepwater Horizon (DWH) oil spill in 2010 impacted reproduction and health of coastal bottlenose dolphins (*Tursiops truncatus*) in the northern Gulf of Mexico [10].

Considering that marine mammals are common, highly visible, charismatic, and potentially vulnerable to oil, it is somewhat surprising that we know relatively little about the effects of oil on individuals and populations. The majority of what has been published in books and peer-reviewed journals comes from a handful of laboratory experiments and the investigations on marine mammals that followed the EVOS.

Oil spills can affect marine mammals through a variety of direct and indirect pathways. Direct pathways include inhalation, ingestion, and dermal exposure, each of which can initiate a suite of physiological responses with health and long-term survival and/or reproduction consequences. For most

marine mammals, the most serious acute health threat may be severe damage to the respiratory system through inhalation of the volatile and highly toxic aromatic components of oil. Ingestion of oil through grooming or consumption of contaminated prey would be expected to harm various internal organs (e.g., liver, kidney, and intestines) and organ systems (e.g., digestive and urogenital). Mild dermal exposure would cause at least short-term injuries to mucus membranes, eyes, and other external soft tissue areas, while severe oiling could result in death by smothering. For those species that rely on fur for insulation, external oiling can be life threatening due to extreme hypothermia. Perhaps equally important, but less well understood, are indirect effects of oil spills. These can include:

1. Short-term reductions in prey availability
2. Long-term injury to prey habitats, prey populations, and prey availability
3. Selective mortality disrupting social bonds
4. Reduced reproduction within structured subpopulations
5. Cumulative effects on individuals, populations, and the ecosystem

In this chapter, we examined what is known about the individual effects and population impacts of spilled oil on marine mammals. We divided marine mammals into five groups (sea otters; seals and sea lions; sea cows; polar bears; and whales, dolphins, and porpoises) to allow a more complete discussion of the pertinent literature for each group and to highlight the wide differences in our understanding of the effects of oil spills and oil-related activities across groups. Most marine mammals are large animals that range widely well out to sea. They are relatively difficult to maintain in captivity for detailed study and few individuals and populations have been followed during and after an oil spill. Thus, our understanding of how oil exploration, development, production, transportation, and spills impact marine mammals is spotty. We know most about species that can be maintained in captivity or spend the majority of their life in the nearshore environment. However, even for those species, many questions persist such as:

1. Do exploration and development activities (e.g., noise and associated human activities, temporary structures, small chronic releases, and transportation infrastructure) have significant effect on individuals?
2. What are the short- and long-term effects on individuals from acute exposure to the most toxic volatile components of oil?
3. What are the long-term health effects on individuals from chronic exposure?
4. Do oil dispersants reduce or increase oil constituent exposure and related effects to individuals?
5. Do spills or development activities cause measurable impacts at the population or subpopulation level?

6. Are ecosystem-wide effects following a large spill sufficiently widespread to impact marine mammals at the population level?

Despite our limited understanding of these important questions, it remains clear that oil spills can, and frequently do, harm at least some individuals of certain species of marine mammals. The insatiable need of modern industrialized societies for large volumes of oil to drive their economies is resulting in exploration, production, and transportation of oil in heretofore unexploited areas, such as the deep ocean and the Arctic. These areas have long been sanctuaries for many marine mammals and the increase in oil-related activities in these areas significantly increases their vulnerability to potentially catastrophic impacts from a large spill or many spills over time. While other forms of energy may replace oil in the future, we expect that oil will remain a primary source of energy for decades to come. Through understanding and reducing long-term impacts of oil on marine mammal populations, we will position ourselves to better address potential population impacts from other forms of energy in the future.

The short synopses below provide some highlights from the taxa-specific sections that follow. For brevity, these synopses do not contain references to foundational literature, which is presented in the taxa-specific discussions.

18.1.1 Sea Otters

Sea otters (*Mustelidae*) are among the most vulnerable marine mammals to an oil spill because they rely on fur for insulation and spend most of their time nearshore on the sea surface where oil and the most toxic components of oil accumulate. Unlike most marine mammals, the physical effects of external oil contamination to sea otters may be as damaging as the toxicological effects. For example, during the EVOS, moderately to heavily oiled sea otters suffered from permanent injury to their eyes, pinna, and pelage from the oil and the excessive grooming they did in an attempt to remove the oil. Even small amounts of external oil fouls the insulating fur covering of sea otters and significantly increases the food required to maintain core body temperature. This is a serious health challenge for an animal that normally consumes about 25% of their body weight each day. To stave off hypothermia, oiled sea otters must consume more food and spend more time grooming. In river otters (*Lontra canadensis*), hypothermia results in (i) short- and long-term injury to the lungs, liver, kidneys, and brain from hypoxia and ischemic necrosis and (ii) reductions in foraging dive times and depths. If this is also true for oiled sea otters, then at a time when their energy needs are extreme their foraging ability is likely impaired and their internal organs are suffering permanent damage.

Long-term monitoring of moderately to heavily oiled adult sea otters kept in captivity following the EVOS demonstrated extended life-threatening problems. For example,

necropsies of these otters showed that nearly 75% had persistent interstitial emphysema and 50% had liver necrosis. The accumulation and persistence of oil in nearshore habitats preferred by sea otters, and certain seals and sea lions, result in prolonged human disturbance during the spill cleanup phase, an extended period of acute exposure, years of low-level chronic exposure, and ongoing impacts to prey resources.

18.1.2 Seals and Sea Lions

Unlike otters, our understanding of the effects of oil on seals and sea lions (pinnipeds) is surprisingly limited. Although there have been more than two dozen documented examples in which oil has contacted free-ranging pinnipeds, the difficulty in obtaining data on exposed animals has resulted in small sample sizes and limited knowledge. Due to their similar anatomy and physiology, it can be safely assumed that, except for metabolic concerns related to how these species maintain their core body temperatures, pinnipeds would respond to acute and long-term chronic exposure to oil similarly to sea otters. The mucous membranes, eyes, ears, external genitalia, and internal organ systems exposed to oil would be negatively affected. However, the magnitude of the harm and its long-term consequence to individuals and local populations remain unknown. For those pinnipeds that rely primarily on blubber for insulation, such as most sea lions, seals, and the walrus (*Odobenus rosmarus*), it appears that external oiling does not significantly impact their ability to maintain their core body temperature. The vulnerability of seals and sea lions to an oil spill probably will be determined by the degree and time course of exposure. Those species that range widely and do not congregate in nearshore waters except to breed and molt, such as elephant seals (*Mirounga spp.*), likely would be less vulnerable. In contrast, some age and sex classes of sea lions and other seals that spend most of their time nearshore and in estuaries and river mouths, likely would be more vulnerable. Fur seals, like sea otters, rely mostly on fur rather than blubber for insulation and likely would face a serious challenge in maintaining their core body temperature if oiled. Not only are individual fur seals vulnerable to spilled oil, but population-level impacts likely would occur if oil was spilled near the rookeries where these seals annually mass to breed. An ill-timed large spill in the vicinity of a fur seal breeding colony could be devastating.

18.1.3 Sea Cows

The four extant species of sea cows or sirenians, which are unique among the marine mammals in being aquatic herbivores with a limited tropical to subtropical distribution, are all considered vulnerable to extinction by the International Union for Conservation of Nature (IUCN). Although their warm water distributions overlap with some of the world's major areas of oil development, extraction, shipping, and refining, there is scant evidence oil has affected sea cows. The single

published study that examined sirenian tissue did not find any petroleum aromatic hydrocarbons (PAH). However, because vertebrates typically rapidly metabolize PAHs, this finding is not unexpected. Sirenians would be affected if spilled oil contaminated sea grasses, their primary food, or the sea grasses were destroyed during cleanup operations. However, even this effect may be temporary as oil has not been shown to persist in and severely impact tropical sea grass beds.

18.1.4 Polar Bears

Polar bears (*Ursus maritimus*) primarily rely on fur to protect them from the extreme arctic temperatures, and, like sea otters and fur seals, they are vulnerable to hypothermia if oiled during a spill. Similar to sea otters, polar bears are known to groom themselves regularly to maintain the insulating properties of their fur and an oiled bear would be expected to ingest significant quantities of oil during grooming. Laboratory observations of two polar bears forced into a pool with oil for 15 min demonstrated that indeed these marine mammals expended considerable effort to remove the oil from their body and the ingestion of that oil during grooming resulted in critically severe to terminal effects on their gastrointestinal tract, kidneys, liver, blood, and respiratory systems. Those oiled bears also showed hair loss, anemia, anorexia, acute inflammation of the nasal passages, increased metabolic rates, elevated skin temperatures, marked epidermal responses, and stress. In addition, the ingestion of oil by polar bears likely would not be confined to grooming as hungry bears would be expected to scavenge oiled wildlife and have been observed to directly consume refined oil products.

The increasing exploration, development, and transportation of oil and gas in the arctic, combined with the decreasing amount of permanent ice and frozen permafrost, suggests that polar bears, their preferred seal prey, and the oil industry soon will be squeezed closer together. It seems inevitable that a significant oil spill from a ship, pipeline, or production platform will greatly impact polar bear populations through direct mortality and impaired health of survivors. In addition, the processes of acquiring and transporting oil likely will disturb and/or displace bears and their seal prey. The risk faced by polar bears and their prey will be greatest in fall or spring during the formation or breakup of ice when bears concentrate in prime feeding areas over the continental shelf. At that time, oil would accumulate in open leads and polynyas, areas of high activity for polar bears and seals. Nevertheless, over the past 30 years there is little evidence that oil production and development in the arctic has affected polar bears.

18.1.5 Whales, Dolphins, and Porpoises

Very little is known about the effects of oil on whales, dolphins, and porpoises, collectively known as cetaceans. There are few published accounts of wild cetaceans in oiled water

and few necropsies of cetaceans that have been oiled. Oil does not adhere to their relatively slick skin and it would not be expected to accumulate in or around the eyes, mouth, blow hole, or other potentially sensitive external areas. Insulation is provided by a layer of blubber rather than hair or fur, so it is unlikely oil would compromise the thermoregulatory system of cetaceans. These marine mammals do not drink large volumes of sea water, do not groom, and likely would not scavenge oil-contaminated prey. Thus, it seems unlikely they would ingest significant quantities of oil. Probably the greatest risk to most cetaceans from an oil spill would occur if they surface to breathe in an oil slick and inhale oil and toxic petroleum vapors.

For certain species that frequent or live in nearshore waters, a spill may pose significant risk. For example, populations of coastal-oriented dolphins likely would be impacted by a spill oiling nearshore waters because they show strong site fidelity to restricted nearshore habitats. If those habitats were oiled, the dolphins could experience both acute and chronic exposure through their respiratory system and through ingestion of contaminated prey. Other coastal-oriented cetaceans, such as gray whales (*Eschrichtius robustus*), could be affected by a spill if the oil sank to the bottom, as these whales scoop up significant quantities of bottom sediments during feeding. Still, other species may be at risk from the oil and the oil cleanup operations disrupting important but fragile social bonds.

18.2 SEA OTTERS

Behavior, morphology, physiology, and natural history conspire to make sea otters exceptionally vulnerable to the effects of oil contamination. Morphologically, this species is unique among marine mammals due to their small body size and primary reliance on air trapped in their fur for insulation [11]. Both characteristics make thermoregulation in water challenging for sea otters even under normal circumstances [12]. During an oil spill, these same characteristics present a liability that leads to comparatively high levels of mortality. Coupled with a natural history that includes a reliance on nearshore habitats where oil can accumulate and persist and prolonged periods of time on the water surface for resting, feeding, grooming, and caring for young, this marine mustelid represents a species of great concern during an oil spill.

This recognition of acute vulnerability has led to numerous studies and the compilation of considerable information regarding the effects of oil exposure on sea otter health. Controlled studies have examined the impact of crude oil on sea otter fur and physiology [13–16]. Extensive field monitoring and rehabilitation of wild sea otters following the EVOS provide a remarkable resource of information for understanding the effects of acute oiling [5,6,9,17,18], as well as for treating oiled otters [19,20]. Long-term effects of subacute initial oiling and chronic exposure to oil included reduced survival [4,5,8], leading to protracted recovery of affected populations [6,9].

During the EVOS, 357 sea otters were treated at rehabilitation centers and over 100 were necropsied. These efforts resulted in a unique data set detailing the physiological and behavioral responses of a marine mammal to oil contamination (See [19] for further details). The following is based largely on this data set that involved Prudhoe Bay crude oil spilled in cold Alaskan waters. Because crude oils can vary markedly in petroleum hydrocarbon composition and toxicity, it is important to know the chemical makeup of released oil to anticipate and effectively address the likely impacts on otters. The nature of the impact, especially in terms of toxicity to animals, will differ between spills and within an individual spill as the oil weathers. Environmental factors such as air and water temperatures as well as water action will alter the composition of spilled oil and the threat it poses to otters and the environment. Shoreline habitats strongly influence the potential for oil to be sequestered in nearshore sediments and present a long-term exposure threat.

18.2.1 External Exposure

As with most marine mammals, exposure of sea otters to petroleum hydrocarbons in crude oil can occur through several routes. The most common are (i) ingestion, (ii) inhalation, and (iii) dermal absorption (Fig. 18.1). Since sea otters spend considerable time on the water surface, the first contact with an oil slick generally results in external contamination of the fur and inhalation of volatile petroleum hydrocarbons. External contamination leads to transdermal absorption of hydrocarbons, which is accompanied by ingestion of oil during grooming and feeding. These quickly lead to widespread internal contamination, which will impact many organ systems, especially those involved in detoxification and excretion [22].

In some ways, the physical effects of external oil may be as damaging to sea otters as the toxicological effects. Depending on the chemical composition of the oil, irritation of sensitive tissues including the interdigital webbing of the hind flippers, as well as membranes around the eyes, nose, mouth and urogenital areas occurs rapidly. In extreme cases, sea otters contaminated with fresh crude oil will bite irritated areas and groom excessively thereby causing permanent damage to the cornea of the eyes, tips of the pinnae, and pelage [23]. In addition, sea otters actively spread even small amounts of oil across their entire body during grooming, thereby exacerbating the problem.

The absence of an insulating blubber layer makes external oil contamination especially problematic for sea otters. Disruption of the air layer in the fur due to contact with oil destroys the heat retaining properties of the pelage and exposes the otter's skin to water. Because water transfers heat 24–25 times faster than air at the same temperature, hypothermia quickly results [24]. The typical daily fluctuations in core body temperature of wild sea otters [2] are intensified when an animal becomes oiled and rectal temperatures of oiled sea otters can fluctuate markedly during all phases of

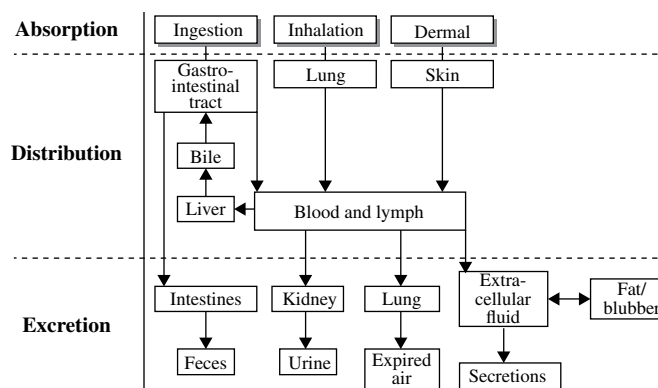


FIGURE 18.1 Major pathways for petroleum hydrocarbon movement in oiled sea otters. Following initial absorption, the chemical constituents of oil can be distributed throughout the body via the skin, gastrointestinal tract, and pulmonary and vascular systems. Petroleum hydrocarbons may be subsequently stored in the fat or blubber layers or excreted through several organ systems. Redrawn from [21] and presented in [19].

oiling and rehabilitation activities [15,20]. For example, during the EVOS, more than 36% of the sea otters arriving at rehabilitation facilities were hypothermic, with the lowest recorded body temperature reaching 8.4°C below normal levels [19]. Conversely, 27% of the arriving oiled otters were hyperthermic due to excessive grooming and hyperactivity after being removed from the water for rehabilitation.

In addition to direct mortality associated with low core body temperatures, hypothermia can instigate long-term organ damage and dysfunction in association with a general collapse of the cardiovascular system and related organ congestion. The severity of vascular congestion and tissue damage in sea otters is correlated to the degree of external oiling. The resultant reduction in blood flow to organs can lead to hypoxia and ischemic necrosis in the lungs, liver, kidneys, and brain with the former two organs showing the greatest injury [19].

The extent of the tissue damage during hypothermia will depend on a variety of factors including the duration and severity of vascular collapse, with some oxygen-sensitive organs never recovering. Consequently, while an oiled sea otter may survive a hypothermic event it may suffer permanent or long-term impaired organ function as a result of hypoxic damage. All of this may occur in the absence of internal contamination or toxic insults from the oil. Thus, responders to an oil spill should be prepared for sea otters that range widely in both internal and external levels of contamination from lightly oiled animals with high levels of internal tissue damage to heavily oiled animals that need more than washing. The level of external contamination should not be considered an accurate predictor of internal contamination [19].

18.2.2 Internal Exposure

Oiled sea otters display a suite of medical disorders related to the toxicity of the oil encountered (Table 18.1). As might be expected, heavily oiled otters contaminated early in a

TABLE 18.1 Medical disorders of oiled sea otters during the early (toxic) phase and later (nontoxic) phase of an oil spill

Early phase

1. Thermoregulatory disorders (hypothermia, hyperthermia)
2. Petroleum hydrocarbon toxicosis
3. Respiratory injury/interstitial and subcutaneous emphysema
4. Hypoglycemia
5. Shock/seizures

Late phase

1. Gastrointestinal disorders
2. Hepatic dysfunction
3. Renal dysfunction
4. Anemia
5. Stress

Category designations are based on the level of PAHs present in the oil and the assumption that crude oil will weather over time.

spill show the severest medical problems and consequently, the highest rate of mortality. As the oil dissipates and the level of PAHs declines with weathering, the severity of disorders diminishes. Four commonly diagnosed disorders in oiled otters requiring immediate veterinary intervention are (i) hypothermia and hyperthermia as discussed earlier, (ii) hypoglycemia, (iii) subcutaneous and interstitial emphysema, and (iv) gastrointestinal injury.

Wild sea otters compensate for their exceptionally high metabolic demands by relying on a predictable schedule of food intake for thermoregulation [12]. If feeding is impaired, as can occur during a spill, sea otters are prone to hypoglycemia (abnormally low blood glucose levels). Underlying reasons for the development of this condition vary and may involve an inability to forage or find prey in a spill zone, impaired liver function or intestinal absorption following contamination, fasting during capture and transport for rehabilitation purposes, or stress/shock. Regardless of the cause, hypoglycemia will contribute to thermoregulatory and metabolic problems as well as seizures in oiled sea otters.

Respiratory distress is common in oiled sea otters and was especially apparent during the first 3 weeks of the EVOS (Fig. 18.2). Injury to respiratory tissues ranges markedly in severity from irritation of the nasopharyngeal membranes and sinusitis to bullous subcutaneous and interstitial emphysema. The subcutaneous emphysema is characterized by air pockets detected on palpation below the skin along the axillary region, and in the most severe cases along the sides of the neck, thorax, and spine [19]. Postmortem examination of oiled sea otters has demonstrated that the air forming subcutaneous emphysema bullae may originate from ruptured membranes in the lungs.

The pathogenesis of emphysema in oiled sea otters is not completely understood. Several contributing factors have been identified and include weakening of the respiratory mucosa by petroleum hydrocarbon exposure coupled with forcible inhalation/exhalation. Ventilatory exertion, as may occur with respiratory distress or with pre- and post-dive periods during foraging, has been implicated in the development of spontaneous emphysema in diving humans [25]. A similar mechanism may explain the development of this condition in oiled sea otters. In addition, the incidence of both interstitial and subcutaneous emphysemas during the initial weeks of the EVOS (Fig. 18.2) suggests that the inhalation and dermal absorption of volatile petroleum hydrocarbons were the underlying causes.

Chemical composition of the oil and environmental factors associated with oil weathering will obviously alter the timeline for respiratory injury in sea otters. Lighter aromatic hydrocarbons (i.e., benzene, toluene, xylene, and ethylene) may evaporate over a period of days to weeks in an acute spill depending on water and air temperatures. In some cases, as in Alaska following the EVOS, toxins from unweathered oil have persisted for decades [4].

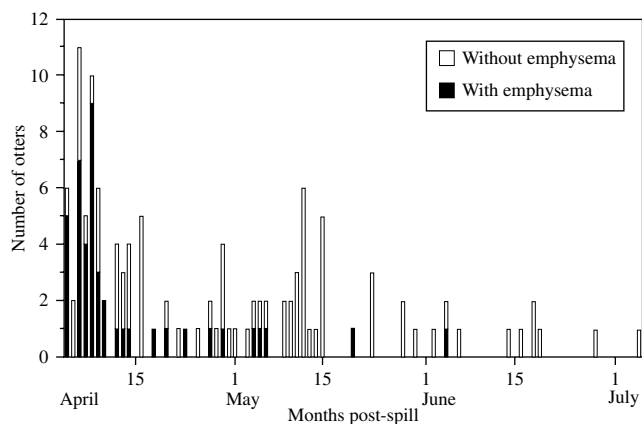


FIGURE 18.2 The incidence of interstitial and subcutaneous emphysema in sea otters in relation to date following the March 24, 1989 EVOS. Height of the bars indicate the total number of otters with (black bars) and without (white bars) evidence of emphysema following necropsy. Note the decrease in occurrence of emphysema three weeks after the spill. From [19].

Such chemical compounds are considered the most toxic of the major classes of petroleum hydrocarbons in crude oil and are known to cause damage to the lungs and mucous membranes of the airways [26]. In Alaska, more than 80% of the documented cases of emphysema in sea otters occurred within 14 days of the grounding of the *Exxon Valdez*. During this period, nearly 70% of the sea otters that died exhibited some form of interstitial emphysema. In contrast, continued release of fresh crude oil in a chronic event such as the DWH spill in the Gulf of Mexico will prolong the period of exposure to tissue damaging chemical compounds. Clearly, the acute or chronic nature of a spill must be considered in assessing potential impacts on the respiratory system as well as other organs and organ systems.

The last of the four major disorders, gastrointestinal injury, is a common problem in oiled sea otters throughout rehabilitation, and affects the ability of the animals to process food. Focal hemorrhaging and ulceration are most evident in the stomach (Fig. 18.3) rather than the intestines, suggesting a hypothermic event rather than toxic lesions per se [27]. Gastrointestinal erosions also occur in stressed sea otters whether the animal has undergone a hypothermic event or not. Based on these findings, the combined effects of hypothermia, stress, shock, captivity during rehabilitation, and overall oil contamination rather than oil ingestion are the primary factors leading to gastrointestinal injury in oiled sea otters [17,18].

In addition to these major disorders, oiled sea otters may display a variety of behavioral problems and symptoms. Seizures, lethargy, hyperactivity, labored breathing, and anorexia have all been documented for sea otters with different degrees of external oiling. Many of these are symptomatic of underlying organ damage. For example, liver dysfunction associated with tissue necrosis due to vascular congestion and oil toxicity has been reported for heavily oiled sea otters. While impairing the animal's ability to assimilate food, damage to the liver also impedes

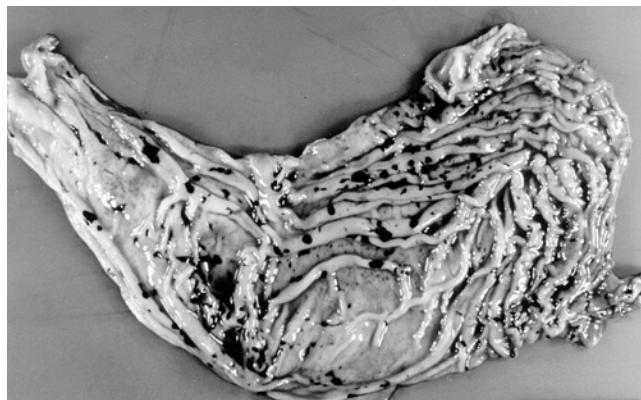


FIGURE 18.3 Internal surface of the stomach of an oiled sea otter showing areas of focal hemorrhage. Although similar in color, the dark areas are hemorrhage sites not ingested crude oil. From [19].

its role in detoxifying and excreting foreign chemicals, such as oil. Acute renal insufficiency due to injury to the kidneys can also impair the ability of the animal to excrete toxicants [19].

Adrenal hyperplasia, immunosuppression, and anemia have been identified as potential problems for other oiled wildlife, particularly during rehabilitation [28–30]. Of these, anemia can be a long-term problem for oiled sea otters and will dictate the timing of release from rehabilitation programs due to impaired diving capabilities associated with this condition. The combined effects of stress and oil toxicosis instigate many of these conditions and illustrate the range of insults that may affect the health of sea otters during an oil spill event and affect the success of its reintroduction to the wild following rehabilitation.

18.2.3 Long-Term Effects

The incidence and duration of injury to various organ systems following oil contamination will differ in sea otters according to the toxicity of the oil, duration of exposure, original health of the animal, environmental conditions, and organ-specific recovery rates [19]. It is also important to note that there is no “typical” clinical, macroscopic, and microscopic profile for oiled sea otters. Not all otters will exhibit the same symptoms or spectrum of lesions nor recover along the same timeline. In addition, as noted earlier, the response to acute and chronic exposure to oil will differ. Despite these caveats, several noteworthy trends regarding tissue damage have been observed.

Interstitial and subcutaneous emphysema, gastrointestinal lesions, and severe organ congestion associated with hypothermia are most likely to occur in the presence of volatile petroleum hydrocarbons characteristic of fresh crude oil. The incidence and severity of these injuries are often limited to the first few weeks of a catastrophic spill and are most evident in heavily oiled otters. Organ dysfunction concomitant with vascular congestion may persist for several months and in some cases will result in permanent damage to kidney and liver function in sea otters.

Anemia is another long-term condition that may develop days to weeks after the original exposure to oil. The condition may persist for over 3 months in severely oiled otters and can hinder release back to the wild. Prolonged anemia represents a challenge for the foraging animal because oxygen stores in the blood are important for supporting aerobic diving by sea otters [31]. For another species of otter, the North American river otter, anemia associated with oiling resulted in fewer dives and a potential decrease of 64% in the capture rate of prey [32]. Thus, the severity and duration of anemia associated with oil exposure may ultimately dictate the ability of contaminated as well as rehabilitated sea otters to survive in the wild.

Lastly, long-term monitoring of moderately to heavily oiled adult sea otters that were placed in aquariums following

the EVOS has demonstrated several conditions that can remain life-long problems. Nearly 75% of these captive otters showed evidence of persistent interstitial emphysema upon necropsy 10 years later. Liver necrosis was found in half of the animals (T.M. Williams, unpublished data). Either condition would have challenged the survival of the otters in the wild had they been released.

Continued observation of wild sea otters in the oil spill zone of Prince William Sound has demonstrated the exceptional persistence of crude oil and oiling effects across decades and generations of sea otters [6]. Specifically, elevated mortality across age classes, including those born after the spill, has resulted in decreased survival compared to unexposed populations and coincident long-term population effects [5]. These effects have persisted for more than two decades with chronic mortality losses approaching or exceeding the acute mortality of sea otters immediately following the oil spill. Exposure rates to lingering oil approached over 24 contact times per year for some individual sea otters in 2011–2012 [9]. Overall, the results of recent studies suggest that residual oil can affect wildlife populations on time scales much longer than previously believed and that the cumulative chronic effects can be as significant as acute effects [8].

In summary, sea otters are one of the most vulnerable mammalian species to the impacts of oil contamination. This is evident from the wide variety of medical problems encountered following experimental and accidental oiling, and the protracted period of individual and population recovery. The EVOS was the first oil spill to impact large numbers of sea otters, and neither the response nor the wildlife community were adequately prepared to fully address the suite of problems that ensued. With knowledge gained during the EVOS, advancements in treatment protocols, and increased, response capabilities and resources following the passage of the Oil Pollution Act of 1990, wildlife personnel are better equipped to address oiled sea otters in a future oil spill. In addition, this increase in resources and knowledge will help us to better understand population-level effects. However, the unique biology, behavioral patterns, and nearshore distribution of sea otters ensures that they will remain a species at high risk during an oil spill.

18.3 SEALS AND SEA LIONS

Seals and sea lions, collectively called pinnipeds, are marine mammals of the order Carnivora. They are distributed from the poles to the tropics and are the most amphibious marine mammal group. Pinnipeds spend hours to months at sea foraging and return to land or ice to rest, molt, and reproduce. This group includes three families and 36 species: the Otariidae comprises 16 fur seal and sea lion species; the Phocidae, or true seals, contains 19 species; and the Odobenidae is represented by a single species, the walrus.

Our understanding of the impact oil has on pinnipeds is surprisingly limited. Oil has been documented to come in contact with free ranging pinnipeds at least 30 times, but small sample sizes and difficult field conditions have precluded any definitive conclusions about the effect of the oil [33]. Researchers have followed oiled and unoiled animals of two species after a spill, but have not been able to detect a difference in survival between the oiled and unoiled individuals [34,35]. Further, while some animals were found dead with oil on them, it was not possible to clearly identify the cause of death [34,35]. Even the well-studied EVOS produced equivocal results. For example, 81% of the 585 harbor seals observed during or after the EVOS were reported to have been oiled, and based on data from subsequent aerial and boat surveys, investigators concluded that 302 harbor seals died as a result of the spill [36]. However, subsequent studies found that harbor seals are more mobile than previously assumed and suggested that the missing individuals may have migrated out of the affected area and were not necessarily dead [37]. Finally, observations of Steller sea lion (*Eumetopias jubatus*) colonies within the spill zone were not able to detect an effect on that species [38]. While definitive impacts have been hard to document, the limited amount of data precludes distinguishing between no effect versus an effect that we were unable to document. Furthermore, while acute impacts of oil contamination are the most obvious and easiest to quantify, the persistence of hydrocarbons in the environment can result in continued exposure for many years after an oil spill [4,9,39]. This chronic exposure can lead to both direct effects on the health of the individual animal, as well as to the indirect effects of chronic contamination that reduces prey availability. Together these effects can cause a reduction in population viability and/or recovery such as has been reported for sea otters after the EVOS [9,39].

18.3.1 Direct Effects

Direct contact with oil can impact pinnipeds in a variety of ways. Oil can coat all or portions of their body surface, they can inhale hydrocarbons, and they can ingest oil directly or in oil-contaminated prey [33]. As sea lions and seals rely on blubber for insulation, their thermoregulatory ability does not seem seriously hampered by contact with oil [40]. However, observations suggest that some individuals have become so encased in oil that they were not able to swim and subsequently drown [36,41]. Studies designed to mimic the small amounts of oil that might be ingested by animals in the wild have been carried out with harp (*Pagophilus groenlandicus*) and ringed (*Pusa hispida*) seals [42,43]. Ingested oil was passed in the feces and the exposed animals were more vocal than control animals. Some changes in liver enzyme levels were noted, but upon euthanasia no relevant organs lesions were observed. Ringed seals placed in a seawater pen with the surface covered with crude oil for 24 h did not ingest the oil, but did exhibit changes in their respiratory

epithelium consistent with inhalation of oil fumes [44]. Some of the oil-exposed seals exhibited liver and kidney pathologies. The eyes, oral cavity, respiratory surfaces, and anal and urogenital surfaces were particularly sensitive to prolonged contact with oil [33]. Behavioral studies have shown that while pinnipeds should be able to detect oil through vision and/or smell they apparently do not avoid oil [33]. They are therefore likely to come in contact with oil if it comes into their habitat. Of the pinnipeds, fur seals, which rely almost entirely on their fur for insulation, are far more sensitive than other species to oiling [40]. Heat transfer doubled in fur seal pelts after oiling, whereas pelts from California sea lions (*Zalophus californianus*), bearded (*Erignathus barbatus*), and Weddell (*Leptonychotes weddellii*) seals showed no change [40]. Further, juvenile northern fur seals (*Callorhinus ursinus*) exhibited a 50% increase in heat loss in water after one-third of their body surface was contaminated with Prudhoe Bay crude oil [45].

18.3.2 Vulnerability and Risk

The potential impact of an oil spill is determined by the probability of coming in contact with the oil and the sensitivity of the species. A population of a sensitive species may never be seriously impacted if its distribution and life history patterns result in very low contact with an oil spill, whereas a population of a relatively insensitive species may be seriously impacted if it is consistently exposed. The worst-case scenario would be for a sensitive species to have a life history pattern or distribution that increases the probability that the majority of the species' entire population could come into contact with oil [46,47]. This is the scenario facing northern fur seals, a relatively sensitive pinniped species to oiling in which much of their breeding population becomes concentrated on a few breeding colonies. During the months of June through November, with a peak in late June and early July, this species aggregates on their largest breeding colonies on the Pribilof Islands (St. Paul and St. George) [48]. During that time, over 80% of the population is on and around the shorelines of these two islands. A moderate-to-large oil spill during the breeding season in the vicinity of these islands could be catastrophic, potentially decimating this species [48]. The various Antarctic fur seal species (*Arctocephalus* spp.), which like their northern cousins rely on air trapped in their fur for insulation, are equally sensitive to the effects of oiling. However, they are not as vulnerable because their breeding colonies are much more widely distributed around the southern oceans. Nevertheless, any single population could be seriously impacted if a spill occurs during the breeding season when the seals are concentrated at their colonies.

In 1990 an excellent overview of the timing of breeding patterns and general distribution of pinnipeds in the context of a potential oil spill was published [47]. For many species, little has changed in our understanding of their migratory and habitat utilization patterns since that time. However, for

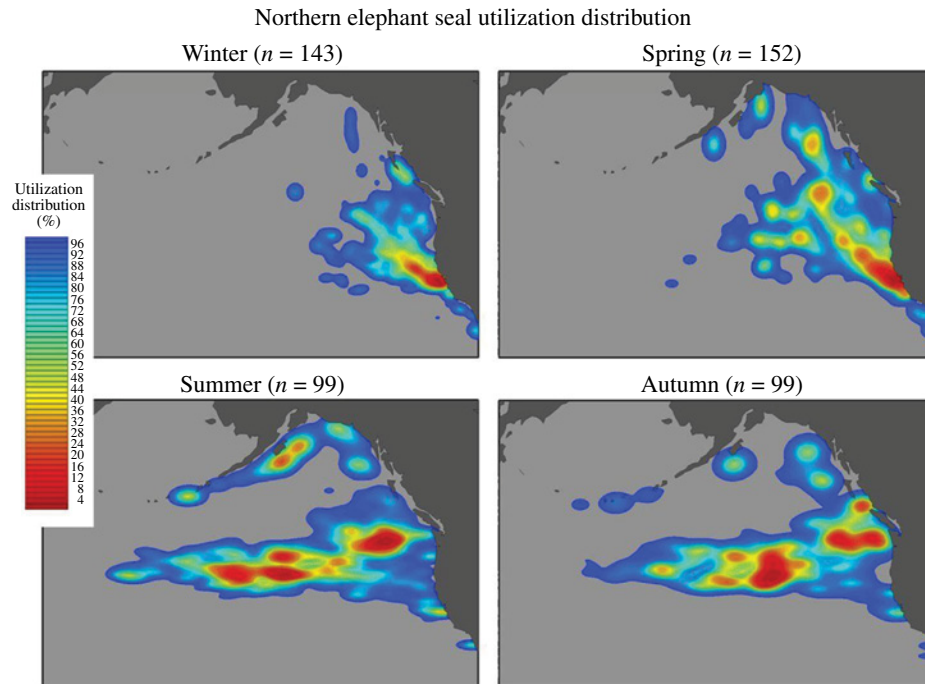


FIGURE 18.4 The seasonal distribution of female northern elephant seals based on movement of ARGOS satellite tagged individuals. It is predicted that these seals will be least vulnerable to an oil spill during summer and autumn when they range most widely offshore.

elephant seals and some fur seals and sea lions there has been a significant increase in knowledge of their movements and habitat utilization patterns [49–55]. In particular, we now know that the seasonal distribution of female northern elephant seals (*Mirounga angustirostris*) is quite variable with some regions of their preferred habitat completely unoccupied during certain seasons (Fig. 18.4). While an analysis of the migratory and habitat utilization patterns of pinnipeds is beyond the scope of this chapter, broad general patterns can be described. Pinnipeds can be classified into migratory and nonmigratory and ice versus land breeding. These differences are further constrained by differences in the breeding biology of the different families.

Unlike cetaceans, pinnipeds are constrained by the need to breed on land or ice, which conflicts with the need to forage at sea. The separation between breeding and feeding habitats has led to the evolution of two general life history patterns. Many phocid (true seals) mothers remain with their pups throughout lactation fasting from birth to weaning. Some phocids, most notably harbor, ringed, and Weddell seals, feed during lactation. Weaning is abrupt and occurs after a minimum of 4 days of nursing for hooded seals (*Cystophora cristata*) to a maximum of 7 weeks for Weddell seals. In contrast, otariid (sea lions and fur seals) mothers stay with their pups for only the first week or so after parturition and then periodically go to sea to feed, returning to suckle their pup on the rookery. Feeding trips vary from 1 to 7 days depending on the species, and shore visits to the pup last 1–3 days. Pups are weaned from a minimum of 4 months in the subpolar fur seals and northern fur seal and up to

3 years in the equatorial Galapagos fur seal (*Arctocephalus galapagoensis*). The remaining otariids breed in temperate climates. In these species, pups are usually weaned within a year of birth, although weaning age can vary both within and between species as a function of seasonal and site specific variations in environmental conditions. For walruses, lactation can last up to 3 years, and the calves stay with or in the vicinity of the mother while she feeds on the benthos [56]. Overall, the breeding characteristics of phocid mothers and their pups make them less susceptible, and otariid mothers and their pups more susceptible to a coastal or near colony oil spill.

The feeding and movement pattern of pinnipeds directly affects their susceptibility to an oil spill. For example, northern elephant seals forage hundreds to thousands of kilometers offshore, while a nursing California sea lion remains relatively close to the coast moving only tens to hundreds of kilometers (Fig. 18.5). Susceptibility is also complicated by differences in the seasonal migratory patterns. During the breeding season, northern and Antarctic fur seals are restricted to a discrete area near the colony, but once the 4-month lactation interval is over, they are highly pelagic, foraging hundreds to thousands of kilometers from their breeding colonies. In contrast, other sea lions and fur seals tend to forage in the coastal zone along the continental shelf [56]. While highly migratory species are likely to leave the area of an oil spill, resident nonmigratory animals will be more susceptible to both the acute and chronic effects of an oil spill. Long-term chronic effects result from direct impacts on their health as well as indirect effects associated with alterations in marine

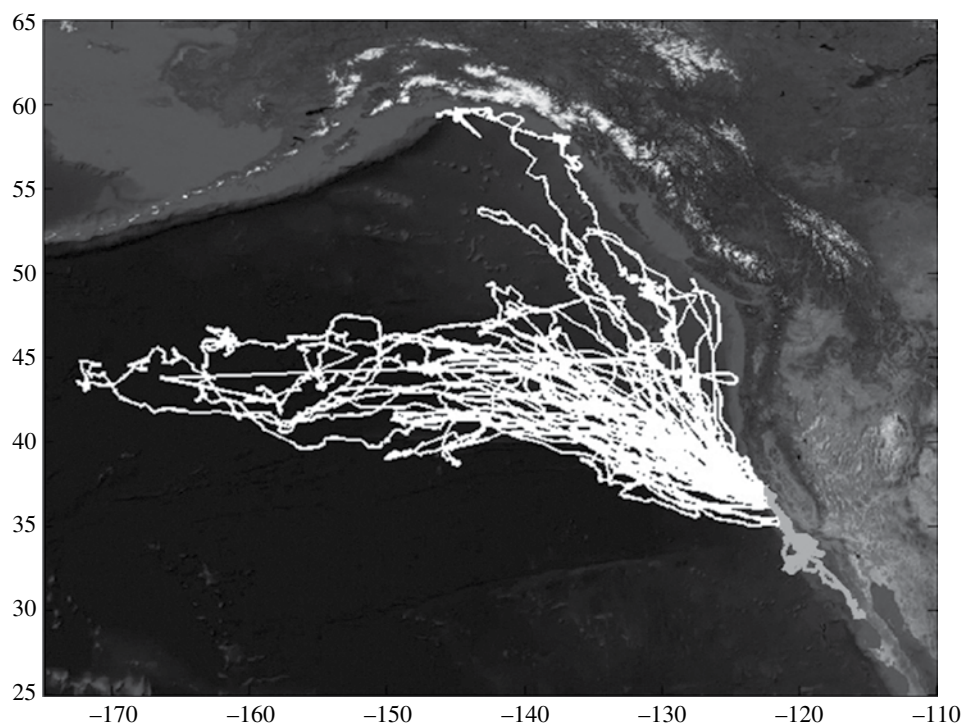


FIGURE 18.5 ARGOS satellite tracks of foraging trips of capital breeding female northern elephant seals (in white) compared to foraging trips of lactating California sea lions (in gray). Elephant seals were foraging from the Año Nuevo colony, California [57], and sea lions from colonies on San Miguel Island, Southern California (Robinson and Costa, unpublished). These foraging patterns strongly indicate California sea lions are more vulnerable than northern elephant seals to an oil spill off the California coast.

food webs, which may result in reductions in prey or increases in predation [4,9,39]. Differences in foraging behavior will also result in differences in exposure after an oil spill. Populations of sea otters and sea ducks have been slow to recover in areas that were oiled compared to areas that were not oiled. The slow recovery is thought to be associated with the continued exposure to oil that has persisted in the sediments years after the EVOS [9,39]. Thus, organisms that feed on nearshore benthic prey are likely to be at greater risk than species that feed in the water column. As such, we might speculate that as a benthic forager, walrus and bearded seals would be, like sea otters, likely to suffer from chronic exposure if there was an oil spill in their foraging grounds.

In summary, pinnipeds are a diverse taxonomic group that is quite variable in their vulnerability to oil contamination. Fur seals are the most vulnerable, with seals and sea lions less sensitive to direct contamination. However, all pinnipeds are likely to be effected by persistent exposure to hydrocarbons consumed in their prey as well as to any reductions in prey availability associated with an oil spill.

18.4 SEA COWS

Sea cows, in the mammalian order Sirenia, include three species of manatees (family Trichechidae) and the dugong (*Dugong dugon*; family Dugongidae). Unlike all other

marine mammals, the extant sirenians are aquatic herbivores limited to tropical and subtropical waters. All four species are of considerable conservation concern and are categorized by the IUCN as “vulnerable,” indicating a high risk of extinction in the wild. Recent comprehensive reviews of the ecology, evolution, and conservation of the Sirenia are available [58,59]. The dugong is exclusively marine and is found in shallow nearshore waters of the Indo-Pacific, the West African manatee (*Trichechus senegalensis*) is euryhaline and occupies coastal and inland waters of the tropical Atlantic coast of Africa, the Amazonian manatee (*Trichechus inunguis*) occupies freshwater habitats of the Amazon Basin and the euryhaline West Indian manatee (*Trichechus manatus*) is found in coastal bays and inland rivers from coastal Brazil to the southeastern United States.

The warm waters within the ranges of the sirenians include some of the world’s major areas of oil development, extraction, shipping, and refining. Examples include facilities in the Gulf of Arabia (dugong), the Gulf of Mexico and the Orinoco Petroleum Belt of Venezuela (West Indian manatee), oil fields in the Amazon Basin (Amazonian manatee), and offshore development in Nigeria and Angola (West African manatee). Despite this juxtaposition of sirenians and oil development, there has been very limited documentation of effects of oil spills on sirenians.

18.4.1 Direct Effects

There have been no published accounts that provide conclusive documentation linking deaths of sirenians to oil spills. There is circumstantial evidence suggesting that about 150 dugongs died as a result of the 1983–1984 Nowruz oil spill in the Arabian Gulf, one of the largest oil spills in history [60,61]. Dugong deaths were noted coincident with this event (37 dead strandings on shores of Saudi Arabia and Bahrain), but no necropsy data were gathered [60–62]. Similarly, in 1991, 14 dugongs were seen dead in the region encompassed by the Gulf War oil spill [63]. No West Indian manatee deaths due to oil or dispersants were confirmed during the 2010 DWH spill in the Gulf of Mexico.

Both the immediate and the long-term chronic effects of exposure to oil are unknown for sirenians. The only published study that examined sirenian tissues for the presence of PAHs and related compounds did not find any of these chemicals [64], which is not surprising as vertebrates are known to efficiently metabolize aromatic hydrocarbons [65,66]. Additionally, this study was not conducted during a major spill nor did it involve sirenians suspected of being exposed to oil. Similarly, no information exists related to potential sublethal effects of exposure to oil on sirenians. Toxic effects of oil and associated vapors on the eyes and respiratory system would likely be similar to those seen in other marine mammals [26,67,68]. The skin of sirenians has a thick dermis and lacks a pelage coat. However, the sparsely distributed sensory hairs may have a function in orientation [69,70] that could be negatively affected if coated in oil. Sirenians spend considerable time with muzzles in the sediment while feeding, and manatees feed on shoreline vegetation [58], so ingestion of residual oil and associated dispersants can be expected in areas impacted by oil spills. While the effects of oil ingestion on sirenians are undocumented, it seems likely they would respond like other large mammalian herbivores. Horses, like sirenians, are hindgut digesters and seem to be more tolerant of oil ingested in water than ruminants. In contrast, horses seem to be more susceptible to oil ingestion from soil than ruminants [71]. Sirenians can be very susceptible to collisions with boats and entanglement in ropes and lines [58,72]. When spills occur in areas frequented by sirenians, response personnel must take extra care to avoid collisions with manatees or dugongs and regularly monitor potential shoreline entanglement hazards resulting from oil recovery efforts.

18.4.2 Indirect Effects

An oil spill could have substantial impact on sirenians by reducing the abundance and quality of their food. Oil has been experimentally shown to cause mortality and sublethal harmful effects on freshwater aquatic vegetation consumed by manatees in the Amazon and elsewhere [73], and oil spills have impacted sea grass meadows in areas used by dugongs or

manatees [60,61,74]. In addition, major diebacks of sea grass beds and multiple short-term toxic effects of oil and dispersants on aquatic vegetation have been documented from oil spills [75–77]. However, the effects of oil on sirenian food resources in tropical climates may not persist for long periods as evidenced by the substantial recovery of sea grasses in the Gulf of Arabia 1 year after the Gulf War spill [78].

Faced with a substantial reduction in food quantity or quality, some sirenians may move to other feeding sites. However, this option may not be available to all individuals given the considerable heterogeneity in scales of movement exhibited by sirenians and the degree of an individual's familiarity with potential alternative unimpacted feeding areas [79,80].

18.5 POLAR BEARS

Polar bears occur throughout the Arctic. There are 19 recognized subpopulations with a total population of 20,000–25,000. About 60% of the bears occur in Canada [81]. In Alaska, they have been observed as far south in the Bering Sea as St. Matthew Island and the Pribilof Islands, but they are most commonly found within 180 mi of the Alaskan coast of the Chukchi and Beaufort seas, from the Bering Strait to the Canadian border. Two stocks occur in Alaska: the Bering–Chukchi seas stock without a reliable population estimate and the southern Beaufort Sea stock with an estimated 1526 bears [82].

18.5.1 Direct and Indirect Effects

Polar bears primarily rely on their fur to protect them from the extreme arctic temperatures. Oil significantly reduces the insulating value of fur and, if not removed, an oiled bear would be unable to survive the resulting heat loss [83]. Polar bears are known to groom themselves regularly to maintain the insulating properties of their fur and an oiled bear would be expected to ingest significant quantities of oil during the grooming process [84]. In 1981, three polar bears were forced into a pool of oil for 15–50 min and observed [83]. Immediately upon exiting the pool, the bears began licking oil from their paws and forelegs, and for the next 5 days, they regularly groomed their fur attempting to remove the oil. After 26 days, one bear died, another was euthanized 3 days later, and one recovered. Necropsies of the two bears that died revealed gastrointestinal fungus-containing ulcers, degenerated kidney tubules, low-grade liver lesions, biochemical changes indicative of stress, depressed lymphoid activity, and liver and kidney failure [83]. Other observed effects included loss of hair, anemia, anorexia, acute inflammation of the nasal passages, increased metabolic rates, elevated skin temperatures, marked epidermal responses, and stress [85,86]. A bear living and feeding near a recent oil spill likely would be exposed to the toxic volatile components of a

spill and may suffer substantial damage to the respiratory and central nervous systems and mucus membranes.

Polar bears are curious and are likely to investigate oil spills and oil-contaminated wildlife [84,85]. Hungry bears are likely to scavenge oil-contaminated seals, as they have shown no aversion to eating and ingesting oil [85,86]. Polar bears may even be attracted to oil as some bears have chosen to consume various refined hydrocarbon products such as antifreeze and hydraulic fluids, which in some instances resulted in death [87].

Polar bears feed on ringed and bearded seals and it seems likely that a large oil spill in the vicinity of these seals would have the same effect on them as the EVOS had on harbor seals [8,88–91], but see Ref. [37]. The spill would either result in high mortality of the seals and a glut of easily available toxic prey or the seals would leave the area and create a prey shortage for the bears. Even if high mortality resulted in an initial glut of prey, that bounty would soon become a prey shortage if the spill was sufficiently large or potent [14,92].

18.5.2 Vulnerability and Risk

The Arctic distribution of polar bears overlaps with many active and planned oil and gas operations within 25 mi of the coast or offshore. Although no major oil spills in the marine environment have occurred within the range of polar bears, terrestrial pipeline spills have occurred in the vicinity of polar bear habitat and denning areas (e.g., Komi Republic, Russia 1994) [93]. The largest terrestrial Alaskan oil spill came from a corroded pipeline leak in the North Slope oil fields in March 2006. This leak released an estimated minimum 4785 barrels of oil. There were no known impacts to polar bears [94]. Despite numerous safeguards to prevent spills, an average of 70 oil and 234 oil waste product spills occurred each year between 1977 and 1999 in the North Slope oil fields [91]. The Bureau of Ocean Energy Management (formerly the Minerals Management Service) [95] estimated there was an 11% chance that the Beaufort Sea Multiple Lease Sale would result in a marine oil spill greater than 1000 barrels.

Expansion of Arctic circumpolar oil and gas development, coupled with expansions in shipping and development of offshore and land-based pipelines, increases the probability that an oil spill will negatively affect polar bears and/or their habitat [91,96,97]. Future declines in the Arctic sea ice are likely to result in increased tanker traffic in high bear use areas, which would increase the chances of an oil spill from a tanker accident, ballast discharge, or discharges during the loading and unloading of oil [98]. The additional open water ship traffic also may disturb the movement patterns of polar bears and their prey [99]. A 5912-barrel oil spill scenario, the largest spill thought possible from a pipeline in polar bear habitat from the Northstar offshore oil production facility in the southern Beaufort Sea, was modeled [100]. For the purposes of the scenario, it was assumed that a polar bear would die if it came in contact with the oil. The study estimated that 0–27 bears could potentially be oiled during the open water

conditions in September and from 0 to 74 bears during the mixed ice conditions in October. The number of polar bears affected would be highest if the spill spread to areas of seasonal polar bear aggregations in the fall, such as the area near Kaktovik, Alaska, and could result in a significant impact to the southern Beaufort Sea population.

Spills in fall or spring during the formation or breakup of ice present the greatest risk to polar bears because of difficulties associated with cleanup during these periods and the presence of bears in their prime feeding areas over the continental shelf. The release of oil trapped under the ice from an underwater spill during the winter or from incomplete cleanup of a spill during the previous year could be catastrophic during spring breakup [101]. During the autumn freeze-up and spring breakup periods, any spilled oil in the marine environment would be expected to concentrate and accumulate in open leads and polynyas, areas of high activity for polar bears and seals, where both would be oiled [84,100,101]. In autumn, bears are not only found in more vulnerable areas but they are also two to five times more abundant nearshore compared with summer [102]. This trend has been increasing in recent years in the Beaufort Sea [103].

During the summer open water season, most polar bears remain offshore in the pack ice and are not typically present in high vessel traffic areas. Barges and vessels associated with industry activities travel in open water and avoid large ice floes. During the ice-covered season, mobile, nondenning bears would have a higher probability of encountering oil or other production wastes than the nonmobile, denning females.

Documented direct impacts on polar bears by the oil and gas industry during the past 30 years are minimal and the mortality that has occurred has been associated with human–bear interactions as opposed to a release of oil. However, oil and gas activities are increasing as development continues to expand throughout the U.S. Arctic and arctic regions of Russia, Canada, and Greenland, including polar bear terrestrial and marine habitats. Disturbance from activities associated with oil and gas development could result in direct or indirect effects on polar bears and their habitat. Direct disturbances include displacement of bears or their primary prey due to the movement of equipment, personnel, and ships through polar bear habitat. Female polar bears tend to select secluded areas for denning, presumably to minimize disturbance during the critical periods of pregnancy and early cub development. Direct disturbance may cause abandonment of established dens before cubs are fit to leave. For example, expansion of the network of roads, pipelines, well pads, and infrastructure associated with oil and gas activities may force pregnant females into marginal denning locations [104,105]. The potential effects of human activities are much greater in areas where there is a high concentration of dens such as Wrangel Island, Russia. Although bear behavior is highly variable among individuals and sample sizes are small, some denning bears have shown a degree of tolerance to human activity [106].

It is reasonable to assume that full-scale industrial activities in the waters off the North Slope will have a cumulative negative impact on polar bears. Such cumulative effects would be expected to displace bears and ringed seals from preferred habitats, increase mortality, and decrease reproductive success. When the predicted effects of climate warming are also factored in, the cumulative impacts on polar bears and ringed seals are likely to result in serious population-level concerns [92]. However, others believe that given the limited geographical scope of industrial activities when combined with proper management controls, the potential for catastrophic population-level effects on polar bears from oil and gas exploration and development activities is probably low [104–106]. Regardless, increased industrial activities in the Arctic marine environment coupled with increasing vessel traffic will require ongoing vigilant monitoring and increased preparedness to reduce the potential risk to polar bears and other Arctic marine mammals.

18.6 WHALES, DOLPHINS, AND PORPOISES

Whales, dolphins, and porpoises, collectively known as cetaceans, are marine mammals of the order Cetartiodactyla. These animals are restricted to aquatic habitats for their entire lives. The group includes about 88 species of toothed and baleen whales. The 74 species of toothed whales, the Odontoceti, include sperm whales (*Physeter macrocephalus*), pygmy and dwarf sperm whales (*Kogia breviceps* and *K. sima*, respectively), beaked whales (Ziphiidae), narwhals (*Monodon monoceros*), belugas (*Delphinapterus leucas*), dolphins (*Delphinidae*), river dolphins, and porpoises (*Phocoenidae*). The 14 species of baleen whales, the Mysticeti, include right whales (*Eubalaena spp.*), gray whales, and rorquals such as blue (*Balaenoptera musculus*), fin (*B. physalus*), and minke whales (*Balaenoptera acutorostrata* and *bonaerensis*).

Cetaceans can be exposed to crude and weathered oils through direct contact with the skin, eyes, mouth, and blowhole(s), and they can also inhale volatile petroleum fractions at the water's surface, ingest oil directly, and consume oil components in food [84,107]. They are thought to be at risk from oil in marine and some freshwater environments because they lack the ability to leave the water to avoid oil, their fish and invertebrate prey can become oiled, and cetaceans must surface periodically to breathe, potentially bringing them into contact with floating oil and volatile toxic components. Nevertheless, comparatively little is known about the effects of oil on cetaceans, as there have been few oil exposure experiments, only a small number of reported observations of wild cetaceans in or near oil, and little published information from necropsies of carcasses of cetaceans known to have been exposed to oil.

Based in part on the scant records of cetacean mortalities associated with oil spills from 1969 to 1989, it has been suggested that an oil spill may only affect small numbers of cetaceans [108]. Other reasons proffered for their potentially

low vulnerability are that cetaceans appear to be able to detect oil. They lack hair or fur so oil does not compromise their insulation, their skin is nearly impermeable to the components of oil, they do not drink large volumes of sea water and would not ingest much oil, their foraging strategies likely do not include scavenging on oil-killed prey, and the toxic volatile components of oil can dissipate quickly so exposure to toxins through inhalation may be minimal.

18.6.1 Direct Effects

Oil does not readily penetrate cetacean skin, which is characterized by tight intercellular bridges and an unusually thick epidermis, 10–20 times that of humans [107]. Experimental direct application of various petroleum fractions to dolphin skin resulted only in subtle histological changes, which were reversed within a week of exposure [26]. The absence of hairs and the frequent sloughing of skin cells provide little opportunity for oil to adhere to cetacean bodies.

Few surveys have evaluated the presence and nature of petroleum constituents in cetaceans [107]. Low concentrations of PAHs were detected in muscle of 26 harbor porpoises in the United Kingdom [109]. Low concentrations of low molecular weight PAHs were found in the blubber of seven stranded sperm whales in the southern North Sea and in muscle from five species of cetaceans from the Northwest Atlantic, including beluga, sperm whale, minke whale, common dolphin (*Delphinus delphis*), and Atlantic white-sided dolphin (*Lagenorhynchus acutus*) [110,111]. Large variations in PAH concentrations were found in gray whale stomachs [112].

Cetaceans primarily feed on live invertebrate or vertebrate prey. They are not scavengers, so it is not likely they will consume petroleum compounds in food that has died from oil exposure. However, it is possible that cetaceans could capture prey contaminated with oil, but which had not died, or they might ingest oil inadvertently while digging into sediments in search of prey.

Potential indirect impacts of oil on feeding of baleen whales were investigated through exposure of baleen plates to oil. The structural and chemical integrity of isolated baleen plates of seven species of whales were reported to remain intact when they were soaked in crude oil, gasoline, or tar over long periods. When plates were exposed to oil in continuous-flow flumes, minor decreases in filtration rates due to fouling were observed, with variation in impairment based on the type of oil [26]. Based on findings from harbor seals during the EVOS, marine mammals probably metabolize hydrocarbons rapidly and efficiently, mediated through the induction of mixed-function oxidases [107]. This is supported by the absence of firm evidence of contamination of tissues or toxicological effects for cetaceans from the EVOS [113]. In addition, no clinical, hematological, or biochemical effects were noted in a captive bottlenose dolphin dosed daily with 5 ml of machine oil for 99 days, suggesting captive dolphins can tolerate small amounts of ingested oil [26].

The few laboratory experiments on the potential impact of oil on cetacean physiology have produced mixed results. The renal cells of spotted dolphins (*Stenella* spp.) were exposed to No. 1 fuel oil to determine the toxicity of the oil and elucidate some of the mechanisms of cytopathology in a standardized preparation [114]. Cell survivability was reduced in a dose-dependent manner and early morphologic changes reflecting cytotoxicity were revealed by transmission electron microscopy. Programmed cell death (apoptosis) studies of the dolphin renal cells exposed to fuel oil for 12, 24, and 48 h showed that the number of cells undergoing early apoptosis increased after 24 h, clearly demonstrating a dose response to No. 1 fuel oil for cultured cells. Although it had been speculated that PAHs induced tumors in St. Lawrence River estuary belugas through the formation of DNA adducts, DNA adducts occurred at similar levels in livers of belugas from remote locations without significant PAH contamination [107,115,116].

Several authors suggest that the threat of most immediate concern to cetaceans is inhalation of volatile toxic fractions at the air–water interface, rather than from ingesting contaminated prey or absorbing oil through skin [84,108,117,118]. This risk is greatest near the source of a fresh spill because volatile toxic vapors disperse relatively quickly. When concentrated vapors are inhaled, mucous membranes may become inflamed, lungs can become congested, and pneumonia may ensue [119]. Inhaled fumes from oil may accumulate in blood and other tissues, leading to possible liver damage and neurological disorders [117]. Respiratory intervals vary between cetacean species, ranging from minutes to more than an hour, but all have the potential to expose cetaceans to toxic fumes from oil spills. One researcher concluded: "...it is clear that for the short time they persist, vapors are one feature of an oil spill that can threaten the health of a cetacean" [108].

The prospect of oil disrupting reproductive behavior is remote for offshore species, but more of a concern for inshore reproducers such as gray whales, humpback whales (*Megaptera novaeangliae*), narwhals, belugas, or resident populations of dolphins or porpoises [120]. For highly social species, the disruption of social groups from loss of some key individuals could potentially impact reproductive success. Potential support for this hypothesis comes from studies of Prince William Sound killer whales before and after the EVOS. Two killer whale pods photo-identified 5 years prior to the spill were followed by photo-identification for 16 years after the spill [7]. These two pods suffered losses of 33 and 41% in the year following the spill, with losses of adult females from these maternally organized groups leading to suppressed reproduction [4,7,113]. After 16 years, one pod had not recovered to prespill numbers, and the other has continued to decline and is now listed as depleted under the Marine Mammal Protection Act.

18.6.2 Vulnerability and Risk

Based on available knowledge of cetacean life history and ecology, hypothetical risks to different taxa of cetaceans were ranked within five subjective criteria: (i) range (large to small), (ii) habitat (oceanic to coastal, ice dwelling, and riverine), (iii) prey diversity (diverse to limited diet), (iv) behavioral flexibility (adaptable to sensitive to stress), and (v) population size (abundant to endangered) [120]. Baleen whales may be at highest risk because of their small populations, their specialized feeding patterns and structures (baleen), and their selected localized habitats for feeding and reproduction. In general, exposure to oil is likely to be most problematic for species inhabiting restricted habitats or those with restricted ranges, and that feeding locations within the water column may also affect exposure. Many cetacean species inhabiting offshore or open coastal waters are highly mobile and range widely, so their contact with an oil spill may be relatively brief. In contrast, some species have very specific habitat requirements for feeding and/or reproduction, and annually move between specific locations [120,121]. For example, baleen whales such as gray whales and humpback whales engage in long annual migrations between specific inshore feeding and breeding areas. These movements are timed to optimize the availability of appropriate food supplies or conditions for successful calving and breeding. Disruptions from oil spills and associated response actions at either terminus could place individuals, and possibly populations, in jeopardy. Species that have more restricted ranges or strong habitat requirements may experience prolonged exposure if they do not shift their ranges to avoid oil. Freshwater dolphin species such as the boto (*Inia geoffrensis*) or tucuxi (*Sotalia fluviatilis*) in South American rivers and the Ganges River dolphin (*Platanista gangetica*) and riverine populations of the Irrawaddy River dolphin (*Orcaella brevirostris*) in southern Asia face extreme restrictions of their ranges to river courses and would be unable to avoid upstream oil spills. Ice-edge species such as narwhals would be similarly vulnerable to spills in their limited habitat.

Strong site fidelity to restricted habitats may place certain species at risk for prolonged exposure to oil [120]. For example, in many parts of their range, bottlenose dolphins are long-term residents of specific bays, sounds, and estuaries [122]. Along the west coast of Florida, year-round resident populations have been studied for more than four decades, and currently span up to five generations of related dolphins [123]. The long-term persistence of these localized populations despite epizootic disease events, catastrophic harmful algal blooms that decimate prey fish stocks, major hurricanes that alter physiography and create high levels of pollution, and intensive and increasing human activities, has led to the hypothesis that these animals live in "ecological cul-de-sacs" where they either cannot or will not shift their ranges in response to major environmental changes and this would potentially include oil spills [124].

Cetacean diets and feeding locations within the water column contribute to defining potential exposure to oil [120]. Cetaceans with limited diets or that take advantage of seasonally abundant or geographically restricted food would be most affected by an overlapping oil spill. The occurrence and magnitude of nutritional effects would depend on the intensity and spread of the oil and its impact on possible alternative prey. The trophic level of cetacean food also might affect their exposure to oil and dispersants, with some feeding on aggregations of small invertebrates such as krill, copepods, and mysids or schools of small fish, and others preying on larger fish, squid, and mammals. Each trophic level has a specific potential to retain and transfer petroleum hydrocarbon residues. Some benthic invertebrates concentrate these compounds in their tissues, whereas teleost fishes and most other invertebrates metabolize and rapidly excrete them [120].

Spilled oil spreads across the water's surface, attaches to particles and sinks to the seafloor or is broken by dispersants into very small droplets that scatter in the water column [84]. There are no data or models indicating how much dispersant or dispersed oil a cetacean may ingest, but it is likely that bottom feeders could inadvertently ingest significant quantities of oil and surface feeders also might engulf a mouthful of oil. Baleen whales exhibit a variety of surface feeding patterns, such as skim feeding performed by right (*Eubalaena* spp.) and bowhead (*Balaena mysticetus*) whales, bubble net feeding by humpback whales, and lunge feeding performed by a number of rorqual whales (*Balaenopteridae*), that have the potential for ingesting oil and/or fouling baleen plates used for filtering food from the large quantities of water that pass through them [121]. Gray whales, which feed by ingesting mats of invertebrates on the seafloor, might be at risk for ingesting settled oil. Most toothed whales would not face these problems, except possibly when dolphins drive prey schools to the surface [120].

Few published observations of cetaceans feeding in the presence of oil exist. Humpback whales, fin whales, and Atlantic white-sided dolphins were observed feeding in the slick from the vessel *Regal Sword* that sank in 1979 off the east coast of the United States and gray whales were reportedly feeding in natural oil seeps around Santa Barbara, California [125].

Avoidance by cetaceans of oil at the water's surface requires that they be able to detect the oil, and that the spill is not so large that it cannot be avoided. Captive bottlenose dolphins can visually discriminate between oil and uncontaminated water, and they can detect oil with an optical density greater than 0.20–0.34 (corresponding to a 1 mm thick film) [108]. The skins of both toothed and baleen whales may be capable of receiving cutaneous signals from contact with oil [108]. Free-ranging dolphins should be able to detect the thicker concentrations of oil that occur near a spill and weathered fractions forming "pancakes" of much thicker viscous oils, but the lighter fractions that disperse into sheens and lightly colored refined products such as

gasoline, diesel fuel, and solvents that rapidly disperse into thin films likely would not be detected easily, if at all [108,126]. It seems likely that a dolphin's ability to detect the more transparent substances may, in part, depend on prior exposure.

Experiments with captive bottlenose dolphins showed they avoided oil on the surface of the water [127]. When presented with a dark-colored, nontoxic oil slick confined to a portion of the seawater holding pen, these dolphins detected the oil and hesitated to swim beneath it, and they startled in their few contacts with the oil. Subsequent experiments under day and night light conditions using clear mineral oil, dark-tinted mineral oil, and refined motor oil found that dolphins avoided oil during both day and night, but the response broke down when the oil was a thin sheen, particularly at night, suggesting a threshold for the dolphins' ability to detect oil or their inclination to avoid it [128]. Dolphins appear to rely on tactile clues to detect and avoid oil and they likely would not be unknowingly subjected to prolonged or repeated exposure to oil in the wild. Indirect support for this conclusion comes from the 1991 Gulf War oil spill in which live dolphins and carcasses were not observed in the aftermath of the spill, but they were observed back in the spill zone by 1992 [129].

Because groups of toothed whales (*Odontoceti*) are constantly communicating, enhanced sensory integration may allow them to more efficiently detect oil, and therefore avoid it as a group [120]. However, avoidance of oil by wild dolphins does not occur under all circumstances. Unidentified "porpoises" rode at the bow of a research vessel in areas of heavy oiling from the 1979 Ixtoc spill off Mexico, without indications of avoiding oil other than veering to avoid tar balls [130]. Bottlenose dolphins and Indo-Pacific humpback dolphins (*Sousa chinensis*) surfaced in oil sheen following the 1991 Gulf War spill [131]. Bottlenose dolphins in Texas waters have been observed on multiple occasions swimming though extensively oiled areas despite the presence of less-oiled waters nearby [118,132–134]. Following the EVOS, cetaceans in Prince William Sound, Alaska, did not appear to alter their behaviors in oiled areas and only a single oiled Dall's porpoise (*Phocoenoides dalli*), exhibiting labored breathing, appeared stressed [135].

The most detailed observations published to date of the behavior of dolphins near oil come from the 1990 *Mega Borg* spill off Galveston, Texas, USA, [118]. Aerial observations of nine bottlenose dolphin groups over a total of 5.6 h were conducted 6–9 days after the initial spill of 109,000 barrels of light-grade Angolan crude oil. Surface oil was classified as sheen, slick, or mousse, with dolphins apparently detecting the latter two, but not the sheen. In contrast to the consistent avoidance demonstrated in the captive dolphin experiments described earlier, wild dolphins hesitated and milled briefly upon encountering an oil slick, but eventually, they dove under or in small oil patches, and they swam through more extensive areas of oil. However, these free ranging dolphins consistently avoided mousse by

swimming under or around it, and group integrity was altered. Bottlenose dolphins may respond to thick oils by tightening their ranks, decreasing respiration rates, and increasing dive durations and heading changes. These alterations in behavior may represent attempts by cetaceans to minimize contact with surface oil as suggested by similar observations of bottlenose dolphins from the 1990 *Apex* oil spill near Galveston, Texas, and gray whales decreasing surface time and respiration rates and changing swimming speeds through natural oil seep slicks [118,136,137]. The detection, but lack of consistent avoidance of slicks and the apparent lack of detection of sheen, may increase risk of exposure to harmful petroleum fractions.

Outside of the 1989 EVOS and the 2010 DWH spill, systematic studies addressing the population-level impact of a large oil spill on cetaceans are rare. Only a few anecdotal cetacean behavioral observations are available from the very large 1979 Ixtoc spill in the Gulf of Mexico [130]. Seventy-nine cetaceans were known to have died in Saudi Arabia and Bahraini waters during the 1991 Gulf War, but no obvious link to oil was noted [131]. Spatiotemporal comparisons of mortality, population structures, diets, and concentrations of vanadium, nickel, and porphyrines in small delphinids, seals, and otters from the French Atlantic coasts following the 1999 *Erika* oil spill found no measurable effect of the spill on dolphins [138].

Limited data on the impact of the DWH spill on cetaceans has been made available on the U.S. National Oceanic and Atmospheric Administration (NOAA) natural resource damage assessment (NRDA) website [10] and a few scientific papers have addressed the health of two Gulf of Mexico bottlenose dolphin populations examined after the spill [139,140]. In 2011, comparative bottlenose dolphin capture–release health assessments were conducted in Barataria Bay, Louisiana, USA, which was heavily oiled for a prolonged time during the DWH spill, and in an area that was not oiled, Sarasota Bay, Florida, USA, where health assessments have been performed on long-term resident dolphins for decades [141–143]. While quantitative

information on the amount of DWH oil that entered Barataria Bay has not been published, Grand Isle, Louisiana, which is immediately adjacent to Barataria Bay and near to where the animals were captured for the health assessments, showed a 45-fold increase in the bioavailable concentration of PAHs after the DWH spill [144].

The Barataria Bay dolphins exhibited severe health problems that were not seen in dolphins from the unoled Sarasota area and have not been seen in previous studies of dolphins from other sites along the Atlantic coast or the Gulf of Mexico (Table 18.2) [139]. Many of the Barataria Bay dolphins were underweight, had low hormone and blood sugar levels, and some showed signs of liver and/or lung damage. The disease conditions observed are uncommon in dolphins, but consistent with those seen in other marine mammals exposed to oil [17,18,83]. The dolphins of Barataria Bay were potentially exposed to oil by inhaling vapors at the water's surface, ingesting oil from sediments or the water while feeding, eating fish harboring chemical contaminants from oil, and/or via absorption through their skin [unpublished, NOAA NRDA].

Many of the serious health conditions found during assessments of Barataria Bay dolphins are suggestive of exposure to oil from the DWH spill, but comparative health data on these dolphins from before the spill are not available. Therefore, it is possible that environmental conditions in Barataria Bay before the spill increased the vulnerability of the resident dolphin population to the DWH spill or these dolphins were already unhealthy prior to the spill. However, it is highly unlikely the severity and prevalence of diseases observed in Barataria Bay dolphins would have gone unnoticed and these dolphins ranked very low in concentrations of a large suite of pesticides and other chemicals when compared with dolphins from 14 other coastal sites [139,140]. Regardless, findings released over the next few years by NOAA scientists and others from the numerous as yet unpublished DWH studies conducted following this spill, including follow-up health assessments in Barataria Bay in 2013 and

TABLE 18.2 Summary comparison of bottlenose dolphin health measures in 2011 from Barataria Bay, Louisiana (heavily oiled by DWH), and Sarasota Bay, Florida (uniled) [139,140]

Health measure	Barataria Bay, (heavily oiled)	Sarasota Bay, (uniled)
Body condition (below reference values relating mass to length)	25% of animals	4% of animals
Extensive tooth loss	19% of animals	None
Inflammation indicators (elevation of one or more of neutrophils, lymphocytes, eosinophils, monocytes, and basophils and/or increased serum globulin or decreased albumin)	41% of animals	8% of animals
Hypoglycemia (glucose below low reference limit)	22% of animals	None
Iron panel (elevation of two or more of serum iron, total iron binding capacity, % saturation of transferrin)	22% of animals	None
Hepatobiliary (abnormal value for two or more enzymes: ALT, AST, GGT, or LDH)	19% of animals	None
Moderate to severe lung disease (as evidenced by alveolar–interstitial syndrome, masses in the lungs, and pulmonary consolidation)	34% of animals	7% of animals
Cortisol levels (below minimums measured elsewhere)	44% of animals	None
Aldosterone levels (below assay detection limit)	53% of animals	8% of animals
Prognosis in 2011	48% guarded or worse; 17% poor or grave, with little expectation of survival	7% guarded; all others good or fair

2014 and Mississippi Sound in 2013, should greatly improve our understanding of the impacts of oil on cetaceans.

REFERENCES

- [1] Frost, K.J., L.F. Lowry, E.H. Sinclair, J. Ver Hoef, and D.C. McAllister, Impacts on distribution, abundance, and productivity of harbor seals, *Marine Mammals and the Exxon Valdez*, T.R. Loughlin (ed.), Academic Press, San Diego, 97, 1994.
- [2] Bodkin, J.L. and M.S. Udevitz, An intersection model for estimating sea otter mortality along the Kenai Peninsula, *Marine Mammals and the Exxon Valdez*, T.R. Loughlin (ed.), Academic Press, San Diego, 81, 1994.
- [3] Piatt, J.F. and R.G. Ford, How many seabirds were killed by the Exxon Valdez oil spill? *Proceedings of the Exxon Valdez oil spill*, S.D. Rice, R.B. Spies, D.A. Wolfe, and B.A. Wright (eds.), Symposium No. 18, American Fisheries Society, 712, 1996.
- [4] Peterson, C.H., S.D. Rice, J.W. Short, D. Esler, J.L. Bodkin, et al., Long-term ecosystem response to the Exxon Valdez oil spill. *Science*, 302, 2082, 2003.
- [5] Monson, D.H., D.F. Doak, B.E. Ballachey, A. Johnson, and J.L. Bodkin, Long-term impacts of the Exxon Valdez oil spill on sea otters, assessed through age-dependent mortality patterns. *PNAS*, 97, 6562, 2000.
- [6] Bodkin, J.L., B.E. Ballachey, T.A. Dean, A.K. Fukuyama, S.C. Jewett, et al., Sea otter population status and the process of recovery from the 1989 Exxon Valdez oil spill, *MEPS*, 241, 237, 2002.
- [7] Matkin, C.O., E.L. Saulitis, G.M. Ellis, P. Olesiuk, and S.D. Rice, Ongoing population-level impacts on Killer Whales, *Orcinus orca*, following the Exxon Valdez oil spill in Prince William Sound, Alaska, *Mar. Ecol. Prog. Ser.*, 356, 269, 2008.
- [8] Monson, D.H., D.F. Doak, B.E. Ballachey, and J.L. Bodkin, Could residual oil from the Exxon Valdez spill create a long-term population sink for sea otters in Alaska? *Ecol. Apps.*, 21, 2917, 2011.
- [9] Bodkin, J.L., B. E. Ballachey, H.A. Coletti, G.G. Essinger, K.A. Kloeckeri, et al., Long-term effects of the Exxon Valdez oil spill: Sea otter foraging in the intertidal as a pathway of exposure to lingering oil, *MEPS*, 447, 273, 2012.
- [10] NOAA NRDA, *Gulf Dolphins Questions and Answers*, http://www.gulfspillrestoration.noaa.gov/2012/03/gulf-dolphins-answers/?utm_source=Barataria+Bay+Dolphins&utm_campaign=Gulf+Dolphins+Email&utm_medium=email, 2012. Accessed August 14, 2014.
- [11] Kenyon, K.W., The sea otter in the eastern Pacific Ocean, *North Am. Fauna*, 68, 1, 1969.
- [12] Yeates, L.C., *Physiological capabilities and behavioral strategies for marine living by the smallest marine mammal, the sea otter (Enhydra lutris)*, PhD dissertation, University of California Santa Cruz, CA, 2006.
- [13] Costa, D.P. and G.L. Kooyman, Oxygen consumption, thermoregulation, and the effects of fur oiling and washing on the sea otter, *Enhydra lutris*, *Can. J. Zool.*, 60, 2761, 1982.
- [14] Siniiff, D.B., T.D. Williams, A.M. Johnson, and D.L. Garshelis, Experiments on the response of sea otters, *Enhydra lutris*, to oil contamination, *Biol. Conserv.*, 23, 261, 1982.
- [15] Davis, R.W., T.M. Williams, J.A. Thomas, R.A. Kastelein, and L.H. Cornell, The effects of oil contamination and cleaning on sea otters (*Enhydra lutris*), II. Metabolism, thermoregulation, and behavior, *Can. J. Zool.*, 66, 2782, 1988.
- [16] Williams, T.M., R.A. Kastelein, R.W. Davis, and J.A. Thomas, The effects of oil contamination and cleaning on sea otters (*Enhydra lutris*). I. Thermoregulatory implications based on pelt studies, *Can. J. Zool.*, 66, 2776, 1988.
- [17] Lipscomb, T.P., R.K. Harris, R.B. Moeller, J.M. Pletcher, R.J. Haebler, et al., Histopathologic lesions in sea otters exposed to crude oil, *Vet. Pathol.*, 30, 1, 1993.
- [18] Lipscomb, T.P., R.K. Harris, A.H. Rebar, B.E. Ballachey, and R.J. Haebler, Pathology of sea otters, *Marine Mammals and the Exxon Valdez*, T.R. Loughlin (ed.), Academic Press, San Diego, 265, 1994.
- [19] Williams, T.M. and R.W. Davis (eds.), *Emergency Care and Rehabilitation of Oiled Sea Otters: A Guide for Oil Spills Involving Fur-bearing Marine Mammals*, University of Alaska Press, Alaska, 1995.
- [20] Jessup, D.A., L.C. Yeates, S. Toy-Choutka, D. Casper, M.J. Murray, et al., Washing oiled sea otters, *Wildl. Soc. Bull.*, 36, 6, 2012.
- [21] Klaassen, C.D. and K. Rozman, Absorption, distribution, and excretion of toxicants, *Toxicology: The Basic Science of Poisons*, M.O. Amdur, J. Doull, and C.D. Klaassen (eds.), McGraw Hill, New York, 50, 1991.
- [22] Mulcahy, D.M. and B.E. Ballachey, Hydrocarbon residues in sea otter tissues, *Marine Mammals and the Exxon Valdez*, T.R. Loughlin (ed.), Academic Press, San Diego, 313, 1994.
- [23] Williams, T.M., Evaluating the long term effects of crude oil exposure in sea otters, *Wildl. J.*, 13, 42, 1990.
- [24] Dejours, P., Water and air physical characteristics and their physiological consequences, *Comparative Physiology: Life in Water and on Land*, P. Dejours, L. Bolis, C.R. Taylor, and E.R. Weibel (eds.), *Fidia Research Series*, IX-Liviana Press, Padova, 9, 3, 1987.
- [25] Parker, G.S., D.A. Mosborg, R.W. Foley, and C.M. Stiernberg, Spontaneous cervical and mediastinal emphysema, *Laryngoscope*, 100, 938, 1990.
- [26] Geraci, J.R. and D.J. St. Aubin (eds.), *Sea Mammals and Oil: Confronting the Risks*, Academic Press, San Diego, 1990.
- [27] Paton, B.C., Accidental hypothermia, *Thermoregulation: Pathology, Pharmacology, and Therapy*, E. Schonbaum and P. Lomax (eds.), Pergamon Press, New York, 397, 1991.
- [28] Øritsland, N.A., F.R. Engelhardt, F.A. Juck, R.J. Hurst, and P.D. Watts, *Effects of crude oil on polar bears*, Environmental Studies Report No. 24, Department of Indian Affairs and Northern Development, Ottawa, Canada, 1981.
- [29] Leighton, F.A., The toxicity of petroleum oils to birds: An overview, *The Effects of Oil on Wildlife: Research, Rehabilitation, and General Concerns*, J. White and L. Frink (eds.), Sheridan Press, Hanover, 43, 1991.
- [30] White, J., Current treatment for anemia in oil-contaminated birds, *The Effects of Oil on Wildlife: Research, Rehabilitation, and General Concerns*, J. White and L. Frink (eds.), Sheridan Press, Hanover, 67, 1991.
- [31] Kooyman, G.L., *Diverse Divers: Physiology and Behavior*, Springer-Verlag, Heidelberg, 1989.

- [32] Ben-David, M., T.M. Williams, and O.A. Ormseth, Effects of oiling on exercise physiology and diving behavior of river otters: A captive study, *Can. J. Zool.*, 78, 1380, 2000.
- [33] St. Aubin, D.J., Physiological and toxic effects on pinnipeds, *Sea Mammals and Oil: Confronting the Risks*, J.R. Geraci and D.J. St. Aubin (eds.), Academic Press, San Diego, 103, 1990.
- [34] Davis, J.E. and S.S. Anderson, Effects of oil pollution on breeding grey seals, *Mar. Pol. Bull.*, 7, 115, 1976.
- [35] Le Boeuf, B.J., Oil contamination and elephant seal mortality a negative finding, *Biological and Oceanographical Survey of the Santa Barbara Channel Oil Spill 1969-1970, Vol. I. Biology and Bacteriology*, D. Straughan (ed.), Allan Hancock Foundation, University of Southern California, Los Angeles, 277, 1971.
- [36] Lowry, L.F., K.J. Frost, and K.W. Pitcher, Observations of oiling of harbor seals in Prince William Sound, *Marine Mammals and the Exxon Valdez*, T.R. Loughlin (ed.), Academic Press, San Diego, 209, 1994.
- [37] Hoover-Miller, A., K.R. Parker, and J.J. Burns, A reassessment of the impact of the *Exxon Valdez* oil spill on harbor seals (*Phoca vitulina richardsi*) in Prince William Sound, Alaska, *Mar. Mam. Sci.*, 17, 111, 2001.
- [38] Calkins, D.G., E.A. Becker, T.R. Spraker, and T.R. Loughlin, Impacts on Steller Sea lions, *Marine Mammals and the Exxon Valdez*, T.R. Loughlin (ed.), Academic Press, San Diego, 119, 1994.
- [39] Jewett, S.C., T.A. Dean, B.R. Woodin, M.K. Hoberg, and J.J. Stegeman, Exposure to hydrocarbons 10 years after the *Exxon Valdez* oil spill: Evidence from cytochrome P4501A expression and biliary FACs in nearshore demersal fishes, *Mar. Envir. Res.*, 54, 21, 2002.
- [40] Kooyman, G.L., R.W. Davis, and M.A. Castellini, Thermal conductance of immersed pinniped and sea otter pelts before and after oiling with Prudhoe Bay crude, *Fate and Effects of Petroleum Hydrocarbons in Marine Ecosystems and Organisms*, D.A. Wolfe (ed.), Pergamon Press, Oxford, 151, 1977.
- [41] Davies, J.L., Observations on the gray seal (*Halichoerus grypus*) at Ramsey Island, Pembrokeshire, *Proc. Zoo. Soc. Lon.*, 119, 673, 1949.
- [42] Geraci, J.R. and T.G. Smith, Direct and indirect effects of oil in ringed seals (*Phoca hispida*) of the Beaufort Sea. *J. Fish. Res. Bd. Can.*, 33, 1976, 1976.
- [43] Engelhardt, F.R., Hydrocarbon metabolism and cortisol balance in oil-exposed ringed seals, *Phoca hispida*, *Comp. Bio. Physiol. C*, 72, 133, 1982.
- [44] Engelhardt, F.R., J.R. Geraci, and T.G. Smith, Uptake and clearance of Petroleum hydrocarbons in the ringed seal, *Phoca hispida*, *J. Fish. Res. Bd. Can.*, 34, 1143, 1977.
- [45] Kooyman, G.L., R.L. Gentry, and W.B. McAllister, *Physiological Impact of Oil on Pinnipeds*, R.N.W.F.C.N.M.F. Service (ed.), NOAA, Department of Commerce, Seattle, 1976.
- [46] Harwood, J. and B. Wilson, The implications of developments on the Atlantic Frontier for marine mammals, *Cont. Shelf Res.*, 21, 1073, 2001.
- [47] McLaren, I.A., Pinnipeds and oil: Ecological perspectives, *Sea Mammals and Oil: Confronting the Risks*, J.R. Geraci and D.J. St. Aubin (eds.), Academic Press, San Diego, 55, 1990.
- [48] French, D.P., M. Reed, J. Calambokidis, and J.C. Cubbage, A Simulation Model of Seasonal Migration and Daily Movements of the Northern Fur Seal, *Ecol. Mod.*, 48, 193, 1989.
- [49] Biuw, M., L. Boehme, C. Guinet, M. Hindell, D. Costa, et al., Variations in behavior and condition of a Southern Ocean top predator in relation to *in situ* oceanographic conditions. *PNAS*, 104, 13705, 2007.
- [50] Simmons, S.E., D.E. Crocker, J.L. Hassrick, C.E. Kuhn, P.W. Robinson, et al., Climate-scale hydrographic features related to foraging success in a capital breeder, the northern elephant seal *Mirounga angustirostris*, *End. Spec. Res.*, 10, 233, 2010.
- [51] Fadely, B.S., B.W. Robson, J.T. Sterling, A. Greig, and K.A. Call, Immature Steller sea lion (*Eumetopias jubatus*) dive activity in relation to habitat features of the eastern Aleutian Islands, *Fish. Oceanog.*, 14, 243, 2005.
- [52] Robson, B.W., M.E. Goebel, J.D. Baker, R.R. Ream, T.R. Loughlin, et al., Separation of foraging habitat among breeding sites of a colonial marine predator, the northern fur seal (*Callorhinus ursinus*), *Can. J. Zool.*, 82, 20, 2004.
- [53] Costa, D.P., D.E. Crocker, M.E. Goebel, M.A. Fedak, B.I. McDonald, et al., Climate change and habitat selection of seals in the western Antarctic peninsula, *Int. Comp. Bio.*, 6, 1018–1030, 2010.
- [54] Page, B., J. McKenzie, M.D. Sumner, M. Coyne, and S.D. Goldsworthy, Spatial separation of foraging habitats among New Zealand fur seals, *Mar. Eco. Prog. Ser.*, 323, 263, 2006.
- [55] Staniland, I.J., N. Gales, N.L. Warren, S.L. Robinson, S.D. Goldsworthy, et al., Geographical variation in the behaviour of a central place forager: Antarctic fur seals foraging in contrasting environments, *Mar. Bio.*, 157, 2383, 2010.
- [56] Costa, D.P., M.J. Weise, and J.P.Y. Arnould, Potential influences of whaling and the status and trends of pinniped populations, *Whales, Whaling and Ocean Ecosystems*, J.A. Estes, T.M. Williams, D. Doak, D.D. DeMaster, and R. Brownell (eds.), University of California Press, Berkeley, 344, 2006.
- [57] Robinson, P.W., S.E. Simmons, D.E. Crocker, and D.P. Costa, Measurements of foraging success in a highly pelagic marine predator, the Northern Elephant Seal, *J. Ani. Ecol.*, 79, 1146, 2010.
- [58] Marsh, H., T.J. O'Shea, and J.E. Reynolds, III, *Ecology and Conservation of the Sirenia: Dugongs and Manatees*, Cambridge University Press, Cambridge, UK, 2011.
- [59] Hines, E. M., J.E. Reynolds III, L.V. Aragones, A. Mignucci-Giannoni, and M. Marmontel (eds.), *Sirenian Conservation: Issues and Strategies in Developing Countries*, University of Florida Press, Gainesville, 2012.
- [60] Preen, A., Distribution, abundance and conservation status of dugongs and dolphins in the Southern and Western Arabian Gulf, *Biol. Conserv.*, 118, 205, 2004.
- [61] Preen A., H. Das, M. Al-Rumaidh, and A. Hodgson, Dugongs in Arabia, *Sirenian Conservation: Issues and Strategies in Developing Countries*, E.M. Hines, J.E. Reynolds III, L.M. Aragones, A.A. Mignucci-Giannoni, and M. Marmontel (eds.), University Press of Florida, Gainesville, 10, 91, 2012.
- [62] Preen, A., *The Status and Conservation of the Dugong in the Arabian Region*, Final Report, Vols 1–2, Meteorology and Environmental Protection Administration, Saudi Arabia, 1988.

- [63] Preen, A., Marine protected areas and dugong conservation along Australia's Indian Ocean Coast, *Environ. Manage.*, 22, 173, 1998.
- [64] Wetzel, D.L., E. Pulster, and J.E. Reynolds III, Organic contaminants and sirenians, *Sirenian Conservation: Issues and Strategies in Developing Countries*, E.M. Hines, J.E. Reynolds III, L.M. Aragones, A.A. Mignucci-Giannoni, and M. Marmontel (eds.), University Press of Florida, Gainesville, 22, 196, 2012.
- [65] Varanasi, U., J.E. Stein, and M. Nishimoto, Biotransformation and deposition of polycyclic aromatic hydrocarbons (PAH) in fish, *Metabolism of Polycyclic Aromatic Hydrocarbons in the Aquatic Environment*, U. Varanasi (ed.), CRC Press, Boca Raton, FL, 1989.
- [66] Neff, J.M., *Bioaccumulation in Marine Organisms: Effect of Contaminants from Oil Well Produced Water*, Elsevier Ltd., Amsterdam, 2002.
- [67] St. Aubin, D.J. and V.J. Lounsbury, Oil effects on manatees: Evaluating the risks, *Sea Mammals and Oil: Confronting the Risks*, J.R. Geraci and D.J. St Aubin (eds.), Academic Press, San Diego, 11, 241, 1990.
- [68] Dierauf, L.A. and F. Gulland (eds.), *CRC Handbook of Marine Mammal Medicine: Health, Disease, and Rehabilitation*, 2nd edition, CRC Press, Boca Raton, FL, 2001.
- [69] Reep, R.L., C.D. Marshall, and M.L. Stoll, Tactile hairs on the postcranial body in Florida manatees: A mammalian lateral line? *Brain Behav. Evol.*, 59, 141, 2002.
- [70] Sarko, D.K., R.L. Reep, J.E. Mazurkiewicz, and F. L. Rice, Adaptations in the structure and innervation of follicle-sinus complexes to an aquatic environment as seen in the Florida manatee (*Trichechus manatus latirostris*), *J. Comp. Neurol.*, 504, 217, 2007.
- [71] American Petroleum Institute, *Protecting Livestock: Frequently Asked Questions About Livestock Exposure to Crude Oil in Oilfield Operations*, American Petroleum Institute Publication 10PL06, Washington, DC, 2006.
- [72] Beck, C.A. and N.B. Barros, The impact of debris on the Florida manatee, *Mar. Pollut. Bull.*, 22, 508, 1991.
- [73] Lopes, A., S.M. da Rosa-Osman, and M.T. Fernandes-Piedade, Effects of crude oil on survival, morphology, and anatomy of two aquatic macrophytes from the Amazon floodplains, *Hydrobiologia*, 636, 295, 2009.
- [74] Mignucci-Giannoni, A., Assessment and rehabilitation of wildlife affected by an oil spill in Puerto Rico, *Environ. Pollut.*, 104, 323, 1999.
- [75] Zieman, J.C., R. Orth, R.C. Phillips, G. Thayer, and A. Thorhaug, The effects of oil on seagrass ecosystems, *Restoration of Habitats Impacted by Oil Spills*, A.L. Buikema, Jr. and J. Cairns, Jr. (eds.), Butterworth-Heinemann Publishers, Burlington, MA, 2, 37, 1984.
- [76] Peters, E.C., N. J. Gassman, J.C. Firman, R.M. Richmond, and E.A. Power, Ecotoxicology of tropical marine ecosystems, *Environ. Toxicol. Chem.*, 16, 12, 1997.
- [77] National Oceanic and Atmospheric Administration, *Adverse Effects from Oil Spill Appendix D*, http://www.darrp.noaa.gov/library/pdf/IAD_AP-D.PDF, Damage Assessment, Remediation, and Restoration Program, 2011. Accessed August 14, 2014.
- [78] Kenworthy, W.J., M.J. Durako, S.M.R. Fatemy, H. Valavi, and G. Thayer, Ecology of seagrasses in northeastern Saudi Arabia one year after the Gulf War oil spill, *Mar. Pollut. Bull.*, 27, 213, 1993.
- [79] Deutsch, C.J., J.P. Reid, R.K. Bonde, D.E. Easton, H.I. Kochman, et al., Seasonal movements, migratory behavior, and site fidelity of West Indian manatees along the Atlantic Coast of the United States, *Wildl. Monogr.*, 151, 1, 2003.
- [80] Sheppard, J.K., A.R. Preen, H. Marsh, I.R. Lawler, S.D. Whiting, et al., Movement heterogeneity of dugongs, *Dugong dugon* (Müller), over large spatial scales, *J. Exper. Mar. Biol. Ecol.*, 344, 64, 2006.
- [81] Obbard, M.E., G.W. Thiemann, E. Peacock, and T.D. DeBruyn (eds.), *Polar Bears: Proceedings of the 15th Working Meeting of the IUCN/SCC Polar Bear Specialist Group, Copenhagen, Denmark, 29 June–3 July 2009*, IUCN, Gland, Switzerland and Cambridge, UK, vii+, 2010.
- [82] Regehr, E.V., S.C. Amstrup, and I. Stirling, *Polar bear population status in the southern Beaufort Sea*, Open-File Report 1337, U. S. Geological Survey, Alaska Science Center, Anchorage, 2006.
- [83] Ortisland, N.A., F.R. Engelhardt, F.A. Juck, R.J. Hurst, and P.D. Watts, Effect of crude oil on polar bears, environmental study no. 24, Canadian Department of Northern Affairs, Ottawa, 1981.
- [84] Neff, J.M., Composition and fate of petroleum and spill-treating agents in the marine environment, *Sea Mammals and Oil: Confronting the Risks*, J.R. Geraci and D.J. St Aubin (eds.), Academic Press, San Diego, 1990.
- [85] St. Aubin, D.J., Physiologic and toxic effects on polar bears, *Sea Mammals and Oil: Confronting the Risks*, J.R. Geraci and D.J. St Aubin (eds.), Academic Press, San Diego, 235, 1990.
- [86] Derocher, A.E. and I. Stirling, Oil contamination of two polar bears, *Polar Rec.*, 27, 160 1991.
- [87] Amstrup, S.A., C. Gardner, K.C. Myers, and F.W. Oehme, Ethylene glycol (antifreeze) poisoning of a free-ranging polar bear, *Vet. Human Toxi.*, 31, 317, 1989.
- [88] Frost, K.J., C.A. Manen, and T.L. Wade, Petroleum hydrocarbons in tissues of harbor seal from Prince William Sound and the Gulf of Alaska, *Marine Mammals and the Exxon Valdez*, T.R. Loughlin (ed.) Academic Press, San Diego, 331, 1994.
- [89] Lowry, L.F., K.J. Frost, and K.W. Pitcher, Observations of oiling of harbor seals in Prince William Sound, *Marine Mammals and the Exxon Valdez*, T.R. Loughlin (ed.), Academic Press, San Diego, 209, 1994.
- [90] Spraker, T.R., L.F. Lowry, and K.J. Frost, Necropsy and histopathological lesions found in harbor seals, *Marine Mammals and the Exxon Valdez*, T.R. Loughlin (ed.), Academic Press, San Diego, 281, 1994.
- [91] Federal Register/Vol. 71, No. 148/Wednesday, August 2, 2006/Rules and Regulations 43936.
- [92] National Research Council, *Cumulative Environmental Effects of Oil and Gas Activities on Alaska's North Slope*, The National Academies Press, Washington, DC, 2003.
- [93] <http://www1.american.edu/ted/KOMI.HTM>. TED Case Studies. Case number 265 - The Russian Arctic Oil Spill. Accessed August 14, 2014.

- [94] http://dec.alaska.gov/spar/perp/response/summary06/060302301/060302301_index.htm. GC-2 Oil Transit Line Release (final). Accessed August 14, 2014.
- [95] Minerals Management Service, Environmental Assessment Proposed Oil and Gas Lease 195, Beaufort Sea planning Area, OCS EIS/EA MMS 2004-028, 2004.
- [96] Stirling, I., Polar bears and oil: Ecological perspectives, *Sea Mammals and Oil: Confronting the Risks*, J.R. Geraci and D.J. St. Aubin (eds.), Academic Press, San Diego, 223, 1990.
- [97] Amstrup, S.C., B.G. Marcot, and D.C. Douglas, *Forecasting the range-wide status of polar bears at selected times in the 21st century*, U.S. Geological Survey Administrative Report, Reston, Virginia, 2007.
- [98] Frantzen, B. and A. Bambulyak, *Oil transport from the Russian part of the Barents region*, Report to the Barents Secretariat, Svanhovd Environmental Centre, Norway, 2003.
- [99] Granier, C., U. Niemeier, J.H. Jungclauss, L. Emmons, P. Hess, et al., Ozone pollution from future ship traffic in the Arctic northern passages, *Geophys. Res. Lett.*, 33, L13807, 2006.
- [100] Amstrup, S.C., G.M. Durner, T.L. McDonald, and W.R. Johnson, *Estimating potential effects of hypothetical oil spills on polar bears*, Unpublished Report, U.S. Geological Survey, Alaska Science Center, Anchorage, 2006.
- [101] Amstrup, S.C., G.M. Durner, and T.L. McDonald, Estimating potential effects of hypothetical oil spills from the Liberty oil production island on polar bears, Liberty Development and Production Plan Draft Environmental Impact Statement, Minerals Management Service, Alaska OCS Region, OCS EIS/EA, MMS 2001-001, Volume III (J-1), 2000.
- [102] Durner, G.M., S.C. Amstrup, and T.L. McDonald, Estimating the impacts of oil spills on polar bears, *Arctic Res.*, 14, 2000.
- [103] Schliebe, S.L., K.D. Rode, J.S. Gleason, J. Wilder, K. Proffitt, et al., Effects of sea ice extent and food availability on spatial and temporal distribution of polar bears during the fall open-water period in the Southern Beaufort Sea, *Polar Biol.*, 31, 2008.
- [104] Lentfer, J.W. and R.J. Hensel, Alaskan polar bear denning, *International Conference on Bear Research and Management*, 4, 101, 1980.
- [105] Amstrup, S.C., I. Stirling, and J.W. Lentfer, Past and present status of polar bears in Alaska, *Wildl. Soc. Bull.*, 14, 1986.
- [106] Amstrup, S.C., Human disturbances of denning polar bears in Alaska, *Arctic*, 46, 1993.
- [107] O'Hara, T.M. and T.J. O'Shea, Toxicology, *CRC Handbook of Marine Mammal Medicine, 2nd Edition*, L.A. Dierauf and F.M.D. Gulland (eds.), CRC Press, Boca Raton, FL, 471, 2001.
- [108] Geraci, J.R., Physiologic and toxic effects on cetaceans, *Sea Mammals and Oil: Confronting the Risks*, J.R. Geraci and D.J. St. Aubin (eds.), Academic Press, San Diego, 167, 1990.
- [109] Law, R.J. and J.A. Whinnet, Polycyclic aromatic hydrocarbons in muscle tissue of harbor porpoises from U.K. waters, *Mar. Pollut. Bull.*, 24, 550, 1992.
- [110] Holsbeek, L., C.R. Joiris, V. Debacker, I.B. Ali, P. Roose, et al., Heavy metals, organochlorines, and polycyclic aromatic hydrocarbons in sperm whales stranded in the southern North Sea during the 1994/1995 Winter, *Mar. Pollut. Bull.*, 38, 304, 1999.
- [111] Hellou, J., G. Stenson, I.-H. Ni, and J.F. Payne, Polycyclic aromatic hydrocarbons in muscle tissue of marine mammals from the Northwest Atlantic, *Mar. Pollut. Bull.*, 21, 469, 1990.
- [112] Varanasi, U., J.E. Stein, K.L. Tilbury, J.P. Meador, C.A. Sloan, et al., Chemical contaminants in gray whales stranded along the west coast of North America, *Sci. Total Environ.*, 145, 29, 1994.
- [113] Loughlin, T.R. (ed.), *Marine Mammals and the Exxon Valdez*, Academic Press, San Diego, 1994.
- [114] Pfeiffer, C.J., L.V. Sharova, and L. Gray, Functional and ultrastructural cell pathology induced by fuel oils in cultured dolphin renal cells, *Ecotox. Environ. Safe.*, 47, 210, 2000.
- [115] Martineau, D., A. Lagace, P. Beland, R. Higgins, D. Armstrong, et al., Pathology of stranded beluga whales from the St. Lawrence Estuary, Quebec, *Can. J. Comp. Pathol.*, 98, 287, 1988.
- [116] Ray, S., B.P. Dunn, J.F. Payne, L. Fancey, R. Helbig, et al., Aromatic DNA-carcinogen adducts in beluga whales from the Canadian Arctic and Gulf of St. Lawrence, *Mar. Pollut. Bull.*, 22, 392, 1992.
- [117] Geraci, J.R. and D.J. St. Aubin, *Study of the effects of oil on cetaceans*, Final Report, Contract No. AA 551-CT9-29, U.S. Department of the Interior, Bureau of Land Management, Washington, DC, 1982.
- [118] Smultea, M.A. and B. Würsig, Behavioral reactions of bottlenose dolphins to the *Mega Borg* oil spill, Gulf of Mexico 1990, *Aquat. Mamm.*, 21, 171, 1995.
- [119] Hansen, D.J., *The potential effects of oil spills and other chemical pollutants on marine mammals occurring in Alaskan Waters*, Report No. MMS 85-0031 U.S. Department of the Interior, Minerals Management Service, Alaska Outer Continental Shelf Region, Anchorage, 1985.
- [120] Würsig, B., Cetaceans and oil: Ecologic perspectives, *Sea Mammals and Oil: Confronting the Risks*, J.R. Geraci and D.J. St. Aubin (eds.), Academic Press, San Diego, 129, 1990.
- [121] Wells, R.S., D.J. Boness, and G.B. Rathbun, Behavior, *Biology of Marine Mammals*, J.E. Reynolds, III and S.A. Rommel (eds.), Smithsonian Institution Press, Washington, DC, 324, 1999.
- [122] Wells, R.S. and M.D. Scott, Bottlenose dolphin *Tursiops truncatus* (Montagu, 1821), *Handbook of Marine Mammals, Vol. 6, the Second Book of Dolphins and Porpoises*, S.H. Ridgway and R. Harrison (eds.), Academic Press, San Diego, 137, 1999.
- [123] Wells, R.S., Dolphin social complexity: Lessons from long-term study and life history, *Animal Social Complexity: Intelligence, Culture, and Individualized Societies*, F.B.M. de Waal and P.L. Tyack (eds.), Harvard University Press, Cambridge, 32, 2003.
- [124] Wells, R.S., Feeling the heat-Potential climate change impacts on bottlenose dolphins, *Whalewatcher, J. Am. Cetacean Soc.*, 39, 12, 2010.
- [125] Goodale, D.R., M.A.M. Hyman, and H.E. Winn, *Cetacean responses in association with the regal sword oil spill, 1979* Annual Report, Cetacean and Turtle Assessment Program, University of Rhode Island, Kingston, 1981.

- [126] Geraci, J.R., D.J. St. Aubin, and R.J. Reisman, Bottlenose dolphins, *Tursiops truncatus*, can detect oil, *Can. J. Fish. Aquat. Sci.*, 40, 1516, 1983.
- [127] Smith, T.G., J.R. Geraci, and D.J. St. Aubin, Reaction of bottlenose dolphins, *Tursiops truncatus*, to a controlled oil spill, *Can. J. Fish. Aquat. Sci.*, 40, 1522, 1983.
- [128] St. Aubin, D.J., J.R. Geraci, T.G. Smith, and T.G. Friesen, How do bottlenose dolphins, *Tursiops truncatus*, react to oil films under different light conditions? *Can. J. Fish. Aquat. Sci.*, 42, 430, 1985.
- [129] Robineau, D. and P. Fiquet, Cetaceans of Dawhat Ad-Dafi and Dawhat Al-Musallamiya (Saudi Arabia) one year after the Gulf War oil spill, *Courier Forsch. Inst. Senckenberg*, 166, 76, 1994.
- [130] Bergey, M., *The Ixtoc oil spill—Effects on marine mammals and turtles*, An observational report from 6–28 September 1979, Unpublished, 1979.
- [131] Preen, A., *Report of the die-off of marine mammals associated with the Gulf War oil spill*, Final Report, The National Commission for Wildlife Conservation and Development, Riyadh, Kingdom of Saudi Arabia, 1, 1991.
- [132] Shane, S.H., *The Population Biology of the Atlantic Bottlenose Dolphin, Tursiops truncatus, in the Aransas Pass Area of Texas*, M.S. Thesis, Texas A&M University, College Station, Texas, 1, 1977.
- [133] Shane, S.H. and D.J. Schmidley, *The population biology of the Atlantic bottlenose dolphin, Tursiops truncatus, in the Aransas Pass Area of Texas*, U.S. Marine Mammal Commission Report No. MMC-76-11, Washington, DC, 1, 1978.
- [134] Gruber, J.A., *Ecology of the Atlantic Bottlenose Dolphin (Tursiops truncatus) in the Pass Cavallo Area of Matagorda Bay, Texas*, M.S. Thesis, Texas A&M University, College Station, Texas, 1, 1981.
- [135] Harvey, J.T. and M.E. Dahlheim, Cetaceans in oil, *Marine Mammals and the Exxon Valdez*, T.R. Loughlin (ed.), Academic Press, San Diego, 257, 1994.
- [136] Kent, D.B., S. Leatherwood, and L. Yohe, *Responses of migrating gray whales, Eschrichtius robustus, to oil on the sea surface*, Report of the Hubbs-Sea World Research Institute, San Diego, 1, 1981.
- [137] Evans, W.E., A study to determine if gray whales detect oil, *Study of the Effects of Oil on Cetaceans, Final Report, Contract No. AA 551-CT9-29*, J.R. Geraci and D.J. St. Aubin (eds.), U.S. Department of the Interior, Bureau of Land Management, Washington, DC, 47, 1982.
- [138] Ridoux, V., L. Lafontaine, P. Bustmante, F. Caurant, W. Dabin, et al., The impact of the “Erika” oil spill on pelagic and coastal marine mammals: Combining demographic, ecological, trace metals and biomarker evidences, *Aquat. Living Resour.*, 17, 379, 2004.
- [139] Schwacke, L.H., C.R. Smith, F.I. Townsend, R.S. Wells, L.B. Hart, et al., Health of common bottlenose dolphins (*Tursiops truncatus*) in the Gulf of Mexico following the Deepwater Horizon oil spill, *Environ. Sci. Technol.*, 48, 93–103, 2014.
- [140] Schwacke, L.H., C.R. Smith, F.I. Townsend, R.S. Wells, L.B. Hart, et al., Response to comment on health of common bottlenose dolphins (*Tursiops truncatus*) in Barataria Bay, Louisiana following the Deepwater Horizon oil spill, *Environ. Sci. Technol.*, 48, 4209, 2014.
- [141] Wells, R.S., H.L. Rhinehart, L.J. Hansen, J.C. Sweeney, F.I. Townsend, et al., Bottlenose dolphins as marine ecosystem sentinels: Developing a health monitoring system, *EcoHealth*, 1, 246, 2004.
- [142] Wells, R.S., Social structure and life history of common bottlenose dolphins near Sarasota Bay, Florida: Insights from four decades and five generations. *Primates and Cetaceans: Field Research and Conservation of Complex Mammalian Societies*, Primatology Monographs, J. Yamagiwa and L. Karczmarski (eds.), Springer, Tokyo, 149–172, 2014.
- [143] Hart, L.B., R.S. Wells, and L.H. Schwacke, Reference ranges for body condition in wild bottlenose dolphins (*Tursiops truncatus*), *Aquat. Biol.*, 18, 63–68, 2013.
- [144] Allan, S.E., B.W. Smith, B.W., and K.A. Anderson, Impact of the Deepwater Horizon oil spill on bioavailable polycyclic aromatic hydrocarbons in Gulf of Mexico coastal waters, *Environ. Sci. Technol.*, 46 (4), 2033–2039, 2012.

OIL SPILL IMPACT AND RECOVERY OF COASTAL MARSH VEGETATION

QIANXIN LIN

Department of Oceanography and Coastal Sciences, School of the Coast and Environment, Louisiana State University,
Baton Rouge, LA, USA

19.1	Introduction	477
19.2	Toxicity and Impact as a Function of Oil Type and Oil Weathering Degree	477
19.3	Sensitivity to Oil Varies by Plant Species	478
19.4	Effects of Oil Exposure Modes on Severity of Oil Impacts	479
19.5	Effects of Oil Spill Cleanup Procedures on Marsh Recovery	481

19.1 INTRODUCTION

Coastal marshes are one of the most important ecosystems because of their high biological productivity, fisheries' support, wildlife habitats, storm mitigation, and shoreline protection. However, coastal wetlands are at high risk of oil spill impacts given that intensive petroleum oil exploration, production, transportation, and refinery activities occur along coasts throughout the world. Not only do oil spills in coastal marshes, such as pipeline ruptures, or near shore oil facility incidents impact these ecosystems, but offshore spilled oil as well. The recent *Deepwater Horizon* oil platform incident on April 20, 2010, in the Gulf of Mexico, 80km from the Louisiana shoreline, transported oil ashore and severely damaged the coastal marshes. Impacts of oil spills on coastal marshes vary widely and depend upon numerous factors, such as oil type, oil amounts and concentration, oil weathering degree, oil exposure mode, species exposed to oil, cleanup methods, and others. Although, all organisms could be affected in oil impacted marshes, in this chapter, the focus is on plants since they are the foundation components of wetlands; healthy vegetation is vital to sustain wetland structure and function to promote important wetland ecosystem services.

19.2 TOXICITY AND IMPACT AS A FUNCTION OF OIL TYPE AND OIL WEATHERING DEGREE

Oil type and oil weathering degree determine the toxicity in wetland environments. Light, small molecule oil components contribute more to chemically toxic effects on marsh plants; however, heavy, large molecule oil components may have more physical suffocating, coating, and fouling effects. Diesel and No. 2 fuel oil are typical examples of light refined products containing higher proportions of smaller molecule hydrocarbons. Crude oils, mixture of various oil components, and No. 6 fuel oil are generally heavier than the light refined product. Different sources of crude oils can have very different hydrocarbon compositions, and thus have different toxicity; South Louisiana crude (SLC) oil that is composed of relatively high proportion of lighter-weight hydrocarbons is a light crude oil, and is more toxic to biota than heavy crude, such as San Joaquin or Venezuela crude [1]. Spilled oils, especially for crude oils with a full range of hydrocarbons, become heavier by losing lighter hydrocarbon components with volatilization, dissolution, degradation, photooxidation, and emulsification during the oil weathering processes; thus, oil weathering processes change the chemical composition and physical properties and reduce the toxicity of the spilled oil.

Crude oils, in general, are less toxic to marsh plants than light refined oil products. *Spartina alterniflora*, one of the most dominant salt marsh plant species along the northern Gulf of Mexico and the east coast of the United States, has been widely studied in oil spills. Generally, *S. alterniflora* has a good chance of recovering from light to moderate crude oil spills [2,3]. Initial impacts of SLC oil on *S. alterniflora* may increase with increasing shoot coverage of the oil; however, the plants can recover from as much as 100% shoot coverage

of crude oil usually in a growing season [3]. New shoot production may begin as soon as days to weeks after oiling, although complete shoot fouling of *S. alterniflora* with crude oil could cause the death of all oiled leaves and shoots [3,4]. *S. alterniflora*, *Spartina patens*, and *Sagittaria lancifolia* could generally recover from light to moderate crude oiling (such as 21m^{-2}) in a growing season, although initial effects of oil shoot coverage can be significant [2,5]. However, large amount of crude oil or heavy fuel on/in the marsh soil may also cause long-term impacts to marsh vegetation as discussed in the following oil exposure mode section.

Light refined oil products, such as No. 2 fuel oil and diesel fuel, can severely damage marsh vegetation and may cause long-term impacts to coastal marshes and hamper recovery of marsh plants. Complete shoot coverage of No. 2 fuel oil can rapidly kill above-ground plant material; regrowth from rootstock may not occur even 1 year after oiling [6]. A pipeline rupture of No. 2 fuel severely affected *S. alterniflora* salt marsh; 95% of the surface area denuded of vegetation by the oil remained unvegetated 7 years after the spill [7]. In a spill of No. 2 and No. 6 fuel oils, heavily oiled *Spartina* marshes showed continuing oil impacts 7 years after the spill [8]. Even four decades after the spill of No. 2 fuel oil from *Barge Florida* in West Falmouth, MA, stem density and above- and belowground biomass of *S. alterniflora* was decreased in oiled areas, which led to unconsolidated sediments, increased topographical variation and, ultimately, loss of salt marsh habitats [9]. Light, small molecule oil components may penetrate soil more readily than heavy oil components. In addition, small molecule oil components may be absorbed from foliage to roots and rhizomes, and affect plant regeneration from belowground rhizomes [6]. All these studies indicate that oil type determines the toxicity; a larger proportion of small molecular components in light refined oil has higher toxicity to marsh plants and reduces the chance of recovery of marsh plants.

Oil weathering processes change oil chemical composition, as a result, changing oil toxicity. In general, toxicity of spilled oil decreases with oil weathering processes by volatilization, degradation, and dissolution of smaller molecular hydrocarbon components. Fresh SLC oil in the soil at oil dosages less than 41m^{-2} affected *S. alterniflora* and *S. patens*. Dosages between 16 and 241m^{-2} can completely kill these marsh plants; however, the same 16 and 241m^{-2} dosages of SLC oil weathered in the soil 2 years with residual TPH concentrations less than 400mg g^{-1} did not significantly affect the transplants of *S. alterniflora* and *S. patens*, indicating that the weathering process greatly reduced oil toxicity [10,11].

Emulsification, mixing of water-in-oil in water turbulence, also alters physical and chemical properties of oil; emulsified oils that may contain water content more than 50% are more viscous, sticky, and dense, although the oil toxicity decreases by dissolution and degradation of smaller molecule hydrocarbon components during oil emulsification. Fresh, unweathered light oil generally coats a thin oil film over plant



FIGURE 19.1 Viscous, emulsified oil added extra weight to shoots of marsh grasses, prevented the shoots from returning to their vertical position, and killed the grasses (*Deepwater Horizon* (DWH) oil spill, Northern Barataria Bay, LA, USA, January and April 2011).

shoots and leaves. However, emulsified oil may thickly coat plant leaves, shoots, and marsh soil surface due to its high viscosity. The viscous, emulsified oil can add extra weight to the shoots of marsh grasses, preventing them from returning to their vertical position. Laid over shoots can be likely more prone to being saturated with oil and/or repeatedly reoiled during tidal cycles, and thereby, impacts can be greater (Fig. 19.1). Therefore, effects of oiling on marsh vegetation are more complex than just chemical toxicity of oil.

19.3 SENSITIVITY TO OIL VARIES BY PLANT SPECIES

Plant species exhibit a great variation of responses to oil spills. Usually annual plant species are more susceptible to oil than perennials probably because they have smaller belowground reserves for regrowth after plants have been affected by the



FIGURE 19.2 *S. alterniflora* and *Distichlis spicata* were recovering with new shoots emerging following crude oil impact; however, *J. roemerianus* did not initiate new shoot growth (DWH oil spill, Northern Barataria Bay, LA, USA, January 2011).

oil. In a 4-year study of an oil spill in a freshwater marsh, Burk observed that all of the 23 species that were relatively unaffected or more abundant following the spill were perennials [12]. Dalby observed that perennial species with large rhizomes survived much better than annuals, but annuals were returning because they are opportunistic species biologically adapted to disturbed sites that are often ephemeral in nature [13]. Natural recovery may begin by invasion of the impacted areas with opportunistic annuals and rhizome spreading of perennials after oil spills [14].

Even among perennials, there is also a large variation in plant species in responding to oil spills in wetlands. A mesocosm study of effects of SLC oil at dosages of 0, 4, 8, 16, and 241m^{-2} revealed that there are great differences in tolerance of oil in the soil among perennial marsh plant species. *S. patens* was relatively sensitive to oil with significant impact at dosage of 41m^{-2} ; *S. alterniflora* showed more tolerance to the oil than *S. patens*; surprisingly, *S. lancifolia* showed a great oil tolerance with no adverse effect of oil even at



FIGURE 19.3 New live branches of *P. australis* grew from shoot nodes that have been heavily covered by crude oil, although the existing oiled leaves died (DWH oil spill, near the mouth of the Mississippi River, LA, USA, July 2010).

241m^{-2} probably due to its large belowground rhizomes and thick cuticle layer on its leaf surface [10]. A similar trend of oil impacts among these plants was reported in another study [2]. *Juncus roemerianus* and *S. alterniflora* often codominate in coastal salt marshes; recovery of *J. roemerianus* is much more severely affected by crude oil coverage of shoots than *S. alterniflora*, (Fig. 19.2) although these two species exhibited similar tolerance to moderate oiling in/on the soil and were severely affected by heavy oiling initially [3]. Morphologically, *J. roemerianus* has no real, rigid stems; leaves of *Juncus* grow from the soil surface up. Oil that covers *Juncus* leaves may readily translocate to their much closer belowground rhizome and roots, and affect their belowground components. Although complete thick oil coverage of plant shoots may cause mortality of the existing oiled shoots for most marsh plant species, shoots of *Phragmites australis* (common reed) may survive from oil coverage; new branches can grow from shoot nodes that have been covered by crude oil (Fig. 19.3). All these indicate that there are great differences in oil sensitivity among marsh plant species, and different oil spill cleanup procedures may be needed for different types of marshes.

19.4 EFFECTS OF OIL EXPOSURE MODES ON SEVERITY OF OIL IMPACTS

Spilled oil may come in contact with coastal marsh plants by either/both coating marsh plant shoots and leaves, thereby affecting the plants from their aerial portion or/and fouling and penetrating the soil, thus impacting the plants from their belowground rootstock. Oil coverage of shoots and leaves of marsh plants may result in instant effects, such as physically clogging leaf stomata, thus instantly inhibiting photosynthesis

and transpiration, two of the most important plant physiological processes. In addition to physical effects of oil, smaller molecule oil components may directly disturb cell membranes, disrupt the integrity of chloroplasts, and cause leaf necrosis. Crude oil coverage of the entire leaf can immediately cease photosynthetic activity of marsh plant species such as *S. alterniflora* and *J. roemerianus* [3,15]. Generally, plant leaves and shoots that have been covered by oil will die eventually within days to weeks dependant on oil toxicity. Thus, initial impacts of oil coverage are usually evident. However, most marsh plants may recover well if the oil does not severely affect their rhizomes. When crude oil primarily covers just the plant shoots, *S. alterniflora* is likely to regrow new shoots from surviving belowground rhizomes (Fig. 19.4) and recover to similar aboveground density and biomass values over time, although the existing oiled shoots die eventually [3]. Similar to crude oil, No. 6 fuel (a heavy fuel oil) coverage of the majority of shoots can kill the oiled aboveground portion of *S. alterniflora*; however, the coverage did not detrimentally affect a plant's new growth the following spring [16]. On the other hand, for light refined oil products, such as No. 2 fuel, even with oil primary coverage of shoots and leaves, small molecule oil components may be absorbed from foliage to plant belowground organs or penetrate the soil to the root zone, affect the viability of roots and rhizomes, thus affecting the plant regrowth and recovery after the oil coverage [6].

Oil floating on the water surface nearshore may enter coastal marshes with currents, winds, storms, and tides. Spilled oil that floats over the water surface in permanently or semi-permanently flooded marshes may prevent new shoots growing through the floating oil layer. In a marsh dominated by *P. australis* near the mouth of Mississippi River, crude oil that was contained in booms floating over an inundated marsh for a year prevented new shoots from emerging through the floating oil layer. New young leaves and shoots came in contact with the floating oil and died. As



FIGURE 19.4 *S. alterniflora* initiated recovery following a crude oil spill by growing new shoots from their surviving rhizomes, although the oil covered shoots died (DWH oil spill, Northern Barataria Bay, LA, USA, January 2011).

existing no oil-coated old shoots senesced and no new shoots regenerated, complete plant mortality occurred within the booms in the following growing season [17]. Furthermore, the floating oil layer may cause repeated oiling when oil over the standing water fluctuates with tides; repeated oiling may consume or eventually deplete belowground carbon and nutrient reserves that are used to generate new shoots. Without the acquisition of enough new carbon from photosynthesis, marsh vegetation may eventually die from repeated oil coverage. Therefore, floating oil in marshes should be removed as soon as possible.

Effects of oil that fouls the marsh soil depend upon the oil amount and oil toxicity. Marsh plants may survive from moderate crude oil on/in the soil. Light to moderate crude oil concentration on/in the soil may not severely affect the recovery of *S. alterniflora* and *J. roemerianus* [3,18,19]. However, oil concentrations on/in the soil ultimately determine the severity of impact to marsh plants and their recovery [3,20]. Heavy, thick and high concentrations of oil (Fig. 19.5), even when highly weathered, emulsified and not deeply penetrating the soil (Fig. 19.6), can still cause complete plant mortality. The *Metula* spill of 47,000 tons of light Arabic crude in the Strait of Magellan, Chile, occurred in August 1974; some of the spilled oil landed on shores and killed marsh vegetation. Even 17 years after the spill, thick oil/mousse deposits with soft and fresh appearance under the surface skin were visible on the marsh surface; there was very little plant recolonization and recovery in the areas with thick deposits [21]. Oil penetration of soil may come in contact with roots and rhizomes, and directly affect plant belowground rootstock. However, water content in the soil, oil viscosity, soil organic matters, and soil texture may affect the degree of oil penetration of soil. Heavier and more viscous oil may have less chance of penetrating into small pores in the soil. Coarse soil texture may have larger pores for oil



FIGURE 19.5 Beneath the thin, weathered surface oil residue, thick (>1 cm) and relatively continuous emulsified crude killed and prevented marsh plants from re-growing (DWH oil spill, Northern Barataria Bay, LA, USA, January 2011).



FIGURE 19.6 Thick (>1 cm) surface oil residues and emulsified crude oil did not always penetrate deeply into the soils, but still killed coastal salt marsh plants (*DWH* oil spill, Northern Barataria Bay, LA, USA, April 2011).

penetration. Secondary source of sediment porosity, such as crab burrows, existing plant shoot and root channels, desiccation cracks, and so on may enhance oil penetration of sediment [22,23]. Oil tends to affiliate to organic matter; higher organic matter content may have greater capacity for absorption of oil [10]. Saturated soil with water occupying pores in the soil can reduce oil entering the soil since water and oil generally repel each other. Combination of these conditions can potentially modify oil penetration of the soil.

19.5 EFFECTS OF OIL SPILL CLEANUP PROCEDURES ON MARSH RECOVERY

In addition to the aforementioned factors that control impacts and recovery of wetlands, oil spill cleanup procedures can also affect marsh vegetation by either accelerating or delaying their recovery. Wetland oil spill cleanup and restoration may include cutting the oiled vegetation, low pressure water flushing, pooled oil vacuuming, oiled surface soil stripping, *in situ* burning, restoration by vegetative planting, and other methods [24,25]. In general, wetland cleanup procedures should promote recovery of wetland structure and function in addition to oil removal and aesthetics.

Intensive physical disturbance during cleanup may do additional damage to marshes other than oil itself. Heavy foot traffic may break plant belowground rhizomes, thus affecting regeneration of wetland plants. Foot traffic can also trample the plants and soil surface and mix oil into the substrate; oil in the subsurface soil may persist longer than in the surface because of slower oil degradation under anaerobic conditions in deep soil. Walking boards may reduce the damage of foot traffic and may be needed when the marsh surface is soft.

Generally, the purpose of the oiled vegetation cutting is to avoid animal contamination when animals enter or pass through oiled wetlands. In addition, cutting the heavily oiled vegetation is also to remove laid-over heavily oiled vegetation that was trapping a thick layer of emulsified oil on the marsh surface, such as in the case of *Deepwater Horizon* (*DWH*) oil spill. However, cutting may require heavy foot traffic in marshes and may cause adverse effects. In addition, vegetation cutting may open and expose wetland plant aerenchyma (air channel in the shoots and roots of many wetland plants, which allows exchange of gases between plant shoots and roots) to oil, thus potentially resulting in oil translocation to plant belowground components, thereby affecting plant roots and rhizomes and marsh regeneration capability. Due to the detrimental effects of cutting, marshes should not be cut when impacted by light oils, where high flushing rates are present, or where reoiling would be likely [26].

Any cleanup procedures that may affect the wetland soil integrity generally should be avoided. Low pressure, large volume water flushing may refloat some oil on the marsh soil surface and herd the floating oil out of marshes to a central collection area; subsequently the herded oil may be collected by skimmers or other methods. However, high-pressure flushing should be avoided since it will most likely damage the integrity of the marsh soil surface. Some pooled oil may be vacuumed; however, vacuuming can also remove the surface sediment, thus disturbing the integrity of marsh surface soil structure. Stripping oiled surface sediment can do more damage to wetlands than oil itself. For coastal marshes, most live plant roots and rhizomes are located at the top 0–20 cm of soil depth. Live marsh plant roots are vital to bind soil and maintain soil shear strength and integrity, thus limiting or slowing erosion. Soil stripping can remove plant roots and rhizomes in the top soil, eliminate vegetation recovery from rhizomes, lower the elevation of the marsh, and expose the subsurface soil that contains fewer living roots and rhizomes and therefore has lesser shear strength. As a result, soil stripping may lead to accelerated marsh erosion. Under most circumstances, excessive removal of surface soils should be avoided. In the case of the *Amoco Cadiz* oil spill, rapid erosion occurred after removing oiled surface sediments up to 50 cm depth in some areas; 12 years after spill, marsh area was reduced by 22–38%, partly due to the initial sediment removal [27,28]. If sediment stripping is necessary in some cases of heavily oiled marshes, sediment backfilling to the original elevation and subsequently vegetative replanting can be helpful for restoration of the oiled marshes [29].

In situ burning may effectively remove bulk oil and accelerate marsh recovery. *In situ* burning is likely suitable for many herbaceous marsh types, but not for forested or shrub wetlands. Standing water over the soil surface is one of the most important factors that control the post-burning recovery of marsh vegetation. As little as several centimeters of standing water over the marsh surface may protect roots and rhizomes from burning or heat scorch, which adversely

TABLE 19.1 Effects of oil spills and cleanup on recovery of coastal marsh vegetation

Oil exposure route	Controlling factors	Impacts	Recovery time	Cleanup	Advantage of cleanup	Disadvantage of cleanup	References
Oil coverage of shoots/leaves	Oil type, oil weathering degree, plant species, oil thickness of coverage	Immediately clog stomata and inhibit leaf photosynthesis and transpiration, cause leaf necrosis and shoot mortality for most plants	Months to years	No cleanup if light oiling Manually cutting oiled shoots	No additional impacts from cleanup Reduces wildlife contacting oil	Aesthetic only Trampling can break roots and rhizomes, push or mix oil into the sediments	[2-4,6,23,33,36]
Floating oil layer in permanently or semi-permanently flooded marshes	Oil type, oil weathering degree, plant species, repeated oiling, oil thickness, duration of flooding, duration of oil presence	Prevent new shoots from growing through the floating oil layer, may cause repeated oiling, and oil contacting soil when standing water table fluctuates	May recover after removal of floating oil	In situ burning Vacuuming Low pressure, large volume water flush	Cleanup large area in a short time For small area, patch, pooled oil Herd oil out of marshes	May cause root burn and delay recovery if marshes are too dry May also suck in surface soil in shallow standing water May not be effective for large area	[1,17,24,30,31,36]
Oil on/in the soil or/and combined with oiled shoots	Oil type, oil weathering degree, plant species, substrate characteristic, thickness and coverage of oil, depth of oil penetration or burial	Impact to belowground components, such as affecting plant roots from uptaking nutrients and rhizomes from reproducing new shoots or/and impact to aboveground components	Years to decades dependant on severity of oiling or erosion may occur before recovery	In-situ burn Low pressure, large volume water flushing Oiled surface sediment stripping Cutting lain-over oiled vegetation, raking, scraping and scooping oil off the soil surface	Effectively removing the floating oil, benefit to vegetation recovery Lifting and refloating surface oil to water surface Remove heavily oiled sediment, may need soil backfilled and re-planting Reduce oil content, enhance surface oil weathering	Relatively short window of opportunity, burning in low tide may flood and suffocate shoot stubbles during high tide Need fine control, oil accumulating in low elevation area Damage soil integrity by removing top root zone, likely enhance erosion Trampling, push or mix oil into the sediments	[7,21,27,28] [1,9,26,32,37]
Restoration by replanting				In-situ burning	Removing oiled shoots	Not effective for removing oil in the soil, may cause root burn and affect recovery if soil dry	
Restore and stabilize marshes, transplants may also enhance oil degradation via phytoremediation				Need intensive labor, may cause physical disturbance during replanting			

affects plant regrowth and recovery [30,31]. *In situ* burning is generally effective in removing the oil floating over the water surface and oil coating on aboveground plant shoots; however, burning is not effective for removing oil in or on the soil [32,33]. It is better to burn oiled marshes as soon as possible after spills to prevent the oil from spreading and contaminating adjacent environments and penetrating into soil. *In situ* burning successfully removed an estimated 80–90% of bulk oiling from a spill during Hurricane Katrina, even 40 days after the initial release [33]. Plants can start growing in days to weeks after *in situ* burning and may completely recover in one to two growing seasons [33–36].

Replanting may be necessary to restore heavily oiled marshes if oiling has killed or is likely to kill the below-ground roots and rhizomes. Wetland erosion could occur if natural regrowth and recovery of marsh plants do not occur in a relatively short timeframe [7,20]. Transplants of *S. alterniflora* grew well in soil contaminated with No. 2 fuel oil, with aboveground plant biomass comparable to reference conditions 3 years after transplanting [7]. However, without transplanting, oiled marsh remained unvegetated after 7 years and experienced severe erosion [7]. Thus, replanting native marsh plants could be an effective procedure to promote marsh recovery and prevent erosion. However, it is sometimes difficult to determine if marshes will naturally recover without assistance of restoration. In general, marshes constantly generate new, young shoots during the growing season. If there are not any new shoots produced within a few months or a single growing season after an oil spill, it may indicate that the oil has detrimentally affected plant rhizomes and their ability to generate new shoots and recovery. In this case, replanting most likely is of benefit to assist marsh recovery. Replanting in a timely manner can restore marshes and limit erosion.

The primary factors likely controlling oil impacts and recovery are summarized in Table 19.1. Marsh oil spills are case specific; cleanup and restoration need to be tailored specially to the oil spill and ecological conditions.

ACKNOWLEDGMENTS

This article was made possible through the support from the Gulf of Mexico Research Initiative (GoMRI) to Louisiana State University. The findings in this article are those of the author and do not necessarily represent the views of GoMRI. In addition, the author thanks anonymous reviewers, especially reviewer 2, for their very helpful comments.

REFERENCES

[1] Mendelssohn, I.A., G.L. Anderson, D.M. Baltz, R.H. Caffey, K.R. Carmen, J.W. Fleeger et al., Oil impacts to coastal Wetland: Implications for the mississippi river delta ecosystem after the Deepwater Horizon oil spill, *Bioscience*, 62, 562, 2012.

[2] DeLaune, R.D., S.R. Pezeshki, A. Jugsujinda, and C.W. Lindau, Sensitivity of US Gulf of Mexico coastal marsh vegetation to crude oil: Comparison of greenhouse and field responses, *Aquat. Ecol.*, 37, 351, 2003.

[3] Lin, Q. and I.A. Mendelssohn, Impacts and recovery of the Deepwater Horizon oil spill on vegetative structure and function of coastal salt marsh in the Northern Gulf of Mexico, *Environ. Sci. Technol.*, 46, 3737, 2012.

[4] Pezeshki, S.R., R.D. DeLaune, J.A. Nyman, R.R. Lessard, and G.P. Canevari, Removing oil and saving oiled marsh grass using a shoreline cleaner, *IOSC*, 203, 1995.

[5] Delaune, R.D. and A.L. Wright, Projected impact of Deepwater Horizon oil spill on U.S. Gulf Coast Wetlands, *SSSAJ*, 75, 1602, 2011.

[6] Webb, J.W. and S.K. Alexander, No. 2 fuel oil effects on *Spartina alterniflora* in a Texas salt marsh, *Contrib. Mar. Sci.*, 32, 9, 1991.

[7] Bergen, A., C. Alderson, R. Bergfors, C. Aquila, and M.A. Matsil, Restoration of a *Spartina alterniflora* salt marsh following a fuel oil spill, New York City, NY, *Wetlands Ecol. Manage.*, 8, 185, 2000.

[8] Michel, J., Z. Nixon, J. Dahlin, D. Betenbaugh, M. White, M. Burton et al., Recovery of interior brackish marshes seven years after the chalk point oil spill, *Mar. Pollut. Bull.*, 58, 995, 2009.

[9] Culbertson, J.B., I. Valiela, M. Pickart, E.E. Peacock, and C.M. Reddy, Long-term consequences of residual petroleum on salt marsh grass, *J. Appl. Ecol.*, 45, 1284, 2008.

[10] Lin, Q. and I.A. Mendelssohn, A comparative investigation of the effects of Louisiana crude oil on the vegetation of fresh, brackish, and salt marsh, *Mar. Pollut. Bull.*, 32, 202, 1996.

[11] Lin, Q. and I.A. Mendelssohn, The combined effects of phytoremediation and biostimulation in enhancing habitat restoration and oil degradation of petroleum contaminated wetlands, *Ecol. Eng.*, 10, 263, 1998.

[12] Burk, C.J., A four year analysis of vegetation following an oil spill in a freshwater marsh, *J. Appl. Ecol.*, 14, 515, 1977.

[13] Dalby, D.H., Some observations on oil pollution of salt marshes in Milford Haven, *Biol. Conserv.*, 1, 295, 1969.

[14] Baca, B.J., T.E. Lankford, and E.R. Gundlach, Recovery of Brittany coastal marshes in the eight years following the Amoco Cadiz incident, *IOSC*, 459, 1987.

[15] Pezeshki, S.R. and R.D. DeLaune, Effect of crude oil on gas exchange functions of *Juncus roemerianus* and *Spartina alterniflora*, *Water Air Soil Pollut.*, 68, 461, 1993.

[16] Webb, J.W., G.T. Tanner, and B.H. Koerth, Oil spill effects on smooth cord grass *Spartina alterniflora* in Galveston Bay Texas USA, *Contrib. Mar. Sci.*, 24, 107, 1981.

[17] Lin, Q., I.A. Mendelssohn, C.B. Henry, M.W. Hester, and E.C. Webb, Effects of oil cleanup methods on ecological recovery and oil degradation of *Phragmites* marshes, *IOSC*, 511, 1999.

[18] Lin, Q. and I.A. Mendelssohn, Evaluation of tolerance limits for restoration and phytoremediation with *Spartina alterniflora* in crude oil-contaminated coastal salt marshes, *IOSC*, 829, 2008.

[19] DeLaune, R.D., W.H. Patrick, and R.J. Buresh, Effect of crude oil on a Louisiana *Spartina alterniflora* salt marsh, *Environ. Pollut.*, 20, 21, 1979.

- [20] Silliman, B.R., J. van de Koppel, M.W. McCoy, J. Diller, G.N. Kasozi, K. Earl et al., Degradation and resilience in Louisiana salt marshes after the BP-Deepwater Horizon oil spill, *PNAS*, 109, 11234, 2012.
- [21] Baker, J.M., L.M. Guzman, P.D. Bartlett, D.I. Little, and C.M. Wilson, Long-term fate and effects of untreated thick oil deposit on salt marshes, *IOSC*, 395, 1993.
- [22] Hayes, M.O., J. Michel, T.M. Montello, D.V. Aurand, A.M. Al-Mansi, A.H. Al-Momen et al., Distribution and weathering of shoreline oil one year after the Gulf War oil spill. *Mar. Pollut. Bull.*, 27, 135, 1993.
- [23] Zengel, S.A., M.O. Hayes, B. Benggio, and F. Lopez, Oil penetration and vegetation recovery in the Lajas Creek Marsh, Puerto Rico, *IOSC*, 545, 2001.
- [24] Hoff, R.Z., Responding oil spills in coastal marshes: The fine line between help and hindrance, *NOAA HAZMAT Report 96-1*, Seattle, WA, 1995.
- [25] Zengel, S.A. and J. Michel, Deepwater Horizon oil spill: Salt marsh oiling conditions, treatment testing, and treatment history in northern Barataria Bay, Louisiana, *NOAA Tech. Report, Office of Response and Restoration*, Seattle, WA, 2011.
- [26] Zengel, S.A. and J. Michel, Vegetation cutting as a clean-up method for salt and brackish marshes impacted by oil spills: A review and case history of the effects on plant recovery, *Mar. Pollut. Bull.*, 32, 876, 1996.
- [27] Long, B.F. and J.H. Vandermeulen, Geomorphological impact of cleanup of an oiled salt marsh (Ile Grande, France), *IOSC*, 501, 1983.
- [28] Gilfillan, E.S., N.P. Maher, C.M. Krejsa, M.E. Lanphear, C.D. Ball, J.B. Meltzer et al., Use of remote sensing to document changes in marsh vegetation following the Amoco Cadiz oil spill (Brittany, France, 1978), *Mar. Pollut. Bull.*, 30, 780, 1995.
- [29] Krebs, C.T. and C.E. Tanner, Restoration of oiled marshes through sediment stripping and *Spartina* propagation, *IOSC*, 386, 1981.
- [30] Lin, Q., I.A. Mendelssohn, K. Carney, N.P. Bryner, and W.D. Walton, Salt marsh recovery and oil spill remediation after *ins-situ* burning: Effects of water depth and burn duration, *Environ. Sci. Technol.*, 36, 576, 2002.
- [31] Lin, Q., I.A. Mendelssohn, N.P. Bryner, and W.D. Walton, *In-situ* burning of oil in coastal marshes: 1. Vegetation recovery and soil temperature as a function of water depth, oil type and marsh type, *Environ. Sci. Technol.*, 39, 1848, 2005.
- [32] Lin, Q., I.A. Mendelssohn, K. Carney, S.M. Miles, N.P. Bryner, N.P. Walton et al., *In-situ* burning of oil in coastal marshes: 2. Oil spill cleanup efficiency as a function of oil type, marsh type and water depth, *Environ. Sci. Technol.*, 39, 1854, 2005.
- [33] Merten, A.A., C.B. Henry, and J. Michel, Decision-making process to use in-situ burning to restore an oiled intermediate marsh following Hurricane Katrina and Rita, *IOSC*, 545, 2008.
- [34] Lindau, C.W., R.D. Delanne, A. Jugsujinda, and E. Sajo, Response of *Spartina alterniflora* vegetation to oiling and burning of applied oil, *Mar. Pollut. Bull.*, 38, 1216, 1999.
- [35] Lindau, C.W., R.D. Delanne, and A. Jugsujinda, Marsh sensitivity to burning of applied crude oil, *Spill Sci. Technol. Bull.*, 8, 404, 2003.
- [36] Baustian, J., I.A. Mendelssohn, Q. Lin, and J. Rapp, *In-situ* burning restores the ecological function and structure of an oil-impacted coastal marsh. *Environ. Manage.*, 46, 781, 2010.
- [37] Pezeshki, S.R., M.W. Hester, Q. Lin, and J.A. Nyman, The effects of oil spill and clean-up on dominant US Gulf coast marsh macrophytes: A review. *Environ. Pollut.*, 108, 129, 2000.

PART X

NATURAL DISPERSION

A REVIEW OF NATURAL DISPERSION MODELS

MERV FINGAS

Spill Science, Edmonton, Alberta, Canada

20.1	Introduction	487
20.2	The Mackay Approach	487
20.3	The Audunson Approach	489
20.4	The Delvigne Approach	490
20.5	Residence in the Water Column	492
20.6	Comparison of the Models	492
20.7	Conclusions	494

20.1 INTRODUCTION

Natural dispersion occurs when fine droplets of oil are transferred into the water column by wave action or turbulence. Smaller oil droplets (<20 µm or 0.020 mm) are stable in water for short periods of time. Larger droplets (>~50 µm) rise quickly to the surface. Depending on oil conditions and the amount of sea energy available, natural dispersion can be insignificant or it can temporarily displace some of the oil. In 1993, the oil from a stricken ship, the *Braer*, dispersed and sedimented almost entirely as a result of high seas off Scotland at the time of the spill and the dispersible nature of the oil cargo [1]. It should be noted that natural dispersion may just be an intermediary in the oil-sediment reaction and subsequent sedimentation. A more accurate view of the *Braer* spill is that it was largely sedimented as a result of oil-fines interaction.

Natural dispersion is dependent on both the oil properties and the amount of sea energy [2]. Heavy oils such as Bunker C or a heavy crude will not disperse naturally to any significant extent, whereas diesel fuel and even light crudes can disperse significantly if the saturate content is high. In addition, significant wave action is needed to disperse oil. In 40 years of monitoring spills on the oceans, those spills where oil has dispersed naturally have all occurred in very energetic seas—up to Beaufort 7. Further, many of these spills involved sedimentation.

The long-term fate of naturally dispersed oil is not known. The oil may degrade to some extent as it consists primarily of saturate components. Some of the dispersed oil may rise and form another surface slick or it may become associated with sediment and be precipitated to the bottom.

20.2 THE MACKAY APPROACH

MacKay et al. pursued the topic of natural dispersion using experimental data as well as a theoretical approach, the latter largely consisting of propositions [3]. In the end, the theoretical approach was finally used with approximate experimental data only used to confirm the values in the theoretical equations. The MacKay approach recognized that most droplets would resurface and that only the smallest might remain in the water for a long time.

The laboratory experiments were conducted in a smaller laboratory vessel and a small flume, both of which were also used to test chemical dispersants. Different types of waves or energy were generated in these vessels. Samples were taken, and the oil in these samples was measured using infrared (IR). No particle size measurements were taken. Results were only compared to that resulting from theoretical approaches. The conclusions of the experimental study were that there are two separate mechanisms of oil spill dispersion into the water column—for non-breaking waves and breaking waves. The non-breaking wave mechanism is purportedly a stretching–compression mechanism and that of the breaking wave is just that.

The theoretical approach begins with the assumption that [3]:

$$R_D = D(dC/dZ) = C_s K_1 \quad (20.1)$$

where, R_D is the rate of diffusion of particles (g/m²·s)

D is the rate of diffusion (m/s)

dC/dZ is the gradient of diffusion (g/l·m)

C_s is the concentration of small particles (g)

K_1 is the mass transfer coefficient rate (m/s).

Assuming a steady state:

$$R_c = V_L C_L + V_S C_S \quad (20.2)$$

where, R_c is the rate of diffusion of particles in $\text{g/m}^2 \cdot \text{s}$

c is the droplet concentration

V_L is the rising velocity flux of the large particles

C_L is the concentration of the large particles

V_S is the rising velocity flux of the small particles

C_s is the concentration of the small particles

After some manipulation and separation of the large and small droplets:

$$C_S = (F_N R_N + F_B R_B) / (V_S + K_1) \quad (20.3)$$

where, C_s is the concentration of the small particles

F_N is the fraction of small droplets produced by non-breaking waves

R_N is the rate of small droplet production by non-breaking waves

F_B is the fraction of small droplets produced by breaking waves

R_B is the rate of small droplet production by breaking waves

V_S is the rising velocity flux of the small particles

K_1 is the mass transfer coefficient rate (m/s)

For large droplets:

$$C_L = (1 - F_N) R_N ((1 - F_B) R_B) / V_L \quad (20.4)$$

where, C_s is the concentration of the small particles

F_N is the fraction of small droplets produced by non-breaking waves

R_N is the rate of small droplet production by non-breaking waves

F_B is the fraction of small droplets produced by breaking waves

R_B is the rate of small droplet production by breaking waves

V_L is the rising velocity flux of the small particles

It was proposed that the large droplets be ignored and that the following relationships might apply to add the effect of sea energy [3]:

$$R_N = K_2 X^n = K_3 S^m X^n \quad (20.5)$$

where, R_N is the dispersion rate ($\text{g/m}^2 \cdot \text{s}$)

K_2 is a constant depending on sea state

X^n is the slick thickness in m

K_3 is a constant

S^m is the sea state, the exponent, m , is proposed to be unity

The loss of small oil droplets then is stated as (presuming they do not rise):

$$F_N R_N = K_3 S x^{-0.25} = \rho dx / dt \quad (20.6)$$

where, $F_N R_N$ is the dispersion rate in $\text{g/m}^2 \cdot \text{s}$

F_N is the fraction of small droplets produced by non-breaking waves

R_N is the rate of small droplet production by non-breaking waves

K_3 is a constant

S is the sea state

x is the oil thickness in m

ρ is the oil density

dx/dt is the change in oil concentration at the surface

Integrating and substituting the expression for the lifetime of a slick is derived (not counting the rise of the droplets):

$$t = x_o^{1.25} \frac{\rho}{1.25 k_3 S} \quad (20.7)$$

where, t is the lifetime in seconds (not counting rising)

x_o is the starting slick thickness

ρ is the oil density

k_3 is a constant

S is the sea state

It should be noted that this construct requires the following considerations:

- the development only represents the amount going in the water column and does not count the rise,
- the development is purely based on suggestion and does not contain either "pure" theoretical or empirical evidence, and
- the relationship of oil thickness to dispersion and is not also based on theoretical or empirical evidence.

Examples are given of the calculated lifetimes if values of ρ , k_3 , and S are forced to give a value of 10^{-10} [3]. These values are ranging from a lifetime of 4 min for a slick of $1 \mu\text{m}$ to 16 days for a slick of 1 mm. It is then presumed that since these values seem reasonable that k_2 and k_3 would then typically have values of 10^{-4} giving typical dispersion rates of $10^{-3} \text{g/m}^2 \cdot \text{s}$.

The assumptions were applied to the breaking wave situation as well. It was assumed that the concentration of small droplets under breaking wave conditions rose within an hour. This would imply that U/V_s is 1 h and since U is about 0.5 m, V_s is about 0.0002 m/s. Assuming that F_B is 0.005, R_B becomes $8 \text{g/m}^2 \cdot \text{s}$. Then the concentration of small droplets becomes:

$$C_s = F_B R_B / V_s = 0.04 / V_s = 200 \quad (20.8)$$

where, C_s is the concentration of small droplets, g/m^3

F_N is the fraction of small droplets produced by breaking waves

R_B is the rate of small droplet production by breaking waves

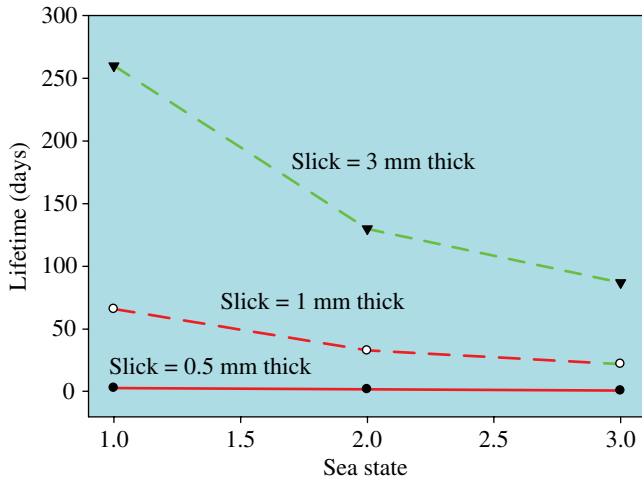


FIGURE 20.1 Natural dispersion for the Mackay model as depicted as lifetime versus sea state.

V_s is the velocity of the small droplets which is approximately 0.0002 m/s

These equations and further assumptions are combined into the following equations which use some of the above material:

$$F = K_A (U + 1)^2 \quad (20.9)$$

where, F = fraction of the sea surface subject to dispersion per second

U is the wind speed in m/s

K_A is a constant

$$F_B = \frac{1}{(1 + K_B \mu^{0.5} x \gamma)} \quad (20.10)$$

where F_B is the fraction of droplets below the critical size

K_B is a constant

μ is the viscosity

x is the slick thickness, m

γ is the oil-water interfacial tension

It should be noted that the Mackay model of natural dispersion should have the following considerations:

- The development only represents the amount going in the water column and does not count the rise, except near the end of development, where it is presumed that the small droplets stay permanently in the water column (which is not true).
- The development does not proceed to a readily usable modeling equation. Equation 20.7 is the most frequently used.
- The development is purely based on suggestion and does not contain either theoretical or empirical evidence.

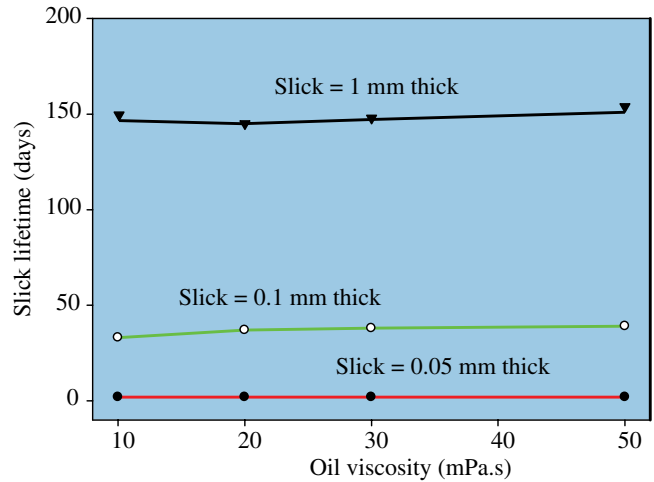


FIGURE 20.2 Natural dispersion for the Mackay model as depicted as lifetime versus oil viscosity. In both Figures 20.1 and 20.2, it can be seen that slick thickness is the most important factor.

- The inclusion of slick thickness as a major factor is questionable, especially as it has a stronger effect than either sea state or oil viscosity.
- The relationship of oil thickness, viscosity, and interfacial tension to dispersion and is not based on theoretical or empirical evidence.

Graphs showing how the Mackay model relates to the input factors of sea state and oil viscosity are shown in Figures 20.1 and 20.2. These show that slick thickness is much more important in this model than either sea state or oil density (here taken as viscosity equivalent).

20.3 THE AUDUNSON APPROACH

The Audunson approach was similar to that of MacKay in that propositions were made and these tested with hypothetical data [4–6].

Audunson proposed that the following could describe the amount of oil on the surface:

$$\frac{dQ}{dt} + \lambda_n Q = q(1 - f(t)) \quad (20.11)$$

where, Q is the amount of oil on the surface at a time

λ_n is the coefficient of natural dispersion

$\lambda_n Q$ is then the loss of oil by natural dispersion

$q(1 - f(t))$ is the loss of oil by evaporation

Estimations of these parameters from the *Bravo* blowout yielded a value of λ_n as 0.1/day. This would imply that being linear, the oil would dissipate in about 10 days. This is also equivalent to a half-life of 7 days or 1 week.

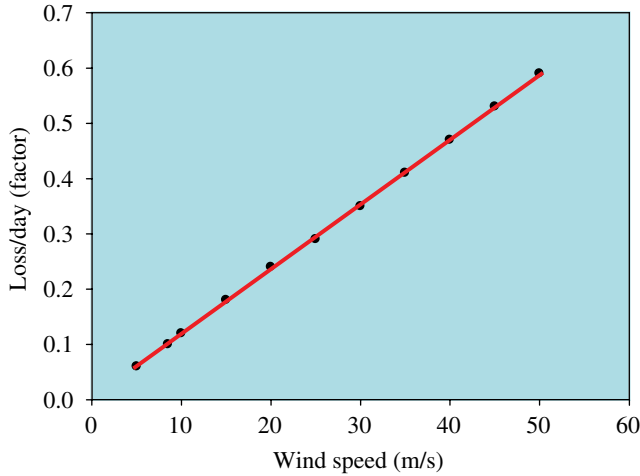


FIGURE 20.3 The dispersion predicted by the Audunson model. Note that the only input is the wind speed which linearly changes the dispersion. Also note that at high wind speeds, the oil would disappear within a day.

Audunson further proposed that the rate or coefficient of natural dispersion should change with the wind speed as:

$$\lambda_n = \lambda_o \left(\frac{U}{U_o} \right)^2 \quad (20.12)$$

where, λ_n is the coefficient of natural dispersion

λ_o is the base coefficient of natural dispersion

U_o is the wind speed at which λ_o was estimated, here taken as 8.5 m/s

U is the wind speed in question

Substituting the values in the equation, one obtains:

$$\lambda_n = 0.1 \left(\frac{U}{8.5} \right)^2 \quad (20.13)$$

where the items are above and λ_n would be given as per day.

Audunson tested this on the *Bravo* blowout findings and found that this appeared to fit the empirical data. No quantitative testing or measurement of oil at sea was carried out, however.

Considerations in using the Audunson model include the following:

- There are no inputs other than wind speed and the all-important factor of oil properties was not included.
- The loss is linear with wind speed; most other studies have found a wind or sea threshold.
- There were no specific studies carried out to develop the model only some overflights of the *Bravo* blowout,

which happened to persist for weeks on the surface and was not closely monitored.

- The model was never verified by experiments.
- The model vastly overpredicts natural dispersion.

Figure 20.3 shows the variation of dispersion with wind speed using the Audunson model. This shows a high linearity with wind speed with no wind onset threshold.

20.4 THE DELVIGNE APPROACH

Delvigne and associates studied the natural dispersion of oil in a series of wave tanks and a series of hydrological apparatuses [7–12]. The turbulence energy was related to the creation of naturally dispersed droplets. The model began with the creation of the following quasi-empirical equation:

$$Q_{(d)} = C_o D^{0.57} d^{0.7} \Delta d S_{cov} F_{wc} \quad (20.14)$$

where $Q_{(d)}$ is the entrained mass rate of droplet sizes in the interval around d per unit surface area and per unit time—given in $\text{kg/m}^2\cdot\text{s}$, D is the energy dissipation of the breaking wave per unit surface area (J/m^2), C_o is a constant for a given oil, a light oil is about 1000–1800, a medium oil about 500–1000, and a heavier oil less than 500, d , Δd is the droplet size and range of droplet size (interval) in m, S_{cov} is the fraction of the sea covered by oil (0–1), and F_{wc} is the fraction of sea surface affected by breaking waves per unit time (s^{-1}).

This was developed further by defining portions of the above equation:

$$F_{wc} = C_b (U - U_i) / T_w \quad (20.15)$$

where F_{wc} is the fraction of sea surface affected by breaking waves per unit time (s^{-1}) as in the equation above

C_b is a constant approximately 0.032 s/m

U is the wind speed (m/s)

U_i is the wind speed at the initiation of breaking waves ($\sim 5 \text{ m/s}$), and

T_w is the wave period (s)

So the equation above can be rewritten as:

$$F_{wc} = 0.032(U - 5) / T_w \quad (20.16)$$

Also, the energy dissipation (D) has been proposed as:

$$D = 0.0034 \rho_w g H_{rms}^2 \quad (20.17)$$

where D is the energy dissipation of the breaking wave per unit surface area (J/m^2)

ρ_w is the density of water (kg/m^3) which is 1030 for typical seawater

g is the acceleration due to gravity (m/s^2) which is 9.81

H_{rms} is the r.m.s. value of the wave height (m)

This then becomes:

$$D = 34.4 H_{\text{rms}}^2 \quad (20.18)$$

Substituting both of these into Equation 20.14 we get:

$$Q_{(d)} = C_o (34.4 H_{\text{rms}}^2)^{0.57} d^{0.7} \Delta d S_{\text{cov}} (0.032(U-5)/T_w) \quad (20.19)$$

where $Q_{(d)}$ is the entrained mass rate of droplet sizes in the interval around d per unit surface area and per unit time—given in $\text{kg/m}^2\cdot\text{s}$, C_o is a constant for a given oil, a light oil is about 1000–1800, a medium oil about 500–1000, and a heavier oil less than 500, H_{rms} is the r.m.s. value of the wave height (m), d , Δd is the droplet size and range of droplet size (interval) in m, S_{cov} is the fraction of the sea covered by oil (0–1), and T_w is the wave period (s).

An analysis of this equation using typical values shows that the most important factor is the wave height. This is shown in Figure 20.4. This is obvious as this factor is a square in the equation and the 0.57 power factor does not remove the effect entirely. The values in Figure 20.4 are plotted with the base lines fixed as the speed of wind is 10 m/s, wave height is 0.5 m, droplet size is 50 μm , sea coverage is 0.3, wave period is 10, and the oil constant is 500. The parameters in the model were varied as follows: wind from 5 to 50 m/s, wave period from 1 to 40 s, the oil constant from 100 to 1200, and the droplet size from 10 to 300 μm .

Several issues have been noted about the formation developed above. These are as follows:

1. The natural dispersion predicted was measured as a temporary phenomenon—that is the instantaneous

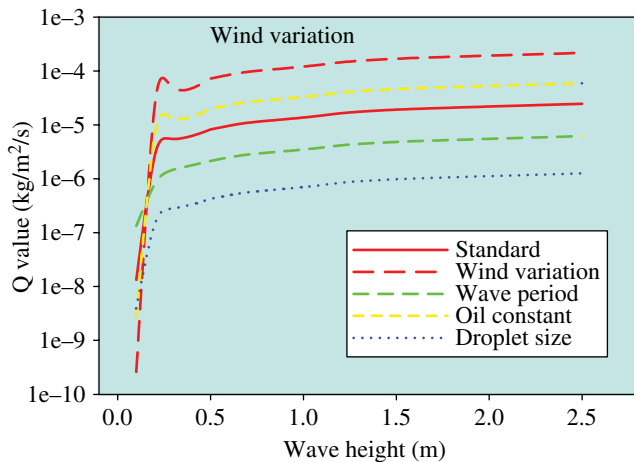


FIGURE 20.4 The relationship of dispersion in the early Delvigne formulation to illustrate the relationship versus various parameters.

input of droplets into the water column. The droplet persistence was not measured. The equation was designed to yield only the temporary input into the water column. Later workers assumed that this amount was permanently dispersed.

2. The equation overpredicts natural dispersion in most cases, especially in cases of low sea states.
3. The given Q is a rate with no input factor, thus mass on the ocean is not input or defined, further, it was stated that this is independent of the oil on the surface, also stated to be independent of oil thickness.
4. The oil constants appear to be arbitrary and the rules that they are 1 per viscosity does not work for cSt.
5. The wave periods in the wave tank experiments were very short.
6. The initiation wind should be greater than 5 m/s—perhaps 10–20 m/s.

These can be partially solved in terms of the Delvigne tank experiments. First, the experiments were mostly conducted with a thickness of 0.6 mm; this constitutes an oil density of 0.6 kg/m^2 . Dividing Equation 20.14 times this factor we get:

$$F_{(d)} = 1.67 C_o (34.4 H_{\text{rms}}^2)^{0.57} d^{0.7} \Delta d S_{\text{cov}} (0.032(U-5)/T_w) \quad (20.20)$$

where $F_{(d)}$ is the fraction of entrained mass rate of droplet sizes in the interval around d per unit surface area and per unit time—given in (s^{-1}), C_o is a constant for a given oil, a light oil is about 1000–1800, a medium oil about 500–1000, and a heavier oil less than 500, H_{rms} is the r.m.s. value of the wave height (m), d , Δd is the droplet size and range of droplet size (interval) in m, S_{cov} is the fraction of the sea covered by oil (0–1), U is the wind speed in m/s, and T_w is the wave period, s.

The droplet size is an issue. Delvigne had suggested a diameter of 300 μm ; however, examination by a number of parties shows that only about 20 μm is relatively stable for several hours [9]. An oil droplet with a diameter of 300 μm has a half life in the water column less than a second or two. Thus substituting 20 μm with a width of 10 μm into Equation 20.20 and assuming that 1/2 of the sea surface is covered in oil:

$$F_{(d)} = 1.75 \times 10^{-8} C_o (34.4 H_{\text{rms}}^2)^{0.57} (0.032(U-5)/T_w) \quad (20.21)$$

where $F_{(d)}$ is the fraction of entrained mass rate of droplet sizes in the interval around from 10 to 30 μm —given in (s^{-1}), C_o is a constant for a given oil, a light oil is about 1000–1800, a medium oil about 500–1000, and a heavier oil less than 500, H_{rms} is the r.m.s. value of the wave height (m), U is the wind speed in m/s, and T_w is the wave period, s.

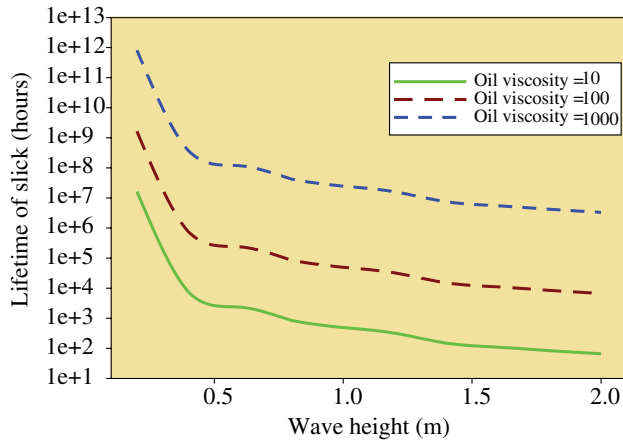


FIGURE 20.5 The dispersion of oil in the Delvigne model compared to oils of various viscosities. This uses the later formulation described in the text.

The oil constant (C_o) can be corrected by multiplying the viscosity value in cSt or mPa·s by 10^{-6} . Then the reciprocal becomes the constant noted in Delvigne's work. An example of this is if we have a medium crude with a viscosity of 120 mPa·s, then the oil constant becomes $1/100 \times 10^{-6}$ or 0.83. It should be noted that the rule-of-thumb given in the Delvigne papers does not come out to the constant he used [9]. This follows the Delvigne papers verbal description but not the mathematical examples. Further the units need to be converted correctly. So converting Equation 20.8 to include the viscosity of the oil rather than the constant and changing the time to hours we get:

$$F_{(d)} = 6.3 \times 10^{-4} / \rho^{1.5} (34.4 H_{rms}^2)^{0.57} (0.032(U - 15)/T_w) \quad (20.22)$$

where $F_{(d)}$ is the fraction of entrained mass rate of droplet sizes in the interval around from 10 to 30 μm —given in /hour,

ρ is the viscosity of the oil in cSt or mPa·s, H_{rms} is the r.m.s. value of the wave height (m), U is the wind speed in m/s, and T_w is the wave period, s.

Let us see if this is reasonable. Figure 20.5 shows the hours until the slick is completely dissipated using the new formulation. The wave height is coupled to the wind and the period so that only one axis is plotted. This figure shows a reasonable pattern where the lightest oil would be completely dissipated in about 60h under energetic conditions, and the heavier oils are little affected under light conditions. So this now seems reasonable compared to some formulations that showed even heavy oils being dissipated in a few hours.

20.5 RESIDENCE IN THE WATER COLUMN

The most important force in resurfacing of oil droplets from dispersion is gravitational separation [13]. Droplets in an emulsion tend to move upward when their density is

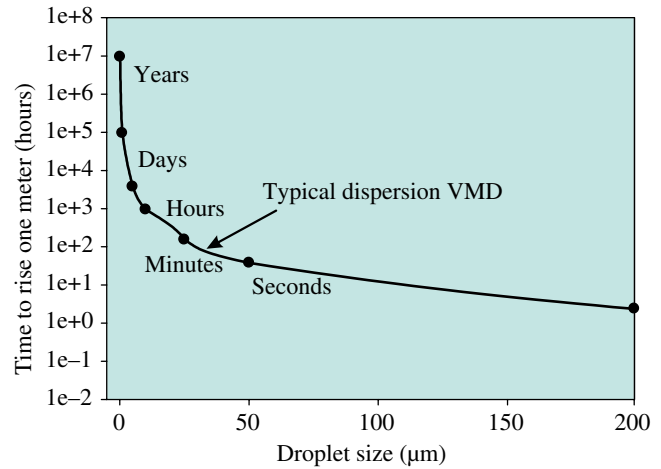


FIGURE 20.6 The Stokes predicted oil droplet rise time from 1 m. Note that typical natural dispersions have a droplet distribution that would rise to the surface in seconds to minutes.

lower than that of water. This is true for almost all crude oil and petroleum dispersions as they usually have droplets with a density lower than that of the surrounding water. Dense or “heavy” oils are poorly, if at all, dispersible. The rate at which oil droplets will rise due to gravitational forces is dependent on the difference in density of the oil droplet and the water, the droplet size (Stokes' law as presented below), and the rheology of the continuous phase.

The classic Stokes' equation is:

$$s = \frac{2\Delta\rho g a^2}{9\Delta\eta} \quad (20.23)$$

where s is the rise rate

$\Delta\rho$ is the density difference between the oil and water (disperse and droplet phases)

g is the gravitational constant

a being the droplet radius

$\Delta\eta$ is the difference between the viscosity of the disperse and droplet phases.

This equation is very important in terms of understanding the resurfacing of oil spill dispersions. It shows that for the smallest droplets at 1 m below the slick, the rise time would be about a year (or forever) and for the largest droplets immediately below the slick, rise time is a few seconds. This is illustrated in Figure 20.6. It is important to note that the most important droplet sizes here would rise to the surface from 1 m in a matter of minutes to seconds.

20.6 COMPARISON OF THE MODELS

The three models presented here are quite different and yield different results. Table 20.1 shows some basic inputs and results of the various models. Figure 20.7 shows a comparison of the three models when dealing with a 10 mPa·s oil, and

TABLE 20.1 A comparison of dispersion models

Parameters	Model		
	Audunson	Delvigne	MacKay
Inputs	Wind speed	Wave height/ energy % of breaking waves Wind speed	Slick thickness (droplet large or small) Oil density
Typical		Oil constants Droplet size	
Days to 100% for 10 mPa-s oil	3	65	1400
Days to 100% for 200 mPa-s oil	3	3800	1800
Treatment of inputs			
Wind speed	Linear	x^2	$\sim x^2$
Oil properties	Not included	$\sim 1/\text{viscosity}^{1.5}$	$\sim 1/\text{density}$
Droplet size	Not included	Chosen spectra	Small vs. large
Slick thickness	Not included	Not included	Thickness ^{1.25}

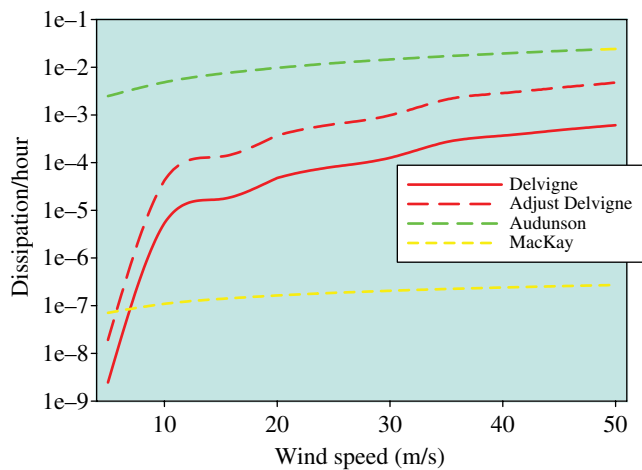
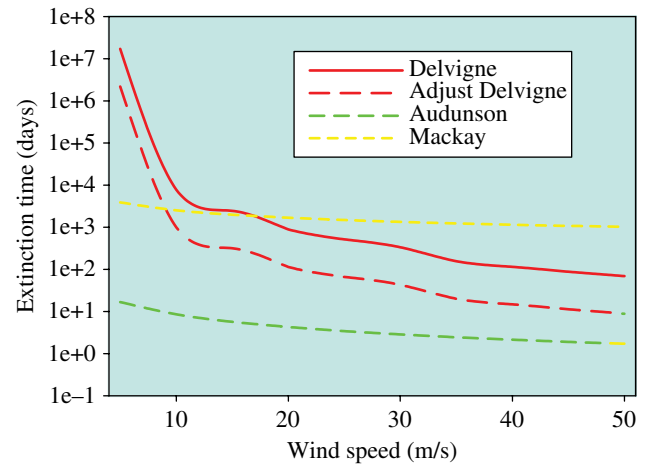
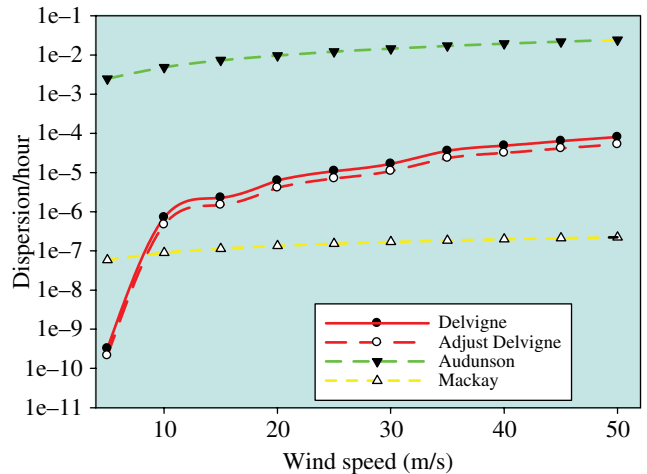
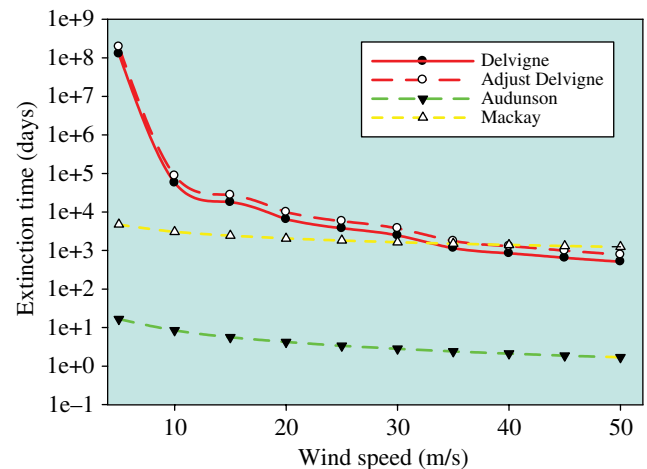
**FIGURE 20.7** A comparison of the four models by dispersion rate. This is for a light oil of 10 mPa-s.

Figure 20.8 shows the same comparison in terms of extinction time. Figure 20.9 shows a comparison of the three models when dealing with a 200 mPa-s oil, and Figure 20.10 shows the same comparison in terms of extinction time.

These figures show clearly that:

- The Audunson model in every case predicts that the slicks would diminish in a few days irrespective of oil type.
- The MacKay model is the most conservative, however, does not vary much with oil type nor with wind speed.
- The two versions of the Delvigne model, the original and the one adjusted by the present author to account directly for oil viscosity, are slightly different at lower oil viscosity, but close at an oil viscosity of about 200 mPa-s.

**FIGURE 20.8** A comparison of the four models by extinction time. This is for a light oil of 10 mPa-s.**FIGURE 20.9** A comparison of the four models by dispersion rate. This is for a heavier oil of 200 mPa-s.**FIGURE 20.10** A comparison of the four models by extinction time. This is for a heavier oil of 200 mPa-s.

- Only the Delvigne model shows a wind threshold before natural dispersion sets in.
- The Delvigne model shows differences in oil types by viscosity, the Audunson not at all, and the Mackay model only very slightly as this model uses the density of the oil, not the viscosity.

20.7 CONCLUSIONS

Several conclusions might be made about natural dispersion models. They are as follows:

1. In all cases, natural dispersion models predicted the input of droplets into the water column and suggestions were made about predicting rise and resurfacing. In no case, was the resurfacing of the droplets actually modeled, although authors such as Delvigne suggested approaches.
2. The natural dispersion predicted was measured as a temporary phenomenon—that is the instantaneous input of droplets in the water column. Droplet persistence in the water column was not measured. The equation was designed to yield only the temporary displacement into the water. Later workers assumed that this amount was permanently dispersed.
3. The Audunson equation overpredicts natural dispersion, especially in cases of low sea states or winds.
4. The Delvigne and Mackay model reach somewhat similar conclusions; however, the MacKay model has less inputs and no wind threshold.
5. Many of the constants in all three models appear to be arbitrary and unnecessary in some cases.
6. Only in the case of the Delvigne model were there direct correlations to experimental data, whereas the other models are largely constructs.
7. Some of the models do not incorporate what one would think are appropriate inputs, for example, the Audunson model does not incorporate oil properties of any type nor does it consider oil droplet size. This particular model only considers wind speed.
8. Given the rather arbitrary nature of these models, it is suggested that natural dispersion not be included in oil spill models. Such inclusion is quite misleading as natural dispersion has not been quantitatively measured at any actual spill.

REFERENCES

- [1] Lunel, T., *The Braer Spill: Oil Fate Governed by Dispersion*, IOSC, Long Beach, CA, p. 790, 1995.
- [2] Farwell, C., C.M. Reddy, E. Peacock, R.K. Nelson, L. Washburn, and D.L. Valentine, *Weathering and the Fallout Plume of Heavy Oil from Strong Petroleum Seeps Near Coal Oil Point, CA*, *Environmental Science and Technology*, Vol. 43, pp. 3542–3548, 2009.
- [3] Mackay, D., I. Buist, R. Mascarenhas, and S. Paterson, *Oil Spill Processes and Models*, EE-8, Environment Canada, Ottawa, 96 p., 1980.
- [4] Audunson, T., *The Fate and Weathering of Surface Oil from the Bravo Blowout*, *Marine Environmental Research*, Vol. 3, pp. 35–61, 1980.
- [5] Audunson, T., H.K. Celius, O. Johansen, P. Steinbakke, and S.E. Sorstrom, *The Experimental Oil Spill on Haltenbanken 1982*, Publication No. 112, Institut For Kontinental-sokkelundersokelser (IKU), Trondheim, Norway, 109 p., 1984.
- [6] Audunson, T., V. Dalen, J.P. Mathisen, J. Haldorsen, and F. Krogh, *SLIKFORCAST—A Simulation Program for Oil Spill Emergency Tracking and Long Term Contingency Planning*, *PETROMAR*, EUROCEAN, Monaco, pp. 513–541, 1981.
- [7] Delvigne, G.A.L., *Experiments on Natural and Chemical Dispersion of Oil in Laboratory and Field Circumstances*, Publication No. 327, Delft Hydraulic Laboratory, Delft, the Netherlands, 24 p., 1984.
- [8] Delvigne, G.A.L., *Natural and Chemical Dispersion of Oil*, *Journal of Advanced Marine Technology Conference*, Vol. 11, pp. 23–40, 1994.
- [9] Delvigne, G.A.L. and C.E. Sweeney, *Natural Dispersion of Oil*, *Oil and Chemical Pollution*, Vol. 4, pp. 281–310, 1988.
- [10] Delvigne, G.A.L. and C.E. Sweeney, *Natural Dispersion of Oil*, Publication No. 399, Delft Hydraulic Laboratory, Delft, the Netherlands, 30 p., 1989.
- [11] Delvigne, G.A.L., J.A. van der Stel, and C.E. Sweeney, *Measurement of Vertical Turbulent Dispersion and Diffusion of Oil Droplets and Oiled Particles*, Report No. Z 75-2, Delft Hydraulic Laboratory, Delft, the Netherlands, 406 p., 1987.
- [12] Delvigne, G.A.L. and L.J.M. Hulsen, *Simplified Laboratory Measurement of Oil Dispersion Coefficient: Application in Computations of Natural Oil Dispersion*, *AMOP*, Environment Canada, Ottawa, pp. 173–187, 1994.
- [13] Fingas, M., *Models of Oil Spill Dispersion Stability*, *AMOP*, Environment Canada, Ottawa, pp. 555–586, 2010.

PART XI

COLD REGION SPILLS

ARCTIC AND ANTARCTIC SPILLS

D.M. FILLER,¹ MAHLON C. KENNICUTT II,² IAN SNAPE,³ STEPHEN T. SWEET,⁴ AND ANDREW G. KLEIN⁵

¹*Department of Civil, Environmental, and Construction Engineering, University of Central Florida, Orlando, FL, USA*

²*Department of Oceanography, Texas A&M University, College Station, TX, USA*

³*Australian Antarctic Division, Environmental Protection and Change Program, Kingston, Tasmania, Australia*

⁴*Texas A&M University, College Station, TX, USA*

⁵*Department of Geography, Texas A&M University, College Station, TX, USA*

21.1	Introduction	497
21.1.1	Occurrences	498
21.1.2	Scale of the Problem	499
21.1.3	Environments	499
21.1.4	Regulatory Framework	501
21.2	Terrestrial Spills	502
21.2.1	Petroleum Transport and Fate	502
21.2.2	Mitigation and Countermeasures	506
21.2.3	Remediation and Lessons Learned	506
21.3	Marine Spills	507
21.3.1	Petroleum Transport and Fate	507
21.3.2	Mitigation and Countermeasures	508
21.3.3	Remediation and Lessons Learned	508
21.4	Policy	508

21.1 INTRODUCTION

The Arctic and Antarctic oceans are relatively pristine when compared to the rest of the world's oceans and seas that are chronically impacted by pollution from industrial, shipping, and fishing activities due to the proximity of population centers. However, polar waters have not been immune to oil and fuel spills, and these environments have been impacted by releases from ships, shore-based operations, and other human activities. Prior to landmark environmental legislation in the 1970s, Arctic and Antarctic coastal waters in proximity to research stations were used for the disposal of wastes of various kinds. The Protocol on Environmental Protection to the Antarctic Treaty (adopted in 1998) exhorts nations to reduce, as far as possible, local waste disposal and minimize impacts and interferences with the natural values of Antarctica. The protocol also encourages the removal of waste from the continent and the cleanup of past and current

disposal sites. The 1991 Arctic Environmental Protection Strategy (the impetus for the Arctic Monitoring and Assessment Program) and various subsequent national and international Arctic marine protection laws have curtailed dumping in Arctic waters.

The Antarctic Treaty and related agreements, collectively called the Antarctic Treaty System, sets the framework for international affairs in Antarctica. Consequently, mineral resource development is prohibited and Antarctica is designated as a natural reserve devoted to peace and science. Most research stations are located in the ice-free areas along the coastal margins and that is where most spills have occurred. Most spills in Antarctica occur when fuel is being transferred or dispensed. Abandoned waste disposal sites are also known to release hydrocarbons to the adjacent environment as well. Several shipping-related marine spills have been documented in Antarctica and the Southern Ocean. The largest fuel spill to date was the *Bahia Paraíso*, and that case study is presented in Chapter 23.

The Arctic does not have a treaty, and oil and gas development on coastal plains and continental shelves is the largest contributor of oil pollution to land, rivers, bays and estuaries. Shipping-related marine spills have been rare in sub-Arctic waters, Arctic shipping routes are few and seasonal, and extracted oil is typically transported within and from the region through pipeline networks to processing and distribution facilities. However, further inland, some of the worst oil spill disasters on record have occurred in the Russian Arctic [1]. Other sources of hydrocarbon pollution in the Arctic include mining, power generation, wood processing activities, military installations, and naturally occurring oil seeps.

This chapter summarizes anthropogenic oil and fuel spills in Polar Regions. Naturally occurring terrestrial and submarine

seeps documented in the Arctic, but introductions related to human activities, will be emphasized in this review.

21.1.1 Occurrences

Oil impacts in Polar Regions can be classified as “legacy” or “modern.” For purpose of this review, legacy spills are defined as those that predate the 1980s, when much less public attention was paid to the environmental consequences of human activities. Legacy impacts due to oil and fuel releases often reflected contemporary practices at a time when it was acceptable to dispose of toxic materials by dumping them in landfills or releasing them untreated into the marine environment. Waste oil or fuel was commonly abandoned on land, disposed of in the ocean, bulldozed onto sea ice with the expectation that this would raft the material into deeper waters, or containerized and buried. Examples of “modern” spills are shipping mishaps (e.g., run-a-grounds and bilge releases), tanker releases, fuel transfer accidents, and pipeline vandalism. While modern spills are generally classified as accidental, there has also been nonpoint chronic release of hydrocarbons to the environment by practices on

land such as disposal of spent crankcase oil and oily storm-water discharges. While individual nonpoint source releases are mostly considered low level, the pervasive nature of these releases results in this being a major source of petroleum to the environment. In Polar Regions, where human populations are much less than in temperate climates, impacts from nonpoint sources of petroleum contamination are expected to be proportionately less.

21.1.1.1 The Arctic Oil spills in the Arctic are primarily associated with oil and gas industry activity (Fig. 21.1). Spills generally occur at exploration and processing infrastructure sites, from distribution pipelines, and along transportation corridors. To a lesser degree, oil spills are also encountered during fuel dispensing operations (work camps and population centers), mining, and vandalism. Legacy spills are often associated with former military facilities and associated dump sites. Oil drums and containers that wash ashore (i.e., shoreline detritus) are also usually of an historic nature. Spills and releases include crude oil, oil byproducts (e.g., heating oil, refined fuels, and lubricants), and oil-chemical mixtures of various kinds.

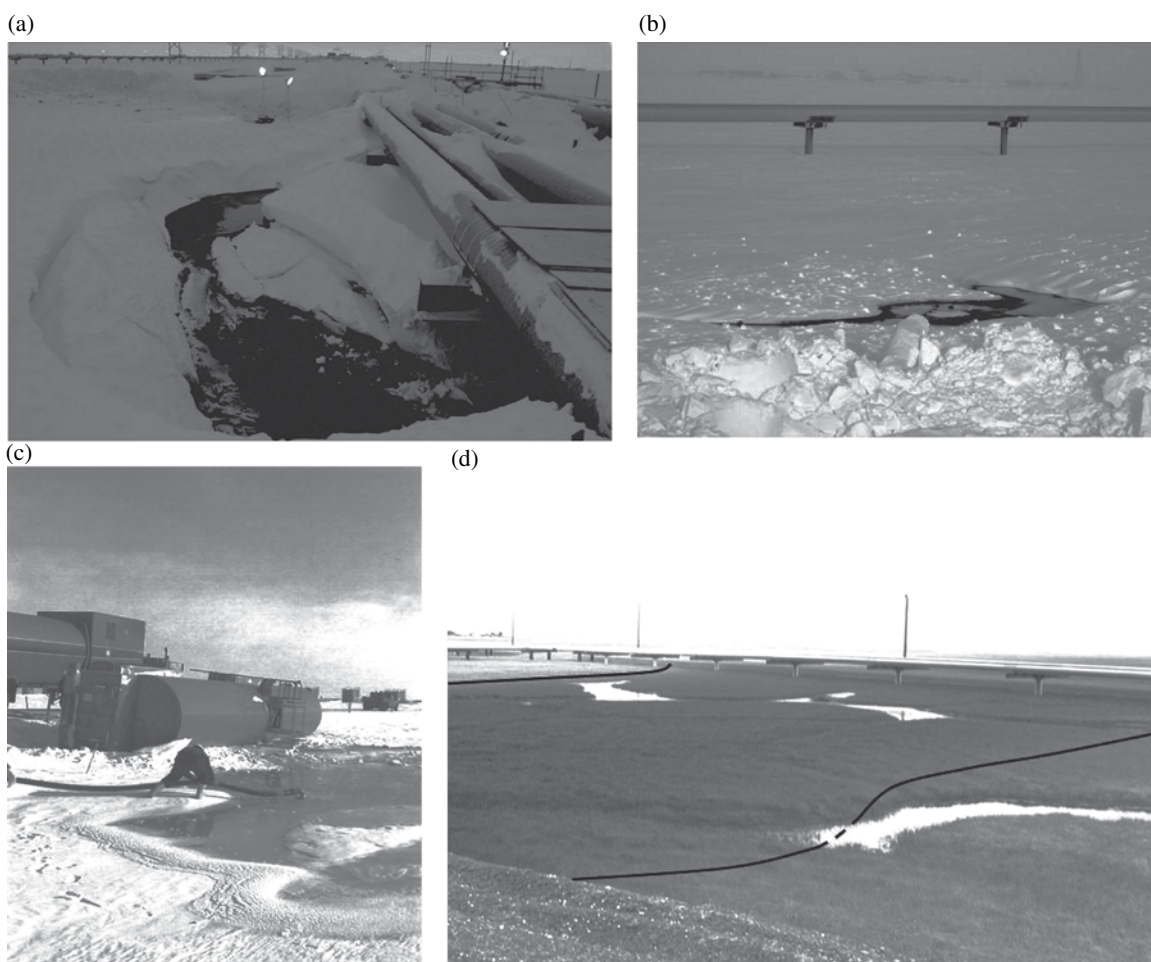


FIGURE 21.1 (a) March 2006 transit oil pipeline corrosion leak at Prudhoe Bay, Alaska, and (b) oil migration across snow-covered tundra (c) diesel tanker rollover with spilled fuel in snow-covered tundra; and (d) flowline oil overspray on tundra (Photographs courtesy of Alaska Department of Environmental Conservation).

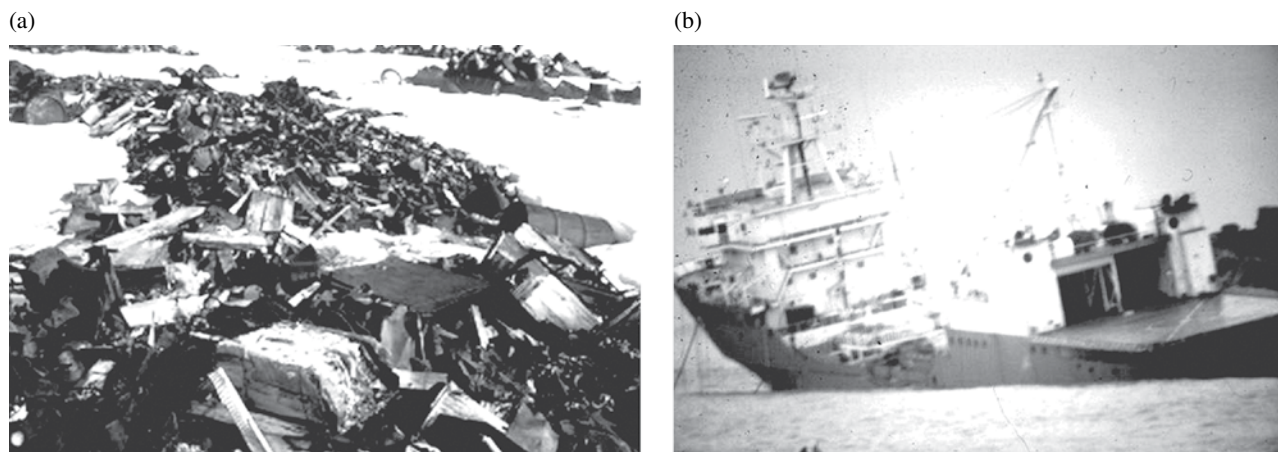


FIGURE 21.2 (a) Waste dump, Wilkes Station, Antarctica, and (b) *Bahia Paraiso* foundering in Port Arthur, Antarctica (Photo courtesy of National Science Foundation).

21.1.1.2 Antarctica Terrestrial releases in Antarctica are primarily fuel oil (Antarctic blend or similar light diesel fuels), kerosene, or JP-8 jet fuel. Spills are known to occur at scientific stations, and during aircraft and vehicle operations and refueling activities. Petroleum contamination of coastal marine environments has been caused by dumping (a former practice), runoff from dump sites, plumes that produce a pulse of contamination each summer during thaw events, and discharges from ship operations [2]. Surface runoff from scientific stations also transports contaminants to adjacent marine environments (Fig. 21.2a).

21.1.2 Scale of the Problem

Alaska, Canada, Finland, Iceland, Norway, and Sweden have assembled inventories of their Arctic and sub-Arctic petroleum-contaminated spills within their national boundaries. Estimates of oil spills in these countries are summarized in Table 21.1 and Figure 21.3. Although the data includes sub-Arctic spills, the estimates provide a perspective on the extent and magnitude of cold regions petroleum contamination.

Currently, small numbers of petroleum-contaminated sites are documented near Arctic coastlines at energy development facilities and former or active military facilities. Antarctica has few contaminated sites, most of which are located at scientific stations in coastal areas where logistical operations are concentrated (Fig. 21.3). The Russian Federation, on the other hand, has reported *contaminated regions* in the Arctic. The distinction between a “contaminated site” and a “contaminated region” is size. Contaminated sites often involve contamination of tens to hundreds of square meters and in some cases even a few hectares (or acres). In contrast, the United Nations Environment Program/Global Environment Facility (or UNEP/GEF Project) has documented large regions of the Russian Arctic where oil contamination is spread over hundreds of square kilometers [1]. Ecological devastation at these sites is enormous (Fig. 21.4).

In Figure 21.4, 11 *impact regions* are identified, with Franz Josef Land Archipelago contamination highlighted as one example. In accordance with UNEP/GEF environmental impact classifications, eight of the impact regions are classified as catastrophic or in crisis state, two others are critical, and one is strained. UNEP/GEF defines a catastrophic environment as one where deep and irreversible damage has occurred to the land and biota (i.e., uninhabitable), a crisis environment as that in which destructive changes to biota and ecosystems are generally irreversible, and a critical environment implies that loss of biota and ecosystem damage can be reversed, but only with significant artificial stimulation of restoration and reclamation processes. UNEP/GEF further defines a strained environment as having some negative changes, but natural restoration of the ecosystem and biota is possible with conservation efforts [1]. The reader is directed to UNEP/GEF [1] and AMAP Assessments 2007 and 2009 for comprehensive assessments of the Russian Federation’s environmental problems.

In the whole of Antarctica, it is estimated that between 100,000 and 1 million m³ of petroleum-contaminated soil exist [3] within the continent’s 330,000 km² of ice-free area. For comparison, Russia’s Komi impact region alone contains over 126,000 tonnes of crude oil spilled over 186 km², which is equivalent to 9.3 million m³ of soil contaminated to a depth of 50 cm. The Russian Federation’s oil contamination problem is magnitudes of scale greater than all other Arctic nations.

21.1.3 Environments

Polar environments present significant challenges to oil spill mitigation. Extreme cold, snow and ice cover, frozen ground, variably wet and organic rich soils, undulating surface cover (e.g., tundra, muskeg, and tussocks), and short summers hamper recovery and remediation of oil spilled in the Arctic. Recovery strategies for a summer spill on wet tundra can differ significantly from those for

TABLE 21.1 Estimates of oil spill impacts in cold regions

Country	Terrestrial contaminated sites			Marine contamination volume estimates (m ³)
	Estimated total no. of sites ^a	Volume estimates (m ³)	Remediation planned or completed ^a	
Alaska (US)	6,400	1482 (crude oil 1995–2007) ^b 8870 (TAPS crude oil 1977–2006) ^b	3400	255 (1944 <i>Jonathan Harrington</i>) ^c 37,000 (1989 <i>Exxon Valdez</i>) 1,270 (2004 <i>Selendang Ayu</i>)
Canada	~2400	~4000 (crude and diesel 1972–2005) ^d	37 ^e	~725 (crude and diesel to freshwater aquatic and marine environments 1972–2005) ^d
Greenland	na	na	1	na
Iceland	>230	na	0	na
Norway	~210	19442 (oil and fuel 1987–2004) ^f	246	885 (oil fields and shipping) ^f 750 (2003 <i>Draugen</i>)
Sweden	11,100	na	444	na
Finland	>20,000 ^g	6.6 million (est. total soil contaminated) ^g	1898	na
Antarctica	~200	10 ^h to 1 million ^a	1	600 (1989 <i>Bahia Paraiso</i>)

^aData from Ref. 3.
^bEstimated from Alaska Department of Environmental Conservation (ADEC) Spill Database (<http://dec.alaska.gov/applications/spar/SpillsDBQuery/search.asp>). TAPS is Trans-Alaska Pipeline System.
^cFrom declassified U.S. military records.
^dEstimated from Government Northwest Territories hazardous materials spill and Indian and Northern Affairs Canada northern contaminants program databases at <http://www.enr.gov.nt.ca> and <http://www.ainc-inac.gc.ca>.
^eFrom Northern Contaminants Program database at <http://www.ainc-inac.gc.ca>, Indian and Northern Affairs Canada.
^fEstimated from Ref. 4.
^gEstimates from Järvinen and Sakari [5].
na, not available.

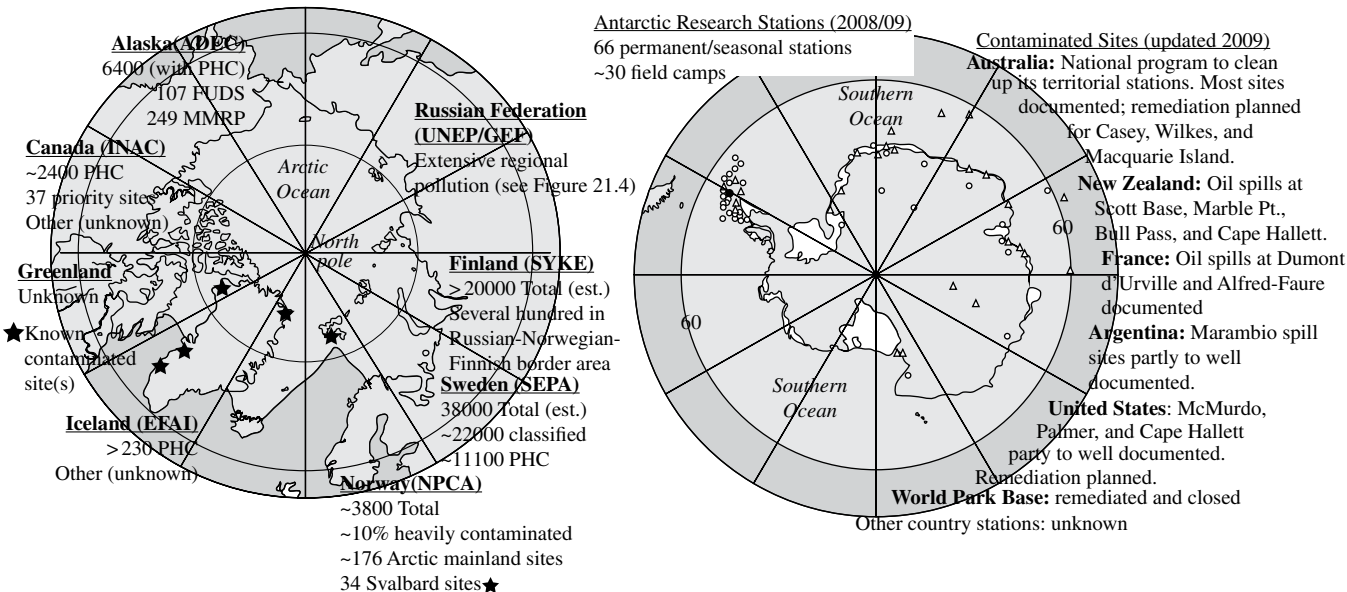


FIGURE 21.3 Estimates of total contaminated sites in the Arctic and Antarctica. PHC, petroleum hydrocarbons; FUDS, formerly used defense sites; MMRP, military munitions response program; ADEC, EFAI, SYKE, SEPA, and NPCA, environmental regulatory agencies in the respective countries.

a winter spill on frozen tundra at the same location [6]. Spill response can cause more damage to tundra than the contamination, and fuel that volatilizes at warm

temperatures becomes refractory in freezing or frozen ground. Furthermore, lack of replacement mineral soil or tundra mat (i.e., seed material) favor in situ treatments

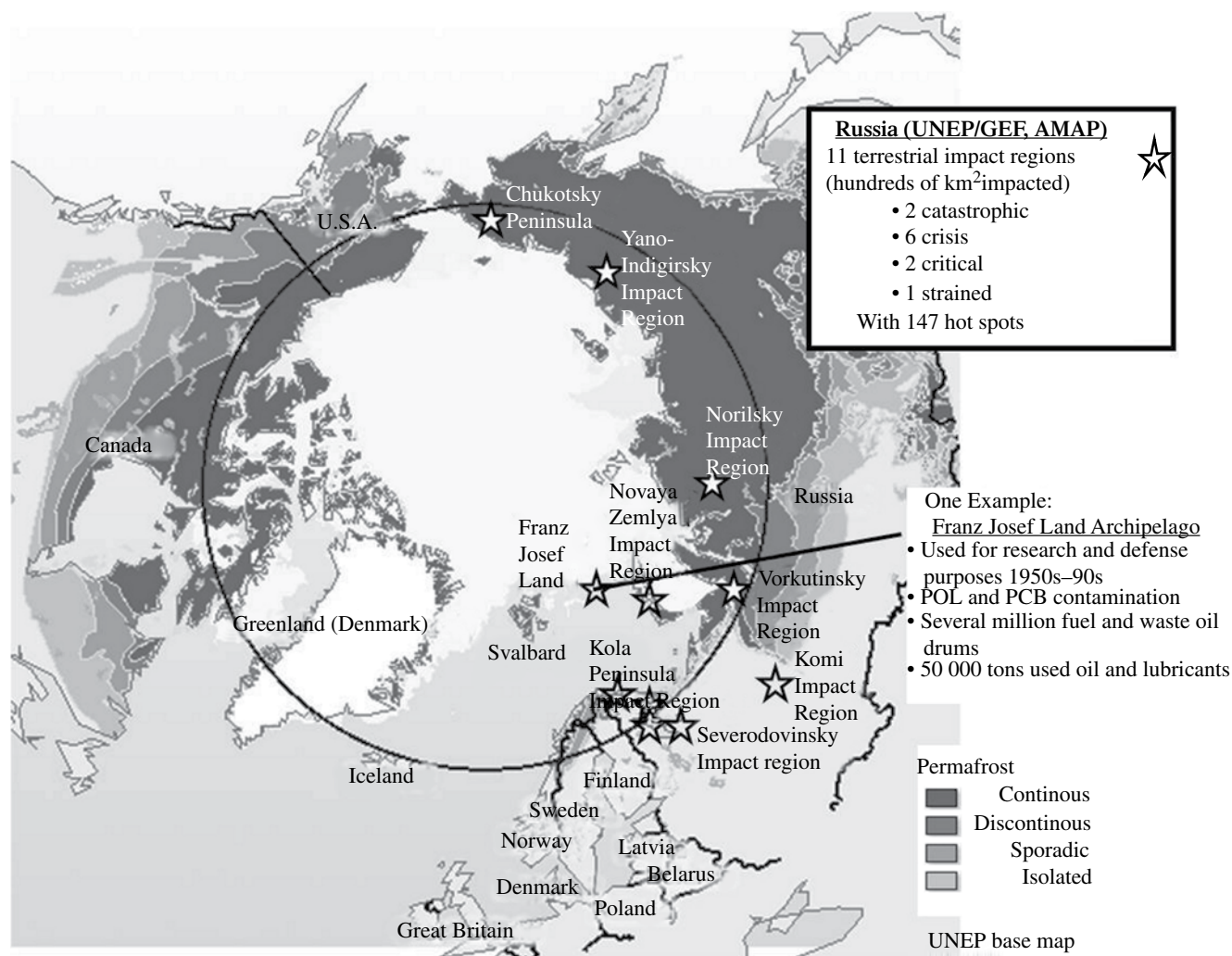


FIGURE 21.4 Oil impact regions in the Russian Federation Arctic. POL, petroleum, oil, and lubricants; PCB, polychlorinated biphenyls; AMAP, Arctic Monitoring and Assessment Program.

that take longer to reduce contaminant concentrations and extend responsible party liability.

In Polar Regions, marine spill responders have to contend with near freezing waters that are subject to strong currents and winds, sea ice, and fog. An oil spill in open ocean polynya would be a challenging scenario as crews would have to maneuver from boats with response equipment that is inadequate to deal with oil–ice interactions. Perhaps the worst case scenario would be a coastal polynya spill in a bay or estuary. While we have experiences with terrestrial spills from which some response tactics and treatment methods are derived, we have little to go on in dealing with marine spills in polar waters.

21.1.4 Regulatory Framework

Arctic oil exploration during the 1950s and 1960s was subject to much less stringent environmental regulations than today. In the 1970s, North America and other western nations enacted major new environmental laws that changed the situation dramatically. By the 1980s and

1990s, environmental regulations and procedures had significantly matured setting standards for air, water, and soil quality. The Antarctic Treaty's Protocol on Environmental Protection, adopted in 1998, was precedent-setting as well for ecological stewardship in Antarctica. Presently, world events, increasing energy demands, rising energy costs, and climate change have focused attention on exploitation of the vast reserves believed to be present above the Arctic Circle [7]. The Arctic is now the focus of countries vying for these natural resources, and a regulatory framework for sustainable development and ecological protection is not yet developed.

While interest in Arctic resources is growing, cold regions environmental science, spill response, and remediation are still underdeveloped. Although advances have been made in understanding Arctic geocryology, hydrology, and environmental remediation, much remains to be learned about how to manage spills in these cold and harsh environments.

North America and the Scandinavian countries are working at environmental stewardship of their Arctic territories. Canada and the United States are working toward developing scientifically defensible contaminant standards for the terrestrial Arctic. However, Greenland and Iceland currently have little resources available to apply toward environmental science and ecological protection [3]. Environmental cleanup is an enormous issue for Russia; others are subsidizing their pollution assessments [1].

21.2 TERRESTRIAL SPILLS

Oil spills that occur in permafrost environments are difficult to mitigate and clean up. Permafrost terrain is complex and dynamic, sensitive to heat, and slow to recover from impacts. Although soil science has significantly advanced our understanding of permafrost soils over the past three decades, understanding the behavior of oil pollution in freezing and frozen ground is still basic.

In this section, we discuss the current state of oil fate and transport in permafrost soil. First, we describe soil formation, and hydrologic processes are described to establish a basis for understanding the complexities of oil-frozen ground interactions. Next, we examine recent advances in understanding the oil movement and interaction within cold soils. Finally, spill countermeasures and environmental remediation are examined to establish the current state of our response capabilities in cold terrestrial environments.

21.2.1 Petroleum Transport and Fate

The following discussions provide an overview of oil migration in polar soils. Soils are characterized, important soil–fluid transport parameters are identified, and consideration is given to movement of oil in the unsaturated active layer and upper permafrost. For an in-depth study of flow of immiscible fluid flow in porous media, the reader should consult seminal works by Bear [8] and Mercer and Cohen [9].

21.2.1.1 Permafrost Soils Permafrost soils occupy 13% of Earth's land area. Permafrost underlies 65% of Russia, 40% of Canada and Norway, about 90% of Greenland, 85% of Alaska, and most of Antarctica [10]. Arctic and Antarctic soils are generally classified as *cryosols*. Cryosols are underlain by permafrost, primarily affected by mechanical weathering, characterized by the absence of well-developed soil horizons, and classified on the basis of soil temperature and moisture [11].

Formed predominately by repeated glaciations and erosional processes, cryosols are seasonally frozen in the active layer or perennially frozen in underlying permafrost. Coastal areas are often underlain by marine deposits associated with glacial rebound and sea-level changes, while further inland

alluvium (sediment deposited by flowing water) and colluvium (sediment deposited at the base of cliffs and on slopes) prevail. Arctic permafrost areas are often characterized by patterned ground forms (e.g., ice or sand wedge polygons, sorted and non-sorted circles, nets, stripes, and steps) over mineral deposits [12]; peaty surface deposits can be found in coastal marshes and lowlands. Arctic vegetation is a nearly continuous cover of shrub-tundra in the south, transitioning to sparse cover of dwarf shrubs, herbs, mosses, and lichens in the north [13]. Upland bedrock outcrops and High-Arctic terrain usually exhibit mineral soils devoid of vegetative cover and little organic content [14].

Cryopedogenic (soil forming) *processes* govern active layer and permafrost soil development [12,15]. Cryoturbation (frost churning and sorting) is the dominant process. Others are freeze-thaw, frost heave, ice segregation, ice buildup (ice wedges, *aufeis*, and other icing forms), thermal cracking, cryodesiccation (soil freeze drying), and thixotrophy (silt sorting by liquefaction). Cryoturbation favors silty parent material, imperfect drainage, frequent freeze-thaw cycles, and shallow (<1 m deep) permafrost [16,17]. Fox [18] and Washburn [12] describe cryoturbation as particle sorting, heaving, stirring, and wedging, with pore formation due to ice segregation and thermal cracking.

Cryoturbated soils (Fig. 21.5) exhibit irregular or broken horizons, contain material from other horizons, irregular textural bands (involutions and diapirs), vertical sorting (e.g., perversion—silt migration along a freezing front), horizontal sorting (oriented stones, silt caps, and ice- and composite wedges), and inclusions of retransported organic matter in marshy areas (paludification) and on permafrost (humus retinization) [12,19]. Other geochemical and biochemical (secondary) processes that affect Arctic soils include gleying (the bacterial iron reduction and accumulation as hard pan in a restricted wet soil horizon); leaching (removal of soil materials—primarily Ca, Mg, K, and Na—in solution); eluviation (removal of soil materials—primarily Ca, Mg, K, and Na—in suspension); salinization (salt accumulation in a mineral soil horizon); brunification (formation of iron-rich minerals, giving soil brownish or reddish-brown color); and podzolization (soil bleaching).

While soils generally deposit and consolidate as distinct and often uniform layers in temperate regions, they do not in Polar Regions. Figure 21.5 represents contrasting examples of Arctic and Antarctic coastal soil profiles. Figure 21.6 illustrates the types of Arctic tundra with hydrologic aspect.

21.2.1.2 Petroleum in a Thawing Active Layer A characteristic of Arctic terra firma so vital to our management of oil spills is the distinction between the active layer and permafrost. The active layer is the upper realm of soil above permafrost that experiences seasonal freezing and thawing. In the High Arctic, the ground thaws to about 45 cm and a small soil thermal gradient is established during summer. Southern Arctic soils experience seasonal thaw to 100 cm and develop more pronounced thermal profiles in the active

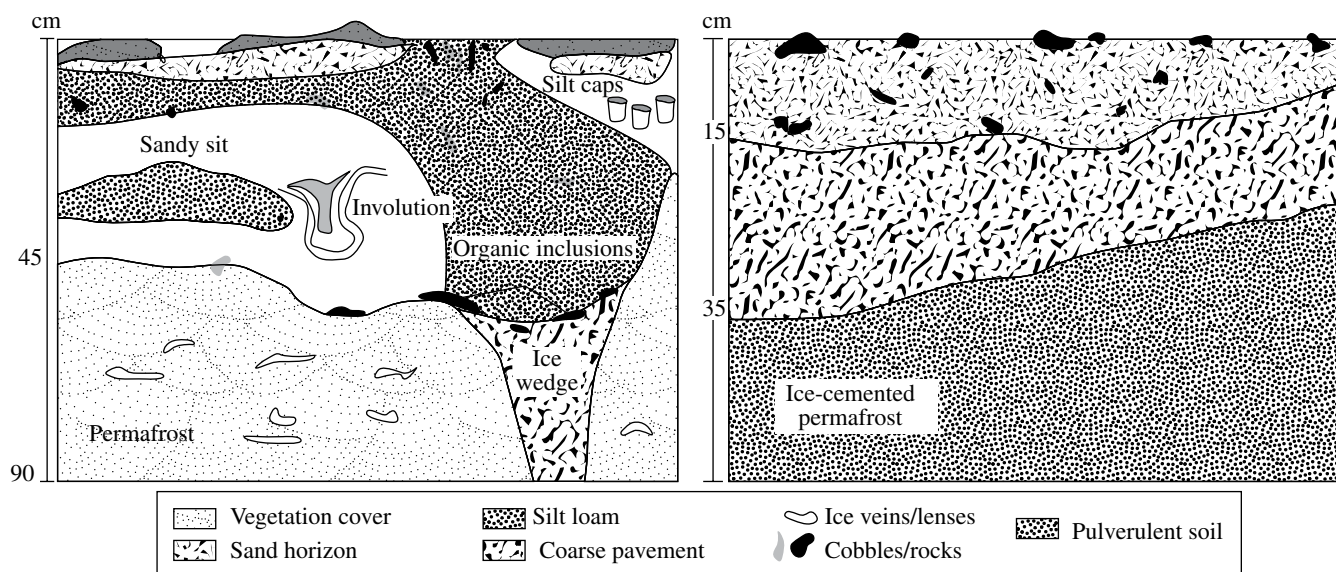


FIGURE 21.5 Comparison of Arctic and Antarctic coastal soil profiles. Arctic coastal patterned (or polygon) ground with stone rings between discontinuous cryoturbated soil horizons above permafrost (at left) and Antarctic coastal weathered till of coarse surface *pavement* with rounded boulders and particles >2 mm typically exceeding 50%, over pulverulent soil, over ice-cemented permafrost (at right).

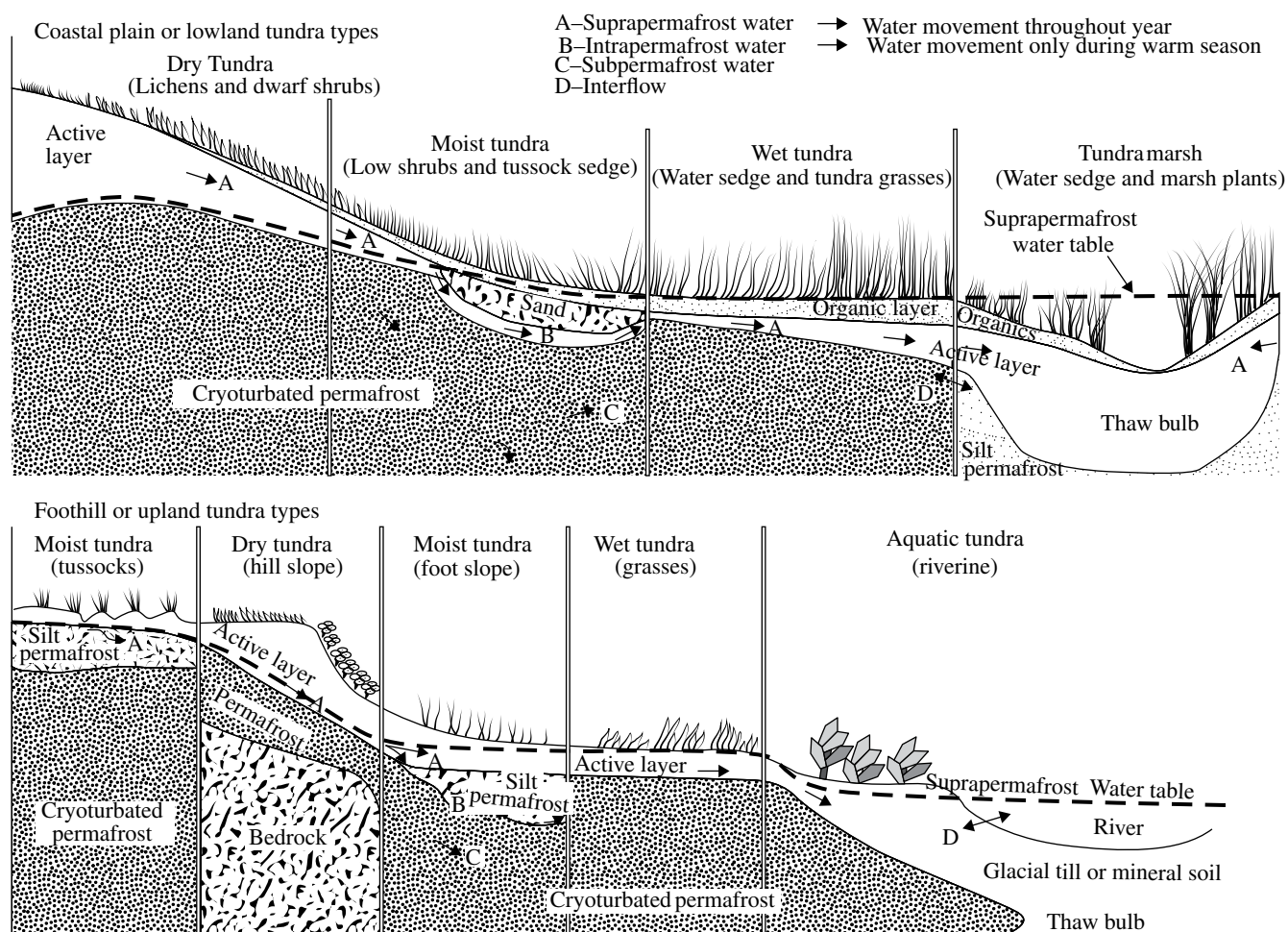


FIGURE 21.6 Pedons illustrating general types of Arctic tundra with hydrologic aspect. After Refs. [20] and [21].

layer. Because the thickness of the active layer fluctuates as a function of climate variability, and a shallow permafrost table, the top of permafrost is also dynamic. Furthermore, the active layer can be an open or closed system. A closed active layer (common to Arctic coastal plains) exhibits ice-saturated upper and lower parts and a middle realm of dry soil with high open porosity. Freezing fronts that converge from the surface downward and upward from the top of permafrost tend to confine fluid movement within this layer. With an open active layer, such as that depicted with dry coarse mineral soil over pulverized fines in Figure 21.5 (at right), released oil can reach permafrost more readily.

Thermodynamics, hydrology, and freeze-thaw cycling govern oil movement within the active layer. While some cryopedogenic processes are fairly well understood, we do not have a complete understanding of how the various cryoprocesses interact to manipulate soil structure and hydrology. For example, we understand moisture migration along thermal gradients, processes driven by water-to-ice phase change, the importance of soil (and ice) saturation and pore ice content to fluid transport, and thermal contraction of frozen material by continued rapid cooling. However, variability in contaminant transport results from laboratory trials [22–25], and field studies [6,26–28] attest to the complexity of the active layer and permafrost. Furthermore, we know little about cryoturbation influence and its potential role in vertical and horizontal movement of soil, water, and oil.

To illustrate, consider the two contrasting models used to explain cryoturbation: (1) the Cryostatic Model [29–31] and (2) the Convective Cell Equilibrium Model [32]. The former involves two opposing freezing fronts, one moving downward from the surface and the other upward from the permafrost table. The converging fronts cause pressure on unfrozen material between them, and the front with greater moisture transfer governs vertical movements. In the convection-cell model, heave-subsidence processes at the ground surface produce net downward and outward movement of materials, and those above the permafrost table produce net upward and inward movements. The combined heave-subsidence affects yield a slow upward cell-type circulation.

Oil contamination in the unsaturated active layer may be present in four physical states: gas, sorbed to soil and ice (solids), dissolved in water, or immiscible liquid. Characteristics of oil and subsurface materials govern pore-scale and field-scale transport. At the pore scale, the following parameters are important to oil migration and distribution:

- Density (ρ) is a temperature-dependent parameter usually expressed in terms of specific gravity (SG). If the SG of oil is less than 1.0, it is less dense than water and will float on it. The density of oil increases as temperature decreases.
- Viscosity is the resistance of oil to flow. Oil viscosity increases as temperature decreases. The greater the

viscosity, the more energy required for the oil to flow in soil.

- Interfacial tension is the surface energy (or force of molecular attraction) between two immiscible fluids (water and oil) in contact.
- Wettability is the tendency of one immiscible fluid to spread on or adhere to a solid surface in the presence of another fluid. The wetting fluid will preferentially wet the solid surface and occupy smaller pore spaces.
- Capillary pressure (P_c) is the tendency of soil to attract a wetting fluid and repel that which is non-wetting. It is a measure of the relative molecular attraction of a liquid to itself (cohesion) and to that of a solid surface (adhesion). In general, capillary pressure increases with decreasing pore size and moisture content, and increasing interfacial tension.
- Relative permeability (k_r) is the ratio of the permeability of the soil to a fluid (oil) at a specified saturation to that of 100% saturation. Values range between 0 and 1.
- Saturation (S) is the relative fraction of total pore space containing fluid in a representative volume of soil. Residual saturation (S_r) refers to the saturation level where a continuous mass of oil becomes discontinuous and immobilized by capillary forces.

Of these, capillary pressure-saturation-relative permeability (or P_c - S - k_r) relationships are the important constituents necessary to characterize two-phase (contaminant and water) flow behavior in the ground. However, because of complex interactions of many factors, including initial water saturation in the soil, wettability of soil particles to a particular fluid, contact angles between fluids and soil particles, pore and particle size distributions, interfacial tensions, hysteresis, and types of heterogeneities, it is generally not possible (nor practical) to measure unique P_c - S - k_r curves [33]. It is those heterogeneities (e.g., intensity and distribution of microcracks and channels, shape and connectivity of microchannels occupied by water, oil discontinuity, and soil wettability to both fluids) that further complicate our understanding of contaminant mobility in freezing and frozen soils. Consequently, environmental practitioners usually treat a contaminated domain as a homogeneous medium and develop site-specific mobility parameters (e.g., permeability, hydraulic conductivity) and relationships (e.g., P_c - S or k_r - S curves) that are order-of-magnitude approximations for use along with field observations in remedial design.

Consider oil released to a thawing active layer in an Arctic coastal-plain setting (Fig. 21.5, at left). Early on, the wet tundra accommodates lateral spread of the oil which coats vegetation and exposed mineral soil but limits vertical penetration because of high soil-water saturation. Nevertheless, with time, the oil can migrate downward with thaw progression and soil saturation changes [6,28,34–36].

Mobility of the oil is related to its saturation in soil as a function of relative permeability, and the magnitude of its residual saturation is highly variable due to those heterogeneities previously mentioned. Brooks and Corey [37] and Farr et al. [38] developed the P_c - S relationships for water and oil in soil as a function of depth below the ground surface. As rederived for the thawing active layer condition in Margesin [13], the total liquid saturation (water and oil, S_T) as a function of capillary pressure between air and oil (P_c^{ao}), and water saturation (S_w) as a function of oil and water capillary pressures are

$$S_T = S_w + S_o = (1 - S_r) \left(\frac{P_c^{ao}}{P_d^{ao}} \right)^{-\lambda} + S_r \quad (21.1)$$

and

$$S_w = (1 - S_r) \left(\frac{P_c^{ow}}{P_d^{ow}} \right)^{-\lambda} + S_r \quad (21.2)$$

In these expressions, S_o is oil saturation, S_r is residual saturation (assumed the same for both liquids), λ is the pore size distribution coefficient, and P_d^{ao} and P_d^{ow} the displacement pressures between air and oil and oil and water, respectively. The capillary pressures between fluids are expressed as

$$P_c^{ao} = \rho_o g(z - T_o) \quad (21.3)$$

and

$$P_c^{ow} = \rho_w g(z - b) + \rho_o g(T_o - z) \quad (21.4)$$

where ρ_o and ρ_w are oil and water densities, g is the gravitational constant, z is the elevation above the top of permafrost, b is the saturated zone thickness prior to oil impact, and T_o the thickness of oil as measured in a monitoring well screened through the saturated zone.

Barnes and Chuvilin [39] investigated prespill water saturation influence on petroleum saturation for a hypothetical 1.5 m-thick sandy-loam vadose zone above permafrost using Equations (21.1) through (21.4). Assuming hydrostatic conditions, no hysteresis (e.g., no difference between wetting and drying soil-water-retention curves), and a spilled oil thickness T_o of 0.7 m, they estimated petroleum saturation as a function of depth for different values of water saturated zone thicknesses of 0.4, 0.3, 0.2, and 0.1 m prior to oil impact. In examining petroleum saturation versus elevation above the top of permafrost for the various water saturation thicknesses they observed the following:

- maximum petroleum saturation occurred at about 0.8 m above permafrost for all water-saturation levels;
- an increase in maximum petroleum saturation with decreasing water saturated zone thickness;

- uniformly increasing petroleum saturation rates in the upper active soil layer;
- a high rate of decrease in petroleum saturation below the maximum threshold depth (0.8 m for 0.4 m water saturation thickness); and
- a slight rate of decrease in petroleum saturation below the maximum threshold depth for 0.1 m water saturation thickness.

The petroleum released to the active layer with a shallow water saturated zone is initially more highly mobile vertically than that for a spill on a thicker water saturated zone. In general, with greater water saturation in the upper active layer, oil is more likely to spread laterally before penetrating vertically.

Oil migration at the field scale is best described using Darcy's Law. For oil-saturated conditions, Darcy's one-dimensional flow model is used to evaluate mobility in terms of oil physical properties as

$$v = -kg \left(\frac{\rho}{\mu} \right)_o \left(\frac{dh}{dl} \right) \quad (21.5)$$

where v is Darcy velocity, k is soil intrinsic permeability, μ is oil dynamic viscosity, and dh/dl is the hydraulic gradient of oil mass. From this equation, we recognize that soil hydraulic conductivity is proportional to the density and inversely proportional to the viscosity of the oil. By comparing ratios of density to viscosity for various fluids, we get an order-of-magnitude approximation of their mobility in soil.

Only within the last decade have soil scientists and environmental engineers been able to examine soil microstructure to comprehend cryoturbation and oil-soil interactions. Since 1997, researchers using optical and scanning electron microscopes began to reveal cryoturbation-oil contaminant interaction in freezing soils. Williams [40,41] recognized that soil pore ice could influence contaminants in cold soil, and White and Williams [42] reported that soil microstructure influenced hydraulic properties of petroleum-contaminated freezing soil. Conversely, White and Coutard [43] suggested that oil contaminants in freezing ground might alter silt microstructure and also reported that soil microstructure governed thermodynamic properties and free energy of water in freezing and frozen ground. It was these breakthroughs that birthed the science of *Contaminants in Freezing Ground*.

Most recently researchers using modified computed tomography (CT scanning) with visualization and analysis software have shown that freeze-thaw alters petroleum's mobility in soil. Torrance and others [44] subjected intact frozen soil samples with various oil-water ratios to rapid unidirectional downward freezing. CT scanning indicated that oil and water were redistributed during freezing along preferential flow paths and within micropores. Haghighi and others [45] used CT scanning to evaluate freeze-thaw effects on laboratory soil columns contaminated with gasoline. They

reported that (i) porosity changed with soil freezing and that these changes were reversible upon thawing; (ii) fuel became discontinuous with soil freezing and formed individual *blobs*; and (iii) freeze-thaw increased the mean volume of blobs at migration locations, and the blobs became more spherical. Fourie and others [46] used CT scanning coupled with Comsol Multiphysics software to model contaminant mobility in laboratory soil columns. These researchers demonstrated that (i) ice that forms in soil pores influences the movement of petroleum by creating preferential flow paths, and that (ii) microscopic modeling of incompressible fluid flow with the Navier–Stokes equation

$$\rho \left(\frac{\partial v}{\partial t} + v \cdot \nabla v \right) = -\nabla p + \mu \nabla^2 v + g \quad (21.6)$$

mirrors the Darcy (Eq. 21.5) macroscopic results. Here, v is flow velocity, g is gravity (per unit volume), ∇ is the del (or vector differential) operator, and all other parameters are as previously defined. From Equation (21.6), we note that on the left, inertia (per volume) comprises unsteady and convective acceleration, and the terms on the right are stress divergence (pressure gradient and viscosity) and the force of gravity. It is now possible to directly calculate fluid tortuosity and dispersivity and describe advection transport of oil in frozen soil at the pore scale.

In general, oil spills impact the active layer before migrating down to permafrost. When released to unfrozen saturated tundra, oil initially spreads laterally, but can penetrate vertically as thawing progresses and with soil saturation changes. In the absence of soil moisture, oil penetration into frozen or unfrozen mineral soils can be rapid; with increasing soil saturation and ice content, its penetration into frozen soil decreases. Freeze-thaw can alter porosity and form preferential flow paths for vertical migration of oil in frozen soil. We know little about oil movement in permafrost beneath the active layer. However, evidence from field trials [26,28] suggests that ice-rich permafrost tends to act as a barrier to oil penetration while dry porous permafrost does not.

21.2.2 Mitigation and Countermeasures

In 1991, the governments of the eight Arctic nations agreed to the Arctic Environmental Protection Strategy (AEPS). This charter of international cooperation was intended to protect and preserve the Arctic environment. AEPS primary objectives are (i) Arctic protection and preservation, (ii) development of a framework of response to environmental emergencies, and (iii) assessment of potential environmental impacts of development activities. Five working groups were established to implement these objectives:

- Arctic Monitoring and Assessment Program (AMAP)
- Emergency Prevention, Preparedness, and Response (EPPR) program

- Protection of the Arctic Marine Environment (PAME)
- Conservation of Arctic Flora and Fauna (CAFF)
- Sustainable Development and Utilization (SDU)

Of these, the EPPR and AMAP working groups focus on spill mitigation and countermeasures, and pollution monitoring. EPPR emphasis is on protection strategies for the Arctic marine environment. AMAP issues biennial reports on circumpolar Arctic pollution in support of the third objective.

The AEPS charter has been successful because of its ability to garner stakeholder cooperation. Researchers, agencies, and industry have worked together to produce useful tools for protection and preservation of Arctic ecosystems. Since implementation of the AEPS charter, national environmental protection agencies of some countries have made significant contributions toward protection of the Arctic. Seminal examples of guidance standards used today for oil spill mitigation and treatment efforts in the Arctic are:

- Alaska Department of Environmental Conservation's *Tundra Treatment Guidelines: A Manual for Treating Oil and Hazardous Substance Spills to Tundra*. This compendium provides tactics that are used after initial recovery efforts to treat and monitor tundra impacted by spills of crude oil, petroleum products, seawater, and other contaminants. The manual provides a framework for identifying treatment goals and appropriate tactics for an effective overall treatment strategy. This manual is available at http://dec.alaska.gov/Spar/perp/r_d/ttman/web/Tundra%20Treatment%20Guidelines%203rd%20Ed.%202010.pdf.
- EPPR's *Field Guide for Oil Spill Response in Arctic Waters*. This guide provides oil-spill countermeasures and treatment methods for response to ocean, lake, river, and shoreline impacts. It offers a unique icon-based alpha and numeric system of method identification, considers season and impact conditions (e.g., oil on surface, submerged oil, oil mixed in ice), and rates method effectiveness based on spill conditions. This guide is available at <http://www.arctic-council.org/eppr/completed-work/oil-and-gas-products/field-guide-for-oil-spill-response/>.

21.2.3 Remediation and Lessons Learned

The knowledge base of oil spill remediation in the Arctic is predominately derived from terrestrial experiences as resource exploration and exploitation has only recently moved into offshore regions. There are only a few shipping-related spills with impacted adjacent shorelines. Petroleum-contaminated sites have been assessed and successfully cleaned up in the Arctic [47–50]. In Antarctica, several countries have assessed oil pollution at research stations and other contaminated sites [51–53] and have tested remediation strategies [54–56].

Antarctica has a well-developed legal framework that encourages environmental stewardship. Because of its remoteness, human activities on the continent, including spills, have been limited. In general, spills of fuel oils or JP-8 range from 200 to ~80,000 l and have mostly occurred at scientific stations and refueling locations. Antarctic nations in general have increased efforts to identify, assess, and remediate their contaminated sites during the past decade. For example, Australia has committed to cleaning up all of its stations and dump sites. Remediation strategies are planned for Casey and Wilkes stations, and trials are underway at Macquarie Island [3]. Greenpeace has mitigated its diesel contamination at the former World Park Base [57]. The United States has been stabilizing or removing historic landfills and monitoring oil pollution at McMurdo Station, Antarctica's largest research installation, since 1999 [58]. The United States has remediated a number of other sites over the years. New Zealand, France, and Argentina have implemented remediation trials at some of their stations to clean up contamination [59,60]. The United States Antarctic Program requires training for participants on how to respond to spills in the field and mandates reporting of all releases no matter how minor.

Through these experiences, bioremediation and landfarming have emerged as the most practical and cost-effective methods for treating petroleum-contaminated sites in Polar Regions [61–63]. In Filler, Snape, and Barnes [62], the collective experiences of thirty-one environmental scientists and remediation practitioners working in the Arctic and Antarctica are compiled as a comprehensive bioremediation and landfarming guidebook specific to cold regions. Polar microbiology, with emphasis on Antarctic soils, is thoroughly discussed in [63].

21.3 MARINE SPILLS

Petroleum derived from tanker accidents is believed to account for 10–15% of the oil released to the environment each year [64]. The majority of oil spill studies in the past have generally been restricted to temperate climates. However, the continued development of Arctic energy reserves, increased ship traffic and tourist activities in both Polar Regions, and recent catastrophic releases of petroleum in the Russian Arctic have increased concerns about high latitude releases. Extensive investigations of the fate and effects of petroleum in the Arctic were undertaken in response to the development of oil reserves in northern Alaska and the subsequent construction of a trans-Alaska pipeline [64–66]. On the other hand, little knowledge is available on the effects of oil on southern polar ecosystems and extrapolation from findings in the Arctic may be inappropriate [67]. Increasingly, man's activities in the Southern Ocean have raised concerns about human impacts on what is seen as one of the last

pristine areas on earth. Highlighting these concerns was the accidental fuel spill from the *Bahia Paraiso* (see Chapter 23) near Anvers Island on the Antarctic Peninsula in 1989.

21.3.1 Petroleum Transport and Fate

The fate and effect of petroleum spills in Antarctic waters is largely dependent on the composition of the petroleum product and the physicochemical and biological processes acting upon the spill. Several factors including the volume of material released, environmental conditions, volatility, mechanical dispersal, dissolution, mousse formation, drifting, photolysis, adsorption and sedimentation, biodegradation, and ice and shoreline interactions act together to determine the ultimate fate of petroleum once released to the environment.

- Dispersal of oil on the water surface is a dynamic process that changes with time as the oil undergoes evaporation, dissolution, and photolytic degradation. Oil viscosity and the surface tension of the water control the rate and mean thickness of the slick. As the slick is dispersed, the relative surface area increases resulting in the loss of volatiles through evaporation.
- Evaporation is the fastest acting process and the dominant removal mechanism for refined products. Evaporation is a function of the SG of the oil, wind stress, and temperature.
- Dissolution of hydrocarbons into the water is based on polarity with the concentration of oil peaking in the upper few meters, then dropping off significantly with depth [68]. Photo-oxidation can promote the formation of polar compounds from the oil, thereby aiding in dissolution into the water column.
- Emulsification (mousse formation) is a function of the oil composition (e.g., higher molecular weight constituents such as surfactants, paraffins, and asphaltenes) and physical processes acting on the spill (e.g., turbulence and wind stress). Water in oil composition can range from 30 to 80% in the most stable emulsions. Stability is inversely related to temperature.
- Drifting is the movement of the slick in response to wind speed and currents.
- Photochemical processes are oxidative, resulting from the adsorption of ultraviolet radiation producing polar compounds (e.g., phenols, ketones, and carboxylic acids). These photolytic reactions can degrade the oil and initiate polymerization. The viscosity of a spill is increased and tar balls are formed. These processes are slower acting than evaporation and dissolution.
- Biodegradation processes generally occur slowly and consequently have limited initial effect on marine oil spills. Microbial degradation of the oil is a function

of the composition of the hydrocarbons, type and abundance of microbial species, temperature, and nutrient bioavailability. Biodegradation potential is probably greatest in bottom sediments and along shorelines.

- Shoreline interactions represent the greatest potential for deleterious effects to the ecosystem through oiling of the biota, fouling of fine-grained intertidal sediments, and impacts to subtidal macroinfauna.

These transport and transformation processes are discussed in depth in Part V.

21.3.2 Mitigation and Countermeasures

There have been few Antarctic and sub-Arctic marine oil spills to date. Although much has been learned from these few experiences in regards to cleanup and mitigation strategies, countermeasure methods have mostly been developed through laboratory testing and a few simulated oil spills off Svalbard and the Mackenzie River Delta.

The preeminent think tank for oil spill response research and development is the U.S. Department of the Interior's Minerals Management Service (MMS) Arctic Oil Spill Response Research (OSRR) program, and Ohmsett, the national oil spill response test facility in Leonardo, New Jersey. Ohmsett is the premier hands-on training site for state and federal agency, private industry, and foreign spill response personnel. It represents a necessary intermediate step between small-scale bench testing and open water testing of response equipment. MMS maintains a library of research developments. OSRR research since 1997 can be obtained from <http://www.bsee.gov/Research-and-Training/Oil-Spill-Response-Research/index/>.

Other good marine spill response resources are EPPR's *Field Guide for Oil Spill Response in Arctic Waters* and Environment Canada (EC), Canada's national environmental protection agency. EC offers spill contingency planning and shoreline cleanup and assessment workshops (<http://www.ec.gc.ca>).

21.3.3 Remediation and Lessons Learned

The January 1989 grounding of the Bahia Paraiso remains the largest spill in the Antarctic. More than 600,000 l of petroleum were released near Palmer Station, a U.S. Antarctic research station [69]. The physical setting limited the extent of the spill to within a few kilometers of Arthur Harbor. The majority of the fuel released was diesel fuel Arctic (DFA) which contains a range of normal, branched, and cyclic aliphatic hydrocarbons (C8–C30) and semi-volatile aromatic hydrocarbons (e.g., naphthalenes and fluorenes). Refined products such as DFA are characterized by a

narrow, low-boiling point range since high-molecular-weight hydrocarbons are removed during refining. Consequently, little residue survives after weathering.

The immediate effects of the Bahia Paraiso spill were restricted to within a few kilometers of the wreck over a several-week period. The size of the spill, physical dispersal of surface slicks from rough seas immediately following the spill, and prevailing offshore winds and currents limited the impact of the spill. The intertidal zone was most directly affected with oil fouling of macroalgae, limpets, birds, sediments, and rocks [69]. Limpet mortality was high, reducing populations by 50% during the first few days after the spill. The impact on macroinfauna indicated the oil was restricted to subtidal depths. Shorelines in the vicinity of Arthur Harbor are rocky, which afforded limited opportunity for the oil to mix with fine-grained sediments.

The waters of Antarctica have been designated as a Special Area under the MARPOL 73/78 Convention, and all discharges of oils from ships are banned. In 2005, efforts were begun to ban the use of heavy fuel oil (HFO) in Antarctic Treaty Areas. HFO regulation is expected to be passed in March 2010 and take effect in 2011. Also, in March 2009, an International Maritime Organization (IMO) subcommittee on Bulk Liquids and Gases advanced an amendment to MARPOL to include intermediate fuel oil. Similar bans on HFO are being brought forward for the Arctic. These fuel regulations should lessen ecological impacts from inadvertent releases by fuels that have greater volatile components and fewer high-molecular-weight hydrocarbons.

21.4 POLICY

Oil exploitation of the Arctic Basin (Fig. 21.7) and consequential growth in economic activity across the Arctic is inevitable. Climate change has greatly reduced the extent of Arctic sea ice in the past 5 years, which has opened up new opportunities for trans-Arctic shipping into the future. In the Antarctic, tourism, scientific research, and fishing are all on the increase. Where people use fuel and oil, there will be spills. The critical issues for the fragile Polar Regions are how to minimize the likelihood of spills, and how we respond to those emergencies when they happen.

Experience and history have shown that spill prevention and remediation practices are driven almost entirely by regulation and the economic sanctions imposed on polluters. The key to sustainable development of the Arctic Basin is international consensus on appropriate development and spill response. The key to improved response and impact mitigation from fuel spills in both the Arctic and Antarctic is clearly defined: scientifically based cleanup criteria and standards, and heavy penalties for polluting. In recent years, the Antarctic Treaty Parties

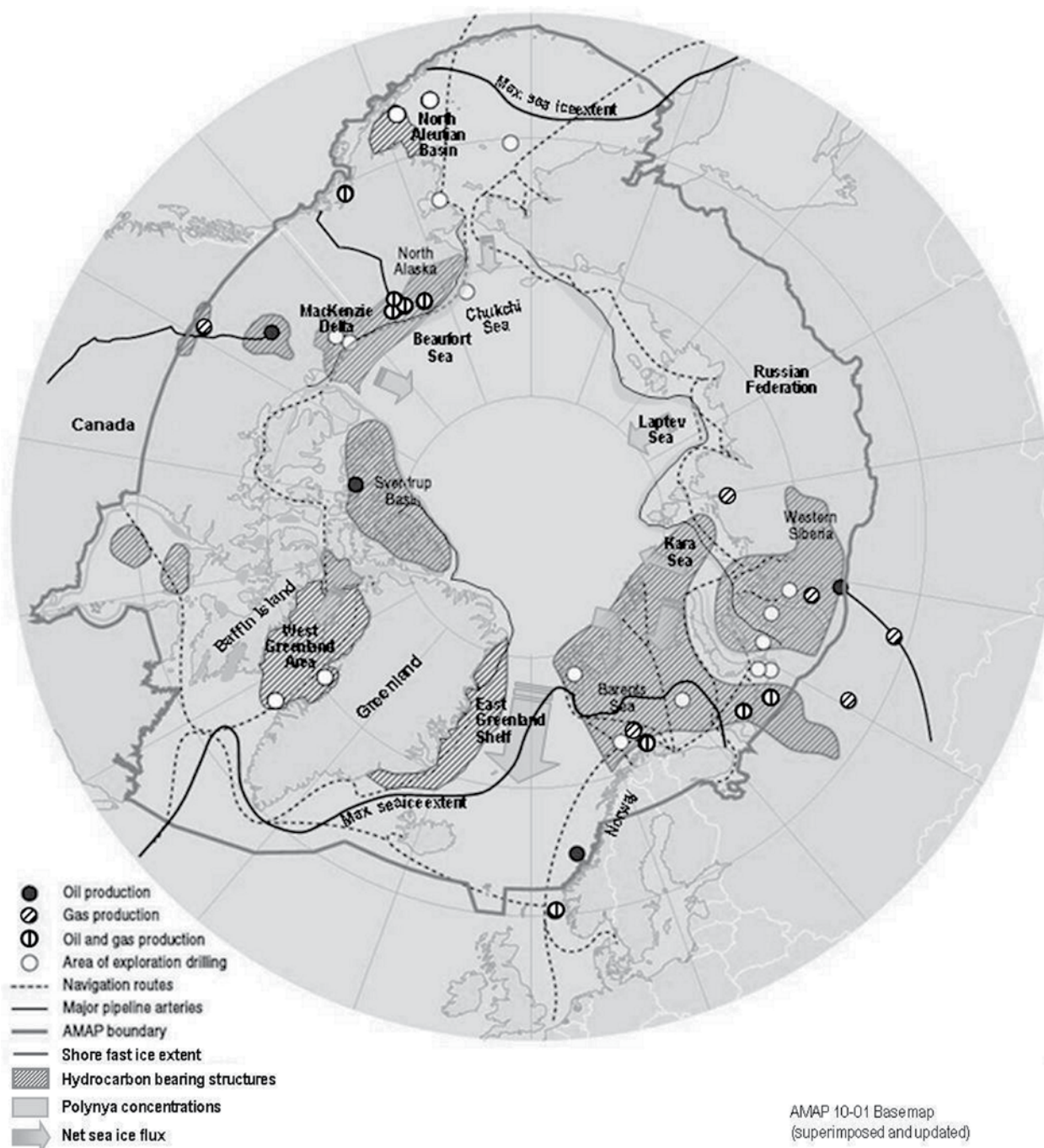


FIGURE 21.7 Regions of concern for coastal and terrestrial oil impacts in the Arctic. Projection includes major areas of oil and gas exploration and development, existing and planned major shipping routes, ice formations and net sea ice flux, and major pipelines.

have agreed to a Liability Annex that would assess monetary penalties for environmental damage. Where individuals, companies, organizations, and national programs are held directly responsible, cleanup responses are swift and impacts can be minimized. Where regulations are weak, ill defined, not legislated and enforced, and there are no penalties, impacts are often long-lived (decades) and extensive (square kilometer or regional).

Prevention is always the preferred choice instead of mitigation and remediation after the incident.

The challenge for scientists and policy makers is to advance policies that allow truly sustainable development and operations in these extreme environments, while minimizing impacts and preventing environmental damage. The difficulty and high costs of prevention and remediation can limit responses to spills in Polar Regions.

REFERENCES

- [1] UNEP/GEF, *UNEP/GEF Project—Russian Federation: Support to the National Programme of Action for the Protection of the Arctic Marine Environment*, Second Steering Committee report, Reykjavik, 289, 2007.
- [2] Bargagli, R., Environmental Contamination in Antarctic Ecosystems, *Sci Total Environ* 400, 212, 2008.
- [3] Snape, I., L. Acomb, D.L. Barnes, S. Bainbridge, R. Eno et al., Contamination, Regulation, and Remediation: An Introduction to Bioremediation of Petroleum Hydrocarbons in Cold Regions, *Bioremediation of Petroleum Hydrocarbons in Cold Regions*, Chap. 1, D.M. Filler, I. Snape, and D.L. Barnes (eds.), Cambridge University Press, 2008.
- [4] Klungsøyr, J., S. Dahle, D.J. Thomas, A. Bambulyak, S. Boitsov et al., Sources, Inputs, and Concentrations of Petroleum Hydrocarbons, Polycyclic Aromatic Hydrocarbons, and Other Contaminants Related to Oil and Gas Activities in the Arctic, Chap. 4, *AMAP Assessment 2007*, Arctic Monitoring and Assessment Programme, Oslo, 2010.
- [5] Järvinen, K. and S. Sakari, *Remediation Costs of Contaminated Sites in Finland*, Memorandum report #82108191 to Finnish Environment Institute (SYKE), Helsinki, 2004.
- [6] Filler, D.M. and D.L. Barnes, Technical Procedures for Recovery and Evaluation of Chemical Spills on Tundra, *Cold Reg Sci Technol* 37, 121, 2003.
- [7] Verma, M.K., L.P. White, and D.L. Gautier, *Engineering and Economics of the USGS Circum-arctic Oil and Gas Resource Appraisal (CARA) Project: U.S. Geological Survey Open-File Report 2008-1193*, Reston, VA, 2008.
- [8] Bear, J. *Dynamics of Fluids in Porous Media*, Elsevier, New York, 1972.
- [9] Mercer, J.W. and R.M. Cohen, A Review of Immiscible Fluids in the Subsurface: Properties, Models, Characterization and Remediation, *J Contam Hydrol* 6, 107, 1990.
- [10] Soil Survey Staff, *Soil Taxonomy: A Basic System of Soil Classification for Making and Interpreting Soil Surveys* (2nd Ed.), Agriculture Handbook 436, USDA Natural Resources Conservation Service, Washington, D.C., 1999.
- [11] Bockheim, J.G., G. Mazhitova, J.M. Kimble, and C. Tarnocai, Controversies on the Genesis and Classification of Permafrost-Affected Soils, *Geoderma* 137, 33, 2006.
- [12] Washburn, A.L., *Geocryology*. John Wiley, New York, 1980.
- [13] Margesin, R. (ed.), *Permafrost Soils*, Springer-Verlag, Heidelberg, 2009.
- [14] Bunting, B.T., High Arctic Soils Through the Microscope: Prospect and Retrospect, *Annals Assoc Am Geog* 73(4), 609, 1983.
- [15] Bryan, K., Cryopedology: The Study of Frozen Ground and Intensive Frost Action with Suggestions on Nomenclature, *Am J Sci* 244, 622, 1946.
- [16] Van Vliet-Lanoë, B., Frost Effects in Soils, *Soils and Quarterly Landscape Evolution*, J. Boardman (ed.), John Wiley, London, 117, 1985.
- [17] Vandenberghe, J., *Cryoturbation*, *Advances in Periglacial Geomorphology*, M.J. Clark (ed.), John Wiley, New York, 179, 1988.
- [18] Fox, C.A., Micromorphology of Permafrost Affected Soils, *Proceedings of the Meeting on Classification, Correlation, and Management of Permafrost-Affected Soils*, J.M. Kimble and R. Ahrens (eds.), Alaska and Yukon and Northwest Territories, U.S. Department of Agriculture, Soil Conservation Service, 51, 1994.
- [19] Bockheim, J.G. and C. Tarnocai, Recognition of Cryoturbation for Classifying Permafrost-Affected Soils, *Geoderma* 81, 281, 1998.
- [20] Walker, D.A., K.R. Everett, P.J. Webber, and J. Brown, *Geobotanical Atlas of the Prudhoe Bay Region, Alaska*, CRREL Report 80-14, U.S. Army Corp of Engineers, Cold Region Research Engineering Laboratory, Hanover, NH, 1980.
- [21] Walker, M.D., D.A. Walker, and K.R. Everett, *Wetland Soils and Vegetation, Arctic Foothills, Alaska*, National Ecology Research Center, U.S. Fish and Wildlife Service Biological Report 89(7), Washington, D.C., 1989.
- [22] Biggar, K.W. and J.C.R. Neufeld, Vertical Migration of Diesel into Silty Sand Subject to Cyclic Freeze-Thaw, *Proceedings of the Eighth International Conference on Cold Regions Engineering*, University of Alaska, Fairbanks, AK, 116, 1996.
- [23] Chuvilin, E.M., N.S. Naletova, E.C. Miklyaeva, and E.V. Kozlova, Factors Affecting Spreadability and Transportation of Oil in Regions of Frozen Ground, *Polar Rec* 37(202), 229, 2001.
- [24] Greshishev, S.G., A. Instanes, J.B. Sheshin, A.B. Pavlov, and O.V. Greshischeva, Laboratory Studies of the Oil-Contaminated Fine-Grained Soils Freezing and Their Negative Temperature Fabric Model, *Cryosphere Earth* N2, 48, 2001.
- [25] Barnes, D.L., S.M. Wolfe, and D.M. Filler, Equilibrium Distribution of Petroleum Hydrocarbons in Freezing Ground, *Polar Rec* 40, 245, 2004.
- [26] Biggar, K.W., S. Haidar, M. Nahir, and P.M. Jarrett, Site Investigations of Fuel Spill Migration into Permafrost, *J Cold Regions Eng* 12, 84, 1998.
- [27] Biggar, K.W. and M. Nahir, The Behavior of Petroleum Spills in Permafrost Soils, *Proceedings of the Assessment and Remediation of Contaminated Sites in Arctic and Cold Climates*, Edmonton, Canada, 45, 1999.
- [28] McCarthy, K., L. Walker, and L. Vigoren, Subsurface Fate of Spilled Petroleum Hydrocarbons in Continuous Permafrost, *Cold Reg Sci Technol* 38, 43, 2004.
- [29] Van Vliet-Lanoë, B., Differential Frost Heave, Load Casting and Convection: Converging Mechanisms: A Discussion of the Origin of Cryoturbation, *Permafrost Periglacial Proc* 2, 123, 1991.
- [30] Vandenberghe, J., Cryoturbations: A Sediment Structural Analysis, *Permafrost Periglacial Proc* 3, 343, 1992.
- [31] Shur, Y., J. Brown, and F. Nelson, Bottom-Up Freezing of the Active Layer: Local and Global Implications, *Proceedings of the 25th Arctic Workshop*, Laval, Canada, 177, 1995.
- [32] Mackey, J.R., The Origin of Hummocks, Western Arctic Coast, Canada, *Can J Earth Sci* 13, 889, 1980.
- [33] Das, D.B., M. Mahsanam, and N. Widdows, Non-Uniqueness in Capillary Pressure-Saturation-Relative Permeability Relationships for Two-Phase Flow in Porous Media: Interplay

- Between Intensity and Distribution of Random Micro-heterogeneities, *Chem Eng Sci* 61, 6786, 2006.
- [34] Mackey, D., M.E. Charles, and C.R. Phillips, *The Physical Aspects of Crude Oil on Northern Terrain, Northern Pipelines*, Task Force on Northern Oil Development, Environmental-Social Committee, Report 74-25, Ottawa, Canada, 1974.
- [35] Mackey, D., M.E. Charles, and C.R. Phillips, *The Physical Aspects of Crude Oil on Northern Terrain (Final Report)*, Arctic Land Use Research Program, Northern Natural Resources and Environmental Branch, Department of Indian Affairs and Northern Development, INA Publication No QS 8060-00-EE-A1, Ottawa, Canada, 1975.
- [36] Johnson, L.A., E.B. Sparrow, T.F. Jenkins, C.M. Collins, C.V. Davenport et al., *The Fate and Effect of Crude Oil Spilled on Subarctic Permafrost Terrain in Interior Alaska*, EPA-600/3-80-040, Environmental Protection Agency, Corvallis Environmental Research Laboratory, Office of Research and Development, Corvallis, NM, 1980.
- [37] Brooks, R.H. and A.T. Corey, *Hydraulic Properties of Porous Media*, Hydrology Paper 3, Colorado State University, Fort Collins, 27 pp, 1974.
- [38] Farr, A.M., R.J. Houghtalen, and D.B. McWhorter, Volume Estimation of Light Nonaqueous Phase Liquids in Porous Media, *Ground Water* 28, 48, 1990.
- [39] Barnes, D.L. and E. Chuvilin, Migration of Petroleum in Permafrost-Affected Regions, *Permafrost Soils*, Chap. 18, R. Margesin (ed.), Springer-Verlag, Heidelberg, 2009.
- [40] Williams, P.J., The Freezing of Soils: Ice in a Porous Medium and Its Environmental Significance, *Proceedings of the NATO Advanced Study Institute*, Springer-Verlag, Berlin, 219, 1997.
- [41] Williams, P.J., Contaminants and Microstructure in Frozen Ground, *Proceedings of the NATO Advanced Study Institute*, Springer-Verlag, Erice, Italy, 1997.
- [42] White, T.L. and P.J. Williams, The Influence of Microstructure on Hydraulic Properties of Hydrocarbon Contaminated Freezing Ground, *Polar Record* 35(192), 25, 1999.
- [43] White, T.L. and J.-P. Coutard, Modification of Silt Microstructure by Hydrocarbon Contamination in Freezing Ground, *Polar Record* 35(192), 41, 1999.
- [44] Torrance, J.K., T. Elliot, R. Heck, and R. Martin, Computed Tomography of Oil-Contaminated Frozen Soil, *Abstracts and Proceedings of the Geological Society of Norway, Number 2, 5th International Conference Contaminants in Freezing Ground*, 99, Erice, Italy, 2006.
- [45] Haghighi, S.K. and S. Ghoshal, Freeze-Thaw Induced Mobilization of Gasoline in Soils, *Proceedings of the Assessment and Remediation of Contaminated Sites in Arctic and Cold Climates 2007*, K. Biggar, G. Cotta, M. Nahir, A. Mullick, J. Buchko et al. (eds.), Oslo, Norway, 178, 2007.
- [46] Fourie, W., R. Said, P. Young, and D.L. Barnes, The Simulation of Pore Scale Fluid Flow with Real World Geometries Obtained from X-ray Computed Tomography, *Proceedings of the Comsol Conference*, Boston, 2007.
- [47] Reynolds, C.M., M. Travis, W.A. Braley, and R.J. Scholze, Applying Field Expedient Bioreactors and Landfarming in Cold Climates, *Hydrocarbon Bioremediation*, R. Hinchee, R.N. Miller, and R.E. Hoeppe (eds.), Boca Raton, Lewis, 100, 1994.
- [48] Braddock, J.F., L.N.A. Harduar, J.E. Lindstrom, and D.M. Filler, Efficacy of Bioaugmentation Versus Fertilization only for Treatment of Diesel Contaminated Soil at an Arctic Site, *Proceedings of the 23rd Arctic and Marine Oilspill (AMOP) Technical Seminar*, 991, Edmonton, Canada, 2000.
- [49] Filler, D.M., J.E. Lindstrom, J.F. Braddock, R.A. Johnson, and R. Nickalaskai, Integral Biopile Components for Successful Bioremediation in the Arctic, *Cold Reg Sci Technol* 32(2-3), 143, 2001.
- [50] Van Stempvoort, D.R., G. Bickerton, S. Lesage, and K. Miller, Cold-Climate, In Situ Biodegradation of Petroleum Fuel in Ground Water, Moose Factory, Canada, *Proceedings of the '04 Petroleum Hydrocarbons and Organic Chemicals in Ground Water: Prevention, Assessment, and Remediation Conference*, National Ground Water Association (ed.), 131, Vancouver, Canada, 2004.
- [51] Aislabie, J., M. Balks, N. Astori, G. Stevenson, and R. Symons, Polycyclic Aromatic Hydrocarbons in Fuel-Oil Contaminated Soils, Antarctica, *Chemosphere* 39, 2201, 1999.
- [52] Deprez, P.P., M. Arens, and E. Locher, Identification and Assessment of Contaminated Sites at Casey Station, Wilkes Land, Antarctica, *Polar Rec* 35, 299, 1999.
- [53] Mazzera, D.M., T. Hayes, D.H. Lowenthal, and B. Zeilinska, Quantification of Polycyclic Aromatic Hydrocarbons in Soil at McMurdo Station, Antarctica, *Sci Total Environ* 229, 65, 1999.
- [54] COMNAP-AEON, *Summary and Environmental Monitoring Activities in Antarctica*, Council of Managers of National Antarctic Programs, Baltimore, MD, 2001.
- [55] Webster, J., K. Webster, P. Nelson, and E. Waterhouse, The Behavior of Residual Contaminants at a Former Station Site, Antarctica, *Environ Pollut* 123, 163, 2001.
- [56] Stark, J.S., I. Snape, and M.J. Riddle, Abandoned Antarctic Waste Disposal Sites: Monitoring Remediation Outcomes and Limitations at Casey Station, *Ecol Manage Rest* 7, 21, 2006.
- [57] Roura, R., Monitoring and Remediation of Hydrocarbon Contamination at the Former Site of Greenpeace's World Park Base, Cape Evans, Ross Island, Antarctica, *Polar Rec* 40, 51, 2004.
- [58] Klein, A.G., S.T. Sweet, T.L. Wade, J.L. Sericano, and M.C. Kennicutt II, Spatial Patterns of Total Petroleum Hydrocarbons (TPH) in the Terrestrial Environment at McMurdo Station, Antarctica, *Antarct Sci* 24(5), 450-466, 2012.
- [59] Aislabie, J.M., M.R. Balks, J.M. Foght, and E.J. Waterhouse, Hydrocarbon Spills on Antarctic Soils: Effects and Management, *Environ Sci Technol* 38(5), 1265, 2004.
- [60] Delille, D., E. Pelletier, F. Coulon, G. Feller, and B. Delille, Tools for Bioremediation of Sub-Antarctic Soils Exposed to Petroleum Hydrocarbons, *Newslett Can Antarct Res Netw* 21, 11, 2006.
- [61] Filler, D.M., C.M. Reynolds, I. Snape, A.J. Daugulis, D.L. Barnes et al., Advances in Engineered Remediation for Use in the Arctic and Antarctica, *Polar Rec* 42, 111, 2006.
- [62] Filler, D.M., I. Snape, and D.L. Barnes (eds.), *Bioremediation of Petroleum Hydrocarbons in Cold Regions*, Cambridge University Press, 2008.

- [63] Asim, K.B., J. Aislabie, and R.M. Atlas (eds.), *Polar Microbiology: The Ecology, Biodiversity and Bioremediation Potential of Microorganisms in Extremely Cold Environments*, CRC Press and Taylor & Francis Group, Boca Raton, 2010.
- [64] National Academy of Sciences, *Oil in the Sea, Inputs, Fates, and Effects*, 1985.
- [65] Arctic Marine Oil Spill Program, 1978–1982, Technical Seminars: 1st 1978; 2nd 1979; 3rd 1980; 4th 1981; 5th 1982, Environmental Protection Service, Environmental Emergency Branch, Canada
- [66] Rice, S.D., J.F. Karinen, and C.C. Brodersen, Effects of oiled sediment on juvenile king crab. *Outer Continental Shelf Environmental Assessment Program*. Final Reports of Principal Investigators, Vol. 29, 287–310, 1981.
- [67] George, R.Y., Dissimilar and Similar Trends in Antarctic and Arctic Marine Benthos, *Polar Oceans*, M.J. Dunbar (ed.), Arctic Institute of North America, Montreal, 391, 1977.
- [68] Mackey, D. and C.D. McAuliff, Fate of Hydrocarbons Discharged at Sea, *Oil Chem Pollut* 5, 1, 1988.
- [69] Kennicutt II, M.C., Oil Spillage in Antarctica: Initial Report of the National Science Foundation-Sponsored Quick Response Team on the Grounding of the Bahia Paraiso, *Environ Sci Tech* 24(5), 620, 1990.

PART XII

CASE STUDIES

THE *PRESTIGE* OIL SPILL

JOAN ALBAIGÉS,¹ ANA BERNABEU,² SONIA CASTANEDO,³ NÚRIA JIMÉNEZ,^{1,6}
CARMEN MORALES-CASELLES,^{4,7} ARACELI PUENTE,³ AND LUCÍA VIÑAS⁵

¹Department of Environmental Chemistry, IDAEA-CSIC, Barcelona, Spain

²Department of Marine Geosciences, University of Vigo, Vigo, Spain

³Environmental Hydraulics Institute (IH Cantabria), Universidad de Cantabria, Parque Científico y Tecnológico de Cantabria (PCTCAN), Santander, Spain

⁴Intergovernmental Oceanographic Commission, UNESCO, Paris, France

⁵Instituto Español de Oceanografía, Centro Oceanográfico de Vigo, Vigo, Spain

⁶Federal Institute for Geosciences and Natural Resources (BGR), Geozentrum Hannover, Hannover, Germany

⁷Associated Unit of Pathology and Environmental Quality, University of Cádiz and Institute of Marine Sciences in Andalusia (CSIC), Puerto Real, Cádiz, Spain

22.1	Introduction	515
22.2	The Ocean and Coastal Dynamics in the NW Iberia and their Influence on the Spill	516
22.2.1	Oceanographic Conditions	516
22.2.2	Oil Spill Forecasting	519
22.3	Oil Monitoring and Fate	521
22.3.1	Fuel Oil Composition	521
22.3.2	Fuel at Sea	521
22.3.3	Spatial and Temporal Distribution in Seawater	525
22.3.4	Continental Shelf Contamination	526
22.3.5	Accumulation in Biota	528
22.4	The Assessment of Effects	531
22.4.1	Bioassays under Laboratory Conditions	531
22.4.2	Field Studies	532
22.5	Environmental Restoration	537
22.5.1	Oil Recovery at Sea	537
22.5.2	Coastal Contamination and Cleanup Efforts	537
22.5.3	Natural Attenuation Processes	539
22.6	Conclusion	541

22.1 INTRODUCTION

On November 13, 2002, the 26-year-old single-hulled oil tanker *Prestige*, operated by a Greek shipping company under the Bahamas flag and carrying 77,000 tonnes of heavy fuel oil from St. Petersburg (Russia) to Singapore, was reported in trouble when a severe storm associated with strong winds and extreme sea conditions (waves 8 m high) hit the NW of the Iberian Peninsula. The tanker suffered a severe structural

failure of the starboard cargo tanks and started to leak oil 50 km off the Finisterre coast (Fig. 22.1). At this point, the crew was evacuated excepting the captain, the first mate and the chief mechanic that stayed onboard trying to control the ship. However, the engine malfunctioned and the *Prestige* went adrift, dangerously approaching the coast.

On November 14, considering the risk of serious pollution of Costa da Morte and Rías Baixas, one of the prime mussel producing regions worldwide, the authorities decided to tow away the ship. At this time, a crack of 35 m opened in the starboard side, and an approximately 100 km long oil slick was already visible to satellites (Fig. 22.1). After some unsuccessful efforts, the oil tanker was finally towed, traveling northeastward. The next day, it was towed southward, turning to SW on November 16 to avoid Portuguese waters but progressively moving away from the Galicia coast. Finally, on November 19, at 9 P.M., the tanker broke in two, 130 nautical miles from the Galicia southcoast, after the spill of about 20,000 tonnes of fuel that first hit the coast between capes Finisterre and Touriñán (Costa da Morte), later acknowledged as the ground zero zone.

The two parts of the wreck sank on the southwestern part of the Galicia Seamount, in the Galicia continental margin (NW Atlantic Spanish margin): the stern at 3565 m water depth (42 10.6 N 012 03.0 W) and the bow at 3830 m water depth (42 10.8 N 012 03.6 W). The 58,000 tonnes of fuel oil remaining in the tanker continued to ooze from several cracks in the bow, giving rise to an additional spill of about

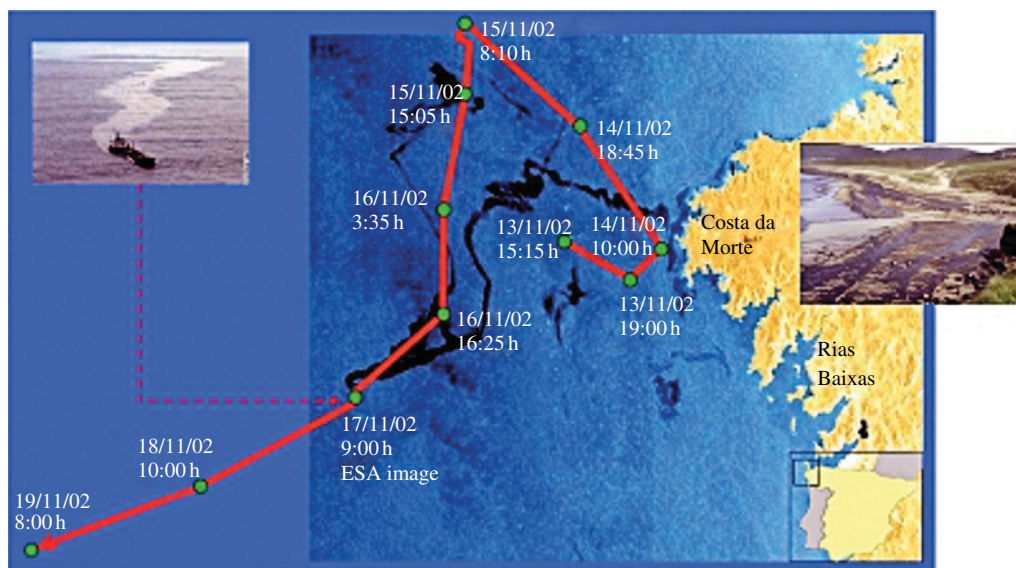


FIGURE 22.1 Towing track of the tanker from November 13 to 19, 2002 and satellite image of the spill (ESA) in November 17. Adapted from Ref. 1 with permission. © Elsevier.

40,000 tonnes until the recovery operations of the fuel in the wreck started in summer 2003.

The sinking area was recognized early on as potentially threatening for the stability of the 13,000 tons of oil remaining in the wreck, so a detailed evaluation of the geological hazard of the sinking area was carried out. The geomorphological studies established that *Prestige* stern and bow were located on conduits for water mass-movement flows [2]. Despite this, detailed sedimentological studies revealed that the turbid sedimentation mainly stopped since the last 11,000 years, resulting in the classification of the geohazard potential as moderate to low [3].

The *Prestige* oil spill (POS) attracted an exceptionally high level of public attention and concern due to the large extension of the area affected and the perceived high ecological and socioeconomic impacts. The successive black tides released from the tanker affected more than 800 km of the Spanish Atlantic shores, including 743 beaches out of the 1064 existing between the borders of Portugal and France and sensitive areas of ecological and touristic value like the Atlantic Islands National Park. The spill also affected the coasts of Portugal and France and had dramatic economic consequences for the Galicia coastal ecosystem, one of the prime producers of mussels worldwide, which had to be closed to commercial harvesting.

In the absence of a contingency plan, the Spanish authorities launched an urgent strategic action and a midterm scientific response plan to manage funds earmarked for the research response in order to ensure translation of the scientific achievements into the adoption of best operational practices. The plan was organized in six main subject areas, encompassing the oil behavior in the sunken tanks, seismic risks for the wreck, the fate of the oil in the environment, biological effects, socioeconomic impacts, and definition

and implementation of contingency plans, including operational oceanography systems for the prediction of oil trajectories in the open sea. A technical office to support these activities was also established at the University of Vigo (<http://otvm.uvigo.es>).

In the following sections, we will summarize the main outcomes of this significant effort.

22.2 THE OCEAN AND COASTAL DYNAMICS IN THE NW IBERIA AND THEIR INFLUENCE ON THE SPILL

22.2.1 Oceanographic Conditions

Meteorological conditions and ocean dynamics account for the drift of oil slicks toward the shoreline. Although the drift of an oil spill is mainly driven by surface winds, during the POS, the dynamics in the continental shelf and slope played a fundamental role.

The oceanographic dynamics of the Galicia continental shelf exhibits a complex pattern, considering the different water masses involved, the combination of some hydrographic phenomena and the high influence of seasonality of winds. In this sense, this system is not completely understood, but the main features of circulation have been recently described [4,5].

During POS, the conditions were typical of an autumn–winter period, with the combination of a river plume and a poleward current (Fig. 22.2). The river plume corresponds to the so-called western Iberian buoyant plume (WIBP), which is generated by the discharge of continental waters, mainly from the Miño River, that extends along the coast and flows northward, with salinity of less than 35.7.

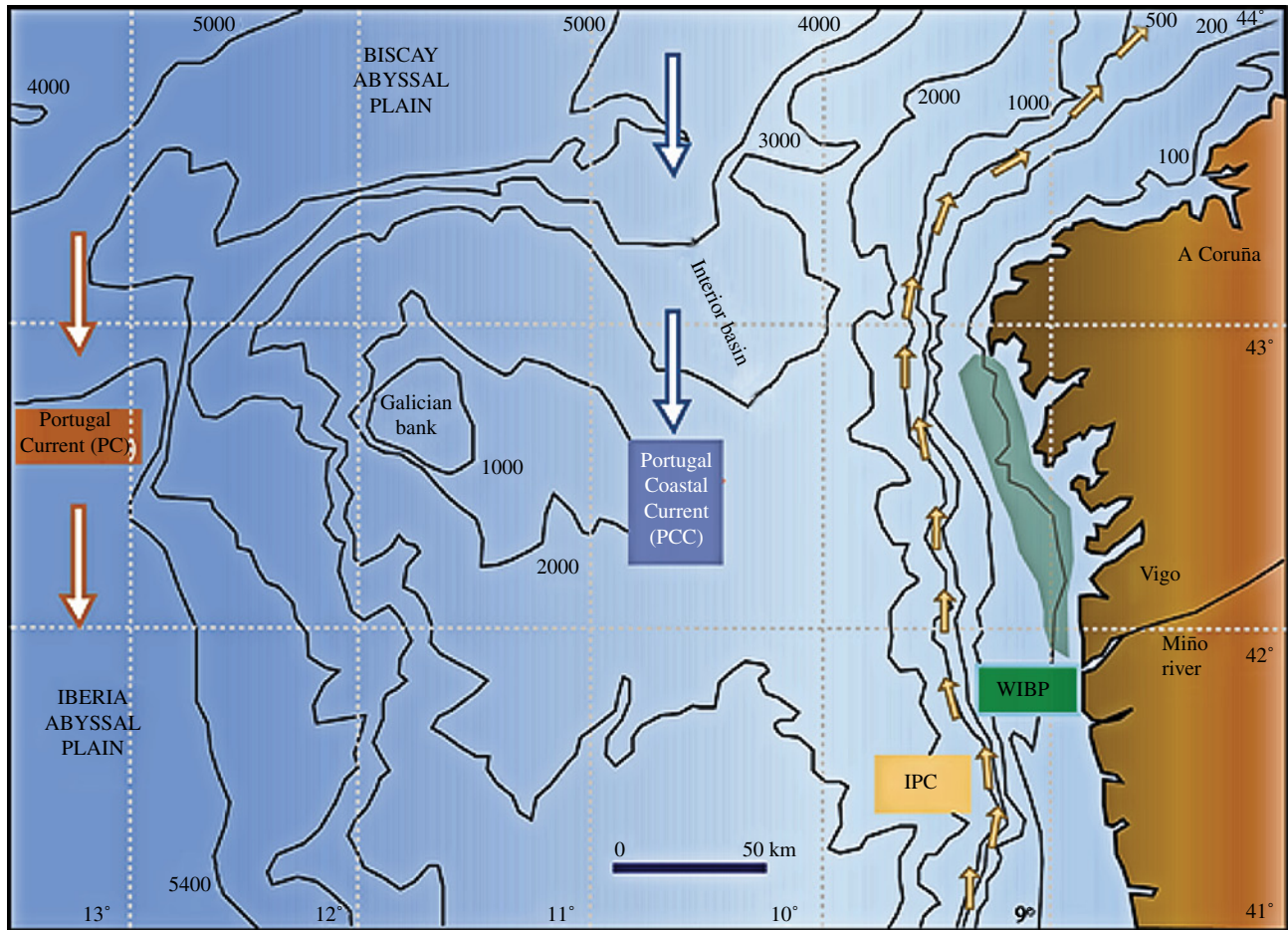


FIGURE 22.2 Schematic diagram with the main water circulation features of the area of the spill.

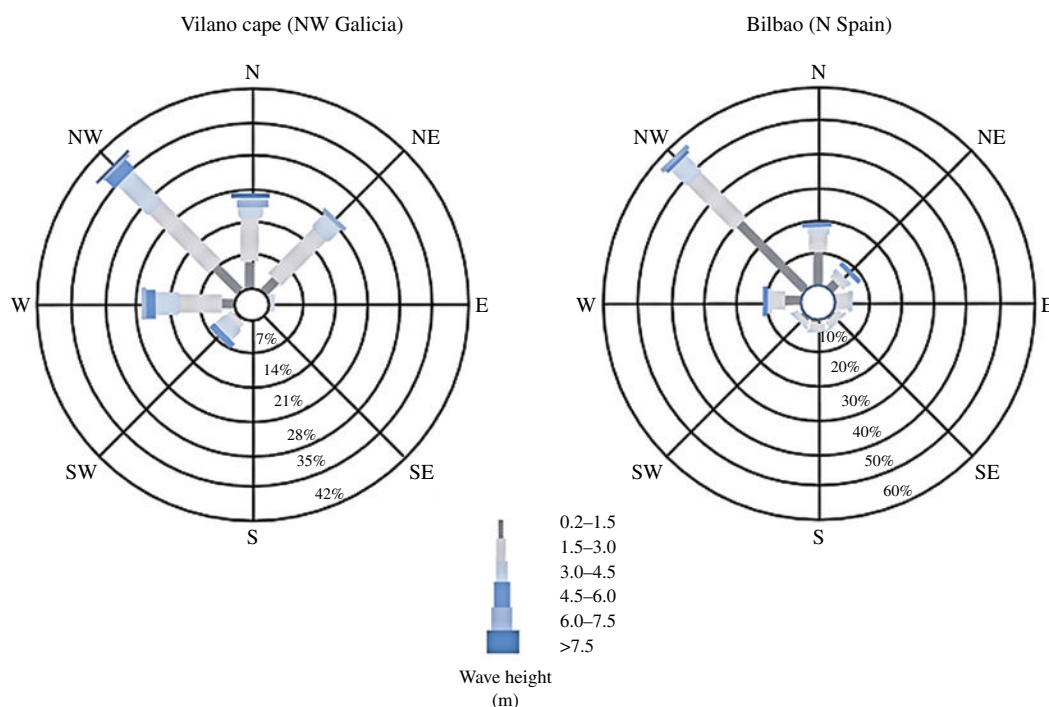
The northward current, known as Iberian poleward current (IPC), mainly appears at the end of the upwelling season, by the end of autumn and during winter, when south westerly winds prevail in the area [6,7]. IPC transports warm and salty waters northward at 10–30 cm/s, along the shelf and the slope off Rías Baixas, opposing to the predominant southern currents, the Portugal current (PC) and Portugal coastal current (PCC), typical of the eastern margins of the oceans (Fig. 22.2). PC flows over the abyssal plain and PCC over the internal basin of Galicia bank, respectively. At the summer period, IPC weakens and moves to higher depths and offshore, whereas during winter it is intensified and enters into the Galicia continental shelf at shallower depths.

During November–December 2002, a marked convergence front between IPC and WIBP acted as a physical barrier to prevent the oil from entering into Rías Baixas, reducing the impact on the shellfish populations intensively cultured inside these embayments, but the northward flow of both currents moved the oil along the Galicia margin, greatly threatening Costa da Morte [8]. After Finisterre Cape, where the WIBP basically disappears, part of the oil moved with IPC, surrounding the Spanish coast and directing to the Cantabria margin and the south of the Bay of Biscay.

The wind regime in this area also conditions the wave climate. The Galicia Atlantic coast is generally exposed to energetic swells from NW to SW (Fig. 22.3a). The most frequent direction is from the NW (40–50%), followed by the W (30–35%). In both cases, waves could be higher than 6 m. Finally, the waves from the SW tend to occur less frequently (<10%) but are normally associated with stormy conditions with waves higher than 5 m.

During the winter 2002–2003, wave heights were unusually high off the NW Galicia coast, with four important storms with wave heights of more than 5 m and duration of more than three consecutive days (Fig. 22.3b). The first of these took place during the days following the accident, between November 19 and 22, 2002, with a maximum wave height of 9.34 m and a period of 15.5 s, coming from the WNW (282°). Moreover, the most frequent wave directions were likewise unusual, with no waves arriving from the north and an increase in the number of those arriving from the southwest, which are frequently associated with storm events. During the following months, the sea became progressively smoother, with significant wave height and period adopting typical winter values (mean H_s = 2.4 m and mean T_s = 8.56 s) and approximately 20% of waves arriving from the north.

(a)



(b)

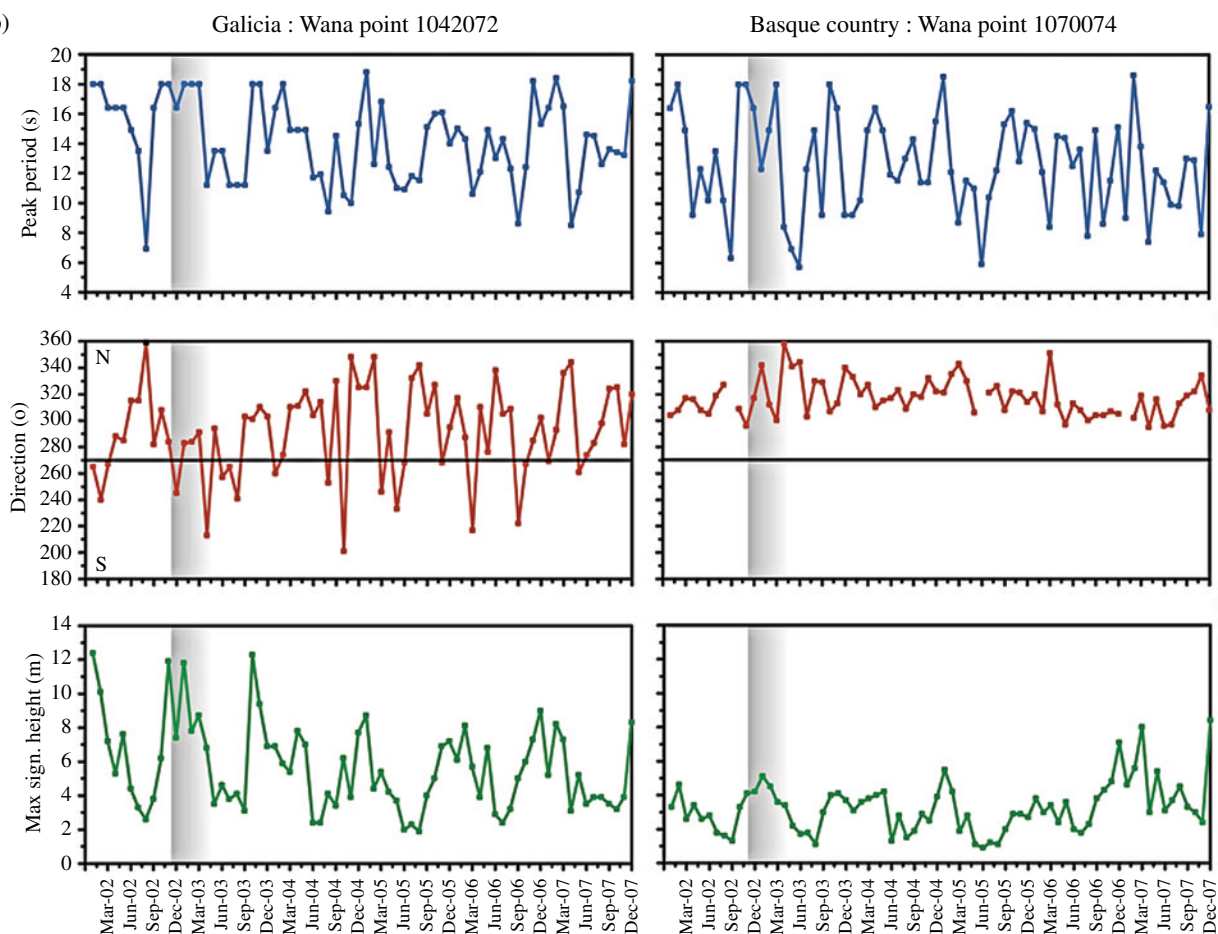


FIGURE 22.3 Wave climate conditions: (a) general conditions represented by a wave rose corresponding to 2005 for NW Galicia and N Spanish coast; (b) specific conditions of wave height, period, and direction from March 2002 to December 2007 for Galicia and Basque Country coasts. Reprinted with permission from Ref. 9. © American Chemical Society.

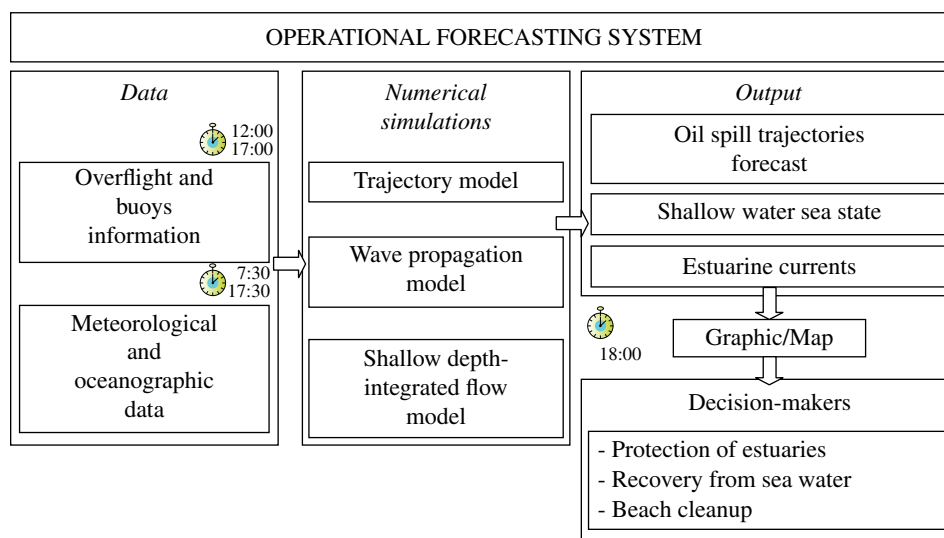


FIGURE 22.4 Structure of the operational forecasting system established in Cantabria. Adapted with permission from Ref. 11. © CERF.

In contrast to the Galicia situation, 800 km away, on the Basque coast, wave climate parameters were typical of an average winter when the *Prestige* oil began to arrive, with mean $H_s = 1.5$ m and mean $T_s = 13$ s.

This information was incorporated into forecasting models for oil spill trajectories and was an important part of a management plan of the oil recovery tasks at sea and response in the coastal zone.

22.2.2 Oil Spill Forecasting

From the first stages of the *Prestige* accident, different Spanish institutions and public agencies started to work on the monitoring and forecasting the oil spill. Several operational forecast systems were built in different regions along the northern coast of Spain with a common objective of helping to manage the crisis. In Galicia, the regional government and the meteorological service (MeteoGalicia) promoted the creation of the Office of Nearshore Surveillance, Unidade de Observación Próxima (UOP), whose main objectives were to monitor the oil spill and operationally forecast its fate [10]. The operational oceanographic systems developed in Cantabria and the Basque Country pursued similar objectives [11,12].

The goal of the operational systems was to forecast weather conditions, wave climate, tidal and wind currents, and oil spill trajectories to provide the decision makers with technical assessments to respond to the POS. The main components of these forecasting systems were overflight information, meteorological and oceanographic data collection, and numerical models. All these elements were connected following a procedure similar to the one shown in Figure 22.4, corresponding to Cantabria.

22.2.2.1 Overflight and Buoy Data One of the main components of the forecasting system was the overflight

information from aircraft belonging to different international and national institutions. The oil slick position charts were elaborated using aerial observations by the Spanish and the local governments by fax and e-mail on daily basis.

Another valuable source of information was the drifter buoys. A set of satellite tracked Lagrangian floats was released between December 2002 and January 2003 (Fig. 22.5). Most of them were placed near the Galicia coast to track the biggest *Prestige* oil slicks right after the accident and some of them were used to infer the path of potential spills of the remaining fuel in the wreck. The buoy data were particularly useful to calibrate oil spill dispersion models.

As Figure 22.5 shows, buoys 23,249 and 23,250, released over the wreck location, moved to the south and drifted off the Galicia coast. The buoys released on the Iberian shelf drifted around Cape Finisterre into the Bay of Biscay following the coastal and shelf shape according to the main trend of the IPC (see Section 22.2.1). A detailed explanation about the buoys motion can be found in the literature [14].

22.2.2.2 Meteorological and Oceanographic Data In order to forecast the fate of spilled oil in the marine environment, data regarding meteorological and oceanographic conditions were needed. Although data from coastal stations and meteorological buoy stations would be more precise, direct observations and measurements at the place of the incident were almost nonexistent. Moreover, only a limited number of wave buoys and tidal gauges as well as meteorological stations were available at nearby locations. For that reason, the output of numerical models was used as the regular data source.

International, national, and regional institutes (NCEP, NRLPOM, AEMET, Puertos del Estado, MeteoGalicia, etc.) provided numerical outputs (48 h forecast of wind, sea state conditions, and currents) to feed the oil spill transport models running in each operational system.

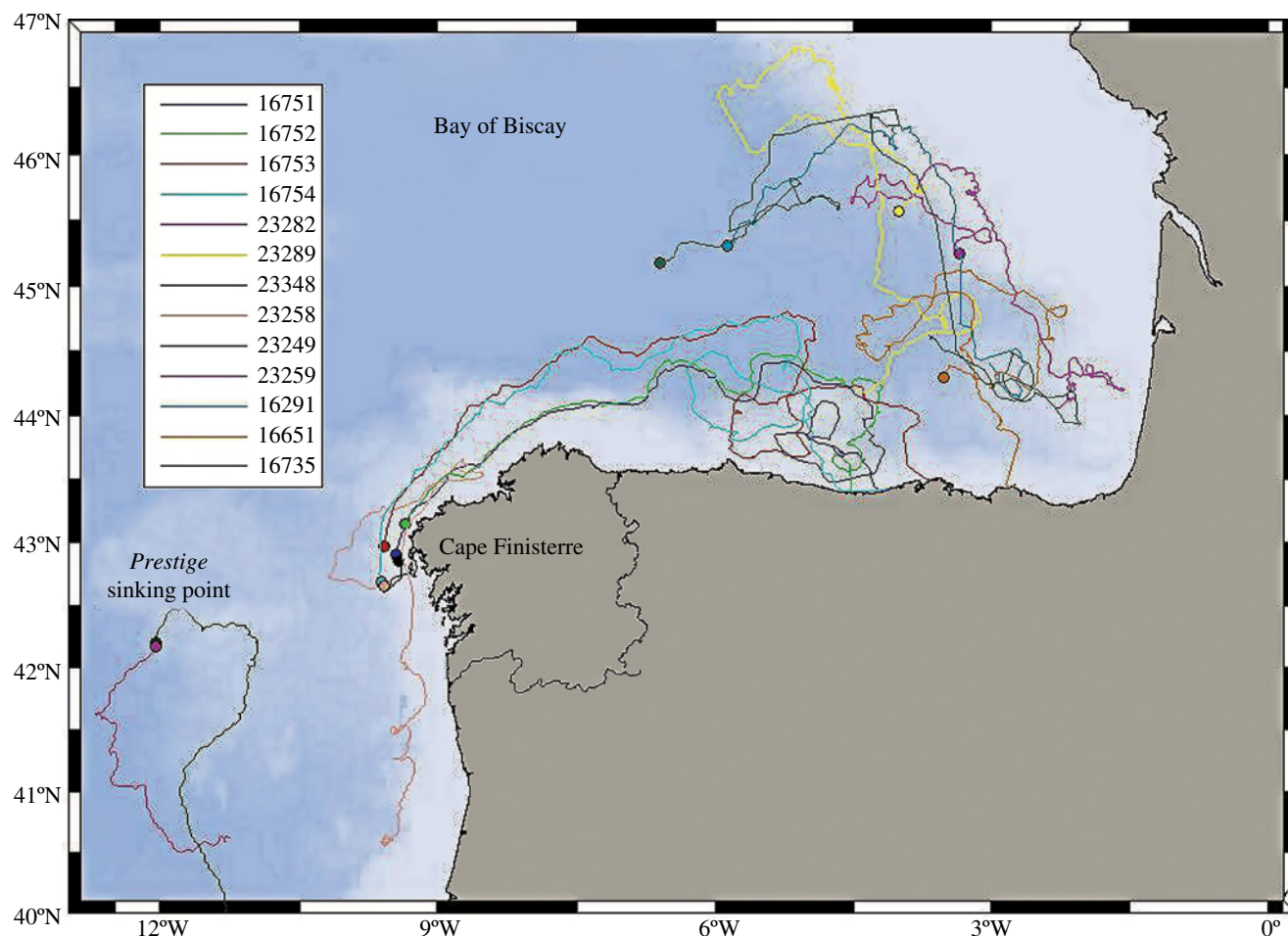


FIGURE 22.5 Buoys trajectory evolution during the study period. The drifter identification numbers are indicated on the legend. Reprinted with permission from Ref. 13. © CERF.

22.2.2.3 Numerical Models Different oil spill numerical model outputs, such as MOTHY from MeteoFrance and GNOME from NOAA, were used to simulate the different processes undergone by the POS at sea [15,16]. Moreover, in Galicia, the MeteoMohid model coupled with a Lagrangian Mohid module was used to obtain oil tracks, and in Cantabria, a two-dimensional (2D) Lagrangian model named PICH1 was developed and applied [10,11].

To test the accuracy of the prediction tools, a periodical comparison between drift buoys trajectories and numerical predicted paths was carried out. The model parameters were corrected by means of a trial-and-error procedure. Specifically, in Cantabria, a study on the relative importance of the different forcing (wind, wave, currents) was undertaken as part of the calibration process. This study found that although wind drift and surface currents were the major advective transport mechanisms, wave-induced Stokes drift could not be discarded and, on several occasions, wave-driven transport became the most important factor in the transport of the floating oil slicks.

Another way of testing the performance of the numerical models consisted of a continuous oil slick

tracking. However, when considering the oil spill that arrived at the Bay of Biscay, it was not an easy task due to several reasons. During rough seas, which are quite frequent along the Cantabria coast, the work of the aircraft became very difficult and was often unable to provide spill data. The submerging of oil was another important factor that contributed to difficulty of oil slick tracking. When the oil spill reached the Cantabria coast, the density of the oil approached that of the water, and the oil patches, emulsified with about 80% water, became “overwashed” by wave action, making them very difficult to track. Once the oil stranded on the coast it was too viscous to penetrate the sand and could therefore float off at the next high tide, be carried and deposited at a different location. All of this made the oil slick tracking difficult.

22.2.2.4 The ESEOO Project The experience gained with the *Prestige* preoperational systems and the funding opportunity provided by the Spanish Ministry of Education and Science gave birth to a 3-year project (2004–2006), the Establecimiento de un Sistema Español de Oceanografía Operacional (ESEOO)—Implementation of a Spanish

Operational Oceanography System (www.esooo.org). The ESEOO partners constituted a multidisciplinary team coordinated by Puertos del Estado. The basic objective of the project was to develop OO at the national level by creating new tools and by improving the interinstitutional and international coordination. Nowadays, the ESEOO modeling products are integrated into SASEMAR (search and rescue institution) procedures, being used to provide forecasts of drifting persons and objects as well as providing basic tools for dealing with accidental marine pollution [17].

22.3 OIL MONITORING AND FATE

Soon after the accident, a large effort was made to monitor the spatial distribution and temporal evolution of hydrocarbons in different marine biotic and abiotic compartments, along the Northern Spanish coast. This involved the sampling of drifting oil, water, sediments, indigenous populations of mussels, and other biota species [18–26].

22.3.1 Fuel Oil Composition

The oil carried by the *Prestige* was a heavy fuel oil (M-100 type) with a viscosity of 100,000 cSt at 15°C, a measured density of 0.992 kg/l at 15°C (11.04° API), 2.28% of sulfur, and a chemical composition of 22% of aliphatic hydrocarbons, 50% of aromatic hydrocarbons, and 28% of resins and asphaltenes.

The total ion chromatogram corresponding to the aliphatic fraction is characterized by a bimodal distribution of *n*-alkanes centered at *n*-C14 and *n*-C24 and extending up to at least *n*-C40, typical of a petroleum residue diluted with a middle distillate, possibly to comply with the commercial specifications (Fig. 22.6a). The series of regular acyclic isoprenoids C14–C20 is also present, with a pristane/phytane ratio of 0.9.

The oil source correlation was made on the basis of some molecular marker and PAH indices, proposed for differentiating sources of spilled oils [27–29]. The triterpane and sterane profiles are shown in Figure 22.6b. Diagnostic ratios used as source indicators are shown in Table 22.1. The *Prestige* oil is characterized by tetra and pentacyclic terpane (27Ts and 29 $\alpha\beta$) and C29 $\alpha\alpha$ S/R and $\beta\beta/\alpha\alpha$ sterane indices significantly below 50. These four parameters were found to be the most meaningful to highlight the *Prestige* oil pollution in sediment, and biota surveys were carried out in the region after the accident [20,21].

The distribution of parent and alkylated PAHs is shown in Figure 22.7. The ratios of C2 and C3 alkyl dibenzothiophenes and phenanthrene/anthracenes (D2/P2 and D3/P3), exhibiting relatively higher values according to the S content of the oil, were also found of diagnostic value.

22.3.2 Fuel at Sea

Following the oil spill, an extensive survey was carried out by the Spanish Marine Safety Agency (SASEMAR) at the northern coast of Spain to obtain a comprehensive picture of the fate of the spill in the marine environment and, indirectly, identify the molecular indicators to be used for oil source recognition, in case of the possible occurrence of illegal discharges in the area after the spill (Fig. 22.8). More than 200 oil samples were collected in the region (at the sea, at the continental shelf, and stranded on the coast) between December 2002 and December 2003 and characterized by chemical fingerprinting of both the aliphatic and aromatic fractions.

The median values of the source indices corresponding to the collected samples along the whole sampling period are shown in Table 22.1. Stout et al. reported that the analytical precision that can be expected in the calculation of these indices is generally high [29]. An RSD variation less than 5% seems reasonable as a threshold for source confirmation. As shown in Table 22.1, this level of variation is well attained in the analyzed samples, confirming their common origin. The higher variability of the pristane/phytane ratio could be attributed to the effect of weathering. Slight deviations of the other ratios from the values of the *Prestige* oil were also found, possibly due to weathering as well, because the trends are consistent with those observed in a field remediation study carried out in the area [30].

On the other hand, 17% of the total samples analyzed during this period did not match the *Prestige* oil, and most of these (52%) were found off A Coruña (Fig. 22.8) where the city harbor and a refinery support an intense maritime traffic. This demonstrates the continued occurrence of oil discharges at sea and the need for a more strict surveillance of the areas with heavy tanker traffic.

During this survey, the *Prestige* oil was drifting on the seawater surface for almost 1 year and thus being highly exposed to major weathering processes (e.g., emulsification, evaporation, dissolution, photo-oxidation, and biodegradation); thus, it was a good opportunity to monitor the resulting compositional changes for assessing the molecular indicators to be used for oil source recognition [18].

A major change observed in the aliphatic fraction of the collected samples was the gradual decrease of *n*-alkanes in less than *n*-C20 range (Fig. 22.9). Based on laboratory evaporative studies and the values estimated by the oil depletion equation established by Douglas et al., a maximum of approximately 5% of the oil would only be lost by evaporation, due to its heavy nature [31].

Usually, the rate of *n*-alkanes evaporation at sea is rapid in the first weeks after the spill and subsequently slows down until it becomes negligible. However, in the present case, a steady depletion trend was observed during the whole period, probably due to the patchy nature of the spilled product.

Some of the oil components that are subject to evaporation, namely, the low molecular weight aromatic hydrocarbons, can

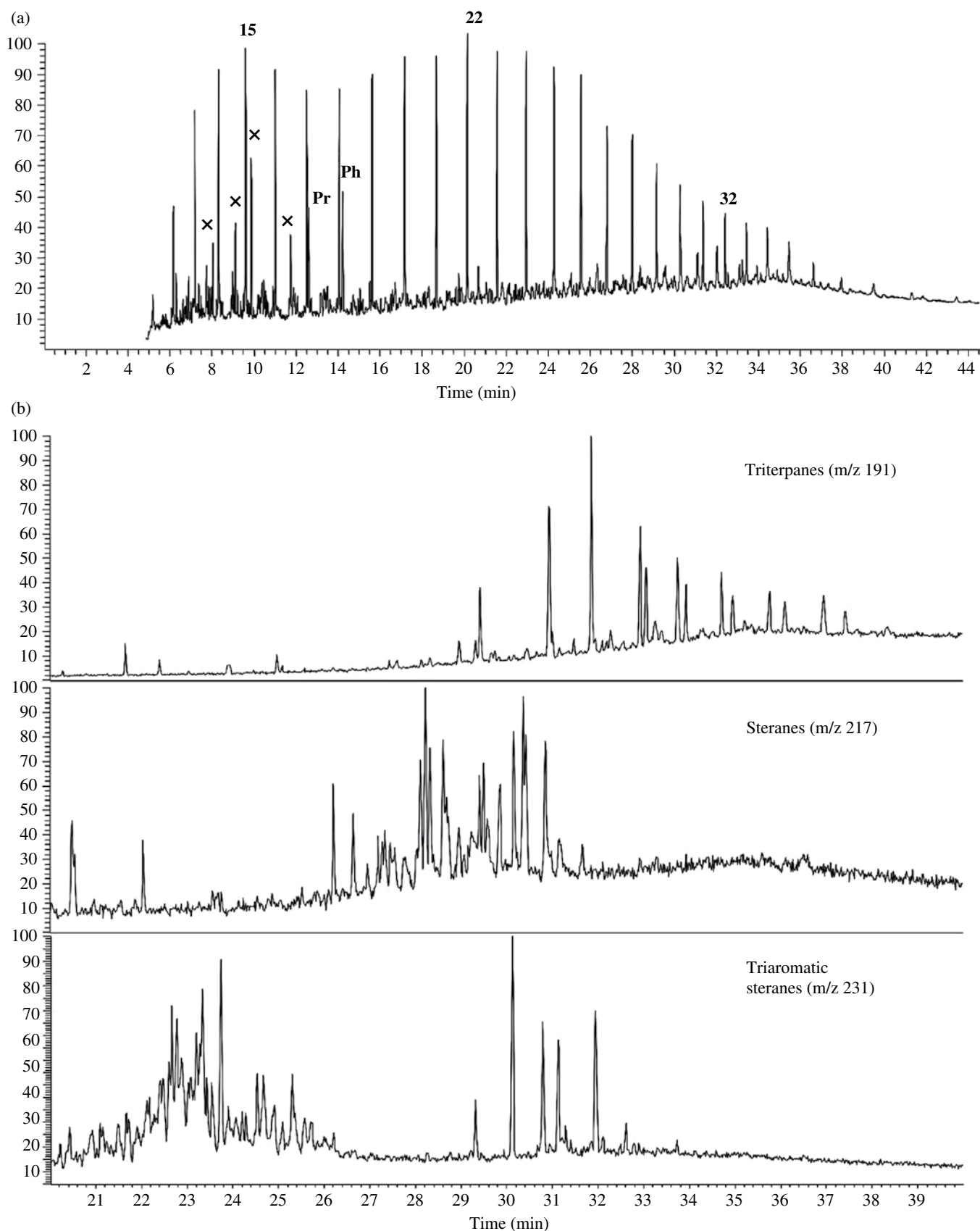


FIGURE 22.6 The total ion chromatogram of the aliphatic fraction of the *Prestige* oil (a) and triterpane and sterane molecular marker distributions (b). The numbers indicate the carbon atoms of the *n*-alkanes. Ph, phytane; Pr, pristane; X, isoprenoid hydrocarbons.

TABLE 22.1 Diagnostic ratios used as source indicators for the oil samples and median values given for the *Prestige* oil residues ($n = 152$)

Diagnostic ion (m/z)	Index	Definition	Structures	<i>Prestige</i> oil	
				Original oil	Oil at sea (%RSD) Biodegraded oil
113	Pr/Ph	Pristane/phytane	Pr: 2,6,10,14-tetramethylpentadecane Ph: 2,6,10,14-tetramethylhexadecane	0.9	0.8 ± 6.2 —
191	%27Ts	$100 \times \text{Ts}/(\text{Ts} + \text{Tm})$	Ts: 18 α (H)-22,29,30-trisnorhopane Tm: 17 α (H)-22,29,30-trisnorhopane	22	23.1 ± 3.7 22
191	%29 $\alpha\beta$	$100 \times 29\alpha\beta/(29\alpha\beta + 30\alpha\beta)$	29 $\alpha\beta$: 17 α (H),21 β (H)-30-norhopane 30 $\alpha\beta$: 17 α (H),21 β (H)-hopane	43	42.2 ± 3.7 42
217	%27dia	$100 \times 27d(R + S)/[27d(R + S) + 27\beta\beta(R + S)]$	27d: 13 β (H),17 α (H)—diacholestane (20S and 20R) 27 $\beta\beta$: 14 β (H),17 β (H)—cholestane (20R and 20S)	36	35.1 ± 3.1 29
217	%29 $\alpha\alpha$ S	$100 \times 29\alpha\alpha S/(29\alpha\alpha S + 29\alpha\alpha R)$	29 $\alpha\alpha$: 24-ethyl-14 α (H),17 α (H)—cholestane (20S and 20R)	45	48.7 ± 2.9 49
217	%29 $\beta\beta$ RS	$100 \times 29\beta\beta(R + S)/[29\beta\beta(R + S) + 29\alpha\alpha(R + S)]$	29 $\beta\beta$: 24-ethyl-14 β (H),17 β (H)—cholestane (20R and 20S)	47	47.9 ± 3.4 57
218	%27 $\beta\beta$	$100 \times [27\beta\beta(R + S)]/[27\beta\beta(R + S) + 28\beta\beta(R + S) + 29\beta\beta(R + S)]$	27 $\beta\beta$: 14 β (H),17 β (H)—cholestane (20R and 20S)	37	34.9 ± 3.0 7
218	%28 $\beta\beta$	$100 \times [28\beta\beta(R + S)]/[27\beta\beta(R + S) + 28\beta\beta(R + S) + 29\beta\beta(R + S)]$	28 $\beta\beta$: 24-methyl-14 β (H),17 β (H)—cholestane (20R and 20S)	27	25.3 ± 4.1 35
218	%29 $\beta\beta$	$100 \times [29\beta\beta(R + S)]/[27\beta\beta(R + S) + 28\beta\beta(R + S) + 29\beta\beta(R + S)]$	29 $\beta\beta$: 24-ethyl-14 β (H),17 β (H)—cholestane (20R and 20S)	36	38.9 ± 1.9 58
231	%26TA	$100 \times 26TAS/(26TAS + 28TAS)$	TAS: triaromatic sterane (20S and 20R)	27	26.7 ± 1.6 15
212/206	D2/P2	$100 \times \text{C2-DBT}/(\text{C2-DBT} + \text{C2-P})$	DBT: dibenzothiophene	34	31.6 ± 3.2 25
226/220	D3/P3	$100 \times \text{C3-DBT}/(\text{C3-DBT} + \text{C3-P})$	P: phenanthrene	40	38.4 ± 2.0 33
212/256	D2/C2	$100 \times \text{C2-DBT}/(\text{C2-DBT} + \text{C2-C})$	C: chrysene	67	66.1 ± 1.9 12
226/270	D3/C3	$100 \times \text{C3-DBT}/(\text{C3-DBT} + \text{C3-C})$	—	70	68.4 ± 1.8 51

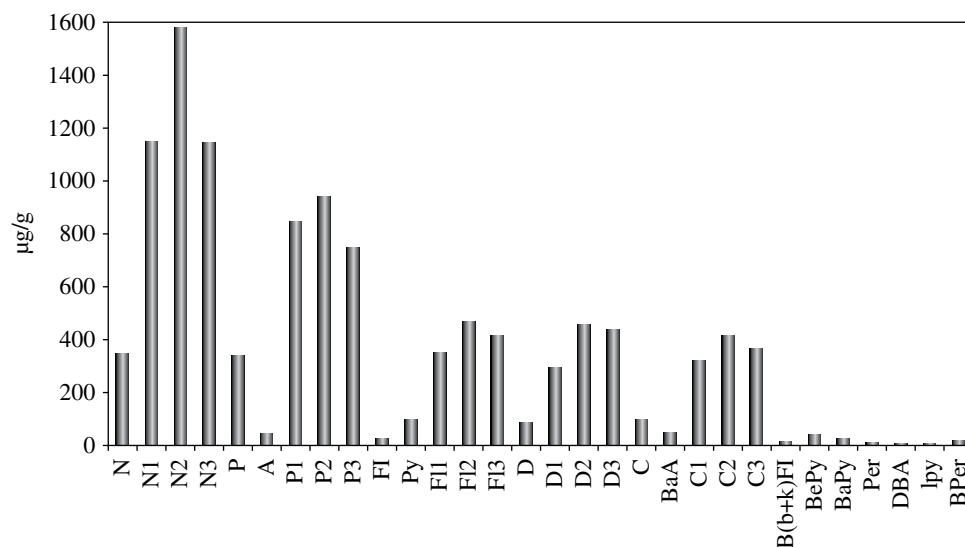


FIGURE 22.7 Distribution of PAHs. A, anthracene; BaA, benz[a]anthracene; B(b + k)FI, benzo[b + k]fluoranthenes; BaPy, benzo[a]pyrene; BePy, benzo[e]pyrene; BPer, benzo[ghi]perylene; C, chrysene + triphenylene; C1–C3, C1–C3-chrysenes; D, dibenzothiophene; D1–D3, C1–C3-dibenzothiophenes; DBA, dibenzo[ah]anthracene; FI, fluoranthene; FI1–FI3, C1–C3-fluoranthene/pyrenes; Ipy, indeno[1,2,3-cd]pyrene; N, naphthalene; N1–N3, C1–C3-naphthalenes; P, phenanthrene; P1–P3, C1–C3-phenanthrenes; Per, perylene; Py, pyrene.

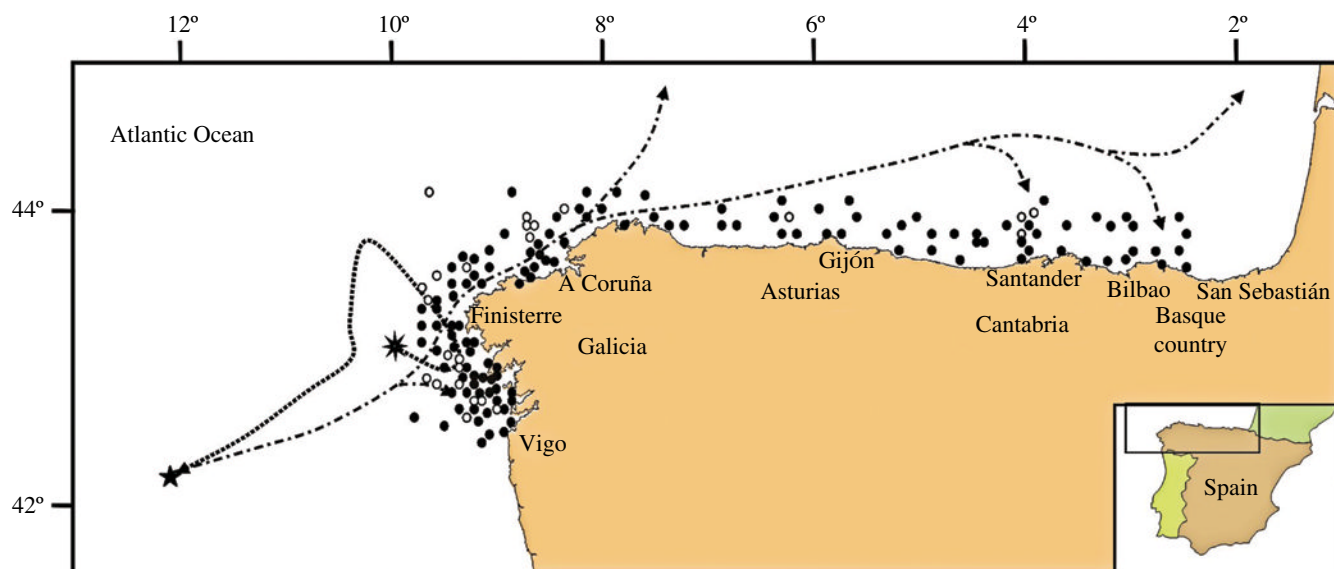


FIGURE 22.8 Sample locations along the Northern Spanish coast with indication of the main oil trajectories → tanker towing route. ★ shipwreck position. → oil trajectories. ● oil samples (full and empty circles correspond to *Prestige* and non-*Prestige* samples, respectively). Reprinted with permission from Ref. 17. © American Chemical Society.

also dissolve into the water column, largely influenced by the hydrodynamic conditions of the surface waters. Thus, evaporation and dissolution are competitive processes. Although the volume loss of spilled oil by dissolution can be negligible from a practical perspective, it can be significant from the ecotoxicological standpoint.

The most important change observed in the aromatic fraction of the collected samples was the decrease of the relative abundance of naphthalene and methylnaphthalenes to

below detection limits. The relative loss of these compounds with respect to C2-naphthalenes, defined by the $[(N + N1) / N2]$ ratio, was particularly evident during the initial phase of the spill, as illustrated in Figure 22.9. The loss of these components accounts for less than 2% of the original oil.

Biodegradation originating compositional changes are dominated by the molecular structure of the hydrocarbons. In this respect, *n*-alkanes are degraded at faster rates than acyclic isoprenoids, and the early effect of microbial degradation

is currently monitored by the *n*-C17/pristane and *n*-C18/phytane ratios [32]. Figure 22.9 indicates a delay of about 2 months before the degradation of *n*-alkanes is evidenced, and after a certain progress, it does not go further for the rest of the year. It is possible that the limited extension of degradation can be due to the fact that the oil is in the form of compact patches, which are only available to bacteria at the surface. Therefore, it appears that although biodegradation might have played a role in the oil weathering, it is not dominant, as already has been observed in other oil spills [33,34].

As opposed to biodegradation, there is evidence that alkyl-substituted aromatic hydrocarbons are photochemically oxidized at a faster rate than the parent compounds [35]. However, microbial degradation results in the depletion

of unsubstituted species relative to their alkylated homologs, so that it is likely that concurrent photo- and biodegradation may give rise, at moderate levels, to profiles similar to those of the fresh oil. The corresponding values of the collected samples did not exhibit any noticeable temporal trend. Therefore, taking into account that, as shown earlier, biodegradation of the samples was rather limited, this may indicate that photo-oxidation has neither been significant at sea during that period.

In summary, the data showed the high persistence of the spilled heavy oil at sea, 1 year after the accident, with a very low evidence of the natural weathering processes. These were only slightly enhanced when the oil was stranded on the shorelines, thus stressing the need for mechanical removal from the sea surface and the coastal areas.

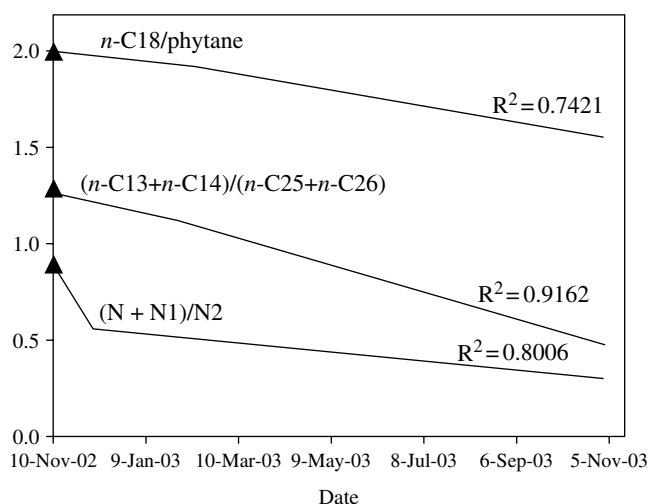


FIGURE 22.9 Weathering ratios of oil samples collected along the Northern Spanish coast. (▲) *Prestige* oil ratios.

22.3.3 Spatial and Temporal Distribution in Seawater

Seawater samples collected at three depths (subsurface, mid depth, and bottom) from 68 stations along the Northern Spanish coast (Fig. 22.10) were analyzed for dissolved/dispersed petroleum aromatic hydrocarbons by UV fluorescence and for 25 individual compounds by GC-MS. Sampling was performed in December 2002, just after the POS, and in February, March, and September 2003 [19].

Higher concentrations of total aromatic hydrocarbons were found at all depths in the samples collected during December 2002 off the Galicia coast, with levels ranging between 0.1 and 0.46 $\mu\text{g/l}$ $\Sigma 16$ PAHs (Fig. 22.11). The higher concentrations were found in the subsurface samples along the Costa da Morte, the area most heavily affected by the spill. These values decreased in the following cruises, down to 0.09 $\mu\text{g/l}$ in September 2003, possibly representing the background levels for the region.

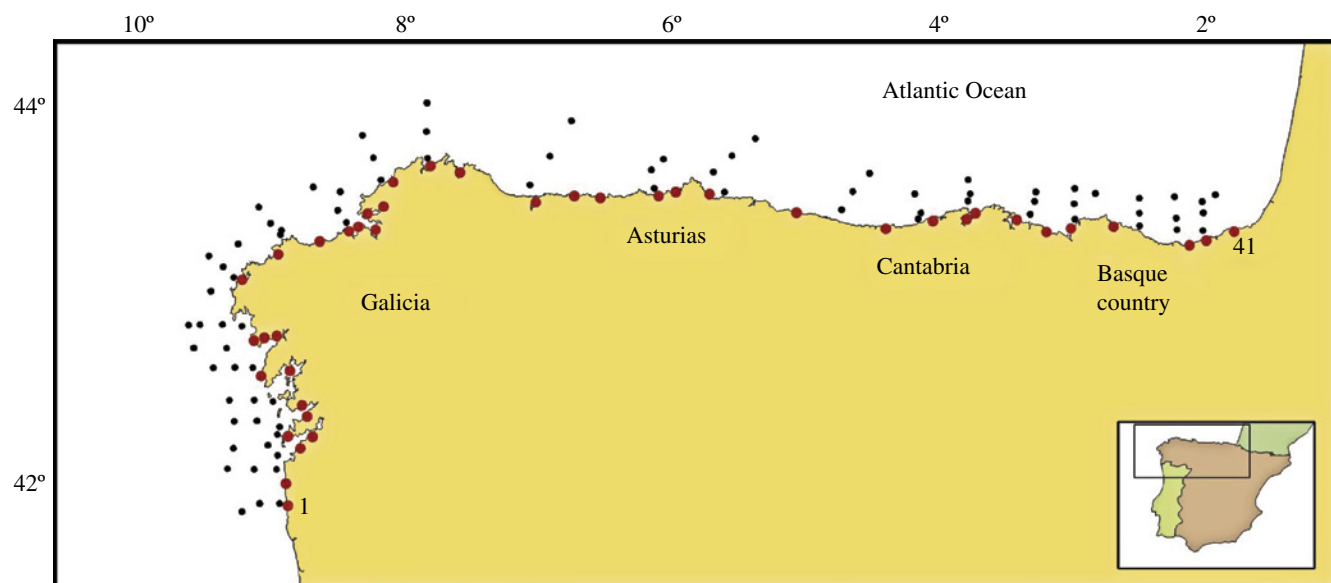


FIGURE 22.10 Sampling stations. Water and sediment (●) and biota (●).

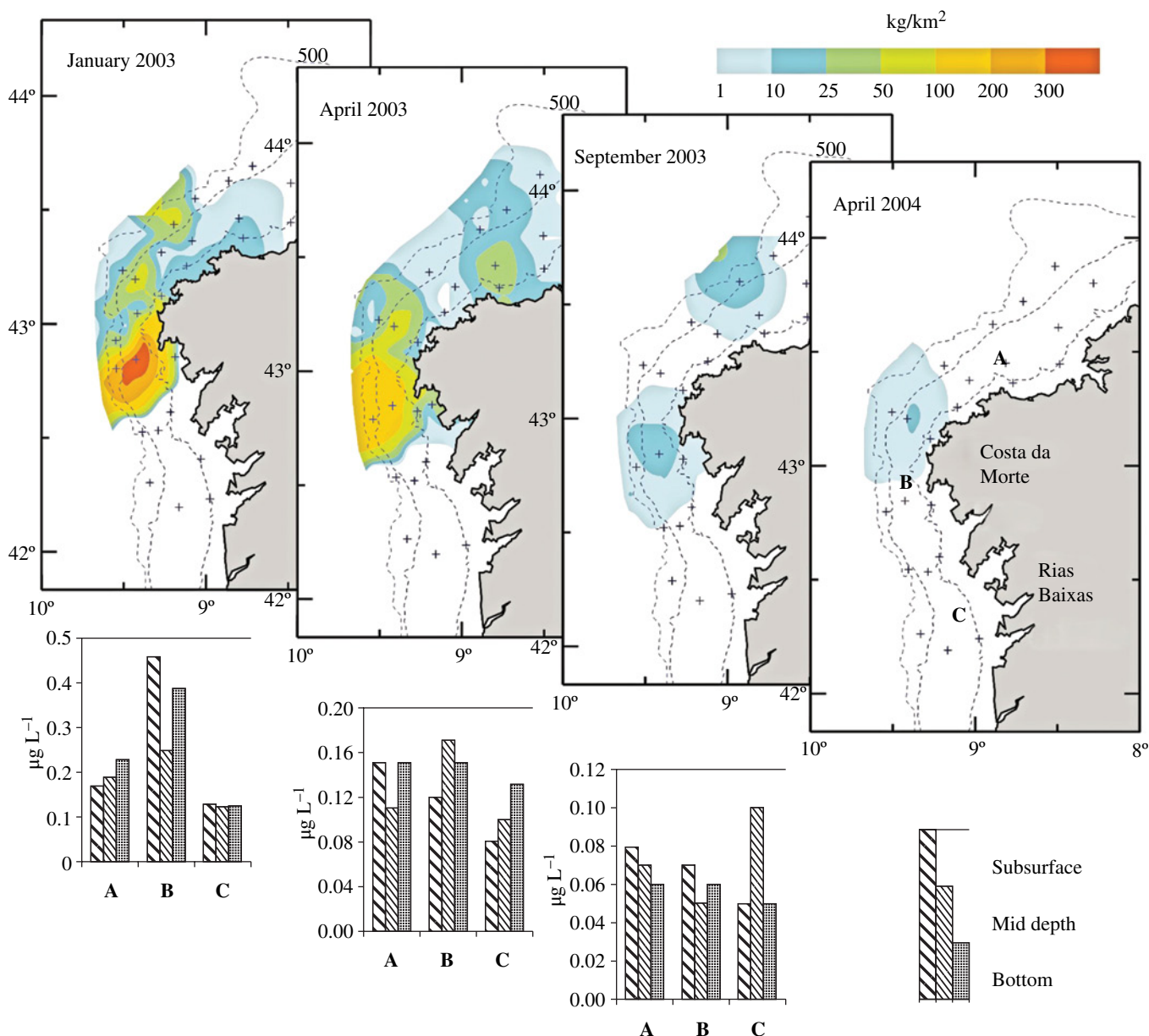


FIGURE 22.11 Temporal variation of concentrations of fuel oil residues in the Galicia continental shelf (in kg/km^2) and of dissolved/dispersed hydrocarbons in the water column (in $\mu\text{g}/\text{l}$).

In the Cantabria coast, the concentrations followed similar trends as in Galicia, namely, decreasing offshore and downward the water column. The highest values, similar to those found in Galicia in December 2002, were found in March 2003 at the subsurface waters of the eastern edge of the coast, consistently with the oil trajectories and the late arrival of the fuel oil to this area. In the last cruise (September 2003), the values decreased to levels similar to those of the Galicia coast, considered as the background values for the region.

The individual PAH distributions in the December 2002 sampling off Galicia were dominated by alkyl naphthalene derivatives, consistently with the pattern distribution shown by the fuel oil–water–accommodated fraction. A PAH distribution dominated by alkyl naphthalenes may be particularly indicative of a recent petroleum input.

In general, the concentrations found after the POS were in the lower range of those quoted in other oil spills (e.g., *Exxon Valdez*, *Baltic Carrier*, and *Ekofisk*) in spite of the amount of the spilled fuel. This was probably due to the heavy nature of the spilled product that predominantly produced floating stable oil–water emulsions and was barely dispersed in the seawater.

22.3.4 Continental Shelf Contamination

In order to assess the extension to which the *Prestige* fuel oil was incorporated onto the seafloor, 80 sediment stations along the North Atlantic Spanish continental shelf (Fig. 22.10) were sampled during three cruises in December 2002, just after the accident, and in February and September

2003. The samples were analyzed for aliphatic hydrocarbons, to identify the hydrocarbon sources, following the molecular marker approach, and PAHs for the particular concern of their possible effects on benthic biota.

The GC profiles of the aliphatic fractions exhibited the general features of coastal environments, with the predominance of terrestrial *n*-alkanes and some evidence of petrogenic contamination, based on the occurrence of C25–C33 *n*-alkanes with high odd–even carbon number predominance and a slight unresolved complex mixture of hydrocarbons, respectively [20]. The presence in all samples of fossil markers, namely steranes and triterpanes, indicated the widespread occurrence of petrogenic contamination but a detailed comparison of the distributions with those characteristic of the *Prestige* oil (Table 22.1) showed clear differences. The sterane distribution, depleted in the C27 components, reflected a highly weathered petrogenic residue, consistent with old chronic pollution. However, the values displayed by some samples collected in the area of Costa da Morte were in an intermediate position, suggesting a possible mixture of the *Prestige* oil with the preexisting (chronic) pollution of the sediments.

The apparently low incidence of the oil on the continental shelf, despite the spreading and movement of the spill, can be attributed to the heavy nature of the product that was barely dispersed in the water column and mainly stranded on the shoreline or deposited in the form of patches or tar aggregates. These residues were collected in the continental shelf during the study of bottom fauna by beam trawling with a mesh size of 1 cm [36].

Concentrations of 300 kg/km² of fuel were found in January 2003 at depths of 120–200 m off the Costa da Morte (Fig. 22.11). During spring and summer 2003, the maximum oil concentration moved slightly northward, preserving the depth of accumulation (100–200 m) and diminishing progressively until reaching very low levels (0.5 kg/km²) in October 2004, probably due to the natural processes of sediment transport and accumulation and because no new processes carrying oil to the bottom took place. For the first survey, the estimation of total oil volume

in the Galicia shelf was 526.3 tons that decreased to 283.8 tons in the second survey and continued to decrease later.

Another sampling was performed in the Cantabria margin during spring, following the indications of the buoys trajectories (Fig. 22.5). The oil was absent along the coast with the exception of an area in front of the Basque Country, near the French border. Obviously, this type of residues is unlikely to be collected with the small area sampled by the box core used for the analysis of sediments and may explain the results obtained in the following study.

The *Prestige* oil contained a significant amount of PAHs (Fig. 22.7), and a number of diagnostic ratios of target alkylated PAH species or methyl isomers have been used as indicators for oil spill identification [27,31,37,38]. Moreover, pyrogenic PAHs are nearly ubiquitous components of marine sediments, which include a number of well-known carcinogens and mutagens, so the assessment of the presence and corresponding sources of PAHs in sediments after the POS was a target.

Concentrations of PAHs ($\Sigma 13$ parent components) were in the range of 1–47 530 $\mu\text{g/kg dw}$, the highest values corresponding to coastal urban/industrial hot spots of Asturias and Basque Country. The median values, however, were in the range of 67–613 $\mu\text{g/kg dw}$ depending on the region and decreasing offshore. Baumard et al. considered that values of the same 12 PAHs in Western Mediterranean coastal sediments below 100 $\mu\text{g/kg}$ could be indicative of low pollution, whereas values higher than 1000 $\mu\text{g/kg}$ corresponded to chronically polluted industrial areas and harbors [39]. Thus, the concentrations found in the continental shelf indicate a low to moderate pollution. Concentrations in the range of 20–50 $\mu\text{g/kg dw}$ were considered to be the baseline values in the region [20].

The detailed study of the distributions suggested a rather uniform mixture of petrogenic and pyrolytic PAH sources along the continental shelf, reflecting the chronic inputs of hydrocarbons in the area, with a decrease of the combustion signature moving away from the potential coastline sources.

Two representative examples are shown in Figure 22.12, where the repeatability of the values for the different sampling campaigns is also evidenced. The larger variability of the

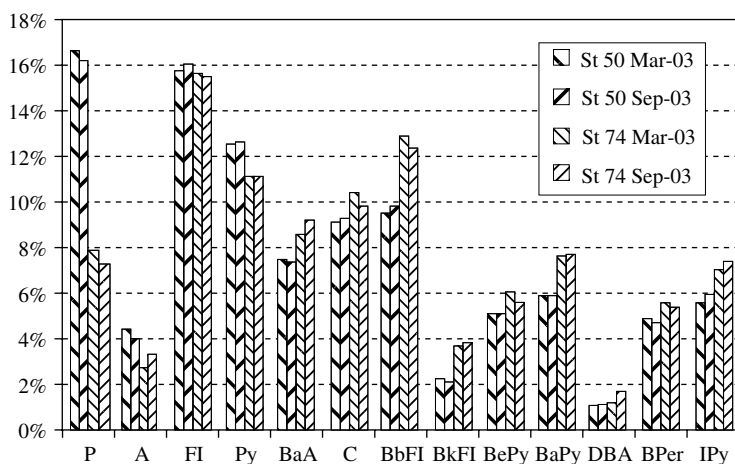


FIGURE 22.12 Average distribution of parent PAHs in surface sediment samples of the Cantabria coast.

relative concentrations of the different compounds corresponds to phenanthrene, increasing from 7 to 17% with the sediment depth. Conversely, the relative content of benzo [b] + [k] fluoranthenes is rather constant, suggesting a relative decrease of the combustion signature moving away from the potential coastline sources.

The uniformity of the general patterns may well reflect the end point of a mature or weathered input of PAHs, as already evidenced for the petrogenic hydrocarbons, by the distribution of specific molecular markers (e.g., by the prevalence of C29 steranes) [20].

The failure to detect the presence of the spilled oil above the background pollution in the sediments, also observed in the case of the *Erika* accident, may be a general feature of heavy oil spills, which, besides oiling the shorelines and intertidal sediments, may sink offshore but distributing a patchy contamination that is more difficult to document [40]. At the same time, the geochemical analysis of the surface sediments of the sinking area also proved that they were unpolluted despite the presence of the *Prestige* wreck.

22.3.5 Accumulation in Biota

The assessment of the accumulation of hydrocarbons in marine biota after an oil spill is a major issue for regulatory purposes regarding public health issues. In the case of the *Prestige*, this was particularly relevant because the affected area, the Galicia coast, was one of the first producers of commercial shellfish worldwide, including mussels, clams, cockles, oysters, sea urchins, razor shells, goose barnacles, and so on.

Bivalves are useful bioindicators of chemical contamination and have been recommended by the International Conventions, such as the OSPAR Commission, the Barcelona Convention and the Helsinki Commission, for coastal pollution monitoring. The Mussel Watch concept was also used in this case for assessing the spatial and temporal

extents of the impacts caused by the oil spill on the coastal ecosystem. Sampling campaigns of wild mussels (*Mytilus galloprovincialis*) were carried out in February, June, and November 2003 and November 2004 at 41 stations along the Atlantic coast, from A Guarda (Galicia) to Hondarribia (Basque Country) (Fig. 22.10). These stations have been regularly monitored for parent PAHs within the Instituto Español de Oceanografía (IEO) monitoring program, so that the existence of previous data was important for comparing contamination levels before and after the spill, identifying the hot spots, and establishing the baseline reference values.

As in the case of sediments, the samples were analyzed for aliphatic and aromatic hydrocarbons by GC-MS to identify the suspected source, namely, the *Prestige* fuel oil, by molecular fingerprinting [21,22]. The diagnostic molecular parameters of the fuel oil (Table 22.1) compared satisfactorily with those displayed by the mussel samples collected in the area of Costa da Morte (stations 9, 12–14) (Fig. 22.10) in the following months after spill, clearly confirming the fuel oil contribution, whereas the more distant stations exhibited patterns with markedly different values, consistent with the widespread occurrence of petrogenic contamination. In turn, the profiles displayed by some samples of the Cantabria coast (e.g., stations 36 and 40) were in an intermediate position, suggesting a possible mixture of the *Prestige* oil with the preexisting (chronic) pollution.

The spatial distribution of PAH concentrations found in the first sampling period also revealed the central area (Costa da Morte) as the most affected by the oil spill. In these stations, concentrations up to 7780 µg/kg dw of the sum of 13 parent PAHs were found 2–3 months after the spill (Fig. 22.13). The levels markedly decreased at most of the stations in the second sampling and recovered to the levels found before the spill 8 months after the accident (29–279 µg/kg dw, av. 133 ± 83 µg/kg dw) [21,23]. However, a certain increase was observed later in some sites of the Cantabria coast probably due to the

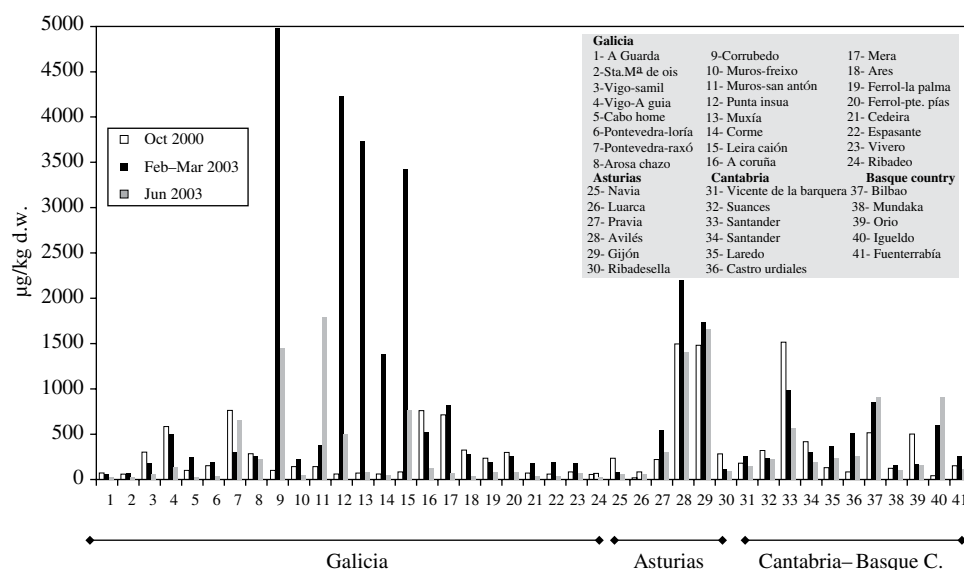


FIGURE 22.13 Concentrations of PAHs in mussels collected along the Spanish Atlantic coast at the indicated dates. Numbers correspond to the stations indicated in Figure 22.10.

continuous arrival of fuel slicks after early summer 2003. The survey also evidenced the existence of two major hot spots in Asturias (stations 28 and 29) [22].

The relative abundances of the parent PAHs may also contribute to illustrate the effect of the spill. A common

feature in the collected samples after the spill is the predominance of chrysene (Fig. 22.14). This was also found after the *Aegean Sea* and *Erika* oil spills and can be used for assessing the time span of the influence of the spill [40,41]. The temporal profiles shown in Figure 22.15 illustrate the

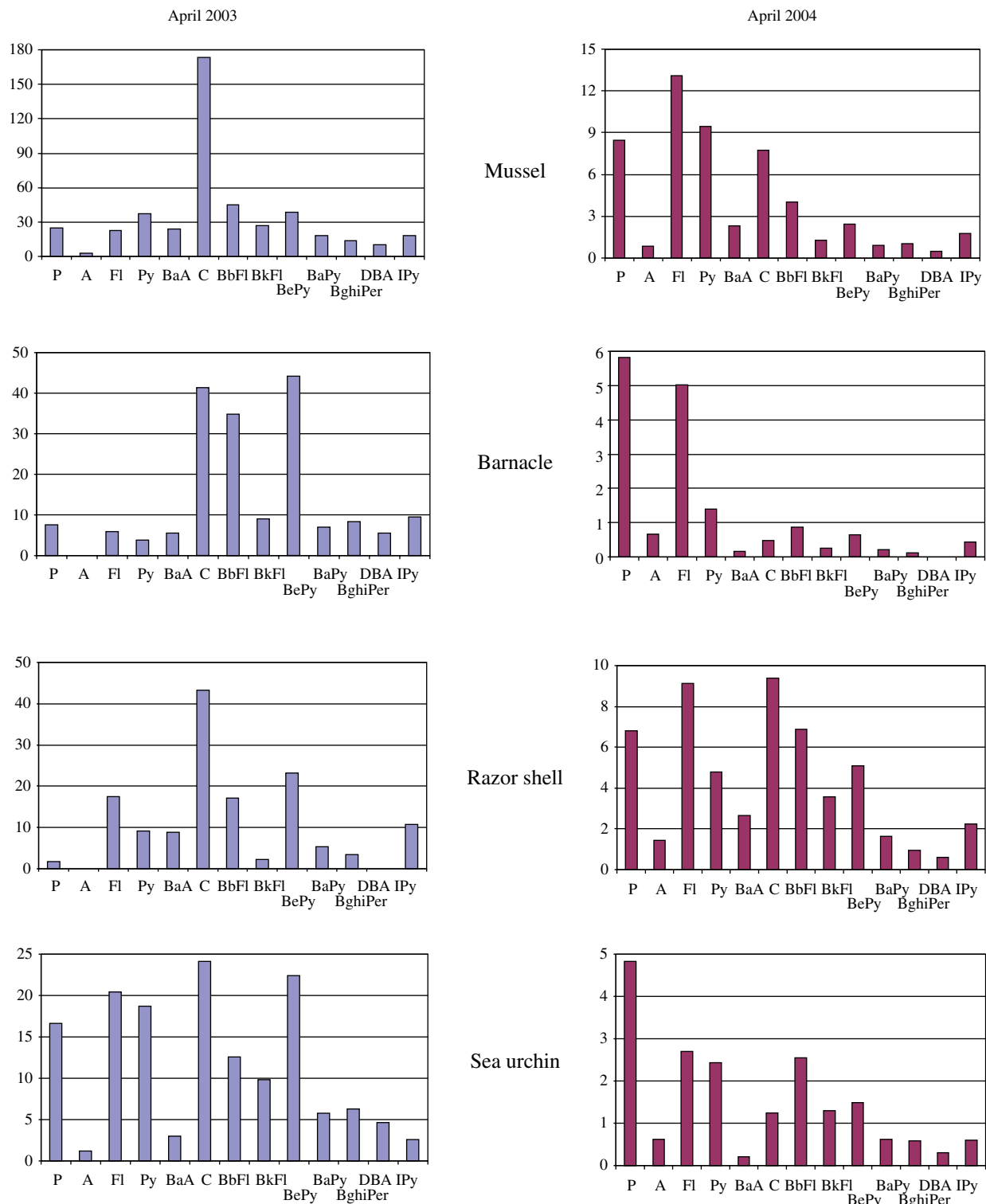


FIGURE 22.14 Representative PAH distributions in barnacle, razor shell, sea urchin, and mussel samples collected at station 12 (Fisterra) just after the spill and 1 year later. Concentrations in µg/kg dw. A, anthracene; BaA, benz[a]anthracene; BaPy, benzo[a]pyrene; BbFl, benzo[b]fluoranthene; BePy, benzo[e]pyrene; BkFl, benzo[k]fluoranthene; BPer, benzo[ghi]perylene; C, chrysene; DBA, dibenz[ah]anthracene; Fl, fluoranthene; IPy, indeno[1,2,3-cd]pyrene; P, phenanthrene; Py, pyrene. Reprinted with permission from Ref. 26. © Elsevier.

Oil spill (Nov–2002)

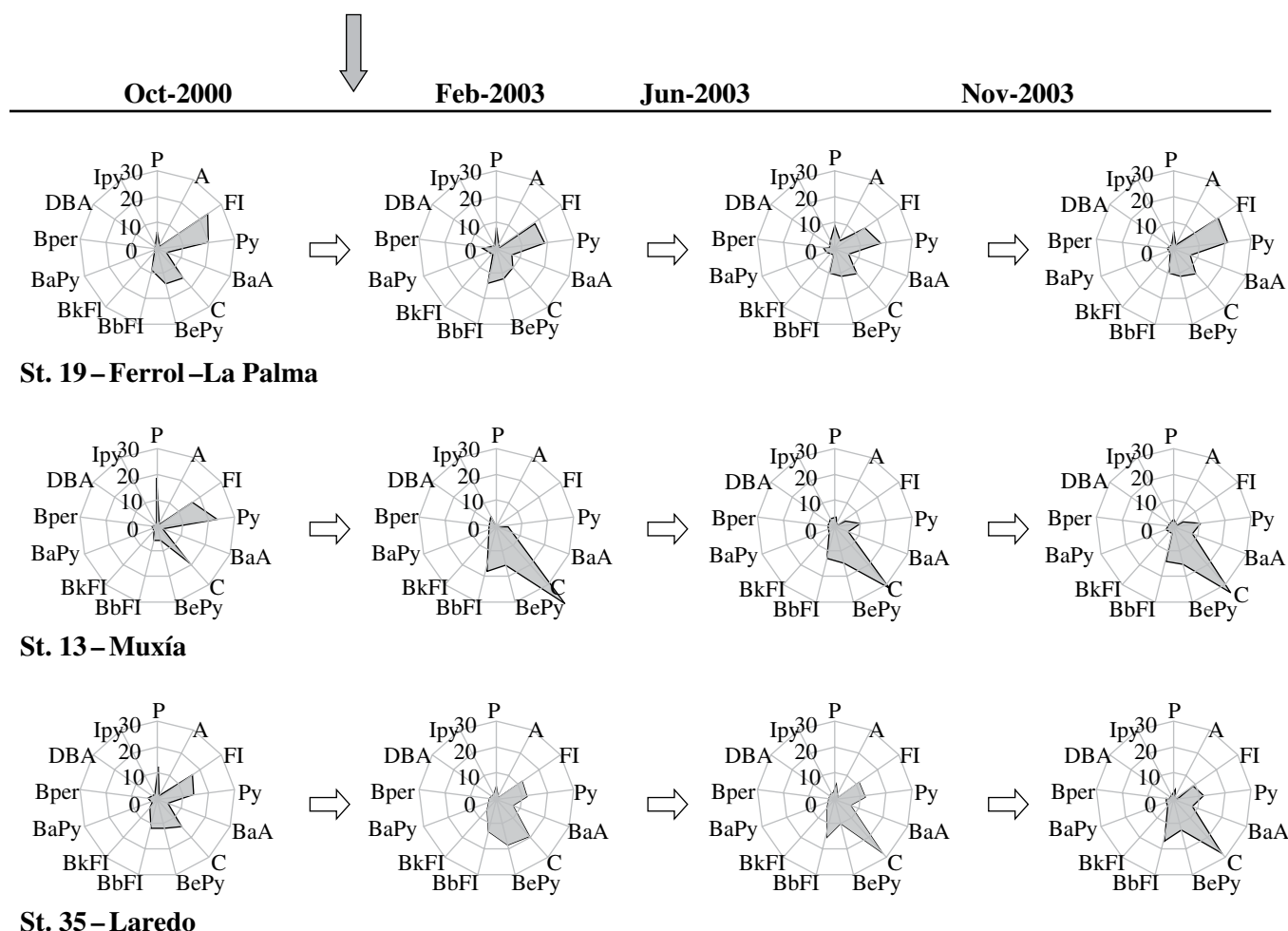


FIGURE 22.15 Radial representation of the PAH distributions in mussels from stations 13, 19, and 35 in October 2000 and February, June, and November 2003. Reprinted with permission from Ref. 21. © Elsevier.

situation of different stations. The distribution profile of Ferrol-La Palma station was rather conservative from October 2000 to November 2003, showing no effect of the *Prestige* event. In turn, the station of Muxía (Costa da Morte) exhibited the characteristic oil accumulation from February to November 2003, whereas in the Cantabria coast (e.g., Laredo), this was delayed according to the late arrival of the oil.

Aliphatic and aromatic hydrocarbons were also determined in other species of commercial shellfish, namely, goose barnacle (*Pollicipes cornucopia*), razor shells (*Ensis arcuatus* and *Ensis siliqua*), and sea urchin (*Paracentrotus lividus*), living in different habitats and exhibiting different feeding behaviors, to get further insight into the bioaccumulation pathways and their suitability for monitoring purposes [26].

The aliphatic fractions were mostly dominated by biogenic hydrocarbons, reflecting the diet composition of the organisms and their low metabolic capacity. The analysis of the aromatic fractions revealed the

occurrence of three- to six-ring parent and alkylated PAHs, which is consistent with a mixed petrogenic–pyrolytic origin, with the common feature of the predominance of chrysene in all samples collected after the spill (Fig. 22.14).

These features indicate that the three species, goose barnacles, razor shells, and sea urchins, responded to the spill, accumulating petrogenic hydrocarbons (also verified by the quantitative analysis discussed in the following) and, therefore, being potentially useful for oil spill biomonitoring. However, it is interesting to notice the relative differences observed in the profiles among the species. Barnacles and sea urchins seem to preserve preferentially the lower components when the direct oiling comes to an end, whereas razor shells have a more conservative behavior for all components.

Observations relating uptake to feeding strategy have explained differences in the profiles of the accumulated PAHs in marine invertebrates [42,43]. Physiological factors, including the uptake and elimination (metabolism,

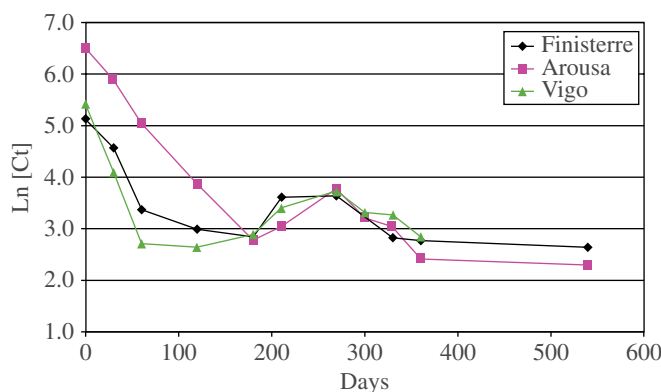


FIGURE 22.16 Temporal trends of total PAH concentrations ($\Sigma 13$) in barnacles collected at three sites along the studied period. Reprinted with permission from Ref. 26. © Elsevier.

diffusion, and excretion) rates, also determine PAH body distributions. Thus, species apparently occupying the same habitat may actually be “sampling” different compartmental hydrocarbons during normal feeding and other life activities. The present profiles seem to reflect in the case of razor shells their association to the sedimentary habitat, and in the case of sea urchins and barnacles their feeding on water suspended plankton. The PAH profiles of these two compartments are strikingly similar to those of the inhabiting organisms. In general, the plankton profiles collected in the region after the oil spill exhibited a marked predominance of the alkylated low molecular weight components (two–three aromatic rings), paralleling those of the seawater-dissolved hydrocarbons [24]. On the other hand, the sediment samples were relatively enriched in the higher PAHs (four–five aromatic rings), which are characteristic hydrocarbons of the surface runoff [20].

The PAH concentrations ($\Sigma 13$) increased significantly after the spill and decreased 6–7 months later to background levels (Fig. 22.16). The slight increase of PAHs during winter can be attributed to the bad weather that may have reintroduced oil residues into the water column. One year after the accident, the median values were 58 $\mu\text{g}/\text{kg}$ for razor shells, 26 $\mu\text{g}/\text{kg}$ for barnacles, and 25 $\mu\text{g}/\text{kg}$ for sea urchins. Although mussels exhibit a higher accumulation rate of hydrocarbons, the results of this study demonstrate that barnacles can also be suitable species for oil spill monitoring.

The temporal evolution of the PAH concentrations along the survey period was used to estimate loss rates for bioavailable PAHs. Half-life values were in the order of 30 and 60 days for barnacles and sea urchins, respectively, similar to those of mussels [23].

In conclusion, even though heavy oils are barely dispersed in the water column, they can be uptaken by bivalves and other shellfish and recognized in their tissues using the molecular marker approach. The levels, however, decreased to background concentrations about 6 months after the spill.

22.4 THE ASSESSMENT OF EFFECTS

The impact of the oil on biota was one of the key issues to be studied considering the economic and health implications of the accident. Studies were performed under laboratory and field conditions, at the level of biomarker responses, bacterioplankton, some intertidal organisms, as well as different shelf communities and their trophic structure.

22.4.1 Bioassays under Laboratory Conditions

Experiments made under controlled laboratory conditions for testing the potential effects of the spill provided useful information on the toxicity and bioavailability of the heavy fuel oil and contaminated water or sediment. The marine organisms used in these experiments included marine invertebrates such as bacteria, amphipods, lugworms, sea urchins, bivalves, and crabs in addition to seaweeds and different species of fish.

Organisms were exposed to the water-accommodated fractions of the fuel or to sediments fortified with different concentrations of fuel oil for a certain period of time (usually 10 days), and the mortality or induction of selected biomarkers or biochemical responses were determined (Fig. 22.17).

The water-accommodated fractions of the fuel were toxic to microalgae and sea urchins, and dose-related mortality was observed in other invertebrates (Fig. 22.18) [44–47]. Comet assay results reflected an increase in the DNA damage in mussels associated to oil exposure related to the higher aqueous total PAHs content, whereas a certain level of toxicity was also observed as increased lipid peroxidation levels in gills of mussels [48,49]. On the other hand, a laboratory experiment carried out to study the immune function alteration of the mussel *M. galloprovincialis* revealed no differences between fuel-treated and control animals in the cellular immune parameters measured (hemocyte viability, phagocytic activity, nitric oxide production, and chemiluminescence emission), indicating that

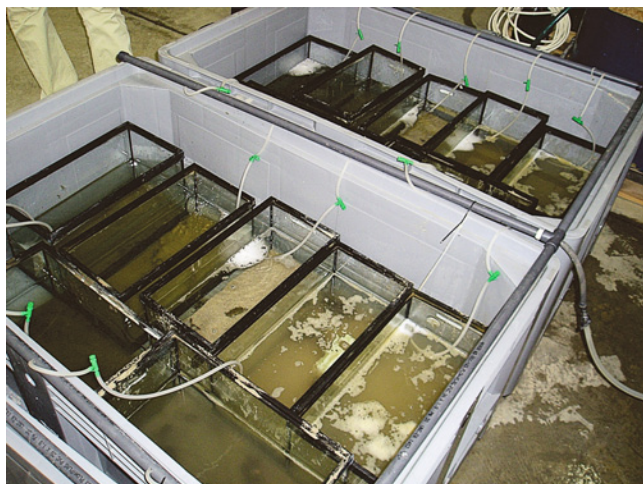


FIGURE 22.17 Laboratory bioassay with the crab *Carcinus maenas* exposed to *Prestige* oil-contaminated sediment.

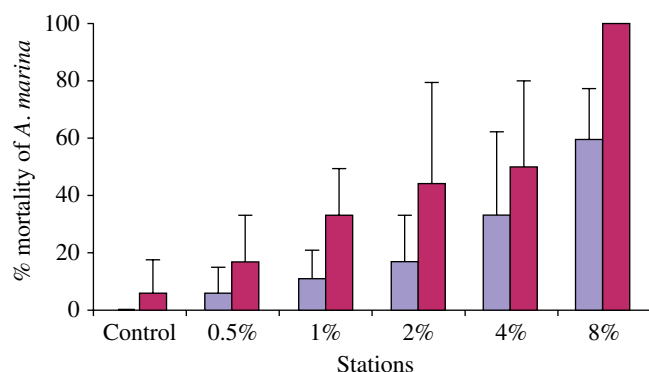


FIGURE 22.18 Average and standard deviations of the percentage of mortality of the polychaete *Arenicola marina* after 10 (left bar) and 21 (right bar) days of exposure to each dilution of *Prestige* fuel oil. Reprinted with permission from Ref. 47. © Springer.

the mussel immune system was not significantly affected by exposure to the fuel oil [50].

Results obtained after exposing juveniles of turbot (*Scophthalmus maximus*) to different concentrations of the *Prestige* fuel oil through their diet suggested the ability of the fuel oil to alter hepatic biotransformation enzymes and to disrupt endogenous hormone levels [51]. The authors indicate that depressed circulating levels of testosterone in juvenile turbot could be associated with a specific inhibitory effect of hydroxylated PAH metabolites on the biosynthesis of testosterone and hypothesize that increased energy requirements for detoxifying functions and xenobiotic clearance in exposed fish may increase physiological stress and, hence, decrease energy for growth and reproduction, an effect that is likely to occur in field specimens exposed to an oil spill.

Sediments collected in affected coastal sites (Atlantic Islands National Park) were also used to test their toxicity. Acute effects determined by Microtox® on amphipod, sea urchin, and lugworm were associated with the content of

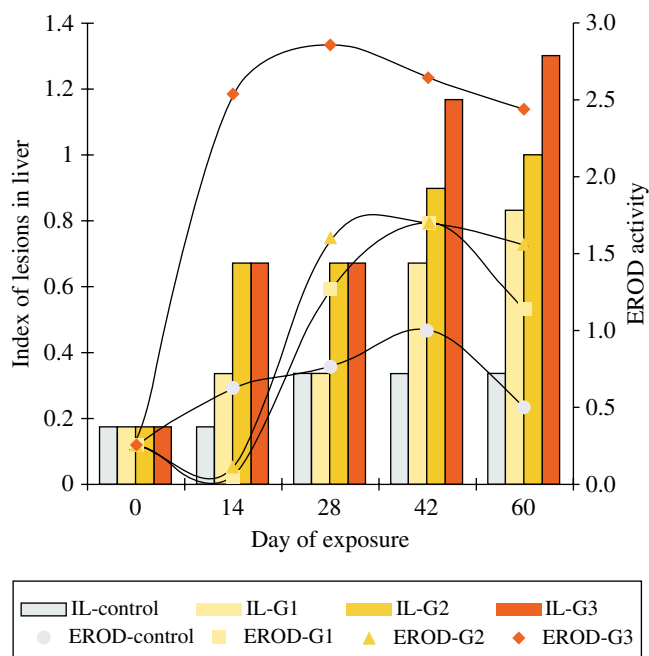


FIGURE 22.19 Curves of EROD activity (pmol/mg/min of protein) and histopathological damage in the liver of *Sparus aurata* exposed to *Prestige* oil-contaminated sediment (G3 > G2 > G1) [52,53].

PAHs in the tested sediments. Bioassays using juveniles of sea bream (*Sparus aurata*) and flatfish (*Solea Senegalensis*) showed induction of biomarkers related to organic detoxification systems (ethoxyresorufin-O-deethylase (EROD) and glutathione-S-transferase (GST) activities) as well as stress symptoms (stimulation of GPX and glutathione reductase (GR) activities). Histopathological lesions were also detected in the liver and gills of the exposed organisms (Fig. 22.19).

In the fish exposed to sediments from the station G3, it seemed that there was a first phase where EROD activity was induced (days 0–28), while when the activity reaches a maximum and begins to decrease (days 28–60), however, the histopathological alterations and the frequency of lesions increase.

Correlations between organics, metals, and biological responses in *Arenicola marina* were observed, with DNA damage measured using the Comet assay, forming the largest contribution toward explaining the observed differences. Four years after the oil spill, a remarkable decrease of toxicity was detected by acute and chronic bioassays [54].

22.4.2 Field Studies

22.4.2.1 Sublethal Effects at Individual Level (Biomarkers)

The comprehensive determination of chemical and biochemical markers in coastal bivalves and fish is a sound procedure for assessing pollution exposure in coastal areas. Cajaraville et al. assessed the biological effects of the POS on coastal ecosystems using mussels (*M. galloprovincialis*) as sentinel organisms [55]. They were sampled at 22 locations

along the coast of Galicia and the Bay of Biscay in April, July, and September 2003 and in February, April, July, and October 2004. Several cell- and tissue-level biomarkers were measured in digestive glands. AOX activity, a marker of exposure to peroxisome proliferating compounds including PAHs, was particularly low in Galicia in 2003 and further markedly increased in several localities in 2004. Values of the labilization period (LP) of the lysosomal membrane were low in all the studied localities, especially in Galicia in 2003. In 2004, LP values raised, evidencing a certain recovery in mussel's health. Significant correlations between several biomarkers and total PAHs were found, overall indicating a certain degree of disturbance in areas most impacted by the oil spill (Galicia) that were able to recover during 2004, related to a decrease in total PAH concentrations in mussels.

Postlarval recruits of mussels *M. galloprovincialis* were also sampled in February 2003 at seven localities along the Galicia coast exhibiting different levels of impact from the POS [56]. The concentrations of PAHs as well as different biochemical (proteins, carbohydrates, glycogen, and lipids) and ecophysiological variables (size–frequency distributions and size–weight relationships) were determined in mussel tissues as indicators of the toxic impact of the spilled oil. The study determined sublethal effects in wild mussel seed populations sampled 3 months after the oil spill. These effects were shown in the form of survival indices and alterations of lipid metabolism.

On the other hand, growth of mussels was investigated for the first cultured generation following the oil spill [57]. Seeds from three natural populations along the Galician coastline were transplanted to a raft culture system. The growth patterns of mussels from the area most affected by the oil spill showed significantly less growth by weight than the other populations, resulting in a lower yield at harvest.

In fish, induction of cytochrome P4501A (CYP1A) together with the determination of hydroxylated PAH metabolites in bile has been successfully used as a biomarker of oil exposure [58]. The metabolism of fuel components by different CYP isoenzymes may yield oxidized products that can be more toxic than the parent compound, resulting in deleterious physiological effects. Some of these intermediate products can cause oxidative stress, and therefore, a number of antioxidant enzymes, such as of EROD, GST, GR, and catalase (CAT), were used as putative biomarkers of fuel exposure [59,60].

Different fish species were selected for a field study: the four-spotted megrim (*Lepidorhombus boscii*), the dragonet (*Callionymus lyra*), and the pouting (*Trisopterus luscus*). Fish were collected along the Northern Iberian coast to provide a wide coverage of the area (Fig. 22.20). The simultaneous use of these species enables gathering of information on pollution exposure in different shelf environments: 70–120 m depth (*T. luscus* and *C. lyra*) and 200–500 m depth (*L. boscii*).

The biochemical markers indicated significant differences among sampling sites and different types of stress along the study area. EROD activity in *T. luscus* and *L. boscii* showed a spatial variation along the middle/outer and inner shelf, coinciding with PCB and DDT residues in muscle tissue but not with bile PAH metabolites [60]. Considering *L. boscii*, EROD activity was about fivefold higher in E (Basque Country), C (Asturias), B (North Galicia), and A (South Galicia) than in the other sites, indicating the presence of CYP1A-inducing agents in those sampling stations, which were mainly characterized by having urban and industrial settlements nearby. EROD activity in *L. boscii* 1 year after the accident (3.5–16 pmol/min/mg protein) was lower than that reported 6 months after the POS

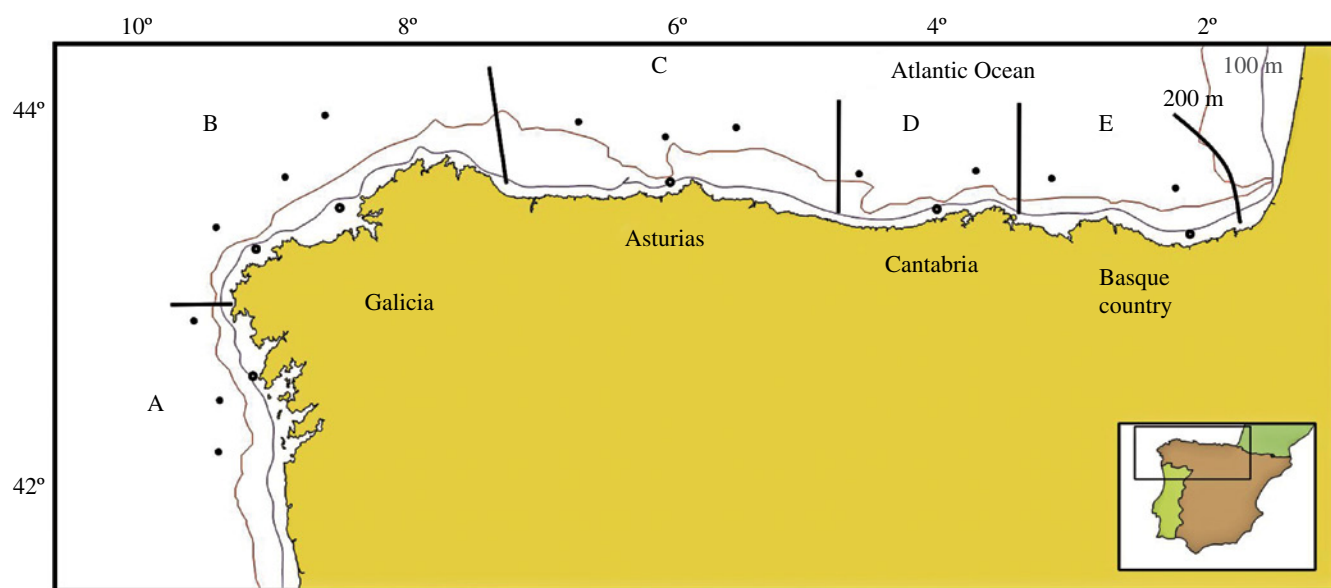


FIGURE 22.20 Sampling sites for fish collection. Open circles: *Trisopterus luscus* and *Callionymus Lyra*. Filled circles: *Lepidorhombus boscii*.

(20–50 pmol/min/mg protein) [59]. The observed differences can be attributed to decreased exposure to oil spill-derived pollutants 1 year after the accident but also to seasonal variability on EROD activity.

Regarding exposure to PAHs, both *T. luscus* and *L. boscii* showed high levels of hydroxylated PAHs in bile in Cantabria and Basque Country areas (Fig. 22.21). Higher levels of hydroxylated-PAHs were observed in *T. luscus* (inner shelf) than in *L. boscii* (middle/outer shelf); this is in agreement with recent studies that reported higher concentrations of PAHs in sediments from the inner shelf than offshore [35]. The results highlight the anthropogenic pressure near coastlines and the chronic pollution of the Cantabria and Basque Country inner shelf due to urban and industrial activities. When considering OH-PAH metabolites, both species showed a similar geographical pattern. 1-Pyrenol, regarded as the best general indicator of PAH exposure in fish, was particularly abundant in fish from Asturias (C), Cantabria (D), and Basque Country (E), while fish from Galicia (A and B) were mainly enriched in 1-naphthol, a marker of recent exposure to petrogenic compounds [61]. In fact, small tar aggregates were still present on the Galicia continental shelf almost 1 year after the *Prestige* accident, and fish inhabiting the area, particularly benthic fish, might have been exposed to those PAHs [35]. Significant amounts of 1-naphthol (35–53%) were also detected in the bile of fish from C and E areas, indicating exposure to PAHs of petrogenic origin 1 year after the accident [60].

22.4.2.2 Effects at Community Level Effects in Estuarine Areas Estuarine areas enclose some of the most valuable, sensitive, and endangered aquatic habitats. In fact, most of

the estuaries located in the north coast of Spain are Special Areas of Conservation (SAC) according to the European Habitats Directive [62]. Fortunately, the effects of POS in these ecosystems were barely significant, despite the fact that some surfaces were oiled and contamination of water and filtering organisms were detected [63,64].

First, the potential contamination of estuaries was minimized by the priority protection strategy applied to these habitats (installation of containment booms, picking up the fuel at the estuary mouths, and immediate manual gathering of oiled wastes) [11,63]. Second, the nature of the substrate (composed of fine grain-size, low-permeability, and water-saturated sediments) prevented substantial penetration of the heavy oil and thus the risk of deleterious effects on benthic communities.

As a result, only some surfaces of the high intertidal fringe suffered substantial impacts. In these sites the fuel coated the rocky substrates, most of them artificial protection structures, and the outer macrophytic individuals of vegetated salt marshes. The most affected species were *Halimione portulacoides* and *Juncus* sp., which frequently colonize these intertidal areas. It should be mentioned that the oiled individuals were removed as soon as possible, preventing further contamination of the whole community [63].

Regarding intertidal macroinfaunal communities, studies carried out in four unaffected and five oil-affected estuaries (18 soft-bottom stations) did not detect significant changes in community structure, overall richness, or diversity [64]. However, the absence of previous data, the high variability of benthic communities, and the confounding effects of other contamination sources introduce some uncertainty regarding the possible effects.

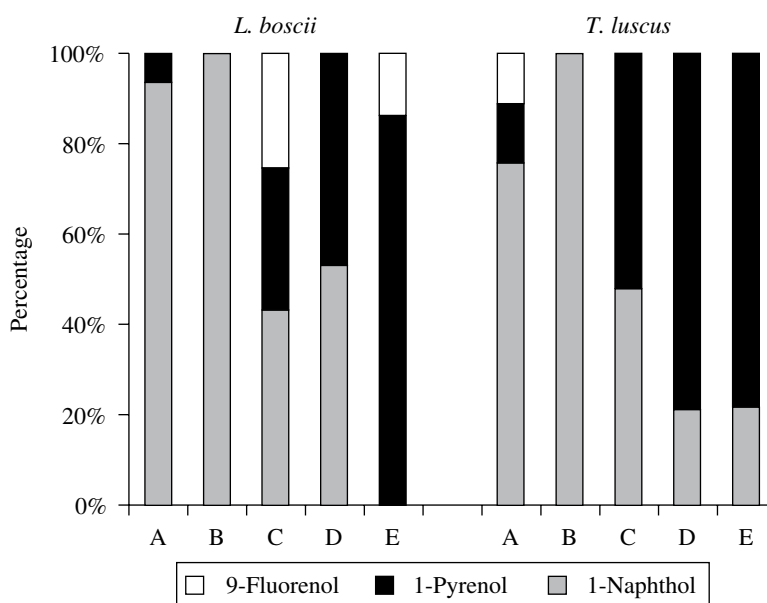


FIGURE 22.21 Percentage of hydroxylated PAH metabolites in bile of *Lepidorhombus boscii* and *Trisopterus luscus* collected along the Northern Iberia coast. A (S Galicia), B (N Galicia), C (Asturias), D (Cantabria), and E (Basque Country). Reprinted with permission from Ref. 60. © Elsevier.

Effects in Intertidal Coastal Areas Extended intertidal coastal areas were affected by the POS, both sandy beaches and rocky shores. The oiled sites were distributed along the Spanish North Atlantic coast, reaching also some coastal areas of France and Portugal.

The sandy shores closest to the accident area, at the Galicia coast, were the most affected soft bottoms. De la Huz et al. and Junoy et al. studied the effects of POS on the macrofauna

of 18 Galicia sandy beaches (Fig. 22.22) [65,66]. Based on previous data, the authors identified changes in the community structure and a decrease in the species richness, reaching a loss of 67% of the total species in the most affected beaches (Fig. 22.23). The isopod genus *Eurydice* and the polychaete *Scolecopsis squamata* were the most affected taxa. Also, Rodríguez et al. reported a decrease in the abundance of meio-benthic Oligochaeta in some of the Galicia beaches strongly



FIGURE 22.22 Location of the beaches studied by de la Huz et al. [65] and Junoy et al. [66].

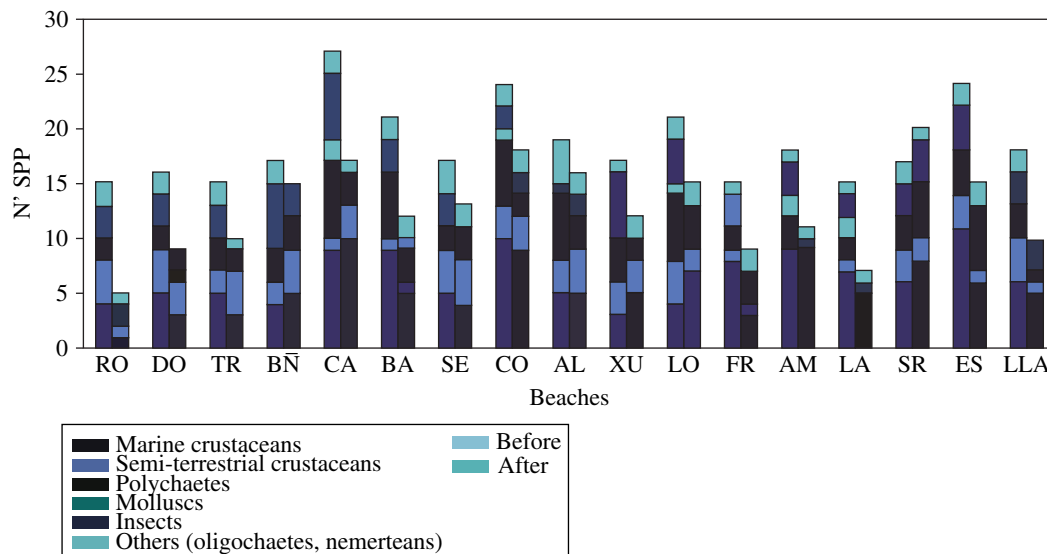


FIGURE 22.23 Number of species of the main groups of macrofauna on Galicia sandy beaches, before and after the POS. Reprinted with permission from Ref. 65. © Elsevier.

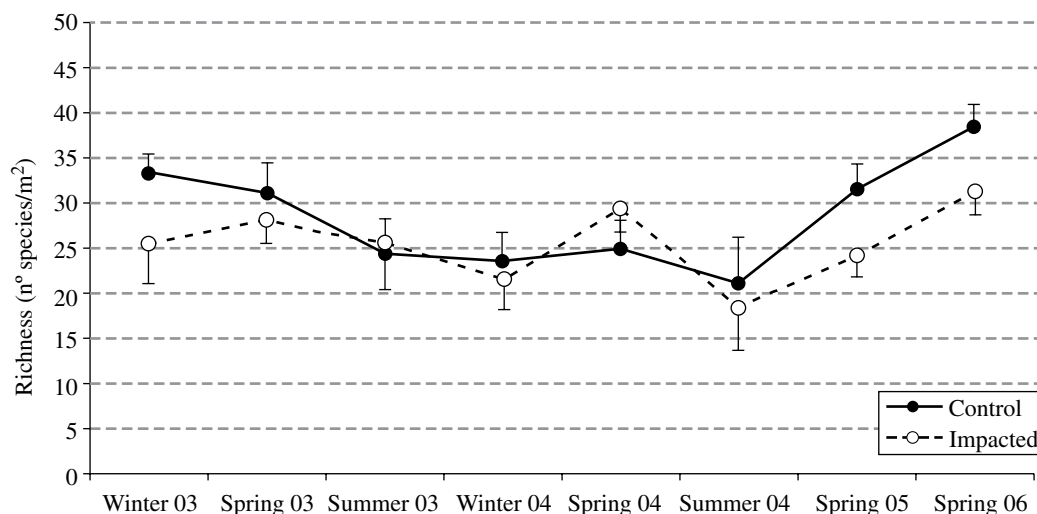


FIGURE 22.24 Temporal changes of macroinvertebrate richness in the mean intertidal of impacted and nonimpacted sites of Cantabrian coasts [64].

affected by the POS [67]. However, in all cases the impacts were described as being lower than expected in comparison with other accidents. No effects in benthic communities were reported for other Atlantic sandy beaches.

On rocky shores the cleaning tasks were more difficult; therefore, many sites remained oiled over a longer period of time. However, the impact on the community structure of macroinvertebrates and the coverage of macroalgae assemblages was much lower than expected, as different authors pointed out [64,68,69]. None of these studies detected high mortalities or significant differences in overall richness, diversity, or coverage of intertidal coastal benthic communities affected by the POS (Fig. 22.24). Neither changes in the proportional abundance of characteristic and opportunistic species were found. These studies concluded that natural spatial and temporal variability of intertidal assemblages are much higher than any possible change driven by the oil contamination.

One of the main reasons for this low impact was because the fuel was deposited in the supralittoral and upper littoral zone. It should be mentioned that the tidal range in this coast is 4.5 m. This intertidal fringe is characterized by very low species richness, diversity, and biological coverage. Thus, lichens (*Verrucaria maura*), barnacles (*Chthamalus* spp.), and limpets (*Patella* spp.), dominant at this level, were the most affected organisms, as a result of the plastering effect [63,70]. Conversely, mid and low intertidal, colonized by diverse benthic communities were not coated by the oil. This fact was promoted by the slippery surface of seaweeds that usually completely cover the substrate at these levels. Typical species in this fringe are *Corallina* spp., *Bifurcaria bifurcata*, *Stypocaulon scoparium*, *Mastocarpus stellatus*, *Himanthalia elongata*, and *Fucus* spp.

In addition, the prevailing rough hydrodynamic conditions of the Cantabrian Sea and the season in which the accident occurred (winter) contributed to the cleaning and dispersion of the fuel. It must be pointed out that the POS did not affect sites exposed to the wave action, such as cliffs, whereas the

oil was mostly deposited in protected or semiexposed sites. On the other hand, due to oceanographic conditions, a water-oil emulsion or “mousse” was generated that magnified the size and persistence of the spill but at the same time reduced its toxicity [71]. Thus, the direct impact on macrofauna by deposition, asphyxia, or acute toxicity was not as powerful as in other oil spills or at least the impact was not as high.

In conclusion, significant effects on benthic estuarine or coastal communities have not been detected after the POS. Nonetheless, it should be pointed out that baseline data in the affected areas were scarce and thus the detection of low magnitude impacts is difficult. Therefore, the contamination of water and bioaccumulation in filtering organisms were detected; it is not possible to ensure that any particular species, sensitive to oil, has not been affected.

Effects in the Subtidal and Continental Shelf Contrary to what occurred at the intertidal area, the amounts of oil deposited in the shallow subtidal bottoms were low, except in some specific sites (Fig. 22.11). Consequently, no significant deleterious effects have been reported for this type of habitat, characterized by the dominance of seaweeds assemblages such as *Gelidium sesquipedale*, *Laminaria* spp., or *Cystoseira* spp. [63].

Studies carried out in the Galicia continental shelf showed low or irrelevant deleterious effects. Serrano et al. performed five surveys (from winter 2002 to autumn 2004) to study the epibenthic, suprabenthic, and infauna assemblages of the Galicia continental shelf between 70 and 300 m depth [36]. No significant changes in richness, diversity, and biomass related to the oil were detected. On the contrary, a decrease in the densities of some epifauna species was registered the first year, although those organisms recovered 1 year later.

Sánchez et al. analyzed the effects of the POS on abundance, distribution, and food habitats of some selected key benthic and demersal populations along the Galician and

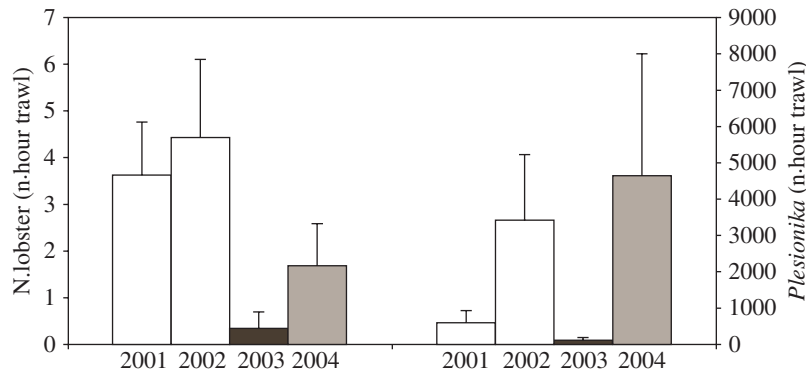


FIGURE 22.25 Mean densities of Norway lobster and *Plesionika heterocarpus* (number.hour trawl \pm SE) in the zone of maximum impact (2001–2004). Reprinted with permission from Ref. 72. © Elsevier.

Cantabrian Sea [72]. Those authors detected significant reductions in the abundance of Norway lobster (*Nephrops norvegicus*), pandalid shrimp (*Plesionika heterocarpus*), and four-spot megrim (*L. boscii*) in the ground zero zone (Costa da Morte), although the shrimp and the megrim recovered in 2004 (Fig. 22.25). No significant effects were detected on hake (*Merluccius merluccius*) populations, neither on the feeding pattern of any of the species analyzed.

Regarding the pelagic communities, Varela et al. reported a lack of impact on zooplankton and phytoplankton, comparing data taken monthly during 2003 with extensive previous data series available at five locations of the N–NW Spanish coast [73]. This was attributed to both the type of oil, barely dispersed in water, and the active planktonic life cycle.

22.5 ENVIRONMENTAL RESTORATION

22.5.1 Oil Recovery at Sea

Once in the water, the fuel underwent a strong emulsification (containing 40–50% of water) and patching, an aspect that greatly complicated the operation of the specialized vessels in oil recovery and that was to be taken into account in assessing the amounts of oil recovered. Large oil recovery vessels with pumping systems were not operational and the contribution of fishing boats was invaluable. Every day, local and regional fishing fleets were mobilized to collect oil slicks at sea, in the different areas, based on the information generated by the operational forecasting systems [11,12]. Due to the fuel characteristics, converted fishing vessels were used for open water cleaning operations (Fig. 22.26). Conventional vessels had to be outfitted including containers and other capabilities to be prepared for manual recovery. The recovered oil, water, and debris mixture from the fishing boats was stored directly in temporary containers that were offloaded at harbors and disposed at specific sites for treatment. Table 22.2 summarizes the recovery of polluted material, at sea and on land, from the sinking date until July 20, 2004 [12].

22.5.2 Coastal Contamination and Cleanup Efforts

When oil finally arrived onshore, different coastal environments (cliffs, gravel, and sandy beaches) were affected. The North Atlantic Spanish coast presents a relationship between sandy beach and total coastal length of 15% (lower than the 25% estimated for a whole Spanish coast). The high rocky coast usually is of difficult access and very exposed to wave action. On one hand, this is a disadvantage, since the cleanup resources did not arrive to most of these areas. On the other hand, the stranded oil was mainly eliminated naturally by waves and transported to adjacent areas by coastal currents. The oil only persisted above the high tide level.

In gravel beaches, the cleanup effort was extensive. In those beaches, similarly to the *Exxon Valdez* spill, the oil percolated to depth increasing its persistence. Manual procedures were used to preserve the beach, and the volunteers moved each gravel grain, cleaned up and replaced in its initial position. Fortunately, the number of gravel beaches in the Northern Spanish coast is limited.

Despite the lower extension of sandy beaches with respect to the total coast, they focus important economic activities and their preservation is one of the priorities of coastal management. In this sense, the major effort during POS was concentrated around the assessment and cleanup of affected sandy beaches.

After POS the affected sandy beaches presented both stranded surficial oil and deep oil contamination. Surface oil was reliably detected by aerial survey and direct inspection on foot. The first priority in the cleanup operations was to remove the surface oil as quickly as possible and ideally by means of manual mechanisms to protect the environment. In the POS, the cleanup response carried out by thousands of volunteers and soldiers with shovels to Northern Spanish coast and the manual oil retrieval was the main mechanism of clean up on sandy beaches (Fig. 22.27). Mechanical means as bulldozers and earthmovers were used in exceptional cases where some economic activity was at risk (Fig. 22.27).



FIGURE 22.26 Manual recovery using fishing vessels.

TABLE 22.2 Oil recovery, at sea and on land, from the sinking date until July 20, 2004

Oil recovery	Galicia	Asturias	Cantabria	Euskadi	France	Tonnes
Oil tonnes recovered on land	66,220	5,300	16,964	3,211	26,050	117,745
Oil tonnes recovered at sea by European vessels	15,500	470	150	—	1,325	17,445
Oil tonnes recovered at sea by fishing fleet	7,825	741	5,362	21,095	1,383	36,406
% Oil recovered by fishing fleet	21.5	2.0	14.7	57.9	3.8	—
% Oil recovered by fishing fleet in the Bay of Biscay	—	2.6	18.8	73.8	4.8	—
Oil recovery ratio: sea oil tonnes/land oil tonnes	0.35	0.23	0.32	6.57	0.10	—
Total oil recovery	89,545	6,511	22,476	24,306	28,758	171,596



FIGURE 22.27 Cleaning sandy beaches.

The subsurface oil contamination was a bit more complex problem to deal with. The previous knowledge was mainly based on the amazing effort done during years studying the *Exxon Valdez* oil spill. However, the characteristics of the Alaska and Spanish beaches are completely different, mainly in the grain size of sediment, and consequently the burial oil

mechanism, without considering the differences between the two spilled oils.

The subsurface oil in sandy beaches affected by POS was able to reach depth up to 4 m, and the main mechanism of burial was directly related to the beach morphodynamics more than to the oil properties. Besides, the assessment of

these beaches showed different oil appearances (e.g., small tar balls, sand coatings, and oil emulsions), evidencing changes in the oil forms after burial. All these new discoveries were based on the application of a beach-optimized suction corer (BOSC) to sample the deeper layer of sand in the intertidal beach zone [9]. As a consequence of monitoring and assessment of sandy beaches, a model of oil burial and behavior in these beaches was proposed (Fig. 22.28) [74].

The stranded oil in the intertidal area is directly subjected to the action of the wave breaking. This mechanism is responsible for the initial fragmentation of the large layers of oil present on the beaches [75] and the active mixing between the oil and the sediment. Tarballs of several centimeters were generated, spreading on the intertidal area of the beaches. In fair weather conditions, the transport of sediment from the lower part (subtidal) toward the higher part (intertidal) of the beach profile was activated, burying the oil up to several meters.

However, the morphodynamic behavior of the beaches not only affects the phenomenon of burial and mixing of oil but also determines the natural cleanup capacity of the beach. In this sense, the dynamics of high-energy beaches favors the burial–exhumation cycle of the oil and its transport, together with the sediment, from the subtidal area to the intertidal area, and vice versa. During this transport, the interaction between the oil and the sediment intensifies abrasion, where the tarballs diminish in size progressively, until they form particles of about mean grain size or less. In the moderate-energy beaches, the mobilization of the sediment is less frequent and the oil remains embedded for longer. The flow of water on the sand core induced by tidal variations favors the dissolution of the hydrocarbons in the interstitial water, pumping and diffusing the oil along the sedimentary column. The appearance of oil coatings on sediment grains forming layers, which in some cases reached more than a meter of thickness, is presented as an indicator of this diffusion process in the sedimentary column.

All these findings were integrated in the strategy design of the POS assessment, and hence the remedial treatment of oiled beaches.

22.5.3 Natural Attenuation Processes

Historical chronic or acute contamination episodes over the last 50 years on the NW Iberian shores (in which more than 50 important tanker accidents have occurred) resulted in highly adapted indigenous bacterial communities readily able to transform or degrade oily products, which can increase rapidly after new oil spills.

Since 1988, Bode et al. monitored the abundance and activity (leucine uptake) of bacterioplankton in impacted coastal areas near A Coruña on a monthly basis and found a significant enhancement of its activity after the spill, although no changes in its abundance were observed [76].

Moreover, the apparent oxygen utilization increased and the production rates were high, which could be related to hydrocarbon degradation.

Likewise, Medina-Bellver et al. used the dissolved inorganic carbon isotopic fractionation in polluted water from the Ons Island to assess the biological degradation of oil components and concluded that there was a strongly active degrading microbial community in some sites [77]. They also performed counts of hydrocarbon degraders by the most probable number method using several carbon sources (undecane, naphthalene, anthracene, phenanthrene, and pyrene) and found higher numbers in the polluted sites. These results agree with those obtained by Alonso-Gutiérrez et al., who 3 months after the oil spill, detected a bacterial community in polluted sediments with a high population of total heterotrophs and alkane degraders but a smaller proportion of aromatic-degrading bacteria [78].

Gallego et al. observed the existence of highly complex microbial communities in which not only bacteria but also fungi were present and speculated that Cyanobacteria and fungi may have a role in fuel biodegradation [79].

Bacterial communities found in impacted sites, particularly in sandy beaches, exhibited a high diversity (Fig. 22.29). However, the same phylogenetic groups (mainly alpha and Gammaproteobacteria and Actinobacteria) prevailed regardless of the study area, accompanied by other less abundant taxons (Firmicutes and Bacteroidetes) [78,80,81]. Moreover several genera (e.g., *Rhodococcus* and *Roseobacter*) have been detected in polluted sites 100 km apart from each other, and some (e.g., *Staphylococcus pasteurii*) have been isolated from very different samples.

Hydrocarbonoclastic bacteria such as *Alcanivorax borkumensis* (considered a model of alkane degrader) or *Cycloclasticus pugetii* (aromatic degrader) were found in recently impacted sediments of Ría de Vigo, where N and P are not limiting, suggesting that they play a key role in the first stages of biodegradation [80].

Other genera, such as *Rhodococcus*, commonly associated with long-chain *n*-alkanes degradation, could be predominant in longer term together with other members of Corynebacterineae, Sphingomonadaceae, or Rhodobacteraceae, which seemed to be related to PAH degradation [80,81].

Several studies conducted after the *Nakhodka* oil spill concluded that the total population of bacteria was almost stable and the accident had no long-term effects on its composition [82–89]. The degraders of oil components showed maximum population levels immediately after the oil spill and then returned to their original level. Similar results were found by Gallego et al. in the case of POS [85].

As it is known that the populations of degrading microorganisms and their effect on the concurrent hydrocarbons can be enhanced by the addition of nutrients, several natural attenuation studies have been reported following the POS. Different laboratory-scale biostimulation assays have proven the usefulness of adding nitrogen and

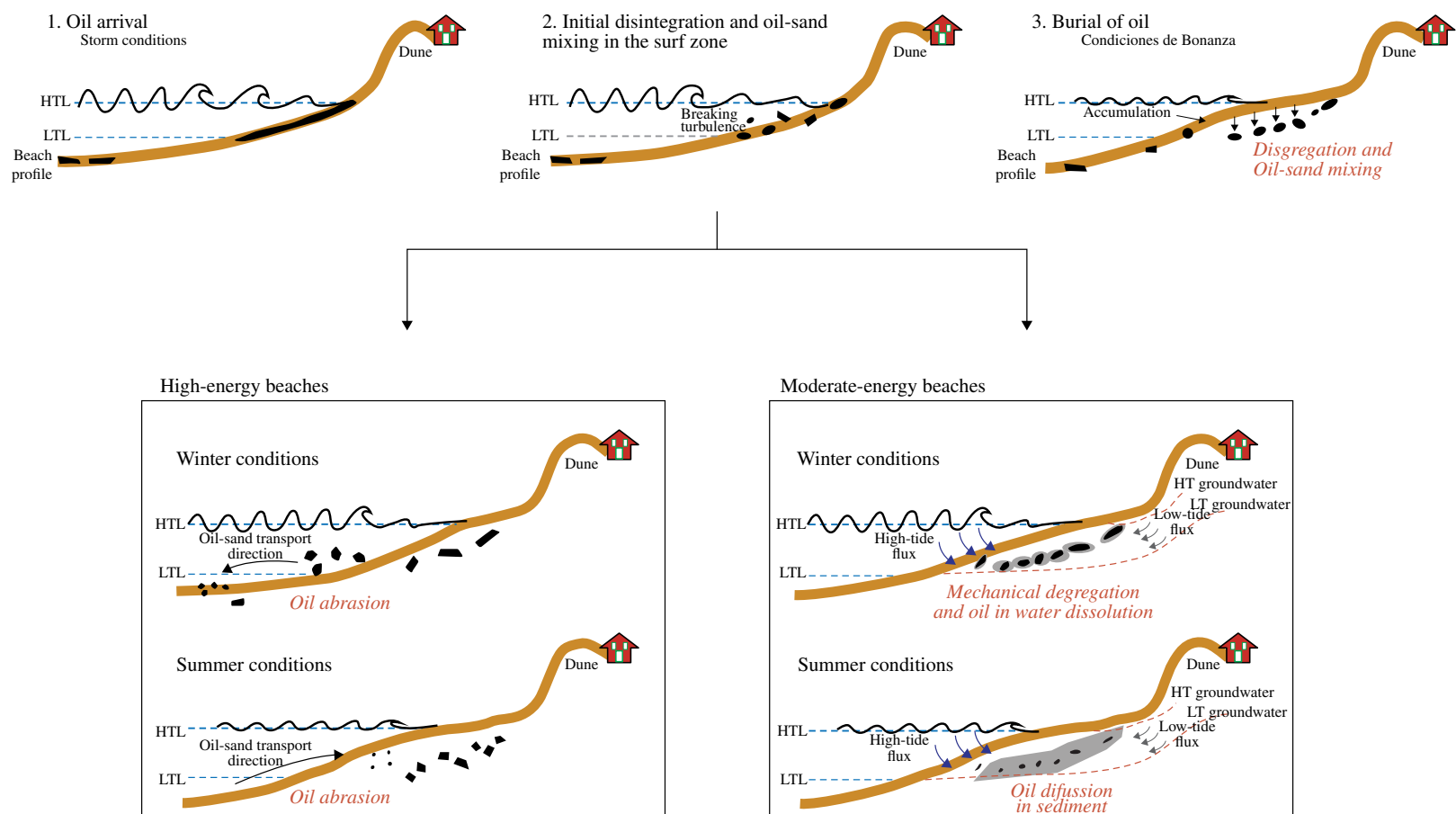


FIGURE 22.28 Model of burial and subsequent fate of the oil in the sediment of the intertidal zone of a beach.

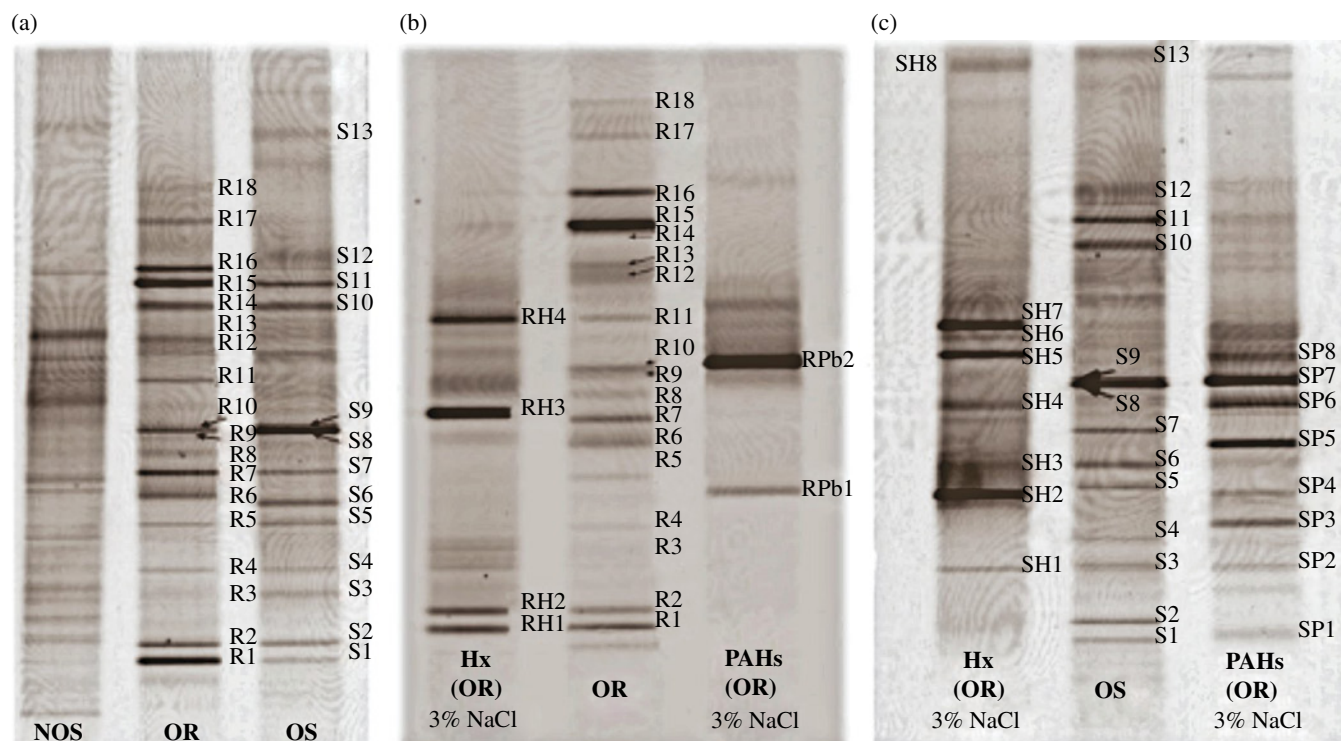


FIGURE 22.29 (a) Microbial diversity present in a nonoiled (NOS) and rocky and sandy oiled (OR and OS) stations. (b) and (c) are enrichments made in *n*-hexadecane and PAHs with oiled rocks and sand. Reprinted with permission from Ref. 80. © American Society for Microbiology.

phosphorus sources [77,85,86]. In addition, Díez et al. found that an oleophilic fertilizer (*S200*, similar to *Inipol EAP22*) significantly enhanced the biodegradation carried out by two different microbial consortia [86]. Several field assays have also been conducted using this oleophilic fertilizer and other amendments [30,79,87,88]. A field bioremediation assay was carried out 10 months after the POS in a beach of the Cantabria coast (North Spain) using *S200* [30]. The field survey showed that the fertilizer enhanced significantly the biodegradation rate, particularly of high molecular weight *n*-alkanes, alkylcyclohexanes and benzenes, and alkylated PAHs, paralleling the results previously found *in vitro* by Díez et al. [86]. This study provided useful information for assessing the potential biodegradability of the spilled product and allowed understanding the degradation pathways and predicting the long-term weathering of the spilled oil. As shown in Table 22.1, the most significant molecular bioremediation indicators were the depletion of diasteranes and C27 sterane components. Enhanced isomeric selectivity was also observed within the C1-phenanthrenes and dibenzothiophenes. Through the analysis of some target aliphatic and aromatic hydrocarbons a number of chemical indicators for assessing the efficiency of field bioremediation as well as identifying the source of highly weathered samples collected in the area after the spill were defined.

The authors suggest that the oleophilic fertilizer would not only provide the necessary nutrients but also improve

the solubilization (and thus bioavailability) of heavier PAHs and *n*-alkanes. In a pilot-scale experiment, Gallego et al. found that the use of the fertilizer together with a surfactant enhanced the degradation of linear alkanes and PAHs [85].

On the other hand, Fernández et al. tested several bioremediation treatments in rocky and sandy substrates, including bioaugmentation with two different commercial products (B350, aerobic and facultative hydrocarbon-degrading bacteria with micronutrients, and L1800, aerobic and facultative anaerobic hydrocarbon-degrading bacteria, micronutrients, and a biodegradable surfactant) and an autochthonous fuel-degrading microbial consortium obtained by enrichment from an environmental sample [87,88]. They also used a commercial hydrophylic fertilizer (Nitrophoska® Suprem) and a sunflower biodiesel (B100) and tried to combine different amendments. However, none of the treatments could enhance the natural bioattenuation processes, although the use of biodiesel resulted in cleaner rocks, mainly due to water washing.

22.6 CONCLUSION

A general conclusion to be drawn from these studies is that with the exception of the coastal areas directly oiled by the spill, it was difficult to identify major physical (e.g., sediment contamination) and toxicological (e.g., PAH

bioaccumulation) impacts in the subtidal zone and the continental shelf. This may be attributed to the physical characteristics of the oil, highly refractory to weathering but forming patches or tar lumps poorly dispersed in the coastal waters. Other than the most affected area (Costa da Morte), the PAH profiles in sediments and associated biota were similar to those generally found in coastal areas influenced by urban/industrial runoff, but even in that area, PAHs in wild mussels declined to background levels about 6 months after the spill.

Populations of benthic species in Costa da Morte (e.g., megrim, lobster, and shrimp) decreased in 2003 but recovered in 2004, whereas no significant effects were detected in demersal communities even though recruits were bound to the same drift of the oil. Yet, the small oil effect upon fish populations, which are generally overexploited, led to many being baffled by the closing of the fishing season declared after the spill.

The biological effects reported in many opportunistic studies carried out during this period cannot be properly assessed by the lack of an adequate methodology for analyzing the results in the context of the temporal data variability. Overall, conclusions could be drawn in this review as the final assessment was supported by the availability of pre-spill data in several areas, for example, PAH concentrations in biota, bacterioplankton activity, abundance and distribution of fish resources, and fishing activity.

REFERENCES

- [1] Albaigés, J., B. Morales, and F. Vilas, The *Prestige* Oil Spill: A Scientific Response. *Mar. Pollut. Bull.*, 53, 205, 2006.
- [2] Ercilla, G. and F. Vilas, Geological Characterization of the Galicia Bank Region (Atlantic Ocean, NW Iberia): The Marine Geology Community's Response to the *Prestige* Disaster, *Mar. Geol.*, 249, 1, 2008.
- [3] Rey, D., B. Rubio, K. Mohamed, F. Vilas, B. Alonso, et al., Detrital and Early Diagenetic Processes in Late Pleistocene and Holocene Sediments from the SW Galicia Bank Inferred from High-Resolution Enviromagnetic and Geochemical Records, *Mar. Geol.*, 249, 64, 2008.
- [4] Varela, R.A., G. Rosón, J.L. Herrera, S. Torres-López, and A.A. Fernández-Romero, A General View of Hydrographic and Dynamical Patterns of the Rías Baixas Adjacent Sea Area, *J. Mar. Syst.*, 54, 97, 2005.
- [5] Ruiz-Villareal, M., C. González-Pola, G. Díaz del Río, A. Lavín, P. Otero, et al., Oceanographic Conditions in the North and Northwest Iberia and their Influence on the *Prestige* Oil Spill, *Mar. Pollut. Bull.*, 53, 220, 2006.
- [6] Peliz, A., T.L. Rosa, A.M.P. Santos, and J.L. Pisarra, Fronts, Currents and Counter-Flows in the Western Iberian Upwelling System, *J. Mar. Syst.*, 35, 61, 2002.
- [7] Haynes, R. and E.D. Barton, A Poleward Flow along the Atlantic Coast of Iberian Península, *J. Geophys. Res.*, 95 (C7), 11425, 1990.
- [8] Álvarez-Salgado, X.A., J.L. Herrera, J. Gago, P. Otero, J.A. Soriano, et al., Influence of the Oceanographic Conditions During Spring 2003 on the Transport of the *Prestige* Tanker Fuel Oil to the Galicia Coast, *Mar. Pollut. Bull.*, 53, 239, 2006.
- [9] Bernabeu, A.M., D. Rey, B. Rubio, F. Vilas, C. Dominguez, et al., Assessment of Cleanup Needs of Oiled Sandy Beaches, Lessons from the *Prestige* Oil Spill, *Environ. Sci. Technol.*, 43, 2470, 2009.
- [10] Montero, P., J. Blanco, J.M. Cabanas, J. Maneiro, Y. Pazos, et al., Oil Spill Monitoring and Forecasting on the *Prestige*-Nassau Accident, *Environment Canada's 26th Arctic and Marine Oil Spill (AMOP) Technical Seminar*, Ottawa, Canada, 1013, 2003.
- [11] Castanedo, S., R. Medina, I.J. Losada, C. Vidal, F.J. Mendez, et al., The *Prestige* Oil Spill in Cantabria (Bay of Biscay). Part I: Operational Forecasting System for Quick Response, Risk Assessment and Protection of Natural Resources, *J. Coastal Res.*, 22, 1474, 2006.
- [12] Gonzalez, M., A. Uriarte, R. Pozo, and M. Collins, The *Prestige* Crisis: Operational Oceanography Applied to Oil Recovery, by the Basque Fishing Fleet, *Mar. Pollut. Bull.*, 53, 369, 2006.
- [13] Abascal, A.J., S. Castanedo, F.J. Mendez, F.R. Medina, and I.J. Losada, Calibration of a Lagrangian Transport Model Using Drifting Buoys Deployed During the *Prestige* Oil Spill, *J. Coastal Res.*, 25, 80, 2009.
- [14] Garcia-Ladona, E., J. Font, E. del Rio, A. Julia, J. Salat, et al., The Use of Surface Drifting Floats in the Monitoring of Oil Spills, The *Prestige* case, *Proceedings of the 19 Biennial International Oil Spill Conference (IOSC)*, Miami: CD-ROM; 14718A, 2005.
- [15] Daniel, P., F. Marty, P. Josse, C. Skandrani, and R. Benshila, Improvement of Drift Calculation in Mothy Operational Oil Spill Prediction System, *Proceedings of the 2003 International Oil Spill Conference (IOSC)*, Washington, DC: American Petroleum Institute; 6, 2003.
- [16] Beegle-Krause, C.J., J. Callahan, and C. O'Connor, NOAA Model Extended to Use Nowcast/forecast Currents, *IOSC 2003 Proceedings*, Vancouver, BC: API Publication No. 14730; 4, 2003.
- [17] Alvarez-Fanjul, E., I. Losada, J. Tintoré, J. Menéndez, M. Espino, et al., The ESEOO Project: Developments and Perspectives for Operational Oceanography at Spain, *Proceedings of the International Offshore and Polar Engineering Conference*, Lisbon, Portugal, 1708, 2007.
- [18] Díez, S., E. Jover, J.M. Bayona, and J. Albaigés, *Prestige* Oil Spill. III. Fate of a Heavy Oil in the Marine Environment, *Environ. Sci. Technol.*, 41, 3075, 2007.
- [19] González, J.J., L. Viñas, M.A. Franco, J. Fumega, J.A. Soriano, et al., Spatial and Temporal Distribution of Dissolved/Dispersed Aromatic Hydrocarbons in Seawater in the Area Affected by the *Prestige* Oil Spill, *Mar. Pollut. Bull.*, 53, 250, 2006.
- [20] Franco, M.A., L. Viñas, J.A. Soriano, D. de Armas, J.J. González, et al., Spatial Distribution and Ecotoxicity of Petroleum Hydrocarbons in Sediments from the Galicia Continental Shelf (NW Spain) after the *Prestige* Oil Spill, *Mar. Pollut. Bull.*, 53, 260, 2006.
- [21] Soriano, J.A., L. Viñas, M.A. Franco, J.J. González, L. Ortiz, et al., Spatial and Temporal Trends of Petroleum Hydrocarbons

- in Wild Mussels from the Galicia Coast (NW Spain) Affected by the *Prestige* Oil Spill, *Sci. Total Environ.*, 370, 80, 2006.
- [22] Soriano, J.A., L. Viñas, M.A. Franco, J.J. González, M.H. Nguyen, et al., Spatial and Temporal Trends of Polycyclic Aromatic Hydrocarbons in Wild Mussels from the Cantabria Coast (N Spain) after the *Prestige* Oil Spill, *J. Environ. Monit.*, 9, 1018, 2007.
- [23] Nieto, Ó., J. Aboigor, R. Buján, M. N'Diaye, J. Graña, et al., Temporal Variation in the Levels of Polycyclic Aromatic Hydrocarbons (PAHs) off the Galicia Coast after the "Prestige" Oil Spill, *Mar. Ecol. Prog. Ser.*, 328, 41, 2006.
- [24] Salas, N., L. Ortiz, M. Gilcoto, M. Varela, J.M. Bayona, et al., Fingerprinting Petroleum Hydrocarbons in Plankton and Surface Sediments During the Spring and Early Summer Blooms in the Galicia Coast (NW Spain) after the *Prestige* Oil Spill, *Mar. Environ. Res.*, 62, 388, 2006.
- [25] Pérez, C., A. Velando, I. Munilla, M. López-Alonso, and O. Daniel, Monitoring Polycyclic Aromatic Hydrocarbon Pollution in the Marine Environment after the *Prestige* Oil Spill by Means of Seabird Blood Analysis, *Environ. Sci. Technol.*, 42, 707, 2008.
- [26] Viñas, L., M.A. Franco, J.A. Soriano, J.J. González, L. Ortiz, et al., Accumulation Trends of Petroleum Hydrocarbons in Commercial Shellfish from the Galicia Coast (NW Spain) Affected by the *Prestige* Oil Spill, *Chemosphere*, 75, 534, 2009.
- [27] Wang, Z.D., M. Fingas, and G. Sergy, Chemical Characterization of Crude-oil Residues from an Arctic Beach by GC/MS and GC/FID, *Environ. Sci. Technol.*, 29, 2622, 1995.
- [28] Douglas, G.S., A.E. Bence, R.C. Prince, S.J. McMillen, and E.L. Butler, Environmental Stability of Selected Petroleum Hydrocarbon Source and Weathering Ratios, *Environ. Sci. Technol.*, 30, 2332, 1996.
- [29] Stout, S.A., A.D. Uhler, and K.J. McCarthy, A Strategy and Methodology for Defensibly Correlating Spilled Oil to Source Candidates, *Environ. Forensics*, 2, 87, 2001.
- [30] Jimenez, N., M. Viñas, J. Sabate, S. Diez, J.M. Bayona, et al., The *Prestige* Oil Spill. II. Enhanced Biodegradation of a Heavy Fuel Oil under Field Conditions by the Use of an Oleophilic Fertilizer, *Environ. Sci. Technol.*, 40, 2578, 2006.
- [31] Douglas, G. S., R.C. Prince, E.L. Butler, and W.G. Steinhauer, The use of Internal Chemical Indicators in Petroleum and Refined Products to Evaluate the Extent of Biodegradation, *Hydrocarbon Bioremediation*, Hinchee, R.E., Alleman, B.C., Hoeppe, R.E., Miller, R.N., Eds., Ann Arbor, Lewis Publishers, 1994.
- [32] Atlas, R.M., *Petroleum Microbiology*, New York, MacMillan Publishers, 1984.
- [33] Boehm, P.D., J.E. Barak, D.L. Fiest, and A.A. Elskus, A Chemical Investigation of the Transport and Fate of Petroleum-Hydrocarbons in Littoral and Benthic Environments—the Tsesis Oil-Spill, *Mar. Environ. Res.*, 6, 157, 1982.
- [34] Ezra, S., S. Feinstein, I. Pelly, D. Bauman, and I. Miloslavsky, Weathering of Fuel Oil Spill on the East Mediterranean Coast, Ashdod, Israel, *Org. Geochem.*, 31, 1733, 2000.
- [35] Garrett, R.M., I.J. Pickering, C.E. Haith, and R.C. Prince, Photooxidation of Crude Oils, *Environ. Sci. Technol.*, 32, 3719, 1998.
- [36] Serrano, A., F. Sánchez, I. Preciado, S. Parra, and I. Frutos, Spatial and Temporal Changes in Benthic Communities of the Galicia Continental Shelf after the *Prestige* Oil Spill, *Mar. Pollut. Bull.*, 53, 315, 2006.
- [37] Bence, A.E., K.A. Kvenvolden, and M.C. Kennicutt II, Organic Geochemistry Applied to Environmental Assessments of Prince William Sound, Alaska, after the Exxon Valdez Oil Spill—A Review, *Org. Geochem.*, 24, 7, 1996.
- [38] Sauer, T.C., J. Michel, M.O. Hayes, and D.V. Aurand, Hydrocarbon Characterization and Weathering of Oiled Intertidal Sediments Along the Saudi Arabian Coast Two Years after the Gulf War Oil Spill, *Environ. Int.*, 24, 43, 1998.
- [39] Baumard, P., H. Budzinski, Q. Michon, P. Garrigues, T. Burgeot, et al., Origin and Bioavailability of PAHs in the Mediterranean Sea from Mussel and Sediment Records, *Estuar. Coast. Shelf Sci.*, 47, 77, 1998.
- [40] Tronczynski, J., C. Munschy, K. Héas-Moisán, N. Guiot, I. Truquet, et al., Contamination of the Bay of Biscay by Polycyclic Aromatic Hydrocarbons (PAHs) Following the T/V "Erika" Oil Spill, *Aquat. Living Resour.*, 17, 243, 2004.
- [41] Porte, C., X. Biosca, D. Pastor, M. Sole, and J. Albaigés, The Aegean Sea Oil Spill, 2. Temporal Study of the Hydrocarbons Accumulation in Bivalves, *Environ. Sci. Technol.*, 34, 5067, 2000.
- [42] Meador, J.P., J.E. Stein, W.L. Reichert, and U. Varanasi, Bioaccumulation of Polycyclic Aromatic Hydrocarbons by Marine Organisms, *Rev. Environ. Contam. Toxicol.*, 143, 79, 1995.
- [43] Law, R. and J. Hellou, Contamination of Fish and Shellfish Following Oil Spill Incidents, *Environ. Geosci.*, 6, 90, 1999.
- [44] Marino-Balsa, J.C., P. Pérez, P. Estévez-Blanco, L. Saco-Álvarez, E. Fernández, et al., Assessment of the Toxicity of Sediment and Seawater Polluted by the *Prestige* Fuel Spill Using Bioassays with Clams (*Venerupis pullastra*, *Tapes decussatus* and *Venerupis rhomboideus*) and the *Microalga Skeletonema costatum*, *Ciencias Marinas*, 29, 115, 2003.
- [45] Beiras, R. and L. Saco-Álvarez, Toxicity of Seawater and Sand Affected by the *Prestige* Fuel-oil Spill Using Bivalve and Sea Urchin Embryogenesis Bioassays, *Water, Air, Soil Pollut.*, 177, 457, 2006.
- [46] Fernández, N., A. Cesar, M.J. Salamanca, and A. DelValls, Toxicological Characterisation of the Aqueous Soluble Phase of the *Prestige* Fuel-oil Using the Sea-urchin Embryo Bioassay, *Ecotoxicology*, 15, 593, 2006.
- [47] Morales-Caselles, C., J. Ramos, I. Riba, and A. DelValls, Using the Polychaete *Arenicola Marina* to Determine Toxicity and Bioaccumulation of PAHs Bound to Sediments, *Environ. Monitor. Assess.*, 142, 219, 2008.
- [48] Pérez-Cadahía, B., B. Laffon, E. Pásaro, and J. Méndez, Evaluation of PAH Bioaccumulation and DNA Damage in Mussels (*Mytilus galloprovincialis*) Exposed to Spilled *Prestige* Crude Oil, *Comp. Biochem. Physiol. C*, 138, 453, 2004.
- [49] Solé, M., A. Buet, L. Ortiz, F. Maynou, J.M. Bayona, et al., Bioaccumulation and Biochemical Responses in Mussels Exposed to the Water-Accommodated Fraction of the *Prestige* Fuel Oil, *Sci. Mar.*, 71, 373, 2007.
- [50] Ordás, M.C., J. Albaigés, J.M. Bayona, A. Ordás, and A. Figueras, Assessment of In-vivo Effects of the *Prestige* Fuel Oil Spill on the Mediterranean mussel Immune System, *Arch. Environ. Contam. Toxicol.*, 52, 200, 2007.

- [51] Martin-Skilton, R., F. Saborido-Rey, and C. Porte, Endocrine Alteration and other Biochemical Responses in Juvenile Turbot Exposed to the Prestige Fuel Oil, *Sci. Total Environ.*, 404, 68, 2008.
- [52] Morales-Caselles, C., N. Jiménez-Tenorio, M.L.G. De Canales, C. Sarasquete, and T.Á. DelValls, Ecotoxicity of Sediments Contaminated by the Oil Spill Associated with the Tanker "Prestige" Using Juveniles of the Fish *Sparus aurata*, *Arch. Environ. Contam. Toxicol.*, 51, 652, 2006.
- [53] Morales-Caselles, C., N. Jiménez-Tenorio, I. Riba, C. Sarasquete, and T.A. DelValls, Kinetics of Biomarker Responses in Juveniles of the Fish *Sparus aurata* Exposed to Contaminated Sediments, *Environ. Monitor. Assess.*, 131, 211, 2007.
- [54] Morales-Caselles, C., I. Riba, C. Sarasquete, and T. Ángel DelValls, Using a Classical Weight-of-evidence Approach for 4-years' Monitoring of the Impact of an Accidental Oil Spill on Sediment Quality, *Environ. Int.*, 34, 514, 2008.
- [55] Cajaraville, M.P., L. Garmendia, A. Orbea, R. Werding, A. Gómez-Mendikute, et al., Signs of Recovery of Mussels Health Two Years After the Prestige Oil Spill, *Mar. Environ. Res.*, 62 (Suppl. 1), S337, 2006.
- [56] Labarta, U., M.J. Fernández-Reiriz, J.L. Garrido, J.M.F. Babarro, J.M. Bayona, et al., Response of Mussel Recruits to Pollution from the "Prestige" Oil Spill along the Galicia Coast, a Biochemical Approach, *Mar. Ecol. Prog. Ser.*, 302, 135, 2005.
- [57] Peteiro, L.G., J.M.F. Babarro, U. Labarta, and M.J. Fernández-Reiriz, Growth of *Mytilus galloprovincialis* after the Prestige Oil Spill, *ICES J. Mar. Sci.*, 63, 1005, 2006.
- [58] Krahn, M.M., G.M. Ylitalo, J. Buzitis, and J.L. Bolton, Analyses for Petroleum-Related Contaminants in Marine Fish and Sediments Following the Gulf Oil Spill, *Mar. Pollut. Bull.*, 27, 285, 1993.
- [59] Martínez-Gómez, C., J.A. Campillo, J. Benedicto, B. Fernández, J. Valdés, et al., Monitoring Biomarkers in Fish (*Lepidorhombus boschii* and *Callionymus lyra*) from the Northern Iberian Shelf after the Prestige Oil Spill, *Mar. Pollut. Bull.*, 53, 305, 2006.
- [60] Fernandes, D., O. Andreu-Sánchez, M.J. Bebianno, and C. Porte, Assessment of Pollution along the Northern Iberian Shelf by the Combined Use of Chemical and Biochemical Markers in Two Representative Fish Species, *Environ. Pollut.*, 153, 327, 2008.
- [61] Ruddock, P.J., D.J. Bird, and D.V. McCalley, Bile Metabolites of Polycyclic Aromatic Hydrocarbons in Three Species of Fish from the Severn Estuary, *Ecotox. Environ. Safety*, 51, 97, 2002.
- [62] Council Directive, On the conservation of Natural Habitats and of Wild fauna and Flora, Council Directive 92/43/EEC, *Off. J. L.*, 206, 7, 1992.
- [63] Juanes, J.A., A. Puente, J.A. Revilla, C. Álvarez, A. García, et al., The Prestige Oil Spill in Cantabria (Bay of Biscay), Part II. Environmental Assessment and Monitoring of Coastal Ecosystems, *J. Coastal Res.*, 23, 978, 2007.
- [64] Puente, A., J.A. Juanes, G. Calderón, B. Echavarri-Erasun, A. García, et al., Medium-Term Assessment of the Effects of the Prestige Oil Spill on Estuarine Benthic Communities in Cantabria (Northern Spain, Bay of Biscay), *Mar. Pollut. Bull.*, 58, 487, 2009.
- [65] de la Huz, R., M. Lastra, J. Junoy, C. Castellanos, and J.M. Viéitez, Biological Impacts of Oil Pollution and Cleaning in the Intertidal Zone of Exposed Sandy Beaches: Preliminary Study of the "Prestige" Oil Spill, *Estuar. Coastal Shelf Sci.*, 65, 19, 2005.
- [66] Junoy, J., C. Castellanos, J.M. Viéitez, M.R. de la Huz, and M. Lastra, The Macroinfauna of the Galician Sandy Beaches (NW Spain) Affected by the Prestige Oil-Spill, *Mar. Pollut. Bull.*, 50, 526, 2005.
- [67] Rodríguez, J.G., M. Incera, R. de la Huz, J. López, and M. Lastra, Polycyclic Aromatic Hydrocarbons (PAHs), Organic Matter Quality and Meiofauna in Galician Sandy Beaches, 6 Months after the Prestige Oil-Spill, *Mar. Pollut. Bull.*, 54, 1031, 2007.
- [68] Lobón, C.M., C. Fernández, J. Arrontes, J.M. Rico, J.L. Acuña, et al., Effects of the "Prestige" Oil Spill on Macroalgal Assemblages: Large-scale Comparison, *Mar. Pollut. Bull.*, 56, 1192, 2008.
- [69] Díez, I., A. Secilla, A. Santolaria, and J.M. Gorostiaga, Ecological Monitoring of Intertidal Phytobenthic Communities of the Basque Coast (N. Spain) Following the Prestige Oil Spill, *Environ. Monitor. Assess.*, 159 (1), 555, 2008.
- [70] Acuña, J.L., R. Anadón, A. Puente, C. Fernández, M.L. Vera, et al., Large Scale Fuel Deposition Patterns in Northern Spanish Shores Following the "Prestige" Oil Spill, *J. Mar. Biol. Assoc. UK*, 88, 463, 2008.
- [71] Kingston, P.F., I.M.T. Dixon, S. Hamilton, and D.C. Moore, The Impact of the Braer Oil Spill on the Macrobenthic Infauna of the Sediments off the Shetland Islands, *Mar. Pollut. Bull.*, 30, 445, 1995.
- [72] Sánchez, F., F. Velasco, J. Cartes, I. Olaso, I. Preciado, et al., Monitoring the Prestige Oil Spill Impacts on Some Key Species of the Northern Iberian Shelf, *Mar. Pollut. Bull.*, 53, 332, 2006.
- [73] Varela, M., A. Bode, J. Lorenzo, M.T. Álvarez-Ossorio, A. Miranda, et al., The Effect of the Prestige Oil Spill on the Plankton in the N-NW Spanish Coast, *Mar. Pollut. Bull.*, 53, 272, 2006.
- [74] Bernabeu, A.M., M. Nuez de la Fuente, D. Rey, R. Rubio, F. Vilas, et al., Beach Morphodynamics Forcements in Oiled Shorelines, Coupled Physical and Chemical Processes During and after Fuel Burial, *Mar. Pollut. Bull.*, 52, 1156, 2006.
- [75] Santas, R. and P. Santas, Effects of Wave Action on the Bioremediation of Crude Oil Saturated Hydrocarbons, *Mar. Pollut. Bull.*, 5, 434–439, 2000.
- [76] Bode, A., N. González, J. Lorenzo, J. Valencia, M.M. Varela, et al., Enhanced Bacterioplankton Activity after the "Prestige" Oil Spill off Galicia, NW Spain, *Aquat. Microb. Ecol.*, 43, 33, 2006.
- [77] Medina-Bellver, J.I., P. Marín, A. Delgado, A. Rodríguez-Sánchez, E. Reyes, et al., Evidence for *in situ* Crude Oil Biodegradation after the Prestige Oil Spill, *Environ. Microbiol.*, 7, 773, 2005.
- [78] Alonso-Gutiérrez, J., M.M. Costa, A. Figueras, J. Albaigés, M. Viñas, et al., Alcanivorax Strain Detected among the Cultured Bacterial Community from Sediments Affected by the Prestige Oil-spill, *Mar. Ecol. Prog. Ser.*, 362, 25, 2008.
- [79] Gallego, J.R., E. González-Rojas, A.I. Peláez, J. Sánchez, M.J. García-Martínez, et al., Natural Attenuation and

- Bioremediation of Prestige Fuel Oil along the Atlantic Coast of Galicia (Spain), *Org. Geochem.*, 37, 1869, 2006.
- [80] Alonso-Gutiérrez, J., A. Figueras, J. Albaigés, N. Jiménez, M. Viñas, et al., Bacterial Communities from the Shoreline Environments “Costa da Morte” (NW Spain)) Affected by the Prestige Oil-spill, *Appl. Environ. Microbiol.*, 11, 3407, 2009.
- [81] Jiménez, N., M. Viñas, J.M. Bayona, A.M. Solanas, and J. Albaigés, The *Prestige* oil Spill, Bacterial Community Dynamics During a Field Biostimulation Assay, *Appl. Microbiol. Biotechnol.*, 77, 935, 2007.
- [82] Kasai, Y., H. Kishira, T. Sasaki, K. Syutsubo, K. Watanabe, et al., Predominant Growth of *Alcanivorax* Strains in Oil-Contaminated and Nutrient-Supplemented Sea Water, *Environ. Microbiol.*, 4, 141, 2002.
- [83] Kasai, Y., H. Kishira, K. Syutsubo, and S. Harayama, Molecular Detection of Marine Bacterial Populations on Beaches Contaminated by the Nakhodka Tanker Oil-Spill Accident, *Environ. Microbiol.*, 3, 246, 2001.
- [84] Maruyama, A., H. Ishiwata, K. Kitamura, M. Sunamura, T. Fujita, et al., Dynamics of Microbial Populations and Strong Selection for *Cycloclasticus pugetii* Following the *Nakhodka* Oil Spill, *Microb. Ecol.*, 46, 442, 2003.
- [85] Gallego, J.R., J.R. Fernández, F. Díez-Sanz, S. Ordoñez, H. Sastre, et al., Bioremediation for Shoreline Cleanup, In situ vs. On-site Treatments, *Environ. Eng. Sci.*, 24, 493, 2007.
- [86] Díez, S., J. Sabaté, M. Viñas, J.M. Bayona, A.M. Solanas, et al., The *Prestige* Oil Spill. I. Biodegradation of a Heavy Fuel Oil under Simulated Conditions, *Environ. Toxicol. Chem.*, 24, 2203, 2005.
- [87] Fernández-Álvarez, P., J. Vila, J.M. Garrido, M. Grifoll, and J.M. Lema, Trials of Bioremediation on a Beach Affected by the Heavy Oil Spill of the *Prestige*, *J. Haz. Mat.*, 137, 1523, 2006.
- [88] Fernández-Álvarez, P., J. Vila, J.M. Garrido, M. Grifoll, G. Feijoo, et al., Evaluation of Biodiesel as Bioremediation Agent for the Treatment of the Shore Affected by the Heavy Oil Spill of the *Prestige*, *J. Haz. Mat.*, 147, 914, 2007.

THE GROUNDING OF THE *BAHÍA PARAÍSO*, ARTHUR HARBOR, ANTARCTICA: DISTRIBUTION AND FATE OF OIL SPILL RELATED HYDROCARBONS

STEPHEN T. SWEET,¹ MAHLON C. KENNICUTT II,² AND ANDREW G. KLEIN³

¹Texas A&M University, College Station, TX, USA

²Department of Oceanography, Texas A&M University, College Station, TX, USA

³Department of Geography, Texas A&M University, College Station, TX, USA

23.1	Introduction and Background	547
23.2	Environmental Sampling	550
23.2.1	Surface Slicks and Water Column	550
23.2.2	Intertidal Macroalgae	550
23.2.3	Intertidal Beaches	550
23.2.4	Intertidal Limpets	551
23.2.5	Subtidal Sediments	553
23.2.6	Impacts on Other Wildlife	553
23.3	Conclusions	555

23.1 INTRODUCTION AND BACKGROUND

Enroute to resupply an Argentine Antarctic base, the *Bahía Paraíso* ran aground on January 28, 1989, and began leaking (Fig. 23.1). The vessel contained a cargo of diesel fuel arctic (DFA), JP-1 aviation fuel, gasoline, and compressed gas cylinders totaling more than one million liters. The primary contaminant was DFA, which is a mixture of diesel and jet fuel used in cold regions to combat gelling or solidification. An estimated 600,000 l of DFA was released during the initial phase of the spill.

Within 1 day of the spill, Palmer Station support personnel and scientists began comprehensive sampling efforts including collection of water samples, intertidal organisms, beach sediments, and oil slicks. Samples were routinely collected at regular intervals at established sites to provide information on the location, fate, and effects of the spill. Visual observations from the 29th to 30th of January 1989 suggested that the spill remained concentrated in Arthur Harbor near the vessel and Torgersen Island. On the 31st of January, winds, currents, and tides freed the *Bahía Paraíso* causing it to drift to its present location near DeLaca Island

(Fig. 23.1). Flowing to the east into Biscoe Bay and the seaward side of Laggard and Jacobs Islands, the oil slick's impact expanded to include nearby islands.

From the 4th through the 7th of February, the Chilean and Argentine navies surveyed the wreck and installed containment booms. The U.S. National Science Foundation (NSF) organized an emergency spill-response team composed of experts from the U.S. Navy, U.S. Department of Commerce National Oceanic and Atmospheric Administration (NOAA), the U.S. Coast Guard, and private contractors. This team of experts arrived at Palmer Station on the 7th of February with 52 tons of fuel-spill response equipment for the initial survey and cleanup. By the 9th of February, a site assessment was performed and skimming operations began. Three weeks after the spill, currents extensively flushed Biscoe Bay and the remaining contamination was concentrated around Arthur Harbor as evidenced by macroalgae contamination (Fig. 23.2).

By mid-March, the released oil was greatly diminished and macroalgae oil staining was restricted to areas in close proximity to the wreck (Bonaparte Point; DeLaca and Janus Islands). Pumping of fuel oil from the ship, skimming operations, and preliminary sealing of hull leaks were completed. The cleanup/salvage teams departed Palmer Station and a NSF-sponsored Quick Response Team arrived to assess the environmental effects of the *Bahía Paraíso* spill. The team consisted of benthic ecologists, algal physiologists, avian biologists, microbiologists, and hydrocarbon chemists and arrived in the area in early March 1989 to expand assessment activities [1].

Additional sampling was undertaken in March 1990 and 1991, 1 and 2 years after the spill [2–7]. In late 1992, a



FIGURE 23.1 Basemap of Palmer Station and vicinity including the initial impact and final location of the *Bahía Paraíso*.

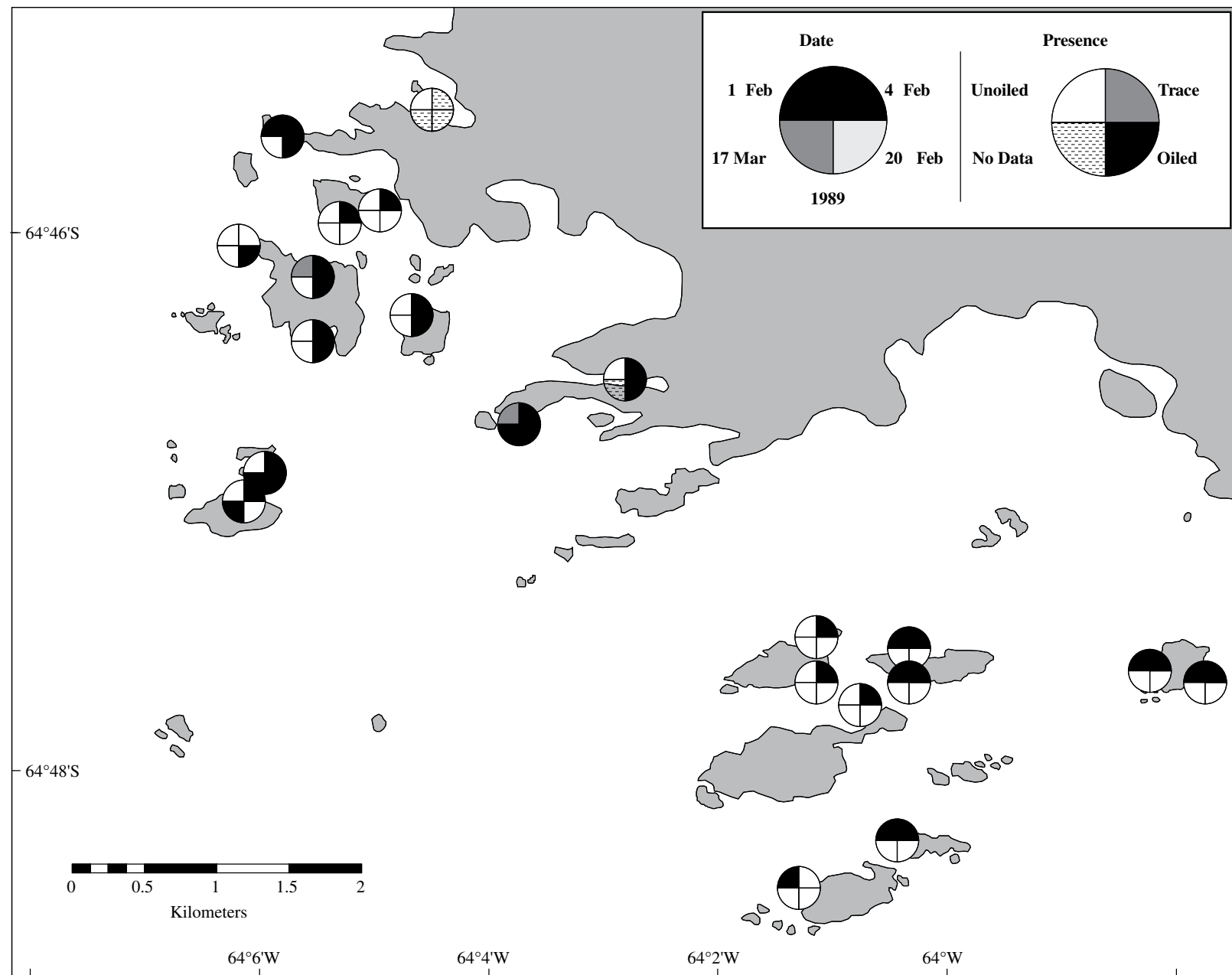


FIGURE 23.2 Qualitative indication of the presence or absence of DFA in intertidal areas based on fluorescence analysis of macroalgae extracts [2].

successful operation by the Argentine Republic and the Kingdom of the Netherlands recovered most of the remaining fuel from the wreck. Water samples collected in 2002 documented that fuel continued to leak from the *Bahía Paraíso*, but it was judged that contamination of local biota was minimal [8]. A small slick around the wreck, accompanied by a hydrocarbon odor emanating from minute amounts of lubricants, continues to leak from the ship.

23.2 ENVIRONMENTAL SAMPLING

The sampling program conducted following the *Bahía Paraíso* spill provides a picture of the spill's initial spatial extent, its quick demise and impacts on local fauna. A variety of samples was collected and analyzed (Table 23.1) during the initial investigation. Samples from the intertidal and subtidal (sediments, macroalgae, and limpets) zones were hand collected by divers or taken from the shoreline. Sediment samples from the deeper portions of the bays were sampled using a Smith-MacIntyre grab sampler operated from the R/V Polar Duke. Water samples were collected at various depths in the water column and oil slicks collected by surface skimming. Refined products were collected from the *Bahía Paraíso*, R/V Polar Duke, Palmer Station, and Old Palmer Station including JP-1, DFA, lube oil, heating fuel, and hydraulic fluid for comparison to the environmental samples collected.

23.2.1 Surface Slicks and Water Column

Surface slicks were sampled throughout the initial 6-week sampling period with collection beginning the day following the spill. The slick composition differed significantly from the DFA stored in drums on the ship's deck and remained constant throughout the initial sampling period [6].

TABLE 23.1 Analytical methodologies

Sample type	Analytical methodology
Water column	Solvent extraction, screening by GC/FID and UV fluorescence
Sediments	Solvent extraction, purification, quantitative GC/FID and GC/MS
Tissues	
Limpets	Solvent extraction, quantitative PAHs by GC/MS
Macroalgae	Solvent extraction, screening by UV fluorescence ^a
Bird feathers	Solvent extraction, screening by UV fluorescence ^a
Plankton tows	Solvent extraction, purification, quantitative GC/FID and GC/MS
Miscellaneous organisms	Solvent extraction, quantitative PAHs by GC/MS
Slicks and fuels	Screening by GC/FID and GC/MS

Source: Kennicutt et al. [9].

^aSamples showing significant fluorescence responses were analyzed further by GC/FID and GC/MS.

GC/FID, gas chromatography/flame ionization detector; GC/MS, gas chromatography/mass spectrometry; UV, ultra violet.

Detectable hydrocarbons in water samples were restricted to early stages of the spill and to areas directly beneath the oil slicks with total polynuclear aromatic hydrocarbon (PAH) concentrations ranging from 50 to 100 µg/l. The hydrocarbon composition closely resembled that of the slick samples which suggests that finely dispersed oil droplets were responsible for the detectable hydrocarbons. Visible evidence of small-scale leakage from the *Bahía Paraíso* still exists. In 2002, Janiot et al. observed and sampled a patchy oil film emanating from the wreck in the vicinity and characterized the hydrocarbon composition present in water samples and slick as DFA [10]. Plankton tows taken in March–April 1989 at 20 locations throughout a 3.2 km radius of Palmer Station failed to recover any residue or tar balls attributable to the spill [6].

23.2.2 Intertidal Macroalgae

Intertidal macroalgae (*Leptosomia simplex*, *Monostroma* sp.) served as a passive sampler and were repeatedly stained by released DFA. Macroalgae staining was consistent with visual observations of slick movement. Fluorescence intensity and spectra were used to detect the presence of petroleum hydrocarbons [8]. Four separate samplings were performed during the initial investigation in 1989 which are illustrated in Figure 23.2. By February 1, 1989, intertidal contamination of macroalgae in the vicinity of the wreck and the seaward edges of the outer islands (Norsel Point, Laggard, Jacobs, Limitrophe, and Cormorant Islands) became apparent. At the end of the first week of February, the wind-driven slick was concentrated in Arthur Harbor and the central portion of Biscoe Bay as documented by the oiling of macroalgae. At other locations, macroalgae recovered from exposure to the DFA due to the limited exposure time and were cleansed within a few days of exposure by evaporative, wave action, and dissolution processes. Resampling the intertidal macroalgae at the same locations a year later failed to detect any evidence of exposure [6].

23.2.3 Intertidal Beaches

Intertidal beaches were sampled during the initial response and during the two subsequent samplings. Most beaches are composed of pebble size or larger sediments which provided few places for the DFA to concentrate protected from wave and wind action. In general following oiling, intertidal beaches were cleansed by wind and wave action within days to weeks. One notable exception was the intertidal beaches on Christine Island which remained oiled for several weeks after other intertidal areas appeared cleansed. Sampling expanded to include additional beaches in 1990 with the vast majority found to contain no detectable hydrocarbons [6]. Two beaches located on Hermit and Cormorant Islands exhibited low level contamination of weathered DFA. Beach samples collected in 1991 were unusually high in PAH contamination as compared to previous samplings

[6]. No ready explanation is evident, however, leakage from the ship continued at a low level throughout the first 3 years of sampling. Quiescent periods of weather and periodic releases of fluids from the *Bahía Paraíso* may account for this accumulation of contaminants in areas protected from the winds and waves. The areas adjacent to Christine, Limitrophe, and Hermit Islands were observed to be contaminated with DFA on a number of occasions over the first 2 years following the incident. The relatively high concentrations of volatile PAH in 1991 indicated a recent re-oiling of these areas. Concurrent sampling of limpets at these areas also revealed elevated PAH levels. These contaminated sites are some of the few locations in the vicinity of Palmer Station where a depositional environment exists and it is reasonable to expect that slicks migrating into these areas would persist due to the relatively low energy environment.

23.2.4 Intertidal Limpets

Intertidal limpets (*Nacella concinna*) were found to be contaminated with DFA over a 6- to 7-week period following the spill. By February 1989, a 50% mortality of intertidal limpets was estimated and algal mats in the littoral zone initially appeared dead [1]. Total PAH concentrations in limpet tissue samples were as high as 125,000 ng/g during the initial phases of the spill (Table 23.2).

The location of the most intense contamination varied with time as is illustrated in Figure 23.3. On February 1, 1989, limpets with highest PAH concentrations were collected from islands to the southeast of the station, Limitrophe, Christine, and Hermit, with greater PAH concentrations on

the side of the islands facing the spill site. On February 4th, the areas with the highest concentrations had shifted to islands to the west and north of the spill site including DeLaca and Litchfield. This is consistent with visual observations of the spill and macroalgae staining.

Within 3 weeks after the first spillage, most PAH concentrations were reduced by a factor of 3–5, and within 6–7 weeks PAH concentrations in tissues were more than an order of magnitude lower than during the most intense exposure. In general, limpet hydrocarbon composition was indicative of oil adsorbed or coated on exterior tissues and not biological uptake; that is, a fractionation enhancing lower molecular weight material hydrocarbons in tissues was not evident [2]. Limpet tissues collected in 1990 generally contained lower PAH concentrations except in close proximity to the wreck, at beach locations exhibiting sediment contamination, and near the dock at Palmer Station. The sampling of intertidal limpets 2 years after the spill demonstrated that contamination continued to decrease (Table 23.2 and Fig. 23.3). Tissue contaminants at this time were dominated by naphthalenes. Limpet tissues containing higher PAH concentrations also contained phenanthrenes [6]. As with beaches, relatively high tissue PAH concentrations were observed at Christine, Limitrophe, and Hermit Islands. Higher concentrations of PAH in limpets coincided with the presence of PAH in the adjacent intertidal sediments. Fluorenes and phenanthrenes were often the most abundant aromatic contaminants in tissues with higher PAH concentrations. Though below the method detection limit, traces of high molecular weight combustion PAH were also present. This may indicate a common origin with the PAH detected in sediments adjacent to the wreck.

TABLE 23.2 PAH in tissues

Sampling location (map location)	Approximate distance from <i>Bahía Paraíso</i> (km)	February 1, 1989 (ng/g dw)	February 4, 1989 (ng/g dw)	February 20, 1989 (ng/g dw)	March 17, 1989 (ng/g dw)	March 22, 1990 (ng/g dw)	March 31, 1991 to April 15, 1991 (ng/g dw)
DeLaca (11)	0.2	698	125,147	1,260	3893	1001	177
Janus (12)	0.3	1,029	4,120	1,272	1882	>10ppb	32
Litchfield-A (7)	0.8	527	21,203	4,996	2791	1070	382
Torgersen (8)	1.2	549	10,162	1,819	>10ppb	523	186
Litchfield-B (5)	1.3	329	78,248	9,639	2111	276	248
Bonaparte Point (10)	1.4	164	3,673	17,653	2094	919	276
Litchfield-C (6)	1.4	194	2,178	227	2264	259	43
Humble-A (3)	1.7	571	15,495	1,090	1861	233	198
Humble-B (4)	1.8	1,542	36,395	3,267	2511	324	36
Norsel Point (2)	2.1	1,399	1,723	76	780	>10ppb	54
Hero Inlet (9)	2.1	677	5,387	6,262	473	544	57
Christine-A (13)	3.5	21,959	17,211	4,279	925	>10ppb	174
Christine-B (14)	3.6	35,775	11,322	2,749	1198	1181	337
Hermit (15)	4.0	16,969	24,874	3,244	2138	907	528
Limitrophe-A (16)	4.1	75,301	23,833	1,722	2413	672	471
Limitrophe-B (17)	4.2	2,687	15,946	1,683	901	>10ppb	84
Laggard (18)	4.4	2,707	1,888	1,242	515	21	68
Jacobs (19)	4.7	5,648	25,856	3,077	N/A	>10ppb	71
Comorant-A (20)	5.7	1,440	48,883	54,347	1203	622	35
Comorant-B (21)	6.0	1,403	628	1,315	460	>10ppb	80

Source: Kennicutt and Sweet [12].

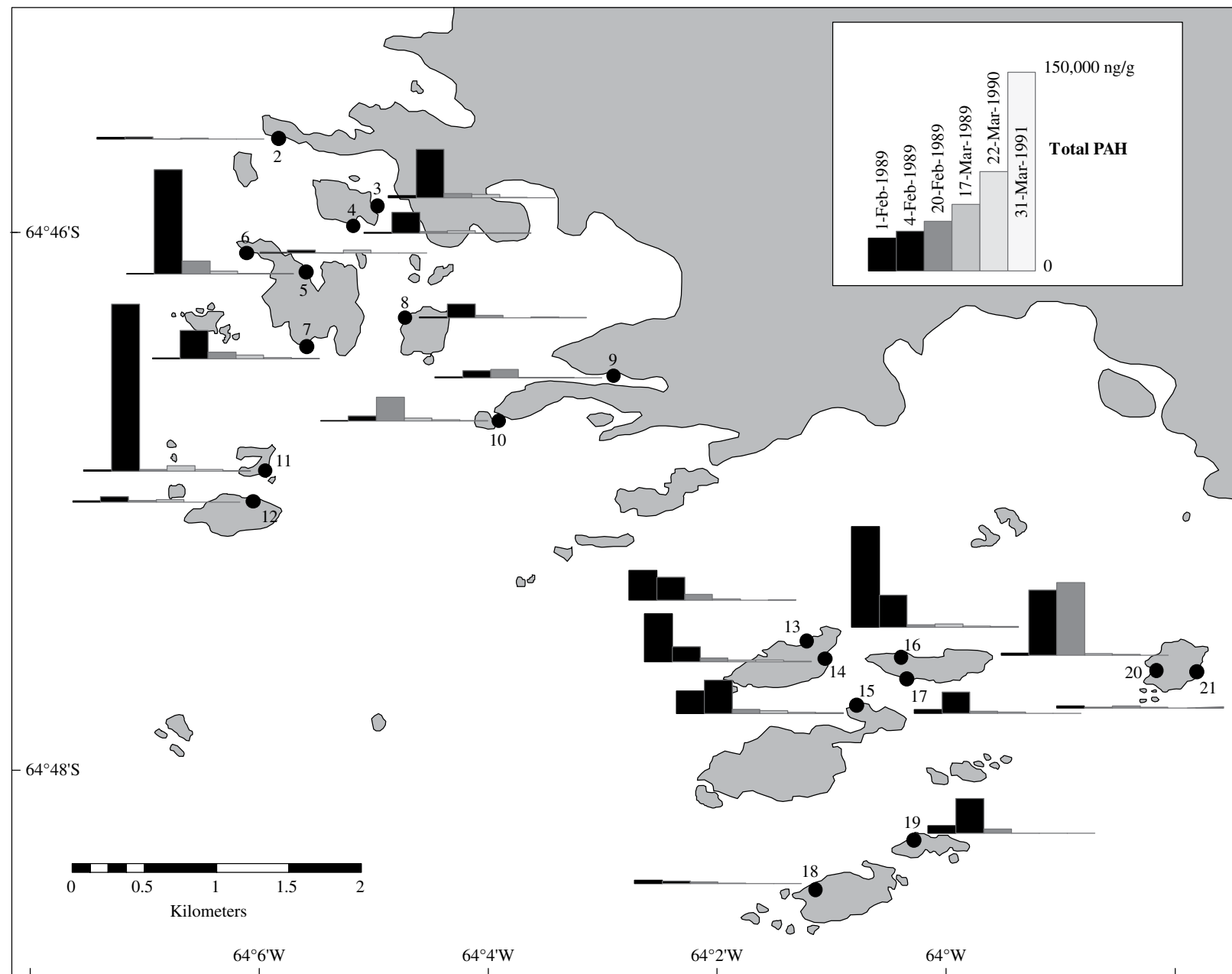


FIGURE 23.3 Bar graphs indicating the total PAH (ng/g dry weight) detected in limpets on six dates at selected sampling locations.

23.2.5 Subtidal Sediments

Subtidal sediment sampling locations and total PAH concentrations collected over a 3-year period are shown in Figure 23.4 with total PAH concentrations listed in Table 23.3. Sediments collected in 1989 from the central portions of the bays typically were fine-grained and low in carbonate (<1%) and organic carbon (~0.4%). Spill-associated hydrocarbons were typified by high levels of naphthalenes and fluorenes associated with suite of *n*-alkanes from *n*-C15 to *n*-C29 [2]. Total *n*-alkanes and PAH concentrations were highest in subtidal sediments near (within tens of meters) the *Bahía Paraíso* [2].

The molecular composition of sediment hydrocarbons suggests multiple sources. Subtidal sediments contaminated with DFA are present in the center of Arthur Harbor and at a few locations in close proximity to the wreck. Sediments in Arthur Harbor contained combustion-related aromatics, PAH from lube oil and/or hydraulic fluid, and biodegraded fuel oil residues.

During the 1990, sampling most subtidal sediments contained little or no PAH [6]. However, in 1991, subtidal sediment PAH concentrations were similar to those observed in 1989 (Table 23.3). This inter-annual heterogeneity in concentration suggests that local inputs other than the spill controlled contaminant distribution [3]. Bottom currents, storms, and ice movement combined to transport sediments away from the Arthur Harbor area. One indication of the dynamic nature of sediments in the harbor was that gravel was retrieved at several locations where finer sediments had previously been sampled.

In 1991, sediments within tens of meters of the wreck contained a different suite of PAH contaminants than found previously [2]. These sediment contaminants were depleted in volatile aromatics and normal alkanes, consistent with microbial degradation of alkanes and dissolution of aromatics into the surrounding water [13]. Previous microbiological studies suggest an indigenous hydrocarbon oxidizing bacterial community within the sediments of Arthur Harbor [1,14]. The half-life for hydrocarbon oxidation by bacteria was estimated to range from months to years [14].

A second change in the contaminant field in 1991 was differences in combustion-related PAH in samples adjacent to the ship, possibly due to the rupture of the ship's engine compartments and subsequent release of spent oil [6]. There were distinct differences in composition when the leakage was active where normal alkanes and low molecular weight, alkylated aromatics were the most abundant PAH [2]. An alternative source of combustion products in the vicinity cannot be ruled out, but the close proximity of these contaminants to the wreck suggests it is the source.

23.2.6 Impacts on Other Wildlife

Clam tissues (*Laternula elliptica*) collected in 1989 exhibited elevated levels of PAH near the wreck (total PAH 17,498 ng/g) and lower levels farther away in the central

portion of Arthur Harbor (total PAH 1212 ng/g). The clams contained large amounts of sediment in their stomach and as with the fish; ingestion of contaminated sediment appears to be the most likely mode of exposure. Clam tissues also contained significant amounts of chrysenes, which were found in bay sediments, confirming a sedimentary source of PAH. Examination of the subtidal macroinfauna suggested little impact in these environments [15].

Benthic and benthic-associated fish did not appear greatly affected by the spill. However, the presence of DFA was detected in stomach contents from Harpagifer fishes (*Notothenia coriiceps neglecta*) collected near the wreck in March 1989 (total PAH 9095; 25,854; and 6259 ng/g). Incorporation of DFA into fish muscle was not apparent as PAH was absent from muscle tissue. The DFA present in the stomach contents was unweathered and likely ingested with sediment during feeding [6].

The *Bahía Paraíso* spill occurred toward the middle-to-end of the breeding season for seven bird species and could have potentially impacted 40,000 birds. During the initial phase of the spill, adult diving birds including shags and penguins experienced minimal losses from oil fouling. However, blue-eyed shag nestlings died of toxicity and abandonment [1]. Surface-feeding birds did not appear to have experienced direct effects of the oil. Fluorescence analysis of bird feathers collected during March and April 1989, 6–8 weeks after the spill, from cormorants (*Phalacrocorax atriceps*), skuas (*Catharcta maccormicki*), gulls (*Larus dominicanus*), and penguins (*Pygoscelis adeliae*) near the wreck showed little or no evidence of exposure to the spill. This could be due to reduced concentrations of the slick present at that time, molting, and/or shifting of bird populations along the peninsula.

The initial impact on seabirds in the area varied with time and with species. Among the breeding populations of giant petrels and brown skuas, the effect of the spill appeared minimal [16]. The South Polar Skua (*Stercorarius maccormicki*) experienced a widespread mortality that appeared linked to the spill; a combination of weather conditions, food limitation, and behavior changes were hypothesized to be the causal factors [17].

The kelp gull (*L. dominicanus*) was indirectly affected by the spill [18]. Adult gulls did not appear affected at the time of the spill and the number of active nest sites in the area exposed to the oil spill has shown a steady decline since 1989. During the breeding season, males defend intertidal limpet populations for themselves and their mates. Fraser and Patterson proposed that the damage done to the intertidal limpet populations accelerated the depletion of this resource in an area where resource limitation was severe, thus driving limpet densities below the threshold levels needed to maintain gull reproduction [16].

Initial surveys of all local Adélie penguin (*P. adeliae*) colonies indicated that more than 80% of the birds had been exposed to the spill. Although few dead birds were observed, most adult birds appeared to have been exposed to the fuel

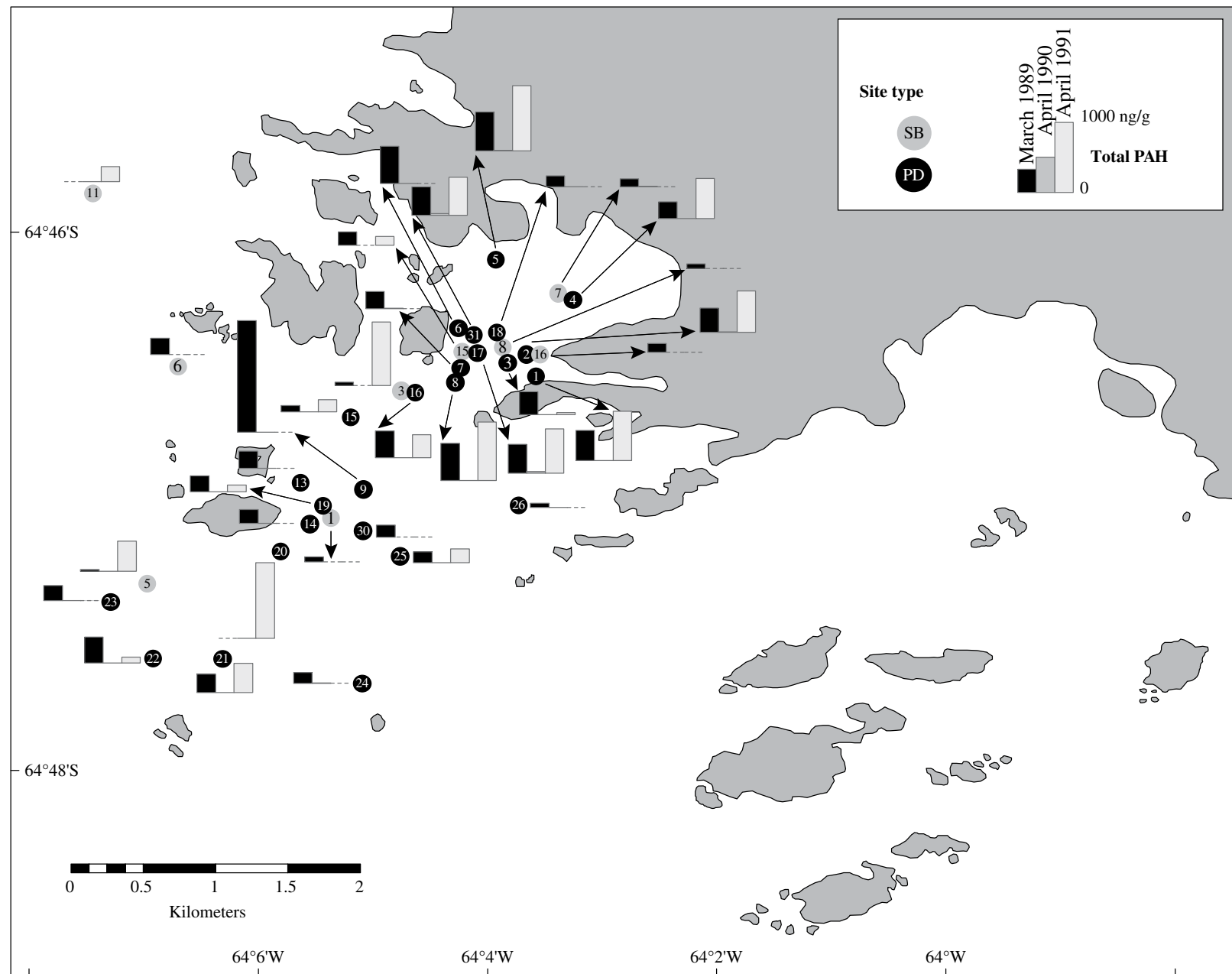


FIGURE 23.4 Bar graphs indicating the total PAH (ng/g) detected in intertidal sediments in 1990, 1991, and 1992 in Arthur Harbor and surrounding areas.

TABLE 23.3 PAH in marine sediment

Station Number	March 1989 (ng/g dw)	April 1990 (ng/g dw)	April 1991 (ng/g dw)
PD-1	425	MDL	699
PD-2	339	MDL	581
PD-3	323	MDL	29
PD-4	238	36	570
PD-5	547	MDL	920
PD-6	523	MDL	NS
PD-7	239	MDL	NS
PD-8	525	MDL	828
PD-9	1573	MDL	NS
PD-10	230	MDL	423
PD-11	414	MDL	NS
PD-13	242	MDL	NS
PD-14	200	MDL	NS
PD-15	92	MDL	172
PD-16	380	MDL	324
PD-17	408	24	626
PD-18	152	MDL	NS
PD-19	224	MDL	91
PD-20	NS	MDL	1068
PD-21	262	MDL	416
PD-22	363	MDL	82
PD-23	214	MDL	NS
PD-24	153	10	NS
PD-25	156	MDL	194
PD-26	62	MDL	NS
PD-30	176	NS	NS
PD-31	400	22	538
SB-1 (PD-19)	70 ^a	NS	NS
SB-3 (PD-16)	50 ^a	NS	897
SB-5 (PD-22)	21 ^a	MDL	425
SB-6	228	NS	NS
SB-7 (PD-4)	108 ^a	MDL	NS
SB-8 (PD-17)	67 ^a	NS	NS
SB-10	117	MDL	143
SB-15 (PD-7)	185 ^a	NS	121
SB-16 (PD-2)	125 ^a	NS	NS
SB-11	NS	MDL	213

Source: Kennicutt and Sweet [11].

MDL-ΣPAH are below the detection limit (<10 ppb for individual PAH).
 ΣPAH=[C1–C4 naphthalenes, phenanthrenes, chrysenes; C0–C3 fluorenes, dibenzothiophenes; C0–C1 fluoranthenes, pyrene; indenopyrene, dibenzanthracene, benzoperylene, benzofluoranthenes plus benzopyrenes].

^aAverage of two to four replicate boxcores.

DW, dry weight; NS, no sample.

oil [16]. Adélie penguin chicks fledged several weeks after the spill and were thus exposed at that time. Cormorants (*P. atriceps*) were documented to have nearly 100% chick mortality from the spill. In a later season, the number of active nests decreased by approximately 85% as a consequence to exposure to the fuel spill in bathing and foraging areas [18].

The exposure of the various species of seabirds in the area to the effects of the spill depended on their behavior. Adults were exposed primarily through feeding on krill and fish. As the spill occurred during the peak period of chick growth for many species, chicks were exposed both to oiled parents and oiled food. Continued studies on various components of the

ecosystem have shown different levels of impact for different species. While the Adélie penguin colonies closest to the spill site no longer exist, changes in overall population numbers remain within the range of natural variability. Active nests of cormorants near the spill have remained reduced by more than 60%, while those away from the spill remained constant. A steady decline in active Kelp Gull nests has persisted, suggesting the initial damage to its mollusk food source drove the bird populations down and recovery is inhibited [16]. Marine mammals were generally absent from the area during February and March of 1989 so there was minimal impact on their populations.

23.3 CONCLUSIONS

For the most part, the spill was dissipated by natural processes. The nature and volume of the fluids spilled from the *Bahía Paraíso* combined with the weather and sea conditions contributed to the rapid removal of spill related hydrocarbons from Arthur Harbor. Components of the ecosystem were contaminated to varying degrees during the spill, including birds, limpets, macroalgae, bivalves, bottom-feeding fish, and sediments. The spill impacts were limited to an area within a few kilometers of the wreck covering a several-week period due to reduction in leakage, cleanup efforts, spill weathering, and flushing of the area. The most direct effect was in the intertidal zone where oil fouled macroalgae, limpets, birds, sediments, and rocks. Staining of macroalgae and analysis of PAH concentrations in limpets and subtidal sediments provide independent lines of evidence that support the conclusion that spill's effects were limited both spatially and temporally. Less than 2 years after, and at many locations within a few weeks, sediment and intertidal organism PAH content returned to background levels. Most contaminants detected in subtidal sediments away from general vicinity of the wreck appear due to ship, boating, and station activities not related to the *Bahía Paraíso*. The action of winds and waves, even within the relatively protected areas of Arthur Harbor, minimized the length of time the area was exposed to potentially harmful contaminants.

REFERENCES

- [1] Kennicutt, M.C. II, S.T. Sweet, W. Fraser, M.E. Culver, W.L. Stockton, et al., Oil Spillage in Antarctica: Initial Report of the National Science Foundation-Sponsored Quick Response Team on the Grounding of the *Bahía Paraíso*, *Environ. Sci. Technol.* 24, 620, 1990.
- [2] Kennicutt, M.C. II, S.T. Sweet, W.R. Fraser, W.L. Stockton, and M. Culver, Grounding of the *Bahía Paraíso* at Arthur Harbor, Antarctica: Distribution and Fate of Oil Spill Related Hydrocarbons, *Environ. Sci. Technol.* 25, 509, 1991.
- [3] Kennicutt, M.C. II, T.J. McDonald, G.J. Denoux, and S.J. McDonald, Hydrocarbon Contamination on the Antarctic

- Peninsula I: Arthur Harbor-Subtidal Sediments, *Mar. Pollut. Bull.* 24, 499, 1992.
- [4] Kennicutt, M.C. II, T.J. McDonald, G.J. Denoux, and S.J. McDonald, Hydrocarbon Contamination on the Antarctic Peninsula II: Arthur Harbor Intertidal and Subtidal Limpets (*Nacella concinna*), *Mar. Pollut. Bull.* 24, 506, 1992.
- [5] Kennicutt, M.C. II, S.J. McDonald, J.L. Sericano, P. Boothe, J. Oliver, et al., Human Contamination of the Marine Environment, Arthur Harbor and McMurdo Sound, Antarctica, *Environ. Sci. Technol.* 29, 1279, 1995.
- [6] Kennicutt, M.C. II and S.T. Sweet, Hydrocarbon Contamination in the Antarctic Peninsula III: The *Bahía Paraíso* Two Years after the Spill, *Mar. Pollut. Bull.* 25, 303, 1992.
- [7] Kennicutt, M.C. II and S.J. McDonald, Marine Disturbance—Contaminants, *Foundations for Ecosystem Research in the Western Antarctic Peninsula*, L. Quetin, R. Ross, and E. Hofmann (eds.), American Geophysical Union, Washington, D.C., 401, 1996.
- [8] Janiot, L.J., J.L. Sericano, and O. Marcucci, Evidence of Oil Leakage from the *Bahía Paraíso* Wreck in Arthur Harbor, Antarctica, *Mar. Pollut. Bull.* 46, 1615, 2003.
- [9] Kennicutt, M.C. II, S.T. Sweet, W.R. Fraser, W.L. Stockton, and M. Culver, Grounding of the *Bahía Paraíso* at Arthur Harbor, Antarctica: Distribution and Fate of Oil Spill Related Hydrocarbons, *Environ. Sci. Technol.* 25, 510, 1991.
- [10] Brooks, J.M., M.C. Kennicutt II, and B.C. Carey, Origins of Hydrocarbons in Bering Sea Sediments I: Aliphatic Hydrocarbons and Fluorescence, *Oil Gas J.* 84, 66, 1980.
- [11] Kennicutt, M.C. II and S.T. Sweet, Hydrocarbon Contamination in the Antarctic Peninsula III: The *Bahía Paraíso* Two Years after the Spill, *Mar. Pollut. Bull.* 25, 305, 1992.
- [12] Kennicutt, M.C. II and S.T. Sweet, Hydrocarbon Contamination in the Antarctic Peninsula III: The *Bahía Paraíso* Two Years after the Spill, *Mar. Pollut. Bull.*, 25, 304, 1992.
- [13] Kennicutt, M.C. II, The Effect of Biodegradation on Crude Oil Bulk and Molecular Composition, *Oil Chem. Pollut.* 4, 89, 1988.
- [14] Karl, D.M., The Grounding of the *Bahía Paraíso*: Microbial Ecology of the 1989 Antarctic Oil Spill, *Microb. Ecol.* 24, 77, 1992.
- [15] Hyland, J., D. Laur, J. Jones, J. Shrake, D. Cadian, and L. Harris, Effects of an Oil Spill on the Soft-Bottom Macrofauna of Arthur Harbor, Antarctica Compared with Long-Term Natural Change, *Ant. Sci.* 6(1), 37, 1994.
- [16] Fraser, W.R. and D.L. Patterson, Human Disturbance and Long-Term Changes in Adélie Penguin Populations: A Natural Experiment at Palmer Station, Antarctic Peninsula, *Antarctic Communities: Species, Structure and Survival*, B. Battaglia, J. Valencia, and D.W.H. Walton (eds.), Cambridge University Press, New York, 445, 1997.
- [17] Eppley, Z.A. and M.A. Rubega, Indirect Effects of an Oil Spill: Reproductive Failure in a Population of South Polar Skuas Following the *Bahía Paraíso* Oil Spill in Antarctica, *Mar. Ecol. Prog. Ser.* 60, 1, 1997.
- [18] Penhale, P.A., J. Coosen, and E.R. Marschoff, The *Bahía Paraíso*: A Case Study in Environmental Impact, Remediation and Monitoring, *Antarctic Communities: Species, Structure and Survival*, B. Battaglia, J. Valencia, and D.W.H. Walton (eds.), Cambridge University Press, New York, 437, 1997.

TASMAN SPIRIT OIL SPILL AT KARACHI COAST, PAKISTAN

HINA AHSAN SIDDIQI AND ALIA BANO MUNSHI

Centre for Environmental Studies, Pakistan Council of Scientific and Industrial Research (PCSIR), Karachi, Sindh, Pakistan

24.1	Introduction	557
24.2	Immediate Response to the Impact: Actions and Remediation	557
24.2.1	Oil Recovery and Coast Cleaning	558
24.2.2	Oil Spill Monitoring	559
24.2.3	Socioeconomic Impact and Damage to Coastal Marine Life Damage	560
24.2.4	Human Health Impacts	561
24.3	The DDWP Project by Ministry of Science and Technology (MoST)	561
24.4	Hydrodynamics and Meteorological Data	562
24.4.1	Oceanographic Conditions	562
24.4.2	The Assessment of Oil Transport: Numerical Models	562
24.5	Oil Monitoring and Fate	564
24.5.1	Oil Composition	564
24.5.2	Spatial and Temporal Distribution in Seawater	564
24.5.3	Biota Affected by Oil Pollution	566
24.5.4	Oil Content of Sediment	566
24.6	Effects of Oil Impact at the Community Level	568
24.6.1	The Effects on the Benthic System	568
24.6.2	The Effects on the Pelagic System	569
24.7	Bioremediation/Natural Attenuation Processes	572
24.8	Conclusions	572

channel to Karachi harbor. The spot where it was aground was away from the centre of the port channel, so vessel did not hinder the operations of the port and it remained open for the movement of ships.

On August 11, 2003, the tanker began to show signs of breaking up. Since water was low and the ship had more drift, it was grounded on the sand just outside the entrance. The pilot asked the Port to try pull the vessel out of sand to refloat the grounded ship; on the Pilot's request, five tugs from the Karachi Port Authorities were deployed along with two Navy tugs to pull her out (Fig. 24.1). But since she was laden with 67,000 tons of oil, all the efforts after 2 days of pulling resulted in widening the crack and structural collapse occurred overnight 13/14 August, causing extensive spillage of oil and about 27,000 tons of the crude oil gushed out into the sea, leaving 14,500 tons on board. Another 3000 tons of the crude oil spilled subsequently, thus bringing the total loss to about 31,000 tons (10,000,000 gallons). The salvagers were able to remove 37,000 tons of the crude oil and 440 tons of bunker fuel. The oil spill continued from the tanker during the evening of August 13, 2003, up to the first week of September 2003 (Fig. 24.2).

24.1 INTRODUCTION

On July 27, 2003, the Greek oil tanker Tasman Spirit, a 24-year-old single hull, owned by Polembros Company of Greece, flying a Maltese flag, under the charter of Pakistan National Shipping Corporation to carry 67,535 tons of Iranian light crude oil for the Pakistan Refinery Limited, and about 450 tons of bunker fuel, ran aground in the access

24.2 IMMEDIATE RESPONSE TO THE IMPACT: ACTIONS AND REMEDIATION

Different international, national, and regional institutes such as UNDP, UNEP, EPA-Sindh, NIO, SUPARCO, Sindh Fisheries Department, Zoological Survey Department, Sindh Wildlife Department, IUCN—Department of Forestry, Environment Department of DHA, and IBA provided



FIGURE 24.1 Efforts of pulling out the grounded ship vessel.



FIGURE 24.2 Oil spilling in the sea from broken ship.

immediate response to the largest oil spill impacting coastal marine life and economy of Karachi with the common objective of helping to manage the crisis.

24.2.1 Oil Recovery and Coast Cleaning

The impacted area covered about 2062 km² while oil affected the sea bed sediments of an area of 270 km² (Fig. 24.3).

International Tanker Owners Pollution Federation Ltd (ITOPF) was notified of the incident on Day 1 by the P&I insurer, the American Club, and was requested to stand by to attend the incident on-site. Over the next few days, a full evaluation was made of the incident and the area potentially under the threat of pollution. The availability of suitable spill response equipment and personnel was ascertained locally, regionally, and globally (OSRL, EARL, NRC). Contact was maintained with the American Club's correspondents in Karachi and general advice was provided through them to

the Karachi Port Trust (KPT), and the government authority in charge of oil spill response activity. Approval for large-scale dispersant use was given by KPT and the Pakistan Environment Protection Agency (Pak-EPA). Immediately after the spill, dispersants (Inipol EAP-22) were applied offshore from the ADDS pack in response to two distinct pollution events on 14 and 22 August involving the progressive break-up of the tanker. About 15 tons of dispersant were initially applied to prevent floating oil from drifting toward the dense mangrove forests to the east of Karachi. Also, for cleaning operations, KPT used booms and oleophilic disk skimmers to protect the main channel to keep it open for vessel traffic. But ITOPF started operations on August 14, 2003, after the oil had already exposed Clifton Beach.

Onshore, pollution reached Clifton Beach (next to Karachi), with an estimated volume of 300 m³ covering some 6 km. Some areas around the harbor and some mangrove swamps were also affected. About 1800 m³ of hydrocarbons remained onboard, including lubricating oil and 200 m³ of heavy propulsion fuel (IFO 180). The most viscous products were recovered with a TK-80 pump from Europe. After this new spill, aerial spraying was implemented again. The volume of dispersants used, rose to 31 tons from the Hercules C-130 aircraft (with aerial dispersant spraying equipments, ADDS pack) and 6 tons from the boats. It was the only option to remove oil from the sea surface to restore oxygen supply and light to marine life, particularly when mechanical recovery is not possible. Offshore recovery operations became difficult because of the presence of the amounts of debris in the oil. According to OSRL, 143 m³ had been pumped out of the vessel in the harbor on 23 August and 0.5–2 m³ was recovered each day.

On the coast, various recovery techniques were used. A coarse cleaning operation was carried out manually and by mechanical recovery, and then by natural cleaning (Fig. 24.4). Oil entering the port of Karachi was confined by deploying booms at suitable collection sites, and in total, 140 tons of oil were recovered by skimmers. Nevertheless, pollution remained deeply buried in different places. In order to avoid accumulation of small unpolluted waste, this pollution was left for natural degradation. Some 2500 tons of polluted materials (mainly polluted sand) were collected.

Clean-up work was hampered by the lack of suitable disposal sites for collected oily waste. Agreement was eventually reached to dispose of collected oily sand at one of the municipal waste sites serving Karachi City. All Oil-soaked sand and debris were removed with spades and bare hands and the same were dumped initially at a site designated by DHA and finally transported to a so-called landfill location at Surjani/Jam Chakro solid waste dump site of the City Government some 30 km distant from the beach. Around 3400 plastic bags containing about 1–1.2 metric tons of the material were dumped at this site after treatment with lime. The main problem with the aftermath of oil spill was in fact restoration of about 200 m wide and 11.5 km long beach that was polluted with an estimated 6000 tons of light crude oil.

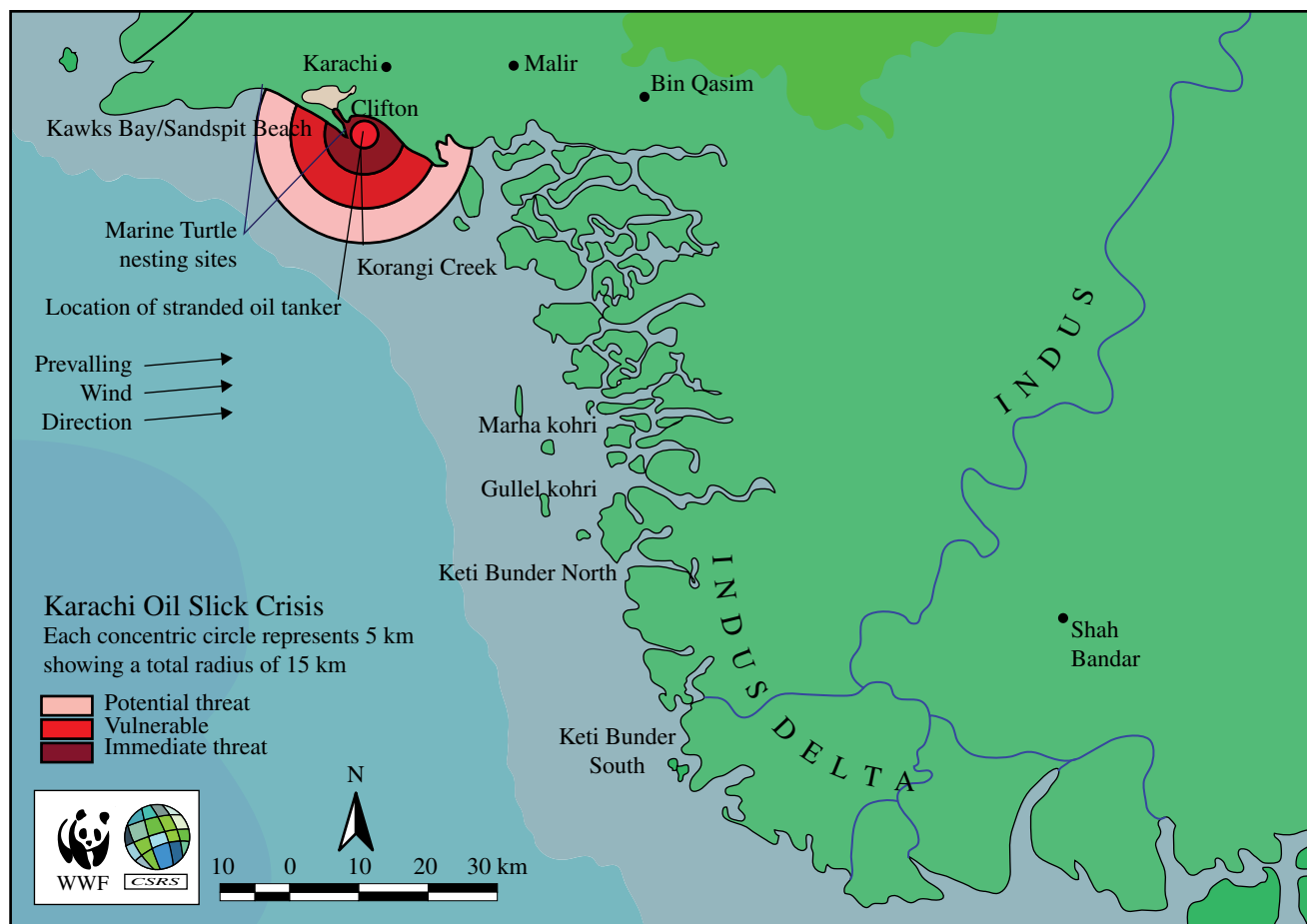


FIGURE 24.3 Spill incident location (Map courtesy of ITOPF).



FIGURE 24.4 Oil before cleaning, on the Karachi shoreline.

Part of this oil had penetrated down to depths of 2 and 3 m in places of high impact and had also deposited on boulders which presented an ugly sight. After several interruptions, the salvors succeeded in removing over 35,000 tons of cargo and most of the 440 tons of heavy fuel oil bunkers from Tasman Spirit. After completion of the cargo transfer operation, about 1000 tons remained unrecovered due to the

constant agitation by wave action in damaged tanks. Later on the ship was towed by the SMIT Salvage in two pieces to Gadani where she was dismantled. SMIT Salvage was contracted to remove the wreck. The wreck removal operation was extremely challenging. The SMIT team not only encountered strong currents, access difficulties and zero visibility, but also had to deal with the fact that the vessel was embedded in a trench around 6 m deep. The wreck was removed from the entrance, using tugs, sheerlegs, and barges. The operation was completed successfully in a time-frame of about 3 months [1–4].

24.2.2 Oil Spill Monitoring

After the accident, different institutes and public organizations started working on monitoring to evaluate the distribution of the oil spill. The meteorological data were provided by the Pakistan Meteorological Department, and oceanographic conditions were measured by National Institute of Oceanography, while satellite remote sensing to supplement the process of oil spill monitoring was done by Space and Upper Atmosphere Research Commission (SUPARCO). The overcast monsoon sky during August, 2003, rendered

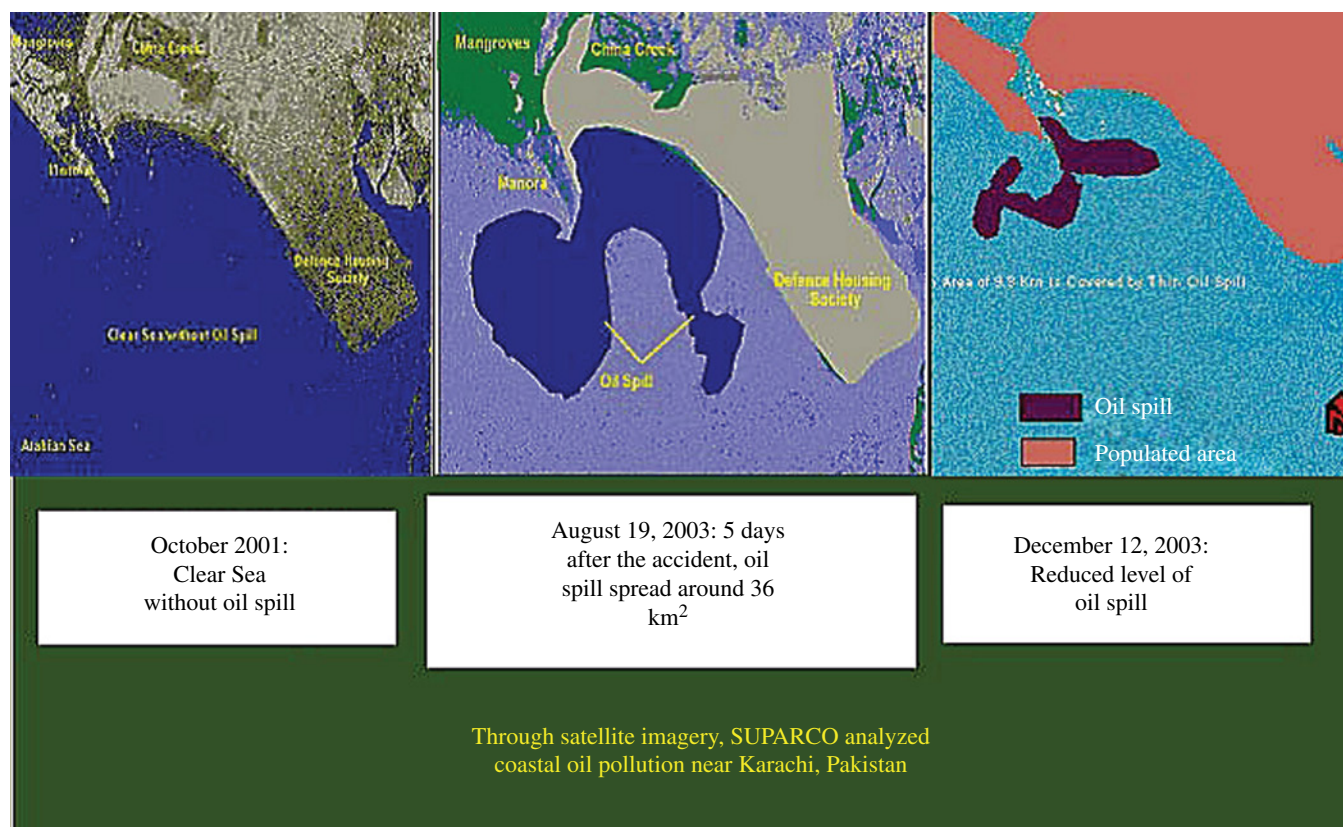


FIGURE 24.5 Satellite image of coast before and after the spill (Map courtesy of SUPARCO).

visual technique and optical satellite images were unsuitable for mapping of oil spill, so Canada's Radarsat images were used for before (October 2001) and after the oil spill (August and December, 2003) over the Arabian Sea including the coastal area of Karachi (Fig. 24.5). The Radarsat equipped with Synthetic Aperture Radar system works in the microwave region of the spectrum. The affected area as indicated in the August 19 image is 37 km², of which 8 km² area around the disastrous ship has been worst affected and seen to have thick slick. Due to natural dispersion and the remediation measures taken, the oil slick condition on December 12, 2003, image was seen to be reduced. The patches of slick were seen around 9 km² off the coast [5].

24.2.3 Socioeconomic Impact and Damage to Coastal Marine Life Damage

Most of the oil impacted the coastal areas of Clifton and DHA beaches, Karachi Harbor, and the offshore area adjacent to Clifton and Defense Housing Authority (DHA) beaches. Despite a massive beach cleaning operation, oil contamination remained highly visible on the beaches and in adjacent seawater for the next 6 months and moderately visible for the next 12 months after the incident. Ecologically sensitive creek areas with mangroves are present on the southeastern coast of Karachi. To the west of the grounding site are known turtle nesting sites along Hawks Bay and

Sand Pit. Within the port of Karachi, there are salt ponds, mangrove forests, and the harbor, mainly used for the shrimp fishery, as well as shipyard facilities, oil terminals, Pakistan Navy installations, and a seawater intake. These are all potentially sensitive areas to oil contamination. To the east of the grounding site are mangrove forests. This area and the area offshore of the grounding site are rich fishing grounds.

The Karachi coastal area impacted by the oil spill is one of the most productive areas of the coast. The area is known to be rich in biological productivity. It includes habitats for sea turtles, dolphins, porpoises, beaked whales, and several species of lizards and snakes. More than 200 species of fish are known to exist in the Karachi Coastal waters. Many fish and shrimp species that constitute commercial and traditional fisheries use the oil-impacted areas for feeding and nursery grounds. Over 50 species of birds (resident and migratory) utilize this area for feeding. The coastal area of Karachi impacted by the Tasman Spirit Oil Spill also includes ecologically sensitive mangrove ecosystems in Indus Delta creeks and Karachi Harbor areas. These provide feeding and nursery grounds for important components of the coastal marine food web. On August 16, the oil spill, started to have its toll over the economic interest of the country and impacted the facilities located in the Manora Channel with an area of about 60 km². The Karachi Fish Harbor, the Naval establishments, salt works, three large areas under mangrove forest cover and the villages around the shoreline of the Channel

were all witness to the creeping oil slick. The fish harbor located at the far end of the Karachi Port toward West Wharf, and catering to the needs of around 2300 boats having an annual catch of about 650,000 tons of fish and shrimps, started receiving the foul smell of the oil, and the Marine Fisheries Department issued directives to the fishermen to be careful in lighting any fire due to the fear that the petroleum vapor may catch fire.

Fishermen belonging to 13 coastal villages with a population of more than 0.2 million were among those directly affected by the oil spill, according to a survey conducted by the Pakistan Fisherfolk Forum, a non-governmental organization. The livelihood of more than 90,000 registered fishermen of Sindh was at stake as the oil slick in fishing zone led to a sharp decline in the sale of seafood in the city markets. Prices of different fish species came down by 60–70%. Owing to the low off-take, traders at fish harbor had to curtail bulk procurement which forced fishermen to fishing the coastal areas of Thatta and Badin rather than in the affected zone and also to dispose off their catch at whatever rate offered. A 3-month fishing ban was imposed by the Marine Fisheries Department along the coastline directly affected by oil, extending five nautical miles offshore. Loss of productivity over the impacted area affected the potential yield of demersal fish estimated at 5.8 g/m², that is, about three to four times the value for primary productivity in terms of carbon. The fish catch in the impacted area has been found to be about 11 tons per day or about 4000 tons per year. It was estimated that the loss of demersal fish for this area spread over 6 years could be a tremendous quantity of over 24,000 tons.

On August 15, 2003, the Government of Pakistan formed an Environmental Impact Evaluation Committee (EIEC) to evaluate the impact caused by the Tasman Spirit Oil Spill (TSOS) and to propose an appropriate restoration plan. The EIEC was composed by government agencies, non-governmental organizations, and experts on natural resources studies and management. The Ministry of Environment contacted United Nations Development Programme (UNDP), United Nations Environment Programme (UNEP), and International Union for Conservation of Nature (IUCN) for assistance. Consequently, Professor Richard G. Steiner of University of Alaska and Mr. Stefan Micallae, Chief, Disasters Management Branch, UNEP, traveled to Pakistan to assist EIEC to prepare a report in consultation with local officials. The in-country office of the UNDP facilitated the work through monetary and technical support. The EIEC submitted its preliminary assessment report on September 9, 2003. The report estimated that, despite of all response efforts, the area impacted by the spill covered at least 40 km².

There was extensive hydrocarbon contamination in seawater samples; counts of 1000 dead fish at a single sampling station in a day; cell damage in phytoplankton communities; reduced numbers of polychaete worms, shellfish, and starfish in the surface sands of Clifton Beach; and loss of regeneration of mangrove growth. Reports also stated that turtle population was reduced; oil contamination destroyed turtles'

foods such as grasses and weeds, and probably forced them to migrate to other places. Oil impacted approximately 78 km² of mangrove forest area, which dropped mangrove seedling survival rate from 30%, a loss of 51,135,000 seedlings for the mangrove, *Avicennia marina*. Drastic decrease in the growth of vegetative parts and seedling of mangroves was also observed due to oil contamination which would result in the loss of production of 2526 tons of shrimp and fish per year [2,6].

24.2.4 Human Health Impacts

It was estimated that about 300,000 people were exposed to petroleum hydrocarbons vapor representing the largest exposure to humans of any oil spill in history. The initial assessment reports estimated that about 11,000 tons of volatile organic compounds were released in the air from the oil spill. The severe pollution of Clifton Beach created very strong oil vapors causing considerable discomfort to local residents and clean-up personnel. Local hospitals reported many cases of headaches, nausea, fainting, dizziness, and nose bleeding, and schools in the vicinity were closed for a short period.

A study was started after the spill by Aga Khan Medical University in Karachi in collaboration with University of Alabama in the United States. According to the results [7], among 500 people examined, coast dwellers suffered with many health problems than the other two groups of people living 2- and 20 km from the coast. They had prevalence of eye, skin, and gastrointestinal problems, as well as respiratory infections caused by fumes from oil.

One study on human health hazards [8] demonstrated that crude oil exposure adversely affected the lung function and this effect primarily showed an obstructive pattern of airways disease. However, this impairment was reversible and lung functions impairment was reversed and improved after 1 year when the exposed group was kept away from the oil exposure.

24.3 THE DDWP PROJECT BY MINISTRY OF SCIENCE AND TECHNOLOGY (MOST)

After the spill, all disastrous outcomes for the local environment due to lack of institutional basis for prevention of such accidents, gave a funding opportunity by the Pakistan Ministry of Science and Technology to establish a system to manage such accidents through a monitoring of their consequences. The project cost 31.32 million rupees for a period of 2 years was approved in Departmental Developmental Working Party (DDWP) meeting held on October 22, 2003. The basic objective of the project was to develop facilities to handle and monitor such accidents at national level by creating new tools and by improving the inter-institutional and international coordination. The project was joint venture of National Institute of Oceanography (NIO) for physical and biological

aspects, Pakistan Council of Scientific and Industrial Research (PCSIR) for chemical aspects, and Centre for Molecular Genetics (CMG), University of Karachi, for bioremediation aspects of the project.

In this chapter, Sections 24.4, 24.6, and 24.7 have been compiled from Tasman Spirit Oil Spill project report.

24.4 HYDRODYNAMICS AND METEOROLOGICAL DATA

24.4.1 Oceanographic Conditions

The water depths in the area are relatively shallow with a maximum depth of about 30 m at the southwest corner. The bathymetry and coastal topography (Fig. 24.6) show a distinct shallow area at the mouth of the dominant tributaries, the Korangi and the Phitti creeks.

Wave climate conditions are presented in Figure 23.7. The predominant monsoon is the southwest (SW) monsoon that occurs between May and September. The SW monsoon winds, having an average speed of about 15 m/s, generate strong waves and currents in the area. The strong and persistent winds generate swells with a period of about 12 s, which strike Karachi coastline from SW direction. During the winter, the northeast (NE) monsoon prevails in the region. During this season, predominantly northeasterly winds with an average speed of 5 m/s prevail. The winds from southwesterly direction are about 10% of the winds in the NE monsoon

season. Since the oil spill occurred in the SW monsoon period, strong mixing with landing of oil on the beach (north side) was observed. However, the movements of polluted sediments were expected toward S and SE area in the NE monsoon and with the passage of time. The winds in the transition periods are mixed, and predominantly weak southwesterly wind prevails in the Karachi and surrounding region.

The observed directions of currents of the area matched with the common reversal of tides during the whole tidal cycles. In general, currents are stronger during ebb tide and attain maximum speed of about 35 cm/s in the Phitti Creek area. Therefore, it seems the shape of coastline, tidal exchange, and the topography of the coast create an area between Oyster Rocks and the mouth of the channel where flushing is weak. In this area, the stranding or beaching of floating objects occurs (i.e., when the floating object encounters a beach and gets stranded).

24.4.2 The Assessment of Oil Transport: Numerical Models

To determine the transport, redistribution and spatial extent of oil-polluted sediments in the coastal waters of oil spill affected area, hydrodynamic modeling of the wind and tide-drive currents and waves were carried out. The impact of river discharges was also included in the numerical simulation. The observed daily wind speed and direction for 2004, predicated tides, and mean river discharges within the area were used as inputs into the model. Using the simulated

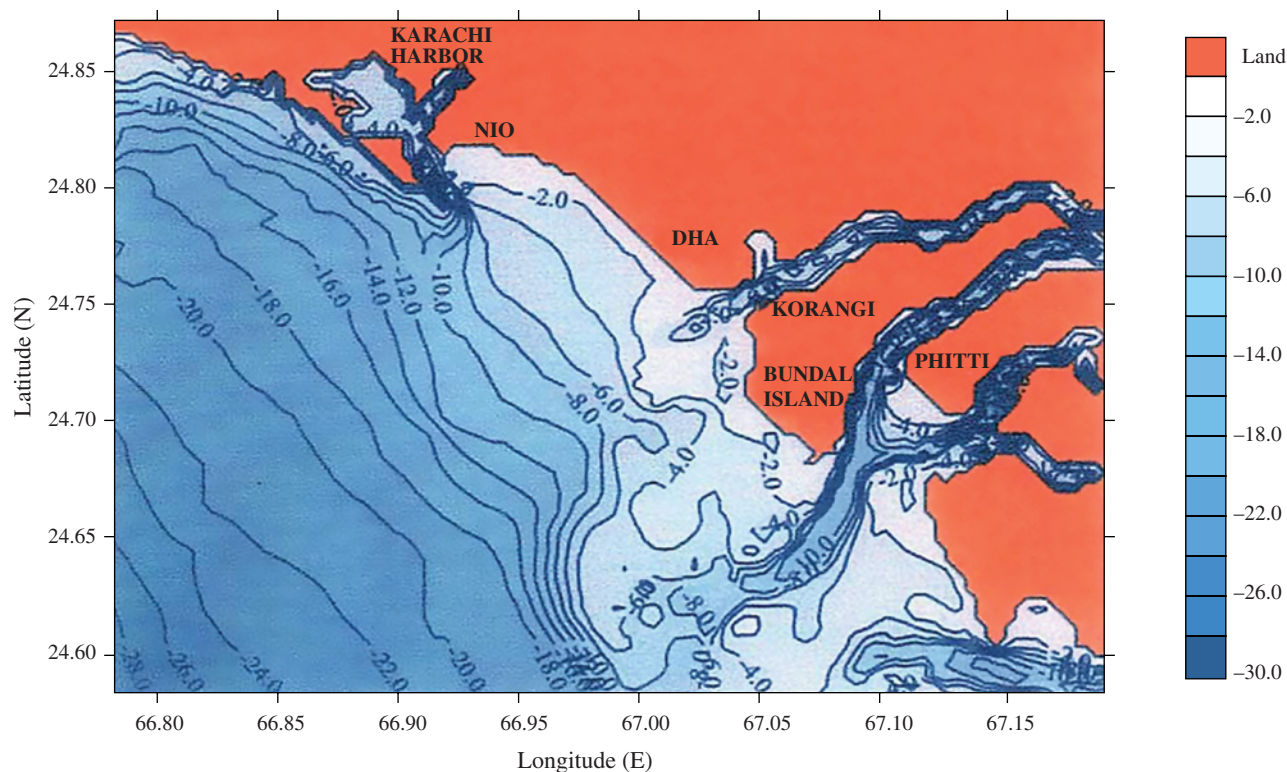


FIGURE 24.6 Coastal configuration and bathymetric contours of affected area.

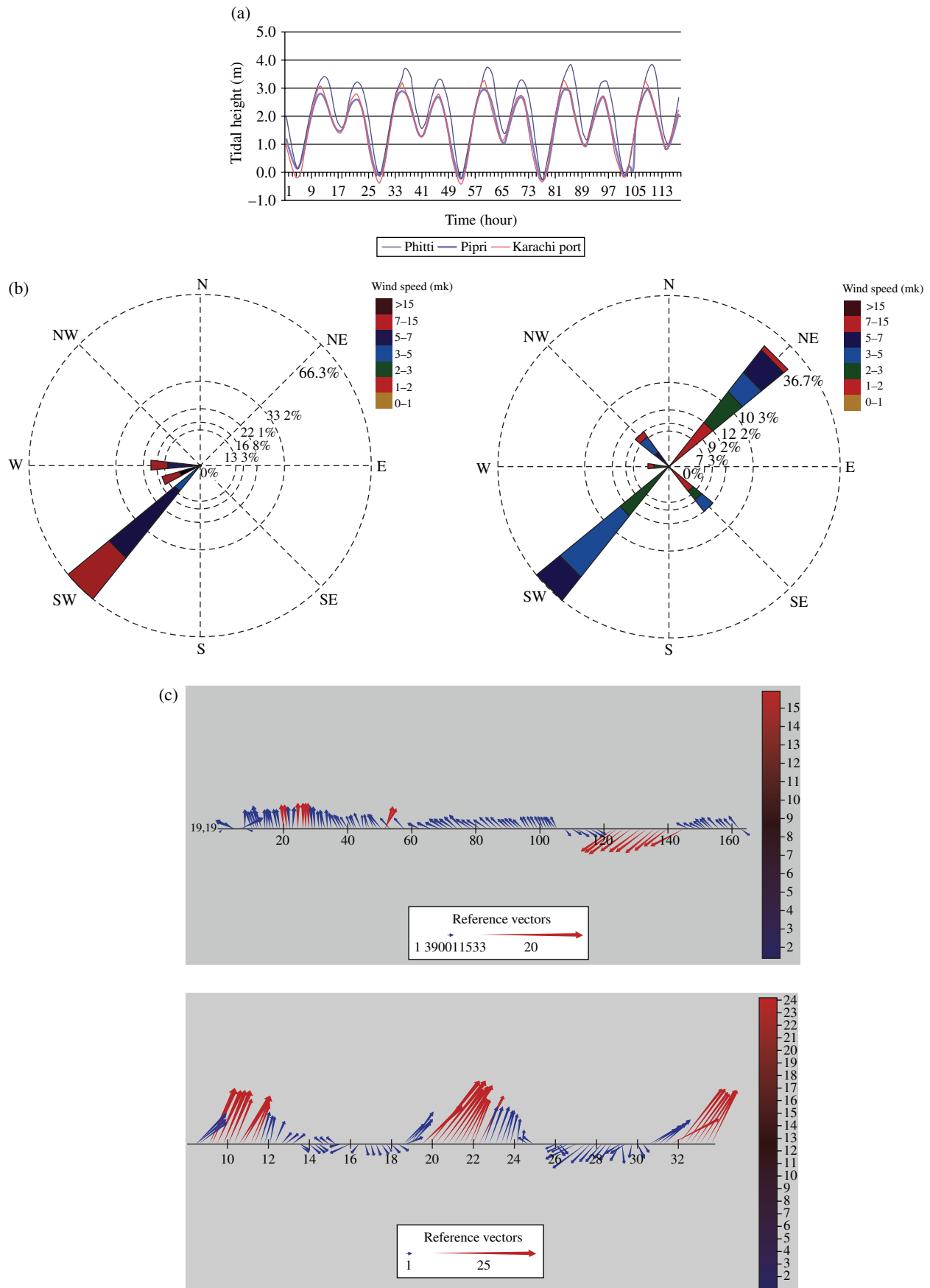


FIGURE 24.7 Wave climate conditions: (a) tidal behavior; (b) cumulative percentage of winds for Karachi Coast during summer (SW) monsoon and winter (NE) monsoon; (c) current pattern in December 2005 and March 2006.

currents, tides, and waves, the suspended and bed-load sediment transport was also modeled around the area of interest.

Different oil spill numerical models such as coastal circulation model, the Boussinesq wave model, the PEERS wave model (PWM), the bed-load sediment transport model, a suspended sediment transport model, and contaminated sediment transport model were used to simulate different processes (oil slick tracking) undergone by the *Tasman Spirit* oil spill at sea [9,10].

The results of the hydrodynamic model showed that wind-driven currents in the area of study ranged from 1 to 15 cm/s with the stronger currents confined in the shallow areas near Bundal Island southeast of the study area. The wind-driven currents showed slight amplification in the channel areas of Korangi and Phitti creeks. Strong tide-driven currents were simulated within these channels with depth-averaged values exceeding 50 cm/s. The effect of combined wind, tide, and river discharges showed even stronger currents within the channels and in the shallow areas. However, the influence of river discharges was found insignificant as far as the coastal circulation is concerned (current magnitude and direction).

For the simulation of short period waves, the PWM was applied using hourly wind data. This model includes the effect of tide and currents in the coastal areas with variable bathymetry and coastal geometry. The model results showed the propagation of high swells in the study area with wave heights ranging from 0.5 to 3.5 m.

The simulated suspended load showed that the shallow areas often experience elevated sediments concentrations that may exceed 50 mg/l with average values of about 20–25 mg/l. The shallow areas have relatively higher concentrations than the deeper areas. This is because of the stronger action of wind-generated waves and currents in shallow areas. It should be noted that the wind stress has a more dominating influence in shallow areas than in deep areas. As the resulting current-induced and wave-induced stress are higher in shallow areas, higher resuspension fluxes are expected in the shallow areas in front of Bundal Island and the adjacent shallow coastal areas to the northwest and southeast of the Korangi and Phitti River mouths.

Finally, using the simulated suspended-load and bed-load sediment transport, the model showed that contaminated sediments were redistributed to the south and southeast of the grounded tanker. The maximum oil polluted sediment layer of about 20 cm was shown by the model to be slowly dispersed by the currents and waves. The first year of the oil spill incident showed that the area and volume of contaminated sediments increased due to the combined dispersive effect of currents and waves. The thickness of the polluted sediment layer began to decrease months after the oil spill incident. Reduction of the polluted sediments layer to less than 8 cm in areas near the grounded tanker was simulated after a year by the end of 2005 (Fig. 24.8).

In terms of spatial extent, the polluted sediments initially occupied an area of about 54 km². About 4 months later, the simulated area of polluted sediments showed a maximum of 223 km² in April 2004. By the end of September 2005, the extent of contaminated sediments was reduced to 138 km².

On the other hand, the volume of contaminated sediments was simulated to be initially about 10.8 million cubic meters (MCM) in January 2004. At the end of January 2004, this was increased to about 17.7 MCM which was reduced to about 4.7 MCM by the end of September 2005 (Fig. 24.9).

Simulated reduction of polluted sediments is reasonable, it is possible however, that only the upper sediments could be cleansed by the combined action of currents and waves. It is postulated that the inner sediments below 10 cm may remain polluted until such time that extreme currents and waves during stormy conditions are able to erode, resuspend, and transport them away for the area. Cleansing of the upper sediments can be accelerated by bacterial action and seaweed absorption.

24.5 OIL MONITORING AND FATE

24.5.1 Oil Composition

The oil carried by *Tasman Spirit* was Iranian light crude oil with a measured density of 0.856 kg/l at 15°C, viscosity of 11 cP, low-energy dispersibility of 40%, and high-energy dispersibility of 80% by volume. It had 1.35% sulfur, about 5% alkanes, with 57% of aromatic hydrocarbons (AH) and 41% of resins and asphaltenes.

24.5.2 Spatial and Temporal Distribution in Seawater

Seawater samples collected at three depths (subsurface, mid depth, and bottom) from 10 stations in a circle around the broken ship, along the Clifton Coast, were analyzed for dissolved/dispersed petroleum aromatic hydrocarbons by UV fluorescence and for 16 individual polycyclic aromatic hydrocarbons (PAHs) compounds by Gas Chromatography-Flame Ionization Detector (GC-FID). Sampling was performed periodically in the year 2003, 2004, 2005, and 2006.

During August–December 2003, higher concentrations of total hydrocarbons were found with levels ranging from 8.2 to 26.4 µg/l (Σ 16 PAHs) and from 5.2 to 21 µg/l (Σ 16 AHs), respectively, in subsurface samples collected from the area around the incident location of the *Tasman Spirit* oil spill. Here the remaining oil spilled out for a longtime from broken oil tanks of the ship; however, in general, the different station transects exhibited decreasing gradients far away from the grounded ship and down through the water column and also with time (Fig. 24.10). The mean values of total oil content in the sea water samples declined from 0.93 l to 0.54 µg/l during 2006. There was a significant decrease in hydrocarbon concentration with distance from the *Tasman Spirit*. It is interesting to note that the higher values in this area

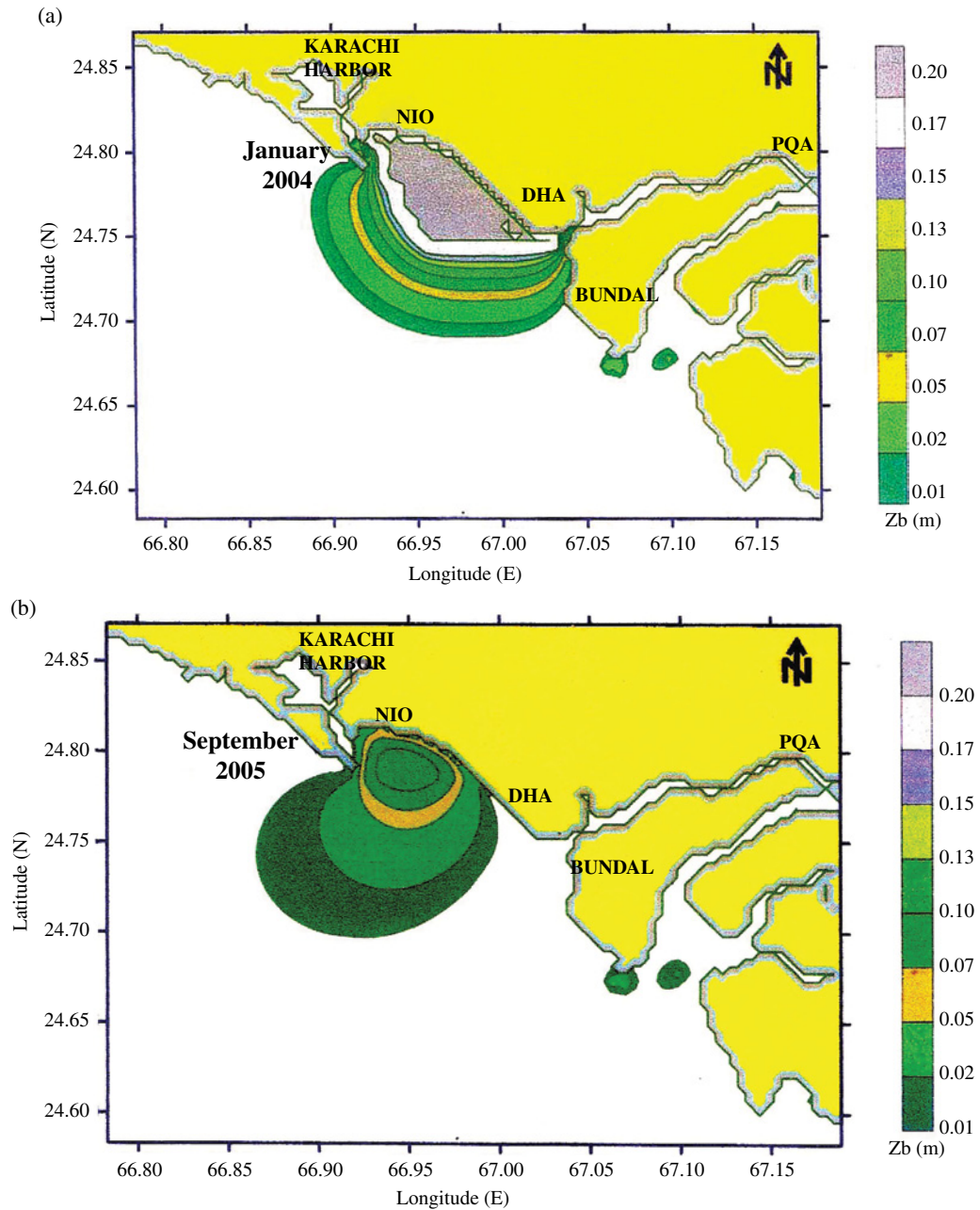


FIGURE 24.8 Simulated contaminated sediment layer: (m) (a) 2004 and (b) 2005.

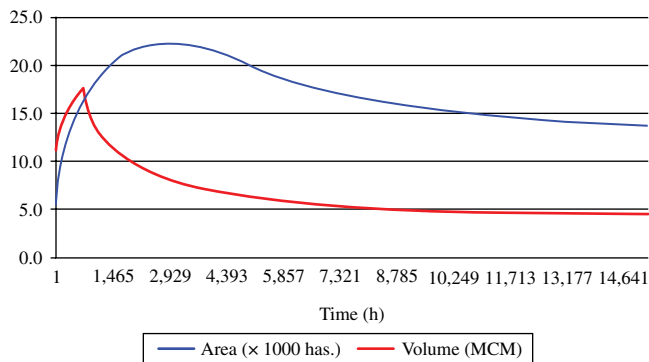


FIGURE 24.9 Simulated area and volume of polluted sediments of the coast.

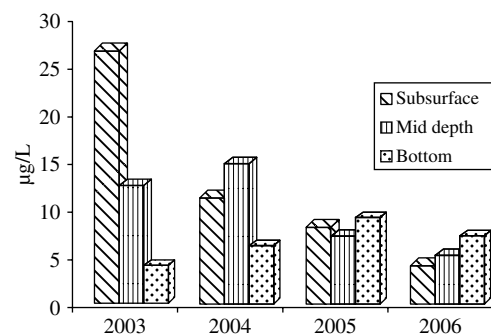


FIGURE 24.10 Temporal distribution of concentration of hydrocarbons (Σ PAHs & AHs, $\mu\text{g/l}$) in sea water.

were found near the bottom in November 2005, probably due to resuspension of the accumulated oil in sediments [11]. Findings in 2006 are similar to that of end of 2005.

24.5.3 Biota Affected by Oil Pollution

A sampling campaign was carried out throughout the project period of 3 years (2003–2006), including all available species of fish, shell fish, crabs, shrimps, molluscs, and echinoderms. Shell fishes compared to fish were found more contaminated because lobsters and bivalves are not migratory types; they are resident species of the environment. As recommended by International Conventions such as OSPAR Convention, Barcelona Convention, and Helsinki Convention, bivalves are useful bioindicators of chemical contamination for coastal pollution monitoring.

Concentrations of 16 PAHs were 2985 µg/g. Individual PAHs were in the range 0.001–602.2 µg/g, while total PAHs were found in the range 1.5–731.7 µg/g, which is well below the data presented from other parts of the world.

High levels of PAHs have been observed in all marine organisms, averaging from 0.02 to 139.3 µg/g, caught from oil impacted area after 28 months of spill comparative to the previous monitoring at the same site made after 18 months by TSOS-NRDA team ranging from 0.001 to 0.07 µg/g on average, as an evidence of bioaccumulation of PAHs; see Figure 24.11 [12]. Further studies are being carried out at PCSIR Laboratories to investigate whether more bioaccumulation or either depuration (decrease to background level) has occurred, as no background data was available for the contaminants.

Individual PAH distributions were dominated by naphthalene in fishes found at their highest concentration ranging between 0.04 and 602.2 µg/g among all PAHs accounting up to 45% of total PAHs, and this might be an indication of a recent petroleum input, followed by benzo(g,h,i)perylene and pyrene. Collectively in all fauna including shell fish, PAH distribution was dominated by benzo(g,h,i)perylene for upto 33% of total PAH concentration (Fig. 24.11). Overall PAH distribution is random, and low and high molecular weight PAHs were both found in fauna as two-ring and six-ring components were high in concentration, 999.98 and 1429.77 µg/g, respectively, which is consistent with a mixed petrogenic-pyrolytic origin.

The temporal profile shown in Figure 24.12 illustrates the situation of contamination in fauna from 2003 to 2006, showing the general pattern of bioaccumulation in the year 2004 with slight (negligible) decrease in 2005/2006.

24.5.4 Oil Content of Sediment

In case of sediments, aliphatic and aromatic fractions have been examined to assess the extent of hydrocarbon distribution which showed strong evidence of petrogenic input.

Total oil content in sediments was found up to 1600 µg/g in initial surveys. About 10–20 cm surface sediments layers around the grounded tanker and in an undetermined area within shallow coastal waters adjacent to Clifton Beach were affected by the crude oil; this thickness persisted for 4 months after the spill. Both aliphatic hydrocarbons (AH) and aromatic hydrocarbons (PAH) are often used to identify hydrocarbon sources. Origin of

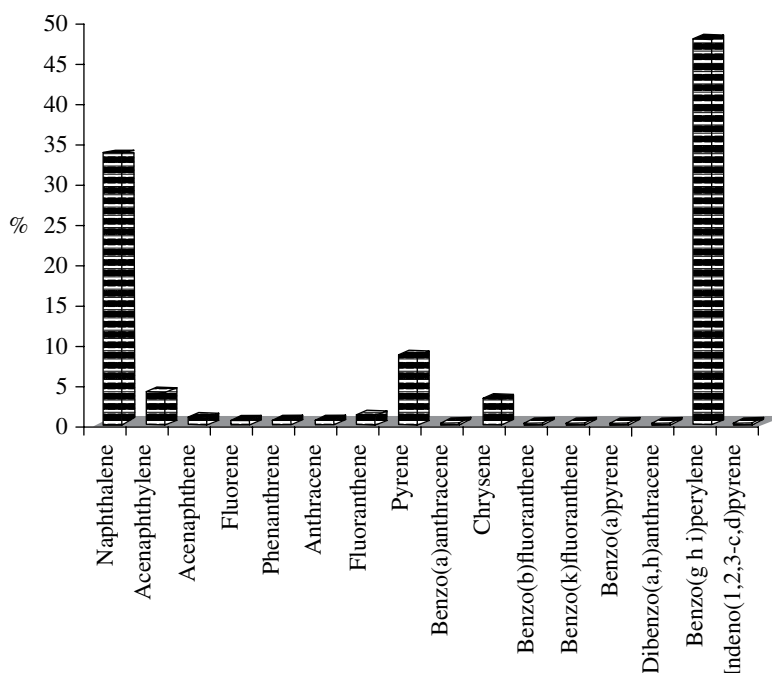


FIGURE 24.11 Average distribution of PAH in fauna.

aliphatic hydrocarbons can be petrogenic and biogenic while origin of PAHs can be pyrolytic; incomplete combustion of fossil fuels, petrogenic; discharge of petroleum and its products and biogenic; post depositional transformation of biogenic precursors. Terrestrial plant waxes, marine phytoplankton, volcanic eruption, biomass combustion, and natural oil seeps contribute to natural inputs of hydrocarbons [12,13].

Concentrations of aliphatic hydrocarbons (*n*-alkanes) ranging from C10 to C40 were 1–95 µg/g (dry weight) with the predominance of C25–C35 *n*-alkanes chains ensuring the evidence of petrogenic contamination. Further pristane/phytane ratio was also found lower than 1 which is a good indication of petroleum contamination [14].

Concentration of 16 PAHs was in the range 1.5–80 µg/g dw, much lower than the values reported for other areas of the world (Table 24.1) [13,15,16]. High levels of dibenzo(a,h)anthracene were found in the sediment samples at maximum range 5–55 µg/g accounting up to 41% of total PAHs concentration followed by phenanthrenes accounting about 20% of total PAHs concentration (Fig. 24.13). The average concentration of individual PAHs recorded were in the range of 0.2–20 µg/g except for dibenzo(a,h)anthracene having concentration values higher than the Effect Range Median value (44,792 ng/g = 44.792 µg/g), which may cause adverse effects on biological systems [17].

Phe/Ant and Flu/Pyr ratio values have been used to confirm the PAHs origin. Petroleum often contains more

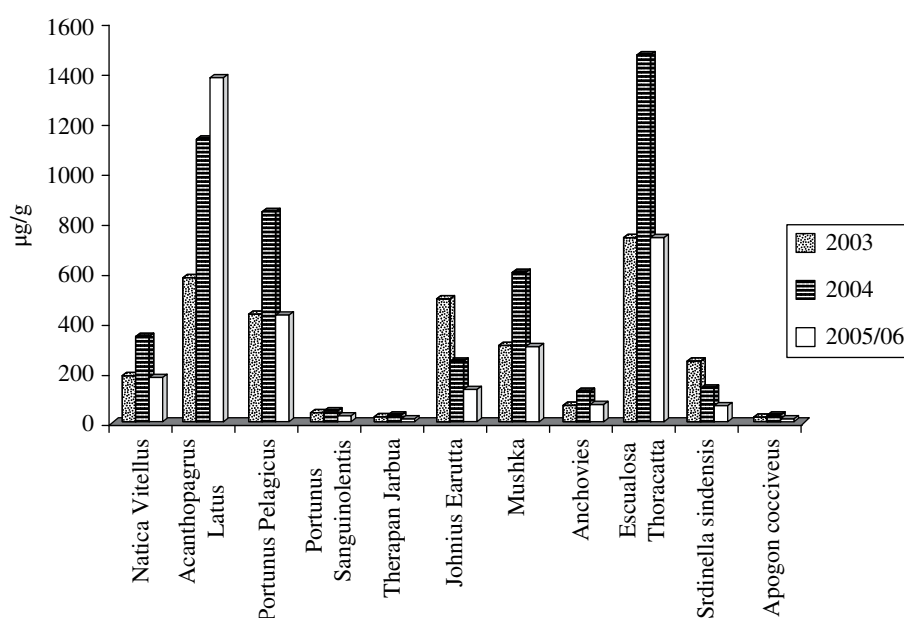


FIGURE 24.12 Temporal trends of total PAH concentration ($\Sigma 16$) in different groups of organisms.

TABLE 24.1 Worldwide concentrations of total hydrocarbons in sediments (ng/g dw)

Area	Total AHs	Total PAHs	References
Kuwait, Gulf	200		Fowler et al. (1993) ^a
Saudi Arabia, Gulf	900–23,000		Fowler et al. (1993)
Oman, Gulf	100–1200		Fowler et al. (1993)
Xiamen Harbor, China		2900–61,000	Hong et al. (1995) ^a
Saudi Arabia, Gulf	200–280	11,000–6,900,000	Readman et al. (1996) ^a
Kitimat Harbor, Canada		ND–10,000,000	Simpson et al. (1996) ^a
Lazaret Bay, France		1600–48,090	Benlahcen et al. (1997) ^a
Gironde estuary, France		622–4888	Budzinski et al. (1997) ^a
Crete, Eastern Mediterranean	100–900	500–5700	Gogou et al. (2000) ^a
Boston Harbor, USA		7300–358,000	Wang et al. (2001) ^a
Santander Bay, Spain		20–25,800	Viguri et al. (2002) ^a
Sochi, Black Sea, Russia	700–3400		Redman et al. (2002) ^a
Hsin-ta Harbor, Taiwan		1155–3382	Fang et al. (2003) ^a
Spanish northern continental shelf		22–47,528	Vinas et al. (2010) ^b
Northwestern Mediterranean			Tolosa et al. (1996) ^c

^aFull details found in Ref. 13.

^bFull details found in Ref. 15.

^cFull details found in Ref. 16.

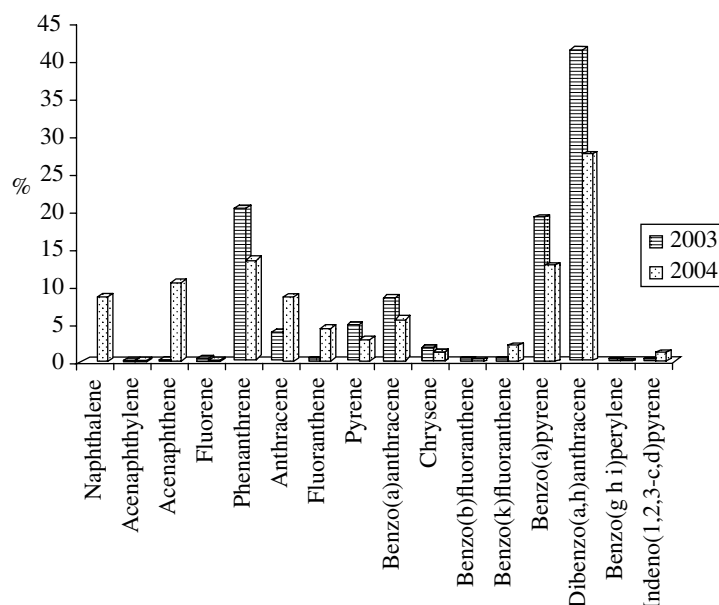


FIGURE 24.13 Average distribution of PAHs in sediment samples from the Clifton Coast.

phenanthrene relative to anthracene as phenanthrene is more a thermodynamically-stable tricyclic aromatic isomer than anthracene, so a Phe/Ant ratio is observed to be very high in PAH petrogenic pollution [18,19]. In sediment samples from Tasman Spirit oil spill affected area, Phe/Ant ratio was higher (>10) indicating the major inputs was petrogenic. As Budzinski et al. suggested sediments with Phe/Ant greater than 10 were mainly contaminated by petrogenic inputs and Phe/Ant less than 10 was typical of pyrolytic sources [20]. Further, a ratio of fluoranthene/pyrene (Flu/Pyr) less than 1 also confirms the contamination to be petrogenic [14].

24.6 EFFECTS OF OIL IMPACT AT THE COMMUNITY LEVEL

24.6.1 The Effects on the Benthic System

The growth of seaweed in Pakistan is seasonal; during the summer period, there is actually no growth and shores are barren without any algae. However, with the onset of the NE monsoonal season (winter), the algae begin appearing and by December and January they establish themselves, covering the entire rocky shore with their luxuriant growth [21–23]. After the spill, overall damage to seaweed occurred due to physical contact with oil, growth in highly oiled areas decreased but as the oil was removed the growth of *Enteromorpha* sp. *Ulva* sp. increased due to more nitrogen availability. The damage to seaweed is the damage to biologically structured communities associated with seaweed including nursery habitat for animals [24,25].

The main dominant group among seaweed was *Sargassum* species that also plays an important role in controlling marine pollution and abatement of pests' activities. Several species of *Sargassum* are known to accumulate toxic heavy metal from the polluted seawater and render it clean for use

by marine organisms apart from acting as primary producers and supporting a wide variety of epifaunal communities [24]. Thus (*S. tenerrimum*, *S. wightii*, *S. johnstonii*, etc.) they serve as biofilters to prevent the coasts from the land-based pollution [26]. All the polluted and nonpolluted stations showed heavy growth of *Sargassum* and *Ulva* species.

The effect of oil itself on the benthic organisms was impossible to access because of the absence of historical data with which it could be compared, and because of the large number of activities that started just after the spill-like dredging for reclamation and for cleaning purposes, overwhelming effects of toxic dispersants applied to the shores, changes and coastal development activities from recreational point of view have drastically changed the benthic communities of this area and they need much longer time than was initially anticipated to start recolonization in their natural habitat.

24.6.1.1 Intertidal Zone The coastal area affected by *Tasman Spirit* oil spill has a history of supporting large colonies of suspension feeders (oysters, mussels, and cockles). They often make up a large proportion of the animals that live in and on the seabed and affect exchanges between the water column and the seabed (such as nutrients and sediment) oyster rocks, and unfortunately oil spillage took place very close to oyster community.

The oil pollution not only decreased the growth rate and inhibited photosynthesis but the diversity of organisms was also badly affected and overall biomass was found to be very low. In samples of intertidal region, a clear difference in the type and diversity of species was observed in the spilled areas when compared with previous studies, which showed complete dominance of large centric diatoms, for example, *Coscinodiscus* sp. and *Shroederella* sp. and *Ditylium* sp.

Oil spills have exerted varied, slight to moderate effects on intertidal organisms, and thus perturbed communities have recovered within a few years. This resistance and

resilience are due to the hardness of intertidal organisms, their rapid reproduction, and the relatively rapid removal of oil from the intertidal zone by waves.

24.6.1.2 Subtidal Zone Mussels are identified as the hydrocarbon vector in the nearshore predator population. In subtidal sediment macro-faunal communities are relatively protected from contact with oil which usually floats but it is sufficient to effect faunal assemblages even in subtidal regions. Intertidal species are more vulnerable than subtidal species, and open water fisheries are not as vulnerable as inshore subtidal fisheries. Nekto-benthos was mostly found to be dominated by flat fishes and crabs. Flat fishes when compared with the earlier studies immediately after the spill, showed drastic decreases in numbers as well as type of specie present. *P. sanguinolentus* was found to be the most adaptable and resistant species of crabs which survived this disaster and remain dominant in the area. Fishes like mullets, gizzard shads, many flat fishes, skates, and rays prefer to live on soft bottom and feed on bottom detritus. These fishes were either absent or were in less number compared to crabs.

The low percentage of flat fishes in coastal waters and decreases in number of Mugil fish from coastal stations which were their natural habitat, clearly reflects the damage caused by the oil spill. Similarly among crustaceans, decreases in number of shrimps and high percentage of opportunistic and hardy species of crabs like *P. sanguinolentus* at all stations indicate the major shift of crustacean community from this area. Mostly the macro benthic communities are dominated by polychaete community occupying more the 80% of total faunal assemblage both in polluted and nonpolluted area, Crustacean fauna was next dominate group found in these samples from the subtidal region but its percentage never exceeds more than 40% (Fig. 24.14).

The catastrophic effects of Tasman Spirit crude oil on subtidal benthos in the Clifton area have caused massive kills of large numbers of dead bottom animals, including lobsters, stomatopods, star fishes, and bivalves were washed ashore. Evidence indicated that the oil pollution spread only in the shallow areas and deeper areas were free from oil.

In present situation, just after the spill, the proliferation of seaweed was an indication of beginning of recolonization process. It will take time as naturally a rule of succession in marine organisms is followed; this is the only way that the system can be brought back to normal. But recovery through succession may still take several years and it is not necessary that same species will occur again and establish their habitat. There is more than a 50% chance that opportunistic species with more resistance and adaptability for the present situation will come as permanent residents.

24.6.2 The Effects on the Pelagic System

24.6.2.1 Zooplankton Overall diversity among the zooplankton community was also greatly affected by the presence of weathered oil fractions in sediments close to the

shore. The main polluted stations showed complete dominance of different crab species as compared to the nonpolluted station where different fish types were observed and total number of animals per catch was much greater than catches at polluted stations. As the fish community due to its strong mobility avoids polluted areas and moves away from them, crustaceans like crabs are not so mobile and they are considered as highly resistant species. The stations slightly away from the affected area and comparatively nonpolluted contained a small population of fish which was low in number and poor in diversity in the catch of 2006 (Fig. 24.15).

Mullets from Mugilidae family are a common fish inhabiting coastal marine waters and estuaries and are the most commonly found fish throughout the coastal belt. This family was completely absent from the spill-affected areas; not a single station showed the presence of these species. While the handbook of fisheries statistics of Pakistan reports its average catch of about 16,955 tons for the years 1993–1999.

Cynoglossidae, *Soleidae*, and *Bothidae* were the only groups of fish found commonly in bottom trawl samples in 2005 and 2006 in small numbers. But immediately after the spill in 2003, these were present in large numbers in trawl catches.

Nemipteridae, *Parascolopsis eriomma*, large specimens of these species, were observed when collection was done just after the spill in 2003, but in next 2 years, these were found in very small numbers. Only juveniles were caught in one trawl and they were completely absent from other trawls.

Portunidae family dominated the fish trawl samples of coastal stations of shallow depth. Mostly *P. sanguinolentus* was observed in large numbers than other species. It was found covered with oil especially, egg masses attached to female fishes were black in color due to oil deposition when collected just after the spill, but these not only managed to maintain their biomasses rather they increased twofold greater than before.

The Penaeidae family contains the greatest number of commercially important species of shrimps in Pakistan. Just after the spill, shrimp were found in low number, but in 2005 and 2006 their number has increased, may be due to proximity of mangrove area that usually supports the growth of shrimps.

24.6.2.2 Phytoplankton Phytoplankton community showed a similar trend for centric, pinnate, and dinoflagellates, that is, high diversity at nonpolluted stations and low at polluted stations. Tintinnids followed the same pattern as that of phytoplankton. Overall data showed lower biomass of centric diatoms. While after spill these stations showed dominance of small centric or pinnate diatoms and presence of other groups in distinct percentages. Dinoflagellates and large number of tintinnids were also observed (Fig. 24.16).

According to an estimate, early developmental stages can be especially vulnerable to hydrocarbon exposure, and recruitment failure in chronically contaminated habitats may be related to direct toxic effects of hydrocarbons

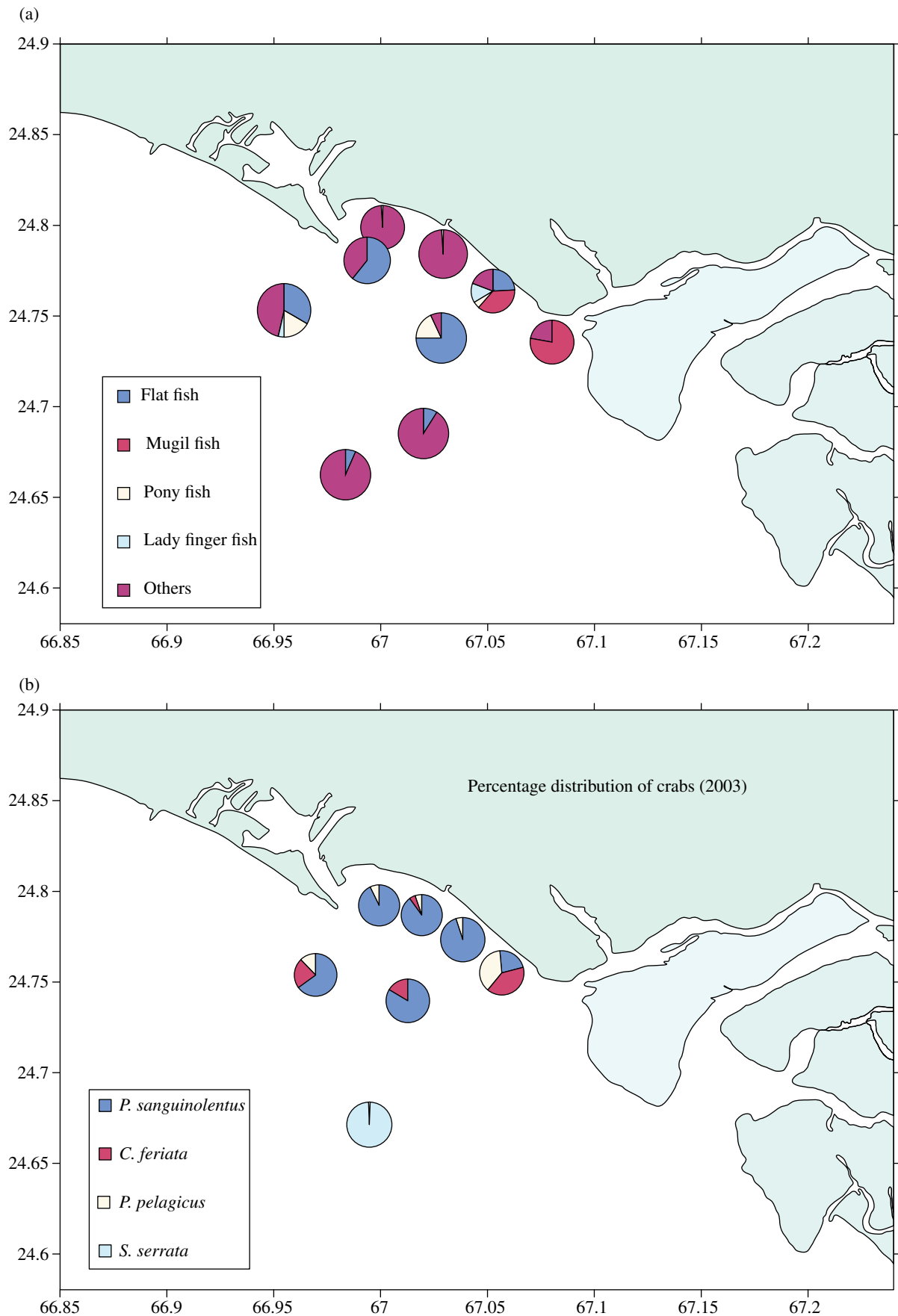


FIGURE 24.14 Percentage composition of (a) flat fishes and (b) crab community.

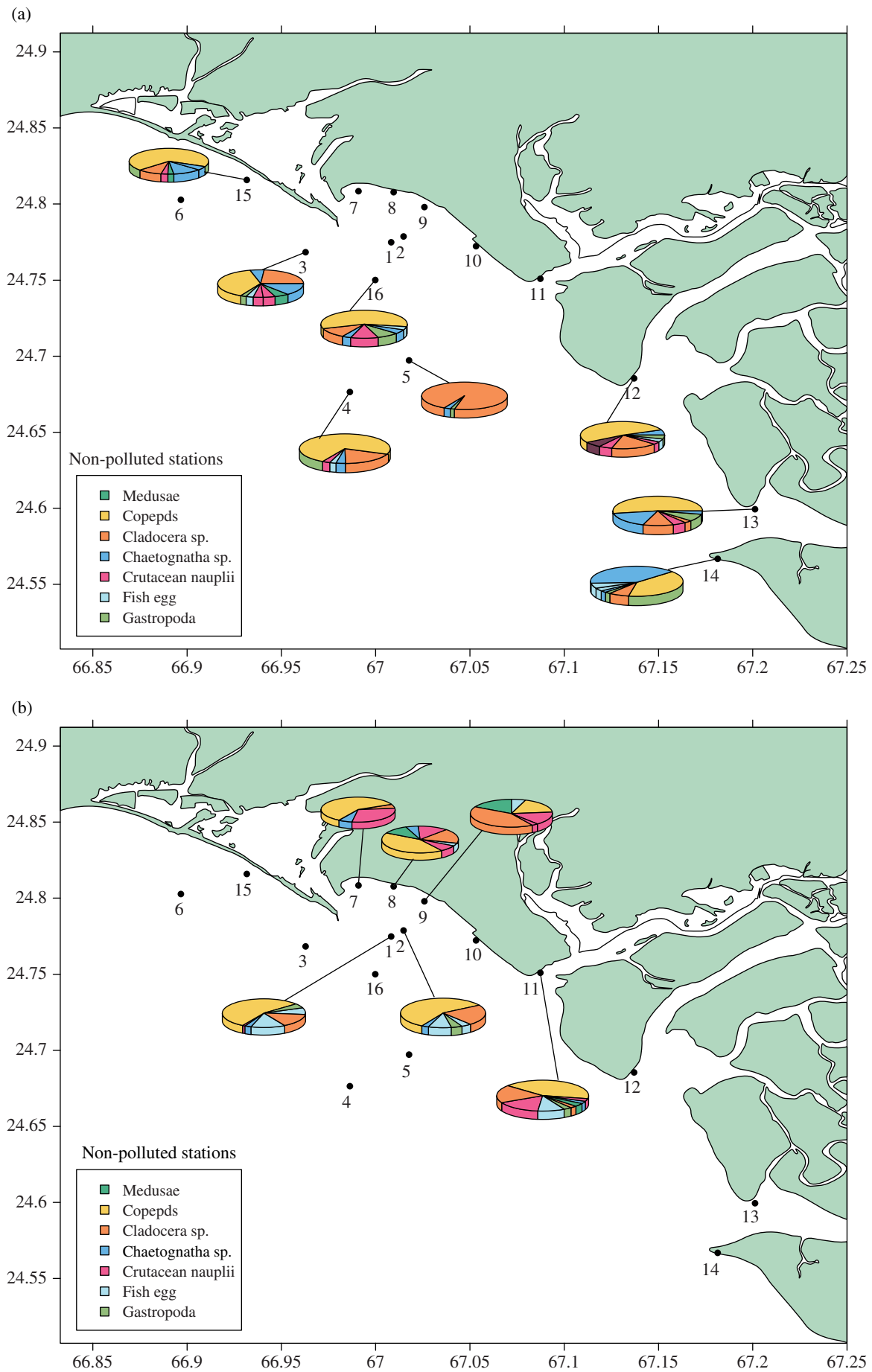


FIGURE 24.15 Percentage composition of zooplankton at (a) nonpolluted and (b) polluted stations.

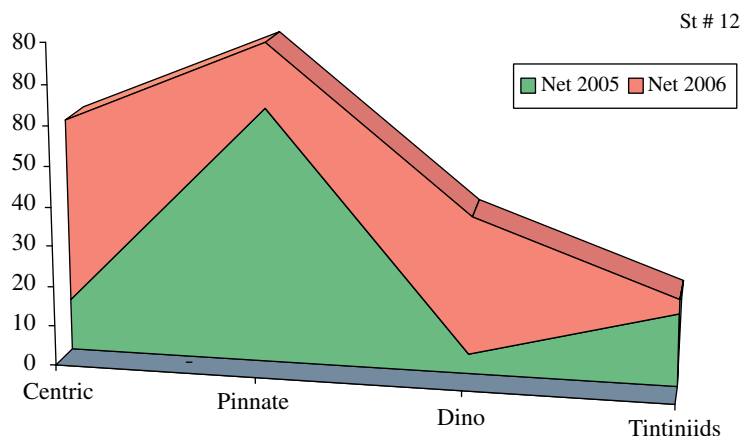


FIGURE 24.16 Percentage distribution of phytoplankton biomass.

contaminated sediments. When the *Tasman Spirit* oil spill occurred in the coastal waters of Clifton Karachi, it was the pre-NE monsoonal period during which pelagic larval stages of fish species were developing near the sea surface, many or most of these larvae died, fish eggs were completely absent from polluted stations and at nonpolluted stations were present in very low percentage.

24.7 BIOREMEDIATION/NATURAL ATTENUATION PROCESSES

Several bacterial strains detected and isolated from oil contaminated soil, belong to *Pseudomonas aeruginosa*, *Pseudomonas stutzeri*, and *Bacillus subtilis*.

Two different microbial consortia were tested in field and laboratory for biodegradation of hydrocarbons. It is known that nutrients enhance the growth of degrading microorganisms and their microbial activity for bioremediation of oil contaminated environments. After TSOS, various field bioremediation assays have been carried out which proved urea to be the most appropriate nutrient for oil removal. It enhanced biodegradation rates up to 100%. But at some sites, addition of fertilizer did not increase the oil degradation rate or even reduced the biodegradation rate; this might be due to high carbon content or imbalance nutrient level in soil also because that site may require longer time period and reinoculation of culture for decontamination.

Treatment with both consortia revealed significant loss of *n*-hexane and *n*-octane.

While quantitative analysis of samples revealed that degradation of naphthalene, acenaphthalene, fluorene, phenanthrene, and anthracene with the help of added consortia were found to be slow in comparison to the other PAHs like pyrene, benz(a)anthracene, chrysene, benzo(b)fluoranthene, benzo(a)pyrene, etc. Subsequent sampling may reveal their complete removal due to bacterial activity.

24.8 CONCLUSIONS

The overall conclusion by these studies is that the oil spill exerted slight to moderate effects on the marine environment. Effects on biotic and abiotic compartments were destructive; however, it was temporary and recovery occurred in the next 2 years. Although bioaccumulation of PAHs was observed, this was not clear which could be more precisely seen by further study of the area as background data was not available for the affected areas. Temporal variation of hydrocarbons in seawater and sediments showed a gradual decreasing trend either by weathering effects or by natural degradation processes. Numerical models for sediment transport also showed reduction in contaminated sediment layers in 1 year after the spill.

Present findings suggest for regular monitoring of fisheries for decrease and increase in hydrocarbon level and studies should be focused on determining the effects of oil on fish reproduction and physiological changes, crab spawning mainly for those species of commercial interest, and further effect on food chain. And strict improvements in existing environmental legislation should be made to cover all aspects of pollution control management, within the country.

ACKNOWLEDGMENTS

Authors wish to thank Ministry of Science and Technology (MoST), Pakistan, for approval and funding this project, and to project directors, coproject directors, and project associates as well. All mentioned and unmentioned agencies, organizations, institutions, departments, and individual personnel who made effort for managing and controlling this crises in any way are really appreciated for their technical and nontechnical assistance.

Authors are specially thankful for courtesy of Dr. Tariq Masood Khan, Dr. Hina Saeed Baig, and Dr. Nuzhat Ahmed

for physical, biological, and bioremediation sections of the chapter; without these sections, chapter on an oil spill would may remain incomplete.

REFERENCES

- [1] Parker, H. Tasman Spirit: The incident and response—A technical perspective. PAJ International Oil Spill Symposium, *New Dimensions in Oil Spill Response After the PRESTIGE-Compensation and Response Technology*, Tokyo, Japan, 4 pp, 2004.
- [2] Baig, M.A.A. Ecological impact of the Tasman Spirit oil spill, DAWN sciences. http://cmsdata.iucn.org/downloads/sindh_soed.pdf, July 2010. Accessed February 7, 2004.
- [3] Tasman Spirit. http://www.cedre.fr/en/spill/tasman_spirit/tasman_spirit.php, September 2010. Accessed August 14, 2014.
- [4] Tasman Spirit. <http://www.smit.com/sitefactor/page.asp?pageid=694>, September 2010. Accessed August 14, 2014.
- [5] Jilani, R. and M. Haq. Monitoring disasters in Pakistan using satellite data. Space & Atmospheric Science Division, *Pakistan Space and Upper Atmosphere Research Commission (SUPARCO)*. http://www.isnet.org.pk/downloadables/remote_sensing_applications2.pdf. Accessed July, 2013.
- [6] Alrai, M.I.S. and S.H.N. Rizvi. Natural resource damage assessment programme for Tasman Spirit oil spill in Pakistan, *International Oil Spill Conference*, Karachi, Pakistan, 4 pp, 2005.
- [7] Janjua, N.Z., P.M. Kasi, H. Nawaz, S.Z. Farooqui, U.B. Khuwaja, Najam-ul-Hassan, S.N. Jafri, S.A. Lutfi, M.M. Kadir, and N. Sathiakumar. Acute health effects of the Tasman Spirit oil spill on residents of Karachi, Pakistan. *BMC Public Health*, 6, 84, 2006.
- [8] Meo, S.A., A.M. Al-Drees, I.M.U. Meo, and M.M. Al-Saadi. Lung function in subjects exposed to crude oil spill into sea water. *Marine Pollution Bulletin*, 56, 88, 2008.
- [9] Rivera, PC. A highly accurate and efficient environmental pollution prediction method based on PEERS pollution model (PPM). *PEERS technical report No. 3*, 2002.
- [10] Rivera, PC. Development and application of the PEERS wave-current model (PWM) for realistic prediction of coastal wave propagation and transformation. *PEERS technical report No. 2*, 2001.
- [11] Munshi, A.B., F.A. Ansari, H.A. Siddiqi and M. Zeeshan. Distribution of petroleum hydrocarbons in coastal/deep sea sediments along the Clifton Beach after Tasman Spirit oil spill. *Pakistan Journal of Scientific and Industrial Research. Series A: Physical Sciences*, 54 (2), 90–97, 2011.
- [12] Siddiqi, H.A., F.A. Ansari, and A.B. Munshi. Assessment of hydrocarbons concentration in marine fauna due to Tasman Spirit oil spill along the Clifton Beach at Karachi Coast. *Environmental Monitoring and Assessment*, 148, 139, 2009.
- [13] El Nemr, A., A. Khaled, A. El-Sikaily, T.O. Said, and A.M.A. Abd-Allah. Distribution and sources of polycyclic aromatic hydrocarbons in surface sediments of the Suez Gulf. *Environmental Monitoring and Assessment*, 111(1–3), 333–358, 2005.
- [14] El Nemr, A., T.O. Said, A. Khaled, A. El-Sikaily, and A.M.A. Abd-Allah. The distribution and sources of polycyclic aromatic hydrocarbons in surface sediments along the Egyptian Mediterranean coast. *Environmental Monitoring and Assessment*, 124, 343, 2007.
- [15] Vinas, L, M.A. Franco, J.A. Soriano, J. José González, J. Pon, and J. Albaigés. Sources and distribution of polycyclic aromatic hydrocarbons in sediments from the Spanish northern continental shelf. Assessment of spatial and temporal trends. *Environmental Pollution*, 158 (5), 1551–1560, 2010.
- [16] Tolosa, I, J.M. Bayona, and J. Albaigés. Aliphatic and polycyclic aromatic hydrocarbons and sulfur/oxygen derivatives in northwestern Mediterranean sediments: Spatial and temporal variability, fluxes, and budgets. *Environmental Science and Technology*, 30, 2495–2503, 1996.
- [17] Long, E.R., D.D. MacDonald, S.L. Smith, and F.D. Calder. Incidence of adverse biological effects within ranges of chemical concentrations in marine and estuarine sediments. *Environmental Management*, 19, 81, 1995.
- [18] Gschwend, P.M. and R.A. Hites. Fluxes of polycyclic aromatic hydrocarbons to marine and lacustrine sediments in the northeastern United States. *Geochimica et Cosmochimica Acta*, 45, 2359, 1981.
- [19] Soclo, H.H., P.H. Garrigues, and M. Ewald. Origin of polycyclic aromatic hydrocarbons (PAHs) in coastal marine sediments: Case studies in Cotonou (Benin) and Aquitaine (France) areas. *Marine Pollution Bulletin*, 40, 387, 2000.
- [20] Budzinski, H., I. Jones, J. Bellocq, C. Pierard, and P. Garrigues. Evaluation of sediment contamination by polycyclic aromatic hydrocarbons in the Gironde estuary. *Marine Chemistry*, 58, 85, 1997.
- [21] Dar, A., H.S. Baig, S.M. Saifullah, V.U. Ahmed, S. Yasmeen, and M. Nizamuddin. Effect of seasonal variation on the anti-inflammatory activity of Sargassum wightii (Greville) J. Agardh extracts from Northern Arabian Sea. *Journal of Experimental Marine Biology and Ecology*, 351, 1–9, 2005.
- [22] Baig, H.S. and I. Zehra. Seasonal variation in sessile and mobile epifauna associated with brown seaweed form rocky shores of Pakistan. *Pakistan Journal of Oceanography*, 2, 1, 2005.
- [23] Baig, H.S. Pharmacological activity of Sargassum and study of associated harmful dinoflagellate in the coastal waters of Pakistan. Thesis published, University of Karachi, Karachi, Pakistan, 2004.
- [24] Baig, H.S., N. Khurshid, and S. Ishaq. Base-line ecological studies of coastal communities of Hingol National Park, Park report, Karachi, Pakistan, 2006.
- [25] Zehra, I., S. Shaukat, and H.S. Baig. Diversity of Algal Associated Epifaunal Communities from the Northern Arabian Sea. In *Proceedings of the Pakistan US Conference*, Karachi, Pakistan, 87, 1995.
- [26] Baig, H.S., S. Yasmeen, A. Dar, and S.M. Saifullah. Preliminary study of analgesic activity of extracts of two Sargassum species collected in different seasons from coastal areas of Pakistan. *International Centre for Chemical Sciences (ICCS)*, University of Karachi, Karachi, Pakistan, poster-123, 2002.

PART XIII

APPENDICES

APPENDIX A

THE OIL PROPERTIES DATA APPENDIX

BRUCE P. HOLLEBONE

Emergencies Science and Technology Section (ESTS), Environment Canada, Ottawa, Ontario, Canada

This appendix provides important oil property data on many common oils. Most of the data is from the Environment Canada website and the Environment Canada laboratory on oil properties. Methodologies and data comparisons are given in my article on oil properties in the forepart of this book.

Each data item is on a standard format, whether or not all data on that type of oil are available. This should aid in seeking and comparing data.

A brief description of each data point follows:

Evaporation Equation: This is an empirical data equation that follows either a natural logarithm with time (\ln) or a square root of time (for diesel fuel or similar materials). This equation is true for oil thicknesses about 1.5 mm or less. Since this is typical for oils spilled at sea and thicker oils are rare at sea, correction may not be required. A correction for oils thicker than 1.5 mm has been measured and is given in the paper by M. Fingas in the forepart of this book.

API Gravity: API gravity is based on the density of pure water which has an arbitrarily assigned API gravity value of 10°. Oils with progressively lower specific gravities have higher API gravities. The following is the formula for calculating API gravity: $\text{API gravity} = [141.5 \div (\text{density at } 15.5^\circ\text{C (60}^\circ\text{F)})] - 131.5$. Oils with high densities have low API gravities and vice versa.

Weathering by Percent: There are three or four columns in each listing showing the weathering of the oil by percent by mass loss. This is important as the properties of the oils change significantly as the oil loses components by evaporation.

Density: Density is the mass (weight) of a given volume of oil and is typically expressed in grams per cubic centimeter

or per milliliter (g/cm^3 or g/ml). It is the property used by the petroleum industry to define light or heavy crude oils. Density is also important as it indicates whether a particular oil will float or sink in water. As the density of water is 1.0 g/cm^3 at 15°C and the density of most oils ranges from 0.7 to 0.99 g/cm^3 , most oils will float on water. As the density of seawater is 1.03 g/cm^3 , even heavier oils will usually float on it. The density of oil increases with time of exposure, as the light fractions evaporate.

Viscosity: Viscosity is the resistance to flow in a liquid. The lower the viscosity, the more readily the liquid flows. For example, water has a low viscosity and flows readily, whereas peanut butter, with a high viscosity, flows poorly. The viscosity of the oil is largely determined by the amount of lighter and heavier fractions that it contains. The greater the percentage of smaller molecules and the lesser the amount of macromolecules such as asphaltenes, the lower the viscosity. As with other physical properties, viscosity is affected by temperature, with a lower temperature giving a higher viscosity. For most oils, the viscosity varies as the logarithm of the temperature, which is a very significant variation. Oils that flow readily at high temperatures can become a slow—moving, viscous mass at low temperatures. In terms of oil spill cleanup, viscosity can affect the oil's behaviour. Viscous oils do not spread rapidly, do not disperse in water readily, do not penetrate soil as readily, and affect the ability of pumps and skimmers to handle the oil.

Flash Point: The flash point of an oil is the temperature at which the liquid gives off sufficient vapors to ignite upon exposure to an open flame. A liquid is considered to be flammable if its flash point is less than 60°C . There is a broad

range of flash points for oils and petroleum products, many of which are considered flammable, especially when fresh. Gasoline, which is flammable under all ambient conditions, poses a serious hazard when spilled. Many fresh crude oils have an abundance of volatile components and may be flammable for as long as 1 day until the more volatile components have evaporated. On the other hand, Bunker C and heavy crude oils typically are not flammable when spilled.

Sulfur Content: This is the mass fraction of sulfur in the oil. Sulfur content is undesirable as it causes problems in refining processes.

Pour Point: The pour point of an oil is the temperature at which it takes longer than a specified time to flow in a standard measuring vessel. As oils are made up of hundreds of compounds, some of which may still be liquid at the pour point, the pour point is not the temperature at which the oil is a solid mass. The nature of some components within the oil, such as waxes, to separate and form a solid surface layer, or crust, can create a situation in which the bulk oil will flow at temperatures below the measured pour point, yet will not flow under the conditions of the test. Pour point has limited use as an indicator of the state of the oil. In the past, this measurement has been overused as a parameter to predict oil behavior in the environment, such as spreading and evaporation.

Surface Tension: Surface tension or the oil/air interfacial tension is the force of attraction or repulsion between the surface molecules of oil and air.

Interfacial Tension Sea Water or Fresh Water: The oil/water interfacial tension is the force of attraction or repulsion between the surface molecules of oil and water. Together with viscosity, surface tension is an indication of how rapidly and to what extent an oil will spread on water. The lower the interfacial tension with water, the greater the extent of spreading. In actual practice, the interfacial tension must be considered along with the viscosity because it has been found that interfacial tension alone does not account for spreading behavior.

Adhesion: The measured quantity of oil adhering to a given surface area.

SARA Content:

Saturates: The saturate group of components in oils consists primarily of alkanes, which are compounds of hydrogen and carbon with the maximum number of hydrogen atoms around each carbon. Thus, the term “saturate” is used because the carbons are “saturated” with hydrogen. The saturate group also includes cyclo-alkanes, which are compounds made up of the same carbon and hydrogen constituents, but with the carbon atoms bonded to each other in rings or circles. Larger saturate compounds are often referred to as “waxes.”

Aromatics: The aromatic compounds include at least one benzene ring of six carbons. Three double carbon-to-carbon

bonds float around the ring and add stability. Because of this stability, aromatic rings are very persistent and can have toxic effects on the environment. The most common smaller and more volatile compounds found in oil are often referred to as BTEX, or benzene, toluene, ethyl-benzene, and xylenes. Polyaromatic hydrocarbons or PAHs are compounds consisting of at least two benzene rings. PAHs make up between 0 and 60% of the composition of oil.

Resins: In the petroleum industry, the smallest polar compounds are called “resins.” Polar compounds are those that have a significant molecular charge as a result of bonding with atoms such as sulfur, nitrogen, or oxygen, known collectively as heteroatoms. The “polarity” or charge that the molecule carries results in behavior that may be different than that of unpolarized compounds.

Asphaltenes: The larger compound fraction of polar compounds. Asphaltenes are large, relatively unknown compounds typically containing several aromatic rings, heteroatoms, and hydrocarbon chains. The more asphaltenes in a oil, the more viscous and the more prone to form water-in-oil emulsions.

Waxes: A subgroup of saturate compounds. The waxes are the straight-chain alkanes from a carbon number of 20 and above. They are important in that they can precipitate out of an oil solution, interact as a group to form a crust or internal matrix, and alter the interfacial properties of the oil, which can significantly affect oil behavior.

Emulsion Formation:

Type: The type of water-in-oil emulsion formed. This includes “does not form” or unstable; meso-stable, stable, and entrained.

Water Content: The measured water content in mass percent of that type of emulsion formed in the laboratory.

Viscosity: The viscosity of the water-in-oil product formed in the laboratory.

Chemical Dispersibility with Corexit 9500: The percent dispersion of the oil with the dispersant Corexit 9500 using the ASTM F-2059 procedure.

Distillation Data: Distillation fractions of an oil represent the fraction, here given by mass, of an oil that is boiled off at a given temperature. This data is obtained on most crude oils so that oil companies can adjust parameters in their refineries to handle the oil. This data also provides environmentalists with useful insights into the chemical composition of oils. For example, while 70% of gasoline will boil off at 100°C, only about 5% of a crude oil will boil off at that temperature and an even smaller amount of a typical Bunker C. The distillation fractions correlate strongly to the composition as well as to other physical properties of the oil.

Cross-Index of the Oils

Algeria	Saharan Blend
Angola	Lago, Lucula, Malongo, Takula
ASMB	Alberta Sweet Mixed Blend
Australia	Barrow Island, Thevenard Island
Automotive Gas Oil	Diesel
Bunker C	Bunker C, Heavy Fuel Oil
China	Taching
Colombia	Cano Limon, Cusiana, Vasconia
Cook Inlet	Endicott, Granite Point, Swanson River
Ecuador	Oriente
FCC	Fluid Catalytic Cracker
Furnace Oil	Fuel Oil no. 2
Hydraulic	Lubricating oil (hydraulic)
Indonesia	Sumatran, Udang
Isopar	IPAR
Kuwait	Hout, Kuwait
Malaysia	Tapis
Marinus	Lubricating oil (turbine)
Mexico	Isthmus, Maya
Motor Oil	Lubricating oil
Newfoundland	Avalon, Hebron, Hibernia, Terra Nova, White Rose
North Sea	Brent, Ninian
North Slope	Alaska, Prudhoe Bay
Northern Pipeline	Alaska North Slope
Norway	Ekofisk, Gullfaks, Heirdrun, Oseberg, Statfjord, Troll
Nova Scotia	Cohasset, Panuke, Sable Island
Russia	Condensate, Scotia light
Sakhalin	Chavyo, Odoptu, Sakhalin
Southern Pipeline	Alaska North Slope
Spartan	Lubricating oil (industrial)
Teresso	Lubricating oil (industrial)
Venezuela	Lago Treco, Lagomedio, Orimulsion
Voltesso 35	Electrical insulating oil
Zaire	Zaire

Oil name**Alaska North Slope 2010****Origin and description**

Alaska North Slope crude oil

Evaporation equation

$$\%Ev = (2.58 + 0.045T)\ln t$$

Where Ev = weight percent evaporated, T = surface temperature (°C), t = time (min)

API gravity

31.56

Weathering % by weight

(all units at 15°C)

Units**Density**

g/ml

Viscosity

mPa·s or cP

(dynamic—values at 15°C)

Flash point

°C

Sulfur content

%

Pour point

°C

Surface tension

mN/m

(air–oil at 15°C)

IFT sea water

mN/m

IFT fresh water

mN/m

Adhesiong/m³**SARA content (saturate, aromatic, resin, asphaltene) %****Saturate**

%

Aromatic

%

Resin

%

Asphaltene

%

Waxes

%

Emulsion formation (type formed and water content %)**Type****Water content**

%

Viscosity

mPa·s or cP

Chemical dispersibility with Corexit 9500

%

Distillation data (% at temperature)

Boiling point (°C)

40

60

80

100

120

140

160

180

200

250

300

400

500

600

700

Oil name Alaska North Slope (Middle Pipeline)
Origin and description Alaska, USA; a.k.a. ANS, North Slope, Middle Pipeline

Evaporation equation $\%Ev = (2.64 + 0.045T)\ln(t)$
 Where Ev = weight percent evaporated, T = surface temperature (°C), t = time (min)

API gravity	29.2	Weathering % by weight			
(all units at 15°C)	Units	0	31		
Density	g/ml	0.8761	0.9418		
Viscosity	mPa·s or cP	16	900		

(dynamic—values at 15°C)

Flash point	°C	−23	> 95		
Sulfur content	%	1.16	1.43		
Pour point	°C	−54	14		
Surface tension	mN/m	27	31.5		

(air–oil at 15°C)

IFT sea water	mN/m	19.9	14.7		
IFT fresh water	mN/m	21.9	19.3		
Adhesion	g/m ³	28	33		

SARA content (saturate, aromatic, resin, asphaltene) %

Saturate	%	52	42		
Aromatic	%	35	38		
Resin	%	9	12		
Asphaltene	%	5	7		
Waxes	%				

Emulsion formation (type formed and water content %)

Type	Unstable	Meso-stable		
Water content	%	62		
Viscosity	mPa·s or cP	2600		

Chemical dispersibility with Corexit 9500

%	46	5		
---	----	---	--	--

Distillation data (% at temperature)

Boiling point (°C)				
40	3			
60	4			
80	7			
100	10			
120	13			
140	16			
160	19			
180	22			
200	25			
250	33	5		
300	42	16		
400	60	43		
500	76	65		
600	88	81		
700	95	92		

Oil name Alaska North Slope (Northern Pipeline)
Origin and description Alaska, USA; a.k.a. ANS, North Slope

Evaporation equation $\%Ev = (2.64 + 0.045T)\ln(t)$
 Where Ev = weight percent evaporated, T = surface temperature (°C), t = time (min)

API gravity	30.6	Weathering % by weight			
(all units at 15°C)	Units	0	31		
Density	g/ml	0.8719	0.9402		
Viscosity	mPa·s or cP	14	748		

(dynamic—values at 15°C)

Flash point	°C	−19	> 90		
Sulfur content	%	1.14	1.39		
Pour point	°C	−55	8		
Surface tension	mN/m	26.8	31.4		

(air–oil at 15°C)

IFT sea water	mN/m	20.6	21.5		
IFT fresh water	mN/m	22.5	22.4		
Adhesion	g/m ³	26	23		

SARA content (saturate, aromatic, resin, asphaltene) %

Saturate	%	51	44		
Aromatic	%	34	37		
Resin	%	9	12		
Asphaltene	%	5	7		
Waxes	%				

Emulsion formation (type formed and water content %)

Type	Unstable	Meso-stable		
Water content	%	70		
Viscosity	mPa·s or cP	1400		

Chemical dispersibility with Corexit 9500

%	33	6		
---	----	---	--	--

Distillation data (% at temperature)

Boiling point (°C)				
40	4			
60	5			
80	8			
100	11			
120	14			
140	17			
160	20			
180	23			
200	26			
250	34	6		
300	43	17		
400	62	43		
500	77	66		
600	88	81		
700	96	92		

Oil name Alaska North Slope (B)
Origin and description Alaska, USA; a.k.a. ANS, North Slope
 Oil used during the SOCSEX experiment

Evaporation equation

Where E_v = weight percent evaporated, T = surface temperature ($^{\circ}\text{C}$), t = time (min)

API gravity	25	Weathering % by weight			
(all units at 15 $^{\circ}\text{C}$)	Units	0	15	22	
Density	g/ml	0.8814	0.8967		
Viscosity	mPa·s or cP				

(dynamic—values at 15 $^{\circ}\text{C}$)

Flash point	$^{\circ}\text{C}$				
Sulfur content	%	1.11			
Pour point	$^{\circ}\text{C}$	21			
Surface tension	mN/m				

(air–oil at 15 $^{\circ}\text{C}$)

IFT sea water	mN/m				
IFT fresh water	mN/m				
Adhesion	g/m ³	22	19	32	

SARA content (saturate, aromatic, resin, asphaltene) %

Saturate	%	53	52	47	
Aromatic	%	37	38	40	
Resin	%	6	7	9	
Asphaltene	%	4	3	5	
Waxes	%				

Emulsion formation (type formed and water content %)

Type				
Water content	%			
Viscosity	mPa·s or cP			

Chemical dispersibility with Corexit 9500

%				
---	--	--	--	--

Distillation data (% at temperature)

Boiling point ($^{\circ}\text{C}$)				
40	2			
60	2			
80	5			
100	8	1		
120	10	3		
140	13	6	1	
160	15	9	3	
180	18	13	5	
200	21	16	8	
250	28	25	17	
300	37	35	27	
400	55	56	49	
500	71	74	68	
600	83	86	82	
700	91	94	92	

Oil name Alaska North Slope (Southern Pipeline)
Origin and description Alaska, USA; a.k.a. ANS, North Slope

Evaporation equation

$$\%E_v = (2.47 + 0.045T)\ln(t)$$

Where E_v = weight percent evaporated, T = surface temperature ($^{\circ}\text{C}$), t = time (min)

API gravity	29.8	Weathering % by weight			
(all units at 15 $^{\circ}\text{C}$)	Units	0	30		
Density	g/ml	0.8766	0.9431		
Viscosity	mPa·s or cP	18	961		

(dynamic—values at 15 $^{\circ}\text{C}$)

Flash point	$^{\circ}\text{C}$	−21	> 95		
Sulfur content	%	1.13	1.46		
Pour point	$^{\circ}\text{C}$	−30	14		
Surface tension	mN/m	27	31.4		

(air–oil at 15 $^{\circ}\text{C}$)

IFT sea water	mN/m	21.7	17.7		
IFT fresh water	mN/m	23.4	20.2		
Adhesion	g/m ³	28	30		

SARA content (saturate, aromatic, resin, asphaltene) %

Saturate	%	54	42		
Aromatic	%	32	39		
Resin	%	8	13		
Asphaltene	%	6	7		
Waxes	%				

Emulsion formation (type formed and water content %)

Type	Unstable	Meso-stable		
Water content	%	53		
Viscosity	mPa·s or cP	1900		

Chemical dispersibility with Corexit 9500

%	45	6		
---	----	---	--	--

Distillation data (% at temperature)

Boiling point ($^{\circ}\text{C}$)				
40	3			
60	4			
80	7			
100	9			
120	12			
140	15			
160	18			
180	20			
200	23			
250	31	5		
300	39	16		
400	58	43		
500	75	67		
600	86	83		
700	94	95		

Oil name **Alaska North Slope (C)**
Origin and description Alaska, USA (drawn as a line sample off the TAPS pipeline where it spurs off to the Petrostar Refinery in Valdez on March 19, 2002); a.k.a. ANS

Evaporation equation $\%Ev = (2.86 + 0.045T)\ln t$
 Where Ev = weight percent evaporated, T = surface temperature ($^{\circ}C$), t = time (min)

API gravity	30.89	Weathering % by weight			
		0	10	22.5	30.5
(all units at 15 $^{\circ}C$)	Units				
Density	g/ml	0.8663	0.894	0.9189	0.934
Viscosity	mPa-s or cP	11.5	31.8	152	624.7
(dynamic—values at 15 $^{\circ}C$)					
Flash point	$^{\circ}C$	< -8	19	75	115
Sulfur content	%	1.11	1.2	1.38	1.5
Pour point	$^{\circ}C$	-32	-20	-9	-6
Surface tension	mN/m	26.4	28.4	30.4	31.8
(air-oil at 15 $^{\circ}C$)					
IFT sea water	mN/m	20.2	23.1	24.2	25.6
IFT fresh water	mN/m	23.6	25.5	27.7	30.2
Adhesion	g/m ³	20	35	38	40

SARA content (saturate, aromatic, resin, asphaltene) %

Saturate	%	75	72.1	69.2	64.8
Aromatic	%	15	16	16.5	18.5
Resin	%	6.1	7.4	8.9	10.3
Asphaltene	%	4	4.4	5.4	6.4
Waxes	%	2.6	2.9	3.3	3.6

Emulsion formation (type formed and water content %)

Type	Unstable	Unstable	Unstable	Meso-stable
Water content	%			72.9

Viscosity mPa-s or cP

Chemical dispersibility with Corexit 9500

%	47	45	34	15
---	----	----	----	----

Distillation data (% at temperature)

Boiling point ($^{\circ}C$)				
40	2.5	0.1		
60	3.9	0.5		
80	6.5	1.4		
100	10	3.6		
120	13.4	6.6	0.1	
140	16.6	9.8	0.6	
160	19.8	13.1	2	
180	22.6	16.3	4.4	
200	25.2	19.2	7.3	0.5
250	32.6	27.4	16.6	7.5
300	40.7	36.4	27	18.7
400	57.7	55.3	48.7	42.8
500	72.8	72.1	68.2	64.2
600	84.1	84.7	82.6	79.9
700				

Oil name **Alberta Sweet Mixed Blend Reference #4**
Origin and description Alberta, Canada; a.k.a ASMB

Evaporation equation $\%Ev = (3.24 + 0.054T)\ln(t)$
 Where Ev = weight percent evaporated, T = surface temperature ($^{\circ}C$), t = time (min)

API gravity	36.1	Weathering % by weight			
		0	14	26	39
(all units at 15 $^{\circ}C$)	Units				
Density	g/ml	0.8434	0.8712	0.8902	0.9078
Viscosity	mPa-s or cP	7	15	44	168
(dynamic—values at 15 $^{\circ}C$)					
Flash point	$^{\circ}C$	-22	35	79	> 95
Sulfur content	%	0.58	0.63	0.73	0.86
Pour point	$^{\circ}C$	-27	-9	3	14
Surface tension	mN/m	25.8	28.2	28.5	30.6
(air-oil at 15 $^{\circ}C$)					
IFT sea water	mN/m	12.2	10.8	11.5	10.4
IFT fresh water	mN/m	15	14.5	14.3	13.9
Adhesion	g/m ³	13	22	35	61

SARA content (saturate, aromatic, resin, asphaltene) %

Saturate	%	65	60	57	54
Aromatic	%	27	31	32	33
Resin	%	5	6	6	7
Asphaltene	%	3	3	3	5
Waxes	%	4.3	6	7	8

Emulsion formation (type formed and water content %)

Type				
Water content	%			
Viscosity	mPa-s or cP			

Chemical dispersibility with Corexit 9500

%	40			
---	----	--	--	--

Distillation data (% at temperature)

Boiling point ($^{\circ}C$)				
40	1.6			
60	2			
80	2.5			
100	7	2		
120	12.8	4		
140	17.3	8		
160	22	12	2	
180	26.5	17	5	
200	30.6	21	9	
250	40.9	33	22	7
300	51.5	45	36	22
400	71.2	68	62	54
500	86.6	85	82	78
600	95.2	95	94	92
700			100	99

Oil name **Alberta Sweet Mixed Blend**
Origin and description Alberta, Canada (ESTD storage, originally from ESSO, Alberta, Canada);
a.k.a ASMB #5

Evaporation equation $\%Ev = (3.35 + 0.0457T)\ln t$
Where Ev = weight percent evaporated, T = surface temperature ($^{\circ}\text{C}$), t = time (min)

API gravity	35.72	Weathering % by weight			
(all units at 15°C) Units		0	12.6	24.3	36.8
Density g/ml		0.8404	0.8676	0.8852	0.9017
Viscosity mPa·s or cP		6.1	13.8	31.5	123.2

(dynamic—values at 15°C)

Flash point $^{\circ}\text{C}$	−4.3	27.8	67.8	> 110
Sulfur content %	0.63	0.7	0.78	0.89
Pour point $^{\circ}\text{C}$	−18	−12	−12	9
Surface tension mN/m	25.5	27.2	28	29.9

(air–oil at 15°C)

IFT sea water mN/m	23.1	23.1	24.1	23.2
IFT fresh water mN/m	14.3	16	15.3	14.3
Adhesion g/m ³	4.8	25	33.6	43.7

SARA content (saturate, aromatic, resin, asphaltene) %

Saturate %	77.3	77	76.5	72.4
Aromatic %	16.8	15.7	15.4	18
Resin %	4.2	5.4	5.7	6.5
Asphaltene %	1.7	2	2.4	3.1
Waxes %	3.2	3.5	4	4.4

Emulsion formation (type formed and water content %)

Type	Meso-stable	Meso-stable	Stable	Stable
Water content %	89.6	92.9	87.7	86
Viscosity mPa·s or cP				

Chemical dispersibility with Corexit 9500

%	28.1	26.6	17.2	10.9
---	------	------	------	------

Distillation data (% at temperature)

Boiling point ($^{\circ}\text{C}$)				
40	2.4	0.2		
60	3.8	0.8	0.1	
80	6.5	1.6	0.1	
100	10.2	3.4	0.1	
120	13.6	6.1	0.2	
140	17.4	9.5	1.1	
160	21.5	13.8	3.4	
180	25.9	18.2	7.2	0.1
200	29.7	22.4	11.4	1.1
250	39.4	32.8	23.1	10.4
300	49.5	43.5	35.5	24.5
400	68	63.5	58.6	51.6
500	82.2	78.9	76.5	72.7
600	90.4	87.7	86.6	84.7
700				

Oil name **Albian Heavy Synthetic**
Origin and description Alberta, Canada

Evaporation equation

Where Ev = weight percent evaporated, T = surface temperature ($^{\circ}\text{C}$), t = time (min)

API gravity		Weathering % by weight		
(all units at 15°C) Units		0	22.6	
Density g/ml		0.9371	1.0174	
Viscosity mPa·s or cP		6.34E+06	3.74E+05	

(dynamic—values at 15°C)

Flash point $^{\circ}\text{C}$	−23	168	
Sulfur content %	2.28	2.91	
Pour point $^{\circ}\text{C}$	< −30	9	
Surface tension mN/m	28.9	NM	

(air–oil at 15°C)

IFT sea water mN/m	23.2	NM	
IFT fresh water mN/m	26.5	NM	
Adhesion g/m ³			

SARA content (saturate, aromatic, resin, asphaltene) %

Saturate %	41.5	31.4	
Aromatic %	27	29.3	
Resin %	26.2	36.3	
Asphaltene %	6	6.8	
Waxes %			

Emulsion formation (type formed and water content %)

Type	Stable	Entrained	
Water content %	89.4	16.2	
Viscosity mPa·s or cP			

Chemical dispersibility with Corexit 9500

%	15.2	< 10%	
---	------	-------	--

Distillation data (% at temperature)

Boiling point ($^{\circ}\text{C}$)			
40			
60			
80			
100			
120			
140			
160			
180			
200			
250			
300			
400			
500			
600			
700			

Oil name **Anadarko HIA-376**
Origin and description Louisiana, USA

Evaporation equation $\%Ev(w/w) = [2.66 + 0.013T(°C)] t^{1/2}$
 (min)

Where Ev = weight percent evaporated, T = surface temperature (°C), t = time (min)

API gravity	33.8	Weathering % by weight			
(all units at 15°C)	Units	0	8.3	16.4	26.6
Density	g/ml	0.8507	0.8662	0.8759	0.8871
Viscosity	mPa-s or cP	10.8	18.4	30.2	70
(dynamic—values at 15°C)					
Flash point	°C	< 0	46	78	115
Sulfur content	%	0.36	0.4	0.5	0.52
Pour point	°C	−35	−32	−30	−27
Surface tension	mN/m	25.7	27.9	29.6	30.7
(air–oil at 15°C)					
IFT sea water	mN/m	20.1	20.2	19.6	14.7
IFT fresh water	mN/m	21.3	19	15.4	15.3
Adhesion	g/m ³	13	23	32	41

SARA content (saturate, aromatic, resin, asphaltene) %

Saturate	%	88.65	87.81	86.69	85.09
Aromatic	%	8.09	9.06	9.41	10.84
Resin	%	3.27	3.14	3.9	4.07
Asphaltene	%	0	0	0	0
Waxes	%	1.7	1.7	1.5	1.9

Emulsion formation (type formed and water content %)

Type	Unstable	Unstable	Unstable	Unstable
Water content	%			
Viscosity	mPa-s or cP			

Chemical dispersibility with Corexit 9500

%	46	24.9	26.4	14.3
---	----	------	------	------

Distillation data (% at temperature)

Boiling point (°C)				
40				
60				
80				
100	2.2	0.8		
120	4.9	2.4	0.1	
140	7.5	4.5	0.5	
160	10.7	7.5	1.9	
180	14.1	11	4.6	0.1
200	17.4	14.5	8	0.9
250	38.2	37.2	32.5	24.3
300	58.5	59.4	56.9	52.2
400	74.5	76.8	76.1	74.4
500	83.8	87	87.1	87.5
600				
700				

Oil name **Arabian Heavy**
Origin and description Saudi Arabia (courtesy of Irving Oil Ltd, Canaport, NB, Canada) 2004

Evaporation equation

Where Ev = weight percent evaporated, T = surface temperature (°C), t = time (min)

API gravity	27	Weathering % by weight			
(all units at 15°C)	Units	0	7.3	15	23.2
Density	g/ml	0.8923	0.9131	0.9315	0.9503
Viscosity	mPa-s or cP	49.7	115.3	393.6	5416.7
(dynamic—values at 15°C)					
Flash point	°C				
Sulfur content	%				
Pour point	°C				
Surface tension	mN/m	27.2	28.3	29.6	
(air–oil at 15°C)					
IFT sea water	mN/m	26.5	28.5	28.6	
IFT fresh water	mN/m	27.8	28.4	30.9	
Adhesion	g/m ³				

SARA content (saturate, aromatic, resin, asphaltene) %

Saturate	%	60.1	58.9	53.3	50
Aromatic	%	24.6	25.2	27.1	27.5
Resin	%	6.3	6	8.9	10.2
Asphaltene	%	9	9.9	10.8	12.2
Waxes	%				

Emulsion formation (type formed and water content %)

Type				
Water content	%			
Viscosity	mPa-s or cP			

Chemical dispersibility with Corexit 9500

%				
---	--	--	--	--

Distillation data (% at temperature)

Boiling point (°C)				
40				
60				
80				
100				
120				
140				
160				
180				
200				
250				
300				
400				
500				
600				
700				

Oil name **Arabian Light (2000)**
Origin and description Saudi Arabia (sampled from Irving Oil Refinery, St. John, NB, 2000)

Evaporation equation $\%Ev = (2.4 + 0.045T)\ln t$
 Where Ev = weight percent evaporated, T = surface temperature ($^{\circ}\text{C}$), t = time (min)

API gravity	31.3	Weathering % by weight			
(all units at 15 $^{\circ}\text{C}$)	Units	0	9.2	17.6	26
Density	g/ml	0.8641	0.866	0.9028	0.9193
Viscosity	mPa·s or cP	13	27.4	59.9	173.7

(dynamic—values at 15 $^{\circ}\text{C}$)

Flash point	$^{\circ}\text{C}$	< -10	36.5	71.7	> 110
Sulfur content	%	1.93	2.17	2.36	2.6
Pour point	$^{\circ}\text{C}$	-21	-15	-8	-9
Surface tension	mN/m	26	27.9	28.4	30.2

(air-oil at 15 $^{\circ}\text{C}$)

IFT sea water	mN/m	21.6	22.8	24.6	20.4
IFT fresh water	mN/m	23.8	22	25.7	22.4
Adhesion	g/m ³	17	28	30	35

SARA content (saturate, aromatic, resin, asphaltene) %

Saturate	%	75.5	73.3	72.4	70.1
Aromatic	%	15.2	16.9	16.7	16.3
Resin	%	5.7	6	6.6	8.8
Asphaltene	%	3.6	3.8	4.3	4.8
Waxes	%	2.7	2.9	3.2	3.6

Emulsion formation (type formed and water content %)

Type		Meso-stable	Meso-stable	Stable	Stable
Water content	%	91.1	88.6	83.8	83.8
Viscosity	mPa·s or cP				

Chemical dispersibility with Corexit 9500

%	19	13.8	10	7.9
---	----	------	----	-----

Distillation data (% at temperature)

Boiling point ($^{\circ}\text{C}$)				
40	0.1			
60	1.3			
80	1.7			
100	4.7	1.2		
120	6.8	2.9	0.1	
140	9.6	5.3	0.6	
160	12.6	8.2	2	
180	15.9	11.7	4.7	0.2
200	19.1	15	8	1.2
250	26.8	23.5	17.3	8.6
300	35.1	32.4	27.3	19.4
400	51.4	50.1	47	41.4
500	65.5	65.4	64	60.5
600	76.2	77	76.8	75
700				

Oil name **Arabian Medium**
Origin and description Saudi Arabia; a.k.a. Khursaniyah

Evaporation equation $\%Ev = (1.89 + 0.045T)\ln(t)$
 Where Ev = weight percent evaporated, T = surface temperature ($^{\circ}\text{C}$), t = time (min)

API gravity	29.5	Weathering % by weight			
(all units at 15 $^{\circ}\text{C}$)	Units	0	13	21	31
Density	g/ml	0.8783	0.9102	0.9263	0.9495
Viscosity	mPa·s or cP	29	91	275	2155

(dynamic—values at 15 $^{\circ}\text{C}$)

Flash point	$^{\circ}\text{C}$	-13	52	90	> 95
Sulfur content	%	1.6	3.16	3.44	3.86
Pour point	$^{\circ}\text{C}$	-10	-4	-2	7
Surface tension	mN/m	27	28.7	29.9	31.3

(air-oil at 15 $^{\circ}\text{C}$)

IFT sea water	mN/m	20.8	24.4	23.3	20
IFT fresh water	mN/m	21.7	25.4	25.3	23
Adhesion	g/m ³	26	28	39	65

SARA content (saturate, aromatic, resin, asphaltene) %

Saturate	%	54	42	40	33
Aromatic	%	32	44	46	54
Resin	%	7	7	8	9
Asphaltene	%	6	7	7	7
Waxes	%	6	5	5	5

Emulsion formation (type formed and water content %)

Type		Stable	Stable	Stable	Stable
Water content	%	85	77	73	65
Viscosity	mPa·s or cP	41,000	20,000	21,000	46,000

Chemical dispersibility with Corexit 9500

%	23	17	7	6
---	----	----	---	---

Distillation data (% at temperature)

Boiling point ($^{\circ}\text{C}$)				
40				
60				
80	1			
100	2			
120	8	1		
140	11	3		
160	13	5	1	
180	16	8	2	
200	18	11	4	
250	26	20	13	2
300	33	29	22	11
400	49	47	42	34
500	64	63	59	54
600	76	77	74	71
700	86	87	86	84

Oil name **Asphalt Primer**
Origin and description

Evaporation equationWhere E_v = weight percent evaporated, T = surface temperature ($^{\circ}\text{C}$), t = time (min)

API gravity	18.6	Weathering % by weight		
(all units at 15°C)	Units	0		
Density	g/ml	0.9421		
Viscosity	mPa·s or cP	3280		
(dynamic—values at 15°C)				
Flash point	$^{\circ}\text{C}$	16		
Sulfur content	%			
Pour point	$^{\circ}\text{C}$	-17		
Surface tension	mN/m	28.3		
(air-oil at 15°C)				
IFT sea water	mN/m	24.7		
IFT fresh water	mN/m	27.8		
Adhesion	g/m^3			

SARA content (saturate, aromatic, resin, asphaltene) %

Saturate	%			
Aromatic	%			
Resin	%			
Asphaltene	%			
Waxes	%			

Emulsion formation (type formed and water content %)

Type			
Water content	%		
Viscosity	mPa·s or cP		

Chemical dispersibility with Corexit 9500

%			
---	--	--	--

Distillation data (% at temperature)

Boiling point ($^{\circ}\text{C}$)			
40			
60			
80			
100			
120			
140			
160			
180			
200			
250			
300			
400			
500			
600			
700			

Oil name **Athabasca Bitumen**
Origin and description Alberta, Canada

Evaporation equationWhere E_v = weight percent evaporated, T = surface temperature ($^{\circ}\text{C}$), t = time (min)

API gravity	7.7–9.0	Weathering % by weight	
(all units at 15°C)	Units	0	
Density	g/ml	1.006–1.016	
Viscosity	mPa·s or cP	19,000–300,000	
(dynamic—values at 15°C)			
Flash point	$^{\circ}\text{C}$		
Sulfur content	%	4.41–5.44	
Pour point	$^{\circ}\text{C}$		
Surface tension	mN/m		
(air-oil at 15°C)			
IFT sea water	mN/m		
IFT fresh water	mN/m		
Adhesion	g/m^3		

SARA content (saturate, aromatic, resin, asphaltene) %

Saturate	%		
Aromatic	%		
Resin	%		
Asphaltene	%	4–5	
Waxes	%		

Emulsion formation (type formed and water content %)

Type		
Water content	%	
Viscosity	mPa·s or cP	

Chemical dispersibility with Corexit 9500

%		
---	--	--

Distillation data (% at temperature)

Boiling point ($^{\circ}\text{C}$)		
40		
60		
80		
100		
120		
140		
160		
180		
200		
250		
300		
400		
500		
600		
700		

Oil name **Atkinson**
Origin and description Beaufort Sea, Canada

Evaporation equation

Where E_v = weight percent evaporated, T = surface temperature ($^{\circ}\text{C}$), t = time (min)

API gravity	23.7	Weathering % by weight			
(all units at 15°C)	Units	0	19		
Density	g/ml	0.911	0.9438		
Viscosity	mPa·s or cP	65	533		
(dynamic—values at 15°C)					
Flash point	$^{\circ}\text{C}$				
Sulfur content	%	0.86	1.07		
Pour point	$^{\circ}\text{C}$	−46			
Surface tension mN/m		28.8	26.6		
(air–oil at 15°C)					
IFT sea water mN/m		17.9	10.9		
IFT fresh water mN/m		23.2	21.2		
Adhesion	g/m^3				

SARA content (saturate, aromatic, resin, asphaltene) %

Saturate	%	48			
Aromatic	%	36			
Resin	%	14			
Asphaltene	%	3			
Waxes	%	1			

Emulsion formation (type formed and water content %)

Type				
Water content	%			
Viscosity	mPa·s or cP			

Chemical dispersibility with Corexit 9500

%				
---	--	--	--	--

Distillation data (% at temperature)

Boiling point ($^{\circ}\text{C}$)				
40				
60				
80				
100				
120				
140				
160				
180				
200				
250				
300				
400				
500				
600				
700				

Oil name **Avalon**
Origin and description Newfoundland, Canada

Evaporation equation

Avalon: $\%E_v = (1.41 + 0.0457)\ln(t)$

Avalon J-34: $\%E_v = (1.58 + 0.0457)\ln(t)$

Where E_v = weight percent evaporated, T = surface temperature ($^{\circ}\text{C}$), t = time (minutes)

API gravity	36	Weathering % by weight		
(all units at 15°C)	Units	0	9	20
Density	g/ml	0.844	0.856	0.886
Viscosity	mPa·s or cP	11	83	438
(dynamic—values at 15°C)				
Flash point	$^{\circ}\text{C}$	14	33	66
Sulfur content	%	0.71	0.86	
Pour point	$^{\circ}\text{C}$			
Surface tension mN/m		26.4	25.8	27.9
(air–oil at 15°C)				
IFT sea water mN/m		20.5	25.6	26.7
IFT fresh water mN/m		29.1		
Adhesion	g/m^3			

SARA content (saturate, aromatic, resin, asphaltene) %

Saturate	%	83		
Aromatic	%	13		
Resin	%	2		
Asphaltene	%	2		
Waxes	%	13		

Emulsion formation (type formed and water content %)

Type			
Water content	%		
Viscosity	mPa·s or cP		

Chemical dispersibility with Corexit 9527

%	10		
---	----	--	--

Distillation data (% at temperature)

Boiling point ($^{\circ}\text{C}$)			
40			
60	1		
80	2		
100	4		
120	6		
140	7		
160	10		
180	13		
200	15		
250	23		
300	31		
400	48		
500	66		
600	80		
700	91		

Oil name Aviation Gasoline 80
Origin and description a.k.a. Avgas 80

Evaporation equation $\%Ev = (15.4 + 0.0457)\ln(t)$
 Where Ev = weight percent evaporated, T = surface temperature (°C), t = time (min)

API gravity	71.8	Weathering % by weight		
(all units at 15°C) Units		0		
Density	g/ml	0.6953		
Viscosity	mPa·s or cP	1		
(dynamic—values at 15°C)				
Flash point	°C			
Sulfur content	%	0.04		
Pour point	°C			
Surface tension mN/m		19		
(air–oil at 15°C)				
IFT sea water mN/m		33.1		
IFT fresh water mN/m		31.7		
Adhesion	g/m ³			

SARA content (saturate, aromatic, resin, asphaltene) %				
Saturate	%			
Aromatic	%			
Resin	%			
Asphaltene	%			
Waxes	%			

Emulsion formation (type formed and water content %)				
Type				
Water content	%			
Viscosity	mPa·s or cP			

Chemical dispersibility with Corexit 9500				
%				

Distillation data (% at temperature)				
Boiling point (°C)				
40				
60				
80				
100				
120				
140				
160				
180				
200				
250				
300				
400				
500				
600				
700				

Oil name Aviation Gasoline 100
Origin and description a.k.a. Avgas 100

Evaporation equation
 Where Ev = weight percent evaporated, T = surface temperature (°C), t = time (min)

API gravity	66.2	Weathering % by weight		
(all units at 15°C) Units		0		
Density	g/ml	0.7151		
Viscosity	mPa·s or cP	1		
(dynamic—values at 15°C)				
Flash point	°C			
Sulfur content	%			
Pour point	°C			
Surface tension mN/m		20		
(air–oil at 15°C)				
IFT sea water mN/m		42.2		
IFT fresh water mN/m		42.2		
Adhesion	g/m ³			

SARA content (saturate, aromatic, resin, asphaltene) %				
Saturate	%			
Aromatic	%			
Resin	%			
Asphaltene	%			
Waxes	%			

Emulsion formation (type formed and water content %)				
Type				
Water content	%			
Viscosity	mPa·s or cP			

Chemical dispersibility with Corexit 9500				
%				

Distillation data (% at temperature)				
Boiling point (°C)				
40				
60				
80				
100				
120				
140				
160				
180				
200				
250				
300				
400				
500				
600				
700				

Oil name Aviation Gasoline 100LL
Origin and description a.k.a. Avgas 100 LL

Evaporation equation $\ln(\%Ev) = (0.5 + 0.045T)\ln(t)$
 Where Ev = weight percent evaporated, T = surface temperature (°C), t = time (min)

API gravity	66.6	Weathering % by weight		
(all units at 15°C)	Units	0	33	60
Density	g/ml	0.7143	0.7258	0.7292
Viscosity	mPa·s or cP	1	1	1
(dynamic—values at 15°C)				
Flash point	°C	< 1	0	0
Sulfur content	%	0.06	0.08	0.12
Pour point	°C	< -75	< -75	< -75
Surface tension	mN/m	20.1	20.6	21
(air-oil at 15°C)				
IFT sea water	mN/m	24	23.4	21.9
IFT fresh water	mN/m	28.8	3	26.6
Adhesion	g/m ³	1	1	1

SARA content (saturate, aromatic, resin, asphaltene) %				
Saturate	%			
Aromatic	%			
Resin	%			
Asphaltene	%			
Waxes	%	0	0	0

Emulsion formation (type formed and water content %)				
Type				
Water content	%			
Viscosity	mPa·s or cP			

Chemical dispersibility with Corexit 9500				
%				

Distillation data (% at temperature)				
Boiling point (°C)				
40	2.7			
60	3.5	0.1		
80	4	0.2		
100	24.2	18.1	15.9	
120	80.8	78.5	72.7	
140	84.4	84.6	82.7	
160	85	85.4	84.1	
180	85.4	86.1	85.1	
200	85.8	86.6	85.9	
250	86.2	87.2	86.8	
300	86.5	87.5	87.2	
400	86.5	87.6	87.4	
500				
600				
700				

Oil name Barrow Island
Origin and description Australia

Evaporation equation $\%Ev = (4.67 + 0.045T)\ln(t)$
 Where Ev = weight percent evaporated, T = surface temperature (°C), t = time (min)

API gravity	36.7	Weathering % by weight			
(all units at 15°C)	Units	0	17	32	48
Density	g/ml	0.841	0.87	0.8906	0.9075
Viscosity	mPa·s or cP	2	4	11	23
(dynamic—values at 15°C)					
Flash point	°C	< -30	42	80	> 95
Sulfur content	%	0.04	0.03	0.05	0.06
Pour point	°C	< -60	-62	-46	-27
Surface tension	mN/m	26.2	28.3	29.8	31
(air-oil at 15°C)					
IFT sea water	mN/m	15.9	14.9	12.7	12.1
IFT fresh water	mN/m	18.1	16.3	15.3	14.3
Adhesion	g/m ³	6	11	20	24

SARA content (saturate, aromatic, resin, asphaltene) %					
Saturate	%	64	66	61	59
Aromatic	%	32	30	35	36
Resin	%	4	4	4	6
Asphaltene	%	0	0	0	0
Waxes	%	0	1	1	1

Emulsion formation (type formed and water content %)					
Type					
Water content	%				
Viscosity	mPa·s or cP				

Chemical dispersibility with Corexit 9500					
%	61	36	27	23	

Distillation data (% at temperature)					
Boiling point (°C)					
40					
60					
80	4				
100	9				
120	14	3			
140	19	6			
160	24	12	1		
180	31	19	5		
200	37	26	11	1	
250	55	47	35	18	
300	71	66	58	45	
400	88	86	83	78	
500	96	96	94	92	
600	99	99	98	98	
700					

Oil name	Belridge Heavy		
Origin and description	California, USA		
Evaporation equation	$\%EV = (0.03 + 0.013T)\sqrt{(t)}$		
Where Ev = weight percent evaporated, T = surface temperature (°C), t = time (min)			
API gravity	13.6	Weathering % by weight	
(all units at 15°C)	Units	0	3
Density	g/ml	0.9849	0.977
Viscosity	mPa·s or cP	12,610	17,105
(dynamic—values at 15°C)			
Flash point	°C	> 90	> 90
Sulfur content	%	1.03	1.03
Pour point	°C	2	4
Surface tension	mN/m	31.2	32.9
(air—oil at 15°C)			
IFT sea water	mN/m	20	30.4
IFT fresh water	mN/m	25.1	
Adhesion	g/m ³	88	83
Saturate	%	28	29
Aromatic	%	39	38
Resin	%	30	30
Asphaltene	%	3	4
Waxes	%	1	1
Type		Entrained	Entrained
Water content	%	54	60
Viscosity	mPa·s or cP	42,000	47,000
Chemical dispersibility with Corexit 9500			
	%	4	7

Distillation data (% at temperature)

Boiling point (°C)

40			
60			
80			
100			
120			
140			
160	1		
180	1	1	
200	2	2	
250	9	8	
300	17	17	
400	39	39	
500	62	62	
600	79	78	
700	91	89	

Oil name		Bent Horn A-02		
Origin and description		Northwest Territories, Canada		
Evaporation equation		$\%Ev = (3.19 + 0.045T)\ln(t)$		
Where Ev = weight percent evaporated, T = surface temperature (°C), t = time (min)				
API gravity	41.5	Weathering % by weight		
(all units at 15°C)	Units	0	20	33
Density	g/ml	0.8177	0.8484	0.8615
Viscosity	mPa·s or cP	12	100	525
(dynamic—values at 15°C)				
Flash point	°C	−14		
Sulfur content	%	0.76	0.81	0.89
Pour point	°C	−16	−2	11
Surface tension	mN/m	25.4	27.9	28.7
(air—oil at 15°C)				
IFT sea water	mN/m	17.6	1.7	2.3
IFT fresh water	mN/m	26.6	13.8	11.4
Adhesion	g/m ³			
SARA content (saturate, aromatic, resin, asphaltene) %				
Saturate	%			
Aromatic	%			
Resin	%			
Asphaltene	%	0		
Waxes	%	9		
Emulsion formation (type formed and water content %)				
Type				
Water content	%			
Viscosity	mPa·s or cP			
Chemical dispersibility with Corexit 9500				
	%			

Distillation data (% at temperature)

Boiling point (°C)

40			
60			
80			
100			
120			
140			
160			
180			
200			
250			
300			
400			
500			
600			
700			

Oil name **Bent Horn**
Origin and description Northwest Territories, Canada

Evaporation equation

Where E_v = weight percent evaporated, T = surface temperature ($^{\circ}\text{C}$), t = time (min)

API gravity	41.3	Weathering % by weight		
(all units at 15°C)	Units	0	20	33
Density	g/ml	0.8181	0.8472	0.8619
Viscosity	mPa·s or cP	24	60	5820
(dynamic—values at 15°C)				
Flash point	$^{\circ}\text{C}$	−9		
Sulfur content	%	0.82		
Pour point	$^{\circ}\text{C}$	−18	−7	−8
Surface tension	mN/m	26.2	28.2	25
(air–oil at 15°C)				
IFT sea water	mN/m	38.5	2.2	7.4
IFT fresh water	mN/m	39.1	16.6	15.4
Adhesion	g/m^3			

SARA content (saturate, aromatic, resin, asphaltene) %

Saturate	%	94		
Aromatic	%	5		
Resin	%	0		
Asphaltene	%	0	0	
Waxes	%	7		

Emulsion formation (type formed and water content %)

Type			
Water content	%		
Viscosity	mPa·s or cP		

Chemical dispersibility with Corexit 9500

%	25		
---	----	--	--

Distillation data (% at temperature)

Boiling point ($^{\circ}\text{C}$)			
40			
60	1		
80	1		
100	3		
120	6		
140	9		
160	12		
180	15		
200	19		
250	28		
300	38		
400	56		
500	72		
600	84		
700	91		

Oil name **Brent Blend**
Origin and description North Sea, UK

Evaporation equation

$$\%E_v = (3.39 + 0.048T)\ln(t)$$

Where E_v = weight percent evaporated, T = surface temperature ($^{\circ}\text{C}$), t = time (min)

API gravity	37.8	Weathering % by weight			
(all units at 15°C)	Units	0	14	26	40
Density	g/ml	0.8351	0.8624	0.8796	0.8996
Viscosity	mPa·s or cP	6	14	39	256
(dynamic—values at 15°C)					
Flash point	$^{\circ}\text{C}$	< −30	27	71	> 95
Sulfur content	%	0.39	0.38	0.44	0.52
Pour point	$^{\circ}\text{C}$	−6	5	9	12
Surface tension	mN/m	25.5	28	29.4	30.5
(air–oil at 15°C)					
IFT sea water	mN/m	22.5	22.7	25	23.5
IFT fresh water	mN/m	22.7	23.2	24.8	23.8
Adhesion	g/m^3	12	20	36	53

SARA content (saturate, aromatic, resin, asphaltene) %

Saturate	%	72	61	56	53
Aromatic	%	23	31	35	34
Resin	%	4	7	7	11
Asphaltene	%	1	2	2	2
Waxes	%	7	7	8	9

Emulsion formation (type formed and water content %)

Type				
Water content	%			
Viscosity	mPa·s or cP			

Chemical dispersibility with Corexit 9500

%				
---	--	--	--	--

Distillation data (% at temperature)

Boiling point ($^{\circ}\text{C}$)				
40	3			
60	4			
80	4	1		
100	5	3		
120	19	6		
140	22	10	1	
160	25	14	3	
180	29	18	7	
200	32	22	11	
250	42	33	23	6
300	52	44	36	20
400	70	65	60	36
500	85	83	80	75
600	95	93	93	91
700	99	99	99	99

Oil name	Bunker C Fuel Oil (Alaska)
Origin and description	a.k.a. Fuel Oil No. 6, Residual/Heavy Fuel Oil

Evaporation equation Short-term (< 5 days): %Ev = $(-0.13 + 0.013T)\sqrt{t}$
Long-term: %Ev = $(0.31 + 0.045T)\ln(t)$

Where Ev = weight percent evaporated, T = surface temperature (°C), t = time (min)

API gravity	11.4	Weathering % by weight		
(all units at 15°C)	Units	0	8	
Density	g/ml	0.9891	1.005	
Viscosity	mPa·s or cP	8,706	280,000	
(dynamic—values at 15°C)				
Flash point	°C	83	> 95	
Sulfur content	%	0.53	0.56	
Pour point	°C	−2	23	
Surface tension	mN/m	32.5		
(air–oil at 15°C)				
IFT sea water	mN/m			
IFT fresh water	mN/m			
Adhesion	g/m ³	85	421	

SARA content (saturate, aromatic, resin, asphaltene) %

Saturate	%	25	23	
Aromatic	%	47	42	
Resin	%	17	20	
Asphaltene	%	11	15	
Waxes	%	2	2	

Emulsion formation (type formed and water content %)

Type		Entrained	Unstable	
Water content	%	35	6	
Viscosity	mPa·s or cP	28,000		

Chemical dispersibility with Corexit 9500

%	14	6	
---	----	---	--

Distillation data (% at temperature)

Boiling point (°C)			
40			
60			
80			
100			
120			
140			
160	1		
180	2		
200	4		
250	12	4	
300	17	10	
400	33	27	
500	57	53	
600	73	72	
700	88	87	

Oil name	Bunker C Fuel Oil
Origin and description	

Evaporation equation Short-term (< 5 days): %Ev = $(0.35 + 0.13T)\sqrt{t}$
Long-term: %Ev = $(-0.21 + 0.045T)\ln(t)$

Where Ev = weight percent evaporated, T = surface temperature (°C), t = time (min)

API gravity	12.3	Weathering % by weight		
(all units at 15°C)	Units	0		
Density	g/ml	0.983		
Viscosity	mPa·s or cP	45,030		
(dynamic—values at 15°C)				
Flash point	°C	98		
Sulfur content	%	2.4		
Pour point	°C	15		
Surface tension	mN/m	NM		
(air–oil at 15°C)				
IFT sea water	mN/m	NM		
IFT fresh water	mN/m	NM		
Adhesion	g/m ³			

SARA content (saturate, aromatic, resin, asphaltene) %

Saturate	%	24		
Aromatic	%	55		
Resin	%	15		
Asphaltene	%	7		
Waxes	%	12		

Emulsion formation (type formed and water content %)

Type		entrained		
Water content	%	26		
Viscosity	mPa·s	110,000		

Chemical dispersibility with Corexit 9500

%	7		
---	---	--	--

Distillation data (% at temperature)

Boiling point (°C)			
40			
60			
80			
100			
120			
140			
160	1		
180	1		
200	2		
250	5		
300	8		
400	20		
500	33		
600	51		
700	81		

Oil name **Bunker C Light Fuel Oil**
Origin and description

Evaporation equation $\%Ev = (0.0035 + 0.0026T)\sqrt{(t)}$
 Where Ev = weight percent evaporated, T = surface temperature (°C), t = time (min)

API gravity		Weathering % by weight		
(all units at 15°C)	Units			
Density	g/ml			
Viscosity	mPa·s or cP			
(dynamic—values at 15°C)				
Flash point	°C			
Sulfur content	%			
Pour point	°C			
Surface tension mN/m				
(air–oil at 15°C)				
IFT sea water mN/m				
IFT fresh water mN/m				
Adhesion	g/m ³			

SARA content (saturate, aromatic, resin, asphaltene) %

Saturate	%			
Aromatic	%			
Resin	%			
Asphaltene	%			
Waxes	%			

Emulsion formation (type formed and water content %)

Type			
Water content	%		
Viscosity	mPa·s or cP		

Chemical dispersibility with Corexit 9500

%	5		
---	---	--	--

Distillation data (% at temperature)

Boiling point (°C)			
40			
60			
80			
100			
120			
140			
160			
180			
200	1		
250	7		
300	19		
400	54		
500	69		
600	76		
700	89		

Oil name **California API 15**
Origin and description California, USA

Evaporation equation $\%Ev = (-0.14 + 0.013T)\sqrt{(t)}$
 Where Ev = weight percent evaporated, T = surface temperature (°C), t = time (min)

API gravity	13.2	Weathering % by weight		
(all units at 15°C)	Units	0		
Density	g/ml	0.977		
Viscosity	mPa·s or cP	6400		
(dynamic—values at 15°C)				
Flash point	°C	12		
Sulfur content	%	5.5		
Pour point	°C	–9		
Surface tension mN/m		33.6		
(air–oil at 15°C)				
IFT sea water mN/m				
IFT fresh water mN/m				
Adhesion	g/m ³			

SARA content (saturate, aromatic, resin, asphaltene) %

Saturate	%	19		
Aromatic	%	35		
Resin	%	23		
Asphaltene	%	22		
Waxes	%	1		

Emulsion formation (type formed and water content %)

Type	Entrained		
Water content	%	39	
Viscosity	mPa·s or cP		

Chemical dispersibility with Corexit 9500

%	0		
---	---	--	--

Distillation data (% at temperature)

Boiling point (°C)			
40			
60			
80			
100			
120			
140	3		
160	5		
180	7		
200	8		
250	12		
300	17		
400	27		
500	39		
600	54		
700	69		

Oil name		California API 11		
Origin and description		California, USA		
Evaporation equation		$\%Ev = (-0.13 + 0.013T)\sqrt[3]{(t)}$		
Where Ev = weight percent evaporated, T = surface temperature (°C), t = time (min)				
API gravity	10.3	Weathering % by weight		
(all units at 15°C)	Units	0		
Density	g/ml	0.9882		
Viscosity	mPa·s or cP	34,000		
(dynamic—values at 15°C)				
Flash point	°C	28		
Sulfur content	%	3.30		
Pour point	°C	0		
Surface tension	mN/m	37		
(air–oil at 15°C)				
IFT sea water	mN/m			
IFT fresh water	mN/m			
Adhesion	g/m ³			
SARA content (saturate, aromatic, resin, asphaltene) %				
Saturate	%			
Aromatic	%			
Resin	%			
Asphaltene	%	16		
Waxes	%	1		
Emulsion formation (type formed and water content %)				
Type		Entrained		
Water content	%	35		
Viscosity	mPa·s or cP			
Chemical dispersibility with Corexit 9500				
	%	0		
Distillation data (% at temperature)				
Boiling point (°C)				
40				
60				
80				
100		1		
120		1		
140		3		
160		4		
180		5		
200		7		
250		12		
300		17		
400		28		
500		49		
600		56		
700		71		

Oil name		Cano Limon			
Origin and description		Colombia			
Evaporation equation		$\%Ev = (1.71 + 0.045T)\ln(t)$			
Where Ev = weight percent evaporated, T = surface temperature (°C), t = time (min)					
API gravity	28.8	Weathering % by weight			
(all units at 15°C)	Units	0	7	14	21
Density	g/ml	0.8817	0.8961	0.9077	0.92
Viscosity	mPa·s or cP	46	103	254	1350
(dynamic—values at 15°C)					
Flash point	°C	13	58	88	> 100
Sulfur content	%	0.38	0.45	0.46	0.51
Pour point	°C	8	11	10	13
Surface tension	mN/m	28	29.1	29.5	
(air–oil at 15°C)					
IFT sea water	mN/m	28.9	23.5		
IFT fresh water	mN/m	28.7	25.6		
Adhesion	g/m ³	34	37	47	112
SARA content (saturate, aromatic, resin, asphaltene) %					
Saturate	%	60	57	56	51
Aromatic	%	24	25	25	28
Resin	%	8	8	8	10
Asphaltene	%	8	9	10	11
Waxes	%	4	4.2	4.9	5.9
Emulsion formation (type formed and water content %)					
Type					
Water content	%				
Viscosity	mPa·s or cP				
Chemical dispersibility with Corexit 9500					
	%				
Distillation data (% at temperature)					
Boiling point (°C)					
40		0.2			
60		0.8	0.2	0.2	0.2
80		1.4	0.3	0.3	0.3
100		2.9	0.4	0.3	0.3
120		4.6	0.9	0.3	0.3
140		6.8	2	0.3	0.3
160		10	4.4	0.8	0.3
180		13.5	7.6	2.5	0.3
200		16.7	10.8	5.1	0.7
250		26.6	21.4	15.6	8
300		37.4	32.9	27.8	20.6
400		59.4	56.2	52.5	47.7
500		77	74.9	72.8	70.1
600		88.6	87.4	86.4	85.3
700					

Oil name	Canola Oil			
Origin and description				
API gravity		Oil type		
(all units at 15°C)	Units	Degummed	Refined	
Density	g/ml	0.9205	0.9205	
Viscosity	mPa·s or cP	83	86	
(dynamic—values at 15°C)				
Flash point	°C			
Sulfur content	%			
Pour point	°C			
Surface tension mN/m				
(air–oil at 15°C)				
IFT sea water mN/m				
IFT fresh water mN/m				
Adhesion	g/m ³			
SARA content (saturate, aromatic, resin, asphaltene) %				
Saturate	%			
Aromatic	%			
Resin	%			
Asphaltene	%			
Waxes	%			
Emulsion formation (type formed and water content %)				
Type				
Water content	%			
Viscosity	mPa·s or cP			
Chemical dispersibility with Corexit 9500				
%				
Distillation data (% at temperature)				
Boiling point (°C)				
40				
60				
80				
100				
120				
140				
160				
180				
200				
250				
300				
400				
500				
600				
700				

Oil name		Carpinteria		
Origin and description		California, USA		
Evaporation equation		$\%Ev = (1.68 + 0.045T)\ln(t)$		
Where Ev = weight percent evaporated, T = surface temperature (°C), t = time (min)				
API gravity	22.9	Weathering % by weight		
(all units at 15°C)	Units	0	10	15
Density	g/ml	0.9155	0.9299	0.9482
Viscosity	mPa·s or cP	164	755	3426
(dynamic—values at 15°C)				
Flash point	°C	0.1	0.1	< 0.1
Sulfur content	%	1.88	2.01	2.04
Pour point	°C	−21	6	12
Surface tension	mN/m	27.8	28.6	33.3
(air–oil at 15°C)				
IFT sea water	mN/m	23.7	21.3	30
IFT fresh water	mN/m	26	24.7	35.5
Adhesion	g/m ³	57	61	76
SARA content (saturate, aromatic, resin, asphaltene) %				
Saturate	%	44	40	31
Aromatic	%	30	30	36
Resin	%	17	19	22
Asphaltene	%	9	11	11
Waxes	%	7	5	4
Emulsion formation (type formed and water content %)				
Type		Unstable	Meso-stable	Meso-stable
Water content	%	9	72	54
Viscosity	mPa·s or cP		21,000	29,000
Chemical dispersibility with Corexit 9500				
	%	16	7	7
Distillation data (% at temperature)				
Boiling point (°C)				
	40	2		
	60	2		
	80	3		
	100	6	1	
	120	8	1	
	140	11	3	
	160	13	5	
	180	15	7	1
	200	18	9	3
	250	24	17	10
	300	32	25	19
	400	47	44	38
	500	64	63	59
	600	78	78	75
	700	89	89	86

Oil name **Fluid Catalytic Cracker Medium Cycle Oil**
Origin and description

Evaporation equation $\%Ev = (-0.16 + 0.013T)\sqrt{(t)}$
 Where Ev = weight percent evaporated, T = surface temperature (°C), t = time (min)

API gravity	12.3	Weathering % by weight		
(all units at 15°C)	Units	0		
Density	g/ml	0.9835		
Viscosity	mPa·s or cP	31		
(dynamic—values at 15°C)				
Flash point	°C			
Sulfur content	%	0.27		
Pour point	°C	−6		
Surface tension	mN/m	32.7		
(air–oil at 15°C)				
IFT sea water	mN/m	22.8		
IFT fresh water	mN/m	27.3		
Adhesion	g/m ³	21		

SARA content (saturate, aromatic, resin, asphaltene) %

Saturate	%	30		
Aromatic	%	62		
Resin	%	7		
Asphaltene	%	1		
Waxes	%	2		

Emulsion formation (type formed and water content %)

Type			
Water content	%		
Viscosity	mPa·s or cP		

Chemical dispersibility with Corexit 9500

%			
---	--	--	--

Distillation data (% at temperature)

Boiling point (°C)			
40			
60			
80			
100			
120			
140			
160			
180			
200	1		
250	5		
300	24		
400	93		
500			
600			
700			

Oil name **Catalytic Cracking Feed**
Origin and description

Evaporation equation $\%Ev = (-0.18 + 0.013T)\sqrt{(t)}$
 Where Ev = weight percent evaporated, T = surface temperature (°C), t = time (min)

API gravity	23.2	Weathering % by weight		
(all units at 15°C)	Units	0	2	
Density	g/ml	0.9139	0.9144	
Viscosity	mPa·s or cP	780	938	
(dynamic—values at 15°C)				
Flash point	°C	> 90	> 90	
Sulfur content	%	0.29	0.28	
Pour point	°C	25	23	
Surface tension	mN/m	32.3	31.9	
(air–oil at 15°C)				
IFT sea water	mN/m	27.7	26.3	
IFT fresh water	mN/m	31.5	30.5	
Adhesion	g/m ³	116	124	

SARA content (saturate, aromatic, resin, asphaltene) %

Saturate	%	53	53	
Aromatic	%	38	38	
Resin	%	7	8	
Asphaltene	%	2	1	
Waxes	%	12	4	

Emulsion formation (type formed and water content %)

Type			
Water content	%		
Viscosity	mPa·s or cP		

Chemical dispersibility with Corexit 9500

%	10		
---	----	--	--

Distillation data (% at temperature)

Boiling point (°C)			
40			
60			
80			
100			
120			
140			
160			
180			
200	1		
250	3	3	
300	8	8	
400	31	31	
500	66	67	
600	90	90	
700	98	98	

Oil name		Chayvo 6			
Origin and description		Russia (Exxon-Mobil)			
Evaporation equation		$Ev\% = (3.52 + 0.45T) \ln t$			
Where Ev = weight percent evaporated, T = surface temperature (°C), t = time (min)					
API gravity	37.91	Weathering % by weight			
(all units at 15°C)	Units	0	14.4	22.1	32.9
Density	g/ml	0.8471	0.8542	0.8609	0.8542
Viscosity	mPa·s or cP	4	12	21	33
(dynamic—values at 15°C)					
Flash point	°C	< −10	47	70	105
Sulfur content	%	0.34	0.38	0.4	0.48
Pour point	°C	−4	−1	8	8
Surface tension	mN/m	26.6	28.1	28.6	28.4
(air–oil at 15°C)					
IFT sea water	mN/m	15.8	12.4	9.7	28.4
IFT fresh water	mN/m	13.8	13.1	13.2	29
Adhesion	g/m ³	7.1	11	17	27
SARA content (saturate, aromatic, resin, asphaltene) %					
Saturate	%	87.86	85.52	80.63	81.03
Aromatic	%	8.59	9.99	11.7	11.5
Resin	%	3.4	4.31	7.46	7.13
Asphaltene	%	0.15	0.18	0.21	0.28
Waxes	%	5	6.1	7.6	7.3
Emulsion formation (type formed and water content %)					
Type					
Water content	%				
Viscosity	mPa·s or cP				
Chemical dispersibility with Corexit 9500					
	%	41	47.7	29.2	23.6
Distillation data (% at temperature)					
Boiling point (°C)					
40		1.1			
60		1.1			
80		2.6			
100		5.4	0.4		
120		9.8	2.2	0.1	
140		14	5.3	0.9	
160		18.4	9.6	3.2	
180		23	14.6	7.5	0.4
200		27.2	19.6	12.4	2.3
250		39.9	34.6	28.5	17.1
300		52.8	50.2	45.5	36.9
400		73.2	74.5	72.1	68.7
500		85.2	88.8	87.9	87.6
600		89.6	94.2	93.8	94.8
700					

Oil name		Coal Oil Point Seep Oil		
Origin and description		California, USA		
Evaporation equation				
Where Ev = weight percent evaporated, T = surface temperature (°C), t = time (min)				
API gravity	11.7	Weathering % by weight		
(all units at 15°C)	Units	0		
Density	g/ml	0.9872		
Viscosity	mPa·s or cP	165,750		
(dynamic—values at 15°C)				
Flash point	°C	> 95		
Sulfur content	%	2.51		
Pour point	°C	8		
Surface tension	mN/m			
(air–oil at 15°C)				
IFT sea water	mN/m			
IFT fresh water	mN/m			
Adhesion	g/m ³	396		
SARA content (saturate, aromatic, resin, asphaltene) %				
Saturate	%	21		
Aromatic	%	35		
Resin	%	24		
Asphaltene	%	21		
Waxes	%	0.9		
Emulsion formation (type formed and water content %)				
Type		As starting		
Water content	%	32		
Viscosity	mPa·s or cP	280,000		
Chemical dispersibility with Corexit 9500				
	%			
Distillation data (% at temperature)				
Boiling point (°C)				
40				
60				
80				
100		0.1		
120		0.1		
140		0.1		
160		0.2		
180		0.6		
200		1.2		
250		5		
300		13.3		
400		34.6		
500		56.6		
600		76.6		
700				

Oil name **Cohasset**
Origin and description Nova Scotia, Canada

Evaporation equationWhere E_v = weight percent evaporated, T = surface temperature ($^{\circ}\text{C}$), t = time (min)

API gravity	47.5	Weathering % by weight		
(all units at 15°C)	Units	0	11	26
Density	g/ml	0.79	0.8046	0.8367
Viscosity	mPa-s or cP			
(dynamic— values at 15°C)				
Flash point	$^{\circ}\text{C}$	32	40	82
Sulfur content	%			
Pour point	$^{\circ}\text{C}$	-30	-18	-12
Surface tension	mN/m	25.6	25.2	26.8
(air-oil at 15°C)				
IFT sea water	mN/m	16.5	12.5	13
IFT fresh water	mN/m			
Adhesion	g/m^3			

SARA content (saturate, aromatic, resin, asphaltene) %

Saturate	%			
Aromatic	%			
Resin	%			
Asphaltene	%	0	0	0
Waxes	%			

Emulsion formation (type formed and water content %)

Type			
Water content	%		
Viscosity	mPa-s or cP		

Chemical dispersibility with Corexit 9500

%			
---	--	--	--

Distillation data (% at temperature)

Boiling point ($^{\circ}\text{C}$)			
40			
60			
80			
100			
120			
140			
160			
180			
200			
250			
300			
400			
500			
600			
700			

Oil name **Cold Lake Bitumen**
Origin and description Alberta, Canada; a.k.a. Cold Lake Crude

Evaporation equationWhere E_v = weight percent evaporated, T = surface temperature ($^{\circ}\text{C}$), t = time (min)

API gravity	9.8	Weathering % by weight		
(all units at 15°C)	Units	0		
Density	g/ml	1.0002		
Viscosity	mPa-s or cP	235,000		
(dynamic—values at 15°C)				
Flash point	$^{\circ}\text{C}$	81		
Sulfur content	%	6.9		
Pour point	$^{\circ}\text{C}$	9		
Surface tension	mN/m			
(air-oil at 15°C)				
IFT sea water	mN/m			
IFT fresh water	mN/m			
Adhesion	g/m^3			

SARA content (saturate, aromatic, resin, asphaltene) %

Saturate	%			
Aromatic	%			
Resin	%			
Asphaltene	%	13		
Waxes	%	2		

Emulsion formation (type formed and water content %)

Type			
Water content	%		
Viscosity	mPa-s or cP		

Chemical dispersibility with Corexit 9500

%			
---	--	--	--

Distillation data (% at temperature)

Boiling point ($^{\circ}\text{C}$)			
40			
60			
80			
100			
120			
140			
160			
180			
200	1		
250	3		
300	8		
400	22		
500	37		
600	54		
700	69		

Oil name **Cold Lake Blend**
Origin and description Alberta, Canada; a.k.a. Cold Lake Dilbit

Evaporation equationWhere E_v = weight percent evaporated, T = surface temperature ($^{\circ}\text{C}$), t = time (min)

API gravity	22.6	Weathering % by weight		
(all units at 15°C)	Units	0		
Density	g/ml	0.9172		
Viscosity	mPa·s or cP	150		
(dynamic—values at 15°C)				
Flash point	$^{\circ}\text{C}$	< -35		
Sulfur content	%	4.72		
Pour point	$^{\circ}\text{C}$	-45		
Surface tension mN/m		27.1		
(air-oil at 15°C)				
IFT sea water mN/m		28.1		
IFT fresh water mN/m		21.7		
Adhesion	g/m ³			

SARA content (saturate, aromatic, resin, asphaltene) %

Saturate	%			
Aromatic	%			
Resin	%			
Asphaltene	%			
Waxes	%			

Emulsion formation (type formed and water content %)

Type			
Water content	%		
Viscosity	mPa·s or cP		

Chemical dispersibility with Corexit 9500

%			
---	--	--	--

Distillation data (% at temperature)

Boiling point ($^{\circ}\text{C}$)			
40	7		
60	7		
80	11		
100	13		
120	15		
140	17		
160	18		
180	19		
200	20		
250	23		
300	28		
400	41		
500	54		
600	69		
700	82		

Oil name **Cold Lake Diluent**
Origin and description Alberta, Canada; condensate used to dilute bitumen

Evaporation equationWhere E_v = weight percent evaporated, T = surface temperature ($^{\circ}\text{C}$), t = time (min)

API gravity	69.3	Weathering % by weight		
(all units at 15°C)	Units	0		
Density	g/ml	0.704		
Viscosity	mPa·s or cP	1		
(dynamic—values at 15°C)				
Flash point	$^{\circ}\text{C}$	< -35		
Sulfur content	%	0.25		
Pour point	$^{\circ}\text{C}$	< -75		
Surface tension mN/m		19.9		
(air-oil at 15°C)				
IFT sea water mN/m		6.8		
IFT fresh water mN/m		8.3		
Adhesion	g/m ³			

SARA content (saturate, aromatic, resin, asphaltene) %

Saturate	%			
Aromatic	%			
Resin	%			
Asphaltene	%			
Waxes	%			

Emulsion formation (type formed and water content %)

Type			
Water content	%		
Viscosity	mPa·s or cP		

Chemical dispersibility with Corexit 9500

%			
---	--	--	--

Distillation data (% at temperature)

Boiling point ($^{\circ}\text{C}$)			
40			
60			
80			
100			
120			
140			
160			
180			
200			
250			
300			
400			
500			
600			
700			

Oil name **Cook Inlet (2003)**
Origin and description Alaska, USA

Evaporation equation

Where Ev = weight percent evaporated, T = surface temperature (°C), t = time (min)

API gravity	34	Weathering % by weight			
(all units at 15°C)	Units	0	11.4	25	34.4
Density	g/ml	0.8544	0.8794	0.9028	0.9194
Viscosity	mPa·s or cP	8.2	16.8	56.4	238.9
(dynamic—values at 15°C)					
Flash point	°C				
Sulfur content	%				
Pour point	°C				
Surface tension	mN/m	24.8	27.8	29.9	30.6
(air–oil at 15°C)					
IFT sea water	mN/m	23.7	23.8	27.4	29.1
IFT fresh water	mN/m	25	26.1	27.7	30
Adhesion	g/m ³				

SARA content (saturate, aromatic, resin, asphaltene) %

Saturate	%	66.7	66.1	63.4	61.6
Aromatic	%	25.2	24.2	24.8	25.1
Resin	%	5.1	6.3	7.3	7.3
Asphaltene	%	3.1	3.5	4.5	6
Waxes	%				

Emulsion formation (type formed and water content %)

Type				
Water content	%			
Viscosity	mPa·s or cP			

Chemical dispersibility with Corexit 9500

%				
---	--	--	--	--

Distillation data (% at temperature)

Boiling point (°C)				
40				
60				
80				
100				
120				
140				
160				
180				
200				
250				
300				
400				
500				
600				
700				

Oil name **Cusiana**
Origin and description Colombia

Evaporation equation

$$\%Ev = (3.39 + 0.0457T)\ln(t)$$

Where Ev = weight percent evaporated, T = surface temperature (°C), t = time (min)

API gravity	38.3	Weathering % by weight			
(all units at 15°C)	Units	0	13	24	38
Density	g/ml	0.8328	0.8598	0.8773	0.8965
Viscosity	mPa·s or cP	7	10	31	326
(dynamic—values at 15°C)					
Flash point	°C	−28	24	60	> 100
Sulfur content	%	0.27	0.22	0.24	0.28
Pour point	°C	−19	−13	2	23
Surface tension	mN/m	25.9	27.7	28.9	34.7
(air–oil at 15°C)					
IFT sea water	mN/m	21.2	21.8	20.1	
IFT fresh water	mN/m	22.5	22.2	21.9	
Adhesion	g/m ³	11	12	17	94

SARA content (saturate, aromatic, resin, asphaltene) %

Saturate	%	76	71	70	71
Aromatic	%	20	23	23	22
Resin	%	3	5	5	5
Asphaltene	%	1	1	2	2
Waxes	%	5	5.6	6.2	6.8

Emulsion formation (type formed and water content %)

Type				
Water content	%			
Viscosity	mPa·s or cP			

Chemical dispersibility with Corexit 9500

%				
---	--	--	--	--

Distillation data (% at temperature)

Boiling point (°C)				
40	1.7			
60	3	0.1		
80	5.4	0.7	0.1	0.1
100	9.1	2.8	0.2	0.2
120	12.7	5.7	0.4	0.3
140	16.4	9.4	1.4	0.3
160	20.5	13.7	4	0.3
180	24.6	18.2	8.1	0.4
200	28.2	22.2	12.3	0.9
250	39.4	34.5	26.1	11
300	51	47.3	40.6	27.7
400	71.9	70.3	66.8	59.6
500	87.7	87	85.8	82.8
600	93.6	94.1	93.9	92.5
700				

Oil name	Diesel 2002				
Origin and description	Retailer, Ottawa, Canada (Stinson's Gas); a.k.a. "Summer" Diesel, Fuel Oil No. 2				
Evaporation equation	$\%Ev = (0.02 + 0.013T) \sqrt{t}$				
Where Ev = weight percent evaporated, T = surface temperature (°C), t = time (min)					
API gravity	37.52	Weathering % by weight			
(all units at 15°C)	Units	0	7.2	14.2	22
Density	g/ml	0.831	0.835	0.8383	0.8416
Viscosity	mPa-s or cP	2.76	3.27	3.42	4.18
(dynamic—values at 15°C)					
Flash point	°C	54	65	76	85
Sulfur content	%	0.09	0.1	0.1	0.1
Pour point	°C	−50	−49	−43	−41
Surface tension	mN/m	27.5	27.7	28.1	28.3
(air–oil at 15°C)					
IFT sea water	mN/m	18.1	19.5	20.7	21.9
IFT fresh water	mN/m	21.6	23.9	24.3	25.7
Adhesion	g/m ³	2	12	13	8
SARA content (saturate, aromatic, resin, asphaltene) %					
Saturate	%	88.2	86.1	86.1	85.6
Aromatic	%	10.2	11.9	11.7	11.4
Resin	%	1.7	2	2.2	3
Asphaltene	%	0	0	0	0
Waxes	%	1.7	1.8	2	1.8
Emulsion formation (type formed and water content %)					
Type		Unstable	Unstable	Unstable	Unstable
Water content	%				
Viscosity	mPa-s or cP				
Chemical dispersibility with Corexit 9500					
	%	72	71	64	66

Distillation data (% at temperature)				
Boiling point (°C)				
40				
60				
80	0.2	0.1		
100	0.5	0.1		
120	1.2	0.1		
140	2.8	0.7	0.1	
160	7.8	4	1.4	0.3
180	16.4	11.8	7.1	3.2
200	26.8	22.4	17	11.2
250	57.4	55.4	51.7	46.7
300	84.1	84.5	83.3	81.4
400	97.9	99.7	99.8	97.8
500	98.2			
600	98.4			
700				

Oil name	Diesel Fuel Oil (Alaska)		
Origin and description	a.k.a. Automotive gas oil		
Evaporation equation	Long-term: %Ev = (4.54 + 0.045 <i>T</i>)ln(<i>t</i>) Short-term (< 5 days): %Ev = (0.51 + 0.013 <i>T</i>)√(<i>t</i>)		
Where Ev = weight percent evaporated, <i>T</i> = surface temperature (°C), <i>t</i> = time (min)			
API gravity	38.8	Weathering % by weight	
(all units at 15°C)	Units	0	37
Density	g/ml	0.83	0.8515
Viscosity	mPa-s or cP	2	5
(dynamic—values at 15°C)			
Flash point	°C	40	> 95
Sulfur content	%	0.21	0.33
Pour point	°C	−36	−22
Surface tension	mN/m	27.4	28.5
(air–oil at 15°C)			
IFT sea water	mN/m	34.5	21.1
IFT fresh water	mN/m	35.4	28.4
Adhesion	g/m ³	2	11
SARA content (saturate, aromatic, resin, asphaltene) %			
Saturate	%	74	75
Aromatic	%	24	23
Resin	%	1	1
Asphaltene	%	0	0
Waxes	%		
Emulsion formation (type formed and water content %)			
Type		Unstable	Unstable
Water content	%		
Viscosity	mPa-s or cP		
Chemical dispersibility with Corexit 9500			
	%	70	39

Distillation data (% at temperature)			
Boiling point (°C)			
40			
60			
80			
100	1		
120	2		
140	5		
160	12		
180	21		
200	29	3	
250	56	32	
300	85	74	
400			
500			
600			
700			

Oil name Diesel Fuel Oil (Canada)
Origin and description Automotive gas oil

Evaporation equation Short-term (< 5 days): %Ev = $(0.31 + 0.018T)\sqrt{t}$
Long-term: %Ev = $(5.8 + 0.045T)\ln(t)$

Where Ev = weight percent evaporated, T = surface temperature (°C), t = time (min)

API gravity	39.4	Weathering % by weight		
(all units at 15°C)	Units	0	28	
Density	g/ml	0.8245	0.835	
Viscosity	mPa·s or cP	2		
(dynamic—values at 15°C)				
Flash point	°C	> 40		
Sulfur content	%	0.1		
Pour point	°C	−30		
Surface tension	mN/m	26.5		
(air–oil at 15°C)				
IFT sea water	mN/m	28		
IFT fresh water	N/m	29.4		
Adhesion	g/m ³			

SARA content (saturate, aromatic, resin, asphaltene) %

Saturate	%			
Aromatic	%			
Resin	%			
Asphaltene	%			
Waxes	%	1		

Emulsion formation (type formed and water content %)

Type			
Water content	%		
Viscosity	mPa·s or cP		

Chemical dispersibility with Corexit 9500

%			
---	--	--	--

Distillation data (% at temperature)

Boiling point (°C)			
40	1		
60	1		
80	1		
100	1		
120	1		
140	3		
160	11		
180	23		
200	34		
250	65		
300	91		
400			
500			

Oil name Diesel Fuel Oil (Southern USA, 1994)
Origin and description a.k.a. Automotive gas oil

Evaporation equation Long-term: %Ev = $(2.18 + 0.045T)\ln(t)$
Short-term (< 5 days): %Ev = $(-0.02 + 0.013T)\sqrt{t}$

Where Ev = weight percent evaporated, T = surface temperature (°C), t = time (min)

API gravity	37.2	Weathering % by weight		
(all units at 15°C)	Units	0	8	16
Density	g/ml	0.8389	0.8427	0.8447
Viscosity	mPa·s or cP	5	5	6
(dynamic—values at 15°C)				
Flash point	°C	70	> 95	> 95
Sulfur content	%	0.22	0.21	0.27
Pour point	°C	−7	−7	−4
Surface tension	mN/m	28.5	28.9	29
(air–oil at 15°C)				
IFT sea water	mN/m	18.8	13.7	15.1
IFT fresh water	mN/m	24.1	21.1	21.5
Adhesion	g/m ³	9	8	15

SARA content (saturate, aromatic, resin, asphaltene) %

Saturate	%	76	78	78
Aromatic	%	22	20	20
Resin	%	2	2	2
Asphaltene	%	0	0	0
Waxes	%	10	11	11

Emulsion formation (type formed and water content %)

Type	Unstable	Unstable	Unstable
Water content	%		
Viscosity	mPa·s or cP		

Chemical dispersibility with Corexit 9500

%	52	45	53
---	----	----	----

Distillation data (% at temperature)

Boiling point (°C)			
40			
60			
80			
100			
120	1		
140	1		
160	3		
180	5	1	
200	8	3	
250	27	20	15
300	62	58	54
400	99	99	98
500			
600			
700			

Oil name Diesel Fuel Oil (Southern USA, 1997)
Origin and description a.k.a. Automotive gas oil

Evaporation equation Long-term: $\%Ev = (-0.02 + 0.013T)\sqrt{t}$
 Short-term (< 5 days): $\%Ev = (0.03 + 0.013T)\sqrt{t}$
 Where Ev = weight percent evaporated, T = surface temperature (°C), t = time (min)

API gravity	37.6	Weathering % by weight		
(all units at 15°C)	Units	0	8	14
Density	g/ml	0.8362	0.84	0.842
Viscosity	mPa·s or cP	4	5	6

(dynamic—values at 15°C)

Flash point	°C	66	95	> 95
Sulfur content	%	0.4	0.43	0.43
Pour point	°C	−14	−9	−7
Surface tension	mN/m	27.3	28.5	28.6

(air–oil at 15°C)

IFT sea water	mN/m	22.8	20.5	16.8
IFT fresh water	mN/m	24	21.9	21
Adhesion	g/m ³	6	6	8

SARA content (saturate, aromatic, resin, asphaltene) %

Saturate	%	76	75	79
Aromatic	%	23	23	19
Resin	%	1	1	2
Asphaltene	%	0	0	0
Waxes	%			

Emulsion formation (type formed and water content %)

Type			
Water content	%		
Viscosity	mPa·s or cP		

Chemical dispersibility with Corexit 9500

%	36	32	20
---	----	----	----

Distillation data (% at temperature)

Boiling point (°C)

40			
60			
80			
100			
120	1		
140	2		
160	3		
180	6	2	
200	11	5	2
250	31	26	21
300	63	61	58
400	99	99	98
500			
600			
700			

Oil name Dos Cuadras
Origin and description California, USA

Evaporation equation $\%Ev = (1.88 + 0.045T)\ln(t)$
 Where Ev = weight percent evaporated, T = surface temperature (°C), t = time (min)

API gravity	25.6	Weathering % by weight		
(all units at 15°C)	Units	0	11	20
Density	g/ml	0.9	0.927	0.9359
Viscosity	mPa·s or cP	51	187	741

(dynamic—values at 15°C)

Flash point	°C	< −30	53	> 90
Sulfur content	%	1.24	1.17	1.42
Pour point	°C	−30	−3	6
Surface tension	mN/m	28.1	28.7	30.6

(air–oil at 15°C)

IFT sea water	mN/m	21.2	22.6	21
IFT fresh water	mN/m	21.6	24.1	23.1
Adhesion	g/m ³	29	38	56

SARA content (saturate, aromatic, resin, asphaltene) %

Saturate	%	48	42	41
Aromatic	%	30	31	31
Resin	%	17	20	19
Asphaltene	%	6	7	9
Waxes	%	6	4	6

Emulsion formation (type formed and water content %)

Type		Unstable	Meso-stable	Meso-stable
Water content	%		48	69
Viscosity	mPa·s or cP		800	9800

Chemical dispersibility with Corexit 9500

%	37	15	7
---	----	----	---

Distillation data (% at temperature)

Boiling point (°C)

40	2		
60	3		
80	4		
100	6	1	
120	9	1	
140	11	3	
160	14	5	
180	17	8	1
200	19	10	3
250	28	19	12
300	36	28	22
400	54	48	44
500	72	68	66
600	87	83	81
700	96	92	92

Oil name Ekofisk
Origin and description North Sea, Norway

Evaporation equation $\%Ev = (4.92 + 0.045T)\ln(t)$
 Where Ev = weight percent evaporated, T = surface temperature (°C), t = time (min)

API gravity	39.2	Weathering % by weight			
(all units at 15°C)	Units	0	26	37	48
Density	g/ml				
Viscosity	mPa·s or cP	5		1277	
(dynamic—values at 15°C)					
Flash point	°C	−14	46	> 95	133
Sulfur content	%	0.15		0.26	
Pour point	°C	−29	15	15	27
Surface tension	mN/m	25.5		30.1	
(air–oil at 15°C)					
IFT sea water	mN/m	11		10.3	
IFT fresh water	mN/m	15.7		16.2	
Adhesion	g/m ³	7		23	

SARA content (saturate, aromatic, resin, asphaltene) %					
Saturate	%	68		60	49
Aromatic	%	25		26	41
Resin	%	7		13	8
Asphaltene	%	1		1	1
Waxes	%	5		7	8

Emulsion formation (type formed and water content %)					
Type					
Water content	%				
Viscosity	mPa·s or cP				

Chemical dispersibility with Corexit 9500					
%					

Distillation data (% at temperature)					
Boiling point (°C)					
40	5				
60	5				
80	7				
100	10				
120	14				
140	18				
160	23				
180	28				
200	32				
250	43		8		
300	54		23		
400	71		50		
500	85		72		
600	94		86		
700	99		95		

Oil name Electrical Insulating Oil (Votesso 35)
Origin and description

Evaporation equation $\%Ev = (-0.18 + 0.013T)\sqrt{t}$
 Where Ev = weight percent evaporated, T = surface temperature (°C), t = time (min)

API gravity	31.8	Weathering % by weight		
(all units at 15°C)	Units	0		
Density	g/ml	0.8711		
Viscosity	mPa·s or cP			
(dynamic—values at 15°C)				
Flash point	°C	> 95		
Sulfur content	%	0.17		
Pour point	°C	−45		
Surface tension	mN/m	29.9		
(air–oil at 15°C)				
IFT sea water	mN/m	43.4		
IFT fresh water	mN/m	42.6		
Adhesion	g/m ³	14		

SARA content (saturate, aromatic, resin, asphaltene) %				
Saturate	%	74		
Aromatic	%	24		
Resin	%	1		
Asphaltene	%	0		
Waxes	%			

Emulsion formation (type formed and water content %)				
Type				
Water content	%			
Viscosity	mPa·s or cP			

Chemical dispersibility with Corexit 9500				
%				

Distillation data (% at temperature)				
Boiling point (°C)				
40				
60				
80				
100				
120				
140				
160				
180				
200				
250	1			
300	22			
400	96			
500				
600				
700				

Oil name **Empire**
Origin and description Louisiana, USA; a.k.a. Louisiana heavy

Evaporation equation $\%Ev = (2.21 + 0.0457T)\ln(t)$
 Where Ev = weight percent evaporated, T = surface temperature (°C), t = time (min)

API gravity	33.8	Weathering % by weight		
	Units	0	10	20
(all units at 15°C)				
Density	g/ml	0.8554	0.8721	0.8839
Viscosity	mPa-s or cP	11	20	42
(dynamic—values at 15°C)				
Flash point	°C	−9	52	> 90
Sulfur content	%			
Pour point	°C	−41	−9	−1
Surface tension mN/m		27.4	28	28.7
(air–oil at 15°C)				
IFT sea water mN/m		15.9	16.1	16.7
IFT fresh water mN/m		18.7	21.3	20.6
Adhesion	g/m ³	20	27	34

SARA content (saturate, aromatic, resin, asphaltene) %				
Saturate	%	67	67	65
Aromatic	%	25	27	27
Resin	%	7	6	6
Asphaltene	%	1	1	1
Waxes	%	5	4	4

Emulsion formation (type formed and water content %)			
Type			
Water content	%		
Viscosity	mPa-s or cP		

Chemical dispersibility with Corexit 9500			
%	31		

Distillation data (% at temperature)			
Boiling point (°C)			
40	1	1	
60	2	1	
80	3	1	
100	5	1	
120	7	2	
140	10	4	
160	13	7	
180	16	10	1
200	19	13	4
250	30	25	16
300	44	40	33
400	68	66	62
500	58	85	83
600	94	94	94
700	99	99	99

Oil name **Endicott**
Origin and description Alaska, USA; a.k.a. Cook Inlet

Evaporation equation $\%Ev = (0.90 + 0.0457T)\ln(t)$
 Where Ev = weight percent evaporated, T = surface temperature (°C), t = time (min)

API gravity	23	Weathering % by weight		
	Units	0	8	13
(all units at 15°C)				
Density	g/ml	0.9149	0.9318	0.9401
Viscosity	mPa-s or cP	84	321	682
(dynamic—values at 15°C)				
Flash point	°C			
Sulfur content	%	1.34	1.34	1.4
Pour point	°C	−2	8	14
Surface tension mN/m		29.1	27.7	30.9
(air–oil at 15°C)				
IFT sea water mN/m		25.8	26	23
IFT fresh water mN/m		25.4	24.4	25.5
Adhesion	g/m ³			

SARA content (saturate, aromatic, resin, asphaltene) %			
Saturate	%		
Aromatic	%		
Resin	%		
Asphaltene	%	4	4
Waxes	%	8	

Emulsion formation (type formed and water content %)			
Type			
Water content	%		
Viscosity	mPa-s or cP		

Chemical dispersibility with Corexit 9500			
%	10		

Distillation data (% at temperature)			
Boiling point (°C)			
40	1		
60	1		
80	3		
100	5		
120	7		
140	7		
160	8		
180	9		
200	11		
250	17		
300	24		
400	43		
500	63		
600	78		
700	87		

Oil name Eugene Island Block 32
Origin and description Gulf of Mexico, USA

Evaporation equation $\%Ev = (0.77 + 0.045T)\ln(t)$
 Where Ev = weight percent evaporated, T = surface temperature (°C), t = time (min)

API gravity	36.9	Weathering % by weight			
(all units at 15°C)	Units	0	6	13	20
Density	g/ml	0.8399	0.8418	0.8453	0.8481
Viscosity	mPa·s or cP	9	9	16	21
(dynamic—values at 15°C)					
Flash point	°C	21	79	> 95	> 95
Sulfur content	%	0.02	0.03	0.03	0.04
Pour point	°C	7	9	12	13
Surface tension	mN/m	27.5	28.5	27.9	27.9
(air–oil at 15°C)					
IFT sea water	mN/m	18.5	23.5	23.7	21.3
IFT fresh water	mN/m	21.7	25.2	26.7	21.8
Adhesion	g/m ³	10	13	20	20

SARA content (saturate, aromatic, resin, asphaltene) %

Saturate	%	84	81	82	81
Aromatic	%	14	16	15	16
Resin	%	2	2	2	3
Asphaltene	%	1	1	1	1
Waxes	%	10	10	11	12

Emulsion formation (type formed and water content %)

Type				
Water content	%			
Viscosity	mPa·s or cP			

Chemical dispersibility with Corexit 9500

%	44	30	22	18
---	----	----	----	----

Distillation data (% at temperature)

Boiling point (°C)				
40				
60				
80	1			
100	2			
120	3			
140	4	1		
160	5	2		
180	7	4		
200	10	6	2	
250	23	20	14	9
300	46	44	40	34
400	82	81	80	78
500	96	95	95	94
600	99	99	99	99
700				

Oil name Eugene Island Block 43
Origin and description Gulf of Mexico, USA

Evaporation equation $\%Ev = (1.57 + 0.045T)\ln(t)$
 Where Ev = weight percent evaporated, T = surface temperature (°C), t = time (min)

API gravity	36.8	Weathering % by weight			
(all units at 15°C)	Units	0	7	16	24
Density	g/ml	0.8404	0.8515	0.8594	0.8665
Viscosity	mPa·s or cP	13	21	36	65
(dynamic—values at 15°C)					
Flash point	°C	12	65	> 95	> 95
Sulfur content	%	0.18	0.1	0.1	0.11
Pour point	°C	0	7	7	11
Surface tension	mN/m	27.5	28.5	29.2	29.7
(air–oil at 15°C)					
IFT sea water	mN/m	2.9	3.6	4.2	8
IFT fresh water	mN/m	4.5			
Adhesion	g/m ³	18	19	20	25

SARA content (saturate, aromatic, resin, asphaltene) %

Saturate	%	81	78	77	78
Aromatic	%	25	17	15	16
Resin	%	3	4	7	5
Asphaltene	%	0	1	1	1
Waxes	%	8	9	8	9

Emulsion formation (type formed and water content %)

Type				
Water content	%			
Viscosity	mPa·s or cP			

Chemical dispersibility with Corexit 9500

%	22	11		
---	----	----	--	--

Distillation data (% at temperature)

Boiling point (°C)				
40				
60				
80				
100	1			
120	1	1		
140	2	2		
160	6	4		
180	13	6	1	
200	16	10	3	
250	27	21	14	7
300	43	38	32	24
400	71	68	65	61
500	90	88	87	85
600	98	97	96	96
700				

Oil name	Everdell			
Origin and description	Alberta, Canada			
Evaporation equation	$\%Ev = (3.38 + 0.045T)\ln(t)$			
Where Ev = weight percent evaporated, T = surface temperature (°C), t = time (min)				
API gravity	44	Weathering % by weight		
(all units at 15°C)	Units	0	15	29
Density	g/ml	0.8064	0.8355	0.852
Viscosity	mPa·s or cP	4	9	25
(dynamic—values at 15°C)				
Flash point	°C	−27	18	62
Sulfur content	%	0.08	0.05	0.05
Pour point	°C	−21	0	8
Surface tension	mN/m	24.7	27	28.5
(air–oil at 15°C)				
IFT sea water	mN/m	11	12.6	6.3
IFT fresh water	mN/m	15.1	15.7	
Adhesion	g/m ³	3	6	15
SARA content (saturate, aromatic, resin, asphaltene) %				
Saturate	%	79	77	77
Aromatic	%	19	21	21
Resin	%	2	2	2
Asphaltene	%	0	0	0
Waxes	%	4.3	4.7	5.5
Emulsion formation (type formed and water content %)				
Type				
Water content	%			
Viscosity	mPa·s or cP			
Chemical dispersibility with Corexit 9500				
	%			

Distillation data (% at temperature)				
Boiling point (°C)				
40	2.8			
60	3.5			
80	4.1	0.1		
100	8.8	1.9		
120	15.2	6.7	0.2	
140	19.3	10.6	1.3	
160	23.8	15.2	4	
180	27.9	19.7	8	
200	31.5	23.7	12.1	0.5
250	41.3	34.8	24.5	9.2
300	52.3	47.1	38.5	25.2
400	72.8	70.1	65.1	57.8
500	87.8	87	84.7	81.8
600	96	96.1	95.2	94.7
700				

Oil name	Federated (1998)				
Origin and description	Alberta, Canada				
Evaporation equation	$\%Ev = (3.45 + 0.045T)\ln(t)$				
Where Ev = weight percent evaporated, T = surface temperature ($^{\circ}\text{C}$), t = time (min)					
API gravity	38.9	Weathering % by weight			
(all units at 15°C)	Units	0	13	25	39
Density	g/ml	0.8298	0.8562	0.8735	0.8931
Viscosity	mPa·s or cP	5	9	23	88
(dynamic—values at 15°C)					
Flash point	$^{\circ}\text{C}$	−26	27	64	> 95
Sulfur content	%	0.34	0.33	0.39	0.48
Pour point	$^{\circ}\text{C}$	−22	−2	7	15
Surface tension	mN/m	25.3	27.2	28.6	29.7
(air–oil at 15°C)					
IFT sea water	mN/m	15.8	15.1	14.2	
IFT fresh water	mN/m	16.9	17.4	18	
Adhesion	g/m^3	5	8	14	42
SARA content (saturate, aromatic, resin, asphaltene) %					
Saturate	%	72	70	65	64
Aromatic	%	22	24	28	27
Resin	%	4	4	5	6
Asphaltene	%	2	2	2	3
Waxes	%	2	207	3.4	4.8
Emulsion formation (type formed and water content %)					
Type					
Water content	%				
Viscosity	mPa·s or cP				
Chemical dispersibility with Corexit 9500					
	%				

Distillation data (% at temperature)				
Boiling point (°C)				
40	1.8			
60	3.2	0.1	0.1	0.1
80	6	0.7	0.1	0.1
100	10.7	3	0.1	0.1
120	14.5	5.8	0.3	0.1
140	18.5	9.6	1.1	0.1
160	23.1	14.5	3.8	0.1
180	28	19.8	8.3	0.1
200	32.1	24.3	13.1	0.8
250	42.3	35.7	26	10.2
300	52.8	47.2	39.2	25.4
400	72.2	68.7	63.9	55.7
500	87.2	85.5	83.2	79.4
600	95.5	94.9	94	92.6
700				

Oil name **Fluid Catalytic Cracker Heavy Cycle Oil**
Origin and description

Evaporation equation $\%Ev = (0.17 + 0.013T)\sqrt{t}$
 Where Ev = weight percent evaporated, T = surface temperature (°C), t = time (min)

API gravity	24.3	Weathering % by weight		
(all units at 15°C) Units		0	4	9
Density	g/ml	0.9075	0.9102	0.9127
Viscosity	mPa-s or cP	3	3	4
(dynamic—values at 15°C)				
Flash point	°C	69	83	>90
Sulfur content	%	0.14	0.16	0.14
Pour point	°C	−58	−58	−55
Surface tension	mN/m	31	29.5	30.4
(air–oil at 15°C)				
IFT sea water	mN/m	26.2	23.6	23.6
IFT fresh water	mN/m	27.1	25	24.2
Adhesion	g/m ³	3		2

SARA content (saturate, aromatic, resin, asphaltene) %

Saturate	%	34		29
Aromatic	%	64		69
Resin	%	2		2
Asphaltene	%	0		0
Waxes	%	0		1

Emulsion formation (type formed and water content %)

Type			
Water content	%		
Viscosity	mPa-s or cP		

Chemical dispersibility with Corexit 9500

%			
---	--	--	--

Distillation data (% at temperature)

Boiling point (°C)			
40	1		
60	1		
80	1		
100	1		
120	2		
140	3		
160	3		
180	5		1
200	11		6
250	59		56
300	95		94
400			
500			
600			
700			

Oil name **Fluid Catalytic Cracker Light Cycle Oil**
Origin and description

Evaporation equation $\%Ev = (-0.17 + 0.013T)\sqrt{t}$
 Where Ev = weight percent evaporated, T = surface temperature (°C), t = time (min)

API gravity	1.6	Weathering % by weight		
(all units at 15°C) Units		0		
Density	g/ml	7418		
Viscosity	mPa-s or cP			
(dynamic—values at 15°C)				
Flash point	°C			
Sulfur content	%	1.062		
Pour point	°C	1		
Surface tension	mN/m	34		
(air–oil at 15°C)				
IFT sea water	mN/m			
IFT fresh water	mN/m			
Adhesion	g/m ³	77		

SARA content (saturate, aromatic, resin, asphaltene) %

Saturate	%	17		
Aromatic	%	58		
Resin	%	4		
Asphaltene	%	20		
Waxes	%	1		

Emulsion formation (type formed and water content %)

Type			
Water content	%		
Viscosity	mPa-s or cP		

Chemical dispersibility with Corexit 9500

%			
---	--	--	--

Distillation data (% at temperature)

Boiling point (°C)			
40			
60			
80			
100			
120			
140			
160			
180			
200	1		
250	4		
300	10		
400	37		
500	87		
600	97		
700			

Oil name **Fuel Oil No. 2**
Origin and description a.k.a. Diesel fuel oil, furnace oil,
and home heating oil

Evaporation equation

Where E_v = weight percent evaporated, T = surface
temperature ($^{\circ}\text{C}$), t = time (min)

API gravity		Weathering % by weight		
(all units at 15°C)		Units	0	
Density	g/ml		0.866	
Viscosity	mPa·s or cP			
(dynamic—values at 15°C)				
Flash point	$^{\circ}\text{C}$		91	
Sulfur content	%		0.36	
Pour point	$^{\circ}\text{C}$		−27	
Surface tension mN/m			27.4	
(air–oil at 15°C)				
IFT sea water mN/m			13.6	
IFT fresh water mN/m			14.7	
Adhesion	g/m^3			
SARA content (saturate, aromatic, resin, asphaltene) %				
Saturate	%			
Aromatic	%			
Resin	%			
Asphaltene	%			
Waxes	%			

Emulsion formation (type formed and water content %)

Type			
Water content	%		
Viscosity	mPa·s or cP		

Chemical dispersibility with Corexit 9500

%			
---	--	--	--

Distillation data (% at temperature)

Boiling point ($^{\circ}\text{C}$)			
40			
60			
80			
100			
120			
140			
160			
180			
200			
250			
300			
400			
500			
600			
700			

Oil name **Fuel Oil No. 5 (2000)**
Origin and description New Jersey, USA (via US Dept.
Int., M.M.S., OHMSETT, NJ,
2000); a.k.a. Bunker B

Evaporation equation

$$\%E_v = (-0.14 + 0.0137) \sqrt{t}$$

Where E_v = weight percent evaporated, T = surface temperature ($^{\circ}\text{C}$),
 t = time (min)

API gravity		Weathering % by weight		
(all units at 15°C)		Units	0	7.2
Density	g/ml		0.9883	1.0032
Viscosity	mPa·s or cP		1410	4530
(dynamic—values at 15°C)				
Flash point	$^{\circ}\text{C}$		94	136
Sulfur content	%		1	1.08
Pour point	$^{\circ}\text{C}$		−19	−3
Surface tension mN/m				
(air–oil at 15°C)				
IFT sea water mN/m				
IFT fresh water mN/m				
Adhesion	g/m^3		34	47

SARA content (saturate, aromatic, resin, asphaltene) %

Saturate	%	44.2	39.9	
Aromatic	%	39.5	39.1	
Resin	%	8	8.3	
Asphaltene	%	8.4	12.8	
Waxes	%	2.3	2.5	

Emulsion formation (type formed and water content %)

Type	Stable	Stable	
Water content	%	78.3	72.8
Viscosity	mPa·s or cP		

Chemical dispersibility with Corexit 9500

%	15	7	
---	----	---	--

Distillation data (% at temperature)

Boiling point ($^{\circ}\text{C}$)			
40			
60			
80			
100			
120	0.1		
140	0.2		
160	0.6		
180	1.3		
200	2.3	0.2	
250	7.2	3.8	
300	14.6	11.3	
400	39.9	38	
500	66.2	66.2	
600	80.4	81.5	

Oil name **Garden Banks Block 387**
Origin and description Gulf of Mexico, USA

Evaporation equation $\%Ev = (1.84 + 0.045T)\ln(t)$
 Where Ev = weight percent evaporated, T = surface temperature (°C), t = time (min)

API gravity	29.5	Weathering % by weight			
		0	7	15	23
(all units at 15°C) Units					
Density	g/ml	0.8782	0.8979	0.9144	0.9287
Viscosity	mPa-s or cP	29	64	181	579
(dynamic—values at 15°C)					
Flash point	°C	−28	33	80	> 95
Sulfur content	%	1.52	1.45	1.55	1.68
Pour point	°C	−39	−34	−29	−25
Surface tension	mN/m	27.5	28.7	30.1	31
(air–oil at 15°C)					
IFT sea water	mN/m	22.9	23.2	22.9	18.6
IFT fresh water	mN/m	25	24.4	25.9	22.3
Adhesion	g/m ³	22	37	33	27

SARA content (saturate, aromatic, resin, asphaltene) %

Saturate	%	53	51	51	46
Aromatic	%	36	38	37	40
Resin	%	10	11	11	13
Asphaltene	%	1	1	1	2
Waxes	%				

Emulsion formation (type formed and water content %)

Type	Unstable	Unstable	Unstable	Meso-stable
Water content				37
Viscosity				6835

Chemical dispersibility with Corexit 9500

%	27	30	17	0
---	----	----	----	---

Distillation data (% at temperature)

Boiling point (°C)				
40	2			
60	2			
80	2			
100	4	1		
120	6	3		
140	9	5		
160	11	7	1	
180	14	10	3	
200	17	13	6	
250	24	20	14	6
300	33	31	26	16
400	52	51	47	29
500	70	70	67	64
600	83	84	83	81
700	92	93	93	92

Oil name **Garden Banks Block 426**
Origin and description Gulf of Mexico, USA

Evaporation equation $\%Ev = (3.44 + 0.045T)\ln(t)$
 Where Ev = weight percent evaporated, T = surface temperature (°C), t = time (min)

API gravity		Weathering % by weight			
		0	12	25	38
(all units at 15°C) Units					
Density	g/ml	0.8285	0.8561	0.8779	0.8993
Viscosity	mPa-s or cP	6	13	34	136
(dynamic—values at 15°C)					
Flash point	°C	−24	24	68	> 95
Sulfur content	%	0.94	0.76	1.06	1.17
Pour point	°C	−22	−7	−2	6
Surface tension	mN/m	23.3	26.3	28.2	30.1
(air–oil at 15°C)					
IFT sea water	mN/m	23.2	26.6	25.2	21.8
IFT fresh water	mN/m	24.7	26.8	26.7	24.1
Adhesion	g/m ³	13	18	37	39

SARA content (saturate, aromatic, resin, asphaltene) %

Saturate	%	70	61	62	56
Aromatic	%	24	30	28	32
Resin	%	5	8	8	10
Asphaltene	%	1	1	2	3
Waxes	%				

Emulsion formation (type formed and water content %)

Type	Unstable	Unstable	Unstable	Stable
Water content				65
Viscosity				9159

Chemical dispersibility with Corexit 9500

%	43	22	16	18
---	----	----	----	----

Distillation data (% at temperature)

Boiling point (°C)				
40	3			
60	3			
80	4			
100	8	3		
120	12	5		
140	16	9	1	
160	20	14	3	
180	25	18	7	
200	29	22	11	1
250	39	33	24	9
300	49	44	36	23
400	67	63	60	51
500	81	79	78	73
600	90	88	89	87
700	95	94	96	95

Oil name Gasoline (Unleaded)
Origin and description a.k.a. Automotive fuel; petrol

Evaporation equation $\%Ev = (13.2 + 0.21T)\ln(t)$
 Where Ev = weight percent evaporated, T = surface temperature ($^{\circ}C$), t = time (min)

API gravity		Weathering % by weight		
(all units at 15°C)	Units	0		
Density	g/ml	0.750–0.850		
Viscosity	mPa·s or cP			
(dynamic—values at 15°C)				
Flash point	$^{\circ}C$	–30		
Sulfur content	%			
Pour point	$^{\circ}C$			
Surface tension	mN/m			
(air–oil at 15°C)				
IFT sea water	mN/m			
IFT fresh water	mN/m			
Adhesion	g/m ³			

SARA content (saturate, aromatic, resin, asphaltene) %

Saturate	%			
Aromatic	%			
Resin	%			
Asphaltene	%			
Waxes	%			

Emulsion formation (type formed and water content %)

Type			
Water content	%		
Viscosity	mPa·s or cP		

Chemical dispersibility with Corexit 9500

%			
---	--	--	--

Distillation data (% at temperature)

Boiling point ($^{\circ}C$)			
40	26		
60	30		
80	44		
100	70		
120	84		
140	85		
160	88		
180	95		
200	98		
250			
300			
400			
500			
600			
700			

Oil name Genesis
Origin and description Gulf of Mexico, USA

Evaporation equation $\%Ev = (2.12 + 0.0457T)\ln(t)$
 Where Ev = weight percent evaporated, T = surface temperature ($^{\circ}C$), t = time (min)

API gravity	28.4	Weathering % by weight			
(all units at 15°C)	Units	0	8	15	23
Density	g/ml	0.8841	0.9074	0.9223	0.9364
Viscosity	mPa·s or cP	26	66	157	543
(dynamic—values at 15°C)					
Flash point	$^{\circ}C$	–22	35	71	> 100
Sulfur content	%	1.38	1.36	1.51	1.73
Pour point	$^{\circ}C$	–62	–41	–26	–24
Surface tension	mN/m	26.8	28.5	28.9	30.6
(air–oil at 15°C)					
IFT sea water	mN/m	22.9	21.5	21.2	16.4
IFT fresh water	mN/m	23.4	24.2	22.8	19.1
Adhesion	g/m ³	31	33	22	24

SARA content (saturate, aromatic, resin, asphaltene) %

Saturate	%	59	56.9	57	47.7
Aromatic	%	29.7	32	30.3	27.8
Resin	%	9.7	9.3	10.6	21.2
Asphaltene	%	1.6	1.8	2.1	3.3
Waxes	%	0.9	0.9	1.1	1.2

Emulsion formation (type formed and water content %)

Type	Unstable	Unstable	Unstable	Meso-stable
Water content	%			62
Viscosity	mPa·s or cP			10,510

Chemical dispersibility with Corexit 9500

%	23	13	24	19
---	----	----	----	----

Distillation data (% at temperature)

boiling point ($^{\circ}C$)				
40	0.9			
60	1.2			
80	1.9	0.2		
100	3.3	0.8		
120	4.5	1.7	0.1	
140	5.9	2.9	0.4	
160	7.6	4.7	1.3	
180	9.5	6.6	2.9	0.1
200	11.3	8.5	4.8	0.7
250	16.7	14.3	11	5.6
300	23.1	21.1	18.5	13.4
400	37.9	36.9	35.7	32
500	53.5	53.6	53.9	51.7
600	66.6	67.7	69.6	68.6
700				

Oil name	Granite Point			
Origin and description	Cook Inlet, Alaska, USA; a.k.a Cook Inlet			
Evaporation equation	$\%Ev = (4.54 + 0.0457T)\ln(t)$			
Where Ev = weight percent evaporated, T = surface temperature (°C), t = time (min)				
API gravity	39	Weathering % by weight		
(all units at 15°C)	Units	0	45	
Density	g/ml	0.8293	0.9028	
Viscosity	mPa·s or cP	4	75	
(dynamic—values at 15°C)				
Flash point	°C	−23	> 95	
Sulfur content	%	0.06	0.08	
Pour point	°C	−37	2	
Surface tension	mN/m	25.6	30.7	
(air–oil at 15°C)				
IFT sea water	mN/m	20.7	14.6	
IFT fresh water	mN/m	21.6	19.5	
Adhesion	g/m ³	8	39	
SARA content (saturate, aromatic, resin, asphaltene) %				
Saturate	%	72	62	
Aromatic	%	22	28	
Resin	%	5	7	
Asphaltene	%	1	3	
Waxes	%			
Type		Unstable	Meso-stable	
Water content	%		83	
Viscosity	mPa·s or cP		16,000	
Chemical dispersibility with Corexit 9500				
	%	41	14	

Distillation data (% at temperature)			
Boiling point (°C)			
40	4		
60	4		
80	7		
100	12		
120	17		
140	22		
160	27		
180	31		
200	36		
250	47	9	
300	58	26	
400	77	59	
500	90	82	
600	96	93	
700	99	98	

Oil name		Green Canyon Block 65			
Origin and description		Gulf of Mexico, USA			
Evaporation equation		$\%Ev = (1.56 + 0.0457T)\ln(t)$			
Where Ev = weight percent evaporated, T = surface temperature ($^{\circ}\text{C}$), t = time (min)					
API gravity	19.5	Weathering % by weight			
(all units at 15°C)	Units	0	8	13	23
Density	g/ml	0.9365	0.9509	0.9559	0.9716
Viscosity	mPa·s or cP	177	457	800	4250
(dynamic—values at 15°C)					
Flash point	$^{\circ}\text{C}$	−4	59	82	> 95
Sulfur content	%	1.87	2.32	2.15	2.68
Pour point	$^{\circ}\text{C}$	−28	−17	−17	−6
Surface tension	mN/m	29.4	30.4	30.8	31.8
(air–oil at 15°C)					
IFT sea water	mN/m	23.9	22.7	20.6	22.9
IFT fresh water	mN/m	27.6	26.1	27.7	NM
Adhesion	g/m^3	41	35	40	77
SARA content (saturate, aromatic, resin, asphaltene) %					
Saturate	%	38	38	36	32
Aromatic	%	40	42	44	45
Resin	%	14	15	15	16
Asphaltene	%	8	5	4	8
Waxes	%	1	1	1	1
Emulsion formation (type formed and water content %)					
Type					
Water content	%				
Viscosity	mPa·s or cP				

Chemical dispersibility with Corexit 9500			
%	15		
Distillation data (% at temperature)			
Boiling point (°C)			
40			
60	1		
80	1		
100	3		
120	4	1	
140	5	2	
160	7	3	1
180	9	5	3
200	11	7	5
250	18	13	11
300	26	21	20
400	43	39	38
500	61	56	57
600	76	72	74
700	88	85	88

Oil name **Green Canyon Block 109**
Origin and description Gulf of Mexico, USA

Evaporation equation $\%Ev = (1.58 + 0.045T)\ln(t)$
 Where Ev = weight percent evaporated, T = surface temperature ($^{\circ}C$), t = time (min)

API gravity	27	Weathering % by weight			
(all units at 15°C)	Units	0	8	14	22
Density	g/ml	0.8921	0.9101	0.9218	0.9341
Viscosity	mPa·s or cP	39	98	225	690
(dynamic—values at 15°C)					
Flash point	$^{\circ}C$	0	59	> 95	> 95
Sulfur content	%	1.89	1.92	1.92	2.07
Pour point	$^{\circ}C$	−36	−27	−21	−16
Surface tension	mN/m	28	29.7	30.7	31.2
(air–oil at 15°C)					
IFT sea water	mN/m	21.5	22.8	21.1	16.1
IFT fresh water	mN/m	23.5	25.7	23.7	18.5
Adhesion	g/m ³	23	25	27	34

SARA content (saturate, aromatic, resin, asphaltene) %

Saturate	%	51	46	44	42
Aromatic	%	34	43	44	43
Resin	%	9	10	11	14
Asphaltene	%	1	1	1	1
Waxes	%	2	2	2	2

Emulsion formation (type formed and water content %)

Type				
Water content	%			
Viscosity	mPa·s or cP			

Chemical dispersibility with Corexit 9500

%	20			
---	----	--	--	--

Distillation data (% at temperature)

Boiling point ($^{\circ}C$)				
40				
60				
80				
100	1			
120	1	1		
140	2	2		
160	7	4		
180	12	6	1	
200	15	9	3	
250	22	17	11	3
300	30	27	22	13
400	48	48	44	38
500	66	68	65	61
600	79	83	82	80
700	88	94	93	92

Oil name **Green Canyon Block 184**
Origin and description Gulf of Mexico, USA

Evaporation equation $\%Ev = (3.55 + 0.045T)\ln(t)$
 Where Ev = weight percent evaporated, T = surface temperature ($^{\circ}C$), t = time (min)

API gravity	39.4	Weathering % by weight			
(all units at 15°C)	Units	0	12	26	38
Density	g/ml	0.8314	0.8575	0.8824	0.9043
Viscosity	mPa·s or cP	5	11	31	117
(dynamic—values at 15°C)					
Flash point	$^{\circ}C$	−18	18	67	> 95
Sulfur content	%	0.94	1	1.15	1.32
Pour point	$^{\circ}C$	−44	−35	−28	−25
Surface tension	mN/m	25	27	28.9	30.2
(air–oil at 15°C)					
IFT sea water	mN/m	23.3	23.2	25.2	19.3
IFT fresh water	mN/m	23.7	24.2	24.7	20.5
Adhesion	g/m ³	6	7	19	21

SARA content (saturate, aromatic, resin, asphaltene) %

Saturate	%	69	61	58	54
Aromatic	%	24	30	33	34
Resin	%	6	8	8	11
Asphaltene	%	1	1	1	1
Waxes	%				

Emulsion formation (type formed and water content %)

Type	Unstable	Unstable	Unstable	Meso-stable
Water content	%			69
Viscosity	mPa·s or cP			8255

Chemical dispersibility with Corexit 9500

%	47	33	25	22
---	----	----	----	----

Distillation data (% at temperature)

Boiling point ($^{\circ}C$)				
40	2			
60	3			
80	4			
100	8	3		
120	12	6		
140	16	10	1	
160	21	15	3	
180	25	20	7	
200	29	24	12	1
250	39	34	24	10
300	48	45	36	24
400	66	65	59	51
500	81	80	77	73
600	90	90	89	88
700	95	96	96	96

Oil name **Green Canyon Block 200**
Origin and description Louisiana, USA (BP)

Evaporation equation %Evaporated = $(3.11 + 0.045T)\ln(t)$
 Where Ev = weight percent evaporated, T = surface temperature (°C), t = time (min)

API gravity (all units at 15°C)	Units	Weathering % by weight			
		0	12	19.1	30.7
Density	g/ml	0.8501	0.8758	0.8876	0.9071
Viscosity	mPa·s or cP (dynamic—values at 15°C)	11.4	22	38.9	121
Flash point	°C	< 0	38	60	109
Sulfur content	%	0.87	1.08	1.18	1.35
Pour point	°C	−10	−25	−17	−15
Surface tension	mN/m (air–oil at 15°C)	27.1	28.7	30.7	30.8
IFT sea water	mN/m	27.1	29.5	28	25.1
IFT fresh water	mN/m	24.2	29.1	27.7	21.1
Adhesion	g/m ³	8	19	22	18

SARA content (saturate, aromatic, resin, asphaltene) %					
Saturate	%	82.29	80.84	79.76	77.16
Aromatic	%	10.05	10.82	11.59	12.6
Resin	%	6.88	7.57	7.72	8.83
Asphaltene	%	0.78	0.78	0.93	1.41
Waxes	%	1.7	1.9	1	2

Emulsion formation (type formed and water content %)					
Type		Unstable	Unstable	Unstable	Meso-stable
Water content	%				78.2
Viscosity	mPa·s or cP				

Chemical dispersibility with Corexit 9500					
%		45.8	28.6	35.5	15

Distillation data (% at temperature)					
Boiling point (°C)					
40		1.8			
60		2.8			
80		5.9			
100		9.1	1.1	0.1	
120		12	3	0.5	
140		15.4	6	1.8	
160		19.4	10	4.6	
180		23.3	14.3	8.4	0.3
200		26.7	18.2	12.2	1.6
250		25.3	28.2	22.5	10.8
300		44.2	38.5	33.3	23
400		61.1	57.9	53.8	46.6
500		75	73.9	70.7	66.1
600		84.5	84.6	82	79.2
700					

Oil name **Gullfaks**
Origin and description North Sea, Norway

Evaporation equation %Ev = $(2.29 + 0.034T)\ln(t)$
 Where Ev = weight percent evaporated, T = surface temperature (°C), t = time (min)

API gravity (all units at 15°C)	Units	Weathering % by weight			
		0	10	19	30
Density	g/ml	0.8701	0.8891	0.9017	0.9129
Viscosity	mPa·s or cP (dynamic—values at 15°C)	13	31	91	202
Flash point	°C	−8	50	92	> 95
Sulfur content	%	0.3	0.41	0.48	0.49
Pour point	°C	−32	−32	−27	−15
Surface tension	mN/m (air–oil at 15°C)	27.7	29.5	30.5	31.4
IFT sea water	mN/m	25.4	23.3	21.8	19.2
IFT fresh water	mN/m	25.9	24.1	23.7	21.4
Adhesion	g/m ³	23	35	31	33

SARA content (saturate, aromatic, resin, asphaltene) %					
Saturate	%	60	59	50	46
Aromatic	%	35	34	38	42
Resin	%	5	6	11	12
Asphaltene	%	1	1	1	1
Waxes	%	4		3	4

Emulsion formation (type formed and water content %)					
Type					
Water content	%				
Viscosity	mPa·s or cP				

Chemical dispersibility with Corexit 9500					
%		25			

Distillation data (% at temperature)					
Boiling point (°C)					
40		1			
60		1	1	1	1
80		1	1	1	1
100		2	1	1	1
120		9	2	1	1
140		12	4	1	1
160		15	7	1	1
180		18	11	2	1
200		21	14	5	1
250		31	25	17	6
300		41	37	30	20
400		61	59	54	47
500		79	78	76	72
600		90	91	90	89
700		97	98	98	97

Oil name **Heavy Fuel Oil 6303 (2002)**
Origin and description Imperial Oil, Nova Scotia, Canada;
a.k.a. Bunker C, Land Bunker

Evaporation equation $\%Ev = (-0.16 + 0.013T) t^{1/2}$
Where Ev = weight percent evaporated, T = surface temperature ($^{\circ}\text{C}$), t = time (min)

API gravity	11.47	Weathering % by weight		
(all units at 15°C)	Units	0	2.5	
Density	g/ml	0.9888	0.9988	
Viscosity	mPa·s or cP	22,800	149,000	
(dynamic—values at 15°C)				
Flash point	$^{\circ}\text{C}$	111	133	
Sulfur content	%	1.48	1.5	
Pour point	$^{\circ}\text{C}$	-1	11	
Surface tension	mN/m			
(air–oil at 15°C)				
IFT sea water	mN/m			
IFT fresh water	mN/m			
Adhesion	g/m^3	100	240	

SARA content (saturate, aromatic, resin, asphaltene) %				
Saturate	%	42.5	38.8	
Aromatic	%	29	26.9	
Resin	%	15.5	16.6	
Asphaltene	%	13	17.7	
Waxes	%	2.5	2.7	

Emulsion formation (type formed and water content %)				
Type		Entrained	Entrained	
Water content	%	57.7	24.1	
Viscosity	mPa·s or cP			

Chemical dispersibility with Corexit 9500				
	%	9	6	

Distillation data (% at temperature)				
Boiling point ($^{\circ}\text{C}$)				
40				
60				
80				
100				
120	0.1			
140	0.2			
160	0.3			
180	0.6			
200	1.2	0.2		
250	5.5	3.5		
300	12.5	10.2		
400	33.5	31.5		
500	41.2	39.7		
600	55.7	54.8		
700				

Oil name **Heavy Reformate**
Origin and description

Evaporation equation $\%Ev = (-0.17 + 0.013T)\sqrt{t}$
Where Ev = weight percent evaporated, T = surface temperature ($^{\circ}\text{C}$), t = time (min)

API gravity	10.1	Weathering % by weight		
(all units at 15°C)	Units	0		
Density	g/ml	0.9226		
Viscosity	mPa·s or cP	1321		
(dynamic—values at 15°C)				
Flash point	$^{\circ}\text{C}$			
Sulfur content	%	1.24		
Pour point	$^{\circ}\text{C}$	28		
Surface tension	mN/m	NM		
(air–oil at 15°C)				
IFT sea water	mN/m	NM		
IFT fresh water	mN/m	NM		
Adhesion	g/m^3	80		

SARA content (saturate, aromatic, resin, asphaltene) %				
Saturate	%	43		
Aromatic	%	50		
Resin	%	7		
Asphaltene	%	0		
Waxes	%	12		

Emulsion formation (type formed and water content %)				
Type				
Water content	%			
Viscosity	mPa·s or cP			

Chemical dispersibility with Corexit 9500				
	%	20		

Distillation data (% at temperature)				
Boiling point ($^{\circ}\text{C}$)				
40				
60				
80				
100				
120				
140				
160	1			
180	1			
200	1			
250	5			
300	11			
400	47			
500	88			
600				
700				

Oil name **Hebron M-04**
Origin and description Newfoundland, Canada

Evaporation equation $\%Ev = (1.01 + 0.045T)\ln(t)$
 Where Ev = weight percent evaporated, T = surface temperature (°C), t = time (min)

API gravity	22.5	Weathering % by weight			
(all units at 15°C)	Units	0	9	16	23
Density	g/ml	0.9189	0.9344	0.9423	0.9564
Viscosity	mPa·s or cP	154	676	1442	7369
(dynamic—values at 15°C)					
Flash point	°C	9	55	82	> 100
Sulfur content	%				
Pour point	°C	−2	9	12	20
Surface tension	mN/m	28.3	28.8	34.6	
(air–oil at 15°C)					
IFT sea water	mN/m	24.9	NM	NM	
IFT fresh water	mN/m	26	NM	NM	
Adhesion	g/m ³	41	64	76	222

SARA content (saturate, aromatic, resin, asphaltene) %

Saturate	%	48.7	46.4	40.1	38.4
Aromatic	%	31.1	31.9	34.6	32.2
Resin	%	9.1	9.1	11.5	12.7
Asphaltene	%	11.1	12.7	13.8	16.7
Waxes	%	5.1	5.7	5.9	6.3

Emulsion formation (type formed and water content %)

Type				
Water content	%			
Viscosity	mPa·s or cP			

Chemical dispersibility with Corexit 9500

%	< 10	< 10	< 10	< 10
---	------	------	------	------

Distillation data (% at temperature)

Boiling point (°C)				
40	0.3			
60	0.3			
80	1.4			
100	3.3	0.4		
120	5.2	1	0.1	
140	7.4	2.3	0.3	
160	10.3	4.5	1.2	
180	13.1	7.1	3	
200	15.8	9.9	5.4	0.2
250	23.8	18.4	14	5.1
300	33.1	28.3	24.6	15.8
400	51.2	47.8	45.1	38.6
500	70.1	68	66.5	62.4
600	85.2	84.2	83.5	81.5
700				

Oil name **Hebron**
Origin and description Newfoundland, Canada

Evaporation equation
 Where Ev = weight percent evaporated, T = surface temperature (°C), t = time (min)

API gravity	20.1	Weathering % by weight		
(all units at 15°C)	Units	0	3	7
Density	g/ml	0.931	0.935	0.938
Viscosity	mPa·s or cP	680	1065	1338
(dynamic—values at 15°C)				
Flash point	°C	61	89	112
Sulfur content	%			
Pour point	°C	< −16	−15	−9
Surface tension	mN/m	33.7	35	35.3
(air–oil at 15°C)				
IFT sea water	mN/m	16.9	16.6	16
IFT fresh water	mN/m			
Adhesion	g/m ³			

SARA content (saturate, aromatic, resin, asphaltene) %

Saturate	%			
Aromatic	%			
Resin	%			
Asphaltene	%			
Waxes	%			

Emulsion formation (type formed and water content %)

Type			
Water content	%		
Viscosity	mPa·s or cP		

Chemical dispersibility with Corexit 9500

%			
---	--	--	--

Distillation data (% at temperature)

Boiling point (°C)			
40			
60			
80			
100			
120			
140			
160			
180			
200			
250			
300			
400			
500			
600			
700			

Oil name **Heidrun**
Origin and description Norwegian Sea, Norway

Evaporation equation $\%Ev = (1.95 + 0.045T)\ln(t)$
 Where Ev = weight percent evaporated, T = surface temperature (°C), t = time (min)

API gravity	28.6	Weathering % by weight			
	Units	0	8	15	23
(all units at 15°C)					
Density	g/ml	0.8835	0.9013	0.9128	0.9222
Viscosity	mPa·s or cP	18	38	76	152
(dynamic—values at 15°C)					
Flash point	°C	−19	49	91	> 95
Sulfur content	%	0.53	0.49	0.55	0.61
Pour point	°C	−45	−30	−27	−25
Surface tension	mN/m	28.1	29.6	30.5	30.6
(air–oil at 15°C)					
IFT sea water	mN/m	18.6	18.1	17.4	14.5
IFT fresh water	mN/m	23.7	24	22.8	20.7
Adhesion	g/m ³	9	19	34	26

SARA content (saturate, aromatic, resin, asphaltene) %					
Saturate	%	55	57	52	52
Aromatic	%	35	33	38	36
Resin	%	9	9	9	10
Asphaltene	%	1	1	1	1
Waxes	%	4			

Emulsion formation (type formed and water content %)				
Type				
Water content	%			
Viscosity	mPa·s or cP			

Chemical dispersibility with Corexit 9500				
%				

Distillation data (% at temperature)				
Boiling point (°C)				
40	3			
60	4			
80	6	1		
100	8	2		
120	8	2		
140	10	4		
160	13	6	1	
180	16	9	3	
200	19	12	5	1
250	30	24	18	10
300	43	38	32	25
400	65	62	59	55
500	83	82	80	78
600	93	93	92	91
700	99	99	99	98

Oil name **Hibernia**
Origin and description Newfoundland, Canada

Evaporation equation $\%Ev = (1.95 + 0.045T)\ln(t)$
 Where Ev = weight percent evaporated, T = surface temperature (°C), t = time (min)

API gravity	35	Weathering % by weight		
	Units	0	11	22
(all units at 15°C)				
Density	g/ml	0.85	0.863	0.879
Viscosity	mPa·s or cP	30	141	150
(dynamic—values at 15°C)				
Flash point	°C		19	26
Sulfur content	%	0.37		
Pour point	°C	9	3	12
Surface tension	mN/m	28.8	30.5	31.7
(air–oil at 15°C)				
IFT sea water	mN/m	9.2	10	17.1
IFT fresh water	mN/m			
Adhesion	g/m ³			

SARA content (saturate, aromatic, resin, asphaltene) %			
Saturate	%	79	
Aromatic	%	15	
Resin	%	4	
Asphaltene	%	1	
Waxes	%	10	

Emulsion formation (type formed and water content %)			
Type			
Water content	%		
Viscosity	mPa·s or cP		

Chemical dispersibility with Corexit 9500			
%			

Distillation data (% at temperature)			
Boiling point (°C)			
40			
60			
80			
100			
120			
140			
160			
180			
200			
250			
300			
400			
500			
600			
700			

Oil name **Hibernia (1999)**
Origin and description Newfoundland

Evaporation equation $\%Ev = (2.18 + 0.045T)\ln(t)$
 Where Ev = weight percent evaporated, T = surface temperature (°C), t = time (min)

API gravity	34.9	Weathering % by weight			
	Units	0	10	21	33
(all units at 15°C)					
Density	g/ml	0.8504	0.8753	0.8893	0.9075
Viscosity	mPa·s or cP	13	35	99	2172
(dynamic—values at 15°C)					
Flash point	°C	−17	30	71	> 100
Sulfur content	%				
Pour point	°C	10	15	18	28
Surface tension mN/m		26.5	28.1	28.9	50
(air–oil at 15°C)					
IFT sea water mN/m		21.6	26.3	24.9	
IFT fresh water mN/m		23.9	27.2		
Adhesion	g/m ³	12	27	51	160

SARA content (saturate, aromatic, resin, asphaltene) %

Saturate	%	73.4	71	60.6	55.9
Aromatic	%	18.2	18.7	28.7	29.2
Resin	%	6.7	8	8.3	11.4
Asphaltene	%	1.7	2.3	2.4	3.5
Waxes	%	5.3	5.6	6	7.7

Emulsion formation (type formed and water content %)

Type				
Water content	%			
Viscosity	mPa·s or cP			

Chemical dispersibility with Corexit 9500

%	21	17	15	11
---	----	----	----	----

Distillation data (% at temperature)

Boiling point (°C)				
40	1.1			
60	1.2			
80	22	0.1		
100	4.7	1		
120	9.3	3.7	0.1	
140	12.5	6.3	0.6	
160	16.4	10	2.3	
180	20.2	13.8	5.4	
200	23.6	17.4	8.9	0.3
250	33	27.4	19.9	7.5
300	43.2	38.4	32.3	20.8
400	62.6	59.3	55.9	48.1
500	79.4	77.6	76.4	72
600	90.2	89.6	89.7	87.7
700				

Oil name **Hibernia (EPA 86)**
Origin and description Newfoundland, Canada; from EPA, OHMSETT, 1986

Evaporation equation
 Where Ev = weight percent evaporated, T = surface temperature (°C), t = time (min)

API gravity	28.3	Weathering % by weight		
	Units	0	9	18
(all units at 15°C)				
Density	g/ml	0.8849	0.9011	0.9138
Viscosity	mPa·s or cP	44	207	1471
(dynamic—values at 15°C)				
Flash point	°C	−14		
Sulfur content	%	0.65	0.64	
Pour point	°C	15	18	21
Surface tension mN/m		26.2	26.5	27
(air–oil at 15°C)				
IFT sea water mN/m		13.5	16.7	19.1
IFT fresh water mN/m		16.2	16.8	20.9
Adhesion	g/m ³			

SARA content (saturate, aromatic, resin, asphaltene) %

Saturate	%	82		
Aromatic	%	14		
Resin	%	2		
Asphaltene	%	4		
Waxes	%			

Emulsion formation (type formed and water content %)

Type			
Water content	%		
Viscosity	mPa·s or cP		

Chemical dispersibility with Corexit 9500

%			
---	--	--	--

Distillation data (% at temperature)

Boiling point (°C)			
40			
60			
80			
100			
120			
140			
160			
180			
200			
250			
300			
400			
500			
600			
700			

Oil name **Hondo Monterey**
Origin and description California, USA

Evaporation equationWhere Ev = weight percent evaporated, T = surface temperature (°C), t = time (min)

API gravity	18.3	Weathering % by weight		
(all units at 15°C)	Units	0	9	18
Density	g/ml	0.9377	0.9705	0.9917
Viscosity	mPa·s or cP	1599	17,880	1,867,000
(dynamic—values at 15°C)				
Flash point	°C	−12	59	> 100
Sulfur content	%	4.34	4.41	4.7
Pour point	°C	−9	4	25
Surface tension	mN/m	29.3	45.5	
(air–oil at 15°C)				
IFT sea water	mN/m	24.1		
IFT fresh water	mN/m	24.6		
Adhesion	g/m ³	86	139	1187

SARA content (saturate, aromatic, resin, asphaltene) %

Saturate	%	34	25	21
Aromatic	%	31	35	33
Resin	%	20	22	23
Asphaltene	%	15	17	23
Waxes	%	1.7	2	2.1

Emulsion formation (type formed and water content %)

Type			
Water content	%		
Viscosity	mPa·s or cP		

Chemical dispersibility with Corexit 9500

%			
---	--	--	--

Distillation data (% at temperature)

Boiling point (°C)			
40	0.7	0.1	0.1
60	1.1	0.3	0.3
80	1.9	0.4	0.4
100	3.2	0.5	0.4
120	4.3	0.9	0.4
140	5.7	1.6	0.4
160	7.2	2.8	0.5
180	8.7	4.3	0.5
200	102	5.9	0.6
250	14.7	10.9	3.4
300	19.7	16.4	8.9
400	31.1	29.1	22.8
500	44.7	44.2	39.6
600	61.7	63	60.5
700			

Oil name **Hondo**
Origin and description California, USA

Evaporation equation

$$\%Ev = (1.49 + 0.0457)\ln(t)$$

Where Ev = weight percent evaporated, T = surface temperature (°C), t = time (min)

API gravity	19.6	Weathering % by weight		
(all units at 15°C)	Units	0	17	32
Density	g/ml	0.9356	0.9674	0.9881
Viscosity	mPa·s or cP	735	9583	449,700
(dynamic—values at 15°C)				
Flash point	°C	−5	71	> 90
Sulfur content	%	4.3	4.6	4.8
Pour point	°C	−15	3	21
Surface tension	mN/m	29.2	30.3	
(air–oil at 15°C)				
IFT sea water	mN/m	15.8	22.8	
IFT fresh water	mN/m	22.5	59.8	
Adhesion	g/m ³	79	124	437

SARA content (saturate, aromatic, resin, asphaltene) %

Saturate	%	33	27	27
Aromatic	%	31	33	28
Resin	%	24	29	32
Asphaltene	%	12	12	13
Waxes	%	4	4	4

Emulsion formation (type formed and water content %)

Type		Stable	Stable	Unstable
Water content	%	81	66	
Viscosity	mPa·s or cP	110,000	190,000	

Chemical dispersibility with Corexit 9500

%	8	6	4
---	---	---	---

Distillation data (% at temperature)

Boiling point (°C)			
40	2		
60	3		
80	5		
100	6		
120	6		
140	8	1	
160	10	2	
180	12	3	
200	14	5	
250	20	11	2
300	26	18	9
400	41	35	28
500	56	52	48
600	70	68	65
700	83	83	81

Oil name **Hout**
Origin and description Kuwait/Iraq Divided Zone

Evaporation equation $\%Ev = (2.29 + 0.045T)\ln(t)$
 Where Ev = weight percent evaporated, T = surface temperature (°C), t = time (min)

API gravity	32.4	Weathering % by weight			
(all units at 15°C) Units		0	9	22	30
Density	g/ml	0.8628	0.8881	0.9117	0.9277
Viscosity	mPa·s or cP	15	37	146	726
(dynamic—values at 15°C)					
Flash point	°C	−18	34	88	> 95
Sulfur content	%	1.88	1.92	2.2	2.43
Pour point	°C	−14	−14	−5	8
Surface tension	mN/m	26.7	28.3	30	31
(air–oil at 15°C)					
IFT sea water	mN/m	15.2	15.7	18.7	15.2
IFT fresh water	mN/m	17.2	17.3	20.1	19.3
Adhesion	g/m ³	23	24	33	38

SARA content (saturate, aromatic, resin, asphaltene) %

Saturate	%	56	50	46	44
Aromatic	%	32	35	37	38
Resin	%	8	8	10	11
Asphaltene	%	5	6	7	7
Waxes	%	3	4	6	6

Emulsion formation (type formed and water content %)

Type				
Water content	%			
Viscosity	mPa·s or cP			

Chemical dispersibility with Corexit 9500

%	18			
---	----	--	--	--

Distillation data (% at temperature)

Boiling point (°C)				
40	4			
60	5			
80	7	1		
100	9	2		
120	11	3		
140	14	5		
160	17	8		
180	20	12	2	
200	23	15	5	
250	31	24	14	4
300	39	33	24	15
400	55	50	44	38
500	69	65	63	59
600	80	78	77	75
700	88	86	87	86

Oil name **IF-30 Fuel Oil**
Origin and description Svalbard, Norway

Evaporation equation $\%Ev = (-0.04 + 0.045T)\ln(t)$
 Where Ev = weight percent evaporated, T = surface temperature (°C), t = time (min)

API gravity	18.3	Weathering % by weight		
(all units at 15°C) Units		0		
Density	g/ml	0.9437		
Viscosity	mPa·s or cP	760		
(dynamic—values at 15°C)				
Flash point	°C	87		
Sulfur content	%	0.61		
Pour point	°C	−12		
Surface tension	mN/m	31.6		
(air–oil at 15°C)				
IFT sea water	mN/m	28.7		
IFT fresh water	mN/m	30.8		
Adhesion	g/m ³	34		

SARA content (saturate, aromatic, resin, asphaltene) %

Saturate	%			
Aromatic	%			
Resin	%			
Asphaltene	%			
Waxes	%			

Emulsion formation (type formed and water content %)

Type			
Water content	%		
Viscosity	mPa·s or cP		

Chemical dispersibility with Corexit 9500

%			
---	--	--	--

Distillation data (% at temperature)

Boiling point (°C)			
40			
60			
80			
100			
120			
140			
160	1		
180	2		
200	3		
250	9		
300	15		
400	33		
500	62		
600	86		
700	97		

Oil name Intermediate Fuel Oil 180
Origin and description Used in SOCSEX experiment

Evaporation equation

Where E_v = weight percent evaporated, T = surface temperature ($^{\circ}\text{C}$), t = time (min)

API gravity	14.7	Weathering % by weight		
(all units at 15°C)	Units	0	2	
Density	g/ml	0.967	0.9685	
Viscosity	mPa·s or cP	2324	3232	
(dynamic—values at 15°C)				
Flash point	$^{\circ}\text{C}$			
Sulfur content	%			
Pour point	$^{\circ}\text{C}$			
Surface tension	mN/m			
(air-oil at 15°C)				
IFT sea water	mN/m			
IFT fresh water	mN/m			
Adhesion	g/m^3			

SARA content (saturate, aromatic, resin, asphaltene) %

Saturate	%	29	32	
Aromatic	%	51	45	
Resin	%	11	12	
Asphaltene	%	10	11	
Waxes	%			

Emulsion formation (type formed and water content %)

Type			
Water content	%		
Viscosity	mPa·s or cP		

Chemical dispersibility with Corexit 9500

%			
---	--	--	--

Distillation data (% at temperature)

Boiling point ($^{\circ}\text{C}$)			
40			
60			
80			
100			
120			
140			
160	1		
180	1	1	
200	2	2	
250	12	12	
300	24	23	
400	39	38	
500	48	46	
600	62	60	
700	86	82	

Oil name Intermediate Fuel Oil 180
Origin and description

Evaporation equation

$$\%E_v = (-0.12 + 0.013T)\sqrt{(t)}$$

Where E_v = weight percent evaporated, T = surface temperature ($^{\circ}\text{C}$), t = time (min)

API gravity	14.7	Weathering % by weight		
(all units at 15°C)	Units	0	8	
Density	g/ml	0.967	0.984	
Viscosity	mPa·s or cP	2324	27,280	
(dynamic—values at 15°C)				
Flash point	$^{\circ}\text{C}$	91	> 95	
Sulfur content	%	1.54	1.64	
Pour point	$^{\circ}\text{C}$	-10	6	
Surface tension	mN/m	31.4	33.1	
(air-oil at 15°C)				
IFT sea water	mN/m	30.7		
IFT fresh water	mN/m	37.2		
Adhesion	g/m^3	49		

SARA content (saturate, aromatic, resin, asphaltene) %

		129		
Saturate	%	29	28	
Aromatic	%	51	39	
Resin	%	11	17	
Asphaltene	%	10	15	
Waxes	%	2	2	

Emulsion formation (type formed and water content %)

Type		Entrained	Entrained	
Water content	%	69	58	
Viscosity	mPa·s or cP	53,000	150,000	

Chemical dispersibility with Corexit 9500

%	0	0	
---	---	---	--

Distillation data (% at temperature)

Boiling point ($^{\circ}\text{C}$)			
40			
60			
80			
100			
120		1	
140		1	
160	1	1	
180	1	1	
200	2	1	
250	12	6	
300	24	18	
400	39	34	
500	48	43	
600	62	56	
700	86	77	

Oil name Intermediate Fuel Oil 300
Origin and description

Evaporation equation $\%Ev = (-0.15 + 0.013T)\sqrt{t}$
 Where Ev = weight percent evaporated, T = surface temperature (°C), t = time (min)

API gravity	11.9	Weathering % by weight		
(all units at 15°C)	Units	0	5	
Density	g/ml	0.9859	0.9996	
Viscosity	mPa·s or cP	14,470	220,000	
(dynamic—values at 15°C)				
Flash point	°C	> 100	> 100	
Sulfur content	%	1.72	1.8	
Pour point	°C	−6	12	
Surface tension	mN/m	32.6		
(air–oil at 15°C)				
IFT sea water	mN/m	37.3		
IFT fresh water	mN/m			
Adhesion	g/m ³	91	358	

SARA content (saturate, aromatic, resin, asphaltene) %				
Saturate	%	26	24	
Aromatic	%	52	28	
Resin	%	12	30	
Asphaltene	%	10	17	
Waxes	%	2	2	

Emulsion formation (type formed and water content %)			
Type		Entrained	Unstable
Water content	%	52	
Viscosity	mPa·s or cP	97,000	

Chemical dispersibility with Corexit 9500			
	%	0	0

Distillation data (% at temperature)			
Boiling point (°C)			
40			
60			
80			
100			
120			
140			
160			
180			
200			
250			
300			
400			
500			
600			
700			

Oil name IPAR 3
Origin and description Synthetic isoparaffin

Evaporation equation
 Where Ev = weight percent evaporated, T = surface temperature (°C), t = time (min)

API gravity	22.2	Weathering % by weight		
(all units at 15°C)	Units	0	0.1	
Density	g/ml	0.8198		
Viscosity	mPa·s or cP	6		
(dynamic—values at 15°C)				
Flash point	°C	> 100		
Sulfur content	%	0		
Pour point	°C	−56		
Surface tension	mN/m	27.9		
(air–oil at 15°C)				
IFT sea water	mN/m	27.2		
IFT fresh water	mN/m	28.3		
Adhesion	g/m ³	8		

SARA content (saturate, aromatic, resin, asphaltene) %			
Saturate	%		
Aromatic	%		
Resin	%		
Asphaltene	%		
Waxes	%	0.1	

Emulsion formation (type formed and water content %)			
Type			
Water content	%		
Viscosity	mPa·s or cP		

Chemical dispersibility with Corexit 9500			
	%		

Boiling point (°C)			
40			
60			
80			
100			
120			
140			
160			
180			
200	0.1		
250	5.6		
300	42.2		
400	90.8		
500			
600			
700			

Oil name Iranian Heavy
Origin and description Iran

Evaporation equation $\%Ev = (2.27 + 0.045T)\ln(t)$
Where Ev = weight percent evaporated, T = surface temperature (°C), t = time (min)

API gravity	30	Weathering % by weight		
(all units at 15°C)	Units	0	14	25
Density	g/ml	0.8756	0.9046	0.9247
Viscosity	mPa-s or cP	20	70	255
(dynamic—values at 15°C)				
Flash point	°C	−15	43	> 90
Sulfur content	%	1.2	1.88	2.22
Pour point	°C	−22	−2	1
Surface tension	mN/m	26.1	28	29.5
(air–oil at 15°C)				
IFT sea water	mN/m	22.5	20.8	23.2
IFT fresh water	mN/m	22.5	23.3	24.7
Adhesion	g/m ³	17	20	23

SARA content (saturate, aromatic, resin, asphaltene) %

Saturate	%	53	46	44
Aromatic	%	30	35	36
Resin	%	11	12	13
Asphaltene	%	6	7	7
Waxes	%	5	5	5

Emulsion formation (type formed and water content %)

Type			
Water content	%		
Viscosity	mPa-s or cP		

Chemical dispersibility with Corexit 9500

%	14		
---	----	--	--

Distillation data (% at temperature)

Boiling point (°C)			
40	2		
60	2	1	
80	4	1	
100	6	2	
120	9	3	
140	11	4	
160	15	7	
180	18	11	2
200	21	14	4
250	28	23	12
300	36	33	22
400	53	53	43
500	69	72	62
600	82	87	76
700	91	97	87

Oil name Issungnak
Origin and description Beaufort Sea, Canada

Evaporation equation $\%Ev = (1.56 + 0.045T)\ln(t)$
Where Ev = weight percent evaporated, T = surface temperature (°C), t = time (min)

API gravity	35	Weathering % by weight		
(all units at 15°C)	Units	0	15	25
Density	g/ml	0.849	0.8682	0.8773
Viscosity	mPa-s or cP			
(dynamic—values at 15°C)				
Flash point	°C			
Sulfur content	%	0.08	0.07	0.1
Pour point	°C		11	13
Surface tension	mN/m	26.2	27.7	28.5
(air–oil at 15°C)				
IFT sea water	mN/m	16.8	17	12.5
IFT fresh water	mN/m	16.7	23.4	21.5
Adhesion	g/m ³			

SARA content (saturate, aromatic, resin, asphaltene) %

Saturate	%	92		
Aromatic	%	3		
Resin	%	0		
Asphaltene	%	0		
Waxes	%			

Emulsion formation (type formed and water content %)

Type			
Water content	%		
Viscosity	mPa-s or cP		

Chemical dispersibility with Corexit 9500

%			
---	--	--	--

Distillation data (% at temperature)

Boiling point (°C)			
40			
60			
80	5		
100	7		
120	10		
140	11		
160	12		
180	16		
200	20		
250	35		
300	54		
400	82		
500	96		
600	99		
700			

Oil name **Isthmus**
Origin and description Mexico

Evaporation equation $\%Ev = (2.48 + 0.045T)\ln(t)$
 Where Ev = weight percent evaporated, T = surface temperature (°C), t = time (min)

API gravity	32	Weathering % by weight		
(all units at 15°C)	Units	0	29	
Density	g/ml	0.8645	0.9228	
Viscosity	mPa·s or cP	13	324	
(dynamic—values at 15°C)				
Flash point	°C	−13	> 95	
Sulfur content	%	1.37	1.75	
Pour point	°C	−32	−3	
Surface tension	mN/m	26.7	30.7	
(air–oil at 15°C)				
IFT sea water	mN/m	23	18.5	
IFT fresh water	mN/m	22.1	20.1	
Adhesion	g/m ³	23	23	

SARA content (saturate, aromatic, resin, asphaltene) %

Saturate	%	60	48	
Aromatic	%	28	36	
Resin	%	6	9	
Asphaltene	%	5	7	
Waxes	%	1		

Emulsion formation (type formed and water content %)

Type			
Water content	%		
Viscosity	mPa·s or cP		

Chemical dispersibility with Corexit 9500

%			
---	--	--	--

Distillation data (% at temperature)

Boiling point (°C)			
40	0.7		
60	1.6		
80	3.2		
100	5.6		
120	7.9		
140	10.8		
160	14.6		
180	18.6		
200	22.1		
250	31.3	7	
300	41.3	19	
400	60.6	45	
500	76.7	67	
600	88.8	82	
700		91	

Oil name **Jet A/Jet A-1**
Origin and description a.k.a. Aviation turbine fuel (kerosene type), turbo fuel A, turbo fuel A-1

Evaporation equation $\%Ev = (0.59 + 0.013T)\sqrt{t}$
 Where Ev = weight percent evaporated, T = surface temperature (°C), t = time (min)

API gravity	41.8	Weathering % by weight			
(all units at 15°C)	Units	0	12	23	37
Density	g/ml	0.8159	0.8193	0.8216	0.8244
Viscosity	mPa·s or cP	2	2	2	2
(dynamic—values at 15°C)					
Flash point	°C	54	66	71	76
Sulfur content	%	0.03	0.03	0.04	0.06
Pour point	°C	−55	−55	−50	−44
Surface tension	mN/m	26.4	27.2	27	
(air–oil at 15°C)					
IFT sea water	mN/m	31.2	31	29	29
IFT fresh water	mN/m	37	33.2	33.8	33.1
Adhesion	g/m ³	1	0	1	6

SARA content (saturate, aromatic, resin, asphaltene) %

Saturate	%	94	98	96	98
Aromatic	%	6	2	3	2
Resin	%	0	0	1	0
Asphaltene	%	0	0	0	0
Waxes	%				

Emulsion formation (type formed and water content %)

Type				
Water content	%			
Viscosity	mPa·s or cP			

Chemical dispersibility with Corexit 9500

%	57	43	50	
---	----	----	----	--

Distillation data (% at temperature)

Boiling point (°C)				
40				
60				
80				
100				
120				
140				
160				
180				
200				
250				
300				
400				
500				
600				
700				

Oil name	Jet B		
Origin and description	a.k.a. Turbo fuel B, wide boiling range aviation turbine fuel		
Evaporation equation	Short-term (< 5 days): $\%Ev = (1.06 + 0.013T)\sqrt{t}$ Long-term: $\%Ev = (7.19 + 0.045T)\ln(t)$ Where Ev = weight percent evaporated, T = surface temperature (°C), t = time (min)		
API gravity	42.9	Weathering % by weight	
(all units at 15°C)	Units	0	53
Density	g/ml	0.8111	0.8354
Viscosity	mPa·s or cP	2	3
(dynamic—values at 15°C)			
Flash point	°C	42	86
Sulfur content	%	0.08	0.13
Pour point	°C	−54	−44
Surface tension	mN/m	26.3	27.8
(air–oil at 15°C)			
IFT sea water	mN/m	39.1	30.5
IFT fresh water	mN/m	39.8	29
Adhesion	g/m ³	3	6
SARA content (saturate, aromatic, resin, asphaltene) %			
Saturate	%	81	80
Aromatic	%	19	19
Resin	%	0	0
Asphaltene	%	0	0
Waxes	%		
Emulsion formation (type formed and water content %)			
Type		Unstable	Unstable
Water content	%		
Viscosity	mPa·s or cP		
Chemical dispersibility with Corexit 9500			
%	78	33	
Distillation data (% at temperature)			
Boiling point (°C)			
40			
60			
80			
100			
120	2		
140	7		
160	18		
180	33	1	
200	47	8	
250	82	61	
300	99	99	
400			
500			
600			
700			

Oil name	Jet B—A		
Origin and description	a.k.a. Turbo fuel B, wide boiling range aviation turbine fuel		
Evaporation equation	Where Ev = weight percent evaporated, T = surface temperature (°C), t = time (min)		
API gravity		Weathering % by weight	
(all units at 15°C)	Units	0	63
Density	g/ml	0.7567	0.7915
Viscosity	mPa·s or cP	1	1
(dynamic—values at 15°C)			
Flash point	°C	−23	
Sulfur content	%		
Pour point	°C	< −23	
Surface tension	mN/m	23	
(air–oil at 15°C)			
IFT sea water	mN/m	10.8	
IFT fresh water	mN/m	12.4	
Adhesion	g/m ³		
SARA content (saturate, aromatic, resin, asphaltene) %			
Saturate	%		
Aromatic	%		
Resin	%		
Asphaltene	%		
Waxes	%		
Emulsion formation (type formed and water content %)			
Type			
Water content	%		
Viscosity	mPa·s or cP		
Chemical dispersibility with Corexit 9500			
%			
Distillation data (% at temperature)			
Boiling point (°C)			
40			
60			
80			
100			
120			
140			
160			
180			
200			
250			
300			
400			
500			
600			
700			

Oil name **Kuwait**
Origin and description Kuwait, a.k.a Kuwait export

Evaporation equationWhere Ev = weight percent evaporated, T = surface temperature (°C), t = time (min)

API gravity	30.6	Weathering % by weight		
(all units at 15°C)	Units	0	10	21
Density	g/ml	0.8722	0.8977	0.9165
Viscosity	mPa·s or cP	22	56	182
(dynamic—values at 15°C)				
Flash point	°C	< 25		
Sulfur content	%	2.52	2.69	3.18
Pour point	°C	−18	−9	3
Surface tension	mN/m	27.8	27.9	30.5
(air–oil at 15°C)				
IFT sea water	mN/m	22.9	18.2	18.5
IFT fresh water	mN/m	28.6	21.1	27
Adhesion	g/m ³			

SARA content (saturate, aromatic, resin, asphaltene) %

Saturate	%			
Aromatic	%			
Resin	%			
Asphaltene	%			
Waxes	%			

Emulsion formation (type formed and water content %)

Type			
Water content	%		
Viscosity	mPa·s or cP		

Chemical dispersibility with Corexit 9500

%			
---	--	--	--

Distillation data (% at temperature)

Boiling point (°C)			
40			
60			
80			
100			
120			
140			
160			
180			
200			
250			
300			
400			
500			
600			
700			

Oil name **Lago Treco**
Origin and description Venezuela

Evaporation equation

$$\%Ev = (1.12 + 0.0457)\ln(t)$$

Where Ev = weight percent evaporated, T = surface temperature (°C), t = time (min)

API gravity	22.6	Weathering % by weight		
(all units at 15°C)	Units	0	16	
Density	g/ml	0.923	0.9661	
Viscosity	mPa·s or cP	272	16,160	
(dynamic—values at 15°C)				
Flash point	°C	−3	> 95	
Sulfur content	%	2.59	2.75	
Pour point	°C	−20	−1	
Surface tension	mN/m	28.7	40	

(air–oil at 15°C)

IFT sea water	mN/m	19.3		
IFT fresh water	mN/m	24.4		
Adhesion	g/m ³	62	96	
Saturate	%	38	32	
Aromatic	%	38	38	
Resin	%	14	15	
Asphaltene	%	11	15	
Waxes	%	0.8		
Type				
Water content	%			
Viscosity	mPa·s or cP			

Chemical dispersibility with Corexit 9500

%	10	< < 10	
---	----	--------	--

Distillation data (% at temperature)

Boiling point (°C)			
40	0.6		
60	1.3		
80	2.3		
100	3.6		
120	4.8		
140	6.4		
160	8.4		
180	10.6		
200	12.7		
250	19.3	4	
300	27.1	12	
400	44.8	34	
500	70.6	55	
600	79.8	71	
700		83	

Oil name		Lago		
Origin and description		Angola		
Evaporation equation		$\%Ev = (1.13 + 0.0457T)\ln(t)$		
Where Ev = weight percent evaporated, T = surface temperature (°C), t = time (min)				
API gravity	27.3	Weathering % by weight		
(all units at 15°C)	Units	0	11	17
Density	g/ml	0.8907	0.9128	0.923
Viscosity	mPa.s or cP	153	7819	18,900
(dynamic—values at 15°C)				
Flash point	°C	−13	90	> 95
Sulfur content	%	0.3	0.3	0.32
Pour point	°C	21	25	30
Surface tension	mN/m			
(air–oil at 15°C)				
IFT sea water	mN/m			
IFT fresh water	mN/m			
Adhesion	g/m ³	65	96	800
SARA content (saturate, aromatic, resin, asphaltene) %				
Saturate	%	56	51	53
Aromatic	%	31	33	30
Resin	%	11	14	14
Asphaltene	%	3	2	3
Waxes	%	10	8	8
Emulsion formation (type formed and water content %)				
Type				
Water content	%			
Viscosity	mPa.s or cP			
Chemical dispersibility with Corexit 9500				
	%	10	< 10	
Distillation data (% at temperature)				
Boiling point (°C)				
40				
60				
80		1		
100		2		
120		4		
140		6		
160		8	1	
180		10	2	
200		12	4	
250		18	111	5
300		25	18	13
400		40	37	33
500		58	58	56
600		73	76	74
700		84	88	88

Oil name		Lagomedio		
Origin and description		Venezuela		
Evaporation equation				
Where Ev = weight percent evaporated, T = surface temperature (°C), t = time (min)				
API gravity	30.6	Weathering % by weight		
(all units at 15°C)	Units	0	9	15
Density	g/ml	0.872	0.891	0.897
Viscosity	mPa·s or cP	41	84	265
(dynamic—values at 15°C)				
Flash point	°C	57		
Sulfur content	%	1.17		
Pour point	°C	−26		
Surface tension	mN/m	28.2	27.5	29.6
(air–oil at 15°C)				
IFT sea water	mN/m	12.4	14.4	17.1
IFT fresh water	mN/m	23.2	23.7	20.5
Adhesion	g/m ³			
SARA content (saturate, aromatic, resin, asphaltene) %				
Saturate	%			
Aromatic	%			
Resin	%			
Asphaltene	%	5		
Waxes	%	10		
Emulsion formation (type formed and water content %)				
Type				
Water content	%			
Viscosity	mPa·s or cP			
Chemical dispersibility with Corexit 9500				
	%			
Distillation data (% at temperature)				
Boiling point (°C)				
40				
60				
80				
100	2			
120	3			
140	6			
160	9			
180	12			
200	15			
250	23			
300	32			
400	51			
500	67			
600	81			
700	91			

Oil name Louisiana
Origin and description Louisiana, USA

Evaporation equation $\%Ev = (2.39 + 0.045T)\ln(t)$
 Where Ev = weight percent evaporated, T = surface temperature (°C), t = time (min)

API gravity	34.5	Weathering % by weight			
(all units at 15°C)	Units	0	10	21	32
Density	g/ml	0.8518	0.8696	0.8837	0.8953
Viscosity	mPa·s or cP	8	16	36	80
(dynamic—values at 15°C)					
Flash point	°C	−11	47	> 95	> 95
Sulfur content	%	0.45	0.53	0.58	0.66
Pour point	°C	−28	−23	−12	−8
Surface tension	mN/m	25.9	28.3	29.6	30.2
(air–oil at 15°C)					
IFT sea water	mN/m	19.6	18.6	15.8	15.4
IFT fresh water	mN/m	21.1	21.1	19.6	19.7
Adhesion	g/m ³	18	22	27	34

SARA content (saturate, aromatic, resin, asphaltene) %					
Saturate	%	73	69	66	64
Aromatic	%	21	25	27	29
Resin	%	4	5	6	7
Asphaltene	%	1	0	0	0
Waxes	%	4	3	4	4

Emulsion formation (type formed and water content %)					
Type					
Water content	%				
Viscosity	mPa·s or cP				

Chemical dispersibility with Corexit 9500					
%	34				

Distillation data (% at temperature)					
Boiling point (°C)					
40	1				
60	1				
80	1				
100	1				
120	8	2			
140	12	4			
160	14	7			
180	18	11	2		
200	21	15	4		
250	33	27	17	6	
300	46	42	33	23	
400	69	66	62	57	
500	86	84	82	80	
600	95	94	93	93	
700	99	99	98	99	

Oil name Low Sulfur Waxy Gas Oil
Origin and description

Evaporation equation
 Where Ev = weight percent evaporated, T = surface temperature (°C), t = time (min)

API gravity	43.8	Weathering % by weight		
(all units at 15°C)	Units	0		
Density	g/ml	0.807		
Viscosity	mPa·s or cP			
(dynamic—values at 15°C)				
Flash point	°C	> 95		
Sulfur content	%	0.03		
Pour point	°C	> 50		
Surface tension	mN/m			
(air–oil at 15°C)				
IFT sea water	mN/m			
IFT fresh water	mN/m			
Adhesion	g/m ³			

SARA content (saturate, aromatic, resin, asphaltene) %			
Saturate	%		
Aromatic	%		
Resin	%		
Asphaltene	%	2	
Waxes	%	> 95	

Emulsion formation (type formed and water content %)			
Type			
Water content	%		
Viscosity	mPa·s or cP		

Chemical dispersibility with Corexit 9500			
%			

Distillation data (% at temperature)			
Boiling point (°C)			
40			
60			
80			
100			
120			
140			
160			
180			
200			
250			
300			
400			
500			
600			
700			

Oil name **Low Sulfur Waxy Residuuum**
Origin and description

Evaporation equation

Where E_v = weight percent evaporated, T = surface temperature ($^{\circ}\text{C}$), t = time (min)

API gravity	39.5	Weathering % by weight		
(all units at 15 $^{\circ}\text{C}$)	Units	0		
Density	g/ml	0.827		
Viscosity	mPa-s or cP			
(dynamic—values at 15 $^{\circ}\text{C}$)				
Flash point	$^{\circ}\text{C}$	> 95		
Sulfur content	%	0.05		
Pour point	$^{\circ}\text{C}$	> 50		
Surface tension mN/m				
(air–oil at 15 $^{\circ}\text{C}$)				
IFT sea water mN/m				
IFT fresh water mN/m				
Adhesion	g/m ³			

SARA content (saturate, aromatic, resin, asphaltene) %

Saturate	%			
Aromatic	%			
Resin	%			
Asphaltene	%	14		
Waxes	%	85		

Emulsion formation (type formed and water content %)

Type			
Water content	%		
Viscosity	mPa-s or cP		

Chemical dispersibility with Corexit 9500

%			
---	--	--	--

Distillation data (% at temperature)

Boiling point ($^{\circ}\text{C}$)			
40			
60			
80			
100			
120			
140			
160			
180			
200			
250			
300			
400			
500			
600			
700			

Oil name **Lubricating Oil (Engine, Gasoline)**
Origin and description a.k.a. Crankcase oil, motor oil

Evaporation equation

Where E_v = weight percent evaporated, T = surface temperature ($^{\circ}\text{C}$), t = time (min)

API gravity	28.3	Motor oil grades			
(all units at 15 $^{\circ}\text{C}$)	Units	5W30	10W30	10W40	Used
Density	g/ml	0.8848			0.8848
Viscosity	mPa-s or cP				175
(dynamic—values at 15 $^{\circ}\text{C}$)					
Flash point	$^{\circ}\text{C}$	214	218	222	
Sulfur content	%				0.29
Pour point	$^{\circ}\text{C}$	–39	–36	–36	–36
Surface tension mN/m					31
(air–oil at 15 $^{\circ}\text{C}$)					
IFT sea water mN/m					21
IFT fresh water mN/m					24.4
Adhesion	g/m ³				

SARA content (saturate, aromatic, resin, asphaltene) %

Saturate	%				
Aromatic	%				
Resin	%				
Asphaltene	%				
Waxes	%				

Emulsion formation (type formed and water content %)

Type				
Water content	%			
Viscosity	mPa-s or cP			

Chemical dispersibility with Corexit 9500

%				
---	--	--	--	--

Distillation data (% at temperature)

Boiling point ($^{\circ}\text{C}$)				
40				
60				
80				
100				
120				
140				
160				
180				
200				
250				
300				
400				
500				
600				
700				

Oil name **Lubricating Oil (Gear, Industrial, Spartan EP-680)**

Origin and description

Evaporation equation $\%Ev = (-0.66 + 0.045T)\ln(t)$
Where Ev = weight percent evaporated, T = surface temperature (°C), t = time (min)

API gravity	26.2	Weathering % by weight		
(all units at 15°C)	Units	0		
Density	g/ml	0.8963		
Viscosity	mPa·s or cP	4210		
(dynamic—values at 15°C)				
Flash point	°C	> 95		
Sulfur content	%	0.35		
Pour point	°C	−12		
Surface tension mN/m		32.5		
(air–oil at 15°C)				
IFT sea water mN/m				
IFT fresh water mN/m				
Adhesion	g/m ³	46		

SARA content (saturate, aromatic, resin, asphaltene) %

Saturate	%	70		
Aromatic	%	25		
Resin	%	4		
Asphaltene	%	0		
Waxes	%			

Emulsion formation (type formed and water content %)

Type			
Water content	%		
Viscosity	mPa·s or cP		

Chemical dispersibility with Corexit 9500

%			
---	--	--	--

Distillation data (% at temperature)

Boiling point (°C)			
40			
60			
80			
100			
120			
140			
160			
180			
200			
250	1		
300	3		
400	13		
500	29		
600	70		
700	95		

Oil name **Lubricating Oil (Hydraulic, Esso XD3-10)**

Origin and description

Evaporation equation

Where Ev = weight percent evaporated, T = surface temperature (°C), t = time (min)

API gravity	30.6	Weathering % by weight		
(all units at 15°C)	Units	0		
Density	g/ml	0.8727		
Viscosity	mPa·s or cP	102		
(dynamic—values at 15°C)				
Flash point	°C	> 95		
Sulfur content	%	0.26		
Pour point	°C	−27		
Surface tension mN/m		21.4		
(air–oil at 15°C)				
IFT sea water mN/m		7.9		
IFT fresh water mN/m		8.8		
Adhesion	g/m ³			

SARA content (saturate, aromatic, resin, asphaltene) %

Saturate	%			
Aromatic	%			
Resin	%			
Asphaltene	%	0		
Waxes	%	3		

Emulsion formation (type formed and water content %)

Type			
Water content	%		
Viscosity	mPa·s or cP		

Chemical dispersibility with Corexit 9500

%			
---	--	--	--

Distillation data (% at temperature)

Boiling point (°C)			
40			
60			
80			
100			
120			
140			
160			
180			
200			
250			
300	1		
400	40		
500	95		
600	98		
700	99		

Oil name **Lubricating Oil (Industrial, Teresso 46)**
Origin and description

Evaporation equation $\%Ev = (-0.67 + 0.045T)\ln(t)$
 Where Ev = weight percent evaporated, T = surface temperature (°C), t = time (min)

API gravity	30.3	Weathering % by weight		
(all units at 15°C) Units		0		
Density	g/ml	0.874		
Viscosity	mPa·s or cP	150		
(dynamic—values at 15°C)				
Flash point	°C	> 95		
Sulfur content	%	0.16		
Pour point	°C	−29		
Surface tension mN/m		31.3		
(air–oil at 15°C)				
IFT sea water mN/m		7		
IFT fresh water mN/m		9.2		
Adhesion	g/m ³	20		

SARA content (saturate, aromatic, resin, asphaltene) %				
Saturate	%	80		
Aromatic	%	18		
Resin	%	2		
Asphaltene	%	0		
Waxes	%			

Emulsion formation (type formed and water content %)				
Type				
Water content	%			
Viscosity	mPa·s or cP			

Chemical dispersibility with Corexit 9500				
%				

Distillation data (% at temperature)				
Boiling point (°C)				
40				
60				
80				
100				
120				
140				
160				
180				
200				
250				
300				
400	23			
500	87			
600				
700				

Oil name **Lubricating oil (Industrial, Teresso 150)**
Origin and description

Evaporation equation $\%Ev = (-0.68 + 0.045T)\ln(t)$
 Where Ev = weight percent evaporated, T = surface temperature (°C), t = time (min)

API gravity	27.8	Weathering % by weight		
(all units at 15°C) Units		0		
Density	g/ml	0.8872		
Viscosity	mPa·s or cP	1000		
(dynamic—values at 15°C)				
Flash point	°C	> 95		
Sulfur content	%	0.22		
Pour point	°C	−15		
Surface tension mN/m		32		
(air–oil at 15°C)				
IFT sea water mN/m				
IFT fresh water mN/m		7.1		
Adhesion	g/m ³	39		

SARA content (saturate, aromatic, resin, asphaltene) %				
Saturate	%	72		
Aromatic	%	25		
Resin	%	2		
Asphaltene	%	0		
Waxes	%			

Emulsion formation (type formed and water content %)				
Type				
Water content	%			
Viscosity	mPa·s or cP			

Chemical dispersibility with Corexit 9500				
%				

Distillation data (% at temperature)				
Boiling point (°C)				
40				
60				
80				
100				
120				
140				
160				
180				
200				
250				
300				
400	2			
500	44			
600	98			
700				

Oil name **Lubricating Oil (Industrial, Teresso 220)**
Origin and description

Evaporation equation $\%Ev = (-0.66 + 0.045T)\ln(t)$
 Where Ev = weight percent evaporated, T = surface temperature (°C), t = time (min)

API gravity	27.1	Weathering % by weight		
(all units at 15°C) Units		0		
Density	g/ml	0.8916		
Viscosity	mPa·s or cP	1170		
(dynamic—values at 15°C)				
Flash point	°C	> 95		
Sulfur content	%	0.19		
Pour point	°C	−15		
Surface tension mN/m		32.5		
(air–oil at 15°C)				
IFT sea water mN/m				
IFT fresh water mN/m		7.9		
Adhesion	g/m ³	40		

SARA content (saturate, aromatic, resin, asphaltene) %

Saturate	%	69		
Aromatic	%	28		
Resin	%	3		
Asphaltene	%	0		
Waxes	%			

Emulsion formation (type formed and water content %)

Type			
Water content	%		
Viscosity	mPa·s or cP		

Chemical dispersibility with Corexit 9500

%			
---	--	--	--

Distillation data (% at temperature)

Boiling point (°C)			
40			
60			
80			
100			
120			
140			
160			
180			
200			
250			
300			
400	2		
500	26		
600	95		
700			

Oil name **Lubricating Oil (Turbine, Marinus ISO46)**
Origin and description Synthetic esters. From Maryn lubricants

Evaporation equation $\%Ev = (-0.68 + 0.045T)\ln(t)$
 Where Ev = weight percent evaporated, T = surface temperature (°C), t = time (min)

API gravity	21	Weathering % by weight		
(all units at 15°C) Units		0		
Density	g/ml	0.9271		
Viscosity	mPa·s or cP	140		
(dynamic—values at 15°C)				
Flash point	°C	> 95		
Sulfur content	%	0.57		
Pour point	°C	−36		
Surface tension mN/m		33.1		

(air–oil at 15°C)				
IFT sea water mN/m		6		
IFT fresh water mN/m		7.9		
Adhesion	g/m ³	20		
Saturate	%	2		
Aromatic	%	1		
Resin	%	98		
Asphaltene	%	0		
Waxes	%			

Emulsion formation (type formed and water content %)

Type			
Water content	%		
Viscosity	mPa·s or cP		

Chemical dispersibility with Corexit 9500

%			
---	--	--	--

Distillation data (% at temperature)

Boiling point (°C)			
40			
60			
80			
100			
120			
140			
160			
180			
200			
250			
300	1		
400	2		
500	8		
600	46		
700			

Oil name Lubricating Oil (Turbine, Marinus ISO32)**Origin and description** Made from synthetic esters. From
Maryn Lubricants**Evaporation equation** $\%Ev = (-0.68 + 0.045T)\ln(t)$ Where Ev = weight percent evaporated, T = surface temperature (°C), t = time (min)

API gravity	23.9	Weathering % by weight		
(all units at 15°C)	Units	0		
Density	g/ml	0.9097		
Viscosity	mPa·s or cP	70		

(dynamic—values at 15°C)

Flash point	°C	> 95		
Sulfur content	%	0.57		
Pour point	°C	−30		
Surface tension	mN/m	32.9		

(air–oil at 15°C)

IFT sea water	mN/m	2.7		
IFT fresh water	mN/m	6.6		
Adhesion	g/m ³	37		

SARA content (saturate, aromatic, resin, asphaltene) %

Saturate	%	5		
Aromatic	%	1		
Resin	%	94		
Asphaltene	%	0		
Waxes	%			

Emulsion formation (type formed and water content %)

Type			
Water content	%		
Viscosity	mPa·s or cP		

Chemical dispersibility with Corexit 9500

%			
---	--	--	--

Distillation data (% at temperature)

Boiling point (°C)			
40			
60			
80			
100			
120			
140			
160			
180			
200			
250			
300	1		
400	3		
500	10		
600	93		
700	99		

Oil name Lubricating Oil (Turbine, STO 120)**Origin and description** a.k.a. Gulf S turbolene**Evaporation equation** $\%Ev = (-0.68 + 0.045T)\ln(t)$ Where Ev = weight percent evaporated, T = surface temperature (°C), t = time (min)

API gravity	30.7	Oil type		
(all units at 15°C)	Units	0	Used	
Density	g/ml	0.8714	0.8693	
Viscosity	mPa·s or cP			

(dynamic—values at 15°C)

Flash point	°C	> 95	> 95	
Sulfur content	%	0.14	0.14	
Pour point	°C	−21	−20	
Surface tension	mN/m	31.3	31.3	

(air–oil at 15°C)

IFT sea water	mN/m	20.5	10	
IFT fresh water	mN/m	23.3	16.2	
Adhesion	g/m ³	18	39	

SARA content (saturate, aromatic, resin, asphaltene) %

Saturate	%	86	85	
Aromatic	%	12	13	
Resin	%	1	1	
Asphaltene	%	0	0	
Waxes	%			

Emulsion formation (type formed and water content %)

Type			
Water content	%		
Viscosity	mPa·s or cP		

Chemical dispersibility with Corexit 9500

%			
---	--	--	--

Distillation data (% at temperature)

Boiling point (°C)			
40			
60			
80			
100			
120			
140			
160			
180			
200			
250			
300			
400	7	30	
500	99	94	
600			
700			

Oil name **Lubricating Oil (Air Compressor)**
Origin and description

Evaporation equation $\%Ev = (-0.68 + 0.045T)\ln(t)$
 Where Ev = weight percent evaporated, T = surface temperature (°C), t = time (min)

API gravity	30.5	Type		
(all units at 15°C)	Units	0	Used	
Density	g/ml	0.8734	0.8746	
Viscosity	mPa·s or cP	220	230	
(dynamic—values at 15°C)				
Flash point	°C	> 95	> 95	
Sulfur content	%	0.14	0.12	
Pour point	°C	−28	−25	
Surface tension	mN/m	31.4	31.4	
(air–oil at 15°C)				
IFT sea water	mN/m	12.7	15.9	
IFT fresh water	mN/m	18	21.3	
Adhesion	g/m ³	34	36	

SARA content (saturate, aromatic, resin, asphaltene) %				
Saturate	%	84	81	
Aromatic	%	13	16	
Resin	%	2	3	
Asphaltene	%	0	0	
Waxes	%			

Emulsion formation (type formed and water content %)				
Type				
Water content	%			
Viscosity	mPa·s or cP			
Chemical dispersibility with Corexit 9500				
	%			

Distillation data (% at temperature)				
Boiling point (°C)				
40				
60				
80				
100				
120				
140				
160				
180				
200				
250				
300	1			
400	7	14		
500	86	73		
600				
700				

Oil name **Lubricating Oil (Electrical)**
Origin and description Ontario Hydro; a.k.a. Lube 27

Evaporation equation
 Where Ev = weight percent evaporated, T = surface temperature (°C), t = time (min)

API gravity	30.5	Weathering % by weight		
(all units at 15°C)	Units	0	Used	
Density	g/ml	0.8728	0.8737	
Viscosity	mPa·s or cP	144	145	
(dynamic—values at 15°C)				
Flash point	°C	> 110	> 110	
Sulfur content	%	0.43	0.43	
Pour point	°C	−24	−27	
Surface tension	mN/m	31.2	31	
(air–oil at 15°C)				
IFT sea water	mN/m	13.6	11.4	
IFT fresh water	mN/m	19.4	22	
Adhesion	g/m ³			

SARA content (saturate, aromatic, resin, asphaltene) %				
Saturate	%			
Aromatic	%			
Resin	%			
Asphaltene	%			
Waxes	%			

Emulsion formation (type formed and water content %)				
Type				
Water content	%			
Viscosity	mPa·s or cP			
Chemical dispersibility with Corexit 9500				
	%			

Distillation data (% at temperature)				
Boiling point (°C)				
40				
60				
80				
100				
120				
140				
160				
180				
200				
250				
300				
400				
500				
600				
700				

Oil name	Lucula			
Origin and description	Angola			
Evaporation equation	$\%Ev = (2.17 + 0.045T)\ln(t)$			
Where Ev = weight percent evaporated, T = surface temperature (°C), t = time (min)				
API gravity	33.4	Weathering % by weight		
(all units at 15°C)	Units	0	11	15
Density	g/ml	0.8574	0.8821	0.8904
Viscosity	mPa·s or cP	43	5214	6118
(dynamic—values at 15°C)				
Flash point	°C	−10	44	68
Sulfur content	%	0.17	0.16	0.12
Pour point	°C	18	28	30
Surface tension	mN/m			
(air—oil at 15°C)				
IFT sea water	mN/m			
IFT fresh water	mN/m			
Adhesion	g/m ³	43	115	116
SARA content (saturate, aromatic, resin, asphaltene) %				
Saturate	%	67	64	62
Aromatic	%	22	23	26
Resin	%	8	8	9
Asphaltene	%	4	4	4
Waxes	%	13	10	11
Emulsion formation (type formed and water content %)				
Type				
Water content	%			
Viscosity	mPa·s or cP			
Chemical dispersibility with Corexit 9500				
	%	20		

Distillation data (% at temperature)				
Boiling point (°C)				
40				
60				
80	3			
100	6	1		
120	8	2		
140	11	4	1	
160	13	7	3	
180	16	10	5	
200	18	12	8	
250	25	20	16	4
300	32	29	25	14
400	48	48	45	37
500	65	67	66	61
600	77	81	81	79
700	86	92	92	91

Oil name	Macondo			
Origin and description	Louisiana oil from Deepwater Horizon Blowout, typical area sample			
Evaporation equation	$\%Ev = (3.0 + 0.045T) \ln t$			
Where Ev = weight percent evaporated, T = surface temperature (°C), t = time (min)				
API gravity	35.2	Weathering % by weight		Emulsified at sea
(all units at 15°C)	Units	0%	30.5	40.1
Density	g/ml	0.839	0.882	0.897
Viscosity	mPa·s or cP	4	45	90
(dynamic—values at 15°C)				
Flash point	°C	< −8	54	100
Sulfur content	%			
Pour point	°C	< −9	6	6
Surface tension	mN/m			
(air–oil at 15°C)				
IFT sea water	mN/m	23.3	22.6	22.5
IFT fresh water	mN/m			
Adhesion	g/m ³			
SARA content (saturate, aromatic, resin, asphaltene) %				
Saturate	%			
Aromatic	%			
Resin	%			
Asphaltene	%			
Waxes	%			
Emulsion formation (type formed and water content %)				
Type	Did not form			Mostly stable
Water content	%			~60
Viscosity	mPa·s or cP			10–82k
Chemical dispersibility with Corexit 9500				
	%			

Distillation data (% at temperature)				
Boiling point (°C)				
40	IBP			
60	3			
80	10			
100	15			
120	25			
140	35			
160	38			
180	40			
200				
250				
300				
400				
500				
600				
700				

Oil name Main Pass Block 37
Origin and description Gulf of Mexico, USA

Evaporation equation $\%Ev = (3.04 + 0.045T)\ln(t)$
 Where Ev = weight percent evaporated, T = surface temperature ($^{\circ}C$), t = time (min)

API gravity	38.8	Weathering % by weight			
(all units at 15°C)	Units	0	16	30	50
Density	g/ml	0.8311	0.8543	0.8689	0.8855
Viscosity	mPa-s or cP	7	16	36	115
(dynamic—values at 15°C)					
Flash point	$^{\circ}C$	−6	48	> 95	> 95
Sulfur content	%	0.16	0.31	0.46	0.39
Pour point	$^{\circ}C$	−3	4	15	17
Surface tension	mN/m	24	28	29	31.2
(air–oil at 15°C)					
IFT sea water	mN/m	19.7	22.6	23.2	21.7
IFT fresh water	mN/m	20.6	23.4	24	25.1
Adhesion	g/m ³	10	18	38	52

SARA content (saturate, aromatic, resin, asphaltene) %

Saturate	%	73	73	70	66
Aromatic	%	21	21	23	24
Resin	%	5	5	6	8
Asphaltene	%	1	1	1	2
Waxes	%	8	6	7	8

Emulsion formation (type formed and water content %)

Type				
Water content	%			
Viscosity	mPa-s or cP			

Chemical dispersibility with Corexit 9500

%	33	26	16	14
---	----	----	----	----

Distillation data (% at temperature)

Boiling point ($^{\circ}C$)				
40	2			
60	2			
80	5			
100	8	1		
120	12	2		
140	16	4		
160	20	8	1	
180	25	13	3	
200	29	18	6	
250	41	31	20	4
300	53	45	36	19
400	74	69	64	54
500	89	87	84	80
600	97	96	95	94
700			99	99

Oil name Main Pass Block 306
Origin and description Gulf of Mexico, USA

Evaporation equation $\%Ev = (2.86 + 0.045T)\ln(t)$
 Where Ev = weight percent evaporated, T = surface temperature ($^{\circ}C$), t = time (min)

API gravity	32.8	Weathering % by weight			
(all units at 15°C)	Units	0	12	24	37
Density	g/ml	0.8606	0.8849	0.9034	0.9203
Viscosity	mPa-s or cP	9	19	54	219
(dynamic—values at 15°C)					
Flash point	$^{\circ}C$	< −30	44	> 95	> 95
Sulfur content	%	0.28	0.31	0.33	0.38
Pour point	$^{\circ}C$	−53	−35	−32	−16
Surface tension	mN/m	26.9	28.6	30.1	31.2
(air–oil at 15°C)					
IFT sea water	mN/m	16.5	18.3	17.4	13.6
IFT fresh water	mN/m	20.3	21.9	22.3	17.5
Adhesion	g/m ³	11	14	28	41

SARA content (saturate, aromatic, resin, asphaltene) %

Saturate	%	65	63	58	55
Aromatic	%	29	29	32	33
Resin	%	5	8	10	11
Asphaltene	%	1	1	1	1
Waxes	%	3	2	2	3

Emulsion formation (type formed and water content %)

Type				
Water content	%			
Viscosity	mPa-s or cP			

Chemical dispersibility with Corexit 9500

%	27	23	18	17
---	----	----	----	----

Distillation data (% at temperature)

Boiling point ($^{\circ}C$)				
40				
60				
80				
100	2	1		
120	2	2		
140	5	5		
160	14	9		
180	23	13	2	
200	26	17	5	
250	37	229	18	4
300	49	42	32	18
400	70	65	59	51
500	86	83	80	75
600	96	94	92	91
700		99	99	98

Oil name		Malongo			
Origin and description		Angola			
Evaporation equation		$\%Ev = (1.67 + 0.045T)\ln(t)$			
Where Ev = weight percent evaporated, T = surface temperature (°C), t = time (min)					
API gravity	31	Weathering % by weight			
(all units at 15°C)	Units	0	12	16	22
Density	g/ml	0.8701	0.897	0.9026	0.9141
Viscosity	mPa·s or cP	63	6359	10,950	25,600
(dynamic—values at 15°C)					
Flash point	°C	−9	66	91	> 95
Sulfur content	%	0.2	0.18	0.19	0.2
Pour point	°C	21	27	31	32
Surface tension	mN/m	28.7			
(air–oil at 15°C)					
IFT sea water	mN/m	22.1			
IFT fresh water	mN/m	23.3			
Adhesion	g/m ³	19	46	159	203
SARA content (saturate, aromatic, resin, asphaltene) %					
Saturate	%	62	60	55	54
Aromatic	%	25	28	29	28
Resin	%	9	10	13	15
Asphaltene	%	4	3	3	4
Waxes	%	10	9	9	9
Emulsion formation (type formed and water content %)					
Type					
Water content	%				
Viscosity	mPa·s or cP				
Chemical dispersibility with Corexit 9500					
	%	15			
Distillation data (% at temperature)					
Boiling point (°C)					
40					
60					
80		2			
100		4			
120		6	1		
140		8	2		
160		10	3	1	
180		13	5	2	
200		15	8	4	
250		21	15	11	5
300		29	24	20	14
400		44	42	40	35
500		62	63	62	59
600		75	78	79	77
700		85	90	91	91

Oil name	Marine Intermediate Fuel Oil		
Origin and description	St. John, New Brunswick; a.k.a. Interfuel 380		
Evaporation equation	Where Ev = weight percent evaporated, T = surface temperature (°C), t = time (min)		
API gravity	12.9	Weathering % by weight	
(all units at 15°C)	Units	0	
Density	g/ml	0.9787	
Viscosity	mPa·s or cP	8200	
(dynamic—values at 15°C)			
Flash point	°C		
Sulfur content	%	2.6	
Pour point	°C		
Surface tension	mN/m	33.6	
(air–oil at 15°C)			
IFT sea water	mN/m	35.5	
IFT fresh water	mN/m		
Adhesion	g/m ³		
SARA content (saturate, aromatic, resin, asphaltene) %			
Saturate	%		
Aromatic	%		
Resin	%		
Asphaltene	%	10	
Waxes	%		
Emulsion formation (type formed and water content %)			
Type			
Water content	%		
Viscosity	mPa·s or cP		
Chemical dispersibility with Corexit 9500			
%			
Distillation data (% at temperature)			
Boiling point (°C)			
40			
60			
80			
100			
120			
140			
160			
180	1		
200	2		
250	8		
300	16		
400	28		
500	34		
600	57		
700	82		

Oil name **Mars TLP—A**
Origin and description Gulf of Mexico, USA, 2004

Evaporation equationWhere Ev = weight percent evaporated, T = surface temperature (°C), t = time (min)

API gravity	26.8	Weathering % by weight			
(all units at 15°C)	Units	0	8.4	17.2	26.2
Density	g/ml	0.8933	0.9162	0.9353	0.9537
Viscosity	mPa·s or cP	33	93	404	2237
(dynamic—values at 15°C)					
Flash point	°C				
Sulfur content	%				
Pour point	°C				
Surface tension	mN/m	26.2	28	29.6	30.8
(air–oil at 15°C)					
IFT sea water	mN/m	21.3	21.1	16.2	
IFT fresh water	mN/m	24.8	21.8	19.7	
Adhesion	g/m ³				

SARA content (saturate, aromatic, resin, asphaltene) %

Saturate	%	58.4	55	52.2	46.7
Aromatic	%	27.5	27.1	28.3	30.1
Resin	%	9.5	11.5	12.4	14.7
Asphaltene	%	4.7	6.3	7.1	8.5
Waxes	%				

Emulsion formation (type formed and water content %)

Type				
Water content	%			
Viscosity	mPa·s or cP			

Chemical dispersibility with Corexit 9500

%				
---	--	--	--	--

Distillation data (% at temperature)

Boiling point (°C)				
40				
60				
80				
100				
120				
140				
160				
180				
200				
250				
300				
400				
500				
600				
700				

Oil name **Mars TLP**
Origin and description Gulf of Mexico, USA

Evaporation equation

$$\%Ev = (2.18 + 0.045T)\ln(t)$$

Where Ev = weight percent evaporated, T = surface temperature (°C), t = time (min)

API gravity	27.6	Weathering % by weight			
(all units at 15°C)	Units	0	8	17	26
Density	g/ml	0.8883	0.9122	0.9331	0.952
Viscosity	mPa·s or cP	33	93	404	2,237
(dynamic—values at 15°C)					
Flash point	°C	–26	26	71	> 100
Sulfur content	%	2.07	1.97	2.13	2.37
Pour point	°C	–28	–16	–17	–7
Surface tension	mN/m	26.2	28	29.6	30.8
(air–oil at 15°C)					
IFT sea water	mN/m	21.3	21.1	16.2	
IFT fresh water	mN/m	24.8	21.8	19.7	
Adhesion	g/m ³	24	25	23	61

SARA content (saturate, aromatic, resin, asphaltene) %

Saturate	%	59.7	55	50.4	48.8
Aromatic	%	24.2	28.1	29.9	29
Resin	%	10.6	10.7	12.6	12.5
Asphaltene	%	5.5	6.2	7.1	9.7
Waxes	%	1.5	1.4	1.9	2.2

Emulsion formation (type formed and water content %)

Type	Unstable	Meso-stable	Meso-stable	Meso-stable
Water content	%	63	65	62
Viscosity	mPa·s or cP	5836	10,520	30,660

Chemical dispersibility with Corexit 9500

%	36	34	16	2
---	----	----	----	---

Distillation data (% at temperature)

Boiling point (°C)				
40	0.8			
60	1.1	0.1		
80	2	0.3		
100	3.4	1.2		
120	4.7	2.2	0.1	
140	6	3.5	0.3	
160	7.8	5.3	1	
180	9.7	7.3	2.5	
200	11.4	9.2	4.2	0.2
250	16.3	14.7	9.8	3.6
300	21.9	20.9	16.4	10.5
400	34.6	35	31.2	27.1
500	48.6	50.7	47.8	45.7
600	62.3	66.3	64.3	64
700				

Oil name		Maya		
Origin and description		Mexico 1997		
Evaporation equation		$\%Ev = (1.38 + 0.045T)\ln(t)$		
Where Ev = weight percent evaporated, T = surface temperature (°C), t = time (min)				
API gravity	21.8	Weathering % by weight		
(all units at 15°C)	Units	0	19	
Density	g/ml	0.9219	0.9762	
Viscosity	mPa·s or cP	299	99,390	
(dynamic—values at 15°C)				
Flash point	°C	−7	> 95	
Sulfur content	%	3.3	3.65	
Pour point	°C	−20	3	
Surface tension	mN/m	28		
(air–oil at 15°C)				
IFT sea water	mN/m	27.3		
IFT fresh water	mN/m	27.6		
Adhesion	g/m ³	69	341	
SARA content (saturate, aromatic, resin, asphaltene)				
%				
Saturate	%	39	29	
Aromatic	%	34	35	
Resin	%	11	14	
Asphaltene	%	16	21	
Waxes	%			
Emulsion formation (type formed and water content %)				
Type				
Water content	%			
Viscosity	mPa·s or cP			
Chemical dispersibility with Corexit 9500				
%		15	13	
Distillation data (% at temperature)				
Boiling point (°C)				
40		5		
60		6		
80		8		
100		10		
120		10		
140		12		
160		14		
180		17		
200		20		
250		27	5	
300		34	14	
400		52	35	
500		69	56	
600		84	73	
700		96	86	

Oil name		Maya—A			
Origin and description		Gulf of Mexico, Mexico, 2004			
Evaporation equation					
Where Ev = weight percent evaporated, T = surface temperature (°C), t = time (min)					
API gravity	20.2	Weathering % by weight			
(all units at 15°C)	Units	0	5.5	11.4	16.7
Density	g/ml	0.9321	0.9499	0.9662	0.9791
Viscosity	mPa·s or cP	576.7	2080	10,990	115,000
(dynamic—values at 15°C)					
Flash point	°C				
Sulfur content	%				
Pour point	°C				
Surface tension	mN/m	28.4			
(air–oil at 15°C)					
IFT sea water	mN/m	30.1			
IFT fresh water	mN/m	28.4			
Adhesion	g/m ³				
SARA content (saturate, aromatic, resin, asphaltene) %					
Saturate	%	46.5	42.7	39.2	35.3
Aromatic	%	25.4	24.7	26	24.2
Resin	%	12.7	15.3	15.6	18.8
Asphaltene	%	15.5	17.3	19.2	21.7
Waxes	%				
Emulsion formation (type formed and water content %)					
Type					
Water content	%				
Viscosity	mPa·s or cP				
Chemical dispersibility with Corexit 9500					
	%				
Distillation data (% at temperature)					
Boiling point (°C)					
40					
60					
80					
100					
120					
140					
160					
180					
200					
250					
300					
400					
500					
600					
700					

Oil name Maya—B
Origin and description Mexico

Evaporation equation $\%Ev = (1.45 + 0.045T)\ln(t)$
 Where Ev = weight percent evaporated, T = surface temperature (°C), t = time (min)

API gravity	21.3	Weathering % by weight			
(all units at 15°C)	Units	0	9	15	22
Density	g/ml	0.9255	0.9515	0.9657	0.9868
Viscosity	mPa·s or cP	280	1980	8670	405,000
(dynamic—values at 15°C)					
Flash point	°C	−9	54	93	> 95
Sulfur content	%	3	3.74	3.98	4.18
Pour point	°C	−15	−9	−2	17
Surface tension	mN/m	28.2	29.7	30.9	
(air–oil at 15°C)					
IFT sea water	mN/m	27	26		
IFT fresh water	mN/m	28.5	28.5		
Adhesion	g/m ³	71	82	102	594

SARA content (saturate, aromatic, resin, asphaltene) %

Saturate	%	38	33	31	28
Aromatic	%	39	41	41	39
Resin	%	8	8	10	11
Asphaltene	%	16	18	17	22
Waxes	%	33	3	4	4

Emulsion formation (type formed and water content %)

Type				
Water content	%			
Viscosity	mPa·s or cP			

Chemical dispersibility with Corexit 9500

%				
---	--	--	--	--

Distillation data (% at temperature)

Boiling point (°C)				
40				
60				
80	1			
100	1			
120	6	1		
140	8	2		
160	9	4		
180	11	6	2	
200	13	8	3	
250	19	15	10	2
300	25	22	17	9
400	38	37	33	27
500	52	52	49	44
600	65	67	65	62
700	78	79	78	76

Oil name Mississippi Canyon Block 72
Origin and description Gulf of Mexico, USA

Evaporation equation $\%Ev = (2.15 + 0.045T)\ln(t)$
 Where Ev = weight percent evaporated, T = surface temperature (°C), t = time (min)

API gravity	32	Weathering % by weight			
(all units at 15°C)	Units	0	9	18	26
Density	g/ml	0.8649	0.8827	0.8966	0.9095
Viscosity	mPa·s or cP	16	34	76	195
(dynamic—values at 15°C)					
Flash point	°C	−5	41	82	> 95
Sulfur content	%	0.39	0.36	0.4	0.48
Pour point	°C	−28	−6	−1	1
Surface tension	mN/m	27.1	28.6	29.7	30.8
(air–oil at 15°C)					
IFT sea water	mN/m	25.5	29	27.9	21.8
IFT fresh water	mN/m	27.1	29.1	28.3	22.1
Adhesion	g/m ³	12	22	40	39

SARA content (saturate, aromatic, resin, asphaltene) %

Saturate	%	64	57	58	52
Aromatic	%	27	33	32	34
Resin	%	7	8	9	11
Asphaltene	%	2	2	2	3
Waxes	%				

Emulsion formation (type formed and water content %)

Type	Unstable	Unstable	Meso-stable	Stable
Water content	%		52	74
Viscosity	mPa·s or cP		4899	32,990

Chemical dispersibility with Corexit 9500

%	31	24	19	18
---	----	----	----	----

Distillation data (% at temperature)

Boiling point (°C)				
40	1			
60	1			
80	2			
100	4	1		
120	7	2		
140	10	5		
160	13	8	1	
180	16	11	4	
200	20	15	7	1
250	29	25	17	9
300	39	36	30	22
400	59	59	54	49
500	76	77	75	72
600	87	90	83	88
700	94	98	97	97

Oil name Mississippi Canyon Block 194
Origin and description Gulf of Mexico, USA

Evaporation equation $\%Ev = (2.62 + 0.045T)\ln(t)$
 Where Ev = weight percent evaporated, T = surface temperature (°C), t = time (min)

API gravity	35.2	Weathering % by weight			
	Units	0	10	21	35
(all units at 15°C)					
Density	g/ml	0.8483	0.8655	0.8762	0.8874
Viscosity	mPa·s or cP	7	11	21	51
(dynamic—values at 15°C)					
Flash point	°C	−6	54	> 95	> 95
Sulfur content	%	0.21	0.19	0.21	0.26
Pour point	°C	−40	−28	−22	16
Surface tension mN/m		27.2	28.5	29.6	30.3
(air–oil at 15°C)					
IFT sea water mN/m		18.1	19.3	17	15.8
IFT fresh water mN/m		19.7	22.7	21.7	19.3
Adhesion	g/m ³	8	10	22	41

SARA content (saturate, aromatic, resin, asphaltene) %

Saturate	%	71	71	69	67
Aromatic	%	25	23	24	26
Resin	%	4	6	6	7
Asphaltene	%	0	0	0	0
Waxes	%	5	4	4	5

Emulsion formation (type formed and water content %)

Type				
Water content	%			
Viscosity	mPa·s or cP			

Chemical dispersibility with Corexit 9500

%	29	22	17	15
---	----	----	----	----

Distillation data (% at temperature)

Boiling point (°C)				
40				
60				
80				
100	1			
120	1	1		
140	3	3		
160	11	6		
180	18	10	2	
200	23	14	4	
250	37	29	20	6
300	52	47	39	27
400	75	72	68	62
500	90	88	86	83
600	97	96	96	94
700		99	99	99

Oil name Mississippi Canyon Block 807 (2002)
Origin and description Louisiana, USA (shell offshore)

Evaporation equation $\%Ev(w/w) = (2.28 + 0.045T) \ln t$
 Where Ev = weight percent evaporated, T = surface temperature (°C), t = time (min)

API gravity	17.5	Weathering % by weight			
	Units	0	11.7	22.4	35.9
(all units at 15°C)					
Density	g/ml	0.9461	0.9202	0.9562	0.9693
Viscosity	mPa·s or cP	4.8	165	396	1472
(dynamic—values at 15°C)					
Flash point	°C	< 0	51	75	115
Sulfur content	%	0.83	0.86	0.9	1.22
Pour point	°C	−57	−56	−35	−23
Surface tension mN/m		28.2	29.9	30.5	
(air–oil at 15°C)					
IFT sea water mN/m		26.6	22.6	22.7	
IFT fresh water mN/m		24.1	22.3	22.3	
Adhesion	g/m ³	27	40	23	27

SARA content (saturate, aromatic, resin, asphaltene) %

Saturate	%	73.7	69.42	66.18	63.11
Aromatic	%	15.45	16.35	16.93	16.27
Resin	%	6.22	8.11	9.71	10.91
Asphaltene	%	5.03	6.12	7.18	9.7
Waxes	%	0.6	0.8	0.8	1

Emulsion formation (type formed and water content %)

Type		Meso-stable	Stable	Stable	Stable
Water content	%	79.7	79.7	76.2	72.1
Viscosity	mPa·s or cP				

Chemical dispersibility with Corexit 9500

%				
---	--	--	--	--

Distillation data (% at temperature)

Boiling point (°C)				
40	1.9			
60	3.2	0.4	0.3	0.1
80	6.3	0.8	0.3	0.2
100	8.5	1.3	0.3	0.2
120	10.5	2.2	0.4	0.2
140	12.8	3.7	0.7	0.2
160	15.6	6.1	1.8	0.2
180	18.3	8.8	3.8	0.3
200	20.7	11.3	6.1	0.8
250	26.9	18.1	13.3	6.3
300	33.2	25	20.9	14.7
400	46.1	39	36.4	32.4
500	59.2	53	52	50.3
600	70.5	65.1	65.4	65.4
700				

Oil name Mississippi Canyon Block 807-A
Origin and description Gulf of Mexico, USA

Evaporation equation $\%Ev = (2.05 + 0.045T)\ln(t)$
 Where Ev = weight percent evaporated, T = surface temperature (°C), t = time (min)

API gravity	27.5	Weathering % by weight			
(all units at 15°C)	Units	0	9	16	26
Density	g/ml	0.8894	0.9187	0.9375	0.9582
Viscosity	mPa·s or cP	41	127	491	3454
(dynamic—values at 15°C)					
Flash point	°C	< -30	29	75	> 95
Sulfur content	%	2.19	2.13	2.31	2.51
Pour point	°C	-34	-33	-26	-5
Surface tension	mN/m	26.4	28.5	30.1	32
(air-oil at 15°C)					
IFT sea water	mN/m	23.3	25	20.5	
IFT fresh water	mN/m	25.9	26.3	24.9	
Adhesion	g/m ³	29	33	32	54

SARA content (saturate, aromatic, resin, asphaltene) %

Saturate	%	47	39		31
Aromatic	%	35	41		43
Resin	%	12	13		18
Asphaltene	%	6	7		8
Waxes	%				

Emulsion formation (type formed and water content %)

Type		Meso-stable	Meso-stable	Stable	Stable
Water content	%	60	68	68	65
Viscosity	mPa·s or cP	6199	10,130	17,850	33,640

Chemical dispersibility with Corexit 9500

%	19	17	0	0
---	----	----	---	---

Distillation data (% at temperature)

Boiling point (°C)				
40	2			
60	3			
80	4			
100	7	2		
120	9	4		
140	12	6	1	
160	15	9	3	
180	18	12	5	
200	21	15	8	1
250	28	23	16	6
300	36	32	26	15
400	53	50	46	38
500	69	68	65	59
600	82	82	80	77
700	92	93	92	90

Oil name Morpeth Block EW921
Origin and description Louisiana, USA (AGIP)

Evaporation equation
 Where Ev = weight percent evaporated, T = surface temperature (°C), t = time (min)

API gravity	25.1	Weathering % by weight			
(all units at 15°C)	Units	0	9.3	15.2	24
Density	g/ml	0.8996	0.9282	0.9426	0.9619
Viscosity	mPa·s or cP	45.1	195	551	3697
(dynamic— values at 15°C)					
Flash point	°C	< 0	40	67	123
Sulfur content	%	1.73	2.01	2.29	2.68
Pour point	°C	-65	-52	-30	-17
Surface tension	mN/m	26.4	28.1	29.6	
(air-oil at 15°C)					
IFT sea water	mN/m	23.8	20.7	19.8	
IFT fresh water	mN/m	22.7	21.1	20	
Adhesion	g/m ³	29	37	43	52

SARA content (saturate, aromatic, resin, asphaltene) %

Saturate	%	70.63	68.59	65.88	60.39
Aromatic	%	16.48	16.79	18.2	18.51
Resin	%	8.42	9.46	10.17	12.92
Asphaltene	%	4.1	5.16	5.76	8.18
Waxes	%	0.7	0.9	0.9	1

Emulsion formation (type formed and water content %)

Type		Unstable	Meso-stable	Stable	Stable
Water content	%		75.5	73.6	69.4
Viscosity	mPa·s or cP				

Chemical dispersibility with Corexit 9500

%	26.6	17.4	13.5	7.8
---	------	------	------	-----

Distillation data (% at temperature)

Boiling point (°C)				
40				
60				
80				
100	2.1	0.9		
120	4.2	2.2	0.1	
140	6.3	4	0.6	
160	8.8	6.4	2	
180	11.3	9	4.1	
200	13.5	11.4	6.4	0.3
250	19.6	18.3	13.4	4.9
300	26.3	25.7	21.2	13.1
400	40.5	41.3	37.7	31.4
500	54.7	57	54.3	49.9
600	67	71.1	68.9	66.2
700				

Evaporation equation $\%Ev = (0.62 + 0.045T)\ln(t)$
Where Ev = weight percent evaporated, T = surface temperature ($^{\circ}\text{C}$), t = time (min)

SARA content (saturate, aromatic, resin, asphaltene) %			
Saturate	%		
Aromatic	%		
Resin	%		
Asphaltene	%	0	
Waxes	%		

Chemical dispersibility with Corexit 9500			
%			

Boiling point (°C)			
40			
60			
80			
100	1		
120	2		
140	3		
160	4		
180	5		
200	7		
250	17		
300	37		
400	74		
500	92		
600	98		
700			

Evaporation equation $\%Ev = (3.75 + 0.045T)\ln(t)$
Where Ev = weight percent evaporated, T = surface temperature ($^{\circ}\text{C}$), t = time (min)

API Gravity	31.2	Weathering % by weight			
(all units at 15°)	Units	0	8	15	23
Density	g/ml	0.8687	0.8826	0.8925	0.8986
Viscosity	mPa-s or cP	17	42	84	187
(dynamic—values at 15°C)					
Flash point	°C	2	54	89	> 100
Sulfur content	%	0.29	0.32	0.27	0.36
Pour point	°C	−1	9	17	19
Surface tension	mN/m	27.8	28.9	29.6	30.1
(air-oil at 15°C)					
IFT sea water	mN/m	21.2	19.3	18.3	14.9
IFT fresh water	mN/m	21.5	21.4	20.9	16.8
Adhesion	g/m ³	18	32	33	42

SARA content (saturate, aromatic, resin, asphaltene) %					
Saturate	%	65	63	62	61
Aromatic	%	28	29	29	29
Resin	%	6	6	7	8
Asphaltene	%	1	2	2	2
Waxes	%	4.1	4.4	4.5	4.5

Emulsion formation (type formed and water content %)					
Type		Unstable	Unstable	Meso-stable	Stable
Water content	%			48	63
Viscosity	mPa.s or cP			14,120	31,240

Chemical dispersibility with Corexit 9500				
%	29	21	16	14

Boiling point (°C)	0.2	0.3	0.4	0.5
40	0.2			
60	0.3			
80	1	0.1		
100	2.2	0.3	0.2	
120	3.5	0.8	0.2	0.3
140	4.9	1.8	0.3	0.3
160	6.7	3.4	0.7	0.3
180	8.7	5.5	2	0.4
200	10.6	7.7	4.1	0.7
250	17	15.1	12.4	0.9
300	24.9	24.1	22.9	18.3
400	43.5	44.6	46.1	44.5
500	61.6	63.7	66.9	67.6
600	73.1	76.5	80.6	82.6
700				

Oil name	Nerlerk		
Origin and description	Beaufort Sea, Canada; a.k.a. Nerlerk M-98A		
Evaporation equation	$\%Ev = (2.01 + 0.045T)\ln(t)$		
Where Ev = weight percent evaporated, T = surface temperature (°C), t = time (min)			
API gravity	23.9	Weathering % by weight	
(all units at 15°C)	Units	0	
Density	g/ml	0.9095	
Viscosity	mPa·s or cP		
(dynamic—values at 15°C)			
Flash point	°C		
Sulfur content	%	0.14	
Pour point	°C		
Surface tension	mN/m	29	
(air-oil at 15°C)			
IFT sea water	mN/m	11	
IFT fresh water	mN/m	15.6	
Adhesion	g/m ³		
SARA content (saturate, aromatic, resin, asphaltene) %			
Saturate	%		
Aromatic	%		
Resin	%		
Asphaltene	%	0	
Waxes	%	2	
Emulsion formation (type formed and water content %)			
Type			
Water content	%		
Viscosity	mPa·s or cP		
Chemical dispersibility with Corexit 9500			
	%		
Distillation data (% at temperature)			
Boiling point (°C)			
40			
60			
80	1		
100	2		
120	3		
140	5		
160	7		
180	10		
200	13		
250	28		
300	47		
400	74		
500	90		
600	97		
700			

Oil name		Ninian Blend		
Origin and description		North Sea, UK		
Evaporation equation		%Ev = (2.65 + 0.045 <i>T</i>)ln(<i>t</i>)		
Where Ev = weight percent evaporated, <i>T</i> = surface temperature (°C), <i>t</i> = time (min)				
API gravity	36.1	Weathering % by weight		
(all units at 15°C)	Units	0	15	30
Density	g/ml	0.8435	0.8655	0.8889
Viscosity	mPa.s or cP	8	16	62
(dynamic—values at 15°C)				
Flash point	°C	−20	29	> 90
Sulfur content	%	0.36	0.36	0.45
Pour point	°C	−9	6	15
Surface tension	mN/m	25.8	28.1	31.5
(air-oil at 15°C)				
IFT sea water	mN/m	21	19.9	12.4
IFT fresh water	mN/m	22.1	20.4	22.8
Adhesion	g/m ³	17	22	32
SARA content (saturate, aromatic, resin, asphaltene) %				
Saturate	%	61	61	55
Aromatic	%	30	29	34
Resin	%	8	7	10
Asphaltene	%	2	2	2
Waxes	%	6	5	7
Emulsion formation (type formed and water content %)				
Type				
Water content	%			
Viscosity	mPa.s or cP			
Chemical dispersibility with Corexit 9500				
	%			
Distillation data (% at temperature)				
Boiling point (°C)				
40	4			
60	5	1		
80	7	2		
100	10	4		
120	10	5		
140	12	7		
160	16	10	1	
180	19	14	2	
200	23	17	5	
250	32	28	15	
300	44	39	28	
400	65	61	54	
500	82	80	76	
600	93	92	89	
700	99	98	97	

Oil name **Norman Wells**
Origin and description Northwest Territories, Canada

Evaporation equation $\%Ev = (3.11 + 0.045T)\ln(t)$
 Where Ev = weight percent evaporated, T = surface temperature (°C), t = time (min)

API gravity	38.4	Weathering % by weight		
(all units at 15°C)	Units	0	10	20
Density	g/ml	0.832		
Viscosity	mPa·s or cP	5		
(dynamic—values at 15°C)				
Flash point	°C	3		
Sulfur content	%	0.37		
Pour point	°C	< -50	< -50	< -50
Surface tension	mN/m	23.6		
(air-oil at 15°C)				
IFT sea water	mN/m	16.4		
IFT fresh water	mN/m	20.1		
Adhesion	g/m ³			

SARA content (saturate, aromatic, resin, asphaltene) %

Saturate	%	86	82	80
Aromatic	%	11	12	13
Resin	%	2	3	4
Asphaltene	%	0	3	3
Waxes	%	2	2	2

Emulsion formation (type formed and water content %)

Type			
Water content	%		
Viscosity	mPa·s or cP		

Chemical dispersibility with Corexit 9500

%	35		
---	----	--	--

Distillation data (% at temperature)

Boiling point (°C)			
40	1		
60	1		
80	4		
100	8		
120	11		
140	15		
160	9		
180	23		
200	27		
250	38		
300	48		
400	68		
500	83		
600	93		
700	99		

Oil name **Odoptu**
Origin and description Russia (Exxon-Mobil)

Evaporation equation $\%Ev = (4.27 + 0.45T) \ln t$
 Where Ev = weight percent evaporated, T = surface temperature (°C), t = time (min)

API gravity	32.87	Weathering % by weight			
(all units at 15°C)	Units	0	13.6	29.3	41.2
Density	g/ml	0.8556	0.8759	0.8941	0.9072
Viscosity	mPa·s or cP	5.3	8.7	18.4	38.2
(dynamic—values at 15°C)					
Flash point	°C	< -10	35.8	74.8	> 110
Sulfur content	%	0.33	0.38	0.44	0.52
Pour point	°C	-48	-42	-29	-17
Surface tension	mN/m	26.7	28.2	29.6	30.5
(air-oil at 15°C)					
IFT sea water	mN/m	23.2	25.1	24.6	23.8
IFT fresh water	mN/m	23.4	24.6	25.7	19.2
Adhesion	g/m ³	0	12	15	31

SARA content (saturate, aromatic, resin, asphaltene) %

Saturate	%	73.4	70.5	62.5	59.3
Aromatic	%	26.6	29.5	37.5	40.7
Resin	%	5.46	5.42	7.31	7.72
Asphaltene	%	0.78	0.75	0.68	0.65
Waxes	%	7.78	7.94	10.41	12.05

Emulsion formation (type formed and water content %)

Type				
Water content	%			
Viscosity	mPa·s or cP			

Chemical dispersibility with Corexit 9500

%	54	40	24	18
---	----	----	----	----

Distillation data (% at temperature)

Boiling point (°C)				
40	1.1	0.3		
60	3.5	1.7		
80	6.2	2.5		
100	10	3.5		
120	16.2	6.9		
140	21.9	12	0.5	
160	27.2	17.5	2.3	
180	33	23.9	6.8	0.2
200	38	29.6	12.4	1.8
250	51.5	45.2	31	17.5
300	63.4	59.1	48	37.1
400	81.2	79.7	73.3	67.4
500	91.9	92.9	88.7	85.9
600	96.6	95.5	92.9	91
700				

Oil name **Oriente**
Origin and description Ecuador

Evaporation equation $\%Ev = (1.45 + 0.0457)\ln(t)$
 Where Ev = weight percent evaporated, T = surface temperature ($^{\circ}C$), t = time (min)

API gravity	25.9	Weathering % by weight		
(all units at 15°C)	Units	0	21	
Density	g/ml	0.8981	0.9426	
Viscosity	mPa·s or cP	85	6124	
(dynamic—values at 15°C)				
Flash point	$^{\circ}C$	−1	> 95	
Sulfur content	%	1.31	1.52	
Pour point	$^{\circ}C$	−4	13	
Surface tension mN/m		27.7		
(air–oil at 15°C)				
IFT sea water mN/m		26.6		
IFT fresh water mN/m		26.8		
Adhesion	g/m ³	30	215	

SARA content (saturate, aromatic, resin, asphaltene) %

Saturate	%	48	41	
Aromatic	%	32	33	
Resin	%	9	11	
Asphaltene	%	12	15	
Waxes	%	1.5		

Emulsion formation (type formed and water content %)

Type			
Water content	%		
Viscosity	mPa·s or cP		

Chemical dispersibility with Corexit 9500

%			
---	--	--	--

Distillation data (% at temperature)

Boiling point ($^{\circ}C$)			
40	0.6		
60	1.4		
80	2.4		
100	4.4		
120	6.2		
140	8.5		
160	11.2		
180	14		
200	16.6		
250	24.7	6	
300	34	16	
400	53.4	40	
500	70.9	61	
600	85.1	76	
700		86	

Oil name **Orimulsion-100**
Origin and description

Evaporation equation $\%Ev = (3.00 + 0.0457)\ln(t)$ water loss
 Where Ev = weight percent evaporated, T = surface temperature ($^{\circ}C$), t = time (min)

API gravity	8.2	Water loss %		
(all units at 15°C)	Units	0	26	
		26% water	No water	
Density	g/ml	1.0123	0.019	
Viscosity	mPa·s or cP	623	6,700,000	
(dynamic—values at 15°C)				
Flash point	$^{\circ}C$	> 95	> 95	
Sulfur content	%	2.32		
Pour point	$^{\circ}C$	2	40	
Surface tension mN/m		34.6		

(air–oil at 15°C)			
IFT sea water mN/m			
IFT fresh water mN/m			
Adhesion	g/m ³		

SARA content (saturate, aromatic, resin, asphaltene) %

Saturate	%	17	
Aromatic	%	47	
Resin	%	16	
Asphaltene	%	20	
Waxes	%		

Emulsion formation (type formed and water content %)

Type			
Water content	%		
Viscosity	mPa·s or cP		

Chemical dispersibility with Corexit 9500

%			
---	--	--	--

Distillation data (% at temperature)

Boiling point ($^{\circ}C$)			
40			
60			
80			
100			
120			
140			
160			
180			
200			
250		1	
300		5	
400		18	
500		35	
600		53	
700		72	

Oil name **Orimulsion-400**
Origin and description Venezuela, 1999

Evaporation equation

Where E_v = weight percent evaporated, T = surface temperature ($^{\circ}\text{C}$), t = time (min)

API gravity	8.7	Water Loss % by weight		
(all units at 15°C)	Units	0		
Density	g/ml	1.0084		
Viscosity	mPa·s or cP	380		
(dynamic—values at 15°C)				
Flash point	$^{\circ}\text{C}$	> 100		
Sulfur content	%			
Pour point	$^{\circ}\text{C}$	1		
Surface tension mN/m				
(air–oil at 15°C)				
IFT sea water mN/m				
IFT fresh water mN/m				
Adhesion	g/m^3			

SARA content (saturate, aromatic, resin, asphaltene) %

Saturate	%			
Aromatic	%			
Resin	%			
Asphaltene	%			
Waxes	%			

Emulsion formation (type formed and water content %)

Type			
Water content	%		
Viscosity	mPa·s or cP		

Chemical dispersibility with Corexit 9500

%			
---	--	--	--

Distillation data (% at temperature)

Boiling point ($^{\circ}\text{C}$)			
40			
60			
80			
100			
120			
140			
160			
180			
200			
250			
300			
400			
500			
600			
700			

Oil name **Oseberg**
Origin and description North Sea, Norway

Evaporation equation

$$\%E_v = (2.68 + 0.045T)\ln(t)$$

Where E_v = weight percent evaporated, T = surface temperature ($^{\circ}\text{C}$), t = time (min)

API gravity	34.4	Weathering % by weight		
(all units at 15°C)	Units	0	14	28
Density	g/ml	0.8522	0.8839	0.8961
Viscosity	mPa·s or cP	10	29	70
(dynamic—values at 15°C)				
Flash point	$^{\circ}\text{C}$	−24	51	> 90
Sulfur content	%	0.28	0.34	0.39
Pour point	$^{\circ}\text{C}$	−9	0	3
Surface tension mN/m		26.2	27.8	29.1
(air–oil at 15°C)				
IFT sea water mN/m		20.2	21.2	19.9
IFT fresh water mN/m		22.6	22.7	22.5
Adhesion	g/m^3	20	32	33

SARA content (saturate, aromatic, resin, asphaltene) %

Saturate	%	65	58	55	36
Aromatic	%	25	30	32	52
Resin	%	8	10	13	10
Asphaltene	%	2	2	1	2
Waxes	%	5	4	5	2

Emulsion formation (type formed and water content %)

Type				
Water content	%			
Viscosity	mPa·s or cP			

Chemical dispersibility with Corexit 9500

%	15			
---	----	--	--	--

Distillation data (% at temperature)

Boiling point ($^{\circ}\text{C}$)				
40	6			
60	8			
80	9	1		
100	10	1		
120	11	1		
140	13	3		
160	16	5		
180	20	9	2	
200	23	12	5	
250	33	23	16	
300	44	36	30	
400	64	59	55	
500	81	79	77	
600	92	91	90	
700	98	98	98	

Oil name	Panuke				
Origin and description	Nova Scotia, Canada				
Evaporation equation		$\%Ev = (7.12 + 0.045T)\ln(t)$			
Where Ev = weight percent evaporated, T = surface temperature ($^{\circ}\text{C}$), t = time (min)					
API gravity	50.8	Weathering % by weight			
(all units at 15°C)	Units	0	32	47	53
Density	g/ml	0.7757	0.8021	0.8168	
Viscosity	mPa·s or cP				
(dynamic—values at 15°C)					
Flash point	$^{\circ}\text{C}$	−30	32	64	
Sulfur content	%	0.04	0.02	0.04	0.02
Pour point	$^{\circ}\text{C}$	−36	−21	−18	
Surface tension	mN/m				
(air–oil at 15°C)					
IFT sea water	mN/m				
IFT fresh water	mN/m				
Adhesion	g/m^3				
SARA content (saturate, aromatic, resin, asphaltene) %					
Saturate	%				
Aromatic	%				
Resin	%				
Asphaltene	%	0	0	1	0
Waxes	%	2			
Emulsion formation (type formed and water content %)					
Type					
Water content	%				
Viscosity	mPa·s or cP				
Chemical dispersibility with Corexit 9500					
%					
Distillation data (% at temperature)					
Boiling point ($^{\circ}\text{C}$)					
40	1				
60	3				
80	9				
100	18				
120	29				
140	36				
160	44				
180	51				
200	57				
250	71				
300	85				
400	98				
500					
600					
700					

Oil name	Petroleum ether		
Origin and description	a.k.a. Ligroin, Skelly Solvent		
Evaporation equation		$\%Ev = (7.12 + 0.045T)\ln(t)$	
Where Ev = weight percent evaporated, T = surface temperature ($^{\circ}\text{C}$), t = time (min)			
API gravity		Weathering % by weight	
(all units at 15°C)	Units	0	
Density	g/ml	0.6404	
Viscosity	mPa·s or cP	0.3	
(dynamic—values at 15°C)			
Flash point	$^{\circ}\text{C}$		
Sulfur content	%		
Pour point	$^{\circ}\text{C}$		
Surface tension	mN/m	17.5	
(air–oil at 15°C)			
IFT sea water	mN/m	43.8	
IFT fresh water	mN/m	44.4	
Adhesion	g/m^3		
SARA content (saturate, aromatic, resin, asphaltene) %			
Saturate	%		
Aromatic	%		
Resin	%		
Asphaltene	%		
Waxes	%		
Emulsion formation (type formed and water content %)			
Type			
Water content	%		
Viscosity	mPa·s or cP		
Chemical dispersibility with Corexit 9500			
%			
Distillation data (% at temperature)			
Boiling point ($^{\circ}\text{C}$)			
40			
60			
80			
100			
120			
140			
160			
180			
200			
250			
300			
400			
500			
600			
700			

Oil name **Petronius Block VK786A**
Origin and description Louisiana, USA (Chevron-Texaco)

Evaporation equation $\%Ev = (2.27 + 0.013T)\sqrt{t}$
 Where Ev = weight percent evaporated, T = surface temperature (°C), t = time (min)

API gravity	30	Weathering % by weight			
		0	8.4	15.8	23.6
(all units at 15°C) Units					
Density	g/ml	0.8713	0.8858	0.8978	0.9096
Viscosity	mPa-s or cP	27.6	55	146	327

(dynamic—values at 15°C)

Flash point	°C	< 0	52	83	117
Sulfur content	%	0.34	0.38	0.41	0.45
Pour point	°C	−19	−6	−2	−2
Surface tension	mN/m	28	29.1	30.2	30.8

(air–oil at 15°C)

IFT sea water	mN/m	25.3	25.3	26.4	25.6
IFT fresh water	mN/m	26.9	25.6	25.1	24.5
Adhesion	g/m ³	31	25	40	34

SARA content (saturate, aromatic, resin, asphaltene) %

Saturate	%	84.02	82.94	81.45	79.2
Aromatic	%	8.91	9.46	9.87	10.18
Resin	%	5.52	5.85	6.62	7.88
Asphaltene	%	1.55	1.75	2.06	2.74
Waxes	%	2.7	2.9	3.4	3.5

Emulsion formation (type formed and water content %)

Type	Unstable	Meso-stable	Meso-stable	Meso-stable
Water content		78.3	78.9	78.4
Viscosity	mPa-s or cP			

Chemical dispersibility with Corexit 9500

%	36.8	38.7	21.5	18.4
---	------	------	------	------

Distillation data (% at temperature)

Boiling point (°C)				
40				
60				
80				
100	2.1	0.4		
120	4.9	1.6		
140	7.4	3.4	0.2	
160	10.5	6.2	1.1	
180	13.7	9.4	3.2	
200	16.6	12.4	5.9	0.6
250	25	21.3	15.3	7.6
300	34.4	31.3	26.3	19
400	52.8	50.9	48.1	42.6
500	68.6	67.6	66.6	62.7
600	79.8	79.2	79.5	76.7
700				

Oil name **Pitas point**
Origin and description California, USA

Evaporation equation $\%Ev = (7.04 + 0.045T)\ln(t)$
 Where Ev = weight percent evaporated, T = surface temperature (°C), t = time (min)

API gravity	38	Weathering % by weight		
		0	24	47
(all units at 15°C) Units				
Density	g/ml	0.8341	0.8537	0.8688
Viscosity	mPa-s or cP	2	2	4

(dynamic—values at 15°C)

Flash point	°C	17	46	
Sulfur content	%	0.61	0.76	
Pour point	°C	< −60	< −65	< −51
Surface tension	mN/m	26.3	27.1	26.4

(air–oil at 15°C)

IFT sea water	mN/m	7.3	8.9	3.7
IFT fresh water	mN/m	10.5	10.4	8.3
Adhesion	g/m ³	2	4	

SARA content (saturate, aromatic, resin, asphaltene) %

Saturate	%	80	62	
Aromatic	%	18	35	
Resin	%	3	2	
Asphaltene	%	0	0	
Waxes	%	0	0	

Emulsion formation (type formed and water content %)

Type	Unstable	Unstable	
Water content			
Viscosity	mPa-s or cP		

Chemical dispersibility with Corexit 9500

%	65	66	
---	----	----	--

Distillation data (% at temperature)

Boiling point (°C)			
40	1		
60	1		
80	2		
100	3	1	
120	7	1	
140	20	7	
160	31	15	
180	44	28	
200	54	40	
250	76	68	
300	88	84	
400	98	97	
500			
600			
700			

Oil name **Platform Elly**
Origin and description California, USA

Evaporation equationWhere Ev = weight percent evaporated, T = surface temperature (°C), t = time (min)

API gravity	15.7	Weathering % by weight			
(all units at 15°C)	Units	0	4.6	7.9	13.3
Density	g/ml	0.9608	0.9732	0.9801	
Viscosity	mPa·s or cP	3860	13,348	34,193	382,333
(dynamic—values at 15°C)					
Flash point	°C				
Sulfur content	%				
Pour point	°C				
Surface tension	mN/m				
(air–oil at 15°C)					
IFT sea water	mN/m				
IFT fresh water	mN/m				
Adhesion	g/m ³				

SARA content (saturate, aromatic, resin, asphaltene) %

Saturate	%	34.6	31.4	28.8	25.8
Aromatic	%	32.4	32.6	31.1	31.5
Resin	%	19.4	21.1	23.7	22.9
Asphaltene	%	13.6	14.9	16.4	19.8
Waxes	%				

Emulsion formation (type formed and water content %)

Type				
Water content	%			
Viscosity	mPa·s or cP			

Chemical dispersibility with Corexit 9500

%				
---	--	--	--	--

Distillation data (% at temperature)

Boiling point (°C)				
40				
60				
80				
100				
120				
140				
160				
180				
200				
250				
300				
400				
500				
600				
700				

Oil name **Platform Gail**
Origin and description California, USA

Evaporation equation

$$\%Ev = (1.68 + 0.045T)\ln(t)$$

Where Ev = weight percent evaporated, T = surface temperature (°C), t = time (min)

API gravity	20.6	Weathering % by weight			
(all units at 15°C)	Units	0	7	13	21
Density	g/ml	0.9297	0.9489	0.9645	0.981
Viscosity	mPa·s or cP	406	1450	7092	161,500
(dynamic—values at 15°C)					
Flash point	°C	–25	32	76	> 100
Sulfur content	%	4.08	4.27	4.42	4.56
Pour point	°C	–20	–12	–1	13
Surface tension	mN/m	27.8	29	30.5	
(air–oil at 15°C)					
IFT sea water	mN/m				
IFT fresh water	mN/m				
Adhesion	g/m ³	65	69	82	280

SARA content (saturate, aromatic, resin, asphaltene) %

Saturate	%	39	35	32	27
Aromatic	%	28	32	28	29
Resin	%	21	21	25	25
Asphaltene	%	12	13	15	19
Waxes	%	1.5	1.6	1.6	2.2

Emulsion formation (type formed and water content %)

Type		Stable	Stable	Stable	Entrained
Water content	%	76	75	67	44
Viscosity	mPa·s or cP	35,820	69,520	112,800	398,200

Chemical dispersibility with Corexit 9500

%	22	4	0	0
---	----	---	---	---

Distillation data (% at temperature)

Boiling point (°C)				
40	1.3	0.1	0.2	0.2
60	1.9	0.6	0.6	0.7
80	3.2	1	0.7	0.9
100	5.2	1.9	0.8	0.9
120	7.1	3.1	0.8	0.9
140	9	4.7	1.2	0.9
160	11.2	6.7	2.2	0.9
180	13.4	8.8	3.9	0.9
200	15.4	10.9	5.9	1.2
250	21.4	17.2	12.5	5.7
300	27.5	23.7	19.5	12.7
400	40.3	37.3	34	28.4
500	54.5	52.4	50.1	46.6
600	68.8	67.6	66.3	65.7
700				

Oil name		Platform Holly			
Origin and description		California, USA			
Evaporation equation		$\%Ev = (1.09 + 0.045T)\ln(t)$			
Where Ev = weight percent evaporated, T = surface temperature (°C), t = time (min)					
API gravity	11	Weathering % by weight			
(all units at 15°C)	Units	0	24	54	78
Density	g/ml	0.9928	1.0003	1.0066	1.0705
Viscosity	mPa·s or cP	3314	4068	399,700	304,550
(dynamic—values at 15°C)					
Flash point	°C	11	> 95	> 95	> 95
Sulfur content	%	1.43	1.87	1.98	2.23
Pour point	°C	−9	12	23	
Surface tension	mN/m	29.1			
(air–oil at 15°C)					
IFT sea water	mN/m	32			
IFT fresh water	mN/m				
Adhesion	g/m ³	61	564	889	938
SARA content (saturate, aromatic, resin, asphaltene) %					
Saturate	%	54	29	36	19
Aromatic	%	14	30	25	26
Resin	%	15	19	17	19
Asphaltene	%	17	24	22	36
Waxes	%	1.6			
Emulsion formation (type formed and water content %)					
Type		Same	Same	Same	Same
Water content	%	77	60	49	34
Viscosity	mPa·s or cP	150,000	360,000	670,000	800,000
Chemical dispersibility with Corexit 9500					
	%				
Distillation data (% at temperature)					
Boiling point (°C)					
40		0.5			
60		1.7			
80		2.7			
100		3.9			
120		5.2			
140		6.8			
160		9			
180		11.5			
200		13.8			
250		20.9			
300		28.4			
400		44.3			
500		61.3			
600		78.7			
700					

Oil name		Platform Irene	
Origin and description		California, USA	
Evaporation equation		Short-term (< 5 days): %Ev = (−0.05 + 0.013 <i>T</i>)√(<i>t</i>) Long-term: %Ev = (0.74 + 0.045 <i>T</i>)ln(<i>t</i>)	
Where Ev = weight percent evaporated, <i>T</i> = surface temperature (°C), <i>t</i> = time (min)			
API gravity	11.2	Weathering % by weight	
(all units at 15°C)	Units	0	
Density	g/ml	0.9907	
Viscosity	mPa·s or cP	76,000	
(dynamic—values at 15°C)			
Flash point	°C	−2	
Sulfur content	%	1.4	
Pour point	°C	12	
Surface tension	mN/m	37.2	
(air–oil at 15°C)			
IFT sea water	mN/m		
IFT fresh water	mN/m		
Adhesion	g/m ³	1342	
SARA content (saturate, aromatic, resin, asphaltene) %			
Saturate	%	26	
Aromatic	%	29	
Resin	%	22	
Asphaltene	%	22	
Waxes	%	2	
Emulsion formation (type formed and water content %)			
Type		Entrained	
Water content	%	62	
Viscosity	mPa·s or cP	390,000	
Chemical dispersibility with Corexit 9500			
	%		
Distillation data (% at temperature)			
Boiling point (°C)			
40			
60			
80			
100			
120			
140			
160			
180			
200			
250			
300			
400			
500			
600			
700			

Oil name **Point Arguello Comingled**
Origin and description California, USA

Evaporation equation $\%Ev = (1.43 + 0.045T)\ln(t)$
 Where Ev = weight percent evaporated, T = surface temperature (°C), t = time (min)

API gravity	21.4	Weathering % by weight			
(all units at 15°C)	Units	0	9	16	22
Density	g/ml	0.9248	0.9528	0.9688	0.9853
Viscosity	mPa·s or cP	533	4988	41,860	2,266,000
(dynamic—values at 15°C)					
Flash point	°C	−5	44	83	> 95
Sulfur content	%	3.64	3.64	3.81	4.09
Pour point	°C	−12	−7	7	28
Surface tension	mN/m	27.5	30.2		
(air–oil at 15°C)					
IFT sea water	mN/m	28.2			
IFT fresh water	mN/m	26.3			
Adhesion	g/m ³	81	104	187	1137

SARA content (saturate, aromatic, resin, asphaltene) %

Saturate	%	36	31	27	24
Aromatic	%	25	33	33	33
Resin	%	23	19	21	21
Asphaltene	%	16	17	19	22
Waxes	%	8	4	4	5

Emulsion formation (type formed and water content %)

Type		Stable	Stable	Entrained	Unstable
Water content	%	82	68	30	5
Viscosity	mPa·s or cP	180,000	150,000	140,000	

Chemical dispersibility with Corexit 9500

%	3	0	0	0
---	---	---	---	---

Distillation data (% at temperature)

Boiling point (°C)				
40				
60				
80	2			
100	5	1		
120	6	2		
140	8	3		
160	10	5	1	
180	12	7	2	
200	14	10	4	
250	20	16	11	4
300	25	23	18	11
400	37	37	34	28
500	50	52	51	46
600	64	75	68	64
700	76	81	83	80

Oil name **Point Arguello Heavy**
Origin and description California, USA

Evaporation equation $\%Ev = (0.94 + 0.045T)\ln(t)$
 Where Ev = weight percent evaporated, T = surface temperature (°C), t = time (min)

API gravity	18.2	Weathering % by weight		
(all units at 15°C)	Units	0	9	18
Density	g/ml	0.9447	0.9706	0.9914
Viscosity	mPa·s or cP	3250	59,390	4,953,000
(dynamic—values at 15°C)				
Flash point	°C	0	72	> 95
Sulfur content	%	3.44	3.93	4.22
Pour point	°C	−4	6	30
Surface tension	mN/m	23.8		
(air–oil at 15°C)				
IFT sea water	mN/m	28.4		
IFT fresh water	mN/m	30.5		
Adhesion	g/m ³	155	276	1231

SARA content (saturate, aromatic, resin, asphaltene) %

Saturate	%	32	26	25
Aromatic	%	32	35	34
Resin	%	17	18	21
Asphaltene	%	19	20	22
Waxes	%	6	4	4

Emulsion formation (type formed and water content %)

Type		Stable	Entrained	Unstable
Water content	%	73	28	
Viscosity	mPa·s or cP	150,000		

Chemical dispersibility with Corexit 9500

%	0	0	0
---	---	---	---

Distillation data (% at temperature)

Boiling point (°C)			
40			
60			
80			
100	2		
120	4		
140	6	1	
160	8	2	
180	9	3	
200	11	5	
250	17	12	3
300	23	19	10
400	35	35	28
500	48	52	46
600	62	67	63
700	75	81	78

Oil name **Point Arguello Light**
Origin and description California, USA

Evaporation equation $\%Ev = (2.37 + 0.045T)\ln(t)$
 Where Ev = weight percent evaporated, T = surface temperature (°C), t = time (min)

API gravity	30.3	Weathering % by weight			
(all units at 15°C)	Units	0	10	19	28
Density	g/ml	0.8739	0.8979	0.9132	0.9289
Viscosity	mPa-s or cP	22	76	183	671
(dynamic—values at 15°C)					
Flash point	°C	−6	49	87	> 95
Sulfur content	%	1.1	1.18	1.26	1.44
Pour point	°C	−22	−12	−12	8
Surface tension	mN/m	27.1	28.9	29.9	30
(air–oil at 15°C)					
IFT sea water	mN/m	24	25.8	25.5	
IFT fresh water	mN/m	27	25.4	24.6	
Adhesion	g/m ³	29	40	46	47

SARA content (saturate, aromatic, resin, asphaltene) %					
Saturate	%	57	54	48	45
Aromatic	%	27	30	31	32
Resin	%	9	9	12	12
Asphaltene	%	7	8	9	11
Waxes	%	6	6	7	8

Emulsion formation (type formed and water content %)					
Type		Stable	Stable	Stable	Stable
Water content	%	93	89	86	80
Viscosity	mPa-s or cP	67,000	280,000	270,000	140,000

Chemical dispersibility with Corexit 9500					
	%	13	20	13	4

Distillation data (% at temperature)					
Boiling point (°C)					
40	1				
60	2				
80	3				
100	6				
120	9	2			
140	12	4			
160	15	7	1		
180	19	11	3		
200	22	14	6		
250	31	25	17	6	
300	40	35	28	17	
400	58	57	52	43	
500	74	76	73	66	
600	87	90	88	82	
700	94	98	97	92	

Oil name **Port Hueneme**
Origin and description California, USA

Evaporation equation $\%Ev = (0.30 + 0.045T)\ln(t)$
 Where Ev = weight percent evaporated, T = surface temperature (°C), t = time (min)

API gravity	14.8	Weathering % by weight		
(all units at 15°C)	Units	0	4	8
Density	g/ml	0.9662	0.9745	0.9787
Viscosity	mPa-s or cP	4131	7833	20,990
(dynamic—values at 15°C)				
Flash point	°C	−11	> 90	> 90
Sulfur content	%	3.73	3.69	3.63
Pour point	°C	−9	−9	0
Surface tension	mN/m	30.8	30	31.1
(air–oil at 15°C)				
IFT sea water	mN/m	23.2	28.4	28.6
IFT fresh water	mN/m	30.2	30.1	32.6
Adhesion	g/m ³	67	91	124

SARA content (saturate, aromatic, resin, asphaltene) %				
Saturate	%	24	23	23
Aromatic	%	43	41	37
Resin	%	20	21	28
Asphaltene	%	12	14	13
Waxes	%	5	3	3

Emulsion formation (type formed and water content %)				
Type		Entrained	Entrained	Entrained
Water content	%	38	45	43
Viscosity	mPa-s or cP	16,000	46,000	71,000

Chemical dispersibility with Corexit 9500			
%	12	5	0

Distillation data (% at temperature)			
Boiling point (°C)			
40	1		
60	1		
80	1		
100	1		
120	2		
140	2		
160	3	1	
180	4	1	
200	5	3	1
250	11	8	6
300	17	15	12
400	33	32	30
500	51	51	50
600	70	69	68
700	84	82	82

Oil name **Prudhoe Bay—A**
Origin and description Alaska, USA, 1995

Evaporation equation $\%Ev = (2.37 + 0.045T)\ln(t)$

Where Ev = weight percent evaporated, T = surface temperature (°C), t = time (min)

API gravity	28.5	Weathering % by weight			
		0	9	18	27
(all units at 15°C) Units					
Density	g/ml	0.8837	0.9048	0.9204	0.9352
Viscosity	mPa·s or cP	22	55	148	623
(dynamic—values at 15°C)					
Flash point	°C	−17	45	87	> 95
Sulfur content	%	0.96	1.01	1.13	1.24
Pour point	°C	−15	−9	8	12
Surface tension	mN/m	27.6	29.5	30.2	30.9
(air–oil at 15°C)					
IFT sea water	mN/m	3.9	11.5	14.2	15.5
IFT fresh water	mN/m	4.2	15.5	16.5	16.5
Adhesion	g/m ³	28	30	24	29

SARA content (saturate, aromatic, resin, asphaltene) %

Saturate	%	53	51	52	43
Aromatic	%	34	35	32	38
Resin	%	10	1	12	15
Asphaltene	%	4	3	4	5
Waxes	%	4	5	5	5

Emulsion formation (type formed and water content %)

Type	Meso-stable	Stable	Unstable	Meso-stable
Water content	43	85	5	20
Viscosity	mPa·s or cP	500	46,000	1600

Chemical dispersibility with Corexit 9500

%	10	18	0	0
---	----	----	---	---

Distillation data (% at temperature)

Boiling point (°C)				
40	1			
60	1			
80	3			
100	6	1		
120	9	2		
140	12	5		
160	15	8	1	
180	19	11	3	
200	22	15	6	
250	32	25	17	7
300	42	36	29	19
400	62	58	54	47
500	79	77	75	71
600	91	90	89	87
700	99	99	98	98

Oil name **Prudhoe Bay—B**
Origin and description Alaska, USA (USEPA reference standard) (2004)

Evaporation equation

Where Ev = weight percent evaporated, T = surface temperature (°C), t = time (min)

API gravity	26.6	Weathering % by weight			
		0	6.3	13.1	19.7
(all units at 15°C) Units					
Density	g/ml	0.8947	0.9112	0.9235	0.9336
Viscosity	mPa·s or cP	38.9	102.8	318.4	864.7
(dynamic—values at 15°C)					
Flash point	°C				
Sulfur content	%				
Pour point	°C				
Surface tension	mN/m	28.7	29.8	30.8	
(air–oil at 15°C)					
IFT sea water	mN/m	28.1	23.8	22.4	
IFT fresh water	mN/m	31.3	25.2	24.5	
Adhesion	g/m ³				

SARA content (saturate, aromatic, resin, asphaltene) %

Saturate	%	60.8	60.4	58.5	53.9
Aromatic	%	28.3	27.7	27	25.2
Resin	%	7.7	8.2	10.1	15.7
Asphaltene	%	3.2	3.8	4.4	5.2
Waxes	%				

Emulsion formation (type formed and water content %)

Type				
Water content	%			
Viscosity	mPa·s or cP			

Chemical dispersibility with Corexit 9500

%				
---	--	--	--	--

Distillation data (% at temperature)

Boiling point (°C)				
40				
60				
80				
100				
120				
140				
160				
180				
200				
250				
300				
400				
500				
600				
700				

Oil name		Prudhoe Bay		
Origin and description		Alaska, USA		
Evaporation equation		$\%Ev = (1.69 + 0.045T)\ln(t)$		
Where Ev = weight percent evaporated, T = surface temperature ($^{\circ}\text{C}$), t = time (min)				
API gravity	24.8	Weathering % by weight		
(all units at 15°C)	Units	0		
Density	g/ml	0.905		
Viscosity	mPa.s or cP	68		
(dynamic—values at 15°C)				
Flash point	$^{\circ}\text{C}$			
Sulfur content	%			
Pour point	$^{\circ}\text{C}$	0		
Surface tension	mN/m	28.3		
(air–oil at 15°C)				
IFT sea water	mN/m	9.7		
IFT fresh water	mN/m	16.9		
Adhesion	g/m^3			
SARA content (saturate, aromatic, resin, asphaltene) %				
Saturate	%	78		
Aromatic	%	18		
Resin	%	3		
Asphaltene	%	2		
Waxes	%	4		
Emulsion formation (type formed and water content %)				
Type				
Water content	%			
Viscosity	mPa.s or cP			
Chemical dispersibility with Corexit 9500				
	%	10		
Distillation data (% at temperature)				
Boiling point ($^{\circ}\text{C}$)				
40		1		
60		1		
80		2		
100		4		
120		6		
140		9		
160		11		
180		14		
200		16		
250		24		
300		33		
400		52		
500		69		
600		82		
700		90		

Oil name	Prudhoe Bay (1995)				
Origin and description	Alaska, USA, sample procured by Env. Canada in 1995 from ARCO				
Evaporation equation	$\%Ev = (2.37 + 0.045T)\ln(t)$				
Where Ev = weight percent evaporated, T = surface temperature ($^{\circ}\text{C}$), t = time (min)					
API gravity	28.5	Weathering % by weight			
(all units at 15°C)	Units	0	9	18	27
Density	g/ml	0.8837	0.9048	0.9204	0.9352
Viscosity	mPa·s or cP	22	55	148	623
(dynamic—values at 15°C)					
Flash point	$^{\circ}\text{C}$	−17	45	87	> 95
Sulfur content	%	0.96	1.01	1.13	1.24
Pour point	$^{\circ}\text{C}$	−15	−9	8	12
Surface tension	mN/m	27.6	29.5	30.2	30.9
(air–oil at 15°C)					
IFT sea water	mN/m	3.9	11.5	14.2	15.5
IFT fresh water	mN/m	4.2	15.5	16.5	16.5
Adhesion	g/m^3	28	30	24	29
SARA content (saturate, aromatic, resin, asphaltene) %					
Saturate	%	53	51	52	43
Aromatic	%	34	35	32	38
Resin	%	10	10	12	15
Asphaltene	%	4	3	4	5
Waxes	%	4	5	5	5
Emulsion formation (type formed and water content %)					
Type		Meso-stable	Stable	Unstable	Meso-stable
Water content	%	43	46,000		1600
Viscosity	mPa·s or cP	500	85		20
Chemical dispersibility with Corexit 9500					
	%	10	18	0	0
Distillation data (% at temperature)					
Boiling point ($^{\circ}\text{C}$)					
40		1			
60		1			
80		3			
100		6	1		
120		9	2		
140		12	5		
160		15	8	1	
180		19	11	3	
200		22	15	6	
250		32	25	17	7
300		42	36	29	19
400		62	58	54	47
500		79	77	75	71
600		91	90	89	87
700		99	99	98	98

Oil name **Rangely**
Origin and description Colorado, USA

Evaporation equation $\%Ev = (1.89 + 0.045T)\ln(t)$
 Where Ev = weight percent evaporated, T = surface temperature ($^{\circ}C$), t = time (min)

API gravity	33.7	Weathering % by weight			
(all units at 15°C)	Units	0	11	21	30
Density	g/ml	0.8567	0.8765	0.892	0.9059
Viscosity	mPa·s or cP	33	61	173	6320
(dynamic—values at 15°C)					
Flash point	$^{\circ}C$	−2	49	94	> 95
Sulfur content	%	0.35	0.64	0.69	0.77
Pour point	$^{\circ}C$	17	18	21	29
Surface tension	mN/m	27.1	28.4	29.8	
(air–oil at 15°C)					
IFT sea water	mN/m	21.7	22.4	23	
IFT fresh water	mN/m	22.1	23.4	26.5	
Adhesion	g/m ³	26	32	71	214

SARA content (saturate, aromatic, resin, asphaltene) %					
Saturate	%	71	68	65	61
Aromatic	%	21	24	24	27
Resin	%	5	5	6	6
Asphaltene	%	4	3	4	6
Waxes	%	10	9	10	10

Emulsion formation (type formed and water content %)				
Type				
Water content	%			
Viscosity	mPa·s or cP			

Chemical dispersibility with Corexit 9500				
%				

Distillation data (% at temperature)				
Boiling point ($^{\circ}C$)				
40				
60	1			
80	2			
100	4	1		
120	6	2		
140	8	4		
160	11	7		
180	14	10	2	
200	17	14	4	
250	26	24	14	4
300	36	35	27	16
400	57	57	52	45
500	75	77	74	69
600	87	88	87	84
700	93	95	95	93

Oil name **Sable Island Condensate**
Origin and description Nova Scotia, Canada

Evaporation equation
 Where Ev = weight percent evaporated, T = surface temperature ($^{\circ}C$), t = time (min)

API gravity	39.9	Weathering % by weight			
(all units at 15°C)	Units	0	41	71	82
Density	g/ml	0.823	0.869	0.87	0.899
Viscosity	mPa·s or cP	2	6	320	2450
(dynamic—values at 15°C)					
Flash point	$^{\circ}C$	−11	81	135	147
Sulfur content	%	0.03			
Pour point	$^{\circ}C$	−51	3	18	27
Surface tension	mN/m				
(air–oil at 15°C)					
IFT sea water	mN/m				
IFT fresh water	mN/m				
Adhesion	g/m ³				

SARA content (saturate, aromatic, resin, asphaltenes) %				
Saturate	%	88		
Aromatic	%	11		
Resin	%	0		
Asphaltenes	%	1		
Waxes	%	2		

Emulsion formation (type formed and water content %)				
Type				
Water content	%			
Viscosity	mPa·s or cP			

Chemical dispersibility with Corexit 9500				
%				

Distillation data (% at temperature)				
Boiling point ($^{\circ}C$)				
40				
60				
80				
100				
120				
140				
160				
180				
200				
250				
300				
400				
500				
600				
700				

Oil name	Saharan Blend			
Origin and description	Algeria			
Evaporation equation	Short-term (< 5 days): %Ev = (0.001 + 0.013T) \sqrt{t} Long-term: %Ev = (1.09 + 0.045T)ln(<i>t</i>) Where Ev = weight percent evaporated, <i>T</i> = surface temperature (°C), <i>t</i> = time (min)			
API gravity	43.6	Weathering % by weight		
(all units at 15°C) Units		0	14	28
Density	g/ml	0.8078	0.8336	0.8528
Viscosity	mPa·s or cP	4	7	19
(dynamic—values at 15°C)				
Flash point	°C	−24	28	75
Sulfur content	%	0.1	0.09	0.09
Pour point	°C	−8	−9	0
Surface tension	mN/m	24.8	26.8	27.5
(air–oil at 15°C)				
IFT sea water	mN/m	20.5	22.4	19.1
IFT fresh water	mN/m	22.8	24.8	22.3
Adhesion	g/m ³	2	5	15
SARA content (saturate, aromatic, resin, asphaltene) %				
Saturate	%	76	77	72
Aromatic	%	21	20	23
Resin	%	3	3	4
Asphaltene	%	1	1	1
Waxes	%			
Emulsion formation (type formed and water content %)				
Type				
Water content	%			
Viscosity	mPa·s or cP			
Chemical dispersibility with Corexit 9500				
%				

Distillation data (% at temperature)				
Boiling point (°C)				
40	8			
60	10	1		
80	15	4		
100	19	6		
120	20	7		
140	23	10	1	
160	27	15	3	
180	32	21	7	
200	36	26	12	
250	47	38	26	10
300	57	51	41	27
400	76	72	66	59
500	88	87	84	81
600	96	96	95	93
700	99			99

Oil name	Sakhalin		
Origin and description	Russia		
Evaporation equation	%Ev = (4.16 + 0.045T)ln(<i>t</i>) Where Ev = weight percent evaporated, <i>T</i> = surface temperature (°C), <i>t</i> = time (min)		
API gravity	32.3	Weathering % by weight	
(all units at 15°C) Units		0	42
Density	g/ml	0.8632	0.9201
Viscosity	mPa·s or cP	4	52
(dynamic—values at 15°C)			
Flash point	°C	−10	> 100
Sulfur content	%	0.25	0.39
Pour point	°C	< −75	−32
Surface tension	mN/m	24.4	30.3
(air–oil at 15°C)			
IFT sea water	mN/m	14	11.3
IFT fresh water	mN/m	16.3	15.7
Adhesion	g/m ³	8	29
SARA content (saturate, aromatic, resin, asphaltene) %			
Saturate	%	61	56
Aromatic	%	32	32
Resin	%	6	10
Asphaltene	%	1	2
Waxes	%	0.6	1.1
Emulsion formation (type formed and water content %)			
Type			
Water content	%		
Viscosity	mPa·s or cP		
Chemical dispersibility with Corexit 9500			
%	84	49	31

Distillation data (% at temperature)		
Boiling point (°C)		
40	0.6	
60	1.6	
80	3.8	
100	7.7	
120	12.2	
140	17.1	
160	22.5	
180	28.6	0.2
200	33.5	1.3
250	47.3	15.8
300	59.4	34.7
400	77.8	65
500	90	84.9
600	96	94.4
700		

Oil name		Santa Clara		
Origin and description		California, USA		
Evaporation equation		$\%Ev = (1.63 + 0.045T)\ln(t)$		
Where Ev = weight percent evaporated, T = surface temperature (°C), t = time (min)				
API gravity	22.1	Weathering % by weight		
(all units at 15°C)	Units	0	11	22
Density	g/ml	0.9202	0.9475	0.9672
Viscosity	mPa·s or cP	304	1859	22,760
(dynamic—values at 15°C)				
Flash point	°C	−24	45	> 90
Sulfur content	%	2.85	3.22	3.41
Pour point	°C	−3	6	27
Surface tension	mN/m	28.7	28	31.8
(air–oil at 15°C)				
IFT sea water	mN/m	23.3	21.6	31.6
IFT fresh water	mN/m	25.7	24.9	
Adhesion	g/m ³	55	69	112
SARA content (saturate, aromatic, resin, asphaltene) %				
Saturate	%	36	32	28
Aromatic	%	22	28	32
Resin	%	29	27	23
Asphaltene	%	13	13	17
Waxes	%	6	4	5
Emulsion formation (type formed and water content %)				
Type		Meso-stable	Meso-stable	Meso-stable
Water content	%	61	50	39
Viscosity	mPa·s or cP	2700	20,000	100,000
Chemical dispersibility with Corexit 9500				
	%	6	4	0
Distillation data (% at temperature)				
Boiling point (°C)				
40	2			
60	2	1		
80	6	1		
100	8	2		
120	10	2		
140	11	3		
160	12	5		
180	14	7	1	
200	15	9	2	
250	21	14	7	
300	26	21	14	
400	39	37	32	
500	55	55	52	
600	70	70	69	
700	82	82	82	

Oil name		Scotian Light			
Origin and description		Nova Scotia, Canada			
Evaporation equation		%Ev = (6.90 + 0.045 <i>T</i>)ln(<i>t</i>)			
Where Ev = weight percent evaporated, <i>T</i> = surface temperature (°C), <i>t</i> = time (min)					
API gravity	53.2	Weathering % by weight			
(all units at 15°C)	Units	0	25	49	64
Density	g/ml	0.7655	0.7949	0.8139	0.8356
Viscosity	mPa·s or cP	1	2	2	5
(dynamic—values at 15°C)					
Flash point	°C	< −30	23	53	95
Sulfur content	%	0.02	0.01	0.01	0.02
Pour point	°C	−22	−12	−10	−2
Surface tension	mN/m	23	24.6	26.4	27.8
(air–oil at 15°C)					
IFT sea water	mN/m	21.3	16	17.8	13.2
IFT fresh water	mN/m	22.4	18.8	18.8	16
Adhesion	g/m ³	0	2	3	9
SARA content (saturate, aromatic, resin, asphaltene) %					
Saturate	%	92	89	85	60
Aromatic	%	8	10	14	38
Resin	%	1	1	1	1
Asphaltene	%	0	0	0	0
Waxes	%	8.7	3.7	4.7	9.8
Emulsion formation (type formed and water content %)					
Type					
Water content	%				
Viscosity	mPa·s or cP				
Chemical dispersibility with Corexit 9500					
	%				
Distillation data (% at temperature)					
Boiling point (°C)					
40		3.4			
60		5.6			
80		9.4	0.6		
100		16.2	4.3		
120		22.1	7.9	0.3	
140		26.7	12.6	1.7	
160		32.3	24.8	9	
180		37.8	34.4	18.8	0.3
200		42.1	41.9	28	2.7
250		52.2	59.9	51	20.9
300		61.2	76.4	71.9	42.8
400		69.7	91.8	91.3	64
500		72.4	94.1	94.1	69.5
600		87.4	95.1	95.2	81.9
700					

Oil name Ship Shoal Block 239
Origin and description Gulf of Mexico, USA

Evaporation equation $\%Ev = (2.71 + 0.045T)\ln(t)$
 Where Ev = weight percent evaporated, T = surface temperature (°C), t = time (min)

API gravity	26.1	Weathering % by weight			
(all units at 15°C)	Units	0	17	43	53
Density	g/ml	0.8972	0.9103	0.8977	0.9076
Viscosity	mPa·s or cP	34	70	74	194
(dynamic—values at 15°C)					
Flash point	°C	11	> 95	> 95	> 95
Sulfur content	%	0.39	0.34	0.73	0.87
Pour point	°C	−15	−26	−26	−2
Surface tension	mN/m	27.1	28.6	29.3	30.2
(air–oil at 15°C)					
IFT sea water	mN/m	30.7	30.7	28.3	23.7
IFT fresh water	mN/m	31.5	32.4	29.7	26.4
Adhesion	g/m ³	22	32	30	42

SARA content (saturate, aromatic, resin, asphaltene) %

Saturate	%	68	59	64	60
Aromatic	%	23	19	26	28
Resin	%	7	6	8	9
Asphaltene	%	2	17	2	4
Waxes	%	5	4	4	4

Emulsion formation (type formed and water content %)

Type				
Water content	%			
Viscosity	mPa·s or cP			

Chemical dispersibility with Corexit 9500

%				
---	--	--	--	--

Distillation data (% at temperature)

Boiling point (°C)				
40	1			
60	1			
80	4			
100	8			
120	12			
140	13	2		
160	15	4		
180	20	8	2	
200	24	12	5	
250	34	25	17	5
300	45	37	30	18
400	63	60	55	44
500	76	79	75	67
600	85	91	89	83
700	91	98	98	92

Oil name Ship Shoal Block 269
Origin and description Gulf of Mexico, USA

Evaporation equation $\%Ev = (3.37 + 0.045T)\ln(t)$
 Where Ev = weight percent evaporated, T = surface temperature (°C), t = time (min)

API gravity	38.7	Weathering % by weight			
(all units at 15°C)	Units	0	13	26	39
Density	g/ml	0.8309	0.8517	0.8657	0.8796
Viscosity	mPa·s or cP	5	7	18	44
(dynamic—values at 15°C)					
Flash point	°C	−7	46	84	> 95
Sulfur content	%	0.41	0.47	0.45	0.64
Pour point	°C	−42	−19	−20	−2
Surface tension	mN/m	25.9	27.5	28.6	29.9
(air–oil at 15°C)					
IFT sea water	mN/m	15.1	20.3	20.4	16.7
IFT fresh water	mN/m	20.9	23.8	23.5	20.1
Adhesion	g/m ³	7	15	25	30

SARA content (saturate, aromatic, resin, asphaltene) %

Saturate	%	79	71	70	67
Aromatic	%	15	23	24	26
Resin	%	6	5	6	6
Asphaltene	%	0	0	1	1
Waxes	%	5	5	5	5

Emulsion formation (type formed and water content %)

Type				
Water content	%			
Viscosity	mPa·s or cP			

Chemical dispersibility with Corexit 9500

%	36	27	23	
---	----	----	----	--

Distillation data (% at temperature)

Boiling point (°C)				
40	1			
60	2			
80	4			
100	8	1		
120	12	2		
140	15	6		
160	20	10	1	
180	25	15	4	
200	30	20	8	
250	43	35	20	9
300	56	49	41	28
400	77	73	68	61
500	90	88	85	82
600	97	96	95	94
700		99	99	99

Oil name **Sockeye (2000)**
Origin and description California, USA; a.k.a. Sockeye Sour

Evaporation equation $\%Ev = (1.52 + 0.045T) \ln t$
 Where Ev = weight percent evaporated, T = surface temperature (°C), t = time (min)

API gravity	19.32	Weathering % by weight			
(all units at 15°C) Units		0	6.9	13	19.8
Density g/ml		0.9354	0.9537	0.9692	0.9839
Viscosity mPa-s or cP		761	2720	15,100	247,000
(dynamic—values at 15°C)					
Flash point °C		−4	35	72	> 110
Sulfur content %		4.51	4.95	5.19	5.47
Pour point °C		−25	−18	`	13
Surface tension mN/m		28.8	31.3	32.2	
(air–oil at 15°C)					
IFT sea water mN/m		21.9	23.1		
IFT fresh water mN/m		21.4	24.9		
Adhesion g/m ³		70	70	90	350

SARA content (saturate, aromatic, resin, asphaltene) %

Saturate %	49.2	46.2	44.4	40.3
Aromatic %	17.2	17.6	18	18
Resin %	15.1	16.4	17.1	17.2
Asphaltene %	18.5	19.8	20.5	24.5
Waxes %	1.6	1.7	1.8	2.1

Emulsion formation (type formed and water content %)

Type	Meso-stable	Meso-stable	Entrained	Entrained
Water content %	75.6	73.3	53.4	17.7
Viscosity mPa-s or cP				

Chemical dispersibility with Corexit 9500

%	11.8	9.6	10.1	8.9
---	------	-----	------	-----

Distillation data (% at temperature)

Boiling point (°C)				
40	0.4			
60	0.4			
80	1.5	0.1		
100	3.3	0.7		
120	5.1	1.6		
140	7.1	3.1	0.2	
160	9.2	5	0.9	
180	11.3	7.1	2.3	
200	13.2	9.2	4.1	0.4
250	18.9	15.4	10.5	4.6
300	24.7	21.6	17.1	11.3
400	36.8	34.6	30.9	26.3
500	50.1	49	46.4	43.4
600	63.5	63.2	62.1	60.9
700				

Oil name **Sockeye Comingled**
Origin and description California, USA

Evaporation equation $\%Ev = (1.38 + 0.045T)\ln(t)$

API gravity	19.8	Weathering % by weight		
(all units at 15°C) Units		0		
Density g/ml		0.935		
Viscosity mPa-s or cP		550		
(dynamic—values at 15°C)				
Flash point °C		−6		
Sulfur content %		4.17		
Pour point °C		−24		
Surface tension mN/m		28.7		
(air–oil at 15°C)				
IFT sea water mN/m		18.2		
IFT fresh water mN/m		20.7		
Adhesion g/m ³		68		

SARA content (saturate, aromatic, resin, asphaltene) %

Saturate %	34		
Aromatic %	32		
Resin %	21		
Asphaltene %	13		
Waxes %			

Emulsion formation (type formed and water content %)

Type	Stable		
Water content %	74		
Viscosity mPa-s or cP	39,000		

Chemical dispersibility with Corexit 9500

%	0		
---	---	--	--

Distillation data (% at temperature)

Boiling point (°C)			
40	3		
60	4		
80	6		
100	7		
120	7		
140	9		
160	11		
180	13		
200	16		
250	22		
300	28		
400	44		
500	59		
600	72		
700	83		

Oil name **Sockeye Sour**
Origin and description California, USA

Evaporation equation $\%Ev = (1.32 + 0.045T)\ln(t)$
 Where Ev = weight percent evaporated, T = surface temperature (°C), t = time (min)

API gravity	18.8	Weathering % by weight		
(all units at 15°C)	Units	0	10	19
Density	g/ml	0.9409	0.9682	0.9838
Viscosity	mPa·s or cP	821	8708	475,200
(dynamic—values at 15°C)				
Flash point	°C	−3	67	> 95
Sulfur content	%	4.41	4.71	5.02
Pour point	°C	−22	−3	18
Surface tension	mN/m	28.9	30.8	
(air–oil at 15°C)				
IFT sea water	mN/m	20.1		
IFT fresh water	mN/m	22.9		
Adhesion	g/m ³	75	98	605

SARA content (saturate, aromatic, resin, asphaltene) %

Saturate	%	38	29	26
Aromatic	%	29	31	30
Resin	%	20	22	22
Asphaltene	%	13	17	24
Waxes	%			

Emulsion formation (type formed and water content %)

Type		Stable	Meso-stable	Unstable
Water content	%	74	60	10
Viscosity	mPa·s or cP	32,000	79,000	

Chemical dispersibility with Corexit 9500

%	0	0	0
---	---	---	---

Distillation data (% at temperature)

Boiling point (°C)			
40	3		
60	4		
80	6		
100	7		
120	7		
140	9	1	
160	11	2	
180	13	4	
200	15	6	
250	21	13	4
300	27	20	11
400	42	39	32
500	58	58	53
600	71	74	70
700	83	87	85

Oil name **Sockeye Sweet**
Origin and description California, USA

Evaporation equation $\%Ev = (2.39 + 0.045T)\ln(t)$
 Where Ev = weight percent evaporated, T = surface temperature (°C), t = time (min)

API gravity	29.4	Weathering % by weight			
(all units at 15°C)	Units	0	8	17	27
Density	g/ml	0.8792	0.8945	0.9089	0.9229
Viscosity	mPa·s or cP	20	39	103	321
(dynamic—values at 15°C)					
Flash point	°C	−9	47	83	> 95
Sulfur content	%	1.1	1.53	1.67	1.81
Pour point	°C	−20	−14	−4	5
Surface tension	mN/m	27.7	28.8	30	30.6
(air–oil at 15°C)					
IFT sea water	mN/m	15.9	17.9	18.5	16.5
IFT fresh water	mN/m	14.8	16.3	17.6	16.5
Adhesion	g/m ³	25	21	28	25

SARA content (saturate, aromatic, resin, asphaltene) %

Saturate	%	55	56	50	48
Aromatic	%	31	30	32	33
Resin	%	10	10	13	14
Asphaltene	%	4	4	5	6
Waxes	%				

Emulsion formation (type formed and water content %)

Type		Unstable	Unstable	Meso-stable	Stable
Water content	%	5	1	82	75
Viscosity	mPa·s or cP			8200	48,000

Chemical dispersibility with Corexit 9500

%	16	17	14	15
---	----	----	----	----

Distillation data (% at temperature)

Boiling point (°C)				
40	2			
60	4			
80	7			
100	9			
120	9	2		
140	12	4		
160	16	7	1	
180	20	11	3	
200	23	15	7	
250	34	26	19	
300	44	38	32	
400	63	60	56	
500	81	79	78	
600	92	92	92	
700	99	98	99	

Oil name		Sockeye		
Origin and description		California, USA		
Evaporation equation		$\%Ev = (2.14 + 0.045T)\ln(t)$		
Where Ev = weight percent evaporated, T = surface temperature (°C), t = time (min)				
API gravity	26.2	Weathering % by weight		
(all units at 15°C)	Units	0	13	22
Density	g/ml	0.8965	0.9166	0.9264
Viscosity	mPa·s or cP	45	163	628
(dynamic—values at 15°C)				
Flash point	°C	−17	57	> 90
Sulfur content	%	2.29	2.67	2.87
Pour point	°C	−12	−3	3
Surface tension	mN/m	27.8	29	29.6
(air–oil at 15°C)				
IFT sea water	mN/m	16.8	17.2	19.6
IFT fresh water	mN/m	19.1	20.8	21
Adhesion	g/m ³	31	30	44
SARA content (saturate, aromatic, resin, asphaltene) %				
Saturate	%	48	44	39
Aromatic	%	31	32	34
Resin	%	13	15	15
Asphaltene	%	8	9	11
Waxes	%	6	5	5
Emulsion formation (type formed and water content %)				
Type		Stable	Stable	Stable
Water content	%	87	81	79
Viscosity	mPa·s or cP	690,000	200,000	250,000
Chemical dispersibility with Corexit 9500				
	%	24	9	5

Distillation data (% at temperature)			
Boiling point (°C)			
40	2		
60	2		
80	4	1	
100	6	1	
120	9	1	
140	12	3	
160	15	5	
180	18	8	1
200	21	11	2
250	30	21	11
300	39	31	22
400	57	53	43
500	74	73	64
600	88	88	79
700	98	98	89

Oil name	Sour Blend			
Origin and description	Alberta, Canada			
Evaporation equation				
Where Ev = weight percent evaporated, T = surface temperature ($^{\circ}\text{C}$), t = time (min)				
API gravity	24.8	Weathering % by weight		
(all units at 15°C)	Units	0	10	20
Density	g/ml	0.85		
Viscosity	mPa·s or cP	8		
(dynamic—values at 15°C)				
Flash point	$^{\circ}\text{C}$	7		
Sulfur content	%			
Pour point	$^{\circ}\text{C}$	6	6	9
Surface tension	mN/m	25.6		
(air—oil at 15°C)				
IFT sea water	mN/m	0.8		
IFT fresh water	mN/m	13		
Adhesion	g/m^3			
SARA content (saturate, aromatic, resin, asphaltene) %				
Saturate	%	82	77	73
Aromatic	%	13	15	16
Resin	%	2	4	4
Asphaltene	%	2	5	7
Waxes	%	6	8	10
Emulsion formation (type formed and water content %)				
Type				
Water content	%			
Viscosity	mPa·s or cP			
Chemical dispersibility with Corexit 9500				
	%			

Distillation data (% at temperature)			
Boiling point (°C)			
40			
60			
80			
100			
120			
140			
160			
180			
200			
250			
300			
400			
500			
600			
700			

Oil name South Louisiana (USEPA Reference Standard) (2004)
Origin and description Gulf of Mexico, USA

Evaporation equation

Where E_v = weight percent evaporated, T = surface temperature ($^{\circ}\text{C}$), t = time (min)

API gravity	37.1	Weathering % by weight			
(all units at 15 $^{\circ}\text{C}$)	Units	0	10.3	20.1	30.8
Density	g/ml	0.8389	0.8579	0.8701	0.8815
Viscosity	mPa-s or cP	7.1	12.6	23.8	46.4

(dynamic—values at 15 $^{\circ}\text{C}$)

Flash point	$^{\circ}\text{C}$				
Sulfur content	%				
Pour point	$^{\circ}\text{C}$				
Surface tension mN/m		26.6	28.1	29.2	29.9

(air-oil at 15 $^{\circ}\text{C}$)

IFT sea water mN/m		22	22.7	22.2	19.4
IFT fresh water mN/m		24.9	25	24.6	22.4
Adhesion	g/m ³				

SARA content (saturate, aromatic, resin, asphaltene) %

Saturate	%	79.4	78.2	77.7	73.8
Aromatic	%	16.9	17.1	17.4	18.2
Resin	%	3.4	4.1	4.4	7.2
Asphaltene	%	0.4	0.5	0.5	0.8
Waxes	%				

Emulsion formation (type formed and water content %)

Type				
Water content	%			
Viscosity	mPa-s or cP			

Chemical dispersibility with Corexit 9500

%				
---	--	--	--	--

Distillation data (% at temperature)

Boiling point ($^{\circ}\text{C}$)				
40				
60				
80				
100				
120				
140				
160				
180				
200				
250				
300				
400				
500				
600				

Oil name South Louisiana (2001)
Origin and description Baton Rouge, Louisiana, USA
 (Exxon-Mobil); a.k.a. Louisiana

Evaporation equation

$$\%E_v = (2.74 + 0.045T) \ln t$$

Where E_v = weight percent evaporated, T = surface temperature ($^{\circ}\text{C}$), t = time (min)

API gravity	32.7	Weathering % by weight			
(all units at 15 $^{\circ}\text{C}$)	Units	0	10.9	19.7	27.7
Density	g/ml	0.8562	0.877	0.8906	0.9018
Viscosity	mPa-s or cP	10.1	23.7	48.9	141

(dynamic—values at 15 $^{\circ}\text{C}$)

Flash point	$^{\circ}\text{C}$	< -10	42.3	80.7	> 110
Sulfur content	%	0.49	0.71	0.79	0.88
Pour point	$^{\circ}\text{C}$	-41	-19	-14	-11
Surface tension mN/m		26.1	28.1	29.4	29.8

(air-oil at 15 $^{\circ}\text{C}$)

IFT sea water mN/m		16.8	19.4	22.2	18.4
IFT fresh water mN/m		15.5	15.8	22.3	21.9
Adhesion	g/m ³	24	34	50	28

SARA content (saturate, aromatic, resin, asphaltene) %

Saturate	%	80.8	80.4	78.4	77.3
Aromatic	%	12.6	12.3	12.5	13.3
Resin	%	5.9	6.4	8	8
Asphaltene	%	0.8	0.9	1.1	1.5
Waxes	%	1.7	1.8	2	2.2

Emulsion formation (type formed and water content %)

Type	Unstable	Unstable	Unstable	Unstable
Water content	%			
Viscosity	mPa-s or cP			

Chemical dispersibility with Corexit 9500

%	26.5	23.5	15.8	10.3
---	------	------	------	------

Distillation data (% at temperature)

Boiling point ($^{\circ}\text{C}$)				
40	1.2			
60	1.6			
80	2.1			
100	5.6	0.9		
120	8.2	2.4	0.1	
140	11.1	4.8	0.4	
160	14.1	7.8	1.6	0.1
180	17.5	11.4	4	0.3
200	20.6	14.9	7.2	1.4
250	29.8	25.2	18.1	10.6
300	39.9	36.6	30.6	24.1
400	58.1	57	53.1	49
500	72	72.7	70.4	68.2
600	80.9	82.8	81.5	80.5
700				

Oil name **South Louisiana (US EPA Reference Standard) (2004)**
Origin and description Gulf of Mexico, USA

Evaporation equation

 Where E_v = weight percent evaporated, T = surface temperature ($^{\circ}\text{C}$), t = time (min)

API gravity	37.1	Weathering % by weight			
(all units at 15°C) Units		0	10.3	20.1	30.8
Density	g/ml	0.8389	0.8579	0.8701	0.8815
Viscosity	mPa·s or cP	7.1	12.6	23.8	46.4

(dynamic—values at 15°C)

Flash point	$^{\circ}\text{C}$				
Sulfur content	%				
Pour point	$^{\circ}\text{C}$				
Surface tension	mN/m	26.6	28.1	29.2	29.9

(air—oil at 15°C)

IFT sea water	mN/m	22	22.7	22.2	19.4
IFT fresh water	mN/m	24.9	25	24.6	22.4
Adhesion	g/m^3				

SARA content (saturate, aromatic, resin, asphaltene) %

Saturate	%	79.4	78.2	77.7	73.8
Aromatic	%	16.9	17.1	17.4	18.2
Resin	%	3.4	4.1	4.4	7.2
Asphaltene	%	0.4	0.5	0.5	0.8
Waxes	%				

Emulsion formation (type formed and water content %)

Type				
Water content	%			
Viscosity	mPa·s or cP			

Chemical dispersibility with Corexit 9500

%				
---	--	--	--	--

Distillation data (% at temperature)

Boiling point ($^{\circ}\text{C}$)				
40				
60				
80				
100				
120				
140				
160				
180				
200				
250				
300				
400				
500				
600				
700				

Oil name **South Pass Block 60**
Origin and description Gulf of Mexico, USA

Evaporation equation

$$\%E_v = (2.91 + 0.045T)\ln(t)$$

 Where E_v = weight percent evaporated, T = surface temperature ($^{\circ}\text{C}$), t = time (min)

API gravity	35.8	Weathering % by weight			
(all units at 15°C) Units		0	17	25	38
Density	g/ml	0.8453	0.8709	0.8809	0.8979
Viscosity	mPa·s or cP	9	22	41	161

(dynamic—values at 15°C)

Flash point	$^{\circ}\text{C}$	−4	61	90	> 95
Sulfur content	%	0.28	0.28	0.3	0.38
Pour point	$^{\circ}\text{C}$	−9	−3	9	12
Surface tension	mN/m	26.8	28.7	29.4	30.3

(air—oil at 15°C)

IFT sea water	mN/m	18.7	20.4	18.9	16.2
IFT fresh water	mN/m	19.6	21.3	21.8	18.8
Adhesion	g/m^3	11	13	19	36

SARA content (saturate, aromatic, resin, asphaltene) %

Saturate	%	71	67	64	61
Aromatic	%	20	26	27	28
Resin	%	8	7	8	9
Asphaltene	%	1	1	1	2
Waxes	%	7	6	7	7

Emulsion formation (type formed and water content %)

Type				
Water content	%			
Viscosity	mPa·s or cP			

Chemical dispersibility with Corexit 9500

%	28	21		
---	----	----	--	--

Distillation data (% at temperature)

Boiling point ($^{\circ}\text{C}$)				
40	2			
60	3			
80	8			
100	11			
120	16	1		
140	17	2		
160	19	5		
180	23	9	2	
200	27	13	5	
250	39	26	18	4
300	51	41	34	20
400	71	65	61	52
500	86	82	80	76
600	94	93	92	90
700	99	98	98	98

Oil name South Pass Block 67
Origin and description Gulf of Mexico, USA

Evaporation equation $\%Ev = (2.17 + 0.045T)\ln(t)$
 Where Ev = weight percent evaporated, T = surface temperature (°C), t = time (min)

API gravity	16.4	Weathering % by weight			
(all units at 15°C)	Units	0	22	45	64
Density	g/ml	0.9564	0.9928	0.951	0.9306
Viscosity	mPa·s or cP	39	110	108	236
(dynamic—values at 15°C)					
Flash point	°C	−1	> 95	> 95	> 95
Sulfur content	%				
Pour point	°C	13	7	13	3
Surface tension	mN/m	26.2	29.1	30	30.9
(air–oil at 15°C)					
IFT sea water	mN/m	30.7	30.5	27	25.9
IFT fresh water	mN/m	32.9	31.3	30.7	29.7
Adhesion	g/m ³	30	35	35	40

SARA content (saturate, aromatic, resin, asphaltene) %

Saturate	%				53
Aromatic	%				27
Resin	%				10
Asphaltene	%				10
Waxes	%	5	4	4	7

Emulsion formation (type formed and water content %)

Type				
Water content	%			
Viscosity	mPa·s or cP			

Chemical dispersibility with Corexit 9500

%				
---	--	--	--	--

Distillation data (% at temperature)

Boiling point (°C)				
40	1			
60	2			
80	4			
100	8			
120	12			
140	16	1		
160	21	3		
180	26	6	1	
200	31	10	3	
250	42	24	15	2
300	53	38	31	15
400	72	64	59	48
500	86	82	79	72
600	95	93	91	89
700		99	98	98

Oil name South Pass Block 93
Origin and description Gulf of Mexico, USA

Evaporation equation $\%Ev = (1.50 + 0.045T)\ln(t)$
 Where Ev = weight percent evaporated, T = surface temperature (°C), t = time (min)

API gravity	33.4	Weathering % by weight			
(all units at 15°C)	Units	0	11	21	34
Density	g/ml	0.8574	0.8637	0.8698	0.8832
Viscosity	mPa·s or cP	19	23	32	80
(dynamic—values at 15°C)					
Flash point	°C	−7	58	90	> 95
Sulfur content	%	0.43	0.36	0.35	0.43
Pour point	°C	−15	8	12	16
Surface tension	mN/m	28.2	29	29.6	30.4
(air–oil at 15°C)					
IFT sea water	mN/m	24.7	24.3	26.7	22.6
IFT fresh water	mN/m	26.5	26	28	24.9
Adhesion	g/m ³	25	15	20	40

SARA content (saturate, aromatic, resin, asphaltene) %

Saturate	%	73	74	73	71
Aromatic	%	20	20	21	22
Resin	%	4	4	4	5
Asphaltene	%	3	2	2	3
Waxes	%	8	6	7	8

Emulsion formation (type formed and water content %)

Type				
Water content	%			
Viscosity	mPa·s or cP			

Chemical dispersibility with Corexit 9500

%				
---	--	--	--	--

Distillation data (% at temperature)

Boiling point (°C)				
40	1			
60	2			
80	3			
100	5			
120	7	1		
140	9	2		
160	12	5	1	
180	15	7	3	
200	18	10	5	
250	28	21	16	4
300	42	36	32	19
400	70	65	63	57
500	89	86	85	83
600	98	96	96	96
700		99	99	99

Oil name South Timbalier Block 130**Origin and description** Gulf of Mexico, USA**Evaporation equation** $\%Ev = (2.77 + 0.045T)\ln(t)$ Where Ev = weight percent evaporated, T = surface temperature ($^{\circ}\text{C}$), t = time (min)

API gravity	35.1	Weathering % by weight			
	Units	0	11	22	35
Density	g/ml	0.8487	0.8632	0.8748	0.8877
Viscosity	mPa·s or cP	7	10	19	48

(dynamic—values at 15°C)

Flash point	$^{\circ}\text{C}$	5	58	89	> 95
Sulfur content	%	0.32	0.28	0.38	0.35
Pour point	$^{\circ}\text{C}$	−27	−23	−18	−9
Surface tension	mN/m	26.5	28.4	29.2	30.2

(air–oil at 15°C)

IFT sea water	mN/m	18.6	19.2	18.9	15
IFT fresh water	mN/m	21.1	22.1	20.4	17.3
Adhesion	g/m^3	11	18	28	27

SARA content (saturate, aromatic, resin, asphaltene) %

Saturate	%	78	72	71	68
Aromatic	%	16	22	23	23
Resin	%	5	5	6	8
Asphaltene	%	0	0	0	1
Waxes	%	4	4	4	4

Emulsion formation (type formed and water content %)

Type				
Water content	%			
Viscosity	mPa·s or cP			

Chemical dispersibility with Corexit 9500

%	31			
---	----	--	--	--

Distillation data (% at temperature)Boiling point ($^{\circ}\text{C}$)

40	1			
60	1			
80	4			
100	7			
120	11	1		
140	12	2		
160	15	6		
180	20	11	2	
200	25	16	6	
250	39	32	23	9
300	54	48	41	29
400	76	73	69	63
500	90	89	87	84
600	97	96	96	94
700			99	99

Oil name**Soybean Oil****Origin and description****Evaporation equation**

API gravity	21.6			
(all units at 15°C)	Units	Regular	Dyed	
Density	g/ml	0.9232	0.9232	
Viscosity	mPa·s or cP	73	73	

(dynamic—values at 15°C)

Flash point	$^{\circ}\text{C}$	> 100	> 100	
Sulfur content	%	0	0	
Pour point	$^{\circ}\text{C}$	−10	−10	
Surface tension	mN/m	31.8	31.6	

(air–oil at 15°C)

IFT sea water	mN/m	9.2	7.8	
IFT fresh water	mN/m	10.5	9.8	
Adhesion	g/m^3	15	43	

SARA content (saturate, aromatic, resin, asphaltene) %

Saturate	%	2	3	
Aromatic	%	0	1	
Resin	%	97	96	
Asphaltene	%	0	0	
Waxes	%			

Emulsion formation (type formed and water content %)

Type			
Water content	%		
Viscosity	mPa·s or cP		

Chemical dispersibility with Corexit 9500

%			
---	--	--	--

Distillation data (% at temperature)

Boiling point			
($^{\circ}\text{C}$)			
40			
60			
80			
100			
120			
140			
160			
180			
200			
250			
300			
400			
500			
600			
700			

Oil name		Statfjord			
Origin and description		North Sea, Norway			
Evaporation equation		$\%Ev = (2.67 + 0.060T)\ln(t)$			
Where Ev = weight percent evaporated, T = surface temperature (°C), t = time (min)					
API gravity	37.8	Weathering % by weight			
(all units at 15°C)	Units	0	13	23	37
Density	g/ml	0.8354	0.8642	0.8778	0.8957
Viscosity	mPa·s or cP	6	17	47	241
(dynamic—values at 15°C)					
Flash point	°C	−12	32	72	> 95
Sulfur content	%	0.26	0.3	0.34	0.43
Pour point	°C	−2	3	17	24
Surface tension	mN/m	26.1	28.3	29.4	31
(air–oil at 15°C)					
IFT sea water	mN/m	23.2	24.7	25	22
IFT fresh water	mN/m	24.4	25	25.2	22.9
Adhesion	g/m ³	14	16	20	62
SARA content (saturate, aromatic, resin, asphaltene) %					
Saturate	%	68	62	60	55
Aromatic	%	26	30	32	33
Resin	%	6	7	7	10
Asphaltene	%	2	1	2	2
Waxes	%	8	7	8	0
Emulsion formation (type formed and water content %)					
Type					
Water content	%				
Viscosity	mPa·s or cP				
Chemical dispersibility with Corexit 9500					
	%	40			
Distillation data (% at temperature)					
Boiling point (°C)					
40		2			
60		3			
80		3			
100		5	2		
120		17	4		
140		20	8	1	
160		23	12	3	
180		26	16	6	
200		30	20	10	
250		39	31	22	6
300		49	43	36	20
400		68	65	60	50
500		84	83	81	76
600		94	94	93	91
700		99	99	99	98

Oil name		Sumatran Heavy		
Origin and description		Indonesia; a.k.a. Duri		
Evaporation equation		$\%Ev = (-0.11 + 0.013T)\sqrt{(t)}$		
Where Ev = weight percent evaporated, T = surface temperature (°C), t = time (min)				
API gravity	20.3	Weathering % by weight		
(all units at 15°C)	Units	0	5	
Density	g/ml	0.9312	0.9374	
Viscosity	mPa·s or cP	13,300	12,900	
(dynamic—values at 15°C)				
Flash point	°C	54	> 90	
Sulfur content	%	0.18	0.19	
Pour point	°C	18	22	
Surface tension	mN/m			
(air–oil at 15°C)				
IFT sea water	mN/m			
IFT fresh water	mN/m			
Adhesion	g/m ³	92	115	
SARA content (saturate, aromatic, resin, asphaltene) %				
Saturate	%	46	45	
Aromatic	%	30	32	
Resin	%	13	16	
Asphaltene	%	10	8	
Waxes	%	1.4	4	
Emulsion formation (type formed and water content %)				
Type		Unstable	Unstable	
Water content	%	21	2	
Viscosity	mPa·s or cP			
Chemical dispersibility with Corexit 9500				
	%	10	0	
Distillation data (% at temperature)				
Boiling point (°C)				
40		0.1		
60		0.2		
80		0.4		
100		0.7		
120		1.1		
140		1.8		
160		2.9		
180		4.2	1	
200		5.6	2	
250		11.1	7	
300		18.4	14	
400		33	28	
500		52.7	48	
600		70.8	65	
700			84	

Oil name **Sumatran Light**
Origin and description Indonesia; a.k.a. Minas

Evaporation equation $\%Ev = (0.96 + 0.0457T)\ln(t)$
 Where Ev = weight percent evaporated, T = surface temperature (°C), t = time (min)

API gravity	32.9	Weathering % by weight		
(all units at 15°C)	Units	0		
Density	g/ml	0.86		
Viscosity	mPa·s or cP	41,480		
(dynamic—values at 15°C)				
Flash point	°C	17		
Sulfur content	%	0.07		
Pour point	°C	38		
Surface tension mN/m				
(air–oil at 15°C)				
IFT sea water mN/m				
IFT fresh water mN/m				
Adhesion	g/m ³	9		

SARA content (saturate, aromatic, resin, asphaltene) %

Saturate	%	70		
Aromatic	%	15		
Resin	%	6		
Asphaltene	%	8		
Waxes	%	10.8		

Emulsion formation (type formed and water content %)

Type		unstable		
Water content	%	13		
Viscosity	mPa·s or cP			

Chemical dispersibility with Corexit 9500

%	0		
---	---	--	--

Distillation data (% at temperature)

Boiling point (°C)			
40	0.3		
60	0.8		
80	1.3		
100	2.2		
120	3.2		
140	4.6		
160	6.5		
180	8.9		
200	11.3		
250	18.6		
300	28.1		
400	48.2		
500	71.3		
600	84.4		
700			

Oil name **Swanson River**
Origin and description Cook Inlet, Alaska, USA.; a.k.a. Cook Inlet

Evaporation equation $\%Ev = (3.58 + 0.0457T)\ln(t)$
 Where Ev = weight percent evaporated, T = surface temperature (°C), t = time (min)

API gravity	36.5	Weathering % by weight		
(all units at 15°C)	Units	0	40	
Density	g/ml	0.842	0.9143	
Viscosity	mPa·s or cP	6	152	
(dynamic—values at 15°C)				
Flash point	°C	–23	> 95	
Sulfur content	%	0.13	0.13	
Pour point	°C	–23	10	
Surface tension mN/m		27	30.7	

IFT sea water mN/m	23.8	19.9	
IFT fresh water mN/m	24.6	23.5	
Adhesion	g/m ³	12	23

SARA content (saturate, aromatic, resin, asphaltene) %

Saturate	%	65	56	
Aromatic	%	25	29	
Resin	%	6	7	
Asphaltene	%	5	7	
Waxes	%			

Emulsion formation (type formed and water content %)

Type	Meso-stable	Stable	
Water content	76	81	
Viscosity	mPa·s or cP	2900	29,000

Chemical dispersibility with Corexit 9500

%	36	10	
---	----	----	--

Distillation data (% at temperature)

Boiling point (°C)			
40	4		
60	4		
80	6		
100	9		
120	14		
140	19		
160	23		
180	28		
200	32		
250	42	9	
300	53	24	
400	72	54	
500	86	76	
600	94	89	
700	98	96	

Oil name **Synthetic Crude**
Origin and description Alberta, Canada; synthetic crude derived from Bitumen

Evaporation equation

Where E_v = weight percent evaporated, T = surface temperature ($^{\circ}\text{C}$), t = time (min)

API gravity	32.6	Weathering % by weight		
(all units at 15°C)	Units	0	11	22
Density	g/ml	0.8614	0.8868	0.9058
Viscosity	mPa·s or cP	5	9	19
(dynamic—values at 15°C)				
Flash point	$^{\circ}\text{C}$	< -21		
Sulfur content	%	0.23	0.15	0.2
Pour point	$^{\circ}\text{C}$	-72	-45	-36
Surface tension	mN/m	25.7	28.4	30.1
(air–oil at 15°C)				
IFT sea water	mN/m	29	29.6	15.5
IFT fresh water	mN/m	30.8	30.5	18.2
Adhesion	g/m^3			

SARA content (saturate, aromatic, resin, asphaltene) %

Saturate	%	82		
Aromatic	%	17		
Resin	%	1		
Asphaltene	%	0		
Waxes	%	0		

Emulsion formation (type formed and water content %)

Type			
Water content	%		
Viscosity	mPa·s or cP		

Chemical dispersibility with Corexit 9500

%	40		
---	----	--	--

Distillation data (% at temperature)

Boiling point ($^{\circ}\text{C}$)			
40			
60			
80	2		
100	5		
120	7		
140	10		
160	12		
180	15		
200	19		
250	32		
300	47		
400	79		
500	97		
600			
700			

Oil name **Taching**
Origin and description China; a.k.a. Daqing

Evaporation equation

$$\%E_v = (-0.11 + 0.013T)\sqrt{(t)}$$

Where E_v = weight percent evaporated, T = surface temperature ($^{\circ}\text{C}$), t = time (min)

API gravity	31	Weathering % by weight		
(all units at 15°C)	Units	0		
Density	g/ml	0.87		
Viscosity	mPa·s or cP	51,38,000		
(dynamic—values at 15°C)				
Flash point	$^{\circ}\text{C}$	23		
Sulfur content	%	0.11		
Pour point	$^{\circ}\text{C}$	38		
Surface tension	mN/m			
(air–oil at 15°C)				
IFT sea water	mN/m			
IFT fresh water	mN/m			
Adhesion	g/m^3	103		

SARA content (saturate, aromatic, resin, asphaltene) %

Saturate	%	74		
Aromatic	%	12		
Resin	%	9		
Asphaltene	%	6		
Waxes	%	23		

Emulsion formation (type formed and water content %)

Type			
Water content	%		
Viscosity	mPa·s or cP		

Chemical dispersibility with Corexit 9500

%	9		
---	---	--	--

Distillation data (% at temperature)

Boiling point ($^{\circ}\text{C}$)			
40			
60			
80	1		
100	3		
120	4		
140	5		
160	7		
180	9		
200	10		
250	15		
300	21		
400	38		
500	56		
600	71		
700	85		

Oil name	Takula			
Origin and description	Angola			
Evaporation equation		$\%Ev = (1.95 + 0.045T)\ln(t)$		
Where Ev = weight percent evaporated, T = surface temperature (°C), t = time (min)				
API gravity	32.2	Weathering % by weight		
(all units at 15°C)	Units	0	11	18
Density	g/ml	0.8637	0.886	0.8961
Viscosity	mPa·s or cP	110	844	3148
(dynamic—values at 15°C)				
Flash point	°C	−7	41	> 90
Sulfur content	%	0.18	0.15	0.13
Pour point	°C	15	19	26
Surface tension	mN/m	30.6		
(air–oil at 15°C)				
IFT sea water	mN/m	28.1		
IFT fresh water	mN/m	31.5		
Adhesion	g/m ³	70	78	232
SARA content (saturate, aromatic, resin, asphaltene) %				
Saturate	%	65	62	60
Aromatic	%	22	24	25
Resin	%	8	10	11
Asphaltene	%	2	4	4
Waxes	%	8	8	9
Emulsion formation (type formed and water content %)				
Type		Stable	Stable	Stable
Water content	%	85	81	75
Viscosity	mPa·s or cP	45,000	83,000	110,000
Chemical dispersibility with Corexit 9500				
	%	14	9	6

Distillation data (% at temperature)			
Boiling point (°C)			
40	2		
60	2	1	
80	4	1	
100	6	2	
120	8	3	
140	10	4	
160	12	6	1
180	15	9	2
200	17	11	4
250	24	19	12
300	32	27	21
400	49	46	42
500	67	66	63
600	80	79	79
700	89	90	90

Oil name	Tapis Blend			
Origin and description	Malaysia			
Evaporation equation		$\%Ev = (3.04 + 0.045T)\ln(t)$		
Where Ev = weight percent evaporated, T = surface temperature (°C), t = time (min)				
API gravity	44.9	Weathering % by weight		
(all units at 15°C)	Units	0	14	29
Density	g/ml	0.802	0.8237	0.8396
Viscosity	mPa·s or cP	8	57	800
(dynamic—values at 15°C)				
Flash point	°C	−26	17	68
Sulfur content	%	0.06	0.03	0.03
Pour point	°C	18	28	31
Surface tension	mN/m	27.1	31.1	
(air–oil at 15°C)				
IFT sea water	mN/m	21.2		
IFT fresh water	mN/m	25		
Adhesion	g/m ³	7	34	55
SARA content (saturate, aromatic, resin, asphaltene) %				
Saturate	%	81	77	80
Aromatic	%	15	19	16
Resin	%	2	3	3
Asphaltene	%	2	1	2
Waxes	%			
Emulsion formation (type formed and water content %)				
Type		Unstable	Unstable	Unstable
Water content	%	16	23	9
Viscosity	mPa·s or cP			
Chemical dispersibility with Corexit 9500				
	%	63	69	56

Distillation data (% at temperature)			
Boiling point (°C)			
40	5		
60	5		
80	7	1	
100	11	2	
120	17	7	
140	22	11	1
160	27	17	4
180	32	23	9
200	37	28	14
250	49	42	31
300	62	57	48
400	83	81	77
500	96	95	94
600	99	99	98
700			

Oil name **Tarsuit**
Origin and description Beaufort Sea, Canada

Evaporation equationWhere E_v = weight percent evaporated, T = surface temperature ($^{\circ}\text{C}$), t = time (min)

API gravity	30.1	Weathering % by weight		
(all units at 15°C)	Units	0	12	16
Density	g/ml	0.875	0.89	0.8922
Viscosity	mPa·s or cP	7	13	14
(dynamic—values at 15°C)				
Flash point	$^{\circ}\text{C}$	65		
Sulfur content	%			
Pour point	$^{\circ}\text{C}$			
Surface tension	mN/m	26.5	29.1	27.7
(air–oil at 15°C)				
IFT sea water	mN/m	14.1	13.9	14.3
IFT fresh water	mN/m	18.4	17.9	17.8
Adhesion	g/m^3			

SARA content (saturate, aromatic, resin, asphaltene) %

Saturate	%	92		
Aromatic	%	7		
Resin	%	0		
Asphaltene	%	0		
Waxes	%			

Emulsion formation (type formed and water content %)

Type			
Water content	%		
Viscosity	mPa·s or cP		

Chemical Dispersibility with Corexit 9500

%			
---	--	--	--

Distillation data (% at temperature)

Boiling point ($^{\circ}\text{C}$)			
40			
60			
80			
100			
120			
140			
160			
180			
200			
250			
300			
400			
500			
600			
700			

Oil name **Terra Nova (1994)**
Origin and description Newfoundland, Canada

Evaporation equation

$$\%E_v = (1.36 + 0.045T)\ln(t)$$

Where E_v = weight percent evaporated, T = surface temperature ($^{\circ}\text{C}$), t = time (min)

API gravity	35.7	Weathering % by weight			
(all units at 15°C)	Units	0	12	24	34
Density	g/ml	0.8457	0.8727	0.8909	0.9033
Viscosity	mPa·s or cP	11	28	167	515
(dynamic—values at 15°C)					
Flash point	$^{\circ}\text{C}$	–22	34	85	> 95
Sulfur content	%	0.43	0.42	0.47	0.55
Pour point	$^{\circ}\text{C}$	5	17	22	26
Surface tension	mN/m	26.9	28.6	30.1	32.3
(air–oil at 15°C)					
IFT sea water	mN/m	21.5	22.9	23.3	23.8
IFT fresh water	mN/m	21.8	23.4	22.6	26.4
Adhesion	g/m^3	10	19	38	80

SARA content (saturate, aromatic, resin, asphaltene) %

Saturate	%	62	60	58	51
Aromatic	%	31	31	31	35
Resin	%	6	7	9	11
Asphaltene	%	2	2	2	2
Waxes	%	9	8	10	10

Emulsion formation (type formed and water content %)

Type				
Water content	%			
Viscosity	mPa·s or cP			

Chemical dispersibility with Corexit 9500

%	14			
---	----	--	--	--

Distillation data (% at temperature)

Boiling point ($^{\circ}\text{C}$)				
40	3			
60	4			
80	7			
100	11	2		
120	14	3		
140	17	6		
160	20	10	1	
180	24	14	3	
200	27	17	6	
250	36	27	17	6
300	45	37	29	18
400	63	57	52	45
500	79	75	73	69
600	90	86	87	85
700	97	94	96	96

Oil name Terra Nova—B
Origin and description Newfoundland, Canada; used in SOCSEX experiment

Evaporation equation

Where E_v = weight percent evaporated, T = surface temperature ($^{\circ}\text{C}$), t = time (min)

API gravity	35.7	Weathering % by weight		
(all units at 15°C)	Units	0	18	26
Density	g/ml	0.9457	0.875	0.8849
Viscosity	mPa·s or cP	11	463	568
(dynamic—values at 15°C)				
Flash point	$^{\circ}\text{C}$			
Sulfur content	%			
Pour point	$^{\circ}\text{C}$			
Surface tension mN/m				
(air–oil at 15°C)				
IFT sea water mN/m				
IFT fresh water mN/m				
Adhesion	g/m^3	10	26	34

SARA content (saturate, aromatic, resin, asphaltene) %

Saturate	%	62	59	58
Aromatic	%	31	33	34
Resin	%	6	6	6
Asphaltene	%	2	2	2
Waxes	%	8		

Emulsion formation (type formed and water content %)

Type			
Water content	%		
Viscosity	mPa·s or cP		

Chemical dispersibility with Corexit 9500

%			
---	--	--	--

Distillation data (% at temperature)

Boiling point ($^{\circ}\text{C}$)			
40	3		
60	4		
80	7		
100	11	1	
120	14	2	
140	17	5	1
160	20	8	3
180	24	12	6
200	27	16	10
250	36	25	20
300	45	35	31
400	63	55	53
500	79	72	73
600	90	84	87
700	97	92	96

Oil name Terra Nova
Origin and description Newfoundland, Canada

Evaporation equation

Where E_v = weight percent evaporated, T = surface temperature ($^{\circ}\text{C}$), t = time (min)

API gravity	33.7	Weathering % by weight		
(all units at 15°C)	Units	0		
Density	g/ml	0.856		
Viscosity	mPa·s or cP	22		
(dynamic—values at 15°C)				
Flash point	$^{\circ}\text{C}$			
Sulfur content	%			
Pour point	$^{\circ}\text{C}$	27		
Surface tension mN/m		27.2		
(air–oil at 15°C)				
IFT sea water mN/m		28.8		
IFT fresh water mN/m		28.7		
Adhesion	g/m^3			

SARA content (saturate, aromatic, resin, asphaltene) %

Saturate	%			
Aromatic	%			
Resin	%			
Asphaltene	%	1		
Waxes	%	9		

Emulsion formation (type formed and water content %)

Type			
Water content	%		
Viscosity	mPa·s or cP		

Chemical dispersibility with Corexit 9500

%			
---	--	--	--

Distillation data (% at temperature)

Boiling point ($^{\circ}\text{C}$)			
40			
60			
80			
100			
120			
140			
160			
180			
200			
250			
300			
400			
500			
600			
700			

Oil name		Thevenard Island			
Origin and description		Australia			
Evaporation equation		$\%Ev = (5.74 + 0.045T)\ln(t)$			
Where Ev = weight percent evaporated, T = surface temperature (°C), t = time (min)					
API gravity	48.6	Weathering % by weight			
(all units at 15°C)	Units	0	23	44	59
Density	g/ml	0.7855	0.8301	0.8352	0.8498
Viscosity	mPa·s or cP	1	3	5	9
(dynamic—values at 15°C)					
Flash point	°C	< −30	43	79	> 95
Sulfur content	%	0.01	0.01	0.01	0.03
Pour point	°C	< −70	−12	6	7
Surface tension	mN/m	23.8	25.5	28.1	29.1
(air–oil at 15°C)					
IFT sea water	mN/m	17.2	10.8	15.2	14.6
IFT fresh water	mN/m	19.6	13.8	16.9	17.1
Adhesion	g/m ³	6	7	12	14
SARA content (saturate, aromatic, resin, asphaltene) %					
Saturate	%	85	79	79	75
Aromatic	%	13	19	19	22
Resin	%	2	2	2	3
Asphaltene	%	0	0	0	0
Waxes	%	1	5	7	9
Emulsion formation (type formed and water content %)					
Type					
Water content	%				
Viscosity	mPa·s or cP				
Chemical dispersibility with Corexit 9500					
	%	77			
Distillation data (% at temperature)					
Boiling point (°C)					
40					
60					
80		7			
100		15	1		
120		21	3		
140		27	7		
160		34	14	1	
180		42	23	6	
200		49	32	14	1
250		66	54	42	21
300		80	73	67	53
400		94	93	93	89
500		98	99	99	99
600		100			
700					

Oil name		Transmountain Blend		
Origin and description		Alberta, Canada		
Evaporation equation				
Where Ev = weight percent evaporated, T = surface temperature (°C), t = time (min)				
API gravity	33.8	Weathering % by weight		
(all units at 15°C)	Units	0	19	29
Density	g/ml	0.855	0.8989	0.9127
Viscosity	mPa·s or cP	11	142	577
(dynamic—values at 15°C)				
Flash point	°C	−2		
Sulfur content	%	0.79		
Pour point	°C	2	8	18
Surface tension	mN/m	25	29.1	
(air–oil at 15°C)				
IFT sea water	mN/m	19.3	25.1	
IFT fresh water	mN/m	19.3	26.5	
Adhesion	g/m ³			
SARA content (saturate, aromatic, resin, asphaltene) %				
Saturate	%	81		
Aromatic	%	14		
Resin	%	2		
Asphaltene	%	4		
Waxes	%	7		
Emulsion formation (type formed and water content %)				
Type				
Water content	%			
Viscosity	mPa·s or cP			
Chemical dispersibility with Corexit 9500				
	%			
Distillation data (% at temperature)				
Boiling point (°C)				
40		1		
60		1		
80		3		
100		6		
120		9		
140		12		
160		15		
180		18		
200		21		
250		30		
300		40		
400		60		
500		78		
600		91		
700		98		

Oil name **Troll**
Origin and description Norway

Evaporation equation

Where E_v = weight percent evaporated, T = surface temperature ($^{\circ}\text{C}$), t = time (min)

API gravity	Units	Weathering % by weight			
		0	6.3	13.1	19.4
(all units at 15°C)					
Density	g/ml	0.8852	0.8972	0.906	0.9134
Viscosity	mPa·s or cP	23.5	43.6	79.7	175.4
(dynamic—values at 15°C)					
Flash point	$^{\circ}\text{C}$				
Sulfur content	%				
Pour point	$^{\circ}\text{C}$				
Surface tension mN/m		28.8	29.6	30.2	30.7
(air–oil at 15°C)					
IFT sea water mN/m		22.6	24	25.4	26.8
IFT fresh water mN/m		24.2	25.2	26.1	25.9
Adhesion	g/m^3				

SARA content (saturate, aromatic, resin, asphaltene) %

Saturate	%	66.9	66.2	64.9	62.2
Aromatic	%	26.6	27.2	27.7	28.6
Resin	%	5.8	5.9	6.6	8.1
Asphaltene	%	0.7	0.7	0.7	1.1
Waxes	%				

Emulsion formation (type formed and water content %)

Type				
Water content	%			
Viscosity	mPa·s or cP			

Chemical dispersibility with Corexit 9500

%				
---	--	--	--	--

Distillation data (% at temperature)

Boiling point ($^{\circ}\text{C}$)				
40				
60				
80				
100				
120				
140				
160				
180				
200				
250				
300				
400				
500				
600				
700				

Oil name **Udang**
Origin and description Indonesia

Evaporation equation

Short-term (< 5 days): $\%E_v = (-0.14 + 0.013T)\sqrt{t}$

Long-term: $\%E_v = (0.06 + 0.045T)\ln(t)$

Where E_v = weight percent evaporated, T = surface temperature ($^{\circ}\text{C}$), t = time (min)

API gravity	Units	Weathering % by weight		
		0		
(all units at 15°C)				
Density	g/ml	0.9701		
Viscosity	mPa·s or cP	10,700		
(dynamic—values at 15°C)				
Flash point	$^{\circ}\text{C}$	> 90		
Sulfur content	%	0.94		
Pour point	$^{\circ}\text{C}$	3		
Surface tension mN/m		32.2		
(air–oil at 15°C)				
IFT sea water mN/m		25.4		
IFT fresh water mN/m		32.5		
Adhesion	g/m^3	97		

SARA content (saturate, aromatic, resin, asphaltene) %

Saturate	%	32		
Aromatic	%	41		
Resin	%	24		
Asphaltene	%	3		
Waxes	%	1		

Emulsion formation (type formed and water content %)

Type	Entrained		
Water content	%	37	
Viscosity	mPa·s or cP	32,000	

Chemical dispersibility with Corexit 9500

%	7		
---	---	--	--

Distillation data (% at temperature)

Boiling point ($^{\circ}\text{C}$)			
40			
60			
80			
100			
120			
140			
160	1		
180	2		
200	3		
250	8		
300	15		
400	35		
500	59		
600	76		
700	89		

Oil name **Uviluk**
Origin and description Beaufort Sea, Canada

Evaporation equationWhere E_v = weight percent evaporated, T = surface temperature ($^{\circ}\text{C}$), t = time (min)

API gravity	29.4	Weathering % by weight		
(all units at 15°C)	Units	0	10	20
Density	g/ml	0.8787	0.8978	0.9152
Viscosity	mPa·s or cP	14	28	67
(dynamic—values at 15°C)				
Flash point	$^{\circ}\text{C}$	−9		
Sulfur content	%	0.24	0.17	0.24
Pour point	$^{\circ}\text{C}$	−12	−3	3
Surface tension mN/m		26.7	28	29.8
(air–oil at 15°C)				
IFT sea water mN/m		12.2	13.8	13.9
IFT fresh water mN/m		24.3	23.2	22.8
Adhesion	g/m^3			

SARA content (saturate, aromatic, resin, asphaltene) %

Saturate	%			
Aromatic	%			
Resin	%			
Asphaltene	%			
Waxes	%			

Emulsion formation (type formed and water content %)

Type			
Water content	%		
Viscosity	mPa·s or cP		

Chemical dispersibility with Corexit 9500

%			
---	--	--	--

Distillation data (% at temperature)

Boiling point ($^{\circ}\text{C}$)			
40			
60			
80			
100			
120			
140			
160			
180			
200			
250			
300			
400			
500			
600			
700			

Oil name **Vasconia**
Origin and description Colombia

Evaporation equation

$$\%E_v = (0.84 + 0.045T)\ln(t)$$

Where E_v = weight percent evaporated, T = surface temperature ($^{\circ}\text{C}$), t = time (min)

API gravity	26.3	Weathering % by weight			
(all units at 15°C)	Units	0	9	14	22
Density	g/ml	0.8958	0.9175	0.9291	0.942
Viscosity	mPa·s or cP				
(dynamic—values at 15°C)					
Flash point	$^{\circ}\text{C}$	−3	54	87	> 100
Sulfur content	%	0.56	0.55	0.57	0.63
Pour point	$^{\circ}\text{C}$	72	169	385	1490
Surface tension mN/m		28.6			
(air–oil at 15°C)					
IFT sea water mN/m		25.2			
IFT fresh water mN/m		24.9			
Adhesion	g/m^3	39	38	44	60

SARA content (saturate, aromatic, resin, asphaltene) %

Saturate	%	61	54	54	53
Aromatic	%	26	31	30	28
Resin	%	6	6	6	8
Asphaltene	%	8	9	10	11
Waxes	%	405	4.6	5.1	5.3

Emulsion formation (type formed and water content %)

Type				
Water content	%			
Viscosity	mPa·s or cP			

Chemical dispersibility with Corexit 9500

%				
---	--	--	--	--

Distillation data (% at temperature)

Boiling point ($^{\circ}\text{C}$)				
40	0.5			
60	0.9			
80	1.8	0.1		
100	3.9	0.3		
120	5.8	0.9	0.1	
140	7.9	2.1	0.2	
160	10.5	4.3	0.8	
180	13.1	7.1	2.4	
200	15.6	9.7	4.6	0.3
250	24.7	19.6	14.6	7.3
300	35.8	31.7	27.4	20.2
400	58.4	56.6	53.7	48.4
500	76.1	76	74.1	70.3
600	86.6	87.3	85.9	83
700				

Oil name **Viosca Knoll Block 826**
Origin and description Gulf of Mexico, USA

Evaporation equation $\%Ev = (2.04 + 0.045T)\ln(t)$
 Where Ev = weight percent evaporated, T = surface temperature (°C), t = time (min)

API gravity	31.6	Weathering % by weight			
(all units at 15°C)	Units	0	8	17	24
Density	g/ml	0.8668	0.8842	0.897	0.9067
Viscosity	mPa·s or cP	16	43	132	325
(dynamic—values at 15°C)					
Flash point	°C	−2	41	86	> 95
Sulfur content	%	0.29	0.28	0.34	0.37
Pour point	°C	−4	6	11	16
Surface tension	mN/m	27.7	29.1	30.1	31
(air–oil at 15°C)					
IFT sea water	mN/m	23.6	26.5	26.1	21.1
IFT fresh water	mN/m	25.5	27.5	28.6	22.5
Adhesion	g/m ³	16	39	38	53

SARA content (saturate, aromatic, resin, asphaltene) %

Saturate	%	66	61	62	59
Aromatic	%	26	29	29	29
Resin	%	6	7	6	8
Asphaltene	%	2	3	3	3
Waxes	%				

Emulsion formation (type formed and water content %)

Type		Unstable	Unstable	Unstable	Stable
Water content	%				64
Viscosity	mPa·s or cP				13,660

Chemical dispersibility with Corexit 9500

%	24	17	15	17
---	----	----	----	----

Distillation data (% at temperature)

Boiling point (°C)				
40	1			
60	2			
80	3			
100	5	1		
120	8	3		
140	11	5		
160	13	8	1	
180	16	11	3	
200	19	14	6	1
250	29	24	15	8
300	40	36	29	22
400	62	60	55	51
500	81	79	77	75
600	92	92	91	90
700	98	98	98	98

Oil name **Viosca Knoll Block 990**
Origin and description Gulf of Mexico, USA

Evaporation equation $\%Ev = (3.16 + 0.045T)\ln(t)$
 Where Ev = weight percent evaporated, T = surface temperature (°C), t = time (min)

API gravity	38.1	Weathering % by weight			
(all units at 15°C)	Units	0	12	24	35
Density	g/ml	0.8337	0.8585	0.8752	0.8905
Viscosity	mPa·s or cP	7	12	31	91
(dynamic—values at 15°C)					
Flash point	°C	−17	34	76	> 95
Sulfur content	%	0.22	0.26	0.28	0.26
Pour point	°C	−32	−7	−6	13
Surface tension	mN/m	22.8	25	29.1	30.3
(air–oil at 15°C)					
IFT sea water	mN/m	15	22.5	22.1	18.4
IFT fresh water	mN/m	15.1	22.7	22.6	18.4
Adhesion	g/m ³	13	21	20	26

SARA content (saturate, aromatic, resin, asphaltene) %

Saturate	%	73	69	66	62
Aromatic	%	22	25	26	28
Resin	%	4	6	6	8
Asphaltene	%	1	1	1	2
Waxes	%	2.2	2.1	2.8	3.2

Emulsion formation (type formed and water content %)

Type		Unstable	Unstable	Unstable	Stable
Water content	%				64
Viscosity	mPa·s or cP				9339

Chemical dispersibility with Corexit 9500

%	41	29	22	14
---	----	----	----	----

Distillation data (% at temperature)

Boiling point (°C)				
40	1.3			
60	2.2			
80	4.4	0.3		
100	7.8	1.7		
120	10.7	3.7		
140	14.1	6.6	0.3	
160	18.1	10.6	1.5	
180	22.3	15.1	4.4	
200	26	19.2	8.1	0.4
250	35.9	30.1	20.2	8.5
300	46.6	42	33.9	23.3
400	66.3	63.7	58.9	52
500	81.2	80.2	77.8	73.6
600	90.7	90.6	89.5	86.9
700				

Oil name **Wabasca Heavy**
Origin and description Alberta, Canada

Evaporation equation

Where E_v = weight percent evaporated, T = surface temperature ($^{\circ}\text{C}$), t = time (min)

API gravity	16.3	Weathering % by weight		
(all units at 15°C)	Units	0	10.70	
Density	g/ml	0.9572	1.0069	
Viscosity	mPa-s or cP	1.28E+05	2.79E+05	
(dynamic—values at 15°C)				
Flash point	$^{\circ}\text{C}$	151	164	
Sulfur content	%	4.7	5	
Pour point	$^{\circ}\text{C}$	-6	3	
Surface tension	mN/m	NM	NM	
(air-oil at 15°C)				
IFT sea water	mN/m	NM	NM	
IFT fresh water	mN/m	NM	NM	
Adhesion	g/m^3			

SARA content (saturate, aromatic, resin, asphaltene) %

Saturate	%	41.3	41.3	
Aromatic	%	31.8	23.0	
Resin	%	27.5	38.3	
Asphaltene	%	8.6	8.4	
Waxes	%			

Emulsion formation (type formed and water content %)

Type		Entrained	Entrained	
Water content	%	14.9	11.7	
Viscosity	mPa-s or cP			

Chemical dispersibility with Corexit 9500

%	< 10%	< 10%	
---	-------	-------	--

Distillation data (% at temperature)

Boiling point ($^{\circ}\text{C}$)			
40			
60			
80			
100			
120			
140			
160			
180			
200			
250			
300			
400			
500			
600			
700			

Oil name **Waxy Light Heavy Blend**
Origin and description California, USA

Evaporation equation

$$\%E_v = (1.52 + 0.0457T)\ln(t)$$

Where E_v = weight percent evaporated, T = surface temperature ($^{\circ}\text{C}$), t = time (min)

API gravity	20.4	Weathering % by weight		
(all units at 15°C)	Units	0	12	20
Density	g/ml	0.9311	0.9582	0.9749
Viscosity	mPa-s or cP	184	2002	17,280
(dynamic—values at 15°C)				
Flash point	$^{\circ}\text{C}$	-3	80	> 95
Sulfur content	%	1.01	1.08	1.18
Pour point	$^{\circ}\text{C}$	-30	-12	0
Surface tension	mN/m	29	31.4	33
(air-oil at 15°C)				
IFT sea water	mN/m	17.2	14.2	
IFT fresh water	mN/m	19.1	18.8	
Adhesion	g/m^3	42	70	92

SARA content (saturate, aromatic, resin, asphaltene) %

Saturate	%	39	32	30
Aromatic	%	35	38	35
Resin	%	21	24	28
Asphaltene	%	5	6	6
Waxes	%	4	1	1

Emulsion formation (type formed and water content %)

Type		Unstable	Meso-stable	Meso-stable
Water content	%	4	50	55
Viscosity	mPa-s or cP		6200	44,000

Chemical dispersibility with Corexit 9500

%	9	0	0
---	---	---	---

Distillation data (% at temperature)

Boiling point ($^{\circ}\text{C}$)			
40			
60			
80	1		
100	3		
120	5		
140	7	1	
160	9	1	
180	10	3	
200	12	5	
250	19	12	5
300	27	22	16
400	45	43	40
500	63	65	65
600	76	81	83
700	86	91	95

Oil name **West Delta Block 30**
Origin and description Gulf of Mexico, USA

Evaporation equation

Where E_v = weight percent evaporated, T = surface temperature ($^{\circ}\text{C}$), t = time (min)

API gravity	11.4	Weathering % by weight			
(all units at 15 $^{\circ}\text{C}$)	Units	0	24	42	61
Density	g/ml	0.9894	0.9562	0.9594	0.9598
Viscosity	mPa·s or cP	1180	1350	1560	4970
(dynamic—values at 15 $^{\circ}\text{C}$)					
Flash point	$^{\circ}\text{C}$	46	> 95	> 95	> 95
Sulfur content	%	0.54	0.61	0.64	0.73
Pour point	$^{\circ}\text{C}$	−23	−17	−12	−8
Surface tension	mN/m	30.7	31.5	31.3	32.3
(air–oil at 15 $^{\circ}\text{C}$)					
IFT sea water	mN/m	17.3			
IFT fresh water	mN/m	22.1			
Adhesion	g/m ³	32	65	65	64

SARA content (saturate, aromatic, resin, asphaltene) %

Saturate	%	43	48	46	41
Aromatic	%	24	33	34	36
Resin	%	11	16	15	20
Asphaltene	%	22	3	5	3
Waxes	%	0	0	0	0

Emulsion formation (type formed and water content %)

Type				
Water content	%			
Viscosity	mPa·s or cP			

Chemical dispersibility with Corexit 9500

%				
---	--	--	--	--

Distillation data (% at temperature)

Boiling point ($^{\circ}\text{C}$)				
40				
60				
80				
100				
120	1			
140	1			
160	2			
180	4			
200	5			
250	13	5	1	
300	24	15	9	
400	48	37	34	
500	69	57	57	
600	83	72	73	
700	93	82	84	

Oil name **West Delta Block 97**
Origin and description Gulf of Mexico, USA

Evaporation equation

$$\%E_v = (6.57 + 0.045T)\ln(t)$$

Where E_v = weight percent evaporated, T = surface temperature ($^{\circ}\text{C}$), t = time (min)

API gravity	50.2	Weathering % by weight			
(all units at 15 $^{\circ}\text{C}$)	Units	0	23	48	74
Density	g/ml	0.7783	0.802	0.8191	0.8388
Viscosity	mPa·s or cP	1	1	3	7
(dynamic—values at 15 $^{\circ}\text{C}$)					
Flash point	$^{\circ}\text{C}$	< −30	30	72	> 95
Sulfur content	%	0.07	0.06	0.06	0.12
Pour point	$^{\circ}\text{C}$	−27	−18	−15	−5
Surface tension	mN/m	24	25.7	26.6	28
(air–oil at 15 $^{\circ}\text{C}$)					
IFT sea water	mN/m	26.9	28.2	27.3	22
IFT fresh water	mN/m	29.1	28.8	28.9	25.3
Adhesion	g/m ³	1	4	5	9

SARA content (saturate, aromatic, resin, asphaltene) %

Saturate	%	92	87	87	85
Aromatic	%	7	12	11	14
Resin	%	1	1	3	2
Asphaltene	%	0	0	0	0
Waxes	%	4	3	5	7

Emulsion formation (type formed and water content %)

Type				
Water content	%			
Viscosity	mPa·s or cP			

Chemical dispersibility with Corexit 9500

%	48			
---	----	--	--	--

Distillation data (% at temperature)

Boiling point ($^{\circ}\text{C}$)				
40	3			
60	5			
80	15			
100	23	2		
120	33	6		
140	34	13		
160	39	23	2	
180	47	33	9	
200	55	43	19	
250	72	64	48	10
300	86	82	74	49
400	99	98	97	94
500				
600				
700				

Oil name West Delta Block 143
Origin and description Gulf of Mexico, USA

Evaporation equation

Where Ev = weight percent evaporated, T = surface temperature ($^{\circ}\text{C}$), t = time (min)

API gravity	29.1	Weathering % by weight			
(all units at 15°C)	Units	0	8.5	17.3	25.8
Density	g/ml	0.8806	0.9049	0.9232	0.9431
Viscosity	mPa·s or cP	28.8	71.7	222.7	1214
(dynamic—values at 15°C)					
Flash point	$^{\circ}\text{C}$				
Sulfur content	%				
Pour point	$^{\circ}\text{C}$				
Surface tension	mN/m	27.6	28.5	29.5	
(air–oil at 15°C)					
IFT sea water	mN/m	23.5	26.2	27.7	
IFT fresh water	mN/m	23.9	27.8	29	
Adhesion	g/m^3				

SARA content (saturate, aromatic, resin, asphaltene) %

Saturate	%	61	59	55.8	49.9
Aromatic	%	26.6	28	28.1	28
Resin	%	8.9	9	11.2	15.4
Asphaltene	%	3.6	4	4.9	6.7
Waxes	%				

Emulsion formation (type formed and water content %)

Type				
Water content	%			
Viscosity	mPa·s or cP			

Chemical dispersibility with Corexit 9500

%				
---	--	--	--	--

Distillation data (% at temperature)

Boiling point ($^{\circ}\text{C}$)				
40				
60				
80				
100				
120				
140				
160				
180				
200				
250				
300				
400				
500				
600				
700				

Oil name West Texas Intermediate (2002)
Origin and description Galveston, Texas, USA

Evaporation equation

$$\% \text{Ev} = (3.08 + 0.045T) \ln(t)$$

Where Ev = weight percent evaporated, T = surface temperature ($^{\circ}\text{C}$), t = time (min)

API gravity	34.38	Weathering % by weight			
(all units at 15°C)	Units	0	10.1	21	31.7
Density	g/ml	0.8474	0.8665	0.8827	0.8973
Viscosity	mPa·s or cP	8.6	16.4	37.5	112.3
(dynamic—values at 15°C)					
Flash point	$^{\circ}\text{C}$	< -10	32.8	66	> 110
Sulfur content	%	0.86	1.01	1.11	1.24
Pour point	$^{\circ}\text{C}$	-22	-12	1	7
Surface tension	mN/m	26	27.6	28.7	29.2
(air–oil at 15°C)					
IFT sea water	mN/m	15.6	14.6	12.6	17.3
IFT fresh water	mN/m	15.8	18.1	17.2	17.1
Adhesion	g/m^3	12.4	16.8	27.6	33.2

SARA content (saturate, aromatic, resin, asphaltene) %

Saturate	%	78.5	78.6	76.3	74.8
Aromatic	%	14.8	13.7	14.6	13.8
Resin	%	6	6.9	8	9.9
Asphaltene	%	0.7	0.8	1.1	1.6
Waxes	%	2.8	3.1	3.4	4

Emulsion formation (type formed and water content %)

Type	Unstable	Unstable	Meso stable	Meso stable
Water content	%		82.7	83.6
Viscosity	mPa·s or cP			

Chemical dispersibility with Corexit 9500

%	27.7	23.6	13.3	12.8
---	------	------	------	------

Distillation data (% at temperature)

Boiling point ($^{\circ}\text{C}$)				
40	0.7			
60	0.7			
80	1			
100	5.5	1.8		
120	8.9	4.2	0.1	
140	12.6	7.5	0.9	
160	16.2	11.2	2.8	
180	20	15.3	6.2	0.4
200	23.5	19.2	10.1	1.9
250	32.4	29	21.1	11.4
300	41.2	38.9	32.3	23.7
400	57.5	57	52.9	47
500	70.7	71.7	69.9	66
600	79.8	81.8	81.2	79.1
700				

Oil name West Texas Intermediate
Origin and description Texas, USA

Evaporation equation $\%Ev = (2.77 + 0.045T)\ln(t)$
 Where Ev = weight percent evaporated, T = surface temperature (°C), t = time (min)

API gravity	36.4	Weathering % by weight		
(all units at 15°C)	Units	0	14	29
Density	g/ml	0.842	0.8674	0.8875
Viscosity	mPa-s or cP	7	16	49
(dynamic—values at 15°C)				
Flash point	°C	−17	32	87
Sulfur content	%	0.48	0.49	0.57
Pour point	°C	−23	−15	3
Surface tension	mN/m	26.6	27.6	29.5
(air–oil at 15°C)				
IFT sea water	mN/m	18.9	18.7	18.1
IFT fresh water	mN/m	19.1	21	20.6
Adhesion	g/m ³	15	21	24

SARA content (saturate, aromatic, resin, asphaltene) %

Saturate	%	66	64	60
Aromatic	%	26	27	30
Resin	%	6	7	8
Asphaltene	%	1	1	1
Waxes	%	4	4	5

Emulsion formation (type formed and water content %)

Type			
Water content	%		
Viscosity	mPa-s or cP		

Chemical dispersibility with Corexit 9500

%	15		
---	----	--	--

Distillation data (% at temperature)

Boiling point (°C)			
40	3	1	
60	4	2	
80	6	3	
100	9	4	
120	13	5	
140	17	7	
160	20	11	1
180	2	15	3
200	28	19	6
250	38	30	19
300	49	42	33
400	69	65	59
500	84	82	79
600	94	93	92
700	99	99	98

Oil name West Texas Sour
Origin and description Texas, USA

Evaporation equation $\%Ev = (2.57 + 0.045T)\ln(t)$
 Where Ev = weight percent evaporated, T = surface temperature (°C), t = time (min)

API gravity	30.2	Weathering % by weight		
(all units at 15°C)	Units	0	15	30
Density	g/ml	0.7843	0.9019	0.928
Viscosity	mPa-s or cP	13	39	262
(dynamic—values at 15°C)				
Flash point	°C	−14	36	> 90
Sulfur content	%	1.5	2.37	2.78
Pour point	°C	−27	−1	12
Surface tension	mN/m	27	27.4	31.8
(air–oil at 15°C)				
IFT sea water	mN/m	17.8	22.4	28.3
IFT fresh water	mN/m	22	23.9	31.8
Adhesion	g/m ³	21	24	25

SARA content (saturate, aromatic, resin, asphaltene) %

Saturate	%	51	46	41
Aromatic	%	36	39	41
Resin	%	9	10	13
Asphaltene	%	5	5	5
Waxes	%	5	5	5

Emulsion formation (type formed and water content %)

Type			
Water content	%		
Viscosity	mPa-s or cP		

Chemical dispersibility with Corexit 9500

%	25		
---	----	--	--

Distillation data (% at temperature)

Boiling point (°C)			
40	2		
60	2	1	
80	5	2	
100	8	3	
120	12	4	
140	16	6	
160	19	10	
180	23	113	1
200	26	17	3
250	36	27	14
300	45	37	26
400	64	58	51
500	80	77	73
600	91	90	88
700	99	98	98

Oil name		White Rose			
Origin and description		Newfoundland			
Evaporation equation		$\%Ev = (1.44 + 0.0457)\ln(t)$			
Where Ev = weight percent evaporated, T = surface temperature ($^{\circ}\text{C}$), t = time (min)					
API gravity		Weathering % by weight			
(all units at 15°C)	Units	0	9	15	24
Density	g/ml	0.8738	0.8926	0.9026	0.9143
Viscosity	mPa-s or cP	30	87	253	992
(dynamic—values at 15°C)					
Flash point	$^{\circ}\text{C}$	−10	48	80	> 100
Sulfur content	%				
Pour point	$^{\circ}\text{C}$	13	23	24	30
Surface tension	mN/m	27.7	29.2	29.9	59.3
(air-oil at 15°C)					
IFT sea water	mN/m	28.2	18.4		
IFT fresh water	mN/m	29.1	19.4		
Adhesion	g/m^3	23	26	46	63
SARA content (saturate, aromatic, resin, asphaltene) %					
Saturate	%	62.9	61.4	58.9	58.5
Aromatic	%	27.4	27.8	27.7	27.7
Resin	%	7.3	8.2	10.7	10.2
Asphaltene	%	2.4	2.6	2.8	3.6
Waxes	%	5.5	5.8	6.2	6.9
Emulsion formation (type formed and water content %)					
Type					
Water content	%				
Viscosity	mPa-s or cP				
Chemical dispersibility with Corexit 9500					
	%	21	20	16	16
Distillation data (% at temperature)					
Boiling point ($^{\circ}\text{C}$)					
40		0.6			
60		0.8			
80		0.9			
100		3.1	0.3		
120		6.3	1.6		
140		8.5	3.1	0.3	
160		11.1	5.4	1.2	
180		13.8	8.1	3.1	
200		16.5	10.9	5.7	0.3
250		25	19.9	15	6.5
300		35.4	31	26.8	18.7
400		57.6	54.7	51.9	46.6
500		77.9	76.5	75.1	72.5
600		90.4	89.8	89.2	88.2
700					

Oil name		Zaire			
Origin and description		Zaire			
Evaporation equation		$\%Ev = (1.36 + 0.045T)\ln(t)$			
Where Ev = weight percent evaporated, T = surface temperature ($^{\circ}\text{C}$), t = time (min)					
API gravity	30.7	Weathering % by weight			
(all units at 15°C)	Units	0	6	14	23
Density	g/ml	0.872	0.8872	0.9015	0.902
Viscosity	mPa-s or cP	2070	52,800	94,560	533,100
(dynamic—values at 15°C)					
Flash point	$^{\circ}\text{C}$	−3	31	85	> 95
Sulfur content	%	0.16	0.16	0.13	0
Pour point	$^{\circ}\text{C}$	25	29	32	34
Surface tension	mN/m				
(air–oil at 15°C)					
IFT sea water	mN/m				
IFT fresh water	mN/m				
Adhesion	g/m^3	58	92	161	333
SARA content (saturate, aromatic, resin, asphaltene) %					
Saturate	%	64	61	59	53
Aromatic	%	22	24	26	28
Resin	%	9	9	10	16
Asphaltene	%	5	5	5	5
Waxes	%	20	11	12	13
Emulsion formation (type formed and water content %)					
Type					
Water content	%				
Viscosity	mPa-s or cP				
Chemical dispersibility with Corexit 9500					
	%	0			
Distillation data (% at temperature)					
Boiling point ($^{\circ}\text{C}$)					
40					
60					
80		2			
100		5	1		
120		6	3		
140		8	5		
160		11	7	1	
180		13	10	3	
200		15	12	5	
250		22	20	13	4
300		29	28	22	12
400		45	46	41	34
500		61	66	63	58
600		74	81	78	76
700		84	91	90	88

APPENDIX B

CONVERSIONS

MERV FINGAS

Spill Science, Edmonton, Alberta, Canada

To convert from	Into	Multiply by
acres	hectares	0.405
acres	square meters (m ²)	4047
atmosphere (pressure)	N m ⁻² (Pa)	1.01 × 10 ⁵
atmosphere (pressure)	pounds per square inch (PSI)	14.7
barrel/day	m ³ /day	0.159
barrels	cubic feet (ft ³)	5.61
barrels	cubic meters (m ³)	0.159
barrels	imperial gallons	35
barrels	U.S. gallons	42
barrels	liters (l)	159
barrels (oil)	tonnes	0.159 × density
barrels (oil)	tonnes	0.136 (crude oil)
barrels (oil)	tonnes	0.116 (gasoline)
barrels (oil)	tonnes	0.150 (Bunker C)
barrels/h	m ³ /h	0.159
centipoise (viscosity)	Pa·s	0.001
centipoise (viscosity)	mPa·s	1
cubic feet (ft ³)	cubic meters (m ³)	0.0283
cubic meters (m ³)	barrels	6.29
cubic meters (m ³)	cubic feet (ft ³)	35.3
cubic meters (m ³)	milliliters (ml)	1,000,000
cubic meters (m ³)	imperial gallon	220
cubic meters (m ³)	U.S. gallon	264
cubic meters/h	barrels/h	6.29
fathom	meters (m)	1.83
fathom	feet (ft)	6
feet (ft)	inches (in.)	12
feet (ft)	meters (m)	0.305
gallon (imperial)	liters (l)	4.55
gallon (U.S.)	liters (l)	3.79
gallon (U.S.)	imperial gallon	0.83

To convert from	Into	Multiply by
gallons/acre (U.S.)	l/hectare	9.36
hectares	acres	2.47
inch (in.)	centimeters (cm)	2.54
kilograms (kg)	pounds (lb)	2.2
kilometers (km)	miles	0.62
kilometers (km)	miles (nautical)	0.54
kilometers per hour	knots	0.54
(km/h)		
knots	meters per second (m/s)	0.52
knots	kilometers per hour (km/h)	1.85
liters (l)	U.S. gallon	0.264
liters/min	gpm (U.S.)	0.265
liters/hectare	U.S. gallons/acre	0.107
m ³ /day	barrel/day	6.29
m ³	barrel	6.29
meters (m)	feet (ft)	3.28
metre/second	knots	1.94
miles	kilometers (km)	1.61
miles (nautical)	kilometers (km)	1.85
pound (lb)	grams (g)	453.6
pound (lb)	kilograms (kg)	0.45
PSI (pressure)	kPa	6.89
square feet (ft ²)	square meters (m ²)	0.093
square meters (m ²)	square feet (ft ²)	10.76
tonne (oil)	U.S. gallons	264 (×density)
tonne (oil)	liters (l)	1000 (×density)
ton (long)	pounds (lb)	2240
ton (short)	pounds (lb)	2000
ton (short)	tonnes	0.907
tons/h	barrels/h	6.3
tonne	kilograms (kg)	1000
tonne	ton (short)	1.1

APPENDIX C

ICE NOMENCLATURE

MERV FINGAS

Spill Science, Edmonton, Alberta, Canada

This glossary of ice terminology closely follows that of the World Meteorological Organization (<http://www.aari.nw.ru/gdsidb/XML/volume1.php?lang1=0&lang2=1&arrange=1>)

This classification is considered standard and is nearly identical in several other classifications such as that for Canada and the United States. The most relevant terms to oil-in-ice are given. There exists about 10 times as many terms as presented here.

Brash ice: Accumulations of floating ice made up of fragments not more than 2 m across, the wreckage of other forms of ice.



Brash ice consists of fragments of larger forms of ice. The small fragments in this photo are brash ice (<http://www.photolib.noaa.gov/>).

Broken ice: An unacceptable term that has made its way into oil spill literature. This term should not be used as it appears in no ice dictionary and does not refer to any specific condition. Use the appropriate terms in this glossary instead.

Close ice: Floating ice in which the concentration is 7/10 to 8/10, composed of floes mostly in contact.



A photo of close ice (<http://www.photolib.noaa.gov/>).

Compact ice: Floating ice in which the concentration is 10/10 and no water is visible.



This is a photo of a typical surface scene over compact ice that includes hummocks and snow. The ice itself is not visible (<http://www.photolib.noaa.gov/>).

Compacted ice edge: Close, clear-cut ice edge compacted by wind or current, usually on the windward side of an area of drift ice.

Concentration: The ratio expressed in tenths* describing the amount of the sea surface covered by ice as a fraction of the whole area being considered. Total concentration includes all stages of development that are present, and partial concentration may refer to the amount of a particular stage or of a particular form of ice and represents only a part of the total.

*Note: In historical sea-ice data, octas have been used by some countries.

Consolidated ice: Floating ice in which the concentration is 10/10 and the floes are frozen together.

Deformed ice: A general term for ice which has been squeezed together and in places forced upward (and downward). Subdivisions are rafted ice, ridged ice, and hummocked ice.

Drift ice/pack ice: Term used in a wide sense to include any area of sea ice other than fast ice, no matter what form it takes or how it is disposed. When concentrations are high, that is, 7/10 or more, drift ice may be replaced by the term pack ice*.

*Note: Previously the term pack ice was used for all ranges of concentration.



This image shows a wide field of drift ice (http://en.wikipedia.org/wiki/Drift_ice).

Fast ice: Sea ice that forms and remains fast along the coast, where it is attached to the shore, to an ice wall, to an ice front, between shoals, or grounded icebergs. Vertical

fluctuations may be observed during changes of sea level. Fast ice may be formed in situ from sea water or by freezing of floating ice of any age to the shore, and it may extend a few meters or several hundred kilometers from the coast. Fast ice may be more than 1 year old and may then be prefixed with the appropriate age category (old, second year, or multiyear). If it is thicker than about 2 m above sea level, it is called an ice shelf.

Fast-ice edge: The demarcation at any given time between fast ice and open water.

First-year ice: Sea ice of not more than one winter's growth, developing from young ice; thickness 30 cm–2 m. May be subdivided into thin first-year ice/white ice, medium first-year ice, and thick first-year ice.

Floating ice: Any form of ice found floating in water. The principal kinds of floating ice are lake ice, river ice, and sea ice which form by the freezing of water at the surface, and glacier ice (ice of land origin) formed on land or in an ice shelf. The concept includes ice that is stranded or grounded.

Floe: Any relatively flat piece of sea ice 20 m or more across. Floes are subdivided according to horizontal extent.



This image shows a series of floes in a pack ice field with brash ice in between (http://icdc.zmaw.de/seaicetype_shipobs_ant.html?&L=1).

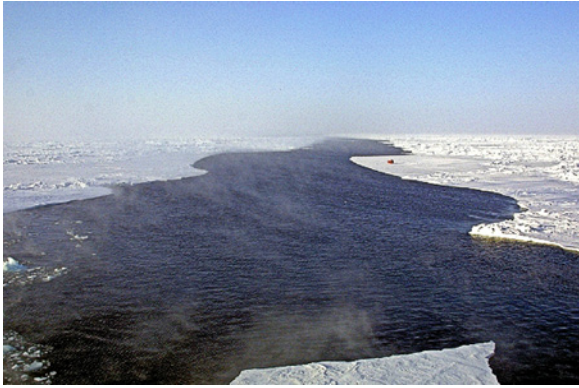
Fracture: Any break or rupture through very close ice, compact ice, consolidated ice, fast ice, or a single floe resulting from deformation processes. Fractures may contain brash ice and/or be covered with nilas and/or young ice. Length may vary from a few meters to many kilometers.

Frazil ice: Fine spicules or plates of ice, suspended in water.

Grease ice: A later stage of freezing than frazil ice when the crystals have coagulated to form a soupy layer on the surface. Grease ice reflects little light, giving the sea a matt appearance.

Ice cover: The ratio of an area of ice of any concentration to the total area of sea surface within some large geographic local; this local may be global, hemispheric, or prescribed by a specific oceanographic entity such as Baffin Bay or the Barents Sea.

Lead: Any fracture or passage-way through sea ice which is navigable by surface vessels.



This image shows a lead in ice (http://icdc.zmaw.de/seaicetype_shipobs_ant.html?&L=1).

Multi-year ice: Old ice up to 3 m or more thick which has survived at least two summers' melt. Hummocks even smoother than in second-year ice, and the ice is almost salt-free. Color, where bare, is usually blue. Melt pattern consists of large inter-connecting irregular puddles and a well-developed drainage system.

New ice: A general term for recently formed ice which includes frazil ice, grease ice, slush, and shuga. These types of ice are composed of ice crystals which are only weakly frozen together (if at all) and have a definite form only while they are afloat.

Old ice: Sea ice that has survived at least one summer's melt; typical thickness up to 3 m or more. Most topographic features are smoother than on first-year ice. May be subdivided into second-year ice and multi-year ice.

Open ice: Floating ice in which the ice concentration is 4/10 to 6/10, with many leads and polynyas, and the floes are generally not in contact with one another.

Open water: A large area of freely navigable water in which sea ice is present in concentrations less than 1/10. No ice of land origin is present.

Pack ice: Term used in a wide sense to include any area of sea ice other than fast ice no matter what form it takes or how it is disposed. Pack ice is often used when concentrations are high, that is, 7/10 or more.



Pack ice is illustrated here (<http://www.photolib.noaa.gov/>).

Pancake ice: Predominantly circular pieces of ice from 30 cm to 3 m in diameter, and up to about 10 cm in thickness, with raised rims due to the pieces striking against one another. It may be formed on a slight swell from grease ice, shuga, or slush or as a result of the breaking of ice rind, nilas or, under severe conditions of swell or waves, of gray ice. It also sometimes forms at some depth at an interface between water bodies of different physical characteristics, from where it floats to the surface; its appearance may rapidly cover wide areas of water.



A close up of pancake ice (<http://www.photolib.noaa.gov/>).



A wide-angle scene of pancake ice (<http://www.photolib.noaa.gov/>).

Rotten ice: Sea ice that has become honeycombed and which is in an advanced state of disintegration.

Sea ice: Any form of ice found at sea which has originated from the freezing of sea water.

Second-year ice: Old ice that has survived only one summer's melt; typical thickness up to 2.5 m and sometimes more. Because it is thicker than first-year ice, it stands higher out of the water. In contrast to multi-year ice, summer melting produces a regular pattern of numerous small puddles. Bare patches and puddles are usually greenish-blue.

Shuga: An accumulation of spongy white ice lumps, a few centimeters across; they are formed from grease ice or slush and sometimes from anchor ice rising to the surface.

Very close ice: Floating ice in which the concentration is 9/10 to less than 10/10.

Very open ice: Floating ice in which the concentration is 1/10 to 3/10 and water preponderates over ice.



The low concentration of ice here is named very open ice (<http://www.photolib.noaa.gov/>).

INDEX

- Acoustic oil-in-ice detection, 386–8
- Adamantane, 122–3, **127**
- Adhesion, 44
- Adsorption to snow or ice, 280
- Aesop project, 367–71
- Alaska north slope crude, 579–82
- Alberta sweet mixed blend crude oil, 582–3
- Albian heavy synthetic crude, 583
- Aliphatic hydrocarbons, 117–18
- Alkane compounds, **56**
- Alkane ratios, 149
- Alkanes, 117–18
- Alkenes *see* Olefins
- Alkyl benzenes, 130
- Alkylated PAHs, 130–136, **131**, **132**, **136**, 137–8
- American Petroleum Institute gravity *see* API gravity
- Anadarko crude, 584
- Antarctic oil spills, 497–509
- Antarctic spill, 547–55
- Antioxidants, **40**
- API gravity, 40, 41, 75, 96
- Appendices, 575–688
- Arabian heavy crude, 584
- Arabian light crude, 585
- Arabian medium crude, 585
- Arctic oil spills, 497–509
- Arctic spill countermeasures, 506, 508
- Arctic terrestrial spills, 502–6
- Aromatic steranes, 138–9
- Aromatics, 98–9, 130–136, **132**
- Asphalt primer, 586
- Asphaltenes, 44, 45, 69, 99
- Athabasca bitumen, 586
- Atkinson crude, 587
- Atmospheric boundary layer, 302–3
- Atmospheric properties, 314
- Audunson natural dispersion model, 489–90
- Avalon crude, 587
- Aviation gasoline 100, 588
- Aviation gasoline 100LL, 589
- Aviation gasoline 80, 588
- Bahía Paraíso, 547–55
- Bahía Paraíso spill, 547–55
- Barrow island crude, 589
- Basic Oil Spill Cost Estimation Model, 25–6
- Belridge heavy crude, 590
- Bent horn crude, 590–591
- Bioaugmentation, 398
- Bioaugmentation strategies, 404
- Biodegradation, 295
 - of aromatics, 146
 - of biomarkers, 144–6
 - effect on composition, 142–6
- Biofuels, 88–9
- Biological organic compounds (BOC), 413
- Biomarker ratios, **148**, 149
- Biopiles, 403
- Bioremediation, 397–404
- Biostimulation, 398
- Biostimulation strategies, 404
- Biosurfactants, 404
- Bird oiling, 431–48
- Bird vulnerability to oil, 433–5
- Bottle effect, 219–20
- Brash ice, 685
- Brent blend crude, 591
- Brewster angle, 319
- Broken ice, 685
- BTEX, 130, **131**
- BTEX compounds, **60–61**
- Bunker C fuel oil, 592–3

- California crude, 593–4
- Cano Limon crude, 594
- Canola oil, 79–91, 595
- Carpinteria crude, 595
- Case studies, 513–74
- Catalytic cracker oil, 596
- CEN method, 191
- Chayvo 6 crude, 597
- Chromatographic fingerprinting, 95–158
- Classifiers, 365–6
- Cleanup effects on marshes, 481–3, **482**
- Close ice, 685
- Coal oil point seep oil, 597
- Cohasset crude, 598
- Cold Lake bitumen, 598
- Cold Lake blend oil, 599
- Cold Lake diluent, 599
- Cold region spills, 495–512
- Compact ice, 685
- Compacted ice edge, 686
- Concentration (ice), 686
- Consolidated ice, 686
- Conversions, 683
- Cook Inlet crude, 49, 600
- Cross plot method, 190–192
- Cusiana crude, 600
- Cycloalkanes, 55, **59**

- Dark formation detection, 363–4
- De Noüy ring, 42
- Deformed ice, 686
- Delvigne natural dispersion model, 490–492
- Density, 40
- Detection and tracking, 313–48, 357–80
- Detection, tracking and remote sensing, 311–94
- Diagnostic ratios, **148**, 148–51, 157, 166–95
- Diamantane, 122–3, **127**
- Diamondoids, 119–20, 122, 125–6
- Diesel fuel, 601–3
- Diffusion regulated models, 213–16
- Dispersant effectiveness, 43
- Dissolution, 295
- Distillation data, 216
- Dolphins and oil, 455–71, 457–8, 467–71
- Dos Cuadras crude, 603
- Double-hull tankers, 11, 29–30
- DR *see* Diagnostic ratios
- Drift ice, 686
- Droplet rising, 492
- Dynamic viscosity, 41

- Ecological risk assessment process, 25
- Effectiveness of dispersants, 43
- Effects of oil on birds, 435–6
- Effects of oil, 429–84
- Ekofisk crude, 604
- Electrical insulating oil, 604
- Elemental composition, 53
- Empire crude, 605
- Emulsification, 290–292
- Emulsification effects, 14

- Emulsion stability, 43
- Endicott crude, 605
- Environmental factors and bioremediation, 399–400
- Environmental sensitivity index, 18–19
- EPA priority PAHS, **65–6**, 130–136, **132**, **136**
- Estimating bird mortality, 441–4
- Eugene island crude, 606
- European Committee for Standardization *see* CEN method
- Evaporation, 207–22, 288–9
 - effect on composition, 141
 - equations, **217–18**
- Evaporative weathering, 46–9
- Everdell crude, 607
- Ex-situ bioremediation, 402–4

- Fast GC analysis, 100–102
- Fast ice, 686
- Fast-ice edge, 686
- Fatty acid content, **80**
- Fault tree analysis, 4, 6–8
- Feature extraction, 364–5
- Federated crude, 607
- Fines, 31–4
- First-year ice, 686
- Flash point, 76
- Floating ice, 686
- Floe, 686
- Fluid catalytic cracker oil, 608
- Forensic case study, 151–8, 197
- Fracture, 686
- Frazil ice, 686
- Fuel oil, 609
 - #2, 609
 - #5, 609
- Future remote sensing trends, 346

- Galicia oil spill, 515–42
- Garden Banks crude, 610
- Gas effect on spreading, 275
- Gas sniffing and detection, 391–2
- Gasoline, 611
- GC measurement of evaporation, 221
- GC-FID, **111**, 112, 111–17, 172–6
- GC-MS, 103–4, 176–95
- Genesis crude, 611
- Granite point crude, 612
- Grease ice, 686
- Green canyon crude, 612–14
- Ground-penetrating radar (GPR), 390–391
- Gullfaks crude, 614

- Heavy fuel oil, 615
- Heavy reformate, 615
- Hebron crude, 616
- Heidrun crude, 617
- Hexane, 57
- Hibernia crude, 617–18
- High performance liquid chromatography, 104
- Hondo crude, 619
- Hout crude, 620
- HPLC *see* High performance liquid chromatography

- Hydrocarbon groups, 44
- Hydrocarbon-degrading organisms, **398**
- Ice cover, 686
- Ice dielectric permittivity, 390
- Ice nomenclature, 685–8
- Ice-infested oil behavior, 271–94
- Identification of compounds, **180**
- Identification of PAHs, **182**
- IFO 180, 621
- IFO 30, 620
- IFO 300, 622
- Impact, 25–8
- Infrared (IR), 323
- In-situ remediation strategies, 400–401
- Integrated airborne sensor systems, 333–4
- Interfacial tension, 40, 41
- Interfacial tension effects, 14
- IPAR 3, 622
- Iranian heavy crude, 623
- Isoprenoid ratios, 149
- Isoprenoids, 117–18
- Issungnak crude, 623
- Isthmus crude, 624
- Jet A fuel, 624
- Jet B fuel, 625
- Karachi oil spill, 557–73
- Kuwait crude, 626
- Lago crude, 627
- Lago Treco crude, 626
- Lagomedio crude, 627
- Lagrangian coherent structures, 308
- Land farming, 402–4
- Land spill bioremediation, 397–404
- Langmuir cells, 306–7
- Large volume injection (LVI), 102–3
- Laser fluorosensors, 325–6
- Lead, 686
- Location effects, 16–18
- Long-term impacts of oil on birds, 444
- Look-alike mapping, 377–8
- Louisiana crude, 628
- Low sulfur waxy gas oil, 628
- Low sulfur waxy residuum, 629
- Lubricating oil, 629–34
- Lucula crude, 635
- MacKay natural dispersion model, 487–9
- Macondo, 635
- Main Pass crude, 636
- Malongo crude, 637
- Marine intermediate fuel oil, 637
- Mars TLP crude, 638
- Marshes, 477–88
- Mass loss by weathering, 147–8
- Maya crude, 639–40
- Mediterranean reconnaissance, 366–7
- Metals, 69, **73**
- Meteorological effects on spilled oil, 301–8
- Methyldibenzothiophenes, 188, 190
- Methylfluoranthenes, 189
- Methylphenanthrenes, 188, 190
- Methylpyrenes, 189
- Microbe-assisted phytoremediation, 407–13
- Microwave
 - radiometers, 326–7
 - scatterometers, 331
 - sensors, 326–31, 360–366
- Middle pipeline crude, 580
- Mississippi Canyon crude, 640–642
- Modeling, 285–310
- Morpeth crude, 642
- Mousse, 225–267
- Movement, 297–9
- Multi-year ice, 687
- Naphthenoaromatic compounds, 58, **67**
- Natural attenuation, 401–2
- Natural dispersion, 293–5, 485–94
- Natural dispersion models, 487–94
- Near infrared, 323–5
- Nektoralik crude, 643
- Neptune spar crude, 643
- Nerlerk crude, 644
- New ice, 687
- Ninian blend crude, 644
- Nitrogen compounds, 69, **71–2**
- Norman wells crude, 645
- Northern pipeline crude, 580
- Nuclear magnetic resonance (NMR), 392
- Nuclear techniques for oil in ice detection, 391
- Oceanographic effects on spilled oil, 301–8
- Odoptu crude, 645
- Oil
 - analysis, 93–204
 - behavior, 205–84
 - behavior in leads, 277–9
 - chemistry, 53–76
 - composition, 53–4, 96–8
 - composition and properties, 51–92
 - density effects, 14
 - detection in ice. 385–92
 - detection with ice. 385–92
 - effects on ice properties, 281
 - evaporation, 207–22
 - fingerprinting, 95–158, 165–201
 - forensics, 165–201
 - on iced shoreline, 281
 - impact on marshes, 477–81
 - movement through ice, 276–7
 - in pack ice, 281
 - properties, 29–49, 37–50, 75–6
 - sample preparation, 105, 109–10
 - thickness effects, 218–19
 - transport, 307–8
 - under multi-year ice, 280
 - viscosity effects, 14
- Oil chromatography, 95–158

- Oil pollution act of 1990, 30–31
- Oil spill
 - emulsions, 225–67
 - identification, 165–201
 - impacts, 18–25
 - on land, 395–428
 - modeling, 287–99
 - risk analysis, 3–34
- Oil Spill Response Cost Effectiveness Analytical Tool, 25–6
- Oiled ice albedo, 280
- Oiled marshes, 477–8
- Oiled otters, 455–71
- Oiled sea mammals, 455–71
- Oiled seabirds, 431–48
- Oiled seals, 455–71
- Oiled whales, dolphins, 455–71
- Oil-fines aggregates (OFA), 295–6
- Oil-fines interaction (OFI), 295–6
- Oil-in-ice behaviour, 271–84
- Oil-in-ice detection, 385–92
- Oil-light interaction, 314–15
- Old ice, 687
- Olefins, 55, 98
- Open ice, 687
- Open water, 687
- Optical oil with ice detection, 386
- Optical satellites, 334–5, 359–60
- Optical sensors, 317–23, 358–60
- Oriente crude, 646
- Orimulsion, 646–7
- Oseberg crude, 647
- Over-washing, 295–7
- Oxygen compounds, 58–9, **70**

- Pack ice, 686, 687
- PAH ratios, 149–50
- PAHs *see* Polycyclic aromatic hydrocarbons (PAHs)
- Pakistan oil spill, 557–73
- Palm kernel oil, 84–5
- Palm oil, 85, 87
- Pancake ice, 687
- Panuke crude, 648
- Paraffins, 97–8
- Pendant/rising droplet interfacial tension, 42
- PEPS case studies, 415–22
- PEPS *see* PGPR-enhanced phytoremediation system
- Permafrost soils, 502–6
- Petroleum ether, 648
- Petronius crude, 649
- PGPR-enhanced phytoremediation system, 414–22
- PGPR-enhanced phytoremediation, 413–14
- Photodegradation weathering, 146–7
- Photooxidation, 295
- Phytane, 98
- Phytoremediation, 407–423
 - costs, 418
 - and regulatory criteria, 421
- Pitas point crude, 649
- Plant growth-promoting rhizobacteria *see* PGPR
- Plant sensitivity to oil, 478–81
- Platform Elly Crude, 49, 650
- Platform Gail crude, 650
- Platform Holly crude, 651
- Platform Irene crude, 651
- Point Arguello crude, 652–3
- Polar bears and oil, 457, 465–7
- Polycyclic aromatic hydrocarbons (PAHs), **62–6**
- Porpoises and oil, 457–8, 467–71
- Port Hueneme crude, 653
- Pour point, 42, 76
- Pour point effects, 14
- Prestige oil spill, 515–42
- Prevention, 3–34, 28–34
- Pristane, 98
- Probability
 - distribution function, 10
 - of spill occurrence, 4
 - of tanker spills, 6
- Programmable temperature variation (PTV), 102–3
- Prudhoe Bay crude, 654–5

- Quality assurance and control, 46

- Radar, 327–31
 - detection methodologies, 361–6
 - false detections, 331
 - satellites, 335–44, **345**
- Radio frequency oil with ice detection, 388–91
- Rangely crude, 656
- Real-time displays, 345
- Rehabilitation of oiled birds, 436–41
- Remote sensing, 313–48, 357–80
- Remote-controlled aircraft, 344–5
- Removal of natural organic compounds, 421–2
- Resins, 44, 45, 69, 99
- Restoration of oiled bird colonies, 446–8
- Risk analysis, 1–36, 3–34
- Risk analysis for policy making, 27–8
- Rotten ice, 687
- Routine surveillance, 345–6

- Sable Island condensate, 656
- Saharan blend crude, 657
- Sakhalin crude, 657
- Sample
 - analysis, 171–95
 - handling, 170–171
- Sampling, 167–70
 - beaches, 169–70
 - tar balls, 167
 - thick layers, 167
 - thin layers, 167–8
 - vessel tanks, 170
- Santa Clara crude, 658
- SARA, 44, 54–5
- Satellite remote sensing, 334–44
- Saturates, 44, 55
- Saturation concentration, 216
- Scotia light crude, 658
- Sea cows and oil, 464–5
- Sea ice, 687
- Sea mammals and oil, 455–71

- Sea otters and oil, 456–7, 458–61
- Sea spray, 306
- Seabird families, **433**
- Seal lions and oil, 457, 461–4
- Seals and oil, 455–71, 461–4
- Second-year ice, 688
- Sediment oil concentrations, **567**
- Sedimentation, 295–6
- Sensitivity, 23–5
- Sensor recommendations, 347
- Sesquiterpanes, 124–30, *128*, **129**
- Ship detection, 377
- Ship pollution detection, 371–4
- Ship Shoal crude, 659
- Shorebird families, **433**
- Shoreline effects on risk, 17
- Shuga, 688
- Single-hull tankers, 11
- Sinking, 295–7
- Skin formation, 220
- Slick
 - sampler, 168
 - thickness measurement, 331–3
- Socio-economic impacts, 14–16
- Sockeye crude, 660–662
- Sour blend crude, 662
- South Louisiana crude, 663–4
- South Pass crude, 664–5
- South Timbalier crude, 666
- Southern pipeline crude, 581
- Soybean oil, 79–91, 666
- Spanish oil spill, 515–42
- Specific gravity, 76
- Spectrographic techniques, 104–5
- Spill Control, and Countermeasures Program (SPCC), 31–2
- Spill
 - prevention, 3–34
 - risk analysis, 3–34
 - volume probability distribution, 9
- Spreading, 297–8
 - on ice, 271–2
 - under ice, 273–4
 - on water, with ice, 274–5
- Statfjord crude, 667
- Steranes, 119, *120–121*, **122**
- Subsurface well blowouts, 308
- Sulfur compounds, 58, **68**
- Sulfur content, 42
- Sumatra heavy crude, 667
- Sumatra light crude, 668
- Surface tension *see* Interfacial tension
- Surface wave radars, 331
- Swanson River crude, 668
- Synthetic crude, 669
- Taching crude, 669
- Takula crude, 670
- Tanker spills, 6, 11
- Tapis Blend crude, 670
- Tar ball formation, 297
- Target analytes, **106–8**
- Tarsuit crude, 671
- Tasman Spirit oil spill, 557–73
- Terpenes, 118–19, *120–121*, **122**
- Terra Nova crude, 671–2
- Thevenard Island crude, 673
- Thickness sensors, 332–3
- Thin layer chromatography, 44
- Transmountain blend crude, 673
- Triaromatic steranes, 186
- Triterpanes, 184, 187
- Troll crude, 674
- Two-dimensional GC Analysis, 102–3
- Udang crude, 674
- UHF radiometer oil in ice detection, 391
- Ultraviolet (UV), 325
- Underwater acoustic oil detection, 388
- Underwater detection, 340
- Uviluk crude, 675
- Vasconcia crude, 675
- Vegetable oil
 - behavior, 87–8
 - biodegradation, 87
 - countermeasures, 88
 - properties, 86–7
 - spills, 79–91, **81**
 - toxicity, 86
- Very close ice, 688
- Very open ice, 688
- Viosca Knoll crude, 676
- Viscosity, 39, 41
- Visible detection of oil, 315–17, 360–362
- Visible sensors, 317–23, 360–362
- Visual slick thickness, 331–2
- Volatilization, 221
- Voltesso, 604
- Wabasca crude, 677
- Water content, 42
- Water currents, 303–4
- Water-in-oil emulsion, 225–67
- Waves, 304–6
- Waxy light-heavy blend crude, 677
- Weather effects on spilled oil, 301–8
- Weathering, 46–9
- Weathering effect, 141–7, 173–6
- West Delta crude, 678–9
- West Texas intermediate crude, 679–80
- West Texas sour crude, 680
- Whales and oil, 457–8, 467–71
- White Rose crude, 681
- Zaire crude, 681

WILEY END USER LICENSE AGREEMENT

Go to www.wiley.com/go/eula to access Wiley's ebook EULA.